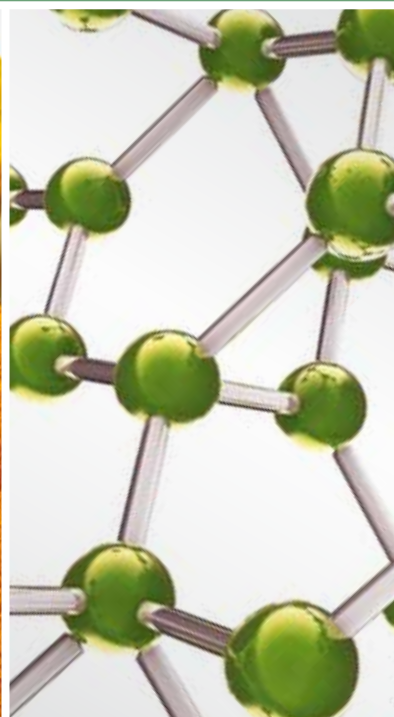


NETWORK PHARMACOLOGY in TRADITIONAL CHINESE MEDICINE

GUEST EDITORS: SHAO LI, TAI-PING FAN, WEI JIA, AIPING LU, AND WEIDONG ZHANG





Network Pharmacology in Traditional Chinese Medicine

Evidence-Based Complementary and Alternative Medicine

Network Pharmacology in Traditional Chinese Medicine

Guest Editors: Shao Li, Tai-Ping Fan, Wei Jia, Aiping Lu,
and Weidong Zhang



Copyright © 2014 Hindawi Publishing Corporation. All rights reserved.

This is a special issue published in "Evidence-Based Complementary and Alternative Medicine." All articles are open access articles distributed under the Creative Commons Attribution License, which permits unrestricted use, distribution, and reproduction in any medium, provided the original work is properly cited.

Editorial Board

- M. A. Abdulla, Malaysia
Jon Adams, Australia
Zuraini Ahmad, Malaysia
U. P. Albuquerque, Brazil
Gianni Allais, Italy
Terje Alraek, Norway
Souliman Amrani, Morocco
Akshay Anand, India
Shrikant Anant, USA
Manuel Arroyo-Morales, Spain
S. M. B. Asdaq, Saudi Arabia
Seddigheh Asgary, Iran
Hyunsu Bae, Republic of Korea
Lijun Bai, China
Sandip K. Bandyopadhyay, India
Sarang Bani, India
Vassya Bankova, Bulgaria
Winfried Banzer, Germany
Vernon A. Barnes, USA
Samra Bashir, Pakistan
Jairo Kenupp Bastos, Brazil
Sujit Basu, USA
David Baxter, New Zealand
Andre-Michael Beer, Germany
Alvin J. Beitz, USA
Y. Chool Boo, Republic of Korea
Francesca Borrelli, Italy
Gloria Brusotti, Italy
Ishfaq A. Bukhari, Pakistan
Arndt Bssing, Germany
Rainer W. Bussmann, USA
Raffaele Capasso, Italy
Opher Caspi, Israel
Han Chae, Korea
Shun-Wan Chan, Hong Kong
I.-M. Chang, Republic of Korea
Rajnish Chaturvedi, India
Chun Tao Che, USA
Hubiao Chen, Hong Kong
Jian-Guo Chen, China
Kevin Chen, USA
Tzeng-Ji Chen, Taiwan
Yunfei Chen, China
Juei-Tang Cheng, Taiwan
Evan Paul Cherniack, USA
Jen-Hwey Chiu, Taiwan
C. S. Cho, Hong Kong
Jae Youl Cho, Korea
S.-H. Cho, Republic of Korea
Chee Yan Choo, Malaysia
Li-Fang Chou, Taiwan
Ryowon Choue, Republic of Korea
Shuang-En Chuang, Taiwan
Joo-Ho Chung, Republic of Korea
Edwin L. Cooper, USA
Gregory D. Cramer, USA
Meng Cui, China
R. K. Nakamura Cuman, Brazil
Vincenzo De Feo, Italy
R. De la P. Vázquez, Spain
Martin Descarreaux, USA
Alexandra Deters, Germany
S. S. K. Durairajan, Hong Kong
Mohamed Eddouks, Morocco
Thomas Efferth, Germany
Tobias Esch, USA
Saeed Esmaeili-Mahani, Iran
Nianping Feng, China
Yibin Feng, Hong Kong
J. Fernandez-Carnero, Spain
Juliano Ferreira, Brazil
Fabio Firenzuoli, Italy
Peter Fisher, UK
W. F. Fong, Hong Kong
Joel J. Gagnier, Canada
Siew Hua Gan, Malaysia
Jian-Li Gao, China
Gabino Garrido, Chile
Muhammad N. Ghayur, Pakistan
Anwarul H. Gilani, Pakistan
Michael Goldstein, USA
Mahabir P. Gupta, Panama
Svein Haavik, Norway
Abid Hamid, India
N. Hanazaki, Brazil
KB Harikumar, India
Cory S. Harris, Canada
Thierry Hennebelle, France
Seung-Heon Hong, Korea
Markus Horneber, Germany
Ching-Liang Hsieh, Taiwan
Jing Hu, China
Sheng-Teng Huang, Taiwan
Benny Tan Kwong Huat, Singapore
Roman Huber, Germany
Angelo Antonio Izzo, Italy
Suresh Jadhav, India
Kanokwan Jarukamjorn, Thailand
Yong Jiang, China
Zheng L. Jiang, China
Stefanie Joos, Germany
Sirajudeen K.N.S., Malaysia
Z. Kain, USA
Osamu Kanauchi, Japan
Wenyi Kang, China
Dae Gill Kang, Republic of Korea
Shao-Hsuan Kao, Taiwan
Krishna Kaphle, Nepal
Kenji Kawakita, Japan
Jong Yeol Kim, Republic of Korea
Youn Chul Kim, Republic of Korea
Cheorl-Ho Kim, Republic of Korea
Yoshiyuki Kimura, Japan
Joshua K. Ko, China
Toshiaki Kogure, Japan
Jian Kong, USA
Nandakumar Krishnadas, India
Yiu Wa Kwan, Hong Kong
Kuang Chi Lai, Taiwan
Ching Lan, Taiwan
Alfred Lngler, Germany
Lixing Lao, Hong Kong
Clara Bik-San Lau, Hong Kong
Jang-Hern Lee, Republic of Korea
Myeong Soo Lee, Republic of Korea
Tat leang Lee, Singapore
Christian Lehmann, Canada
Marco Leonti, Italy
Ping Chung Leung, Hong Kong
Lawrence Leung, Canada
Kwok Nam Leung, Hong Kong
Ping Li, China
Min Li, China
Man Li, China
ChunGuang Li, Australia

Xiu-Min Li, USA
Shao Li, China
Yong Hong Liao, China
Sabina Lim, Korea
Wen Chuan Lin, China
Bi-Fong Lin, Taiwan
Christopher G. Lis, USA
Gerhard Litscher, Austria
I-Min Liu, Taiwan
Ke Liu, China
Gaofeng Liu, China
Yijun Liu, USA
Cun-Zhi Liu, China
Gail B. Mahady, USA
Juraj Majtan, Slovakia
Subhash C. Mandal, India
J. L. Marnewick, South Africa
Virginia S. Martino, Argentina
James H. McAuley, Australia
Karin Meissner, Germany
Andreas Michalsen, Germany
David Mischoulon, USA
Syam Mohan, Saudi Arabia
J. Molnar, Hungary
Valério Monteiro-Neto, Brazil
H.-I. Moon, Republic of Korea
Albert Moraska, USA
Mark Moss, UK
Yoshiharu Motoo, Japan
Frauke Musial, Germany
MinKyun Na, Republic of Korea
Richard L. Nahin, USA
Vitaly Napadow, USA
F. R. F. Nascimento, Brazil
S. Nayak, Trinidad And Tobago
Roland Ndip Ndip, South Africa
Isabella Neri, Italy
T. B. Nguiefack, Cameroon
Martin Offenbaecher, Germany
Ki-Wan Oh, Republic of Korea
Yoshiji Ohta, Japan
Olumayokun A. Olajide, UK
Thomas Ostermann, Germany
Stacey A. Page, Canada
Tai-Long Pan, Taiwan
Bhushan Patwardhan, India
B. Smestad Paulsen, Norway

Andrea Pieroni, Italy
Richard Pietras, USA
Waris Qidwai, Pakistan
Xianqin Qu, Australia
Cassandra L. Quave, USA
Roja Rahimi, Iran
Khalid Rahman, UK
Cheppail Ramachandran, USA
Gamal Ramadan, Egypt
Ke Ren, USA
Man H. Rhee, Republic of Korea
M.-R. Rhyu, Republic of Korea
José L. Ríos, Spain
Paolo R. di Sarsina, Italy
B. Saad, Palestinian Authority
Sumaira Sahreen, Pakistan
Omar Said, Israel
Luis A. Salazar-Olivo, Mexico
Mohd. Zaki Salleh, Malaysia
A. Sandner-Kiesling, Austria
Adair Santos, Brazil
G. Schmeda-Hirschmann, Chile
Andrew Scholey, Australia
Veronique Seidel, UK
Senthamil R. Selvan, USA
Tuhinadri Sen, India
Hongcai Shang, China
Karen J. Sherman, USA
Ronald Sherman, USA
Kuniyoshi Shimizu, Japan
Kan Shimpo, Japan
Byung-Cheul Shin, Korea
Yukihiro Shoyama, Japan
Chang Gue Son, Korea
Rachid Soulimani, France
Didier Stien, France
Shan-Yu Su, Taiwan
Mohd R. Sulaiman, Malaysia
Venil N. Sumantran, India
John R. S. Tabuti, Uganda
Toku Takahashi, USA
Rabih Talhouk, Lebanon
Yuping Tang, China
Wen-Fu Tang, China
Lay Kek Teh, Malaysia
Mayank Thakur, Germany
Menaka C. Thounaojam, India

Mei Tian, China
Evelin Tiralongo, Australia
Stephanie Tjen-A-Looi, USA
Michał Tomczyk, Poland
Yao Tong, Hong Kong
K. V. Trinh, Canada
Karl W.-K. Tsim, Hong Kong
Volkan Tugcu, Turkey
Yew-Min Tzeng, Taiwan
Dawn M. Upchurch, USA
M. Van de Venter, South Africa
Sandy van Vuuren, South Africa
Alfredo Vannacci, Italy
Mani Vasudevan, Malaysia
Carlo Ventura, Italy
Wagner Vilegas, Brazil
Pradeep Visen, Canada
Aristo Vojdani, USA
Y. Wang, USA
Shu-Ming Wang, USA
Chenchen Wang, USA
Chong-Zhi Wang, USA
Kenji Watanabe, Japan
Jintanaporn Wattanathorn, Thailand
Wolfgang Weidenhammer, Germany
Jenny M. Wilkinson, Australia
Darren R. Williams, Republic of Korea
Haruki Yamada, Japan
Nobuo Yamaguchi, Japan
Yong-Qing Yang, China
Junqing Yang, China
Ling Yang, China
Eun Jin Yang, Republic of Korea
Xiufen Yang, China
Ken Yasukawa, Japan
Min Ye, China
M. Yoon, Republic of Korea
Jie Yu, China
Zunjian Zhang, China
Jin-Lan Zhang, China
Wei-Bo Zhang, China
Hong Q. Zhang, Hong Kong
Boli Zhang, China
Ruixin Zhang, USA
Hong Zhang, China
Haibo Zhu, China

Contents

Network Pharmacology in Traditional Chinese Medicine, Shao Li, Tai-Ping Fan, Wei Jia, Aiping Lu, and Weidong Zhang
Volume 2014, Article ID 138460, 2 pages

A Network Pharmacology Approach to Determine Active Compounds and Action Mechanisms of Ge-Gen-Qin-Lian Decoction for Treatment of Type 2 Diabetes, Huiying Li, Linhua Zhao, Bo Zhang, Yuyu Jiang, Xu Wang, Yun Guo, Hongxing Liu, Shao Li, and Xiaolin Tong
Volume 2014, Article ID 495840, 12 pages

dTGS: Method for Effective Components Identification from Traditional Chinese Medicine Formula and Mechanism Analysis, Ji Luo, Yinglong Ren, Hao Gu, Yi Wu, and Yun Wang
Volume 2013, Article ID 840427, 9 pages

A Module Analysis Approach to Investigate Molecular Mechanism of TCM Formula: A Trial on Shu-feng-jie-du Formula, Jianglong Song, Fangbo Zhang, Shihuan Tang, Xi Liu, Yibo Gao, Peng Lu, Yanping Wang, and Hongjun Yang
Volume 2013, Article ID 731370, 14 pages

Study on Incompatibility of Traditional Chinese Medicine: Evidence from Formula Network, Chemical Space, and Metabolism Room, Wei Long, Xiao-Dong Zhang, Hong-Ying Wu, Jin Jin, Guang-Yun Yu, Xin He, Hao Wang, Xiu Shen, Ze-Wei Zhou, Pei-Xun Liu, and Sai-Jun Fan
Volume 2013, Article ID 352145, 8 pages

Bioinformatics Analysis for the Antirheumatic Effects of Huang-Lian-Jie-Du-Tang from a Network Perspective, Haiyang Fang, Yichuan Wang, Tinghong Yang, Yang Ga, Yi Zhang, Runhui Liu, Weidong Zhang, and Jing Zhao
Volume 2013, Article ID 245357, 11 pages

Systemic Revealing Pharmacological Signalling Pathway Networks in the Hippocampus of Ischaemia-Reperfusion Mice Treated with Baicalin, Haixia Li, Yingying Zhang, Yanan Yu, Bing Li, YinYing Chen, Hongli Wu, Jingtao Wang, Jun Li, Xingjiang Xiong, Qiongyong He, Jinzhou Tian, Zhong Wang, and Jie Wang
Volume 2013, Article ID 630723, 11 pages

Network-Based Biomarkers for Cold Coagulation Blood Stasis Syndrome and the Therapeutic Effects of Shaofu Zhuyu Decoction in Rats, Shulan Su, Jinao Duan, Wenxia Cui, Erxing Shang, Pei Liu, Gang Bai, Sheng Guo, Dawei Qian, and Yuping Tang
Volume 2013, Article ID 901943, 15 pages

Erratum to “Xiao-Xu-Ming Decoction Protects against Blood-Brain Barrier Disruption and Neurological Injury Induced by Cerebral Ischemia and Reperfusion in Rats”, Rui Lan, Jun Xiang, Guo-Hua Wang, Wen-Wei Li, Wen Zhang, Li-Li Xu, and Ding-Fang Cai
Volume 2013, Article ID 476749, 1 pages

Expression Profiling and Proteomic Analysis of JIN Chinese Herbal Formula in Lung Carcinoma H460 Xenografts, Luyu Zheng, Weiye Zhang, Miao Jiang, Huarong Zhang, Fei Xiong, Yang Yu, Meijuan Chen, Jing Zhou, Xiaoming Dai, Yuping Tang, Ming Jiang, Mingyan Wang, Ge Cheng, Jinao Duan, Wei Yu, Biaoyang Lin, Haian Fu, and Xu Zhang
Volume 2013, Article ID 160168, 10 pages

Navigating Traditional Chinese Medicine Network Pharmacology and Computational Tools, Ming Yang, Jia-Lei Chen, Li-Wen Xu, and Guang Ji
Volume 2013, Article ID 731969, 23 pages

The Phytochemical Shikonin Stimulates Epithelial-Mesenchymal Transition (EMT) in Skin Wound Healing, Shu-Yi Yin, An-Ping Peng, Li-Ting Huang, Ya-Ting Wang, Chun-Wen Lan, and Ning-Sun Yang
Volume 2013, Article ID 262796, 13 pages

Exploring the Ligand-Protein Networks in Traditional Chinese Medicine: Current Databases, Methods, and Applications, Mingzhu Zhao, Qiang Zhou, Wanghao Ma, and Dong-Qing Wei
Volume 2013, Article ID 806072, 15 pages

Involvement of Endoplasmic Reticulum Stress in Capsaicin-Induced Apoptosis of Human Pancreatic Cancer Cells, Shengzhang Lin, Jianhong Zhang, Hui Chen, Kangjie Chen, Fuji Lai, Jiang Luo, Zhaohong Wang, Heqi Bu, Riyuan Zhang, Honghai Li, and Hongfei Tong
Volume 2013, Article ID 629750, 12 pages

The Predicted Proteomic Network Associated with the Antiarthritic Action of Qingfu Guanjieshu in Collagen-II-Induced Arthritis in Rats, Ting Yu Wang, Hua Zhou, Yuen Fan Wong, Pui Kei Wu, Wen-Luan Wendy Hsiao, Elaine Lai-Han Leung, and Liang Liu
Volume 2013, Article ID 582493, 15 pages

Network Pharmacology: A New Approach for Chinese Herbal Medicine Research, Gui-biao Zhang, Qing-ya Li, Qi-long Chen, and Shi-bing Su
Volume 2013, Article ID 621423, 9 pages

MAPK Signal Transduction Pathway Regulation: A Novel Mechanism of Rat HSC-T6 Cell Apoptosis Induced by FUZHENGHUAYU Tablet, Qi Wang, Hongbo Du, Min Li, Yue Li, Shunai Liu, Ping Gao, Xiaoli Zhang, and Jun Cheng
Volume 2013, Article ID 368103, 13 pages

A Computational Drug-Target Network for Yuanhu Zhitong Prescription, Haiyu Xu, Ye Tao, Peng Lu, Peng Wang, Fangbo Zhang, Yuan Yuan, Songsong Wang, Xuefeng Xiao, Hongjun Yang, and Luqi Huang
Volume 2013, Article ID 658531, 15 pages

Optimizing Combinations of Flavonoids Deriving from Astragali Radix in Activating the Regulatory Element of Erythropoietin by a Feedback System Control Scheme, Hui Yu, Wendy L. Zhang, Xianting Ding, Ken Y. Z. Zheng, Chih-Ming Ho, Karl W. K. Tsim, and Yi-Kuen Lee
Volume 2013, Article ID 541436, 10 pages

Predicting the Drug Safety for Traditional Chinese Medicine through a Comparative Analysis of Withdrawn Drugs Using Pharmacological Network, Mengzhu Xue, Shoude Zhang, Chaoqian Cai, Xiaojuan Yu, Lei Shan, Xiaofeng Liu, Weidong Zhang, and Honglin Li
Volume 2013, Article ID 256782, 11 pages

Xiao-Xu-Ming Decoction Protects against Blood-Brain Barrier Disruption and Neurological Injury Induced by Cerebral Ischemia and Reperfusion in Rats, Rui Lan, Jun Xiang, Guo-Hua Wang, Wen-Wei Li, Wen Zhang, Li-Li Xu, and Ding-Fang Cai
Volume 2013, Article ID 629782, 12 pages

A Systematic, Integrated Study on the Neuroprotective Effects of Hydroxysafflor Yellow A Revealed by ¹H NMR-Based Metabonomics and the NF- κ B Pathway, Yuanyan Liu, Zeqin Lian, Haibo Zhu, Yinghong Wang, Shishan Yu, Tingting Chen, Jing Qu, Jianbei Li, Shuanggang Ma, and Xianhong Chen
Volume 2013, Article ID 147362, 14 pages

An Integrative Platform of TCM Network Pharmacology and Its Application on a Herbal Formula, Qing-Luo-Yin, Bo Zhang, Xu Wang, and Shao Li
Volume 2013, Article ID 456747, 12 pages

A Systems Biology-Based Investigation into the Pharmacological Mechanisms of Wu Tou Tang Acting on Rheumatoid Arthritis by Integrating Network Analysis, Yanqiong Zhang, Danhua Wang, Shufang Tan, Haiyu Xu, Chunfang Liu, and Na Lin

Volume 2013, Article ID 548498, 12 pages

Metabolism of Genipin in Rat and Identification of Metabolites by Using Ultraperformance Liquid Chromatography/Quadrupole Time-of-Flight Tandem Mass Spectrometry, Yue Ding, Jian-Wei Hou, Yong Zhang, Li-Ying Zhang, Tong Zhang, Yi Chen, Zhen-Zhen Cai, and Li Yang

Volume 2013, Article ID 957030, 13 pages

Metabolomic Study of Collagen-Induced Arthritis in Rats and the Interventional Effects of Huang-Lian-Jie-Du-Tang, a Traditional Chinese Medicine, Rongcai Yue, Ling Zhao, Yaohua Hu, Peng Jiang, Shuping Wang, Li Xiang, Wencong Liu, Lei Shan, Weidong Zhang, and Runhui Liu

Volume 2013, Article ID 439690, 12 pages

Metabolomic Strategy for Studying the Intervention and the Synergistic Effects of the Shexiang Baoxin Pill for Treating Myocardial Infarction in Rats, Li Xiang, Peng Jiang, Shuping Wang, Yaohua Hu, Xiaojun Liu, Rongcai Yue, Weidong Zhang, and Runhui Liu

Volume 2013, Article ID 823121, 11 pages

Vitexicarpin Acts as a Novel Angiogenesis Inhibitor and Its Target Network, Bo Zhang, Lu Liu, Shiwen Zhao, Xu Wang, Liyang Liu, and Shao Li

Volume 2013, Article ID 278405, 13 pages

Traditional Chinese Medicine-Based Network Pharmacology Could Lead to New Multicomponent Drug Discovery, Jian Li, Cheng Lu, Miao Jiang, Xuyan Niu, Hongtao Guo, Li Li, Zhaoxiang Bian, Na Lin, and Aiping Lu

Volume 2012, Article ID 149762, 11 pages

Editorial

Network Pharmacology in Traditional Chinese Medicine

Shao Li,¹ Tai-Ping Fan,² Wei Jia,³ Aiping Lu,⁴ and Weidong Zhang⁵

¹ Bioinformatics Division, TNLIST/Department of Automation, Tsinghua University, Beijing, China

² Department of Pharmacology, University of Cambridge, Cambridge, UK

³ University of Hawaii Cancer Center, Honolulu, USA

⁴ School of Chinese Medicine, Hong Kong Baptist University, Hong Kong

⁵ Department of Pharmacy, Second Military Medical University, Shanghai, China

Correspondence should be addressed to Shao Li; shaoli@mail.tsinghua.edu.cn

Received 8 January 2014; Accepted 8 January 2014; Published 24 February 2014

Copyright © 2014 Shao Li et al. This is an open access article distributed under the Creative Commons Attribution License, which permits unrestricted use, distribution, and reproduction in any medium, provided the original work is properly cited.

Network pharmacology is becoming a cutting-edge research field in current drug discovery and drug development thanks to rapid progress in systems biology, network biology, and chemical biology. By integrating reductionist and systems approaches as well as computational and experimental methods, network pharmacology has great potential to act as the next generation mode of drug research. Network pharmacology studies emphasize the paradigm shift from “one target, one drug” to “network target, multicomponent therapeutics,” highlighting a holistic thinking also shared by traditional Chinese medicine (TCM). In TCM, the perspective of holism has long been central to herbal treatments of various diseases. Characterized by holistic theory and rich experience in multicomponent therapeutics, TCM herbal formulae offer bright prospects for the control of complex diseases in a systematic manner. Thus, introducing network pharmacology in TCM will provide novel methodologies and new opportunities for discovering bioactive ingredients and endogenous/exogenous biomarkers, revealing mechanisms of action and exploring scientific evidence of numerous herbs and herbal formulae in TCM on the basis of complex biological systems of human body. Moreover, the integration of TCM and network pharmacology can greatly promote the progress of network pharmacology as well.

Here, we have grouped together 27 papers in this burgeoning field, put forward for publication in this special issue on TCM network pharmacology.

In the special issue, we have firstly published four concise reviews or perspectives across the two fields between

TCM and network pharmacology. The topics range from the research paradigm of network pharmacology based on TCM theory and practice, the available databases and computational tools in TCM network pharmacology, to the applications of network pharmacology in TCM. These papers highlighted some specific themes, such as the concept of network target, mechanisms of TCM herbal formulae, and target identification of herbal active ingredients. For example, a review article provided a perspective regarding TCM-based network pharmacology and its use in multiple compound drug discovery, by following an analysis of the merged networks of differentially expressed genes in rheumatoid arthritis-cold pattern and protein targets related to Fu Zi, Xi Xin and Gui Zhi. Three other review articles comprehensively addressed the origin and development of TCM network pharmacology, the definitions of basic network concepts, the computational tools and data sources regarding TCM network pharmacology, and the significance and approaches of network pharmacology in the TCM field, as well as the target identification methods of herbal active ingredients and the use of ligand-protein networks.

A remarkable feature of TCM is the use of herbal formulae. Understanding the mechanisms of action and combinatorial rules of herbal formulae is of great significance in TCM modernization and is also one of the important steps in modern drug discovery. The emerging TCM network pharmacology offers a unique opportunity to explore systematically not only the molecular complexity of an herbal formula, but also the molecular relationships between an herbal

formula and complex diseases. A practical strategy of TCM network pharmacology is the combined use of network-based computational predictions and experimental validations. In this special issue, we have published 11 interesting research papers covering 10 classic herbal formulae by employing network-based approaches and omics-based experimental studies. For example, two research papers established an integrative platform of TCM network pharmacology on the basis of the concept of “network target, multicomponent therapeutics,” and then applied this platform in the identification of active compounds and mechanisms of action of an herbal formula *Qing-Luo-Yin* for the treatment of rheumatoid arthritis, as well as *Ge-Gen-Qin-Lian* decoction recorded in “*Shang-Han-Lun*” for the treatment of Type 2 diabetes. Moreover, network analysis and omics technologies including genomic, metabolomic, and proteomic studies are always integrated together to understand the molecular actions exerted by herbal formulae at a systematic level. In the special issue, four papers addressed the metabolomic analysis for determining the effects of *Huang-Lian-Jie-Du-Tang* in a rat model of collagen-induced arthritis, the metabolomic analysis for *She-Xiang-Bao-Xin* pill in treating myocardial infarction in rats, the proteomic analysis for determining the possible proteomic network associated with the antiarthritic effects of *Qing-Fu-Guan-Jie-Shu* in collagen-induced arthritis rats, and the experimental study of the protective effect of *Xiao-Xu-Ming* decoction in a rat model of cerebral ischemia and reperfusion. It is known that identifying the target proteins and combinatorial rules of active ingredients in herbal formulae remains to be a difficult issue. There are six papers to address such an issue from the network point of view by using bioinformatics analysis and experiments, for example, the mechanism of antirheumatic actions of *Huang-Lian-Jie-Du-Tang* by network analysis, the molecular mechanism of *Shu-Feng-Jie-Du* formula by a module analysis, drug-target network of *Yuan-Hu-Zhi-Tong* prescription, the pharmacological mechanisms of *Wu-Tou-Tang*, and the mechanism of cell apoptosis induced by *Fu-Zheng-Hua-Yu* tablet.

Herbal active ingredients have long been viewed as a rich source of therapeutic leads in drug discovery. Network pharmacology is expected to be a new strategy and powerful tool to find the bioactive compounds as well as their potential molecular targets from numerous herbs or herbal formulae. For herbal active ingredients, there are eight papers published in this special issue with the efforts to study herbal active ingredients by network pharmacology approaches. For example, a paper predicted the target network of vitexicarpin and experimentally validated the molecular network account for its antiangiogenic activities. A paper proposed a computational method to identify the effective herbal components and mechanisms of action. A paper revealed a pharmacological signaling pathway network of baicalin in the treatment of ischaemia-reperfusion in mice. Three other papers addressed the molecular mechanisms of herbal active ingredients with the help of omics technologies, including the metabolomic analysis of genipin in rats and identification of metabolites by LC/MS, the neuroprotective effects of hydroxysafflor yellow A via the NF- κ B pathway

by NMR-based metabolomics, and expression profiling and proteomic analysis of JIN Chinese herbal formula in lung carcinoma H460 xenografts. Lastly, two experimental studies are published on the epithelial-mesenchymal transition induction of shikonin in skin wound healing and capsacin-induced cancer cell apoptosis through ER stress.

Uncovering the scientific basis of herbal traditional properties especially the molecular association between herbal formulae and TCM syndrome (ZHENG) is absolutely critical to preserve and develop TCM. Four papers in this special issue focus on the traditional properties of TCM. A paper identified the network-based biomarkers for the Cold Coagulation Blood Stasis Syndrome and showed the therapeutic effects of *Shao-Fu-Zhu-Yu* decoction in rats. To identify potent synergistic combinations in herbal formulae, a paper developed an interesting Feedback System Control Scheme to optimize combinations of flavonoids derived from *Astragali Radix*. As the potential adverse effects of herbs have limited their clinical applications, a paper proposed a network-based computational model to predict the safety of herbs through a comparative analysis of withdrawn drugs. Based on combining formula network, chemical space, and metabolic space, a paper analyzed the properties of the incompatible herbal pairs associated with the traditional rule termed “eighteen antagonisms and nineteen mutual inhibitors” in herbal formulae.

In summary, TCM network pharmacology is a new interdisciplinary frontier in both ancient TCM and modern drug discovery and development fields, which represents valuable interactions and exchanges between traditional Chinese medicine and those of network, pharmacological, biomedical and computational sciences. This special issue provides a high-profile venue for dissemination of significant scientific findings in TCM network pharmacology. It is just the beginning. We encourage researchers in TCM and related fields to support the development of this novel and promising direction.

Shao Li
Tai-Ping Fan
Wei Jia
Aiping Lu
Weidong Zhang

Research Article

A Network Pharmacology Approach to Determine Active Compounds and Action Mechanisms of Ge-Gen-Qin-Lian Decoction for Treatment of Type 2 Diabetes

Huiying Li,¹ Linhua Zhao,² Bo Zhang,^{1,3} Yuyu Jiang,⁴ Xu Wang,¹ Yun Guo,²
Hongxing Liu,² Shao Li,¹ and Xiaolin Tong²

¹ MOE Key Laboratory of Bioinformatics, Bioinformatics Division, TNLIST/Department of Automation, Tsinghua University, Beijing 100084, China

² Guang'anmen Hospital, China Academy of Chinese Medical Sciences, Beijing 100053, China

³ Tianjin International Joint Academy of Biotechnology & Medicine, Tianjin 300457, China

⁴ Wuxi Medical School, Jiangnan University, Wuxi 214122, China

Correspondence should be addressed to Shao Li; shaoli@mail.tsinghua.edu.cn and Xiaolin Tong; xiaolintong66@sina.com

Received 23 October 2013; Accepted 11 December 2013; Published 16 January 2014

Academic Editor: Aiping Lu

Copyright © 2014 Huiying Li et al. This is an open access article distributed under the Creative Commons Attribution License, which permits unrestricted use, distribution, and reproduction in any medium, provided the original work is properly cited.

Traditional Chinese medicine (TCM) herbal formulae can be valuable therapeutic strategies and drug discovery resources. However, the active ingredients and action mechanisms of most TCM formulae remain unclear. Therefore, the identification of potent ingredients and their actions is a major challenge in TCM research. In this study, we used a network pharmacology approach we previously developed to help determine the potential antidiabetic ingredients from the traditional Ge-Gen-Qin-Lian decoction (GGQLD) formula. We predicted the target profiles of all available GGQLD ingredients to infer the active ingredients by clustering the target profile of ingredients with FDA-approved antidiabetic drugs. We also applied network target analysis to evaluate the links between herbal ingredients and pharmacological actions to help explain the action mechanisms of GGQLD. According to the predicted results, we confirmed that a novel antidiabetic ingredient from *Puerariae Lobatae radix* (Ge-Gen), 4-Hydroxymephenytoin, increased the insulin secretion in RIN-5F cells and improved insulin resistance in 3T3-L1 adipocytes. The network pharmacology strategy used here provided a powerful means for identifying bioactive ingredients and mechanisms of action for TCM herbal formulae, including Ge-Gen-Qin-Lian decoction.

1. Introduction

Type 2 diabetes (T2D), or noninsulin-dependent diabetes mellitus, is a common complex disease with an increasing prevalence worldwide. In 2012 it was estimated that more than 371 million people have diabetes and that T2D constitutes over 90% of diabetic patients [1]. Furthermore, epidemiological survey analysis suggests that the prevalence of diabetes is accelerating [2]. T2D is characterized by high blood glucose levels due to insufficient insulin secretion, insulin resistance, and impaired insulin action [3]. T2D is influenced by lifestyle factors, such as age, pregnancy, and obesity, but has a strong genetic predisposition [4]. Multiple genes are involved in genetic susceptibility, each making

a small contribution to T2D risk [5, 6]. Alterations in multiple signaling pathways, for example, JAK-STAT, MAPK, VEGF, PPAR, P13K, and Wnt were implicated in the pathogenesis of the disease [7–9]. Treatments aimed at controlling high-level blood glucose, as well as therapies that prevent diabetic complications, have all shown specific therapeutic activity in T2D patients, such as metformin, alpha-glucosidase inhibitors, sulfonylureas, thiazolidinediones (TZDs), and insulin injections [10]. However, these treatments have shown limited efficacy and are associated with various side effects such as flatulence and diarrhea [11]. Therefore, as a complicated disease, T2D may require complex therapeutic approaches such as traditional Chinese medicine (TCM) [12].

In TCM, T2D is treated as “Xiaoke” and the related herbal formulae have been used over thousands of years. The therapeutic effects of Chinese medicines used for the treatment of T2D have been documented based on clinical trials or the use of animal T2D models [13, 14]. One such herbal formula is the Ge-Gen-Qin-Lian decoction (GGQLD), an ancient and effective treatment for “dampness-heat” ZHENG causing diarrhea and dysentery, which originated from “*Shanghan Lun*” compiled by ZhongJing Zhang. GGQLD consists of four herbs: *Puerariae Lobatae radix* (Ge-Gen) as the principle herb, *Scutellariae radix* (Huang-Qin), *Coptidis rhizoma* (Huang-Lian), and *Glycyrrhizae Radix et Rhizoma Praeparata cum Melle* (Gan-Cao) used as adjuvant herbs to assist the effects of Ge-Gen. It has been reported that puerarin from Ge-Gen reduced blood sugar in diabetic mice, and improved insulin resistance and hyperlipidemia in rats [15–17]. Baicalin from Huang-Qin had antihyperglycemic effects on diabetic rats [18]. Berberine from Huang-Lian lowered blood glucose significantly by increasing insulin receptor expression [19]. Furthermore, amorfrutins from Gan-Cao have potent antidiabetic activity [20]. Intriguingly, recent studies also showed that GGQLD had good clinical effects on T2D and the anti-diabetic activities of GGQLD *in vivo* and *in vitro* were investigated [21, 22]. Although research has indicated that GGQLD, composed of multiple biologically active compounds, helps in T2D treatment, the mechanism of this formula remains unknown due to its complex nature, as well as a lack in appropriate methods.

As complex mixtures of herbs, TCM formulae consist of many small molecular compounds, which may simultaneously, transiently (short residue time), or weakly (low affinity) bind with multiple target proteins [23, 24]. The systematic therapeutic strategy of a formula is realized through collectively targeting the disease-specific molecular network. Its increased efficacy and decreased toxicity may arise as a result of complex synergistic or antagonistic interactions among different formula components. Such features of TCM herbal formulae meet the requirements of complex disease (e.g., T2D) treatment in a systematic manner. Interestingly, the holistic philosophy of TCM is consistent with the key idea of emerging network pharmacology [25, 26]. Recently, TCM network pharmacology has been proposed by Li et al. [25, 27–30], which integrates TCM theory with interaction networks and uses a “network target” as a mathematical and computable representation of various connections between herbal formulae and diseases [31, 32]. The combinatorial rules and holistic regulation effects of herbal formulae can be conveyed using the network properties arising directly from network topology and dynamics, such as the network parameters including connectivity, centrality, modularity, and propagation [33–37]. Therefore, TCM network pharmacology can be used to understand the scientific basis of TCM herbal formulae at the molecular level and from a system perspective.

Our previous studies have shown that the “network target” as a key concept of TCM network pharmacology can help to decipher the molecular mechanisms of the therapeutic effects of TCM herbal formulae and to determine their active ingredients or combinations [25, 31, 32, 38]. Here, to better understand the molecular basis of the therapeutic

effects of GGQLD on T2D, we computationally recognized the active ingredients and mechanisms in GGQLD using integrative analysis based on our TCM network pharmacology platform and experimentally validated the antidiabetic activity of the candidate ingredients. Network target analysis showed that GGQLD can regulate key biological processes in T2D development, such as glucose homeostasis and response to insulin stimulus. Moreover, we revealed that 4-Hydroxymephenytoin, a core component of Ge-Gen, was involved in the antidiabetic ingredients of GGQLD, which can stimulate endogenous insulin secretion and ameliorate insulin resistance in 3T3-L1-based insulin resistance models. These results provide new insight into the molecular mechanisms of the antidiabetic activity of GGQLD and accelerate drug discovery on the basis of GGQLD.

2. Methods and Materials

2.1. Computational Prediction of Antidiabetic Ingredients from GGQLD Using Network Target Analysis

2.1.1. Data Collection. We collected the TCM herbal ingredients imported from the Herb BioMap database (China Copyright of Computer Software, 2011SR076502), which contains information on 621 herbs and 10,805 distinct chemical ingredients. To identify the active ingredients in GGQLD, a total of 287 available chemical ingredients were collected, with 42 found in Ge-Gen, 57 found in Huang-Qin, 22 found in Huang-Lian, and 166 found in Gan-Cao. The chemical information on GGQLD ingredients (structure, canonical name, and CID number) employed for computational analysis was downloaded from the PubChem Compound database (<http://pubchem.ncbi.nlm.nih.gov/>) [39]. A data set of 80 T2D-related genes and the true targets of 19 FDA-approved antidiabetic drugs were retrieved from the OMIM Morbid Map and DrugBank databases, respectively [40, 41].

2.1.2. Network-Based Prediction of Herbal Ingredient Target Profiles. *In silico* prediction of comprehensive target profiles of TCM ingredients is the first step in TCM network pharmacology. Compared with virtual screening based on docking analysis, the network-based computational approach for drug target identification is not restricted to the target protein structures. In this study, a network-based regression model (drugCIPHER) for target profile prediction was carried out. The drugCIPHER method scored the likelihood of drug-target interactions by integrating structural similarities of drugs and protein-protein interactions in a heterogeneous network that correlated chemical and genomic spaces [42]. Briefly, drugCIPHER was performed to predict the target profiles of each GGQLD ingredient. The drugCIPHER score represented the likelihood of an ingredient-target interaction, which was obtained from the correlation between the query ingredient’s structural similarity vector in chemical space and the target protein’s closeness vector in genomic space. Finally, the top 100 proteins were selected as target profiles for each ingredient since the top 100 targets reach the high prediction

TABLE 1: Nineteen FDA-approved antidiabetic drugs compiled from the Drugbank database.

Category	Name	CID
Sulfonylurea drug	Tolbutamide	5505
	Glyburide	3488
	Glipizide	3478
	Gliquidone	91610
	Glimepiride	3476
	Gliclazide	3475
Biguanide drug	Metformin	4091
	Phenformin	8249
	Acarbose	441184
	Voglibose	444020
	Miglitol	441314
Euglycemic agent	Pioglitazone	4829
	Rosiglitazone	77999
Euglycemic agent (Nonsulfonylurea)	Repaglinide	65981
	Staris (TN)	443871
Aldose reductase inhibitor	Tolrestat	53359
	Alrestatin	2120
Other oral antidiabetic drugs	Sitagliptin	4369359
	Rimonabant	104850

accuracy (77.3%) in general and can be a representation of the whole target profile [42].

2.1.3. Cluster Analysis of Target Profiles for Computational Identification of Antidiabetic Ingredients. Two-dimensional hierarchical clustering of target profiles was used to determine possible antidiabetic ingredients by comparing the GGQLD ingredients and antidiabetic drug profiles [43]. For the purpose of comparison and cluster analysis, 19 FDA-approved antidiabetic drugs were compiled (Table 1) and their target profiles were generated using drugCIPHER. Clustering was executed using MATLAB (Mathworks Matlab R2013a) and standard hierarchical clustering of a matrix dependence on drugs or ingredient target profiles. The clustering coefficient between GGQLD ingredients and antidiabetic drug profiles was estimated and the cutoff value was set >0.5 . The similarity networks of herbal ingredients and drugs (clustering coefficient of target profiles >0.5) were created using network visualization software CytoScape 2.8.

2.1.4. Network Pharmacology for Predicting Synergistic Herbal Ingredient Combinations. Prediction of synergistic herbal ingredient combinations was performed as described previously [32]. We adapted a synergy score that predicted how strong disease molecular networks were perturbed with herbal ingredient combinations. In this study, berberine in Huang-Lian was used to search possible synergistic combinations with the 286 GGQLD ingredients. Different features of the disease molecular network were combined to quantify the synergy, such as node importance and shortest path distance between berberine and other ingredient target profiles. The calculation details have been described previously [32].

Statistical significance of the synergistic herbal ingredient combinations was estimated using P value.

2.1.5. Network Target Analysis of Mechanisms of Action of GGQLD. Identification and characterization of the action mechanism of GGQLD were performed using network target analysis as depicted previously [38]. Briefly, a gene ontology (GO) enrichment analysis tool from the DAVID database was used to identify statistically significant enriched GO biological process (BP) terms of assembled T2D-related genes (P value < 0.05 after Benjamini's correction), which were selected as common biological functions and pathways for T2D [44]. Secondly, the target profile of each antidiabetic GGQLD ingredient inferred by cluster analysis and the gene set of enriched GO BP terms of T2D-related genes were mapped simultaneously onto the protein-protein interaction (PPI) network assembled PPI data from public databases [38]. Thirdly, the possible biological functions of each antidiabetic ingredient were predicted by the network-based algorithm of drug function identification developed previously, which integrated important network parameters such as node importance and shortest path distance between the herbal ingredients' target gene set and T2D-related gene set [45]. Fourthly, we constructed a large GGQLD herbal ingredient-function network with GO BP terms and herbal ingredients as nodes and the links extracted from the P value calculated above. Lastly, a more biologically meaningful subnetwork representing the action mechanisms of GGQLD was produced, which was visualized by CytoScape software.

2.2. Experimental Validation for Computational Prediction Results Using Insulin Secretion Assay and Insulin Resistance Model

2.2.1. Drugs and Reagents. Two FDA-approved antidiabetic drugs (nateglinide and pioglitazone), a known antidiabetic herbal ingredient (berberine), the newly discovered GGQLD herbal antidiabetic (4-Hydroxymephenytoin), and palmitic acid (PA, P0500) were obtained from Sigma Chemical Co. (St. Louis, Missouri, USA). The RPMI 1640 medium, high-glucose DMEM medium, 3-isobutyl-1-methylxanthine, trypsin, and fetal bovine serum for cell culture were purchased from GIBCO (Grand Island, New York, USA). The MTT detection kit, insulin ELISA kit, and glucose detection kit were obtained from R&D (Minneapolis, USA).

2.2.2. Cell Cultures and Treatment. RIN-5F cells derived from rat insulinoma and 3T3-L1 preadipocytes derived from 3T3 mouse embryo fibroblast were purchased from the American Type Culture Collection (Manassas, VA; ATCC no.: CRL-2058 and CL-173, resp.). The RIN-5F cells were cultured in RPMI 1640 medium containing 10% FBS, 100 U/mL penicillin, and 100 μ g/mL streptomycin under an atmosphere of 5% CO_2 /95% humidified air at 37°C. The medium was renewed every 3 days. The cells were used at passages 20–25. The 3T3-L1 preadipocytes were grown and differentiated into adipocytes as described previously [46]. Briefly, preadipocytes were differentiated in high-glucose

DMEM, 10% FBS with dexamethasone (0.25 μ M), insulin (10 μ g/mL), and 3-isobutyl-1-methylxanthine (0.5 mM) for 48 h and then treated with insulin (1 μ g/mL) for an additional 48 h. Adipocytes were maintained in and refed every 2 days with high-glucose DMEM and 10% FBS until being used for experiments 8–12 days after the addition of differentiation factors, when between 90 and 95% of cells exhibited an adipocyte phenotype. For antidiabetic drugs or herbal ingredient treatment of cells, RIN-5F and 3T3-L1 adipocytes were cultured for the indicated time in the corresponding medium containing BSA (2%) and glucose (5.4 mM) in the absence of nateglinide, pioglitazone, berberine, and 4-Hydroxymephenytoin. After that, other assays were performed.

2.2.3. MTT Assay. A total of 1×10^4 cells were plated in 96-well flat-bottom plates in 100 μ L of medium. The next day, cells were exposed to the antidiabetic drugs and potential herbal ingredients at different concentrations. After one day from the last drug addition, 20 μ L of 5 mg/mL MTT solution in PBS was added to each well for 4 h. The medium was removed, and 200 μ L DMSO was added to each well to dissolve the formazan crystals. Absorption at 570 nm was determined using a Bio Rad microplate reader (Model 3550 microplate reader, Bio-Rad Laboratories, Richmond, CA). Triplicate wells were assayed for each condition, and standard deviations were determined. The concentrations of each agent with survival rates >90% were selected for use in the following assays.

2.2.4. Insulin Secretion. The RIN-5F cells were seeded in 12-multiwell plates at a density of 10^7 cells/mL. After 24 h, the medium was discarded, and the cells were washed twice for 30 min at 37°C with PBS. The cells were incubated in the presence or absence of increasing concentrations of glucose for different periods of time. To study herbal ingredient-induced insulin secretion, RIN-5F cells were incubated for the last indicated time at 37°C in the medium with different glucose content in the presence or absence of different concentrations of nateglinide, berberine, and 4-Hydroxymephenytoin. Aliquots of the supernatant were collected and stored at -20°C for subsequent insulin amount determination by ELISA.

2.2.5. Oil Red O Staining. Oil red O was used to stain lipids in the 3T3-L1 adipocytes. Cells were washed three times with PBS and then once in 60% isopropanol. Oil red O was added and the cells were incubated for 20 min at room temperature. Cells were washed three times in PBS and then once in 60% isopropanol again. Slides were rinsed and counterstained with haematoxylin. Mounting solution and coverslips were added.

2.2.6. Insulin-Resistance Model and Glucose Consumption Assay. The 3T3-L1 adipocytes were cultured for 12 h in serum-free DMEM with 0.2% BSA. The cells were then cultured in DMEM containing 1% BSA for 24 h (normal group); or in DMEM containing 0.5 mM PA and 2% BSA (model

group); or in DMEM containing 0.5 mM PA, 0.1, 1, and 10 μ M pioglitazone, berberine, and 4-Hydroxymephenytoin, and 2% BSA (treatment group) for 24 h [47]. The 3T3-L1 preadipocytes were differentiated to adipocytes in a 12-well plate. After serum starvation in 0.2% BSA DMEM overnight, the cells were incubated with DMEM containing 0.5 mM PA and various concentrations of pioglitazone, berberine, and 4-Hydroxymephenytoin for 24 h. The medium was removed and its glucose concentrations were determined by the glucose oxidase method. The amount of glucose consumption was calculated by subtracting the remaining glucose in the plate from the glucose concentrations of blank wells. Three replicate wells were established. Additionally, an MTT assay was employed to determine cell number and viability.

2.2.7. Statistical Analysis. Data were expressed as means \pm standard deviation (SD). Multigroup comparisons were carried out by analysis of variance (ANOVA) with SPSS 16.0. Values of $P < 0.05$ were considered statistically significant.

3. Results and Discussion

3.1. Computational Prediction Based on Network Pharmacology for GGQLD. Cells employ complex signaling networks to drive biological processes. Genetic or epigenetic alterations in signaling pathways and networks might result in imbalanced signaling of islet cells, which then leads to T2D phenotypes. The successful application of GGQLD in T2D therapy not only demonstrated the feasibility of TCM herbal formulae but also showed that increasing the complexity of proposed therapies by targeting different pathological processes in disease development should more efficiently treat complex diseases. Interestingly, the network-based therapeutic strategies are evidence based presumably in agreement with the properties of TCM herbal formulae [48]. Previously, we showed that integrative TCM network pharmacology and its application provided insight into the combinatorial role of an antirheumatoid arthritis herbal formula and identified the active ingredients [38]. To gain further insight into the underlying mechanism of GGQLD, we applied a network-based approach to predict the target profiles of each herbal GGQLD ingredient and 19 FDA-approved antidiabetic drugs (Table 1). Here, the target profiles of herbal compounds and 19 FDA-approved antidiabetic drugs will be compared and clustered to predict the actions of herbal compounds. Note that although the FDA-approved drugs have their known targets, we need to predict the target profile of these FDA drugs by drugCIPHER, making the target and activity information more complete and more comprehensive for the FDA drugs. The reliability and precision of the target profiles predicted by drugCIPHER have been evaluated for FDA-approved small molecular drugs [42]. The genes involved in target profiles were defined by all genes within the assembled PPI network. We also restricted our analysis to the top 100 genes present in each target profile.

3.1.1. Identifying Antidiabetic Ingredients from GGQLD Using Cluster Analysis. To computationally determine antidiabetic

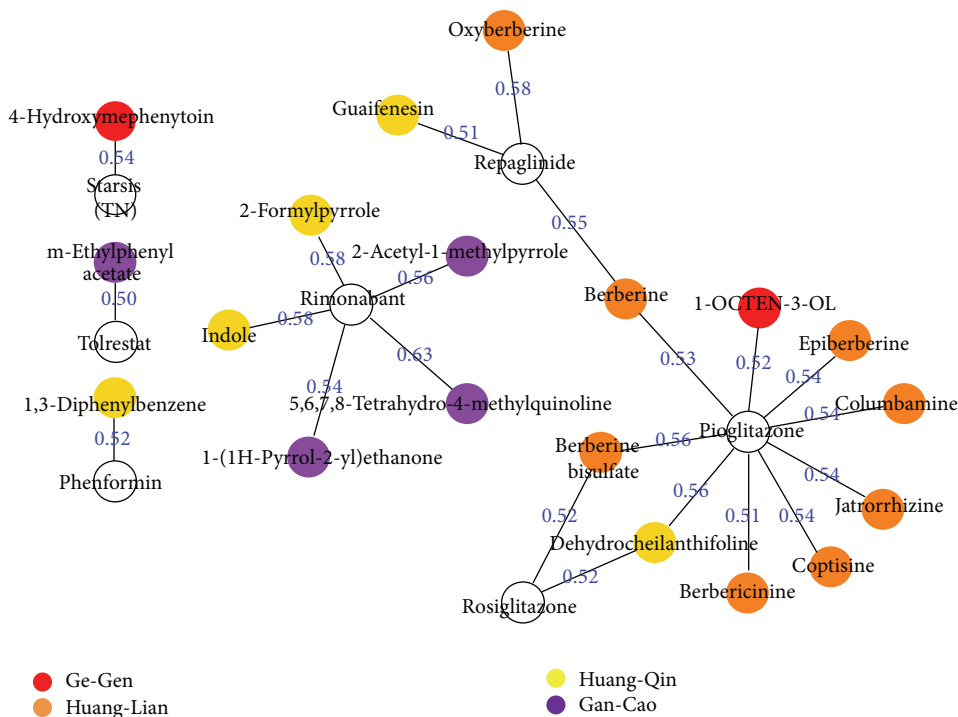


FIGURE 1: The herbal ingredient-drug networks based on the target profile cluster analysis. Each node represents a herbal ingredient or drug. The color of herbal ingredient represents its source herbs. Two nodes between herbal ingredients and drugs are linked by an edge if their similarity score is above the predefined threshold >0.5.

herbal ingredients and understand the molecular basis of GGQLD, we hypothesized that the potential antidiabetic herbal ingredients and FDA-approved antidiabetic drugs were likely to share similar target profile patterns or similar biological functions and pharmacological action. In line with prior research [38], we measured the similarity between the target profiles of herbal ingredients and the selected drugs using the hierarchical clustering algorithm, which revealed that certain herbal ingredients were associated with antidiabetic drugs with diverse action mechanisms. After cluster analysis using target profiles, the herbal ingredients with coefficients of more than 0.5 were analyzed in greater detail and a similarity network with weighted edges based on differences in the target profiles of herbal ingredients and drugs was generated (Figure 1). This network represented similar relationships or common mechanisms between herbal ingredients and drugs. Table 2 shows that 19 herbal ingredients in this network were identified as potential antidiabetic ingredients in GGQLD, of which two, nine, four, and four ingredients were from Ge-Gen, Huang-Lian, Huang-Qin, and Gan-Cao, respectively. To demonstrate whether these ingredients had antidiabetic properties, a literature search was performed using SciFinder [49] and PubMed. This search identified 13 of the 19 herbal ingredients as known antidiabetic compounds supported by at least one independent item of evidence [50–63]. These ingredients were linked to diverse antidiabetic activities in previous studies and were computationally confirmed here. For example, 1-OCTEN-3-OL from Ge-Gen and 2-Acetyl-1-methylpyrrole from Gan-Cao

were found to be antioxidants involved in the improvement of diabetes [50, 63, 64]; guaifenesin from Huang-Qin promoted neurite outgrowth and protected diabetic mice from neuropathy [61]. In particular, several core ingredients from Huang-Lian, berberine bisulfate, columbamine, coptisine, epiberberine, jatrorrhizine, oxyberberine, dehydrocheilanthifoline, and berberine were reported to have hypoglycemic and antidiabetic actions through the regulation of glucose metabolic effects and reduction of oxidative stress injury [51–59]. These results demonstrated the reliability of our approach and provided possible explanations for the molecular basis and mechanisms of action of GGQLD [21, 22]. For the remaining six ingredients not reported in the literature, 4-Hydroxymephenytoin was commercially available and was tested in *in vitro* antidiabetic assay below.

3.1.2. Determining Combinatorial Rules of GGQLD Using Network Pharmacology. From the computational screening of the pooled GGQLD herbal ingredients, a known antidiabetic ingredient (berberine in Huang-Lian) was selected as a core component to combine with other ingredients, resulting in 287 unique ingredient pairs. We used significant synergy scores to identify potent ingredient pairs. Table 3 shows the potent berberine-ingredient pairs with significant *P* values (*P* < 0.05). Berberine treats T2D by lowering blood glucose and improving insulin-resistant states. The significant top ranked herbal ingredient pairs suggest that berberine combined with oxyberberine in Huang-Lian and guaifenesin in Huang-Qin may produce synergistic antidiabetic actions.

TABLE 2: Potential antidiabetic ingredients in Ge-Gen-Qin-Lian formula by network target analysis.

Ingredients	Herbs	CID	Literature evidence
4-Hydroxymephenytoin	Ge-Gen	119507	/
1-OCTEN-3-OL	Ge-Gen	18827	[50]
Berbericine	Huang-Lian	19009	/
Berberine bisulfate	Huang-Lian	12457	[51]
Columbamine	Huang-Lian	72310	[52]
Coptisine	Huang-Lian	72322	[53]
Epiberberine	Huang-Lian	160876	[54, 55]
Jatrorrhizine	Huang-Lian	72323	[55, 56]
Oxyberberine	Huang-Lian	11066	[57]
Dehydrocheilanthifoline	Huang-Lian	3084708	[58]
Berberine	Huang-Lian	2353	[59]
Indole	Huang-Qin	798	[60]
1,3-Diphenylbenzene	Huang-Qin	7076	/
2-Formylpyrrole	Huang-Qin	13854	/
Guaifenesin	Huang-Qin	3516	[61]
1-(1H-Pyrrol-2-yl)ethanone	Gan-Cao	14079	[62]
2-Acetyl-1-methylpyrrole	Gan-Cao	61240	[63]
m-Ethylphenyl acetate	Gan-Cao	76462	/
5,6,7,8-Tetrahydro-4-methylquinoline	Gan-Cao	185667	/

/: no evidence.

TABLE 3: Herbal ingredients in GGQLD with potential synergistic antidiabetic effects on berberine.

Herb name	Chemical name	Synergy score	P value
Gan-Cao	5,6,7,8-Tetrahydro-4-methylquinoline	0.532	0.001
Huang-Qin	Indole	0.463	0.001
Ge-Gen	SA3	0.452	0.001
Huang-Lian	Oxyberberine	0.372	0.006
Huang-Qin	Guaifenesin	0.453	0.011
Gan-Cao	1-(1H-Pyrrol-2-yl)ethanone	0.359	0.042

This result was indirectly validated by the synergistic combinations of FDA-approved antidiabetic drugs with similar target profiles. For example, the combination of repaglinide and pioglitazone has acceptable safety with greater reductions in glycemic parameters than treatment using either agent alone [65]. In addition, the combinational effects of berberine with other ingredients in GGQLD were also predicted, which needs further experimental verification. We suspect that the synergistic mechanisms of berberine with 5,6,7,8-Tetrahydro-4-methylquinoline/1-(1H-Pyrrol-2-yl)ethanone in Gan-Cao or indole in Huang-Qin might be due to their different antidiabetic mechanisms, as the similarity network found the difference of target profiles.

3.1.3. Understanding the Action Mechanisms of GGQLD Using Network Target Analysis. Comodule analysis by mapping disease genes and drug target profiles into the integrative PPI network suggests an underlying link between disease and drugs if the two gene sets coexist within the same module or the distance between them is very close in the network. The network-based approach could therefore provide predictable power for the pharmacological actions of herbal ingredients. Consequently, to identify which T2D-related biological processes were regulated by the predicted herbal ingredients from GGQLD, network target analysis was performed with the T2D-related genes enriched GO terms and target profiles

of herbal ingredients. Because the network distribution of T2D genes was considered a specific network target, the relationship between T2D pathological processes and herbal ingredients was evaluated using node importance and shortest path distance, as previously described [45]. The network target analysis enabled a comprehensive understanding of the action mechanisms of GGQLD so that the resulting network could be used to explain the combinatorial activities of herbal ingredients in GGQLD. Figure 2 shows that the key biological processes involved in T2D (glucose homeostasis, regulation of glucose import, regulation of glucose transport, regulation of glucose metabolic process, and response to insulin stimulus) were regulated by different ingredients from GGQLD. This suggests that GGQLD can treat T2D by regulating the complex network related to multiple pathological processes of T2D.

Furthermore, our previous studies found that Cold ZHENG and Hot ZHENG in the classic theory of TCM were characterized by imbalance in the metabolic and immune networks, considering from a biological or molecular correlate between the ZHENG and diseases [27, 66, 67]. There are two therapeutic strategies, one direct and one indirect, for attempting to recover the Yin and Yang balance in the human body. For example, “clearing heat” is used in the direct treatment of Hot ZHENG, while the therapeutic principle of “nourishing Yin and clearing heat” is used in

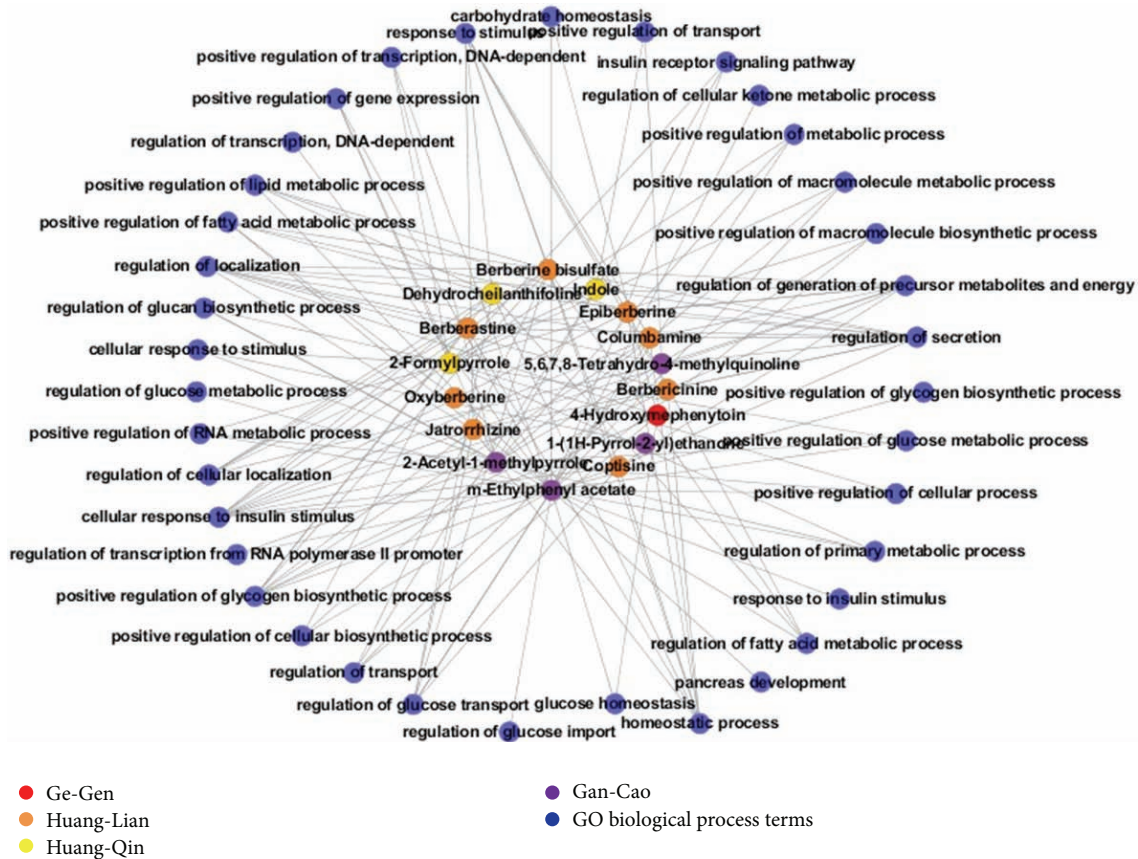


FIGURE 2: Relationships between antidiabetic ingredients and their perturbed GO Biological Processes. Blue nodes represent T2D-related GO Biological Processes; other color nodes represent ingredients from different herbs. This network can be regarded as a perturbed network targeted by various ingredients from GGQLD.

the indirect treatment of Hot ZHENG. GGQLD with cold-dominated herbs is now routinely used for treating “damp-heat syndrome” in TCM clinics. As shown in Figure 2, GGQLD mainly affected the positive regulation of many types of metabolic processes, suggesting that GGQLD can efficiently treat T2D by improving the imbalanced state of metabolic processes in T2D patients. These results showed that the therapeutic strategy of GGQLD is indirect and also implied that the “damp-heat syndrome” treated by GGQLD may be one of the phenotypes caused by “Yin deficiency,” such as the reduced secretion of insulin.

3.2. Experimental Validation of the Antidiabetic Effect of 4-Hydroxymephenytoin. Patients who develop T2D have a complex phenotype with disordered insulin secretion, increased hepatic glucose production, and resistance to the action of insulin, which all contribute to the development of overt hyperglycemia [68]. The therapeutic action mechanisms of antidiabetic agents on T2D might be related to their effect of ameliorating glucose metabolism disorders, improving insulin resistance, and increasing tissue sensitivity to insulin. In this study, we investigated the activities of 4-Hydroxymephenytoin on insulin secretion and resistance *in vitro* to validate its antidiabetic potential, as shown in Figure 3(a).

3.2.1. Effect of 4-Hydroxymephenytoin on Insulin Secretion. To assess the stimulatory effect of 4-Hydroxymephenytoin on insulin secretion *in vitro*, we used a rat insulin enzyme-immunoassay to determine activity based on the insulin levels released from RIN-5F cells under both basal and hyperglycemic conditions, which contained 1 and 20 mM glucose, respectively. As shown in Figure 3(b), insulin secretion was augmented when the glucose concentration increased from 1 to 20 mM. Although nateglinide, berberine, and 4-Hydroxymephenytoin in the presence of 1 mM glucose did not significantly induce insulin secretion from the cells, exposure to 4-Hydroxymephenytoin (0.1, 0.3, and 3 μ M) in the presence of 20 mM glucose stimulated a significant increase in insulin secretion in a concentration-dependent manner ($P < 0.01$). Interestingly, RIN-5F cells responded better to 4-Hydroxymephenytoin than to nateglinide and berberine in insulin secretion. Maximum activity was observed with 0.3 μ M of 4-Hydroxymephenytoin. At 20 mM glucose, 4-Hydroxymephenytoin induced a 1.9-fold increase in insulin secretion compared to that without 4-Hydroxymephenytoin, whereas 4-Hydroxymephenytoin in 1 mM glucose showed lower activity. Toxicity profiles of nateglinide, berberine, and 4-Hydroxymephenytoin in the RIN-5F cells were determined at 0.1–10 μ M of nateglinide, berberine and 4-Hydroxymephenytoin by cell proliferation assay

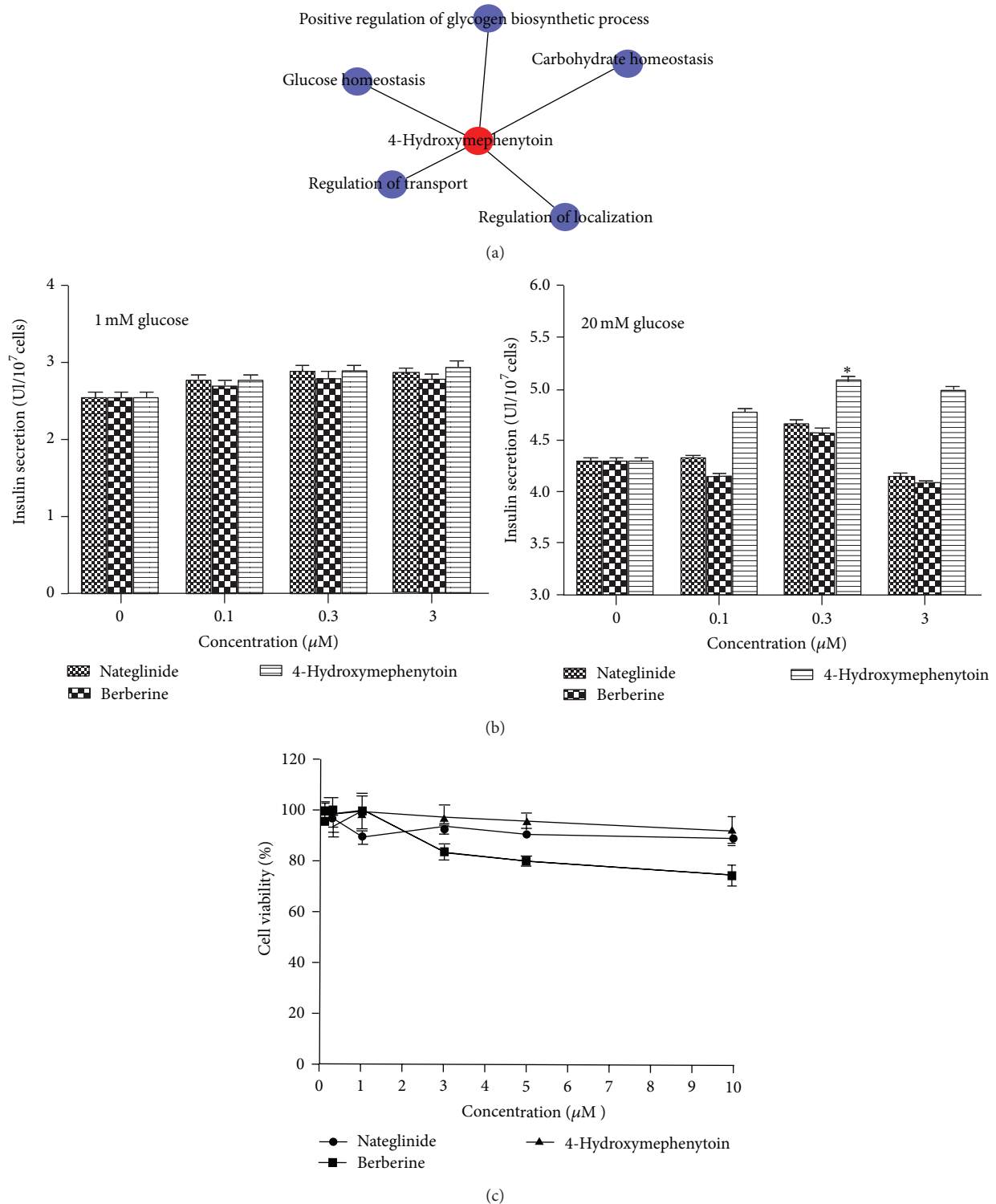


FIGURE 3: 4-Hydroxymephenytoin induced insulin secretion in RIN-5F cells at a nontoxic concentration. (a) Subnetwork targeted by 4-Hydroxymephenytoin. (b) Effects of nateglinide, berberine, and 4-Hydroxymephenytoin on glucose-stimulated insulin secretion from RIN-5F islet cells. Cells were incubated with various concentrations of nateglinide, berberine, and 4-Hydroxymephenytoin for 2 h to induce insulin secretion. Glucose with different concentrations was used as the control for basal and hyperglycemic conditions. Values are means \pm SD of five replicate experiments in each group. * $P < 0.05$ and ** $P < 0.01$ are compared with the control group of 20 mM glucose. (c) Effects of nateglinide, berberine, and 4-Hydroxymephenytoin on cytotoxicity in RIN-5F islet cells. Cells were incubated with various concentrations of nateglinide, berberine, and 4-Hydroxymephenytoin, respectively for 24 h in the presence of 20 mM glucose. Cell viability was measured using MTT assay. Values are means \pm SD of seven replicate experiments in each group.

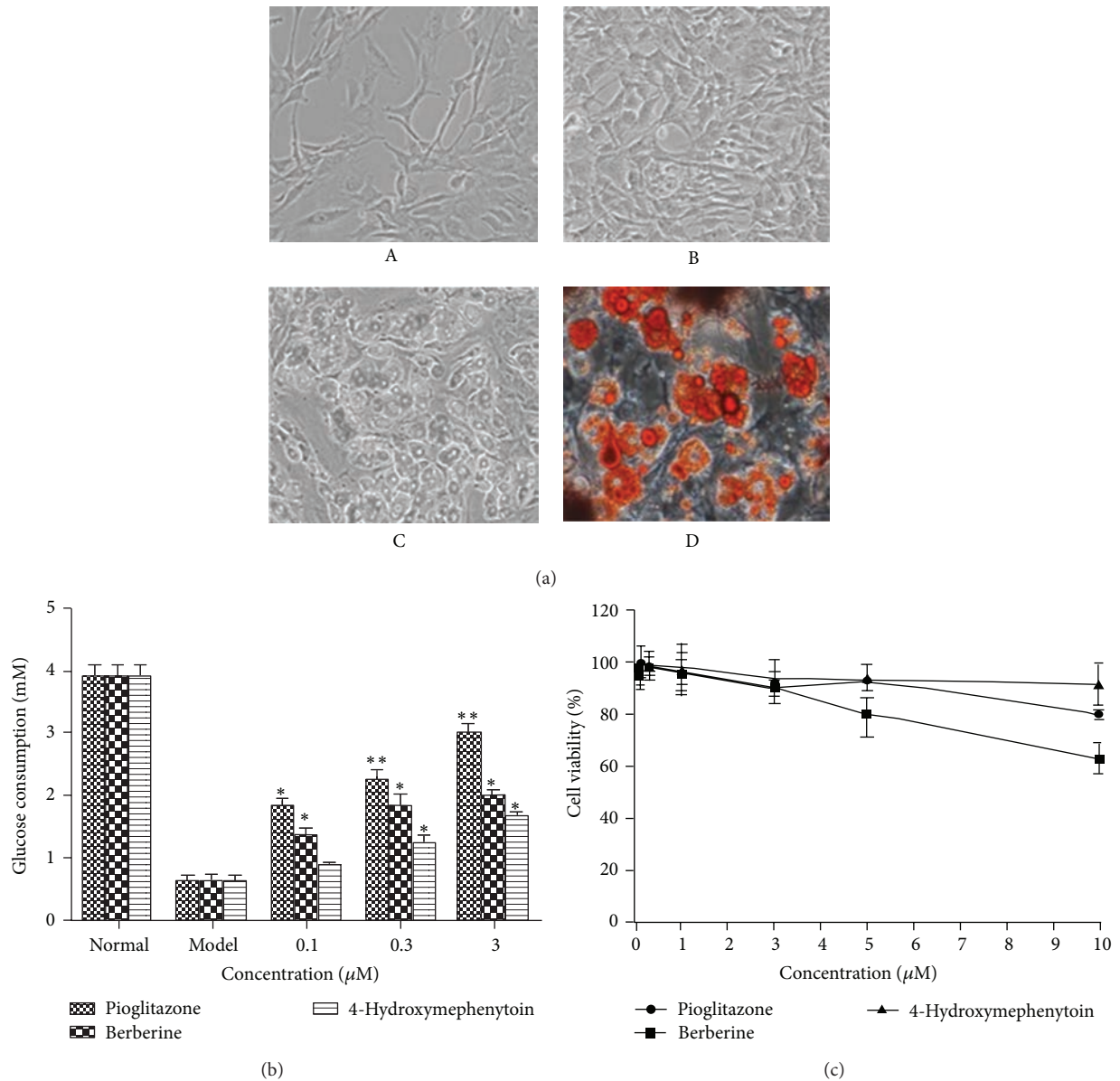


FIGURE 4: 4-Hydroxymephenytoin induced insulin-induced glucose consumption in 3T3-L1 adipocytes. (a) General view of differentiation of 3T3-L1 preadipocytes into adipocytes as seen in inverted phase contrast microscope (A–D). Large lipid droplets are the main characteristics of the cytoplasm of the cells (C). Intracellular lipid content was measured by oil red O staining. (b) Effects of pioglitazone, berberine, and 4-Hydroxymephenytoin on glucose consumption in 3T3-L1 adipocytes. Differentiated 3T3-L1 adipocytes in 96-well plates were preincubated with DMEM containing 0.2% BSA for 12 h and then incubated with various concentrations (0.1, 0.3, and 3 μM) of pioglitazone, berberine, and 4-Hydroxymephenytoin for 24 h. Glucose consumption amount was obtained from the difference in glucose concentrations between initial and final states for the indicated time from the culture medium. Values are means \pm SD of five replicate experiments in each group. * $P < 0.05$ and ** $P < 0.01$ are compared with model group. (c) Effects of pioglitazone, berberine, and 4-Hydroxymephenytoin on cytotoxicity in 3T3-L1 adipocytes. Cells were incubated with various concentrations of pioglitazone, berberine, and 4-Hydroxymephenytoin for 24 h. Cell viability was measured using MTT assay. Values are means \pm SD of seven replicate experiments in each group.

(Figure 3(c)). The incubation period for the induction of insulin secretion was insufficient to detect cytotoxicity. Therefore, the cultures were incubated for 24 h. 4-Hydroxymephenytoin did not show apparent cytotoxicity up to 1 μM , indicating that the activities of 4-Hydroxymephenytoin on insulin secretion were not due to their toxicity. Moreover, toxic concentrations of 4-Hydroxymephenytoin were higher than these of nateglinide and berberine.

3.2.2. Improvement of 4-Hydroxymephenytoin on Insulin Resistance and Glucose Consumption. We investigated the effects of 4-Hydroxymephenytoin on improving insulin resistance induced by PA in 3T3-L1 adipocytes. Differentiated 3T3-L1 adipocytes from preadipocytes were used as a cellular model to evaluate the activity of 4-Hydroxymephenytoin for the improvement of insulin resistance. Adipocyte differentiation was induced in the 3T3-L1 preadipocytes using

3-isobutyl-1-methylxanthine and dexamethasone, and lipid droplets were detected with oil red O staining. Because increased adiposity in the 3T3-L1 adipocytes may be due to increased adipocyte differentiation, adipogenesis is shown in Figure 4(a). The 3T3-L1 adipocytes were treated with PA (0.5 mM, 24 h) to induce insulin resistance. Insulin-induced glucose consumption was measured to determine insulin sensitivity. The results showed that insulin-induced glucose consumption was ~8 times higher than that in the normal group but was inhibited by as much as 87.5% after incubation with PA for 24 h, which was consistent with previous free-fatty acid-induced insulin resistance studies [69]. However, intervention with 0.1, 0.3, and 3 μ M of pioglitazone, berberine and 4-Hydroxymephenytoin reversed the condition somewhat. Insulin-induced glucose consumption was increased by 43.8%, 100%, and 162.5% after intervention with 0.1, 0.3 and 3 μ M of 4-Hydroxymephenytoin, respectively for 2 h and were both dose- and time-dependent. In addition, the insulin-induced glucose consumption increased by 368.8% and 212.5%, respectively, in the 3 μ M pioglitazone and berberine groups (Figure 4(b)). As shown in Figure 4(c), nontoxic concentrations of each agent were selected in this study. Together, these results suggest that 4-Hydroxymephenytoin can improve insulin resistance and increase glucose consumption in the 3T3-L1 adipocytes, albeit less efficiently than pioglitazone and berberine at 0.3 μ M.

4. Conclusions

A practical application of the network-based approach was illustrated in GGQLD and the results demonstrate that this approach is an effective strategy for TCM modern research. Increased coverage, quality, and variety of herbal ingredients data involved in each herb will, in turn, enable further opportunities for molecular basis of TCM herbal formulae. Integrating chemical, target protein binding, gene and protein expression, pharmacokinetic and pharmacodynamic or diagnostic and clinical information hold further promise for determining relationships between diseases and TCM herbal formula at multiple levels. At present, the success of network-based active ingredient identification and mechanism prediction supports the notion that TCM herbal formulae target a disease-specific network [26] and that the key to understanding the mechanisms of action and combinatorial rules of TCM herbal formulae is encoded in the molecular network. The antidiabetic activities of the GGQLD herbal ingredients were identified in this work through network pharmacology methods and can serve as potential antidiabetic ingredients for future experimental validation, and 4-Hydroxymephenytoin from Ge-Gen is such a representation validated in this study.

Conflict of Interests

The authors declare that there is no conflict of interests regarding the publication of this paper.

Authors' Contribution

Shao Li and Xiaolin Tong conceived the study and designed the experiments. Huiying Li, Linhua Zhao, Bo Zhang, Yuyu Jiang, Xu Wang, Yun Guo, and Hongxing Liu performed the experiments. Huiying Li, Linhua Zhao, Bo Zhang, Xiaolin Tong, and Shao Li analyzed the data and wrote the paper. Huiying Li and Linhua Zhao are regarded as joint first authors.

Acknowledgments

This work is supported by the NSFC projects (nos. 81225025, 60934004, and 81303139), the 973 Project (no. 2010CB530601), and the Tsinghua-Giti project.

References

- [1] International Federation of Diabetes, IDF diabetes atlas, <http://www.diabetesatlas.org/>.
- [2] F. M. Ashcroft and P. Rorsman, "Diabetes mellitus and the β cell: the last ten years," *Cell*, vol. 148, no. 6, pp. 1160–1171, 2012.
- [3] B. B. Kahn, "Type 2 diabetes: when insulin secretion fails to compensate for insulin resistance," *Cell*, vol. 92, no. 5, pp. 593–596, 1998.
- [4] R. F. Hamman, "Genetic and environmental determinants of non-insulin-dependent diabetes mellitus (NIDDM)," *Diabetes/Metabolism Reviews*, vol. 8, no. 4, pp. 287–338, 1992.
- [5] A. Bonnefond, P. Froguel, and M. Vaxillaire, "The emerging genetics of type 2 diabetes," *Trends in Molecular Medicine*, vol. 16, no. 9, pp. 407–416, 2010.
- [6] I. Prokopenko, M. I. McCarthy, and C. M. Lindgren, "Type 2 diabetes: new genes, new understanding," *Trends in Genetics*, vol. 24, no. 12, pp. 613–621, 2008.
- [7] A. J. Richard and J. M. Stephens, "Emerging roles of JAK-STAT signaling pathways in adipocytes," *Trends in Endocrinology and Metabolism*, vol. 22, no. 8, pp. 325–332, 2011.
- [8] V. T. Samuel and G. I. Shulman, "Mechanisms for insulin resistance: common threads and missing links," *Cell*, vol. 148, no. 5, pp. 852–871, 2012.
- [9] H. J. Welters and R. N. Kulkarni, "Wnt signaling: relevance to β -cell biology and diabetes," *Trends in Endocrinology and Metabolism*, vol. 19, no. 10, pp. 349–355, 2008.
- [10] N. Morral, "Novel targets and therapeutic strategies for type 2 diabetes," *Trends in Endocrinology and Metabolism*, vol. 14, no. 4, pp. 169–175, 2003.
- [11] R. G. Larkins, "New concepts for treatment of non-insulin-dependent diabetes mellitus," *Trends in Endocrinology and Metabolism*, vol. 8, no. 5, pp. 187–191, 1997.
- [12] A. Pujol, R. Mosca, J. Farrés, and P. Aloy, "Unveiling the role of network and systems biology in drug discovery," *Trends in Pharmacological Sciences*, vol. 31, no. 3, pp. 115–123, 2010.
- [13] L. H. Zhao, F. M. Lian, H. Y. Ji, Q. Zhou, L. Xia, and X. L. Tong, "Clinical examples of treatment for type 2 diabetes by professor Tong Xiao-lin using Ge-Gen-Qin-Lian decoction," *Chinese Journal of Experimental Traditional Medical Formulae*, vol. 17, no. 4, pp. 249–251, 2011.
- [14] L. H. Zhao, H. Y. Ji, B. W. Ji, J. Song, and X. L. Tong, "Exploration of Ge-Gen-Qin-Lian Decoction's effect on diabetes mellitus in theory," *China Journal of Traditional Chinese Medicine and Pharmacy*, vol. 27, no. 2, pp. 280–283, 2012.

- [15] W. Zhang, C.-Q. Liu, P.-W. Wang et al., "Puerarin improves insulin resistance and modulates adipokine expression in rats fed a high-fat diet," *European Journal of Pharmacology*, vol. 649, no. 1–3, pp. 398–402, 2010.
- [16] F.-L. Hsu, I.-M. Liu, D.-H. Kuo, W.-C. Chen, H.-C. Su, and J.-T. Cheng, "Antihyperglycemic effect of puerarin in streptozotocin-induced diabetic rats," *Journal of Natural Products*, vol. 66, no. 6, pp. 788–792, 2003.
- [17] Y. M. Liu, Q. J. Feng, X. Niu, Q. Song, X. Zhang, and Y. M. Kang, "Puerarin reduces blood sugar in the diabetic mice and improves hyperlipidemia in rats," *The FASEB Journal*, vol. 20, p. A298, 2006.
- [18] H.-T. Li, X.-D. Wu, A. K. Davey, and J. Wang, "Antihyperglycemic effects of baicalin on streptozotocin–nicotinamide induced diabetic rats," *Phytotherapy Research*, vol. 25, no. 2, pp. 189–194, 2011.
- [19] H. Zhang, J. Wei, R. Xue et al., "Berberine lowers blood glucose in type 2 diabetes mellitus patients through increasing insulin receptor expression," *Metabolism*, vol. 59, no. 2, pp. 285–292, 2010.
- [20] C. Weidner, J. C. de Groot, A. Prasad et al., "Amorfrutins are potent antidiabetic dietary natural products," *Proceedings of the National Academy of Sciences of the United States of America*, vol. 109, no. 19, pp. 7257–7262, 2012.
- [21] X.-L. Tong, L.-H. Zhao, F.-M. Lian et al., "Clinical observations on the dose-effect relationship of Gegen Qin Lian Decoction on 54 out-patients with type 2 diabetes," *Journal of Traditional Chinese Medicine*, vol. 31, no. 1, pp. 56–59, 2011.
- [22] C. H. Zhang, G. L. Xu, Y. H. Liu et al., "Anti-diabetic activities of Ge-Gen-Qin-Lian Decoction in high-fat diet combined with streptozotocin-induced diabetic rats and in 3T-L1 adipocytes," *Phytomedicine*, vol. 20, no. 3–4, pp. 3221–3229, 2013.
- [23] F. Bai, Y. Xu, J. Chen et al., "Free energy landscape for the binding process of Huperzine A to acetylcholinesterase," *Proceedings of the National Academy of Sciences of the United States of America*, vol. 110, no. 11, pp. 4273–4278, 2013.
- [24] S. Ohlson, "Designing transient binding drugs: a new concept for drug discovery," *Drug Discovery Today*, vol. 13, no. 9–10, pp. 433–439, 2008.
- [25] S. Li and B. Zhang, "Traditional Chinese medicine network pharmacology: theory, methodology and application," *Chinese Journal of Natural Medicines*, vol. 11, no. 2, pp. 110–120, 2013.
- [26] A. L. Hopkins, "Network pharmacology: the next paradigm in drug discovery," *Nature Chemical Biology*, vol. 4, no. 11, pp. 682–690, 2008.
- [27] S. Li, Z. Q. Zhang, L. J. Wu, X. G. Zhang, Y. D. Li, and Y. Y. Wang, "Understanding ZHENG in traditional Chinese medicine in the context of neuro-endocrine-immune network," *IET Systems Biology*, vol. 1, no. 1, pp. 51–60, 2007.
- [28] S. Li, "Framework and practice of network-based studies for Chinese herbal formula," *Journal of Chinese Integrative Medicine*, vol. 5, no. 5, pp. 489–493, 2007.
- [29] S. Li, "Network systems underlying traditional Chinese medicine syndrome and herb formula," *Current Bioinformatics*, vol. 4, no. 3, pp. 188–196, 2009.
- [30] S. Li, B. Zhang, D. Jiang, Y. Wei, and N. Zhang, "Herb network construction and co-module analysis for uncovering the combination rule of traditional Chinese herbal formulae," *BMC Bioinformatics*, vol. 11, supplement 11, article S6, 2010.
- [31] S. Li, "Network target: a starting point for traditional Chinese medicine network pharmacology," *Zhongguo Zhongyao Zazhi*, vol. 36, no. 15, pp. 2017–2020, 2011.
- [32] S. Li, B. Zhang, and N. Zhang, "Network target for screening synergistic drug combinations with application to traditional Chinese medicine," *BMC Systems Biology*, vol. 5, supplement 1, article S10, 2011.
- [33] U. Stelzl, U. Worm, M. Lalowski et al., "A human protein-protein interaction network: a resource for annotating the proteome," *Cell*, vol. 122, no. 6, pp. 957–968, 2005.
- [34] H. Jeong, S. P. Mason, A.-L. Barabási, and Z. N. Oltvai, "Lethality and centrality in protein networks," *Nature*, vol. 411, no. 6833, pp. 41–42, 2001.
- [35] L. H. Hartwell, J. J. Hopfield, S. Leibler, and A. W. Murray, "From molecular to modular cell biology," *Nature*, vol. 402, no. 6761, pp. C47–C52, 1999.
- [36] D. B. Goldstein, "Common genetic variation and human traits," *New England Journal of Medicine*, vol. 360, no. 17, pp. 1696–1698, 2009.
- [37] E. E. Schadt, "Molecular networks as sensors and drivers of common human diseases," *Nature*, vol. 461, no. 7261, pp. 218–223, 2009.
- [38] B. Zhang, X. Wang, and S. Li, "An integrative platform of TCM network pharmacology and its application on a Herbal Formula, Qing-Luo-Yin," *Evidence-Based Complementary and Alternative Medicine*, vol. 2013, Article ID 456747, 12 pages, 2013.
- [39] Y. Wang, J. Xiao, T. O. Suzek, J. Zhang, J. Wang, and S. H. Bryant, "PubChem: a public information system for analyzing bioactivities of small molecules," *Nucleic Acids Research*, vol. 37, no. 2, pp. W623–W633, 2009.
- [40] A. Hamosh, A. F. Scott, J. S. Amberger, C. A. Bocchini, and V. A. McKusick, "Online Mendelian Inheritance in Man (OMIM), a knowledgebase of human genes and genetic disorders," *Nucleic Acids Research*, vol. 33, pp. D514–D517, 2005.
- [41] D. S. Wishart, C. Knox, A. C. Guo et al., "DrugBank: a knowledgebase for drugs, drug actions and drug targets," *Nucleic Acids Research*, vol. 36, no. 1, pp. D901–D906, 2008.
- [42] S. Zhao and S. Li, "Network-based relating pharmacological and genomic spaces for drug target identification," *PLoS ONE*, vol. 5, no. 7, Article ID e11764, 2010.
- [43] A. B. Parsons, R. L. Brost, H. Ding et al., "Integration of chemical-genetic and genetic interaction data links bioactive compounds to cellular target pathways," *Nature Biotechnology*, vol. 22, no. 1, pp. 62–69, 2004.
- [44] D. W. Huang, B. T. Sherman, and R. A. Lempicki, "Systematic and integrative analysis of large gene lists using DAVID bioinformatics resources," *Nature Protocols*, vol. 4, no. 1, pp. 44–57, 2009.
- [45] L. S. Li, N. B. Zhang, and S. Li, "Ranking effects of candidate drugs on biological process by integrating network analysis and Gene Ontology," *Chinese Science Bulletin*, vol. 55, no. 26, pp. 2974–2980, 2010.
- [46] A. Kaiden Student, R. Y. Hsu, and M. D. Lane, "Induction of fatty acid synthetase synthesis in differentiating 3T3-L1 preadipocytes," *Journal of Biological Chemistry*, vol. 255, no. 10, pp. 4745–4750, 1980.
- [47] B. A. Nelson, K. A. Robinson, and M. G. Buse, "High glucose and glucosamine induce insulin resistance via different mechanisms in 3T3-L1 adipocytes," *Diabetes*, vol. 49, no. 6, pp. 981–991, 2000.
- [48] H. Kitano, "A robustness-based approach to systems-oriented drug design," *Nature Reviews Drug Discovery*, vol. 6, no. 3, pp. 202–210, 2007.

- [49] A. B. Wagner, "SciFinder Scholar 2006: an empirical analysis of research topic query processing," *Journal of Chemical Information and Modeling*, vol. 46, no. 2, pp. 767–774, 2006.
- [50] S.-J. Lee, K. Umano, T. Shibamoto, and K.-G. Lee, "Identification of volatile components in basil (*Ocimum basilicum* L.) and thyme leaves (*Thymus vulgaris* L.) and their antioxidant properties," *Food Chemistry*, vol. 91, no. 1, pp. 131–137, 2005.
- [51] L. J. Xu, F. E. Lu, and S. C. Wei, "Use of berberine derivative in preparing medicament for treating type-2 diabetes, adjusting blood sugar and blood fat," Patents Number: CN100404534C, 2008.
- [52] G. Y. Yeh, D. M. Eisenberg, T. J. Kaptchuk, and R. S. Phillips, "Systematic review of herbs and dietary supplements for glycemic control in diabetes," *Diabetes Care*, vol. 26, no. 4, pp. 1277–1294, 2003.
- [53] Z. Zhen, B. Chang, M. Li et al., "Anti-diabetic effects of a coptis chinensis containing new traditional Chinese medicine formula in type 2 diabetic rats," *American Journal of Chinese Medicine*, vol. 39, no. 1, pp. 53–63, 2011.
- [54] J. C. Li, X. F. Shen, and X. L. Meng, "A traditional Chinese medicine JiuHuangLian (*Rhizoma coptidis* steamed with rice wine) reduces oxidative stress injury in type 2 diabetic rats," *Food and Chemical Toxicology*, vol. 59, pp. 222–229, 2013.
- [55] X. F. Jiang, L. J. Wang, X. G. Li, Z. Q. Zhao, and J. Y. Zhu, "Isolation of Jatrorrhizine and Epiberberine in *Coptis chinensis* and their in vitro Hypoglycemic Effect," *Guizhou Agricultural Sciences*, vol. 39, no. 9, pp. 44–46, 2011.
- [56] Y. Fu, B. R. Hu, Q. Tang et al., "Effect of jatrorrhizine, berberine, Huanglian Decoction and compound-mimic prescription on blood glucose in mice," *Chinese Traditional and Herbal Drugs*, vol. 36, no. 4, pp. 548–551, 2005.
- [57] A. Shirwaikar, K. Rajendran, and I. S. R. Punitha, "Antidiabetic activity of alcoholic stem extract of *Coscinium fenestratum* in streptozotocin-nicotinamide induced type 2 diabetic rats," *Journal of Ethnopharmacology*, vol. 97, no. 2, pp. 369–374, 2005.
- [58] S. Ali, J. Igoli, C. Clements et al., "Antidiabetic and antimicrobial activities of fractions and compounds isolated from *Berberis brevissima* Jafri and *Berberis parkeriana* Schneid," *Bangladesh Journal of Pharmacology*, vol. 8, no. 3, pp. 336–342, 2013.
- [59] Y. S. Lee, W. S. Kim, K. H. Kim et al., "Berberine, a natural plant product, activates AMP-activated protein kinase with beneficial metabolic effects in diabetic and insulin-resistant states," *Diabetes*, vol. 55, no. 8, pp. 2256–2264, 2006.
- [60] D. Diengott and I. A. Mirsky, "Hypoglycemic action of indole-3-acetic acid by mouth in patients with diabetes mellitus," *Proceedings of the Society for Experimental Biology and Medicine*, vol. 93, no. 1, pp. 109–110, 1956.
- [61] M. B. Hadimani, M. K. Purohit, C. Vanampally et al., "Guaifenesin derivatives promote neurite outgrowth and protect diabetic mice from neuropathy," *Journal of Medicinal Chemistry*, vol. 56, no. 12, pp. 5071–5078, 2013.
- [62] X. Su, F. Pradaux-Caggiano, N. Vicker et al., "Adamantyl ethanone pyridyl derivatives: potent and selective inhibitors of human 11 β -hydroxysteroid dehydrogenase type 1," *ChemMedChem*, vol. 6, no. 9, pp. 1616–1629, 2011.
- [63] G. Bartosz, *Food Oxidants and Antioxidants: Chemical, Biological, and Functional Properties*, CRC Press, 2013.
- [64] R. Rahimi, S. Nikfar, B. Larjani, and M. Abdollahi, "A review on the role of antioxidants in the management of diabetes and its complications," *Biomedicine and Pharmacotherapy*, vol. 59, no. 7, pp. 365–373, 2005.
- [65] L. Jovanovic, D. R. Hassman, B. Gooch et al., "Treatment of type 2 diabetes with a combination regimen of repaglinide plus pioglitazone," *Diabetes Research and Clinical Practice*, vol. 63, no. 2, pp. 127–134, 2004.
- [66] R. Li, T. Ma, J. Gu, X. Liang, and S. Li, "Imbalanced network biomarkers for traditional Chinese medicine Syndrome in gastritis patients," *Scientific Reports*, vol. 3, article 1543, 2013.
- [67] B. Jiang, X. Liang, Y. Chen et al., "Integrating next-generation sequencing and traditional tongue diagnosis to determine tongue coating microbiome," *Scientific Reports*, vol. 2, article 936, 2012.
- [68] C. J. Schofield and C. Sutherland, "Disordered insulin secretion in the development of insulin resistance and Type 2 diabetes," *Diabetic Medicine*, vol. 29, no. 8, pp. 972–979, 2012.
- [69] M. Van Epps-Fung, J. Williford, A. Wells, and R. W. Hardy, "Fatty acid-induced insulin resistance in adipocytes," *Endocrinology*, vol. 138, no. 10, pp. 4338–4345, 1997.

Research Article

dTGS: Method for Effective Components Identification from Traditional Chinese Medicine Formula and Mechanism Analysis

Ji Luo,¹ Yinglong Ren,¹ Hao Gu,¹ Yi Wu,² and Yun Wang¹

¹ Beijing University of Chinese Medicine, School of Chinese Pharmacy No. 6, Zhonghuan South Road, Wangjing, Chaoyang, Beijing 100102, China

² Pennsylvania State University Erie, The Behrend College, School of Engineering, 5101 Jordan Road, Erie, PA 16563, USA

Correspondence should be addressed to Yun Wang; wangyun@bucm.edu.cn

Received 24 July 2013; Revised 27 September 2013; Accepted 27 September 2013

Academic Editor: Weidong Zhang

Copyright © 2013 Ji Luo et al. This is an open access article distributed under the Creative Commons Attribution License, which permits unrestricted use, distribution, and reproduction in any medium, provided the original work is properly cited.

Because of the complexity of the components in Traditional Chinese Medicine formula (TCM formula), it is still a challenge to identify its effective components, to elucidate the mechanism of the components, and to discover the relationship between components and therapy objectives. In this paper, a method called directed TCM grammar systems (dTGS) for effective component identification was proposed using entity grammar systems (EGS) as the theoretical framework. The component-disease relationship of a TCM formula (i.e., Bai-Hu decoction plus Wasting-Thirsting formula, BHDWT) and one disease (i.e., type 2 diabetes mellitus) treated with it was studied, and the effective component groups (ECGs) were identified. 19 compounds were found acting on 20 proteins in type 2 diabetes mellitus (T2D) disease network, and 15 compounds were determined as the candidate effective components. Results indicated that this method can be used to identify the effective components and provide an innovative way to elucidate the molecular mechanism of TCM formulas.

1. Introduction

The components in Traditional Chinese Medicine formula (TCM formula) were very complex and their molecular mechanism was unclear. For the treatment of one disease, some components may be favorable and others may not. Identification of favorable components and analysis of their action mechanisms will benefit the optimization of cultivation condition, processing technology, extraction process, and new drug development. At present, experiment screening was still the main method for the identification of effective components and effective component groups (ECGs). For example, high-performance liquid chromatography-mass spectrometry (HPLC-MS) was used to analyze the active constituents of Xiao-Xu-Ming decoction [1]; drosophila transgenic models were used to identify combinatorial drug, such as suberoylanilide hydroxamic acid (SAHA) and geldanamycin, for the treatment of Huntington's disease [2]; cell-based assays technology was used to screen two-component combinations for the treatment of cancer, infectious diseases, and CNS disorders [3]. However, the results identified

through experimental screening were limited, due to the complexity of components and the high cost associated with experiments.

Recently, computational systems biology was used to study TCM because of the technical advantages of studying large and complex systems and the relative lower cost compared to experimental screening. The applications of complex network analysis techniques, in particular, led to many new findings. For instance, microarray technology and connectivity maps were integrated into the research of molecular mechanisms of Si-Wu decoction (composed of four herbs: Radix Rehmanniae preparata, Radix Angelicae Sinensis, Rhizoma Ligustici Chuanxiong, and Radix Paeoniae Alba) [4]. Multilayer map of "Phenotype network-Biological network-Herb network" was applied to uncover the underlying network systems of TCM syndromes and herb formulas [5]; the drug-target network was implemented to elucidate the mechanism of one TCM formula for the treatment of T2D [6]. Although those applications of computational systems biology in the study of TCM formulas are still in the exploratory stages, they demonstrate the feasibility of

integrating the biological network and the experiences in traditional medicines for the analysis of TCM formulas.

To date, graph theory is a primary approach for network research [7]. It is viable to study a network graph composed of dozens or hundreds of nodes through visual inspection. However, it is not practical to analyze a network containing massive nodes or complex relations between them, even with the help of three-dimensional display techniques. Most methods developed for complex networks, such as the path-length method and the nodes-distribution method [8], focus on the topological structure instead of the specific relationship between nodes. Therefore, it is still challenging to study a complex disease network with intercrossing pathways and to understand the final effects of the components of TCM formulas based on the biological signal pathways. In addition, those biological effects may be ambiguous (positive through one pathway, while negative through the other one) plus some proteins affected by the components of TCM which have not been identified as disease targets. In order to solve these issues and to discover components with positive effect from TCM formulas, we proposed a new approach called directed TCM grammar systems (dTGS) to identify effective components from TCM formula based on an entity grammar system (EGS). In dTGS, the TCM component-protein network and the disease network are viewed as grammar systems and the ECGs can be identified through syntax rules. Bai-Hu decoction plus Wasting-Thirsting formula (BHDWT) was selected as an example in this paper to illustrate the basic idea of the method.

2. Materials and Methods

2.1. Definition of dTGS Model in the Framework of EGS. EGS is a formal grammar system that aims at complex biological system modeling [9]. Because of its scalable feature, EGS has already been used to establish the flow graph models of chemical processes [10] and to illustrate the mechanisms of TCM [11]. The details for establishing a specific EGS were described in [9] and are briefly summarized here.

An entity grammar system G is a quintuple, $G = (V_N, V_T, F, P, S)$, whereas $V_N \cup V_T = V$, V_N is a finite set of nonterminal symbols, V_T is a finite set of terminal symbols, and $V_N \cap V_T = \Phi$, F is a finite set of relations for V ; P is a set of rules to deduce relationships between entities, and S is the starting entity.

dTGS has the same structure as EGS: set V contains different types of nodes (compounds, proteins, T2D, apoptosis, inflammation, etc.); set F contains different types of relationships between adjacent nodes; set P defines the rules to derive the relationship of nodes, as described by the following:

$$V = V_1 \cup V_2 \cup V_3 \cup V_4. \quad (1)$$

V_1 is the set of the compounds in TCM formulas, V_2 is the set of proteins in the disease network on which the compounds in TCM formulas act directly, V_3 is the set of the rest proteins in the disease network, and V_4 is the

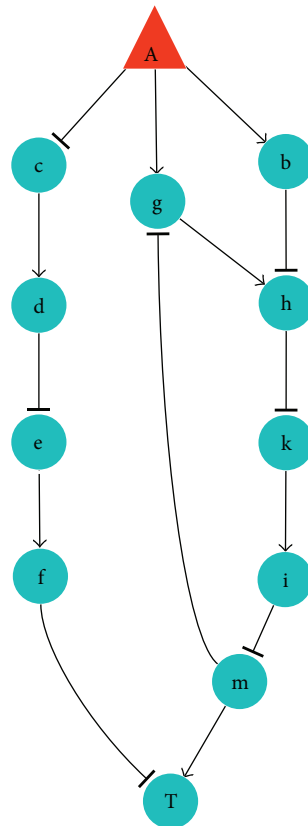


FIGURE 1: Network used in dTGS for deduction. Red triangle node: chemical compound; blue circle node: protein; “ \rightarrow ”: one chemical component or one protein enables the expression of the next protein, raises the expression, or enhances the activity of the next protein. “ \dashv ”: one chemical component or one protein inhibits the expression of the next protein, lowers the expression, or weakens the activity of the next protein.

set of nonprotein nodes in the disease network (e.g., T2D, apoptosis, inflammation, etc.). Consider

$$F = \{cp(X, Y, Z), pp(X, Y, Z), draw(X, Y, Z), tag(X)\}. \quad (2)$$

In $cp(X, Y, Z)$, $X \in V_1$, $Y \in V_2$, $Z \in \{\text{pos}, \text{neg}\}$; in $pp(X, Y, Z)$, $X, Y \in V_3 \cup V_4$, $Z \in \{\text{pos}, \text{neg}\}$; in $draw(X, Y, Z)$, $X, Y \in V$, $Z \in \{\text{pos}, \text{neg}\}$; in $tag(X)$, $X \in V$.

$cp(X, Y, Z)$ defines that X (compound in TCM formulas) acts on Y (protein directly reacts to compound) with an effect described in Z . $pp(X, Y, Z)$ defines that X (protein) acts on Y (protein) with an effect described in Z . $tag(X)$ labels nodes of interest. $draw(X, Y, Z)$ extracts tagged nodes, and their relationships defined in $cp(X, Y, Z)$ or $pp(X, Y, Z)$ in dTGS; $E(V, F)$ refers to all entities composed by the elements in V , with the structure $cp(X, Y, Z)$, $pp(X, Y, Z)$, $draw(X, Y, Z)$, or $tag(X)$. Consider

$$P = P_1 \cup P_2 \cup P_3 \cup P_4 \cup P_5 \cup P_6,$$

$$P_1 = \{pp(X, Y, \text{pos}), pp(Y, M, \text{pos}) \implies pp(X, M, \text{pos})\},$$

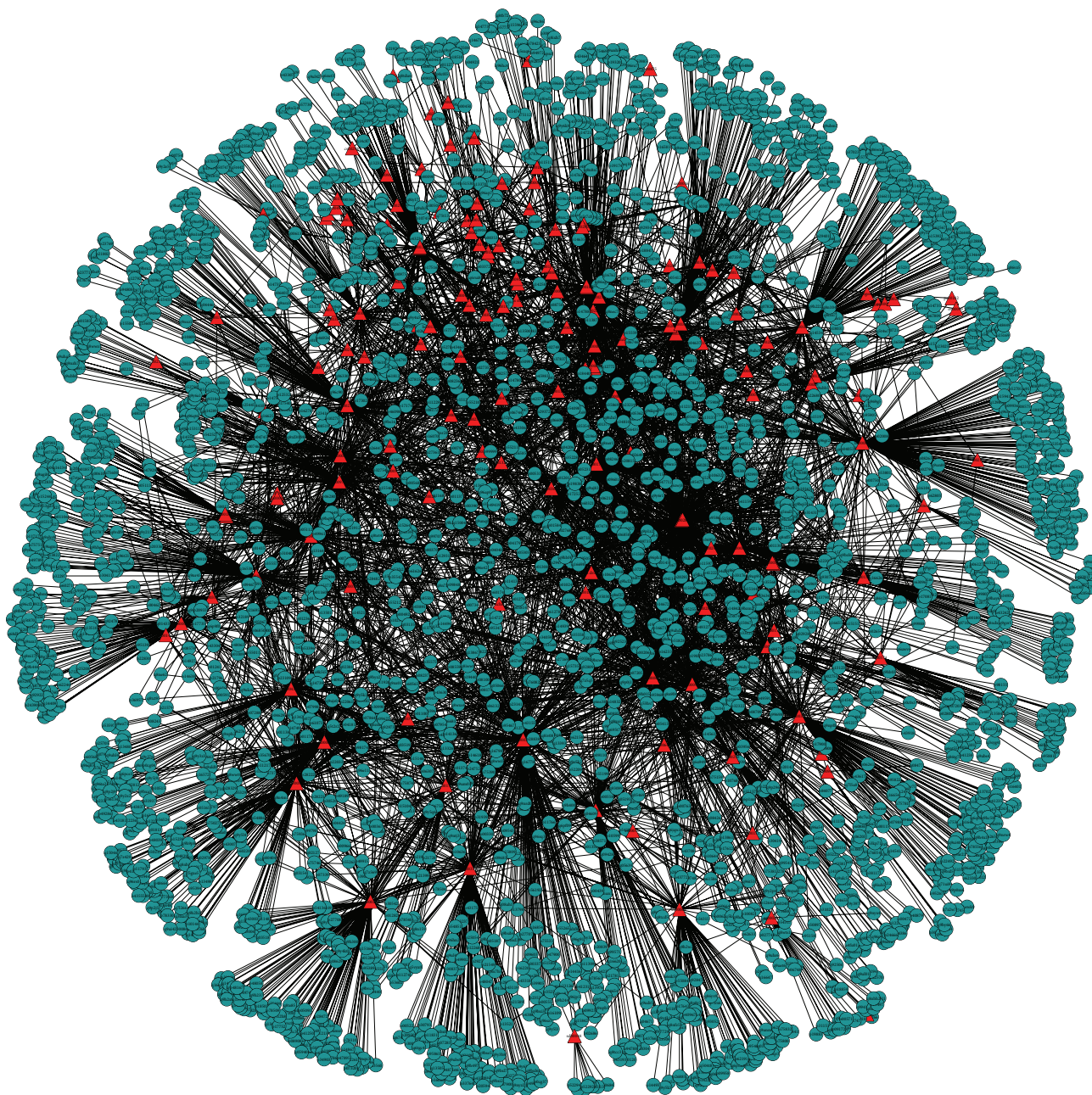


FIGURE 2: Compound-protein network of BHDWT. Red triangle node: compound in BHDWT; blue circle node: protein.

$$\begin{aligned}
 P_2 &= \{pp(X, Y, \text{neg}), pp(Y, M, \text{neg}) \implies pp(X, M, \text{pos})\}, \\
 P_3 &= \{pp(X, Y, \text{pos}), pp(Y, M, \text{neg}) \implies pp(X, M, \text{neg})\}, \\
 P_4 &= \{pp(X, Y, \text{neg}), pp(Y, M, \text{pos}) \implies pp(X, M, \text{neg})\}, \\
 P_5 &= \{pp(X, Y, Z), \text{tag}(X) \implies \text{draw}(X, Y, Z), \text{tag}(Y)\}, \\
 P_6 &= \{cp(X, Y, Z), \text{tag}(X) \implies \text{draw}(X, Y, Z), \text{tag}(Y)\}.
 \end{aligned}
 \tag{3}$$

$P_1 \cup P_2 \cup P_3 \cup P_4$ is the set of rules to deduce the eventual effects of chemical compounds on the disease. P_1 indicates

that if the effect of X to Y is positive and the effect of Y to M is positive too, then the effect of X to M is positive. Similar derivations are defined in P_2 , P_3 , and P_4 . They may be used as many times as necessary to the final disease node. P_5 and P_6 are the rules to extract the nodes for the network. They can also be used to draw the subnetwork when the original networks are too complicated to analyze. P_5 indicates that if X (protein) acts on Y (protein) with the effect of Z and X is tagged, then this relation is extracted and Y is also labeled for further derivation. P_6 is similar to P_5 except that the starting entity is chemical compound X . In the construction

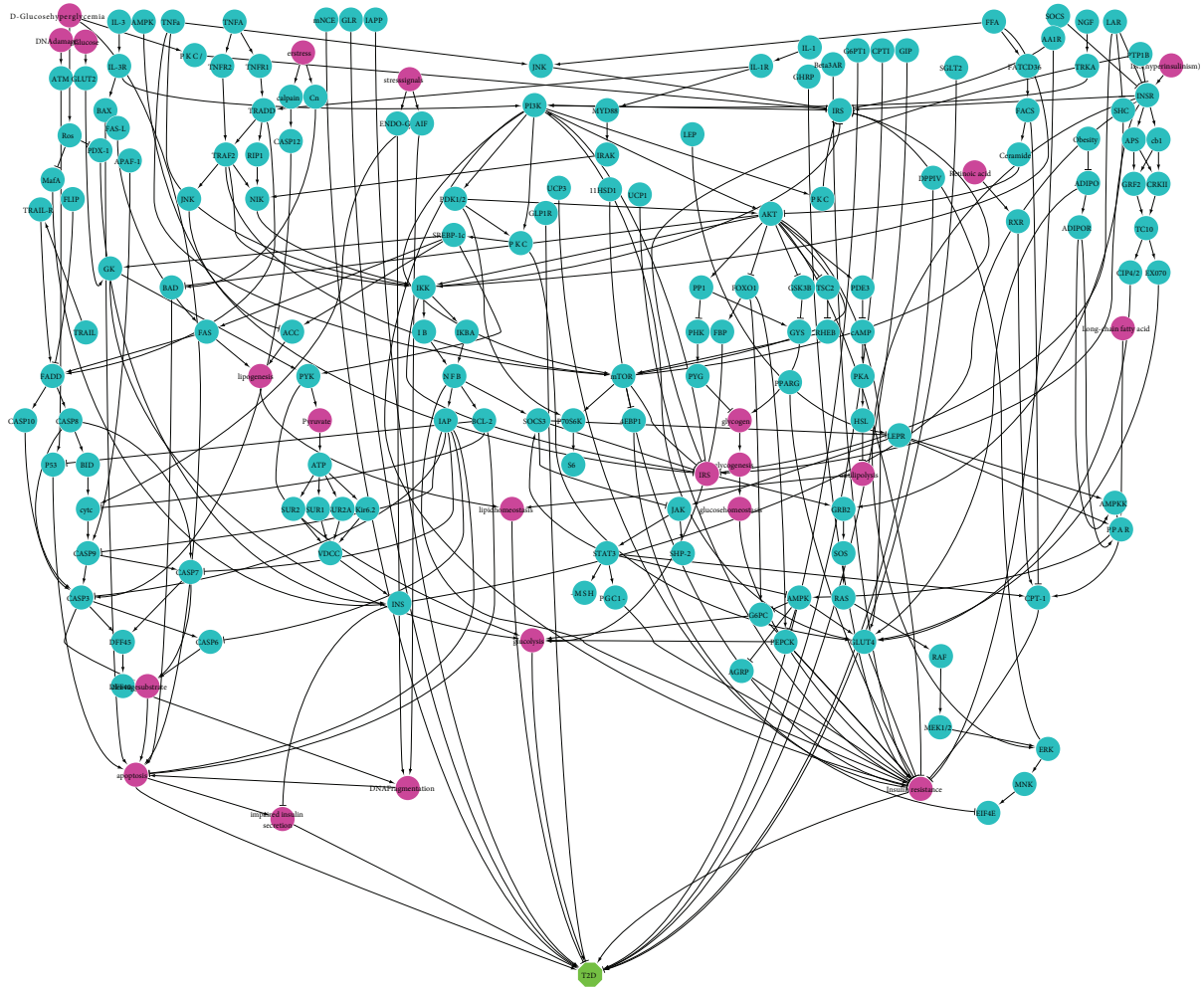


FIGURE 3: Biological network of T2D. Blue circle node: protein; purple circle node: nonprotein node; green octagon nodes: type 2 diabetes; “ \rightarrow ”: one node enables the expression of the next node, raises the expression, or enhances the activity of the next node; “ $-$ ”: one node inhibits the expression of the next node, lowers the expression, or weakens the activity of the next node.

of network, P_6 will be used once and P_5 may be used as many times as necessary to the target.

The modes of action between nodes include the positive (pos) and the negative (neg) effects. If we define the positive effect as “1” and the negative effect as “-1,” the ultimate influence of intervention will depend on the product of each step in the whole signal pathway. For example, compound A in Figure 1 influences protein T through 3 paths. The effect of A to T is negative through the path “A-c-d-e-f-T” and the path “A-b-h-k-i-m-T.” This effect is uncertain through the third path “A-g-h-k-i-m-T,” taking into account the negative effect from the feedback path m to g. In this paper, we neglected the effects produced through feedback because the role of feedback is expected to regulate the magnitude of effect but not to alter the overall mode of action of effect. So, the effect is positive through the third path. After the effects of one compound on the ultimate node (i.e., T in Figure 1) through all signal pathways are determined, we can select the effective compounds based on the desired effect. If the desired effect on the ultimate node is positive, the compounds

with positive effects through all pathways will be selected as active components. The compounds with negative effects through all pathways will be ruled out. The components with both effects through different pathways need further analysis on molecular mechanism. If their undesired effects can be countered by other compounds, they may also be selected as effective components to be used together with the countering compounds. The opposite analysis will be done if the desired effect on the ultimate node is negative. Consider

$$S = S_1 \cup S_2. \quad (4)$$

S_1 is the set of entities with structure $cp(X, Y, Z)$ or $pp(X, Y, Z)$ in biological network of disease, which are the background for deduction. S_2 is the set of labeled compounds or proteins, expressed by $tag(X)$. S_2 is the initial conditions for deduction.

2.2. Data for Construction of Component-Protein Network of BHDWT Formula. For decades, BHDWT has been used to treat T2D at the Beijing Guang-An-Men Hospital [12].

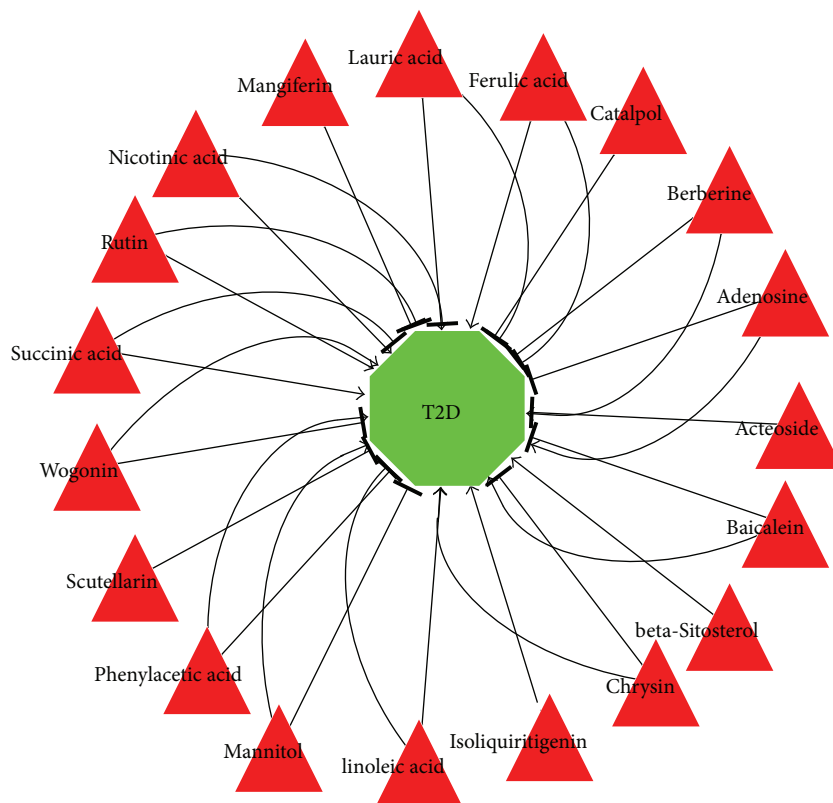


FIGURE 4: The effect of compound of BHDWT on T2D. Red triangle node: chemical compound; green octagon nodes: type 2 diabetes; “+”: one compound has the positive effect on T2D; “-”: one compound has the negative effect on T2D.

BHDWT has a positive effect on blood glucose control and symptom control for some patients in the early stages of T2D. The BHDWT formula consists of eight herbs, including gypsum, *Anemarrhena asphodeloides* Bunge, rehmannia dried rhizome, radix trichosanthis, *Ophiopogon japonicus* Ker Gawl, *Coptis chinensis* Franch, *Scutellaria baicalensis* Georgi, and *Glycyrrhiza uralensis*.

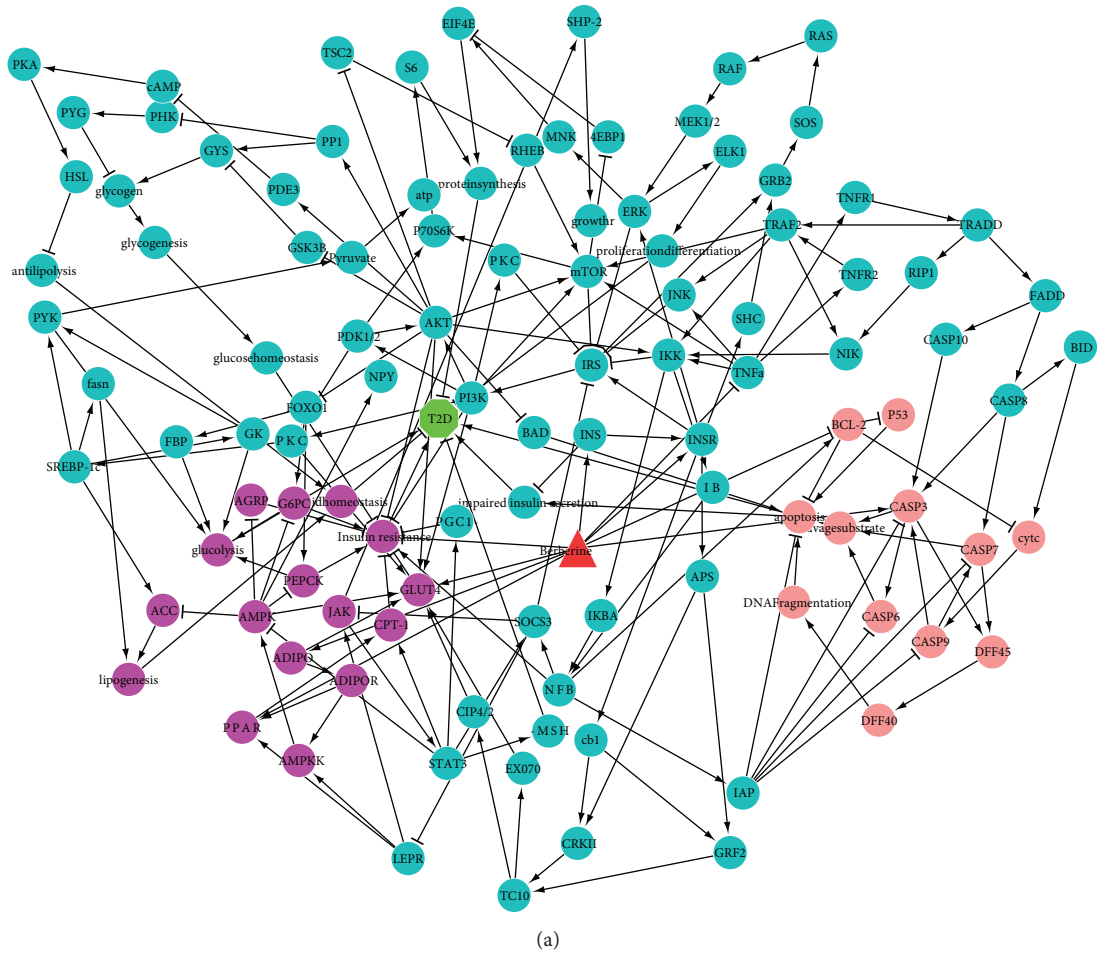
The components of the BHDWT formula came from the Traditional Chinese Medicines Database (TCMD) [13], the State Administration of Traditional Chinese Medicine Basic Information Database (<http://dbshare.cintcm.com/ZhongYaoJiChu/>), and *A Handbook on the Analysis of the Active Composition in Traditional Chinese Medicine* [14].

The compound-targeted proteins were derived from the STITCH system (<http://stitch.embl.de/>) [15]. By entering the names or identifiers of compounds or proteins of interest, STITCH provides the list of proteins with matching or higher confidence score that the user specified, up to the number the user specified. The required confidence score represents the possibility of interaction between the entities. In order to obtain more general results, the parameter of the required confidence score was set higher than 0 and the interacting entities number was set to be 500. The interacting entities with clear mode of action (positive or negative) were chosen for further analysis.

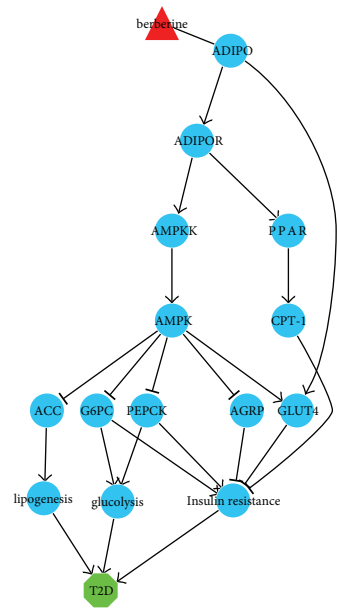
2.3. Data for the Construction of T2D Biological Network. To construct the T2D network, we used the data collected from the Kyoto Encyclopedia of Genes and Genomes (KEGG) and therapeutic targets database (TTD). KEGG lists the signal pathways related to T2D and TTD lists the chemical components used to treat T2D. The biological network of T2D (Figure 3) was constructed using the signal pathways from KEGG, the chemical components from TTD, and the positive or negative relationship between targets and T2D from STITCH. The networks were visualized with the software Cytoscape [16].

3. Results and Discussion

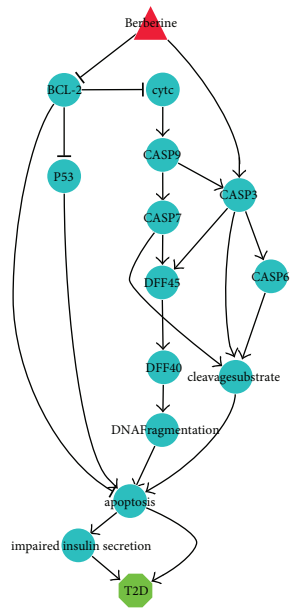
3.1. Compound-Protein Network of BHDWT Formula and the Biological Network of T2D. We first constructed the component-protein network of BHDWT using the data from Section 2.2 (Figure 2, additional file 1 in Supplementary Material available online at <http://dx.doi.org/10.1155/2013/840427>). In this network, there are 144 compounds and 2865 proteins. The red triangle nodes represent the compound in BHDWT and the blue circle nodes represent the proteins. The biological network of T2D (Figure 3) was derived from the data in Section 2.3 using P_5 and P_6 defined in Section 2.1, with T2D as the ultimate node. Biological network of T2D contains 146 proteins. The effects of each



(a)



(b)



(c)

FIGURE 5: Sub-network affected by berberine. (a) Sub-network of berberine acting on six proteins. (b) Sub-network of berberine acting on ADIPO. (c) Sub-network of berberine acting on BCL-2 and caspase 3.

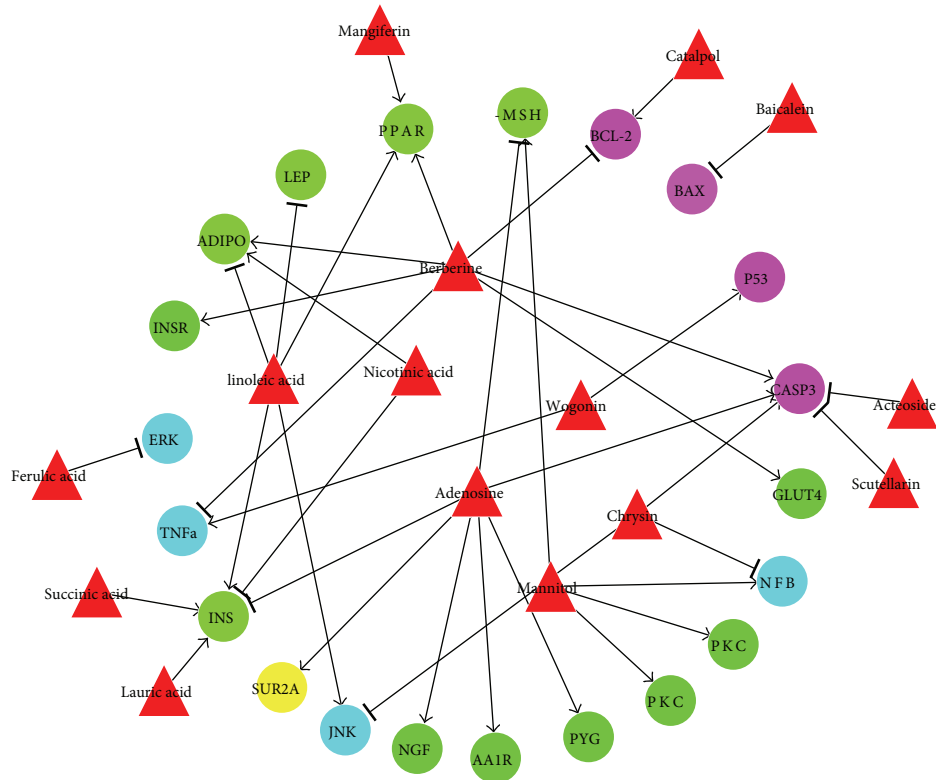


FIGURE 6: Relationship between effective components of BHDWT and reactive proteins. Red triangle node: active chemical component. Green nodes: proteins in the first category (related to insulin resistance). Purple nodes: proteins in the second category (related to apoptosis). Blue nodes: proteins in the third category (related to both insulin resistance and apoptosis). Yellow nodes: proteins in the fourth category (related to insulin secretion).

compound in BHDWT on T2D were derived using P_1 , P_2 , P_3 , and P_4 rules defined in Section 2.1.

3.2. The Effect of Chemical Components on T2D. The ultimate effects of each compound of BHDWT on T2D can be found by combining Figures 2 and 3 through dTGS. We applied rule P_6 for each compound node in Figure 3 as X , with the linked protein with X to be Y in P_6 rule. As a result, all the compounds in Figure 2 that have clear modes of action on linked protein were labeled. The proteins presented in both Figures 2 and 3 were also labeled by applying P_6 . With the labeled protein as X and the connected node as Y , the pathway describing the relationship can be extracted by applying P_5 . Those compounds' ultimate effects on T2D (Figure 4) can be derived through P_1 , P_2 , P_3 , and P_4 . Totally, 45 compounds in 7 TCMs (except gypsum) showed effects on 61 proteins in the T2D biological network. Among 45 compounds, 19 (additional file 2) have a clear mode of action (positive or negative) recorded in STITCH. Three kinds of effect were found: positive, negative, and bidirectional effects. The desired effect on T2D is negative. Among these 19 compounds, β -sitosterol, isoliquiritigenin played a positive effect on T2D (i.e., negative effect on the treatment of T2D) and four compounds (i.e., scutellarin, catalpol, mangiferin, and acteoside) have negative effects on T2D (i.e., positive effect on the treatment of T2D). The rest of the 13 compounds

show bidirectional effects and will be studied further in the next section.

3.3. Extraction of the Subnet and Effective Components. For each of the 13 bidirectional compounds, we extracted the subnetworks affected by each of them to study their effects in more detail. The method of extracting the subnetwork has been explained in Section 2.1. We found through subnetworks that the negative effect of rutin and phenylacetic acid on T2D originates from the feedback pathways, being not expected to override the positive effect through direct pathways. So, these two compounds were not considered as candidate effective components. Some other bidirectional components have a complex sub-network. For example, berberine acts on six proteins. The derived sub-network including all six proteins is too complex for further analysis (Figure 5). Therefore, we derived six sub-networks including one or two proteins reacting with berberine. Two of those sub-networks were shown in Figures 5(b) and 5(c). Through analyzing these six sub-networks, we found that berberine's negative effect on T2D arises from the direct pathway. Finally, all 13 bidirectional components except rutin and phenylacetic acid were selected as candidate effective components. They together with the other four negative compounds (i.e., scutellarin, catalpol, mangiferin, and acteoside) form 15 candidate

effective components combinations and will be screened further in the next section.

3.4. Combination of Candidate Effective Components. In this section, we try to find out which proteins each of the 15 effective components affects. This will help us figure out how to combine those components to achieve optimal results. According to the literature, insulin resistance and impaired insulin secretion are two major etiological factors of T2D [17], and β -cell apoptosis was considered as one reason for the impaired insulin secretion [18]. Therefore, we divided the proteins into four categories. The first category is only related to insulin resistance; the second category is only related to apoptosis; the third category is related to both insulin resistance and apoptosis; the fourth category is only related to insulin secretion. Then, the effects of each active component were screened according to the category of proteins (Figure 6). For instance, mangiferin acts on insulin resistance related proteins (PPAR α) and catalpol acts on apoptosis related proteins (BCL-2); hence, the combination of mangiferin and catalpol was predicted to treat T2D by ameliorating insulin resistance and inhibiting apoptosis. It is worth noting that Figure 6 missed one protein in additional file 2, that is, CASP9. This is due to the fact that beta-sitosterol, the only compound which enables CASP9, was ignored because of beta-sitosterol's positive effect on T2D. The rest of the compounds in Figure 6 did not act on CASP9.

Some of the findings revealed in Figure 6 are consistent with numerous studies on the treatment of T2D. Ferulic acid showed antidiabetic effects in experiments on diabetic mice [19]. Mangiferin exhibited the potential to improve blood lipids in T2D [20]. Baicalein was demonstrated to protect pancreatic beta-cells from apoptosis and ameliorates hyperglycemia in a mouse model of T2D [21]. The experiment in vitro indicated that berberine can improve glucose consumption (GC) over 30% when the concentration is above 5×10^{-6} mol/L; at the same time, berberine also depressed cell growth remarkably at the same concentration [22]. This finding was consistent with our analysis that berberine promotes cell apoptosis by promoting caspase 3 and inhibiting BCL-2.

The compounds that have multiple and counterpart pathways in Figure 6 were still selected as candidate effective components to treat T2D because their unfavorable effects may not be dominant or counteracted by other compounds, as demonstrated in clinical practice. For example, some physicians have used berberine to treat hyperglycemia agent in China for many years [23].

Figure 6 also discloses some information useful for designing or analyzing component combination. Although the hepatotoxicity or pancreatotoxicity (typically resulting from enhanced cell apoptosis) induced by berberine has never been observed in clinics, Figure 6 indicated that its toxicity may be counteracted while constructing drug combinations with the components that can inhibit cell apoptosis, such as catalpol, scutellarin, acteoside, and baicalein. In clinical practice, BHDWT was used to treat early stages

of T2D when the main disease factor is insulin resistance [8]. This can be explained by several effective components acting on green nodes (i.e., proteins related to insulin resistance) in Figure 6. Similar effects to suppress the insulin resistance can also be achieved by the combinations of some of these effective components according to Figure 6, such as (i) the combinations of berberine and mangiferin, (ii) the combinations of berberine and catalpol (or scutellarin or acteoside or baicalein), and (iii) of berberine, mangiferin combination and catalpol (or scutellarin or acteoside or baicalein). Some of these combinations have been validated by the work from other researchers: the combination of berberine and mangiferin was granted a patent [24], and the combination of berberine and catalpol [25] has been filed for a patent. All of the results indicate that TCM formula plays its role through synergistic effects of multiple components.

4. Conclusions

This paper proposed dTGS as an innovative method to study TCM formulas. It integrates the research achievements from three fields: TCM chemistry, drug discovery, and the network biology. The findings include the action trends of chemical components against one disease (T2D) and the active component combinations from BHDWT formula. It can also be applied on other TCM formulas to benefit the research on the mechanism of TCM formulas.

In addition, our work would benefit the development of fixed-dose combinations. Nowadays, drug combinations or fixed-dose combinations (FDCs) are widely used in the treatment of complex diseases because of the low cost and the clinical efficiency. TCM formulas, due to their characteristics of multicomponents, multitargets, and multipath effects, may embody some component combinations or combination principles beneficial to the design of drug combination. Our method provides a systemic approach to reveal those principles.

Last but not least, our method provided a novel idea for network analysis. Our method is different from the primary approach in network research (e.g., graph theory) in that we proposed a series of inference rules derived from the relationship of the nodes and provided a new theoretical framework for analyzing the complex network. The feasibility of this theoretical framework was proved by its success to identify the effective component combinations in TCM formulas.

Acknowledgments

This work is supported and sponsored by the Natural Science Foundation of China (NSFC 81373985, NSFC 81173568), Program for New Century Excellent Talents in University (NCET-11-0605), and Key Projects in the National Science & Technology Pillar Program during the Eleventh Five-Year Plan Period (2008BAI51B01).

References

- [1] Y. Wang, C. Ding, C. Wu et al., "HPLC-MS and HPLC-MS/MS analysis of seven active constituents of Xiao-Xu-Ming decoction and application to a pharmacokinetic study after oral administration to rat," *Acta Pharmaceutica Sinica B*, vol. 2, no. 2, pp. 188–197, 2012.
- [2] N. Agrawal, J. Pallos, N. Slepko et al., "Identification of combinatorial drug regimens for treatment of Huntington's disease using *Drosophila*," *Proceedings of the National Academy of Sciences of the United States of America*, vol. 102, no. 10, pp. 3777–3781, 2005.
- [3] A. A. Borisy, P. J. Elliott, N. W. Hurst et al., "Systematic discovery of multicomponent therapeutics," *Proceedings of the National Academy of Sciences of the United States of America*, vol. 100, no. 13, pp. 7977–7982, 2003.
- [4] Z. Wen, Z. Wang, S. Wang et al., "Discovery of molecular mechanisms of traditional Chinese medicinal formula Si-Wu-Tang using gene expression microarray and connectivity map," *PLoS One*, vol. 6, no. 3, Article ID e18278, 2011.
- [5] S. Li, "Network systems underlying traditional Chinese medicine syndrome and herb formula," *Current Bioinformatics*, vol. 4, no. 3, pp. 188–196, 2009.
- [6] J. Gu, H. Zhang, L. Chen, S. Xu, G. Yuan, and X. Xu, "Drug-target network and polypharmacology studies of a traditional Chinese medicine for type II diabetes mellitus," *Computational Biology and Chemistry*, vol. 35, no. 5, pp. 293–297, 2011.
- [7] M. E. J. Newman, "The structure and function of complex networks," *Society for Industrial and Applied Mathematics Review*, vol. 45, no. 2, pp. 167–256, 2003.
- [8] R. Albert and A.-L. Barabási, "Statistical mechanics of complex networks," *Reviews of Modern Physics*, vol. 74, no. 1, pp. 47–97, 2002.
- [9] Y. Wang, "Entity grammar systems: a grammatical tool for studying the hierarchal structures of biological systems," *Bulletin of Mathematical Biology*, vol. 66, no. 3, pp. 447–471, 2004.
- [10] R. Zheng, K. S. Wang, and Y. Wang, "Regulating flow graph model of chemical processes in framework of entity grammar systems," *Computer Engineering and Applications*, vol. 46, pp. 245–248, 2010.
- [11] J. Yan, Y. Wang, S.-J. Luo, and Y.-J. Qiao, "TCM grammar systems: an approach to aid the interpretation of the molecular interactions in Chinese herbal medicine," *Journal of Ethnopharmacology*, vol. 137, no. 1, pp. 77–84, 2011.
- [12] L. Lin, *Contemporary Diabetes Mellitus in Traditional Chinese Medicine*, People's Medical Publishing House, Beijing, China, 2008.
- [13] H. B. Liu, Y. X. Qiao, B. Liu, and J. J. Zhou, "Transformation of traditional Chinese medicine database into data warehouse," *Chinese Pharmaceutical Journal*, vol. 9, pp. 645–648, 2006.
- [14] X. Q. Chang and L. X. Ding, *A Handbook on Analysis of the Active Composition in Traditional Chinese Medicine*, Academy Press, Beijing, China, 2002.
- [15] M. Kuhn, C. von Mering, M. Campillos, L. J. Jensen, and P. Bork, "STITCH: interaction networks of chemicals and proteins," *Nucleic Acids Research*, vol. 36, supplement 1, pp. D684–D688, 2008.
- [16] P. Shannon, A. Markiel, O. Ozier et al., "Cytoscape: a software Environment for integrated models of biomolecular interaction networks," *Genome Research*, vol. 13, no. 11, pp. 2498–2504, 2003.
- [17] F. Halperin, X. Lopez, R. Manning, C. R. Kahn, R. N. Kulkarni, and A. B. Goldfine, "Insulin augmentation of glucose-stimulated insulin secretion is impaired in insulin-resistant humans," *Diabetes*, vol. 61, no. 2, pp. 301–309, 2012.
- [18] M. Y. Donath, J. A. Ehses, K. Maedler et al., "Mechanisms of β -cell death in type 2 diabetes," *Diabetes*, vol. 54, supplement 2, pp. S108–S113, 2005.
- [19] M. S. Balasubashini, R. Rukkumani, and V. P. Menon, "Protective effects of ferulic acid on hyperlipidemic diabetic rats," *Acta Diabetologica*, vol. 40, no. 3, pp. 118–122, 2003.
- [20] T. Miura, N. Iwamoto, M. Kato et al., "The suppressive effect mangiferin with exercise on blood lipids in type 2 diabetes," *Biological and Pharmaceutical Bulletin*, vol. 24, no. 9, pp. 1091–1092, 2001.
- [21] C.-H. Chen, L. L. H. Huang, C.-C. Huang, C.-C. Lin, Y. Lee, and F.-J. Lu, "Baicalein, a novel apoptotic agent for hepatoma cell lines: a potential medicine for hepatoma," *Nutrition and Cancer*, vol. 38, no. 2, pp. 287–295, 2000.
- [22] J. Yin, R. Hu, M. Chen et al., "Effects of berberine on glucose metabolism in vitro," *Metabolism*, vol. 51, no. 11, pp. 1439–1443, 2002.
- [23] J. Yin, H. Xing, and J. Ye, "Efficacy of berberine in patients with type 2 diabetes mellitus," *Metabolism*, vol. 57, no. 5, pp. 712–717, 2008.
- [24] G. A. Xu, "Drug composition for treating 2 type diabetes and diabetic chronicity complications," US. publication no. 2009/0176816 A1.
- [25] J. Young, "Method of treating non-insulin dependent diabetes mellitus and related complications," US. publication no. 2005/0019435 A1.

Research Article

A Module Analysis Approach to Investigate Molecular Mechanism of TCM Formula: A Trial on Shu-feng-jie-du Formula

Jianglong Song,¹ Fangbo Zhang,² Shihuan Tang,² Xi Liu,¹ Yibo Gao,¹ Peng Lu,^{1,2} Yanping Wang,³ and Hongjun Yang²

¹ Institute of Automation, Chinese Academy of Sciences, Beijing 100190, China

² Institute of Chinese Materia Medica, China Academy of Chinese Medical Sciences, Beijing 100700, China

³ Institute of Basic Research in Clinical Medicine, China Academy of Chinese Medical Sciences, Dongzhimen, Beijing 100700, China

Correspondence should be addressed to Yanping Wang; wang4816@yahoo.com.cn and Hongjun Yang; hongjun0420@vip.sina.com

Received 12 September 2013; Revised 8 October 2013; Accepted 11 October 2013

Academic Editor: Aiping Lv

Copyright © 2013 Jianglong Song et al. This is an open access article distributed under the Creative Commons Attribution License, which permits unrestricted use, distribution, and reproduction in any medium, provided the original work is properly cited.

At the molecular level, it is acknowledged that a TCM formula is often a complex system, which challenges researchers to fully understand its underlying pharmacological action. However, module detection technique developed from complex network provides new insight into systematic investigation of the mode of action of a TCM formula from the molecule perspective. We here proposed a computational approach integrating the module detection technique into a 2-class heterogeneous network (2-HN) which models the complex pharmacological system of a TCM formula. This approach takes three steps: construction of a 2-HN, identification of primary pharmacological units, and pathway analysis. We employed this approach to study Shu-feng-jie-du (SHU) formula, which aimed at discovering its molecular mechanism in defending against influenza infection. Actually, four primary pharmacological units were identified from the 2-HN for SHU formula and further analysis revealed numbers of biological pathways modulated by the four pharmacological units. 24 out of 40 enriched pathways that were ranked in top 10 corresponding to each of the four pharmacological units were found to be involved in the process of influenza infection. Therefore, this approach is capable of uncovering the mode of action underlying a TCM formula via module analysis.

1. Introduction

With the development and evolution for thousands of years, Traditional Chinese Medicine (TCM) has become a sound and complete theory based on distinct principles and foundation from Western Medicine. TCM formulae, characterized by abundant ingredients and vast associated targets, are usually effective alternatives to western drugs for various multifactorial disorders [1]. Influenced by the decreased efficiency of new drug invention in recent years, the pattern of drug design has to evolve from traditional “one drug, one target” to “multicomponent, multitarget” drug discovery [2, 3]. As multicomponent agent with potential treatment effects, TCM formula holds great promise to promote the process of multitarget drug discovery based on molecular networks

[1, 4]. Thus, the investigation of molecular mechanism of TCM formula plays an important role for better understanding the essence of TCM therapies and multicomponent drug discovery.

Currently, network-based approaches become crucial in unveiling and interpreting the mode of action of a TCM formula, with the accumulation of volume “omics” data and the emerging of network pharmacology. So far, lots of researchers have made great effort to acquire and collect “omics” data through advanced in vivo and in vitro techniques [5–7]. Among various “omics” data, interaction knowledge such as compound-protein interaction (CPI) and protein-protein interaction (PPI), as well as Gene Ontology (GO) and pathway annotation, make it possible to describe and analyze complex TCM formula in a holistic manner by

using computational techniques. On the other hand, network pharmacology brought new insight into drug discovery once it was put forth [8]. The research interests of drug discovery extend from simple disease-drug-gene relations to some new spots such as promiscuity, synergistic effect, and functional modules [9–11]. Consequently, the focus in pharmacology research has shifted to the exploration of multicomponent multitarget drugs [3, 12]. In fact, plenty of work investigated the intrinsic regulating mechanism between many drugs and numerous targets or synergistic effects of drug combinations from a network perspective [13, 14]. Meanwhile, numerous network-based methods have been developed to decipher the pathological pattern underlying complex disorders and uncover the mode of action of TCM herbs or formulae [15, 16]. Moreover, network target was introduced as a new subject for studying the pharmacological action of TCM herbs rather than individual target or target set [17]. By using network-based techniques, several TCM formulae such as Liu-wei-di-huang have been particularly observed and studied in order to discover the underlying mode of action at the molecular level [18]. Therefore, it is essential to investigate the molecular mechanism of TCM formula using network-based methods, especially in TCM pharmacology research [1].

Notably, module analysis technique based on network model holds great promise to deal with most widely-used TCM formulae of unexpected complexity at the molecular level. In general, a TCM formula contains hundreds of chemical constituents and may associate with thousands of potential targets. It is a challenging task to identify the effective bioactive compounds or even discover the pharmacological action of numerous constituents of a TCM formula [1]. Thus, it is of great importance to capture the dominant modules of the molecular network representing a TCM formula. Two common types of dominant modules we are interested in are functional module and pharmacological unit. A functional module usually represents a group of genes or proteins sharing similar molecular functions, while a pharmacological unit is a connected subnetwork in which a set of compounds with similar physiochemical properties modulate the activities of a group of function-similar gene products. Typically, functional modules or pharmacological units within the molecular network usually hold some significant properties that are helpful in revealing the mode of action of TCM formula. In fact, numbers of researchers proposed diverse methods to detect functional modules from interaction networks [11, 19, 20]. On the contrary, there are few researches on identifying pharmacological units for multicomponent drugs [18]. On the other hand, network clustering algorithms, also known as module detection methods, developed from statistical physics are usually capable of finding significant communities enriched with explicit real-world meaning [21, 22]. As a matter of fact, several algorithms accomplished important tasks in biological field such as identifying protein complexes [23–25]. Additionally, to identify functional modules or pharmacological units is obviously another application of network clustering methods, which is crucial in the investigation of pharmacological action of TCM formula. Hence, applying classic module detection algorithms to the molecular network of TCM

formula may contribute to better understanding of its mode of action at the molecular level.

We here proposed a computational approach combining clustering algorithm with heterogeneous network to investigate the molecular mechanism of TCM formula. This approach takes a three-step procedure. At first, we constructed a 2-class heterogeneous network (2-HN) comprised of herbal ingredients and associated targets for a TCM formula under study. Then, a classic module detection algorithm was applied to the 2-HN and we identified pharmacological units from the 2-HN. Finally, we finely selected primary pharmacological units and investigated them by pathway analysis. This approach is apparently applicable for any TCM formula. In this paper, we use Shu-feng-jie-du formula (SHU formula) as an example to illustrate the procedure of the approach. The pathway analysis of four pharmacological units identified from the 2-HN for SHU formula showed that 24 out of 40 enriched pathways that were ranked in top 10 corresponding to each of the four pharmacological units were directly or indirectly involved in the process of influenza development.

2. Methods

The novel approach is aimed at discovering the molecular mechanism of TCM formula based on a heterogeneous network together with a clustering algorithm. The procedure of this approach mainly consists of three steps: the construction of a heterogeneous network, module detection from the network, and the pathway analysis of selected primary pharmacological units. In practice, we investigated the mode of action of Shu-feng-jie-du formula by using this approach.

2.1. Construct Heterogeneous Network. Since our approach takes advantage of the network to study a TCM formula, we should firstly construct a heterogeneous network comprised of herbal ingredients and potential targets. At the beginning, the specific composition of each herb in a given TCM formula must be acquired. Typical ways to collect the chemical ingredients of herbs include literature mining, TCM database retrieval, and identification test. By diverse means, we can collect the chemical constituents together with their geometric structure for all herbs in the TCM formula. Subsequently, the interaction data and potential targets could be computed and retrieved, respectively, based on the chemical knowledge for the studied TCM formula.

First of all, we acquire the interaction data between herbal compounds by computational chemistry techniques. Although various kinds of interaction knowledge is available, compound pairs with similar chemical structures are widely used in network-based pharmacology and drug discovery research. The rationale is a well-known assumption that similar compounds have similar properties [26]. In other words, similar chemicals may share common targets and are likely to perform synergistic action on complex diseases. Thus, we evaluate compound pairs by calculating the pairwise chemical similarity using the geometric structure previously curated. In the field of cheminformatics, various methods

were proposed to compute the structural similarity between compounds. Notably, fingerprint-based similarity is practically preferable to Maximum Common Subgraph (MCS) and other methods in dealing with a large number of compound pairs. We here employ Pybel, a Python wrapper for the Openbabel toolkit, to calculate fingerprint-based chemical similarity [27]. In the similarity measure, Tanimoto Coefficient is used to evaluate the commonness of fingerprints derived from two corresponding compounds as follows:

$$s_{TC}(c_1, c_2) = \frac{c}{a + b - c}, \quad (1)$$

where c_1 and c_2 are two compounds; a and b are bit lengths of c_1 and c_2 fingerprints, respectively; and c is the number of common bits between c_1 and c_2 fingerprints. In addition, a threshold θ is predefined to determine whether two compounds are similar in structure. Compound pairs are considered to be similar only if the pairwise similarity is equal to or greater than the threshold. In the end, similar compound pairs are collected as one of the sources for the construction of the heterogeneous network.

Next, we retrieve potential targets from some authentic databases according to the chemical constituents within the TCM formula under study. When retrieving a specific database such as DrugBank, CTD, and STITCH, we regard the gene products that interact with herbal compounds as potential targets. Note that only gene products of *homo sapiens* (human) will be taken into consideration. Once the initial set of potential targets is achieved, the potential targets should be carefully selected in order to avoid contingency. It is understood that “hub” targets usually associate with two or more chemicals due to the promiscuous property of potential target in pharmacological space [9, 13]. So we here define Promiscuity Index of a target simply by the number of chemicals interacting with that target. Similarly, the Promiscuity Index of a chemical can be measured by the number of its binding targets. A threshold δ is specified beforehand to eliminate peripheral targets curated for the TCM formula. Gene products with Promiscuity Index no less than δ are eventually selected into the target set for the TCM formula. Note that the threshold δ is a small integer but is greater than one, for instance, 2 or 3.

Then, we collect interaction relations between gene products in the target set from some authentic databases. Recent findings demonstrated that proteins always function in cooperation with others rather than in isolation inside or out of a cell [13]. That is, gene products tend to form functional modules to participate in certain biological processes or accomplish specific physiological functions. Lots of databases, such as HPRD, BioGrid, IntAct, and DIP, gather plenty of acknowledged protein-protein interactions (PPIs) across diverse species. We usually select one database as the source of PPI data due to the diverse reliability of PPIs in different databases. Therefore, the interactome knowledge is introduced to the heterogeneous network by retrieving PPIs between gene products in the target set.

Finally, we construct an integrated network on the basis of heterogeneous data acquired before. Since compounds and gene products are present in this integrated network

at the same time, we consider such a network as a 2-class heterogeneous network (2-HN). In brief, 2-class heterogeneous network (2-HN) is an abstract network model involving two distinct groups of objects. As a matter of fact, heterogeneous network, sometimes viewed as multilayer network, has been employed in recent work to study complex drug-target interactions and predict disease genes [18, 28, 29]. In our case, the 2-HN describes a complex pharmacological system relating the TCM formula under study to its treatable diseases. From a local point of view, the 2-HN can be divided into three subnetworks in chemical, pharmacological and genomic space in terms of three types of links in the 2-HN (Figure 1) [30]. In most cases, it is difficult to investigate and analyze the 2-HN for the TCM formula due to its complexity. Moreover, dense modules identified from the 2-HN may reveal some important pathways enriched in a subset rather than the whole set of genes related to the TCM formula. Therefore, to identify the pharmacological units from the 2-HN by module detection methods is always necessary to uncover the molecular mechanism of the TCM formula (Figure 1).

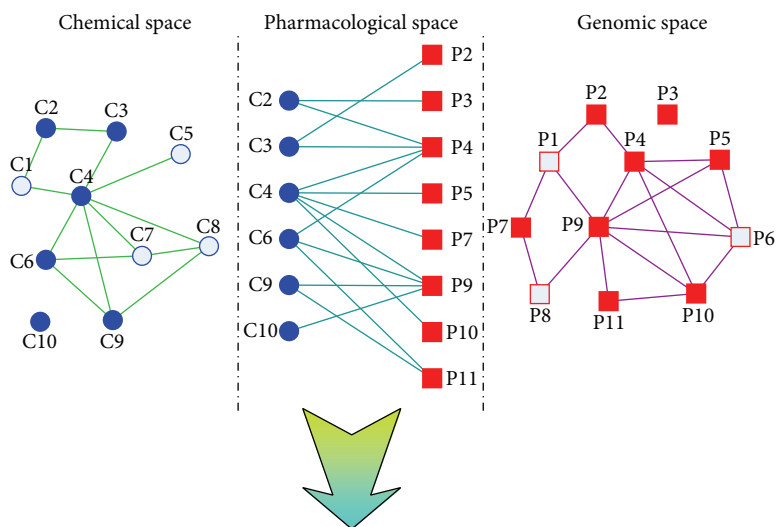
2.2. Detect Significant Modules. Since the complex network theory emerged, module detection has become one of the major techniques to promote the application and development of complex network. A great quantity of algorithms have been devised and implemented to find significant modules from connected networks [21–23]. Among various classic methods, a well-known method, Girvan-Newman algorithm, is capable to detect communities of a complex system and identify community structure [22]. Girvan-Newman algorithm is performed by iteratively removing edges with highest betweenness from the original network. In this way, the community structure could be viewed as a dendrogram. We employ clusterMaker, an implementation of Girvan-Newman algorithm in Cytoscape, to identify significant modules within the 2-HN for the TCM formula [31, 32].

After the clustering partition is detected from the network, we need a measure to quantify the significance of identified modules. Notably, modularity is an outstanding quality function measuring the goodness of network partition [33, 34]. Consequently, we use a measure similar to the definition of modularity to evaluate whether a module is significant or not in the original network. For an undirected simple graph, the modularity of a module C can be expressed as follows:

$$Q(C) = \frac{l_C}{m} - \left(\frac{d_C}{2m} \right)^2, \quad (2)$$

where $l_C = \sum_{ij \in C} w_{ij}$ is the summation of weights of edges in module C ; $d_C = \sum_{n \in C} \deg(n)$ is the summation of degrees of nodes in module C ; and $m = (1/2) \sum_{i,j \in G} w_{ij}$ is the size of the graph G . Obviously, a significant module corresponds to a modularity larger than zero. A “good” module always has a large modularity; otherwise, a small modularity indicates the “poor” significance of a network module. Moreover, according to the definition above,

(a) The 2-HN for TCM formula



(b) Pharmacological unit

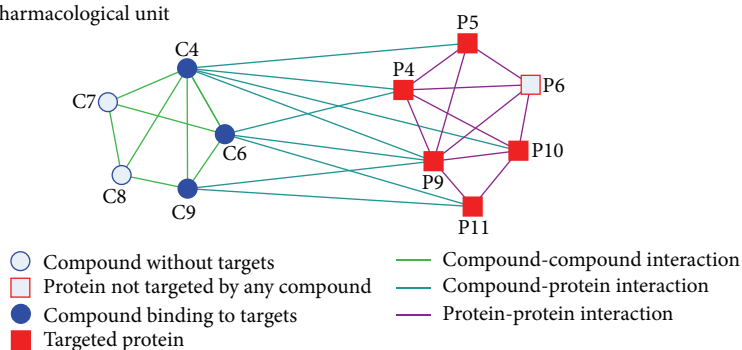


FIGURE 1: (a) A 2-class heterogeneous network (2-HN) modeling the complex system of a TCM formula and its molecular targets. A 2-HN can be simply divided into three subnetworks in chemical, pharmacological, and genomic space in terms of the type of links. (b) A pharmacological unit identified from the 2-HN in (a). A pharmacological unit includes a set of structure-similar herbal compounds and a group of function-similar target genes, indicating that the herbal compounds modulate the activities of gene products.

the modularity of a clustering partition of a given network is just the summation of modularities over all modules in the partition.

2.3. Analyze Pharmacological Units. The significant modules identified from the 2-HN of the TCM formula need to be examined before conducting further analysis. First, modules should be excluded if they are only comprised of compounds or gene products. Since compound-protein interactions (CPIs) relate herbal ingredients to potential targets, modules without any CPI make little contribution to uncover the pharmacological action of herbal compounds in the TCM formula. Second, modules with small modularity close to zero should be eliminated. Generally, a module may not be significant enough to be considered as a rational pharmacological unit for the TCM formula if it has a fairly small modularity. Third, modules should be paid less attention if the ratio of preserved compound-protein interactions is particularly low. The ratio of preserved CPIs is defined as the number of CPIs in a module divided by the total number of

CPIs in the 2-HN. The ratio for a module C can be expressed as

$$R(C) = \frac{|\{e_{cg} \mid c, g \in C\}|}{|\{e_{cg} \mid c, g \in G\}|}, \quad (3)$$

where c is a compound and g is a gene product; $|\cdot|$ is the norm of a set, that is, the number of elements in the set. If the ratio is low or few CPIs are present in a module, the module is unlikely to represent the primary interacting pattern that links herbal compounds and potential targets for the TCM formula under study. After these examinations, the remaining modules can be simply regarded as primary pharmacological units responsible for the studied TCM formula taking effect on complex diseases.

We investigate and analyze the primary pharmacological units by pathway analysis. Pathway analysis always play an essential role of discovering possible biological processes that the genes in the input list participate in. A lot of databases collect many curated pathways concerning metabolism, cellular processes, and diseases, such as KEGG, BioCarta, Reactome, GeneGo, and Ingenuity. Besides, Gene Ontology (GO),

another kind of pathways, usually reveals the physiological functions and cellular locations of a group of genes or gene products. Thus, pathway and GO supply us with sufficient knowledge about molecular regulation and gene function. Other analysis methods, for instance, disease analysis using gene overlapping and biomarkers, could provide new insight to understand the underlying functions of the TCM formula. In this paper, we use MetaDrug, a platform of systems pharmacology and toxicity, to perform pathway analysis for the identified primary pharmacological units [35]. Then, the molecular mechanism underlying the studied TCM formula could be uncovered through analyzing the enriched pathways or GO terms for primary pharmacological units.

To illustrate the workflow of the approach in detail, we apply the approach to an effective agent for influenza, Shu-feng-jie-du formula. Instead of Shufeng-jie-du formula, we use SHU formula for short in following sections. Following the procedure of the approach, we can investigate the mode of action underlying SHU formula.

3. Results and Discussion

3.1. 2-HN for SHU Formula. We firstly acquired the herb composition of SHU formula and collected chemical constituents within each herb. In fact, SHU formula mainly consists of 8 herbs: Bai-Jiang-Cao (Herba Patriniae), Ban-Lan-Gen (Radix Isatidis), Chai-Hu (Radix Bupleuri), Gan-Cao (Radix Glycyrrhizae), Hu-Zhang (Rhizoma Polygoni Cuspidati), Lian-Qiao (Fructus Forsythiae), Lu-Gen (Rhizoma Phragmitis), and Ma-Bian-Cao (Herba Verbenae) (Table 1). According to the herb composition, we collected 243 nonredundant chemical constituents for this formula. All constituents of SHU formula were retrieved from the Chemistry Database founded by Shanghai Institute of Organic Chemistry (<http://www.organchem.csdb.cn>). The 2D structures of herbal constituents were downloaded from PubChem Compound database according to unique CAS Registry Number. Then, we evaluated the similar compound pairs based on the fingerprint-based Tanimoto similarity. The threshold θ for similarity score was set to 0.7 as stated in [27]. In this way, 562 pairs of compounds were collected and considered to be similar because they had comparable structural similarities to the threshold. In the next step, we searched Comparative Toxicogenomics Database (CTD) for potential targets interacting with herbal ingredients in SHU formula [36]. The threshold δ for Promiscuity Index of potential targets was set to 3. Namely, we only selected gene products targeted by at least 3 herbal compounds, as well as the interactions between those proteins and chemicals. As a result, 238 potential targets were collected from CTD, which associated with herbal compounds by 1101 interactions. At last, we extracted acknowledged interactions between 238 gene products extracted before from BioGRID database [37]. There were 718 nonredundant PPIs between the curated potential targets. Based on these data, a 2-HN, an integrated network for SHU formula, was constructed. Since we focused on the largest connected component of the 2-HN for SHU

TABLE 1: Herb composition of Shu-feng-jie-du formula (SHU formula).

English translation	Pharmaceutical name	Simplified Chinese script
Hu-Zhang	Rhizoma Polygoni Cuspidati	虎杖
Lian-Qiao	Fructus Forsythiae	连翘
Ban-Lan-Gen	Radix Isatidis	板蓝根
Chai-Hu	Radix Bupleuri	柴胡
Bai-Jiang-Cao	Herba Patriniae	败酱草
Ma-Bian-Cao	Herba Verbenae	马鞭草
Lu-Gen	Rhizoma Phragmitis	芦根
Gan-Cao	Radix Glycyrrhizae	甘草

formula, the resultant network contained 171 herbal compounds and 238 potential targets after discarding small-size components (Table 2).

The 2-HN of SHU formula has some interesting properties in topology. As shown in Table 2, two groups of nodes in the 2-HN (rectangle for compounds and ellipse for gene products) are connected by three types of links. It is obvious that the pharmacological subnetwork is a bipartite, which is comprised of all CPIs (Table 2). So the 2-HN for SHU formula is beyond a bipartite by including compound interactions and PPIs (Table 2). The network heterogeneity decreases from 2.531 of the pharmacological subnetwork to 1.588 of the 2-HN for SHU formula. This is because compound interactions and PPIs bring many extra links to the “nonhub” chemicals and gene products, respectively [38]. In addition, the chemical subnetwork has 34 connected components of which 17 are isolated compounds (Table 2). Regardless of the isolated nodes, each of the remaining connected components has 9.059 compounds in average. That is, herbal compounds in SHU formula tend to form multiple components in terms of similar structure. As for the genomic subnetwork, there are 57 connected components, among which 55 are comprised of isolated proteins (Table 2). In fact, nearly all of the nonisolated proteins connect to a giant component with 181 nodes and 717 links in the genomic subnetwork. It suggests that the giant component determines the mode of action of SHU formula to a large extent. Different from the phenomenon in chemical subnetwork, target proteins of SHU formula tend to form a single large component instead of multiple components. Furthermore, only a small fraction (50 out of 171) of the involved herbal compounds (blue rectangles) take direct or indirect actions on the 238 gene products in the 2-HN (Table 2). Apart from the incompleteness of chemical-protein knowledge, we could see that only limited number of compounds have acknowledged therapeutic effects in SHU formula. Among these 50 compounds, there are several “hub” compounds associated with many targets, such as quercetin and resveratrol, which may exhibit high activities against influenza progression.

The “hub” compounds usually play an essential role to achieve the expected effect of SHU formula treating influenza. We listed four “hub” herbal compounds in Table 3 and investigated their pharmacological functions at the same time.

TABLE 2: Topological properties of the 2-HN for SHU formula and its three subnetworks.

Property		CSN	PSN	GSN	2-HN
Node	Compounds	171	50	0	171
	Proteins	0	238	238	238
Edge	CCIs	481	0	0	481
	CPIs	0	1101	0	1101
	PPIs	0	0	718	718
	Connected components	34	1	57	1
	Isolated nodes	17	0	55	0
	Clustering coefficient	0.662	0.0	0.198	0.414
	Network density	0.033	0.027	0.025	0.028
	Network heterogeneity	0.664	2.531	1.287	1.588

* CCI is short for compound-compound interaction, CPI is compound-protein interaction, and PPI is protein-protein interaction. CSN represents the chemical subnetwork of the 2-HN for SHU formula, PSN the pharmacological subnetwork, and GSN the genomic subnetwork.

* All the topological properties were calculated using Cytoscape 2.8 [32].

TABLE 3: “Hub” herbal compounds identified from the pharmacological subnetwork of the 2-HN for SHU formula.

Name	CAS RN	PubChem CID	PI	Action	Reference
Quercetin	117-39-5	5280343	222	(i) Quercetin and rutin exhibit prooxidant effect in healthy and antioxidant activity in influenza—infected animals.	[39]
				(ii) Quercetin and oseltamivir exhibited antiviral effect on the Toll-like receptor 7 (TLR7) signaling pathway when dendritic cells and macrophages were infected with H1N1.	[40]
Resveratrol	501-36-0	445154	218	Resveratrol inhibited the replication of influenza virus in MDCK cells.	[43]
Kaempferol	520-18-3	5280863	67	Kaempferol inhibited influenza A nucleoprotein production in human lung epithelial (A549) cells infected with the H5N1 virus strain A/Thailand/Kan-1/04 in non-toxic concentrations.	[44]
Eugenol	97-53-0	3314	61	Eugenol could inhibit autophagy and influenza A virus replication, inhibit the activation of ERK, p38MAPK and IKK/NF- κ B signal pathways.	[45]

* PI is Promiscuity Index of individual compound, that is, the number of binding targets in the 2-HN for SHU formula.

Two outstanding compounds are quercetin and resveratrol with far larger Promiscuity Index (222 and 218, resp.) than other compounds (the third largest is 67 for kaempferol). Previous works revealed the underlying functions of these four compounds in defending against influenza. For instance, quercetin could relieve the oxidative stress caused by experimental influenza virus infection in organisms like lungs and liver [39]. Another work demonstrated that quercetin together with oseltamivir exhibited antiviral effect on the Toll-like receptor 7 (TLR7) signaling pathway when dendritic cells and macrophages were infected with H1N1 [40]. Several quercetin derivatives such as quercetin-3-rhamnoside and isoquercetin also served as anti-influenza agents by inhibiting the replication of influenza virus [41, 42]. Additionally, resveratrol was found to inhibit the replication of influenza virus in MDCK cells, which involved the blockade of the nuclear-cytoplasmic translocation of viral ribonucleoproteins [43]. Moreover, kaempferol could inhibit the influenza A nucleoprotein production in human lung epithelial cells infected by the H5N1 virus [44] and eugenol could inhibit autophagy and influenza A virus replication by suppressing

the activation of ERK, p38MAPK, and IKK/NF- κ B signal pathways [45]. Therefore, these four “hub” herbal compounds, characterized by large Promiscuity Index, indeed take effect to defend against influenza.

Although the general effect of SHU formula could be observed by studying the “hub” herbal compounds in the 2-HN, we still needed module analysis to further investigate the biological pathways that SHU formula actually influences and regulates. We firstly identified primary pharmacological units from the 2-HN for SHU formula and then investigated the particular mode of action of SHU formula treating influenza.

3.2. Pharmacological Units from the 2-HN. Through detecting modules using Girvan-Newman algorithm, 12 significant modules were identified from the 2-HN for SHU formula. However, not all the modules are fairly important and need to be analyzed in detail. We selected primary pharmacological units from the 12 modules according to three principles explained before. As shown in Table 4, module 11 is only comprised of compounds and thus excluded because it is

TABLE 4: Metrics of detected modules from the 2-HN for SHU formula.

Module	Compounds	Proteins	Valid	Modularity	Ratio of preserved CPIs
1	20	121	Yes	0.121375	0.257039
2	37	58	Yes	0.075361	0.15168
3	31	2	Yes	0.040522	0.003633
4	3	30	Yes	0.037876	0.023615
5	17	14	Yes	0.021214	0.014532
6	19	1	Yes	0.030336	0.001817
7	12	4	Yes	0.014417	0.003633
8	9	5	Yes	0.013261	0.004541
9	11	1	Yes	0.009457	0.000908
10	7	1	Yes	0.006564	0.000908
11	3	0	No	0.001104	0.0
12	2	1	Yes	0.000873	0.000908

not a valid pharmacological unit (including compounds and gene products). We chose 0.02 as the threshold for modularity and consequently five more modules, 7, 8, 9, 10, and 12, were discarded due to the low significance in the original network. The threshold for the ratio of preserved CPIs was set to 0.01 and another two modules, 3 and 6, were eliminated as they included too few CPIs. In the end, four modules, 1, 2, 4, and 5, were selected and considered as primary pharmacological units. From the topological perspective, modules 1, 2, 4, and 5 are highly connected in the background network of the 2-HN characterized by relatively large modularities. Besides, these four pharmacological units are of great importance to represent the pharmacological essence of SHU formula due to the large amount of preserved CPIs from the original system. So we made great effort to investigate these four pharmacological units by pathway analysis.

We analyzed the underlying biology by performing enrichment analysis with pathways from GeneGo database. For each primary pharmacological unit, we employed the genes within the module as input gene list to search for enriched pathways in GeneGo database. The top 10 enriched pathways corresponding to each module were illustrated in Figure 2. The pathways were sorted according to the *P* value which measured the significance of a given pathway enriched in the gene list of a pharmacological unit. The bioactive compounds in every pharmacological unit potentially acting on the enriched pathways were also highlighted in Figure 2. The associated herbal compounds were ranked by Promiscuity Index, which was defined as the number of targets connected to a given compound by the preserved CPIs in an identified module (Materials and Methods). From the viewpoint of pathway category, the bioactive compounds in every primary pharmacological unit seemed to particularly interfere with pathways from one or two specific categories. For example, compounds in module 1 generally participate in the processes of cell cycle (4 pathways) and development (4 pathways); the highly enriched pathways of module 2 exhibit high relevance to metabolism (9 pathways), especially the estradiol metabolism (3 pathways); module 4 mostly influence the biological processes related to apoptosis and survival (10 pathways); and module 5 interfere in the activities

of cell adhesion (4 pathways) and cytoskeleton remodeling (3 pathways) as well as immune response (3 pathways). Despite of the redundancy of GeneGo pathways, we could see that each of the four pharmacological units tends to regulate relevant pathways from specific categories, which implies that SHU formula carries out pharmacological efficacy by simultaneously intervening pathological activities from distinct aspects at the pathway level. Since the module analysis approach was applied to SHU formula generated explicit results as exhibited in Figure 2, we should verify the reliability of the prediction and evaluate the relevance of SHU formula to influenza infection.

According to Figure 2, we could find that compounds in all four pharmacological units had potential effects on influenza infection. At first, 40 enriched pathways in Figure 2 were regulated to some extent by corresponding herbal compounds in each module, which can be explained by the acknowledged regulatory relations between compounds and pathway components from CTD. For example, resveratrol influences the EGFR signaling pathway through binding to EGFR protein and thus decreasing the phosphorylation of EGFR protein [46]. However, since not all enriched pathways were involved in the activities of influenza infection, we particularly focused on those related to influenza progression and the regulatory relations between SHU formula and those pathways. As shown in Table 5, 24 of the 40 enriched pathways were found to directly or indirectly participate in the processes of influenza virus invasion, production, proliferation, and transition, and to account for the influenza-induced syndromes as well, such as inflammation. Here we primarily studied the specific action of herbal compounds in each pharmacological unit on 24 influenza-related pathways, while the participation of these pathways in the progression of influenza would be analyzed in following section. For module 1, resveratrol together with other compounds blocked the G1/S-phase transition [47], inhibited the EGFR/HER2 signaling pathway [46], and regulated the PTEN/AKT pathway [46]. Quercetin and kaempferol together with other bioactive compounds in module 2 showed inhibitory effect on the *in vitro* hepatic metabolism of 17 β -estradiol [48] and on the hydroxylation of benzo[a]pyrene [49]. Additionally,

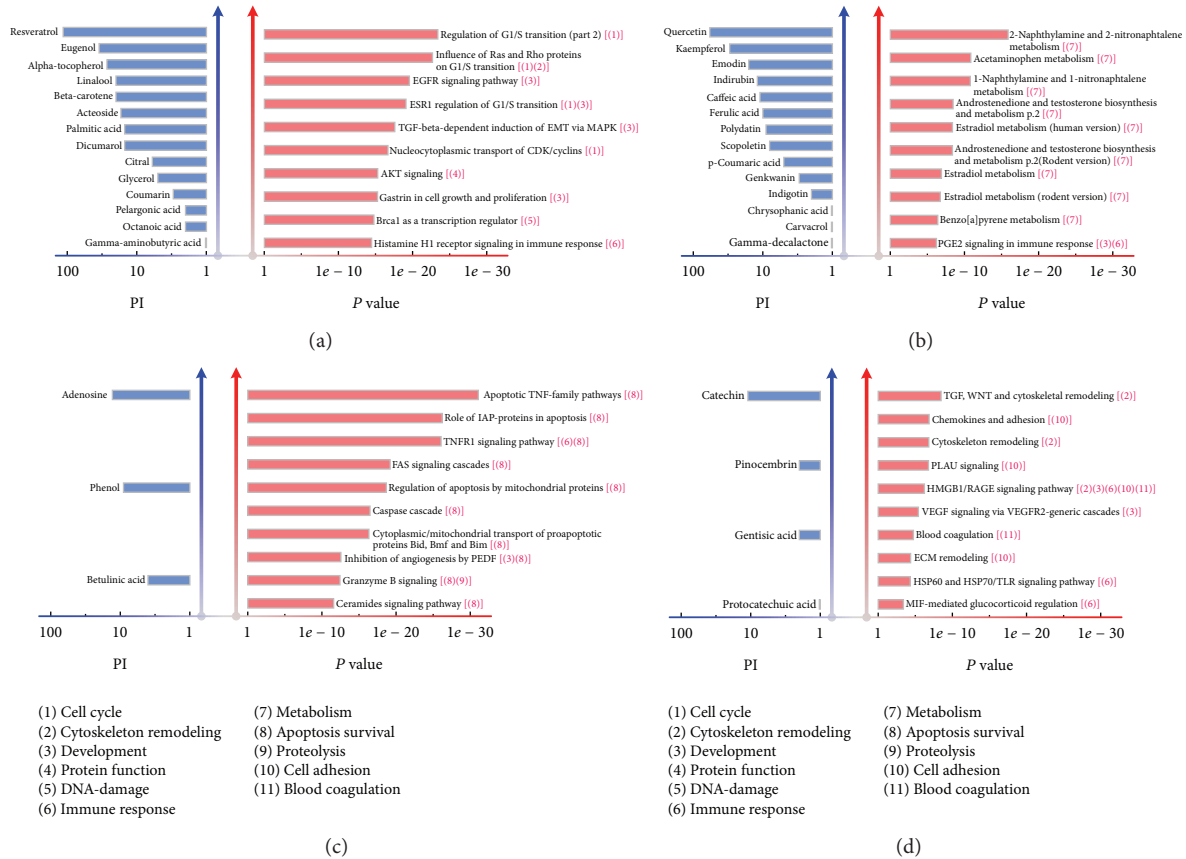


FIGURE 2: (a), (b), (c), and (d) Top 10 enriched pathways and associated herbal compounds corresponding to module 1, 2, 4, and 5, respectively. The herbal compounds are ranked by Promiscuity Index (PI), which is defined as the number of targets connected to a given compound by the preserved CPIs in a detected module. Note that only compounds with PI greater than zero are listed in this figure. The enriched pathways are ranked by the P values calculated in MetaDrug. The circled numbers in brackets after pathway name indicate the major category that pathway belongs to. For example, “ESR1 regulation of G1/S transition” belongs to category 1 and 3, that is, cell cycle and development. The category knowledge is curated from the classification tree of GeneGo pathways in MetaDrug. All pathways in this figure are significant with P values lower than 0.001.

quercetin also suppressed COX-2 expression and PGE2 production [50]. Herbal compounds in module 4 such as adenosine, phenol, and betulinic acid tended to inhibit IL-12 and TNF- α production [51], downregulate the expression of IAP2 [52], and trigger CD95 (APO-1/Fas)- and p53-independent apoptosis [53]. Compounds in module 5 like catechin could inhibit the endotoxin-induced HMGB1 release [54] and block the TLR signaling pathway [55]. Moreover, the remaining 16 pathways were also likely to correlate with influenza infection, although there has been no literature support for those pathways so far. In brief, 24 influenza-related pathways elucidated the potential effects of SHU formula against influenza infection from diverse aspects at the pathway level.

Moreover, by exploring the development of influenza, we could explicitly see how the enriched pathways modulated by bioactive components in SHU formula led human physiological system to a serious disease state. These pathways either promoted the production and replication of viral RNAs or proteins or induced host immune response and inflammation. The participation of these pathways in the pathological process of influenza infection, discussed in

the next section, explained how SHU formula treated against influenza infection by intervening various pathways in different stages and cellular locations.

3.3. SHU Formula Treating Influenza. When Influenza A virus (H1N1) enters host cells, it induces host cell cycle arrest in G(0)/G(1) phase and creates favorable conditions for viral replication. The nonstructural protein 1 (NS1) of influenza A virus induces G(0)/G(1) cell cycle arrest mainly through interfering with the RhoA/pRb signaling pathway, thus providing beneficial conditions for viral protein replication and accumulation [56]. The concentration and activity of RhoA protein is pivotal for G(1)/S phase transition, which were decreased with overexpressing NS1 [56]. When viral macromolecules interact with host proteins. High-mobility-group box (HMGB) proteins bind to the nucleoprotein (NP) component of viral ribonucleoproteins (vRNPs) in the absence of viral RNA, and HMGB1 protein plays a significant role in intranuclear replication of influenza viruses [74]. PI3K/Akt signaling pathway is activated by NS1 protein and inhibition of the PI3K/Akt pathway is an anti-influenza

TABLE 5: Literature-verified pathways related to influenza infection corresponding to four pharmacological units.

Module	Enriched pathways	<i>P</i> -value	Rank	Reference
1	Regulation of G1/S transition (part 2)	$4.137e - 24$	1	[56]
	Influence of Ras and Rho proteins on G1/S Transition	$2.156e - 23$	2	
	EGFR signaling pathway	$2.803e - 20$	3	[57]
	TGF-beta-dependent induction of EMT via MAPK	$2.603e - 18$	5	[58]
	AKT signaling	$5.258e - 16$	7	[59]
	Brcal as a transcription regulator	$1.710e - 15$	9	[60]
	Histamine H1 receptor signaling in immune response	$3.503e - 15$	10	[61]
2	Estradiol metabolism (human version)	$4.213e - 9$	5	[62]
	Estradiol metabolism	$1.293e - 7$	7	
	Estradiol metabolism (rodent version)	$1.832e - 7$	8	[63]
	Benzo[a]pyrene metabolism	$4.024e - 7$	9	
	PGE2 signaling in immune response	$6.146e - 7$	10	
4	Apoptotic TNF-family pathways	$8.253e - 32$	1	[65]
	Role of IAP-proteins in apoptosis	$6.132e - 27$	2	[66]
	FAS signaling cascades	$6.374e - 20$	4	[67]
	Inhibition of angiogenesis by PEDF	$2.792e - 13$	8	[68]
	Granzyme B signaling	$3.712e - 13$	9	[69]
	Ceramides signaling pathway	$2.652e - 12$	10	[70]
5	TGF, WNT, and cytoskeletal remodeling	$3.303e - 9$	1	[71]
	Chemokines and adhesion	$1.360e - 7$	2	[72]
	Cytoskeleton remodeling	$1.502e - 7$	3	[73]
	HMGB1/RAGE signaling pathway	$5.901e - 7$	5	[74]
	HSP60 and HSP70/TLR signaling pathway	$4.805e - 5$	9	[75]
	MIF-mediated glucocorticoid regulation	$3.981e - 4$	10	[76]

*The rank is the order of ascending *P* values of enriched pathways corresponding to each primary pharmacological unit.

strategy which is still in an early phase of preclinical development [59]. In addition, influenza virus infection activates three distinct MAPKs, ERK, p38 MAPK, and JNK, to participate to various extents in the induction of PGE2 synthesis from arachidonic acid in human bronchial epithelial cells [64]. Metabolized benzo[a]pyrene (BaP) reduced viral IFN induction by approximately 80% assessed in LLC-MK2 cell [63].

Airway epithelium play an important role in host immune response. Many diverse viruses target a polarized epithelial monolayer during host invasion. The polarized epithelium restrict the movement of pathogens across the mucosa. This regulation can be attributed to the presence of a junctional complex between adjacent cells and to an intricate network of actin filaments [73]. Virus-infected alveolar epithelium regulate CCL2/CCR2-dependent monocyte transepithelial migration dependent on both classical beta(1) and beta(2) integrins but also junctional adhesion molecule pathways during influenza infection [72]. The epithelial response to inhaled pathogens in airway epithelium that deposit on the airway epithelial surface includes EGFR signaling cascades [57].

Influenza virus invasion is associated with host immunity and inflammation. Inflammatory cytokines such as TNF- α , IFN- γ , and ET-1 may trigger the occurrence of AMI [65]. Toll-like receptors (TLRs) play an important role in early, innate viral inhibition in naturally occurring influenza

with inflammatory cytokine responses [75]. Histamine mediates the acute inflammatory and immediate hypersensitivity responses, and it has also been demonstrated to affect chronic inflammation and regulate several essential events in the immune response [61]. Type V collagen [col(V)] overexpression and IL-17-mediated anti-col(V) immunity are key contributors to obliterative bronchiolitis pathogenesis. IL-17 is shown to induce EMT, TGF- β mRNA expression, and SMAD3 activation, whereas downregulating SMAD7 expression in vitro [58]. Macrophage migration inhibitory factor (MIF) is involved in inflammatory responses to H5N1 influenza virus infections by induction of pulmonary inflammatory cytokines and chemokines [76]. BRCA1 regulates inflammation-induced endothelial cell function and limits endothelial cell apoptosis and dysfunction [60]. Pigment epithelial-derived factor (PEDF) suppresses inflammation by inhibiting lipopolysaccharide-driven macrophage activation in vitro and in vivo [68]. GzmB deficiency associated with pathology, morbidity, and mortality results in exacerbation of lymphocytic inflammation during bleomycin-induced acute lung injury [69]. Ceramide is the core of sphingolipid metabolism, and phosphorylation of ceramide by ceramide kinase gives rise to ceramide-1-phosphate which has also been shown to participate in inflammation [70].

Besides immune responses in host defence, influenza A virus infection induces endoplasmic reticulum stress, Fas-dependent apoptosis, and TGF- β production in a variety of

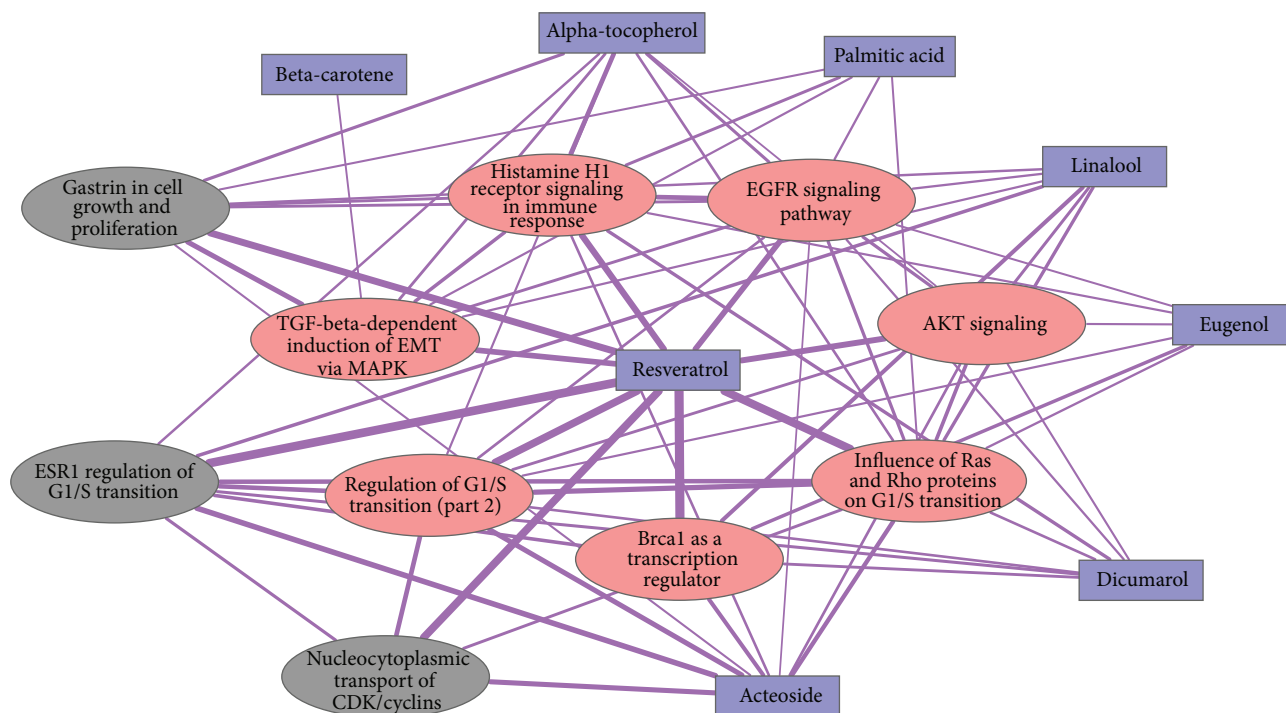


FIGURE 3: An illustration of SHU formula intervening the influenza development through multiple pathways. The blue rectangle is bioactive herbal compounds derived from SHU formula. The ellipse represents biological pathways that the compounds modulate. The red ones are literature-verified pathways that participate in the process of influenza infection, while the gray ones are not verified yet. A thick edge indicates many common hits (pathway components that are also associated targets of herbal compounds) between two pathways or between a compound and a pathway.

cells [71]. Inhibitor of apoptosis proteins (IAPs) influence ubiquitin-dependent pathways that modulate innate immune signaling via activation of nuclear factor κ B (NF- κ B) [66]. Multiple influenza virus factors have been identified that can activate intrinsic or extrinsic apoptotic induction pathways. dsRNA, NS1, NA, and PB1-F2 are influenza virus inducers of apoptosis. dsRNA and NA act via an extrinsic mechanism involving proapoptotic host-defense molecules: PKR by induction of Fas-Fas ligand and NA by activation of TGF- β . PB1-F2 act intrinsically by localization and interaction with the mitochondrial-dependent apoptotic pathway [67].

The symptoms of influenza virus infection are related to gender. Females suffer a worse outcome from influenza A virus infection than males, which can be reversed by administration of estradiol to females and reflects differences in the induction of proinflammatory responses [62].

3.4. Discussion. According to the results of pathway analysis, we built a simple network to illustrate the pharmacological action of SHU formula against influenza infection (Figure 3). This network was constructed based on module 1 identified by Girvan-Newman algorithm from the 2-HN of SHU formula. The edge connecting a compound and a pathway indicates the cooccurrence of associated targets of the compound and pathway components, while the edge between two pathways represents the commonness of hits (pathway components that are also associated targets of herbal compounds) corresponding to both pathways. As shown in Figure 3, 8

bioactive compounds of module 1 modulate 10 enriched pathways related to influenza infection. From the perspective of topology, resveratrol is the most important to regulate the involved pathways compared to other compounds. It is obvious that resveratrol is connected to all 10 pathways through strong links, indicating that resveratrol mediates multiple gene products in these pathways. Besides, resveratrol is found to modulate the G1/S-phase transition (P value $4.1e-24$) [47], the EGFR/HER2 signaling pathway (P value $2.8e-20$) [46], and the PTEN/AKT pathway (P value $5.3e-16$) [46]. Other compounds like Acteoside also perform similar functions on the involved pathways [77]. Of the top 10 enriched pathways, 7 (red ellipse) are found to participate in the development of influenza and its induced symptoms, illustrated in Table 5. Thus, the herbal compounds in Figure 3 are likely to intervene in the invasion, production, proliferation, and transition of influenza virus, through mediating multiple relevant pathways. Three pathways (grey ellipse) regulated by the compounds in Figure 3 hold great promise to influence the influenza development, while such prediction needs further work to test and verify.

In this paper, we presented a computational approach based on module analysis to investigate the molecular mechanism of TCM formula. This approach has several advantages. On one hand, we employed a precise model, 2-class heterogeneous network (2-HN), to represent the pharmacological system of a TCM formula. Since a 2-HN is structurally more complete than a bipartite by incorporating interactions

within the same categories, so additional information is integrated into such a comprehensive model. In case of the 2-HN for SHU formula, besides the regulatory relations between chemicals and gene products, similar compounds within SHU formula and interactions between gene products are also taken into consideration when studying the mode of action of SHU formula. This additional information represented by compound-compound interactions (CCIs) and PPIs is critical to systematic investigation of multicomponent drugs, while traditional methods always disregard knowledge like this or use it separately [15]. On the other hand, the approach presented in this paper takes advantage of module detection technique to uncover the molecular mechanism of a TCM formula. Different from conventional methods, we analyze small-size yet topologically significant pharmacological units rather than the whole drug-target system of unexpected complexity. Generally, the pharmacological units identified by module detection methods are more reliable in topology than the original system. This is because the pharmacological units are significantly components in the original network featured by dense intraconnections. So a 2-HN together with module detection technique could deal with the challenging task of discovering the molecular mechanism of a TCM formula from its pharmacological system with hundreds of herbal compounds and thousands of targets, as well as unpredictable amount of interactions.

Although the approach provides new insight into molecular mechanism of TCM formula, it can be improved in three aspects. First, the compound interaction is not limited to structurally similar compound pair. The derivative or isometric relation, similarity in physicochemical property, and ontology similarity between compounds may outperform structural similarity to some extent. Second, the module detection methods could be improved in order to (i) identify modules with overlapping nodes and edges and (ii) take into account the differences of interactions in a 2-HN. Generally, a compound may have diverse therapeutic functions and a gene may participate in diverse biological processes. In other words, a node should be assigned to two or more modules representing diverse functions or processes. So overlapping modules detected from a 2-HN may be more consistent with reality. In addition, CPIs in a 2-HN should be paid more attention than CCIs and PPIs when detecting pharmacological units. This is because CPIs are indispensable in a pharmacological unit that is a connected subnetwork containing compounds and gene products. Third, we could adopt improved pathway analysis to uncover the biology underlying identified pharmacological units. As elaborated in [78], pathway enrichment analysis has two inevitable shortcomings. It treats every gene equally when finding pathways enriched in the input gene list. Besides, it does not take the pathway dependence into account, which results in three “Estradiol metabolism” pathways enriched in module 2 gene list (Figure 2). So precise pathway techniques are in need to find rational and reliable pathways underlying each primary pharmacological units from the 2-HN for a given TCM formula. With these improvements, the module analysis-based approach will be more capable of uncovering explicit molecular mechanism of TCM formula.

4. Conclusion

We here propose a computational approach based on module analysis to investigate the molecular mechanism underlying TCM formula. The approach incorporates the module detection technique with a 2-class heterogeneous network, a precise model to depict the complex system of a TCM formula. This approach mainly consists of three steps: network construction, module detection, and pathway analysis. The application of this approach to Shu-feng-jie-du formula outputs good results, which identified four primary pharmacological units uncovering key herbal compounds and essential pathways they modulated. 24 out of 40 enriched pathways that were ranked in top 10 corresponding to each of the four pharmacological units were found to be relevant to the process of influenza infection and some induced symptoms like inflammation. This demonstrates the effectiveness of our approach in discovering the molecular mechanism of a TCM formula. Although effective, this approach still requires improvement with regard to chemical similarity, module detection algorithm and accurate pathway analysis of identified modules. After all, our approach provides new insight into discovering the molecular basis of TCM formula and further promotes the large-scale exploration of the pharmacological action of multicomponent drugs in a low-cost manner, especially TCM formulae.

Conflict of Interests

The authors declare that they do not have a direct financial relation with any commercial identity including the one mentioned in the paper. None of the authors have a conflict of interests to declare.

Authors' Contribution

Jianglong Song, Fangbo Zhang, and Shihuan Tang contributed equally to this work.

Acknowledgments

This work was supported by the Special Research Foundation for Traditional Chinese Medicine (Grant no. 200907001-5), the National Science Foundation for Post-doctoral Scientists of China (Grant no. 2012M510733), and the National Science Foundation of China (Grant no. 81303152).

References

- [1] J. Zhao, P. Jiang, and W. Zhang, “Molecular networks for the study of TCM pharmacology,” *Briefings in Bioinformatics*, vol. 11, no. 4, Article ID bbp063, pp. 417–430, 2009.
- [2] F. Sams-Dodd, “Target-based drug discovery: is something wrong?” *Drug Discovery Today*, vol. 10, no. 2, pp. 139–147, 2005.
- [3] G. R. Zimmermann, J. Lehár, and C. T. Keith, “Multi-target therapeutics: when the whole is greater than the sum of the parts,” *Drug Discovery Today*, vol. 12, no. 1-2, pp. 34–42, 2007.
- [4] E. L. Leung, Z. W. Cao, Z. H. Jiang, H. Zhou, and L. Liu, “Network-based drug discovery by integrating systems biology and

- computational technologies,” *Briefings in Bioinformatics*, vol. 14, no. 4, pp. 491–505, 2013.
- [5] M. Ashburner, C. A. Ball, J. A. Blake et al., “Gene ontology: tool for the unification of biology,” *Nature Genetics*, vol. 25, no. 1, pp. 25–29, 2000.
 - [6] C. Knox, V. Law, T. Jewison et al., “Drugbank 3.0: a comprehensive resource for “Omics” research on drugs,” *Nucleic Acids Research*, vol. 39, no. 1, pp. D1035–D1041, 2011.
 - [7] L. Salwinski, C. S. Miller, A. J. Smith, F. K. Pettit, J. U. Bowie, and D. Eisenberg, “The database of interacting proteins: 2004 update,” *Nucleic Acids Research*, vol. 32, pp. D449–D451, 2004.
 - [8] A. L. Hopkins, “Network pharmacology: the next paradigm in drug discovery,” *Nature Chemical Biology*, vol. 4, no. 11, pp. 682–690, 2008.
 - [9] G. V. Paolini, R. H. B. Shapland, W. P. van Hoorn, J. S. Mason, and A. L. Hopkins, “Global mapping of pharmacological space,” *Nature Biotechnology*, vol. 24, no. 7, pp. 805–815, 2006.
 - [10] M. Cokol, H. N. Chua, M. Tasan et al., “Systematic exploration of synergistic drug pairs,” *Molecular Systems Biology*, vol. 7, article 544, 2011.
 - [11] S. Suthram, J. T. Dudley, A. P. Chiang, R. Chen, T. J. Hastie, and A. J. Butte, “Network-based elucidation of human disease similarities reveals common functional modules enriched for pluripotent drug targets,” *PLoS Computational Biology*, vol. 6, no. 2, Article ID e1000662, 2010.
 - [12] J. J. Lu, W. Pan, Y. J. Hu, and Y. T. Wang, “Multi-target drugs: the trend of drug research and development,” *PLoS ONE*, vol. 7, no. 6, Article ID e40262, 2012.
 - [13] M. A. Yildirim, K. I. Goh, M. E. Cusick, A. L. Barabasi, and M. Vidal, “Drug—target network,” *Nature Biotechnology*, vol. 25, pp. 1119–1126, 2007.
 - [14] J. Jia, F. Zhu, X. Ma, Z. W. Cao, Y. X. Li, and Y. Z. Chen, “Mechanisms of drug combinations: interaction and network perspectives,” *Nature Reviews Drug Discovery*, vol. 8, no. 2, pp. 111–128, 2009.
 - [15] Y. Sun, R. Zhu, H. Ye et al., “Towards a bioinformatics analysis of anti-alzheimer’s herbal medicines from a target network perspective,” *Briefings in Bioinformatics*, vol. 14, no. 3, pp. 327–343, 2013.
 - [16] L. Wang, G.-B. Zhou, P. Liu et al., “Dissection of mechanisms of Chinese medicinal formula realgar-indigo naturalis as an effective treatment for promyelocytic leukemia,” *Proceedings of the National Academy of Sciences of the United States of America*, vol. 105, no. 12, pp. 4826–4831, 2008.
 - [17] S. Li, B. Zhang, and N. Zhang, “Network target for screening synergistic drug combinations with application to traditional Chinese medicine,” *BMC Systems Biology*, vol. 5, no. 1, article S10, 2011.
 - [18] S. Li, B. Zhang, D. Jiang, Y. Wei, and N. Zhang, “Herb network construction and co-module analysis for uncovering the combination rule of traditional Chinese herbal formulae,” *BMC Bioinformatics*, vol. 11, no. 11, article S6, 2010.
 - [19] S. G. A. Konietzny, L. Dietz, and A. C. McHardy, “Inferring functional modules of protein families with probabilistic topic models,” *BMC Bioinformatics*, vol. 12, article 141, 2011.
 - [20] M. T. Dittrich, G. W. Klau, A. Rosenwald, T. Dandekar, and T. Müller, “Identifying functional modules in protein-protein interaction networks: an integrated exact approach,” *Bioinformatics*, vol. 24, no. 13, pp. i223–i231, 2008.
 - [21] S. Fortunato, “Community detection in graphs,” *Physics Reports*, vol. 486, no. 3–5, pp. 75–174, 2010.
 - [22] M. Girvan and M. E. J. Newman, “Community structure in social and biological networks,” *Proceedings of the National Academy of Sciences of the United States of America*, vol. 99, no. 12, pp. 7821–7826, 2002.
 - [23] G. Palla, I. Derényi, I. Farkas, and T. Vicsek, “Uncovering the overlapping community structure of complex networks in nature and society,” *Nature*, vol. 435, no. 7043, pp. 814–818, 2005.
 - [24] A. J. Enright, S. van Dongen, and C. A. Ouzounis, “An efficient algorithm for large-scale detection of protein families,” *Nucleic Acids Research*, vol. 30, no. 7, pp. 1575–1584, 2002.
 - [25] P. Jiang and M. Singh, “SPICi: a fast clustering algorithm for large biological networks,” *Bioinformatics*, vol. 26, no. 8, Article ID btq078, pp. 1105–1111, 2010.
 - [26] M. Johnson and G. Maggiora, *Concepts and Applications of Molecular Similarity*, Wiley-Interscience, 1990.
 - [27] N. M. O’Boyle, C. Morley, and G. R. Hutchison, “Pybel: a python wrapper for the ppenbabel cheminformatics toolkit,” *Chemistry Central Journal*, vol. 2, no. 1, article 5, 2008.
 - [28] X. Wu, R. Jiang, M. Q. Zhang, and S. Li, “Network-based global inference of human disease genes,” *Molecular Biology of Disease*, vol. 4, article 189, 2008.
 - [29] S. Zhao and S. Li, “Network-based relating pharmacological and genomic spaces for drug target identification,” *PLoS ONE*, vol. 5, no. 7, Article ID e11764, 2010.
 - [30] Y. Yamanishi, M. Araki, A. Gutteridge, W. Honda, and M. Kanehisa, “Prediction of drug-target interaction networks from the integration of chemical and genomic spaces,” *Bioinformatics*, vol. 24, no. 13, pp. i232–i240, 2008.
 - [31] J. H. Morris, L. Apeltsin, A. M. Newman et al., “Clustermaker: a multi-algorithm clustering plugin for cytoscape,” *BMC Bioinformatics*, vol. 12, article 436, 2011.
 - [32] M. E. Smoot, K. Ono, J. Ruscheinski, P.-L. Wang, and T. Ideker, “Cytoscape 2.8: new features for data integration and network visualization,” *Bioinformatics*, vol. 27, no. 3, Article ID btq675, pp. 431–432, 2011.
 - [33] M. E. J. Newman and M. Girvan, “Finding and evaluating community structure in networks,” *Physical Review E*, vol. 69, no. 2, Article ID 026113, 15 pages, 2004.
 - [34] M. E. J. Newman, “Modularity and community structure in networks,” *Proceedings of the National Academy of Sciences of the United States of America*, vol. 103, no. 23, pp. 8577–8582, 2006.
 - [35] S. Ekins, A. Bugrim, L. Brovold et al., “Algorithms for network analysis in systems-ADME/Tox using the metacore and metadrag platforms,” *Xenobiotica*, vol. 36, no. 10–11, pp. 877–901, 2006.
 - [36] A. P. Davis, T. C. Wieggers, R. J. Johnson et al., “Text mining effectively scores and ranks the literature for improving chemical-gene-disease curation at the comparative toxicogenomics database,” *PLoS ONE*, vol. 8, no. 4, Article ID e58201, 2013.
 - [37] A. Chatr-aryamontri, B. J. Breitkreutz, S. Heinicke et al., “The BioGRID interaction database: 2013 update,” *Nucleic Acids Research*, vol. 41, pp. D816–D823, 2013.
 - [38] J. Dong and S. Horvath, “Understanding network concepts in modules,” *BMC Systems Biology*, vol. 1, article 24, 2007.
 - [39] V. M. Savov, A. S. Galabov, L. P. Tantcheva et al., “Effects of rutin and quercetin on monoxygenase activities in experimental influenza virus infection,” *Experimental and Toxicologic Pathology*, vol. 58, no. 1, pp. 59–64, 2006.
 - [40] C. Chen, Z. Y. Jiang, B. Yu et al., “Study on the anti-h1n1 virus effects of quercetin and oseltamivir and their mechanism related

- to tlr7 pathway,” *Journal of Asian Natural Products Research*, vol. 14, no. 9, pp. 877–885, 2012.
- [41] H. J. Choi, J. H. Song, K. S. Park, and D. H. Kwon, “Inhibitory effects of quercetin 3-rhamnoside on influenza A virus replication,” *European Journal of Pharmaceutical Sciences*, vol. 37, no. 3–4, pp. 329–333, 2009.
- [42] Y. Kim, S. Narayanan, and K.-O. Chang, “Inhibition of influenza virus replication by plant-derived isoquercetin,” *Antiviral Research*, vol. 88, no. 2, pp. 227–235, 2010.
- [43] A. T. Palamara, L. Nencioni, K. Aquilano et al., “Inhibition of influenza A virus replication by resveratrol,” *Journal of Infectious Diseases*, vol. 191, no. 10, pp. 1719–1729, 2005.
- [44] P. Sithisarn, M. Michaelis, M. Schubert-Zsilavec, and J. Cinatl Jr., “Differential antiviral and anti-inflammatory mechanisms of the flavonoids biochanin A and baicalein in H5N1 influenza A virus-infected cells,” *Antiviral Research*, vol. 97, no. 1, pp. 41–48, 2013.
- [45] J. P. Dai, X. F. Zhao, J. Zeng et al., “Drug screening for autophagy inhibitors based on the dissociation of beclin1-bcl2 complex using bifc technique and mechanism of eugenol on anti-influenza A virus activity,” *PLoS ONE*, vol. 8, no. 4, Article ID e61026, 2013.
- [46] Y. Wang, T. Romigh, X. He et al., “Resveratrol regulates the PTEN/AKT pathway through androgen receptor-dependent and -independent mechanisms in prostate cancer cell lines,” *Human Molecular Genetics*, vol. 19, no. 22, Article ID ddq354, pp. 4319–4329, 2010.
- [47] M. Savio, T. Coppa, L. Bianchi et al., “The resveratrol analogue 4,4'-dihydroxy-trans-stilbene inhibits cell proliferation with higher efficiency but different mechanism from resveratrol,” *International Journal of Biochemistry and Cell Biology*, vol. 41, no. 12, pp. 2493–2502, 2009.
- [48] W. Schubert, U. Eriksson, B. Edgar, G. Cullberg, and T. Hedner, “Flavonoids in grapefruit juice inhibit the in vitro hepatic metabolism of 17 β -estradiol,” *European Journal of Drug Metabolism and Pharmacokinetics*, vol. 20, no. 3, pp. 219–224, 1995.
- [49] M. K. Buening, R. L. Chang, and M. T. Huang, “Activation and inhibition of benzo(a)pyrene and aflatoxin B1 metabolism in human liver microsomes by naturally occurring flavonoids,” *Cancer Research*, vol. 41, no. 1, pp. 67–72, 1981.
- [50] X. Xiao, D. Shi, L. Liu et al., “Quercetin suppresses cyclooxygenase-2 expression and angiogenesis through inactivation of P300 signaling,” *PLoS ONE*, vol. 6, no. 8, Article ID e22934, 2011.
- [51] G. Haskó, D. G. Kuhel, J.-F. Chen et al., “Adenosine inhibits IL-12 and TNF- α production via adenosine A(2a) receptor-dependent and independent mechanism,” *The FASEB Journal*, vol. 14, no. 13, pp. 2065–2074, 2000.
- [52] D. Yang, T. Yaguchi, T. Nakano, and T. Nishizaki, “Adenosine-induced caspase-3 activation by tuning Bcl-XL/DIABLO/ IAP expression in HuH-7 human hepatoma cells,” *Cell Biology and Toxicology*, vol. 26, no. 4, pp. 319–330, 2010.
- [53] S. Fulda, C. Friesen, M. Los et al., “Betulinic acid triggers CD95 (APO-1/Fas)- and p53-independent apoptosis via activation of caspases in neuroectodermal tumors,” *Cancer Research*, vol. 57, no. 21, pp. 4956–4964, 1997.
- [54] W. Li, M. Ashok, J. Li, H. Yang, A. E. Sama, and H. Wang, “A major ingredient of green tea rescues mice from lethal sepsis partly by inhibiting HMGB1,” *PLoS ONE*, vol. 2, no. 11, Article ID e1153, 2007.
- [55] K.-M. Lee, M. Yeo, J.-S. Choue et al., “Protective mechanism of epigallocatechin-3-gallate against *Helicobacter pylori*-induced gastric epithelial cytotoxicity via the blockage of TLR-4 signaling,” *Helicobacter*, vol. 9, no. 6, pp. 632–642, 2004.
- [56] W. Jiang, Q. Wang, S. Chen et al., “Influenza A virus NS1 induces G₀/G₁ cell cycle arrest by inhibiting the expression and activity of RhoA protein,” *Journal of Virology*, vol. 87, no. 6, pp. 3039–3052, 2013.
- [57] J. L. Koff, M. X. G. Shao, I. F. Ueki, and J. A. Nadel, “Multiple TLRs activate EGFR via a signaling cascade to produce innate immune responses in airway epithelium,” *American Journal of Physiology: Lung Cellular and Molecular Physiology*, vol. 294, no. 6, pp. L1068–L1075, 2008.
- [58] R. Vittal, L. Fan, D. S. Greenspan, E. A. Mickler, and B. Gopalakrishnan, “IL-17 induces type V collagen overexpression and EMT via TGF- β -dependent pathways in obliterative bronchiolitis,” *American Journal of Physiology: Lung Cellular and Molecular Physiology*, vol. 304, pp. L401–L414, 2013.
- [59] W. Li, G. Wang, H. Zhang et al., “Inability of NS1 protein from H5N1 influenza virus to activate pi3k/akt signaling pathway correlates to the enhanced virus replication upon pi3k inhibition,” *Veterinary Research*, vol. 43, article 36, 2012.
- [60] K. K. Singh, P. C. Shukla, A. Quan et al., “Bcr1 is a novel target to improve endothelial dysfunction and retard atherosclerosis,” *The Journal of Thoracic and Cardiovascular Surgery*, vol. 146, no. 4, pp. 949–960, 2013.
- [61] M. Jutel, M. Akdis, and C. A. Akdis, “Histamine, histamine receptors and their role in immune pathology,” *Clinical and Experimental Allergy*, vol. 39, no. 12, pp. 1786–1800, 2009.
- [62] D. P. Robinson, M. E. Lorenzo, W. Jian, and S. L. Klein, “Elevated 17 β -estradiol protects females from influenza A virus pathogenesis by suppressing inflammatory responses,” *PLoS Pathogens*, vol. 7, no. 7, Article ID e1002149, 2011.
- [63] N. Hahon and J. A. Booth, “Benzo[a]pyrene metabolites: effects on viral interferon induction,” *Journal of Interferon Research*, vol. 6, no. 5, pp. 591–602, 1986.
- [64] K. Mizumura, S. Hashimoto, S. Maruoka et al., “Role of mitogen-activated protein kinases in influenza virus induction of prostaglandin E2 from arachidonic acid in bronchial epithelial cells,” *Clinical and Experimental Allergy*, vol. 33, no. 9, pp. 1244–1251, 2003.
- [65] X. Guan, W. Yang, X. Sun et al., “Association of influenza virus infection and inflammatory cytokines with acute myocardial infarction,” *Inflammation Research*, vol. 61, no. 6, pp. 591–598, 2012.
- [66] J. Silke and P. Meier, “Inhibitor of apoptosis (iap) proteins—modulators of cell death and inflammation,” *Cold Spring Harbor Perspectives in Biology*, vol. 5, no. 2, Article ID a008730, 2013.
- [67] R. J. Lowy, “Influenza virus induction of apoptosis by intrinsic and extrinsic mechanisms,” *International Reviews of Immunology*, vol. 22, no. 5–6, pp. 425–449, 2003.
- [68] P. Zamiri, S. Masli, J. W. Streilein, and A. W. Taylor, “Pigment epithelial growth factor suppresses inflammation by modulating macrophage activation,” *Investigative Ophthalmology & Visual Science*, vol. 47, no. 9, pp. 3912–3918, 2006.
- [69] J. A. Hirota, P. R. Hiebert, M. Gold et al., “Granzyme B deficiency exacerbates lung inflammation in mice following acute lung injury,” *American Journal of Respiratory Cell and Molecular Biology*, vol. 49, no. 3, pp. 453–462, 2013.
- [70] A. Gomez-Munoz, P. Gangoiti, L. Arana et al., “New insights on the role of ceramide 1-phosphate in inflammation,” *Biochimica et Biophysica Acta*, vol. 1831, no. 6, pp. 1060–1066, 2013.

- [71] E. C. Roberson, J. E. Tully, A. S. Guala et al., "Influenza induces endoplasmic reticulum stress, caspase-12-dependent apoptosis, and c-Jun N-terminal kinase-mediated transforming growth factor- β release in lung epithelial cells," *American Journal of Respiratory Cell and Molecular Biology*, vol. 46, no. 5, pp. 573–581, 2012.
- [72] S. Herold, W. von Wulffen, M. Steinmueller et al., "Alveolar epithelial cells direct monocyte transepithelial migration upon influenza virus infection: impact of chemokines and adhesion molecules," *Journal of Immunology*, vol. 177, no. 3, pp. 1817–1824, 2006.
- [73] E. Delorme-Axford and C. B. Coyne, "The actin cytoskeleton as a barrier to virus infection of polarized epithelial cells," *Viruses*, vol. 3, no. 12, pp. 2462–2477, 2011.
- [74] D. Moisy, S. V. Avilov, Y. Jacob et al., "HMGB1 protein binds to influenza virus nucleoprotein and promotes viral replication," *Journal of Virology*, vol. 86, no. 17, pp. 9122–9133, 2012.
- [75] N. Lee, C. K. Wong, D. S. Hui et al., "Role of human toll-like receptors in naturally occurring influenza a infections," *Influenza and Other Respiratory Viruses*, vol. 7, no. 5, pp. 666–675, 2013.
- [76] X. Q. Hou, Y. W. Gao, S. T. Yang, C. Y. Wang, Z. Y. Ma, and X. Z. Xia, "Role of macrophage migration inhibitory factor in influenza H5N1 virus pneumonia," *Acta Virologica*, vol. 53, no. 4, pp. 225–231, 2009.
- [77] K.-W. Lee, H. J. Kim, Y. S. Lee et al., "Acteoside inhibits human promyelocytic HL-60 leukemia cell proliferation via inducing cell cycle arrest at G₀/G₁ phase and differentiation into monocyte," *Carcinogenesis*, vol. 28, no. 9, pp. 1928–1936, 2007.
- [78] P. Khatri, M. Sirota, and A. J. Butte, "Ten years of pathway analysis: current approaches and outstanding challenges," *PLoS Computational Biology*, vol. 8, no. 2, Article ID 100237, 2012.

Research Article

Study on Incompatibility of Traditional Chinese Medicine: Evidence from Formula Network, Chemical Space, and Metabolism Room

Wei Long, Xiao-Dong Zhang, Hong-Ying Wu, Jin Jin, Guang-Yun Yu, Xin He, Hao Wang, Xiu Shen, Ze-Wei Zhou, Pei-Xun Liu, and Sai-Jun Fan

Tianjin Key Laboratory of Radiation Medicine and Molecular Nuclear Medicine, Institute of Radiation Medicine, Chinese Academy of Medical Sciences and Peking Union Medical College, Tianjin 300192, China

Correspondence should be addressed to Wei Long; longwaylong@gmail.com and Sai-Jun Fan; fansaijun@irm-cams.com.cn

Received 7 June 2013; Revised 12 August 2013; Accepted 2 September 2013

Academic Editor: Shao Li

Copyright © 2013 Wei Long et al. This is an open access article distributed under the Creative Commons Attribution License, which permits unrestricted use, distribution, and reproduction in any medium, provided the original work is properly cited.

A traditional Chinese medicine (TCM) formula network including 362 TCM formulas was built by using complex network methodologies. The properties of this network were analyzed including network diameter, average distance, clustering coefficient, and average degree. Meanwhile, we built a TCM chemical space and a TCM metabolism room under the theory of chemical space. The properties of chemical space and metabolism room were calculated and analyzed. The properties of the medicine pairs in “eighteen antagonisms and nineteen mutual inhibitors,” an ancient rule for TCM incompatibility, were studied based on the TCM formula network, chemical space, and metabolism room. The results showed that the properties of these incompatible medicine pairs are different from those of the other TCM based on the analysis of the TCM formula network, chemical space, and metabolism room. The lines of evidence derived from our work demonstrated that the ancient rule of TCM incompatibility, “eighteen antagonisms and nineteen mutual inhibitors,” is probably scientifically based.

1. Introduction

Chinese formula is the most common use form of TCM in clinical treatment. The theory of TCM incompatibility is the fundamental principle that should be followed for correct clinical medication, which has a direct relationship with effectiveness and safety of TCM formulas. With the accumulation of practice and experience for thousands of years, the theoretical system of TCM and formulas was gradually taking form and passed it down, such as “Harmony in Four Properties and Five Flavors,” “Sovereign, Minister, Assistant and Guide in Formulas,” and “eighteen antagonisms and nineteen mutual inhibitors,” a special rule for TCM incompatibility in formulas. Since the beginning of the 21st century, the modernization of TCM in China has remarkably proceeded. However, up to present, interpreting ancient theory of TCM in modern scientific language is still a challenging problem for us to make clear the traditional subjects, like the incompatibility of TCM.

The complexity characteristic of traditional Chinese medicine has been generally accepted for many years [1]. The theory of complicated system provides a new cutting point for the present TCM researches. The characteristics of TCM, like complexity and systematicness, make the methodologies of complex system theory adapted naturally to the investigations on TCM. The complex network method is frequently used in studying the complex systems in recent years [2, 3], particularly in biological researches. Thanks to the complex network technologies, to some extent, Systems Biology has been developed from academic theory to practical application [4–7]. In recent years, systems Biology has been introduced into the TCM researches. Li et al. carried out a series of studies centering on TCM Syndrome theory and Chinese herbal property with complex network technology in Systems Biology and made their own achievements [8–13].

On the other hand, the theory of chemical space has drawn widespread attention as soon as it was proposed. Theoretically, chemicals can be characterized by a wide range

of “descriptors,” such as their molecular mass, lipophilicity, and topological features. “Chemical space” is a term often used in place of “multi-dimensional descriptor space”: it is a region defined by a particular choice of descriptors and the limits placed on them. In the context of this insight, chemical space is defined as the total descriptor space that encompasses all the small carbon-based molecules that could in principle be created [14]. It describes things at the standpoint of macrochemical perspective and tends towards conclusions on the integral view. It has been applied preliminarily in TCM studies [15]. Based on the theory of chemical space, we created TCM chemical space and TCM metabolism room in this work by using TCM chemical and metabolic properties.

Up to now, our understanding of the whole law of TCM formula is still poor, due to the complexity of the traditional theories, such as incompatibility of TCM, and less documents available in this field. In order to resolve the mystery of the ancient rule of TCM incompatibility, “eighteen antagonisms and nineteen mutual inhibitors,” scientific experiments based on chemistry and pharmacology were carried out recently [16, 17]. In this study, based on our preliminary work [18], we constructed TCM formula network, chemical space, and metabolism room by collecting massive data with complex network and chemical space methodologies. Property analysis was performed based on the formula network, chemical space, and metabolism room to get the knowledge of TCM formulas, and efforts were made to interpret the ancient rule of TCM incompatibility, “eighteen antagonisms and nineteen mutual inhibitors,” from a new viewpoint.

2. Materials and Methods

2.1. TCM Formula Network

2.1.1. Data Collection. Three hundred and sixty-two TCM formulas were collected into our formula database in the light of *Chinese Medical Formulas* [19], the Textbook for TCM Colleges and Universities edited by the National Educational Ministry. These formulas are all classic and effective and confirmed by numerous clinical studies, with authority and reliability both ensured.

2.1.2. Network Construction. The TCM formula network was constructed with all the 330 Chinese drugs collected in the formula database. The Chinese drugs were defined as the network nodes, and the relationships among these drugs were defined as the network edges. It was stipulated that there was a special relationship between the two Chinese drugs if they appeared in the same formula; then we give them a network edge by connecting the two drugs or two nodes. Consequently, these network nodes and edges make up the whole TCM formula network. Excel combining with programming script was used to process the original data, and then they were converted to Pajek file format by Creatpajek program [20].

2.1.3. Network Analysis. The files obtained above were imported into network analysis software, such as Pajek [21]

and ORA [22, 23]. The frame chart was subsequently drawn, and topology analysis was performed as follows [24].

- (1) The distance (d_{ij}) between the nodes i and j in the network is defined as the number of edges on the shortest path that connected the two nodes. The maximum distance between any of two nodes, which is noted as D , is defined as the diameter in the network. The average path length L in the network is defined as the average distance of any two nodes.
- (2) Assuming a node (i) has K_i sides to connect it with other nodes, then these k_i nodes are called the neighbors of i . Obviously there are at most $k_i(k_i - 1)/2$ sides among k_i nodes. The ratio of the number of sides that actually exist to that which might exist in the overall is defined as clustering coefficient of the node C_i .
- (3) In the properties of individual node, degree is a simple and important concept. The degree of node, k_i , is defined as the number of the other nodes connecting to this node (i). The average of all the degrees is called the average degree of the network. The distribution of degree in the network can be described with a distribution function $P(k)$ which means the probability of a randomly selected degree k . Numerous studies indicate that the distribution of degree can be described in the form of power law:

$$P(k) \propto k^{-\gamma}. \quad (1)$$

The network that is featured by power-law distribution is also called scale-free distribution network.

2.2. TCM Chemical Space. The construction of TCM chemical space was based on the database of Chinese Medicine Chemistry which was developed in our previous work [25], and 383 commonly used TCM are included in this database. The chemical components of every TCM, 8514 compounds in total, are collected in the database. TCM chemical space was constructed according to the following steps shown in Figure 1.

2.2.1. Calculation of Descriptors. The descriptor calculation modules of software CODESSA [26] and MOE [27] were used to calculate the descriptors of all chemical constituents of each TCM in the database. There are 120 descriptors involved in all, including structural descriptors, fragmental descriptors, electrical descriptors, topology descriptors, and space descriptors. These descriptors comprehensively describe the physico-chemical properties of the chemical constituents of each TCM in various perspectives and levels, which paved the way for the construction of TCM chemical space.

2.2.2. Weight Center Treatment. Each of 120 descriptors was defined as a dimensionality. Then all the chemical constituents of each TCM were distributed in a multidimensional chemical space. According to the theory of Chinese medicine chemistry, the property of each TCM is mostly determined

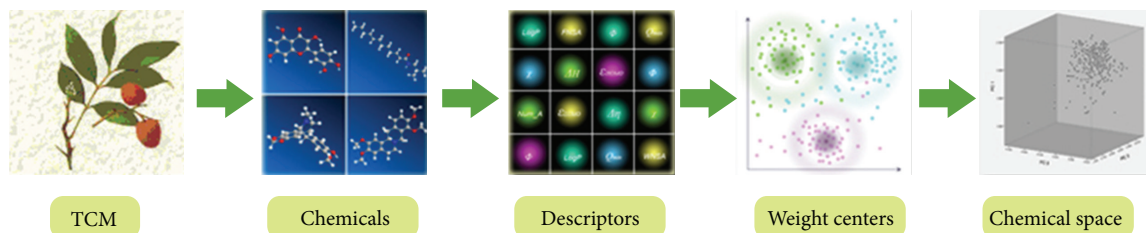


FIGURE 1: The workflow of constructing TCM chemical space.

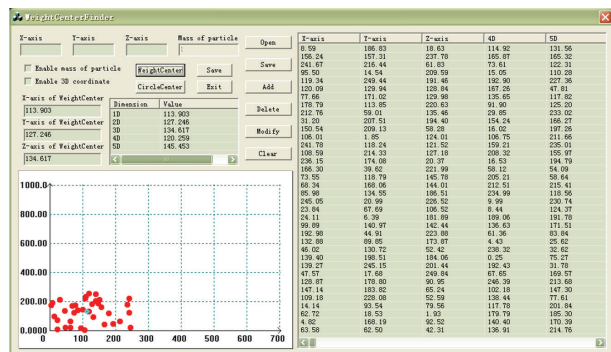


FIGURE 2: Graphical user interface of software "WeightCenterFinder."

by its chemical constituents. However, the number and type of chemical constituents in each TCM vary from tens to hundreds. It is hard to describe the properties of TCM by using such a wide variety of chemical constituents in a chemical space. After instant searches and creations, we developed a new method called weight center treatment that is employed to gather all the constituents of every TCM to a point, which bring together the chemical properties of all the constituents of a TCM and dexterously balance the differences among the chemical constituents. As a result, the whole property of a TCM can be described in a chemical space from a macro perspective. It is assumed that all the particles have the same weight in this work. Each TCM can be presented as a separate unit in the chemical space. Thereby, all the TCM can be redefined chemically by this method of chemical space. The detail of this treatment was described in reference [26]. The weight center treatment is accomplished by the software of "WeightCenterFinder" (Figure 2), which is compiled on Visual C++ 6.0 platform.

2.2.3. Dimension Reduction in Chemical Space. It is difficult to describe the chemical properties of the objects in multidimensional chemical space. In the present study, in order to reduce the chemical dimensions, we employed the method of principal component analysis (PCA) to obtain the eigenvalues and eigenvectors by calculating relevant matrices and diagonalization of the 120 descriptions. Matrix of eigenvectors is used as a transformational matrix to bring the largest percentage of information into the new units of relevant matrix. It can be plotted when the number of units reduced to three. Thereby, the data of multidimensional



FIGURE 3: Graphic user interface of chemical spatial distance calculator.

descriptors can be effectively mapped to 3D diagram. If the cumulative contribution rate of the three main units reaches 80%, it means that the three main units included message of all descriptors basically. The PCA and other statistical analyses were all performed by using SPSS 16.0 [28].

2.2.4. Calculation of Chemical Spatial Distance. The chemical spatial distance can display the relationship of affinity between the two TCM, and the formula for calculating chemical spatial distance is given herein: $D = [(X_j - X_i)^2 + (Y_j - Y_i)^2 + (Z_j - Z_i)^2]^{1/2}$.

Here $(X_i, Y_i, Z_i), (X_j, Y_j, Z_j)$ represent the coordinates of any two dots in chemical space.

The calculation of chemical spatial distance is accomplished by self-developed chemical spatial distance calculator (Figure 3). Affinity and compatible relationship among TCM is analyzed by calculating chemical spatial distance.

2.3. TCM Metabolism Room. In this study, we made a metabolism room involved with P450 enzymes, which are the most important factors that influence the incompatibility property of TCM. Through analysis of this metabolism room, we tried to find evidence for interrupting the rule of "eighteen antagonisms and nineteen mutual inhibitors." All the TCM chemicals were derived from the database of Chinese Medicine Chemistry, with 383 commonly used TCM and 8514 TCM chemicals involved. TCM metabolism room was built by a similar workflow like the TCM chemical space, under the basic theory of chemical space. In the construction process, there were four steps as follows.

2.3.1. Molecular Docking. Fifteen P450 enzymes, the most critical ones related to drug and TCM metabolism, were selected as targets for TCM chemicals in molecular docking. The crystal structures of these enzymes were collected from PDB, with the names and their PDB code as follows: CYP 1A1 (PDB code: 4I8V), CYP 1A2 (PDB code: 2HI4), CYP 1B1 (PDB code: 3PM0), CYP 2A6 (PDB code: 1ZI0), CYP 2A13 (PDB code: 2PB5), CYP 2B4 (PDB code: 3TMZ), CYP 2B6 (PDB code: 3UA5), CYP 2C5 (PDB code: 1NR6), CYP 2C8 (PDB code: 2VN0), CYP 2C9 (PDB code: 1R9O), CYP 2C18 (PDB code: 2H6P), CYP 2C19 (PDB code: 4GQS), CYP 2D6 (PDB code: 3TDA), CYP 2E1 (PDB code: 3T3Z), and CYP 3A4 (PDB code: 3NXU). Molecular docking was implemented by Glide, a docking program in Schrodinger software package. Protein preparation, chemical disposure, and other operations were all carried out in Maestro, the molecular modeling environment of Schrodinger software. The docking score of each TCM chemical towards each P450 enzyme will be assigned as a metabolic value for this chemical. Then, each TCM chemical will have 15 metabolic values corresponding to the 15 P450 enzymes. These metabolic values describe the whole P450 metabolic properties of this chemical from an overall perspective.

2.3.2. Weight Center Treatment. The same treatment used in TCM chemical space was applied in this process. As the treatment result, each TCM will be presented by a weight center, which was concentrated from all the chemicals in this TCM, in a multiple dimensional metabolism room.

2.3.3. Dimension Reduction. The same treatment used in TCM chemical space was applied in this process. The original 15 dimensions were reduced into 3 dimensions by using PCA, with over 80% of the cumulative contribution rate from these 3 main units.

2.3.4. Calculation of Metabolism Room Distance. We applied the same method in TCM chemical space to calculate the metabolism room distance.

3. Results and Discussion

3.1. TCM Formula Network. The TCM formula network we constructed has 330 nodes and 5236 edges in all. The network structure chart is drawn with the software ORA. We can see the results in Figure 4.

The topological parameters of the network were calculated by Pajek; for main parameters, see Table 1.

There are 330 nodes in this network, and the number of edges reached 5258, with 31.7 as the average degree of each node, which indicate a high network density and considerably close connection among TCM. Most of TCM are likely to have good comparability with each other, which is in line with the actual application of TCM. The diameter of the network is 5, and the average path length is 2.17, which indicate that the TCM formula network is featured as a small-world network. Generally, the clustering coefficient of the network ranges from 0 to 1. The bigger the coefficient, the higher the

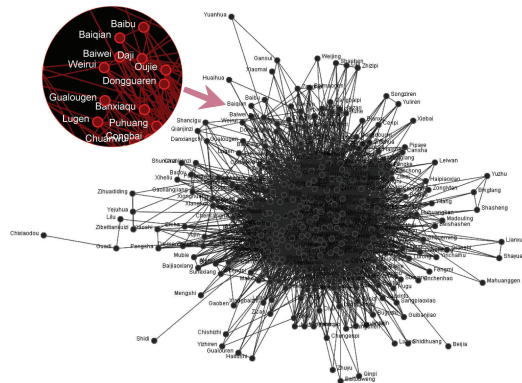


FIGURE 4: The map of TCM formula network (a partial enlarged illustration on the upper left).

TABLE 1: The main topological parameters of TCM formulas network.

Parameter	Value
Network diameter	5
Average distance	2.17
Clustering coefficient	0.726
Average degree	31.7

clustering property. The clustering coefficient of the TCM formulas network is 0.726, which indicates a high clustering property of this network.

As we know, there are hundreds of medicines frequently used in the TCM formulas, and the properties of TCM are different from each other, such as “Four Properties and Five Flavors,” “Ascending, Descending, floating and sinking.” However, the different TCM in the same formula can be used as a whole to cure the same kind of disease. This may be because the TCM of different properties in the same formula interacts with each other, and these interactions make them tended to be homogenous and compatible. Turning to the TCM formula network, the high clustering property of the network probably gives us a clue to explain it. The analysis results of degree distribution showed that the TCM formulas network is featured by partly scale-free property (Figure 5). The degree distribution function is described as follows:

$$P(k) \propto k^{-0.6237}, \quad \gamma = 0.6237. \quad (2)$$

According to the theory of complex networks, the higher the value of power exponent, the less homogenous the network. Thus, a low value of power exponent indicates that the hubs and the key nodes play vital roles in the network. The γ of this network is 0.6237, which is smaller than the general scale-free network, which shows that the key nodes in TCM formula network are in great numbers and play critical roles in this network. It can be concluded that the commonly used TCM occupy an important position in forming of the formulas. Additionally, the scale-free network is usually of robustness, which is also called antistrike capability. Interestingly, the clinical use of TCM formulas exhibits the same characteristic as well. As is known to us,

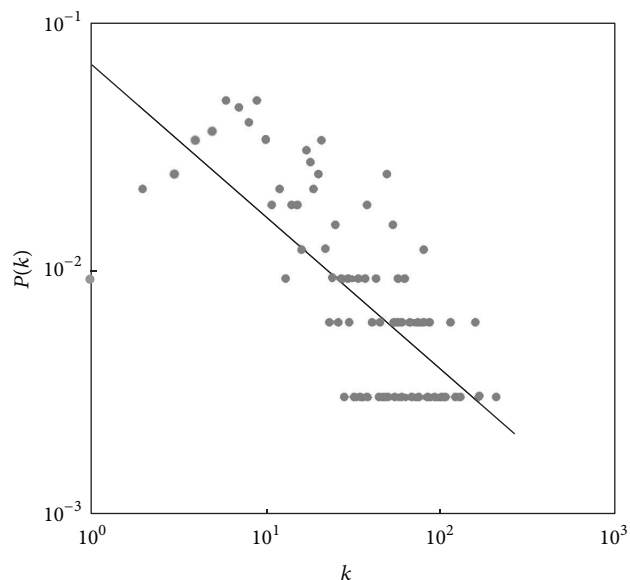


FIGURE 5: The degree distribution chart of TCM formulas network.

some Chinese medicines have substitutes in clinical usage; for instance, rhinoceros horn can be substituted by buffalo horn. It is normal practice for traditional Chinese physicians to substitute, add, and reduce some medicine in the same formula according to actual needs. But it will not change the main property and function of this formula in clinic. A traditional Chinese doctor can still make a prescription by using the principle of substitution in the case of some medicine lacking. On the other hand, they are usually making different prescriptions to the same disease case because of different habits of prescribing, but they can still achieve the same therapeutic purposes. Probably, the robustness property of the TCM formulas network can give us insight on explaining all the phenomena mentioned above.

Network path analysis of the TCM pairs derived from “Eighteen Antagonisms and Nineteen Mutual Inhibitors” was performed based on the formula network (seen in Figure 8). The path distance of the network nodes represents their affinity relationship. The result shows that the average path distance between the TCM pairs in “Eighteen antagonisms and nineteen mutual inhibitions” is 2.46, which is longer than the average path distance of the network, 2.17. Because of the most commonly used TCM in formulas, liquorice root, the network path distance of the medicine pairs in “Eighteen antagonisms and nineteen mutual inhibitions” has been greatly shortened. But the difference between the special medicine pairs and the average path distance still signified that the theory of “Eighteen antagonisms and nineteen mutual inhibitions” is science based from the results of TCM formula network.

3.2. TCM Chemical Space. To further confirm the conclusion, we studied the chemistry basis of “antagonism and mutual restraint” in TCM by using the method of chemical space. The chemical space is constructed containing 383 commonly used

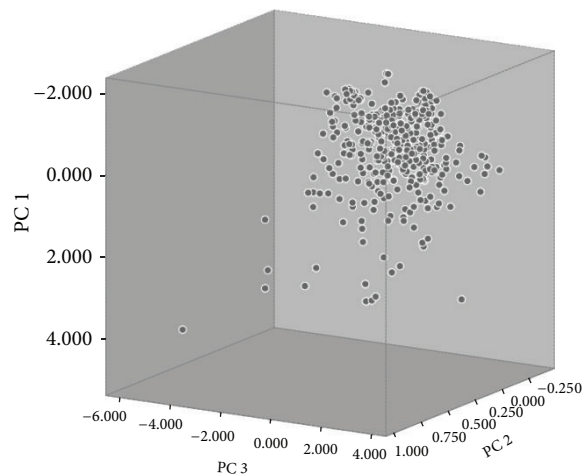


FIGURE 6: The map of TCM chemical space.

TCM with 8514 chemical components. From the PCA results, we found that the variance of the first principle component (PC) was 42.72%, the second PC was 31.64%, and the third PC was 11.78%, with the cumulative rate of three PCs reaching 86.14%. Thus, it means that the three PCs included message of all descriptors basically, and the map of TCM chemical space was constructed based on these three PCs, seen in Figure 6. According to the theory of chemical space, chemical entities with similar functions tend to cluster in a certain special region. In the map of TCM chemical space, we can see that the distribution of TCM in the whole space ranges from loose to dense. But a significant proportion of them cluster at the top right corner of this chemical space. It is inferred that most of TCM are chemically compatible; in other words, they are likely to compose formulas with each other. A small proportion of TCM are dispersed and at intervals with others, which corresponds with the fact that incompatibility exists in a small proportion of TCM.

We measured the spatial distance of TCM in the chemical space, to judge the chemical affinity relationship between every two TCM. The results show that average chemical spatial distance between medicine pairs of “Eighteen antagonisms and nineteen mutual inhibitions” is 2.066, which is much larger than the average distance of all TCM, 1.641. The detailed results for each medicine pair were shown in Figure 8. This implicated that the property of incompatibility among TCM is chemically based, and it is formed by the whole chemical properties of the components contained in each TCM.

3.3. TCM Metabolism Room. It was well demonstrated that the metabolic property of TCM, especially about the P450 enzymes, is always the main factor to cause the in vivo toxicity when two kinds of incompatible TCM are used together [29]. For instance, if the chemical components from two TCM in vivo compete for one special P450 enzyme, the guardian responsible for detoxifying the dangerous drugs or TCM chemical components in the body, one of them is doomed to be left with its untreated form. If this one happened to

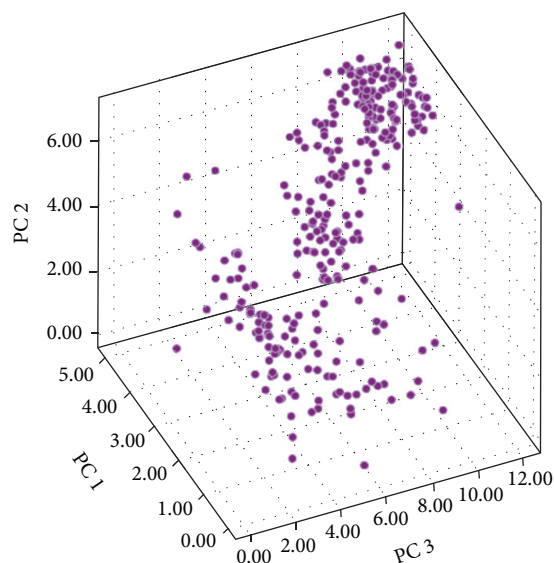


FIGURE 7: The map of TCM metabolism room.

be toxic, the body will be poisoned. In this case, it will be called the incompatibility of TCM. Thus, studying the metabolic property of TCM will be helpful to reveal the incompatibility phenomenon in TCM. Accordingly, we built this TCM metabolism room, where all the TCM will be fixed in their positions by evaluating their activities towards P450 enzymes. In this room, the TCM ones close to each other indicate that they have the close metabolic characteristic. It also implies a potential risk when they are used in a prescription simultaneously. The PCA results showed that the variance of the first PC was 52.13%, the second PC was 30.54%, and the third PC was 9.69%, with the cumulative rate of three PCs reaching 92.36%. Therefore, it means that the three PCs included the most message of all descriptors, and the map of TCM chemical space was constructed based on these three PCs.

In Figure 7, we can see that there is a large proportion of TCM located in the upper inside corner, where most of P450 enzymes keep high activity. It tells us that a large part of TCM is easily metabolized, for many P450 enzymes can undertake this job with enthusiasm. But we also can be implied that a part of TCM favor exclusive enzyme colony, with their particular position being shown in the room. The distance of TCM in the metabolism room was measured, so as to tell the metabolic relationship between every two TCM. The result shows that the average metabolism room distance between the TCM pairs in “Eighteen antagonisms and nineteen mutual inhibitions” is 2.40, which is much shorter than the average distance of all TCM, 4.25. The detailed results for each medicine pairs were shown in Figure 8. It showed that the incompatible TCM pairs tend to compete for the similar P450 enzyme colony, which make the toxic TCM ones obstructed to be metabolized or detoxified. This probably induces the incompatibility phenomenon that occurred.

3.4. Discussion about the Limitation of the Applied Methodology. In the construction of TCM chemical space and

metabolism room, we employed a new methodology, weight center treatment. It is a novel strategy to approach describing TCM by chemical information. Chemistry is easy to be used to describe a single compound by various chemical descriptors. But TCM always contains tens or even hundreds of chemical compounds. It is a difficult problem to apply chemistry to describe a kind of TCM by batches of chemical descriptors derived from its numerous chemical components. Enlightened from geometrics, we applied weight center strategy to obtain an integrated chemical profile of a kind of TCM by treating all its chemical components in a chemical space. This chemical space is multidimension featured, every dimension of which represents a kind of chemical description. In this space, the dispersed chemical components of a kind of TCM concentrate to a pyknois, the weight center, which will be used as the symbol of this TCM. That means a kind of TCM will be described by a series of treated chemical descriptors produced by the original descriptors of all the compounds contained in this kind of TCM. In this study, we assumed that all the “particles” in the chemical space have the same mass; that is to say, all the chemical components are assigned the same content ratios. Apparently, it was not fully considered since the content of the chemical components, in fact, is various in a kind of TCM. However, even though our software WeightCenterFinder is originally designed to be able to assign the components content values, it is impossible, in the present condition, to collect all the exact content data of the TCM chemical components. The reason is that, a part of these data are still absent; on the other hand, the available data are always in disparity because of the different measure methods and conditions. In addition, the number of the chemicals in a kind of TCM is also not completely certain, because there are still new compounds that can be discovered from TCM. But the number of the chemicals is very crucial to position the TCM weight center. These factors, obviously, will bring uncertainty and inaccuracy to the results of this study. Therefore, it is expected that, with the coming of new technologies and more discoveries, this methodology will have further improvement in the future.

4. Conclusion

In this study, the TCM formula network was built by using complex network methodologies. Meanwhile, we built a TCM chemical space and a TCM metabolism room under the theory of chemical space. Then the analysis of general network properties and chemical space was performed. The analysis results showed that the TCM formulas network was a partial scale-free network and also has the feature of small-world network. The analysis of TCM chemical space indicated that the properties of compatibility and incompatibility among TCM had chemical foundation. In addition, we found that the incompatible TCM pairs were different from the other ones in metabolism room. The ancient rule for incompatibility of TCM, “Eighteen Antagonisms and Nineteen Mutual Inhibitors,” was evidenced by our analysis from TCM formula network, chemical space, and metabolism room constructed in this work. Taken together,

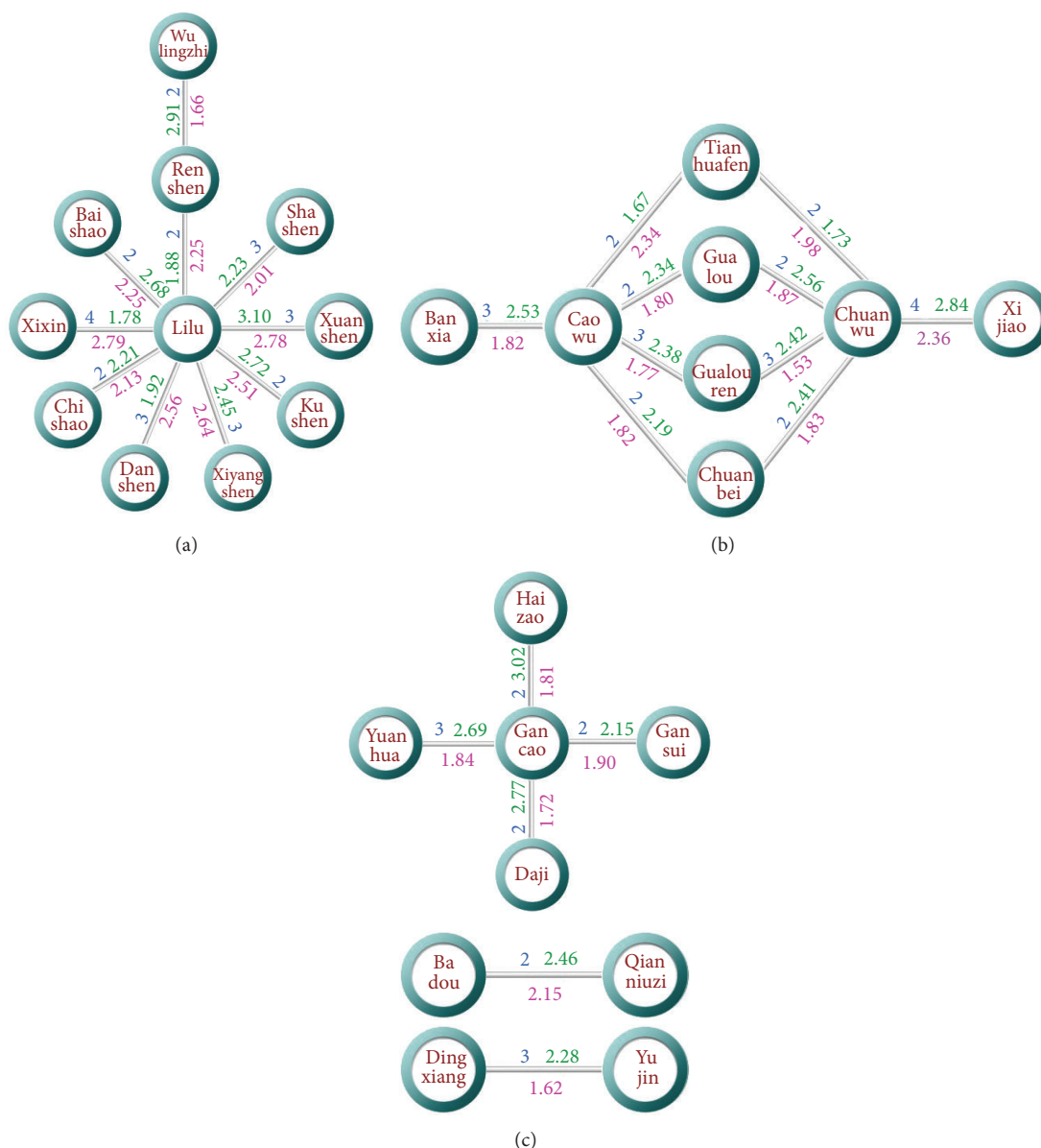


FIGURE 8: The network path distance (blue numbers), chemical spatial distance (pink numbers), and metabolism room distance (green numbers) between the medicine pairs of “Eighteen antagonisms and nineteen mutual inhibitions.”

the TCM formula network, chemical space, and metabolism room gave us new insight and standpoint in analyzing the incompatibility property of TCM. We also hope it will bring up some new ideas and enlightenments into solving the problems in investigation of TCM and formulas.

Acknowledgments

The authors are grateful for the financial support provided by the National Natural Science Foundation of China (no. 81202153), PUMC Youth Fund and the Fundamental Research Funds for the Central Universities (no. 3332013104), Research Fund for the Doctoral Program of Higher Education of China (no. 20121106120042), and Development Fund of Institute of

Radiation Medicine, Chinese Academy of Medical Sciences (nos. SF1227, SZ1337).

References

- [1] H. F. Bao, “More considerations on the complexity of TCM Science: preliminary study on TCM standardization,” *Acta Universitatis Traditionis Medicalis Sinensis Pharmacologiaeque Shanghai*, vol. 17, no. 3, pp. 3–6, 2003.
- [2] D. J. Watts and S. H. Strogatz, “Collective dynamics of ‘small-world’ networks,” *Nature*, vol. 393, no. 6684, pp. 440–442, 1998.
- [3] A.-L. Barabási and R. Albert, “Emergence of scaling in random networks,” *Science*, vol. 286, no. 5439, pp. 509–512, 1999.
- [4] A.-L. Barabási and Z. N. Oltvai, “Network biology: understanding the cell’s functional organization,” *Nature Reviews Genetics*, vol. 5, no. 2, pp. 101–113, 2004.

- [5] P. F. Jonsson and P. A. Bates, "Global topological features of cancer proteins in the human interactome," *Bioinformatics*, vol. 22, no. 18, pp. 2291–2297, 2006.
- [6] T. Ideker and R. Sharan, "Protein networks in disease," *Genome Research*, vol. 18, no. 4, pp. 644–652, 2008.
- [7] I. Feldman, A. Rzhetsky, and D. Vitkup, "Network properties of genes harboring inherited disease mutations," *Proceedings of the National Academy of Sciences of the United States of America*, vol. 105, no. 11, pp. 4323–4328, 2008.
- [8] R. Li, T. Ma, J. Gu, X. Liang, and S. Li, "Imbalanced network biomarkers for traditional Chinese medicine syndrome in gastritis patients," *Scientific Reports*, vol. 3, p. 1543, 2013.
- [9] B. Zhang, X. Wang, and S. Li, "An integrative platform of TCM network pharmacology and its application on an herbal formula, *Qing-Luo-Yin*," *Evidence-Based Complementary and Alternative Medicine*, vol. 2013, Article ID 456747, 12 pages, 2013.
- [10] S. Li, B. Zhang, and N. Zhang, "Network target for screening synergistic drug combinations with application to traditional Chinese medicine," *BMC Systems Biology*, vol. 5, no. 1, article S10, 2011.
- [11] S. Li, B. Zhang, D. Jiang, Y. Wei, and N. Zhang, "Herb network construction and co-module analysis for uncovering the combination rule of traditional Chinese herbal formulae," *BMC Bioinformatics*, vol. 11, no. 11, article S6, 2010.
- [12] T. Ma, C. Tan, H. Zhang, M. Wang, W. Ding, and S. Li, "Bridging the gap between traditional Chinese medicine and systems biology: the connection of Cold Syndrome and NEI network," *Molecular BioSystems*, vol. 6, no. 4, pp. 613–619, 2010.
- [13] S. Li, Z. Q. Zhang, L. J. Wu, X. G. Zhang, Y. D. Li, and Y. Y. Wang, "Understanding ZHENG in traditional Chinese medicine in the context of neuro-endocrine-immune network," *IET Systems Biology*, vol. 1, no. 1, pp. 51–60, 2007.
- [14] C. M. Dobson, "Chemical space and biology," *Nature*, vol. 432, no. 7019, pp. 824–828, 2004.
- [15] X.-D. Li, Q. Huang, and X.-J. Xu, "Target-Ligand space distribution of the compound sets from Xuefu Zhuyu decoction, a traditional Chinese medicinal recipe," *Acta Physico-Chimica Sinica*, vol. 24, no. 4, pp. 547–551, 2008.
- [16] S. L. Su, J. A. Duan, W. L. Li, Y. P. Tang, and X. S. Fan, "Exploration the toxicity/increase virulence mechanisms of "eighteen incompatible medicaments" based on chemical substances," *Chinese Journal of Experimental Traditional Medical Formulae*, vol. 16, no. 1, pp. 123–129, 2010.
- [17] C. Wang, Y. G. Wang, Q. D. Liang, W. Q. Rang, C. R. Xiao, and Y. Gao, "Analysis of chemical composition in combination of aconitum and fritillaria by UPLC/Q-TOFMS with multivariate statistical analysis," *Acta Chimica Sinica*, vol. 69, no. 16, pp. 84–92, 2011.
- [18] W. Long, X. Pi, J. Xiang, P. X. Liu, and Z. M. Zou, "Network of Chinese medical formulas and Chinese medicinal chemical space," *Journal of Beijing University of Traditional Chinese Medicine*, vol. 34, no. 11, pp. 729–732, 2011.
- [19] Z. J. Deng, *Chinese Medical Formulas*, China Press of Traditional Chinese Medicine, Beijing, China, 2003.
- [20] <http://www.fas.at/science/downloads/index.htm#creatpajek>.
- [21] V. Batagelj and A. Mrvar, Pajek software 1.24, 2009.
- [22] K. M. Carley, ORA software 1.9.5.4.0, 2009.
- [23] <http://www.casos.cs.cmu.edu/projects/ora/>.
- [24] X. F. Wang, X. Li, and G. R. Chen, *Theory and Application of Complex Networks*, Tsinghua University Press, Beijing, China, 2006.
- [25] W. Long, P. Liu, J. Xiang, X. Pi, J. Zhang, and Z. Zou, "A combination system for prediction of Chinese Materia Medica properties," *Computer Methods and Programs in Biomedicine*, vol. 101, no. 3, pp. 253–264, 2011.
- [26] CODESSA, *Comprehensive Descriptors for Structural and Statistical Analysis, Version 2.7.10*, Semichem, Inc., 2007.
- [27] MOE, *Molecular Operating Environment, Version 2008. 10*, Chemical Computing Group Inc., 2008.
- [28] SPSS 16.0, SPSS Inc., Chicago, Ill, USA, 1987–2007.
- [29] Y. Wang, Z. Ma, Q. Liang et al., "Study on the eighteen incompatible pairs based on cytochrome P450," *World Science and Technology-Modernization of Traditional Chinese Medicine*, vol. 13, no. 1, pp. 36–40, 2011.

Research Article

Bioinformatics Analysis for the Antirheumatic Effects of Huang-Lian-Jie-Du-Tang from a Network Perspective

Haiyang Fang,¹ Yichuan Wang,¹ Tinghong Yang,¹ Yang Ga,² Yi Zhang,³
Runhui Liu,⁴ Weidong Zhang,⁴ and Jing Zhao^{1,4}

¹ Department of Mathematics, Logistical Engineering University, Chongqing 401311, China

² Tibet Traditional Medical College, Lhasa 850000, China

³ The National Medical College, Chengdu University of TCM, Chengdu 610075, China

⁴ Department of Natural Medicinal Chemistry, Second Military Medical University, Shanghai 200433, China

Correspondence should be addressed to Weidong Zhang; wdzhangy@hotmail.com and Jing Zhao; zhaojanne@gmail.com

Received 16 July 2013; Accepted 11 September 2013

Academic Editor: Aiping Lv

Copyright © 2013 Haiyang Fang et al. This is an open access article distributed under the Creative Commons Attribution License, which permits unrestricted use, distribution, and reproduction in any medium, provided the original work is properly cited.

Huang-Lian-Jie-Du-Tang (HLJDT) is a classic TCM formula to clear “heat” and “poison” that exhibits antirheumatic activity. Here we investigated the therapeutic mechanisms of HLJDT at protein network level using bioinformatics approach. It was found that HLJDT shares 5 target proteins with 3 types of anti-RA drugs, and several pathways in immune system and bone formation are significantly regulated by HLJDT’s components, suggesting the therapeutic effect of HLJDT on RA. By defining an antirheumatic effect score to quantitatively measure the therapeutic effect, we found that the score of each HLJDT’s component is very low, while the whole HLJDT achieves a much higher effect score, suggesting a synergistic effect of HLJDT achieved by its multiple components acting on multiple targets. At last, topological analysis on the RA-associated PPI network was conducted to illustrate key roles of HLJDT’s target proteins on this network. Integrating our findings with TCM theory suggests that HLJDT targets on hub nodes and main pathway in the Hot ZENG network, and thus it could be applied as adjuvant treatment for Hot-ZENG-related RA. This study may facilitate our understanding of antirheumatic effect of HLJDT and it may suggest new approach for the study of TCM pharmacology.

1. Introduction

Rheumatoid arthritis (RA) is a chronic, systemic inflammatory joint disorder that principally attacks flexible (synovial) joints, leading to the destruction of articular cartilage and fusion of the joints. It can also affect other tissues throughout the body. RA is considered as a systemic autoimmune disease, whose cause and pathogenesis remain largely unknown.

Currently there is no cure for RA. The aim of the treatment is to reduce inflammation, relieve pain, suppress disease activity, prevent joint damage, and slow disease progression, so as to maintain the patient’s quality of life and ability to function. Clinical treatments for RA include non-steroidal anti-inflammatory drugs (NSAIDs), disease modifying antirheumatic drugs (DMARDs), glucocorticoids, and biological response modifiers. Even so, current RA treatment

medications are limited by several well-characterized clinical side effects, such as hepatotoxicity [1, 2], gastrointestinal effects [3], and cardiotoxic effects [4]. Therefore, there is a need to explore new or alternative anti-RA agents.

Huang-Lian-Jie-Du-Tang (HLJDT; oren-gedoku-to in Japanese), a classic TCM formula to clear “heat” and “poison,” is an aqueous extract of four herbal materials, Rhizoma Cop-tidis, Radix Scutellariae, Cortex Phellodendri, and Fructus gardeniae. It has been used to treat gastrointestinal disorders, inflammation, liver disease, hypertension, and cerebrovascular disease [5]. Earlier studies have demonstrated that HLJDT possesses antiobesity [6], antitumor [7], neuroprotection [8], and anti-inflammatory activities [9, 10]. A series of experimental studies by one of our laboratories on HLJDT’s effects on collagen-induced arthritis in rats suggested that HLJDT exhibits antirheumatic activity [11–13]. On the other hand,

many compounds have been identified as active ingredients of HLJDT, including baicalin, baicalein, wogonoside, wogonin, berberine, coptisine, palmatine, jatrorrhizine, crocin, crocetin, chlorogenic acid, and geniposide [14], some of which have been reported to show antirheumatic effects [15–18].

It has been known that complex chronic diseases including RA are usually caused by an unbalanced regulating network resulting from the dysfunctions of multiple genes or their products [19–22]. Meanwhile, as multicomponent and multitarget agent, the therapeutic effectiveness of a TCM formula is believed to be achieved through collectively modulating the molecular network of the body system by its active ingredients [23, 24]. Thus there is a need to study the therapeutic mechanism of TCM formulae on complex diseases from the viewpoint of network-based systems biology [23–28].

In this work, we studied antirheumatic effects of HLJDT as compared to FDA-approved anti-RA drugs from network perspective. We first collected genes associated with RA, proteins inhibited by main active compounds of HLJDT, and targets of FDA-approved anti-RA drugs. Then we study the drug targets in the context of RA-associated pathway and protein networks. HLJDT's targets were mapped onto the drug-target network of FDA-approved anti-RA drugs and the RA pathway in the KEGG database to investigate their potential anti-RA functions. The network-based antirheumatic effect score was defined to quantitatively analyze the antirheumatic effect of HLJDT and compare it with those of FDA-approved anti-RA drugs. Topological analysis on the RA-associated PPI network was conducted to explore the roles that HLJDT's target proteins play on this network.

2. Materials and Methods

2.1. Data Preparing

2.1.1. RA-Associated Genes. We collected genes associated with RA from three resources as follows.

- (1) The Online Mendelian Inheritance in Man (OMIM) database [29]: it is a database that catalogues all the known diseases with a genetic component and when possible links them to the relevant genes in the human genome and provides references for further research and tools for genomic analysis of a catalogued gene. We searched the OMIM database with a keyword “rheumatoid arthritis” and found 7 causal genes: CD244, HLA-DR1B, MHC2TA, NFKB1L1, PAD, SLC22A4, and PTPN8.
- (2) Genetic Association Database (GAD) [30]: it is an archive of human genetic association studies of complex diseases and disorders and includes summary data extracted from published papers in peer-reviewed journals on candidate gene and GWAS studies. We searched the GAD database with a keyword “rheumatoid arthritis” and found 82 genes whose association with RA was shown “Y.” Five of the seven

RA causal genes in the OMIM database are also included in the 82 genes collected from the GAD.

- (3) Kyoto Encyclopedia of Genes and Genomes (KEGG) Pathway Database [31]: this is a collection of online databases dealing with genomes, enzymatic pathways, and biological chemicals. A total of 92 genes appear on the rheumatoid arthritis pathway in the KEGG database. These genes are considered to be associated with RA.

Based on the above three databases, we obtained 163 distinct genes that are associated with RA (see Table S1 in Supplementary Material available online at <http://dx.doi.org/10.1155/2013/245357>).

2.1.2. FDA Approved Anti-RA Drugs and Their Target Proteins. The data of FDA-approved anti-RA drugs and their targets was downloaded from the DrugBank database [32], which was updated in May 2013. We searched the DrugBank database with a keyword “rheumatoid arthritis” and extracted all of the FDA-approved anti-RA drugs and their corresponding targets (32 drugs and 51 protein targets). Four classes of drugs are used clinically for the treatment of RA. They are nonsteroidal anti-inflammatory drugs (NSAID) such as flurbiprofen, disease-modifying antirheumatic drugs (DMARDs) such as sulfasalazine, glucocorticoids such as cortisone acetate, and biological response modifiers such as etanercept and abatacept. See Supplementary Table S2 for detail.

2.1.3. Target Proteins of HLJDT's Main Ingredients. Based on our previous study and literature reports, fourteen active components are identified in HLJDT: baicalin, baicalein, wogonoside, wogonin, berberine, magnoflorine, phellodendrine, coptisine, palmatine, jatrorrhizine, crocetin, crocin, chlorogenic acid, and geniposide [10, 14]. Data about target proteins for HLJDT's main compounds was collected from Herbal Ingredients' Targets Database (HIT) [33], a well-known herb ingredient target database (<http://lifecenter.sgst.cn/hit/>), with a keyword of each ingredient name. According to HIT, 10 ingredients can find the corresponding drug target proteins. They are baicalein, berberine, chlorogenic, coptisine, crocetin, crocin, geniposide, jatrorrhizine, palmatine, and wogonin, in which crocin's only one target could not be found on the PPI network we used. Thus crocin is not included in our network analysis. A total of 91 distinct target proteins of HLJDT were found in the HIT database. The detailed data are shown in Supplementary Table S3.

2.1.4. Protein-Protein Interaction Data. Protein-protein interactions between human proteins were downloaded from the version 9.05 of STRING [34]. STRING includes both physical and functional interactions integrated from numerous sources, including experimental repositories, computational prediction methods, and public text collections. It uses a scoring system to weigh the evidence of each interaction. The interaction scores were normalized to the interval [0, 1]. We first extracted interactions weighted at least 0.9 to

construct a protein-protein interaction network with high confidence. Then we checked if the genes we studied, that is, RA-associated genes, FDA-approved anti-RA drugs' target proteins, and target proteins of HLJDT's main ingredients, are included in this network. For those genes missing in this network but appearing in the STRING database, we added their interactions with the highest weights which are less than 0.9. In this way, we constructed a weighted PPI network with 9289 nodes and 57179 edges.

2.2. Construction of Drug-Target Network. A drug-target network is defined as a bipartite network for the drug-target associations consisting of two disjoint sets of nodes [35]. One set of nodes corresponds to all drugs under consideration, and the other set corresponds to all the proteins targeted by drugs in the study set. A protein node and a drug node are linked if the protein is targeted by that specific drug according to the DrugBank information.

2.3. Pathway Enrichment Analysis. We used pathway enrichment analysis [36] to determine whether a pathway is significantly regulated by HLJDT. Hypergeometric cumulative distribution was applied to quantitatively measure whether a pathway is more enriched with HLJDT's targets than would be expected by chance [37]. Generally, if we randomly draw n samples from a finite set, the probability of getting i samples with the desired feature by chance obeys hypergeometric distribution as

$$f(i) = \frac{\binom{K}{i} \binom{N-K}{n-i}}{\binom{N}{n}}, \quad (1)$$

where N is the size of the set and K is the number of items with the desired feature in the set. Then the probability of getting at least k samples with the desired feature by chance can be represented by hypergeometric cumulative distribution defined as P value:

$$P = 1 - \sum_{i=0}^{k-1} f(i) = 1 - \sum_{i=0}^{k-1} \frac{\binom{k}{i} \binom{N-K}{n-i}}{\binom{N}{n}}. \quad (2)$$

Given significance level α , a P value smaller than α demonstrates low probability that the items with the desired feature are chosen by chance. In our case, if all pathways under study include N distinct genes, in which K genes are HLJDT's targets, for a pathway with n genes, a P value $< \alpha$ implies a low probability that the k HLJDT's targets appear in the pathway by chance; that is, this pathway can be regarded as significantly regulated by HLJDT.

2.4. Network Scoring of Antirheumatic Effects of Drugs

2.4.1. Scoring Network Effect of a Group of Seed Nodes. We applied the algorithm of random walk with restart to score the effect of a group of seed nodes on all the nodes in the network under study [38, 39]. The network is the weighted human PPI network, while the seeds could be disease-associated genes or protein targets of drugs.

A random walk starts at one of the seed nodes in the set S . At each step, the random walker either moves to a randomly chosen neighbor $u \in N$ of the current node v or it restarts at one of the nodes in the seed set S . The probability of restarting at a given time step is a fixed parameter denoted by r . For each restart, the probability of restarting at $v \in S$ suggests the degree of association between v and the seed set S . For each move, the probability of moving to interacting partner u of the current node v is proportional to the reliability of the interaction between u and v . After a sufficiently long time, the probability of being at node v at a random time step provides a measure of the functional association between v and the genes in seed set S . This process could be denoted as follows:

$$x^{t+1} = (1-r)Px^t + rx^0, \quad (3)$$

where P is the adjacency matrix of the weighted PPI network, representing the coupling strength of nodes in the network; $r \in [0, 1]$ is a parameter denoting the restart probability which needs to be calibrated with real data; x^t is a vector in which $x^t(v)$ denotes the probability that the random walker will be at node v at time t ; x^0 is a vector corresponding to the strength of seed nodes. The effect strength of seed set S to each nodes in the network is defined by steady-state probability vector x^∞ when $x^{t+1} = x^t$.

The algorithm of random walk with start has been successfully used in the prioritization of candidate disease genes and $r = 0.3$ appeared to be a robust choice [40]. Thus we took $r = 0.3$ in this study.

2.4.2. Scoring RA's Effect on the Human PPI Network. In this case the seed nodes are defined as RA-associated genes we collected. Theoretically, the degree in which different RA-associated gene correlates with RA is varying, and thus the initial strength values of different seed nodes should be different. For simplicity, we treated all RA-associated genes equally and defined the initial vector x^0 as $x^0(v) = 1$ if v is a seed; otherwise, $x^0(v) = 0$.

Then random walk with restart was used to compute the RA effect score of each node in the human network and we get a disease effect vector x_{RA} .

2.4.3. Scoring a Drug's Effect on the Human PPI Network. In this case, the seed nodes are defined as the drug's protein targets and the initial strength value of a seed node should be the binding strength or affinity of the drug to the corresponding target. In theory, the affinities could be measured in biochemical assays, which are not always available. Some studies used chemical proteomics data as a proxy for binding strengths [41, 42]. Here we study HLJDT's effect on the human PPI network by comparison with those of FDA-approved anti-RA drugs; thus, our focus is on the relative binding affinities of western drugs and HLJDT's components to target proteins. It has been known that the inhibition potency of natural compounds on protein targets is usually much lower than that of specifically designed drug molecules; for example, our earlier study found that the IC50 value of natural compound Astragaloside IV against proteins CN and ACE was approximately two orders higher than the

corresponding western drugs cyclosporine A and enalapril, respectively [43]. Therefore, for an FDA-approved anti-RA drug, we defined the initial vector \mathbf{x}^0 as $x^0(v) = 1$ if v is a seed; otherwise, $x^0(v) = 0$. Meanwhile, we defined the initial vector \mathbf{x}^0 of a HLJDT's component as $x^0(v) = 0.01$ if v is a target of this component; otherwise, $x^0(v) = 0$.

For each drug, random walk with restart was used to compute its effect score on each node in the human network and we get its drug effect vector \mathbf{x}_{drug} .

2.4.4. Scoring the Antirheumatic Effects of a Drug. We applied the inner product between the vectors of disease effect and drug effect to measure how the drug impacts the human interactome under the influence of the disease [42]. $E = \langle \mathbf{x}_{\text{RA}}, \mathbf{x}_{\text{drug}k} \rangle$ is defined specifically as the antirheumatic effect score of the k th drug under study. The effect score of a drug was then compared with that of its random counterparts by z -score.

2.5. Z-Score. Z -score was applied to quantify the difference between the antirheumatic effect scores of a drug and its random counterparts as

$$z = \frac{E - \bar{E}_r}{\Delta E_r}, \quad (4)$$

where E is the score of antirheumatic effect of a drug and \bar{E} and ΔE_r are the mean and standard deviation of the corresponding metric for the random counterparts. The higher the absolute value of a z -score, the more significant the difference.

2.6. Construction of RA-Associated PPI Network. We defined RA-associated PPI network as a subnetwork of human PPI network consisting of nodes with high RA effect score. We sorted RA's effect scores and collected the top 3% proteins. Then these proteins and their interactions were extracted from human PPI network to construct the RA-associated PPI network.

2.7. Topological Features of Nodes in RA-Associated PPI Network

Node Degree. The degree of a node in a network is the number of connections it has to other nodes.

k -Core. A k -core of a graph is a maximal connected subgraph in which every vertex is connected to at least k vertices in the subgraph [44]. A k -core subgraph of a graph can be generated by recursively deleting the vertices from the graph whose present degree is less than k . This process can be iterated to gradually zoom into the more connected parts of the network. A node located in higher-level core indicates its higher centrality in the network.

Betweenness Centrality. Betweenness centrality is a measure of a node's centrality in a network [45]. It is equal to the number of the shortest paths from all vertices to all others that pass through that node. Betweenness centrality is a more

useful measure (than just connectivity) of both the load and importance of a node. The betweenness centrality of a node v is given by the following equation:

$$g(v) = \sum_{s \neq v \neq t} \frac{\sigma_{st}(v)}{\sigma_{st}}, \quad (5)$$

where σ_{st} is the total number of shortest paths from node s to node t and $\sigma_{st}(v)$ is the number of those paths that pass through node v .

3. Results and Discussion

3.1. HLJDT's Targets in the Drug-Target Network for Anti-RA Drugs. It would be interesting to bridge HLJDT and existing FDA-approved anti-RA drugs via their common drug targets. This is expected to provide alternative insights for deducing the therapeutic mechanism of HLJDT. We constructed the drug-target network for the 32 FDA-approved anti-RA drugs included in DrugBank and their corresponding 51 targets and then mapped the 91 targets of HLJDT onto this network. As shown in Figure 1, this network shows that the active compounds of HLJDT share 5 targets (TNE, PTGS1, PTGS2, AHR, and IL1B) with 3 types of anti-RA drugs, in which PTGS1, PTGS2, and TNF are conformed therapeutic targets for nonsteroidal anti-inflammatory drugs (NSAID) and biological response modifiers, respectively, suggesting that the effect of HLJDT could be a combination of different classes of anti-RA agents.

On the other hand, ZHENG is the key pathological principle in the TCM theory to understand disease pathogenesis and guide the treatment, in which the "Cold" ZHENG and "Hot" ZHENG are the two key statuses which therapeutically direct the use of TCM recipe in the clinical practice. It has been found that two targets of HLJDT, TNF, and IL1B are main hub nodes in the Hot ZENG network, implying the key roles that these proteins play in diseases related to Hot ZENG [46]. Therefore, from TCM theory, HLJDT as a hot-cooling TCM formula clears "heat" and "poison" by targeting the hub nodes of Hot ZENG network.

3.2. Pathways Significantly Regulated by HLJDT. RA is a systemic autoimmune disease which causes recruitment and activation of inflammatory cells, synovial hyperplasia, and destruction of cartilage and bone. The course of RA is accompanied with the prolonged and enhanced activation of the immune system, leading to the disturbance of the balance between bone formation and bone resorption, which results in periarticular bone destruction. Multiple inflammatory signaling pathways such as cytokine pathway and Wnt signaling are known to strigger the generation of bone resorbing osteoclasts [47].

To deduce the possible pathways affected by HLJDT, we mapped HLJDT's targets onto KEGG pathways of basic biological process, including pathways in metabolism, organismal systems, cellular processes, environmental information processing, and genetic information processing. A pathway enrichment analysis was performed to identify the pathways significantly affected by HLJDT, and P values were computed

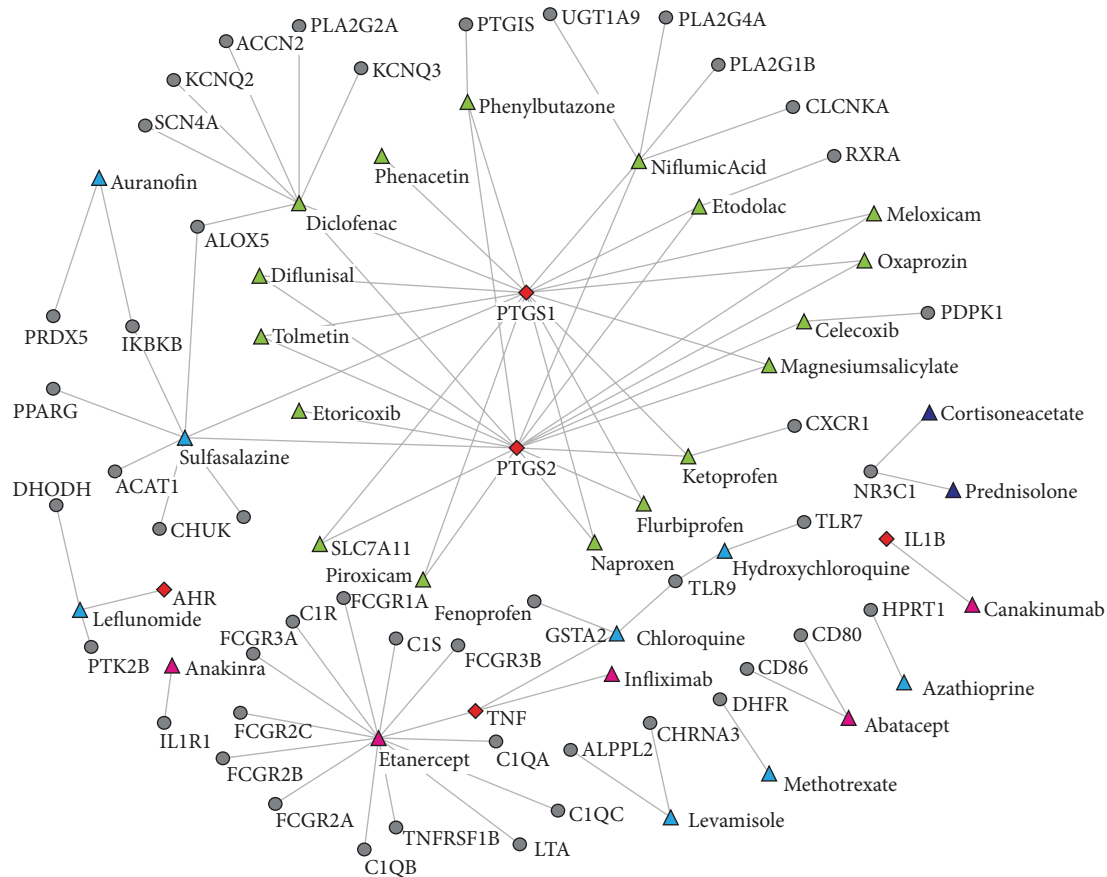


FIGURE 1: Drug-target network for all FDA approved anti-RA drugs in DrugBank. A target protein node and a drug node are linked if the protein is targeted by the corresponding drug. Triangles are drugs, while circles and diamonds are targets. Green: Nonsteroidal anti-inflammatory drugs; Shallow blue: Disease-modifying anti-rheumatic drugs; Dark blue: Glucocorticoids; Pink: Biological response modifiers; Red: Overlapped drug targets of FDA approved anti-RA drugs and HLJDT.

for each of the pathways with HLJDT's targets. Considering that diseases are higher level biological processes caused by the dysfunctions of basic biological processes, we did not include the KEGG pathway section of human diseases in this statistical analysis. The computation generated 32 pathways with values of $P < 0.01$, which may be regarded as key pathways affected by HLJDT (see Supplementary Table S4). In Table 1, we listed the 13 most significantly affected pathways with P value $< 10^{-4}$.

A central feature of RA is inflammation, one of the first responses of the immune system to infection or irritation. As listed in Table 1 and Supplementary Table S4, HLJDT acts on a large fraction of pathways in immune system. Some other pathways, although not classified into immune system in the KEGG database, have been known to be highly associated with the function of immune response, such as apoptosis [48] and MAPK signaling pathway [49]. Table 1 includes specifically several pathways related to pathogen recognition and inflammatory signalling in innate immune defences, in which the most important one is the Toll-like receptor (TLR) signalling pathway. The innate immune system relies on pattern recognition receptors (PRRs) to detect distinct pathogen-associated molecular patterns (PAMPs).

Upon PAMP recognition, PRRs trigger a number of different signal transduction pathways. The pathways induced by PRRs ultimately result in the expression of a variety of proinflammatory molecules, such as cytokines, chemokines, cell-adhesion molecules, and immunoreceptors, which together orchestrate the early host response to infection, mediate the inflammatory response, and also bridge the adaptive immune response together [50]. The family of TLRs is the major class of PRRs [50]. In addition, we also found that HLJDT regulates some proinflammatory molecule-involved pathways, such as the chemokine signaling pathway, natural killer-cell mediated cytotoxicity, and Fc epsilon RI signaling pathway. These pathways indicate the process of innate immune response in the progress of RA. On the other hand, it is known that B and T lymphocytes are responsible for the adaptive immune response [51]. Table 1 shows that HLJDT's targets are involved in B- and T-cell receptor signalling pathways, implying that they regulate the adaptive immune response of RA.

Another prominent feature of RA is enhanced osteoclast formation, which disturbs the balance between bone resorption and bone formation. The osteoclast differentiation pathway is a biological process that maintains bone density and structure through a balance of bone resorption by

TABLE 2: The anti-rheumatic effect scores of representative anti-RA western medicines.

Class of drug	Anti-RA drug	Targets	Effect score
Biological response modifiers	Etanercept	FCGR2C, TNFRSF1B, TNF, LTA, FCGR3B, FCGR3A, FCGR2B, FCGR2A, FCGR1A, CIS, CIR, CIQC, CIQB, CIQA	1.644
	Abatacept	CD86, CD80	0.609
	Infliximab	TNF	0.293
	Anakinra	IL1R1	0.159
DMARDs	Chloroquine	TLR9, TNF, GSTA2	0.463
	Sulfasalazine	SLC7A11, PTGS2 , PTGS1, PPARG, IKBKB , CHUK, ALOX5, ACAT1	0.454
	Hydroxychloroquine	TLR9, TLR7	0.173
	Leflunomide	PTK2B, DHODH, AHR	0.149
	Auranofin	PRDX5, IKBKB	0.14
	Leflunomide	PTK2B, DHODH, AHR	0.061
	Azathioprine	HPRT1	0.053
	Auranofin	PRDX5, IKBKB	0.05
NSAIDs	Flurbiprofen	PTGS2 , PTGS1	0.133
Glucocorticoids	Cortisone acetate	NR3C1	0.063

RA-associated disease genes are marked in bold characters.

compare the antirheumatic effect of HLJDT with those of FDA-approved anti-RA drugs, we chose several representatives from each of the four classes of anti-RA western medicines and then computed the network score for the antirheumatic effect of each drug, respectively. The initial vector x^0 of drug effect was defined as $x^0(v) = 1$ if node v is a drug target; otherwise, $x^0(v) = 0$.

As shown in Table 2, biological response modifiers and disease-modifying antirheumatic drugs (DMARDs) get averagely much higher scores than the other two classes of drugs, nonsteroidal, anti-inflammatory drugs (NSAID) and glucocorticoids. Actually, biological response modifiers are a new type of DMARDs [53], that is, biotech agents, while drugs categorized into the class of DMARDs are small molecular compounds. DMARDs target the part of the immune system that is leading to inflammation and joint damage. Thus they can often slow or stop the progression of RA. From Table 2, we can see that some DMARDs target directly on RA-associated genes such as TNE, CD80, and CD86 [54], supporting their higher antirheumatic effects.

Since RA is an inflammatory disease affecting the joints, it gets worse over time unless the inflammation is stopped or slowed. Thus anti-inflammatory is very important in the treatment. Glucocorticoids and NSAIDs are such class of drugs, in which glucocorticoids are steroidal strong anti-inflammatory drugs that can also block other immune responses while NSAIDs work by inhibiting enzymes that promote inflammation [55]. By reducing inflammation, anti-inflammatory agents help reduce swelling and pain. But they are not effective in reducing joint damage. Thus these drugs alone are not effective in treating the disease and they should be taken in combination with other rheumatoid arthritis medications [56].

We then computed the network score for the antirheumatic effect of HLJDT and its compounds, respectively. Unlike specifically designed drug molecules, HLJDT's active

TABLE 3: The anti-rheumatic effect scores of HLJDT and its main ingredients.

The component of HLJDT	Target numbers	Effect Score	Z-score
HLJDT	78	0.137	21.122
Berberine	52	0.061	9.635
Coptisine	6	0.0139	7.827
Wogonin	26	0.032	7.627
Baicalin	24	0.0215	4.377
Chlorogenic	1	0.001	1.914
Crocetin	1	0.001	1.457
Geniposide	5	0.002	0.468
Palmitine	1	0.0003	-0.011
Jatrorrhizine	1	0.0002	-0.260

compounds are naturally occurring substances; thus, their inhibition potency on targets could be much weaker. Therefore, we defined the initial vector x^0 of HLJDT's components as $x^0(v) = 0.01$ if node v is a target; otherwise, $x^0(v) = 0$. In this way, the antirheumatic effect score of HLJDT and its compounds are obtained as listed in Table 3. It can be seen that the effect score of each component is very small, while the whole HLJDT achieves a much higher effect score, which is in the same order as that of anti-inflammatory agents, including glucocorticoids and NSAIDs. This result quantitatively validates the suggestion that weak inhibition of multiple targets could orchestrate synergistic effect comparable to strong inhibition of a single target [57].

To investigate if the scores of HLJDT and its components suggest significant antirheumatic effect, for each drug, we generated 3000 random target sets, respectively, each of which included the same number of proteins as the drug's targets. The mean effect score and the standard deviation

TABLE 4: The network topology analysis about the overlapped genes and target proteins of HLJDT. It mainly included degree of distribution, betweenness, and K-core analysis.

Gene	Degree	Betweenness	K-coreness	RA disease gene	Targeted by component of HLJDT
IL6	84	0.059	20	Y	Berberine; coptisine; wogonin
IFNG	75	0.047	20	Y	Berberine
IL1B	63	0.029	20	Y	Berberine; coptisine
JUN	59	0.016	20	Y	Berberine; wogonin
IL8	58	0.026	20	Y	Berberine; wogonin
VEGFA	51	0.027	20	Y	Baicalein; berberine
FOS	51	0.024	20	Y	Baicalein; berberine
IL4	50	0.014	20	Y	Berberine
CCL2	41	0.006	20	Y	Berberine; wogonin
CXCL12	33	0.009	19	Y	Berberine
NOS2	9	1.35×10^{-5}	9	Y	Berberine; coptisine; wogonin
TNF	6	4.45×10^{-5}	6	Y	Berberine; coptisine; wogonin
RELA	56	0.012	20	N	Baicalein; berberine; wogonin
SRC	48	0.026	20	N	Baicalein
IL2RA	44	0.003	20	N	Berberine
MAPK1	42	0.016	20	N	Berberine
NFKBIA	42	0.008	20	N	Berberine
AKT1	42	0.010	20	N	Baicalein; wogonin
MMP9	38	0.0130	20	N	Baicalein
EGFR	35	0.004	20	N	Berberine
FN1	34	0.010	15	N	Wogonin
BCL2	33	0.004	20	N	Baicalein; berberine; geniposide; wogonin
PTGS2	30	0.004	20	N	Baicalein; berberine; coptisine; wogonin
RAC1	26	0.002	19	N	Berberine
APP	24	0.006	16	N	Berberine
TP53	24	0.007	18	N	Baicalein; berberine; wogonin
KDR	22	0.003	15	N	Wogonin
NFATC1	20	0.003	18	N	Baicalein

of the 3000 random counterparts were calculated. Hence the z -score of HLJDT and its compounds' antirheumatic effect score were obtained, which were listed in Table 3. The absolute value of z -score bigger than 3 usually suggests a statistically significant deviation between the actual value and the random ones. Thus the z -score 21.12 of HLJDT suggests its significant antirheumatic effect. The z -scores of four active compounds, berberine, coptisine, wogonin, and baicalein, are greater than 3.0, implying the antirheumatic effect of these single compounds. In fact, an earlier study has reported the effects of these compounds on RA [15–18].

3.4. HLJDT's Effects on RA-Associated PPI Network. To see how HLJDT acts on a protein-protein interaction network affected by RA, we first constructed an RA-associated PPI network, which consists of proteins with top 3% RA effect scores and their interactions. This network has 272 nodes and 2803 edges. Of the 163 RA-associated genes under study, 151 ones appear on this network, taking a percentage of 93.79%, suggesting a high correlation of this network to RA's biological process. Then the 91 target proteins of HLJDT were mapped onto this RA-associated PPI network and 28 of which were found on this network, in which half are targeted

by multiple components of HLJDT. As shown in Figure 3, HLJDT acts on 12 RA-associated genes, while some major causative genes of RA in this network, such as TNF and ILs are targeted by HLJDT's multiple components.

To understand the roles that HLJDT's targets play on the RA-associated PPI network, we analyzed three topological features which reflect node centrality in this network, including degree, betweenness, and k -core. The average degree and betweenness of nodes in this network are 20 and 0.0063, respectively, and the highest k -core index is 20. In Table 4 we listed the three topological measures of the 28 HLJDT's targets in this network. It can be seen that most targets located in the highest k -core and have degrees higher than the average, and the betweenness values of more than half targets are higher than the average, suggesting that HLJDT may interfere with RA by acting on proteins in the central locations of the disease network with multiple components.

4. Conclusions

This work studies HLJDT's antirheumatic effects from a network perspective. We have extracted data related to RA's pathogenesis and treatment—RA-associated genes from

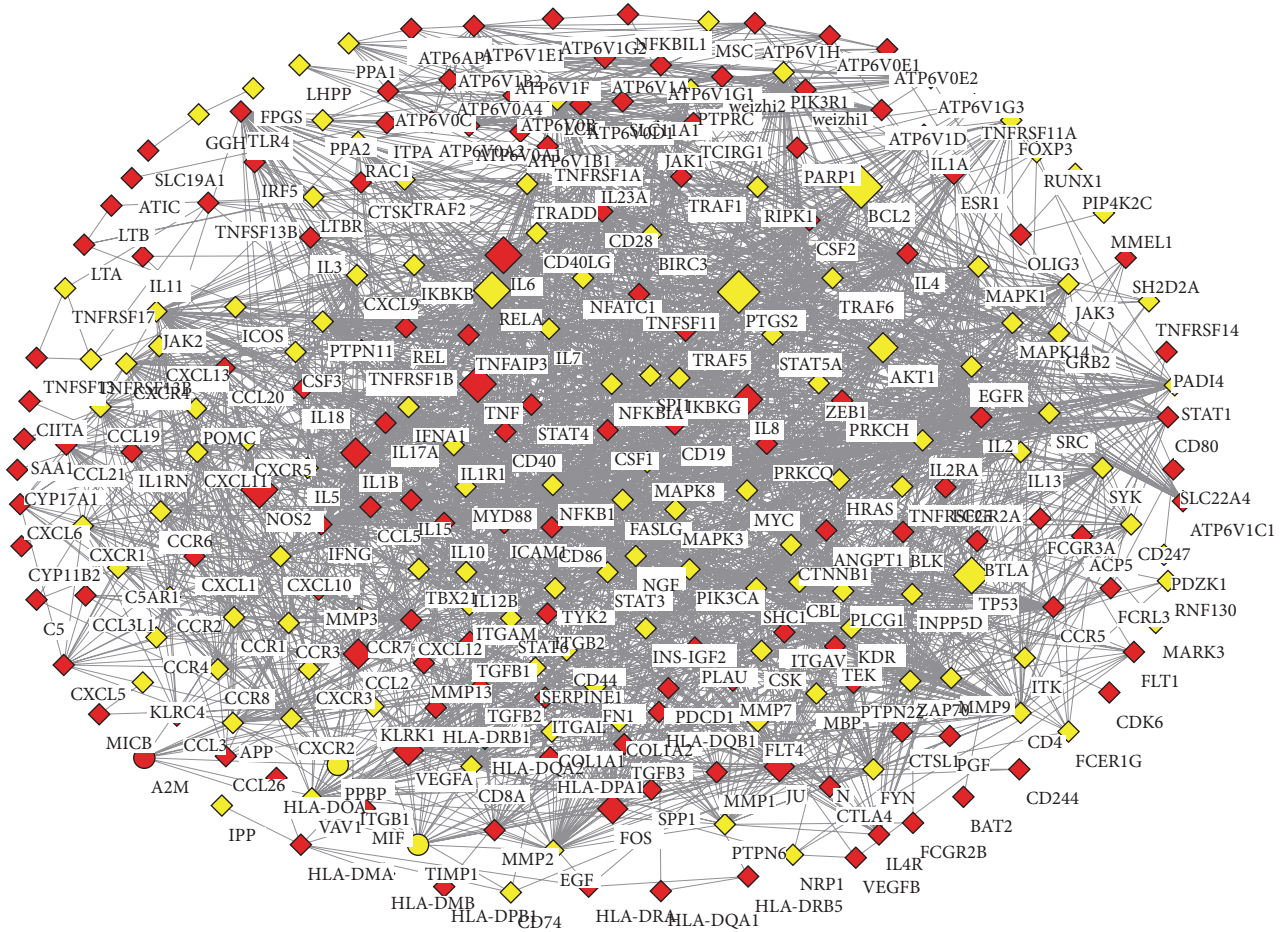


FIGURE 3: HLJDT's effects on RA-associated PPI network. This network consists of proteins with high RA effect score and their interactions. Diamond nodes are overlapped target proteins of HLJDT, while the size of a diamond node corresponds to the number of HLJDT's components targeting on this protein. Red: RA-associated genes; Yellow: other genes.

the OMIM database, GAD and KEGG pathway database, protein targets of FDA-approved anti-RA drugs, and HLJDT, respectively. First, we constructed drug-target network for FDA-approved anti-RA drugs. By mapping HLJDT's targets on this network, we found that 5 targets of HLJDT, TNF, PTGS1, PTGS2, AHR, and IL1B, exist in this network. Then we mapped HLJDT's targets onto KEGG pathways of basic biological process and identified 32 pathways enriched with HLJDT's targets, which include pathways in immune system and bone formation. These pathways are considered as key pathways affected by HLJDT. In addition, 12 targets were found involved in the KEGG RA pathway. These findings indicate that HLJDT could intervene in the biological process of the occurrence and development of RA by targeting on multiple targets associated with immune function and bone modeling, and it may function as a combination of different categories of anti-RA drugs.

We also quantitatively analyzed the antirheumatic effect of HLJDT and compared it with those of FDA-approved anti-RA drugs through a network based antirheumatic effect score. It is found that the antirheumatic effect score of each HLJDT's component is very low, while the whole HLJDT

achieves a much higher effect score, which is comparable to that of FDA approved anti-inflammatory agents. This result suggests a synergistic antirheumatic effect of HLJDT achieved by its multiple components acting on multiple targets.

At last, we conducted topological analysis on the RA-associated PPI network to investigate the roles HLJDT's targets play on this network. We found that most targets own large degree, betweenness, and high k -core index in the network, suggesting that HLJDT may interfere with RA by acting on proteins in the central locations of the disease network with multiple components.

In TCM theory, RA could be related to Cold ZHENG or Hot ZHENG [58]. Our study on drug-target network and pathways also found that HLJDT targets on hub nodes and main pathway in the Hot ZENG network, suggesting that HLJDT could be applied as adjuvant treatment for Hot-ZENG-related RA. Further clinical trial needs to be conducted to confirm this.

This work applied network approach to explain HLJDT's antirheumatic effect. It may shed new lights on the study about the TCM pharmacology and promote the development of nationality medicine.

Conflict of Interests

The authors declare that they have no conflict of interests.

Acknowledgments

This research was supported by the National Natural Science Foundation of China (10971227, 61372194, 81260672, and 81230090) and FP7-PEOPLE-IRSES-2008 (TCMCANCER Project 230232).

References

- [1] C. Salliot and D. van der Heijde, "Long-term safety of methotrexate monotherapy in patients with rheumatoid arthritis: a systematic literature research," *Annals of the Rheumatic Diseases*, vol. 68, no. 7, pp. 1100–1104, 2009.
- [2] N. Alcorn, S. Saunders, and R. Madhok, "Benefit-risk assessment of leflunomide: an appraisal of leflunomide in rheumatoid arthritis 10 years after licensing," *Drug Safety*, vol. 32, no. 12, pp. 1123–1134, 2009.
- [3] D. Schaffer, T. Florin, C. Eagle et al., "Risk of serious NSAID-related gastrointestinal events during long-term exposure: a systematic review," *Medical Journal of Australia*, vol. 185, no. 9, pp. 501–506, 2006.
- [4] P. A. Scott, G. H. Kingsley, C. M. Smith, E. H. Choy, and D. L. Scott, "Non-steroidal anti-inflammatory drugs and myocardial infarctions: comparative systematic review of evidence from observational studies and randomised controlled trials," *Annals of the Rheumatic Diseases*, vol. 66, no. 10, pp. 1296–1304, 2007.
- [5] Y. Ohta, E. Sasaki, K. Nishida et al., "Inhibitory effect of Oren-gedoku-to (Huanglian-Jie-Du-Tang) extract on hepatic triglyceride accumulation with the progression of carbon tetrachloride-induced acute liver injury in rats," *Journal of Ethnopharmacology*, vol. 61, no. 1, pp. 75–80, 1998.
- [6] N. Ikarashi, M. Tajima, K. Suzuki et al., "Inhibition of preadipocyte differentiation and lipid accumulation by Orengedokuto treatment of 3T3-L1 cultures," *Phytotherapy Research*, vol. 26, no. 1, pp. 91–100, 2012.
- [7] Y.-L. Hsu, P.-L. Kuo, T.-F. Tzeng et al., "Huang-Lian-Jie-Du-Tang, a traditional Chinese medicine prescription, induces cell-cycle arrest and apoptosis in human liver cancer cells in vitro and in vivo," *Journal of Gastroenterology and Hepatology*, vol. 23, no. 7, part 2, pp. e290–e299, 2008.
- [8] J. Xu, Y. Murakami, K. Matsumoto et al., "Protective effect of Oren-gedoku-to (Huang-Lian-Jie-Du-Tang) against impairment of learning and memory induced by transient cerebral ischemia in mice," *Journal of Ethnopharmacology*, vol. 73, no. 3, pp. 405–413, 2000.
- [9] H. Zeng, X. Liu, S. Dou et al., "Huang-Lian-Jie-Du-Tang exerts anti-inflammatory effects in rats through inhibition of nitric oxide production and eicosanoid biosynthesis via the lipoxigenase pathway," *Journal of Pharmacy and Pharmacology*, vol. 61, no. 12, pp. 1699–1707, 2009.
- [10] H. Zeng, S. Dou, J. Zhao et al., "The inhibitory activities of the components of Huang-Lian-Jie-Du-Tang (HLJDT) on eicosanoid generation via lipoxigenase pathway," *Journal of Ethnopharmacology*, vol. 135, no. 2, pp. 561–568, 2011.
- [11] R. Yue, L. Zhao, Y. Hu et al., "Rapid-resolution liquid chromatography TOF-MS for urine metabolomic analysis of collagen-induced arthritis in rats and its applications," *Journal of Ethnopharmacology*, vol. 145, no. 2, pp. 465–475, 2013.
- [12] R. Yue, L. Zhao, Y. Hu et al., "Metabolomic study of collagen-induced arthritis in rats and the interventional effects of Huang-Lian-Jie-Du-Tang, a traditional Chinese medicine," *Evidence-Based Complementary and Alternative Medicine*, vol. 2013, Article ID 439690, 12 pages, 2013.
- [13] Y. Hu, Z. Hu, S. Wang et al., "Protective effects of Huang-Lian-Jie-Du-Tang and its component group on collagen induced arthritis in rats," *Journal of Ethnopharmacology*, 2013.
- [14] S. Dou, L. Liu, P. Jiang, W. Zhang, and R. Liu, "LC-DAD and LC-ESI-MS chromatographic fingerprinting and quantitative analysis for evaluation of the quality of Huang-Lian-Jie-Du-Tang," *Chromatographia*, vol. 69, no. 7-8, pp. 659–664, 2009.
- [15] X.-H. Wang, S.-M. Jiang, and Q.-W. Sun, "Effects of berberine on human rheumatoid arthritis fibroblast-like synoviocytes," *Experimental Biology and Medicine*, vol. 236, no. 7, pp. 859–866, 2011.
- [16] J.-W. Lee, A. Iwashashi, S.-I. Hasegawa et al., "Coptisine inhibits RANKL-induced NF- κ B phosphorylation in osteoclast precursors and suppresses function through the regulation of RANKL and OPG gene expression in osteoblastic cells," *Journal of Natural Medicines*, vol. 66, no. 1, pp. 8–16, 2012.
- [17] C.-M. Lin, H. Chang, Y.-H. Chen, S. Y. Li, I.-H. Wu, and J.-H. Chiu, "Protective role of wogonin against lipopolysaccharide-induced angiogenesis via VEGFR-2, not VEGFR-1," *International Immunopharmacology*, vol. 6, no. 11, pp. 1690–1698, 2006.
- [18] Y. Kimura, N. Matsushita, and H. Okuda, "Effects of baicalin isolated from *Scutellaria baicalensis* on interleukin 1β - and tumor necrosis factor α -induced adhesion molecule expression in cultured human umbilical vein endothelial cells," *Journal of Ethnopharmacology*, vol. 57, no. 1, pp. 63–67, 1997.
- [19] K.-I. Goh, M. E. Cusick, D. Valle et al., "The human disease network," *Proceedings of the National Academy of Sciences of the United States of America*, vol. 104, no. 21, pp. 8685–8690, 2007.
- [20] Z.-P. Liu, Y. Wang, X.-S. Zhang, and L. Chen, "Network-based analysis of complex diseases," *IET Systems Biology*, vol. 6, no. 1, pp. 22–33, 2012.
- [21] J. Zhao, S. H. Lee, M. Huss, and P. Holme, "The network organization of cancer-associated protein complexes in human tissues," *Scientific Reports*, vol. 3, article 1583, 2013.
- [22] J. Zhao, J. Chen, T.-H. Yang, and P. Holme, "Insights into the pathogenesis of axial spondyloarthritis from network and pathway analysis," *BMC Systems Biology*, vol. 6, supplement 1, article S4, 2012.
- [23] J. Zhao, P. Jiang, and W. Zhang, "Molecular networks for the study of TCM pharmacology," *Briefings in Bioinformatics*, vol. 11, no. 4, pp. 417–430, 2009.
- [24] S. Li and B. Zhang, "Traditional Chinese medicine network pharmacology: theory, methodology and application," *Chinese Journal of Natural Medicines*, vol. 11, no. 2, pp. 110–120, 2013.
- [25] P. Csermely, T. Korcsmaros, H. J. M. Kiss, G. London, and R. Nussinov, "Structure and dynamics of molecular networks: a novel paradigm of drug discovery: a comprehensive review," *Pharmacology & Therapeutics*, vol. 138, no. 3, pp. 333–408, 2013.
- [26] G. Chen, J. Miao, C. Lv, and A.-P. Lu, "Prediction of therapeutic mechanisms of tripterygium wilfordii in rheumatoid arthritis using text mining and network-based analysis," in *Proceedings of the IEEE International Symposium on IT in Medicine & Education (ITME '09)*, pp. 115–119, Jinan, China, August 2009.
- [27] S. Li, B. Zhang, D. Jiang, Y. Wei, and N. Zhang, "Herb network construction and co-module analysis for uncovering the combination rule of traditional Chinese herbal formulae," *BMC Bioinformatics*, vol. 11, supplement 11, article S6, 2010.

- [28] J. Colinge, U. Rix, K. L. Bennett, and G. Superti-Furga, "Systems biology analysis of protein-drug interactions," *Proteomics*, vol. 6, no. 1-2, pp. 102–116, 2012.
- [29] A. Hamosh, A. F. Scott, J. S. Amberger, C. A. Bocchini, and V. A. McKusick, "Online Mendelian Inheritance in Man (OMIM), a knowledgebase of human genes and genetic disorders," *Nucleic Acids Research*, vol. 33, supplement 1, pp. D514–D517, 2005.
- [30] K. G. Becker, K. C. Barnes, T. J. Bright, and S. A. Wang, "The Genetic Association Database," *Nature Genetics*, vol. 36, no. 5, pp. 431–432, 2004.
- [31] M. Kanehisa and S. Goto, "KEGG: kyoto encyclopedia of genes and genomes," *Nucleic Acids Research*, vol. 28, no. 1, pp. 27–30, 2000.
- [32] D. S. Wishart, C. Knox, A. C. Guo et al., "DrugBank: a comprehensive resource for in silico drug discovery and exploration," *Nucleic Acids Research*, vol. 34, pp. D668–D672, 2006.
- [33] H. Ye, L. Ye, H. Kang et al., "HIT: linking herbal active ingredients to targets," *Nucleic Acids Research*, vol. 39, supplement 1, pp. D1055–D1059, 2011.
- [34] L. J. Jensen, M. Kuhn, M. Stark et al., "STRING 8—a global view on proteins and their functional interactions in 630 organisms," *Nucleic Acids Research*, vol. 37, supplement 1, pp. D412–D416, 2009.
- [35] M. A. Yıldırım, K.-I. Goh, M. E. Cusick, A.-L. Barabási, and M. Vidal, "Drug-target network," *Nature Biotechnology*, vol. 25, no. 10, pp. 1119–1126, 2007.
- [36] R. K. Curtis, M. Orešič, and A. Vidal-Puig, "Pathways to the analysis of microarray data," *Trends in Biotechnology*, vol. 23, no. 8, pp. 429–435, 2005.
- [37] J. Zhao, G.-H. Ding, L. Tao et al., "Modular co-evolution of metabolic networks," *BMC Bioinformatics*, vol. 8, article 311, 2007.
- [38] F. Göbel and A. A. Jagers, "Random walks on graphs," *Stochastic Processes and Their Applications*, vol. 2, no. 4, pp. 311–336, 1974.
- [39] H. Tong, C. Faloutsos, and J.-Y. Pan, "Random walk with restart: fast solutions and applications," *Knowledge and Information Systems*, vol. 14, no. 3, pp. 327–346, 2008.
- [40] M. S. Erten, *Network Based Prioritization of Disease Genes*, Case Western Reserve University, 2009.
- [41] T. R. Burkard, U. Rix, F. P. Breitwieser, G. Superti-Furga, and J. Colinge, "A computational approach to analyze the mechanism of action of the kinase inhibitor bafetinib," *PLoS Computational Biology*, vol. 6, no. 11, Article ID e1001001, 2010.
- [42] J. Colinge, U. Rix, and G. Superti-Furga, "Novel global network scores to analyze kinase inhibitor profiles," in *Proceedings of the 4th International Conference on Computational Systems Biology*, Suzhou, China, 2010.
- [43] J. Zhao, P. Yang, F. Li et al., "Therapeutic effects of astragaloside IV on myocardial injuries: multi-target identification and network analysis," *PLoS ONE*, vol. 7, no. 9, Article ID e44938, 2012.
- [44] S. Wuchty and E. Almaas, "Peeling the yeast protein network," *Proteomics*, vol. 5, no. 2, pp. 444–449, 2005.
- [45] M. E. J. Newman, "The structure and function of complex networks," *SIAM Review*, vol. 45, no. 2, pp. 167–256, 2003.
- [46] S. Li, Z. Q. Zhang, L. J. Wu, X. G. Zhang, Y. D. Li, and Y. Y. Wang, "Understanding ZHENG in traditional Chinese medicine in the context of neuro-endocrine-immune network," *IET Systems Biology*, vol. 1, no. 1, pp. 51–60, 2007.
- [47] S. Herman, G. Krönke, and G. Schett, "Molecular mechanisms of inflammatory bone damage: emerging targets for therapy," *Trends in Molecular Medicine*, vol. 14, no. 6, pp. 245–253, 2008.
- [48] T. N. Mayadas and X. Cullere, "Neutrophil β_2 integrins: moderators of life or death decisions," *Trends in Immunology*, vol. 26, no. 7, pp. 388–395, 2005.
- [49] M. S. Lee and Y.-J. Kim, "Signaling pathways downstream of pattern-recognition receptors and their cross talk," *Annual Review of Biochemistry*, vol. 76, pp. 447–480, 2007.
- [50] T. H. Mogensen, "Pathogen recognition and inflammatory signaling in innate immune defenses," *Clinical Microbiology Reviews*, vol. 22, no. 2, pp. 240–273, 2009.
- [51] A. Bauch and G. Superti-Furga, "Charting protein complexes, signaling pathways, and networks in the immune system," *Immunological Reviews*, vol. 210, no. 1, pp. 187–207, 2006.
- [52] S. R. Goldring and M. B. Goldring, "Eating bone or adding it: the Wnt pathway decides," *Nature Medicine*, vol. 13, no. 2, pp. 133–134, 2007.
- [53] P. A. Rosandich, J. T. Kelley III, and D. L. Conn, "Perioperative management of patients with rheumatoid arthritis in the era of biologic response modifiers," *Current Opinion in Rheumatology*, vol. 16, no. 3, pp. 192–198, 2004.
- [54] J. M. Kremer, M. Dougados, P. Emery et al., "Treatment of rheumatoid arthritis with the selective costimulation modulator abatacept: twelve-month results of a phase IIb, double-blind, randomized, placebo-controlled trial," *Arthritis & Rheumatism*, vol. 52, no. 8, pp. 2263–2271, 2005.
- [55] H. M. Imseis, P. D. Zimmerman, P. Samuels, and D. A. Kniss, "Tumour necrosis factor- α induces cyclo-oxygenase-2 gene expression in first trimester trophoblasts: suppression by glucocorticoids and NSAIDs," *Placenta*, vol. 18, no. 7, pp. 521–526, 1997.
- [56] M. C. Genovese, J. D. McKay, E. L. Nasonov et al., "Interleukin-6 receptor inhibition with tocilizumab reduces disease activity in rheumatoid arthritis with inadequate response to disease-modifying antirheumatic drugs: the tocilizumab in combination with traditional disease-modifying antirheumatic drug therapy study," *Arthritis & Rheumatism*, vol. 58, no. 10, pp. 2968–2980, 2008.
- [57] P. Csermely, V. Ágoston, and S. Pongor, "The efficiency of multi-target drugs: the network approach might help drug design," *Trends in Pharmacological Sciences*, vol. 26, no. 4, pp. 178–182, 2005.
- [58] S. Li, "Advances in TCM symptomatology of rheumatoid arthritis," *Journal of Traditional Chinese Medicine*, vol. 22, no. 2, pp. 137–142, 2002.

Research Article

Systemic Revealing Pharmacological Signalling Pathway Networks in the Hippocampus of Ischaemia-Reperfusion Mice Treated with Baicalin

Haixia Li,¹ Yingying Zhang,² Yanan Yu,² Bing Li,² YinYing Chen,²
Hongli Wu,² Jingtao Wang,¹ Jun Li,¹ Xingjiang Xiong,¹ Qiongyong He,¹
Jinzhou Tian,³ Zhong Wang,² and Jie Wang¹

¹ Department of Cardiology, Guang'anmen Hospital, China Academy of Chinese Medical Sciences, Beixiang 5, Xicheng District, Beijing 100053, China

² Institute of Basic Research in Clinical Medicine, China Academy of Chinese Medical Sciences, Dongzhimen, Beijing 100700, China

³ Geriatric Department, Dongzhimen Hospital Affiliated to Beijing University of Chinese Medicine, Dongzhimen, Beijing 100007, China

Correspondence should be addressed to Zhong Wang; zhonw@vip.sina.com and Jie Wang; wangjie0103@sohu.com

Received 17 May 2013; Accepted 26 July 2013

Academic Editor: Wei Jia

Copyright © 2013 Haixia Li et al. This is an open access article distributed under the Creative Commons Attribution License, which permits unrestricted use, distribution, and reproduction in any medium, provided the original work is properly cited.

Background. Baicalin (BA) exhibits ill understood neuroprotective, anti-inflammatory, and antioxidative effects in brain injury. **Objective.** To identify the differential network pathways associated with BA-related biological effects. **Methods.** MCAO-induced mice received BA 5 mg/Kg (BA group). Controls received vehicle only. Following ischaemia-reperfusion, ArrayTrack analysed the whole genome microarray of hippocampal genes, and MetaCore analysed differentially expressed genes. **Results.** Four reversing pathways were common to BA and controls, but only 6 were in the top 10 for BA. Three of the top 5 signalling pathways in controls were not observed in BA. BA treatment made absent 3 pathways of the top 5 signalling pathways from the top 5 in controls. There were 2 reversing pathways between controls and BA that showed altered gene expression. Controls had 6 networks associated with cerebral ischaemia. After BA treatment, 9 networks were associated with cerebral ischaemia. Enrichment analysis identified 10 significant biological processes in BA and controls. Of the 10 most significant molecular functions, 7 were common to BA and controls, and only 3 occurred in BA. BA and controls had 7 significant cellular components. **Conclusions.** This study showed that the clinical effectiveness of BA was based on the complementary effects of multiple pathways and networks.

1. Introduction

The biochemical and molecular mechanisms underlying cerebral ischaemia, such as reperfusion injuries (common in stroke patients), alterations in multiple genes, proteins, and mechanistic pathways, cumulatively lead to progressive neurological damage and cell death [1]. Cerebral ischaemia mechanisms involve mitogen-activated protein kinases (MAPKs), phosphoinositide 3-kinase/protein kinase B, nuclear factor kappa-light-chain-enhancer of activated B cells, cAMP response element-binding protein, Janus kinase-signal transducer and activator of transcription (STAT) pathway, WNT/beta-catenin pathway, and excessive inflammatory response [2–7]. Elucidating details of these complex mechanisms are difficult despite recent improvements in research

technologies, such as reverse pharmacology. A better understanding is however critical to facilitate development of novel therapeutic agents.

Baicalin (5,6-dihydroxy-7-O-glucuronide flavone) (BA) is a flavonoid compound, extracted from the dry dicotyledonous skullcap root commonly used in traditional Chinese and clinical medicine to treat stroke [1]. BA exerts neuroprotective, anti-inflammatory, and antioxidative effects in a variety of animal models of brain injury [8–14], but its mechanism of action is not well understood. Initial studies of BA's mechanism of action focused on differential gene expression. By identifying many potentially up- or downregulated candidate genes, these studies produced complex and disparate mechanistic data. Genes studied included those involved in TLR2/4 signalling [15, 16], apoptosis [1, 12, 17], reactive

oxygen species scavenging [12], GABAergic signalling [11], calcium signalling, and tight junction proteins in the blood-brain barrier [17, 18].

Several contemporary analytical tools have been developed to determine trends and to assimilate and visualize molecular interaction data, such as Ingenuity Pathway Analysis (IPA) [19] and the Kyoto Encyclopaedia of Genes and Genomes (KEGG) [20] databases. These tools, coupled with computerized databases, allow a better understanding of the gene interactions that cumulatively affect important biological pathways and have analysed the influence of BA on gene molecular functions and network path functions. In a study of a cDNA microarray of 374 genes, ArrayTrack and IPA pathway analysis showed that the genes influenced by BA participated in calcium regulation, cell signal transduction, cell proliferation, and antiapoptotic mechanisms [21]. In a study of a microarray of 16464 genes, ArrayTrack and KEGG pathway analysis showed that BA affected expression of 361 distinct genes was associated with activation of 76 pathways, including those regulating extracellular matrix receptors and ATP-binding cassette transporters [22]. Despite increases in available raw data, limited computing power and small databases have reduced the ability of research efforts to establish associations between numerous and complex cellular mechanisms following ischemic events involving many cell types and pathways. An analysis of the full array of mechanisms that occur following ischaemia requires more advanced software solutions, such as larger datasets and more advanced data retrieval methods. GeneGo MetaCore software [23] uses a unique, proprietary, high-quality, manually curated database of human protein-protein, protein-DNA, and protein-RNA interactions. Unlike previous software systems, MetaCore integrates information on signalling and metabolic pathways and the effects of bioactive molecules [24]. Another benefit is that data are presented within an intuitive graphical model, which allows transcriptomics data to be visualized [25]. MetaCore software was used to identify the differential pathway networks of BA in a rodent model of cerebral ischaemia-reperfusion injury. A microarray of 16,463 genes, analyzed with combined ArrayTrack and MetaCore systems, identified differential pathway networks from gene expression profiles in the hippocampus of mice with cerebral ischaemia following BA administration.

2. Methods

2.1. Animal Subjects. There were 144 healthy, specific pathogen-free, adult male Kunming mice aged 12 weeks of age and weighing 38 to 48 g. They were housed at 25°C with a 12-hour light/dark cycle and randomly divided into 3 groups of 48 mice (BA group, vehicle group, and sham group). Animal use protocols were reviewed and approved by the Ethics Review Committee for Animal Experimentation of the China Academy of Chinese Medical Sciences, and all animal experiments were conducted in accordance with the Prevention of Cruelty to Animals Act of 1986 and National Institute of Health guidelines for care and use of experimental laboratory animals.

2.2. Middle Cerebral Artery Occlusion. For the BA and vehicle groups, mice were anaesthetized with 2% napental (4 mg/Kg, intraperitoneal) then underwent surgery to induce middle cerebral artery occlusion. The middle cerebral artery was ligated with an intraluminal filament for 1.5 hours and then reperfused for 24 hours. For the sham group, the external carotid artery was surgically prepared for insertion of the filament, but no filament was inserted. During the experimental procedures, blood pressure, blood gas level, and glucose levels were monitored. Rectal temperature was maintained at 37.0 to 37.5°C with a heating pad, and body temperature was maintained at 37°C with a thermostatically controlled infrared lamp. Brain temperature was maintained at 36 to 37°C and monitored with a 29-gauge thermocouple in the right corpus striatum and a temperature-regulating lamp. An electroencephalogram was taken to ensure isoelectricity during the ischemic period. Operational success was determined based on infarct volume and subsequent mouse behaviour.

2.3. Drug Administration. BA group mice were administered 5 mg/Kg BA, dissolved in 0.9% normal saline immediately prior to use, by injection into the tail vein 1.5 hours after focal cerebral ischaemia induction. Vehicle and sham group mice were administered only 0.9% normal saline (2 mL/Kg). All BA preparations were standard, validated using fingerprint chromatography, and obtained from the China Natural Institute for the Control of Pharmaceutical and Biological Products or the Beijing University of Traditional Chinese Medicine.

2.4. RNA Isolation. The left hippocampus of 9 mice in each group was homogenized in TRIzol Reagent (Invitrogen, USA), and total RNA was isolated according to the manufacturer's instructions. RNA was further purified to remove genomic DNA contamination and concentrated using an RNeasy micro kit (Qiagen, Valencia, CA, USA). The RNA quality was determined from the 26S/18S ratio, using a Bioanalyzer microchip device (Agilent, Palo Alto, CA, USA).

2.5. Microarrays. A mouse brain array (Boao Capital, Beijing, China) and a microarray chip for the whole genome array for mice containing 16,463 oligoclones (Incyte Genomics, Santa Clara, CA, USA) were used for gene expression profiling. On each chip, duplicate clones were printed, generating 4 technical replicates per clone. A single intensity value for each clone was generated by averaging quadruplet measurements after smoothing spline normalization. All clones were verified by DNA sequencing. RNA from the vehicle group was pooled and labelled with Cy3, and RNA from other groups was labelled with Cy5. Microarrays were hybridized, washed, and scanned according to standard protocols. These procedures were repeated for each group, at least as biological triplicates and technical quadruplets.

2.6. Microarray Data Analysis. All experimental data were uploaded to the ArrayTrack system. Experimental analysis was based on the Minimum Information about Microarray Experiment Guidelines and the Microarray Quality Control Project, and the results were submitted to the Array Express

database. All microarray data were normalized by locally weighted linear regression to reduce experimental variability (smoothing factor, 0.2; robustness iterations, 3). One-way analysis of variance and significance analysis of microarrays were used to compare means of the altered genes between the sham and vehicle groups and between BA and vehicle groups. Genes with a $P < 0.05$ and a >1.5 -fold change were further analysed. An increase in expression level >1.5 -fold or a decrease <0.5 -fold was considered to indicate upregulation or downregulation, respectively. All statistically significant differentially expressed genes were uploaded into the GeneGo system [26] and gene identity numbers were uploaded to MetaCore to determine their associated networks. A cut-off value was set to identify molecules with significantly differentially regulated expressions, and these were labelled as Network Eligible molecules.

Networks of Network Eligible molecules were algorithmically generated based on connectivity. Right-tailed Fisher's exact test was used to calculate P values for the probability that each biological function assigned to a network was due to chance alone. The significance of association between these genes and the canonical pathway was measured in the following 2 ways:

- (1) a ratio calculated using the number of genes from the dataset that maps the pathway divided by the total number of genes that map to the canonical pathway;
- (2) a P value, calculated by Fischer's exact test, determining the probability that the association between the genes and canonical pathway was explained by chance alone. The level of statistical significance was set at $P < 0.05$. Finally, canonical pathways with $P < 0.05$ and a fold change >1.5 were screened and analyzed.

2.7. Network Calculation of Enrichment. Enrichment analysis is a computational method for identifying the functional distribution of genomic/proteomic expression profiles and significantly enriched functional categories [26]. This method is helpful to understand the overall functions of differentially expressed genes and so supply fundamental bioinformatics information. Biological processes, subcellular locations, and molecular function distributions of differentially expressed genes were computed using MetaCore based on Gene Ontology annotations [27], and the network distribution of selected genes was computed using MetaCore based on GeneGo network ontologies.

Auto Expand adds objects until a dense network is created, allowing neighbouring interactions and objects surrounding selected nodes to be visualized. Using the original input list, Analyze Network analyzes the network modularity for selected genes, thus creating a large network which can be subdivided it into smaller subnetworks sets. The resulting networks are evaluated and ranked according to their statistical significance (P values). This high trust P value calculation is also used to evaluate the network's relevance to Gene Ontology Biological Processes classification. The advantage of using this network algorithm is that it may find a well-connected cluster of root nodes without any predefined restrictions and thereby offer more flexibility in

identifying possible connections. These interactions are then assigned to specific biological processes, cellular components, and/or molecular functions to further characterize the underlying condition and provide insight into the underlying mechanisms.

2.8. Statistical Analysis. Significance of enrichment and pathways was calculated using scores produced using the Expression Analysis Systematic Explorer software (National Institute of Health, USA) [28], which employs modified Fisher's exact test [29]. To calculate pathways, the statistical significance of ontological matches was calculated for the probability of a match occurring by chance, taking database size into account. Lower significance, which denoted higher ratings for matched terms, was expected as the number of genes/proteins belonging to a single process/pathway increased, with $P < 0.1$ considered statistically significant.

3. Results

3.1. Pharmacodynamic Results. BA was effective in reducing ischemic infarction volume compared with the vehicle group in our previous study ($P < 0.05$) [25].

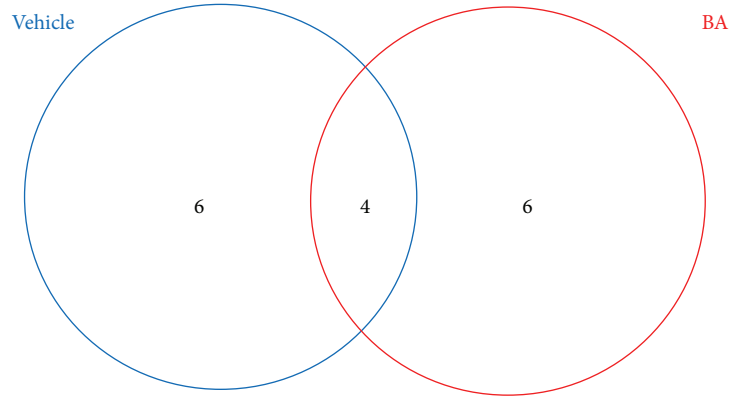
3.2. Pathway Map Analysis of Altered Genes. The MetaCore pathway map analysis of the selected genes was used to identify the 10 most statistically significant pathways, based on calculated P values (see Supplementary Table 5A available online at <http://dx.doi.org/10.1155/2013/630723>). Four reversing pathways were common to both BA and vehicle groups, but only 6 pathways were among the top 10 for only the BA group: "cytoskeleton remodeling: TGF, WNT, and cytoskeletal remodeling"; "development: VEGF signalling via VEGFR2-generic cascades"; "development: TGF-beta-dependent induction of EMT via MAPK"; "transcription: transcription factor Tubby signalling pathways"; "cytoskeleton remodelling: cytoskeleton remodeling"; and "normal and pathological TGF beta-mediated regulation of cell proliferation" (Figure 1). A diagram of BA action in targeting pathways involved in cell apoptosis, and death is shown in Figure 2.

Three of the top 5 most statistically significant signalling pathways in the vehicle group were not observed in the BA group (Figure 1, Supplementary Tables 1A, 1B). Notably, in the "development: G-protein mediated regulation of MAPK-ERK signalling" pathway, 8 genes were upregulated. In the "reproduction: GnRH signalling" pathway, 9 genes were upregulated, while ATF3 was downregulated. In the "development: thyroliberin signalling" pathway, 6 genes were upregulated.

BA treatment also produced 3 of the top 5 most statistically significant signalling pathways, and these were absent from the top 5 in the vehicle group. In the "cytoskeleton remodeling: TGF, WNT, and cytoskeletal remodeling" pathway, 11 genes were upregulated. In the "development: Flt3 signalling" pathway, 8 genes were upregulated. In the "development: VEGF signalling via VEGFR2-generic cascades" pathway, 8 genes were upregulated.

There were 2 reversing pathways between the vehicle and BA groups that nonetheless showed altered gene expression. In the "neurophysiological process: NMDA-dependent

1. Cytoskeleton remodeling_TGF, WNT and cytoskeletal remodelling
2. Development_VEGF signaling via VEGFR2-generic cascades
3. Development_TGF-beta-dependent induction of EMT via MAPK
4. Transcription_transcription factor tubby signalling pathways
5. Cytoskeleton remodeling_cytoskeleton remodeling
6. Normal and pathological TGF-beta-mediated regulation of cell proliferation



1. Development_G-proteins mediated regulation MAPK-ERK signaling
2. Reproduction_GnRH signaling
3. Development_thyroliberin signaling
4. Apoptosis and survival_TNFR1 signaling pathway
5. Development_PIP3 signaling in cardiac myocytes
6. Signal transduction_PKA signaling

1. Neurophysiological process_NMDA-dependent postsynaptic long-term potentiation in CA1 hippocampal neurons
2. G-protein signaling_regulation of p38 and JNK signaling mediated by G-proteins
3. Development_Flt3 signaling
4. G-protein signaling_G-protein alpha-i signaling cascades 4

FIGURE 1: Pathway maps associated with regulated genes in both BA and vehicle groups.

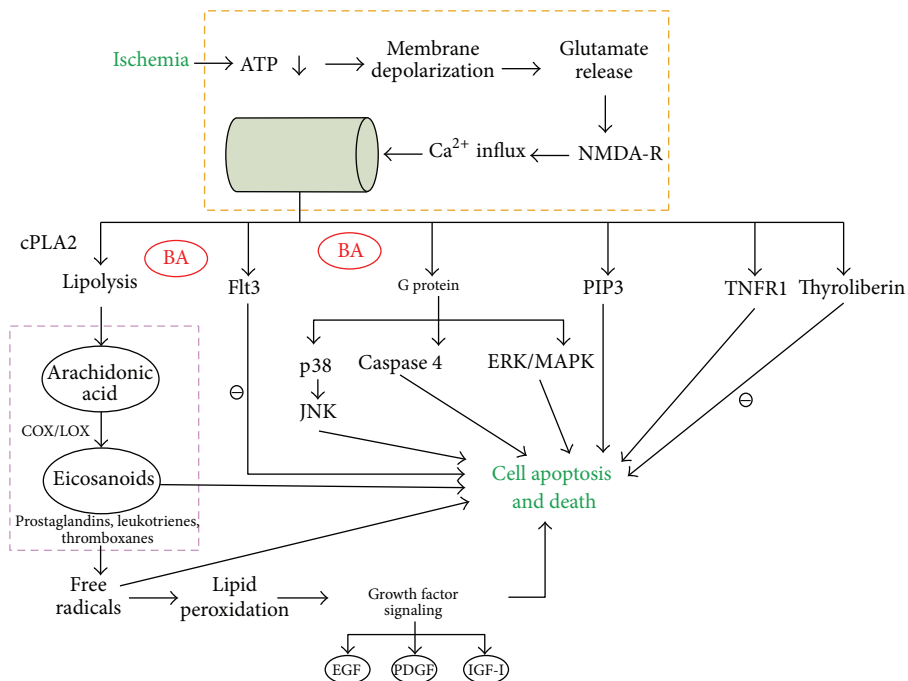


FIGURE 2: Diagram of BA action in targeting pathways involved in cell apoptosis and death.

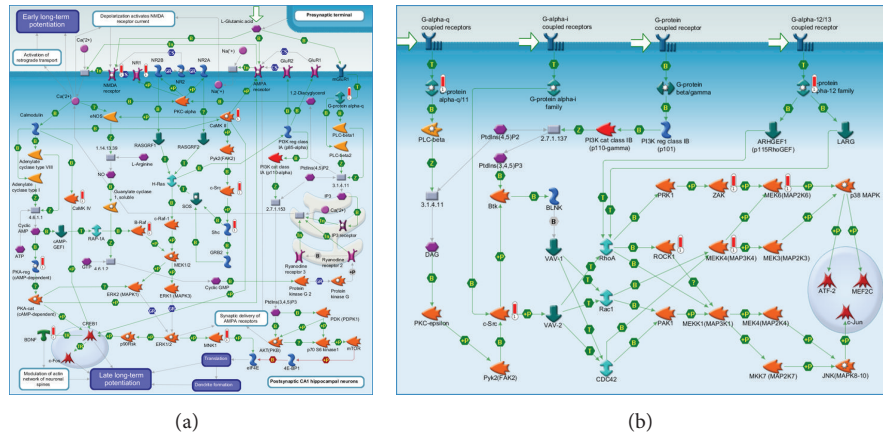


FIGURE 3: Two reversing pathways between the vehicle and baicalin groups. (a) Neurophysiological process: NMDA-dependent postsynaptic long-term potentiation in CA1 hippocampal neurons' pathway. (b) G-protein signalling: regulation of p38 and JNK signalling pathway.

postsynaptic long-term potentiation in CA1 hippocampal neurons' pathway (Figure 3(a)), the following genes were upregulated in the vehicle group: NMDA receptor, NR1, G-protein alpha-q, CaMKII, Pyk2, c-src, CaMKIV, adenylate cyclase type I, Shc, and PKA-cat. After treatment with BA, NMDA receptor, NR1, G-protein alpha-q, CaMKII, and Shc were still dominantly expressed, whereas adenylate cyclase type I and PKA-cat were not, and B-Raf, PKA-reg, BDNF, and MNK1 were upregulated. In the "G-protein signalling: regulation of p38 and JNK signalling" pathway (Figure 3(b)), the following genes were upregulated in the vehicle group: G-protein alpha-12 family, G-protein alpha-q, ARHGEF1, ZAK, c-src, and Pyk2. In the BA group, G-protein alpha-q, G-protein alpha-12 family, ZAK, and c-src were still dominantly expressed, while ARHGEF1 and Pyk2 were no longer dominantly expressed, and MEK6, ROCK1, and MEKK4 were upregulated.

3.3. Process Network Distribution. In the vehicle group, 6 networks were associated with cerebral ischaemia, each with 150 nodes (Supplementary Table 7). The major function of subnetwork 1 was positive regulation of cellular process (Figure 4). The major function of subnetwork 2 was positive regulation of RNA metabolic process. The major function of subnetwork 3 was positive regulation of DNA-dependent transcription. The major function of subnetwork 4 was nucleotide metabolic process. The major function of subnetwork 5 was regulation of cellular metabolic process. The major function of subnetwork 6 was viral genome expression (Supplementary Figure 1, Supplementary Table 7). Subnetwork 1 and subnetwork 5 of vehicle have similar function of cellular process.

After BA treatment, there were 9 networks associated with cerebral ischaemia, with 150 nodes (Supplementary Table 6). The major function of subnetwork 1 was regulation of cellular metabolic process. The major functions of subnetwork 2 were positive regulation of the nitrogen compound metabolic process and positive regulation of the cellular biosynthetic process (Figure 5). The major functions of

subnetwork 3 were intracellular signal transduction and cell surface receptor linked signalling pathway (Supplementary Figure 2). The major function of subnetwork 4 was positive regulation of macromolecule metabolic process (Figure 5). The major function of subnetwork 5 was positive regulation of macromolecule metabolic process. The major function of subnetwork 6 was positive regulation of cellular metabolic process. The major function of subnetwork 7 was regulation of molecular function. The major function of subnetwork 8 was regulation of calcium ion transport via voltage-gated calcium channel activity. The major function of subnetwork 9 was positive regulation of RNA metabolic process (Supplementary Figure 2 and Supplementary Table 6).

Sub-network 1 and sub-network 7 of BA had similar function of cellular metabolic process. Subnetwork 4 and subnetwork 5 of BA had similar function of macromolecule metabolic process.

In the BA group novel subnetwork function includes "positive regulation of the nitrogen compound metabolic process and positive regulation of the cellular biosynthetic process," "intracellular signal transduction and cell surface receptor linked signalling pathway," "macromolecule metabolic process," and "regulation of calcium ion transport via voltage-gated calcium channel activity" (Supplementary Figure 2 and Supplementary Table 6).

3.4. Enrichment Analysis of Biological Processes in the BA and Vehicle Groups. There were 10 significant biological processes identified by enrichment analysis in the BA and vehicle groups ($P < 0.05$) (Supplementary Table 3). The biological processes "positive regulation of cellular process," "signaling," and "signal transduction" were among the top 10 biological processes in all groups, but "positive regulation of molecular function," "cellular response to stimulus," and "intracellular signal transduction" were absent from the BA group. In the BA group, novel biological processes included "positive regulation of biological process," "cell communication," and processes associated with phosphorylation and phosphorus/phosphate metabolism (Figure 6).

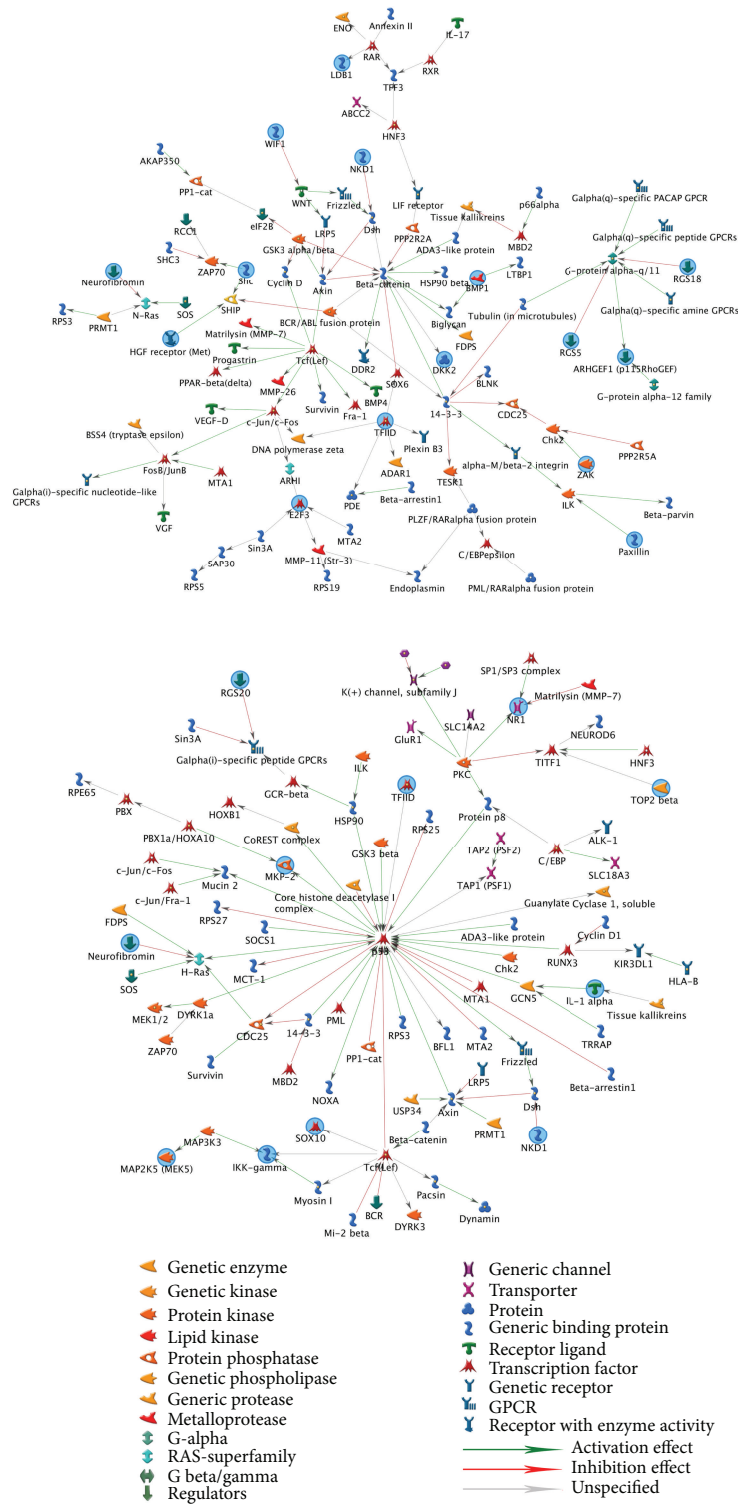


FIGURE 4: Subnetwork 1 and 5 of 6 networks in vehicle group. The subnetwork 1 primarily consisted of G-protein alpha-q, TFIID, ARHGEF1 (p115RhoGEF), Shc, and E2F3, and its major function was positive regulation of cellular process. The centre of subnetwork 5 is p53 whose major function was the regulation of cellular metabolic process.

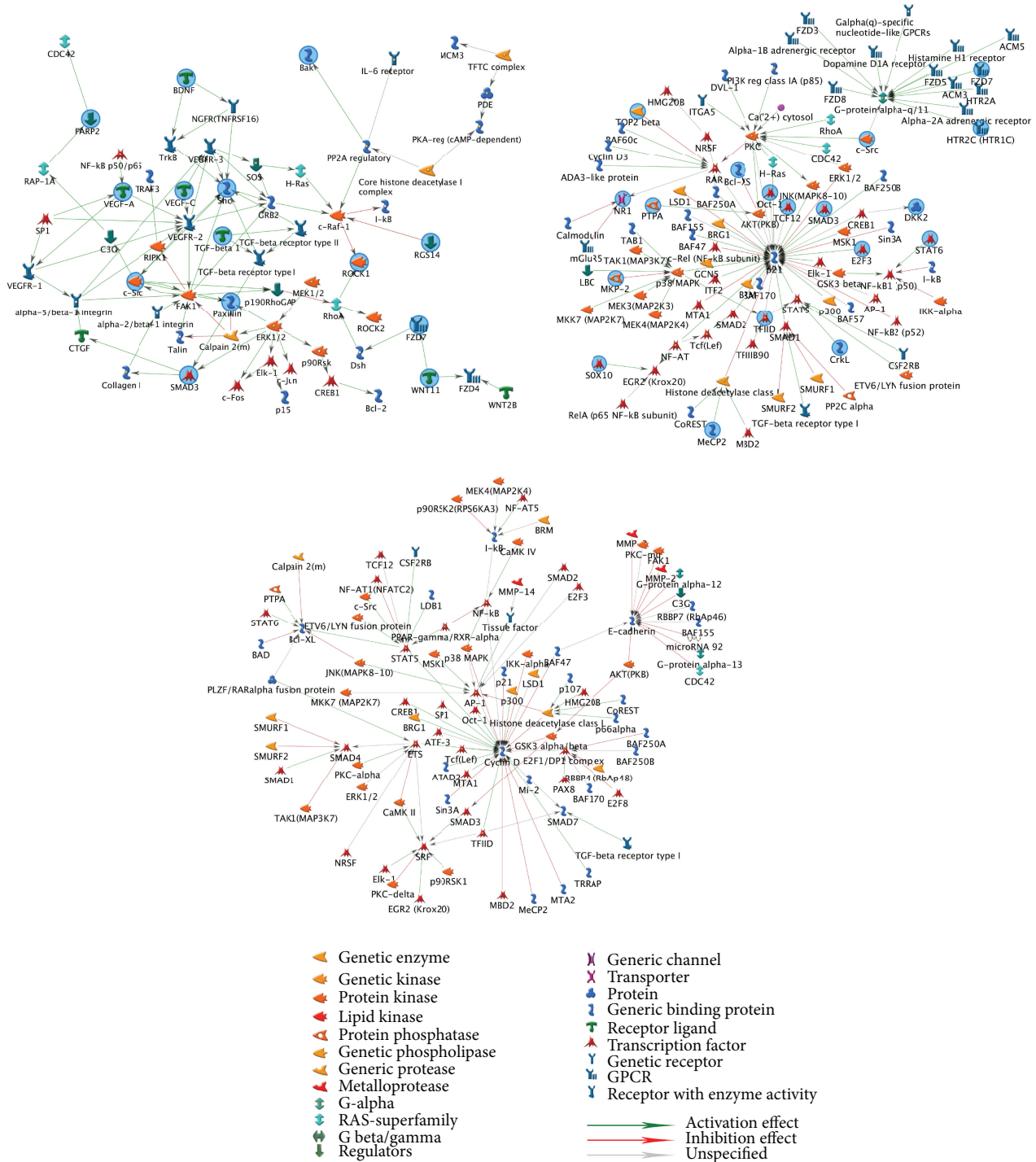


FIGURE 5: Subnetworks 1, 2, and 4 of 9 networks in baicalin group. The subnetwork 1 primarily consisted of Shc, c-src, VEGF-A, paxillin, and SMAD3, and its major function was regulation of cellular metabolic process. The centre of subnetwork 2 is p21 whose major function was positive regulation of nitrogen compound metabolic process and positive regulation of cellular biosynthetic process. The centre of subnetwork 4 is cyclin D whose major function was positive regulation of macromolecule metabolic process.

3.5. Distribution of Molecular Functions in the BA and Vehicle Groups. Of the 10 most significant molecular functions presented in Supplementary Table 4 ($P < 0.05$), seven molecular function categories were common to the BA and vehicle groups, and 3 categories (“phosphotransferase activity with

alcohol group as acceptor,” “protein kinase binding,” and “kinase activity”) only occurred in the BA group (Figure 6).

3.6. Distribution of Cellular Components in the BA and Vehicle Groups. The 10 most significant cellular components

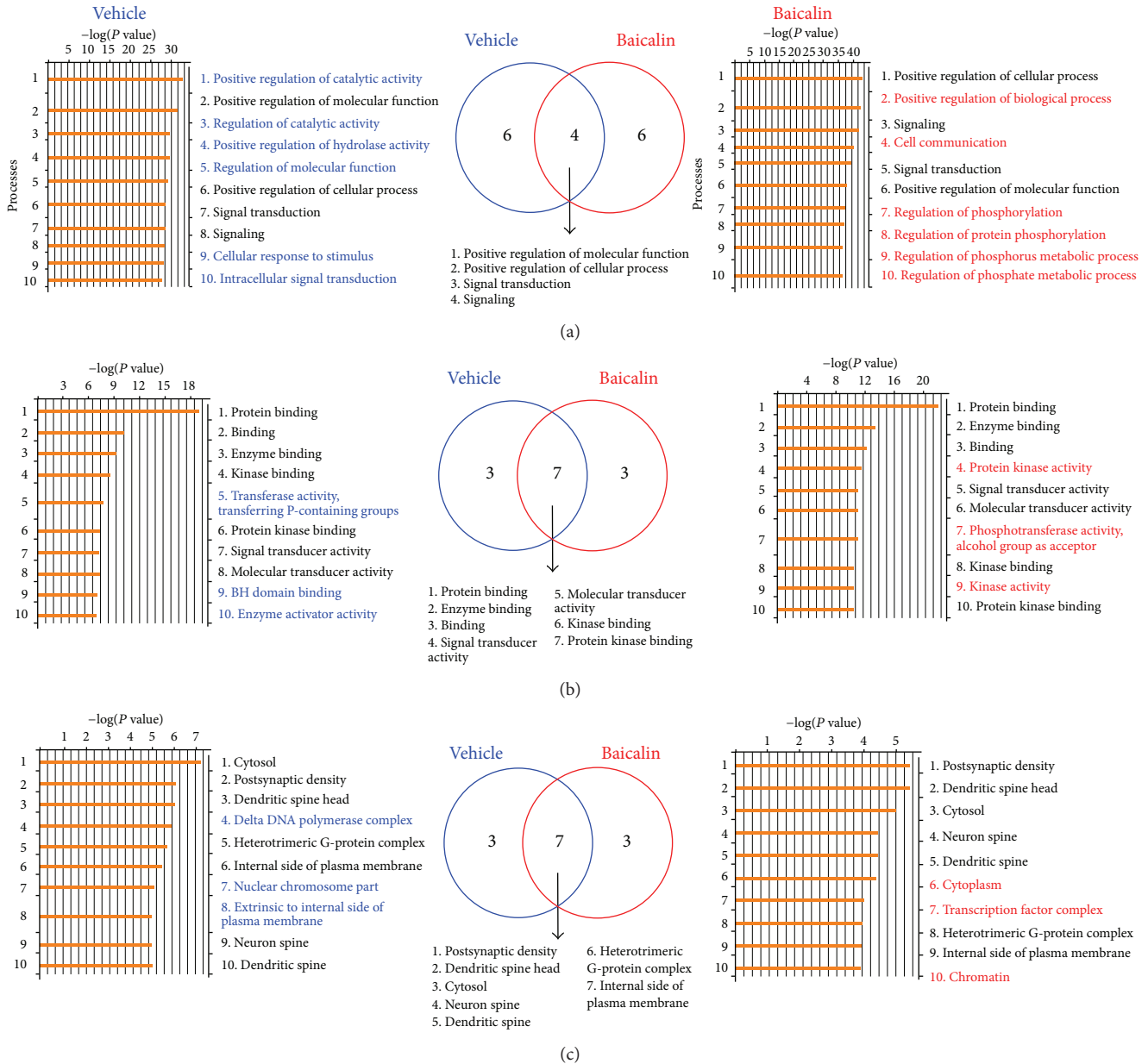


FIGURE 6: Biological process (a), molecular functions (b), and cellular components (c) associated with upregulated genes in both BA and vehicle groups.

($P < 0.05$) associated with the vehicle and BA groups are shown in Supplementary Table 5. Seven cellular components were identified for both groups, and 3 (“cytoplasm,” “transcription factor complex,” and “chromatin”) appeared only in the top 10 of the BA group (Figure 6).

4. Discussion

Although several previous studies have investigated the effects of BA on individual gene expression, none has integrated these various findings into a coherent series of interacting functional pathways and networks [1, 9, 12, 17, 18, 18–20]. The current study is a novel combination of microarray

techniques with 16463 clones analyzed with ArrayTrack and MetaCore, providing an in-depth analysis that extends the breadth of knowledge of changes in gene expression associated with cerebral ischaemia-reperfusion injury. BA pathways most apparently influenced by gene expression were associated with cytoskeleton remodeling, cellular development, VEGF signalling via VEGFR2, and TGF-beta-dependent EMT induction via MAPK. In the vehicle group by contrast, gene expression was primarily associated with G-protein mediated regulation of MAPK-ERK signalling during important developmental processes, reproductive GnRH signalling, developmental thyroliberin signalling, and TNFR1 signalling pathways associated with apoptosis and survival. Notably,

gene expressions in both the BA and the vehicle groups were associated with pathways involved in NMDA-dependent postsynaptic long-term neuron-potential in CA1 hippocampal neurons, G-protein signalling through p38- and JNK-mediated pathways, developmental Flt3 signalling, and G-protein alpha-i signalling cascades. Furthermore, gene expression and likely mechanistic pathways influenced by BA administration were determined with great specificity. The neuroprotective effects of BA treatment relate to selective regulation of pathways, particularly p38 and JNK signalling, NMDA-dependent postsynaptic long-term potentiation, and differentially expressed gene networks, and thereby reduce apoptosis rates and downstream damage due to radical accumulation. Thus, this modern computer-based analysis allows for a more comprehensive understanding of mechanistic pathways in ischaemia-reperfusion injury and subsequent BA treatment than what was previously possible, suggesting that BA treatment induces gene expression that not only prevents apoptosis but also promotes oligodendrocyte survival and myelination signalling.

Two recent studies [24, 25] which used ArrayTrack, IPA, and KEGG-based analysis to better understand the underlying BA mechanisms of action were of limited value because they had relatively small databases. Although numerous databases are currently available for analysis of differential pathway networks, their completeness and accuracy have enormous consequences on data output quality and reliability. Thus, the current study adopted MetaCore due to its novel use of an extensive and manually curated database of human protein-protein, protein-DNA, and protein-RNA interactions, allowing a much more complete integration of signalling and metabolic pathways than previously applied sources.

There were 2 unaltered pathways between the vehicle and BA groups that showed altered gene expression: the “neurophysiological process: NMDA-dependent postsynaptic long-term potentiation in CA1 hippocampal neurons” pathway (Figure 3) and “G-protein signalling: regulation of p38 and JNK signalling” pathway (Figure 3).

Though biochemical evidence strongly indicates apoptotic processes in the postischemic period, morphological evidence interestingly does not widely support standard apoptotic process occurrence, particularly in CA1 pyramidal cells of the hippocampus [30]. BA treatment following stroke has also been demonstrated to have antioxidative and anti-apoptotic properties that may act by increasing superoxide dismutase, glutathione peroxidase and glutathione, and BDNF expression while reducing caspase-3 activity [1, 12]. Consistent with previous reports [12], BA gene expression did limit the action of apoptotic factors, such as caspase-3, but application of BA may have more profound and interesting effects on NMDA-dependent postsynaptic potentiation, associated with delayed neuronal death due to neurotoxicity [31]. Previous studies have indicated that NMDA neuroreceptor NR2A/2B aAbs are independent and sensitive serologic markers for transient ischaemia, indicative of potential elevation of damaging thrombotic (homocysteine, antiphospholipid antibodies, anticardiolipin antibodies), neurotoxic (glutamate), neurochemical markers (neuro-specific enolase,

protein S100, and myelin), and peptide fragments [32]. Thus, these findings indicate that BA-induced genetic expression may potentially act to mediate ischemic damage after an initial insult by mediating cellular metabolism associated with rising neurotoxicity.

The most widely accepted theory of ischemic brain injury suggests that ischaemia causes delayed neuronal death, primarily affecting the vulnerable CA1 region of the hippocampus [33]. In fact, death of CA1 pyramidal cells has been demonstrated to be an immediate result of ischaemia [34], though it has been reported that the majority of cells at the borders of the infarct were not yet dead after 48 hours [32]. In the current study, it was found that BA acted on calcium ion (Ca^{2+})-dependent signalling cascades, shown to play a neuroprotective role in cerebral ischaemia by signalling Ca^{2+} /CaM-dependent ERK activation, and this is consistent with previous findings [35]. In 1999, Lipton noticed that extracellular Ca^{2+} concentration sharply declines in the ischemic core immediately after ischaemia with a concomitant rise in extracellular potassium ions (K^+) (~70 mM) over 2 hours and returns to near normal concentration over 6 to 24 hours [31]. Thus, BA may aid mediation of harmful flux and subsequent cellular response of extracellular Ca^{2+} and K^+ concentration. Furthermore, this hypothesis is supported by the observed impact of BA treatment on regulators of G-protein signalling 5, 6, 14, and 30 observed in the current study, which, with GPCR-kinase 2 (GRK2), may play a role in protecting receptors from overstimulation by induced desensitization [36]. Effects on GABAergic signalling associated with enhanced expression of HSP70 and phosphorylated ERK coupled with decreased levels of phosphorylated JNK and p38 have also been reported [11], consistent with the observations of the current study. Furthermore, BA may act on calcium signalling pathways, tight junction proteins of the blood-brain barrier [14, 19], and neural stem/progenitor cells [9]. Though further study is required, the potential neuroprotective role of BA via G-protein desensitization merits further study.

Consistent with previous studies, [37] the current study indicated that the G-protein network may be associated with apoptosis, as it was readily apparent without BA treatment. The current study similarly showed increasing expression of p53 network and proapoptotic Src homology 2 domain containing transforming protein (Shc) in vehicle group. Isoform p66Shc acts as a downstream target of the tumour suppressor p53 and is indispensable for stress-activated p53 to induce an increase in intracellular oxidant concentration, cytochrome c release, and apoptosis [38]. It could activate and induce apoptosis in a p53-independent manner as well [39] (Figure 5). Network including these networks and genes in vehicle group may play roles in increasing apoptosis and cell death following ischaemia-reperfusion. Conversely, treatment with BA was shown to increase the network processes for the antiapoptotic p21 and SMAD3 (Figure 6), which has been demonstrated to quantitatively affect apoptosis rates [40]. Thus, BA may act through these and other network pathways to limit apoptosis. Furthermore, cyclin D and TGF beta networks were also increased in BA treated group (Figure 6). As a substrate for SMAD3, cyclin D phosphorylated SMAD3

in a cell-cycle-dependent manner and repressed its transcriptional activity. SMAD3 has an inhibitory effect on wound healing, probably by altering the TGF-mediated chemotaxis of monocytes [40]. BA activation of the cyclinD-SMAD3-TGF beta network pathway may improve wound healing after cerebral ischaemia.

As in the use of any proprietary database, although we used Western blotting confirmed results of key proteins in the WNT3 and NF-KB pathways in different groups in our previous study [2], the study results may contain some bias based on the database used, which may not fully represent the actual biological conditions in their entirety. Furthermore, the mouse model may not completely represent the human response to ischaemia-reperfusion and BA treatment. Thus, further clinical assessments will be required to verify these results in humans [41].

5. Conclusion

This study used modern computer databases with extensive manually curated data sets to provide a comprehensive analysis of the pathways and networks involved in the neuroprotective effects of BA treatment for stroke. The study suggests that cerebral ischaemia may induce 10 pathways and alter 6 networks and that BA may recover ischaemia damage cells via 9 networks and 10 pathways, of which 4 are reversing. This study showed that the clinical effectiveness of BA was based on the complementary effects of multiple pathways and networks.

Conflicts of Interests

All authors declare that they have no conflict of interests.

Acknowledgment

This work was supported in part by the Basic Research Fund of Guest Professor Innovation Research Project in China Academy of Chinese Medical Sciences (no. ZZ070803).

References

- [1] Z.-J. Zhang, P. Li, Z. Wang et al., "A comparative study on the individual and combined effects of baicalin and jasminoidin on focal cerebral ischemia-reperfusion injury," *Brain Research*, vol. 1123, no. 1, pp. 188–195, 2006.
- [2] J. Liu, Z. J. Zhang, C. X. Zhou et al., "Outcome-dependent global similarity analysis of imbalanced core signaling pathways in ischemic mouse hippocampus," *CNS & Neurological Disorders*, vol. 11, no. 8, pp. 1070–1082, 2012.
- [3] T. Chen, W. Liu, X. Chao et al., "Neuroprotective effect of osthole against oxygen and glucose deprivation in rat cortical neurons: involvement of mitogen-activated protein kinase pathway," *Neuroscience*, vol. 183, pp. 203–211, 2011.
- [4] Q. Zhang, M. Shen, M. Ding, D. Shen, and F. Ding, "The neuroprotective action of pyrroloquinoline quinone against glutamate-induced apoptosis in hippocampal neurons is mediated through the activation of PI3K/Akt pathway," *Toxicology and Applied Pharmacology*, vol. 252, no. 1, pp. 62–72, 2011.
- [5] V. A. DiNapoli, S. A. Benkovic, X. Li et al., "Age exaggerates proinflammatory cytokine signaling and truncates signal transducers and activators of transcription 3 signaling following ischemic stroke in the rat," *Neuroscience*, vol. 170, no. 2, pp. 633–644, 2010.
- [6] O. A. Harari and J. K. Liao, "NF- κ B and innate immunity in ischemic stroke," *Annals of the New York Academy of Sciences*, vol. 1207, pp. 32–40, 2010.
- [7] Z.-H. Zhang, G.-M. Xi, W.-C. Li, H.-Y. Ling, P. Qu, and X.-B. Fang, "Cyclic-AMP response element binding protein and tau are involved in the neuroprotective mechanisms of nerve growth factor during focal cerebral ischemia/reperfusion in rats," *Journal of Clinical Neuroscience*, vol. 17, no. 3, pp. 353–356, 2010.
- [8] P. W. Zhuang, G. Z. Cui, Y. J. Zhang et al., "Baicalin regulates neuronal fate decision in neural stem/progenitor cells and stimulates hippocampal neurogenesis in adult rats," *CNS Neuroscience & Therapeutics*, vol. 19, no. 3, pp. 154–162, 2013.
- [9] O. Cheng, Z. Li, Y. Han, Q. Jiang, Y. Yan, and K. Cheng, "Baicalin improved the spatial learning ability of global ischaemia/reperfusion rats by reducing hippocampal apoptosis," *Brain Research*, vol. 1470, pp. 111–1118, 2012.
- [10] J. Dai, L. Chen, Y. M. Qiu et al., "Activations of GABAergic signalling, HSP70 and MAPK cascades are involved in baicalin's neuroprotection against gerbil global ischaemia/reperfusion injury," *Brain Research Bulletin*, vol. 90, pp. 1–9, 2013.
- [11] Y. Cao, X. Mao, C. Sun et al., "Baicalin attenuates global cerebral ischemia/reperfusion injury in gerbils via anti-oxidative and anti-apoptotic pathways," *Brain Research Bulletin*, vol. 85, no. 6, pp. 396–402, 2011.
- [12] X.-K. Tu, W.-Z. Yang, R.-S. Liang et al., "Effect of baicalin on matrix metalloproteinase-9 expression and blood-brain barrier permeability following focal cerebral ischemia in rats," *Neurochemical Research*, vol. 36, no. 11, pp. 2022–2028, 2011.
- [13] X. Xue, X.-J. Qu, Y. Yang et al., "Baicalin attenuates focal cerebral ischemic reperfusion injury through inhibition of nuclear factor κ B p65 activation," *Biochemical and Biophysical Research Communications*, vol. 403, no. 3-4, pp. 398–404, 2010.
- [14] Z.-J. Zhang, Z. Wang, X.-Y. Zhang, K. Ying, J.-X. Liu, and Y.-Y. Wang, "Gene expression profile induced by oral administration of baicalin and gardenin after focal brain ischemia in rats," *Acta Pharmacologica Sinica*, vol. 26, no. 3, pp. 307–314, 2005.
- [15] H. Y. Li, Z. Y. Yuan, Y. G. Wang et al., "Role of baicalin in regulating Toll-like receptor 2/4 after ischemic neuronal injury," *Chinese Medical Journal*, vol. 125, no. 9, pp. 1586–1593, 2012.
- [16] X.-K. Tu, W.-Z. Yang, S.-S. Shi et al., "Baicalin inhibits TLR2/4 signaling pathway in rat brain following permanent cerebral ischemia," *Inflammation*, vol. 34, no. 5, pp. 463–470, 2011.
- [17] X.-K. Tu, W.-Z. Yang, S.-S. Shi, C.-H. Wang, and C.-M. Chen, "Neuroprotective effect of baicalin in a rat model of permanent focal cerebral ischemia," *Neurochemical Research*, vol. 34, no. 9, pp. 1626–1634, 2009.
- [18] H. Zhu, Z. Wang, Y. Xing et al., "Baicalin reduces the permeability of the blood-brain barrier during hypoxia in vitro by increasing the expression of tight junction proteins in brain microvascular endothelial cells," *Journal of Ethnopharmacology*, vol. 141, pp. 2714–720, 2012.
- [19] Ingenuity Pathway Analysis™, <http://www.ingenuity.com/>.
- [20] Encyclopaedia of Genes and Genomes, <http://www.genome.jp/kegg/>.

- [21] L. Guo, F. Meng, G. Zhang et al., "Baicalin and jasminoidin effects on gene expression and compatibility in the hippocampus following focal cerebral ischemia," *Neural Regeneration Research*, vol. 6, no. 3, pp. 167–170, 2011.
- [22] Y. Chen, C. Zhou, Y. Yu et al., "Variations in target gene expression and pathway profiles in the mouse hippocampus following treatment with different effective compounds for ischaemia-reperfusion injury," *Naunyn-Schmiedeberg's Archives of Pharmacology*, vol. 385, no. 8, pp. 797–7806, 2012.
- [23] GeneGo MetaCore™ software, <http://www.genego.com/>, <http://www.genego.com/metacore.php>.
- [24] M. Baitaluk, M. Sedova, A. Ray, and A. Gupta, "Biological-Networks: visualization and analysis tool for systems biology," *Nucleic Acids Research*, vol. 34, pp. W466–W471, 2006.
- [25] D. M. van Leeuwen, M. Pedersen, L. E. Knudsen et al., "Transcriptomic network analysis of micronuclei-related genes: a case study," *Mutagenesis*, vol. 26, no. 1, pp. 27–32, 2011.
- [26] A. Subramanian, P. Tamayo, V. K. Mootha et al., "Gene set enrichment analysis: a knowledge-based approach for interpreting genome-wide expression profiles," *Proceedings of the National Academy of Sciences of the United States of America*, vol. 102, no. 43, pp. 15545–15550, 2005.
- [27] T. Werner, "Bioinformatics applications for pathway analysis of microarray data," *Current Opinion in Biotechnology*, vol. 19, no. 1, pp. 50–54, 2008.
- [28] Expression Analysis Systematic Explorer software (National Institute of Health, USA), <http://david.abcc.ncifcrf.gov/ease/ease.jsp>.
- [29] D. A. Hosack, G. Dennis Jr., B. T. Sherman, H. C. Lane, and R. A. Lempicki, "Identifying biological themes within lists of genes with EASE," *Genome Biology*, vol. 4, no. 10, p. R70, 2003.
- [30] P. Lipton, "Ischemic cell death in brain neurons," *Physiological Reviews*, vol. 79, no. 4, pp. 1431–1568, 1999.
- [31] S. A. Dambinova, G. A. Khounteev, G. A. Izykenova, I. G. Zavolokov, A. Y. Ilyukhina, and A. A. Skoromets, "Blood test detecting autoantibodies to N-methyl-D-aspartate neuroreceptors for evaluation of patients with transient ischemic attack and stroke," *Clinical Chemistry*, vol. 49, no. 10, pp. 1752–1762, 2003.
- [32] F. Zhang and C. Iadecola, "Temporal characteristics of the protective effect of aminoguanidine on cerebral ischemic damage," *Brain Research*, vol. 802, no. 1-2, pp. 104–110, 1998.
- [33] Y.-B. Zhang, M.-Y. Kan, Z.-H. Yang et al., "Neuroprotective effects of N-stearoyltyrosine on transient global cerebral ischemia in gerbils," *Brain Research*, vol. 1287, pp. 146–156, 2009.
- [34] I. Ferrer, M. A. Soriano, A. Vidal, and A. M. Planas, "Survival of parvalbumin-immunoreactive neurons in the gerbil hippocampus following transient forebrain ischemia does not depend on HSP-70 protein induction," *Brain Research*, vol. 692, no. 1-2, pp. 41–46, 1995.
- [35] J. Zhao, H.-W. Wu, Y.-J. Chen et al., "Protein phosphatase 2A-negative regulation of the protective signaling pathway of Ca^{2+} /CaM-Dependent ERK activation in cerebral ischemia," *Journal of Neuroscience Research*, vol. 86, no. 12, pp. 2733–2745, 2008.
- [36] C. H. A. Nijboer, A. Kavelaars, A. Vroon, F. Groenendaal, F. van Bel, and C. J. Heijnen, "Low endogenous G-protein-coupled receptor kinase 2 sensitizes the immature brain to hypoxia-ischemia-induced gray and white matter damage," *Journal of Neuroscience*, vol. 28, no. 13, pp. 3324–3332, 2008.
- [37] J. W. Adams and J. H. Brown, "G-proteins in growth and apoptosis: lessons from the heart," *Oncogene*, vol. 20, no. 13, pp. 1626–1634, 2001.
- [38] Uniprot Consortium, <http://www.uniprot.org/uniprot/Q16594>.
- [39] L. Tiberi, A. Faisal, M. Rossi, L. D. Tella, C. Franceschi, and S. Salvioli, "p66Shc gene has a pro-apoptotic role in human cell lines and it is activated by a p53-independent pathway," *Biochemical and Biophysical Research Communications*, vol. 342, no. 2, pp. 503–508, 2006.
- [40] K. Yanagisawa, H. Osada, A. Masuda et al., "Induction of apoptosis by Smad3 and down-regulation of Smad3 expression in response to TGF- β in human normal lung epithelial cells," *Oncogene*, vol. 17, no. 13, pp. 1743–1747, 1998.
- [41] J. Wang and X. J. Xiong, "Current situation and perspectives of clinical study in integrative medicine in China," *Evidence-Based Complementary and Alternative Medicine*, vol. 2012, Article ID 268542, 11 pages, 2012.

Research Article

Network-Based Biomarkers for Cold Coagulation Blood Stasis Syndrome and the Therapeutic Effects of Shaofu Zhuyu Decoction in Rats

Shulan Su,¹ Jinao Duan,¹ Wenxia Cui,¹ Erxing Shang,¹ Pei Liu,¹ Gang Bai,²
Sheng Guo,¹ Dawei Qian,¹ and Yuping Tang¹

¹ Jiangsu Key Laboratory for High Technology Research of TCM Formulae, Nanjing University of Chinese Medicine, Nanjing 210046, China

² College of Pharmacy, State Key Laboratory of Medicinal Chemical Biology, Tianjin Key Laboratory of Molecular Drug Research, Nankai University, Tianjin 300071, China

Correspondence should be addressed to Jinao Duan; duanja@163.com

Received 25 May 2013; Accepted 1 August 2013

Academic Editor: Aiping Lu

Copyright © 2013 Shulan Su et al. This is an open access article distributed under the Creative Commons Attribution License, which permits unrestricted use, distribution, and reproduction in any medium, provided the original work is properly cited.

In this study, the reverse docking methodology was applied to predict the action targets and pathways of Shaofu Zhuyu decoction (SFZYD) bioactive ingredients. Furthermore, Traditional Chinese Medicine (TCM) cold coagulation blood stasis (CCBS) syndrome was induced in female Sprague-Dawley rats with an ice-water bath and epinephrine, and SFZYD was used to treat CCBS syndrome. A metabolomic approach was used to evaluate changes in the metabolic profiles and to analyze the pharmacological mechanism of SFZYD actions. Twenty-three potential protein targets and 15 pathways were discovered, respectively; among these, pathways are associated with inflammation and immunological stress, hormone metabolism, coagulation function, and glycometabolism. There were also changes in the levels of endogenous metabolites of LysoPCs and glucuronides. Twenty endogenous metabolites were identified. Furthermore, the relative quantities of 6 endogenous metabolites in the plasma and 5 in the urine were significantly affected by SFZYD ($P < 0.05$). The pharmacological mechanism of SFZYD was partially associated with glycerophospholipid metabolism and pentose and glucuronate interconversions. In conclusion, our findings demonstrated that TCM CCBS pattern induced by ice water and epinephrine was complex and related to multiple metabolic pathways. SFZYD did regulate the TCM CCBS by multitargets, and biomarkers and SFZYD should be used for the clinical treatment of CCBS syndrome.

1. Introduction

Traditional Chinese medicine (TCM) is guided by the theory of traditional Chinese medical science for clinical application. TCM can be characterized as being holistic, with an emphasis on regulation of the integrity of the human body and the interaction between individuals and their environment. Multiple natural therapeutic methods for patient's management were applied in TCM; among these, the herbal formula was the most typical treatment. Most herbal medicines are prescribed in combination to obtain synergistic effects or diminish possible adverse reactions [1]. This medical approach has played an increasingly important role in evidence-based personalized medicine, which is

a new trend and a hot research topic of medical development.

Based on the theory of TCM, which is rooted in the philosophy of treating the entire body as a whole, multi-pathogenic factors, such as cold coagulation, Qi stagnation, and blood insufficiency, are considered to be the main causes of many diseases or syndromes. In TCM, there are several different disharmony patterns (named ZHENG) such as the syndrome of blood stasis, syndrome of Qi stagnation, and Yin/Yang deficiency syndrome [2]. The TCM ZHENG as a diagnostic approach may provide an invaluable guidance for therapeutic choices and personalized disease management, not only in traditional medical practices but also in modern healthcare systems [3].

Cold coagulation blood stasis (CCBS) is primarily induced by cold-evil, and as a subtype of blood stasis syndrome, it is a critical pattern for many diseases, especially in women. The pathologic mechanisms of CCBS syndrome were recently found to be related to the changes in hemorheological properties including high-blood viscosity, increased erythrocyte aggregation, increased blood sedimentation, decreased erythrocyte deformability, decreased hematocrit, microcirculation disturbance, and coagulant function abnormality [4]. Further research revealed that blood stasis syndrome is closely related to inflammatory factors and the immune response. Inflammatory- and immune-related genes are remarkably dominant in the gene expression profiles of blood stasis syndrome, which may explain the functions of inflammation and the immune response in the occurrence and development of this syndrome [5]. Moreover, it was reported that the occurrence of vasomotor dysfunction in the ovaries and the levels of reproductive hormone decrease in patients with blood stasis syndrome [6], but the complex pathological mechanisms and metabolite profiling changes in CCBS syndrome remain incompletely elucidated.

The famous Chinese herbal formula, Shaofu Zhuyu decoction (SFZYD), which was originally identified by the “*Correction of Errors in Medical Classics*” compiled by Qingren Wang in the Qing dynasty (A.D. 1830), was utilized in the clinic for approximately 200 years to treat blood stasis syndrome in gynecological diseases such as dysmenorrhea, amenorrhea, or menoxenia. SFZYD is considered an effective prescription for the treatment of CCBS syndrome, and it is composed of ten crude drugs: *Angelicae sinensis Radix*, *Chuanxiong Rhizoma*, *Cinnamomi Cortex*, *Foeniculi Fructus*, *Zingiberis Rhizoma*, *Myrrha*, *Trogopteris Faeces*, *Typhae Pollen*, *Paeoniae Radix Rubra*, and *Corydalis Rhizoma* [7]. In the clinic, SFZYD was reported to have over 90% efficacy for the treatment of primary dysmenorrhea with CCBS syndrome [8, 9]. However, the therapeutic mechanisms of SFZYD are still unknown and require a comprehensive investigation.

Metabolomics, which is based on the dynamic changes of low molecular weight metabolites in organisms, indicates the overall physiological status in response to pathophysiological stimuli or genetic, environmental, or lifestyle factors [10]. Metabolites often mirror the end result of genomic and protein perturbations in a disease, and they are most closely associated with phenotypic changes. Furthermore, the pathogenesis of diseases and the mechanisms of action for therapies can be elucidated by identifying biomarkers, analyzing the metabolic pathway, discovering drug-target interactions, and so on. Recently, metabolic profiling has attracted great interest for biomarker discovery and for assessing the holistic effects of many therapeutics used in TCM [11–16].

Network pharmacology, a system biology-based methodology, is a new approach to highlight a holistic thinking and systematical theory of interactions among drugs, targets, and diseases, which is also shared with TCM theory. The remarkable feature of network pharmacology is the “multicomponent therapeutics, network target” [17–19]. In the network

pharmacology-based drug research, a biological network of a disease and a pharmacological network of the candidates are established. So, the network pharmacology applied to TCM research would provide a novel methodology and opportunity for screening bioactive ingredients, synergistic drug combinations [20], and biomarkers, revealing mechanisms of action and exploring scientific evidence of herbs [21] or herbal formulae on the basis of complex biological systems [22].

Here, for the first time, we studied the network targets and pathway of SFZYD bioactive ingredients. Furthermore, the plasma and urine metabolomics of cold coagulation blood stasis syndrome, which was induced by epinephrine and cold evil, and the therapeutic effects of SFZYD in rats were investigated. We used the ultra-high-performance liquid chromatography in tandem with a time-of-flight mass spectrometry (UHPLC-TOF/MS) based metabolomic approach to elucidate the metabolic profiles and phenotype changes between normal rats and model rats and to identify potential biomarkers. A multivariate statistical analysis was used to investigate the pathological variations of cold coagulation blood stasis syndrome and to explore the therapeutic effects of SFZYD.

2. Materials and Methods

2.1. Materials. Ten crude herbs, *Angelicae sinensis Radix*, *Chuanxiong Rhizoma*, *Paeoniae Radix Rubra*, *Cinnamomi Cortex*, *Foeniculi Fructus*, *Zingiberis Rhizoma*, *Myrrha*, *Trogopteris Faeces*, *Typhae Pollen*, and *Corydalis Rhizoma*, were purchased from Minxian (Gansu), Pengzhou (Sichuan), Chifeng (Neimeng), Yulin (Guangxi), Wuwei (Gansu), Yulin (Guangxi), Guangdong, Changzhi (Shanxi), Jiangsu (Yixing), and Songyang (Zhejiang), respectively. The corresponding author authenticated all of the raw materials, and the herbal drugs were verified according to the Chinese pharmacopoeia (Chinese pharmacopoeia, 2010). The voucher specimens (no. NJUTCM-20110818-20110827) were deposited in the Jiangsu Key Laboratory for TCM Formulae Research of Nanjing University of Chinese Medicine.

HPLC grade acetonitrile was purchased from Tedia (Fairfield, OH, USA), and AR grade formic acid was purchased from the Shanghai Reagent Company (Shanghai, China). Ultrapure water for UHPLC analysis was prepared using a Millipore water purification system (Millipore, Milford, MA, USA) and filtered with 0.22 μm membranes prior to use. Sodium citrate (no. 20071107) and epinephrine hydrochloride (no. 0808231) were obtained from Tianjin Biochem Pharmaceutical CO., LTD., and Tianjin King York Amino Acid CO., LTD., respectively.

2.2. Preparation of SFZYD Extract. *Angelicae sinensis Radix*, *Chuanxiong Rhizoma*, *Paeoniae Radix Rubra*, *Cinnamomi Cortex*, *Foeniculi Fructus*, *Zingiberis Rhizoma*, *Myrrha*, *Trogopteris Faeces*, *Typhae Pollen*, and *Corydalis Rhizoma* were mixed at a weight ratio of 3:1:2:1:0.5:2:1:3:1:1, respectively. The mixture (1.5 kg) was decocted with 15 L of water for 2 h. The filtrates were collected, and the residues

were decocted in 12 L of water for 1.5 h. The filtrates from each decoction were combined and concentrated to 1.5 L at 70°C. The concentrated solution was dried with a vacuum, and 28.9 g extract of Shaofu Zhuyu decoction (SFZYD) was produced.

2.3. Network Targets and Pathway Prediction of SFZYD Bioactive Ingredients. Based on our previous studies [23, 24], the ten compounds absorbed into blood were selected to predict the biological targets. The mol2 files of ten compounds are imported into PharmMapper database (<http://59.78.96.61/pharmmapper/>) to predict the targets, then the target numbers were entered into the database (<http://www.uniprot.org/>, <http://bioinfo.capitalbio.com/mas3/>), and the Kyoto Encyclopedia of Genes and Genomes (KEGG) database (<http://www.genome.jp/kegg/>) was used to annotate and analyze the pathway. The chemical structures of ten compounds from SFZYD were shown in Figure 1.

2.4. Animal Handling Procedure and Drug Treatment. Female Sprague-Dawley (SD) rats (180 ± 10 g) were purchased from Nanjing University of Chinese Medicine (rodent license no. SCXK 20080033). The rats were housed under standard laboratory conditions, and food and tap water were provided ad libitum. Experimental procedures were carried out in accordance with the Guide for the Care and Use of Laboratory Animals, and before the animal experiments were carried out, the procedures were approved by the Laboratory Animal Center of Nanjing University of Chinese Medicine.

The experimental groups ($n = 6$) were as follows: (1) normal control (NC), (2) cold- and epinephrine-induced CCBS syndrome (CCBS), and (3) CCBS model rats with SFZYD treatment. The model rats were put into ice water (0°C~1°C) for 5 min daily for 7 days. On the 8th day, they received two subcutaneous injections of hypodermic epinephrine (1 mg·kg⁻¹) at 4-hour intervals. Simultaneously, model rats were administered SFZYD (10.08 g kg⁻¹; 10 times the clinical dose for humans) via gastric irrigation once daily for 7 days. The dose of SFZYD was chosen based on the clinical application dosage of 45 g/day/60 kg body weight. The rats in the normal control group were treated with an equal volume of distilled water as a vehicle control.

2.5. Samples Collection and Preparation. Blood samples were collected in heparinized tubes on the 8th day after the injection of epinephrine. They were then anticoagulated in sodium citricum, centrifuged at 15000 ×g for 10 min, and stored at -20°C until analysis. Urine samples were collected in 12-hour intervals every day for 10 days, then centrifuged at 15000 ×g for 10 min and stored at -20°C until analysis.

Two hundred microliters of plasma was added to 600 μL of acetonitrile, and this mixture was vortexed for 30 s and centrifuged at 15,000 ×g for 10 min to obtain the supernatant. Prior to analysis, the urine samples were thawed at room temperature and centrifuged at 15000 ×g for 10 min. The supernatant liquid (1 mL) was added to 3 mL of acetonitrile, vortex mixed for 30 s, and centrifuged at 15000 ×g for 10 min

to obtain the supernatant. The samples were processed and analyzed in a random order.

The plasma and urine supernatants were removed and evaporated to dryness in a 40°C water bath under a gentle stream of nitrogen. The residues were reconstituted in 200 μL mobile phase of 70% acetonitrile-water solution, centrifuged at 15000 ×g for 5 min, and filtered through a 0.22 μm membrane filter. The filtrates were transferred to an autosampler vial and stored at 4°C. A 5 μL aliquot of each plasma or urine sample was injected for LC/MS analysis. The samples were analyzed in a random order.

2.6. Model Assessment. The hemorheology indexes, coagulation function, and metabolic profiling changes were calculated to evaluate the success of the CCBS syndrome model in rats. The hemorheology indexes of whole blood viscosity and plasma viscosity were measured according to a previously described method [25]. The coagulation function index, including thrombin time (TT), prothrombin time (PT), activated partial thromboplastin time (APTT), and fibrinogen (FIB), was determined to assess the CCBS syndrome model. Thrombin time (TT) was determined using a coagulometer (Model LG-PABER-I, Steellex Co., China). Shortly after adding the thrombin solution, the coagulometer was started and TT was recorded. To establish the standard curve of TT and thrombin concentration, TT was determined by incubating 40 μL of plasma for 3 min at 37°C, and this was followed by the addition of 40 μL of a thrombin solution (different concentrations in Tris-HCl buffer, pH 7.4) and 20 μL of solvent for 3 min at 37°C. TT was examined using the previously described method and converted into thrombin concentration using the indicated regression equation. Prothrombin time (PT), activated partial thromboplastin time (APTT), and fibrinogen content (FIB) were examined with commercial kits, following the manufacturer's instructions with slight modification. PT was determined by incubating 40 μL of plasma solution for 3 min at 37°C, followed by the addition of 40 μL of thromboplastin agent and 20 μL of sample. APTT was determined by incubating 10 μL of the sample solution and 50 μL of plasma with 50 μL of APTT-activating agents for 3 min at 37°C, followed by the addition of 50 μL of CaCl₂. FIB was determined by incubating 10 μL of plasma with 90 μL of imidazole buffer for 3 min at 37°C, followed by the addition of 50 μL of FIB agent and 10 μL of the sample solution. 5-HT, NA, and β-EP were determined according to the methods of ELISA kits described.

2.7. UPLC-QTOF/MS and UPLC-QqQ/MS Analysis. Chromatography was performed on an AcQuity UHPLC system (Waters Corp., Milford, MA, USA) with a conditioned autosampler at 4°C. The separation was carried out on an AcQuity UHPLC BEH C₁₈ column (50 mm × 2.1 mm i.d., 1.7 μm; Waters Corp., Milford, MA, USA), which was maintained at 35°C. The mobile phase consisted of 0.1% formic acid (HOOCH) in water as solvent A and acetonitrile (ACN) as solvent B. The gradient conditions of the mobile phase were as follows: 0~4 min, A: 98%~85%; 4~9 min, A: 85%~70%; 9~12 min, A: 70%~65%; 12~15 min, A: 65%; 15~

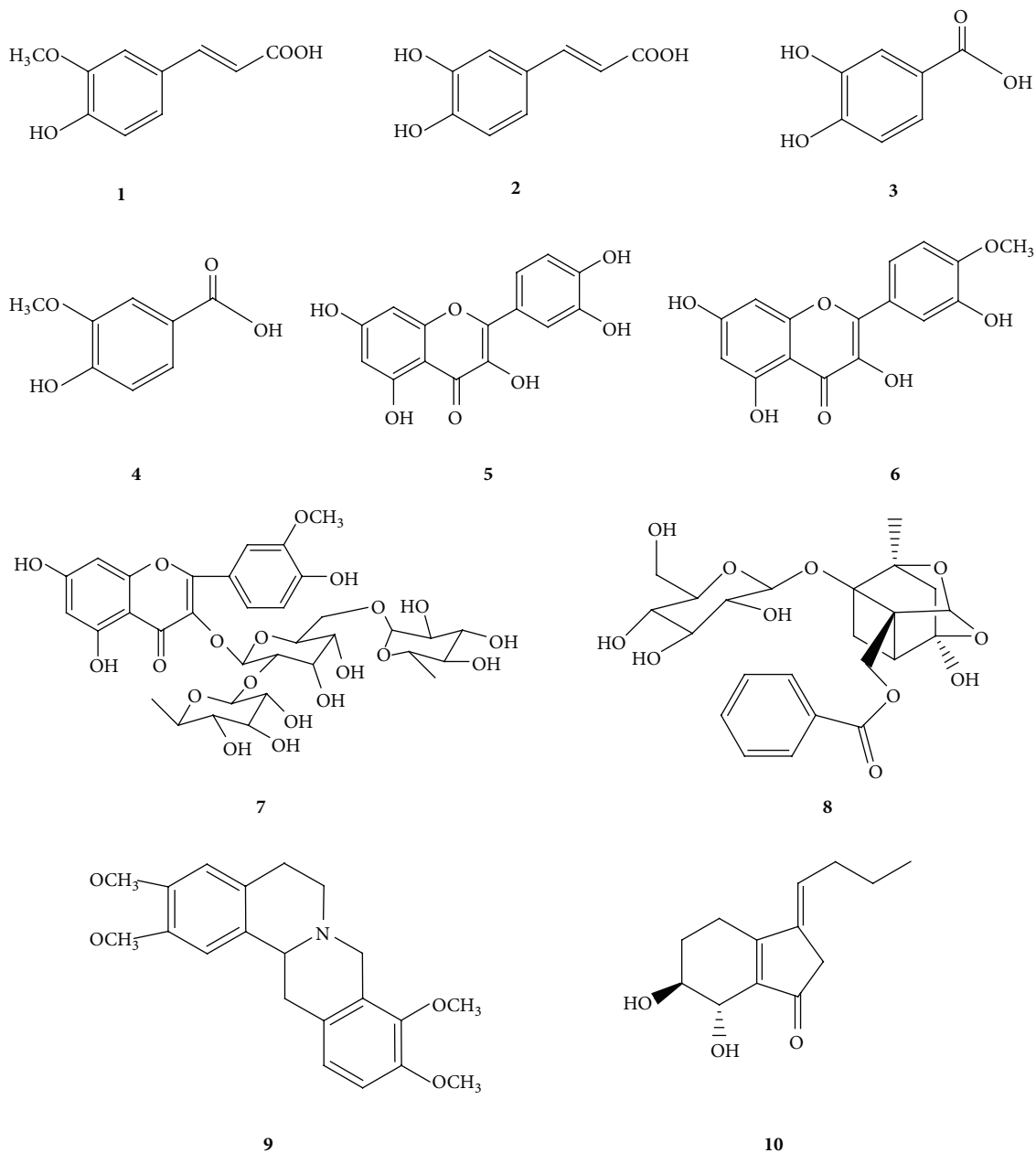


FIGURE 1: The chemical structures of the ten target compounds ((1) ferulic acid; (2) caffeic acid; (3) protocatechuic acid; (4) vanillic acid; (5) quercetin; (6) isorhamnetin; (7) typhaneoside; (8) paeoniflorin; (9) tetrahydropalmatine; (10) senkyunolide I).

18 min, A: 65%~50%; 18~21 min, 50%~25%; 21~22 min, 25%~20%; 22~26 min, 20%~5%; 26~28 min, 5%; and 29~31 min, 98%. The flow rate was 0.40 mL min^{-1} , and the sample injection volume was $2 \mu\text{L}$.

Mass spectrometric detection was carried out on an AcQuity Synapt mass spectrometer equipped with an electrospray ionization (ESI) interface (Waters, Milford, MA, USA). The ESI source was operated in negative and positive ionization modes. The ionization source conditions were as follows: capillary voltage of 3.0 kV, source temperature of 120°C , and desolvation temperature of 350°C . The sampling cone voltage was set to 30 V, the extraction cone voltage was

2.0 V (for plasma sample) or 0.7 V (for urine sample), the trap collision energy was 6.0 V, the transfer collision energy was 4.0 V, the trap gas flow was 1.50 mL min^{-1} , and the ion energy was 1.0 V. Nitrogen and argon were used as cone and collision gases, respectively. The cone and desolvation gas flow were 50 and 600 L h^{-1} , respectively. The scan time was 0.5 s (for plasma sample) or 0.2 s (for urine sample), and an interval scan time of 0.02 s was used throughout, with a collision energy of 6 eV. The mass spectrometric data were collected from m/z 100 to 1000 in centroid mode. Leucine-enkephalin was used as the lock mass, generating an $[\text{M}+\text{H}]^+$ ion (m/z 556.2771) and an $[\text{M}-\text{H}]^-$ ion (m/z 554.2615) at a

concentration of 200 pg mL^{-1} and a flow rate of $100 \text{ } \mu\text{L min}^{-1}$. Dynamic range enhancement was applied throughout the MS experiment to ensure that accurate mass measurements were obtained over a wider dynamic range.

2.8. Metabolomic Data Processing and Multivariate Analysis. UPLC/MS data were detected and noise-reduced in both the UPLC and MS domains such that only true analytical peaks were selected for further processing by the software. A list of the peak intensities detected was then generated for the first chromatogram using the R_t - m/z data pairs as identifiers. The resulting normalized peak intensities form a single matrix, with R_t - m/z pairs for each file in the dataset. All processed data from each chromatogram were normalized and Pareto-scaled prior to the multivariate statistical analysis.

All data from the plasma and urine samples were processed using the MarkerLynx application manager for MassLynx 4.1 and MarkerLynx software (Waters Corp., Milford, USA). The intensity of each ion was normalized with respect to the total ion count to generate a data matrix consisting of the retention time, m/z value, and normalized peak area. The multivariate data matrix was analyzed using EZ info software (Waters Corp., Milford, USA). Unsupervised segregation was examined with a principal component analysis (PCA) using Pareto-scaled data. A partial least squared discriminant analysis (PLS-DA) and an orthogonal partial least-squared discriminant analysis (OPLS-DA) were used to identify the various metabolites responsible for the separation between the model and normal groups. Potential biomarkers of interest were extracted from the S-plots that were constructed following the OPLS-DA analysis, and the biomarkers were chosen based on their contribution to the variation and correlation within the dataset.

An internal 5-fold cross-validation was carried out to estimate the performance of the PLS-DA models. The calculated $R^2 Y_{(\text{cum})}$ estimates how well the model represents the fraction of explained Y-variation, and $Q^2_{(\text{cum})}$ estimates the predictive ability of the model. Models are considered excellent when the cumulative values of $R^2 Y$ and Q^2 are greater than 0.8. In addition to cross-validation, 200 permutation tests were also performed to validate the model. The variable importance in the projection (VIP) value is a weighted sum of squares of the PLS weights that reflects the relative contribution of each X variable to the model. The variables with $VIP > 1$ were considered to be influential for sample separation in the score plots generated from PLS-DA analysis [26]. Ultimately, different metabolic features associated with the model group and the SFZYD treatment group were obtained based on cutoff points of both VIP values from a 5-fold cross-validated PLS-DA model and critical P values from a univariate analysis. In addition, the corresponding fold change was calculated to show the degree of variation in metabolite levels between groups.

2.9. Biomarker Identification and Construction of the Metabolic Pathway. The identities of the potential biomarkers were

confirmed by comparing their mass spectra and chromatographic retention times with the available reference standards and a full spectral library containing MS/MS data obtained in the positive and/or negative ion modes. The Mass Fragment application manager (Waters MassLynx v4.1, Waters Corp., Milford, USA) was used to facilitate the MS/MS fragment ion analysis through the use of chemically intelligent peak-matching algorithms. This information was then used to search multiple databases, either in-house or using online data sources, including ChemSpider database (<http://www.chemspider.com>), Mass Bank (<http://www.massbank.jp/>), PubChem (<http://ncbi.nlm.nih.gov/>), and MetFrag (<http://msbi.ipb-halle.de/MetFrag/>).

To identify the affected metabolic pathways, a construction, interaction, and pathway analysis of potential biomarkers was performed using MetPA (<http://metpa.metabolomics.ca/MetPA/faces/Home.jsp>) based on several database sources, including the KEGG (<http://www.genome.jp/kegg/>), Human Metabolome Database (<http://www.hmdb.ca/>), SMPD (<http://www.smpdb.ca/>), and METLIN (<http://metlin.scripps.edu/>). Potential biological roles were evaluated by an enrichment analysis using MetaboAnalyst.

2.10. Statistical Analysis. All quantitative data analyses were performed using the SPSS 11.5 software package for Windows. Significance was determined using one-way analyses of variance (ANOVAs), followed by Student's t -test. The results were expressed as the mean \pm SD. P values less than 0.05 were considered significant.

3. Results and Discussion

3.1. Potential Targets and Pathway Analysis. The 10 compounds that confirmed the absorption into the blood were imported into the database of PharmMapper to analyze the reverse docking. The results showed that 23 important potential protein targets were found, and these targets were put into the KEGG pathway annotation, the 15 pathways were discovered. Among these pathways there were 8 pathways related to inflammation and immunological stress. They are arachidonic acid metabolism, MAPK, adherens junction, focal adhesion, Fc epsilon RI, VEGF, B cell receptor signaling pathway, and T-cell receptor signaling pathway, respectively. The pathways associated with hormone metabolism are including androgen and estrogen metabolism, GnRH signaling pathway, and ErbB signaling pathway. Figure 2 showed the relationships between the ingredients, targets, and pathways.

3.2. Changes in Blood Indexes and Model Evaluation. Blood viscosity is the measure of how thin or thick the blood fluid is, and it reflects the blood flow and blood flow resistance. When blood is thick, blood flow is sluggish and there is an increased resistance, which tends to hinder normal energy metabolism and can lead to functional disorders in organs and tissues. In this experiment, whole blood viscosity and plasma viscosity indexes were determined for CCBS model rats. The whole blood viscosity (at high and low shear rates of 200 s^{-1} , 30 s^{-1} ,

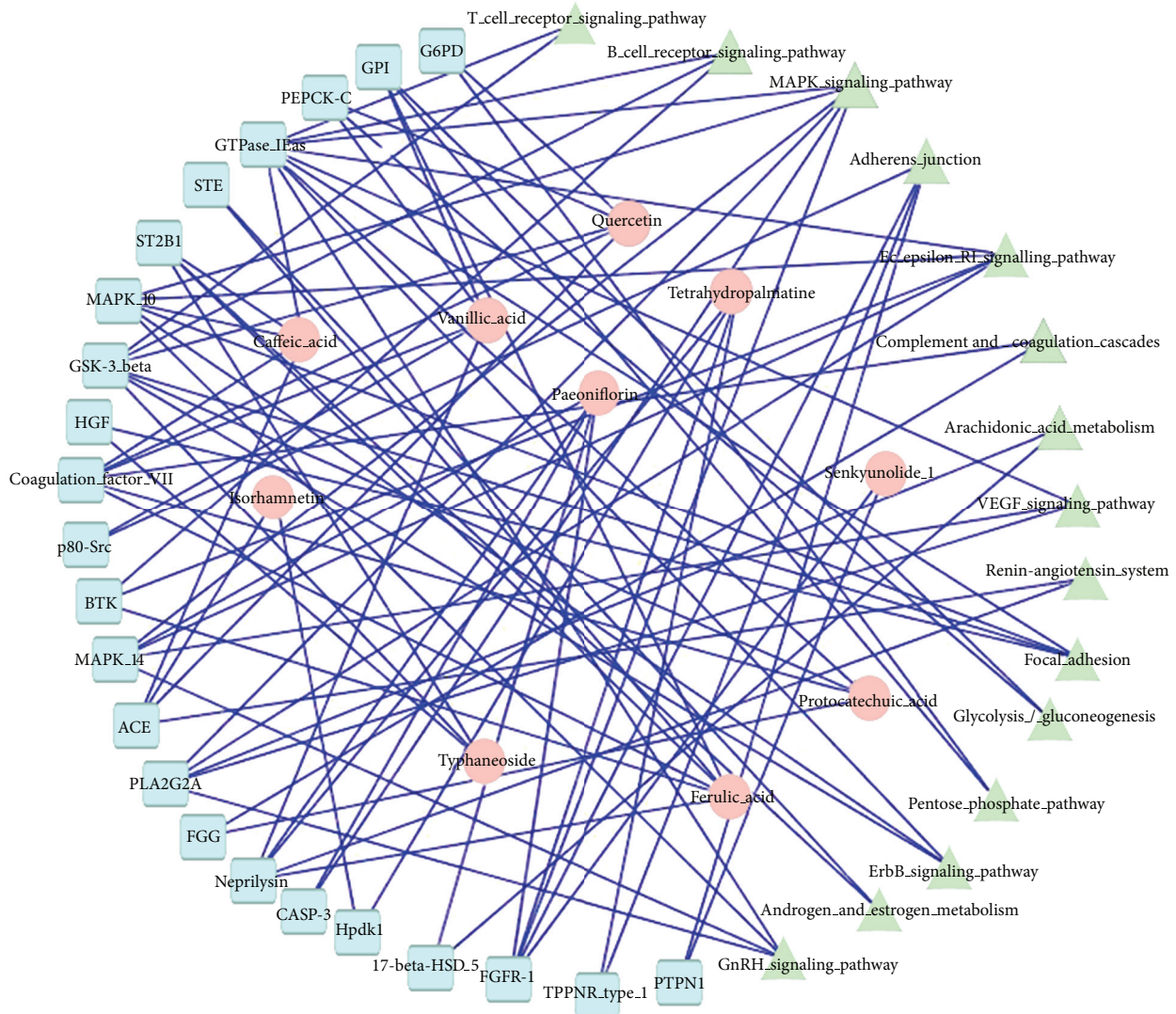


FIGURE 2: The relationships between the ingredients, targets, and pathways based on network biology.

5 s^{-1} , and 1 s^{-1}) and plasma viscosity in model rat plasma were significantly increased ($P < 0.05$ or 0.01) (Table 1), which suggests that the blood of these CCBS syndrome rats is in a viscous or stasis state. SFZYD significantly regulated whole blood viscosity at low shear rates (5 s^{-1} and 1 s^{-1}) in model rats ($P < 0.05$) at 5.04 and 10.08 g kg^{-1} doses, respectively. At a dose of 10.08 g kg^{-1} , SFZYD also significantly decreased whole blood viscosity at high shear rates (30 s^{-1} and 200 s^{-1}) and plasma viscosity ($P < 0.05$ or $P < 0.01$).

Coagulation is one important index for evaluating the state of blood stasis syndrome. The coagulation pathway comprises the complex interaction of many elements of the endothelium, coagulation factors, and platelets. Among these, thrombin plays a pivotal role in blood stasis syndrome. Thrombin acts as a multifunctional serine protease that is generated in response to vascular injury, and it catalyzes the proteolytic cleavage of the soluble plasma-protein fibrinogen to form insoluble fibrin, leading to clot formation. Thrombin

also serves as a potent platelet agonist and amplifies its own generation via feedback activation of several steps in the coagulation cascade.

The PT and APTT assays were developed based on theories and the specific need for testing, without complete knowledge of all the proteins involved in coagulation. Our data showed that in model rats, the TT, PT, APTT, and FIB were remarkably decreased compared with those of normal rats. Furthermore, SFZYD prolonged TT and PT significantly ($P < 0.05$) in the model group (Table 2). At a dosage of 10.08 g kg^{-1} , SFZYD also showed activity toward APTT.

The determined data of 5-HT, NA, and β -EP were listed in Table 3. The results showed that the contents of 5-HT and NA in both brain tissue and plasma and of β -EP in plasma significantly increased in model rat ($P < 0.05$), while the content of β -EP in brain tissue was decreased in model rat ($P < 0.05$). After SFZYD treatment, the abnormal state was regulated remarkably ($P < 0.05$ or $P < 0.01$).

TABLE 1: Changes in the whole blood and plasma shear viscosity of model rats and SFZYD-treated rats ($n = 6, \bar{x} \pm s$).

	Whole blood viscosity (η_b /mPa·s)				plasma viscosity (η_b /mPa·s)
	200 (s^{-1})	30 (s^{-1})	5 (s^{-1})	1 (s^{-1})	
Normal group	4.01 \pm 0.13	4.95 \pm 0.17	7.58 \pm 0.46	14.85 \pm 1.54	2.45 \pm 0.16
Model group	4.24 \pm 0.10 ^Δ	5.46 \pm 0.19 ^{ΔΔ}	8.99 \pm 0.59 ^{ΔΔ}	19.19 \pm 2.01 ^{ΔΔ}	3.08 \pm 0.60 ^Δ
SFZYD group (5.4 g kg ⁻¹)	4.15 \pm 0.18	5.20 \pm 0.23	8.19 \pm 0.49*	16.61 \pm 1.48**	2.84 \pm 0.32
SFZYD group (10.8 g kg ⁻¹)	4.00 \pm 0.11*	5.10 \pm 0.18*	7.89 \pm 0.53**	15.86 \pm 1.63**	2.67 \pm 0.21*

^Δ $P < 0.05$, ^{ΔΔ} $P < 0.01$ normal group versus model group; * $P < 0.05$ model group versus SFZYD group.

TABLE 2: Changes in the plasma coagulation function of model rats and SFZYD-treated rats ($n = 6, \bar{x} \pm s$).

	TT (s)	PT (s)	APTT (s)	FIB (g/L)
Normal group	31.5 \pm 3.9	20.0 \pm 2.3	47.2 \pm 4.7	26.9 \pm 1.8
Model group	22.7 \pm 2.0 ^{ΔΔ}	14.4 \pm 1.7 ^Δ	34.8 \pm 3.1 ^Δ	18.4 \pm 2.9 ^{ΔΔ}
SFZYD group (5.4 g kg ⁻¹)	28.2 \pm 2.3*	19.9 \pm 1.9*	36.6 \pm 3.6	20.9 \pm 2.3
SFZYD group (10.8 g kg ⁻¹)	30.9 \pm 3.3**	20.9 \pm 1.2**	38.9 \pm 2.8*	21.4 \pm 2.5

^Δ $P < 0.05$, ^{ΔΔ} $P < 0.01$ normal group versus model group; * $P < 0.05$ model group versus SFZYD group.

Moreover, we evaluated the model by analyzing metabolic profiling changes based on urine metabolomic data. The base peak intensity (BPI) chromatograms of the urine samples collected in positive ion mode during the eight days of animal model preparation are shown in (see Figure S1 Supplementary Material available online at <http://dx.doi.org/10.1155/2013/901943>). The results revealed that during the first three days of animal model preparation, there was no obvious departure of urine metabolic profiling, as determined by PCA, while pronounced changes were observed after 5 and 7 days of preparation, especially on the eighth day after the injection of hypodermic epinephrine, when there was a remarkable change in the metabolic profile (see Figure S2).

3.3. Metabolic Profiling Analysis. Typical base peak intensity (BPI) chromatograms in positive and negative ion modes of plasma and urine samples collected from normal and model rats are shown in Figure S3. The unsupervised PCA model was used to separate the plasma and urine samples into two blocks, respectively, between the normal group and the model group in positive and negative ion modes (Figures 3(a), 3(b), 3(c), 3(d), 4(a), 4(b), 4(c), and 4(d)). The supervised OPLS-DA, which could improve biomarker discovery and separate the samples into two blocks, was applied to obtain better discrimination between the two groups. The OPLS-DA score plot analysis of the chromatographic data identified the plasma and urine samples of the normal group and the model group based on the differences in their metabolic profiles, which suggested that the metabolic profiles were significantly changed as a result of CCBS syndrome (Figures 5(a), 5(b), 5(c), and 5(d)). The recognition of a different pattern indicates that the endogenous metabolites have changed in CCBS syndrome model rats.

OPLS-DA distinguished normal rat and model rat cohorts with 100% sensitivity and no less than 95% specificity using a leave-one-out algorithm. The R^2Y of this PLS-DA

model was 0.926 and 0.917 (plasma samples) and 0.947 and 0.922 (urine samples) in the positive and negative ion modes, respectively. The Q^2 of the model was 0.849 and 0.853 (plasma samples) and 0.823 and 0.837 (urine samples), respectively. These results indicate that the OPLS-DA models were reliable.

3.4. Metabolites Identification. The ions furthest away from the origin contribute significantly to the clustering of the two groups, and they may be regarded as the potential biomarkers in model rats. Q-TOF was used to determine the precise molecular mass of these compounds within measurement errors (<5 ppm). The potential elemental composition, degree of unsaturation, and fractional isotope abundance of the compounds were obtained. The presumed molecular mass was searched in the METLIN database, Chemspider, Human Metabolome Database, and other databases to identify the possible chemical constitutions, and MS/MS data were used to determine the possible structures of these ions.

Potential markers were extracted from S-plots and constructed following the OPLS analysis. Then, markers were chosen on the basis of their contribution to the variation and correlation within the data set. In the plasma, ten endogenous metabolites that contributed to the separation of the model rats and the normal rats were identified by comparing their molecular ion information and the corresponding fragments of product ions with authentic standards (Table 4). To illustrate the identification of metabolites, we will describe the ion at $t_R = 15.97$ min (m/z 496.3450) as an example. This ion may contain an odd number of nitrogen atoms because its precise molecular weight is 496.3383, and its molecular formula was speculated to be $C_{24}H_{50}NO_7P$, based on the analysis of its elemental composition and fractional isotope abundance. In the positive ion spectrum, the main fragment ions that were analyzed via MS/MS screening were observed at m/z 478.3290, 419.2279, 313.1615, 184.0786, 125.9252, and 104.1071, which could be the $[M+H]^+$ due to the loss of $-H_2O$,

TABLE 3: The contents of 5-HT, NA, and β -EP in plasma and brain tissue of model rats and treatment group ($n = 6$, $\bar{x} \pm s$).

	5-HT (ng/mL)		NA (ng/mL)		β -EP (ng/mL)	
	Brain tissue	Plasma	Brain tissue	Plasma	Brain tissue	Plasma
Normal group	144.39 \pm 30.36	467.71 \pm 86.01	3.92 \pm 0.72	15.23 \pm 2.66	0.28 \pm 0.10	2.57 \pm 0.45
Model group	259.38 \pm 74.48 [#]	549.9 \pm 90.1 [#]	4.8 \pm 1.3 [#]	18.5 \pm 1.9 [#]	0.15 \pm 0.08 [#]	3.47 \pm 1.68 [#]
SFZYD group (5.4 g kg ⁻¹)	183.49 \pm 89.99 [*]	492.79 \pm 72.14 [*]	4.33 \pm 1.46	16.95 \pm 5.11 [*]	0.24 \pm 0.09 [*]	2.38 \pm 1.42 [*]
SFZYD group (10.8 g kg ⁻¹)	153.56 \pm 76.32 ^{**}	458.24 \pm 81.56 ^{**}	3.85 \pm 1.45 [*]	15.87 \pm 4.36 ^{**}	0.34 \pm 0.12 [*]	2.56 \pm 1.89 [*]

5-HT: 5-hydroxytryptamine; NA: Noradrenaline; β -EP: β -endorphin. Data were expressed as Mean \pm SEM. Means between the normal group, model group, low-dose SFZYD-treated group, and high-dose SFZYD-treated group. Significant differences when compared with the model group ^{*} $P < 0.05$, ^{**} $P < 0.01$ and compared with the normal group [#] $P < 0.05$.

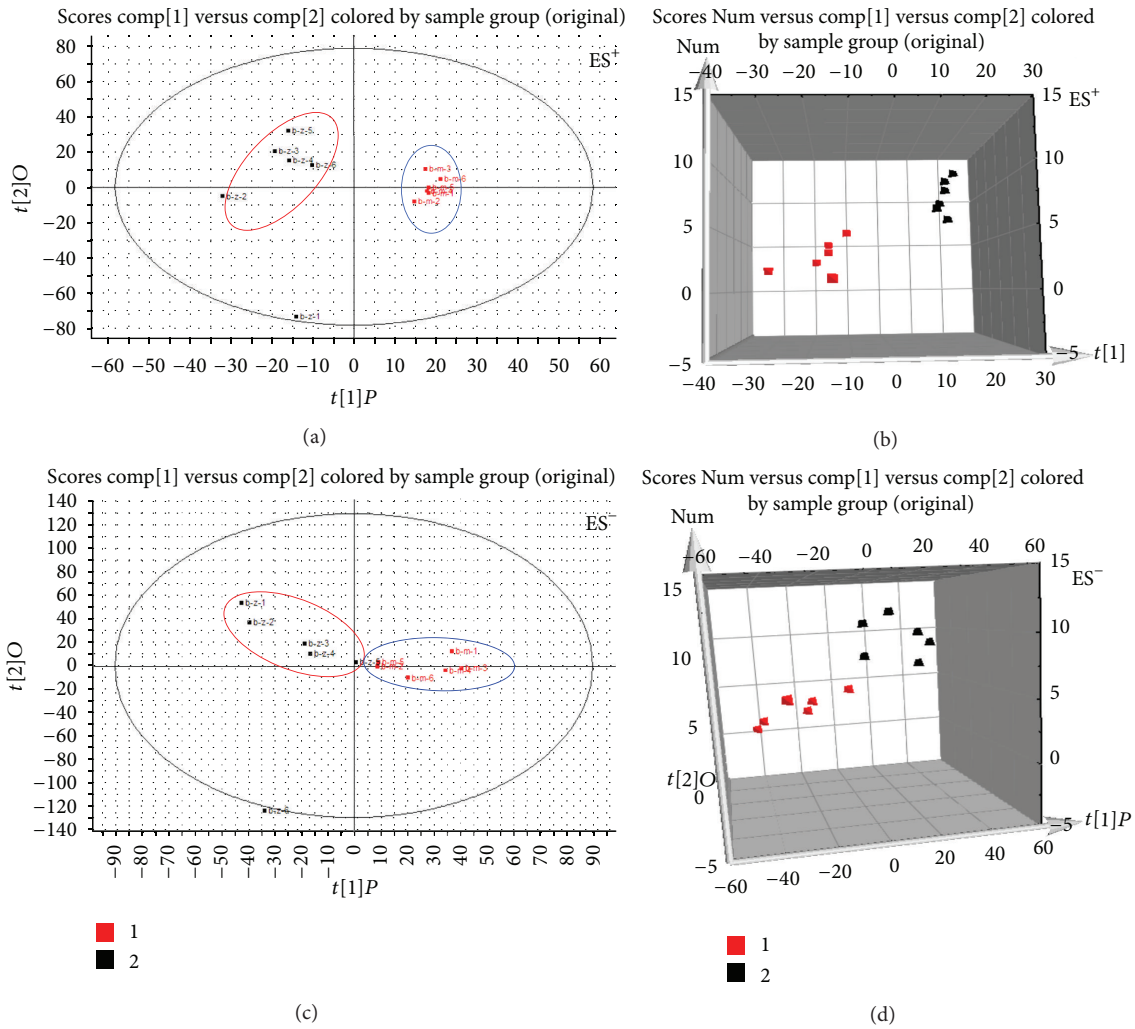


FIGURE 3: PLS-DA model results for samples obtained from the plasma of the normal and model groups and analyzed in positive and negative ion modes (ES⁺: (a) 2-D plot; (b) 3-D plot; ES⁻: (c) 2-D plot; (d) 3-D plot).

$-C_3H_{10}NO$, $-C_5H_{13}NO_4P$, $-C_{19}H_{37}NO_2$, $-C_{22}H_{44}NO_3$, and $-C_{20}H_{42}NO_4P$, respectively. Finally, to define its structure, we searched the HMDB database, and the metabolite was tentatively identified as lysophosphatidylcholine (16:0) [LPC (16:0)].

Compared with normal rats, four metabolites were upregulated ($P < 0.05$) in CCBS syndrome model rats, including 5-dehydro-4-deoxy-*D*-glucarate, 5 α -tetrahydrocorticosterone, PC (13:0/0:0), and 17-phenyl trinor PGF_{2 α} methyl ester.

Alternatively, six metabolites were significantly downregulated ($P < 0.05$) in CCBS syndrome model rats, including LysoPC (22:5 (7Z,10Z,13Z,16Z,19Z)), LysoPC (17:0), PC (0:0/18:0), LysoPC (18:2(9Z,12Z)), LysoPC (16:0), and LysoPC (22:6 (4Z, 7Z, 10Z, 13Z, 16Z, 19Z)) (Table 4).

In urine samples, the significant variables that were identified in positive and negative ion modes are summarized in Table 5. Ten endogenous metabolites were tentatively identified using the methods described above. The

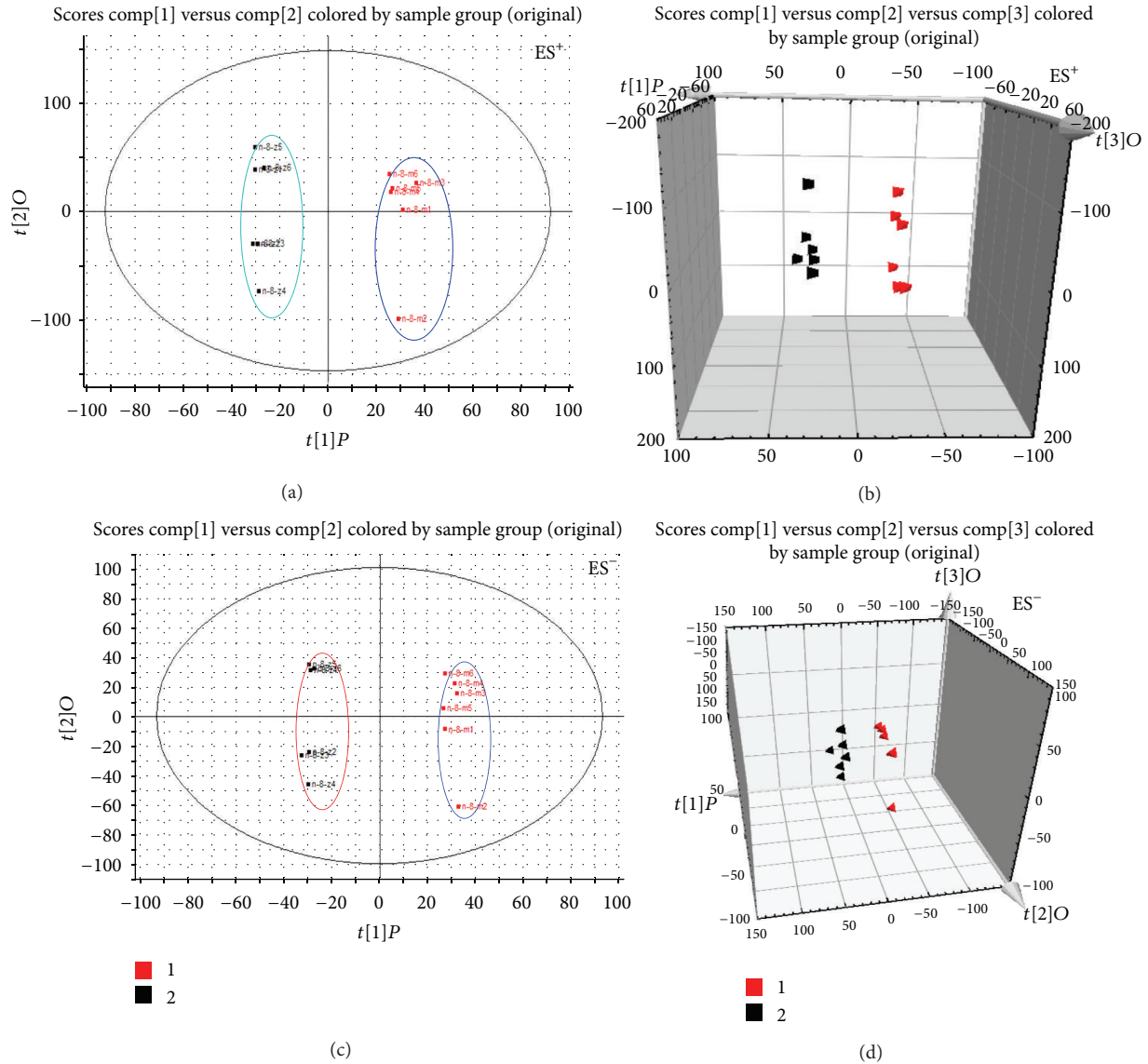


FIGURE 4: PLS-DA model results for the samples obtained from the urine of the normal and model groups and analyzed in positive and negative ion modes (ES⁺: (a) 2-D plot; (b) 3-D plot; ES⁻: (c) 2-D plot; (d) 3-D plot).

metabolites of cholic acid, 3-methoxy-4-hydroxyphenylglycol sulfate, 5-dehydro-4-deoxy-*D*-glucarate, 5 α -tetrahydrocortisol, and 13,14-dihydro PGF_{2 α} were significantly upregulated ($P < 0.05$) in CCBS syndrome model rats, whereas the metabolites of 2-phenylethanol glucuronide, hippuric acid, 6-hydroxy-5-methoxyindole glucuronide, 2,8-dihydroxyquinoline-beta-*D*-glucuronide, and normeperidine acid glucuronide were significantly downregulated ($P < 0.05$). The fact that different metabolites were altered in the plasma and urine may denote the potential of these metabolites as targeted biomarkers that can be used to differentiate between the CCBS syndrome and normal states.

3.5. Metabolic Pathway and Function Analysis. Metabolite profiling is the analysis of a group of metabolites that are related to a specific metabolic pathway in biological states. More detailed analyses of the most relevant pathways and

networks for CCBS were performed using Metaboanalyst, which is a free, web-based tool that combines the results of powerful pathway enrichment analysis with the conditions of the study. Metaboanalyst and directed graph use the high-quality KEGG (<http://www.genome.jp/kegg/>) pathway database as the backend knowledgebase. Consequently, the identification of potential targets using a metabolic pathway analysis (impact value ≥ 0.10) with Metaboanalyst revealed that metabolites that were identified together are important for the host response to CCBS, and they are responsible for pentose and glucuronate interconversions and glycerophospholipid metabolism (see Figure S4). Distinct metabolic pathway analyses (impact value ≥ 0.10) were performed to identify pathways related to CCBS.

3.6. Therapeutic Effects of SFZYD. To more clearly characterize the effects of SFZYD on CCBS model rats,

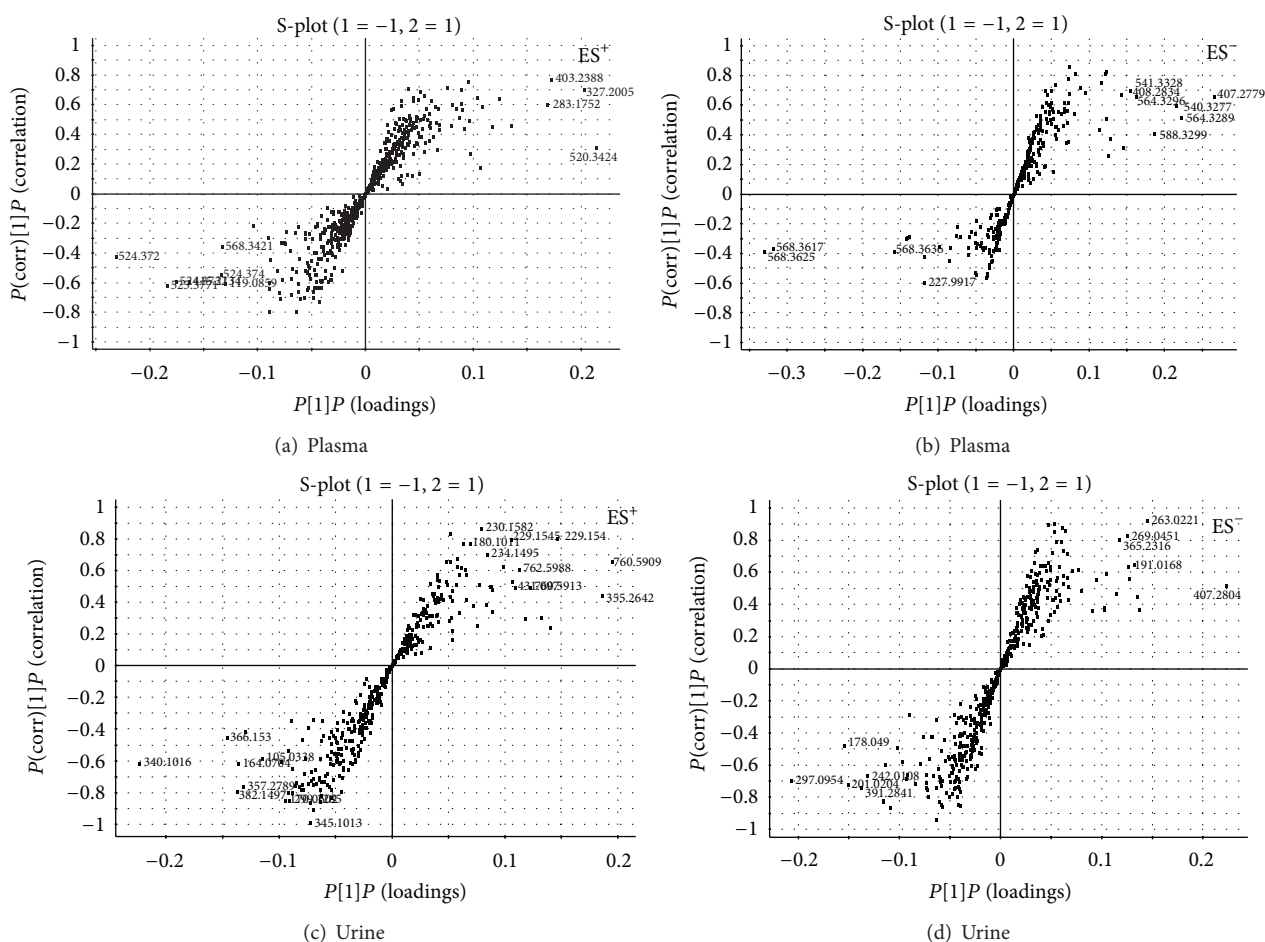


FIGURE 5: S-plot of the OPLS-DA model for the plasma and urine samples from the normal versus model groups (plasma: (a) ES⁺ mode; (b) ES⁻ mode; urine: (c) ES⁺ mode; and (d) ES⁻ mode).

TABLE 4: Identification of differentially expressed metabolites in the plasma that may account for the discrimination between normal and model rats.

No.	Metabolites	Formula	Obsd. $[M + H]^+ / [M - H]^-$ (m/z)	Content variance ^c	FC ^d	P ^e value
1	LysoPC (22:5 (7Z, 10Z, 13Z, 16Z, 19Z))	C ₃₀ H ₅₂ NO ₇ P	568.3436 ^a	↓	-2.33	0.018
2	5-Dehydro-4-deoxy-D-glucarate	C ₆ H ₈ O ₇	191.0197 ^a	↑	2.56	0.022
3	LysoPC (17:0)	C ₂₅ H ₅₂ NO ₇ P	508.3403 ^a	↓	-1.42	0.030
4	5 α -Tetrahydrocorticosterone	C ₂₁ H ₃₄ O ₄	349.2378 ^a	↑	2.56	0.035
5	PC (13:0/0:0)	C ₂₁ H ₄₄ NO ₇ P	452.2774 ^a	↑	1.25	0.021
6	17-phenyl trinar PGF2 α methyl ester	C ₂₄ H ₃₄ O ₅	404.2438 ^b	↑	2.01	0.017
7	PC (0:0/18:0)	C ₂₆ H ₅₄ NO ₇ P	524.3720 ^b	↓	-1.35	0.042
8	LysoPC (18:2 (9Z, 12Z))	C ₂₆ H ₅₀ NO ₇ P	520.3424 ^b	↓	-1.56	0.030
9	LysoPC (16:0)	C ₂₄ H ₅₀ NO ₇ P	496.3450 ^b	↓	-1.78	0.016
10	LysoPC (22:6 (4Z, 7Z, 10Z, 13Z, 16Z, 19Z))	C ₃₀ H ₅₀ NO ₇ P	568.3421 ^b	↓	-2.60	0.026

^aObserved at ES⁻ mode $[M - H]^-$; ^bobserved at ES⁺ mode $[M + H]^+$.

^c↑: content increased; ↓: content decreased.

^dFold change was calculated as the ratio of the mean metabolite levels between two groups. A positive value of fold change indicates a relatively higher concentration of metabolites, while a negative value of fold change indicates a relatively lower concentration of metabolites in model rats as compared to normal rats.

^eP values were calculated from two-tailed Mann-Whitney U test with a threshold of 0.05.

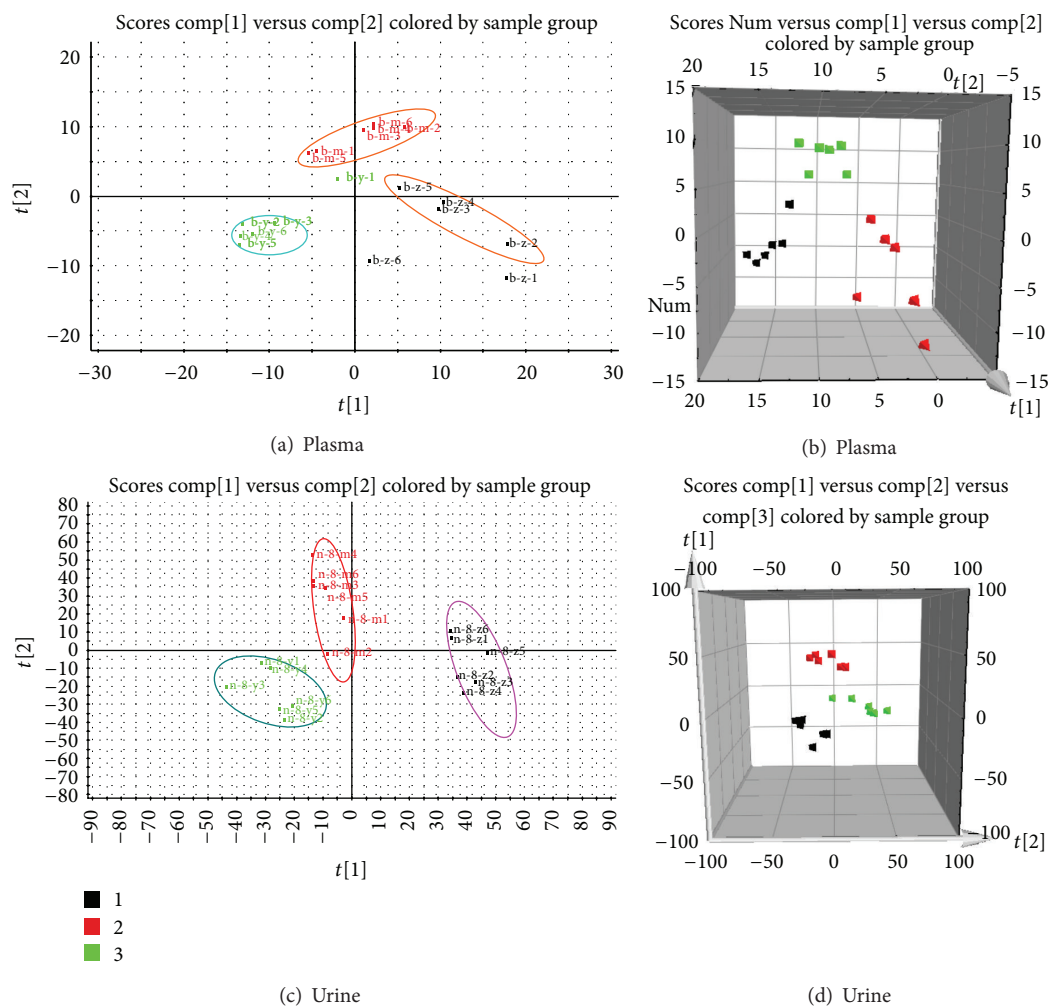


FIGURE 6: PLS-DA model results and loadings plots for the plasma and urine samples obtained from the normal, model, and treatment groups and analyzed in positive ion mode (Plasma: (a) 2-D plot and (b) 3-D plot; Urine: (c) 2-D plot and (d) 3-D plot).

TABLE 5: Identification of differentially expressed metabolites in the urine that may account for the discrimination between normal and model rats.

No.	Metabolites	Formula	Obsd. $[M + H]^+ / [M - H]^- (m/z)$	Content variance ^c	FC ^d	P^e value
1	Cholic acid	$C_{24}H_{40}O_5$	407.2804 ^a	↑	1.56	0.035
2	2-Phenylethanol glucuronide	$C_{14}H_{18}O_7$	297.0954 ^a	↓	-1.69	0.026
3	Hippuric acid	$C_9H_9NO_3$	178.0491 ^a	↓	-1.81	0.040
4	3-Methoxy-4-hydroxyphenylglycol sulfate	$C_9H_{12}O_7S$	263.0221 ^c	↑	2.53	0.025
5	5-Dehydro-4-deoxy-D-glucarate	$C_6H_8O_7$	191.0168 ^a	↑	2.40	0.016
6	5 α -Tetrahydrocortisol	$C_{21}H_{34}O_5$	365.2316 ^a	↑	3.70	0.023
7	6-Hydroxy-5-methoxyindole glucuronide	$C_{15}H_{17}NO_8$	340.1016 ^b	↓	-3.79	0.012
8	2,8-Dihydroxyquinoline-beta-D-glucuronide	$C_{15}H_{15}NO_8$	338.0847 ^b	↓	-2.42	0.028
9	Normeperidinic acid glucuronide	$C_{18}H_{23}NO_8$	382.1497 ^b	↓	-3.21	0.037
10	13,14-dihydro PGF2 α	$C_{20}H_{36}O_5$	357.2724 ^b	↑	2.01	0.028

^aObserved at ES^- mode $[M - H]^-$; ^bobserved at ES^+ mode $[M + H]^+$.

^c ↑: content increased; ↓: content decreased.

^dFold change was calculated as the ratio of the mean metabolite levels between two groups. A positive value of fold change indicates a relatively higher concentration of metabolites while a negative value of fold change indicates a relatively lower concentration of metabolites in model rats as compared to normal rats.

^e P values were calculated from two-tailed Mann-Whitney U test with a threshold of 0.05.

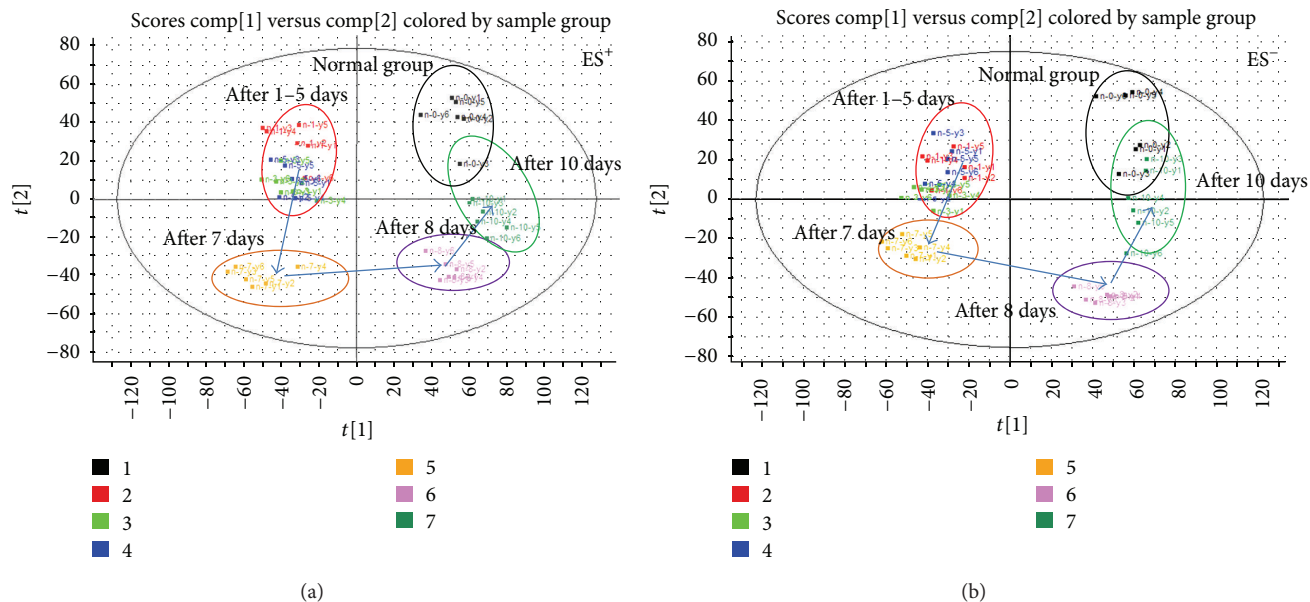


FIGURE 7: Urine metabolic profile changes after days 0, 1, 3, 5, 7, 8, and 10 of SFZYD treatment, as analyzed in positive and negative ion modes ((a) ES⁺ mode; (b) ES⁻ mode) [23].

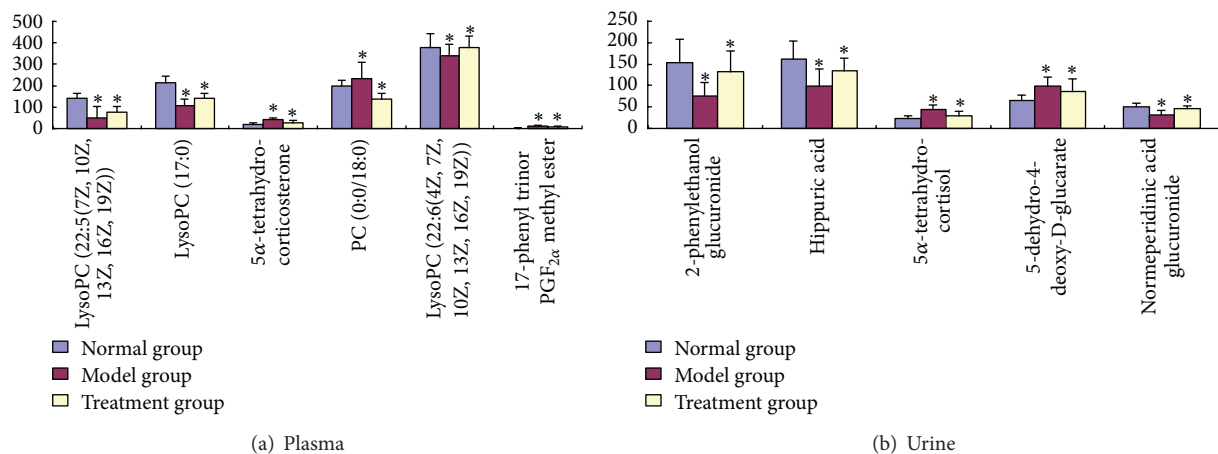


FIGURE 8: Changes in the relative quantities of targeted metabolites in the plasma and urine, identified in different groups. A two-tailed, parametric t -test was used to determine the significance of the changes for each metabolite, in relative quantities. Bars represent the mean relative metabolite concentration and standard deviations. * $P < 0.05$.

a PCA analysis was carried out to determine the changes before and after SFZYD treatment. The results revealed variations between the plasma and urine metabolic profiles of the model group, normal group, and SFZYD group (Figures 6(a), 6(b), 6(c), and 6(d)). To better understand the time-dependent effect of SFZYD, a PCA model was constructed to analyze all the data acquired from the normal group, predose group and treatment group at days 1, 3, 5, 7, and 10 in both positive and negative ion modes (Figures 7(a) and 7(b)). The spot observed in the treatment group at days 1–5 is close to that of the model group, indicating that the cold coagulation and blood stasis syndrome state is dominant. The spots observed in the treatment group at day 7 clustered near the center of the plot with a shift back toward the normal group, which might be an indication

of the accumulated effect of SFZYD. The spot observed in the treatment group at days 8 and 10 ultimately approached the normal state, suggesting that SFZYD treatment had a positive therapeutic effect on the rats. Furthermore, the relative concentrations of 6 endogenous metabolites in the plasma and 5 endogenous metabolites in the urine were significantly affected by SFZYD ($P < 0.05$). All of these metabolites returned to normal levels after SFZYD treatment (Figures 8(a) and 8(b)). Thus, the efficient regulation of these potential biomarkers may account for the effects of SFZYD in model rats.

The prediction and identification of molecular markers (targets) and metabolic pathways have the potential to improve the diagnosis, prognosis, and therapy for ZHENG or diseases [27–30]. We utilized reverse docking method to

predict the biology targets and pathway annotation. Furthermore a metabolomic approach to analyze the changes in the plasma and urine samples of CCBS syndrome model rats, normal rats, and SFZYD-treated rats was applied. We identified 20 endogenous metabolites (10 in the plasma and 10 in the urine) that were upregulated or downregulated ($P < 0.05$ or 0.01) in CCBS syndrome, including LysoPCs and glucuronide metabolites. Furthermore, 11 potential biomarkers (6 metabolites in the plasma and 5 metabolites in the urine) were regulated by SFZYD.

Studies using targeted metabolite analyses have already shown that alterations in critical CCBS syndrome metabolic pathways, such as glycerophospholipid metabolism (impact value 0.24) and pentose and glucuronate interconversions (impact value 0.27), are strongly associated with the development of CCBS syndrome. Phospholipid metabolism and glycometabolism were disturbed in the plasma and urine of CCBS rats, respectively. In urine, the levels of the metabolites of 2-phenylethanol glucuronide, hippuric acid, and normeperidinic acid glucuronide, which are all related to glycometabolism, were significantly decreased in model rats. The low level of glucuronide metabolites implies that energy metabolism decreased and the energy metabolism pathway increased, resulting in abnormal pentose and glucuronate interconversions. Previous studies have also reported that cold exposure increased energy expenditure by activating specific sympathetic pathways [31]. These results agreed well with the SFZYD bioactive ingredients prediction of network targets related to inflammation and immunological stress, hormone metabolism, glycometabolism, and coagulation cascade system.

Ephedrine is known to raise blood pressure, heart rate, and energy expenditure and to increase the levels of multiple circulating metabolites, including glucose, insulin, and thyroid hormones [31]. In this paper, cold and ephedrine mutually induced CCBS syndrome in model rats, and the level of phosphatidylcholine in the plasma decreased. Among the potential markers, 5α -tetrahydrocorticosterone and 17-phenyl trinor PGF_{2 α} methyl ester levels increased in the plasma of the model rats. 5α -Tetrahydrocorticosterone is a corticosteroid hormone, and the hypothalamic-pituitary-adrenal axis was activated in the CCBS model rats induced with cold and epinephrine. The excretion of corticotropin-releasing factor (CRF) by the hypothalamus and pituitarium leads to the release of adrenocorticotrophic hormone, which acts on the adrenal cortex to promote the secretion of corticosteroid hormones [32]. Therefore, the combination of cold and ephedrine could change the metabolism of hormones in CCBS syndrome model rats. Moreover, the levels of LysoPC metabolites were decreased in the plasma of model rats.

It was reported that primary dysmenorrhea patients with CCBS syndrome have high levels of prostaglandin growth factor 2 (PGF2) in their menstrual fluid [33], and PGF2 stimulates myometrial contractions and ischemia and sensitizes nerve endings. In this paper, CCBS syndrome model rats had high levels of 17-phenyl trinor PGF_{2 α} methyl ester, and phospholipid metabolism was disturbed, likely due to the inflammatory response. Future research will focus on

the discovery of additional biomarkers using metabolomics platforms and the validation of explorative biomarkers.

In addition, 11 specific metabolites regulated by SFZYD were identified, including 5α -tetrahydrocortisol, 5-dehydro-4-deoxy-D-glucarate, 2-phenylethanol glucuronide, hippuric acid, and normeperidinic acid glucuronide in the urine and 5α -tetrahydrocorticosterone, PC (0:0/18:0), 17-phenyl trinor PGF_{2 α} methyl ester, LysoPC (22:6(4Z, 7Z, 10Z, 13Z, 16Z, 19Z)), LysoPC (17:0), and LysoPC (22:6 (4Z, 7Z, 10Z, 13Z, 16Z, 19Z)) in the plasma. These biomarkers suggest that the pathogenesis of CCBS syndrome is closely related to glycometabolism and phospholipid metabolism. Based on these findings, further studies would be performed to validate the predicted targets and the changed metabolites and to elucidate the mechanisms underlying these alterations.

Our results also showed that SFZYD improved the status of hemorheology and blood viscosity, and it regulated the coagulation function of TT and APTT. These data imply that the state of CCBS syndrome is closely associated with blood coagulation function. This research also verified that ephedrine-induced platelet aggregation, gluconeogenesis, ischemia, and Ca²⁺ influx in vascular endothelial cells are mediated by CNGA2 channels [34–37]. So, the systems biology and network targets prediction are one of the most important trends for the development of traditional Chinese medicine [38–40].

4. Conclusions

In summary, the reverse docking method and metabolomics-based study provide a powerful approach to evaluate the effects of Chinese herbs and discover potential biomarkers (targets) via the prediction of biological targets and analysis of global changes in an individual's metabolic profile. Here, for the first time, we performed a comprehensive analysis of the network targets, pathways induced by SFZYD bioactive ingredients, and metabolic patterns of CCBS syndrome. Our findings suggest that the proposed approach would be helpful for establishing a suitable model to reasonably evaluate CCBS syndrome, explore its pathological mechanisms, and clarify the mechanisms of action of SFZYD.

Abbreviations

PD:	Primary dysmenorrhea
SFZYD:	Shaofu Zhuyu decoction
MS/MS:	Tandem mass spectrometry
OPLS:	Orthogonal partial least squares
PCA:	Principal components analysis
PLS-DA:	Partial least-squares discriminant analysis
RT:	Retention time
TOFMS:	Time-of-flight mass spectrometry
UPLC:	Ultrapformance liquid chromatography.

Acknowledgments

This work was supported by the Key Research Project in Basic Science of Jiangsu College and University (nos. 06KJA36022

and 11KJA360002) and the National Natural Science Foundation of China (nos. 30973885, 81373889 and 81102898). This work was also supported by the Construction Project for Jiangsu Key Laboratory for High Technology Research of TCM Formulae (BM2010576; BK2010561), the Construction Project for Jiangsu Engineering Center of Innovative Drug from Blood-conditioning TCM Formulae, and a project funded by the Priority Academic Program Development of Jiangsu Higher Education Institutions (ysxk-2010).

References

- [1] T. Xue and R. Roy, "Studying traditional Chinese medicine," *Science*, vol. 300, no. 5620, pp. 740–741, 2003.
- [2] S. Li, Z. Q. Zhang, L. J. Wu, X. G. Zhang, Y. D. Li, and Y. Y. Wang, "Understanding ZHENG in traditional Chinese medicine in the context of neuro-endocrine-immune network," *IET Systems Biology*, vol. 1, no. 1, pp. 51–60, 2007.
- [3] S. B. Su, A. P. Lu, S. Li, and W. Jia, "Evidence-based ZHENG: a traditional Chinese medicine syndrome," *Evidence-Based Complementary and Alternative Medicine*, vol. 2012, Article ID 246538, 2 pages, 2012.
- [4] F. Liao, "Herbs of activating blood circulation to remove blood stasis," *Clinical Hemorheology and Microcirculation*, vol. 23, no. 2–4, pp. 127–131, 2000.
- [5] X.-J. Ma, H.-J. Yin, and K.-J. Chen, "Investigation of gene expression profiles in patients with blood stasis syndrome," *Journal of Chinese Integrative Medicine*, vol. 6, no. 4, pp. 355–360, 2008.
- [6] S. L. Su, J. A. Duan, T. J. Wang, and Y. P. Tang, "Evaluating the effects of Shaofu Zhuyu Decoction on hemorheology and ovarian function in rat model of Han-Ning blood stasis," *Chinese Journal of Experimental Traditional Medicine Formula*, vol. 14, no. 12, pp. 14–34, 2008 (Chinese).
- [7] J. Zhang and C. L. Sun, "Application in gynecology diseases of Shaofu Zhuyu decoction," *Chinese Journal of Natural Medicine*, vol. 4, no. 2, pp. 109–112, 2002 (Chinese).
- [8] M. Fan, "Clinical observation of Shaofu Zhuyu decoction for treating primary dysmenorrhea of cold coagulation and blood stasis," *Beijing Journal of Traditional Chinese Medicine*, vol. 30, no. 6, pp. 455–456, 2011 (Chinese).
- [9] Q. Q. Cheng and Y. Zhu, "Clinical study on primary dysmenorrhea of blood—stasis of cold-coagulation syndrome treated with modified Shaofu Zhuyu decoction," *Journal of Chinese Medicine*, vol. 26, no. 10, pp. 1249–1250 (Chinese).
- [10] J. K. Nicholson and I. D. Wilson, "Understanding "global" systems biology: metabolomics and the continuum of metabolism," *Nature Reviews Drug Discovery*, vol. 2, no. 8, pp. 668–676, 2003.
- [11] C.-X. Liu, "Metabolomics in medical and pharmaceutical research," *Acta Academiae Medicinae Sinicae*, vol. 29, no. 6, pp. 712–718, 2007.
- [12] X. Wang, B. Yang, A. Zhang, H. Sun, and G. Yan, "Potential drug targets on insomnia and intervention effects of Jujuboside A through metabolic pathway analysis as revealed by UPLC/ESI-SYNAPT-HDMS coupled with pattern recognition approach," *Journal of Proteomics*, vol. 75, no. 4, pp. 1411–1427, 2012.
- [13] Y. H. Lu, H. P. Hao, G. J. Wang, and X. H. Chen, "Metabolomics approach to the biochemical differentiation of traditional Chinese medicine syndrome types of hypertension," *Chinese Journal of Clinical Pharmacology Therapeutics*, vol. 12, no. 10, pp. 1144–1150, 2007 (Chinese).
- [14] P. Gong, N. Cui, L. Wu et al., "Chemicalome and metabolome matching approach to elucidating biological metabolic networks of complex mixtures," *Analytical Chemistry*, vol. 84, no. 6, pp. 2995–3002, 2012.
- [15] X. Wang, H. Wang, A. Zhang et al., "Metabolomics study on the toxicity of aconite root and its processed products using ultraperformance liquid-chromatography/electrospray-ionization synapt high-definition mass spectrometry coupled with pattern recognition approach and ingenuity pathways analysis," *Journal of Proteome Research*, vol. 11, no. 2, pp. 1284–1301, 2012.
- [16] H. Y. Zhao, J. Li, X. J. He et al., "The protective effect of Yi Shen Juan Bi Pill in arthritic rats with castration-induced kidney deficiency," *Evidence-Based Complementary and Alternative Medicine*, vol. 2012, Article ID 102641, 8 pages, 2012.
- [17] J. Li, C. Lu, M. Jiang et al., "Traditional Chinese Medicine-based network pharmacology could lead to new multicomponent drug discovery," *Evidence-Based Complementary and Alternative Medicine*, vol. 2012, Article ID 149762, 11 pages, 2012.
- [18] S. Li and B. Zhang, "Traditional Chinese medicine network pharmacology: theory, methodology and application," *Chinese Journal of Natural Medicines*, vol. 11, no. 2, pp. 110–120, 2013.
- [19] B. Zhang, X. Wang, and S. Li, "An integrative platform of TCM network pharmacology and its application on an herbal formula, Qing-Luo-Yin," *Evidence-Based Complementary and Alternative Medicine*, vol. 2013, Article ID 456747, 12 pages, 2013.
- [20] S. Li, B. Zhang, and N. Zhang, "Network target for screening synergistic drug combinations with application to traditional Chinese medicine," *BMC Systems Biology*, vol. 5, supplement 1, article S10, 2011.
- [21] S. Li, B. Zhang, D. Jiang, Y. Wei, and N. Zhang, "Herb network construction and co-module analysis for uncovering the combination rule of traditional Chinese herbal formulae," *BMC Bioinformatics*, vol. 11, supplement 11, article S6, 2010.
- [22] S. Li, "Network systems underlying traditional Chinese medicine syndrome and herb formula," *Current Bioinformatics*, vol. 4, no. 3, pp. 188–196, 2009.
- [23] S. L. Su, W. X. Cui, J. A. Duan et al., "UHPLC-MS simultaneous determination and pharmacokinetic study of three aromatic acids and one monoterpene in rat plasma after oral administration of Shaofu Zhuyu Decoction," *The American Journal of Chinese Medicine*, vol. 41, no. 3, pp. 697–715, 2013.
- [24] S. Su, J. Guo, J.-A. Duan et al., "Ultra-performance liquid chromatography-tandem mass spectrometry analysis of the bioactive components and their metabolites of Shaofu Zhuyu decoction active extract in rat plasma," *Journal of Chromatography B*, vol. 878, no. 3–4, pp. 355–362, 2010.
- [25] H.-X. Li, S.-Y. Han, X.-W. Wang et al., "Effect of the carthamins yellow from *Carthamus tinctorius* L. on hemorheological disorders of blood stasis in rats," *Food and Chemical Toxicology*, vol. 47, no. 8, pp. 1797–1802, 2009.
- [26] E. M. Lenz and I. D. Wilson, "Analytical strategies in metabolomics," *Journal of Proteome Research*, vol. 6, no. 2, pp. 443–458, 2007.
- [27] G. S. Catchpole, M. Beckmann, D. P. Enot et al., "Hierarchical metabolomics demonstrates substantial compositional similarity between genetically modified and conventional potato crops," *Proceedings of the National Academy of Sciences of the United States of America*, vol. 102, no. 40, pp. 14458–14462, 2005.

- [28] J.-Y. Liu, N. Li, J. Yang et al., "Metabolic profiling of murine plasma reveals an unexpected biomarker in rofecoxib-mediated cardiovascular events," *Proceedings of the National Academy of Sciences of the United States of America*, vol. 107, no. 39, pp. 17017–17022, 2010.
- [29] K. Suhre, S. Y. Shin, A. K. Petersen et al., "Human metabolic individuality in biomedical and pharmaceutical research," *Nature*, vol. 477, no. 7326, pp. 54–60, 2011.
- [30] D. D. Andersona, C. M. Quintero, and P. J. Stovera, "Identification of a de novo thymidylate biosynthesis pathway in mammalian mitochondria," *Proceedings of the National Academy of Sciences of the United States of America*, vol. 108, no. 37, pp. 15163–15168, 2011.
- [31] A. M. Cypess, Y. C. Chen, C. Sze et al., "Cold but not sympathomimetics activates human brown adipose tissue in vivo," *Proceeding of the National Academy of Science of the United States of America*, vol. 109, no. 25, pp. 10001–10005, 2012.
- [32] L. Arborelius, M. J. Owens, P. M. Plotsky, and C. B. Nemeroff, "The role of corticotropin-releasing factor in depression and anxiety disorders," *Journal of Endocrinology*, vol. 160, no. 1, pp. 1–12, 1999.
- [33] W. Y. Chan and M. Y. Dawood, "Prostaglandin levels in menstrual fluid of nondysmenorrheic and of dysmenorrheic subjects with and without oral contraceptive or ibuprofen therapy," *Advances in prostaglandin and thromboxane research*, vol. 8, pp. 1443–1447, 1980.
- [34] A. Spalding, H. Vaitkevicius, S. Dill, S. MacKenzie, A. Schmaier, and W. Lockette, "Mechanism of epinephrine-induced platelet aggregation," *Hypertension*, vol. 31, no. 2, pp. 603–607, 1998.
- [35] K. Kim, C. C. Sung, A. Cova, I. S. Jang, and S. C. Park, "Alterations of epinephrine-induced gluconeogenesis in aging," *Experimental and Molecular Medicine*, vol. 41, no. 5, pp. 334–340, 2009.
- [36] B. H. Sung, M. F. Wilson, C. Robinson, U. Thadani, and W. R. Lovallo, "Mechanisms of myocardial ischemia induced by epinephrine: comparison with exercise-induced ischemia," *Psychosomatic Medicine*, vol. 50, no. 4, pp. 381–393, 1988.
- [37] B. Shen, K.-T. Cheng, Y.-K. Leung et al., "Epinephrine-induced Ca^{2+} influx in vascular endothelial cells is mediated by CNGA2 channels," *Journal of Molecular and Cellular Cardiology*, vol. 45, no. 3, pp. 437–445, 2008.
- [38] X. Wang, B. Yang, H. Sun, and A. Zhang, "Pattern recognition approaches and computational systems tools for ultra performance liquid chromatography-mass spectrometry-based comprehensive metabolomic profiling and pathways analysis of biological data sets," *Analytical Chemistry*, vol. 84, no. 1, pp. 428–439, 2012.
- [39] S. L. Su, J. A. Duan, P. J. Wang et al., "Metabolomic study of biochemical changes in the plasma and urine of primary dysmenorrhea patients using UPLC–MS coupled with a pattern recognition approach," *Journal of Proteome Research*, vol. 12, no. 2, pp. 852–865, 2013.
- [40] T. Ma, C. Tan, H. Zhang, M. Wang, W. Ding, and S. Li, "Bridging the gap between traditional Chinese medicine and systems biology: the connection of cold syndrome and NEI network," *Molecular BioSystems*, vol. 6, no. 4, pp. 613–619, 2010.

Erratum

Erratum to “*Xiao-Xu-Ming* Decoction Protects against Blood-Brain Barrier Disruption and Neurological Injury Induced by Cerebral Ischemia and Reperfusion in Rats”

**Rui Lan,¹ Jun Xiang,^{1,2} Guo-Hua Wang,¹ Wen-Wei Li,¹ Wen Zhang,¹
Li-Li Xu,¹ and Ding-Fang Cai¹**

¹ *Department of Integrative Medicine, Zhongshan Hospital, and Laboratory of Neurology, Institute of Integrative Medicine, Fudan University, Shanghai 200032, China*

² *Longhua Hospital, Shanghai University of Traditional Chinese Medicine, Shanghai 200032, China*

Correspondence should be addressed to Ding-Fang Cai; dingfangcai@163.com

Received 19 June 2013; Accepted 27 August 2013

Copyright © 2013 Rui Lan et al. This is an open access article distributed under the Creative Commons Attribution License, which permits unrestricted use, distribution, and reproduction in any medium, provided the original work is properly cited.

The word “GADPH” should be “GAPDH” in line 23 of Section 2.10 and in Figure 6.

Research Article

Expression Profiling and Proteomic Analysis of JIN Chinese Herbal Formula in Lung Carcinoma H460 Xenografts

Luyu Zheng,¹ Weiyi Zhang,² Miao Jiang,¹ Huarong Zhang,² Fei Xiong,¹ Yang Yu,¹ Meijuan Chen,¹ Jing Zhou,¹ Xiaoming Dai,¹ Yuping Tang,¹ Ming Jiang,³ Mingyan Wang,¹ Ge Cheng,¹ Jinao Duan,¹ Wei Yu,² Biaoyang Lin,² Haian Fu,⁴ and Xu Zhang¹

¹ College of Basic Medicine and School of Pharmacy, Nanjing University of Chinese Medicine, Nanjing 210029, China

² Zhejiang California International Nanosystems Institute, Zhejiang University, Hangzhou 310058, China

³ School of Chinese Medicine, Hong Kong Baptist University, Hong Kong

⁴ Department of Pharmacology and Winship Cancer Institute, Emory University School of Medicine, 1510 Clifton Road, Atlanta, GA 30322, USA

Correspondence should be addressed to Xu Zhang; zhangxutcm@gmail.com

Received 28 March 2013; Revised 8 July 2013; Accepted 17 July 2013

Academic Editor: Aiping Lu

Copyright © 2013 Luyu Zheng et al. This is an open access article distributed under the Creative Commons Attribution License, which permits unrestricted use, distribution, and reproduction in any medium, provided the original work is properly cited.

Many traditional Chinese medicine (TCM) formulae have been used in cancer therapy. The JIN formula is an ancient herbal formula recorded in the classic TCM book *Jin Kui Yao Lue* (Golden Chamber). The JIN formula significantly delayed the growth of subcutaneous human H460 xenografted tumors in vivo compared with the growth of mock controls. Gene array analysis of signal transduction in cancer showed that the JIN formula acted on multiple targets such as the mitogen-activated protein kinase, hedgehog, and Wnt signaling pathways. The coformula treatment of JIN and diamminedichloroplatinum (DDP) affected the stress/heat shock pathway. Proteomic analysis showed 36 and 84 differentially expressed proteins between the mock and DDP groups and between the mock and JIN groups, respectively. GoMiner analysis revealed that the differentially expressed proteins between the JIN and mock groups were enriched during cellular metabolic processes, and so forth. The ones between the DDP and mock groups were enriched during protein-DNA complex assembly, and so forth. Most downregulated proteins in the JIN group were heat shock proteins (HSPs) such as HSP90AA1 and HSPA1B, which could be used as markers to monitor responses to the JIN formula therapy. The mechanism of action of the JIN formula on HSP proteins warrants further investigation.

1. Introduction

Nonsmall cell lung cancer is a major cause of cancer-related mortality worldwide and is highly resistant to treatment by classical cytotoxic agents including platinum-based drugs. Traditional Chinese medicine (TCM) aims to correct maladjustments and restore the self-regulatory ability of the body without antagonizing specific pathogenic targets. TCM has been used to treat human diseases and has a long history of safety and efficacy. The approaches used in systems biology and pharmacogenetics are similar to the practices of TCM [1]. The JIN formula is an ancient herbal formula recorded in the classical TCM book *Jin Kui Yao Lue* (Golden Chamber). This formula is composed of *Ophiopogon japonicus* (30 g),

prepared *Rhizoma pinelliae* (15 g), *Ginseng radix* (30 g), *Glycyrrhiza radix* (12 g), peach kernel (15 g), unprepared *Coix lacryma-jobi* seeds (30 g), Chinese wax gourd seed (30 g), and *Phragmites caulis* (30 g). TCM theory indicates that lung cancer is related to Qi and Yin deficiencies, Qi insufficiency in the spleen and lungs, or pathological changes because of Qi stagnation, blood stasis, and phlegm and toxin accumulation. The JIN formula can replenish both Qi and Yin, strengthen the spleen and lungs, and clear the lungs. The JIN formula can also remove phlegm and activate blood circulation to remove stasis. This study focuses on the efficacy of the JIN formula in vivo in a murine xenograft lung cancer model. This study explains the underlying mechanism of the JIN formula by microarray and proteomic analysis.

2. Materials and Methods

2.1. Cell Line and Culture Conditions. Human lung carcinoma (NCI-H460) cells were obtained from the Cell Line Bank (Shanghai, China) and used in the described experiments. The cell line was cultured in Dulbecco's modified Eagle's medium (Gibco, USA) with 10% fetal bovine serum, 100 U/mL penicillin, and 100 mg/mL streptomycin in a cell culture incubator at 37°C under 5% CO₂. The cells were used within 2 passages to 4 passages at the log phase of growth. Aliquots of the cell line were frozen at -80°C until use.

2.2. Experimental Animals. Balb/c athymic (nude) mice (male, 6 wk to 8 wk, $n = 30$) weighing 21 g to 25 g were purchased from the Animal Center of the Academy of Military Medical Sciences (Beijing, China). The mice were housed under specific pathogen-free conditions according to the guidelines of the Institutional Animal Care and Use Committee of Nanjing University of Chinese Medicine. The animal room was controlled for temperature ($22 \pm 2^\circ\text{C}$), light (12 h light/dark cycle), and humidity ($50 \pm 10\%$). All laboratory feed pellets and bedding were autoclaved.

2.3. Xenograft Model. The tumor regression model was successfully applied in nude mice to evaluate antitumor activity. This model was used to evaluate the suppression of solid tumor growth by the JIN formula. A total of 1×10^7 NCI-H460 cells in 0.2 mL of culture medium were injected subcutaneously into the flank of each mouse by using a 26 ga needle. After 7 d of observation, a solid tumor mass was excised from the mice inoculated with NCI-H460 cells. When the tumor volume in the nude mice reached approximately 50 mm³, the xenografted tumor models were randomly distributed into four groups: NCI-H460 + saline (mock group), NCI-H460 + 12 mg/mL/d JIN formula (JIN group), NCI-H460 + 20 µg/mL/d diamminedichloroplatinum (DDP) (DDP group), NCI-H460 + JIN formula + DDP (coformulated group, same dosage as in other groups), and saline (control group, without tumor). Six mice were included in each group. The JIN formula was orally administered daily for 15 d, and DDP was injected abdominally for 15 d. A group with no tumor was administered orally with saline and served as a control group.

2.4. Antitumor Activity In Vivo. All animals were monitored for activity, physical condition, body weight, and tumor growth. The body weight of each animal was measured once every 3 d. The longest (*A*) and shortest (*B*) tumor diameters (mm) were obtained, and the formula for an ellipsoid sphere ($0.52 \times A \times B^2$) was used to calculate the tumor volume every 2 d. The tumor weights were also measured on the basis of the tumor regression on the final day of the experiment after the animals were sacrificed. The antitumor activities of the treatments were expressed as follows: inhibition rate (%) = $(W_{\text{mock}} - W_{\text{treatment}}) / W_{\text{model}} \times 100\%$, where W_{mock} and $W_{\text{treatment}}$ are the tumor weights of the mock and treatment groups, respectively. The xenografted tumors and other vital organs

of the mice were harvested, fixed in 4% formalin, embedded in paraffin, and cut in 4 mm sections for histological study.

2.5. Preparation of Total RNA. Total RNA from the xenografted tumor was isolated with TRIZOL reagent (Invitrogen Life Technologies). We pooled an equal amount of cancer tissues from six individual mouse xenografts in each group (JIN, DPP, JIN + DDP, and the mock groups) to save cost. The RNA was eluted in RNase-free water, and the integrity was verified by electrophoresis on 1.2% agarose gel and visualized with ethidium bromide staining. The concentration was quantified by ultraviolet absorption with a nanodrop spectrophotometer (BioLab Ltd.).

2.6. Expression Profiling Array. The total RNA from the experimental samples was used as a template and reverse-transcribed to generate cDNA. The cDNA was then converted into biotin-labeled cRNA probes by using Biotin-16-dUTP (Roche) by in vitro transcription with the TrueLabeling-AMP linear RNA amplification kit (SuperArray Bioscience). Before hybridization, the cRNA probes were purified with the ArrayGrade cRNA Cleanup Kit (Superarray Bioscience).

The Oligo GEArray microarray series (OHS-044) (SuperArray Inc.) was used to quantify the expression of the 113 genes involved in the 15 signal transduction pathways in cancer (mitogen-activated protein kinase (MAPK), Wnt, hedgehog, signal transducers, and activators of transcription, stress/heat shock, inflammation/nuclear factor-kappa B, survival, androgen/estrogen, and transforming growth factor-beta (TGF-β) pathways, etc).

Purified cRNA probes were hybridized with the membranes at 60°C overnight with slow agitation in a hybridization oven. The hybridized membranes were washed once in saline sodium citrate buffer solution I (2x, 1% sodium citrate/sorbitol buffer) and once in solution II (0.1x, 0.5% sodium dodecyl sulfate (SDS)). Membranes were incubated with alkaline phosphatase-conjugated streptavidin. Thereafter, the membranes were washed and incubated with the CDP-Star chemiluminescent substrate. Detection was performed by exposure to X-ray film. Membrane images were analyzed by the web-based GEArray Expression Analysis Suite software. The relative expression level of each gene was determined by comparing the signal intensity of each gene in the array after background and normalization corrections. For comparison, at least 1 spot intensity had to be more than twice the background intensity, and the spot intensity ratios had to be higher than 2 (for upregulation) or lower than 0.5 and higher than 0 (for downregulation).

2.7. Quantitative Real-Time Polymerase Chain Reaction (PCR). PCR primers were designed by using the Primer 5.0 software (Primer, Canada) based on the special design criteria for real-time PCR primers (Table 1). The forward and reverse primer sequences and lengths of amplified gene products were as follows. The RNA samples were reverse-transcribed by using Moloney murine leukemia virus reverse transcriptase (Epicentre). An oligo-dT primer was used to prime the reverse transcription. Beta-actin was selected as the reference

TABLE 1: Description of the primer sequences.

Gene	Forward and reverse primer sequences	Annealing temperature (°C)	Length of amplified product (bp)
<i>β-actin</i>	F: 5' CCTGTACGCCAACACAGTGC3' R: 5' ATACTCCTGCTTGCTGATCC3'	59	211
<i>CDKN1C</i>	F: 5' CTGCGGTGAGCCAATTTAGAG3' R: 5' CCTTGGGACCAGTGTACCTTCT3'	59	231
<i>PTCH2</i>	F: 5' GGCTTCGTGCTTACTTCCA3' R: 5' TGGCGTGC GG TCTGTAT3'	59	259

gene for the normalization of results. Quantitative real-time PCR was performed by using Rotor-Gene 3000 real-time PCR (Corbett Research) with SYBR green (Molecular Probes) as the detection system. The results were analyzed by Rotor-Gene 6.0 software (Corbett Research). Relative expression levels were determined in three repeat experiments ($n = 3$, mean \pm standard deviation).

2.8. Sample Preparation for Proteomic Analysis. For the proteomic analysis, we pooled an equal amount of cancer tissues from six individual mouse xenografts in each group (JIN, DPP, and the mock groups) to save cost. Cancer tissues were snap-frozen in liquid nitrogen and stored in a -80°C freezer. To extract proteins, the cancer tissues were grinded under liquid nitrogen with a mortar and pestle, and tissue lysis buffer was added. The solution was then sonicated on ice with an ultrasonic processor (Biorblock Scientific, France) for 90 min. The tissue lysis buffer contained 50 mM Tris (pH 7.4), 150 mM NaCl, 1% Triton X-100, 1% sodium deoxycholate, 0.1% SDS, 1x cocktail (0.5 mM Na_3VO_4 , 50 mM NaF, 1x phosphatase inhibitor cocktail, and 5 mM phenylmethanesulfonyl fluoride). The homogenate was then centrifuged at 12,000 g for 1 h at 4°C . Supernatant was collected, and protein concentration was determined by bicinchoninic acid assay. Each sample (70 μg) was separated on 12% SDS polyacrylamide gel. Gels were stained with colloidal coomassie brilliant blue. Twenty-seven individual bands were removed and subjected to gel trypsin digestion by using the In-Gel Tryptic Digestion Kit protocol (Pierce Biotechnology, Rockford, IL, USA). The bands were then analyzed by tandem mass spectrometry (MS/MS).

2.9. Mass Spectrometric Analysis. Tryptic peptide mixtures were separated by Ettan multidimensional liquid chromatography (LC) nanoflow/capillary LC system (GE Healthcare, Pittsburgh, PA, USA) equipped with a trapping column (Dionex/LC Packings μ -Precolumn Cartridge P/N 160454 C18 PepMap 100; 5 μm , 100 \AA , 300 μm internal diameter \times 5 mm; Sunnyvale, CA, USA) and nanocolumn (Dionex/LC Packings P/N 160321; 150 mm \times 0.075 mm inner diameter, C18 PepMap, 3 μm , 100 \AA ; Sunnyvale, CA, USA). The mixtures were then analyzed by using LTQ-Orbitrap (Thermo Finnigan, Bremen, Germany) with a nanospray configuration. The precursor ion scan mass spectra (m/z 300–1600) were obtained in the orbitrap with a resolution of $R = 60,000$ at m/z 400, and the number of accumulated ions was 1×10^6 . The five most intense ions were isolated and fragmented in

a linear ion trap (number of accumulated ions: 3×10^4). The resulting fragment ions were recorded with a resolution of $R = 15,000$ at m/z 400.

2.10. Mass Spectra Analysis. The Extract-MSn of BioWorks V3.2 (Thermo Electron, Inc., Waltham, MA, USA) was used to generate the mass spectrometry (MS) peak list with the default parameters. The Interactive Chemical Information System peak detection algorithm was used. The SEQUEST algorithm (Thermo Fisher Inc.) was used for the SEQUEST database search, and the spectra were searched against the IPI.HUMAN.v3.58.fasta protein database (79,794 entries) (<http://www.ebi.ac.uk/>) by using the BioWorks program V3.2 (Thermo Electron, Inc., Waltham, MA, USA). In the Turbo SEQUEST search parameter setting, the threshold for data generation was 10,000, and the precursor mass tolerance for data generation was 1.4 Da. For the SEQUEST search, peptide tolerance was set at 3 Da, and fragment ion tolerance was set at 0.01 Da. PeptideProphet [2] was used to assess the tandem mass spectra quality. The threshold score for accepting individual tandem mass spectra was $P = 0.9$, which corresponds to a 0.5% error rate in our dataset. One missed tryptic cleavage was permitted.

Carboxyamidomethyl cysteine (Cys_CAM) (+57) was included as a fixed modification for iodoacetamide reduction and alkylation. Given that the proteins were prepared by polyacrylamide gel electrophoresis, cysteines might react with free acrylamide monomers to form propionamide cysteine (Cys_PAM). We included an optional 14 Da in the search to account for potential Cys_PAM. The mass difference between Cys_PAM and Cys_CAM is 14. Methionine oxidation (+15.999 Da) was selected as another optional modification for the database search. Proteins with ProteinProphet P value greater than 0.9 and more than two unique peptide hits were considered as true hits. A randomized database of the IPI.HUMAN.v3.58.fasta was used as a decoy database to calculate the false discovery rate of protein identification. The Perl script used for randomization was obtained from <http://www.matrixscience.com/downloads/decoy.pl.gz>. The false discovery rate (0.568%) was calculated by the ratio of the number of matches in the randomized database to the number of matches in the IPI.HUMAN.v3.58.fasta database. Keratins were removed from the protein list because these proteins often represent contaminations from sample handling.

The MS/MS data from the cancer and control samples were analyzed by the PeptideProphet and ProteinProphet

program for statistical validation by using TPP4.31 [3, 4]. To identify the differential protein expression between two experimental groups (e.g., Sample A versus Sample B), we used the spectral counting method with a Bayesian mixture model [5]. Spectral counts are the average of duplicate LC-MS/MS runs and normalized to the total spectra ($5000 \times$ total spectra of the protein/sum of all total spectra of the proteins in the dataset). Significantly differentially expressed proteins were identified with a posterior probability of >0.95 by using the Bayesian mixture model, and the spectral count difference was greater than 10. GoMiner [6, 7] was used to find statistically represented gene ontology (GO) biological processes (level 3) with $\log_{10}(P) < -2$ (i.e., $P < 0.01$).

2.11. Western Blot Analysis. Cells were lysed in NP-40 buffer (1.0% NP-40, 10 mM hydroxyethyl piperazine ethanesulfonic acid, pH 7.4, 150 mM NaCl, 5 mM NaF, 2 mM Na_3VO_4 , 5 mM $\text{Na}_4\text{P}_2\text{O}_7$, 10 g/mL aprotinin, 10 g/mL leupeptin, and 1 mM phenylmethylsulfonyl fluoride). Equal volumes of cell lysate were subjected to SDS-polyacrylamide gel electrophoresis (12.5% gel). Proteins were then electrotransferred into a nitrocellulose membrane (GE Water and Process Technologies, USA). The membranes were blocked in a solution of 5% nonfat dry milk in Tris-buffered saline—Tween 20 buffer (20 mM Tris, pH 7.6, 500 mM NaCl, and 0.5% Tween 20) for 30 min followed by incubation with a primary antibody for at least 2 h. The membrane was then washed and treated with horseradish peroxidase-conjugated anti-mouse immunoglobulin or anti-rabbit immunoglobulin as indicated. Immunodetection was performed by using West Pico (Pierce Chemical, Rockford, IL) or West Dura (Pierce Chemical) followed by imaging on an Image Station 2000R (Eastman Kodak, USA).

2.12. Statistical Analysis. The data were analyzed by SPSS 19 software and presented as mean \pm standard deviation. The significance of the difference between the mean of the mock and treatment groups was analyzed by using one-way ANOVA followed by Dunnett's *t*-test correction and paired *t*-test. Statistical significance was determined at the level of $P < 0.05$ and $P < 0.01$.

3. Results

3.1. The JIN Formula Has Similar Effects as the Standard DDP Treatment but Is Less Toxic Than DDP. To study the toxicity of the JIN formula, we treated NCI-H460 xenografts that were grown subcutaneously in nude mice with saline, JIN formula, DDP, and JIN formula + DDP (coformulated group) for 15 d. A control group with no tumor was also included. One mouse in the mock group died on the 11th day of treatment. A mouse in the DDP and coformulated group died on the 15th day before sacrifice. Other mice in these two groups significantly lost weight and displayed slower activities and dry skins. All mice in the JIN group were alive and had stable weights, normal activities, and moist skins (Figure 1).

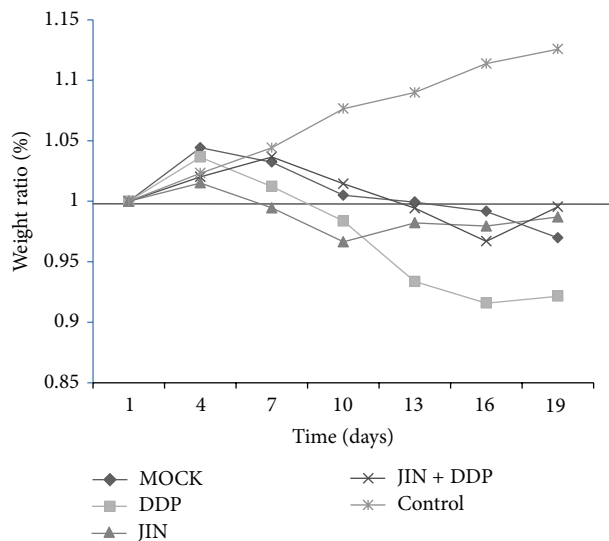


FIGURE 1: Body weights were measured every 3 days and body weight ratio was calculated relative to baseline measurement. The chemotherapy showed the toxicity to the mice, whereas the herbal treatment showed little toxicity compared to the saline group as measured by body weight loss.

This result indicated that herbal treatment and chemotherapy prolonged the lifespan of the mice. However, chemotherapy is toxic to the mice, whereas herbal treatment showed little toxicity compared with the saline group as demonstrated by the body weight loss.

All treatment groups (DDP, JIN, and JIN + DDP) showed inhibited growth of the NCI-H460 cell-transplanted solid tumor compared with the mock group (Figure 2). Significant differences in the final tumor weights ($P < 0.01$) and volume ($P < 0.01$) were found between each treatment group and the mock group after sacrifice (Figure 2). The tumor weights of mice treated with DDP, JIN, and the coformula were inhibited by 63.99%, 55.03%, and 65.79% ($P < 0.01$), respectively, after 15 d of treatment compared with those of mice administered with saline only.

3.2. Histological Changes Induced by JIN Formula Treatment.

Histological examination showed that the tumors of the mock group were solid masses composed of densely arranged cells without distinct cell differentiations. The cells were heteromorphic and had large nuclei that contain vesicles and obvious nucleoli. Reverse proportions between the nucleus and cytoplasm, high rates of mitosis and angiogenesis, infiltrative growths of tumor cells, and large areas of necrosis and hemorrhage were observed. No significant difference in cell morphology was found between each treatment group and the mock group. However, the tumor cells in the treatment group were less densely arranged, with patchy sparse cell arrangements, enlarged intercellular spaces, vacuoles in the cytoplasm, scattered intense stains in nuclei, scattered pyknosis of tumor cells, and varying degrees of degeneration. Tumor cell metastasis was not found in the lungs and liver (data not shown). The results indicated that the formula

TABLE 2: Genes regulated more than 2 folds by JIN treatment in H460 cells.

GeneBank	Symbol	Description	JIN/MOCK	P value
NM_000076	<i>CDKN1C</i>	Cyclin-dependent kinase inhibitor 1C (p57, Kip2)	2.72	0.01
NM_003738	<i>PTCH2</i>	Patched homolog 2 (Drosophila)	0.45	0.04
NM_003202	<i>TCF7</i>	Transcription factor 7 (T-cell specific, HMG-box)	0.39	0.02
NM_015626	<i>WSB1</i>	WD repeat and SOCS box-containing 1	0.13	8.71044E – 05

TABLE 3: Genes regulated more than 2 folds by DDP treatment in H460 cells.

GeneBank	Symbol	Description	DDP/MOCK	P value
NM_002423	<i>MMP7</i>	Matrix metalloproteinase7 (matrilysin, uterine)	3.16	0.003
NM_001429	<i>EP300</i>	E1A binding protein p300	0.35	0.008
NM_022475	<i>HHIP</i>	Hedgehog interacting protein	0.26	0.02
NM_015626	<i>WSB1</i>	WD repeat and SOCS box-containing 1	0.13	8.79479E – 05

can promote the degeneration and death of tumor cells and induce apoptosis, thus inhibiting the growth of lung cancer. These data suggested that the JIN formula could be safely administered as a novel therapeutic agent. Optimization of the dose and dosing schedule might yield a higher antitumor efficacy (Figure 3).

3.3. Gene Expression. To investigate preferentially altered signal transduction pathways in H460 xenografted tumors treated by herbal formula, the Human Q Series Signal Transduction in Cancer Gene Array, which includes marker genes with functions related to cell signal transduction pathways, was used. In the JIN group, the *CDKN1C* gene was upregulated and the *PTCH2*, *TCF7*, and *WSB1* genes were downregulated with twofold differences in ratios, as shown by the *t*-test. The results were reconfirmed by real-time PCR with *CDKN1C* and *PTCH2* primer pairs (Tables 2-3, Figure 4). The expression of these genes indicated the preferential change in the hedgehog and TGF- β signaling pathways in H460 xenografted tumor regulated by the JIN formula.

Furthermore, the coformula treatment of JIN and DDP also inhibited the stress/heat shock pathway, which involves the *HSF1*, *MYC*, and *FOS* genes (Table 4).

3.4. Proteomic Analysis of Cancer Cells Treated with JIN and DDP. We conducted a comprehensive mass spectra analysis of the JIN formula, DDP, and mock groups. We identified 1,131, 831, and 1,326 proteins in the JIN formula, DDP, and mock groups, respectively. By using Booth's Bayesian mixture model to compare the spectral count data for shotgun proteomics [5], we identified 40 (corresponding to 36 proteins) and 178 peptides (corresponding to 84 proteins) that were differentially expressed between the mock and DDP groups and between the mock and JIN formula groups, respectively (see Supplementary Tables 1 to 4 available online at <http://dx.doi.org/10.1155/2013/160168>). We found that the expression of the HSP90AA1 and HSPA1B proteins was significantly reduced in the JIN group compared with that in the mock group. HSPA1B was also significantly reduced in the DDP group compared with that in the mock group.

GoMiner analysis revealed that the differentially expressed proteins between the JIN and mock groups were enriched in GO:0006977 (DNA damage response signal transduction by p53 class mediator resulting in cell cycle arrest), GO:0006915 (apoptosis), and GO:0016032 (viral reproduction) (Table 5). By contrast, the differentially expressed proteins between the DDP and mock groups were enriched in GO:0065004 (protein-DNA complex assembly) and GO:0006414 (translational elongation) (Table 6). These results suggested that the JIN formula and DPP act on different biological processes.

We identified proteins and protein families that were downregulated in the JIN group compared with these in the mock group. These proteins include several histone family proteins and two heat shock proteins (HSPs), namely, heat shock 70 kDa protein 1 β (HSPA1B) and HSP 90 kDa alpha, class A member 1 (HSP90AA1). Several proteasome subunits (PSMA3, PSMA7, and PSMA8) and cellular structural proteins (Lamin A/C, keratin 18, tubulins, transgelin, etc.) were upregulated by the JIN formula relative to the mock control group. We selected HSP90AA1 for validation by Western blot, which shows that HSP90AA1 was downregulated by the JIN and DPP treatments (Figure 5). The downregulation was more significant in the JIN treatment group compared with that in the DPP group.

4. Discussion

Chinese or oriental herbal medicine has long been used for treating cancer. Single herbs are seldom used alone compared with herbal formulae, which uses the synergy and interactions among various phytochemicals present in different herbs to achieve therapeutic efficacy and targets multiple biological and pathological processes while minimizing side effects.

TCM formulae are rich in potential cancer chemopreventive and therapeutic agents. However, rigorous and systematic evaluations are necessary to establish the efficacy of herbal formulae and transform traditional herbal practices into evidence-based medicine. We evaluated the anticancer activities of the JIN formula, which is an ancient herbal

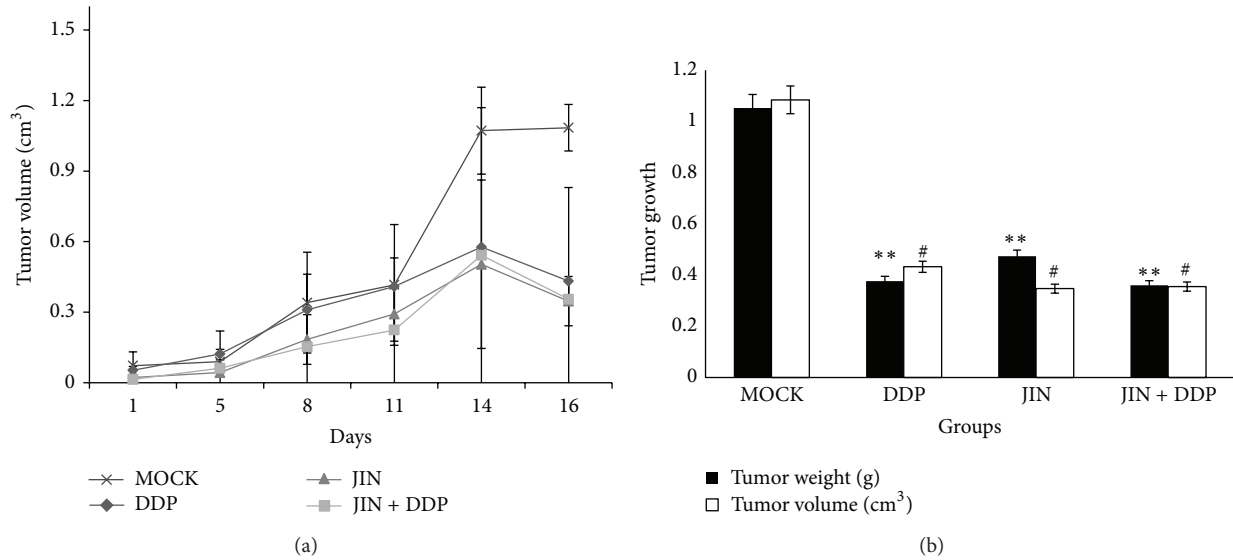


FIGURE 2: Effect of treatment on tumour growth. (a) The effect of JIN, JIN + DDP, and DDP on tumour size. Tumour volumes were measured every 3 days. (b) The effect of JIN, JIN + DDP, and DDP on tumour weight. Data presented are the mean \pm SD at 8–25 days posttumour implantation; groups were compared and analysed using *t*-test. ** $P < 0.01$ tumor weight compared with model group, # $P < 0.05$ tumor volume compared with model group. DDP, JIN, and cofomula inhibited tumor weight by 63.99%, 55.03%, and 65.79%, respectively, ($P < 0.01$) after 15 days of treatment compared to mice administered the vehicle only.

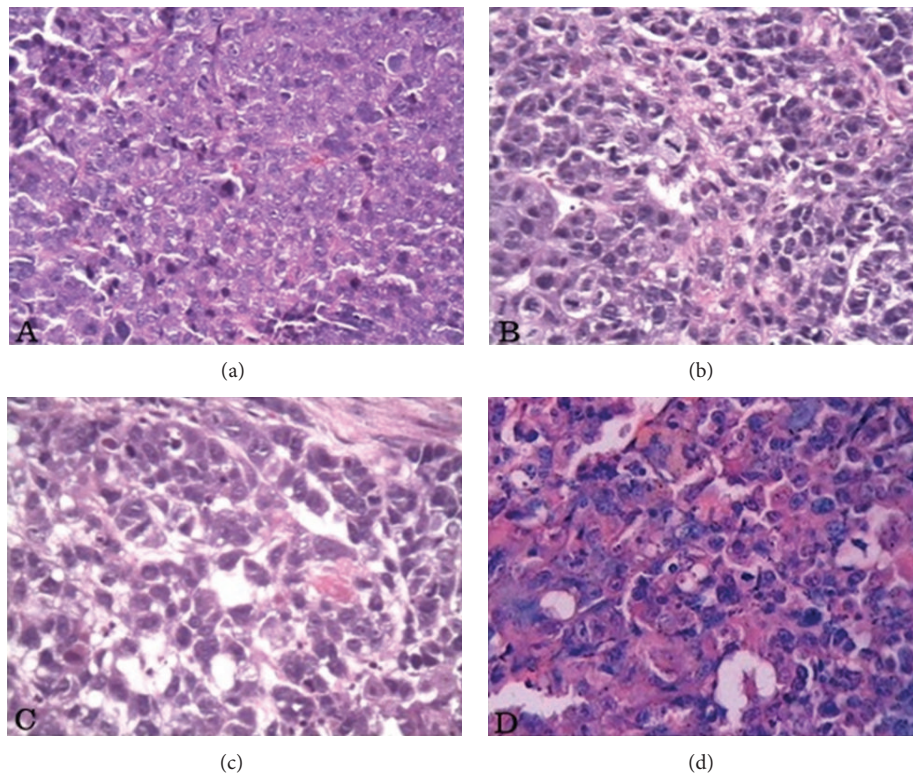


FIGURE 3: (a) MOCK group; (b) JIN group; (c) DDP group; (d) JIN + DDP group. Histological examination showed the tumors of MOCK group were solid masses composed of densely arranged cells without distinct cell differentiation, which are heteromorphic with a large nucleus containing vesicles and an obvious nucleolus, a reverse proportion between nucleus and cytoplasm, much mitosis and angiogenesis, infiltrative growth of tumor cells, and large areas of necrosis and hemorrhage.

TABLE 4: Genes regulated more than 2 folds by JIN + DDP treatment in H460 cells.

GeneBank	Symbol	Description	JIN + DDP/MOCK	P value
NM_000076	CDKN1C	Cyclin-dependent kinase inhibitor 1C (p57, Kip2)	3.24	0.003
NM_001904	CTNNB1	Catenin (cadherin-associated protein), beta 1, 88 kDa	0.26	0.003
NM_005228	EGFR	Epidermal growth factor receptor (erythroblastic leukemia viral (v-erb-b) oncogene homolog, avian)	0.46	0.05
NM_001429	EP300	E1A binding protein p300	0.35	0.007
NM_005252	FOS	V-fos FBJ murine osteosarcoma viral oncogene homolog	0.46	0.03
NM_002133	HMOX1	Hemeoxygenase (decycling) 1	0.42	0.09
NM_005526	HSF1	Heat shock transcription factor 1	0.44	0.02
NM_002467	MYC	V-myc myelocytomatosis viral oncogene homolog (avian)	0.22	0.0008
NM_003738	PTCH2	Patched homolog 2 (Drosophila)	0.40	0.01
NM_003202	TCF7	Transcription factor 7 (T-cell specific, HMG-box)	0.32	0.006
NM_015626	WSB1	WD repeat and SOCS box-containing 1	0.13	8.74349E - 05

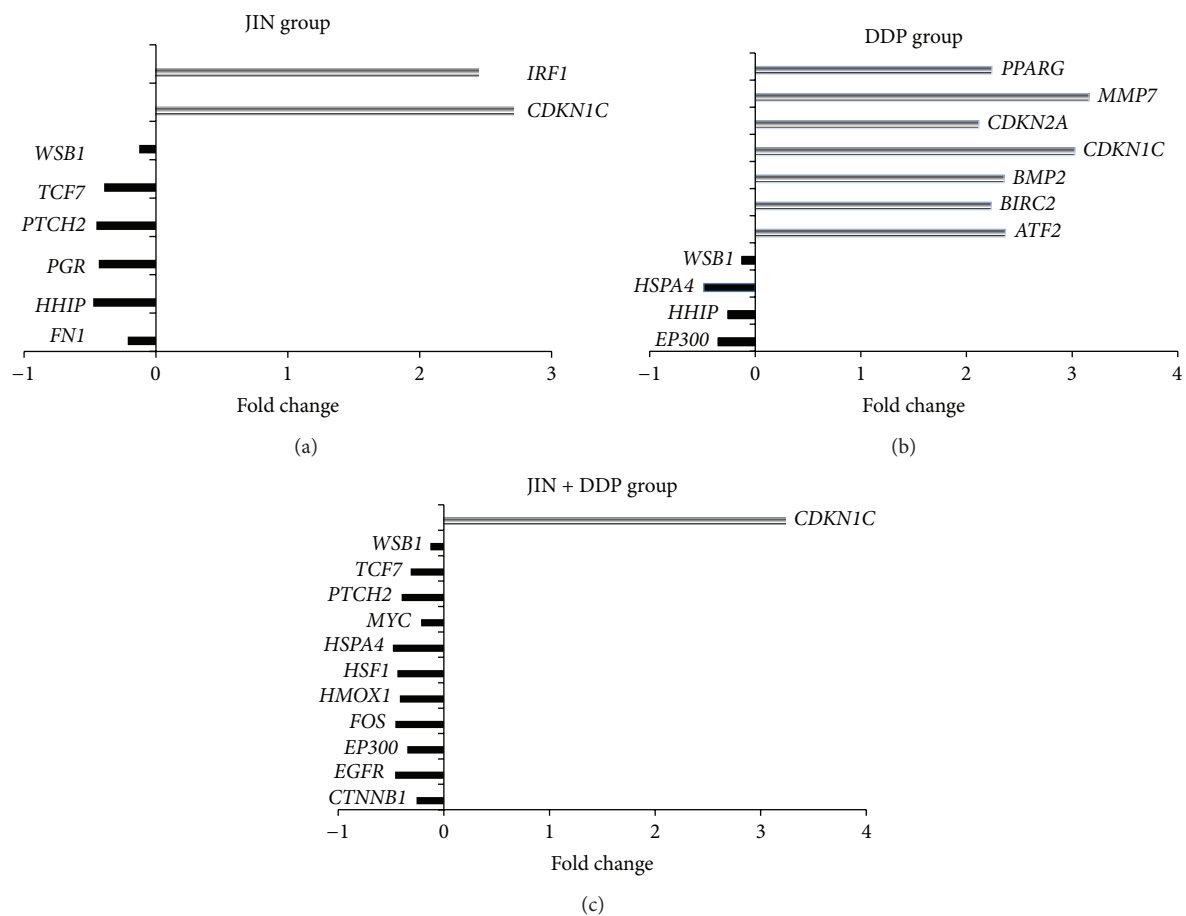


FIGURE 4: (a) Genes regulated more than 2 folds by Jin treatment on H460 cells. Combined with ratio values 2-fold difference, in JIN group, significantly upregulated gene *CDKN1C* and downregulated genes including *PTCH2*, *TCF7*, and *WSB1* passed statistic *t*-test. The results were reconfirmed by real-time PCR with *CDKN1C* and *PTCH2* primer pairs. (b) Genes regulated more than 2 folds by DDP treatment on H460 cells. (c) The cofomula treatment of JIN and DDP also involved the inhibition of the stress/heat shock pathway: *HSPA4*, *HSF1*, *MYC*, *FOS*, and so forth.

TABLE 5: Significantly enriched GO Biological process terms in the differentially expressed proteins between the JIN formula and the MOCK groups.

GO category	Description	Total genes	Changed genes	Enrichment	$\log_{10}(P)$
GO:0044237	Cellular metabolic process	4513	45	1.40	-3.26
GO:0044249	Cellular biosynthetic process	2322	26	1.58	-2.22
GO:0006139	Nucleobase nucleoside nucleotide and nucleic acid metabolic process	2350	26	1.56	-2.14
GO:0016032	Viral reproduction	343	16	6.56	-8.93
GO:0034621	Cellular macromolecular complex subunit organization	364	14	5.41	-6.76
GO:0006915	Apoptosis	784	13	2.33	-2.53
GO:0006414	Translational elongation	97	12	17.41	-11.62
GO:0006977	DNA damage response signal transduction by p53 class mediator resulting in cell cycle arrest	57	4	9.88	-3.16
GO:0072395	Signal transduction involved in cell cycle check point	57	4	9.88	-3.16

TABLE 6: Significantly enriched GO biological process terms in the differentially expressed proteins between the DPP and the MOCK groups.

GO category	Description	Total genes	Changed genes	Enrichment	$\log_{10}(P)$
GO:0006414	Translational elongation	97	3	11.54	-2.68
GO:0065004	Protein-DNA complex assembly	44	2	16.96	-2.22
GO:0071824	Protein-DNA complex subunit organization	51	2	14.64	-2.09

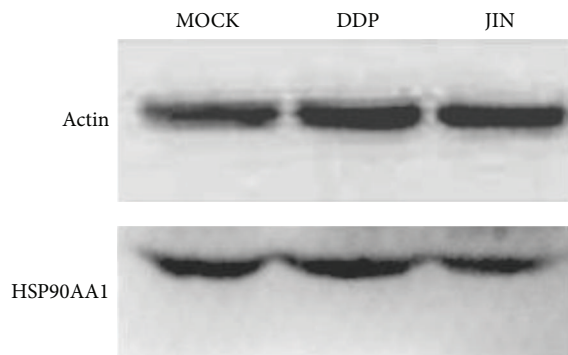


FIGURE 5: Western blot analysis showing that after treated by JIN formula the HSP90AA1 was downregulated significantly than DDP did.

formula recorded in the classic TCM book *Jin Kui Yao Lue* (Golden Chamber). The results showed that the JIN formula significantly delayed the growth of subcutaneous human H460 xenografted tumors in vivo relative to the mock control group.

Gene array analysis of signal transduction in cancer showed that the JIN formula acted on multiple targets in the MAPK, hedgehog, and Wnt signaling pathways in the H460 xenografted tumor. JIN upregulated two tumor suppressors, namely, CDKN1C and interferon regulatory factor-1 (IRF-1). Abnormal cell cycle regulation is the important reason of excessive cell proliferation and tumorigenesis. Cell cycle progression is regulated by balanced interactions between

cyclins and cyclin-dependent kinases (CDKs). The suppressive effect of cyclin-dependent kinase inhibitors (CDKIs) on cyclin/CDK complexes is among the many mechanisms that control normal cell cycle progression. Cell cycle progression is negatively regulated by proteins from two families, the inhibitors of cyclin-dependent kinase 4 (INK4) family [CDKN2A (p16), CDKN2B (p15), CDKN2C (p18), and CDKN2D (p19)] and the CIP/KIP family [CDKN1A (p21), CDKN1B (p27), and CDKN1C (p57)]. The protein encoded by CDKN1C is a tight-binding, strong inhibitor of several G1 cyclin/Cdk complexes and a negative regulator of cell proliferation. Mutations in this gene are implicated in sporadic cancers and the Beckwith-Wiedemann syndrome, thus suggesting that this gene is a tumor suppressor candidate [8]. The anticancer mechanisms of the JIN formula may seek a new breakthrough by the further study of this protein family. IRF-1 was originally identified as a regulator of $\text{IFN}\alpha/\beta$. IRF-1 expression is considerably upregulated during viral infections and stimulations by the interferon family. Increasing evidence supports the theory that IRF-1 functions as a tumor suppressor and represses the transformed phenotype. In human tumors, IRF-1 is deactivated to prevent apoptosis and cell cycle arrest by genetic mechanisms [9].

The downregulated genes *PTCH2*, *TCF7*, and *WSBI* are related to the embryonic signaling pathways Hedgehog and Wnt. The inappropriate reactivation of these pathways in adult cells promotes tumor growth [10]. Many studies showed that lung tumors are caused by the activation of these embryonic regulatory pathways [11, 12]. Hedgehog signaling plays a key role in a variety of processes, such as embryogenesis, maintenance of adult tissue homeostasis, tissue repair

during chronic persistent inflammation, and carcinogenesis. Hedgehog signals protect cancer cells, particularly cancer stem cells [13]. Hedgehog signaling is frequently activated in esophageal cancer, gastric cancer, and pancreatic cancer due to transcriptional upregulation of Hedgehog ligands and epigenetic silencing of HHIP1/HHIP gene, encoding the Hedgehog inhibitor. However, Hedgehog signaling is rarely activated in lung cancer due to negative regulation by the canonical WNT signaling pathway. The Wnt pathway may serve as a potential target in the development of therapeutic agents. The blockade of the Wnt pathway may be considered in formulating new treatment strategies in lung cancer [14]. Given the current and increasing availability of drugs that inhibit Hh and Wnt signaling, an understanding of the role of Hh and Wnt in lung cancer pathogenesis might lead to the development of new therapies. Furthermore, the co-formula treatment of JIN and DDP also targeted the stress/heat shock pathway, specifically for the *HSPA4*, *HSF1*, *MYC*, and *FOS* genes.

HSPs are encoded by several gene families and have essential roles in cell survival, tumorigenesis, and tumor progression. The HSP70 family proteins, which are named according to their approximate relative molecular mass, contain at least eight members that are almost ubiquitously expressed [15]. More than 99% of the amino acids of the two major HSP70 proteins, namely, HSP70-1a and HSP70-1b (encoded by the *HSPA1A* and *HSPA1B* genes, resp.), have been identified. These proteins are initially found in cells under stress [16, 17]. HSP70 is closely involved in programmed cell death protection through interactions with several key regulatory proteins, along with HSP90 and several cochaperones. HSP70-1 proteins are overexpressed in many types of tumor, and this over-expression is often correlated with tumor malignancy, progression, poor prognosis, and metastasis [16]. The overexpression of HSP70-1 induces cell transformation [15]. However, the expression and regulation of HSP70-1 in lung cancer cells are rarely studied. Our analysis showed that *HSPA1B*, which also belongs to the HSP70 family, was highly expressed in the mock group. After JIN formula treatment, the expression of *HSPA1B* was downregulated significantly. Cancer metastasis was not observed in the lungs, liver, and brain of mice from the JIN group, thus suggesting that distant tumor metastases was prevented by the JIN formula.

HSP 90 kDa (HSP90) is a molecular chaperone that maintains the function of numerous intracellular signaling nodes utilized by cancer cells for proliferation and survival. HSP90 is also involved in a number of human pathological states such as ischemia and autoimmune diseases. Lung cancer progression is also influenced by HSP90. HSP90 α is a cytoplasmic protein that is highly conserved in the process of biological evolution. The HSP90 chaperones in humans are encoded by two distinct genes, namely, HSP90 α and HSP90 β . Differences in their respective modes of regulation have been observed; HSP90 α is more inducible than HSP90 β . HSP90 α is required for the conformational maturation and stability of multiple oncogenic kinases that induce signal transduction and proliferation of lung cancer cells. HSP90 α is also important in modulating tumor cell apoptosis. Moreover, HSP90 α facilitates the migration and proliferation of tumor

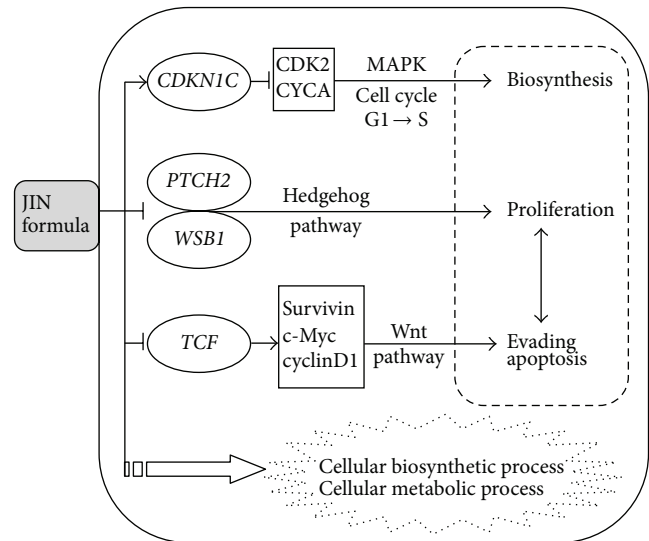


FIGURE 6: Possible cell signaling network regulated by JIN formula on H460-xonografted tumor.

cells and is associated with the poor prognosis of specific cancers. Changes in the proteins encoded by HSP90 may be caused by changes in the nature and expression of HSP90 α . These changes may participate in the development of lung cancer. Considering the increased role of HSP90 in lung cancer incidence and the process of encoding HSP90 α and HSP90AA1 in single nucleotide polymorphisms may be interrelated and associated with lung cancer. HSP90 is an adenosine triphosphate- (ATP-) dependent molecular chaperone that maintains the active conformation of clients in coproteins of cancer cells. The inhibition of HSP90 leads to the inhibition of tumor growth and metastasis [17]. HSP90 is also detected on the plasma membrane of tumor cells and its expression is correlated with metastatic potential [18]. In the current study, we discovered that HSP90AA1 was highly expressed in the mock group. This study is the first to report the downregulation of HSP90AA1 by the JIN formula relative to the mock group. HSP90AA1 might serve as a potential prognostic marker or a candidate therapeutic target of H460. HSP90AA1 might also be a viable marker for H460 without distant metastasis.

We found that GO:0044237 (cellular metabolic process) and GO:0006139 (nucleobase, nucleoside, nucleotide, and nucleic acid metabolic process) (Table 5) were enriched by differentially expressed proteins in the JIN group compared with the mock group. HSP90AA1 and *HSPA1B* were downregulated by the JIN formula. Aldolase A (fructose-bisphosphate) was upregulated in the JIN group compared with that in the mock group. HSP90AA1 is related to GO:0034621 (cellular macromolecular complex subunit organization), GO:0072395 (signal transduction in cell cycle checkpoint), and GO:0044249 (cellular biosynthetic process, etc.). HSP90 is an active ATP-dependent chaperone involved in the assembly and regulation of signal transduction pathways by activating specific client proteins [19]. HSP90AA1

plays an important role in each step of the cell cycle and tumor formation. The function of HSP90 is reflected by the polo-like kinase stability. The inhibition of HSP90AA1 in HeLa cells results in cell cycle arrest either at the G2 stage or metaphase-anaphase transition [20]. Our results suggested that the JIN formula acted on the maintenance of the cell cycle and signaling processes. The potential mechanism of the JIN formula is shown in Figure 6. Further investigation should be conducted to reveal the detailed mechanism of the JIN formula.

Authors' Contribution

X. Zhang, H. Fu, and B. Lin designed the research; L. Zheng, M. Jiang, W. Zhang, H. Zhang, F. Xiong, Y. Yu, M. Chen, J. Zhou, X. Dai, and M. Wang performed the research; L. Zheng, M. Jiang, and W. Zhang contributed equally; Y. Tang, M. Jiang, G. Cheng, and J. Duan designed the herbal formula; L. Zheng, M. Jiang, W. Zhang, H. Zhang, B. Lin, and X. Zhang analyzed the data; and L. Zheng, B. Lin, H. Fu, and X. Zhang wrote the paper.

Acknowledgments

The authors thank the members of the Fu Laboratory of the Emory University and Jiangsu Key Laboratory for their research on the TCM formulae and the Nanjing University of Chinese Medicine for their assistance and enlightening discussions. This study is supported in part by the National Science and Technology Pillar Program in the 11th Five-year Plan of China (Grant no. 2006BAI1B08-01, for H. Fu and X. Zhang), Priority Academic Program Development of Jiangsu Higher Education Institution (for X. Zhang), and the Ministry of Science and Technology of China (Grant no. 2006DFA32950, for B. Lin).

References

- [1] W. Y. Jiang, "Therapeutic wisdom in traditional Chinese medicine: a perspective from modern science," *Discovery Medicine*, vol. 5, no. 29, pp. 455–461, 2005.
- [2] A. I. Nesvizhskii, A. Keller, E. Kolker, and R. Aebersold, "A statistical model for identifying proteins by tandem mass spectrometry," *Analytical Chemistry*, vol. 75, no. 17, pp. 4646–4658, 2003.
- [3] A. Keller and D. Shteynberg, "Software pipeline and data analysis for MS/MS proteomics: the trans-proteomic pipeline," *Methods in Molecular Biology*, vol. 694, pp. 169–189, 2011.
- [4] P. G. A. Pedrioli, "Trans-proteomic pipeline: a pipeline for proteomic analysis," *Methods in Molecular Biology*, vol. 604, pp. 213–238, 2010.
- [5] J. G. Booth, K. E. Eilertson, P. D. B. Olinares, and H. Yu, "A bayesian mixture model for comparative spectral count data in shotgun proteomics," *Molecular and Cellular Proteomics*, vol. 10, no. 8, 2011.
- [6] B. R. Zeeberg, W. Feng, G. Wang et al., "GoMiner: a resource for biological interpretation of genomic and proteomic data," *Genome Biology*, vol. 4, no. 4, p. R28, 2003.
- [7] B. R. Zeeberg, H. Qin, S. Narasimhan et al., "High-throughput GoMiner, an "industrial-strength" integrative gene ontology tool for interpretation of multiple-microarray experiments, with application to studies of Common Variable Immune Deficiency (CVID)," *BMC Bioinformatics*, vol. 6, article 168, 2005.
- [8] E. M. Algar, A. Muscat, V. Dagar et al., "Imprinted CDKN1C is a tumor suppressor in rhabdoid tumor and activated by restoration of SMARCB1 and histone deacetylase inhibitors," *PLoS ONE*, vol. 4, no. 2, Article ID e4482, 2009.
- [9] J. Park, K. Kim, E.-J. Lee et al., "Elevated level of SUMOylated IRF-1 in tumor cells interferes with IRF-1-mediated apoptosis," *Proceedings of the National Academy of Sciences of the United States of America*, vol. 104, no. 43, pp. 17028–17033, 2007.
- [10] S. J. Freemantle and E. Dmitrovsky, "Cyclin E transgenic mice: discovery tools for lung cancer biology, therapy, and prevention," *Cancer Prevention Research*, vol. 3, no. 12, pp. 1513–1518, 2010.
- [11] H. Lemjabbar-Alaoui, V. Dasari, S. S. Sidhu et al., "Wnt and hedgehog are critical mediators of cigarette smoke-induced lung cancer," *PLoS ONE*, vol. 1, no. 1, article e93, 2006.
- [12] J. W. Neal and L. V. Sequist, "Exciting new targets in lung cancer therapy: ALK, IGF-1R, HDAC, and Hh," *Current Treatment Options in Oncology*, vol. 11, no. 1-2, pp. 36–44, 2010.
- [13] Y. Katoh and M. Katoh, "Hedgehog target genes: mechanisms of carcinogenesis induced by aberrant hedgehog signaling activation," *Current Molecular Medicine*, vol. 9, no. 7, pp. 873–886, 2009.
- [14] J. Mazieres, B. He, L. You, Z. Xu, and D. M. Jablons, "Wnt signaling in lung cancer," *Cancer Letters*, vol. 222, no. 1, pp. 1–10, 2005.
- [15] S. Lu, Z. Tan, M. Wortman, S. Lu, and Z. Dong, "Regulation of heat shock protein 70-1 expression by androgen receptor and its signaling in human prostate cancer cells," *International Journal of Oncology*, vol. 36, no. 2, pp. 459–467, 2010.
- [16] S. K. Calderwood, M. A. Khaleque, D. B. Sawyer, and D. R. Ciocca, "Heat shock proteins in cancer: chaperones of tumorigenesis," *Trends in Biochemical Sciences*, vol. 31, no. 3, pp. 164–172, 2006.
- [17] S. A. Eccles, A. Massey, F. I. Raynaud et al., "NVP-AUY922: a novel heat shock protein 90 inhibitor active against xenograft tumor growth, angiogenesis, and metastasis," *Cancer Research*, vol. 68, no. 8, pp. 2850–2860, 2008.
- [18] S. Tsutsumi, B. Scroggins, F. Koga et al., "A small molecule cell-impermeant Hsp90 antagonist inhibits tumor cell motility and invasion," *Oncogene*, vol. 27, no. 17, pp. 2478–2487, 2008.
- [19] M. Dugaard, M. Rohde, and M. Jäättelä, "The heat shock protein 70 family: highly homologous proteins with overlapping and distinct functions," *FEBS Letters*, vol. 581, no. 19, pp. 3702–3710, 2007.
- [20] M. P. Mayer and B. Bukau, "Hsp70 chaperones: cellular functions and molecular mechanism," *Cellular and Molecular Life Sciences*, vol. 62, no. 6, pp. 670–684, 2005.

Review Article

Navigating Traditional Chinese Medicine Network Pharmacology and Computational Tools

Ming Yang,^{1,2} Jia-Lei Chen,¹ Li-Wen Xu,¹ and Guang Ji²

¹ Longhua Hospital Affiliated to Shanghai University of TCM, Shanghai 200032, China

² Institute of Digestive Disease, Longhua Hospital, Shanghai University of Traditional Chinese Medicine, Shanghai 200032, China

Correspondence should be addressed to Guang Ji; jiliver@vip.sina.com

Received 6 June 2013; Accepted 4 July 2013

Academic Editor: Ai-ping Lu

Copyright © 2013 Ming Yang et al. This is an open access article distributed under the Creative Commons Attribution License, which permits unrestricted use, distribution, and reproduction in any medium, provided the original work is properly cited.

The concept of “network target” has ushered in a new era in the field of traditional Chinese medicine (TCM). As a new research approach, network pharmacology is based on the analysis of network models and systems biology. Taking advantage of advancements in systems biology, a high degree of integration data analysis strategy and interpretable visualization provides deeper insights into the underlying mechanisms of TCM theories, including the principles of herb combination, biological foundations of herb or herbal formulae action, and molecular basis of TCM syndromes. In this study, we review several recent developments in TCM network pharmacology research and discuss their potential for bridging the gap between traditional and modern medicine. We briefly summarize the two main functional applications of TCM network models: understanding/uncovering and predicting/discovering. In particular, we focus on how TCM network pharmacology research is conducted and highlight different computational tools, such as network-based and machine learning algorithms, and sources that have been proposed and applied to the different steps involved in the research process. To make network pharmacology research commonplace, some basic network definitions and analysis methods are presented.

1. Background

Traditional Chinese medicine (TCM) has been developed and practiced in China for thousands of years. Although TCM is still being practiced and more countries consider it an alternative treatment [1], several questions need to be addressed: (1) what are the active substances in TCM and how do they work? (2) What are the combinatorial rules of TCM herbal formulae, and why can it be used for the treatment of multiple diseases? (3) What basic biological knowledge underlines TCM? The development of systems biology technology over the past several decades has helped shed light on the effectiveness of TCM and helped to answer the previous questions. Systems biology tools could be used to obtain valuable insights into TCM theories. Recent advancements in “Omics” technologies have led to more accumulated data that require powerful computational tools to study and analyze. Although the most widely used experimental technologies, such as high-throughput gene expression profiling [2], have permitted the characterization

of relationships between complex biological processes and TCM treatment, an obvious limitation of these approaches is that they usually analyze data on a single state (i.e., changes in the expression of specific disease or TCM agent). To be more effective, these novel strategies should integrate systematic information to contextualize the characterization to illustrate the holistic characteristic of TCM. Such relationships could be understood better through building, validation, and analysis of computational models. Similar to complex diseases that require complex therapies, complex data require scale-matched approaches. A network-based approach for pharmacology has been proposed recently. Network pharmacology challenges the traditional “one disease-one target-one drug” paradigm and explores interactions between the body and drug by mapping drug-target-disease networks on a biological level. A recent analysis of network pharmacology highlighted the complexity of both drug action and protein-protein interaction [3–6] and triggered significant changes in strategies for therapies and the drug discovery process [7]. For TCM, Li [8] presented the framework and practice

of network-based studies for understanding the mechanism of Chinese herbal formulae. His group proposed the novel concept of “network target” based on their works [9, 10], which pioneered network pharmacology research on TCM. “Network target” considers the biomolecular disease network as a target through which researchers can design and develop the best drug intervention; the key is to establish a network for drug-gene-disease association. Network pharmacology has the potential not only to accelerate TCM modernization and bridge the gap between traditional and modern medicine but also to change methods for rational design and optimization of drug discovery from herbal formulae. As a meaningful visual interface, the network-based approach is a functional element in tackling complicated problems by enabling data exploration and engaging the human ability to synthesize complex visual inputs into meaningful understanding [11]. However, the construction of a network depends on information about different types of relationships. To make network pharmacology for TCM commonplace, an all-encompassing resource that contains both TCM knowledge and biological processes and different computational algorithm tools should be refined.

In this review, we focus on how TCM network pharmacology research is conducted. We highlight different computational bioinformatics approaches that have been introduced and applied to different steps involved in network pharmacology. The general analysis process can be described as follows: (a) interaction information retrieval from databases; (b) network construction; and (c) knowledge discovery based on network models. Accordingly, this review is organized as follows: the second part contains useful databases and network analysis software. In the third part, we present the methods for constructing networks of different modes. Several basic network definitions and network properties analysis are depicted. The fourth part describes recent developments in TCM network pharmacology and discusses different computational methods that have been proposed so far to address current issues. We further discuss how and what underlying TCM knowledge can be discovered based on network models. In the final part, we discuss challenges to TCM network pharmacology. Our review is not comprehensive. Therefore, we encourage interested readers to write reviews that address another aspect of this subject.

2. Databases and Data Analysis Tools

Research on network pharmacology is supported by large-scale biological databases that offer a wealth of information on interactions of biological entities, such as drug-gene-disease. These databases are developed for different but complementary objectives. With advancements in systems biology of TCM, TCM-related resources can also be obtained from the Web. Table 1 summarizes the most frequently used resources for TCM network pharmacology. The resources are divided into the following four categories based on the type of information in the databases: (1) biomolecular databases that contain large amounts of information on human protein-protein interactions (PPIs), gene ontologies (GOs), protein-DNA interactions, and functional pathways;

(2) disease/phenotype databases on phenotypes of human diseases and their related genes; (3) chemical/drug-related databases that provide many useful cheminformatics and bioinformatics information on drugs or chemical substances, such as 2D and 3D structures, bioactivity, and comprehensive drug target (i.e., sequence, structure, and pathway); and (4) TCM-related databases that provide information on many active ingredients related to TCM drugs and their target proteins. We also focus on the relationships among these databases, mapping them in Figure 1 based on the following principle: if A database is integrated from B database or is annotated from B database, they are connected, with A having an out-degree and B having an in-degree. In other words, the database that has a larger in-degree and smaller out-degree is the source of many others and is called the primary database, whereas the database that has smaller in-degree and larger out-degree is called the secondary database.

Figure 1 shows that among the biomolecular databases, KEGG [12], HPRD [13], PDB [14], and TTD [15] have larger in-degree and smaller out-degree and could thus be considered primary databases. These databases are frequently used and provide extensive information on pathways (KEGG), PPIs (HPRD), protein structure (PDB), and therapeutic target (TTD). However, the ConsensusPathDB (CPDB) [16] and the Human Annotated and Predicted Protein Interaction (HAPPI) database [17] could be considered secondary databases. CPDB may be the largest searching platform database and integrates seven types of functional biological interactions (PPIs, signaling reactions, metabolic reactions, gene regulations, genetic interactions, drug-target interactions, and biochemical pathways) and 30 public resources. HAPPI, which integrates five different resources, was developed by Indiana University. A unified scoring model was applied to measure each PPI at one of the five-star rank levels from 1 to 5. The latest version contains 273,068, 189,150, 71,036, 33,733, and 34,770 PPIs that were ranked from 1 star to 5 stars, respectively, and provides a more flexible selection for researchers to achieve different data confidence levels. OMIM [18] under disease/phenotype databases as well as Drug-Bank [19] and ChEMBL [20] under chemical/drug-related databases are primary databases. TCM-related databases are all secondary databases that require integration with other resources. Although TCM has continued to gain popularity, relatively few resources on TCM are available online. These TCM-related databases complement each other to provide information on active ingredients, herbs, herbal formulae, and even herbal ingredient targets. The connection between TCM-related databases and other categories indicates to some extent the existing complex interactions of TCM-active ingredient-gene-disease. For example, TCMID [21] integrates three types of database, which is the largest data set for a related field. TCMID contains 47,000 prescriptions, 8,159 herbs, 25,210 compounds, 6,828 drugs, 3,791 diseases, and 17,521 related targets that facilitate research on TCM network pharmacology.

Table 2 lists several major network analysis tools that can be used for biological network analysis, although some were originally developed for social network analysis, such as Pajek, Ucinet, and NetMiner. Most of the tools are based

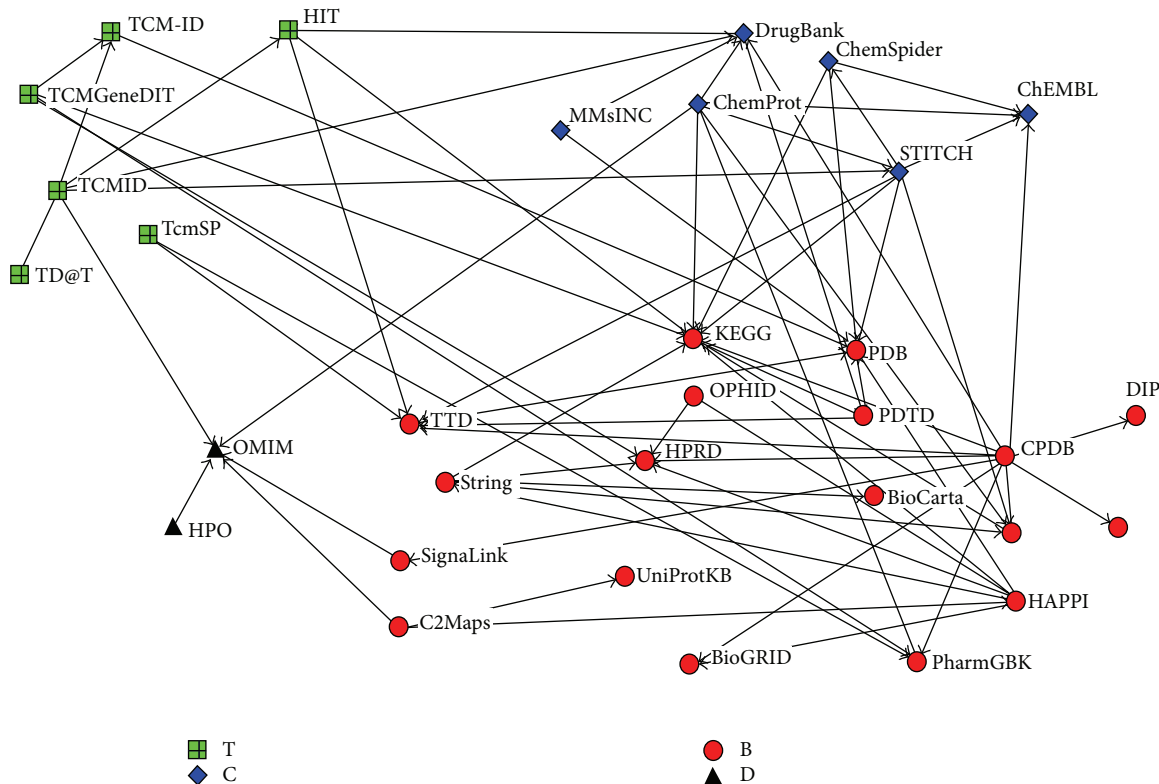


FIGURE 1: Database relationship network.

on Java (Cytoscape) or Python (NetworkX, NetMiner, Guess) language script, which allows researchers to extend the functionality of network analysis by developing specific plugins or apps. More than 150 plugins are integrated in Cytoscape [22, 23], thus increasing its power and versatility. As a tool designed for biological networks, Cytoscape has several specialized plugins that can be used to import and map existing interaction data cataloged in public databases, such as BioGridPlugin [24], MiMI [25], ConsensusPathDB [26], and APID2NET [27]. Some plugins support computational literature mining. For example, AgilentLiteratureSearch [28] can mine literature abstracts from online databases such as OMIM and Medline to determine interactions. Although packages based on Matlab or R are not efficient in analyzing large networks ($\geq 10,000$ nodes), their powerful statistic and data mining toolboxes facilitate further analysis.

3. Computational Measurements for Network Analysis

Network-based approaches have been proven to be helpful in organizing high-dimensional biological data sets and extracting meaningful information. The simplest way to construct a biological network is through graph points, which could be either genes, proteins, or drugs connected by lines that represent the nature of the interaction. Networks are amenable to analysis by using several branches of mathematics [29]. Thus, local and global properties of this map can be evaluated by using network metrics. In this

section, we describe several of the most apparent and least complex measurements of general network analysis. Despite the simplicity of the ideas and definitions, good theoretical reasons (and some empirical evidence) support the view that these basic properties of biological networks must be very important. These measurements are discussed as follows.

3.1. Basic Properties. Network thinking has contributed a number of important insights on biological process. Protein and protein or disease and disease interactions are believed to be more complicated. Identifying the importance of a protein or disease is essential in understanding biological networks. The properties of the network that we are investigating primarily deal with the importance of nodes. If the group composed of important nodes is called the “center” of the biological network, we can evaluate the centrality of the nodes based on three general measurements: degree, betweenness, and closeness. Degree is the number of nodes connected to a given node in a graph. Betweenness and closeness are both related to geodesic distance, which is the number of relations in the shortest possible path from one node to another. In a biological network, a node with a large degree could be regarded as a hub node, and a node with large betweenness is a bottleneck node. Some studies suggested that human-inherited disease genes tend to be hub nodes in the interaction network [30–33]. However, other studies have provided evidence that the “hubness” of inherited disease genes may be only apparent [31] and suggested that bottleneck nodes tend to be essential proteins [34, 35]. The use of

TABLE 1: Useful public databases for TCM network pharmacology.

Type [#]	Name	Description	Application	Webpage	Reference
	OPHID	Online predicted human interaction database: a web-based database of predicted interactions between human proteins, which contains 23889 predicted interactions currently	PPIs retrieval	http://ophid.utoronto.ca	[139]
	STRING	A database of known and predicted protein interactions	PPIs retrieval	http://string-db.org/	[140]
	BioGRID	Biological general repository for interaction datasets: providing protein-protein interaction data from model organisms and humans	PPIs retrieval	http://thebiogrid.org/	[24]
	HPRD	Human protein reference database: depicting and integrating information related to domain architecture, posttranslational modifications, interaction networks, and disease association for each protein in the human proteome	PPIs retrieval	http://www.hprd.org/	[13]
	HAPPI	Human annotated and predicted protein interaction database: containing 142,956 nonredundant, medium to high-confidence level human protein interaction pairs among 10,592 human proteins	PPIs retrieval	http://bio.informatics.iupui.edu/HAPPI/	[17]
	PDB	Protein data bank: a key resource in areas of structural genomics for containing 3D biological macromolecular structure	Protein information retrieval	http://www.rcsb.org/pdb/	[14]
B	PDTD	PDTD: a web-accessible protein database for drug target identification and focusing on those drug targets with known 3D structures	Drug target identification	http://www.dddc.ac.cn/pdtd/	[141]
	TTD	Therapeutic target database: providing information about the known and exploring therapeutic protein and nucleic acid targets, the targeted disease, pathway information, and the corresponding drugs	Drug target identification	http://bidd.nus.edu.sg/group/cjttd/	[15]
	UniProtKB	Universal protein knowledge database: providing protein information in detail	Protein analysis	http://www.uniprot.org/uniprot/	[142]
	PharmGBK	Pharmacogenomics knowledge base: providing information of gene-drug associations and genotype-phenotype relationships	Comprehensive gene-drug-phenotype analysis	http://www.pharmgkb.org/	[143]
	DIP	Database of interacting proteins	PPIs analysis	http://dip.doe-mbi.ucla.edu	[144]
	C2Maps	A network pharmacology database with comprehensive disease-gene-drug connectivity relationships	Comprehensive gene-drug-disease analysis	http://bio.informatics.iupui.edu/	[145]
	MetaCore	An integrated suite for functional analysis of microarray, metabolic, SAGE, proteomics, siRNA, microRNA, and screening data	Comprehensive biological analysis	http://www.genego.com	[146, 147]
	CPDB	A database that integrates different types of functional interactions including protein-protein, genetic, metabolic, signaling, gene regulatory, and drug-target interactions	Comprehensive gene-drug-disease analysis	http://cpdb.molgen.mpg.de/	[16]

TABLE 1: Continued.

Type [#]	Name	Description	Application	Webpage	Reference
	BioCarta	An interactive web-based resource giving four categories information: gene function, proteomic pathways, and research reagents	PPIs and pathway retrieval	http://www.biocarta.com/	[148]
	KEGG	As a collection of online databases, which deals with genomes, enzymatic pathways, and biological chemicals, especially giving pathway map in the forms of molecular networks	PPIs and pathway retrieval	http://www.genome.jp/kegg/	[12]
	SignaLink	A database containing eight major signaling pathways, which can be used for comparative and cross-talk analyses of signaling pathways	Pathway analysis	http://signalink.org/	[149]
	Reactome	Curated knowledge base of biological pathways in humans	Pathway analysis	http://www.reactome.org	[150]
	NetPath	A manually curated resource of signal transduction pathways in humans	Pathway analysis	http://www.netpath.org/	[151]
	OMIM	Database of comprehensive, authoritative compendium of human genes and genetic phenotypes	Disease-gene retrieval	http://www.omim.org/	[18]
D	COSMIC	A database of catalogue of somatic mutations in cancer	Biological information relating to human cancers retrieval	http://cancer.sanger.ac.uk/cancergenome/projects/cosmic/	[152]
	HPO	Human phenotype ontology database: providing a standardized vocabulary of phenotype of human disease	Phenotype retrieval	http://www.human-phenotype-ontology.org/	[153]
	STITCH	Chemical-protein interactions database: providing known and predicted interactions of chemicals and proteins	Chemical-protein interaction retrieval	http://stitch.embl.de/	[154]
	DrugBank	A knowledge base for drugs, drug actions, and drug targets	Comprehensive analysis for approved drugs	http://www.drugbank.ca/	[19]
	ChEMBL	A database of bioactive drug-like small molecules, which contains 2 D structures, calculated properties, and abstracted bioactivities	Ingredient and drug chemoinformatics information retrieval	https://www.ebi.ac.uk/chembl/	[20]
	MMsINC	A large-scale chemoinformatics database	Ingredient and drug chemoinformatics information retrieval	http://mms.dsfarm.unipd.it/MMsINC/search/	[155]
C	CB	A comprehensive chemical structures database	Ingredient and drug chemoinformatics information retrieval	http://www.chemicalbook.com/	[156]
	ChemProt	A comprehensive disease-chemical biology database	Chemical-protein interaction analysis	http://www.cbs.dtu.dk/services/ChemProt-2.0/	[157]
	LookChem	A comprehensive chemical structures database	Ingredient and drug chemoinformatics information retrieval	http://www.lookchem.com/	[158]
	ChemSpider	A chemical structure database providing structures, properties, and associated information of compound	Ingredient and drug chemoinformatics information retrieval	http://www.chemspider.com/	[159]

TABLE 1: Continued.

Type [#]	Name	Description	Application	Webpage	Reference
	HIT	A comprehensive and fully curated database for linking herbal active ingredients to targets	Herbal ingredients' targets identification	http://lifecenter.sgst.cn/hit/	[160]
	CHMIS-C	A comprehensive herbal medicine information system for cancer	Comprehensive analysis for ingredient target of cancer	http://sw16.im.med.umich.edu/chmis-c/	[161]
	TD@T	TCM Database@Taiwan: providing chemical composition of Chinese medicinal herb including two- and three-dimensional structures of each TCM constituent	TCM medical compound retrieval	http://tcm.cmu.edu.tw/	[162]
	TCMGeneDIT	A database for associated traditional Chinese medicine, gene and disease information using text mining	Comprehensive analysis for ingredient-gene disease-effect of TCM	http://tcm.lifescience.ntu.edu.tw/	[163]
T	TCM-ID	Traditional Chinese medicine information database: providing information on formulae, medicinal herbs, and herbal ingredients	TCM formula and medical compound retrieval	http://tcm.cz3.nus.edu.sg/group/tcm-id/tcmid_ns.asp	[164]
	TCMID	Traditional Chinese medicine integrated database: a comprehensive database to provide information on drug-herb and its ingredient, prescription, target, and disease	Comprehensive analysis for TCM biological sciences	http://www.megabionet.org/tcmid/	[21]
	TcmSP	Traditional Chinese medicine systems pharmacology database and analysis platform: providing information on relationships between drugs, targets, and diseases	Comprehensive analysis for TCM biological sciences	http://tcmSPnw.com	[165]
	SIRC-TCM	Traditional Chinese medicine information database: providing information on formulae, medicinal herbs, and herbal ingredients	TCM formula and medical compound retrieval	http://www.tcm120.com/1w2k/tcm_species.asp	[166]

[#] B: biomolecular databases; D: disease/phenotype databases; C: chemical/drug-related databases; T: TCM related-databases.

these metrics for evaluation is illustrated in Figure 2. Two proteins, P1 and P2, interact through three and two proteins, respectively. P1's proteins do not have any interactions except with P1, whereas each of P2's proteins interact with two proteins. P2 would have greater chance of influencing than P1 despite its smaller degree because it has larger betweenness, which allows greater participation in information flow and may coregulate more proteins. These network characteristics can be captured by testing the distance between two nodes. Large distances mean that diffusing information from one node to another may take a longer time or require more steps. Thus, betweenness, which is related to distance, may be more appropriate in reflecting information flow based on biological regulation [36]. However, these network centrality measurements are correlated [37] and appear to complement each other in some cases. Each of these three measurements has been elaborated in a number of ways, and the locations of nodes are described in terms of how close they are to the center of the network. Network analysts are more likely to refer to their approaches as descriptions of centrality.

NIMS [38], which is a network-based approach for screening synergistic drug combinations in TCM, has integrated these three measurements into the topology score, which is used to indicate node importance. To identify genes that change their expression between two conditions, DiffRank, a novel network-based algorithm, was proposed. Betweenness was integrated into DiffRank as a structural scoring measure [39].

Thus, the distance between nodes in a network may be another important characteristic of a biological network based on the assumption that closer proteins have more similar functional annotations [40]. An analysis of network distances between regulated genes found that genes regulated by structurally similar drugs are significantly closer than genes regulated by dissimilar drugs [41]. Random walk, which describes a walker who walks randomly from node to node along edges in a network, was used to identify the relationship between disease and genes by calculating functional distance between nodes [42, 43]. The shortest path distance (SPD) is often used for network topology construction in pharmacology studies [38, 44]. For instance, SPD is applied to measure

TABLE 2: Network analysis tools.

Name/platform	Description	Type	Webpage
Cytoscape	An open source software platform for analyzing and visualizing complex networks: integrating a lot of plugins (Apps) concerning network analysis, communication scripting, and functional enrichment for biological network analysis. In addition, the package allows third-party developers to extend functionality of network analysis based on Java script [22, 23].	Free	http://www.cytoscape.org/
Pajek	A particularly useful package for the analysis of very large networks: integrating many network analysis methods. Thanks to its specific.net data file type, most of the algorithms of network analysis run quickly and scale well [167].	Free	http://pajek.imfm.si/doku.php
NetworkX	A Python-based package for comprehensive analysis of complex networks: integrating many network analysis methods including network structure and analysis measures.	Free	http://networkx.github.io/
Ucinet	A comprehensive package for the analysis of network: providing many network analysis methods as well as multivariate statistics. In addition, the package has strong matrix analysis such as matrix algebra and can be used to analyze different mode network data.	Commercial use	http://www.analytictech.com/ucinet/
NetMiner	An application software for exploratory analysis and visualization of large network data: providing 73 kinds of network analysis modules, 25 kinds of statistic and mining analysis modules, 28 kinds of visualization algorithms, 21 kinds of data transform modules.	Commercial use	http://www.netminer.com/
Guess	An exploratory data analysis and visualization tool for graphs and networks supporting Python which facilitate to the researcher working on graph structures in their own manners.	Free	http://graphexploration.cond.org/
Complex Networks Package for Matlab	Providing a comprehensive framework for both static and dynamic network analysis in Matlab.	Free	http://www.levmuchnik.net/Content/Networks/ComplexNetworksPackage.html
QuACN	An R Package for analyzing complex biological networks: providing function of analysis, classification and comparison for networks by different topological network descriptors [168, 169].	Free	http://cran.r-project.org/web/packages/QuACN/

the similarity between drugs [45] or between the binding site and a ligand [46] in the context of biological interaction networks or to compare entire networks [47, 48].

3.2. Network Mode. A network can be classified into different modes according to the number of kinds of nodes. In general, given a network $G = (V, E)$, where V is a set of nodes and E is a set of edges, if V has k subsets and no two nodes in the same subset are adjacent, G is called a k -partite network or k -mode network [49]. A network with two partitions is a bipartite network. A simple biological network that contains the same type of nodes such as PPIs is a 1-partite network or a standard network, where k equals 1. However, in many cases, biological network databases provide specialized data with different types, and researchers prefer to examine interactions between different types, such as disease-target and drug-target networks. A multi-partite network is difficult to analyze

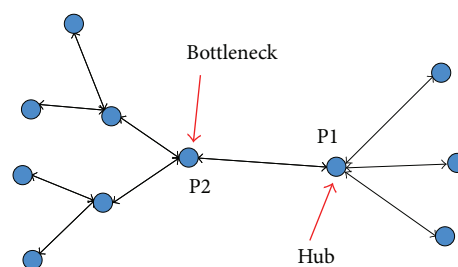


FIGURE 2: Illustrative example for measuring the basic properties of a network.

because of its asymmetry. As most network methods are developed based on the standard network, a multipartite network can be analyzed by transforming it into a single partite network, which can be easily achieved through matrix

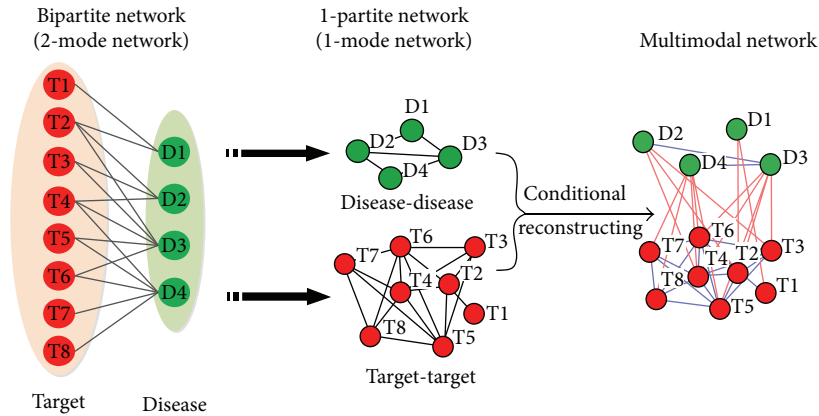


FIGURE 3: Illustrative example of network mode transformation.

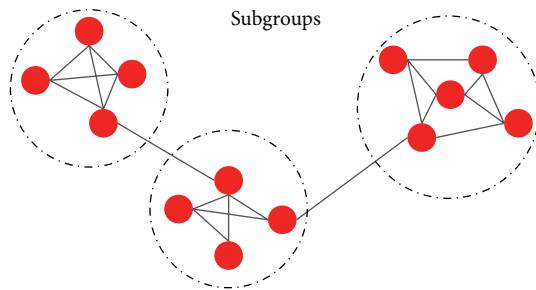


FIGURE 4: Network subgroups.

algebra. Figure 3 shows an example of a bipartite disease-gene network. Disease nodes are D1 (its targets are T1 to T2), D2 (its targets are T2 to T4), D3 (its targets are T2 to T6), and D4 (its targets are T4 to T8). This bipartite network can be represented by matrix M_{ij} , ($i = 1, 2, \dots, 8$, and $j = 1, 2, \dots, 4$), where $M_{ij} = 1$ denotes disease D_j , which has target T_i . This bipartite network can be transformed into two 1-mode networks through matrix multiplication after excluding self-interactions, namely, disease-disease network by $M' * M$ and target-target network by $M * M'$. A disease-disease network is constructed by sharing a target, and a target-target network is constructed by sharing a disease. These two 1-mode networks can be analyzed by using various network methods, such as calculating basic properties. Although analyzing 1-mode networks provides deeper insights into the relationship between the same kind of entities, identifying the interactions between different entities would be more valuable. A supervised learning integration method of a bipartite network was proposed for TCM network pharmacology to identify potential targets based on known drug-protein interactions by using a predicting model [50]. The proposed approach performed better than the nearest neighbor- and weight-based algorithms. Fuzzy clustering and spectral coclustering algorithms were applied for k -partite network analysis in network pharmacology [49, 51]. A tripartite disease-gene-protein complex network was decomposed by using the fuzzy clustering algorithm to determine structures in a network with multiple types of nodes.

A k -partite network that has adjacent nodes in the same subset and is more heterogeneous, which is beyond the definition of a k -partite network, is called a multimodal network (MMN) [52], which is very common in biology. Metabolic pathways, gene regulation networks, and signaling pathways are some examples of MMNs whose structures are modeled heterogeneously. In the above-mentioned bipartite network transformation, two 1-mode networks are given. We reconsider the relationship between diseases based on existing information and stipulate that two diseases are correlated (nodes are adjacent) only when they share two or more targets. A simple MMN is constructed by using matrix combination, as shown in Figure 3 (rightmost portion), and reflects three kinds of relationships: disease-disease, target-target, and disease-target, which provides more information than the k -partite network. Complicated networks require more complicated analysis methods. CIPHER-HIT [53], a hitting time-based method that integrates modularity measure into the network inference, was proposed for the prediction of disease genes and disease subtypes on the phenotype-gene MMN. CIPHER-HIT can significantly improve disease gene predictions on modularity levels and does not require preset parameters, unlike the random walk with restart [53]. A case study on breast cancer by using CIPHER-HIT was also given in this paper; two critical breast cancer subtypes were identified, which could reveal the potential genetic and phenotypic properties of breast cancer [53].

3.3. Community Structure and Subgroup Analysis. Network analysis commonly focuses on certain issues, one of which is subgroup structures. Figure 4 illustrates a simple network with several subgroup structures in which network connections are dense, but between which they are more sparse [54]. Therefore, network structure can be viewed from three different levels: individual, subgroup, and entire network [55]. Divisions of biology entities into groups could be a very important aspect of biological network structure. In addition, analyzing the structures of PPI networks could help biologists identify important biological units such as protein complexes and functional modules [56]. Understanding how biological entities play a role in the entire network

TABLE 3: Network-based subgroup analysis approaches in TCM.

Algorithm	Description	Application and findings
BK	Bron-Kerbosch algorithm: an efficient algorithm for finding all maximal cliques of a network. The recursive procedure for optimizing candidate selection is performed based on the three different sets (R, P, X) of nodes, where R represents the currently growing clique (initially empty), P denotes prospective nodes, and X stands for the nodes already processed [69].	Applied for the discovery of basic formula (BF) in herbal prescriptions of the famous TCM expert. Three BFs for psoriasis and four BFs for eczema were found [58].
K-core	A subnetwork detecting methods to find the required clusters in which all the nodes have at least k degree [64].	Applied for the subnetworks analysis of TCM ingredients target-target network, as well as for the measuring centrality of nodes by “K value” [77]. Applied for clustering symptoms for differentiating TCM syndrome of coronary heart disease based on the symptom-symptom network [76].
IPCA	A network-based clustering algorithm to identify subgroups based on the new topological structure [170].	Applied for clustering functional proteins of PPIs network based on TCM cold and hot syndromes [80] or TCM therapy [123].
CPM	Clique percolation Method for finding such a subgroup that corresponds to fully connected k nodes [56].	Applied for detecting synergistic or antagonistic subgroups of clinical factors networks in TCM tumor treatment [78].
SA	A simulated annealing algorithm, which is a generic probabilistic metaheuristic of the global optimizing for decomposing the networks [73].	Applied for subgroups detecting based on pathway-pathway association network for salvianolic acid B [79].

is important. For instance, in biological networks, some entities may act as bridges between subgroups and could be potential bottleneck nodes, while others may all be related within a single subgroup and could be potential hub nodes that could be important in understanding the biological process. The differences in the functions of entities may result from the different ways that entities are embedded in the structure of subgroups within a network. In TCM, most prescriptions commonly have some relatively smaller fixed composition(s) that can be called a basic formula (BF) [57]. Adding and/or subtracting herbs from BFs are usually carried out to produce a personalized treatment. Therefore, BFs could be implied by subgroups in herb-herb networks [58–60]. An herb-herb network, where subgroups overlap, provides insights into the TCM principle of treating the same disease by using different methods or treating different diseases by using the same method. Approaches to understanding the subgroup structure of a network have been developed. Some of these methods are based on graph theory, such as spectral bisection method [61] and Kernighan-Lin algorithm [62], while some are based on sociological methods, such as k -plexes [63], k -cores [64], CPM [56], and maximal clique algorithms [65–69]. Other approaches are based on clustering methods, such as optimization-related algorithms [70–73] and similarity-related methods [74, 75]. For TCM-related networks, network-based subgroup analysis methods are summarized in Table 3. Several subgroup analysis methods have been applied in the analysis of different types of networks in TCM, such as herb-herb [58], symptom-symptom [76], target-target [77], factor-factor [78], and pathway-pathway networks [79]. Thus, valuable herb combinations (basic formulae) [58], meaningful symptom groups [76], or biological entities [80] for differentiating syndromes, and

instructive therapy combinations for tumor treatment [78] have been obtained and provide a more comprehensive understanding of TCM principles.

4. TCM Network Pharmacology

A general framework for TCM network pharmacology research is shown in Figure 5. The flowchart shows two main types of analysis flows, whose starting points are the TCM object and disease. The key challenge for TCM network pharmacology research is the construction of drug- and disease-related networks, which requires different steps and methods. Although high-throughput experimental technologies offer considerable information, these technologies are often expensive and time consuming. Using existing information from databases appears to be more efficient but is not consistently sufficient. Advancements in systems biology have ensured that any information on both biological/medical resources and methodology can be obtained to facilitate TCM network pharmacology research. TCM network pharmacology and modern systems biology share most resources. This resource sharing explains to some extent why researchers view TCM network pharmacology as a bridge between TCM and modern medical science. The following sections discuss the practice of TCM network pharmacology and the resources and computational methods/tools it uses.

4.1. Network Construction. The key in network pharmacology is the construction of the network. The network pharmacology research process usually begins from the identification of drug- or disease-related biological entities (gene, protein, and metabolite) and then proceeds by constructing drug- or

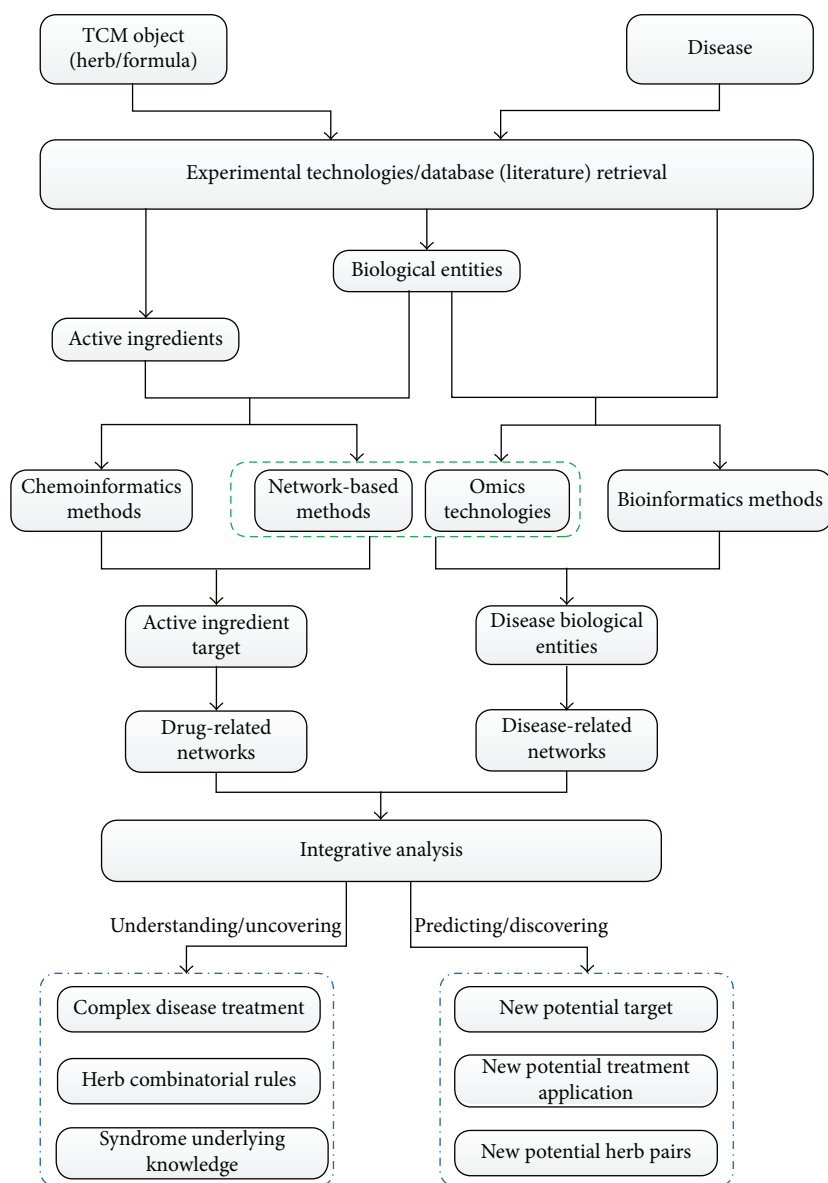


FIGURE 5: General TCM network pharmacology framework.

disease-related networks that could reveal underlying relationships by analyzing network topology properties. However, in TCM, constructing drug-related networks is different. Drug-related networks in TCM include herb/active ingredient (AI)-herb/active ingredient (AI) network and target-target network. Herb/AI-herb/AI network can be constructed by sharing formulae, targets, or disease/phenotypes, whereas target-target network can be constructed by sharing herb/AI. As herbal formulae are a major form for treatment in TCM, herb-herb networks that could reflect herbal combinatorial rules are particularly interesting. Li et al. [59] initiated a TCM network pharmacology based on an herb-herb network and proposed a DMIM method for constructing the network that assessed the herb-herb relationship based on both distance score and mutation information association. Identification of AI in herbs is the first step. TCM modernization in the past

few decades has enabled the retrieval of most known AIs in herbs from the literature or databases, although available data are not comprehensive. The challenge is to detect AI targets. AI identification is an easy method for constructing TCM drug-related networks based on existing resources. However, a shortcoming of current TCM-related interaction databases is that they contain a rather small number of interactions that have been validated experimentally. Many interactions remain unknown. Thus, methods that predict and identify new interactions should be developed. Experimental technologies such as “Omics” technologies are beyond the scope of this review. Table 4 summarizes useful methods or algorithms for AI target identification. Although only a few of these methods have been applied for TCM, all are instructive and could facilitate TCM drug-related network construction. Figure 5 shows the two main computational strategies for

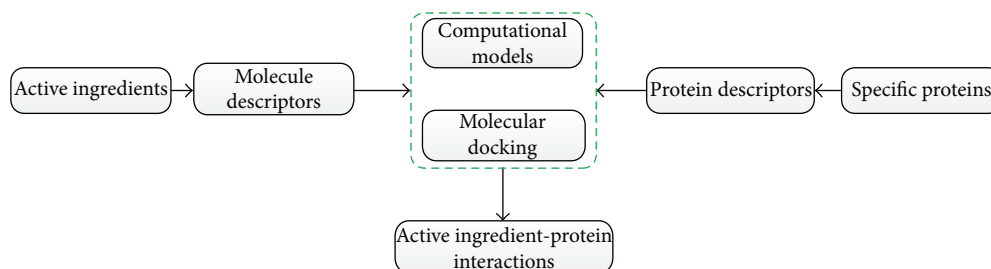


FIGURE 6: General cheminformatics protocol for identifying AI-protein interactions.

AI target identification: cheminformatics and network-based methods. The goal of cheminformatics is to describe relationships between targets and ligand- or structure-based information from AI. The general protocol of cheminformatics for identifying AI-protein interactions is shown in Figure 6. First, structure information of AI is retrieved from databases such as ChEMBL (<https://www.ebi.ac.uk/chembl>) or TCM Database@Taiwan (<http://tcm.cmu.edu.tw>). The structure information is then imported into a chemical software such as Dragon (Talete Inc.), Cerius2 (Accelrys, Inc.), MOE (Chemical Computing Group Inc.), or Sybyl (Tripos Inc.) to calculate the molecular descriptors, while protein descriptors are obtained from databases such as PDB (<http://www.rcsb.org/pdb>). Second, molecular docking is performed to infer the relationship between ligand and protein, or computational models are established to model the relationship between molecular and protein descriptors. Finally, AI-protein interactions are obtained through model prediction or by ranking the dock score. In this strategy, supervised machine learning algorithms such as k-nearest neighbors (KNNs) [81], support vector machine (SVM) [82–84], random forests (RFs) [82, 83], and Bayesian classifiers [85–87] are often used to establish classification models (Table 4). These algorithms require known AI-target information that is usually obtained from DrugBank (<http://www.drugbank.ca>) to train the models to successfully predict unknown information. Li et al. [83] proposed a network-based approach to reveal the mechanisms of action of three representative Chinese herbs (Ligusticum chuanxiong Hort., Dalbergia odorifera T. Chen, and Corydalis yanhusuo WT Wang) that are used to treat cardiovascular disease (CVD). RF and SVM were used to establish the drug-target models based on 6,511 drugs and 3,999 targets extracted from DrugBank databases, which indicates good prediction performance for drug-target interactions [82]. The AI molecular descriptors of the herbs were then calculated by using Dragon, and the structure information of candidate proteins was retrieved from the PDB database. As a result, 261 protein targets related to 64 AIs were predicted for the construction of a drug-target network. In this study, SVM was also used to predict oral bioavailability (OB) for screening AIs such that only AIs with good OB were selected for further analysis. KNN was applied to predict drug-target interactions [81]. In this paper, the common functional groups of drugs, instead of molecular descriptors, and four functional groups of proteins (enzymes, ion channels, G-protein-coupled receptors, and nuclear receptors), instead

of an entire family, were used to establish the classification models. In some cases, unsupervised algorithms such as self-organizing maps are useful [88, 89] and can be used to assess similarities between chemical and protein features. However, most cheminformatic methods often focus on a handful of proteins without considering that similar drug responses may result from their different targets in the same pathway or in the same biological process rather than from having common targets [87, 90, 91]. Information on drugs of one target and its distance in biological space to other targets can support the evaluation of new molecules for one or more novel targets [92]. Recent studies that combine different types of data such as protein-protein interactions have shown how computational analysis can identify drug targets [91, 93, 94]. Network-based approaches such as drugCIPHER [91] and WNBI [93] are good examples (Table 4). DrugCIPHER [91] integrates both drug therapeutic similarity (TS) and chemical similarity (CS) and uses a network topology property, namely, drug-protein closeness based on the PPI network, as drug genomic relatedness to model the relationships between drugs and targets. Three linear regression models, namely, drugCIPHER-TS, drugCIPHER-CS, and drugCIPHER-MS, which relate TS, CS, and their combination, respectively, are established. A comparison indicates that drugCIPHER-MS performs significantly better than the others, having successfully predicted the high-ranking proteins of Oxytocin and Nefazodone in the database. WNBI [93] integrated both drug-based and target-based similarity inference. Node-weighted network-based inference and edge-weighted network-based inference are then proposed by matrix operation. This approach can handle the weighted drug-target interaction network.

Constructing disease-related networks is not easy because disease biology is extremely complex. The progress of high-throughput interaction discovery experimental technologies enhanced the quality of PPI maps, which have become valuable tools that help in understanding the underlying mechanisms of diseases [95]. A prerequisite to the construction of disease networks is the availability of interaction information. Disease-related networks include disease-gene/protein, gene/protein-gene/protein, disease-phenotype, phenotype-phenotype, and disease-disease networks, among others. A critical step for the construction of disease-related networks is the identification of disease-gene/protein interactions. These interactions can be achieved in various ways, which is similar to the identification of AI targets. Most TCM network pharmacology researchers retrieve disease gene/protein based on databases such as

TABLE 4: Computational methods/algorithms for network pharmacology.

Type	Method and algorithm	Description	Application [#]
Network based	drugCIPHER	A network-based method for drug-target identification based on three linear regression models which integrates drug therapeutic similarity, chemical similarity, and the relevance of targets on PPIs network, respectively [91].	^H [91, 124, 132]
	DMIM	A distance-based mutual information model for indicating the relationship of herbs in TCM formulas [59].	^H [59]
	WNBI	A weight network-based inference method for drug-target prediction by integrating drug similarity and known target similarity [93].	^H [93]
	CIPHER	A computational framework based on a regression model which integrates PPIs, disease phenotype similarities, and gene-phenotype relationships [101].	^D [101]
	LMMA	A reliable approach for constructing disease-related gene network, which combines literature mining and microarray analysis [102].	^D [102]
	ClustEx	A two-step method based on module identification in PPIs network by integrating the time-course microarray data for specific disease-related gene discovery [171].	^D [171]
	MIClique	Identifying disease gene subsets by the combination of mutual information and clique analysis for biological networks [103].	^D [103]
	rcNet	A coupling ridge regression model established based on the known phenotype-gene network for predicting the unknown ones by maximizing the coherence between them [172].	^D [172]
	WSM	A similarity based method for weighted networks matching [104].	^D [104]
	SCAN	A structural clustering algorithm based on biological networks for functional modules discovery [173].	^D [173]
	CIPHER-HIT	A hitting-time-based method for predicting disease genes, which combined the modularity measure into the network inference [53].	^I [53]
	ComCIPHER	An efficient approach for identifying drug-gene-disease comodules underlying the gene closeness data [116].	^I [116]
	PPA	Ping-Pong algorithm: an efficient algorithm for predicting drug-gene associations based on multitypes of data [115].	^I [115]
	ISA	Iterative signature algorithm for searching the modules in heterogeneous network [118].	^I [118]
	NSS	A network stratification strategy to analyze conglomerate networks [174].	^I [174]
Machine learning/others	KNN	K nearest neighbor algorithm: a classical supervised classification algorithm based on closest training samples in the feature space.	^H [81]
	SVM	Support vector machine: a supervised kernel based classification algorithm based on the support vectors which are obtained after the training process by transforming original space into kernel space.	^B [82-84, 96, 97, 175]
	GIP	Gaussian Interaction profile: an efficient classification algorithm for predicting drug-target by constructing a kernel function from the known drug-target interaction profiles [176].	^H [176]
	RF	Random forest: an ensemble learning method for classification based on a multitude of trained decision trees.	^B [82, 83, 177]
	Bayesian classifiers	A popular supervised classification method based on probabilistic graphical model.	^B [85-87, 98, 99]
	SOM	Self-organizing maps: a unsupervised technology based on competition among the output neurons for assignment of the input vectors to map input observations to an output space represented by a grid of output neurons for similarity assessment.	^B [88, 89]
	SEM	Similarity ensemble methods: usually based on several similarity index such as Tanimoto coefficient(Tc) [107, 108] or Jaccard coefficient (Jc) [109].	^B [38, 110, 111]

TABLE 4: Continued.

Type	Method and algorithm	Description	Application [#]
	PCA	Principal component analysis: a classical data reduction technique for revealing the interrelationship among many variables by creating linear combinations of them into a few new variables to facilitate clustering and model analysis.	^B [100, 124, 178]

Application[#]: ^Hherb-related networks construction; ^Ddisease-related networks construction; ^Iintegrative analysis; ^Bboth herb- and- disease-related networks construction.

OMIM (<http://www.omim.org>), whereas others develop computational methods to assess the susceptibility of genes to diseases. Some of these methods are based on bioinformatics models such as machine learning algorithms (Table 4). These methods, which are mostly based on gene expression pattern recognition, assume that some disease genes are already known and detect candidate genes based on established classification models; SVM [96, 97] and Bayesian classifiers [98, 99] are often used. Microarray gene expression data sets contain a large number of features. Thus, several dimension reduction methods are useful, such as principal component analysis [100] and maximum relevance minimum redundancy [81]. Other methods are network-based approaches (Table 4) that integrate different types of data for analysis. Wu et al. [101] developed the network-based tool CIPHER to predict disease genes. CIPHER was based on the characteristics of genes that share a mutant phenotype, which are closely linked in the network. This approach integrates phenotype similarity and gene closeness based on the PPI network and uses their correlation as a disease predictor to establish the linear model. LMMA [102] was proposed by the same group and was developed for disease-related network construction, which combined text mining and multivariate statistics. LMMA initially constructs a literature mining-based network (LM) by using literature information from a database such as PubMed (<http://www.ncbi.nlm.nih.gov/pubmed>). The microarray information is then integrated into the approach. The construction of an LMMA-based network is facilitated after the LM-based network was refined through stepwise multiple variable selection. LMMA was applied for the construction of angiogenesis network. Compared with the LM-based approach, LMMA could significantly eliminate false positive relations to obtain a more reliable interaction network. Some recent subgroup analysis-based approaches, such as MIClique [103], WSM [104], and CPM [105], can identify the disease-gene relationship. Most of these approaches were not applied on TCM network pharmacology, but they are all instructive.

Similarity ensemble method (SEM) is widely used in many aspects of network pharmacology research. In contrast to model-based approaches, SEM offers a model-free alternative because of its nonparametric characteristics [106]. Similarity metric, Jaccard similarity coefficient [107], and Tanimoto similarity coefficient [108, 109] are often used in TCM network pharmacology research to assess GO function similarity [38], compound structure similarity [110], or drug-likeness calculation [111]. These methods are adopted because network pharmacology variables are usually binary coded

strings. These methods originated from different cases, but they are mathematically equal [112].

4.2. Integrative Analysis. Integrative analysis is a complicated process in network pharmacology research. Researchers are now compelled to handle different types of lines and nodes because of multiple network construction. An easy solution is the use of functional annotation analysis for common elements based on prior knowledge. For example, 54 targets and 9 signal pathways were extracted from a CVD-related gene network after TCM drug-target network construction. These targets could reveal the biological mechanism of herbs used for treating CVD [83]. A comparison among network topology properties is also useful. Ye et al. [113] investigated the mechanism of Chuanxiong Rhizome-Paeonia Albifora Pall (HP CXR-PAP) in osteoarthritis treatment. Some similar characteristic distributions of network properties between herbal ligand-target network and drug-ligand network (data source from DrugBank) indicate that the mechanism of HP CXR-PAP on this disease has potential drug-likeness or lead-like compounds. Li et al. [59] compared the average shortest path distance (ASPD) between networks and found that ASPD between TCM drug-target and specific disease genes was significantly smaller compared with that between TCM drug-target and a randomly selected disease. This finding implies the rationality of these TCM drugs in treating specific diseases. Some useful alignment methods such as IsoRankN [114] can also identify the best mapping based on clustering and allows multiple network comparison. Module approaches for integrative analysis are more informative. Searching for modules is relatively easy if the network is simple. Thus, several network-based subgroup methods (Table 3) can be used. However, biological networks in most cases are composed of multiple types of nodes and edges. The “comodule” approach, which is another effective computational analysis method, was initially proposed by Kutalik et al. [115] and introduced to TCM pharmacology by Li et al. [59, 116, 117]; “comodule” does not have a precise definition. This approach is an analysis strategy rather than a tool in network pharmacology. The basic idea of comodule is to search modules (subsets) in heterogeneous (multimodal) or multilevel networks with similar patterns and perform an integrative analysis of their connections between or within groups. Li et al. [59] initially performed comodule analysis on multilevel networks to determine the combination rule of TCM formula. The herb, biomolecular, and disease modules in this module were extracted from herb, biological, and disease networks, respectively. Biomolecular modules

support the treatment of specific disease modules by herb modules through overlapping and functional annotation analysis. Comodule analysis also allows the investigation of multiple types of lines and nodes. Table 4 lists a number of comodule methods. ISA [118], PPA [115], and CIPHER-HIT [53] can handle two distinct types of node associations and their shared node modules on the network. comCIPHER can detect modules on a network that has three types of node relationships, such as the drug-gene-disease heterogeneous network. This method handles the dataset as a huge matrix. Row denotes gene space, whereas column denotes drug and disease spaces. Markov chain Monte Carlo was used to initially select genes as modules in the row space. The chain determined by using the Gibbs sampler and the Metropolis-Hastings algorithm is then moved. Partitioning was performed in the row and the column spaces to divide the genes into different modules. The column space (drug and disease) was partitioned into two categories, namely, associated and nonassociated with the same row of gene module. Comodules, including genes and their drugs and diseases, could be achieved through Bayesian partitioning after presenting the distributions of drug-gene and disease-gene profile values. This algorithm has two advantages. First, the drug-gene and disease-gene relationships are simultaneously investigated within the same module to facilitate the identification of potential associations between drugs and diseases. These associations are meaningful and might suggest new drug applications and side effects. This paper shows that comCIPHER successfully identified two drugs (Pranlukast and Minocycline) as new treatment for human cancer. Second, modules obtained by using comCIPHER seem more compressed compared with those obtained by using other module analysis methods such as PPA. This finding might provide a clearer insight into the association between drugs and diseases because of high network interconnections.

4.3. Applications. Network pharmacology, as a distinctive new approach for TCM research, includes the application of network analysis to identify the group of proteins that are most critical in diseases and to recognize chemical molecules that can target that group of proteins. Network pharmacology is similar to other computational tools and generally has two main functions (Figure 5). One function is the understanding/uncovering function, which involves providing a deeper insight or scientific evidence for TCM knowledge or breaking down existing TCM knowledge and identifying them as scientifically proven. The other function is the predicting/discovering function, which involves extending knowledge or providing new hypotheses by building on existing TCM knowledge by using more reliable network models. The following sections discuss these functions in detail.

4.3.1. Understanding/Uncovering the TCM Principle of Treating Complex Diseases. TCM treatments are holistic, considering the patient as a whole rather than focusing solely on the disease. This characteristic agrees with the concept that

various complex diseases result from dysregulation of multiple pathways and changes in expression of a large number of genes, proteins, and metabolites. Network pharmacology provides a deeper insight into TCM treatments and helps uncover action mechanisms on a biological basis. Recent progress in TCM network pharmacology research revealed the biological molecular mechanisms of TCM treatment of many complex diseases (Table 5). CVD is a class of diseases that involves dysfunction of the heart or blood vessels. Zhao et al. [119] identified 1,619 proteins involved in 33 pathways after mapping CVD drug targets from DrugBank. These proteins could be regarded as candidate protein targets related to CVD. Different medications are employed to treat this disease. TCM herbs or formulae that can effectively promote blood circulation for removing blood stasis (“*Huo Xue Hua Yu*”), such as *Salvia Miltiorrhiza*, *Ligustici Chuanxiong*, and *Panax Notoginseng*, are often used. Li et al. [37] constructed a compound-potential target network and a compound-pathway network based on the *Compound Danshen Formula* (CDF). This approach identified 41 potential targets of CDF that are significantly related to CVD and the involvement of three main pathways, namely, PPAR signaling, glucocorticoid and inflammatory, and L-arginine/NO signaling pathways. Wang et al. [120] proposed the network pharmacology method to investigate the mechanisms of four clinically and widely used herbs (*Radix Astragali Mongolici*, *Radix Puerariae Lobatae*, *Radix Ophiopogonis Japonici*, and *Radix Salviae Miltiorrhiza*) for CVD treatment. Twenty-one out of 68, 19 out of 77, 13 out of 34, and 19 out of 77 targets were related to CVD, respectively. Astragaloside IV, one of the main AIs of *Astragalus Membranaceus*, identified 39 distinct proteins as putative targets related to CVD. Thirty-three proteins can be classified into eight functional classes that are related with CVD pathogenesis, such as the regulation of vasoconstriction and vasodilation, blood coagulation, calcium ion related, MAP kinase activity related, and others [119]. Rheumatoid arthritis (RA) is induced by several complex processes, including inflammatory response, excess synovial fluid, and the development of fibrous tissue in the synovium [121]. TCM regards RA as a blockage disease. Thus, the main treatment principle for RA is the removal of dampness and dredging the channel [122]. Several studies in network pharmacology [77, 123, 124] provided biological molecule evidence for the rationality of this principle. Wu-Tou-Tang (WTT) [77] and Qin-Luo-Yin (QLY) [124] are classical TCM formulae that could be used for treating RA. WTT [77] is composed of five herbs, namely, *Radix Aconiti*, *Herba Ephedrae*, *Radix Astragali*, *Radix Paeoniae Alba*, and *Radix Glycyrrhizae*. Yan et al. [77] collected the structure information of 165 compounds of WTT. After analyzing the topological features of both PPI and drug-target networks, nine proteins with higher values of centrality properties were identified as major candidates of effector modules of WTT. Six proteins, namely, ADRB2, ADRA1B, HSP90AA1, STAT3, NR3C1, and TUBB, were significantly associated with RA. Twelve proteins/genes in QLY are related with RA. These proteins were related to angiogenesis, inflammatory response, immune response, and NF- κ B activity.

TABLE 5: TCM network pharmacology for understanding the treatment principle of complex diseases.

Disease/action [#]	Related ingredient/herb/formula	Reference
T2DM	Tangminling pills	[134]
APL	Realgar-indigo naturalis formula	[179]
	Yishen juanbi tablet	[123]
RA	Qing-Luo-Yin	[124]
	Wu Tou Tang	[77]
	Ligusticum Chuanxiong Hort., Dalbergia Odorifera T. Chen and Corydalis Yanhusuo WT Wang	[83]
	Radix Astragali Mongolici, Radix Puerariae Lobatae, Radix Ophiopogonis Japonici, and Radix Salviae Miltiorrhiza	[120]
CVD	Compound Danshen formula	[37, 180]
	Astragaloside IV	[119]
	Salvianolic acid B	[79]
	Radix Curcumae formula	[111]
	Salvia Miltiorrhiza, Safflower, Ligustici Chuanxiong, Herba Erigerontis, Semen Persicae, Panax Notoginseng, Radix Paeoniae Rubra	[181]
	Tiao-Pi-Hu-Xin formula	[182]
OA	Chuanxiong Rhizome, Paeonia Albiflora Pall	[113]
	Tao-Hong-Si-Wu decoction	[183]
Alzheimer	Ginkgo Biloba, Huperzia Serrata, Melissa Officinalis, Salvia Officinalis	[184]
Anti-angiogenesis	Sixty-one herbal ingredients	[38]
Sepsis	Xue-Bi-Jing formula	[185]
Cancer	Kang Ai Pian	[186]
	Ganoderic acid D	[187]
Influenza	Lonicera Japonica and Fructus Forsythiae	[188]
	Maxingshigan-Yinqiaosan formula	[189]
Hepatoprotection	Yin-Chen-Hao-Tang	[190]
GBS	Gui-Zhi-Fu-Ling capsule	[191]
AWI	Zhike Chuanbei Pipa dropping pills	[192]
CKD	Sixty-two herbs	[193]

[#]T2DM: type II diabetes mellitus; APL: acute promyelocytic leukemia; RA: rheumatoid arthritis; CVD: cardiovascular disease; OA: osteoarthritis; GBS: gynecological blood stasis; AWI: airway inflammation; CKD: chronic kidney disease.

4.3.2. *Understanding/Uncovering Herb Combinatorial Rules in TCM.* The role of herbs in TCM formulae should be understood because their combinatorial rules might reflect underlying principles of TCM therapies. TCM formulae are composed of herbs that play different roles during treatment. “Jun” represents the principal component and treats the main disease directly. Other herbs, namely, “Chen” (minister), “Zuo” (adjuvant), and “Shi” (courier) [125], help enhance the effects, treat the accompanying symptoms, and facilitate the delivery of the principal component, respectively. Several researchers [37, 111, 124] provided some good examples to clarify the roles of herbs in formulae at a biological molecular level by using network pharmacology. Zhang et al. [124] examined the roles of herbs in QLY for RA treatment. QLY is composed of four herbs, namely, *Sophora Flavescens* (SF), *Sinomenium Acutum* (SA), *Phellodendron Chinensis* (PC), and *Dioscorea Collettii* (DC). Target network analysis and functional annotation analysis indicate that SF, which is a “Jun” herb, performs principal processes in the development

of RA. These processes include angiogenesis, inflammatory response, and immune response, which are consistent with the function of this herb. Other herbs served as complements by regulating RA-related genes. Other studies [37, 111] examined herb combinatorial rules based on OB prediction before network construction. Tao et al. [111] explained the combinatorial mechanism of *Radix Curcumae* formula (RCF) and predicted the potential targets related to CVD. RCF includes four herbs, namely, *Radix Curcumae* (RC), *Fructus Gardeniae* (FG), *Moschus* (MS), and *Borneolum* (BM). This paper predicted the OB of herbal ingredients based on the developed silicomodel [126]. Drug-likeness index was calculated based on Tanimoto similarity. OB and drug-likeness were used to select candidate compounds. Seventy-four candidate compounds with good OB were obtained. The number of candidate compounds explained the roles of herbs in this formula. Forty-five out of 74 compounds were involved in the “Jun” herb (RC), 19 out of 74 compounds were involved in the “Chen” herb (FG), 12 compounds were

involved in the “Zuo” herb (MS), and only three compounds were involved in the “Shi” herb (BM). The percentage of overlapping targets also supported the combinatorial rule. The number of shared targets between “Jun” and “Chen” was larger than that between “Jun” and “Zuo.” No shared targets were found among “Jun,” “Chen,” and “Shi.” These results illustrate the different roles of herbs in RCF for CVD treatment. Their study investigated the mechanisms of CDF for the same disease. The results also indicate the feasibility of this analysis to uncover the herb combinatorial rules in TCM formulae [37].

4.3.3. Understanding/Uncovering the Underlying Principle of TCM Syndromes. Syndrome is the basic concept in TCM theory. Most of its contents are abstracted and inferred from direct observation and experience. Syndrome differentiation guides TCM therapies. Given the importance of syndrome differentiation, its underlying principle should therefore be investigated. Network pharmacology is a powerful tool for understanding TCM syndrome on a molecular level [10, 127]. Li et al. pioneered this approach [10, 127, 128] and explored relationships between syndrome-related diseases and the neuroendocrine-immune (NEI) system based on the basic properties of a syndrome network (hot and cold) [127, 128]. A hot syndrome network was constructed based on 38 related diseases, and a cold syndrome network was constructed based on 21 related diseases. Biological entities as network nodes were classified into hot and cold genes based on a predefined topological temperature. The study conducted functional annotation analysis for hub nodes of networks and topological temperature comparison, which indicated that the molecular foundation of hot syndrome was mainly associated with immune-related genes, and cold syndrome was primarily based on hormone-related genes [127]. Ma et al. [128] selected 16 family members that have a history of cold syndrome to examine gene expression levels. Twenty-five differentially expressed genes were identified. Thirteen genes interacted with NEI cold or hot genes by expanding the network based on PPIs. Twelve pathways of these interaction genes were identified as metabolism- or energy-related, which indicated the relationship between TCM syndrome and energy metabolism in the context of the NEI network. The natural properties of herbs may indicate the principle behind TCM, such as “cooling the hot and warming the cold.” Two classical formulae, namely, CWHF and HCHF, were applied to the rat model of collagen-induced arthritis after identifying the hub genes of the cold and hot networks. These formulae represent cold syndrome-oriented and hot syndrome-oriented herbal treatments, respectively. CWHF suppresses the hub genes of the cold network, and HCHF tends to affect the hub genes of the hot network [127]. In another study, Li et al. [59] found that major ingredients paired with “warm” herbs caused synergistic proangiogenic activity. Their recent study [129] further explored hot and cold syndromes by using a network balance model. Bioinformatics and clinical information were combined to establish the network model

for identifying biomarkers that reflect network imbalance in hot/cold syndromes to reveal the biological basis of cold and hot syndromes in chronic gastritis patients. Thus, several biomarkers were identified. Higher leptin levels were found in cold syndrome patients, whereas higher CCL2/MCP1 levels were found in hot syndrome patients. These findings further revealed the connections between TCM syndromes and the metabolism and immune system. The potential of tongue-coating microbiome as a biomarker for characterizing TCM syndromes was also discussed [130]. Tongue-coating samples were collected from 19 gastritis patients and 8 healthy volunteers. These patients were categorized into hot and cold syndromes based on traditional tongue diagnosis. Next-generation sequencing data analysis indicated that a total of 381 species-level operational taxonomic units (OTUs) differed significantly between groups. Two hundred fifty-one of these OTUs were classified into 61 genera and 49 species. These genera and species could be regarded as potential biomarkers for characterizing hot/cold syndromes.

Lu et al. explored the molecular mechanism of TCM syndrome on RA patients through network pharmacology [80, 117, 123, 131]. Their findings indicate that the cold and hot syndromes of RA patients can be differentiated based on biological modules. Thirty-three RA patients with cold and hot syndromes were included. Twenty-one significantly differentially expressed genes were identified between cold and hot syndromes after genome-wide expression analysis. RA-related network was constructed by expanding the PPI network by using these genes as seeds. Four significantly and highly connected groups were obtained after subgroup network analysis. Group 1 was mostly associated with signal transduction. Group 2 was related to eicosanoid metabolic processes, oxidation-reduction reactions, and fatty acid metabolic processes. Groups 3 and 4 were involved in cell proliferation [80]. Their other study [131] included healthy volunteers to further explore the difference of biological basis of TCM syndrome between RA and normal patients. Thirty-five differentially expressed genes were identified between the cold syndrome and normal patients, and 21 genes were identified between hot syndrome and normal patients by using similar strategy analysis. Their shared genes were related to the following pathways: autoimmune thyroid disease, cell adhesion molecules, T-cell receptor signaling pathway, rheumatoid arthritis, and proteasome. These pathways also indicated the different molecular basis between RA and the normal patients. Jiang et al. then investigated the mechanism of effect of TCM syndrome on the clinical effectiveness of interventions [123]. Different therapies showed different benefits in treating RA patients with different TCM syndromes. For example, TCM therapy is more appropriate for hot syndrome, whereas biomedical therapy is better for cold syndrome. These results clarify the relationship between biological modules and TCM syndromes.

4.3.4. Predicting/Discovering New Potential Targets and Treatment Applications. The predicting/discovering function of network pharmacology as a computational tool is mainly

based on the assumption that other nodes, which are topologically closely related to them or their neighbors, might also be associated if significant node pairs in the network are known to be associated. The association is not guaranteed, but it can be used to facilitate the direction of laboratory testing or to validate and lead to new discoveries. The predicting/discovering function of new potential targets of drug is valuable for providing new insights into the mechanism of drug action and might lead to new treatment applications. Zhang et al. [132] applied TCM network pharmacology to explore vitexicarpin (VIT). VIT is extracted from the fruits of *Vitex rotundifolia*. They [59] previously found that VIT has antiangiogenic properties, but the mechanism remains unknown. This study used drugCIPHER [91] to predict the target proteins of VIT. The top 10% targets of VIT predicted by drugCIPHER model were selected to construct a drug-target network to identify significant pathways. Fifty-eight targets of FDA-approved drugs that directly targeted VEGF signaling pathways were also collected. Eleven direct target proteins were obtained based on correlations between the profiles of the 58 FDA-approved drugs and VIT. SRC and AKT, whose drugCIPHER scores are ranked at the top 2, were validated by experiments and computational docking analysis. Thus, the potential targets of new VIT predicted by network-based approach illustrate the mechanism of its antiangiogenic activity and lead to its new application as an angiogenesis inhibitor. Another article provides new insights into rhein [133], which is a classical natural substance isolated from rhubarb. This study successfully predicted three new molecular targets for rhein, namely, MMP2, MMP9, and TNF. MMP2 and MMP9 were significantly associated with cancer-related pathways, which further illustrates the potential of rhein and its products to be used for cancer relief in China. Gu et al. [134] conducted network analysis to elucidate the action mechanism of the medical composition, Tangminling Pills (TP). TP was designed for the treatment of type II diabetes mellitus (T2DM). A total of 676 ingredients contained in TP were considered for the construction of drug-target and drug-drug networks. Five ingredients were significantly associated with T2DM through subgroup and topology property analysis, namely, rheidin A, rheidin C, sennoside C, procyanidin C1, and dihydrobaicalin. Their biological activities of T2DM were not reported. These findings might expand the applications of these ingredients. A drug-target network of Yuanhu-Zhitong (YZP) was constructed to explain its molecular mechanism [135]. YZP is a classical formula in TCM and is widely used for the treatment of gastralgia, dysmenorrhea, and headache. The alkaloids of YZP are highly connected with the GABA receptor group, which are close to benzodiazepine receptors. This finding suggests that YZP might serve as an antidepressant and an anti-anxiety drug. These potential treatment applications were validated by computational docking analysis and experiments. Some new indications of CDF (a classical TCM formula) were also reported [37]. Li et al. [37] found that CDF may be potentially applied to treat metabolic diseases because of its high association with metabolism-related targets after network pharmacology analysis. These findings may drive future laboratory or clinical research. However, they have not been further validated.

4.3.5. Predicting/Discovering New Potential Synergistic Herb/Ingredient Pairs. An herb pair, which is the most frequent cooccurrence of two herbs in TCM therapies, is the basic herbal combinatorial form in TCM formulae. Herb pairs may achieve better efficacy according to TCM theory. Hundreds of herb pairs are available in TCM therapies, but their function in the treatment remains unknown. Discovering new potential synergistic herb/ingredient pairs is important for understanding combinatorial rules and designing new TCM drug compositions. Herb pairs can be mathematically denoted as the interaction between two herbs. Edges in the network depict this relationship. Network-based approaches were proposed to explore the relationship of herbs to achieve core herbs, core herb pairs, and core herb formulae [58, 59, 136–138]. Li et al. [59] discovered six new herb pairs related to angiogenic activities by DMIM based on an herb-herb network. Three of these pairs included *Rhizoma Chuanxiong* (RCX), which indicate the importance of this herb. Further network topology analysis also supported the role of RCX as a core herb. This herb-herb network also successfully retrieved most widely known herb pairs and six classical herbal formulae, which indicate its reliability to a certain extent. A new herb pair, RCX and *Flos Carthami* (FC), was chosen to evaluate the combination effect. This work utilized tetramethylpyrazine, a compound isolated from RCX, instead of RCX and hydroxysafflor yellow A, a compound isolated from FC. The results validated the synergistic effect of this herb pair, which also expanded their applications in clinical therapies in TCM. Their study [38] explored 63 agents, including 61 herbs or herb ingredients and their combination effect related to antiangiogenesis by using NIMS. The advantage of NIMS is its ability to integrate two informative parameters, topology score, and agent score, which might increase the reliability and robustness of outputs. Thus, five new synergistic herbal ingredient pairs were reported, which were experimentally validated. The rank order of maximum increased inhibition rate of ingredient pairs obtained from experiments was identical to that predicted by NIMS, which further confirmed the synergistic effect of these ingredient pairs.

5. Perspectives

An overview of TCM network pharmacology and its computational tools was presented. Network pharmacology, as a new research approach, provides revolutionary opportunities for TCM modernization. Recent studies show that sufficient information can be obtained to largely enhance understanding of the underlying principle of TCM when combined with multiple types of data and computational tools. It might predict and explain existing TCM knowledge. Recent successes in TCM network pharmacology research were achieved in the last decade. However, current TCM network pharmacology remains in its infancy, and deducing reliable predictive inferences remains challenging because of a number of reasons. First, network pharmacology largely relies on available data sources. Several biological databases are open source and up to date. Thus, more information on

TCM is needed, including the standardization and identification of active ingredients, which requires additional experimental technologies and further experimental investigations into TCM-related biochemistry research to better understand the mechanisms of TCM drug action. Second, this information is collected from various experiments or literature, thereby resulting in many false positive and false negative interactions that can be partially attributed to the lack of reliability and robustness of network models. Therefore, more powerful computational tools are needed to reevaluate or to refine more informative interactions. Third, network-based algorithms have advantages for the analysis of multiple types of data. However, several current informative network-based algorithms are limited by network scale because of their computational cost. Most algorithms are designed for the analysis of a static network, which ignores the dynamic nature of molecular systems. Thus, high-performance computational tools for analyzing large-scale networks and dynamic networks should be developed for rapid and efficient analysis. Lastly, the results of network pharmacology studies should be validated to verify the inferences. The associations, especially for TCM ingredients and their interactions, may not be strong enough to be easily identified by general experiments. Thus, more sensitive and quantitative experimental techniques are needed. Most TCM network pharmacology studies focus on the efficacy of an herb or formulae. However, concerns over drug toxicity increased significantly in the past decade. Research on the mechanism of adverse side effects or identification of the “off-targets” of TCM drug is valuable for the reevaluation of TCM clinical efficacy and the design of new TCM therapies, which may become the future direction of TCM network pharmacology research. Another interesting aspect is the interactions between TCM and Western medicines, which may illustrate how the combination can achieve better efficacy and fewer side effects. The use of network pharmacology approaches is vital to driving future research on TCM pharmacology.

Acknowledgments

The authors are grateful to the anonymous reviewers and the editors for their helpful comments and suggestions, which substantially improved the quality of this paper. This study was supported by the National Natural Science Foundation of China (81273727), Longhua Medical Project. There is no conflict of interests involved in this paper.

References

- [1] P. M. Barnes, B. Bloom, and R. L. Nahin, “Complementary and alternative medicine use among adults and children: United States, 2007,” *National Health Statistics Reports*, no. 12, pp. 1–23, 2008.
- [2] M. Schena, D. Shalon, R. W. Davis, and P. O. Brown, “Quantitative monitoring of gene expression patterns with a complementary DNA microarray,” *Science*, vol. 270, no. 5235, pp. 467–470, 1995.
- [3] M. A. Yildirim, K.-I. Goh, M. E. Cusick, A.-L. Barabási, and M. Vidal, “Drug-target network,” *Nature Biotechnology*, vol. 25, no. 10, pp. 1119–1126, 2007.
- [4] G. V. Paolini, R. H. B. Shapland, W. P. Van Hoorn, J. S. Mason, and A. L. Hopkins, “Global mapping of pharmacological space,” *Nature Biotechnology*, vol. 24, no. 7, pp. 805–815, 2006.
- [5] J. C. Nacher and J.-M. Schwartz, “A global view of drug-therapy interactions,” *BMC Pharmacology*, vol. 8, article 5, 2008.
- [6] E. Gregori-Puigjané and J. Mestres, “A ligand-based approach to mining the chemogenomic space of drugs,” *Combinatorial Chemistry & High Throughput Screening*, vol. 11, no. 8, pp. 669–676, 2008.
- [7] A. Pujol, R. Mosca, J. Farrés, and P. Aloy, “Unveiling the role of network and systems biology in drug discovery,” *Trends in Pharmacological Sciences*, vol. 31, no. 3, pp. 115–123, 2010.
- [8] S. Li, “Framework and practice of network-based studies for Chinese herbal formula,” *Journal of Chinese Integrative Medicine*, vol. 5, no. 5, pp. 489–493, 2007.
- [9] S. Li, “Network target: a starting point for traditional Chinese medicine network pharmacology,” *Zhongguo Zhongyao Zazhi*, vol. 36, no. 15, pp. 2017–2020, 2011.
- [10] S. Li and B. Zhang, “Traditional Chinese medicine network pharmacology: theory, methodology and application,” *Chinese Journal of Natural Medicines*, vol. 11, no. 2, pp. 110–120, 2013.
- [11] L. Perini, “Explanation in two dimensions: diagrams and biological explanation,” *Biology & Philosophy*, vol. 20, no. 2-3, pp. 257–269, 2005.
- [12] M. Kanehisa, “The KEGG database,” *In Silico Simulation of Biological Processes*, vol. 247, pp. 91–103, 2002.
- [13] T. S. Keshava Prasad, R. Goel, K. Kandasamy et al., “Human protein reference database—2009 update,” *Nucleic Acids Research*, vol. 37, no. 1, pp. D767–D772, 2009.
- [14] H. M. Berman, J. Westbrook, Z. Feng et al., “The protein data bank,” *Nucleic Acids Research*, vol. 28, no. 1, pp. 235–242, 2000.
- [15] F. Zhu, B. Han, P. Kumar et al., “Update of TTD: therapeutic target database,” *Nucleic Acids Research*, vol. 38, supplement 1, pp. D787–D791, 2010.
- [16] A. Kamburov, U. Stelzl, H. Lehrach et al., “The ConsensusPathDB interaction database: 2013 update,” *Nucleic Acids Research*, vol. 41, no. 1, pp. D793–D800, 2013.
- [17] J. Y. Chen, S. R. Mamidipalli, and T. X. Huan, “HAPPI: an online database of comprehensive human annotated and predicted protein interactions,” *BMC Genomics*, vol. 10, supplement 1, article S16, 2009.
- [18] McKusick-Nathans Institute of Genetic Medicine, Johns Hopkins University, “Online Mendelian Inheritance in Man, OMIM,” 2013, <http://omim.org/>.
- [19] C. Knox, V. Law, T. Jewison et al., “DrugBank 3.0: a comprehensive resource for ‘Omics’ research on drugs,” *Nucleic Acids Research*, vol. 39, no. 1, pp. D1035–D1041, 2011.
- [20] J. P. Overington, “ChEMBL: large-scale mapping of medicinal chemistry and pharmacology data to genomes,” *Abstracts of Papers of the American Chemical Society*, vol. 238, 2009.
- [21] R. C. Xue, Z. Fang, M. X. Zhang et al., “TCMID: traditional Chinese medicine integrative database for herb molecular mechanism analysis,” *Nucleic Acids Research*, vol. 41, no. 1, pp. D1089–D1095, 2013.
- [22] P. Shannon, A. Markiel, O. Ozier et al., “Cytoscape: a software environment for integrated models of biomolecular interaction networks,” *Genome Research*, vol. 13, no. 11, pp. 2498–2504, 2003.

- [23] M. E. Smoot, K. Ono, J. Ruscheinski, P.-L. Wang, and T. Ideker, "Cytoscape 2.8: new features for data integration and network visualization," *Bioinformatics*, vol. 27, no. 3, pp. 431–432, 2011.
- [24] A. Chatr-Aryamontri, B. J. Breitkreutz, S. Heinicke et al., "The BioGRID interaction database: 2013 update," *Nucleic Acids Research*, vol. 41, no. 1, pp. D816–D823, 2013.
- [25] J. Gao, A. S. Ade, V. G. Tarcea et al., "Integrating and annotating the interactome using the MiMI plugin for cytoscape," *Bioinformatics*, vol. 25, no. 1, pp. 137–138, 2009.
- [26] K. Pentchev, K. Ono, R. Herwig, T. Ideker, and A. Kamburov, "Evidence mining and novelty assessment of protein-protein interactions with the consensusPathDB plugin for Cytoscape," *Bioinformatics*, vol. 26, no. 21, pp. 2796–2797, 2010.
- [27] J. Hernandez-Toro, C. Prieto, and J. De Las Rivas, "APID2NET: unified interactome graphic analyzer," *Bioinformatics*, vol. 23, no. 18, pp. 2495–2497, 2007.
- [28] A. Vailaya, P. Bluvas, R. Kincaid, A. Kuchinsky, M. Creech, and A. Adler, "An architecture for biological information extraction and representation," *Bioinformatics*, vol. 21, no. 4, pp. 430–438, 2005.
- [29] A. S. Azmi, "Network pharmacology for cancer drug discovery: are we there yet?" *Future Medicinal Chemistry*, vol. 4, no. 8, pp. 939–941, 2012.
- [30] I. Feldman, A. Rzhetsky, and D. Vitkup, "Network properties of genes harboring inherited disease mutations," *Proceedings of the National Academy of Sciences of the United States of America*, vol. 105, no. 11, pp. 4323–4328, 2008.
- [31] K.-I. Goh, M. E. Cusick, D. Valle, B. Childs, M. Vidal, and A.-L. Barabási, "The human disease network," *Proceedings of the National Academy of Sciences of the United States of America*, vol. 104, no. 21, pp. 8685–8690, 2007.
- [32] J. Z. Xu and Y. J. Li, "Discovering disease-genes by topological features in human protein-protein interaction network," *Bioinformatics*, vol. 22, no. 22, pp. 2800–2805, 2006.
- [33] T. K. B. Gandhi, J. Zhong, S. Mathivanan et al., "Analysis of the human protein interactome and comparison with yeast, worm and fly interaction datasets," *Nature Genetics*, vol. 38, no. 3, pp. 285–293, 2006.
- [34] M. M. He, A. S. Smith, J. D. Oslob et al., "Medicine: small-molecule inhibition of TNF- α ," *Science*, vol. 310, no. 5750, pp. 1022–1025, 2005.
- [35] N. J. Moerke, H. Aktas, H. Chen et al., "Small-molecule inhibition of the interaction between the translation initiation factors eIF4E and eIF4G," *Cell*, vol. 128, no. 2, pp. 257–267, 2007.
- [36] H. Y. Yu, P. M. Kim, E. Sprecher, V. Trifonov, and M. Gerstein, "The importance of bottlenecks in protein networks: correlation with gene essentiality and expression dynamics," *PLoS Computational Biology*, vol. 3, no. 4, pp. 713–720, 2007.
- [37] X. Li, X. Xu, J. Wang et al., "A system-level investigation into the mechanisms of Chinese Traditional Medicine: Compound Danshen Formula for cardiovascular disease treatment," *PLoS One*, vol. 7, no. 9, Article ID e43918, 2012.
- [38] S. Li, B. Zhang, and N. Zhang, "Network target for screening synergistic drug combinations with application to traditional Chinese medicine," *BMC Systems Biology*, vol. 5, supplement 1, article S10, 2011.
- [39] O. Odibat and C. K. Reddy, "Ranking differential hubs in gene co-expression networks," *Journal of Bioinformatics and Computational Biology*, vol. 10, no. 1, Article ID 1240002, 2012.
- [40] R. Sharan, I. Ulitsky, and R. Shamir, "Network-based prediction of protein function," *Molecular Systems Biology*, vol. 3, article 88, 2007.
- [41] M. Kotlyar, K. Fortney, and I. Jurisica, "Network-based characterization of drug-regulated genes, drug targets, and toxicity," *Methods*, vol. 57, no. 4, pp. 499–507, 2012.
- [42] S. Köhler, S. Bauer, D. Horn, and P. N. Robinson, "Walking the interactome for prioritization of candidate disease genes," *American Journal of Human Genetics*, vol. 82, no. 4, pp. 949–958, 2008.
- [43] Y. Li and J. C. Patra, "Genome-wide inferring gene-phenotype relationship by walking on the heterogeneous network," *Bioinformatics*, vol. 26, no. 9, pp. 1219–1224, 2010.
- [44] R. K. Pan, N. Chatterjee, and S. Sinha, "Mesoscopic organization reveals the constraints governing *Caenorhabditis elegans* nervous system," *PLoS ONE*, vol. 5, no. 2, Article ID e9240, 2010.
- [45] Y. Y. Wang, K. J. Xu, J. Song et al., "Exploring drug combinations in genetic interaction network," *BMC Bioinformatics*, vol. 13, supplement 7, article S7, 2012.
- [46] A. de Ruyter and C. Oostenbrink, "Protein-ligand binding from distancefield distances and hamiltonian replica exchange simulations," *Journal of Chemical Theory and Computation*, vol. 9, no. 2, pp. 883–892, 2013.
- [47] J. C. Sun and Z. M. Zhao, "A comparative study of cancer proteins in the human protein-protein interaction network," *BMC Genomics*, vol. 11, supplement 1, article S5, 2010.
- [48] M. Choura and A. Rebai, "Topological features of cancer proteins in the human NR-RTK interaction network," *Journal of Receptors and Signal Transduction*, vol. 32, no. 5, pp. 257–262, 2012.
- [49] M. L. Hartspenger, F. Blöchl, V. Stümpflen, and F. J. Theis, "Structuring heterogeneous biological information using fuzzy clustering of k-partite graphs," *BMC Bioinformatics*, vol. 11, article 522, 2010.
- [50] X. Liu, P. Lu, X. Zuo et al., "Prediction of network drug target based on improved model of bipartite graph valuation," *Zhongguo Zhongyao Zazhi*, vol. 37, no. 2, pp. 125–129, 2012.
- [51] C. C. Shen and Y. Liu, "A tripartite clustering analysis on microRNA, gene and disease model," *Journal of Bioinformatics and Computational Biology*, vol. 10, no. 1, Article ID 1240007, 2012.
- [52] L. S. Heath and A. A. Sioson, "Semantics of multimodal network models," *IEEE/ACM Transactions on Computational Biology and Bioinformatics*, vol. 6, no. 2, pp. 271–280, 2009.
- [53] X. Yao, H. Hao, Y. Li, and S. Li, "Modularity-based credible prediction of disease genes and detection of disease subtypes on the phenotype-gene heterogeneous network," *BMC Systems Biology*, vol. 5, article 79, 2011.
- [54] M. E. J. Newman, "Detecting community structure in networks," *European Physical Journal B*, vol. 38, no. 2, pp. 321–330, 2004.
- [55] H. Du, M. W. Feldman, S. Li, and X. Jin, "An algorithm for detecting community structure of social networks based on prior knowledge and modularity," *Complexity*, vol. 12, no. 3, pp. 53–60, 2007.
- [56] S. H. Zhang, X. M. Ning, and X.-S. Zhang, "Identification of functional modules in a PPI network by clique percolation clustering," *Computational Biology and Chemistry*, vol. 30, no. 6, pp. 445–451, 2006.
- [57] Y. Jiang, Z. Deng, R. Li et al., "Basic formulae of Chinese materia medica and its meaning of clinics," *Study Journal of Traditional Chinese Medicine*, vol. 19, no. 4, pp. 382–383, 2001.
- [58] M. Yang, Y. Tian, J. L. Chen et al., "Application of bron-kerbosch algorithm for discovery of basic formulas of traditional Chinese medicine," *Zhongguo Zhong Yao Za Zhi*, vol. 37, no. 21, pp. 3323–3328, 2012.

- [59] S. Li, B. Zhang, D. Jiang, Y. Wei, and N. Zhang, "Herb network construction and co-module analysis for uncovering the combination rule of traditional Chinese herbal formulae," *BMC Bioinformatics*, vol. 11, supplement 11, article S6, 2010.
- [60] S. Li, "Network systems underlying traditional Chinese medicine syndrome and herb formula," *Current Bioinformatics*, vol. 4, no. 3, pp. 188–196, 2009.
- [61] C.-C. Tu and H. J. Cheng, "Spectral methods for graph bisection problems," *Computers and Operations Research*, vol. 25, no. 7-8, pp. 519–530, 1998.
- [62] J. Larsson Träff, "Direct graph k-partitioning with a Kernighan-Lin like heuristic," *Operations Research Letters*, vol. 34, no. 6, pp. 621–629, 2006.
- [63] B. Balasundaram, S. S. Chandramouli, and S. Trukhanov, "Approximation algorithms for finding and partitioning unit-disk graphs into co-k-plexes," *Optimization Letters*, vol. 4, no. 3, pp. 311–320, 2010.
- [64] V. Batagelj and M. Zaveršnik, "Fast algorithms for determining (generalized) core groups in social networks," *Advances in Data Analysis and Classification*, vol. 5, no. 2, pp. 129–145, 2011.
- [65] X. H. Shi, L. LuoLiang, Y. Wan, and J. Xu, "A finding maximal clique algorithm for predicting loop of protein structure," *Applied Mathematics and Computation*, vol. 180, no. 2, pp. 676–682, 2006.
- [66] E. J. Gardiner, P. J. Artymiuk, and P. Willett, "Clique-detection algorithms for matching three-dimensional molecular structures," *Journal of Molecular Graphics and Modelling*, vol. 15, no. 4, pp. 245–253, 1997.
- [67] P. J. Artymiuk, R. V. Spriggs, and P. Willett, "Graph theoretic methods for the analysis of structural relationships in biological macromolecules," *Journal of the American Society for Information Science and Technology*, vol. 56, no. 5, pp. 518–528, 2005.
- [68] F. Kose, W. Weckwerth, T. Linke, and O. Fiehn, "Visualizing plant metabolomic correlation networks using clique-metabolite matrices," *Bioinformatics*, vol. 17, no. 12, pp. 1198–1208, 2001.
- [69] C. Bron and J. Kerbosch, "Algorithm 457: finding all cliques of an undirected graph," *Communications of the ACM*, vol. 16, no. 9, pp. 575–577, 1973.
- [70] D. X. He, J. Liu, B. Yang et al., "An ant-based algorithm with local optimization for community detection in large-scale networks," *Advances in Complex Systems*, vol. 15, no. 8, 2012.
- [71] R. Chandrasekharam, S. Subhranian, and S. Chaudhury, "Genetic algorithm for node partitioning problem and applications in VLSI design," *IEE Proceedings E*, vol. 140, no. 5, pp. 255–260, 1993.
- [72] D. Y. Liu, D. Jin, C. Baquero et al., "Genetic algorithm with a local search strategy for discovering communities in complex networks," *International Journal of Computational Intelligence Systems*, vol. 6, no. 2, pp. 354–369, 2013.
- [73] J. Hou, G.-F. Yan, and Z. Fan, "Memoryless cooperative graph search based on the simulated annealing algorithm," *Chinese Physics B*, vol. 20, no. 4, Article ID 048103, 2011.
- [74] Y. W. Jiang, C. Y. Jia, and J. Yu, "An efficient community detection method based on rank centrality," *Physica A*, vol. 392, no. 9, pp. 2182–2194, 2013.
- [75] J. K. Ochab, "Maximal-entropy random walk unifies centrality measures," *Physical Review E*, vol. 86, no. 6, 2012.
- [76] Q. Shi, H. Zhao, J. Chen et al., "Study on TCM syndrome identification modes of coronary heart disease based on data mining," *Evidence-Based Complementary and Alternative Medicine*, vol. 2012, Article ID 697028, 11 pages, 2012.
- [77] Q. Z. Yan, H. W. Dan, F. T. Shu et al., "A systems biology-based investigation into the pharmacological mechanisms of Wu Tou Tang acting on rheumatoid arthritis by integrating network analysis," *Evidence-Based Complementary and Alternative Medicine*, vol. 2013, Article ID 548498, 12 pages, 2013.
- [78] Y. Ming, J. Lijing, C. Peiqi et al., "Complex systems entropy network and its application in data mining for Chinese medicine tumor clinics," *World Science and Technology*, vol. 14, no. 2, pp. 1376–1384, 2012.
- [79] L. Ye, Y. He, H. Ye et al., "Pathway-pathway network-based study of the therapeutic mechanisms by which salvianolic acid B regulates cardiovascular diseases," *Chinese Science Bulletin*, vol. 57, no. 14, pp. 1672–1679, 2012.
- [80] G. Chen, C. Lu, Q. Zha et al., "A network-based analysis of traditional Chinese medicine cold and hot patterns in rheumatoid arthritis," *Complementary Therapies in Medicine*, vol. 20, no. 1-2, pp. 23–30, 2012.
- [81] Z. He, J. Zhang, X.-H. Shi et al., "Predicting drug-target interaction networks based on functional groups and biological features," *PLoS ONE*, vol. 5, no. 3, Article ID e9603, 2010.
- [82] H. Yu, J. X. Chen, X. Xu et al., "A systematic prediction of multiple drug-target interactions from chemical, genomic, and pharmacological data," *PLoS One*, vol. 7, no. 5, Article ID e37608, 2012.
- [83] B. Li, X. Xu, X. Wang et al., "A systems biology approach to understanding the mechanisms of action of chinese herbs for treatment of cardiovascular disease," *International Journal of Molecular Sciences*, vol. 13, no. 10, pp. 13501–13520, 2012.
- [84] F. Cheng, Y. Zhou, J. Li et al., "Prediction of chemical-protein interactions: multitarget-QSAR versus computational chemogenomic methods," *Molecular BioSystems*, vol. 8, no. 9, pp. 2373–2384, 2012.
- [85] B. A. Krueger, T. Weil, and G. Schneider, "Comparative virtual screening and novelty detection for NMDA-GlycineB antagonists," *Journal of Computer-Aided Molecular Design*, vol. 23, no. 12, pp. 869–881, 2009.
- [86] Y. H. Wang, Y. Li, J. Ding, Y. Wang, and Y. Chang, "Prediction of binding affinity for estrogen receptor α modulators using statistical learning approaches," *Molecular Diversity*, vol. 12, no. 2, pp. 93–102, 2008.
- [87] F. Nigsch, A. Bender, J. L. Jenkins, and J. B. O. Mitchell, "Ligand-target prediction using winnow and naive bayesian algorithms and the implications of overall performance statistics," *Journal of Chemical Information and Modeling*, vol. 48, no. 12, pp. 2313–2325, 2008.
- [88] G. Bouvier, N. Evrard-Todeschi, J.-P. Girault, and G. Bertho, "Automatic clustering of docking poses in virtual screening process using self-organizing map," *Bioinformatics*, vol. 26, no. 1, pp. 53–60, 2010.
- [89] G. Schneider, Y. Tanrikulu, and P. Schneider, "Self-organizing molecular fingerprints: a ligand-based view on drug-like chemical space and off-target prediction," *Future Medicinal Chemistry*, vol. 1, no. 1, pp. 213–218, 2009.
- [90] A. E. Cleves and A. N. Jain, "Robust ligand-based modeling of the biological targets of known drugs," *Journal of Medicinal Chemistry*, vol. 49, no. 10, pp. 2921–2938, 2006.
- [91] S. Zhao and S. Li, "Network-based relating pharmacological and genomic spaces for drug target identification," *PLoS ONE*, vol. 5, no. 7, Article ID e11764, 2010.
- [92] N. M. Penrod, R. Cowper-Sal-Lari, and J. H. Moore, "Systems genetics for drug target discovery," *Trends in Pharmacological Sciences*, vol. 32, no. 10, pp. 623–630, 2011.

- [93] F. Cheng, Y. Zhou, W. Li et al., "Prediction of chemical-protein interactions network with weighted network-based inference method," *PLoS One*, vol. 7, no. 7, Article ID e41064, 2012.
- [94] F. X. Cheng, C. Liu, J. Jiang et al., "Prediction of drug-target interactions and drug repositioning via network-based inference," *PLOS Computational Biology*, vol. 8, no. 5, Article ID e1002503, 2012.
- [95] A. Zanzoni, M. Soler-López, and P. Aloy, "A network medicine approach to human disease," *FEBS Letters*, vol. 583, no. 11, pp. 1759–1765, 2009.
- [96] L. Li, H. M. Chen, C. Liu et al., "A robust hybrid approach based on estimation of distribution algorithm and support vector machine for hunting candidate disease genes," *The Scientific World Journal*, vol. 2013, Article ID 393570, 7 pages, 2013.
- [97] Y. N. Zhu, W. Pan, and X. T. Shen, "Support vector machines with disease-gene-centric network penalty for high dimensional microarray data," *Statistics and Its Interface*, vol. 2, no. 3, pp. 257–269, 2009.
- [98] M. C. Denham and J. C. Whittaker, "A Bayesian approach to disease gene location using allelic association," *Biostatistics*, vol. 4, no. 3, pp. 399–409, 2003.
- [99] L. Zhang, B. Mukherjee, M. Ghosh, and R. Wu, "Bayesian modeling for genetic association in case-control studies: accounting for unknown population substructure," *Statistical Modelling*, vol. 6, no. 4, pp. 352–372, 2006.
- [100] S. Podder and T. C. Ghosh, "Evolutionary dynamics of human autoimmune disease genes and malfunctioned immunological genes," *BMC Evolutionary Biology*, vol. 12, article 10, 2012.
- [101] X. Wu, R. Jiang, M. Q. Zhang et al., "Network-based global inference of human disease genes," *Molecular Systems Biology*, vol. 4, article 189, 2008.
- [102] S. Li, L. Wu, and Z. Zhang, "Constructing biological networks through combined literature mining and microarray analysis: a LMMA approach," *Bioinformatics*, vol. 22, no. 17, pp. 2143–2150, 2006.
- [103] H. Zhang, X. Song, H. Wang, and X. Zhang, "MIClique: an algorithm to identify differentially coexpressed disease gene subset from microarray data," *Journal of Biomedicine and Biotechnology*, vol. 2009, Article ID 642524, 9 pages, 2009.
- [104] A. Bhattacharjee and H. M. Jamil, "WSM: a novel algorithm for subgraph matching in large weighted graphs," *Journal of Intelligent Information Systems*, vol. 38, no. 3, pp. 767–784, 2012.
- [105] P. G. Sun, L. Gao, and S. Han, "Prediction of human disease-related gene clusters by clustering analysis," *International Journal of Biological Sciences*, vol. 7, no. 1, pp. 61–73, 2011.
- [106] J. Achenbach, P. Tiikkainen, L. Franke, and E. Proschak, "Computational tools for polypharmacology and repurposing," *Future Medicinal Chemistry*, vol. 3, no. 8, pp. 961–968, 2011.
- [107] W. P. McCormick, N. I. Lyons, and K. Hutcheson, "Distributional properties of Jaccard index of similarity," *Communications in Statistics-Theory and Methods*, vol. 21, no. 1, pp. 51–68, 1992.
- [108] T. Tanimoto, "IBM internal report," Tech. Rep., 1957.
- [109] J. W. Godden, L. Xue, and J. Bajorath, "Combinatorial preferences affect molecular similarity/diversity calculations using binary fingerprints and Tanimoto coefficients," *Journal of Chemical Information and Computer Sciences*, vol. 40, no. 1, pp. 163–166, 2000.
- [110] Z. X. Meng, D. Z. Shou, Q. C. Chao et al., "Predicting the drug safety for traditional Chinese medicine through a comparative analysis of withdrawn drugs using pharmacological network," *Evidence-Based Complementary and Alternative Medicine*, vol. 2013, Article ID 256782, 11 pages, 2013.
- [111] W. Tao, X. Xu, X. Wang et al., "Network pharmacology-based prediction of the active ingredients and potential targets of Chinese herbal Radix Curcumae formula for application to cardiovascular disease," *Journal of Ethnopharmacology*, vol. 145, no. 1, pp. 1–10, 2013.
- [112] "Jaccard index," 2013, http://en.wikipedia.org/wiki/Jaccard_index.
- [113] H.-Z. Ye, C.-S. Zheng, X.-J. Xu, M.-X. Wu, and X.-X. Liu, "Potential synergistic and multitarget effect of herbal pair Chuanxiong Rhizome-Paeonia Albifora Pall on osteoarthritis disease: a computational pharmacology approach," *Chinese Journal of Integrative Medicine*, vol. 17, no. 9, pp. 698–703, 2011.
- [114] C.-S. Liao, K. Lu, M. Baym, R. Singh, and B. Berger, "IsoRankN: spectral methods for global alignment of multiple protein networks," *Bioinformatics*, vol. 25, no. 12, pp. i253–i258, 2009.
- [115] Z. Kutalik, J. S. Beckmann, and S. Bergmann, "A modular approach for integrative analysis of large-scale gene-expression and drug-response data," *Nature Biotechnology*, vol. 26, no. 5, pp. 531–539, 2008.
- [116] S. Zhao and S. Li, "A co-module approach for elucidating drug-disease associations and revealing their molecular basis," *Bioinformatics*, vol. 28, no. 7, pp. 955–961, 2012.
- [117] J. Li, C. Lu, M. Jiang et al., "Traditional chinese medicine-based network pharmacology could lead to new multicomponent drug discovery," *Evidence-Based Complementary and Alternative Medicine*, vol. 2012, Article ID 149762, 11 pages, 2012.
- [118] S. Bergmann, J. Ihmels, and N. Barkai, "Iterative signature algorithm for the analysis of large-scale gene expression data," *Physical Review E*, vol. 67, no. 3, 18 pages, 2003.
- [119] J. Zhao, P. Yang, F. Li et al., "Therapeutic effects of astragaloside IV on myocardial injuries: multi-target identification and network analysis," *PLoS One*, vol. 7, no. 9, Article ID e44938, 2012.
- [120] X. Wang, X. Xu, W. Y. Tao et al., "A systems biology approach to uncovering pharmacological synergy in herbal medicines with applications to cardiovascular disease," *Evidence-Based Complementary and Alternative Medicine*, vol. 2012, Article ID 519031, 15 pages, 2012.
- [121] C. Bohler, H. Radner, M. Ernst et al., "Rheumatoid arthritis and falls: the influence of disease activity," *Rheumatology*, vol. 51, no. 11, pp. 2051–2057, 2012.
- [122] J. Liu and R.-L. Liu, "The potential role of Chinese medicine in ameliorating extra-articular manifestations of rheumatoid arthritis," *Chinese Journal of Integrative Medicine*, vol. 17, no. 10, pp. 735–737, 2011.
- [123] M. Jiang, C. Lu, G. Chen et al., "Understanding the molecular mechanism of interventions in treating rheumatoid arthritis patients with corresponding traditional chinese medicine patterns based on bioinformatics approach," *Evidence-Based Complementary and Alternative Medicine*, vol. 2012, Article ID 129452, 11 pages, 2012.
- [124] B. Zhang, X. Wang, and S. Li, "An integrative platform of TCM network pharmacology and its application on a herbal formula, Qing-Luo-Yin," *Evidence-Based Complementary and Alternative Medicine*, vol. 2013, Article ID 456747, 12 pages, 2013.
- [125] D.-X. Kong, X.-J. Li, and H.-Y. Zhang, "Where is the hope for drug discovery? Let history tell the future," *Drug Discovery Today*, vol. 14, no. 3-4, pp. 115–119, 2009.
- [126] X. Xu, W. X. Zhang, C. Huang et al., "A novel chemometric method for the prediction of human oral bioavailability," *International Journal of Molecular Sciences*, vol. 13, no. 6, pp. 6964–6982, 2012.

- [127] S. Li, Z. Q. Zhang, L. J. Wu, X. G. Zhang, Y. D. Li, and Y. Y. Wang, "Understanding ZHENG in traditional Chinese medicine in the context of neuro-endocrine-immune network," *IET Systems Biology*, vol. 1, no. 1, pp. 51–60, 2007.
- [128] T. Ma, C. Tan, H. Zhang, M. Wang, W. Ding, and S. Li, "Bridging the gap between traditional Chinese medicine and systems biology: the connection of Cold Syndrome and NEI network," *Molecular BioSystems*, vol. 6, no. 4, pp. 613–619, 2010.
- [129] R. Li, T. Ma, J. Gu, X. Liang, and S. Li, "Imbalanced network biomarkers for traditional Chinese medicine Syndrome in gastritis patients," *Scientific Reports*, vol. 3, article 1543, 2013.
- [130] B. Jiang, X. J. Liang, Y. Chen et al., "Integrating next-generation sequencing and traditional tongue diagnosis to determine tongue coating microbiome," *Scientific Reports*, vol. 2, article 936, 2012.
- [131] C. Lu, X. Niu, C. Xiao et al., "Network-based gene expression biomarkers for cold and heat patterns of rheumatoid arthritis in traditional chinese medicine," *Evidence-Based Complementary and Alternative Medicine*, vol. 2012, Article ID 203043, 17 pages, 2012.
- [132] B. Zhang, L. Liu, S. Zhao et al., "Vitexicarpin acts as a novel angiogenesis inhibitor and its target network," *Evidence-Based Complementary and Alternative Medicine*, vol. 2013, Article ID 278405, 13 pages, 2013.
- [133] A. Zhang, H. Sun, B. Yang, and X. Wang, "Predicting new molecular targets for rhein using network pharmacology," *BMC Systems Biology*, vol. 6, article 20, 2012.
- [134] J. Gu, H. Zhang, L. Chen, S. Xu, G. Yuan, and X. Xu, "Drug-target network and polypharmacology studies of a Traditional Chinese Medicine for type II diabetes mellitus," *Computational Biology and Chemistry*, vol. 35, no. 5, pp. 293–297, 2011.
- [135] X. Haiyu, T. Ye, L. Peng et al., "A computational drug-target network for Yuanhu Zhitong prescription," *Evidence-Based Complementary and Alternative Medicine*, vol. 2013, Article ID 658531, 15 pages, 2013.
- [136] Y. Ming, T. Yu, C. JiaLei et al., "Application of complex systems entropy network for discovering traditional herb-pairs in traditional Chinese medicine prescriptions," *Pharmaceutical Care and Research*, vol. 13, no. 2, pp. 89–92, 2013.
- [137] S. Z. Run, Z. Z. Xue, L. Y. Nai et al., "Study on compounding rules of Chinese herb prescriptions for treating syndrome of liver and spleen disharmony by scale-free network," *World Science and Technology*, vol. 12, no. 6, pp. 882–887, 2010.
- [138] L. Jie, S. L. Hong, H. Wei et al., "Primary study of characteristics of lung cancer TCM treatment by data ming," *World Science and Technology*, vol. 11, no. 5, pp. 753–757, 2009.
- [139] K. R. Brown and I. Jurisica, "Online predicted human interaction database," *Bioinformatics*, vol. 21, no. 9, pp. 2076–2082, 2005.
- [140] A. Franceschini, D. Szklarczyk, S. Frankild et al., "STRING v9.1: protein-protein interaction networks, with increased coverage and integration," *Nucleic Acids Research*, vol. 41, no. 1, pp. D808–D815, 2013.
- [141] Z. T. Gao, H. L. Li, H. L. Zhang et al., "PDTD: a web-accessible protein database for drug target identification," *BMC Bioinformatics*, vol. 9, article 104, 2008.
- [142] W. M. Chan and U. Consortium, "The UniProt Knowledgebase (UniProtKB): a freely accessible, comprehensive and expertly curated protein sequence database," *Genetics Research*, vol. 92, no. 1, pp. 78–79, 2010.
- [143] M. Whirl-Carrillo, E. M. McDonagh, J. M. Hebert et al., "Pharmacogenomics knowledge for personalized medicine," *Clinical Pharmacology & Therapeutics*, vol. 92, no. 4, pp. 414–417, 2012.
- [144] I. Xenarios, Ł. Salwinski, X. J. Duan, P. Higney, S.-M. Kim, and D. Eisenberg, "DIP, the database of interacting proteins: a research tool for studying cellular networks of protein interactions," *Nucleic Acids Research*, vol. 30, no. 1, pp. 303–305, 2002.
- [145] H. Huang, X. G. Wu, R. Pandey et al., "C²Maps: a network pharmacology database with comprehensive disease-gene-drug connectivity relationships," *BMC Genomics*, vol. 13, article S17, 2012.
- [146] S. Schuierer, L.-C. Tranchevent, U. Dengler, and Y. Moreau, "Large-scale benchmark of endeavour using MetaCore maps," *Bioinformatics*, vol. 26, no. 15, pp. 1922–1923, 2010.
- [147] S. Ekins, A. Bugrim, L. Brovold et al., "Algorithms for network analysis in systems-ADME/Tox using the MetaCore and MetaDrug platforms," *Xenobiotica*, vol. 36, no. 10-11, pp. 877–901, 2006.
- [148] D. Nishimura, "BioCarta," *Biotech Software & Internet Report*, vol. 2, no. 3, pp. 117–120, 2001.
- [149] D. Fazekas, M. Koltai, D. Turei et al., "SignaLink 2—a signaling pathway resource with multi-layered regulatory networks," *BMC Systems Biology*, vol. 7, article 7, 2013.
- [150] I. Vastrik, P. D'Eustachio, E. Schmidt et al., "Reactome: a knowledge base of biologic pathways and processes," *Genome Biology*, vol. 8, no. 3, article R39, 2007.
- [151] K. Kandasamy, S. Sujatha Mohan, R. Raju et al., "NetPath: a public resource of curated signal transduction pathways," *Genome Biology*, vol. 11, no. 1, article r3, 2010.
- [152] S. A. Forbes, N. Bindal, S. Bamford et al., "COSMIC: mining complete cancer genomes in the catalogue of somatic mutations in cancer," *Nucleic Acids Research*, vol. 39, no. 1, pp. D945–D950, 2011.
- [153] P. N. Robinson, S. Köhler, S. Bauer, D. Seelow, D. Horn, and S. Mundlos, "The human phenotype ontology: a tool for annotating and analyzing human hereditary disease," *American Journal of Human Genetics*, vol. 83, no. 5, pp. 610–615, 2008.
- [154] M. Kuhn, D. Szklarczyk, A. Franceschini et al., "STITCH 3: zooming in on protein-chemical interactions," *Nucleic Acids Research*, vol. 40, no. 1, pp. D876–D880, 2012.
- [155] J. Masciocchi, G. Frau, M. Fanton et al., "MMsINC: a large-scale chemoinformatics database," *Nucleic Acids Research*, vol. 37, no. 1, pp. D284–D290, 2009.
- [156] "ChemicalBook," 2008, <http://www.chemicalbook.com/>.
- [157] S. K. Kjaerulff, L. Wich, J. Kringelum et al., "ChemProt-2.0: visual navigation in a disease chemical biology database," *Nucleic Acids Research*, vol. 41, no. 1, pp. D464–D469, 2013.
- [158] "LookChem," 2008, <http://www.lookchem.com/>.
- [159] H. E. Pence and A. Williams, "Chemspider: an online chemical information resource," *Journal of Chemical Education*, vol. 87, no. 11, pp. 1123–1124, 2010.
- [160] H. Ye, L. Ye, H. Kang et al., "HIT: linking herbal active ingredients to targets," *Nucleic Acids Research*, vol. 39, no. 1, pp. D1055–D1059, 2011.
- [161] X. Fang, L. Shao, H. Zhang, and S. Wang, "CHMIS-C: a comprehensive herbal medicine information system for cancer," *Journal of Medicinal Chemistry*, vol. 48, no. 5, pp. 1481–1488, 2005.
- [162] C. Y.-C. Chen, "TCM Database@Taiwan: the world's largest traditional Chinese medicine database for drug screening In Silico," *PLoS ONE*, vol. 6, no. 1, Article ID e15939, 2011.

- [163] Y.-C. Fang, H.-C. Huang, H.-H. Chen, and H.-F. Juan, "TCMGeneDIT: a database for associated traditional Chinese medicine, gene and disease information using text mining," *BMC Complementary and Alternative Medicine*, vol. 8, article 58, 2008.
- [164] Traditional Chinese Medicine Information Database, 2005, http://tcm.cz3.nus.edu.sg/group/tcm-id/tcmid_ns.asp.
- [165] Lab of Systems Pharmacology for Chinese Traditional Medicine, "TcmSP: Traditional Chinese Medicine Systems Pharmacology Database and Analysis Platform," 2012, http://tcmispnw.com/login_clearSession.
- [166] "Shanghai R&D Public Service Platform," 2013.
- [167] V. Batagelj and A. Mrvar, "Pajek—analysis and visualization of large networks," *Graph Drawing*, vol. 2265, pp. 477–478, 2002.
- [168] L. A. J. Mueller, K. G. Kugler, A. Graber, F. Emmert-Streib, and M. Dehmer, "Structural measures for network biology using QuACN," *BMC Bioinformatics*, vol. 12, no. 1, article 492, 2011.
- [169] L. A. J. Mueller, K. G. Kugler, A. Dander, A. Graber, and M. Dehmer, "QuACN: an R package for analyzing complex biological networks quantitatively," *Bioinformatics*, vol. 27, no. 1, pp. 140–141, 2011.
- [170] M. Li, J.-E. Chen, J.-X. Wang, B. Hu, and G. Chen, "Modifying the DPPlus algorithm for identifying protein complexes based on new topological structures," *BMC Bioinformatics*, vol. 9, article 398, 2008.
- [171] J. Gu, Y. Chen, S. Li, and Y. Li, "Identification of responsive gene modules by network-based gene clustering and extending: application to inflammation and angiogenesis," *BMC Systems Biology*, vol. 4, article 47, 2010.
- [172] T. H. Hwang, W. Zhang, M. Q. Xie, J. Liu, and R. Kuang, "Inferring disease and gene set associations with rank coherence in networks," *Bioinformatics*, vol. 27, no. 19, pp. 2692–2699, 2011.
- [173] Y. J. Ding, M. J. Chen, Z. C. Liu et al., "atBioNet—an integrated network analysis tool for genomics and biomarker discovery," *BMC Genomics*, vol. 13, article 325, 2012.
- [174] M. Zhang and L. J. Lu, "Investigating the validity of current network analysis on static conglomerate networks by protein network stratification," *BMC Bioinformatics*, vol. 11, article 466, 2010.
- [175] L.-C. Huang, X. Wu, and J. Y. Chen, "Predicting adverse side effects of drugs," *BMC Genomics*, vol. 12, supplement 5, article S11, 2011.
- [176] T. van Laarhoven, S. B. Nabuurs, and E. Marchiori, "Gaussian interaction profile kernels for predicting drug-target interaction," *Bioinformatics*, vol. 27, no. 21, pp. 3036–3043, 2011.
- [177] A. Bureau, J. Dupuis, K. Falls et al., "Identifying SNPs predictive of phenotype using random forests," *Genetic Epidemiology*, vol. 28, no. 2, pp. 171–182, 2005.
- [178] H. Strömbergsson and G. J. Kleywegt, "A chemogenomics view on protein-ligand spaces," *BMC Bioinformatics*, vol. 10, supplement 6, article S13, 2009.
- [179] J. Zhao, P. Jiang, and W. Zhang, "Molecular networks for the study of TCM pharmacology," *Briefings in Bioinformatics*, vol. 11, no. 4, pp. 417–430, 2010.
- [180] X. Li, L. Wu, X. Fan et al., "Network pharmacology study on major active compounds of Fufang Danshen formula," *Zhongguo Zhongyao Zazhi*, vol. 36, no. 21, pp. 2911–2915, 2011.
- [181] F. H. Ming, L. Z. Yan, Z. R. Zhen et al., "Study on mechanism of blood-activating and stasis-dissolving Herbs on Coronary heart disease in molecular level by network pharmacology," *World Science and Technology*, vol. 14, no. 5, pp. 1969–1975, 2012.
- [182] F. Z. Yan, W. X. Zhi, Q. A. Hai et al., "Pharmacodynamic research of spleen-regulating and heart-nourishing formula based on network features," *Traditional Chinese Drug & Research Clinical Pharmacology*, vol. 23, no. 1, pp. 25–29, 2012.
- [183] X. L. Xian, "Network pharmacology-based prediction of the multi-target capabilities of the compounds in Taohong Siwu decoction, and their application in osteoarthritis," *Experimental and Therapeutic Medicine*, pp. 125–132, 2013.
- [184] Y. Sun, R. Zhu, H. Ye et al., "Towards a bioinformatics analysis of anti-Alzheimer's herbal medicines from a target network perspective," *Brief Bioinform*, vol. 14, no. 3, pp. 327–343, 2013.
- [185] S. T. Ma, C. T. Feng, X. L. Zhang et al., "The multi-target capabilities of the compounds in a TCM used to treat sepsis and their in silico pharmacology," *Complementary Therapies in Medicine*, vol. 21, no. 1, pp. 35–41, 2013.
- [186] E. Chan, M. Tan, J. Xin, S. Sudarsanam, and D. E. Johnson, "Interactions between traditional Chinese medicines and Western therapeutics," *Current Opinion in Drug Discovery & Development*, vol. 13, no. 1, pp. 50–65, 2010.
- [187] Q.-X. Yue, Z.-W. Cao, S.-H. Guan et al., "Proteomics characterization of the cytotoxicity mechanism of ganoderic acid D and computer-automated estimation of the possible drug target network," *Molecular and Cellular Proteomics*, vol. 7, no. 5, pp. 949–961, 2008.
- [188] X. Wang, X. Xu, Y. Li et al., "Systems pharmacology uncovers Janus functions of botanical drugs: activation of host defense system and inhibition of influenza virus replication," *Integrative Biology*, vol. 5, no. 2, pp. 351–371, 2013.
- [189] W. Dai, J. X. Chen, P. Lu et al., "Pathway Pattern-based prediction of active drug components and gene targets from H1N1 influenza's treatment with maxingshigan-yinqiaosan formula," *Molecular BioSystems*, vol. 9, no. 3, pp. 375–385, 2013.
- [190] H. Sun, A. H. Zhang, G. L. Yan et al., "Proteomics study on the hepatoprotective effects of traditional Chinese medicine formulae Yin-Chen-Hao-Tang by a combination of two-dimensional polyacrylamide gel electrophoresis and matrix-assisted laser desorption/ionization-time of flight mass spectrometry," *Journal of Pharmaceutical and Biomedical Analysis*, vol. 75, pp. 173–179, 2013.
- [191] X. Wei, C. Liang, F. Qiru et al., "Action mechanism studies of GuizhiFuling Capsule: based on a bio-network analysis," *Computers and Applied Chemistry*, vol. 29, no. 12, pp. 1455–1459, 2012.
- [192] H. Yang, L. Xing, M.-G. Zhou et al., "Network pharmacological research of volatile oil from Zhike Chuanbei Pipa Dropping Pills in treatment of airway inflammation," *Chinese Traditional and Herbal Drugs*, vol. 43, no. 6, pp. 1129–1135, 2012.
- [193] W. Zhu, X. H. Qiu, X. J. Xu, and C. Lu, "Computational network pharmacological research of Chinese medicinal plants for chronic kidney disease," *Science China Chemistry*, vol. 53, no. 11, pp. 2337–2342, 2010.

Research Article

The Phytochemical Shikonin Stimulates Epithelial-Mesenchymal Transition (EMT) in Skin Wound Healing

Shu-Yi Yin, An-Ping Peng, Li-Ting Huang, Ya-Ting Wang,
Chun-Wen Lan, and Ning-Sun Yang

Agricultural Biotechnology Research Center, Academia Sinica, 128 Academia Road, Section 2, Nankang, Taipei 115, Taiwan

Correspondence should be addressed to Ning-Sun Yang; nsyang@gate.sinica.edu.tw

Received 28 November 2012; Accepted 8 May 2013

Academic Editor: Taiping Fan

Copyright © 2013 Shu-Yi Yin et al. This is an open access article distributed under the Creative Commons Attribution License, which permits unrestricted use, distribution, and reproduction in any medium, provided the original work is properly cited.

Although various pharmacological activities of the shikonins have been documented, understanding the hierarchical regulation of these diverse bioactivities at the genome level is unsubstantiated. In this study, through cross examination between transcriptome and microRNA array analyses, we predicted that topical treatment of shikonin *in vivo* affects epithelial-mesenchymal transition (EMT) and the expression of related microRNAs, including 200a, 200b, 200c, 141, 205, and 429 microRNAs, in mouse skin tissues. *In situ* immunohistological analyses further demonstrated that specific EMT regulatory molecules are enhanced in shikonin-treated epidermal tissues. RT-PCR analyses subsequently confirmed that shikonin treatment downregulated expression of microRNA-205 and other members of the 200 family microRNAs. Further, expression of two RNA targets of the 200 family microRNAs in EMT regulation, Sip1 (Zeb2) and Tcf8 (Zeb1), was consistently upregulated by shikonin treatment. Enhancement of these EMT activities was also detected in shikonin-treated wounds, which repaired faster than controls. These results suggest that topical treatment with shikonin can confer a potent stimulatory effect on EMT and suppress the expression of the associated microRNAs in skin wound healing. Collectively, these cellular and molecular data provide further evidence in support of our previous findings on the specific pharmacological effects of shikonin in wound healing and immune modulation.

1. Introduction

Shikonin, a phytochemical derived from *Lithospermum erythrorhizon* (LE), has been shown to exhibit various biological and pharmacological activities [1, 2], including antioxidant [3], wound-healing [2, 4, 5], anti-inflammatory [4, 6, 7], and antitumor properties [8, 9]. Clinically, the use of shikonin dates back to the 5th century A.D. when it was used by Chinese herbalists for the treatment of burns, urticaria, and other allergic diseases [10]. Subsequently, it has been shown that the wound-healing activity of shikonin may result from its effect on the proliferation of fibroblasts, collagen fiber levels of the granuloma tissue [11], and proliferation of CD11b⁺ cells in such tissues [12]. Our group previously demonstrated that shikonin can confer a strong suppressive effect on gene expression of TNF- α at the promoter level in skin tissue [6] and a strong modulatory effect on specific mRNA splicing in human monocytes [7]. These findings suggest that the various pharmacological properties of shikonin may be due

to a multifunctional and hierarchical effect on a spectrum of signaling genes at the genome and cellular levels.

In normal somatic tissues, epithelial-mesenchymal transition (EMT) is not only instrumental in wound healing but also in tissue fibrosis [13–15]. Downregulation of E-cadherin is one of the hallmarks of EMT and can lead to a concomitant increase in expression of specific mesenchymal cell markers (e.g., vimentin and fibroblast specific protein 1) as well as extracellular matrix-remodeling enzymes (i.e., matrix metalloproteinases) that are often observed together with a profound reorganization of the actin cytoskeleton [16, 17]. Previous studies have also shown that specific microRNAs in the microRNA 200 family are involved in the control of EMT activity in human epithelial cells, via repression of the translation of specific regulatory proteins, such as E-cadherin transcriptional repressors ZEB1 and ZEB2 (also known as Smad-interacting protein-1, SIP1) [18, 19]. Notably, we previously demonstrated that shikonin can effectively enhance the wound-healing process in severely damaged

porcine skin tissues [20]. These observations and results together raised the hypothesis that topical treatment with shikonin may hierarchically modulate and facilitate the EMT process in skin tissues.

Profiling global gene expression patterns by DNA microarray analysis provides a useful approach for investigating complex biological phenomena [21], as we have previously shown for immune cell systems [22–24]. In addition, microRNAs, which are small ribonucleotides (~22 nt in length), act as key players in cellular differentiation and tissue development [25–28]. Characterization of the complex relationship between microRNAs and target mRNAs in shikonin-treated skin may thus assist in determining the molecular pathways and cell signaling processes involved in the process.

In this study we investigated the multifaceted effect of shikonin on mouse skin tissue *in vivo* at the transcriptome and the microRNA regulatory levels with an eye to future translational studies. We took advantage of the vast amounts of information obtained from decades of studies on shikonin-treated mammalian tissues [3, 4, 6–9, 11, 12, 20] and employed a network knowledge-based approach to analyze the genome-wide transcriptome activity *in vivo* for possible correlation with specific microRNA expression activities. We found that expressions of various EMT process-related microRNAs, such as microRNA-200a, -200b, -200c, -429, -141, and -205 were suppressed in skin after shikonin treatment. Consistent with these findings, histological results showed that shikonin induced EMT consistent cellular and tissue behavior in the epidermal layer during the process of wound healing. These findings provide cellular and molecular evidence supporting previous studies on the wound-healing [6, 20] and immunomodulatory activities of shikonins [6, 7] and have generated a new integrated strategy for investigating the mode of action of shikonins and other potent phytomedicines.

2. Materials and Methods

2.1. Mice. Female C57BL/6JNarl mice (National Laboratory Animal Breeding and Research Center, Taipei, Taiwan) were maintained under pathogen-free conditions on standard laboratory chow and water in the animal facilities of the Agricultural Biotechnology Research Center, Academia Sinica. All mice used in the experiments were 6–8 weeks old.

2.2. Treatment of Mouse Skin with Shikonin. Solutions containing 10 $\mu\text{g}/\mu\text{L}$ shikonin (*Nacalai Tesque*, Kyoto, Japan) or 100 μM phorbol 12-myristate 13-acetate (*TPA*; *Sigma*, St. Louis) in acetone were prepared immediately before use. Aliquots of 100 μL of the test chemicals were pipetted onto the abdominal skin area of mice, immediately spread evenly, and allowed to air dry completely. Test skin treated with solvent (acetone) alone was used as a negative control. For each treatment, the test area was marked with an ink stamp encircling a surface area of 2.3 cm in diameter (i.e., 4.15 cm²). Animals were sacrificed at 4 or 24 hours after treatment, and treated or untreated skin samples were excised and frozen in liquid nitrogen for further RNA or protein expression analyses. For wound-healing experiments, 20 μL shikonin solution

or control solvent (acetone) was pipetted 3–4 mm beyond the margins of the wound (~40 mm²) on days 0, 2, and 4. The concentration of shikonin for topical application was 5 $\mu\text{g}/\mu\text{L}$ (100 $\mu\text{g}/\text{wound}$), which was selected based on our preliminary wound-healing experiment (data not shown).

2.3. Microarray and MicroRNA Array Analyses. For total RNA extraction, frozen skin samples were homogenized in liquid nitrogen. Subsequently, total RNA was extracted using TRIzol reagent (Invitrogen) according to the manufacturer's instructions and resuspended in 30 μL of diethyl pyrocarbonate-treated (DEPC) water. A total of 8 hybridizations were performed for acetone-treated and shikonin-treated skin samples, and each test time point and treatment was analyzed in duplicate samples on separate chips. Standard Pearson correlation coefficients were used to determine the consistency of gene expression in each replicate array as previously described [24]. For microarray analysis, fluorescent aRNA (antisense RNA) targets were prepared from 2.5 μg total RNA samples using OneArray Amino Allyl aRNA Amplification Kit (Phalanx Biotech Group, Taiwan) and Cy5 dye labeling (Amersham Pharmacia, Piscataway, NJ). Fluorescent targets were hybridized to the Mouse OneArray Whole Genome DNA microarray (Phalanx, Hsinchu, Taiwan) as previously described [29, 30], which contained 29,922 mouse genome probes, with Phalanx hybridization buffer using the Phalanx Hybridization System. After hybridization for 16 h at 50°C, nonspecific binding targets were washed away and the Cy5 fluorescent intensities for each spot were analyzed by GenePix 4.1 software (Molecular Devices, Sunnyvale). Data were analyzed using Spotfire software to determine whether a test gene was present or absent and whether the expression level of a gene in an experimental sample was significantly increased or decreased relatively to the control sample [24]. Changes in expression levels were evaluated as the averages of \log_2 [shikonin treatment/acetone treatment]. The microarray data have been deposited to the Gene Expression Omnibus database at NCBI (GEO; <http://www.ncbi.nlm.nih.gov/projects/geo/>) under the accession number GSE32694.

For microRNA array analysis, Febit's biochips (Geniom Biochip MPEA, *mus musculus*) were used. The probes were designed as the reverse complements of all mature microRNA sequences, which were published in the current Sanger miRBase release (version 14.0, September 2009) [31] for *mus musculus*. The probes on the chips were synthesized with intra-array replicates to increase the statistical confidence and to compensate for potential positional effects. RNA samples obtained from skin tissues treated with acetone or shikonin for 24 hours were subjected to a quality check to determine the quality and quantity of the sample RNA. The quality control was conducted using the Agilent 2100 Bioanalyzer and the RNA 6000 Nano Kit according to the manufacturer's instructions. For each array, test RNA was suspended in Febit's proprietary microRNA hybridization buffer (25 μL per array). Hybridization was performed automatically for 16 hours at 42°C using the Geniom RT Analyzer. Following the labeling procedure, the biochips were stringently washed and the quantile normalization

was performed according to the manufacturer's instructions [32, 33]. A total of 4 hybridizations were performed for acetone-treated and shikonin-treated skin samples, and each treatment was analyzed in duplicate on separate chips. In contrast to genomic DNA microarray analysis, the whole dataset microRNA (710 microRNAs) was systematically analyzed without filtering by "fold change" of expression level. Changes in expression levels were also revealed as averages of \log_2 [shikonin treatment/acetone treatment]. Combined analyses of the microarray and microRNA datasets were performed by using the MetaCore software to predict the modulatory effect of shikonin on skin tissue. The microarray data have been deposited to the database at NCBI (GEO; <http://www.ncbi.nlm.nih.gov/projects/geo/>) under the accession number GSE32695.

2.4. Immunofluorescence and Histological Staining. Skin specimens were fixed with 4% formalin and embedded in paraffin. For histological comparison, 6 μm thick sections were then cut and stained with hematoxylin and eosin (H&E). For immunofluorescence staining, fixed tissue sections were initially immersed in boiling sodium citrate buffer (0.01 M sodium citrate buffer, pH 6.0) for 30 min (antigen retrieval step). Skin sections then were blocked with 5% nonfat milk and incubated with polyclonal anti-FSP-1 antibody (Millipore, 07-2274, 1:200 dilution), monoclonal anti-E-cadherin antibody (Epitomics, 4552-1, 1:100), or monoclonal anti-vimentin antibody (Santa Cruz, sc-21791-PE, 1:200) in 1% nonfat milk for 1 hour at room temperature. Sections were washed with PBS containing 0.1% Tween 20. To detect primary antibodies, some sections were incubated with fluorescein isothiocyanate-conjugated anti-mouse-IgG (Jackson, 111-095-003, 1:200) (for FSP-1). 4',6-Diamidino-2-phenylindole dihydrochloride (1 $\mu\text{g}/\text{mL}$) was used to stain nuclei. Fluorescence microscopy evaluation of immunostained tissue sections was performed using a Zeiss Axiovert 200 M microscope (Carl Zeiss, Heidelberg, Germany). Images were captured with a digital camera (Orca ER, Hamamatsu) and processed using Axiovision 4.6.3 (Carl Zeiss). The number of individual fluorescent spots as test cells was then scored for comparative analysis and the data were exported to Microsoft Excel.

2.5. Real-Time PCR Analysis. To verify the array results, 3 full-thickness skin samples per group were further analyzed as follows. For wound-healing experiments, skin tissues surrounding the wound area (1 cm in diameter) were prepared by removing the subcutaneous fat and connective tissue [34]. Real-time PCR reactions were performed using microRNA- and mRNA-specific primers for Zeb1; Zeb2; microRNA-200a, -200b, -200c, -141, -429, and -205. For mRNA analysis, complementary DNA (cDNA) was randomly primed from 2.0 μg of total RNA using the Superscript reverse transcription kit (Invitrogen) according to the manufacturer's instructions. Reactions were incubated at 50°C for 50 min, and PCR amplification was carried out after denaturing at 95°C for 10 s. The following primers were used: mouse Zeb1, 5'-TGGCAAGACAACGTGAAAGA-3'

(forward), and 5'-AACTGGGAAAA TGCATCTGG-3' (reverse); mouse Zeb2, 5'-TAGCCGGTCCAGAAGAAATG-3' (forward), and 5'-GGCCATCTCTT TCCTCCAGT-3' (reverse); mouse E-cadherin, 5'-AATGGCGGCAATGCAATCCCA AGA-3' (forward), and 5'-TGCCACAGACCGATTGTGGAGATA-3' (reverse); mouse Gapdh, 5'-AGGTCGGTGTGAACGGATTTG-3' (forward), and 5'-TGTAGACCATGT AGTTGAGGTCA-3' (reverse). Real-time PCR amplifications were performed using a LightCycler 2.0 Real-Time PCR System (Roche, Basel, Switzerland), and results were normalized to mouse glyceraldehyde 3-phosphate dehydrogenase (Gapdh) as an internal control. For microRNA analysis, 5 μg of total RNA extracted from each test sample was reverse-transcribed into cDNA using the Mir-X miRNA First-Strand Synthesis Kit (ClonTech). The Mir-X miRNA qRT-PCR SYBR Kit (ClonTech) was then used to quantify microRNAs according to the manufacturer's instructions. The microRNA-specific forward primers contained the following sequences: mouse microRNA-200a, 5'-TAACACTGTCTG GTAACGATGT-3'; microRNA-200b, 5'-TAAT ACTGCCTGGTAATGATGA-3'; microRNA-200c, 5'-TAATACTGCCGGTAATGATGGA-3'; microRNA-141, 5'-TAACACTGTCTGGTA AAGATGG-3'; microRNA-429, 5'-TAATAC TGTCTGGTAATGCCGA-3'; microRNA-205, 5'-TCCTTCATTCCACCGGAGTCTG-3'. A universal reverse primer was used for each microRNA according to the manufacturer's instructions. For microRNA quantification, the delta-delta C_t method was used to determine the level of each microRNA relatively to the level of U6 small nuclear (sn) RNA. Data are mean values \pm S.D. of three independent experiments performed in triplicate.

2.6. Western Blot Analysis. For total protein extraction, acetone- (vehicle) and shikonin-skin samples were immersed in 500 μL of lysis buffer (50 mM Tris-HCl (pH 7.4), 150 mM NaCl, 0.5% Triton X-100, 20 mM EGTA, 1 mM dithiothreitol, 1 mM Na_3VO_4 , and appropriate protease inhibitor cocktail tablets) for 10 min. For isolation of total protein, mouse skin samples were excised, immediately placed in liquid nitrogen, and pulverized with metal beads (2 mm in diameter) at 4°C for 30 min. Lysates were centrifuged at 12,000 $\times g$ for 20 min, and supernatant containing 30 μg of protein was boiled in SDS sample loading buffer for 10 min before electrophoresis on a 8% PAGE BisTris gel (Invitrogen). After electrophoresis for 2 h, proteins in the gel were transferred to a polyvinylidene difluoride membrane (Novex, San Diego, CA), and the blots were blocked with 5% nonfat dry milk in PBST buffer (PBS containing 0.1% Tween 20) for 60 min at room temperature. The membranes were incubated overnight at 4°C with anti-MMP-9 antibody (1:50,000), anti-MMP-2 antibody (1:10,000), anti-E-cadherin antibody (1:3,000), or anti-vimentin antibody (1:3,000). Washed blots were incubated with a 1:10,000 dilution of HRP-conjugated anti-rat, anti-mouse, or anti-rabbit secondary Abs. Equal protein loading was assessed using mouse β -actin (Sigma). All antibodies were purchased from Abcam (Cambridge, UK). The protein bands were visualized on HyperMax film using the ECL system (Amersham Biosciences).

2.7. Wound Creation and Scoring of Wound Tissues. Cohorts of 8- to 12-week old C57BL/6 mice were used for the creation of physical wounds. All test animals were treated according to the guidelines outlined by the Institutional Animal Care and Use Committee. Two standardized full-thickness wounds, 4.5 mm in diameter, were made with a scalpel on mouse abdominal skins, one on each side of the midline. Eight mice were initially sacrificed at day 0, then a group of 16 mice (8 control and 8 shikonin-treated mice) were killed at each of the indicated time points (days 1–5). Therefore, in all, a total of 88 mice were randomly assigned to either the control group or the shikonin-treatment group. Digital images were taken on the day of surgery and each subsequent day. For scoring of wound healing, the wound areas (in mm²) were calculated from wound perimeter tracings and were compared using Image Pro Plus 6.0 software (Media Cybernetics, Maryland). Wound areas were normalized by setting the day 0 wounding level as 100%; relative wound areas on the subsequent days were expressed as a percentage of the day 0 value [35]. After scoring of the wound area, three mice from each group ($n = 8$) were subjected to immunofluorescence observation and the other five mice underwent RNA expression study.

3. Results

3.1. Histological and Physiological Changes in Mouse Skin Tissues in Response to Topical Treatment with Shikonin. We initiated this study by evaluating the histological and physiological effects of shikonin on mouse abdominal skin. Figure 1(a) shows the histological features of typical skin biopsy samples of four representative test mice. A total of 5.3 cm² of skin area was treated for 4 or 24 hours with 100 μ L acetone containing 10 μ g/ μ L (3.5 mM) shikonin or 100 μ M 12-O-tetradecanoylphorbol-13-acetate (TPA), a well-known inflammatory agent. TPA stimulation was used as a positive control for an inflammatory condition in skin tissue. We observed a much thicker epidermal tissue with up to a 5-fold increase in thickness (shown as black bars) in shikonin-treated skin tissues than control skin tissues. The epithelium of skin tissues in the acetone- (vehicle control) treated group exhibited only 2-3 cell layers. Underneath the epithelium, a high population of cells infiltrated into the dermis layer in shikonin-treated skin tissues (Figure 1(a)—(B)) as compared to those treated with acetone (Figure 1(a)—(A)). These results suggest that shikonin can enhance the tissue permeability or cell chemotaxis in test mouse skin tissues, indicating that shikonin can initiate its cellular or physiological effect at a very early stage during the wound-healing process, that is, at 4 h after treatment”. In addition, disorganization and an increased number of fat cell layers were readily observed in shikonin-treated skins (Figure 1(a)-(B)). In mouse skins topically treated with TPA, epidermal cell layers became swollen and thickened, and various cell types penetrated into the stromal/dermal/fat tissue layers (Figure 1(a)-(C)), in a similar fashion as observed for shikonin-treated skin tissue (Figure 1(a)-(B)). However, the shikonin-treated skins still maintained a distinctive border (stratum basale) between the

epidermal layer and the dermal layer; by contrast, in TPA-induced inflamed skin, no boundary between the epidermal and dermal tissues could be detected. These specific and different physiological effects on multiple cell layers of normal skin tissue suggest that although the shikonin-treated skins exhibited some inflammation-associated cellular characteristics, the treatment apparently did not cause damage at the tissue level. These results support previously reported pharmacological activities of the shikonins and the traditional medical use of shikonin-containing *Lithospermum erythrorhizon* plants in skin wound-healing [4–6].

3.2. Shikonin Treatment Results in Differential Gene Expression in Mouse Skin Tissues. In order to systematically evaluate the effects of shikonin on mouse skin tissues, we next compared the gene expression profiles in shikonin-treated versus acetone-treated skin tissues at different time points. Total RNA samples were collected at indicated time points for transcriptome and microRNA array analyses as described previously [22–24]. Only genes showing at least a 2-fold change in the level of RNA transcripts in two independent experiments were considered as significant for further analysis. Differences in gene expression levels were calculated by dividing the signal intensity values obtained from shikonin-treated skin tissues by those from acetone-treated tissues. Gene expression profiling analysis showed that a total of 2,300 and 3,930 genes had markedly changed expression levels after 4 hours and 24 hours of pretreatment with shikonin, respectively. By comparing and grouping the number of shikonin-responsive genes using the MetaCore program, we found that shikonin treatment can result in 5 major cellular/physiological effects with known molecular or biochemical functions (Figure 1(b)). This gene-clustering analysis showed that the top five gene functional groups significantly modulated through shikonin stimulation, either at 4 or 24 h after treatment were cell adhesion (cytoskeleton and cell movement), chemotaxis, inflammation, IL-10-mediated anti-inflammation, and cytokine-mediated immune response. These responses suggest that shikonin treatment induces an integrated tissue-wide response involving cell chemotaxis, attachment, and cellular immune responses.

Next, these responsive genes were grouped and classified according to the P value of the hypergeometric intersection, which indicates the “trend” or the “consistence” of a test dataset in gene-clustering analysis. A lower P value of the entity means higher relevance to the dataset, which appears in the higher rating of the entity [36]. By comparing the $-\log [P \text{ value}]$ level in the different gene clusters, different gene groups can be assigned according to their known cellular and molecular processes, using the MetaCore software. This analysis predicted a list of top ten cellular and molecular processes that may be regulated or affected in skin by topical treatment with shikonin, at 4 (Figure 1(d)) or 24 hours (Figure 1(e)) after treatment. It is important and interesting to note here that the regulation of immunological signaling networks and the control of cell or tissue development signals represent over 80% of the shikonin-responsive gene expression activities. Among them, two are specifically related to cell adhesion or cytoskeleton remodeling. In addition, several key cytokines,

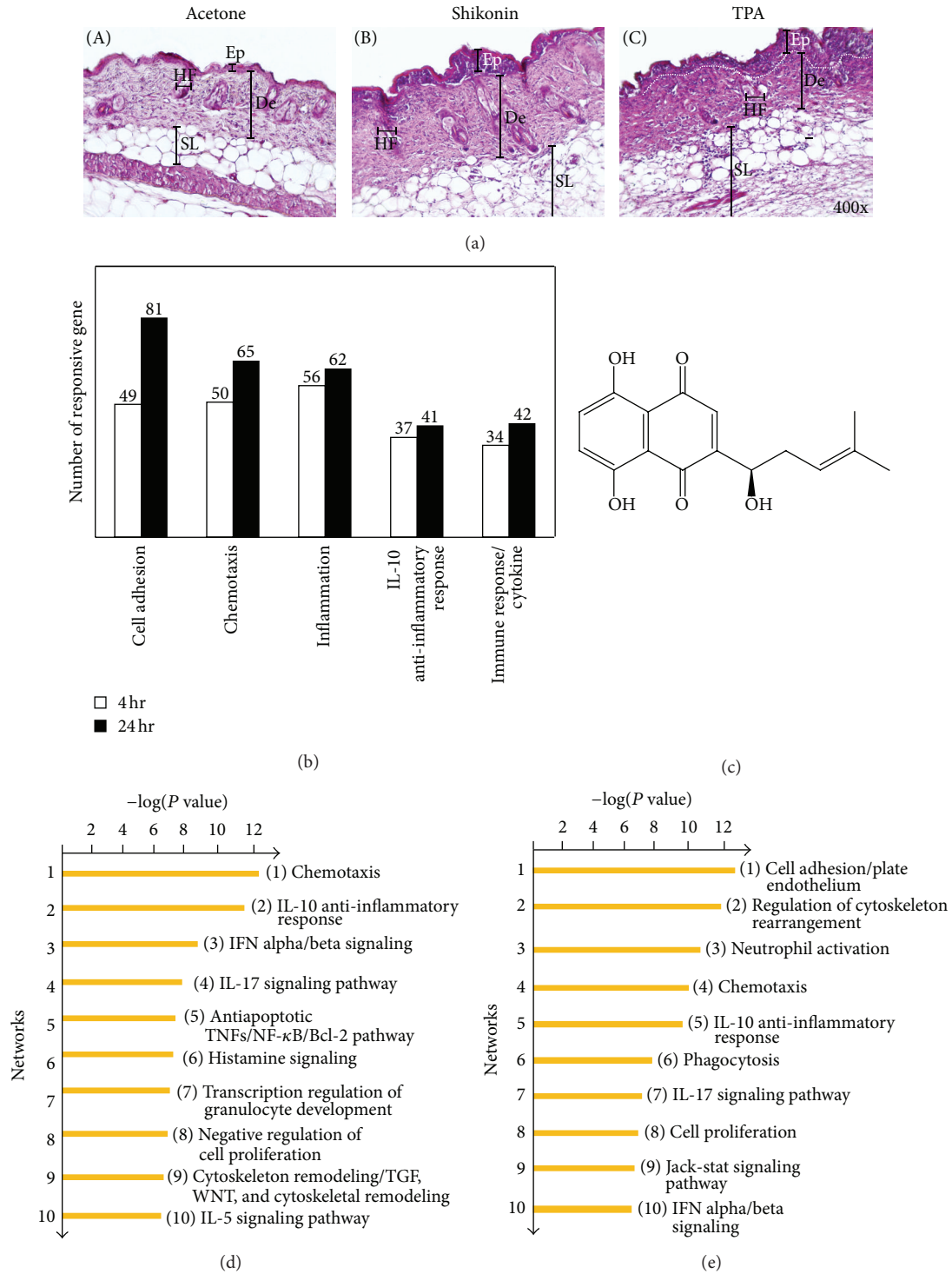


FIGURE 1: Histological analysis shikonin-treated mouse skin and grouping of genes that are responsive to shikonin treatment. (a) The histological characteristics of acetone- (vehicle control), shikonin-, and TPA-treated skin were revealed by H&E staining. Test mice (3 animals per group) were topically treated with (1) 100 μ L acetone, (2) shikonin (3.5 mM in 100 μ L acetone), or (3) TPA (10 nM in 100 μ L acetone) for 24 h. Black bars mark the thickness of the epidermal layer (Ep), dermis (De), subcutaneous layer (SL; also known as hypodermis), and hair follicles (HF). The dotted line in panel 3 indicates a terminally damaged boundary line between the epidermal (stratum spinosum) and dermal layers. (b) Shikonin-responsive genes in skin, as compared to acetone- (vehicle control) treated skin samples, were grouped according to their known molecular, cellular, or biochemical functions. Classified gene groups were then listed according to the abundance in number of responsive genes in skin tissue treated with shikonin for 4 or 24 h. (c) Structure of the naphthoquinone, shikonin. (d and e) GeneGo Pathway Maps processed by MetaCore software analysis. By comparing the $-\log [P \text{ value}]$ of different gene-clustering groups, the top ten responsive processes with specific cellular or molecular functions were predicted for evaluating the effect of shikonin. The orange bars indicate the calculated values generated from 4 h (d) and 24 h (e) datasets, respectively.

including IL-10 and IL-17, were also predicted to play a role in defined cytokine-mediated immune activities in response to shikonin (Figures 1(d) and 1(e)). Interestingly, our analysis further revealed a relationship between shikonin stimulation and activities of specific cell types, such as transcription regulation of granulocyte development and neutrophil activation. These results suggest that shikonin treatment of skin may induce specific growth or differentiation activities according to cell type and may subsequently facilitate the tissue remodeling at the organ level that we had previously observed in mouse and pig skins [6, 20].

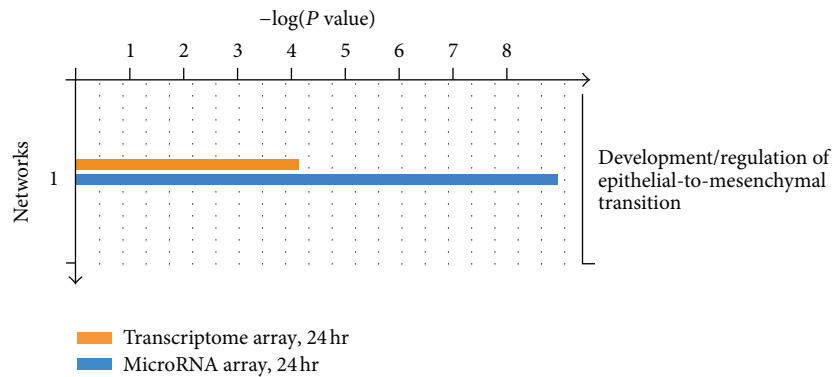
3.3. Combination of Transcriptomic and MicroRNA Array Analyses for Evaluating Signaling Networks Modulated by Shikonin in Skin Tissue. To examine possible hierarchical regulation of the effects of shikonin on gene expression networks at the transcriptome level and to determine the main factors that may coordinate high-level regulation of the stimulatory effects of shikonin on skin tissues, we extended our investigation by combining the use of microRNA array and the transcriptome microarray. In this test, the microRNA expression values for a total 710 microRNAs were obtained from output data. Initial experimental preparations yielded Pearson's correlation values of 0.97 and 0.92 for test biological sample replicates of shikonin- and acetone-treated skins, respectively, confirming the validity of the assay stringency. All microRNAs identified from the normalized data of this analysis were then employed to identify candidate target genes in subsequent studies.

Having analyzed the *in vivo* microRNA expression profiles of cells in skin tissues, we observed that expression levels of a number of microRNA species were consistently regulated after treatment with shikonin for 24 hours. These include the expression of six microRNAs of the microRNA 200 family, microRNA-200a, -200b, -200c, -141, -429, and -205, which were all downregulated (see the left blue bar-containing thermometers in Figure 2(b)). Consistent with this result, the transcriptomic array analysis also showed that the gene expression levels for Zeb1 (*Tcf8*) and Zeb2 (*Sip1*; *Zfhx1b*) were upregulated after shikonin treatment for 24 hours (see the red bar-containing thermometers in Figure 2(b)). Figure 2(a), obtained from the *GeneGo Process* of the MetaCore software, shows the hypothetical or candidate networks of EMT processing revealed by our combined analyses of the representative genes and the microRNAs in coordination as a response to shikonin stimulation. This analysis predicted that the EMT process is the only pathway strongly modulated by shikonin treatment of test mouse skin tissue; however, this conclusion was only obtained when we performed the combined analyses of the datasets obtained from both the transcriptome and the microRNA expression profiles (Figure 2(a)). Taken together, our results therefore strongly suggest that shikonin treatment has a potent suppressive effect on the expression of different members of the microRNA 200 family, and the resultant cascade at the RNA transcript level efficiently activates the EMT process through coordinated and potent activation of the Zeb1 (*Tcf8*) and Zeb2 (*Sip1*) gene expressions, the master regulators of the EMT activity.

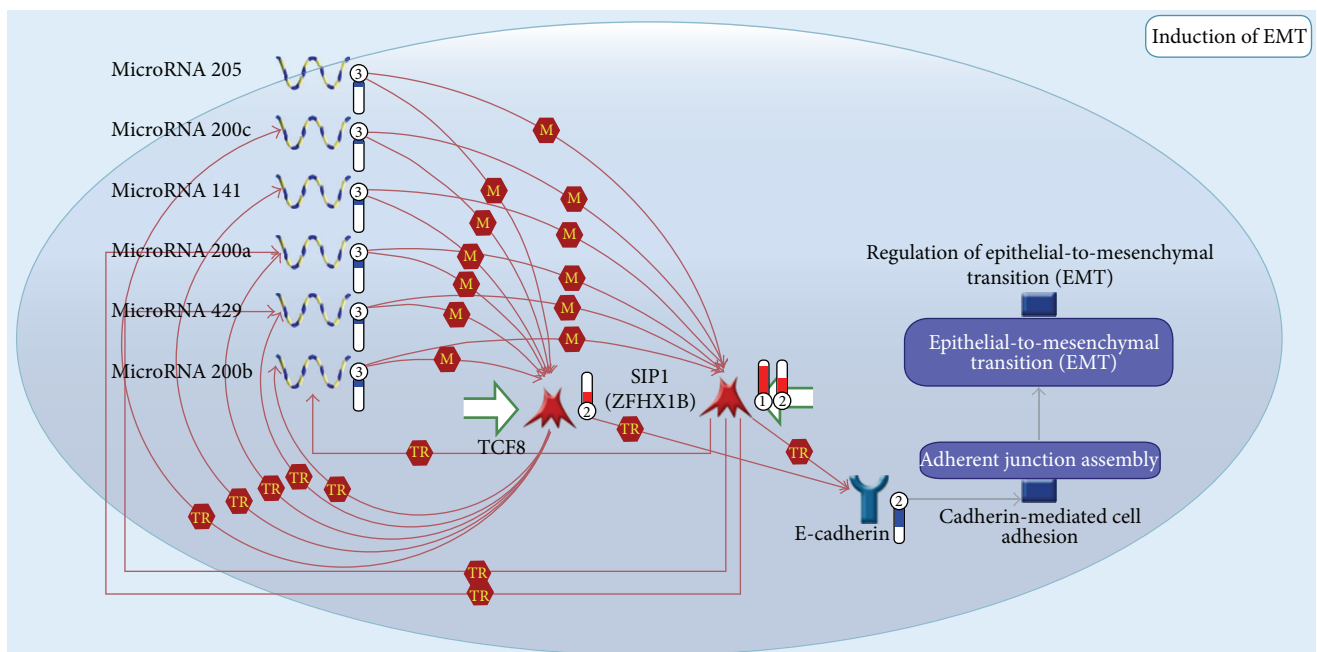
3.4. Induction of EMT Features in Shikonin-Treated Skin Tissue. As a followup, the effect of shikonin on the specific cellular features of the EMT process was evaluated in mouse skin using immunofluorescence staining assay. It is known that epithelial cells undergoing the EMT process, that is, those cells that are localized above the basement membrane zone (BMZ) that have gained specific mesenchymal cell markers, are fibroblast-specific protein 1 (FSP1) and/or vimentin positive [13, 16, 17]. In our study, this layer of epithelial cells was characterized by E-cadherin expression (red staining in Figures 3(a)—1; to 3 and 3(b)—7 to 9). The EMT features in TPA-treated skin tissues were detected as a positive control for inflamed skin tissue (Figure 3(a)—3 and 6; Figure 3(b)—9 and 12). A comparison of shikonin- and acetone-treated skin tissues showed that shikonin-treated skins contained a much higher population of epithelial cells positively stained for FSP1 and/or vimentin (Figure 3(a)—2 and 5; Figure 3(b)—8 and 11). By contrast, the surrounding epithelial cells clearly lacked these mesenchymal markers. In agreement with the result from H&E staining of abdominal skin tissue, the thickness of epithelial cell layers was drastically increased in skins treated with shikonin (Figure 1(a)). Statistical analyses of EMT activity clearly showed that shikonin treatment could activate the EMT process in abdominal skin tissues (Figure 3(c)). These results demonstrate the specific stimulatory effect of shikonin on the EMT process in test mouse skins, strongly supporting the results obtained from the microRNA array and transcriptome analyses.

The effect of shikonin on EMT features was also evaluated in ear skin tissues (Figure 3(b)). We found that some cells exhibiting mesenchymal cell markers were also detectable in the ear skin tissues treated with shikonin. However, the level of change in EMT activities was not as obvious as that detected in abdominal skin (Figure 3(a)—2 and 4). The reason for the difference may be the thickness of the epithelial layers in these two different skin tissues. Shikonin treatment did not result in a significant increase in skin thickness in ear skin tissue, contrary to the results seen in abdominal skin. It is important to note here that ear skins have traditionally been used as a popular model for evaluating different pharmaceutical effects of candidate drugs or therapeutics. Our data suggest that the potency or specificity of shikonin-induced EMT activity may depend on skin tissue and the constituent cell type.

3.5. EMT-Related MicroRNA and Protein Expressions in Skin Tissue Are Regulated by Stimulation with Shikonin. Previous studies have shown that expression of microRNA-200 family members and microRNA-205 in particular is necessary for the maintenance of the epithelial phenotype [18, 19], that is, the reverse of EMT activity; thus, we further validated the RNA transcript and microRNA array expression results. The expression levels of EMT process-related mRNAs (Zeb1 and Zeb2) and microRNAs (microRNA-200a, -200b, -200c, -141, -429, and -205) were quantitatively determined by real-time PCR (RT-PCR). In comparison with the vehicle-control skin samples, the observed decrease in the expression levels of specific microRNAs in shikonin-treated skin, although seeming following a similar pattern, was insignificant at 4



(a)



(b)

FIGURE 2: Combinational analysis of transcriptome/DNA microarray and microRNA array datasets to predict possible effects of shikonin on mouse skin tissue. (a) Functional analysis and prediction by “GeneGo Pathway Maps” processed by MetaCore software. By analyzing the $-\log [P \text{ value}]$ value of different gene-clustering groups in the 24 h treatment datasets obtained from the transcriptomic array and microRNA array analyses, the regulation of the EMT process was predicted to be the major physiological response to shikonin stimulation. The orange and blue bars indicate the calculated value output from transcriptomic array and microRNA array analysis, respectively. (b) Putative signaling networks (microRNA-dependent inhibition of EMT) involved in the modulatory effect of shikonin on skin tissue were predicted from the MetaCore software. In this map, a prototypical cell was constructed from six representative microRNAs and three differentially expressed genes that respond coordinately to an *in vivo* treatment with shikonin for 24 h. Experimental data from transcriptomic array and microRNA array analyses are linked to and visualized on the maps as thermometer-like symbols. Red and blue scales indicate the upregulated and downregulated gene expressions (microRNAs or mRNAs). M: microRNA binding. TR: transcription regulation. TCF8 (Zeb1): transcription factor 8. SIP1 (Zeb2; Zfhx1B): Smad-interacting protein 1.

hours after treatment (Figure 4(a)). However, at 24 hours after treatment, the expression of these microRNAs was significantly suppressed by shikonin treatment (Figure 4(b)). Consistent with this data, the levels of Zeb1 and Zeb2 mRNAs were also significantly increased in skin tissues treated for 24 hours with shikonin. Taken together, our data suggest that suppression of the expression of these microRNAs plays an important role in the shikonin-induced EMT process *in vivo* in mouse skin. Interestingly, the suppression of the expression

of some microRNAs (i.e., microRNA-200a, -200b, and -205) was not statistically significant as conventionally measured by “fold change.” However, when the microRNAs are viewed as a whole, a clear trend in expression could be seen. Based on the pattern of coordinated regulation, our data does support that such less than “substantial fold change” for individual microRNAs, but good alliance in the expression trend as coordinated with across-the-board alteration may confer a good regulatory network for gene expression controls.

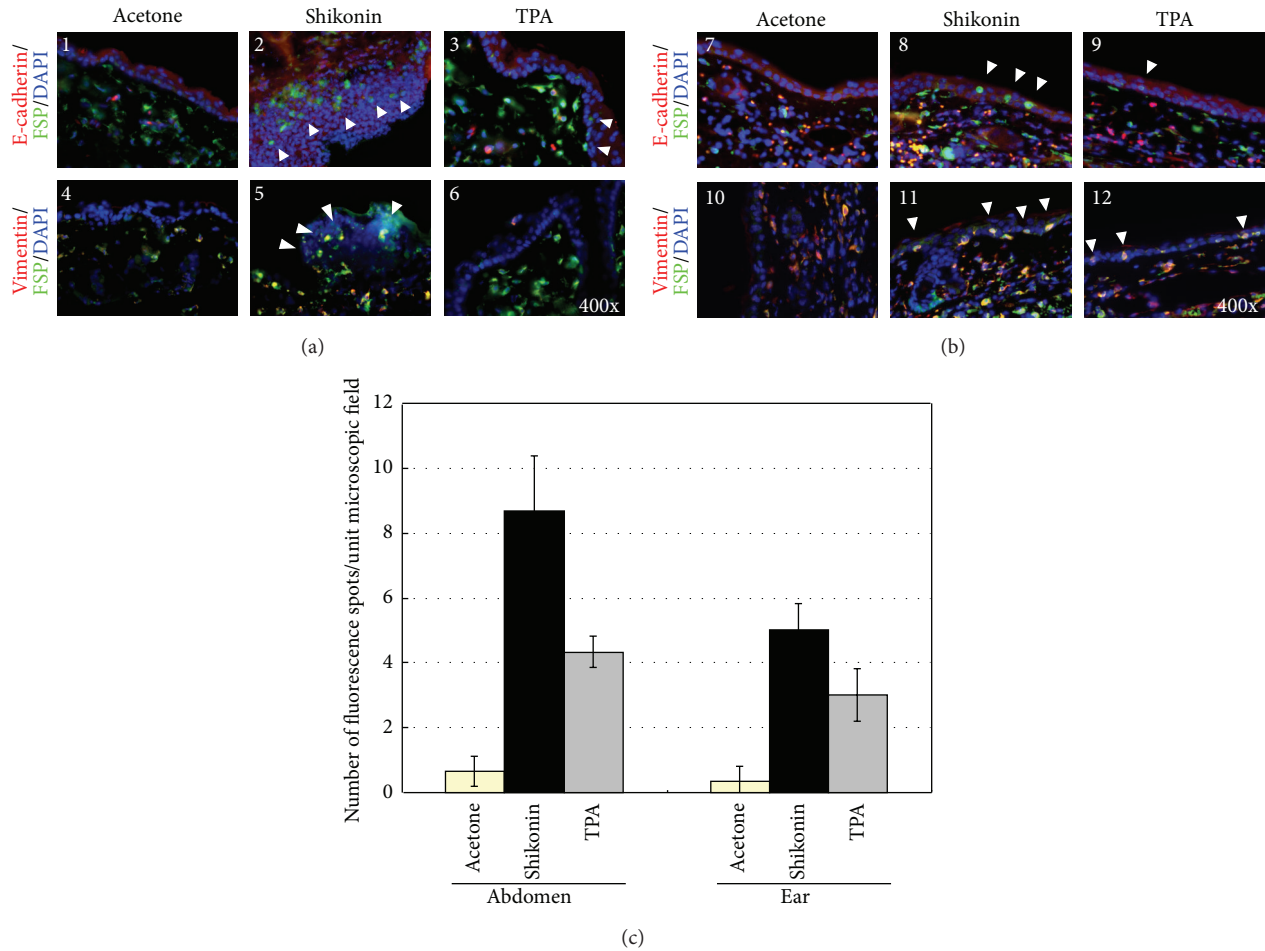


FIGURE 3: Gain of mesenchymal features by epithelial cells in mouse abdominal and ear skin tissues treated with shikonin. (a) At 24 h after treatment, (1) acetone-, (2) shikonin-, and (3) TPA-treated abdominal skin tissues were stained for the presence of E-cadherin (red), FSP1 (green and indicated with arrowheads), and DAPI (blue) to reveal the appearance of mesenchymal cells in epidermis. The presence of vimentin (red) and FSP1 (green) double-stained cells (yellow and indicated with arrowheads) further indicates that these epithelial cells underwent the EMT process in test skin tissues (4–6). (b) Analogous analysis was performed on treated ear epidermis (7–12). (c) Statistical comparison of EMT activity was performed by scoring the number of yellow fluorescence spots (vimentin⁺/FSP1⁺) in (a) and (b). Values shown are the mean \pm SEM of three experiments. The significance of differences was analyzed by one way ANOVA (* $P < 0.05$, ** $P < 0.01$, and *** $P < 0.001$).

Our study may thus also indicate the need for such systematic analyses of trends in microRNA expression profiles.

As shown in Figure 4(c), the expression levels of some mesenchymal-associated protein markers such as MMP2, MMP-9, and vimentin were substantially increased in cells of skin treated with shikonin for 24 hours as compared to those in cells obtained from control skin samples, thus validating the shikonin-induced EMT activity in abdominal skin cells. In addition, we observed significant downregulation of E-cadherin expression, another hallmark of EMT, in shikonin-treated skin tissue, especially at 24 hours after treatment. These data are consistent with the mesenchymal features that we observed histologically in tissue sections.

3.6. Epithelial Cells Located in the Wound Margin of Shikonin-Treated Skin Tissues Acquire Mesenchymal Cell Phenotypes. To evaluate the enhancing effect of shikonin on tissue

repair in skin wounding, aliquots of 20 μ L shikonin solution (5 μ g/ μ L) or control solvent were topically applied to the area surrounding the test wound. Wound closure was measured as the area of epidermal closure (mm^2) from the initial wound after treatment, and the rates of wound closure (area of granulation tissue remaining exposed) were measured for different treatments (Figure 5(a)). The addition of shikonin (100 μ g/wound) significantly accelerated wound-healing activity, especially during the early repair phase (0–2 d), as compared with the acetone-treated mouse skins. This result suggests that topical application of shikonin can increase the rate of wound closure kinetics for skin wound healing.

During the reepithelization phase, epithelial cells in the wound margin tissues can be mobilized through gain-of-mesenchymal features during the wound repair process [34]. Our results above led us to suggest that partial

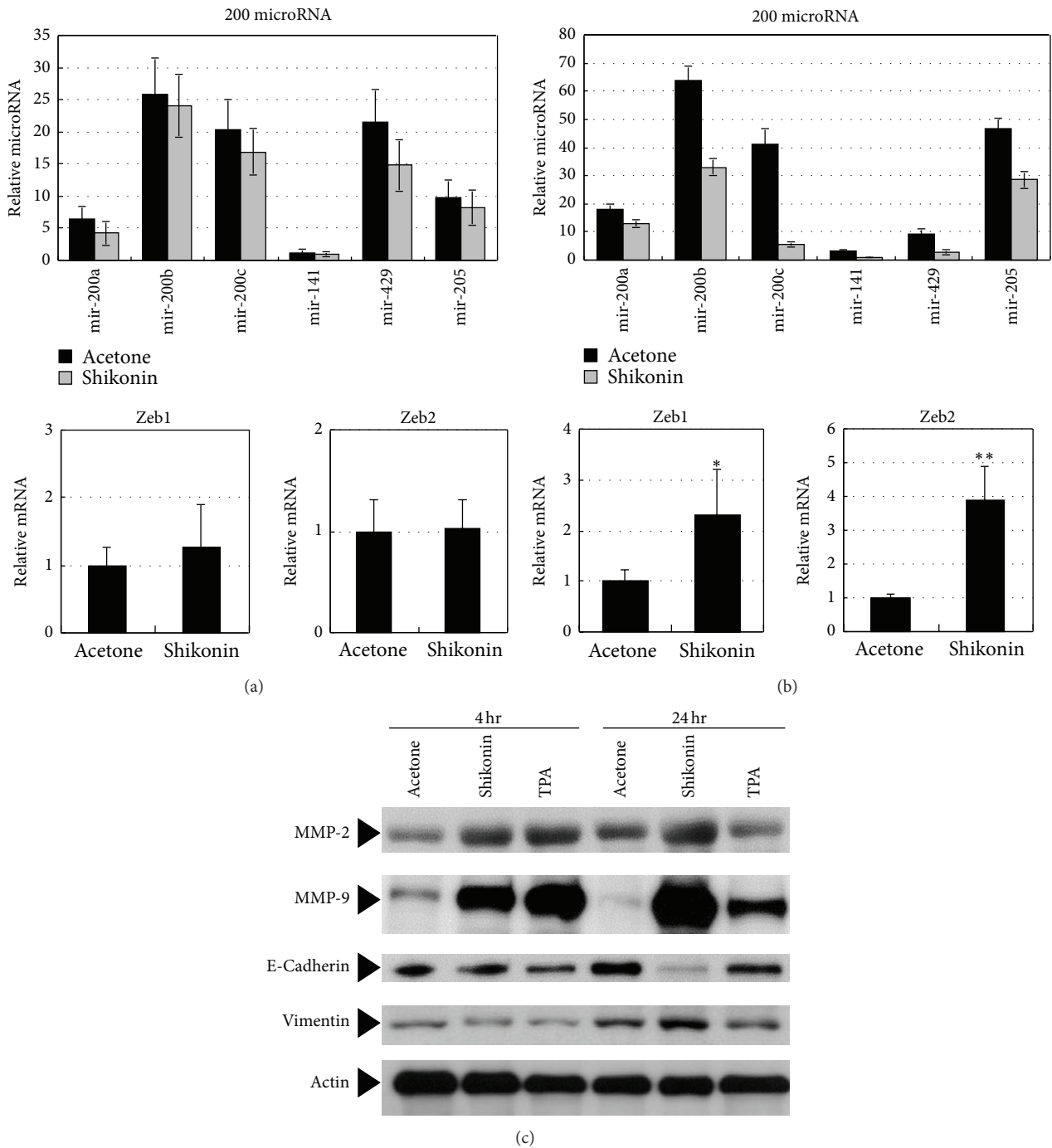


FIGURE 4: Validation of the EMT activity-related expression of microRNAs and proteins. The expression levels of some key mesenchymal-associated microRNAs, that is, mir-200a (microRNA-200a), mir-200b (microRNA-200b), mir-200c (microRNA-200c), mir-141 (microRNA-141), mir-429 (microRNA-429), and mir-205 (microRNA-205), as well as Zeb1 and Zeb2 mRNAs in epidermal cells treated with shikonin for 4 h (a) and 24 h (b) were determined by real-time PCR analyses. Values shown are the mean \pm SEM of three experiments. The significance of differences was analyzed by one way ANOVA (* $P < 0.05$; ** $P < 0.01$). (c) Expression of E-cadherin and other mesenchymal-associated markers, MMP2, MMP-9, and vimentin, were measured by Western blot analysis. β -actin was used as gel loading control. Data are representative of triplicate experiments.

EMT activity is induced by topical application of shikonin onto wounded skin tissues. Therefore, we evaluated mouse skin tissues around the acute wounds during the phase of re-epithelialization. Skin biopsy samples were harvested between 0 and 5 days after the creation of aseptic wounds. As shown in Figure 5(b) through H&E staining, the active migratory tongue of epidermal cells penetrated into the wound tissue bed under the scab at the wound margin (black arrows) at 2 days after stimulation. In these specimens, we observed that many epithelial cells undergoing the EMT process indeed gained mesenchymal markers, such as FSP1 and/or vimentin (Figure 5(b)—3 to 6). A comparison of the shikonin- with acetone-treated skin wounds showed that the migration tongues of shikonin-treated skins contained a significantly higher population of the epithelial cells that were stained positively for FSP1 or vimentin (Figure 5(b)—4 and 5). In addition, expression levels of the 200 family microRNAs in shikonin-treated skin surrounding the wound were also significantly lower than those in the untreated skin, at 2 days after treatment (Figure 5(c)). Consistently, the levels of *Zeb1* and *Zeb2* mRNAs were also significantly increased in the shikonin-treated skin wounds (Figure 5(d)). Taken together, the results shown in Figure 5 are consistent with the data obtained from normal skins which were not subjected to wound creation (Figures 3 and 4). In summary, our data acquired by integrating multiple experimental approaches suggest that shikonin can confer a highly efficacious stimulatory effect on the EMT process, via which epithelial cells can effectively acquire the mesenchymal machinery features to guide cell migration and tissue repair.

4. Discussion

Using a combination of mRNA and microRNA expression profile analyses, we investigated the *in vivo* effects of the medicinal phytochemical shikonin, on cellular, histological, and immune-modulatory activities in mouse skin tissue. In the present study, although the changes in expression levels of some 200 family microRNAs were modest (e.g., 1.4- to 1.8-fold change) in response to shikonin treatment for 24 hours, the high degree of consistency in the trends in expression strongly suggests that these microRNA species together may play important roles in suppressing specific target genes and result in hierarchical control and onset of a shikonin-induced EMT process and the subsequent cascade activities. These results further suggest that because the role of microRNAs in regulation of gene expression is often sequence dependent and virtually always involves coregulation by several microRNA or siRNA components [37–40], measurement of “fold change” of their expression levels may not be a wholly satisfactory method to evaluate and filter responsive microRNAs. Based on the current findings, we hence further suggest that our strategy in combining the profiling and clustering of microRNA expression activities with specific transcriptome activities is a systematic and logical approach for evaluating the effect of certain phytochemicals on specific cellular or physiological functions that are regulated in a coordinated and hierarchical manner. This combinational approach may

be superior to transcriptome or microRNA profiling alone for the evaluation of phytomedicines.

Previously, the skin tissue obtained from the mouse ear has been employed as a mouse skin model applied for treating various dermal diseases or testing drug delivery efficacy. The advantages of this tissue origin may include its relatively simple composition of epidermal or dermal cell layers and the ease with which it can be obtained from test mice. However, the interactive relationships between skin and other tissue layers in the ear can be drastically different from the relationships in other body parts, which often exhibit a more complex interaction with the underneath substratum tissues. In this study, we found that topical application of shikonin could markedly increase the thickness of both the epidermal and the dermal layers of the abdominal skin (Figure 1(a)) but not ear skin. In addition, the level of shikonin-induced EMT activity in ear skin (Figure 3(b)) was much less obvious than that in skin tissues of the abdomen (Figure 3(a)) or thigh (data not shown). These results suggest that the lower EMT activity we observed in ear skin may be due to its relatively simple tissue composition. Such tissue diversity in different skins of the body should be explored for future development of skin remedies or healthcare agents.

The anti-inflammatory effects of shikonin have been investigated in a spectrum of physiological, molecular, and cellular studies [4, 6, 7, 41, 42]. In this study, our data also show that some IL-10-mediated anti-inflammation response-related genes were activated after shikonin treatment for 24 hours (Figure 1(b)). However, a comparison with TPA-induced inflamed skin in this investigation revealed that some proinflammatory histological properties and molecular mediators are also induced in shikonin-treated abdominal skin tissues. These features include the changes in skin thickness (Figure 1(a)), expression of some inflammation-related genes (Figure 1(b)), and expression of some inflammation-related protein molecules, such as MMP2 and MMP9 (Figure 4(c)). The differences between some of our results and previously reported results may reflect the different skin models we used. On the other hand, it has become increasingly evident that different proinflammatory stimuli may differentially affect gene expression profiles and/or genome activities. Similarly, different anti-inflammatory agents may also act differently against different inflammatory conditions. In both cases, interactive and interactive signalings apparently can generate specific tissue and cellular environments for dealing with and responding to different physiological processes or stresses, such as inflammatory activities, stress response, wound repair, and tissue remodeling [43–45]. We previously showed, using time-course experiments, that shikonin can greatly affect human monocyte/dendritic cells involving groups of anti-inflammatory and proinflammatory cytokines/chemokines in “cross-talk” and “overlapping” manner [46]. These findings together with the current results suggest that shikonin might be a promising molecular agent for treatment of various diseases or epithelial tissue damages. However, the optimal dosage for different skin tissues (e.g., ear versus abdomen) for potential future clinical use of shikonin remains to be identified.

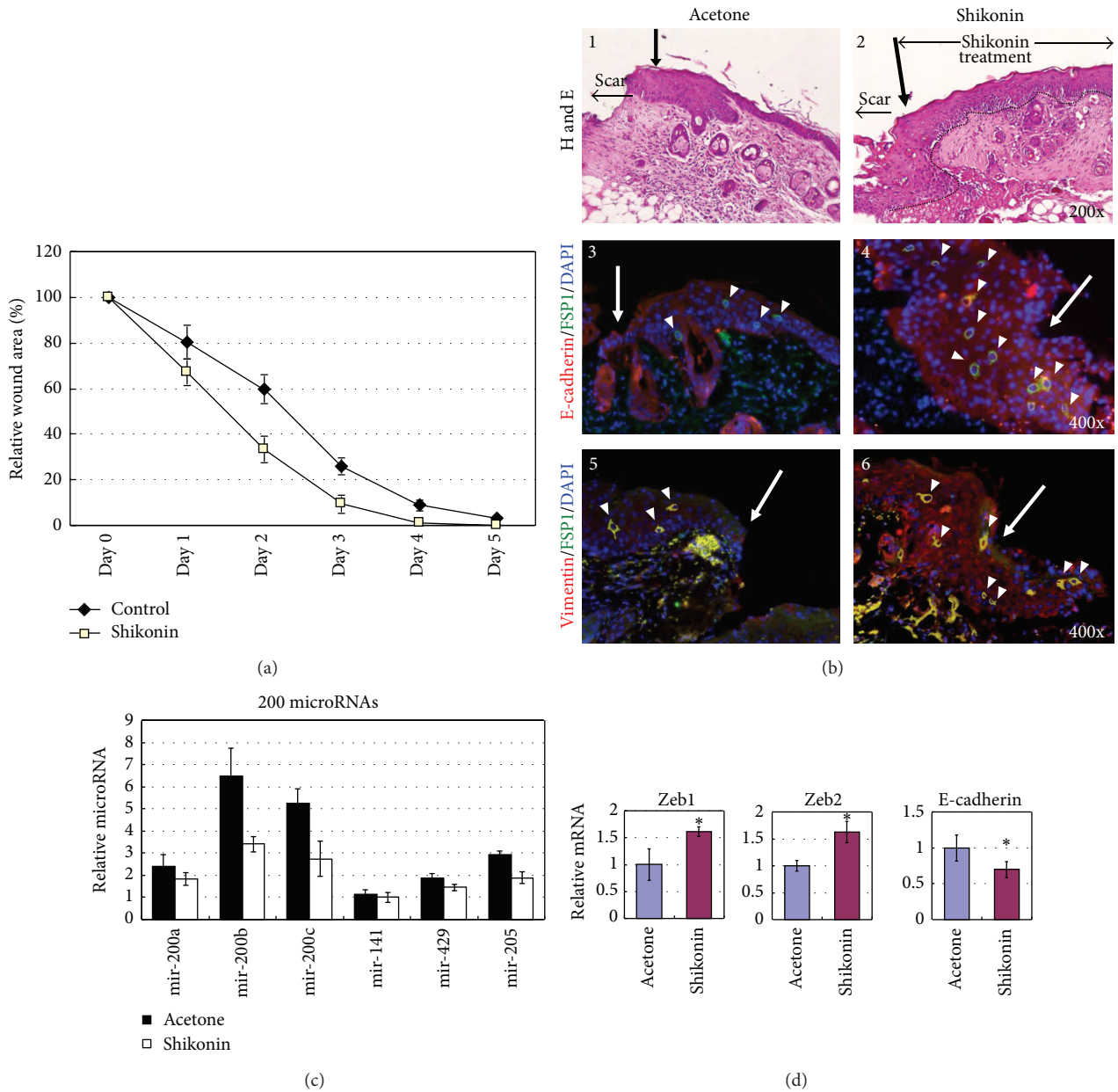


FIGURE 5: Characteristics of EMT in shikonin-treated wound healing in mouse skin tissues. (a) Wound closure rates of skins subjected to different treatments (shikonin versus control). The data represent the mean \pm SEM of six mice. At 2 d after treatment, histological and immunohistochemical characteristics of acetone- (1) and shikonin-treated skins (2) were analyzed. Long arrows indicate the original edges of each wound. The dotted line in panel 2 indicates the terminally damaged boundary line between the epidermal and dermal layers. (b) Tissue biopsy samples from each test group were also stained for the expression of E-cadherin (red), FSP1 (green), and DAPI (blue). Triangle arrows indicate the presence of mesenchymal cells in the epidermis (3 and 4). The presence of vimentin (red) and FSP1 (green) double-stained cells (yellow and indicated with arrowheads) further indicates that these epithelial cells have undergone the EMT process in test skin tissues (5 and 6). (c) Changes in expression levels of mesenchymal-associated microRNAs, including mir-200a, mir-200b, mir-200c, mir-141, mir-429, and mir-205, as well as the Zeb1, Zeb2, and E-cadherin mRNAs (d) in shikonin-treated skin wound, as measured by real-time PCR analyses. The significance of differences was analyzed by one way ANOVA (* $P < 0.05$ and ** $P < 0.01$).

The highly effective wound-healing activity of shikonin has been demonstrated in a number of *in vivo* studies using different animal models [6, 12, 20]; however, the molecular or cellular mechanisms and the derived guidance for supporting this therapeutic use of shikonin are not known in detail. In

fact, some of the reported effects of shikonin, including anti-inflammatory [4, 6, 7] and antiangiogenesis activities [4, 42], may be considered physiologically or biochemically contradictory to its wound-healing activity. In the present study, the specific effect of shikonin on the EMT process and on

related microRNA expression has provided us with valuable information and new insights into the wound-healing activities of shikonin. In wound-healing research, EMT has been shown as a very important cell transdifferentiation process for both acute and fibrotic cutaneous wound-healing activities in human skin [34]. On the other hand, because EMT activity also plays a role in carcinogenesis and neoplasia, there may be concern that shikonin-induced EMT activity could lead to carcinogenesis of local tumors. In 2009, EMTs were classified into three different biological subtypes based on various biological contexts [47, 48]. Among these subtypes, the EMTs associated with wound healing, tissue regeneration, and organ fibrosis are classified as type 2, whereas EMTs assigned for activities in development of localized tumors are classified as type 3. Although the specific signals that delineate the EMTs in the three discrete settings are not totally clear, it is known that the features of EMTs (expression of FSP-1, vimentin, and cell proliferation activity) are transient and reversible for the type 1 and type 2 EMT processes, but not for type 3 EMT. In this study, we observed that specific EMT features were readily detectable during the wound-healing process of mouse skin tissues (data not shown). Moreover, to our knowledge studies indicating the “carcinogenesis-promoting” activity of shikonin have not been previously reported. Taken together, we therefore consider that the beneficial effect of shikonin on skin wound-healing is mainly related to the type 1 EMT process. To add to our current findings, in the future we will investigate the specific targets of shikonin and the mechanistic roles of the specific molecular or cellular components at the tissue/organ level in shikonin-enhanced wound-healing activity.

5. Conclusions

In conclusion, we characterized the specific effects of shikonin in skin wound-healing activities at the molecular and cellular levels by probing the cell transdifferentiation processes and microRNA regulation. We consider that comprehensive analyses using different omics approaches in our *in vivo* experimental system can be usefully employed for integrated evaluation of the pharmacogenomic activities of the shikonins and other phytochemicals from various traditional medicinal herbs that are routinely used as remedies.

Conflict of Interests

The authors declare no conflict of interests.

Acknowledgments

This work was supported by the Academia Sinica Investigator Award (2010–2014), Taiwan. The authors also thank the Febit Company for technical assistance in performing microRNA array tests, Dr. Vani Staniforth for early experimental input on this project, and Ms. Miranda Loney and Dr. Heiko Kuhn of Academia Sinica for paper editing.

References

- [1] K. Touno, J. Tamaoka, Y. Ohashi, and K. Shimomura, “Ethylene induced shikonin biosynthesis in shoot culture of *Lithospermum erythrorhizon*,” *Plant Physiology and Biochemistry*, vol. 43, no. 2, pp. 101–105, 2005.
- [2] F. E. Koehn and G. T. Carter, “The evolving role of natural products in drug discovery,” *Nature Reviews Drug Discovery*, vol. 4, no. 3, pp. 206–220, 2005.
- [3] H. Chung, M. Kang, C. Cho et al., “Inhibition of lipopolysaccharide and interferon-gamma-induced expression of inducible nitric oxide synthase and tumor necrosis factor-alpha by *Lithospermum radix* in mouse peritoneal macrophages,” *Journal of Ethnopharmacology*, vol. 102, no. 3, pp. 412–417, 2005.
- [4] X. Chen, L. Yang, J. J. Oppenheim, and O. M. Zack Howard, “Cellular pharmacology studies of shikonin derivatives,” *Phytotherapy Research*, vol. 16, no. 3, pp. 199–209, 2002.
- [5] M. Hayashi, S. Tsurumi, and H. Fujimura, “Pharmacological activities of *Lithospermum root*,” *Japanese Journal of Pharmacology*, vol. 65, pp. 195–196, 1969.
- [6] V. Staniforth, S. Wang, L. Shyur, and N. Yang, “Shikonins, phytochemicals from *Lithospermum erythrorhizon*, inhibit the transcriptional activation of human tumor necrosis factor alpha promoter *in vivo*,” *Journal of Biological Chemistry*, vol. 279, no. 7, pp. 5877–5885, 2004.
- [7] S. Chiu and N. Yang, “Inhibition of tumor necrosis factor- α through selective blockade of Pre-mRNA splicing by shikonin,” *Molecular Pharmacology*, vol. 71, no. 6, pp. 1640–1645, 2007.
- [8] W. Han, L. Li, S. Qiu et al., “Shikonin circumvents cancer drug resistance by induction of a necroptotic death,” *Molecular Cancer Therapeutics*, vol. 6, no. 5, pp. 1641–1649, 2007.
- [9] K. Nakaya and T. Miyasaka, “A shikonin derivative, β -hydroxyisovalerylshikonin, is an ATP-non-competitive inhibitor of protein tyrosine kinases,” *Anti-Cancer Drugs*, vol. 14, no. 9, pp. 683–693, 2003.
- [10] S. Li, *Ben Cao Gang Mu*, vol. 1, 1590.
- [11] B. S. Kaith, N. S. Kaith, and N. S. Chauhan, “Anti-inflammatory effect of *Arnebia euchroma* root extracts in rats,” *Journal of Ethnopharmacology*, vol. 55, no. 1, pp. 77–80, 1996.
- [12] I. Sakaguchi, M. Tsujimura, N. Ikeda et al., “Granulomatous tissue formation of shikon and shikonin by air pouch method,” *Biological and Pharmaceutical Bulletin*, vol. 24, no. 6, pp. 650–655, 2001.
- [13] E. D. Hay, “An overview of epithelio-mesenchymal transformation,” *Acta Anatomica*, vol. 154, no. 1, pp. 8–20, 1995.
- [14] R. Levayer and T. Lecuit, “Breaking down EMT,” *Nature Cell Biology*, vol. 10, no. 7, pp. 757–759, 2008.
- [15] M. Zeisberg and R. Kalluri, “Fibroblasts emerge via epithelial-mesenchymal transition in chronic kidney fibrosis,” *Frontiers in Bioscience*, vol. 13, no. 18, pp. 6991–6998, 2008.
- [16] H. Acloque, M. S. Adams, K. Fishwick, M. Bronner-Fraser, and M. A. Nieto, “Epithelial-mesenchymal transitions: the importance of changing cell state in development and disease,” *Journal of Clinical Investigation*, vol. 119, no. 6, pp. 1438–1449, 2009.
- [17] G. Moreno-Bueno, H. Peinado, P. Molina et al., “The morphological and molecular features of the epithelial-to-mesenchymal transition,” *Nature protocols*, vol. 4, no. 11, pp. 1591–1613, 2009.
- [18] Y. Katoh and M. Katoh, “Hedgehog signaling, epithelial-to-mesenchymal transition and miRNA (review),” *International Journal of Molecular Medicine*, vol. 22, no. 3, pp. 271–275, 2008.

- [19] P. A. Gregory, A. G. Bert, E. L. Paterson et al., "The miR-200 family and miR-205 regulate epithelial to mesenchymal transition by targeting ZEB1 and SIP1," *Nature Cell Biology*, vol. 10, no. 5, pp. 593–601, 2008.
- [20] J.-H. Wang, K.-F. Lin, S. A. Benson et al., "Tissue array transgene expression system for the evaluation of effect of medicinal herbs on wound-healing," *Journal of Genetics and Molecular Biology*, vol. 14, no. 3, pp. 133–134.
- [21] D. J. Lockhart, H. Dong, M. C. Byrne et al., "Expression monitoring by hybridization to high-density oligonucleotide arrays," *Nature Biotechnology*, vol. 14, no. 13, pp. 1675–1680, 1996.
- [22] C. Wang, M. Chiao, P. Yen et al., "Modulatory effects of *Echinacea purpurea* extracts on human dendritic cells: a cell- and gene-based study," *Genomics*, vol. 88, no. 6, pp. 801–808, 2006.
- [23] C. Wang, V. Staniforth, M. Chiao et al., "Genomics and proteomics of immune modulatory effects of a butanol fraction of *echinacea purpurea* in human dendritic cells," *BMC Genomics*, vol. 9, article 479, 2008.
- [24] S. Yin, W. Wang, P. Wang et al., "Stimulatory effect of *Echinacea purpurea* extract on the trafficking activity of mouse dendritic cells: revealed by genomic and proteomic analyses," *BMC Genomics*, vol. 11, no. 1, article 612, 2010.
- [25] V. Ambros, "A hierarchy of regulatory genes controls a larva-to-adult developmental switch in *C. elegans*," *Cell*, vol. 57, no. 1, pp. 49–57, 1989.
- [26] V. Ambros, "The functions of animal microRNAs," *Nature*, vol. 431, no. 7006, pp. 350–355, 2004.
- [27] H. R. Horvitz, P. W. Sternberg, I. S. Greenwald, W. Fixsen, and H. M. Ellis, "Mutations that affect neural cell lineages and cell fates during the development of the nematode *Caenorhabditis elegans*," *Cold Spring Harbor Symposia on Quantitative Biology*, vol. 48, part 2, pp. 453–463, 1983.
- [28] L. Song and R. S. Tuan, "MicroRNAs and cell differentiation in mammalian development," *Birth Defects Research C*, vol. 78, no. 2, pp. 140–149, 2006.
- [29] Y. Li, Q. Zhang, X. Yin et al., "Generation of iPSCs from mouse fibroblasts with a single gene, Oct4, and small molecules," *Cell Research*, vol. 21, no. 1, pp. 196–204, 2011.
- [30] Y. Zhao, X. Yin, H. Qin et al., "Two supporting factors greatly improve the efficiency of human iPSC generation," *Cell Stem Cell*, vol. 3, no. 5, pp. 475–479, 2008.
- [31] S. Griffiths-Jones, H. K. Saini, S. van Dongen, and A. J. Enright, "miRBase: tools for microRNA genomics," *Nucleic Acids Research*, vol. 36, no. 1, Database issue, pp. D154–D158, 2008.
- [32] W. Huber, A. von Heydebreck, H. Sültmann, A. Poustka, and M. Vingron, "Variance stabilization applied to microarray data calibration and to the quantification of differential expression," *Bioinformatics*, vol. 18, supplement 1, pp. S96–S104, 2002.
- [33] S. Vorwerk, K. Ganter, Y. Cheng, J. Hoheisel, P. F. Stähler, and M. Beier, "Microfluidic-based enzymatic on-chip labeling of miRNAs," *New Biotechnology*, vol. 25, no. 2-3, pp. 142–149, 2008.
- [34] C. Yan, W. A. Grimm, W. L. Garner et al., "Epithelial to mesenchymal transition in human skin wound healing is induced by tumor necrosis factor- α through bone morphogenic protein-2," *American Journal of Pathology*, vol. 176, no. 5, pp. 2247–2258, 2010.
- [35] D. G. Greenhalgh, K. H. Sprugel, M. J. Murray, and R. Ross, "PDGF and FGF stimulate wound healing in the genetically diabetic mouse," *American Journal of Pathology*, vol. 136, no. 6, pp. 1235–1246, 1990.
- [36] S. Schuierer, L. Tranchevent, U. Dengler, and Y. Moreau, "Large-scale benchmark of Endeavour using MetaCore maps," *Bioinformatics*, vol. 26, no. 15, Article ID btq307, pp. 1922–1923, 2010.
- [37] R. W. Carthew and E. J. Sontheimer, "Origins and Mechanisms of miRNAs and siRNAs," *Cell*, vol. 136, no. 4, pp. 642–655, 2009.
- [38] C. M. Croce and G. A. Calin, "miRNAs, cancer, and stem cell division," *Cell*, vol. 122, no. 1, pp. 6–7, 2005.
- [39] A. Khvorova, A. Reynolds, and S. D. Jayasena, "Functional siRNAs and miRNAs exhibit strand bias," *Cell*, vol. 115, no. 2, pp. 209–216, 2003.
- [40] E. J. Sontheimer and R. W. Carthew, "Silence from within: endogenous siRNAs and miRNAs," *Cell*, vol. 122, no. 1, pp. 9–12, 2005.
- [41] X. Chen, J. Oppenheim, and O. M. Z. Howard, "Shikonin, a component of antiinflammatory Chinese herbal medicine, selectively blocks chemokine binding to CC chemokine receptor-1," *International Immunopharmacology*, vol. 1, no. 2, pp. 229–236, 2001.
- [42] T. Hisa, Y. Kimura, K. Takada, F. Suzuki, and M. Takigawa, "Shikonin, an ingredient of *Lithospermum erythrorhizon*, inhibits angiogenesis in vivo and in vitro," *Anticancer Research*, vol. 18, no. 2A, pp. 783–790, 1998.
- [43] S. A. Eming, T. Krieg, and J. M. Davidson, "Inflammation in wound repair: molecular and cellular mechanisms," *Journal of Investigative Dermatology*, vol. 127, no. 3, pp. 514–525, 2007.
- [44] M. Spies, O. Nestic, R. E. Barrow, J. R. Perez-Polo, and D. N. Herndon, "Liposomal IGF-1 gene transfer modulates pro- and anti-inflammatory cytokine mRNA expression in the burn wound," *Gene Therapy*, vol. 8, no. 18, pp. 1409–1415, 2001.
- [45] X. Wang, G. Han, P. Owens, Y. Siddiqui, and A. G. Li, "Role of TGF β -mediated inflammation in cutaneous wound healing," *Journal of Investigative Dermatology Symposium Proceedings*, vol. 11, no. 1, pp. 112–117, 2006.
- [46] S. Chiu, S. Tsao, P. Hwang, S. Vanisree, Y. Chen, and N. Yang, "Differential functional genomic effects of anti-inflammatory phytochemicals on immune signaling," *BMC Genomics*, vol. 11, no. 1, article 513, 2010.
- [47] M. Zeisberg and E. G. Neilson, "Biomarkers for epithelial-mesenchymal transitions," *Journal of Clinical Investigation*, vol. 119, no. 6, pp. 1429–1437, 2009.
- [48] R. Kalluri and R. A. Weinberg, "The basics of epithelial-mesenchymal transition," *Journal of Clinical Investigation*, vol. 119, no. 6, pp. 1420–1428, 2009.

Review Article

Exploring the Ligand-Protein Networks in Traditional Chinese Medicine: Current Databases, Methods, and Applications

Mingzhu Zhao, Qiang Zhou, Wanghao Ma, and Dong-Qing Wei

National Key Laboratory of Microbial Metabolism and College of Life Sciences and Biotechnology, Shanghai Jiao Tong University, 800 Dongchuan Road, Minhang District, Shanghai 200240, China

Correspondence should be addressed to Dong-Qing Wei; dqwei@sjtu.edu.cn

Received 24 February 2013; Revised 6 May 2013; Accepted 7 May 2013

Academic Editor: Weidong Zhang

Copyright © 2013 Mingzhu Zhao et al. This is an open access article distributed under the Creative Commons Attribution License, which permits unrestricted use, distribution, and reproduction in any medium, provided the original work is properly cited.

The traditional Chinese medicine (TCM), which has thousands of years of clinical application among China and other Asian countries, is the pioneer of the “multicomponent-multitarget” and network pharmacology. Although there is no doubt of the efficacy, it is difficult to elucidate convincing underlying mechanism of TCM due to its complex composition and unclear pharmacology. The use of ligand-protein networks has been gaining significant value in the history of drug discovery while its application in TCM is still in its early stage. This paper firstly surveys TCM databases for virtual screening that have been greatly expanded in size and data diversity in recent years. On that basis, different screening methods and strategies for identifying active ingredients and targets of TCM are outlined based on the amount of network information available, both on sides of ligand bioactivity and the protein structures. Furthermore, applications of successful *in silico* target identification attempts are discussed in detail along with experiments in exploring the ligand-protein networks of TCM. Finally, it will be concluded that the prospective application of ligand-protein networks can be used not only to predict protein targets of a small molecule, but also to explore the mode of action of TCM.

1. Introduction

Drug discovery was once an empirical process when the effect of the medicine was purely based on phenotype readout, while the mode of action of drug molecules remained unknown. Later, reductionists began to research on the molecular mechanism of the drug-target interactions, believing that the drug is like a magic bullet towards the functioning targets [1]. This means that a drug takes action on the disease by interacting with one specific therapeutic target. The idea of each drug being like a key (or ligand) matching each “lock” (or protein) has guided the modern drug discovery practice for the last several decades. However, in the recent years, more and more evidence has shown that many drugs exert their activities by modulating multitargets [2–4]. Besides, some drugs interact with antitargets and induce strong side effects [5, 6]. Therefore, it is inappropriate to stick to the paradigm that drug interacts with only one target. How to modulate a set of targets to achieve efficacy while avoiding others to reduce the risk of side effects remains a central challenging task for pharmaceutical industry.

The traditional Chinese medicine (TCM), which has been widely used in China as well as in other Asian countries for a long history, is considered to be the pioneer of the “multicomponent-multitarget” pharmacology [7, 8]. Thousands of years of clinical practices in TCM have accumulated a considerable number of formulae that exhibit reliable *in vivo* efficacy and safety. Based on the methodology of holism, hundreds of different components in a TCM prescription can cure the diseases or relieve the patients by modulating a serial of potential therapeutic targets [9].

In recent years, great efforts have been made on modernization of TCM, most on identification of effective ingredients, and ligands in TCM formulae and functioning targets [10, 11]. Several databases of TCM formulae, ingredients and compounds with chemical structures have been established such as traditional Chinese medicine database (TCMD) [12]. However, the molecular mechanisms responsible for their therapeutic effectiveness are still unclear. On one hand, experimental validation of new drug-target interactions still remains very limiting and expensive, and very few new drugs and targets are identified as clinical applications every

TABLE 1: Basic information for main TCM databases.

Database	Description	URL or ref.
Traditional Chinese medicine database (TCMD)	6760 herbs, 23,033 compounds	[12]
Chinese herb constituents database (CHCD)	240 herbs, 8264 compounds	[15]
3D structural database of biochemical components	2073 herbs, 10,564 compounds	[16]
TCM database@Taiwan	453 herbs, 20,000 compounds	[17]
Traditional Chinese medicine information database (TCM-ID)	1197 formulae, 1313 herbs, ~9000 compounds	[18]
TCM drugs information system	1712 formulae, 2738 herbs, 16,500 compounds, 868 dietotherapy prescription	[19]
Comprehensive herbal medicine information system for cancer (CHMIS-C)	203 formulae, 900 herbs, 8500 compounds	[20]
China natural products database (CNPD)	45,055 compounds	[21]
Marine natural products database (MNPDP)	8078 compounds, 3200 with bioactivity data	[22]
Bioactive plant compounds database (BPCD)	2794 compounds	[15]
acupuncture.com.au	TCM formulations	http://www.acupuncture.com.au/education/herbs/herbs.html/
Dictionary of Chinese herbs	TCM formulae, toxicity, and side effects	http://alternativehealing.org/chinese_herbs_dictionary.htm/
Plants for a future	Herb medical usage and potential side effects	http://www.pfaf.org/

year [13, 14]. On the other hand, the complex composition and polypharmacology of TCM make it even harder to conduct a full set of experiments between compounds and targets and elucidate the multitarget mode of action from the holistic view on the biological network level.

On the contrary, *in silico* methods can predict a large number of new drug-target interactions, construct the drug-target networks, and explore the functional mechanism underlying the multicomponent drug combinations at the molecular level. In the present stage, there have already been successful applications in interpreting the action mechanism of TCM from the perspective of drug-target networks, although the quantity is limited. Compared with the huge amounts of TCM formulae and components, only a small portion of drug-target pairs has been validated by the laborious and costly biochemical experiments. This motivates the needs for constructing models that could predict genuine interacting pairs between ligands and targets, based on the existing small number of known ligand-target bindings.

In this paper, we firstly investigate TCM databases for *in silico* methods that have been greatly expanded in size and data diversity in recent years. On that basis, different screening methods and strategies for identifying active ingredients and targets of TCM are outlined based on the amount of information available, both on sides of ligand bioactivity and the protein structures. Finally, successful applications in this area have been summarized and reviewed, including experimental and computational examples. Learning from the methods in modern western medicine (WM), different computing models and strategies can be used to confirm the effective components and related targets in TCM in order to build the ligand-target networks. One of the research

directions of the modernization of TCM is to clarify the mode of action of TCM based on ligand-protein networks.

2. Databases for TCM

Data availability is the first consideration before any virtual screening or data-mining task could be undertaken. The TCM databases can be classified in accordance with several categories, namely, formulae, herbs, and compounds. The formula of TCM is a combination of herbs for treating a disease, while compounds are the bioactive molecules within herbs. In this section, we have summarized a list of databases for TCM herbs, formulations, and compounds, as shown in Table 1.

The elementary units of TCM databases are compounds, the bioactive components that exert efficacy through binding to therapeutic targets. Most of the compounds in TCM databases have two-dimensional structure, while some of them have three-dimensional structures deduced by force field. In most TCM databases, the information of both herbs and compounds are collected while some even have formulae information as well.

The traditional Chinese medicine database (TCMD) contains 23,033 chemical constituents and over 6760 herbs that mainly come from Yan et al. [12]. The query keywords for the database include molecular formula, substructure, botanical identity, CAS number, pharmacological activity, and traditional indications. Only a small proportion of herbs in TCMD have full coverage of compounds while most have partial coverage. Chinese herb constituents database (CHCD) contains information on 8264 compounds derived from 240 commonly used herbs with both botanical and

Chinese pinyin names, the part of the herbs that contain the compounds, pharmacological and toxicological information, and other useful information [15]. Qiao et al. [16] have developed 3D structural database of biochemical components which covers 10,564 constituents from 2073 herbs with 3D structures built and optimized using the MMFF94 force field [23]. This database uses MySQL as the data engine and contains detailed information such as basic molecular properties, optimized 3D structures, herb origin, and clinical effects. The TCM database@Taiwan was reported to be the world's largest traditional Chinese medicine database. The web-based database contains more than 20,000 pure compounds isolated from 453 TCM herbs [17]. Both simple and advanced query methods are acceptable in terms of molecular properties, substructures, TCM ingredients, and TCM classifications.

In addition to herbs and compounds, traditional Chinese medicine information database (TCM-ID) [18], TCM drugs information system [19], and comprehensive herbal medicine information system for cancer (CHMIS-C) [20] also collect the information of TCM formulae. TCM-ID is developed by Zhejiang University together with National University of Singapore on all aspects of TCM herbs. TCM-ID currently takes in 1197 TCM formulae, 1313 herbs, and around 9000 compounds. It covers ~4000 disease conditions, and more than half of the compounds have valid 3D structures. The data are collected from credible TCM books as well as journals, and the records can be retried by different sets of query keywords. TCM drugs information system based on networks of five large databases has also been developed [19]. It includes information of 1712 formulae, 2738 herbs, 16,500 compounds, and 868 dietotherapy prescriptions from the integration of Chinese herb database, Chinese patent medicine database, effective components database of Chinese herbs, Chinese medical dietotherapy prescription database, and Chinese medical recipe database. Herbal medicine information system for cancer (CHMIS-C) integrates the information of 203 formulae that are commonly used to treat cancer clinically as well as 900 herbs and 8500 compounds. The compounds in this database are linked to the entries in National Cancer Institute's database and drugs approved by the U.S. Food and Drug Administration.

The China natural products database (CNPD) [21], marine natural products database (MNPd) [22], and bioactive plant compounds database (BPCD) [15] only focus on the structures of the compounds in TCM and do not contain pertinent information on formulae and herbs. CNPD is built to meet the needs for drug discovery using natural products including TCM and collects the 2D and 3D structures of more than 45,055 compounds. MNPd has a collection of 8078 compounds from 10,000 marine natural products, of which 3200 have bioactivity data. BPCD contains information on 2794 active compounds against 78 molecular targets, as well as the subunits of the target structures to which the compounds bind.

There are other databases on the internet focusing only on the clinical efficacy or side effects of formulae and herbs, without details of compounds. acupuncture.com.au collects the TCM formulae according to their clinical action and efficacy. Both the English and Chinese names of TCM herbs

are recorded to facilitate studies using both traditional and modern methods. The dictionary of Chinese herbs contains information on both clinical usage and side effects of the TCM herbs. It also includes the samples of TCM formulae for treating diseases such as cancer, dengue fever, diabetes, and hepatitis B. Besides, the compatibility of TCM herbs and certain drugs is listed to provide biochemical explanation for drug designers. The plants for a future database allows querying of herbs with special medicinal usage and also lists the potential side effects, medical usage, and physical characteristics.

3. *In Silico* Methods for Ligand-Protein Interactions

The computational methods for drug discovery based on ligand-protein networks have been increasingly developed and applied in the area of TCM and other drugs in recent years [7, 8]. These methods mainly fall into the territories of ligand-based approach, target-based approach, and machine learning.

3.1. Ligand-Based Approach. The ligand-based approach, also known as the chemical approach, is to reorganize pharmacological characteristics and protein associations, by means of ligand similarities rather than genomic space such as sequence, structural or pathway information. The basic assumption for ligand-based approach is that, regardless that similar chemical structures may interact with proteins in different ways, similar ligands tend to bind to similar targets more than not [24]. The general practice of ligand-based approach is to describe ligands with chemical descriptors, and calculate the similarity coefficient (most commonly, Tanimoto coefficient or T_C [25–27]) between ligands. With the ligand-based descriptions of a protein, one can predict which targets are likely to be hit by a ligand, given its known structure.

In the area of ligand-based virtual screening, researchers have tried to evaluate whether novel ligand-target pairs could be identified, based on the chemical knowledge of ligands and ligand-target interactions. G protein-coupled receptors (GPCRs) are a family of effective drug targets with significant therapeutic value. Many researchers have built support vector machine (SVM) models as well as substructural analysis to describe GPCRs from the perspective of ligand chemogenomics [28]. In particular, the deorphanization of receptors without known ligands was employed using the ligands of the related receptors. For 93% of the orphan receptors, the prediction results are better than random, while for 35% the performance was good.

A powerful ligand-based prediction method based on features of protein ligands is the similarity ensemble approach (SEA), which was originally used to investigate protein similarity based on chemical similarity between their ligand sets with the main idea that similar ligands might tend to share same targets [3]. SEA calculates Z -score and E -value by summing up the T_C over a threshold between two ligand sets as indicators to evaluate the possible interaction between two ligand sets in a way similar to BLAST. The similarity

threshold for T_C is chosen in a way that the Z-score best observes the extreme value distribution (EVD). This method was then applied to predict new molecular targets for known drugs [29]. The author investigated 3000 FDA-approved drugs against hundreds of targets and found 23 new cases of drug-target interactions. By *in vitro* experiments, five of them were validated to be positive with affinities less than 100 nM. Besides Keiser's research, SEA was also used to investigate the off-target effect of some commercial available drugs against the target protein farnesyltransferase (PFTase) [30], and two drugs loratadine and miconazole were found to be able to bind to PFTase.

The pharmacophore model is perhaps the most widely used methods that make use of the 3D structure representations of molecules [31]. A pharmacophore is defined to be the molecular features pertinent to bioactivity aligned in three-dimensional spaces, including hydrogen bonding, charge transfer, and electrostatic and hydrophobic interactions [32]. The underlying methodology of pharmacophore model was defined by different researchers [33]. Recently, this model was successfully applied in mesangial cell proliferation inhibitor discovery and virtual screening of potential ligands for many targets such as HIV integrase and CCR5 antagonist [34–37]. In 3D pharmacophore model, the molecular spatial features and volume constraints represent the intrinsic interactions of small bioactive ligands with protein receptors. Wolber and Langer tried to extract ligand pharmacophores from protein cavities based on a defined set of six types of chemical structures [38] and develop the algorithms for ligand extraction and interpretation as well as pharmacophore creation for multiple targets.

Pharmacophore screening only considers those compounds who are direct mimics of the ligand from which the pharmacophore has been generated and may neglect the other positive binding modes as well. In fact, the pharmacophore model is limited to only one mode of action for small molecules [39]. However, this limitation can be conquered by combining multiple pharmacophore models with different modes of action. This method is called virtual parallel screening and has been successfully applied to the identification of natural products' activity [39, 40]. In such work, The PDB-based pharmacophores were firstly used for target fishing for TCM constituents. Results showed that 16 constituents of *Ruta graveolens* were screened against a database of pharmacophores, and good congruity was found between the potential predictions and their corresponding IC_{50} values.

Quantitative structure-activity relationships (QSARs) were first established in the early 1960s when computational means were used to quantitatively describe pharmacodynamics and pharmacokinetic effects in biology systems and the chemical structures of compounds [41]. Generally speaking, any mathematical model or statistical method that builds relationship between molecular structures and biological properties may be considered as QSAR. The idea of QSAR is easy while training and application of QSAR is much difficult since similar structures may interact with totally different targets due to the diversity and complexity of biology [42]. Furthermore, the intrinsic noise in data to describe both the

chemical space and biological effects brings much trouble in accurate modeling [43]. Despite these difficulties, in case robust biological data is available and few outliers coexist, thousands of QSAR models have been generated and stored in related database in the past 40 years [44, 45].

3.2. Target-Based Approach. The target-based approach predicts ligand-target interactions by the structural information of protein targets as well as ligands. The target-based approach depends highly on the availability of the structural information of targets, either from wet experiments or numerical simulations [46, 47]. On one hand, these methods aim to predict the conformation and orientation of the ligand within the protein cavity. On the other hand, the binding affinity of the ligand and protein is simulated with scoring functions. The main target-based approach is docking, which predicts the preferred orientation of one molecule to another when they bind to each other to form a stable complex [48]. Usually, docking is implemented to search appropriate ligands for known targets with the lowest fitting energy. On the contrary, inverse docking seeks to fish targets from known ligands "from scratch" and also plays an important role in virtual screening.

Despite more than 20 years of research, docking and scoring ligands with proteins are still challenging processes and the performance is highly dependent on targets [49–51]. Docking cannot be applied to proteins whose 3D structures are not identified [52]. The high-resolution structure of the protein target is preferably obtained from X-ray crystallography and NMR spectroscopy. However, approximately half of the currently approved drugs bind to the membrane proteins, whose structures are extremely difficult to be acquired experimentally. Alternatively, homology modeling is usually adopted to build a putative geometry and docking cavity [53]. Besides, threading and ab initio structure prediction together with molecular dynamics (MD) and Monte Carlo simulations are utilized to predict the target structures. However, the fidelity of homology modeling, threading, and ab initio structures is still questioned by many researchers. Other important challenges of docking are the dynamic behavior, the large number of degrees of freedom, and the complexity of the potential energy surface. This confines docking to be a low-throughput method on a very small scale, which fails to predict interactions on the level of millions of ligands and targets.

To alleviate the situation that docking depends on the nature of targets, multiple active sites have been used to compensate the ligand-dependent biases, and the consensus scoring has been also suggested to reduce the false positives in virtual screening [54]. The accuracy of scoring functions still remains the main weakness of docking approach [55]. Also, docking is starting to adopt the conformation information derived from protein-bound ligands as a strategy to overcome the limitations of current scoring functions and can predict the orientation of the ligands into the protein cavity [56]. Besides, molecular-dynamics-assisted docking method has been applied in virtual screening against the individual targets in HIV to search for multitarget drug-like agents, and KNI-765 was identified to be potential inhibitor [57].

Regardless of all limitations, virtual screening based on docking and inverse docking has been successfully utilized to identify and predict novel bioactive compounds in the past 10 years. Using the combinatorial small molecule growth algorithm, Grzybowski applied the docking to the design of picomolar ligands for the human carbonic anhydrase II [58, 59]. Inverse docking was firstly developed to identify multiple proteins to which a small molecule can bind or weakly bind. In some cases, the bioactivity of the TCM compounds is well recognized, while the underlying mode of action is not very clear. In 2001, INVDOCK [60] has been developed to search for the targets for TCM constituents and employed a database of protein cavities derived from PDB entries. The results of inverse docking involving multiple-conformer shape-matching alignment showed that 50% of the computer-predicted potential protein targets were implicated or experimentally validated. The same approach was used to determine potential drug toxicity and side effects in early stages of drug development, and results showed that 83% of the experimentally known toxicity and side effects were predicted [61]. Zahler et al. tried the inverse docking method to find potential kinase targets for three Indirubin derivatives and examined 84 unique protein kinases in total [62]. Recently, one indirubin compound was found to possess therapeutic effects against myelogenous leukemia [63].

Docking is usually used as the second step to further validate the ligand-target binding features after the first round of virtual screening by other ligand-based approaches [64–67]. Wei et al. applied the docking together with similarity search and molecular simulation to search for anti-SAS drugs [68], find the binding mechanism of H5N1 influenza virus with ligands [69], detect possible drug leading to Alzheimer's disease [70, 71], and identify the binding sites for several novel amide derivatives in the nicotinic acetylcholine receptors (AChRs) [72].

3.3. Machine Learning. The ligand-based approach and target-based approach predict potential ligand-target bindings by means of chemical similarity and structural information. Machine learning is a high-throughput method of artificial intelligence that enables computers to learn from data of knowns, including ligand chemistry, structural information, and ligand-protein networks, and to predict unknowns, such as new drugs, targets, and drug-target pairs. This method gains stability and credibility and has strong ability for classifications among large numbers of ligand-protein pairs that otherwise would be impossible to be connected based on chemical similarity alone.

Machine learning is to exact features from data automatically by computers [73]. Basically, machine learning can be categorized into unsupervised learning and supervised learning. In unsupervised learning, the objective is to extract and conjecture patterns and interactions among a series of input variables, and there is no outcome to train the input variables. The common approaches in unsupervised learning are clustering, data compression, and outlier detection, such as principal-component-based methods [74]. In supervised learning, the objective is to predict the value of an outcome variable based on the input variables [75]. The data

is commonly divided into training and validation datasets, which are used in turn to finalize a robust model. The variable the supervised model predicts is typically the binding probability of ligands and targets.

Nidhi et al. trained a multiple-category Laplacian-modified naïve Bayesian model from 964 target classes in WOMBAT and predicted the top three potential targets for compounds in MDDR with or without known targets information [76]. On average, the prediction accuracy with compounds with known targets is 77%. Bayesian classifier was usually used in early prediction, while the Winnow algorithm was reported more recently [77]. With the same training datasets, the prediction result is slightly different with the multiple-category Laplacian model. This indicates that it is necessary to apply different prediction methods and make comparisons even on the same training dataset.

The Gaussian interaction profile kernels, which represented the drug-target interactions, were used in regularized least squares combined with chemical and genomic space to achieve the prediction with precision-recall curve (AUPR) up to 92.7 [78]. Based on simple physicochemical properties extracted from protein sequences, the potential drug targets were related to the existing ones by several models [79]. The supervised bipartite graph inference is used to represent the drug interaction networks and can be solely able to predict new interactions, or together with chemical and genomic space [80, 81]. Besides, semisupervised learning method (Laplacian regularized least square FLapRLS) was also explored to effectively predict the results by integration of genomic and chemical space [82].

The support vector machine (SVM) is a powerful classification tool in which appropriate kernel functions are selected to map the data space into higher-dimensional space without increasing the computational difficulties. The performance of SVM is usually stronger than other probability-based models. Wale and Karypis [83] made comparisons between a Bayes classifier together with binary SVM, cascaded SVM, a ranking-based SVM, ranking perception, and the combination of SVM and ranking perception in terms of the ability to predict the targets for small compounds and found that the cascaded SVM has better performance than the Bayes models and that the combination of SVM and ranking perception has the best performance of all. Kuhn et al. developed an SVM model based on the chemical-protein interactions from STITCH [84] using new features from ligand chemical space and interaction networks. Four new D-amino acid oxidase inhibitors were successfully predicted by this model and validated by wet experiments, and one may have a new application in therapy of psychiatric disorders other than being an antineoplastic agent [85].

Random forest, a form of multiple decision trees, recently has been applied to screen TCM database for potential inhibitors against several therapeutically important targets [86]. With the use of binding information from another database, random forest was performed to find multiple hits out of 8264 compounds in 240 Chinese herbs on an unbalanced dataset. Among all the predictions, 83 herb-target predictions were proved by the literature search. Three Potential inhibitors of the human, aromatase enzyme (CYP19)

myricetin, liquiritigenin, and gossypetin, were screened by random forest as well as molecular docking studies. The virtual screening results were subsequently confirmed experimentally by *in vitro* assay [87].

Linear regression models have also been applied to predict ligand-target pairs. Zhao and Li developed a computational framework, drugCIPHER, to infer drug-target interactions based on pharmacology and genomic space [88]. In this framework, three linear regression models were created to relate drug therapeutic similarity, chemical similarity, and target similarity on the basis of a protein-protein interaction network. The drugCIPHER achieved the performance with AUC of 0.988 in the training set and 0.935 in the test set, and 501 new drug-target interactions were found, implying potential novel applications or side effects.

Although machine learning has strong performance in classification of protein-ligand interactions, its shortcoming is obvious. The process of some machine learning methods is implicit, like a black box, from which we cannot have an intuitive biological or physical relevance between proteins and ligands. SVM maps the classification problem into higher space and acquires excellent performance with high computational efficiency. The tradeoff is that it can hardly explicitly create relationship between a protein and a ligand. Therefore, even with a very strong prediction tool, we can hardly move forward with innovations in theory of protein-ligand interactions.

4. Applications of Ligand-Protein Networks in TCM Pharmacology

Network-based pharmacology explores the possibility to develop a systematic and holistic understanding of the mode of actions of multidrugs by considering their multitargets in the context of molecular networks. It has also been suggested that relatively weak patterns of inhibition of many targets may prove more satisfactory than the highly potent single-target inhibitors routinely developed in the course of a drug discovery program [89]. In drug discovery, the use of networks incorporating multiple components and the corresponding multiple target, is one of the driving forces to propel the current development in TCM pharmacology. Several successful examples have been accumulated both in experiments and *in silico* analysis, as shown in Table 2.

4.1. Experimental Study. Many bioactive compounds in TCM herbs may have synergetic effect with many non-TCM drugs in markets. Tannin, a component derived from a TCM, can be combined with HIV triple cocktail therapy to yield everlasting efforts in preventing HIV virus propagation. The underlying mechanism is that tannin suppresses the activity of HIV-1 reverse transcriptase, protease, and integrase and cuts off virus fusion and virus entry into the host cells [90]. Recently, Li et al. proposed a new idea to induce immune tolerance in T cells by using matrine, a chemical derived from the root of *Sophora flavescens* AIT, targeting both the PKC γ pathway and the NFAT pathway in cocktail preparations for treating AIDS [91].

Lam et al. recently showed in murine colon 38 allograft model that a formula containing 4 herbs (PHY906) has synergetic effect on reducing side effects and enhancing efficacy induced by CPT-11, a powerful anticancer agent with strong toxicity. The reason is that PHY906 can repair the intestinal epithelium by facilitating the intestinal progenitor or stem cells and several Wnt signaling components and suppressing a batch of inflammatory responses like factor kB, cyclooxygenase-2, and inducible nitric oxide synthase [92].

Multicomponent and multitarget interactions are the main mode of action for TCM formula, which exerts synergetic effects as a whole preparation rather than the primary active compound in TCM alone. Xie et al. demonstrated that other components in “Qingfu Guanjiesshu” (QFGJS) could effectively influence the pharmacokinetic behavior and metabolic profile of paeonol in rats, indicating the synergy of herbal components. This synergy may be the result of enhanced adsorption of paeonol in the gastrointestinal tract induced by P-glycoprotein-mediated efflux change [93]. Another similar study showed that paeoniflorin from the root of *Paeonia lactiflora* was markedly enhanced when coadministered with sinomenine, the stem of *Sinomenium acutum*. Sinomenine promotes intestinal transportation via inhibition of P-glycoprotein and affects the hydrolysis of paeoniflorin via interaction with b-glycosidase [94].

Huang-Lian-Jie-Du-Tang (HLJDT) is a TCM formula with anti-inflammatory efficacy, but the action mechanism is still not very clear. Zeng et al. investigated the effects of its component herbs and pure components on eicosanoid generation and found out the active components and their precise targets on arachidonic acid (AA) cascade. Results showed that *Rhizoma coptidis* and *Radix scutellariae* were the key herbs responsible for the suppressive effect of HLJDT on eicosanoid generation. Further experiments on the pure components of HLJDT revealed that baicalein derived from *Radix scutellariae* has significant inhibitory effect on 5-LO and 15-LO while coptisine from *Rhizoma coptidis* shows medium inhibitory effects on LTA(4)H. Besides, baicalein and coptisine were proven to have synergetic inhibition on LTB(4) by the rat peritoneal macrophages [95].

A TCM formula, Realgar-Indigo naturalis formula (RIF), was applied to treat Acute promyelocytic leukemia (APL) and showed a high complete remission (CR rate) [96]. In RIF, multiple agents within one formula were found to work synergistically. A small-scale combinational study using Chou and Talalay combination index method was performed and three main active components of RIF and six core proteins they targets in mediating the anti-tumor effect were identified. The main active ingredients of RIF are tetraarsenic tetrasulfide (A), indirubin (I), and tanshinone IIA (T), from Realgar, *Indigo naturalis*, and *Salvia miltiorrhiza*, respectively. A acts as the principal component of the formula, whereas T and I serve as adjuvant ingredients. ATI leads to ubiquitination/degradation of promyelocytic leukemia (PML) retinoic acid receptor oncoprotein, reprogramming of myeloid differentiation regulators, and G1/G0 arrest in APL cells by mediating multiple targets. Using multiomics technologies, Zhang et al. later proved that the combined use of Imatinib and arsenic sulfide from toxic herbal remedy exerted better

TABLE 2: Summary of multi-target drugs/preparations with TCM pharmacology based on ligand-protein networks.

Disease	Methods and experiments	Formula, herbs, and components	TCM pharmacology	Reference
AIDS	Experiments	Tannin	Tannin suppresses the activity of HIV-1 reverse transcriptase, protease, and integrase and cuts off virus fusion and virus entry into the host cells.	[90]
AIDS	Experiments	Matrine from the root of <i>Sophora flavescens</i>	Matrine is effective in inducing T-cell anergy by targeting both the MAPKs pathway and the NFAT pathway.	[91]
Antitumor	Experiments	PHY906: <i>Glycyrrhiza uralensis</i> Fisch (G), <i>Paeonia lactiflora</i> Pall (P), <i>Scutellaria baicalensis</i> Georgi (S), and <i>Ziziphus jujuba</i> Mill (Z).	PHY906 reduces CPT-11-induced gastrointestinal toxicity in the treatment of colon or rectal cancer by several mechanisms. It both repairs the intestinal epithelium by facilitating the generation of intestinal progenitor or stem cells and several Wnt signaling components and suppresses inflammatory responses like factor kB, cyclooxygenase-2, and inducible nitric oxide synthase.	[92]
Anti-inflammatory and analgesic effects	Experiments	Qingfu Guanjiesshu (QFGJS): paeonol and other components	The pharmacokinetic behavior and metabolites of paeonol are greatly promoted by other components in QFGJS. This may be the result of enhanced adsorption of paeonol in the gastrointestinal tract by P-glycoprotein-mediated efflux change.	[93]
Inflammatory and arthritic diseases	Experiments	Paeoniflorin from the root of <i>Paeonia lactiflora</i> and sinomenine from the stem of <i>Sinomenium acutum</i> .	Paeoniflorin is markedly enhanced when coadministered with sinomenine, which promotes intestinal transportation via the inhibition of P-glycoprotein and affects the hydrolysis of paeoniflorin via interaction with b-glycosidase.	[94]
Anti-inflammatory	Experiments	Huang-Lian-Jie-Du-Tang (HLJDT): <i>Rhizoma coptidis</i> and <i>Radix scutellariae</i>	Baicalein derived from <i>Radix scutellariae</i> showed significant inhibitory effect on 5-LO and 15-LO while coptisine from <i>Rhizoma coptidis</i> showed medium inhibitory effects on LTA(4)H.	[95]
Acute promyelocytic leukemia (APL)	Experiments	Realgar-Indigo naturalis: tetraarsenic tetrasulfide (A), indirubin (I), and tanshinone IIA (T)	ATI leads to ubiquitination/degradation of promyelocytic leukemia (PML) retinoic acid receptor oncoprotein, reprogramming of myeloid differentiation regulators, and G1/G0 arrest in APL cells by mediating multiple targets. A acts as the principal component of the formula, whereas T and I serve as adjuvant ingredients.	[96]
Chronic myeloid leukemia (CML)	Experiments	Imatinib (IM) and arsenic sulfide [As(4)S(4) (AS)]	AS targets BCR/ABL through the ubiquitination of key lysine residues, leading to its proteasomal degradation, whereas IM inhibits the PI3K/AKT/mTOR pathway.	[97]
Inflammation	Pharmacophore-assisted docking	Twelve examples of compounds from CHCD	The screened compounds target cyclooxygenases 1 and 2 (COX), p38 MAP kinase (p38), c-Jun terminal-NH(2) kinase (JNK), and type 4 cAMP-specific phosphodiesterase (PDE4).	[98]
Type II diabetes mellitus (T2DM)	Molecular docking (LigandFit), clustering, and drug-target network analysis	676 compounds in eleven herbs from Tang-min-ling Pills	Multiple active components in Tangminling Pills interact with multiple targets. The 37 targets were classified into 3 clusters, and proteins in each cluster were highly relevant to each other. Ten known compounds were selected according to their network attribute ranking in drug-target and drug-drug network.	[99]
Cardiovascular disease	Similarity search and alignment, docking (LigandFit)	Xuefu Zhuyu decoction (XFZYD): 501 compounds, 489 drug/drug-like compounds	Active components in XFZYD mainly target rennin, ACE, and ACE2 in renin-angiotensin system (RAS), which modulates the cardiovascular physiological function.	[100]

TABLE 2: Continued.

Disease	Methods and experiments	Formula, herbs, and components	TCM pharmacology	Reference
9 types of cancer, 5 diseases with dysfunction, and 2 cardiovascular disorders	Distance-based mutual information model (DMIM)	Liu-wei-di-huang formula (LWDH), Shan-zhu-yu (<i>Fructus Corni</i>), Ze-xie (<i>Rhizoma Alismatis</i>), Dan-pi (<i>Cortex Moutan</i>), Di-huang (<i>Radix Rehmaniae</i>), Fu-ling (<i>Poria Cocos</i>) and Shan-yao (<i>Rhizoma Dioscoreae</i>)	The interactions between TCM drugs and disease genes in cancer pathways and neuro-endocrine-immune pathways were inferred to contribute to the action of LWDH formula.	[101]
Cardiovascular diseases	Quantitative composition-activity relationship model (QCAR) (SVM and linear regression)	<i>Shenmai</i> , Qi-Xue-Bing-Zhi-Fang (QXBZF)	The proportion of active components of <i>Shenmai</i> and QXBZF were optimized based on clinical outcome (collateral and infarct rate of heart) using QCAR. The interactions of multiple weak bindings among different compounds and targets may contribute to the synergetic effect of multicomponent drugs.	[102, 103]
Anticoagulant	Network-based computational scheme utilizing multi-target docking score (LigandFit and AutoDock)	Six argatroban intermediates and a series of components from 24 TCMS widely used for cardiac system diseases	A ligand can have impact on multiple targets based on the docking scores, and those with the highest-target network efficiency are regarded as potential anticoagulant agents. Factor Xa and thrombin are two critical targets for anticoagulant compounds and the catalytic reactions they mediate were recognized as the most fragile biological matters in the human clotting cascade system.	[104]
Alzheimers' disease	Systematical target network analysis framework	<i>Ginkgo biloba</i> , <i>Huperzia serrata</i> , <i>Melissa officinalis</i> , and <i>Salvia officinalis</i>	AD-symptoms-associated pathways, inflammation-associated pathways, cancer-associated pathways, diabetes-mellitus-associated pathways, Ca ²⁺ -associated pathways, and cell-proliferation pathways are densely targeted by herbal ingredients.	[105]
Depression	Literature search and network analysis	Hyperforin (HP), hypericin (HY), pseudohypericin (PH), amentoflavone (AF), and several flavonoids (FL) from St. John's Wort (SJW)	Active components in SJW mainly intervene with neuroactive ligand-receptor interaction, the calcium-signaling pathway, and the gap-junction related pathway. Pertinent targets include NMDA-receptor, CRF1 receptor, 5-hydroxytryptamine receptor 1D, and dopamine receptor D1.	[106]
Rheumatoid arthritis (RA)	Integrative platform of TCM network pharmacology including drugCIPHER	Qing-Luo-Yin (QLY), including four herbs, Ku-Shen (<i>Sophora flavescens</i>), Qing-Feng-Teng (<i>Sinomenium acutum</i>), Huang-Bai (<i>Phellodendron chinensis</i>) and Bi-Xie (<i>Dioscorea collettii</i>), which contain several groups of ingredients such as saponins and alkaloids	The target network of QLY is involved in RA-related key processes including angiogenesis, inflammatory response, and immune response. The four herbs in QLY work in concert to promote efficiency and reduce toxicity. Specifically, the synergetic effect of Ku-Shen (<i>jun</i> herb) and Qing-Feng-Teng (<i>chen</i> herb) may come from the feedback loop and compensatory mechanisms.	[107]

therapeutic effects in a BCR/ABL-positive mouse model of chronic myeloid leukemia (CML) than either drug as a single agent. AS targets BCR/ABL through the ubiquitination of key lysine residues, leading to its proteasomal degradation, whereas IM inhibits the PI3 K/AKT/mTOR pathway [97].

4.2. Computational Framework. To target the complex, multifactorial diseases more effectively, the network biology incorporating ligand-protein networks has been applied in multitarget drug development as well as modernization of traditional Chinese medicine in the systematic and holistic way. Zhao et al. reviewed the available disease-associated networks, drug-associated networks that can be used to assist the drug discovery and elaborate the network-based TCM pharmacology [106]. Klipp et al. discussed the possibility to use networks to aid the drug discovery process and focused on networks and pathways in which the components are related by physical interactions or biochemical process [108]. Leung investigated the possibility of network-based intervention for curing system diseases by means of network-based computational models and using medicinal herbs to develop into new wave of network-based multitarget drugs. It was concluded that further integration across various “omics” platform and computational tools would accelerate the drug discovery based on network [109].

Barlow et al. screened among Chinese herbs for compounds that may be active against 4 targets in inflammation, by means of pharmacophore-assisted docking. The results showed that the twelve examples of compounds from CHCD inhibit multiple targets including cyclooxygenases 1 and 2 (COX), p38 MAP kinase (p38), c-Jun terminal-NH(2) kinase (JNK), and type 4 cAMP-specific phosphodiesterase (PDE4). The distribution of herbs containing the predicted active inhibitors was studied in regard to 192 Chinese formulae, and it was found that these herbs were in the formulae that were traditionally used to treat fever, headache, and so on [98].

Many traditional Chinese medicines (TCMs) are effective to relieve complicated diseases such as type II diabetes mellitus (T2DM). Gu et al. employed the molecular docking and network analysis to elucidate the action mechanism of a medical composition-Tangminling Pills which had clinical efficacy for T2DM. It was found that multiple active components in Tangminling Pills interact with multiple targets in the biological network of T2DM. The 37 targets were classified into 3 clusters, and proteins in each cluster were highly relevant to each other. Ten known compounds were selected according to their network attribute ranking in drug-target and drug-drug network [99].

XFZYD, a recipe derived from Wang Q. R. in Qing dynasty, was widely used in cardiac system disease. From similarity search and alignment, the chemical space of compounds in XFZYD was found to share a lot of similarities with that of drug/drug-like ligands set collected from cardiovascular pharmacology, while the chemical pattern in XFZYD is more diverse than that in drug/drug-like ligands for cardiovascular pharmacology. Docking protocol between compounds in XFZYD and targets related to cardiac system disease using LigandFit shows that many molecules have good binding affinity with the targeting enzymes and most have

interactions with more than one single target. The active components in XFZYD mainly target rennin, ACE, and ACE2 in renin-angiotensin system (RAS), which modulates the cardiovascular physiological function. It was proved that promiscuous drugs in TCM might be more effective for treating cardiosystem diseases, which tend to result from multitarget abnormalities, but not from a single defect [100].

A lot of integrative computational tools and models have been developed and widely used to optimize the combination regimen of multicomponents drugs and elucidate the interactive mechanism among ligand-target networks.

Li et al. built a method called distance-based mutual information model (DMIM) to identify useful relationships among herbs in numerous herbal formulae. DMIM combines mutual information entropy and distance between herbs to score herb interactions and construct herb network. Novel antiangiogenic herbs, Vitexicarpin and Timosaponin A-III, were discovered to have synergistic effects. Based on herb network constructed by DMIM from 3865 collateral-related herbs, the interactions between TCM drugs and disease genes in cancer pathways and neuro-endocrine-immune pathways were inferred to contribute to the action of Liu-wei-di-huang formula, one of the most well-known TCM formulae as potential treatment for a variety of diseases including cancer, dysfunction of the neuro-endocrine-immune-metabolism system, and cardiovascular system [101].

Wang et al. adopted a new method based upon lattice experimental design and multivariate regression to model the quantitative composition-activity relationship (QCAR) of *Shenmai*, a Chinese medicinal formula. This new strategy for multicomponent drug design was then successfully applied in searching optimal combination of three key components (PD, PT, and OP) of *Shenmai*. Experimental outcome of infarct rate of heart in mice with different dosage combination of the three components was finally measured, and the fitted relationship equation showed that the optimal values of PD, PT, and OP were 21.6, 39.2, and 39.2%, respectively [102]. The proportion of two active components of Qi-Xue-Bing-Zhi-Fang, PF and FP, was also optimized in similar way using several fitting techniques like linear regression, artificial neural network, and support vector regression [103]. Although the underlying mechanism of drug synergy for the two formulae was still not very clear, the interactions of multiple weak bindings among different compounds and targets might be the contributory factors.

A network-based multitarget computational scheme for the whole efficacy of a compound in a complex disease was developed for screening the anticoagulant activities of a serial of argatroban intermediates and eight natural products, respectively. Aimed at the phenotypic data of drugs, this scheme predicted bioactive compounds by integrating biological network efficiency analysis with multitarget docking score, which evolves from the traditional virtual screening method that usually predicted binding affinity between single drug molecule and target. A ligand can have impact on multiple targets based on the docking scores, and those with highest-target-network efficiency are regarded as potential anticoagulant agents. Factor Xa and thrombin are two critical targets for anticoagulant compounds, and the catalytic

reactions they mediate were recognized as the most fragile biological matters in the human clotting cascade system [104].

Sun et al. presented a systematic target network analysis framework to explore the mode of action of anti-Alzheimer's disease (AD) herb ingredients based on applicable bioinformatics resources and methodologies on clinical anti-AD herbs and their corresponding target proteins [105]. The results showed that, just as many FDA-approved anti-AD drugs do, the compounds of these herbs bind to targets in AD symptoms-associated pathway. Besides, they also interact closely with many successful therapeutic targets related to diseases such as inflammation, cancer, and dementias. This suggests that the possible cross talks between these complicated diseases are prevalent in TCM anti-AD herbs [110]. Moreover, pathways of Ca(2+) equilibrium maintaining, upstream of cell proliferation and inflammation, were found to be intensively hit by the anti-AD herbal ingredients.

Based on the available experimental results, Zhao et al. analyzed the molecular mechanism with the aid of pathways and networks and theoretically proved the multitarget effect of St. John's Wort [106]. A comprehensive literature search was conducted and the neurotransmitter receptors, transporter proteins, and ion channels on which the SJW active compounds show effects were collected. Three main pathways that SJW intervenes were found by mapping these proteins onto KEGG pathways. Active components in SJW mainly intervene with neuroactive ligand-receptor interaction, the calcium-signaling pathway, and the gap-junction-related pathway, pertinent to targets including NMDA-receptor, CRF1 receptor, 5-hydroxytryptamine receptor 1D, and dopamine receptor D1. The networks show that the effect of SJW is similar to that of combinations of different types of antidepressants. However, the inhibitory effects of the SJW on each of the pathway are lower than other individual agents. Accordingly, the significant antidepressant efficacy and lower side effects are due to the synergetic effect of low-dose multitarget actions.

Zhang et al. established an integrative platform of TCM network pharmacology to discover herbal formulae on basis of systematic network. This platform incorporates a set of state-of-the-art network-based methods to explore the action mechanism, identify active ingredients, and create new synergetic combinations of components. The Qing-Luo-Yin (QLY), an antirheumatoid arthritis (RA) formula, was studied comprehensively using the new platform. It is found that the target network of QLY is involved in RA-related key processes including angiogenesis, inflammatory response, and immune response. The four herbs in QLY work in concert to promote efficiency and reduce toxicity, as the *jun*, *chen*, *zuo*, and *shi* in Chinese, respectively. Specifically, the synergetic effect of Ku-Shen (*jun* herb) and Qing-Feng-Teng (*chen* herb) may come from the feedback loop and compensatory mechanisms [107].

5. Discussion and Conclusion

In recent years, the bottleneck in western medicine has brought unprecedented opportunities in TCM research and development. For decades, the fundamental research has

achieved great success and laid the foundation of modern western medicine, and the philosophical idea of "reductionism" was considered to own the credit.

The counterparty of "reductionism" in Chinese medicine is the philosophical idea of holism, which has thousands years of history of practice in China as well as in other Asian countries. Using this methodology, the effectiveness of TCM can only be verified from a large number of clinical trials given the unclear composition and unknown relationship among various components. This implicit effect without clear clarification at the molecular level has been hindering the modernization of TCM. How to learn from the accumulative knowledge of western medicine in order to identify the effective compositions and explore the molecular mechanism of the efficacy is an urgent problem that needs to be solved in TCM.

The hypothesis of "multidrug, multitarget, multigene" in fact bridges the gap between TCM and western medicine and is also a manifestation of unity of opposites on "reductionism" and "holism." TCM uses the holistic method to investigate the effects of multicomponent formula across the whole organism, such as the use of a variety of "ZHENG" in TCM theory [111]. However, the only option we have to uncover the underlying mechanism of TCM at the molecular level is to make use of the theory of reductionism. Of course, for complex systems, the reduction method can only reach to a certain depth since it becomes more troublesome as we get deeper. Therefore, some researchers tend to reduce the mechanism of TCM to the level of "multidrug, multitarget, multigene" at present, and for further reduction to the level of "single-drug, single-target, single-gene," the problem of emergentism [112] in philosophy needs to be addressed properly. The theory of emergentism believes that some unique features or "ultimate features" of a system can never be reduced to properties at lower levels, nor the former can be predicted or explained by the latter, as shown in Figure 1.

So far, ligand-protein network or "multidrug, multitarget, multigene" is one of the few basic modules that can clearly reveal the pharmacology of TCM and is expected to be the future direction of the modernization of TCM. But just relying on experimental scientists to build ligand-protein interactions nonexhaustively will slow down both the modernization of TCM and the development of its industry. Therefore, the use of cross-platform database (TCM compounds and recipe database; see Section 2 in this paper) and the improvement on modeling technique (computational method of ligand-protein interactions; see Section 3 in this paper) will afford the basis of *in silico* research for future modernization and development of TCM. It can be foreseen that one future direction is to use these TCM databases and predictive models to reveal the pharmacological effect of TCM, through the establishment of ligand-protein networks or, "multidrug, multitarget, multigene" relationships. Nevertheless, the pharmacological mechanism of TCM can be very complex and may not be well explained only with the known ligand-protein network. After all, this is a process of reeling silk from cocoons and also one of the best choices we have right now.

The increasing availability of ligand-protein networks is a unique chance to boost success in the modernization of TCM based on the accumulative knowledge of TCM

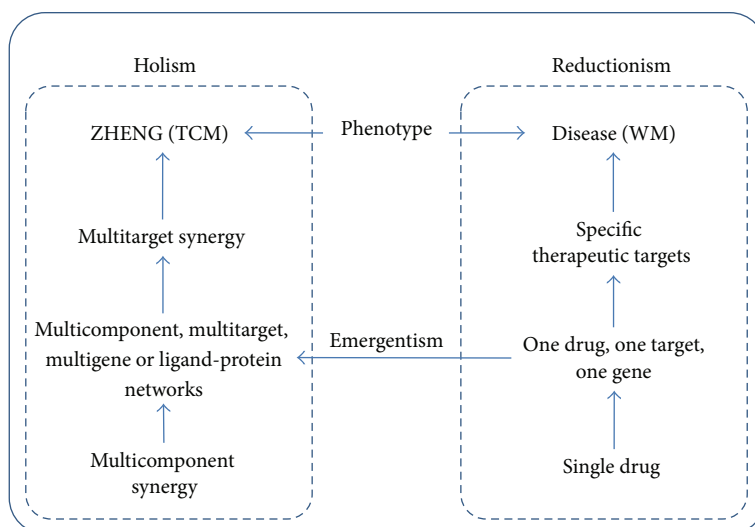


FIGURE 1: Unity of opposites on holism in traditional Chinese medicine and reductionism in western medicine. Emergentism constructs the framework of the understanding of holism in TCM via accumulative practice of reductionism in WM.

formulae and practices based on the assumption that TCM exerts the pharmacological efficacy in multidrug, multitarget way. Although preliminary research has been initiated in this area, there is still a long way to go to further leverage these networks and modeling techniques. Virtual screening and informatics in the drug discovery area have already been proven to be quite useful either to predict potential new drug and target candidates for experimentalists or to explore the functional mechanism at the molecular level. A large number of drug-target interactions have thus been gained and the resulted drug-target networks will also be quite beneficial to investigate the underlying mechanism of multicomponent drugs, such as the TCM. With further applications of these methods in TCM area, we are expecting to reveal the mode of action underlying polypharmacology of TCM. This grants us the possibility to discover novel effective drug leads, understand the synergistic mechanism of drug combinations, and more importantly, develop drug portfolios against epidemic, chronic disease, cancer, and other complex diseases that are almost incurable by western medicine.

Conflict of Interests

The authors declare that they have no conflict of interests.

Acknowledgments

This work is supported by Grants from the National High-Tech R&D Program (863 Program Contract No. 2012AA020307), the National Basic Research Program of China (973 Program) (Contract no. 2012CB721000), the Key Project of Shanghai Science and Technology Commission (Contract no. 11JC1406400), and Ph.D. Programs Foundation of Ministry of Education of China (Contract no., 20120073110057), which were awarded to D. Q. Wei.

References

- [1] S. H. E. Kaufmann, "Paul Ehrlich: founder of chemotherapy," *Nature Reviews Drug Discovery*, vol. 7, no. 5, p. 373, 2008.
- [2] G. V. Paolini, R. H. B. Shapland, W. P. van Hoorn, J. S. Mason, and A. L. Hopkins, "Global mapping of pharmacological space," *Nature Biotechnology*, vol. 24, no. 7, pp. 805–815, 2006.
- [3] M. J. Keiser, B. L. Roth, B. N. Armbruster, P. Ernsberger, J. J. Irwin, and B. K. Shoichet, "Relating protein pharmacology by ligand chemistry," *Nature Biotechnology*, vol. 25, no. 2, pp. 197–206, 2007.
- [4] A. L. Hopkins, "Drug discovery: predicting promiscuity," *Nature*, vol. 462, no. 7270, pp. 167–168, 2009.
- [5] A. Vedani, M. Dobler, and M. A. Lill, "The challenge of predicting drug toxicity *in silico*," *Basic and Clinical Pharmacology and Toxicology*, vol. 99, no. 3, pp. 195–208, 2006.
- [6] T. Klabunde and A. Evers, "GPCR antitarget modeling: pharmacophore models for biogenic amine binding GPCRs to avoid GPCR-mediated side effects," *ChemBioChem*, vol. 6, no. 5, pp. 876–889, 2005.
- [7] S. Ekins, J. Mestres, and B. Testa, "*In silico* pharmacology for drug discovery: methods for virtual ligand screening and profiling," *British Journal of Pharmacology*, vol. 152, no. 1, pp. 9–20, 2007.
- [8] S. Ekins, J. Mestres, and B. Testa, "*In silico* pharmacology for drug discovery: applications to targets and beyond," *British Journal of Pharmacology*, vol. 152, no. 1, pp. 21–37, 2007.
- [9] S. Lukman, Y. He, and S. C. Hui, "Computational methods for Traditional Chinese Medicine: a survey," *Computer Methods and Programs in Biomedicine*, vol. 88, no. 3, pp. 283–294, 2007.
- [10] T. M. Ehrman, D. J. Barlow, and P. J. Hylands, "Phytochemical informatics and virtual screening of herbs used in Chinese medicine," *Current Pharmaceutical Design*, vol. 16, no. 15, pp. 1785–1798, 2010.
- [11] Y. Feng, Z. Wu, X. Zhou, Z. Zhou, and W. Fan, "Knowledge discovery in traditional Chinese medicine: state of the art and

- perspectives," *Artificial Intelligence in Medicine*, vol. 38, no. 3, pp. 219–236, 2006.
- [12] X. Yan, J. Zhou, and Z. Xu, "Concept design of computer-aided study on traditional chinese drugs," *Journal of Chemical Information and Computer Sciences*, vol. 39, no. 1, pp. 86–89, 1999.
- [13] S. J. Haggarty, K. M. Koeller, J. C. Wong, R. A. Butcher, and S. L. Schreiber, "Multidimensional chemical genetic analysis of diversity-oriented synthesis-derived deacetylase inhibitors using cell-based assays," *Chemistry and Biology*, vol. 10, no. 5, pp. 383–396, 2003.
- [14] F. G. Kuruvilla, A. F. Shamji, S. M. Sternson, P. J. Hergenrother, and S. L. Schreiber, "Dissecting glucose signalling with diversity-oriented synthesis and small-molecule microarrays," *Nature*, vol. 416, no. 6881, pp. 653–657, 2002.
- [15] T. M. Ehrman, D. J. Barlow, and P. J. Hylands, "Phytochemical databases of Chinese herbal constituents and bioactive plant compounds with known target specificities," *Journal of Chemical Information and Modeling*, vol. 47, no. 2, pp. 254–263, 2007.
- [16] X. Qiao, T. Hou, W. Zhang, S. Guo, and X. Xu, "A 3D structure database of components from Chinese traditional medicinal herbs," *Journal of Chemical Information and Computer Sciences*, vol. 42, no. 3, pp. 481–489, 2002.
- [17] C. Y. Chen, "TCM Database@Taiwan: the world's largest traditional Chinese medicine database for drug screening *in silico*," *PLoS ONE*, vol. 6, no. 1, Article ID e15939, 2011.
- [18] X. Chen, H. Zhou, Y. B. Liu et al., "Database of traditional Chinese medicine and its application to studies of mechanism and to prescription validation," *British Journal of Pharmacology*, vol. 149, no. 8, pp. 1092–1103, 2006.
- [19] X.-B. Qiao, T.-J. Hou, H.-D. Yu, and X.-J. Xu, "Research and development of traditional Chinese medicine drugs," *Acta Physico-Chimica Sinica*, vol. 18, pp. 394–398, 2002.
- [20] X. Fang, L. Shao, H. Zhang, and S. Wang, "CHMIS-C: a comprehensive herbal medicine information system for cancer," *Journal of Medicinal Chemistry*, vol. 48, no. 5, pp. 1481–1488, 2005.
- [21] J. Shen, X. Xu, F. Cheng et al., "Virtual screening on natural products for discovering active compounds and target information," *Current Medicinal Chemistry*, vol. 10, no. 21, pp. 2327–2342, 2003.
- [22] J. Lei and J. Zhou, "A marine natural product database," *Journal of Chemical Information and Computer Sciences*, vol. 42, no. 3, pp. 742–748, 2002.
- [23] A. Cheng, S. A. Best, K. M. Merz, and C. H. Reynolds, "GB/SA water model for the Merck molecular force field (MMFF)," *Journal of Molecular Graphics and Modelling*, vol. 18, no. 3, pp. 273–282, 2000.
- [24] A. Bender and R. C. Glen, "Molecular similarity: a key technique in molecular informatics," *Organic and Biomolecular Chemistry*, vol. 2, no. 22, pp. 3204–3218, 2004.
- [25] P. Willett, *Similarity and Clustering in Chemical Information Systems*, Chemometrics Series, Research Studies Press, New York, NY, USA, 1987.
- [26] P. Willett, "Searching techniques for databases of two- and three-dimensional chemical structures," *Journal of Medicinal Chemistry*, vol. 48, no. 13, pp. 4183–4199, 2005.
- [27] P. Willett, "Similarity-based virtual screening using 2D fingerprints," *Drug Discovery Today*, vol. 11, no. 23–24, pp. 1046–1053, 2006.
- [28] E. van der Horst, J. E. Peironcelly, A. P. IJzerman et al., "A novel chemogenomics analysis of G protein-coupled receptors (GPCRs) and their ligands: a potential strategy for receptor de-orphanization," *BMC Bioinformatics*, vol. 11, article 316, 2010.
- [29] M. J. Keiser, V. Setola, J. J. Irwin et al., "Predicting new molecular targets for known drugs," *Nature*, vol. 462, no. 7270, pp. 175–181, 2009.
- [30] A. J. DeGraw, M. J. Keiser, J. D. Ochocki, B. K. Shoichet, and M. D. Distefano, "Prediction and evaluation of protein farnesyltransferase inhibition by commercial drugs," *Journal of Medicinal Chemistry*, vol. 53, no. 6, pp. 2464–2471, 2010.
- [31] J. S. Mason, A. C. Good, and E. J. Martin, "3-D pharmacophores in drug discovery," *Current Pharmaceutical Design*, vol. 7, no. 7, pp. 567–597, 2001.
- [32] D. Maclean, J. J. Baldwin, V. T. Ivanov et al., "Glossary of terms used in combinatorial chemistry," *Journal of Combinatorial Chemistry*, vol. 2, no. 6, pp. 562–578, 2000.
- [33] T. Langer and R. D. Hoffmann, *Pharmacophores and Pharmacophore Searches*, Wiley-VCH, Weinheim, Germany; John Wiley & Sons, Chichester, UK, 2006.
- [34] M. C. Nicklaus, N. Neamati, H. Hong et al., "HIV-1 integrase pharmacophore: discovery of inhibitors through three-dimensional database searching," *Journal of Medicinal Chemistry*, vol. 40, no. 6, pp. 920–929, 1997.
- [35] Y. Koide, T. Hasegawa, A. Takahashi et al., "Development of novel EDG3 antagonists using a 3D database search and their structure-activity relationships," *Journal of Medicinal Chemistry*, vol. 45, no. 21, pp. 4629–4638, 2002.
- [36] A. K. Debnath, "Generation of predictive pharmacophore models for CCR5 antagonists: study with piperidine- and piperazine-based compounds as a new class of HIV-1 entry inhibitors," *Journal of Medicinal Chemistry*, vol. 46, no. 21, pp. 4501–4515, 2003.
- [37] Y. Kurogi, K. Miyata, T. Okamura et al., "Discovery of novel mesangial cell proliferation inhibitors using a three-dimensional database searching method," *Journal of Medicinal Chemistry*, vol. 44, no. 14, pp. 2304–2307, 2001.
- [38] G. Wolber and T. Langer, "LigandScout: 3-D pharmacophores derived from protein-bound ligands and their use as virtual screening filters," *Journal of Chemical Information and Modeling*, vol. 45, no. 1, pp. 160–169, 2005.
- [39] J. M. Rollinger, "Accessing target information by virtual parallel screening—the impact on natural product research," *Phytochemistry Letters*, vol. 2, no. 2, pp. 53–58, 2009.
- [40] J. M. Rollinger, D. Schuster, B. Danzl et al., "In silico target fishing for rationalized ligand discovery exemplified on constituents of *Ruta graveolens*," *Planta Medica*, vol. 75, no. 3, pp. 195–204, 2009.
- [41] D. Sharples, "Factors affecting the binding of tricyclic tranquilizers and antidepressants to human serum albumin," *Journal of Pharmacy and Pharmacology*, vol. 28, no. 2, pp. 100–105, 1976.
- [42] R. P. Verma and C. Hansch, "An approach toward the problem of outliers in QSAR," *Bioorganic and Medicinal Chemistry*, vol. 13, no. 15, pp. 4597–4621, 2005.
- [43] J. Polanski, A. Bak, R. Gieleciak, and T. Magdziarz, "Modeling robust QSAR," *Journal of Chemical Information and Modeling*, vol. 46, no. 6, pp. 2310–2318, 2006.
- [44] A. Kurup, "C-QSAR: a database of 18,000 QSARS and associated biological and physical data," *Journal of Computer-Aided Molecular Design*, vol. 17, no. 2–4, pp. 187–196, 2003.
- [45] C. Hansch, D. Hoekman, A. Leo, D. Weininger, and C. D. Selassie, "Chem-bioinformatics: comparative QSAR at the interface between chemistry and biology," *Chemical Reviews*, vol. 102, no. 3, pp. 783–812, 2002.

- [46] B. K. Shoichet, "Virtual screening of chemical libraries," *Nature*, vol. 432, no. 7019, pp. 862–865, 2004.
- [47] G. Klebe, "Virtual ligand screening: strategies, perspectives and limitations," *Drug Discovery Today*, vol. 11, no. 13-14, pp. 580–594, 2006.
- [48] T. Lengauer and M. Rarey, "Computational methods for biomolecular docking," *Current Opinion in Structural Biology*, vol. 6, no. 3, pp. 402–406, 1996.
- [49] D. B. Kitchen, H. Decornez, J. R. Furr, and J. Bajorath, "Docking and scoring in virtual screening for drug discovery: methods and applications," *Nature Reviews Drug Discovery*, vol. 3, no. 11, pp. 935–949, 2004.
- [50] A. R. Leach, B. K. Shoichet, and C. E. Peishoff, "Prediction of protein-ligand interactions. Docking and scoring: successes and gaps," *Journal of Medicinal Chemistry*, vol. 49, no. 20, pp. 5851–5855, 2006.
- [51] P. Manoharan, R. S. K. Vijayan, and N. Ghoshal, "Rationalizing fragment based drug discovery for BACE1: insights from FB-QSAR, FB-QSSR, multi objective (MO-QSPR) and MIF studies," *Journal of Computer-Aided Molecular Design*, vol. 24, no. 10, pp. 843–864, 2010.
- [52] A. C. Cheng, R. G. Coleman, K. T. Smyth et al., "Structure-based maximal affinity model predicts small-molecule druggability," *Nature Biotechnology*, vol. 25, no. 1, pp. 71–75, 2007.
- [53] A. Evers, H. Gohlke, and G. Klebe, "Ligand-supported homology modelling of protein binding-sites using knowledge-based potentials," *Journal of Molecular Biology*, vol. 334, no. 2, pp. 327–345, 2003.
- [54] G. P. A. Vigers and J. P. Rizzi, "Multiple active site corrections for docking and virtual screening," *Journal of Medicinal Chemistry*, vol. 47, no. 1, pp. 80–89, 2004.
- [55] Z. Gao, H. Li, H. Zhang et al., "PDTD: a web-accessible protein database for drug target identification," *BMC Bioinformatics*, vol. 9, article 104, 2008.
- [56] X. Fradera and J. Mestres, "Guided docking approaches to structure-based design and screening," *Current Topics in Medicinal Chemistry*, vol. 4, no. 7, pp. 687–700, 2004.
- [57] J. C. Clemente, L. Govindasamy, A. Madabushi et al., "Structure of the aspartic protease plasmepsin 4 from the malarial parasite *Plasmodium malariae* bound to an allophenylnorstatine-based inhibitor," *Acta Crystallographica Section D: Biological Crystallography*, vol. 62, no. 3, pp. 246–252, 2006.
- [58] B. A. Grzybowski, A. V. Ishchenko, C. Y. Kim et al., "Combinatorial computational method gives new picomolar ligands for a known enzyme," *Proceedings of the National Academy of Sciences of the United States of America*, vol. 99, no. 3, pp. 1270–1273, 2002.
- [59] C. Bissantz, "Conformational changes of G protein-coupled receptors during their activation by agonist binding," *Journal of Receptors and Signal Transduction*, vol. 23, no. 2-3, pp. 123–153, 2003.
- [60] Y. Z. Chen and D. G. Zhi, "Ligand-protein inverse docking and its potential use in the computer search of protein targets of a small molecule," *Proteins*, vol. 43, no. 2, pp. 217–226, 2001.
- [61] Y. Z. Chen and C. Y. Ung, "Prediction of potential toxicity and side effect protein targets of a small molecule by a ligand-protein inverse docking approach," *Journal of Molecular Graphics and Modelling*, vol. 20, no. 3, pp. 199–218, 2001.
- [62] S. Zahler, S. Tietze, F. Totzke et al., "Inverse *in silico* screening for identification of kinase inhibitor targets," *Chemistry and Biology*, vol. 14, no. 11, pp. 1207–1214, 2007.
- [63] M. L. MacDonald, J. Lamerdin, S. Owens et al., "Identifying off-target effects and hidden phenotypes of drugs in human cells," *Nature Chemical Biology*, vol. 2, no. 6, pp. 329–337, 2006.
- [64] W. N. Gao, D. Q. Wei, Y. Li et al., "Agaritin and its derivatives are potential inhibitors against HIV proteases," *Medicinal Chemistry*, vol. 3, no. 3, pp. 221–226, 2007.
- [65] H. Zheng, D. Q. Wei, R. Zhang, C. Wang, H. Wei, and K. C. Chou, "Screening for new agonists against Alzheimer's disease," *Medicinal Chemistry*, vol. 3, no. 5, pp. 488–493, 2007.
- [66] H. Wei, R. Zhang, C. Wang et al., "Molecular insights of SAH enzyme catalysis and implication for inhibitor design," *Journal of Theoretical Biology*, vol. 244, no. 4, pp. 692–702, 2007.
- [67] S. Q. Wang, Q. S. Du, K. Zhao, A. X. Li, D. Q. Wei, and K. C. Chou, "Virtual screening for finding natural inhibitor against cathepsin-L for SARS therapy," *Amino Acids*, vol. 33, no. 1, pp. 129–135, 2007.
- [68] D. Q. Wei, R. Zhang, Q. S. Du et al., "Anti-SARS drug screening by molecular docking," *Amino Acids*, vol. 31, no. 1, pp. 73–80, 2006.
- [69] K. Gong, L. Li, J. F. Wang, F. Cheng, D. Q. Wei, and K. C. Chou, "Binding mechanism of H5N1 influenza virus neuraminidase with ligands and its implication for drug design," *Medicinal Chemistry*, vol. 5, no. 3, pp. 242–249, 2009.
- [70] R. X. Gu, H. Gu, Z. Y. Xie et al., "Possible drug candidates for Alzheimer's disease deduced from studying their binding interactions with $\alpha 7$ nicotinic acetylcholine receptor," *Medicinal Chemistry*, vol. 5, no. 3, pp. 250–262, 2009.
- [71] S. G. Chen, R.-X. Gu, H. Dai, and D.-Q. Wei, "Virtual screening for $\alpha 7$ nicotinic acetylcholine receptor for treatment of Alzheimer's disease," *Journal of Molecular Graphics and Modelling*, vol. 39, pp. 98–107, 2013.
- [72] H. R. Arias, R. X. Gu, D. Feuerbach, B. B. Guo, Y. Ye, and D. Q. Wei, "Novel positive allosteric modulators of the human $\alpha 7$ nicotinic acetylcholine receptor," *Biochemistry*, vol. 50, no. 23, pp. 5263–5278, 2011.
- [73] T. M. Mitchell, *Machine Learning*, McGraw-Hill Series in Computer Science, McGraw-Hill, New York, NY, USA, 1997.
- [74] H. Strömbergsson and G. J. Kleywegt, "A chemogenomics view on protein-ligand spaces," *BMC Bioinformatics*, vol. 10, supplement 6, article S13, 2009.
- [75] L. J. Jensen and A. Bateman, "The rise and fall of supervised machine learning techniques," *Bioinformatics*, vol. 27, no. 24, pp. 3331–3332, 2011.
- [76] Nidhi, M. Glick, J. W. Davies, and J. L. Jenkins, "Prediction of biological targets for compounds using multiple-category bayesian models trained on chemogenomics databases," *Journal of Chemical Information and Modeling*, vol. 46, no. 3, pp. 1124–1133, 2006.
- [77] F. Nigsch, N. J. M. Macaluso, J. B. O. Mitchell, and D. Zmuidinavicius, "Computational toxicology: an overview of the sources of data and of modelling methods," *Expert Opinion on Drug Metabolism and Toxicology*, vol. 5, no. 1, pp. 1–14, 2009.
- [78] T. van Laarhoven, S. B. Nabuurs, and E. Marchiori, "Gaussian interaction profile kernels for predicting drug-target interaction," *Bioinformatics*, vol. 27, no. 21, pp. 3036–3043, 2011.
- [79] Q. Li and L. Lai, "Prediction of potential drug targets based on simple sequence properties," *BMC Bioinformatics*, vol. 8, article 353, 2007.
- [80] Y. Yamanishi, M. Araki, A. Gutteridge, W. Honda, and M. Kanehisa, "Prediction of drug-target interaction networks from the integration of chemical and genomic spaces," *Bioinformatics*, vol. 24, no. 13, pp. i232–i240, 2008.

- [81] K. Bleakley and Y. Yamanishi, "Supervised prediction of drug-target interactions using bipartite local models," *Bioinformatics*, vol. 25, no. 18, pp. 2397–2403, 2009.
- [82] W. Yu, X. Cheng, Z. Li, and Z. Jiang, "Predicting drug-target interactions based on an improved semi-supervised learning approach," *Drug Development Research*, vol. 72, no. 2, pp. 219–224, 2011.
- [83] N. Wale and G. Karypis, "Target fishing for chemical compounds using target-ligand activity data and ranking based methods," *Journal of Chemical Information and Modeling*, vol. 49, no. 10, pp. 2190–2201, 2009.
- [84] M. Kuhn, C. von Mering, M. Campillos, L. J. Jensen, and P. Bork, "STITCH: interaction networks of chemicals and proteins," *Nucleic Acids Research*, vol. 36, no. 1, pp. D684–D688, 2008.
- [85] M. Zhao, H.-T. Chang, Z. Liu, L. Chen, and D. Wei, "Predicting protein-ligand interactions based on chemical preference features with its application to new D-amino acid oxidase inhibitor discovery," *Current Pharmaceutical Design*. In press.
- [86] T. M. Ehrman, D. J. Barlow, and P. J. Hylands, "Virtual screening of Chinese herbs with random forest," *Journal of Chemical Information and Modeling*, vol. 47, no. 2, pp. 264–278, 2007.
- [87] S. Paoletta, G. B. Steventon, D. Wildeboer, T. M. Ehrman, P. J. Hylands, and D. J. Barlow, "Screening of herbal constituents for aromatase inhibitory activity," *Bioorganic and Medicinal Chemistry*, vol. 16, no. 18, pp. 8466–8470, 2008.
- [88] S. Zhao and S. Li, "Network-based relating pharmacological and genomic spaces for drug target identification," *PLoS ONE*, vol. 5, no. 7, Article ID e11764, 2010.
- [89] S. Li and B. Zhang, "Traditional Chinese medicine network pharmacology: theory, methodology and application," *Chinese Journal of Natural Medicines*, vol. 11, no. 2, pp. 110–120, 2013.
- [90] G. Borkow and A. Lapidot, "Multi-targeting the entrance door to block HIV-1," *Current Drug Targets—Infectious Disorders*, vol. 5, no. 1, pp. 3–15, 2005.
- [91] T. Li, V. K. W. Wong, X. Q. Yi, Y. F. Wong, H. Zhou, and L. Liu, "Matrine induces cell anergy in human jurkat T cells through modulation of mitogen-activated protein kinases and nuclear factor of activated t-cells signaling with concomitant up-regulation of anergy-associated genes expression," *Biological and Pharmaceutical Bulletin*, vol. 33, no. 1, pp. 40–46, 2010.
- [92] W. Lam, S. Bussom, F. Guan et al., "Chemotherapy: the four-herb Chinese medicine PHY906 reduces chemotherapy-induced gastrointestinal toxicity," *Science Translational Medicine*, vol. 2, no. 45, article 45ra59, 2010.
- [93] Y. Xie, H. Zhou, Y. F. Wong, H. X. Xu, Z. H. Jiang, and L. Liu, "Study on the pharmacokinetics and metabolism of paeonol in rats treated with pure paeonol and an herbal preparation containing paeonol by using HPLC-DAD-MS method," *Journal of Pharmaceutical and Biomedical Analysis*, vol. 46, no. 4, pp. 748–756, 2008.
- [94] Z. Q. Liu, Z. H. Jiang, K. Chan et al., "Pharmacokinetic interaction of paeoniflorin and sinomenine: pharmacokinetic parameters and tissue distribution characteristics in rats and protein binding ability *in vitro*," *Journal of Pharmaceutical Sciences*, vol. 99, no. 4, pp. 381–391, 2005.
- [95] H. Zeng, S. Dou, J. Zhao et al., "The inhibitory activities of the components of Huang-Lian-Jie-Du-Tang (HLJDT) on eicosanoid generation via lipoxygenase pathway," *Journal of Ethnopharmacology*, vol. 135, no. 2, pp. 561–568, 2011.
- [96] L. Wang, G. B. Zhou, P. Liu et al., "Dissection of mechanisms of Chinese medicinal formula Realgar-Indigo naturalis as an effective treatment for promyelocytic leukemia," *Proceedings of the National Academy of Sciences of the United States of America*, vol. 105, no. 12, pp. 4826–4831, 2008.
- [97] Q. Y. Zhang, J. H. Mao, P. Liu et al., "A systems biology understanding of the synergistic effects of arsenic sulfide and Imatinib in BCR/ABL-associated leukemia," *Proceedings of the National Academy of Sciences of the United States of America*, vol. 106, no. 9, pp. 3378–3383, 2009.
- [98] T. M. Ehrman, D. J. Barlow, and P. J. Hylands, "In silico search for multi-target anti-inflammatories in Chinese herbs and formulas," *Bioorganic and Medicinal Chemistry*, vol. 18, no. 6, pp. 2204–2218, 2010.
- [99] J. Gu, H. Zhang, L. Chen, S. Xu, G. Yuan, and X. Xu, "Drug-target network and polypharmacology studies of a Traditional Chinese Medicine for type II diabetes mellitus," *Computational Biology and Chemistry*, vol. 35, no. 5, pp. 293–297, 2011.
- [100] Q. Huang, X. Qiao, and X. Xu, "Potential synergism and inhibitors to multiple target enzymes of Xuefu Zhuyu Decoction in cardiac disease therapeutics: a computational approach," *Bioorganic and Medicinal Chemistry Letters*, vol. 17, no. 6, pp. 1779–1783, 2007.
- [101] S. Li, B. Zhang, D. Jiang, Y. Wei, and N. Zhang, "Herb network construction and co-module analysis for uncovering the combination rule of traditional Chinese herbal formulae," *BMC Bioinformatics*, vol. 11, supplement 11, article S6, 2010.
- [102] Y. Wang, L. Yu, L. Zhang, H. Qu, and Y. Cheng, "A novel methodology for multicomponent drug design and its application in optimizing the combination of active components from Chinese medicinal formula shenmai," *Chemical Biology and Drug Design*, vol. 75, no. 3, pp. 318–324, 2010.
- [103] Y. Wang, X. Wang, and Y. Cheng, "A computational approach to botanical drug design by modeling quantitative composition-activity relationship," *Chemical Biology and Drug Design*, vol. 68, no. 3, pp. 166–172, 2006.
- [104] Q. Li, X. Li, C. Li et al., "A network-based multi-target computational estimation scheme for anticoagulant activities of compounds," *PLoS ONE*, vol. 6, no. 3, Article ID e14774, 2011.
- [105] Y. Sun, R. Zhu, H. Ye et al., "Towards a bioinformatics analysis of anti-Alzheimer's herbal medicines from a target network perspective," *Briefings in Bioinformatics*, 2013.
- [106] J. Zhao, P. Jiang, and W. Zhang, "Molecular networks for the study of TCM pharmacology," *Briefings in Bioinformatics*, vol. 11, no. 4, pp. 417–430, 2009.
- [107] B. Zhang, X. Wang, and S. Li, "An integrative platform of TCM network pharmacology and its application on a herbal formula, *Qing-Luo-Yin*," *Evidence-Based Complementary and Alternative Medicine*, vol. 2013, Article ID 456747, 12 pages, 2013.
- [108] E. Klipp, R. C. Wade, and U. Kummer, "Biochemical network-based drug-target prediction," *Current Opinion in Biotechnology*, vol. 21, no. 4, pp. 511–516, 2010.
- [109] E. L. Leung, Z. W. Cao, Z. H. Jiang, H. Zhou, and L. Liu, "Network-based drug discovery by integrating systems biology and computational technologies," *Briefings in Bioinformatics*, 2013.
- [110] T. Wang, J. Gu, J. Yuan, R. Tao, Y. Li, and S. Li, "Inferring pathway crosstalk networks using gene set co-expression signatures," *Molecular BioSystems*, 2013.
- [111] R. Kanawong, T. Obafemi-Ajayi, T. Ma, D. Xu, S. Li, and Y. Duan, "Automated tongue feature extraction for ZHENG classification in traditional chinese medicine," *Evidence-Based Complementary and Alternative Medicine*, vol. 2012, Article ID 912852, 14 pages, 2012.

- [112] A. M. Soto and C. Sonnenschein, "Emergentism as a default: cancer as a problem of tissue organization," *Journal of Biosciences*, vol. 30, no. 1, pp. 103–118, 2005.

Research Article

Involvement of Endoplasmic Reticulum Stress in Capsaicin-Induced Apoptosis of Human Pancreatic Cancer Cells

Shengzhang Lin,^{1,2} Jianhong Zhang,² Hui Chen,² Kangjie Chen,¹ Fuji Lai,² Jiang Luo,² Zhaohong Wang,² Heqi Bu,² Riyuan Zhang,² Honghai Li,² and Hongfei Tong²

¹ Department of Hepatobiliary and Pancreatic Surgery, The First Affiliated Hospital, Zhejiang University School of Medicine, Hangzhou, Zhejiang 310003, China

² Department of Hepatobiliary-Pancreatic Surgery, The Second Affiliated Hospital of Wenzhou Medical College, Wenzhou, Zhejiang 325027, China

Correspondence should be addressed to Shengzhang Lin; wzhosldc@163.com

Received 29 September 2012; Revised 31 March 2013; Accepted 23 April 2013

Academic Editor: Taiping Fan

Copyright © 2013 Shengzhang Lin et al. This is an open access article distributed under the Creative Commons Attribution License, which permits unrestricted use, distribution, and reproduction in any medium, provided the original work is properly cited.

Capsaicin, main pungent ingredient of hot chilli peppers, has been shown to have anticarcinogenic effect on various cancer cells through multiple mechanisms. In this study, we investigated the apoptotic effect of capsaicin on human pancreatic cancer cells in both *in vitro* and *in vivo* systems, as well as the possible mechanisms involved. *In vitro*, treatment of both the pancreatic cancer cells (PANC-1 and SW1990) with capsaicin resulted in cells growth inhibition, G0/G1 phase arrest, and apoptosis in a dose-dependent manner. Knockdown of growth arrest- and DNA damage-inducible gene 153 (GADD153), a marker of the endoplasmic-reticulum-stress- (ERS-) mediated apoptosis pathway, by specific siRNA attenuated capsaicin-induced apoptosis both in PANC-1 and SW1990 cells. Moreover, *in vivo* studies capsaicin effectively inhibited the growth and metabolism of pancreatic cancer and prolonged the survival time of pancreatic cancer xenograft tumor-induced mice. Furthermore, capsaicin increased the expression of some key ERS markers, including glucose-regulated protein 78 (GRP78), phosphoprotein kinase-like endoplasmic reticulum kinase (phosphoPERK), and phosphoeukaryotic initiation factor-2 α (phospho-eIF2 α), activating transcription factor 4 (ATF4) and GADD153 in tumor tissues. In conclusion, we for the first time provide important evidence to support the involvement of ERS in the induction of apoptosis in pancreatic cancer cells by capsaicin.

1. Introduction

Pancreatic cancer, an invisible killer to human beings, is the fourth or fifth leading cause of cancer death in the developed countries and widely known for its high mortality rate [1, 2]. Surgery is believed to be the only prospective cure, although the resection rate is relatively low [1]. This is at least partially due to the fact that only 10–20% of pancreatic adenocarcinoma patients are candidates for surgery due to the asymptomatic nature of early stage pancreatic cancer [1, 2]. However, resectional surgery does lead to about a 20% 5-year survival [1]. Administration of fluorouracil chemoradiation and gemcitabine chemotherapy is regarded as the standard first-line treatment for unresectable pancreatic tumors [3]. However, the benefits were very limited due to the inherent resistance to chemotherapeutic agents and their toxicity

[4, 5]. Therefore, it is of especial interest to set new therapeutic strategies aimed at improving the prognostic of this deadly disease.

Some active components of dietary agents and herbs have been reported to possess antiproliferative effect on pancreatic cancer cells, and their molecular mechanisms include generation of reactive oxygen species and activation of mitochondria apoptosis pathway [6]. Furthermore, these components can serve as potent agents to enhance the therapeutic effects of chemotherapy in pancreatic cancer [7, 8]. Capsaicin (8-methyl-N-vanillyl-nonenamide), a homovanillic acid derivative, is the spicy component of hot chili peppers and widely used as a food additive [9, 10]. Some data show that capsaicin has analgesic and anti-inflammatory activities and is currently used in topical creams and gels to mitigate neurogenic pain [11, 12]. Studies reveal that capsaicin inhibits

the growth of human cancer cells by different mechanisms, including generation of reactive oxygen species, disruption of mitochondrial transmembrane potential, and activation of caspase-9 and caspase-3 [6, 13–15]. Recently, a report has shown that capsaicin triggers apoptosis in pancreatic cancer cells via mitochondria-mediated apoptotic pathway [6]. However, the mechanisms underlying capsaicin-induced apoptosis are not well established.

In the present study, we determined whether capsaicin exerted its antiproliferative effect on pancreatic cancer cells via ERS-mediated apoptotic pathway. We showed for the first time that capsaicin induced both *in vitro* and *in vivo* models, an activation of ERS in pancreatic cancer cells with PERK and eIF2 α phosphorylated, as well as ATF4, GRP78, and GADD153 upregulated. Taken together, the present study provides strong evidence supporting an important role of ERS in mediating capsaicin-induced apoptosis in pancreatic cancer cells.

2. Materials and Methods

2.1. Reagents and Antibodies. Capsaicin, propidium iodide (PI), and dimethyl sulfoxide (DMSO) were purchased from Sigma-Aldrich (St. Louis, MO, USA). Dulbecco's Modified Eagle Medium (DMEM), penicillin-streptomycin, fetal bovine serum (FBS), Opti-MEM I reduced serum medium, and trypsin-EDTA were obtained from Gibco BRL (Invitrogen, Grand Island, NY). RNase was obtained from Fermentas (EU). Mouse anti-GADD153, ATF4, and rabbit anti-GRP78 were bought from Abcam (Cambridge, UK). Rabbit phospho-PERK antibody, phospho-eIF2 α antibody, and β -tubulin antibody were purchased from Cell Signaling Technology (Beverly, MA, USA). Bovine serum albumin (BSA), horseradish-peroxidase- (HRP-) conjugated goat anti-rabbit, and anti-mouse secondary antibody were obtained from Beyotime Biotechnology (Beyotime, Haimen, China). [¹⁸F]-fluorodeoxyglucose was provided by Zhejiang University (Hangzhou, China).

2.2. Cell Culture. The human pancreatic cancer cell lines PANC-1 and SW1990 were bought from Shanghai Cell Bank (Shanghai, China). Human pancreatic normal epithelial cells (HPNE) (CHI Scientific INC, Maynard, MA, USA) were stocked in our laboratory. PANC-1, SW1990, and HPNE cells were cultured in DMEM with 10% FBS, 100 units/mL penicillin, and 100 μ g/mL streptomycin at 37°C under a humidified 5% CO₂ atmosphere. Cells were passaged at 70–80% confluence.

2.3. Determination of Cell Viability by CCK-8 Assay. Cell Counting Kit-8 kit (CCK-8 kit) (Dojindo Molecular Technologies, Japan) was used to assess the cells viability. PANC-1, SW1990, and HPNE cells were incubated into 96-well plates at a density of approximately 5×10^3 cells per well and grown for 24 h. The cells were treated with 50, 100, 150, 200, 250, and 300 μ mol/L capsaicin or DMSO (control) for 24 h. Then 10 μ L CCK-8 reagent was added to 100 μ L of media in each well, and the cells were incubated for a further 3 h. The absorbance (A)

of each well was determined with an ELISA reader (Bio-Tek ELx808, Winooski, VT, USA) at a wavelength of 450 nm. Survival rate (%) = $(A_{\text{sample}} - A_{\text{blank}})/(A_{\text{control}} - A_{\text{blank}})$. The experiment was repeated three separate times.

2.4. Flow Cytometry Analysis of Cell Cycle. PANC-1 and SW1990 cells were seeded into 6-well plates at a density of approximately 5×10^5 cells per well, cultured overnight, then various concentrations of capsaicin (0, 150, 200, and 250 μ mol/L for PANC-1 cells; 0, 100, 150, and 200 μ mol/L for SW1990 cells) were added. After 24 h incubation cells were harvested, washed with phosphate buffer saline (PBS), and then fixed with 70% ethanol overnight at 4°C. Cells were stained with 20 μ g/mL RNase and 20 μ g/mL PI for 30 minutes at 37°C in the dark and then analyzed by flow cytometry (Becton Dickinson, San Jose, CA, USA). The experiment was repeated three separate times.

2.5. Flow Cytometry Analysis of Apoptosis. Apoptosis in PANC-1 and SW1990 cells was evaluated using Annexin V-FITC Apoptosis Detection Kit (BioVision, CA, USA), which was performed according to the manufacturer's protocol. Approximately 5×10^5 cells per well were seeded into 6-well plates, allowed to adhere overnight, and then treated with various concentrations of capsaicin (0, 150, 200, and 250 μ mol/L for PANC-1 cells; 0, 100, 150 and 200 μ mol/L for SW1990 cells). Cells were collected after 24 h incubation, washed with PBS, and resuspended in 500 μ L binding buffer containing 5 μ L Annexin V-FITC and 10 μ L PI in the dark for 5 min at room temperature. The apoptotic cells were detected by flow cytometry (Becton Dickinson, San Jose, CA, USA). The experiment was repeated three separate times.

2.6. Protein Extraction and Western Blot Analysis. Total proteins were extracted from cultured cells or tumor tissues using Cell Lysis Buffer (20 mmol/L Tris-HCl pH 7.5, 150 mmol/L NaCl, 1 mmol/L Na₂EDTA, 1 mmol/L EGTA, 1% Triton, 2.5 mmol/L sodium pyrophosphate, 1 mmol/L beta-glycerophosphate, 1 mmol/L Na₃VO₄, 1 μ g/mL leupeptin, 1 mmol/L PMSF). After centrifugation at 14,000 g for 15 min at 4°C, the supernatant was collected and protein concentration was detected using the BCA Protein Assay Kit (Pierce, USA), according to the manufacturer's instructions. Equal amounts of protein were separated on 8% sodium dodecyl sulfate-polyacrylamide gel (SDS-PAGE) and transferred onto polyvinylidene difluoride membrane. After blocking with 5% BSA, membrane was incubated with the specific primary antibodies followed by the incubation with the secondary antibodies. Immunoreactivity was detected using the Enhanced Chemiluminescence Kit (Pierce, USA) according to the manufacturer's instructions. Each experiment was repeated three separate times.

2.7. RNA Preparation and Real-Time PCR. Total RNA was isolated from cultured cells or tumor tissues using the TRIzol reagent (Invitrogen, Carlsbad, CA, USA), according to the manufacturer's instructions. For reverse transcriptase analysis, 1 μ g of total RNA was reversely transcribed in 20 μ L

TABLE 1: Sequences of primers used in the realtime PCR.

Primer name	Primer sequence
GRP78-forward	5' CCAAGACAGCACAGACAGATTG 3'
GRP78-reverse	5' CCACGAACCAGGCCGAAGG 3'
GADD153-forward	5' GCTTGGCTGACTGAGGAGGAG 3'
GADD153-reverse	5' CTGACTGGAATCTGGAGAGTGAGG 3'
RPLP0-forward	5' GAGACAAAGTGGGAGCCAGCGA 3'
RPLP0-reverse	5' ACCCTCCAGGAAGCGAGAATGC 3'

volume, using RevertAid First Strand cDNA Synthesis Kit (KI622, Fermentas, EU). Real-time PCR amplification with one microliter of the reverse transcriptase reaction mixture was performed with SYBR Green Real-time PCR Master Mix-Plus- (Toyobo, Japan). The initial denaturation step was 95°C for 60 s followed by 40 cycles of amplification at 95°C for 15 s, 60°C for 15 s, and 72°C for 45 s. All samples were performed in triplicate, and the experiment was repeated three separate times. The relative amount of the target gene was normalized with the housekeeping gene ribosomal protein, large, P0 (RPLP0). Sequences of primers listed in Table 1 were designed using the software Primer Premier 5.

2.8. Small Interfering RNA (siRNA). Lipofectamine²⁰⁰⁰ reagent (Invitrogen) was used for the transfection of siRNA into pancreatic cancer PANC-1 and SW1990 cells. The GADD153-specific siRNA (sense 5'-GAGCUCUGAUUG-ACCGAAU-3' and antisense 5'-AUUCGGUCAUUCAGAGCUC-3') and nonsilencing scrambled siRNA were obtained from GenePharma (Shanghai, China). Briefly, approximately 5×10^5 cells per well were seeded into 6-well plates and allowed to adhere overnight. For each well, 250 μ L Opti-MEM I reduced serum medium containing 100 pmol siRNA was added to a solution containing 5 μ L lipofectamine²⁰⁰⁰ in 250 μ L Opti-MEM I reduced serum medium. The 500 μ L mixture was mixed gently, incubated for 20 min at room temperature, and then carefully dripped into the cells in 2 mL antibiotic- and serum-free DMEM. Regular growth medium was added 24 h after transfection. Then cells were treated with capsaicin (150 μ mol/L for PANC-1 and 100 μ mol/L for SW1990 cells) for 24 h. Cells were collected for real-time PCR analysis, western blot, and apoptosis assay. Each experiment was repeated three separate times.

2.9. In Vivo Study. BALB/C (nu/nu) four-week-old male mice were purchased from Shanghai Laboratory Animals Center (Shanghai, China) and maintained in specific pathogen-free conditions. Mice were allowed to acclimate for one week before the beginning of the experiments. All animal studies performed in this study were reviewed and approved by the Animal Research and Ethical Committee of Wenzhou Medical College. Orthotopic pancreatic cancer xenograft tumor model was established as described by us previously [16]. Briefly, nude mice were anesthetized with pentobarbital sodium, a small left abdominal flank incision was made, and PANC-1 cells (5×10^6) at exponential stage in 50 μ L serum-free media were injected into the subcapsular

region of pancreas. Two weeks after cell inoculation, a total of 48 nude mice were randomized into four groups with 12 mice per group: control group (PBS), CAP 1 group (capsaicin, 1 mg/kg), CAP 2.5 group (capsaicin, 2.5 mg/kg), and CAP 5 group (capsaicin, 5 mg/kg). Capsaicin was dissolved initially in ethanol and further diluted in PBS before administering to the mice, and the final concentration of ethanol was less than 0.2%. Mice were treated with gavage in 100 μ L PBS containing different concentrations of capsaicin 3 days per week (Monday, Wednesday, and Friday), and the treatment was continued for 3 weeks.

After the first treatment, 6 mice in each group were used for survival study which was carried out up to 60 days. When mice died during the period of survival study, the living days were recorded. At the end of survival study, the living mice were euthanized. One week after the last treatment, the other 6 mice in each group were used for the study of tumors metabolisms detected by micropositron emission tomography (Micro-PET). Then the mice were sacrificed, and the tumors were removed. The tumors were weighted with an electronic balance, and tumor volumes were calculated with a vernier caliper using the following formula: $(4\pi/3) \times (\text{width}/2)^2 \times (\text{length}/2)$. Tumor tissue was stored in liquid nitrogen for western blot and real-time PCR analysis.

2.10. Micro-PET Study. Micro-PET imaging was performed one week after the last treatment. Mice were injected with 0.1 microcuries [¹⁸F]-fluorodeoxyglucose per mouse via the tail vein. Mice were anesthetized with isoflurane and positioned in the cavity of the Micro-PET scanner and then imaged. A 10 min data collection was performed with an uptake time of 1 h after the tracer injection. Static acquisition was performed in three-dimensional mode using a Micro-PET imaging system (R4, Concorde Microsystems, Knoxville, TN, USA). The Micro-PET images were analyzed with the Acquisition Sinogram and Image Processing software that accompanies the Micro-PET. A semiquantitative index of glucose metabolism, the standardized uptake value (SUV), is here used as a marker of growth metabolism in pancreatic cancer xenografts. The SUV is obtained by placing a region of interest (ROI) and dividing the value (in microcuries per cubic centimeter) by the injected dose (in microcuries) divided by the weight (in grams) of the mouse. ROI was manually drawn by creating a volume of interest in the central area of the tumor and in the reference area.

2.11. Statistical Analysis. Data are expressed as mean \pm SD. Statistical analysis was performed using SPSS 13.0. Differences between the capsaicin-treated and DMSO-treated (control) groups were analyzed by the unpaired Student's *t*-test or ANOVA analysis. A value of *P* less than 0.05 was considered statistically significant.

3. Results

3.1. Effects of Capsaicin on the Viability of Pancreatic Cancer and HPNE Cells. To first investigate the antiproliferative effect of capsaicin, PANC-1, SW1990, and HPNE cells were

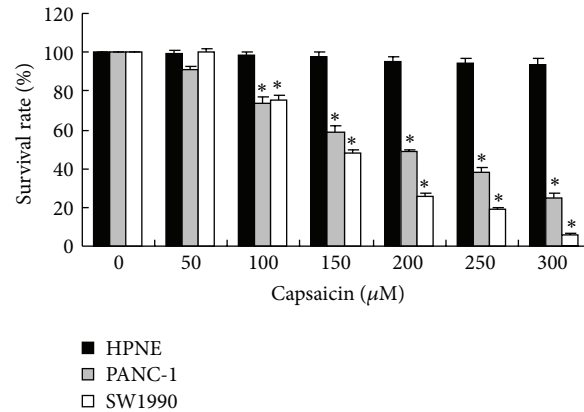


FIGURE 1: Effects of capsaisin on the growth of pancreatic cancer and HPNE cells. PANC-1, SW1990, and HPNE cells were incubated with 50, 100, 150, 200, 250, and 300 $\mu\text{mol/L}$ capsaisin or DMSO (control) for 24 h, and cell viability was measured using CCK-8 assay with six replicates per concentration of capsaisin. Data obtained from three separate experiments are expressed as mean \pm SD and analyzed by one-way ANOVA followed by Dunnett's test, and * $P < 0.01$ compared with DMSO-treated cells.

treated with various concentrations of capsaisin, and then the cell viability was measured by CCK-8 assay. PANC-1 and SW1990 cells viability was inhibited by capsaisin treatment for 24 h in a dose-dependent manner (Figure 1). We found that capsaisin inhibited cell growth more effectively in SW1990 cells (IC_{50} , 150 $\mu\text{mol/L}$) than in PANC-1 cells (IC_{50} , 200 $\mu\text{mol/L}$). Besides, the survival rate of HPNE cells was minimally changed after capsaisin treatment.

3.2. Capsaicin-Induced G0/G1 Phase Arrest and Apoptosis in PANC-1 and SW1990 Cells. We next investigated whether the antiproliferative activity of capsaisin in PANC-1 and SW1990 cells was correlated with cell cycle arrest and apoptosis. As shown in Figure 2(a), the results of cell cycle analysis showed that capsaisin increased the ratio of cells in the G0/G1 phase and decreased those in the S and G2/M phase, in a dose-dependent manner. There were significant differences in the ratio of cells in G0/G1 phase and S plus G2/M phase between capsaisin-treated groups (150, 200, and 250 $\mu\text{mol/L}$ for PANC-1 cells; 150 and 200 $\mu\text{mol/L}$ for SW1990 cells) and control group ($P < 0.05$; Figures 2(b) and 2(c)). Further flow cytometry analysis revealed that capsaisin significantly increased the apoptotic rate of pancreatic cancer cells in a dose-dependent manner. The apoptotic rates in PANC-1 cells (0, 150, 200, and 250 $\mu\text{mol/L}$ capsaisin for 24 h) were $4.72\% \pm 1.40\%$, $16.66\% \pm 1.51\%$, $21.72\% \pm 1.78\%$, and $34.36\% \pm 1.91\%$, respectively (Figures 3(a) and 3(b)). In SW1990 cells treated with 0, 100, 150, and 200 $\mu\text{mol/L}$ capsaisin for 24 h, the apoptotic rates were $6.97\% \pm 1.17\%$, $25.48\% \pm 2.14\%$, $38.59\% \pm 1.80\%$, and $48.11\% \pm 2.97\%$, respectively (Figures 3(a) and 3(c)). Significant differences ($P < 0.01$) in the apoptotic rate of PANC-1 and SW1990 cells were observed in capsaisin-treated groups relative to the control group. These data were consistent with previous studies of cell growth inhibition using the CCK-8 assay, indicating that the loss of viable cells by capsaisin was at least partly due to the G0/G1 phase arrest and apoptosis induction.

3.3. Effects of Capsaicin on the mRNA Expression of GRP78 and GADD153 in PANC-1 and SW1990 Cells. Next, we investigated whether endoplasmic-reticulum-stress- (ERS-) mediated apoptotic pathway was involved in antiproliferative and apoptotic effects of capsaisin in PANC-1 and SW1990 cells. We examined the effect of capsaisin on the mRNA expression of two key ERS markers, GRP78 and GADD153. These results of real-time PCR analysis indicated that capsaisin significantly increased the mRNA expression of GRP78 and GADD153. GRP78 and GADD153 were higher in PANC-1 cells treated with 200 $\mu\text{mol/L}$ capsaisin (3.71-fold and 4.14-fold, $P < 0.01$; Figure 4(a)) compared with DMSO-treated cells. The GRP78 and GADD153 mRNA expression in SW1990 cells treated with 150 $\mu\text{mol/L}$ capsaisin was about 3.69-fold and 5.99-fold more than that of DMSO-treated cells ($P < 0.01$; Figure 4(b)).

3.4. Knockdown of GADD153 by siRNA Attenuated Capsaicin-Induced Apoptosis in PANC-1 and SW1990 Cells. To further confirm the functional role of GADD153 in capsaisin-induced apoptosis in pancreatic cancer cells, GADD153-specific siRNA was employed in this study. Real-time PCR and western blot analysis demonstrated that transfection of siRNA against GADD153 resulted in a suppression of capsaisin-induced GADD153 expression in PANC-1 and SW1990 cells as compared to cells transfected with scrambled siRNA (Figures 5(a) and 5(b)). The apoptotic rates of PANC-1 cells in scrambled siRNA-transfected and GADD153 siRNA-transfected group were $35.34\% \pm 2.48\%$, and $27.99\% \pm 2.05\%$, respectively ($P < 0.05$; Figures 5(c) and 5(d)). And in SW1990 cells, the apoptotic rate in GADD153 siRNA-transfected group was much lower than that in scrambled siRNA-transfected group ($P < 0.05$; Figures 5(c) and 5(d)). These results suggested that GADD153-specific siRNA significantly decreased capsaisin-induced apoptosis in pancreatic cancer cells.

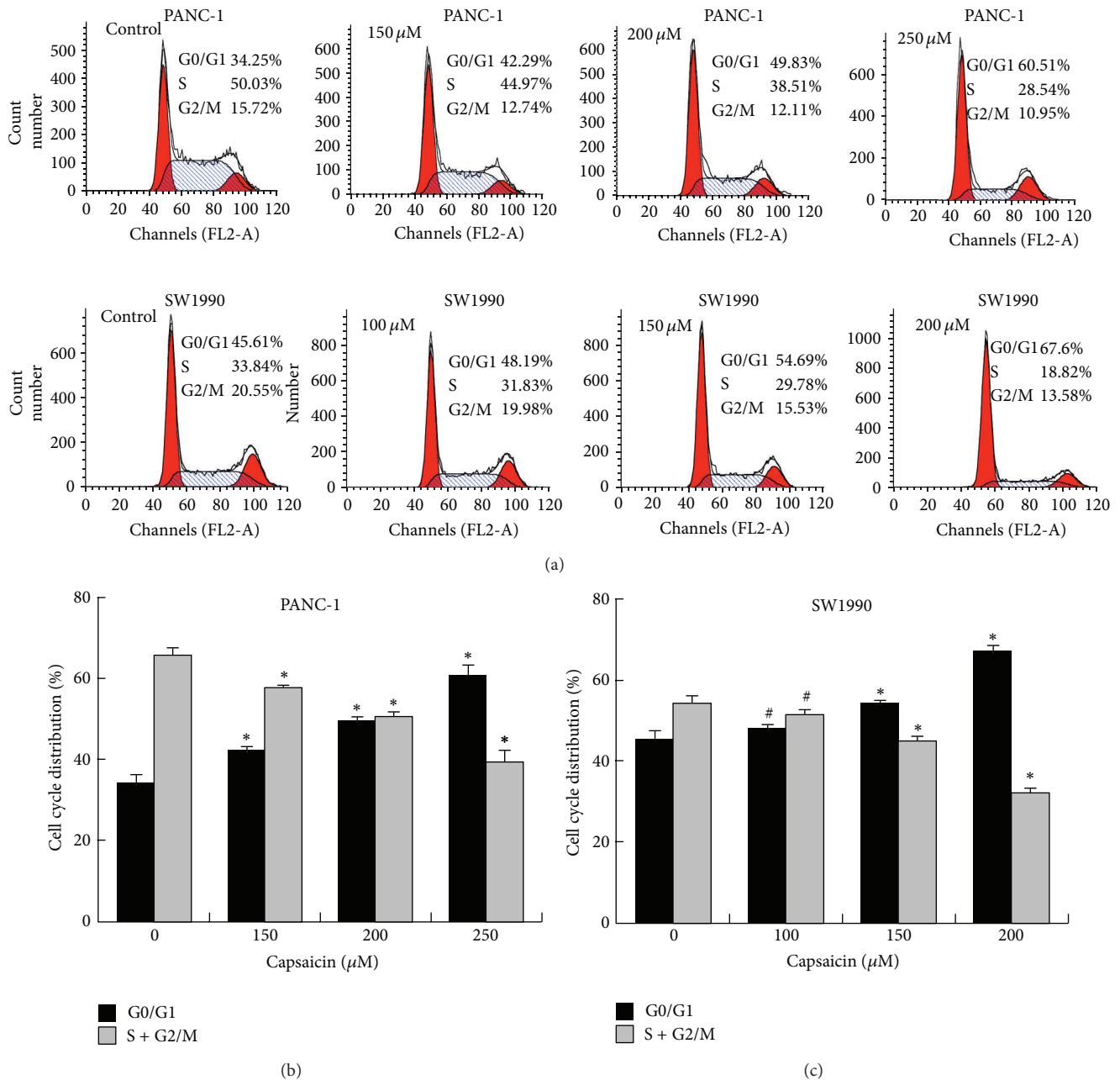
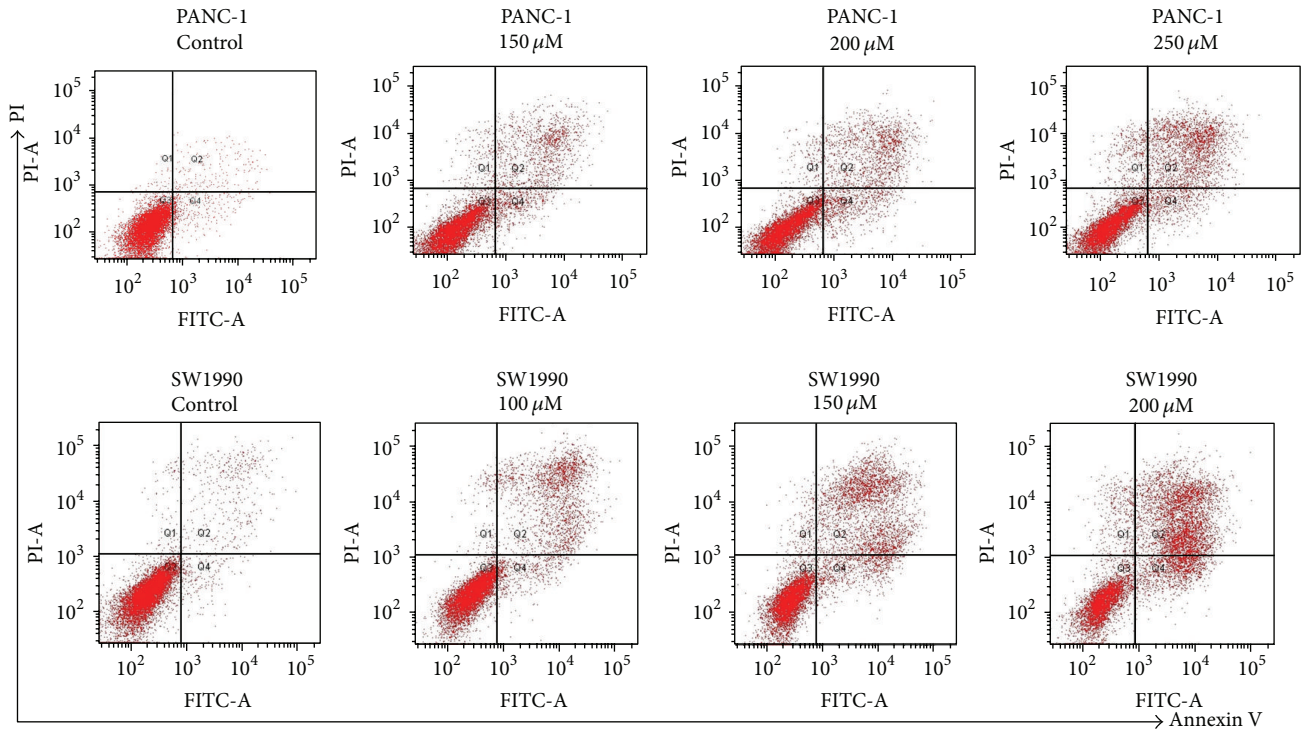


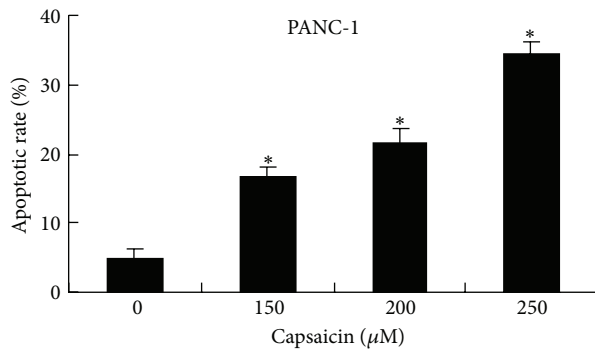
FIGURE 2: Effects of capsaicin on cell cycle in PANC-1 and SW1990 cells. PANC-1 and SW1990 cells were treated with various concentrations of capsaicin (0, 150, 200, and 250 $\mu\text{mol/L}$ for PANC-1 cells; 0, 100, 150, and 200 $\mu\text{mol/L}$ for SW1990 cells) for 24 h. Distribution of treated cells in different phases of cell cycle was analyzed by PI staining followed by flow cytometry. (a) The cell cycle distribution graphs. The results shown are representative of three independent experiments. The ratio of cells in each phase (G0/G1, S, and G2/M) was calculated by using the ModFit software. (b) and (c) The comparison of cell cycle (G0/G1 and S plus G2/M phase) of capsaicin-treated groups and control group in PANC-1 (b) and SW1990 (c) cells. Data obtained from three separate experiments are expressed as mean \pm SD and analyzed by one-way ANOVA followed by Dunnett's test. # $P > 0.05$ and * $P < 0.05$, compared with DMSO-treated cells.

3.5. Antitumoral Effect of Capsaicin in Orthotopic Pancreatic Cancer Xenograft Tumor in Nude Mice. To investigate the antitumoral effect of capsaicin *in vivo*, we established orthotopic pancreatic cancer xenograft tumor in nude mice. As expected, capsaicin exerted significant antitumoral effect in pancreatic cancer *in vivo*. For example, the SUVs in different groups were: control (9.15 ± 0.67), CAP 1 (6.06 ± 0.57), CAP

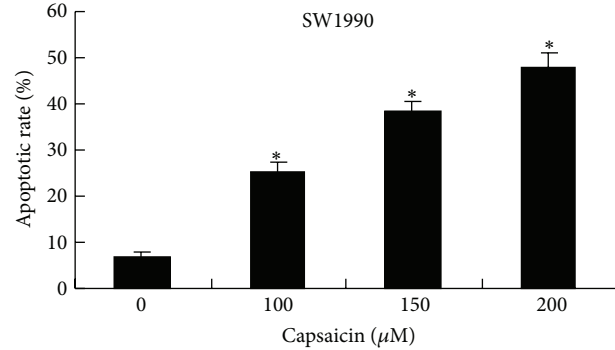
2.5 (3.82 ± 0.37), and CAP 5 (1.63 ± 0.50) (Figure 6(a)). The mean weights of tumors in CAP 1, CAP 2.5, and CAP 5 group were, respectively, 0.71 ± 0.10 , 0.51 ± 0.11 , and 0.37 ± 0.08 g, compared to the control group 0.91 ± 0.11 g (Figure 6(b)). The average tumor volumes in control, CAP 1, CAP 2.5, and CAP 5 group were 766.50 ± 91.29 , 573.56 ± 88.54 , 394.05 ± 98.72 , and 256.62 ± 67.64 mm^3 , respectively (Figure 6(c)).



(a)



(b)



(c)

FIGURE 3: Effects of capsaicin on apoptosis in PANC-1 and SW1990 cells. PANC-1 and SW1990 cells were treated with various concentrations of capsaicin (0, 150, 200, and 250 $\mu\text{mol/L}$ for PANC-1 cells; 0, 100, 150, and 200 $\mu\text{mol/L}$ for SW1990 cells) for 24 h and subsequently stained with Annexin V-FITC/PI followed by flow cytometry. (a) Representative dot plots illustrating apoptotic status in PANC-1 and SW1990 cells. Cells in the lower left quadrant (Annexin V-FITC-/PI-) are viable, those in the lower right quadrant (Annexin V-FITC+/PI-) are early apoptotic, and those in the upper right quadrants (Annexin V-FITC+/PI+) are late apoptotic. (b) and (c) Apoptotic cells (lower right quadrant and upper right quadrants) in PANC-1 (b) and SW1990 (c) cells. Data obtained from three separate experiments are expressed as mean \pm SD and analyzed by one-way ANOVA followed by Dunnett's test, and * $P < 0.01$ compared with DMSO-treated cells.

As shown in Figure 7, capsaicin prolonged the survival time of pancreatic cancer xenograft tumor mice. The median survival time of mice in the groups CAP 1 (42 days), CAP 2.5 (53 days), and CAP 5 (56 days) was significantly longer than that in the control group (30 days) (Figure 7(c)).

To gain further insight into the mechanisms for antitumoral effect of capsaicin *in vivo*, we determined the expression of some markers related to ERS-mediated apoptotic pathway (GRP78, phospho-PERK, phospho-eIF2 α , ATF4, and GADD153) in tumor tissues. The results of western blot analysis showed that the protein expression of GRP78,

phospho-PERK, phospho-eIF2 α , ATF4, and GADD153 was much higher in the tumor tissues of capsaicin-treated mice compared with that of the control group (Figure 8(a)). As shown in Figure 8(b), compared with the control group, GRP78 and GADD153 mRNA expression in CAP 2.5 group was increased (3.81-fold and 4.04-fold, resp.; $P < 0.01$).

4. Discussion

Pancreatic cancer remains a devastating malignancy due to lack of effective therapy. The present study demonstrated that

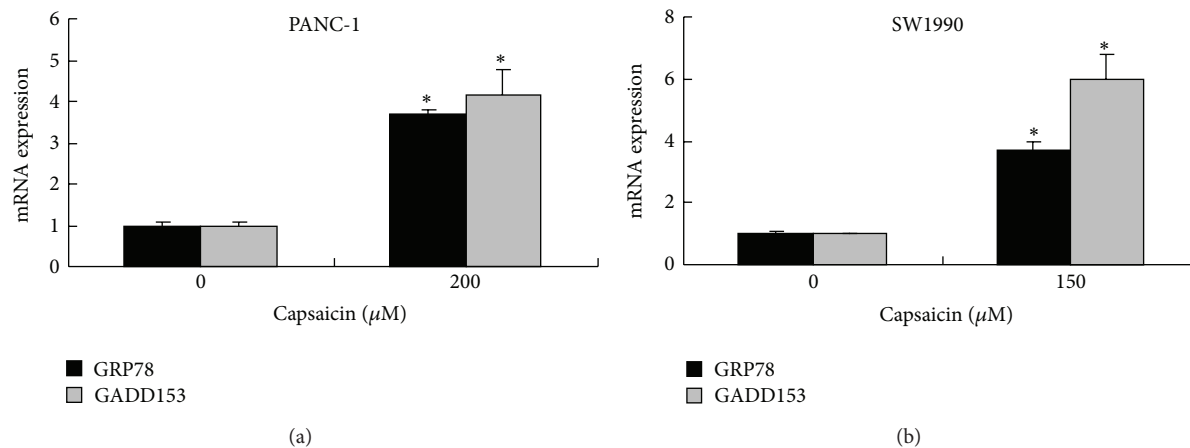


FIGURE 4: Capsaicin promoted the mRNA expression of ERS markers, GRP78 and GADD153. PANC-1 (a) and SW1990 (b) cells were treated with 200 $\mu\text{mol/L}$ and 150 $\mu\text{mol/L}$ capsaicin for 24 h, respectively. Real-time PCR analysis for mRNA expression of GRP78 and GADD153 was performed after capsaicin treatment. All samples were performed in triplicate, and the relative amount of the target gene was normalized with the housekeeping gene RPLP0. Data are expressed as mean \pm SD and analyzed by the unpaired Student's *t*-test, and **P* < 0.01 compared with DMSO-treated cells.

capsaicin was effective in suppressing growth and inducing apoptosis of human pancreatic cancer cells because of its cytostatic and cytotoxic properties. Importantly our studies provided novel evidence for a role of endoplasmic-reticulum-stress- (ERS-) mediated apoptotic pathway in suppressing growth of pancreatic cancer *in vitro* and *in vivo* after capsaicin treatment.

Endoplasmic reticulum is the cell organelle of synthesis and folding of secretory proteins. Perturbation of endoplasmic reticulum homeostasis affects protein folding and causes ERS [17, 18]. The endoplasmic reticulum responds to ERS by activating intracellular signal transduction pathways, collectively termed as the unfolded protein response (UPR), which aims to restore the homeostasis of the organelle [17, 18]. During UPR, GRP78 dissociates from endoplasmic reticulum-resident transmembrane proteins, which leads to autophosphorylation and activation of these transmembrane proteins, such as PERK [19]. Activated PERK phosphorylates eIF2 α and then ATF4 is induced [19]. GRP78, a hallmark of ERS, is a constitutively expressed resident protein of the ER of all eukaryotic cells and belongs to the highly conserved hsp70 protein family [20, 21]. Increasing evidences have showed that elevated GRP78 expression, induced by oxidative stress and chemical toxicity, triggers PERK/eIF2 α /ATF4 signaling pathway and cell death [22–25]. Several reports also have suggested that GRP78 in the early stage may protect the cell against apoptosis by some mechanisms, such as suppressing oxyradical accumulation and stabilizing mitochondrial function [26–28]. In the present study, significantly promoted GRP78 mRNA expression was observed after capsaicin treatment *in vitro*. And the results of western blot analysis and real-time PCR showed that capsaicin significantly increased the protein and mRNA expression of GRP78 in tumor tissues. Moreover, we found that *in vivo* studies capsaicin obviously augmented PERK and eIF2 α phosphorylation and expression of ATF4, a downstream target of eIF2 α . Our results suggested

that capsaicin could trigger ERS and then activate UPR (GRP78/PERK/eIF2 α /ATF4 signaling pathway) in pancreatic cancer cells.

In this study, the critical finding is the elevated expression of GADD153 by capsaicin in pancreatic cancer cells. GADD153, also known as CCAAT/enhancer binding protein homologous protein (CHOP), is one of the components of the ERS-mediated apoptotic pathway [18, 19]. Accumulating evidences have showed that GADD153 plays an important role in ERS-induced apoptosis [17–19, 29, 30]. GADD153 deficiency can protect cells from ERS-induced apoptosis [31]. The mRNA expression of GADD153 is primarily regulated by the PERK/eIF2 α /ATF4 signaling pathway [19, 30]. Although low in normal cells, a variety of stress stimuli can induce the expression of GADD153, including endoplasmic reticulum stress, genotoxic agent, and nutrient depletion [19, 32]. We found capsaicin significantly increased the mRNA and protein expression of GADD153 *in vitro* and *in vivo*. Furthermore, downregulation of GADD153 induced by specific siRNA significantly diminished capsaicin-induced apoptosis. These results suggested that GADD153 was a regulator for capsaicin-triggered apoptosis. However, GADD153 interference only partially abrogated the apoptotic effect of capsaicin in PANC-1 cells, suggesting that other apoptosis-related pathways may also contribute to capsaicin-induced apoptosis. Overexpression of GADD153 has been reported to play a role in growth arrest pathway and to block the cell progression from G1 to S phase [33]. Our results revealed that capsaicin induced G0/G1 phase arrest, which could be the results of upregulation of GADD153. However, effector molecules of apoptosis triggered by GADD153 are not well elucidated. These results suggested that ERS-mediated apoptotic pathway and GADD153 upregulation were involved in antiproliferative effect of capsaicin in pancreatic cancer cells.

We further determined the *in vivo* effects of capsaicin in an orthotopic pancreatic cancer xenograft tumor in BALB/C

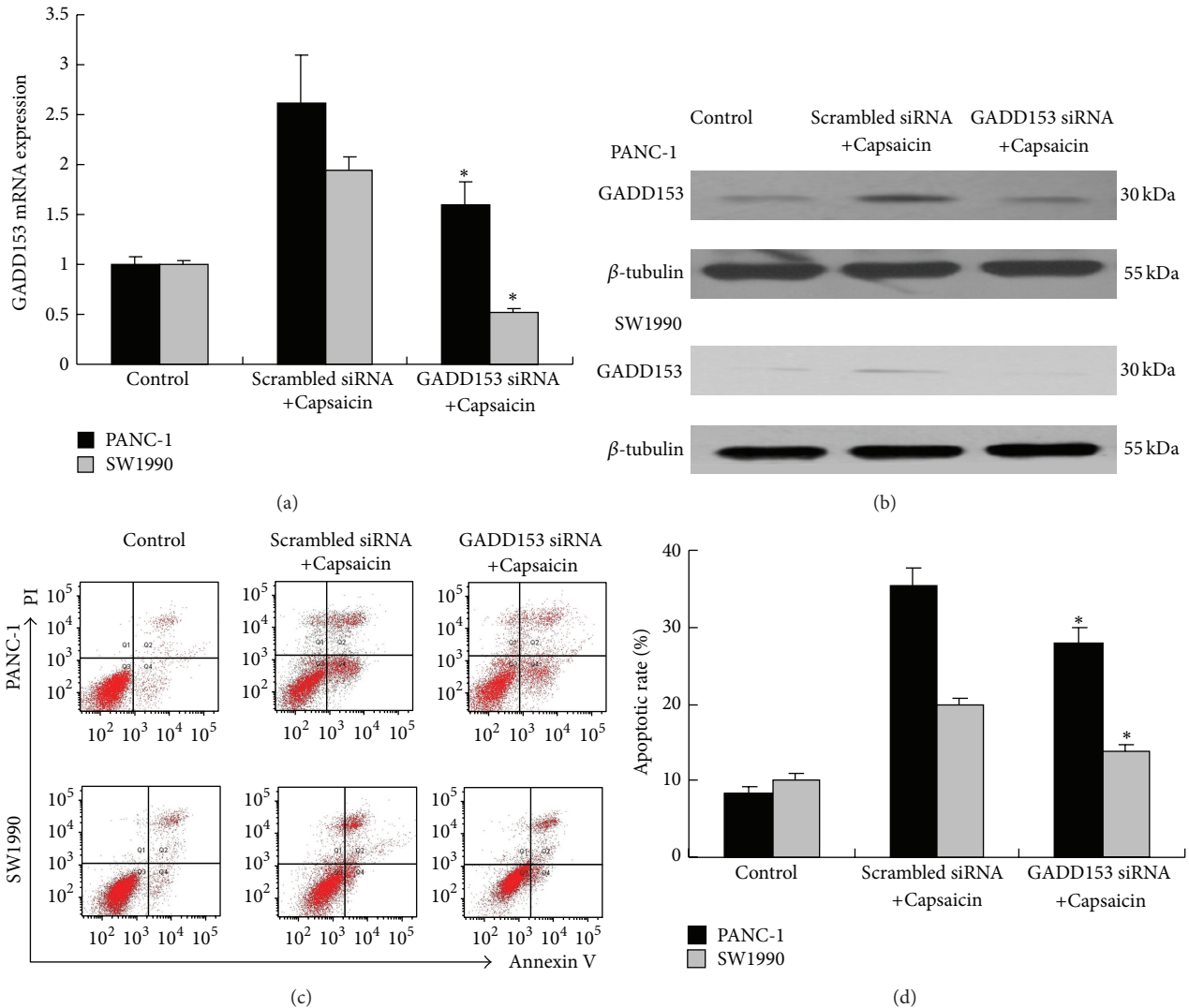


FIGURE 5: Silencing GADD153 by siRNA attenuated capsaicin-induced apoptosis in PANC-1 and SW1990 cells. PANC-1 and SW1990 cells were transfected with GADD153-specific siRNA and scrambled siRNA. 24 h after transfection, cells were treated with capsaicin (150 μ mol/L for PANC-1 and 100 μ mol/L for SW1990 cells) for 24 h. (a) Real-time PCR analysis of GADD153 mRNA expression. All samples were performed in triplicate. Data are expressed as mean \pm SD and analyzed by one-way ANOVA followed by Bonferroni test, and * $P < 0.05$ compared with scrambled siRNA-transfected capsaicin-treated cells. (b) The protein level of GADD153 was determined by western blot. β -tubulin was used as a loading control. The results shown are representative of three independent experiments. (c) and (d) Representative dot plots illustrating apoptotic status (c) and statistical analysis (d) showed that GADD153-specific siRNA decreased capsaicin-induced apoptosis. Data obtained from three separate experiments are expressed as mean \pm SD and analyzed by one-way ANOVA followed by Bonferroni test, and * $P < 0.05$ compared with scrambled siRNA-transfected capsaicin-treated cells.

(nu/nu) mice. Our study showed that capsaicin effectively inhibited tumor growth, as previously reported [6, 13]. Micro-PET imaging, a routine detection used in clinical oncology nowadays, generally employs fluorodeoxyglucose to detect tumors and assess their metabolic activities [34, 35]. Micro-PET imaging is also employed to assess the metabolisms of xenograft tumor model in animals [36]. In the present study, we employed Micro-PET imaging to detect metabolisms of pancreatic cancers in mice. The standardized uptake value (SUV) was used as a marker of metabolism in pancreatic cancer xenografts. The results of Micro-PET imaging showed that

capsaicin treatment markedly decreased tumors SUV and thus inhibited the metabolisms of pancreatic cancers. Besides, the median survival time of mice in the capsaicin-treated groups was significantly longer than that in the control group, which suggested that capsaicin could significantly prolong the survival time of pancreatic cancer xenograft tumor mice. Moreover, increased mRNA and protein expressions of some markers related to ERS-mediated apoptotic pathway were observed in capsaicin-treated group. These *in vivo* results further confirmed the antitumoral effects of capsaicin by inducing ERS-mediated apoptosis in pancreatic cancer.

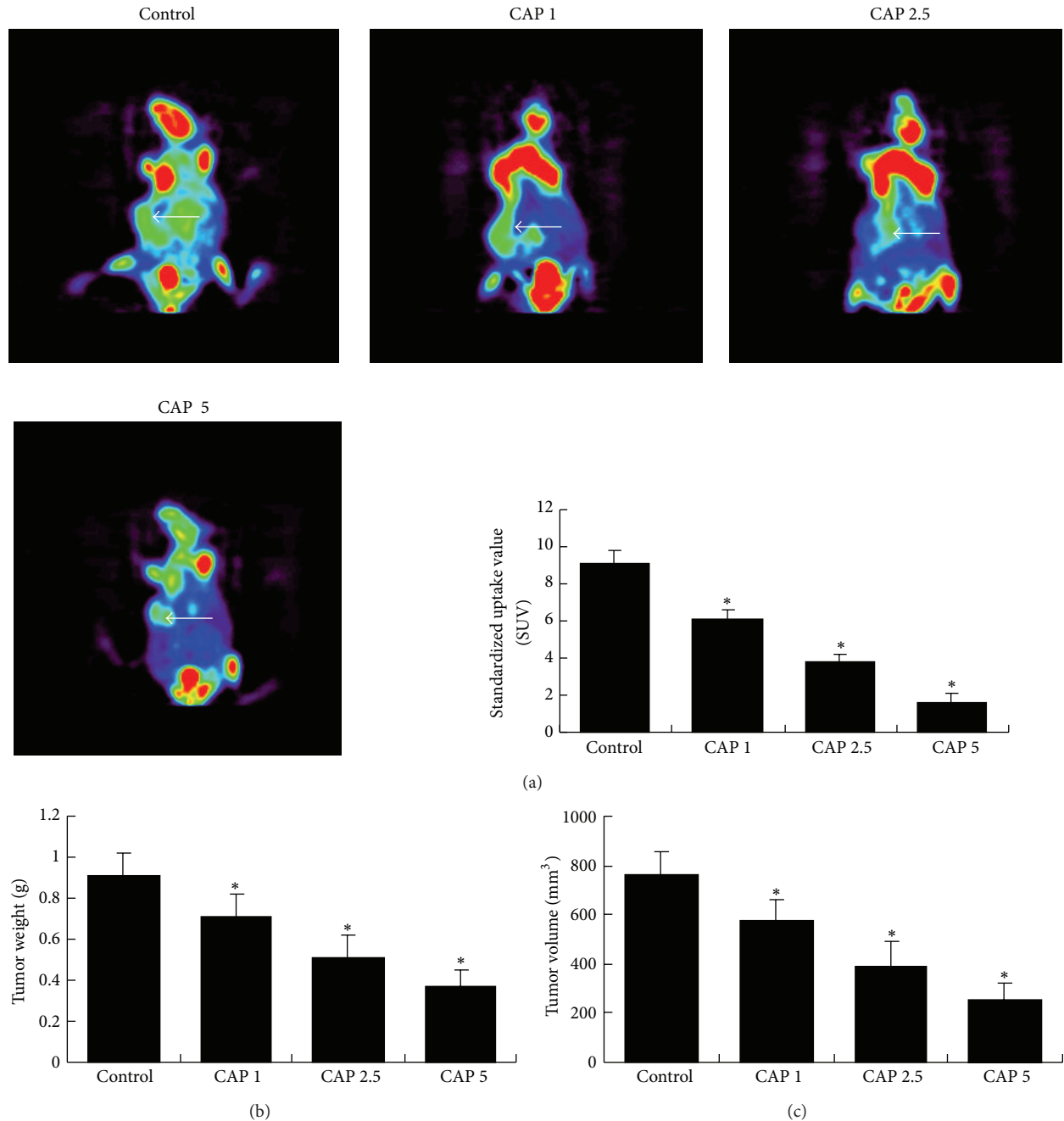


FIGURE 6: Effect of capsaicin on the tumor metabolisms, weights, and volumes in pancreatic cancer xenograft tumor mice (control, PBS; CAP 1, capsaicin, 1 mg/kg; CAP 2.5, capsaicin, 2.5 mg/kg; CAP 5, capsaicin, 5 mg/kg). (a) Micro-PET imaging. Micro-PET imaging was performed one week after the last treatment. The values of SUV are expressed as mean \pm SD and analyzed by one-way ANOVA followed by Dunnett's test, and $*P < 0.01$ compared with the control group. (b) Tumor weights. One week after the last treatment, the mice were sacrificed and tumors were removed. The tumors were weighted with an electronic balance. Data are expressed as mean \pm SD and analyzed by one-way ANOVA followed by Dunnett's test, and $*P < 0.01$ compared with the control group. (c) Tumor volumes. Tumor volumes were calculated with a vernier caliper with the following formula: $(4\pi/3) \times (\text{width}/2)^2 \times (\text{length}/2)$. Data are expressed as mean \pm SD and analyzed by one-way ANOVA followed by Dunnett's test, and $*P < 0.01$ compared with the control group.

Together, our results could provide important evidence for clinical application of capsaicin as an anticancer agent.

In conclusion, to the best of our knowledge, this is the first study on the effect of capsaicin on the ERS-mediated apoptotic pathway of pancreatic cancer both *in vitro* and

in vivo. These findings provide important new insights into the signaling events involved in capsaicin-induced apoptosis and may facilitate the development of chemotherapeutic or chemopreventive strategies based on capsaicin for human pancreatic cancer.

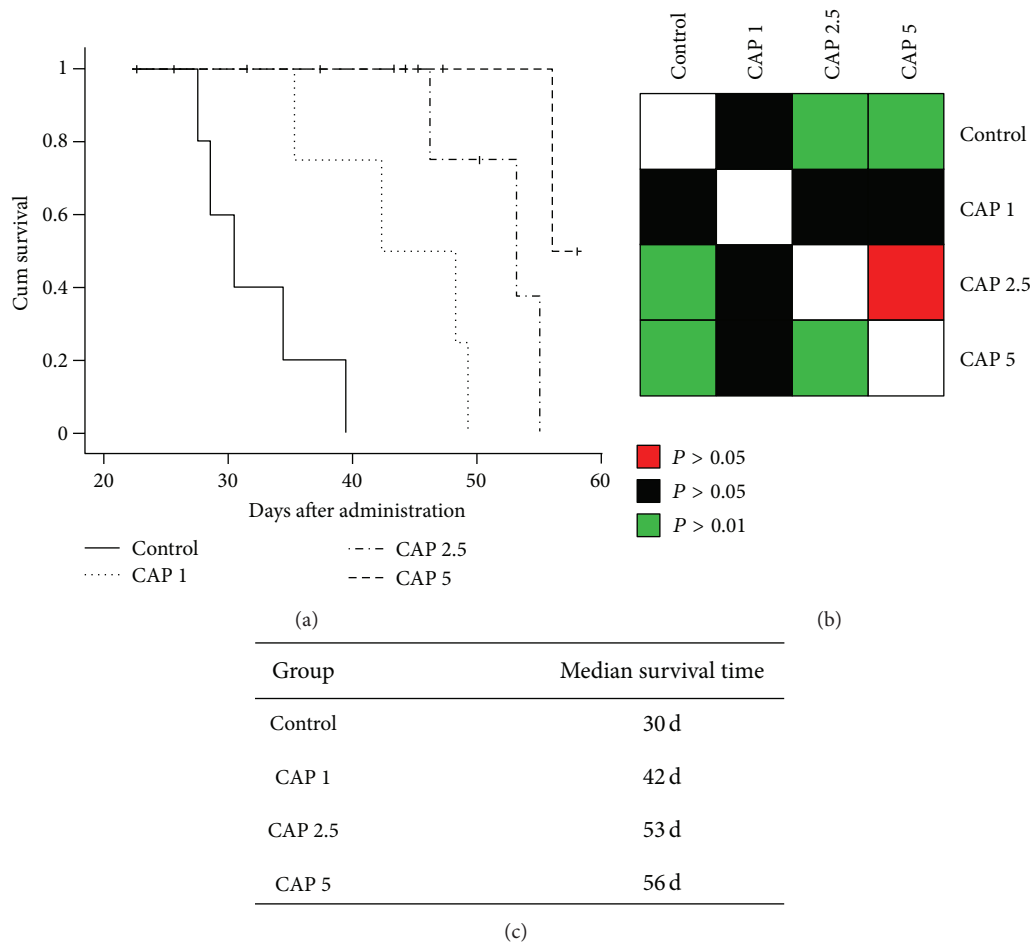


FIGURE 7: Survival analysis of mice orthotopic bearing pancreatic cancer (control, PBS; CAP 1, capsaicin, 1 mg/kg; CAP 2.5, capsaicin, 2.5 mg/kg; CAP 5, capsaicin, 5 mg/kg). The survival study was carried out up to 60 days after the first treatment. The number of living days was recorded when mice died during the period of survival study. (a) Kaplan-Meier curves show survival for mice administrated with different doses of capsaicin. (b) Statistical significance was determined by the log-rank test. A matrix of P values is showed according to a log-rank test between the different groups (red, $P > 0.05$; black, $P < 0.05$; green, $P < 0.01$). (c) Median survival time of different groups.

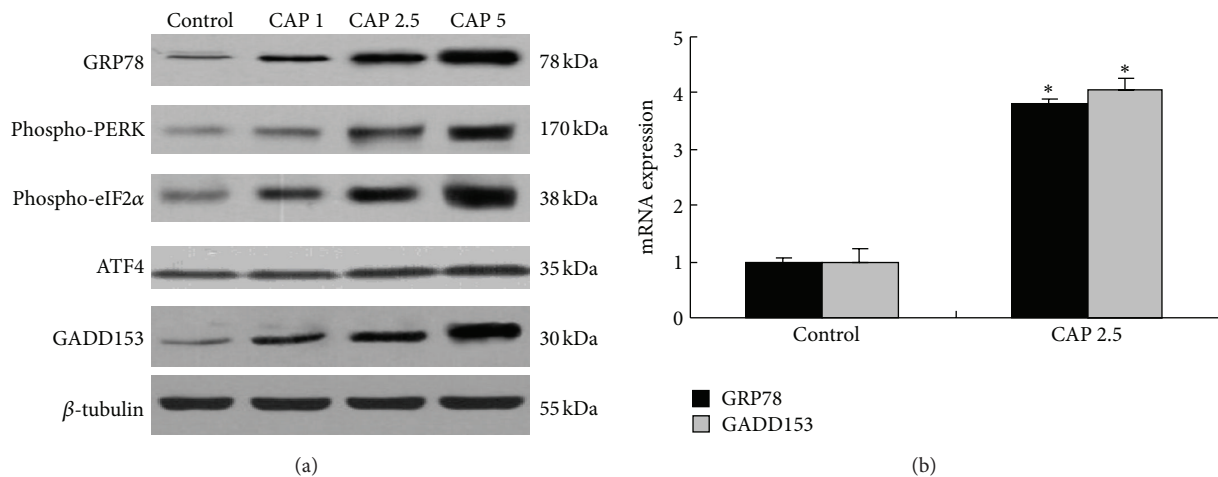


FIGURE 8: Effect of capsaicin on the expression of protein and mRNA of ERS markers in tumor tissues (control, PBS; CAP 1, capsaicin, 1 mg/kg; CAP 2.5, capsaicin, 2.5 mg/kg; CAP 5, capsaicin, 5 mg/kg). (a) Western blot analysis. Capsaicin promoted the protein expression of ERS markers (GRP78, phospho-PERK, phospho-eIF2 α , ATF4, and GADD153) in tumor tissues. β -tubulin was used as a loading control. The results shown are representative of three independent experiments. (b) Real-time PCR analysis for the mRNA expression of GRP78 and GADD153 in the control group and CAP 2.5 group. The relative amount of the target gene was normalized with the housekeeping gene RPLP0. Data are expressed as mean \pm SD and analyzed by the unpaired Student's t -test, and * $P < 0.01$ compared with the control group.

Conflict of Interests

The authors declare that they have no conflict of interests.

Acknowledgments

The authors are grateful for funding support from The Administration of Traditional Chinese Medicine of Zhejiang Province, China (Grant no. 2011ZZ010), Zhejiang Provincial Science Fund for Distinguished Young Scholars (Grant no. LR12H280001), and The National Natural Science Foundation of China (Grant no. 81173606). The authors thank the entire staff of the Animal Experimental Center in scientific research platform of the Second Affiliated Hospital of Wenzhou Medical College, the Animal Experimental Center in Zhejiang University School of Medicine, and Institute of Watershed Science and Environmental Ecology in Wenzhou Medical College for helpful assistance.

References

- [1] S. Raimondi, P. Maisonneuve, and A. B. Lowenfels, "Epidemiology of pancreatic cancer: an overview," *Nature Reviews Gastroenterology and Hepatology*, vol. 6, no. 12, pp. 699–708, 2009.
- [2] A. Vincent, J. Herman, R. Schulick, R. H. Hruban, and M. Goggins, "Pancreatic cancer," *The Lancet*, vol. 378, no. 9791, pp. 607–720, 2011.
- [3] A. Stathis and M. J. Moore, "Advanced pancreatic carcinoma: current treatment and future challenges," *Nature Reviews Clinical Oncology*, vol. 7, no. 3, pp. 163–172, 2010.
- [4] R. Andersson, U. Aho, B. I. Nilsson et al., "Gemcitabine chemoresistance in pancreatic cancer: molecular mechanisms and potential solutions," *Scandinavian Journal of Gastroenterology*, vol. 44, no. 7, pp. 782–786, 2009.
- [5] M. Hartel, F. F. Di Mola, F. Selvaggi et al., "Vanilloids in pancreatic cancer: potential for chemotherapy and pain management," *Gut*, vol. 55, no. 4, pp. 519–528, 2006.
- [6] R. Zhang, I. Humphreys, R. P. Sahu, Y. Shi, and S. K. Srivastava, "In vitro and in vivo induction of apoptosis by capsaicin in pancreatic cancer cells is mediated through ROS generation and mitochondrial death pathway," *Apoptosis*, vol. 13, no. 12, pp. 1465–1478, 2008.
- [7] W. T. Wei, H. Chen, Z. L. Ni et al., "Antitumor and apoptosis-promoting properties of emodin, an anthraquinone derivative from *Rheum officinale* Baill, against pancreatic cancer in mice via inhibition of Akt activation," *International Journal of Oncology*, vol. 39, no. 6, pp. 1381–1390, 2011.
- [8] W. T. Wei, H. Chen, Z. H. Wang et al., "Enhanced antitumor efficacy of gemcitabine by evodiamine on pancreatic cancer via regulating PI3K/Akt pathway," *International Journal of Biological Sciences*, vol. 8, no. 1, pp. 1–14, 2012.
- [9] G. A. Cordell and O. E. Araujo, "Capsaicin: identification, nomenclature, and pharmacotherapy," *The Annals of Pharmacotherapy*, vol. 27, no. 3, pp. 330–336, 1993.
- [10] D. G. Barceloux, "Pepper and capsaicin (Capsicum and Piper species)," *Disease-a-Month*, vol. 55, no. 6, pp. 380–390, 2009.
- [11] M. J. Caterina, M. A. Schumacher, M. Tominaga, T. A. Rosen, J. D. Levine, and D. Julius, "The capsaicin receptor: a heat-activated ion channel in the pain pathway," *Nature*, vol. 389, no. 6653, pp. 816–824, 1997.
- [12] Y. J. Surh, "More than spice: capsaicin in hot chili peppers makes tumor cells commit suicide," *Journal of the National Cancer Institute*, vol. 94, no. 17, pp. 1263–1265, 2002.
- [13] A. M. Sanchez, M. G. Sanchez, S. Malagarie-Cazenave, N. Olea, and I. Diaz-Laviada, "Induction of apoptosis in prostate tumor PC-3 cells and inhibition of xenograft prostate tumor growth by the vanilloid capsaicin," *Apoptosis*, vol. 11, no. 1, pp. 89–99, 2006.
- [14] J. Y. Kim, E. H. Kim, S. U. Kim, T. K. Kwon, and K. S. Choi, "Capsaicin sensitizes malignant glioma cells to TRAIL-mediated apoptosis via DR5 upregulation and survivin downregulation," *Carcinogenesis*, vol. 31, no. 3, pp. 367–375, 2010.
- [15] K. Ito, T. Nakazato, K. Yamato et al., "Induction of apoptosis in leukemic cells by homovanillic acid derivative, capsaicin, through oxidative stress: implication of phosphorylation of p53 at Ser-15 residue by reactive oxygen species," *Cancer Research*, vol. 64, no. 3, pp. 1071–1078, 2004.
- [16] Z. H. Wang, H. Chen, H. C. Guo et al., "Enhanced antitumor efficacy by the combination of emodin and gemcitabine against human pancreatic cancer cells via downregulation of the expression of XIAP in vitro and in vivo," *International Journal of Oncology*, vol. 39, no. 5, pp. 1123–1131, 2011.
- [17] V. I. Rasheva and P. M. Domingos, "Cellular responses to endoplasmic reticulum stress and apoptosis," *Apoptosis*, vol. 14, no. 8, pp. 996–1007, 2009.
- [18] P. Walter and D. Ron, "The unfolded protein response: from stress pathway to homeostatic regulation," *Science*, vol. 334, no. 6059, pp. 1081–1086, 2011.
- [19] S. Oyamomari and M. Mori, "Roles of CHOP/GADD153 in endoplasmic reticulum stress," *Cell Death and Differentiation*, vol. 11, no. 4, pp. 381–389, 2004.
- [20] L. G. Haas, "BiP (GRP78), an essential hsp70 resident protein in the endoplasmic reticulum," *Experientia*, vol. 50, no. 11–12, pp. 1012–1020, 1994.
- [21] R. V. Rao, A. Peel, A. Logvinova et al., "Coupling endoplasmic reticulum stress to the cell death program: role of the ER chaperone GRP78," *The FEBS Letters*, vol. 514, no. 2–3, pp. 122–128, 2002.
- [22] R. J. Kaufman, "Stress signaling from the lumen of the endoplasmic reticulum: coordination of gene transcriptional and translational controls," *Genes & Development*, vol. 13, no. 30, pp. 1211–1233, 1999.
- [23] Q. J. Quinones, G. G. de Ridder, and S. V. Pizzo, "GRP78: a chaperone with diverse roles beyond the endoplasmic reticulum," *Histology and Histopathology*, vol. 23, no. 11, pp. 1409–1416, 2008.
- [24] S. H. Oh and S. C. Lim, "Endoplasmic reticulum stress-mediated autophagy/apoptosis induced by capsaicin (8-methyl-N-vanillyl-6-nonenamide) and dihydrocapsaicin is regulated by the extent of c-jun NH2-terminal kinase/extracellular signal-regulated kinase activation in WI38 lung epithelial fibroblast cells," *Journal of Pharmacology and Experimental Therapeutics*, vol. 329, no. 1, pp. 112–122, 2009.
- [25] S. W. Ip, S. H. Lan, H. F. Lu et al., "Capsaicin mediates apoptosis in human nasopharyngeal carcinoma NPC-TW 039 cells through mitochondrial depolarization and endoplasmic reticulum stress," *Human and Experimental Toxicology*, vol. 31, no. 6, pp. 539–549, 2012.
- [26] R. K. Reddy, C. Mao, P. Baumeister, R. C. Austin, R. J. Kaufman, and A. S. Lee, "Endoplasmic reticulum chaperone protein GRP78 protects cells from apoptosis induced by topoisomerase inhibitors. Role of ATP binding site in suppression of caspase-7 activation," *Journal of Biological Chemistry*, vol. 278, no. 23, pp. 20915–20924, 2003.

- [27] L. H. Zhang and X. Zhang, "Roles of GRP78 in physiology and cancer," *Journal of Cellular Biochemistry*, vol. 110, no. 6, pp. 1299–1305, 2010.
- [28] J. Lee, A. J. Bruce-Keller, Y. Kruman, S. L. Chan, and M. P. Mattson, "2-deoxy-D-glucose protects hippocampal neurons against excitotoxic and oxidative injury: evidence for the involvement of stress proteins," *Journal of Neuroscience Research*, vol. 57, no. 1, pp. 48–61, 1999.
- [29] R. V. Rao, H. M. Ellerby, and D. E. Bredesen, "Coupling endoplasmic reticulum stress to the cell death program," *Cell Death and Differentiation*, vol. 11, no. 4, pp. 372–380, 2004.
- [30] I. Tabas and D. Ron, "Integrating the mechanisms of apoptosis induced by endoplasmic reticulum stress," *Nature Cell Biology*, vol. 13, no. 3, pp. 184–190, 2011.
- [31] H. Zinszner, M. Kuroda, X. Wang et al., "CHOP is implicated in programmed cell death in response to impaired function of the endoplasmic reticulum," *Genes & Development*, vol. 12, no. 7, pp. 982–995, 1998.
- [32] D. Ron and J. F. Habener, "CHOP, a novel developmentally regulated nuclear protein that dimerizes with transcription factors C/EBP and LAP and functions as a dominant-negative inhibitor of gene transcription," *Genes & Development*, vol. 6, no. 3, pp. 439–453, 1992.
- [33] M. V. Barone, A. Crozat, A. Tabaei, L. Philipson, and D. Ron, "CHOP (GADD153) and its oncogenic variant, TLS-CHOP, have opposing effects on the induction of G1/S arrest," *Genes & Development*, vol. 8, no. 4, pp. 453–464, 1994.
- [34] E. Topkan, C. Parlak, A. Kotek, A. F. Yapar, and B. Pehlivan, "Predictive value of metabolic 18FDG-PET response on outcomes in patients with locally advanced pancreatic carcinoma treated with definitive concurrent chemoradiotherapy," *BMC Gastroenterology*, vol. 11, article 23, 2011.
- [35] A. F. Shields, "PET imaging of tumor growth: not as easy as it looks," *Clinical Cancer Research*, vol. 18, no. 5, pp. 1189–1191, 2012.
- [36] C. Zhao, Z. Chen, X. Ye et al., "Imaging a pancreatic carcinoma xenograft model with 11C-acetate: a comparison study with 18F-FDG," *Nuclear Medicine Communications*, vol. 30, no. 12, pp. 971–977, 2009.

Research Article

The Predicted Proteomic Network Associated with the Antiarthritic Action of Qingfu Guanjieshu in Collagen-II-Induced Arthritis in Rats

Ting Yu Wang,^{1,2} Hua Zhou,³ Yuen Fan Wong,² Pui Kei Wu,² Wen-Luan Wendy Hsiao,² Elaine Lai-Han Leung,³ and Liang Liu³

¹ Department of Pharmacy, Shanghai Ninth People's Hospital, Shanghai Jiao Tong University School of Medicine, 639 Zhizaoju Road, Shanghai 200011, China

² Center for Cancer and Inflammation Research, School of Chinese Medicine, Hong Kong Baptist University, Kowloon Tong, Hong Kong

³ State Key Laboratory of Quality Research in Chinese Medicine, Macau University of Science and Technology, Avenida Wai Long, Taipa, Macau

Correspondence should be addressed to Elaine Lai-Han Leung; lhleung@must.edu.mo and Liang Liu; lliu@must.edu.mo

Received 31 January 2013; Accepted 23 April 2013

Academic Editor: Taiping Fan

Copyright © 2013 Ting Yu Wang et al. This is an open access article distributed under the Creative Commons Attribution License, which permits unrestricted use, distribution, and reproduction in any medium, provided the original work is properly cited.

Qingfu Guanjieshu (QFGJS) is an herbal preparation for treating rheumatoid arthritis (RA). Previous studies revealed that QFGJS significantly inhibited experimental arthritis and acute inflammation, accompanied by reduction of proinflammatory cytokines and elevation of anti-inflammatory cytokines. This study aims to identify the targeted proteins and predict the proteomic network associated with the drug action of QFGJS by using 2D gel and MALDI-TOF-MS/MS techniques. Thirty female Wistar rats were evenly grouped as normal and vehicle- and QFGJS-treated CIA rats. The antiarthritic effect of QFGJS was examined with a 19-day treatment course, and the knee synovial tissues of animals from each group were obtained for 2D gel and MALDI-TOF-MS/MS analysis. Results showed that QFGJS significantly ameliorated collagen II-induced arthritis when administered at 2.8 g/kg body weight for 19 days. 2D gel image analysis revealed 89 differentially expressed proteins in the synovial tissues among the normal and vehicle- and QFGJS-treated CIA rats from over 1000 proteins of which 63 proteins were identified by MALDI-TOF-MS/MS analysis, and 32 proteins were included for classification of functions using Gene Ontology (GO) method. Finally, 14 proteins were analyzed using bioinformatics, and a predicted proteomic network related to the anti-arthritic effect of QFGJS was established, and Pgl1 plays a central role.

1. Introduction

Rheumatoid arthritis (RA) is a chronic inflammatory and immunological disease characterized by an invasive synovial hyperplasia that leads to cartilage and bone destruction. RA afflicts generally 0.5~1.0% of the population worldwide and commonly leads to loss of joint function and consequently reduction of life quality and expectancy [1, 2]. The etiology and pathogenesis of RA remain still uncertain, and no ideal therapeutics from conventional medicine is available for treating RA at this moment. Complementary and alternative medicine (CAM), predominantly herbal therapy, has been reported valuable in treating RA due to its effectiveness in

preventing structural damage of the arthritic joints and its highly tolerance to RA patients [3, 4].

Herbal medicine, especially the herbal formulas, has been widely used for treating RA with promising outcomes for long history in China, Japan, and other Asian countries. QFGJS was prepared from five herbs as follows: *Caulis Sinomenii* 12 g, *Radix Aconiti Lateralis Preparata* 9 g, *Rhizoma Curcumae Longae* 6 g, *Radix Paeoniae Alba* 15 g, and *Cortex Moutan* 9 g. Based on the amount of these five herbs in QFGJS, the percentage composition of these five herbs were calculated as 23.53%, 17.65%, 11.76%, 29.41%, and 17.65%, respectively [5]. In our previous studies on QFGJS, it was found that QFGJS administered before the induction or after

the establishment of arthritis could significantly inhibit the onset and progression of the experimental CIA and adjuvant-induced arthritis (AA) in rats, showing marked decrease of the incidence and degree of clinical symptoms of arthritis, paw volume, arthritic score, and erythrocyte sedimentation rate (ESR), as well as reduction of cartilage and bone destruction revealed by radiological and histopathological analyses [5]. Further mechanistic studies showed that the anti-arthritic effect of QFGJS was in association with significant suppression of three major pro-inflammatory cytokines (TNF- α , IL-1 β , and IL-6) in serum during disease progression of AA and CIA in rats [5, 6]. However, both of the protein networks related to the pathogenesis of AA and CIA models and the drug action mechanisms of QFGJS remain unknown.

Autoimmune conditions like RA are characterized by the complexity of systematic pathologies difficult to be elucidated by the conventional biological and biochemical technologies, while the large-scale analysis of proteins expression, interactions, and functions in human clinical or arthritic mouse samples has shown great promise for unlocking many of their pathophysiological mechanisms [7]. For treatment of autoimmune conditions using herbal medicine, there must be significant complexities both in the effective chemical components and drug action mechanisms, while the proteomic analytical technology would be one of the most powerful tools to identify the targeted proteins and networks related to drug actions. Technically, two-dimensional (2D) polyacrylamide gel electrophoresis coupled with matrix-assisted laser desorption/ionization time-of-flight mass spectrum/mass spectrum (MALDI-TOF-MS/MS) has been proven as the most efficient proteomics tool, where thousands of protein spots can be visualized simultaneously, resulting in a global view of the state of a proteome. Using statistical-based bioinformatics analysis, it is capable of employing the vast proteomic data to identify specific disease-associated or drug-targeted proteins with a high level of confidence [8, 9]. Also, changes in individual proteins can be detected and quantified through comparison of the 2D gel spots patterns from different samples.

Accordingly, in the current study we utilized proteomics and bioinformatics technologies to identify the targeted proteins and predict proteomic networks of QFGJS responsible for its anti-arthritic effect in CIA rats as CIA is the most widely adopted animal models for investigating RA pathogenesis and examining drug actions of new therapeutics [10]. Simultaneously, proteomic profiling of the major complicated proteins and of CIA rats could be identified, which provides more scientific data in understanding the pathogenesis and characteristics of CIA at the protein level. In parallel with evaluation of the anti-arthritic action of QFGJS as did before [6], the knee synovial tissues of normal and vehicle- and QFGJS-treated CIA rats were isolated for proteomic analysis using 2D gel and MALDI-TOF-MS/MS techniques. Thereafter, Western blot assay was employed to verify QFGJS-targeted proteins in the same tissue samples, while bioinformatics technology and Genes Ontology (GO) analysis were utilized for classifying the identified proteins as well as establishing the proteomic networks involving anti-arthritic action of QFGJS in CIA rats.

2. Materials and Methods

2.1. Preparation of Collagen II and QFGJS Solutions. Collagen II (CII) solution was prepared by dissolving CII in 0.05 M acetic acid at 2 mg/mL (Chondrex 20022, Redmond, WA, USA) and emulsifying with an equal volume of incomplete Freund's adjuvant (IFA) (Chondrex 7002, Redmond, WA, USA) at 4°C using a high-speed homogenizer. QFGJS was prepared by extracting the five herbs with water, alcohol, and supercritical carbon dioxide followed by drying according to our previous reported method [6]. In brief, samples of the five herbs were refined as coarse powder by pulverization. Caulis Sinomenii was extracted with water, and the water extract was spray dried to obtain Extract 1. Radix Aconiti Lateralis Preparata and Radix Paeoniae Alba were refluxed together with 80% ethanol, and the ethanol extract was spray dried to obtain Extract 2. Cortex Moutan was extracted by supercritical CO₂ to produce Extract 3. The residue after supercritical CO₂ extraction was then refluxed with 80% ethanol and the ethanol extract was spray-dried to obtain Extract 4. Similarly, Rizhoma Curcuma Longae was extracted by supercritical CO₂ to produce Extract 5. The residue after supercritical CO₂ extraction was then refluxed with 80% ethanol, and the ethanol extract was dried with the vacuum drying technique to obtain Extract 6. Finally, Extracts 1–6 were mixed thoroughly to produce QFGJS. The quality consistency of QFGJS was demonstrated by HPLC fingerprint analysis. QFGJS solution at concentration of 0.283 g/mL was prepared by dissolving the drug (batch no. 20040822, granules) in the vehicle of 0.3% (w/v) carboxymethylcellulose (CMC) freshly before use.

2.2. Animals. Thirty female Wistar rats (5–6 weeks old) were purchased from the Laboratory Animal Services Center, the Chinese University of Hong Kong (Hong Kong). The animals were housed five per cage in rooms maintained at 20 ± 1°C with alternating 12-h light-dark cycle. Food and water were provided ad libitum throughout the experiments. Animals were acclimated to their surroundings over 1 week to eliminate the effect of stress prior to initiation of experiments. All of the experimental protocols involving animals and their care were approved by the Committee on Use of Human & Animal Subjects in Teaching and Research of the Hong Kong Baptist University and were carried out according to the regulations of the National Institutes of Health of USA and the Department of Health of Hong Kong Special Administrative Region.

2.3. Induction of CIA and QFGJS Treatment. Twenty female Wistar rats were used for induction of CIA according to the method described previously [5], while ten animals were used as normal control. Briefly, rats were intradermally injected at the base of the tail with 100 μ L CII solution, using a glass syringe with a locking hub and a 27-G needle. On day 7 after the primary immunization, all CIA rats were given a booster injection of CII solution with same dose. For normal rats, they were intradermally given saline in the primary immunization and booster injection.

Previously, we examined the anti-arthritic effect of QFGJS on CIA rats at dose of 1.94 and 3.89 g/kg significantly inhibit the paw swelling and reduce the pro-inflammatory cytokinesis expression [5]. Therefore, we took the average of these two doses and used 2.8 g/kg as the working dosage in this project. The CIA rats were further randomly separated and exposed to once-daily oral administration of QFGJS (2.8 g/kg body weight) or vehicle (0.3% CMC solution) from the day after the onset of arthritis to day 30 of CIA induction. The administration volume (mL) to each rat equaled to one percent of its body weight (g).

2.4. Evaluation of the Development of Arthritis. The rats were inspected daily for the onset of arthritis characterized by edema and/or erythema in the paws. The incidence and severity of arthritis were evaluated using an arthritic scoring system, bi-hind paw volumes, and body weight measurement every 2 consecutive days beginning on the day when arthritic signs were first visible (around day 12 of CIA induction). In the arthritic scoring system, lesions (i.e., the clinical arthritic signs) of the four paws of each rat were graded from 0 to 4 according to the extent of both edema and erythema of the periarticular tissues; 16 was the potential maximum of the combined arthritic scores per animal. The hind paw volumes were measured using a plethysmometer chamber (7140 UGO, Basile, Comerio, Italy) and expressed as the mean volume change of both hind paws of rat. Body weight of the rats was monitored with a 0.1 g precision balance (Sartorius AG, Goettingen, Germany).

2.5. Synovial Tissues Sample Preparation. On day 30 of the experiment, all animals were sacrificed and both hind limbs were taken from rats with sterilized scissors. The limbs were put on the ice, and the synovia were isolated from the knee joints of both hind paws of each rat by removing the skin, muscle, fatty tissues, bone, and tendons of an individual paw. The synovial tissues were immediately snap frozen in liquid nitrogen and then stored in the refrigerator at -80°C .

In aspect of sample preparation for two-dimensional gel electrophoresis, the synovial tissues of each rat were pooled and washed with cold isotonic buffer for three times and centrifuged at 12,000 g for 1 min each time, and then the tissues were frozen in liquid nitrogen and ground into fine powder in an ice bath. For protein extraction, the powder was lysed with 2D lysis buffer (8 M urea, 4 M thiourea, 4% (w/v) CHAPS, and 40 mM DTT) plus 2 $\mu\text{L}/\text{mL}$ Benzonase (Calbiochem, Madison, WI). The lysates were incubated on ice for 20 min with gentle shaking and then centrifuged at 25,000 g at 4°C for 30 min. The supernatants were collected, and protein concentrations were determined by 2D Quant Kit (GE Healthcare, Chalfont St. Giles, UK) according to the manufacturer's instructions.

2.6. Two-Dimensional Gel Electrophoresis. Equal amount of proteins (80 μg) was processed by 2D Clean-up kit (GE Healthcare, Chalfont St. Giles, UK) to remove interfering substances according to the manufacturer's instructions. The purified protein pellets were air dried and resuspended in

250 μL of rehydration buffer (8 M urea, 2 M thiourea, 4% (w/v) CHAPS, 0.5% (v/v) IPG buffer pH 3–10, 1.2% (v/v) destreak reagent (GE Healthcare, Chalfont St. Giles, UK)). Then, the resuspended proteins were subjected to 2D gel electrophoresis. In the first dimension, proteins were separated by IEF with a 13 cm Immobiline DryStrip gel of pH 3–10 (GE Healthcare, Chalfont St. Giles, UK) and rehydrated in a standard strip holder (GE Healthcare, Chalfont St. Giles, UK) at 30 V for 5 hr and then at 60 V for further 5 hr. The protein samples were then separated on a 50 $\mu\text{A}/\text{strip}$ using the Ettan IPGphor 3 System (GE Healthcare, Chalfont St. Giles, UK) with a program of stepwise increase in voltage for 65860 Vh at 20°C using the following program: 100 V step-n-hold for 2 hrs; 500 V step-n-hold for 1 hr; 1000 V step-n-hold for 1 hr; 5000 V step-n-hold for 1 hr; 8000 V gradient for 1 hr; 8000 V step-n-hold for 50000 Vhr. After the first dimension, the strips were equilibrated in SDS equilibration buffer (6 M urea, 75 mM Tris-HCl (pH 8.8), 30% glycerol (v/v), 2% SDS (w/v), and 0.002% (w/v) bromophenol blue) containing 10 mg/mL DTT for 15 min, and thereafter in the SDS equilibration buffer containing 25 mg/mL iodoacetamide (IAA) for 15 min. After equilibration, proteins were separated on 12.5% SDS polyacrylamide gel Laemmli buffer system in an SE 600 standard vertical electrophoresis unit (GE Healthcare, Chalfont St. Giles, UK). The IPG strips were sealed in place with 1% agarose solution. The second dimension electrophoresis was performed at 30 mA at room temperature. Finally, 2D gels were silver stained using a protocol compatible with mass spectrometry for protein spot visualization [11]. The silver stained gels were then scanned with an Image Scanner III (GE Healthcare, Chalfont St. Giles, UK) and analyzed with Progenesis SameSpots software (Nonlinear Dynamics Ltd., UK).

2.7. In-Gel Trypsin Digestion, Mass Spectrometry Analysis, and Database Searching. In-gel trypsin digestion, MS analysis, and database searching were subsequently performed. Protein spots showing significantly altered expression levels among three groups of the synovium samples were excised in duplicate from the silver-stained gels and identified by MALDI-TOF-MS/MS. Briefly, the gel plugs were dehydrated with acetonitrile (ACN), which were then removed and then were vacuum dried. Next, 20 μL of 10 mM DTT in 10 mM NH_4HCO_3 was added, and the proteins were reduced for 30 min at 56°C . The gel plugs were then dehydrated with 200 μL ACN. The supernatants were subsequently replaced with 20 μL of 55 mM iodoacetamide (IAA) in 10 mM NH_4HCO_3 . After 20 min incubation at room temperature in the dark, IAA solution was removed. The gel plugs were washed with 50% ACN in 10 mM NH_4HCO_3 and dehydrated with 100% ACN followed by drying in a vacuum centrifuge. The completely dried gel plugs were incubated with trypsin (trypsin gold, mass spectrometry grade, Promega, USA) solution (12.5 $\mu\text{g}/\text{mL}$ in 10 mM NH_4HCO_3) overnight at 37°C . Peptides were extracted with 1% TFA in 80% acetonitrile and vacuum dried at 45°C for 1.5 hr and then stored at -20°C until mass spectrometry.

MALDI samples were prepared by spotting 1–2 μL digested solution onto a thin layer of α -cyano-4-hydroxy-cinnamic

acid on the 600 μm AnchorChip MALDI probe (Bruker Daltonik, Germany). After reaching dryness at room temperature, the samples were analyzed on a Bruker Autoflex III MALDI TOF/TOF Mass Spectrometer (Bruker Daltonik, Germany). MALDI-MS and MS/MS data were acquired and combined through the BioTools 3.0 program to search the protein database (Swiss-Prot 57.1, 462764 sequences; 163773385 residues) using in-house Mascot software (Matrix Science, London, UK).

2.8. Western Blot Analysis. Proteins were extracted from knee synovial tissues of the normal, CIA, and QFGJS-treated CIA rats according to previous protocols [12]. Forty micrograms of proteins from each group were separated on 12.5% SDS gels and transferred to polyvinylidene difluoride membranes (Millipore, MA, USA). Following the transfer, the membranes were blocked overnight at 4°C using 5% skim milk in Tris-buffered saline (TBS, 20 mM, Tris, 500 mM NaCl, pH 7.5) and then incubated with primary antibodies specifically against Pgk1, Gstp1, Aldh6a1, vimentin (Santa Cruz, Santa Cruz, CA, USA), and beta-actin (Sigma, St. Louis, MO, USA) in TBS for 1 hr at room temperature. The membranes were washed three times with TBST (TBS, 0.1% Tween 20) and then incubated with 1:10,000 dilution of anti-rabbit or anti-mouse IgG secondary antibodies (Zymed, South San Francisco, CA, USA) conjugated to horseradish peroxidase in 2% skim milk in TBST for 1 hr at room temperature. Finally, the membranes were washed three times, and the immunoreactive proteins were detected by enhanced chemiluminescence (ECL) using hyperfilm and ECL reagent (Amersham International Plc., Buckinghamshire, UK).

2.9. Protein Classification and Interaction Analysis. To assess the major biological themes of the differentially regulated proteins by QFGJS in the knee synovial tissues of CIA rats, Gene Ontology (GO) analysis (<http://www.geneontology.org/>) was conducted. The differentially expressed proteins in the normal rats, CIA rats, and QFGJS-treated-CIA rats were classified into different groups. Data filtering was performed based on the gene product type, data source, species, and the term association. The ontology of biological processes, molecular functions, and cellular components was further filtered. The accession item was chosen to get the term lineage, and finally, the classification of a unique protein was determined and presented in Table 1. All the proteins identified by MODI-TOF/TOF of the three different experimental animal groups were classified with this method.

After classification by GO, proteins in the same class were chosen and analyzed by the String database (<http://string.embl.de/>). The tool provides analysis of the functionally related proteins that might be coregulated or physically interacted under CIA condition and upon the QFGJS treatment. Consequently, a predicted network of the newly identified proteins representing their protein-protein interactions related to CIA induction and the anti-arthritis effect of QFGJS can be established.

2.10. Statistical Analysis. For evaluation of the pharmacological arthritic effect of QFGJS, data were expressed as

mean \pm SEM. Statistical analysis was performed with one-way ANOVA followed by post hoc test with least significant difference (LSD) method. All analyses were performed with SPSS 15.0 (SPSS Inc., Chicago, USA). Values were considered as significantly different when $P < 0.05$. For 2D gel results of proteomic analysis, differential software Progenesis SameSpots (Nonlinear Dynamics) was used for identification of the up- and downregulated spots by comparing the relative abundance of each matched protein spot among the normal groups, vehicle-treated CIA, and QFGJS-treated CIA groups ($n = 6$, for each sample). It was considered as significant when the overall fold change of the protein among the three groups of the animals was more than 1.4 and analysis of variance (ANOVA) P value lower than 0.5.

3. Results

3.1. Amelioration of CIA by QFGJS. CIA was induced on day 1, while the inflammatory and arthritic lesions that appeared from day 12 onwards in CIA rats were assessed until day 30 at the end of experiment. Just from day 12, QFGJS was given once per day until day 30 as well. The results showed that QFGJS treatment markedly decreased hind paw volumes and arthritic scores from day 20 and day 24 onward, respectively (Figures 1(a) and 1(b)). Also, QFGJS demonstrated a trend against loss of body weight of CIA rats, although no statistical significance was achieved between the QFGJS-treated and control animals (Figure 1(c)). Regarding changes of the synovial tissues, the average weight of synovial tissues isolated from both knee joints of normal animals was about 10 mg, while it reached at about 15 mg in CIA rats, indicating significant cell proliferations in synovial membranes of the arthritic CIA rats. Previously, we reported the protocol of CIA in rats [5], and the experiment followed the reported protocol. Marked tissues swelling, blood vessels dilation, and accumulation of synovial fluids in the CIA rats were observed while such pathological changes were much less in the QFGJS-treated rats in comparison with the vehicle-treated CIA animals.

3.2. 2-D Gel Protein Spot Images of the Knee Synovial Tissues from Normal and Vehicle- and QFGJS-Treated CIA Rats. To establish a predicted potential proteomic network and identify targeted proteins of QFGJS in treating CIA rats, we employed 2D gel image technique to examine the protein expression profiling in the knee synovial tissues of the vehicle- and QFGJS-treated CIA rats, as well as normal rats. The representative 2D gel images resembling proteome of the knee synovial tissues from three groups of animals are showing in Figure 2. When we compared gels from different groups, one gel was selected as the standard, and every protein spot on this gel was distributed with a rank number by the Progenesis SameSpots software. The software has generated more than 1000 rank numbers, for example, the highest rank number in Figure 2(a) is 1349 on the upper left corner of the gel. To analyze the altered protein spots, we compiled 2D images obtained from 6 random biological replicates for each group of animals using Progenesis SameSpots software (Nonlinear

TABLE 1: Identification of the differentially expressed proteins in the knee synovial tissue samples of the normal and vehicle-treated and QFGJS-treated CIA rats.

Spot no.	Target protein name ^a	Swiss-Prot accession number	Theoretical Mr/pI	Sequence coverage (%)	Mowse scores	Number of unique peptides	Normal	CIA	QFGJS	CIA/Normal	QFGJS/CIA	Max/Min ^b	P value
1	IgG-2a Ig gamma-2A chain C region	P20760	35677/7.72	11	211	3	6.85	7.45	7.40	3.93	0.90	3.93	3.89E - 05
2	Vim vimentin	P31000	53757/5.06	30	282	12	6.34	6.60	6.91	1.82	2.04	3.73	0.011
3	Gstp1 glutathione S-transferase P	P04906	23652/6.89	20	268	3	6.24	6.68	6.55	2.70	0.75	2.70	0.006
4	Apolipoprotein C-III, isoform CRA_b	P06759	7847/4.65	36	163	2	6.03	6.33	5.90	2.00	0.37	2.69	0.011
5	Aldh6a1 methylmalonate-semialdehyde dehydrogenase [acylating], mitochondrial	Q02253	58396/8.44	7	90	3	6.46	6.89	6.56	2.71	0.47	2.71	0.019
6	Ca 3 carbonic anhydrase 3	P14141	29698/6.89	14	109	4	6.46	6.26	6.05	0.64	0.61	2.56	0.026
7	Vdac2 voltage-dependent anion-selective channel protein 2	P81155	32353/7.44	13	104	2	6.45	6.45	6.08	1.00	0.42	2.38	0.045
8	Tpil triosephosphate isomerase	P48500	27345/6.89	13	195	2	7.03	6.81	6.71	0.61	0.79	2.10	2.48E - 04
9	Ces3 carboxylesterase 3	P16303	62393/6.1	2	88	2	6.52	6.20	6.31	0.48	1.28	2.08	0.035
10	Des desmin	P48675	53481/5.21	7	176	3	7.04	6.73	6.79	0.49	1.15	2.06	0.02
11	RGDI560402 similar to phosphoglycerate kinase 1 (Pgkl)	IP100372910	43604/6.15	10	97	3	6.63	6.71	6.39	1.20	0.48	2.08	0.034
12	Pgam1 phosphoglycerate mutase 1	P25113	28928/6.67	12	143	3	7.19	7.47	7.43	1.94	0.91	1.94	0.018
13	Anxa2 isoform short of Annexin A2	Q07936-1	38939/7.55	21	172	7	7.01	6.92	6.73	0.80	0.65	1.92	0.015
14	Gpx1 glutathione peroxidase 1	P04041	22472/7.66	16	121	3	6.61	6.88	6.73	1.90	0.71	1.90	0.033
15	Ivd isovaleryl-CoA dehydrogenase, mitochondrial	P12007	46862/8.03	14	112	5	6.86	6.71	6.59	0.70	0.76	1.86	0.002
16	Crp C-reactive protein	P48199	25737/4.89	21	193	4	6.48	6.63	6.75	1.41	1.31	1.85	0.048
17	Capzb F-actin-capping protein subunit beta	Q5XI32	30952/5.69	15	297	5	7.31	7.22	7.04	0.82	0.66	1.83	0.019
18	Idh3a isocitrate dehydrogenase [NAD] subunit alpha, mitochondrial	Q99NA5	40044/6.47	15	199	5	7.01	6.89	6.75	0.77	0.73	1.79	0.027

TABLE 1: Continued.

Spot no.	Target protein name ^a	Swiss-Prot accession number	Theoretical Mr/pI	Sequence coverage (%)	Mowse scores	Number of unique peptides	Logarithm of average normalized volume		Fold change of average normalized volume between groups		Overall fold change of average normalized volume among three groups		P value
							Normal	CIA	QFGJS	CIA/Normal	QFGJS/CIA	Max/Min ^b	
19	RGDI565368 similar to glyceralddehyde-3-phosphate dehydrogenase	IPI00554039	36045/8.44	12	97	4	7.15	7.01	6.90	0.71	0.78	1.79	0.006
20	Selenbp1 selenium-binding protein 1	Q8VIF7	53069/6.1	16	149	7	7.18	6.99	6.94	0.65	0.90	1.71	0.008
21	Ogn osteoglycin	IPI00362931	34390/5.85	30	284	8	7.64	7.50	7.41	0.72	0.81	1.70	0.007
22	Ldhd L-lactate dehydrogenase B chain	P42123	36874/5.7	11	136	4	7.33	7.20	7.10	0.74	0.81	1.68	0.049
23	Actb actin, cytoplasmic 1	P60711	42052/5.29	13	209	4	7.13	6.99	6.91	0.74	0.83	1.63	0.023
24	Serum albumin	P02770	71244/5.82	9	120	5	6.80	6.73	6.60	0.85	0.73	1.61	0.004
25	S100a4 protein S100-A4	P05942	11997/5.04	52	233	6	7.32	7.53	7.50	1.60	0.95	1.60	0.038
26	Np purine nucleoside phosphorylase	P85973	32566/6.46	12	122	3	7.51	7.64	7.70	1.34	1.15	1.55	0.03
27	Capza2 F-actin-capping protein subunit alpha-2	Q3TIK5	33118/5.57	9	139	2	7.45	7.35	7.27	0.79	0.84	1.52	0.048
28	Mdhl malate dehydrogenase, cytoplasmic	O88989	36631/6.16	12	73	4	7.27	7.17	7.09	0.80	0.83	1.51	0.024
29	Gstol glutathione S-transferase omega-1	Q9Z339	27936/6.25	12	146	3	6.86	6.80	6.70	0.88	0.78	1.46	0.05
30	Apoe apolipoprotein E	P02650	35788/5.23	33	251	11	7.15	7.31	7.24	1.45	0.85	1.45	0.015
31	Aldh2 protein	P11884	53791/5.83	12	396	6	7.35	7.20	7.21	0.71	1.03	1.42	0.045
32	Anxa1 Annexin A1	P07150	39147/6.97	16	316	6	7.38	7.28	7.23	0.79	0.89	1.41	0.033

^aThe differently expressed proteins with fold change of Max/Min less than 1.4 after Progenesis SameSpots software analysis, repetitive proteins analyzed by MALDI-TOF-MS/MS, and unique peptides less than 2 with Mascot software were excluded.

^bDenote as the ratio of maximum (Max) and minimum (Min) average normalized spot volumes among the normal rats, vehicle-treated CIA, rats and QFGJS-treated CIA rats.

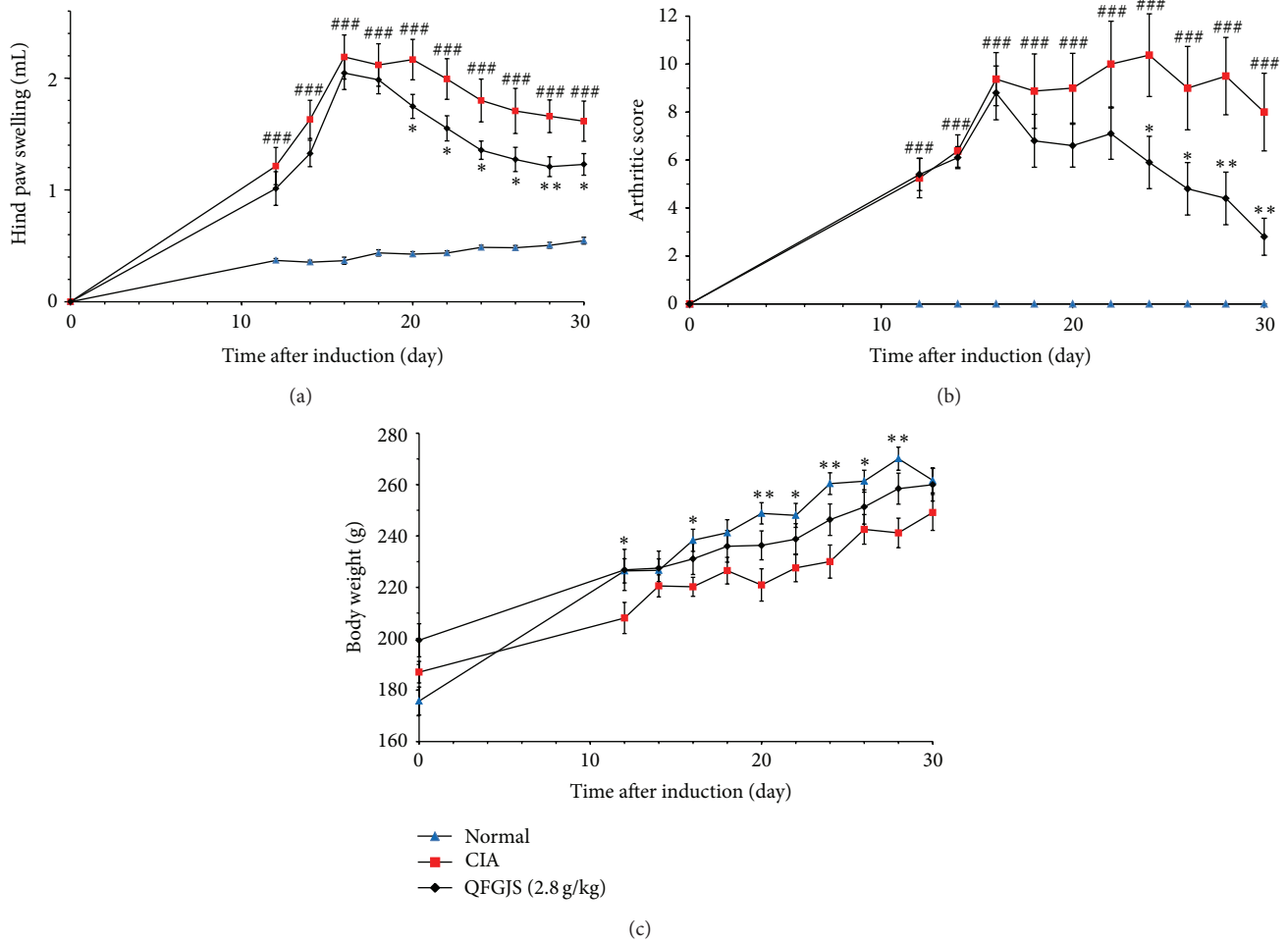


FIGURE 1: Effect of QFGJS on collagen II-induced arthritis (CIA) in rats. (a) paw swelling, (b) arthritic score, and (c) body weight. CIA was induced by intradermal injection of 100 μ L collagen II (CII)/incomplete Freund's adjuvant (IFA) emulsion containing 100 μ g of CII at the tail base of each rat, together with a booster injection of 100 μ g of CII in IFA on day 7 after the primary immunization. Normal rats (blue triangle) were intradermally given with saline at the primary immunization and booster injection. CIA rats were daily given with QFGJS at 2.8 g/kg body weight (black diamond) or vehicle (red square) beginning from day 12 after arthritis induction until day 30. Saline was orally given to the normal rats. Data were expressed as mean \pm SEM ($n = 10$). ### $P < 0.001$, normal rats versus the vehicle-treated CIA rats; * $P < 0.05$; ** $P < 0.01$, QFGJS-treated CIA rats versus vehicle-treated CIA rats.

Dynamics Ltd., UK). A match set was accordingly created by manual editing, and the gel with the most spots and the least background was chosen as a standard gel, and then, all of the other 17 gels were matched to this one automatically so as to match the proteins from different gels point to point. As such, all protein spots from different gels were matched to each other (Figure 2(b)). Overall, 89 differentially expressed protein spots were identified by comparing the normal- versus, vehicle- and vehicle- versus QFGJS-treated CIA rats. Such analysis on the overall fold changes of proteins expressions among three groups can ensure at the most screening of the potential proteins involved both in the pathogenesis of CIA disease and drug action mechanisms of QFGJS, so as to provide sufficient candidate proteins for further analysis using MALDI-TOF-MS/MS technique.

3.3. Identification of the Differentially Expressed Proteins in the Knee Synovial Tissues among Normal and Vehicle- and

QFGJS-Treated CIA Rats. Among 89 differentially expressed protein spots, 63 proteins were successfully identified by MALDI-TOF-MS/MS analysis. For other 25 spots, peptide mapping could not be performed due to insufficient amount of proteins and technical limitation. Proteomic data from MS analysis were acquired and combined through the BioTools 3.0 program, and then the identities of each protein were collected after searching the protein database with Mascot software. Among 63 differentially expressed proteins, the repetitive proteins analyzed by MALDI-TOF-MS/MS (16 spots) or the unique peptides less than 2 (15 spots) analyzed by Mascot software were excluded for further classification and verification. Finally, as shown in Table 1, a total of 32 proteins have been well identified together with their Swiss-Prot accession number, theoretical molecular weight and pI, sequence coverage, Mowse scores, number of unique peptides, logarithm of average normalized volume, and overall fold changes among three groups.

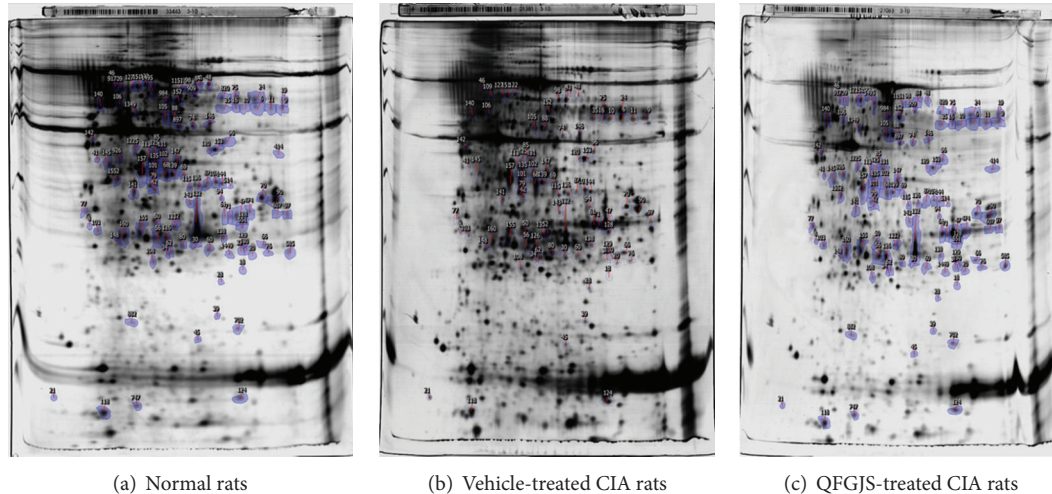


FIGURE 2: The representative images of 2D gel analysis resembling the proteome in the knee synovial tissues of the normal and vehicle- and QFGJS-treated CIA rats ($n = 6$). (a) Normal rats, (b) vehicle-treated CIA rats, and (c) QFGJS-treated CIA rats. After first dimension of IEF and second dimension of electrophoresis, the 2D gels were stained with silver solution. The gel images were scanned with Image Scanner III and analyzed with Progenesis SameSpots software. Protein spots showing the significantly altered expression levels among three groups of animals were marked and then excised for trypsin digestion followed by MALDI-TOF-MS/MS identification and database searching.

Comparing CIA rats to the normal animals, the dominant overexpression proteins in Table 1 include IgG-2a Ig gamma-2A chain C region, Gstp1 glutathione S-transferase P, Aldh6a1 methylmalonate-semialdehyde dehydrogenase, apolipoprotein C-III, isoform CRA-b, Vim vimentin, and Pgam1 phosphoglycerate mutase 1. On the other hand, both in the conditions of CIA rats and QFGJS treatment, some proteins showed a decreased expression such as Ca 3 carbonic anhydrase 3, Tpil triosephosphate isomerase, Anxa2 isoform short of Annexin A2, Ivd isovaleryl-CoA dehydrogenase, mitochondrial, Capzb F-actin-capping protein subunit beta, Idh3a isocitrate dehydrogenase [NAD] subunit alpha, and glyceraldehyde-3-phosphate dehydrogenase. Moreover, in animals treated with QFGJS, it was found not only to suppress proteins expressions related to the pathogenesis of arthritis but even activate expression of some proteins like Vim vimentin, C-reactive protein, and Np purine nucleoside phosphorylase. Another typical changes are phosphoglycerate kinase 1 (Pgk1) which showed only a little bit increase of protein expression under CIA condition but was significantly suppressed by QFGJS treatment, even lower than the level of normal animals. Therefore, due to such complicated changes of protein expressions under CIA condition and QFGJS treatment, our current studies should include all proteomic data from three groups of animals rather than from the treated and nontreated animals, so as to perform a more comprehensive proteomic analysis as well as achieve a global proteomic profiling upon QFGJS treatment for CIA rats.

3.4. Classification of the Differentially Expressed Protein Spots among Normal and Vehicle- and QFGJS-Treated CIA Rats. Gene Ontology (GO) analysis was performed to assess the major biological themes of the differentially expressed proteins in knee synovial tissues samples among three groups of animals. As shown in Table 2, those 32 identified proteins

in Table 1 could be classified into five classes upon their major known functions: 17 proteins are involved in metabolic process; 6 proteins are related to binding activity; 3 proteins can regulate biological processes; 3 proteins are in association with cellular processes, and other 3 proteins belong to the category of others.

3.5. Establishment of the Predicted Proteomic Network among the Major Differentially Identified Proteins Responsible for the Antiarthritic Effect of QFGJS. After classification by GO, the majority of newly identified differentially expressed proteins in the knee synovial tissues of CIA rats responsible for the antiarthritic effect of QFGJS fell into the class of proteins which are heavily involved in metabolic process (17 proteins). Therefore, those 17 proteins were subject to further analysis using String database by which a potential proteomic network was predicted. However, as the apolipoprotein C-III, Pgam1, and Gpx1 with rat origin were not found in the database of String Software, they were excluded for building the network. Other 14 proteins (Gstp1, Tpil1, Ca 3, Ivd, Apoe, Aldh6a, Idh3a, Pgk1, Gapdh, Ldhh, Np, Mdh1, Aldh2, and Gsto1) are well connected in building of the network. As a result, predicted connections and interactions in the proteomic network between 14 proteins have been elucidated in Figure 3, which include neighborhood, gene fusion, cooccurrence, and coexpression. In this network, Pgk1 is a core protein which plays the most important role in phosphoprotein glycolysis and connects with other 13 proteins. Also, Pgk1 is the neighborhood of Tpil1 and can be translocated with Tpil1, leading to protein-protein interaction with Ca 3. Other major connections in the network are Gapdh connects Pgk1 with Np and Mdh1; Mdh1 is the neighborhood of Idh3a and Ldhh; Ldhh connects Mdh1 with Ivd, Aldh2, and Aldh6a1. Besides, Gstp1 is a homologous protein of Gsto1 and Apoe and connects them with Ivd.

TABLE 2: Classification of the differentially expressed proteins revealed in the knee synovial tissues among the normal and vehicle-treated and QFGJS-treated CIA rats.

Classification	Subclassification	Name of proteins	Functions	Spot no.
	Antigen binding	IgG-2a Ig gamma-2A chain C region	Nucleotide sequence and antibody effector functions	1
	Cytoskeletal protein binding	Anxa2 isoform short of Annexin A2	Calcium-regulated membrane-binding protein	13
Binding	Protein binding	Des desmin	Class-III intermediate filaments	10
		Ogn osteoglycin	Induces bone formation in conjunction with TGF-beta-1 or TGF-beta-2	21
		Actb actin, cytoplasmic 1	Involved in various types of cell motility	23
		Serum albumin	Regulation of the colloidal osmotic pressure of blood	24
		Gsto1 glutathione S-transferase omega-1	Exhibits glutathione-dependent thiol transferase and dehydroascorbate reductase activities	29
	Metabolic process	Gstp1 glutathione S-transferase P	Conjugation of reduced glutathione to hydrophobic electrophiles	3
		Pgam1 phosphoglycerate mutase 1	Catalyze the reaction of EC 5.4.2.4 (synthase) and EC 3.1.3.13 (phosphatase)	12
	Lipid metabolic process	Tpi1 triosephosphate isomerase	Belongs to the triosephosphate isomerase family	8
	Lipoprotein metabolic process	Apoe apolipoprotein E	Mediates the binding, internalization, and catabolism of lipoprotein particles	30
	One-carbon metabolic process	Apolipoprotein C-III, isoform CRA_b	Inhibits lipoprotein and hepatic lipase and decreases the uptake of lymph chylomicrons	4
		Ca 3 carbonic anhydrase 3	Involved in the metabolism of xenobiotics and of natural substrates	6
		Aldh2 protein	Aldehyde dehydrogenase (NAD) activity, identical protein binding	31
Metabolic process	Oxidation reduction	Aldh6a1 methylmalonate-semialdehyde dehydrogenase [acylating], mitochondrial	Plays a role in valine and pyrimidine metabolism	5
		Gpx1 glutathione peroxidase 1	Protects the hemoglobin in erythrocytes	14
		Ivd isovaleryl-CoA dehydrogenase, mitochondrial	It is Oxidoreductase	15
		Idh3a isocitrate dehydrogenase [NAD] subunit alpha, mitochondrial	It is Oxidoreductase	18
		Ldhb L-lactate dehydrogenase B chain	Identical protein, NAD or NADH binding, and L-lactate dehydrogenase activity	22
		Mdh1 malate dehydrogenase, cytoplasmic	Oxidoreductase, NAD or NADH binding, and L-malate dehydrogenase activity	28
		RGD1565368 similar to glyceraldehyde-3-phosphate dehydrogenase	Catalytic activity	19
	Nucleobase, nucleoside, nucleotide, and nucleic acid metabolic process	Np purine nucleoside phosphorylase	Transferase, glycosyltransferase, purine-nucleoside phosphorylase activity	26
	Glycolysis	RGD1560402 similar to phosphoglycerate kinase 1 (Pgkl)	Phosphoglycerate kinase activity	11

TABLE 2: Continued.

Classification	Subclassification	Name of proteins	Functions	Spot no.
Regulation of biological process	Actin filament capping	Capzb F-actin-capping protein subunit beta	Blocking the exchange of subunits	17
		Capza2 F-actin-capping protein subunit alpha-2	Blocking the exchange of subunits	27
	Signal transduction	Anxa1 Annexin A1	Promotes membrane fusion and is involved in exocytosis	32
Cellular process	Protein transport	Selenbp1 Selenium-binding protein 1	Involved in the sensing of reactive xenobiotics	20
	Intermediate filament-based process	Vim vimentin	Plays a role in the stability of the cytoplasmic architecture	2
	Transmembrane transport	Vdac2 Voltage-dependent anion-selective channel protein 2	Forms a channel through the mitochondrial outer membrane that allows diffusion of small hydrophilic molecules	7
		Ces3 carboxylesterase 3	Involved in the metabolism of xenobiotics and of natural substrates	9
Other	Acute inflammatory response	Crp C-reactive protein	Displays several functions associated with host defense	16
	Cellular component	S100a4 protein S100-A4	Interacts with PPF1BP1 in a calcium-dependent mode	25

Spot no. denotes the number shown in the first column of Table 1.

The differentially expressed protein spots observed among the normal rats, CIA rats, and QFGJS-treated CIA rats are classified into five classes. 6 proteins are related to binding, 17 proteins are related to metabolic process, 3 proteins are related to biological process, and 3 proteins are related to cellular process and 3 proteins belong to other class.

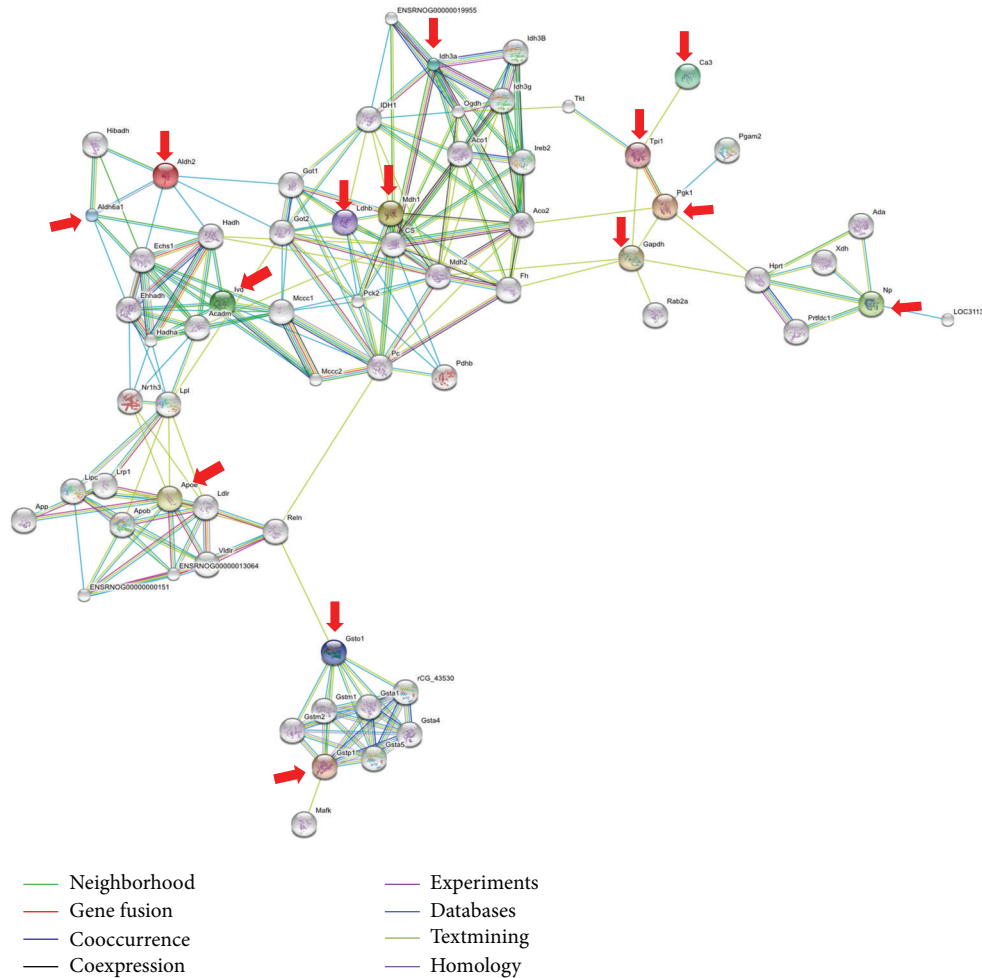


FIGURE 3: The predicted proteomic network identified by String Software resembling potential connections and interactions among the differentially expressed proteins associated with the anti-arthritis effect of QFGJS in CIA rats. The jointed lines represent the predicted protein-protein connections and correlations among the network including neighborhood, gene fusion, cooccurrence, and coexpression. The color points (arrow pointed) represent the proteins identified in the synovial tissues with functions involved in metabolic processes. The white points represent the proteins which have been reported in the literature, databases, text mining or showing homology. Although differential expression of apolipoprotein C-III, Pgam1, and Gpx1 had been demonstrated among the normal and vehicle-treated CIA and QFGJS-treated CIA rats after 2D gel analysis, these proteins with rat's origin were not found in the database of String Software; therefore, they were not included in the diagram.

3.6. *Verification of the Targeted Proteins Responsible for the Antiarthritic Effect of QFGJS Using Western Blot Assay.* To further verify if the major identified proteins are involved in the anti-arthritis effect of QFGJS, three proteins (Pgl1, Gstp1, and Aldh6a1), which were revealed as the most significant alteration of protein expression levels with overall fold change more than 2 and also having the most close connections and interactions in the network diagram, were selected for verification studies using Western blot assay. Vimentin was also selected for verification study because it is an important protein involving inflammatory process although QFGJS showed no suppressive effect on this protein upon 2D gel image analysis. But the Tpi1 and Car3 proteins were not employed for verification purpose due to their weak association with other proteins in the network, although their overall fold change of protein expressions was shown with

more than 2. In general, the results of verification using Western blot assay demonstrated a consistent trend with alterations of the targeted proteins expression in the synovial tissue samples among the normal and vehicle- and QFGJS-treated CIA rats, compared to the results from 2D gel image analysis (Figure 4). For instance, Pgl1, Gstp1, and vimentin showed overexpression in the knee synovial tissues of vehicle-treated CIA rats, while QFGJS treatment could markedly downregulate the expression of Pgl1 protein and slightly reduce the expression of Gstp1 and vimentin. Moreover, the suppressive potency of QFGJS on Pgl1 protein expression seemed to be more prominent in the Western blot assay compared to the results using 2D gel image analysis. Interestingly, Pgl1 has been known as phosphoglycerate kinase that plays a central role of regulating signaling transduction in immunocompetent cells, while in the current study, QFGJS

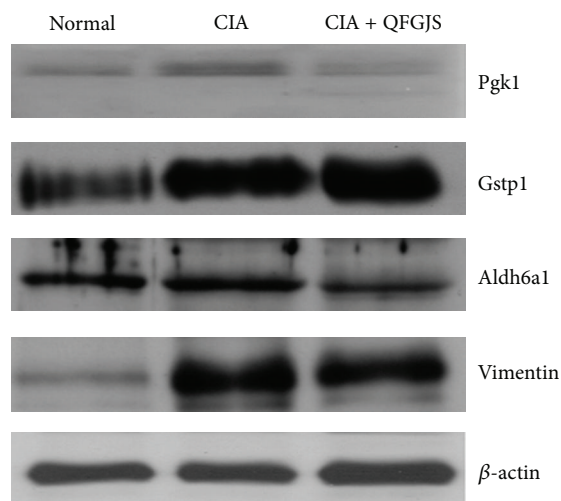


FIGURE 4: Western blot analysis for verification of the representative differentially expressed proteins. Forty micrograms of each tested protein extracted from the knee synovial tissues of normal rats, vehicle-treated CIA rats (CIA), and QFGJS-treated CIA rats (CIA + QFGJS) were separated on 12.5% SDS gels and probed with a specific primary antibody of Pgk1, Gstp1, Aldh6a1, or vimentin. Beta-actin was used as loading control and normalization. The Western blot was a representative of three individual experiments ($n = 3$).

showed to be potent of suppressing this protein. More importantly, Pgk1 demonstrates as a core protein to be well connected with other 13 proteins in the predicted proteomic network induced by QFGJS treatment (Figure 4). Regarding expression of Aldh6a1 protein, compared to the normal animals, it demonstrated upregulatory potency in the vehicle-treated CIA rats determined by Western blot assay against its potency determined by 2D gel analysis. In QFGJS-treated CIA rats, the Aldh6a1 expression was slightly downregulated. Collectively, suppression of protein Pgk1 expression may play central roles in antiarthritis of QFGJS to CIA rats.

4. Discussion

The synovial membranes are a thin lining layer within joint cavities which are responsible for maintaining normal joint functions and homeostasis. The fibroblast-like synovial (FLS) cells within synovial membranes are the cells that are closely associated with the homeostatic function of joints. These cells are the primary source of articular hyaluronic acid and other glycoproteins such as lubricin [13, 14]. In chronic inflammatory and arthritic disorders such as RA, synovial membranes become the major target of a persistent inflammatory process that leads to production of thickening in the synovial lining layer, neovascularization, and lymphocyte infiltration [15–17]. Although the pathogenesis of RA remains unknown, available evidence suggests that it may involve acquisition of a combination of increased proliferative potential and resistance to apoptosis in synovial membranes. This leads to a marked increase in the number of fibroblast-like synoviocytes in synovial membranes, which participate in complex autocrine and paracrine activation networks with

macrophages, lymphocytes, and dendritic cells and serve to sustain the synovitis and to enhance its destructive potential in the arthritic joints [18].

Several proteomic methods such as multidimensional liquid chromatography or 2-dimensional polyacrylamide gel electrophoresis (2D PAGE) in conjunction with mass spectrometry (MS) are increasingly being applied to determine differential mediators and protein markers profiling so as to identify the pathogenesis of joint diseases using samples from the synovium, cartilage, synovial fluid, and serum from patients and animals with arthritis [19–23]. Such systematic biological approaches have also been applied to explore the biomarkers and protein targets associated with therapeutic effects of drugs using RA patients' sera prior to and after therapy [24, 25]; however, application of proteomics on herbal medicine, especially on identification of the targeted proteins, remain limiting. In this study, we have applied 2D gel and MALDI-TOF-MS/MS techniques and identified the targeted proteins associated with CIA and the anti-arthritic effect of QFGJS in this rat model.

QFGJS is a pharmaceutical herbal preparation for treatment in both CIA and AA rat model; however, its molecular mechanism and target proteins have not yet been elucidated. To evaluate the influence of QFGJS on disease progression and protein expression of synovium of CIA rats, we examined the effect of QFGJS on CIA with daily treatment protocol for 19 days (from day 12 to 30 after induction of CIA) and obtained the knee joint synovial tissues for protein expression analysis. The results demonstrated that QFGJS at a dose of 2.8 g/kg body weight once daily treatment for 19 days could significantly ameliorate the arthritis induced by collagen II (Figure 1). For proteomic profiles, we have examined 18 knee synovium samples, that is, 6 normal biological replicates from each group of the normal and vehicle- and QFGJS-treated CIA rats using MALDI-TOF-MS/MS technique. 2D gel analysis revealed 89 proteins differentially expressed among the normal, vehicle- and QFGJS treated CIA rats from over 1000 proteins. Of those 89 proteins, 63 proteins were identified by MALDI-TOF-MS/MS analysis (Figure 2). After elimination of the repetitive and unsatisfied proteins, 32 proteins were selected for further bioinformatics analysis (Table 1). From the data of Table 1, it indicates that simultaneously analyzing the overall fold of change of a protein involved among the normal and vehicle-treated and QFGJS-treated rats is more comprehensive than analyzing the proteomic data from the treated and nontreated animals only.

By comparing protein expression levels among three groups of animals, of those 32 proteins, 10 (IgG-2a, vimentin, Gstp1, apolipoprotein C-III, Aldh6a1, Pgaml, Gpx1, Crp, S100a4, and Apoe) were found upregulated (fold change between the normal and CIA rats: >1.4) and 8 proteins (Ca3, Tpil, Ces3, Des, Ivd, RGD1565368, Selenbp1, and Aldh2) downregulated (fold change between the normal and CIA rats: <0.71), indicating that these proteins might be involved in the pathogenesis of CIA. Of these 18 proteins, 8 upregulated proteins (IgG-2a, Gstp1, apolipoprotein C-III, Aldh6a1, Pgaml, Gpx1, S100a4, and Apoe) and 3 downregulated proteins (Ces3, Des, and Aldh2) in the QFGJS-treated animals showed a tendency of returning the normal level,

suggesting that those 11 proteins might be involved in the anti-arthritic action of QFGJS. However, the expression of two proteins (vimentin and Crp) which have been upregulated in CIA were further enhanced by QFGJS treatment, while the expression of 5 proteins (Ca 3, Tpil, Ivd, RGD1565368, and Selenbp1) which have been down-regulated in CIA rats was further suppressed by QFGJS treatment. However, detailed roles of these proteins need to be further identified either in the pathogenesis of CIA or the anti-arthritic effect of CIA. Under such a situation, the Gene Ontology and proteomic network analysis were employed to elucidate the potential correlations of those 32 proteins and their roles in CIA and QFGJS treatment.

With the software of Gene Ontology, these 32 proteins were classified into five classes (Table 2): the majority of identified proteins (17 proteins) are related to metabolic processes; 6 proteins possess binding functions; 3 proteins are related to biological regulatory processes; 3 proteins are in association with cellular processes; and 3 proteins belong to other classes of proteins. And those 17 proteins involved in metabolic processes are the apolipoprotein C-III, Pgam1, Gpx1, Gstp1, Tpill, Ca 3, Ivd, Apoe, Aldh2, Aldh6a, Idh3a, Pgk1, Gapdh, Ldhh, Np, Mdh1, and Gsto1 and were selected for predicting the proteomic network of QFGJS's action. As apolipoprotein C-III, Pgam1, and Gpx1 are not with rat origin they were excluded for further bioinformatics analysis. Subsequently, a proteomic network with predicted connections and interactions among those 14 proteins has been established in the current study (Figure 3). Especially in this proteomic network, Pgk1 was found to be a core protein with close connection to other proteins. Pgk1 is the neighborhood of and was reported to have gene fusion with Tpill, which can interact with Ca 3. Pgk1 can also connect Gapdh with Np and Mdh1, while Mdh1 is the neighborhood of Idh3a and Ldhh. Ldhh connects Mdh1 with Ivd, Aldh2, and Aldh6a1. Gstp1 is the homologous proteins of Gstp1 and ApoE and connects with Ivd. For further verification, only proteins with overall fold change of more than 2 among three groups and involved in metabolic processes (except vimentin) were selected for further Western blot verification, of which the differential expression of Pgk1, Gstp1, Aldh6a1, and vimentin in the knee synovial samples among the normal and vehicle- and QFGJS-treated CIA rats was further confirmed by Western blot assay. Overall, the protein expression level of the core protein (Pgk1) was prominently changed in vehicle-treated CIA rats, while QFGJS treatment could restore its expression potency into an almost normal level, suggesting a strong correlation between the protein and anti-arthritic effect of QFGJS.

Moreover, Pgk1 is an important kinase for phosphoprotein glycolysis, and it was also identified as an autoantibody of RA reported by mass spectrometry analysis using 110 early untreated RA patients' sera [26]. Our data are also in line with their clinical findings, and Pgk1 was also identified as core responsive target to QFGJS in the rat CIA model, suggesting that using proteomic approach on QFGJS-treated CIA rat model is potentially useful to identify new targets with clinical relevance. Gstp1 is an enzyme that detoxifies carcinogens and protects cells against oxidative stress [27, 28], and the genetic polymorphisms of human *GSTP1* gene

were reported to be associated with disease activity of RA [29]. In our current study, higher protein expressions of Gstp1 and Pgk1 in the synovial membranes of CIA rats were shown in line with the previous clinical reports, while QFGJS treatment could significantly reverse expression levels of these two proteins, indicating that QFGJS is able to reduce the autoimmunity and oxidative stress. Aldh6a1 belongs to the aldehyde dehydrogenases family of proteins and plays a role in the valine and pyrimidine catabolic pathways. The product of this protein, a mitochondrial methylmalonate semialdehyde dehydrogenase, can catalyze the irreversible oxidative decarboxylation of malonate and methylmalonate semialdehydes into acetyl- and propionyl-CoA [30, 31]. In our study, QFGJS could decrease the expression of Aldh6a1 which indicates a suppressive role of oxidative stress by QFGJS. Further studies are needed on the behavior and mechanism of interactions among those proteins in association with the anti-arthritic effect of QFGJS during metabolic process.

Vimentin is an intermediate filament, abundantly expressed in synovial fibroblasts [32], and also a highly dynamic protein that regulates inflammatory responses assembly and disassembly via phosphorylation [33, 34]. Vimentin can be secreted by the activated macrophages through induction of TNF- α during inflammation, but the extracellular vimentin is essential for efficiently killing bacteria [35]. The consequence of secretion or presence of vimentin could lead to autoimmunity against these intermediate filaments. Presence of autoantibodies in autoimmune diseases such as RA has been reported in 40% RA patients' sera, and such antibodies can direct actions against the Sa antigen presence on the surface of citrullinated vimentin [36]. However, our findings in a current study showed no marked correlation between inhibition of vimentin and the antiarthritic effect of QFGJS, which needs further investigations.

In the current study, 2D gel image and MALDI-TOF-MS/MS techniques have been successfully utilized for identification of the global proteomic profiles of the normal and vehicle- and QFGJS-treated CIA rats, as well as the targeted proteins related to the antiarthritic effect of QFGJS in CIA model, in which 32 upregulated or downregulated proteins were identified from the synovial membranes by comparing all proteomic data among three groups of animals. Bioinformatics analysis using the software of Gene Ontology classified those 32 proteins into five classes, of which 17 proteins are considered as the major corresponding ones related to the pathogenesis of CIA as well as the drug actions of QFGJS. Further analysis using String database produced a prediction of the proteomic network related to the antiarthritic action of QFGJS, in which Pgk1 plays a central role.

Previously, we have demonstrated five representative bioactive compounds, that is, sinomenine, paeoniflorin, paeonol, curcumin, and hypaconitine, as the chemical markers of the pharmaceutical preparation of QFGJS [37]. Though sinomenine, paeoniflorin, paeonol, and curcumin have an antiarthritic effect, the effects of herbal medicinal compounds contained in QFGJS on antiarthritis must not be the same with the single bioactive compounds which may be caused by multicomponents and compound-compound interactions. For example, we have previously studied the effect of pure

paeonol and QFGJS containing paeonol, and the results indicated that other components in QFGJS could effectively influence the pharmacokinetic behavior and metabolic profile of paeonol in rats [38]. Therefore, combined use of all 5 herbs might probably be essential to exhibit the real treatment effect of QFGJS. However, it is interesting to further work on which components and what combination of the components providing the optimal treatment effect. Here, in the current studies we have attempted to use proteomics as the system biology platform to elucidate the network target of QFGJS, and optimization of drug combination of the network-based drug will further rely on the tighter integration of system biology and computational technologies [39].

All in all, we have tried to link the network-based treatment principle of herbal medicine with the pharmacological target network, and we believed that the efficient use of systems biology and computational technologies for investigation of medicinal herbs and herbal preparations will function as a powerful engine for multitarget drug discovery and development of network medicine. We hoped that the QFGJS example will arouse attention on how to develop novel and better method to study the network pharmacological effect of the complex herbal formulas.

Abbreviations

QFGJS:	Qingfu Guanjiesshu
RA:	Rheumatoid arthritis
MALDI-TOF-MS/MS:	Matrix-assisted laser desorption/ionization-time of flight-mass spectrum/mass spectrum
2D:	Two-dimensional
(CII):	Collagen II
(CIA):	Collagen II-induced arthritis.

Conflict of Interests

The authors declare no financial or commercial conflict of interests. They do not have a direct financial relation with the commercial identities mentioned in this paper.

Authors' Contribution

Ting Yu Wang and Hua Zhou equally contributed to the paper.

Acknowledgments

This work was supported by the Central Allocation Grant of Research Grant Council of Hong Kong Special Administrative Region (HKSAR) (HKBU2/07C) and Macao Science and Technology Development Fund (Project no. 035/2011/A2). The funders had no role in study design, data collection and analysis, decision to publish, or preparation of the paper. The authors thank Mr. Chi Chung Lee for providing technical support in MALDI-TOF-MS/MS analysis.

References

- [1] G. A. Schellekens, H. Visser, B. A. de Jong et al., "The diagnostic properties of rheumatoid arthritis antibodies recognizing a cyclic citrullinated peptide," *Arthritis and Rheumatism*, vol. 43, pp. 155–163, 2000.
- [2] D. L. Scott, D. P. M. Symmons, B. L. Coulton, and A. J. Popert, "Long-term outcome of treating rheumatoid arthritis: results after 20 years," *The Lancet*, vol. 1, no. 8542, pp. 1108–1110, 1987.
- [3] J. K. Rao, K. Mihaliak, K. Kroenke, J. Bradley, W. M. Tierney, and M. Weinberger, "Use of complementary therapies for arthritis among patients of rheumatologists," *Annals of Internal Medicine*, vol. 131, no. 6, pp. 409–416, 1999.
- [4] K. L. Soeken, S. A. Miller, and E. Ernst, "Herbal medicines for the treatment of rheumatoid arthritis: a systematic review," *Rheumatology*, vol. 42, no. 5, pp. 652–659, 2003.
- [5] X. Cai, H. Zhou, Y. F. Wong et al., "Suppression of the onset and progression of collagen-induced arthritis in rats by QFGJS, a preparation from an anti-arthritic Chinese herbal formula," *Journal of Ethnopharmacology*, vol. 110, no. 1, pp. 39–48, 2007.
- [6] X. Cai, H. Zhou, F. W. Yuen et al., "Suppressive effects of QFGJS, a preparation from an anti-arthritic herbal formula, on rat experimental adjuvant-induced arthritis," *Biochemical and Biophysical Research Communications*, vol. 337, no. 2, pp. 586–594, 2005.
- [7] R. Gobezie, P. J. Millett, D. S. Sarracino, C. Evans, and T. S. Thornhill, "Proteomics: applications to the study of rheumatoid arthritis and osteoarthritis," *The Journal of the American Academy of Orthopaedic Surgeons*, vol. 14, no. 6, pp. 325–332, 2006.
- [8] D. Fenyő and R. C. Beavis, "Informatics and data management in proteomics," *Trends in Biotechnology*, vol. 20, pp. S35–S38, 2002.
- [9] W. Zhang and B. T. Chait, "ProFound: an expert system for protein identification using mass spectrometric peptide mapping information," *Analytical Chemistry*, vol. 72, no. 11, pp. 2482–2489, 2000.
- [10] M. Hegen, J. C. Keith Jr., M. Collins, and C. L. Nickerson-Nutter, "Utility of animal models for identification of potential therapeutics for rheumatoid arthritis," *Annals of the Rheumatic Diseases*, vol. 67, no. 11, pp. 1505–1515, 2008.
- [11] A. Shevchenko, M. Wilm, O. Vorm, and M. Mann, "Mass spectrometric sequencing of proteins from silver-stained polyacrylamide gels," *Analytical Chemistry*, vol. 68, no. 5, pp. 850–858, 1996.
- [12] Y. F. Wong, H. Zhou, J. R. Wang, Y. Xie, H. X. Xu, and L. Liu, "Anti-inflammatory and analgesic effects and molecular mechanisms of JCICM-6, a purified extract derived from an anti-arthritic Chinese herbal formula," *Phytomedicine*, vol. 15, no. 6–7, pp. 416–426, 2008.
- [13] G. D. Jay, D. A. Harris, and C. J. Cha, "Boundary lubrication by lubricin is mediated by O-linked $\beta(1-3)$ Gal-GalNAc oligosaccharides," *Glycoconjugate Journal*, vol. 18, no. 10, pp. 807–815, 2001.
- [14] Y. Yamanishi and G. S. Firestein, "Pathogenesis of rheumatoid arthritis: the role of synoviocytes," *Rheumatic Disease Clinics of North America*, vol. 27, no. 2, pp. 355–371, 2001.
- [15] O. FitzGerald, M. Soden, G. Yanni, R. Robinson, and B. Bresnihan, "Morphometric analysis of blood vessels in synovial membranes obtained from clinically affected and unaffected knee joints of patients with rheumatoid arthritis," *Annals of the Rheumatic Diseases*, vol. 50, no. 11, pp. 792–796, 1991.

- [16] T. J. Smeets, R. J. Dolhain, F. C. Breedveld, and P. P. Tak, "Analysis of the cellular infiltrates and expression of cytokines in synovial tissue from patients with rheumatoid arthritis and reactive arthritis," *The Journal of Pathology*, vol. 186, pp. 75–81, 1998.
- [17] P. P. Tak, T. J. M. Smeets, M. R. Daha et al., "Analysis of the synovial cell infiltrate in early rheumatoid synovial tissue in relation to local disease activity," *Arthritis and Rheumatism*, vol. 40, no. 2, pp. 217–225, 1997.
- [18] G. S. Firestein, "Evolving concepts of rheumatoid arthritis," *Nature*, vol. 423, no. 6937, pp. 356–361, 2003.
- [19] R. Gobeze, A. Kho, B. Krastins et al., "High abundance synovial fluid proteome: distinct profiles in health and osteoarthritis," *Arthritis Research and Therapy*, vol. 9, article R36, 2007.
- [20] H. Liao, J. Wu, E. Kuhn et al., "Use of mass spectrometry to identify protein biomarkers of disease severity in the synovial fluid and serum of patients with rheumatoid arthritis," *Arthritis and Rheumatism*, vol. 50, no. 12, pp. 3792–3803, 2004.
- [21] K. Tilleman, K. Van Steendam, T. Cantaert, F. De Keyser, D. Elewaut, and D. Deforce, "Synovial detection and autoantibody reactivity of processed citrullinated isoforms of vimentin in inflammatory arthritides," *Rheumatology*, vol. 47, no. 5, pp. 597–604, 2008.
- [22] J. Wu, W. Liu, A. Bemis et al., "Comparative proteomic characterization of articular cartilage tissue from normal donors and patients with osteoarthritis," *Arthritis and Rheumatism*, vol. 56, no. 11, pp. 3675–3684, 2007.
- [23] H. Yamagiwa, G. Sarkar, M. C. Charlesworth, D. J. McCormick, and M. E. Bolander, "Two-dimensional gel electrophoresis of synovial fluid: method for detecting candidate protein markers for osteoarthritis," *Journal of Orthopaedic Science*, vol. 8, no. 4, pp. 482–490, 2003.
- [24] Y. C. Chen, P. W. Wang, T. L. Pan, G. Bazylak, and J. J. Shen, "Proteomic analysis of plasma to reveal the impact of short-term etanercept therapy in pediatric patients with enthesitis-related arthritis: a case report," *Combinatorial Chemistry and High Throughput Screening*, vol. 13, no. 6, pp. 469–481, 2010.
- [25] R. C. Dwivedi, N. Dhindsa, O. V. Krokhn, J. Cortens, J. A. Wilkins, and H. S. El-Gabalawy, "The effects of infliximab therapy on the serum proteome of rheumatoid arthritis patients," *Arthritis Research and Therapy*, vol. 11, no. 2, article R32, 2009.
- [26] V. Goëb, M. Thomas-L'Otellier, R. Daveau et al., "Candidate autoantigens identified by mass spectrometry in early rheumatoid arthritis are chaperones and citrullinated glycolytic enzymes," *Arthritis Research and Therapy*, vol. 11, no. 2, article R38, 2009.
- [27] K. D. Tew and D. M. Townsend, "Regulatory functions of glutathione S-transferase P1-1 unrelated to detoxification," *Drug Metabolism Reviews*, vol. 43, no. 2, pp. 179–183, 2011.
- [28] Z. Yin, V. N. Ivanov, H. Habelhah, K. Tew, and Z. Ronai, "Glutathione S-Transferase p elicits protection against H₂O₂-induced cell death via coordinated regulation of stress kinases1," *Cancer Research*, vol. 60, no. 15, pp. 4053–4057, 2000.
- [29] P. B. Grabar, D. Logar, M. Tomšič, B. Rozman, and V. Dolžan, "Genetic polymorphisms of glutathione S-transferases and disease activity of rheumatoid arthritis," *Clinical and Experimental Rheumatology*, vol. 27, no. 2, pp. 229–236, 2009.
- [30] K. L. Chambliss, R. G. F. Gray, G. Rylance, R. J. Pollitt, and K. M. Gibson, "Molecular characterization of methylmalonate semialdehyde dehydrogenase deficiency," *Journal of Inherited Metabolic Disease*, vol. 23, no. 5, pp. 497–504, 2000.
- [31] N. Y. Kedishvili, K. M. Popov, P. M. Rougraff, Y. Zhao, D. W. Crabb, and R. A. Harris, "CoA-dependent methylmalonate-semialdehyde dehydrogenase, a unique member of the aldehyde dehydrogenase superfamily. cDNA cloning, evolutionary relationships, and tissue distribution," *The Journal of Biological Chemistry*, vol. 267, no. 27, pp. 19724–19729, 1992.
- [32] O. A. Osung, M. Chandra, and E. J. Holborow, "Intermediate filaments in synovial lining cells in rheumatoid arthritis and other arthritides are of vimentin type," *Annals of the Rheumatic Diseases*, vol. 41, no. 1, pp. 74–77, 1982.
- [33] J. E. Eriksson, T. He, A. V. Trejo-Skalli et al., "Specific in vivo phosphorylation sites determine the assembly dynamics of vimentin intermediate filaments," *Journal of Cell Science*, vol. 117, no. 6, pp. 919–932, 2004.
- [34] J. L. Martys, C. L. Ho, R. K. H. Liem, and G. G. Gundersen, "Intermediate filaments in motion: observations of intermediate filaments in cells using green fluorescent protein-vimentin," *Molecular Biology of the Cell*, vol. 10, no. 5, pp. 1289–1295, 1999.
- [35] N. Mor-Vaknin, A. Punturieri, K. Sitwala, and D. M. Markovitz, "Vimentin is secreted by activated macrophages," *Nature Cell Biology*, vol. 5, no. 1, pp. 59–63, 2003.
- [36] E. R. Vossenaar, N. Després, E. Lapointe et al., "Rheumatoid arthritis specific anti-Sa antibodies target citrullinated vimentin," *Arthritis Research and Therapy*, vol. 6, no. 2, pp. R142–R150, 2004.
- [37] Y. Xie, Z. H. Jiang, H. Zhou et al., "Combinative method using HPLC quantitative and qualitative analyses for quality consistency assessment of a herbal medicinal preparation," *Journal of Pharmaceutical and Biomedical Analysis*, vol. 43, no. 1, pp. 204–212, 2007.
- [38] Y. Xie, H. Zhou, Y. F. Wong, H. X. Xu, Z. H. Jiang, and L. Liu, "Study on the pharmacokinetics and metabolism of paeonol in rats treated with pure paeonol and an herbal preparation containing paeonol by using HPLC-DAD-MS method," *Journal of Pharmaceutical and Biomedical Analysis*, vol. 46, no. 4, pp. 748–756, 2008.
- [39] E. L. Leung, Z. W. Cao, Z. H. Jiang, H. Zhou, and L. Liu, "Network-based drug discovery by integrating systems biology and computational technologies," *Briefings in Bioinformatics*, 2012.

Review Article

Network Pharmacology: A New Approach for Chinese Herbal Medicine Research

Gui-biao Zhang,¹ Qing-ya Li,^{1,2} Qi-long Chen,¹ and Shi-bing Su¹

¹ Research Center for Traditional Chinese Medicine Complexity System, Shanghai University of Traditional Chinese Medicine, Shanghai 201203, China

² Henan University of TCM, Zhengzhou 450008, China

Correspondence should be addressed to Shi-bing Su; shibingsu07@163.com

Received 26 January 2013; Revised 28 March 2013; Accepted 2 May 2013

Academic Editor: Wei Jia

Copyright © 2013 Gui-biao Zhang et al. This is an open access article distributed under the Creative Commons Attribution License, which permits unrestricted use, distribution, and reproduction in any medium, provided the original work is properly cited.

The dominant paradigm of “one gene, one target, one disease” has influenced many aspects of drug discovery strategy. However, in recent years, it has been appreciated that many effective drugs act on multiple targets rather than a single one. As an integrated multidisciplinary concept, network pharmacology, which is based on system biology and polypharmacology, affords a novel network mode of “multiple targets, multiple effects, complex diseases” and replaces the “magic bullets” by “magic shotguns.” Chinese herbal medicine (CHM) has been recognized as one of the most important strategies in complementary and alternative medicine. Though CHM has been practiced for a very long time, its effectiveness and beneficial contribution to public health has not been fully recognized. Also, the knowledge on the mechanisms of CHM formulas is scarce. In the present review, the concept and significance of network pharmacology is briefly introduced. The application and potential role of network pharmacology in the CHM fields is also discussed, such as data collection, target prediction, network visualization, multicomponent interaction, and network toxicology. Furthermore, the developing tendency of network pharmacology is also summarized, and its role in CHM research is discussed.

1. Introduction

Over the past decades, drug discovery has followed the dominant paradigm of the “one gene, one drug, one disease” and mainly focused on designing exquisitely selective ligands which could avoid side effects [1]. However, owing to the lack of efficacy and safety, the clinical attrition rate of new drug candidates reached up to 30% [2]. Moreover, the large-scale functional genomics studies have revealed that many single-gene knockouts exhibit little effect on the phenotype [3], and only 34% of single-gene knockout resulted in sickness or lethality [4]. Systems biology is a recent trend in bioscience research which focuses on the complex interactions in biological systems from a holistic perspective, rather than altering the single molecular component [5, 6]. Network pharmacology [7, 8], a system biology-based methodology, replaces the corollary of rational drug design of “magic bullets” by the search for multitarget drugs that act on biological networks

as “magic shotguns” [9]. Network biology analysis has also revealed that the deletion of individual nodes has little effect on the disease networks [10]. The increased understanding of the role of network biology systems challenges the dominant assumption of single-target drug discovery [11, 12]. Chinese herbal medicines (CHM) include natural medicines that were discovered by the ancient Chinese and evolved through at least 3000 years of uninterrupted clinical practice. Generally, CHM cures diseases by the synergistic effects of multiple compounds and herbal formula, which is mainly based on the integrative and holistic ways [13]. However, with the growing popularity and great promise of CHM, the ever-increasing demand for illuminating pharmacological mechanisms, potential drug efficacy, and clinical toxicity are major issues that need to be addressed. As a methodology and technology, network pharmacology offers a new approach to integrate the notion of drug discovery based on comprehensive research and synthetic assessment. Obviously, this

principle coincides with the characteristics of syndrome differentiation by traditional Chinese medicine (TCM) and holistic view of CHM treatment [14].

In this review, the concept and significance of network pharmacology is briefly introduced. Its application and potential role in CHM research is also summarized.

2. Concept and Significance of Network Pharmacology

With the rapid growth of available biomedical data in the postgenomic era, systems biology and polypharmacology have provided fresh insight into the drug discovery [15, 16]. The computational biology provides profitable approach to address the scientific suspense through efficacious modeling and theoretical exploration. In 2007, Hopkins created a novel concept of network pharmacology, which is built on the fundamental concept that many effective drugs in therapeutic areas act on multiple rather than single targets [7, 9]. Network pharmacology can be reconstructed with molecular networks that integrate multidisciplinary concepts including biochemical, bioinformatics, and systems biology [8]. It affords a rewarding assistance to forecast the off-target effects at a higher efficiency, which could improve the potency for drug discovery through a novel network mode of “multiple targets, multiple effects, complex diseases” [17].

The advantages of network pharmacology include the following: regulation of the signaling pathway with multiple channels, increase in drug efficacy, reduction of side effects, increase in the success rate of clinical trials, and decrease in the costs of drug discovery. Many complex diseases involve the interactions of multiple genes and functional proteins [18]. Network pharmacology models aim at addressing questions such as how and where in the disease network one target inhibits or activates the disease phenotypes. This ideally leads to therapies that are less vulnerable to drug resistance and lesser side effects by means of attacking the disease network at the systems level through synergistic and lethal interactions. The drug discovery strategies thereby should explore the regulated pathology network and reduce the typically high attrition rates in the disease networks [19]. Many studies have reported the interesting biological findings from these networks, and more than 40% of the drug-activated targets were discovered based on the disease gene networks by meta-analysis [20], which were associated with a number of diseases [21]. Therefore, network pharmacology can assist in systematic characterization of drug targets, thereby helping to decrease the high failure rates in discovery projects.

3. Research Approaches of Network Pharmacology

Network pharmacology can make an impact at two main approaches in the drug development process. One is to establish a pragmatic network model and predict the drug target based on public databases or available data of earlier researches. Subsequently, the mechanism of functional drug should be explored for the network equilibrium principle.

Based on this approach, Gu et al. calculated the effect of Rheidin A and C and Sennoside C, which was the first report on multiple component drugs for type II diabetes [22]. Yan et al. also predicted the new pharmacological action of Ephedra Decoction using virtual screening and network forecast techniques [23].

The other approach is to reconstruct a “drug target disease” network prediction model using the high-throughput screen (HTS) technology and bioinformatics methods. In this approach, the mechanism of drugs in the biological network was analyzed by comparing the interaction between the drug and the model. Many examples on the application of network pharmacology in drug discovery have been reported in the literature. Li et al. [24] used Liuwei Dihuang pill (a CHM formula) to predict the suitable network targets in disease treatment and found that the multilayer networks may underlie the combined mechanisms of herbal formula. Furthermore, nine components were screened in Fufang Danshen formula based on network pharmacology, which could modulate 42 cardiovascular-associated genes [25]. Additionally, by integrating the above research approaches, it was demonstrated that salvianolic acid B was compatible and feasible for cardiovascular disease treatment [26].

4. Process in Network Pharmacology Research

4.1. Data Collection and Validation. Network pharmacology takes into account the aforementioned principles to optimize the efficacy and safety of a candidate drug and their potent combinations. These also represent the two important steps in any experimental study. The first step of network pharmacology is the selection of original data from the experiments to build a biological network. The second is the experimental validation for the predicted network model. The validated data can be quantified using many different integrated methods including genomics, proteomics, metabolomics, and HTS/high-content screening (HCS) technologies [27].

HTS/HCS technologies can rapidly detect millions of data samples, identify substances, and modulate a particular molecular pathway or alter the phenotype of a cell [28, 29]. These have many desirable features such as homogeneous, multidimensional phenotypic detection, real-time, dynamic monitoring, and visualization. Moreover, this dual high-throughput technology also can collect network data from the experiments and validate the network model. For instance, Fakhari and Dittmer created the polymerase chain reaction (PCR) chip technology to detect the gene expression [30]. The results demonstrated that the technology was convenient for the high-throughput studies.

Molecular interaction validation technology is another tool which validates the approach for network pharmacology, reveals the drug activity mechanisms, and verifies the drug network or predicted model. It can help researchers to discover the relationship between the drug and the macromolecules, and it mainly includes surface plasmon resonance (SPR) [31] and bilayer interferometry (BLI) technologies [32]. All of these techniques involve high-throughput, high-precision, label-free, and real-time detection.

4.2. Network Analysis and Visualization. Network analysis focuses on established network using related technology and extracts useful information which is convenient for further studies [33]. Three types of network analysis are available. The first one involves the calculation of the optimal topological structure and statistical properties of network after the extraction of specific network data [34], which is conserved as the hidden information in the network maximally. Secondly, the generation and comparison of random networks is used to check the reliability of the existing network by inducing acceptable modulation [35]. At last, the hierarchical clustering of the network is performed [36], algorithm is applied to predigest the complicated network, and potential information in the network is anticipated.

Network visualization is applied to extract the interaction information from interassociation data and switch them into a visual network using visualization tools [33]. This process contains two steps: (1) enriching network attributes, adding network nodes, and increasing connection power of network; (2) describing the network and taking abundant instrument to describe the architectural feature that clearly and intuitively represents the network. At present, most visualization of network pharmacology is through professional tools such as Cytoscape [37], GUESS [38], and Pajek [39]. Brief information of network pharmacological technologies and tools is shown in Table 1.

5. Application of Network Pharmacology in CHM Research

CHM, the ancient treatment methodology popular in China and surrounding areas, has been recognized as a pharmaceutical area of TCM and holds promise for preventing diseases in a holistic way [40, 41]. In a long period of clinical practice, it is known for its effectiveness and beneficial contribution to public health and disease control. However, the pharmacological mechanisms of CHM have not been fully established. With increasing knowledge of the network of genes and molecular interactions, the researchers adopt network pharmacology for their drug research and development. Figure 1 shows the developing tendency of network pharmacological studies from the data available in Web of Knowledge, PubMed, and CNKI databases from 2007 to 2012. The applications of network pharmacology in CHM were systematically summarized to demonstrate the significant value in this area of research.

5.1. Construction and Application of CHM Database. Building a CHM database is critical for a network pharmacology study. Chen et al. [42] constructed the TCM-ID database including TCM prescriptions, herbal ingredients, and 3D structure of herbal ingredients. It was mainly used for illustrating the mechanism of the effects of herbal ingredients. Ye et al. [43] integrated the text-mining technology, a strict artificial audit and annotation process, and obtained the protein targets of Chinese medicine by determining the effective components based on the mass literature from PubMed.

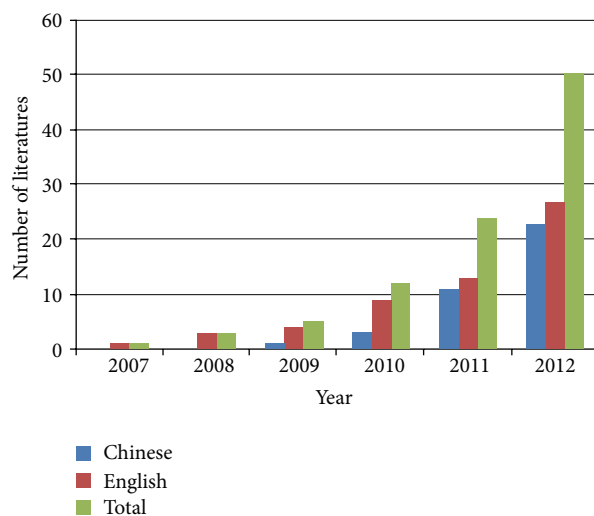


FIGURE 1: Developing tendency of network pharmacology study. The publications of network pharmacology study in Web of Knowledge, PubMed, and CNKI databases from 2007 to 2012. All results were screened in manual way.

Subsequently, the Herbal Ingredients' Targets Database provided the integrated information for the Chinese herbal active ingredient protein target and offered platform to analyze the similarity between the compound formula and protein sequence.

Furthermore, many other TCM databases have been established for network pharmacology research, such as the TCMGeneDIT database [44] and TCM Database@Taiwan [45]. The former mainly focuses on TCM-related gene and disease information, and the latter is applied to CHM screening. In addition, the disease-drug-target databases such as SuperTarget, Matador [46], DrugBank [47], and Therapeutic Target Database [48] are also used for drug-target research on herbal compounds.

5.2. Predictions of CHM Drug Target. Relevant technology can be used to screen the effective herbal substances and discover the drug target. Such technology could also provide theoretical support for detecting new pharmacological effects of Chinese compound formula. Li [49] proposed a methodology termed "network target," which is used to reveal the interactions between herbal compounds/formulas and complex syndrome systems based on network pharmacology and systems biology. Wu et al. [50] predicted the multitarget of *Aconiti Lateralis Radix Praeparata's* multi-compound based on the drug-target data and random forest algorithm. They found that each compound was correlated with 16.3 targets, whereas each target was related to 4.77 compounds. This study reflects the notion of "multi-compound and multitarget" in CHM towards drug discovery.

Yu et al. [51] predicted the new pharmacological effects (antihyperglycemic and antihyperlipidemic) of Fuzheng Huayu Capsule using high-throughput technology and Connectivity Map databases [52]. Using the chemical structure of compounds, target identification, and enrichment analysis,

TABLE 1: Brief introduction of network pharmacological technologies methods and tools.

Mainly experimental techniques and tools in network pharmacology			
Technique	Application fields	Advantage	Literatures
HTS/HCS	Massive data acquisition	Homogeneous, multidimensional phenotypic detection, dynamic real-time monitoring, and visualization	[28, 29]
PCR chip	Massive data acquisition	Dual high throughput, strong specificity, high sensitivity, and good repeatability	[30]
SPR	Massive data acquisition	No marks, high-throughput, high-precision, and real-time detection	[31, 32]
BLI	Massive data acquisition	No marks, high-throughput, high-precision, and real-time detection	[31, 32]
Cytoscape	Network visualization	Graphic operation, construct simple network, plugin support for analysis, and easy to use	[37]
GUESS	Network visualization	Graphic operation, command line, and script support for analysis	[38]
Pajek	Network visualization	Graphic operation, building large-scale network	[39]
Network topology information calculation	Network analysis	Classify and sequence the nodes, reflect hidden information	[34]
Random network creation and comparison	Network analysis	Verify reliability of existing network	[35]
Network layer and clustering	Network analysis	Simplify the complexity of network, find out potential information	[36]

Zhu and Yao [53] successfully predicted the molecular targets of Xiaochaihu Decoction. They found that the potential targets of the 21 compounds mainly involved metabolic, inflammation, and poison degradation processes. Zhang et al. [54] created a new algorithm to predict the molecular targets of rhein, which integrated the protein-protein interactions, pathways, genome expression, and the literature data mining. The results showed that three specific genes were relevant for drug targets, and their functions mainly involved cellular apoptosis, immunity, and transport.

5.3. Network Visualization of the CHM Literature Mining Researches. Essentially, the network visualization of the CHM literature examines the database to find modes or rules [55], detects the literature information, analyzes the selection data, and discovers the novel effects of CHM. For example, Li et al. [56] integrated the microarray and the literature database to design a literature mining and microarray analysis system, which was used to construct biological networks and reveal the related interactions.

Wu et al. [57] collected slices information of TCM from the Chinese Pharmacopoeia by text mining and constructed the TCM slices-symptom network. They discovered 3016 pairs of TCM slice-symptom correlations. Each TCM slice was correlated with 4.67 symptoms, and each symptom was related to 7.47 TCM slices. Furthermore, the network analysis also indicated that network pharmacology approaches could be used to forecast and discover unknown or new effects and channel tropisms of TCM slices. Additionally, Zhang et al. [58] reconstructed three Bayesian belief networks [59] for bitter, sweet, and pungent flavors, which was based on the modern pharmacology of TCM slices and clinical data. The

results suggested that the Bayesian belief network could be used to predict the flavors of Chinese medicinal components and perform further studies of drug properties and drug compatibility.

5.4. CHM Multicomponent and Formula Researches. In order to discover the relationship between Chinese herbal multicomponent and potential pharmacological function, Li et al. [60] applied a network target-based identification of multicomponent synergy (NIMS) algorithms to calculate the component of CHM and demonstrate the synergistic correlation of the multicomponent. The results proposed that the NIMS approach could be beneficial for analyzing the therapeutic effects of CHM multicomponent. In the Tougu Xiaotong capsule (TGXTC) study, Zheng et al. [61] analyzed 514 components using network pharmacology and computational pharmacological methods. By analyzing the network parameters of the TGXTC compound-target and drug-target networks, they revealed the molecular mechanism of multicomponent, multitarget, and multipathway in TGXTC.

Zhu et al. [62] used molecular docking and complex analytical techniques to study the pharmacodynamic function of multicomponent in spleen-regulating heart-nourishing formula. They found that the scale-free feature and node attribute of networks clearly illuminated the pharmacological function of CHM multicomponent. Excitingly, some recent studies revealed the mechanisms of multicomponent efficiency in CHM for the treatment of cardiovascular disease [63, 64] by systematic investigation, which have constructed "CHM components targets" networks based on chemical

components, chemical structures, chemogenomics, and target predictors data.

5.5. CHM Network Toxicology Researches. Network toxicology is based on comprehension of “toxicity (side effects) gene target drug,” which utilizes the network analysis to speculate and estimate toxicity and side effects of drugs. It focuses on the toxic reaction of specific component in a complex system and provides assistance for drug safety evaluation and research. The study of Liu et al. [65] identified that the integrated high-throughput biochip technologies and drug-target network could afford significant values for activated ingredient screening, toxic components exclusion, and molecular mechanisms of CHM research. Fan et al. [66] used network pharmacology method to reconstruct the network model to describe the toxicological properties, which offered valuable information to identify the toxic substances and potential toxicity of known compounds in a complex system. Zhou et al. [67] analyzed the nephrotoxicity of aristolochic acid based on the metabolic network and established an integral and dynamical progression of drug toxicity method.

In addition, the databases such as Comparative Toxicogenomics Database, National Toxicology Program, and Toxicology Data Network are widely used for network toxicology studies [68, 69]. Furthermore, the forecasting toxicity software such as Toxicity Prediction by Komputer-Assisted Technology, HazardExpert, DEREK, and Prediction System of Carcinogenic Toxicity [70] is other available tools for CHM network toxicology studies.

5.6. TCM Syndrome-Based Network Pharmacology Researches. The feature of TCM is based on the syndrome differentiation, which emphasizes the integrating disease and syndrome. Monarch, minister, assistant, and guide in TCM prescription contain many principles of system theory, and the aim of coordination and cooperation of several kinds of CHM is to regulate body functional imbalances and disorders. Therefore, network pharmacology could be used for TCM diagnosis based on “disease-syndrome-formula” model, which integrates the information of “disease-phenotype-gene-drug” and builds a “disease phenotype biological molecule” network [24]. In a study on patients with rheumatoid arthritis (RA), Niu et al. [71] revealed the molecular mechanism of “herbs-pattern correspondence” with heat pattern in TCM, which analyzed the drug-target molecular network. Four common canonical pathways were found to be involved in these: GM-CSF signaling, CLTA4 signaling in cytotoxic T lymphocytes, T-cell receptor signaling, and CD28 signaling in T-helper cells. These uniform pathways implicated that the “herbs-pattern correspondence” could more likely be associated with heat pattern of RA.

ZHENG is a complex concept in TCM. Li et al. [72] reconstructed the neuroendocrine-immune (NEI) network by systems biology approach combined with animal experiments. The results showed that the hormones were predominant in the Cold ZHENG network, whereas immune factors were predominant in the Hot ZHENG network. In

particular, two networks were connected by neurotransmitters, which suggested that ZHENG might have a special molecular mechanism from the background of NEI study. Using the microarray samples of liver-gallbladder dampness-heat syndrome and liver depression and spleen deficiency syndrome in chronic hepatitis B and liver cirrhosis, Guo et al. [73] elucidated the molecular mechanisms of the same TCM syndrome for different diseases and different TCM syndrome for the same disease, which might be related to the G-protein-coupled receptor protein-signaling pathway. Moreover, Shi et al. [74] used a complex network and chi-squared automatic interaction detector decision tree to identify the core syndromes of TCM in coronary heart disease (CHD) and establish TCM syndrome identification modes of CHD based on the four diagnostic information and biological parameters.

6. Discussion and Conclusion

Although TCM has a long history of clinical practice in China, it is considered as a complementary and alternative medicine in the rest of the world. The biggest obstacles of CHM development are the multiple *in vivo* pathways of CHM metabolites from their multiple drug components, which are essential for their pharmacological actions. However, the knowledge on the effective mechanisms of CHM formulas is scarce. Moreover, the CHM mechanism is considered as the synergistic effect of active drug ingredients and results of complex biological interactions. Fortunately, as a novel approach, network pharmacology takes into account the multidisciplinary and cross-disciplinary fields to optimize the efficacy and safety of drug discovery. Hence, researchers started utilizing it to study the drug targets and efficacy of CHM [75]. Network pharmacology has become a helpful tool to understand the details of drug-target, especially for multiple drug components of CHM.

Generally, network pharmacology of CHM has been considered to contain static and dynamic configurations. The static configuration is called a network pharmacy metrology with chromatographic fingerprint, while the dynamic is called a network pharmacodynamics with chromatographic fingerprint (NPDCF). The key problem for CHM formula network pharmacology is how to confirm the parameters of NPDCF by network equilibrium constants [76]. For example, He et al. [77] analyzed the multiple drug components from the parameters of network pharmacokinetic model and found that the effects of CHM formulas were inhibited by pharmacokinetic and pharmacodynamic coefficients [78]. In the static multicomponent studies of CHM formula, Tal et al. [79] predicted the active ingredients and potential targets of Chinese herbal *Radix Curcumae* formula using network pharmacology, which was used for the treatment of cardiovascular disease. However, the network dynamics research of CHM formulas need more evidence.

The characteristics of TCM theory involve the consideration of organic wholeness and treatment based on TCM syndrome differentiation. A diagram is proposed to exhibit the research approach of network pharmacology for CHM

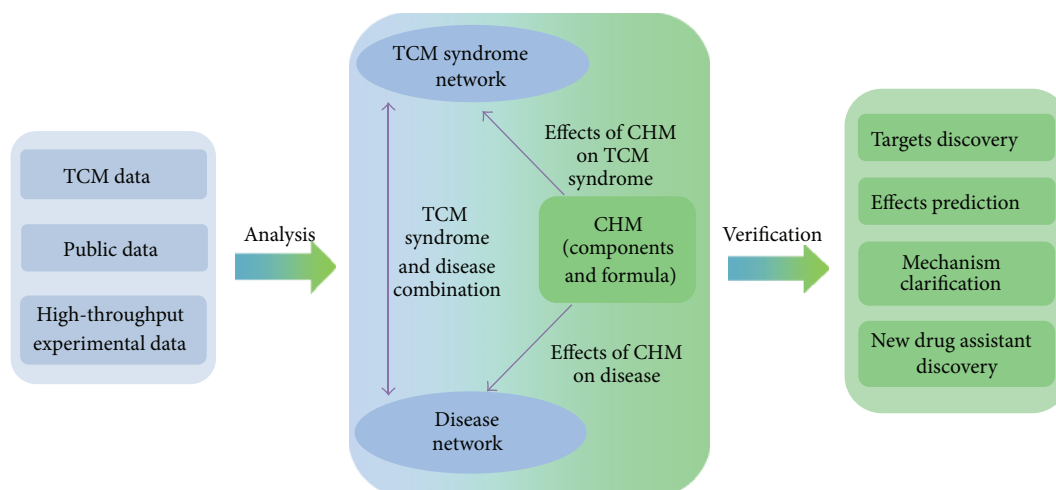


FIGURE 2: Network pharmacology approach for CHM research. For the discovery of CHM-derived targets, effect prediction, mechanism clarification, and new drug assistant discovery using network pharmacology approach. It analyzes the information from public data, high-throughput experimental data, and TCM data and constructs a “CHM-TCM syndrome disease” interaction network using technologies of network expansion, optimization, comparison, knockout, and addition. Finally, it carries out computational and experimental verifications.

(Figure 2). This approach is a combination from “disease-syndrome-CHM” model, which comprises the core values for reflecting disease and TCM syndrome as well as correlates with CHM, TCM syndrome, and multitarget effects. By integrating the chemical predictor, target predictor, and network building, a system of TCM was constructed. It systematically revealed the potential mechanisms of TCM [80]. The appropriate cellular and animal models are conducive to evaluate the effectiveness of TCM [81–83], which could be used to verify the results of network analysis and mutual authentication. However, the systemic characterization is still unclear for the drug-target correlation of CHM. Network pharmacology could be helpful to confirm the effective ingredients and promote drug discovery of CHM.

Network pharmacology has become a helpful tool in understanding the fine details of drug-target interactions. Using network pharmacology to investigate CHM pharmacological effects and drug targets, attention should be paid to degree centrality [84], betweenness centrality [85], and bridging centrality [86]. Network-based tools for analyzing topology and especially dynamics have great potential to identify alternative targets for finding and developing multitarget drugs [87].

In summary, the advancements in systems biology and bioinformatics will make an operational shift from reductionism in favor of network pharmacology and will undoubtedly bring about a conceptual move in drug discovery and make a significant contribution to CHM modernization and globalization.

Acknowledgments

This study was supported by the National Science and Technology Major Project of China (no. 2012ZX10005001-004),

Leading Academic Discipline Project of Shanghai Municipal Education Commission (no. J50301 and no. 2012JW25), Shanghai Municipal Science and Technology Commission Project (12401900401), and E-institutes of Shanghai Municipal Education Commission (no. E 03008).

References

- [1] F. Sams-Dodd, “Target-based drug discovery: is something wrong?” *Drug Discovery Today*, vol. 10, no. 2, pp. 139–147, 2005.
- [2] I. Kola and J. Landis, “Can the pharmaceutical industry reduce attrition rates?” *Nature Reviews Drug Discovery*, vol. 3, no. 8, pp. 711–715, 2004.
- [3] B. P. Zambrowicz and A. T. Sands, “Modeling drug action in the mouse with knockouts and RNA interference,” *Drug Discovery Today*, vol. 3, no. 5, pp. 198–207, 2004.
- [4] M. E. Hillenmeyer, E. Fung, J. Wildenhain et al., “The chemical genomic portrait of yeast: uncovering a phenotype for all genes,” *Science*, vol. 320, no. 5874, pp. 362–365, 2008.
- [5] H. Kitano, “Systems biology: a brief overview,” *Science*, vol. 295, no. 5560, pp. 1662–1664, 2002.
- [6] U. Sauer, M. Heinemann, and N. Zamboni, “Getting closer to the whole picture,” *Science*, vol. 316, no. 5824, pp. 550–551, 2007.
- [7] A. L. Hopkins, “Network pharmacology,” *Nature Biotechnology*, vol. 25, no. 10, pp. 1110–1111, 2007.
- [8] A. L. Hopkins, “Network pharmacology: the next paradigm in drug discovery,” *Nature Chemical Biology*, vol. 4, no. 11, pp. 682–690, 2008.
- [9] B. L. Roth, D. J. Sheffer, and W. K. Kroeze, “Magic shotguns versus magic bullets: selectively non-selective drugs for mood disorders and schizophrenia,” *Nature Reviews Drug Discovery*, vol. 3, no. 4, pp. 353–359, 2004.
- [10] P. Csermely, V. Ágoston, and S. Pongor, “The efficiency of multitarget drugs: the network approach might help drug design,” *Trends in Pharmacological Sciences*, vol. 26, no. 4, pp. 178–182, 2005.

- [11] C. G. Wermuth, "Multitargeted drugs: the end of the "one-target-one-disease" philosophy?" *Drug Discovery Today*, vol. 9, no. 19, pp. 826–827, 2004.
- [12] C. T. Keith, A. A. Borisy, and B. R. Stockwell, "Multicomponent therapeutics for networked systems," *Nature Reviews Drug Discovery*, vol. 4, no. 1, pp. 71–78, 2005.
- [13] G. A. Luo, Q. L. Liang, R. L. Zhang et al., "Study of chemical matteromics and prescription of traditional Chinese medicine—and an analysis of material foundation of compound prescription Qingkailing," *World Science and Technology*, vol. 8, no. 1, pp. 6–15, 2006.
- [14] Z. H. Liu and X. B. Sun, "Network pharmacology: new opportunity for the modernization of traditional Chinese medicine," *Acta Pharmaceutica Sinica*, vol. 47, no. 6, pp. 696–703, 2012.
- [15] A. Friboulet and D. Thomas, "Systems biology—an interdisciplinary approach," *Biosensors and Bioelectronics*, vol. 20, no. 12, pp. 2404–2407, 2005.
- [16] J. T. Metz and P. J. Hajduk, "Rational approaches to targeted polypharmacology: creating and navigating protein-ligand interaction networks," *Current Opinion in Chemical Biology*, vol. 14, no. 4, pp. 498–504, 2010.
- [17] J. H. Pan, "New paradigm for drug discovery based on network pharmacology," *Chinese Journal of New Drugs and Clinical Remedies*, vol. 28, no. 10, pp. 721–726, 2009.
- [18] X. Wu, R. Jiang, M. Q. Zhang et al., "Network-based global inference of human disease genes," *Molecular Systems Biology*, vol. 4, pp. 1–11, 2008.
- [19] Y. Chen, J. Zhu, P. Y. Lum et al., "Variations in DNA elucidate molecular networks that cause disease," *Nature*, vol. 452, no. 7186, pp. 429–435, 2008.
- [20] M. A. Yildirim, K. I. Goh, M. E. Cusick, A. L. Barabási, and M. Vidal, "Drug-target network," *Nature Biotechnology*, vol. 25, no. 10, pp. 1119–1126, 2007.
- [21] A. L. Barabási, N. Gulbahce, and J. Loscalzo, "Network medicine: a network-based approach to human disease," *Nature Reviews Genetics*, vol. 12, no. 1, pp. 56–68, 2011.
- [22] J. Gu, H. Zhang, L. Chen et al., "Drug—target network and polypharmacology studies of a Traditional Chinese Medicine for type II diabetes mellitus," *Computational Biology and Chemistry*, vol. 35, no. 5, pp. 293–297, 2011.
- [23] J. Yan, Y. Wang, S. J. Luo et al., "TCM grammar systems: an approach to aid the interpretation of the molecular interactions in Chinese herbal medicine," *Journal of Ethnopharmacology*, vol. 137, no. 1, pp. 77–84, 2011.
- [24] S. Li, B. Zhang, D. Jiang, Y. Wei, and N. Zhang, "Herb network construction and co-module analysis for uncovering the combination rule of traditional Chinese herbal formulae," *BMC Bioinformatics*, vol. 11, no. 11, article S6, 2010.
- [25] X. Li, L. Wu, X. Fan et al., "Network pharmacology study on major active compounds of Fufang Danshen formula," *China Journal of Chinese Materia Medica*, vol. 36, no. 21, pp. 2911–2914, 2011.
- [26] C. Ma, Y. Yao, Q. X. Yue et al., "Differential proteomic analysis of platelets suggested possible signal cascades network in platelets treated with Salvanolic acid B," *PLoS ONE*, vol. 6, no. 2, Article ID e14692, 2011.
- [27] X. R. Cheng, W. X. Zhou, and Y. X. Zhang, "Experimental techniques in network pharmacology," *Chinese Journal of Pharmacology and Toxicology*, vol. 26, no. 2, pp. 131–137, 2012.
- [28] B. S. Edwards, T. Oprea, E. R. Prossnitz, and L. A. Sklar, "Flow cytometry for high-throughput, high-content screening," *Current Opinion in Chemical Biology*, vol. 8, no. 4, pp. 392–398, 2004.
- [29] F. Miscevic, O. Rotstein, and X. Y. Wen, "Advances in zebrafish high content and high throughput technologies," *Combinatorial Chemistry & High Throughput Screening*, vol. 15, no. 7, pp. 515–521, 2012.
- [30] F. D. Fakhari and D. P. Dittmer, "Charting latency transcripts in Kaposi's sarcoma-associated herpesvirus by whole-genome real-time quantitative PCR," *Journal of Virology*, vol. 76, no. 12, pp. 6213–6223, 2002.
- [31] X. Guo, "Surface plasmon resonance based biosensor technique: a review," *Journal of Biophotonics*, vol. 5, no. 7, pp. 483–501, 2012.
- [32] C. A. Wartchow, F. Podlaski, S. Li et al., "Biosensor-based small molecule fragment screening with bilayer interferometry," *Journal of Computer-Aided Molecular Design*, vol. 25, no. 7, pp. 669–676, 2011.
- [33] L. H. Wu, Y. Wang, and X. Fan, "Tools for network pharmacology study: network visualization and network analysis," *China Journal of Chinese Materia Medica*, vol. 36, no. 21, pp. 2923–2925, 2011.
- [34] L. Cagnolo, A. Salvo, and G. Valladares, "Network topology: patterns and mechanisms in plant-herbivore and host-parasitoid food webs," *Journal of Animal Ecology*, vol. 80, no. 2, pp. 342–351, 2011.
- [35] K. V. Brinda, S. Vishveshwara, and S. Vishveshwara, "Random network behaviour of protein structures," *Molecular Biosystems*, vol. 6, no. 2, pp. 391–398, 2010.
- [36] L. Hou, L. Wang, A. Berg et al., "Comparison and evaluation of network clustering algorithms applied to genetic interaction networks," *Frontiers in Bioscience*, vol. 4, pp. 2150–2161, 2012.
- [37] C. T. Lopes, M. Franz, F. Kazi, S. L. Donaldson, Q. Morris, and G. D. Bader, "Cytoscape web: an interactive web-based network browser," *Bioinformatics*, vol. 26, no. 18, Article ID btq430, pp. 2347–2348, 2010.
- [38] E. Adar and M. Kim, "Soft GUESS: visualization and exploration of code clones in context," in *Proceedings of the 29th International Conference on Software Engineering (ICSE '07)*, pp. 762–765, May 2007.
- [39] D. N. Wouter, M. Andrej, and B. Vladimir, *Exploratory Social Network Analysis With Pajek*, Cambridge University Press, Cambridge, Mass, USA, 2005.
- [40] J. Xu and Y. Yang, "Traditional Chinese medicine in the Chinese health care system," *Health Policy*, vol. 90, no. 2–3, pp. 133–139, 2009.
- [41] F. Cheung, "TCM: made in China," *Nature*, vol. 480, pp. S82–S83, 2011.
- [42] X. Chen, H. Zhou, Y. B. Liu et al., "Database of traditional Chinese medicine and its application to studies of mechanism and to prescription validation," *British Journal of Pharmacology*, vol. 149, no. 8, pp. 1092–1103, 2006.
- [43] H. Ye, L. Ye, H. Kang et al., "HIT: linking herbal active ingredients to targets," *Nucleic Acids Research*, vol. 39, no. supplement 1, pp. D1055–D1059, 2011.
- [44] Y. C. Fang, H. C. Huang, H. H. Chen et al., "TCMGeneDIT: a database for associated traditional Chinese medicine, gene and disease information using text mining," *BMC Complementary and Alternative Medicine*, vol. 8, p. 58, 2008.
- [45] C. Y. Chen, "TCM Database@Taiwan: the world's largest traditional Chinese medicine database for drug screening *In Silico*," *PLoS ONE*, vol. 6, no. 1, Article ID e15939, 2011.

- [46] S. Gunther, M. Kuhn, M. Dunkel et al., "SuperTarget and Matador: resources for exploring drug-target relationships," *Nucleic Acids Research*, vol. 36, pp. D919–D922, 2008.
- [47] C. Knox, V. Law, T. Jewison et al., "DrugBank 3. 0: a comprehensive resource for 'omics' research on drugs," *Nucleic Acids Research*, vol. 39, no. 1, pp. D1035–D1041, 2011.
- [48] F. Zhu, B. Han, P. Kumar et al., "Update of TTD: therapeutic target database," *Nucleic Acids Research*, vol. 38, no. 1, pp. D787–D791, 2009.
- [49] S. Li, "Network target: a starting point for traditional Chinese medicine network pharmacology," *China Journal of Chinese Materia Medica*, vol. 36, no. 15, pp. 2017–2020, 2011.
- [50] L. Wu, X. Gao, L. Wang et al., "Prediction of multi-target of aconiti lateralis radix praeparata and its network pharmacology," *China Journal of Chinese Materia Medica*, vol. 36, no. 21, pp. 2907–2910, 2011.
- [51] S. Yu, Z. Guo, Y. Guan et al., "Combining ZHENG theory and high-throughout expression data to predict new effects of Chinese herbal formulae," *Evidence-Based Complementary and Alternative Medicine*, vol. 2012, Article ID 986427, 8 pages, 2012.
- [52] J. Lamb, E. D. Crawford, D. Peck et al., "The connectivity map: using gene-expression signatures to connect small molecules, genes, and disease," *Science*, vol. 313, no. 5795, pp. 1929–1935, 2006.
- [53] W. Zhu and L. M. Yao, "Potential targets and molecular mechanisms of, 'Xiaochaihu Decoction' by Metadrag software," *Shanghai Journal of Traditional Chinese Medicine*, vol. 45, no. 1, pp. 79–82, 2011.
- [54] A. H. Zhang, S. Hui, Y. Bo et al., "Predicting new molecular targets for rhein using network pharmacology," *BMC Systems Biology*, vol. 6, p. 20, 2012.
- [55] I. H. Witten and E. Frank, *Data Mining Practical Machine Learning Tools and Techniques*, China Machine, Beijing, China, 2005.
- [56] S. Li, L. Wu, and Z. Zhang, "Constructing biological networks through combined literature mining and microarray analysis: a LMMA approach," *Bioinformatics*, vol. 22, no. 17, pp. 2143–2150, 2006.
- [57] L. Wu, X. Gao, Y. Cheng et al., "Symptom-based traditional Chinese medicine slices relationship network and its network pharmacology study," *China Journal of Chinese Materia Medica*, vol. 36, no. 21, pp. 2916–2919, 2011.
- [58] P. Zhang, J. Li, Y. Wang et al., "Bayesian belief network and its application in predicting the five flavors of Chinese medicinal components," *Modernization of Traditional Chinese Medicine and Materia Materia-World Science and Technology*, vol. 10, no. 5, pp. 114–117, 2008.
- [59] R. Montironi, W. F. Whimster, Y. Collan, P. W. Hamilton, D. Thompson, and P. H. Bartels, "How to develop and use a Bayesian belief network," *Journal of Clinical Pathology*, vol. 49, no. 3, pp. 194–201, 1996.
- [60] S. Li, B. Zhang, and N. Zhang, "Network target for screening synergistic drug combinations with application to traditional Chinese medicine," *BMC Systems Biology*, vol. 5, no. 1, article S10, 2011.
- [61] C. S. Zheng, Z. C. Lin, H. F. Xu et al., "Pharmacological research on osteoarthritis treated by tougu xiaotong capsule," *Journal of Fujian University of TCM*, vol. 21, no. 1, pp. 43–47, 2011.
- [62] Y. F. Zhu, Z. W. Xu, H. Q. Ao et al., "Pharmacodynamic research of spleen-regulating and heart-nourishing formula based on network features," *Traditional Chinese Drug Research & Clinical Pharmacology*, vol. 23, no. 1, pp. 25–29, 2012.
- [63] X. Wang, X. Xu, W. Tao et al., "A systems biology approach to uncovering pharmacological synergy in herbal medicines with applications to cardiovascular disease," *Evidence-Based Complementary and Alternative Medicine*, vol. 2012, 15 pages, 2012.
- [64] B. Li, X. Xu, X. Wang et al., "A systems biology approach to understanding the mechanisms of action of Chinese herbs for treatment of cardiovascular disease," *International Journal of Molecular Sciences*, vol. 13, no. 10, pp. 13501–13520, 2012.
- [65] Q. Liu, Z. Zhang, L. Fang et al., "Application of network pharmacology and high through-put technology on active compounds screening from traditional Chinese medicine," *China Journal of Chinese Materia Medica*, vol. 37, no. 2, pp. 134–137, 2012.
- [66] X. Fan, X. Zhao, Y. Jin et al., "Network toxicology and its application to traditional Chinese medicine," *China Journal of Chinese Materia Medica*, vol. 36, no. 21, pp. 2920–2922, 2011.
- [67] M. M. Zhou, P. Liu, W. Jia et al., "Evaluation of therapeutic effects of TCM based on metabolic variation," *Modernization of Traditional Chinese Medicine and Materia Materia-World Science and Technology*, vol. 8, no. 6, pp. 113–119, 2006.
- [68] A. P. Davis, B. L. King, S. Mockus et al., "The comparative toxicogenomics database: update 2011," *Nucleic Acids Research*, vol. 39, no. 1, pp. D1067–D1072, 2011.
- [69] G. H. I. Wolfgang and D. E. Johnson, "Web resources for drug toxicity," *Toxicology*, vol. 173, no. 1-2, pp. 67–74, 2002.
- [70] A. Lagunin, D. Filimonov, A. Zakharov et al., "Computer-aided prediction of rodent carcinogenicity by PASS and CISOC-PSCCT," *QSAR and Combinatorial Science*, vol. 28, no. 8, pp. 806–810, 2009.
- [71] X. Y. Niu, J. Li, C. Lu et al., "The molecular mechanism of 'Herbs-Pattern Correspondence' in RA with heat pattern based on network pharmacology," *Chinese Journal of Experimental Traditional Medical Formulae*, vol. 18, no. 8, pp. 299–303, 2012.
- [72] S. Li, Z. Q. Zhang, L. J. Wu, X. G. Zhang, Y. D. Li, and Y. Y. Wang, "Understanding ZHENG in traditional Chinese medicine in the context of neuro-endocrine-immune network," *IET Systems Biology*, vol. 1, no. 1, pp. 51–60, 2007.
- [73] Z. Guo, S. Yu, Y. Guan et al., "Molecular mechanisms of 'Same TCM Syndrome for Different Diseases' and 'Different TCM Syndrome for Same Disease' in chronic hepatitis B and liver cirrhosis," *Evidence-Based Complementary and Alternative Medicine*, vol. 2012, 9 pages, 2012.
- [74] Q. Shi, H. H. Zhao, J. X. Chen et al., "Study on TCM syndrome identification modes of coronary heart disease based on data mining," *Evidence-Based Complementary and Alternative Medicine*, vol. 2012, Article ID 697028, 2012.
- [75] G. H. Du, Y. H. Wang, R. Zhang et al., "Multi-target and multi-component pattern, a superficial understanding of the action mechanism of Traditional Chinese Medicine," *Modernization of Traditional Chinese Medicine and Materia Materia-World Science and Technology*, vol. 11, no. 4, pp. 480–484, 2009.
- [76] F. Y. He, K. W. Deng, W. L. Liu et al., "Study on theoretical and technologic key problems of network pharmacology and pharmacodynamics for the Chinese Materia Medica Formula," *Pharmacology and Clinics of Chinese Materia Medica*, vol. 28, no. 5, pp. 256–259, 2012.
- [77] F. Y. He, H. H. Zhou, and J. Y. Luo, "Establishment of a network pharmacokinetic model for multiple component drugs and parameter analyses," *Chinese Journal of Clinical Pharmacology and Therapeutics*, vol. 12, no. 12, pp. 1321–1331, 2007.

- [78] F. He, K. Deng, H. Zou, Y. Qiu, F. Chen, and H. Zhou, "Study on differences between pharmacokinetics and chromatopharmacodynamics for Chinese materia medica formulae," *China Journal of Chinese Materia Medica*, vol. 36, no. 2, pp. 136–141, 2011.
- [79] W. Y. Tal, X. Xu, X. Wang et al., "Network pharmacology-based prediction of the active ingredients and potential targets of Chinese herbal *Radix Curcumae* formula for application to cardiovascular disease," *Journal of Ethnopharmacology*, vol. 145, no. 1, pp. 1–10, 2013.
- [80] B. H. Li, X. Xu, X. Wang et al., "A systems biology approach to understanding the mechanisms of action of Chinese herbs for treatment of cardiovascular disease," *International Journal of Molecular Sciences*, vol. 13, no. 10, pp. 13501–13520, 2012.
- [81] M. Wang, X. Zhang, X. Xiong et al., "Efficacy of the Chinese traditional medicinal herb *Celastrus orbiculatus* Thunb on human hepatocellular carcinoma in an orthotopic fluorescent nude mouse model," *Anticancer Research*, vol. 32, no. 4, pp. 1213–1220, 2012.
- [82] M. Hu, M. Zhao, C. An et al., "Real-time imaging of apoptosis induction of human breast cancer cells by the traditional Chinese medicinal herb tubeimu," *Anticancer Research*, vol. 32, no. 7, pp. 2509–2514, 2012.
- [83] B. Zhao, L. Liu, S. Zhao et al., "Vitexicarpin acts as a novel angiogenesis inhibitor and its target network," *Evidence-Based Complementary and Alternative Medicine*, vol. 2013, Article ID 278405, 13 pages, 2013.
- [84] R. Albert, H. Jeong, and A. L. Barabási, "Error and attack tolerance of complex networks," *Nature*, vol. 406, no. 6794, pp. 378–382, 2000.
- [85] H. Yu, P. M. Kim, E. Sprecher, V. Trifonov, and M. Gerstein, "The importance of bottlenecks in protein networks: correlation with gene essentiality and expression dynamics," *PLoS Computational Biology*, vol. 3, no. 4, pp. 713–720, 2007.
- [86] W. C. Hwang, A. Zhang, and M. Ramanathan, "Identification of information flow-modulating drug targets: a novel bridging paradigm for drug discovery," *Clinical Pharmacology and Therapeutics*, vol. 84, no. 5, pp. 563–572, 2008.
- [87] I. J. Farkas, T. Korcsmáros, I. A. Kovács et al., "Network-based tools for the identification of novel drug targets," *Science Signaling*, vol. 4, no. 173, 2011.

Research Article

MAPK Signal Transduction Pathway Regulation: A Novel Mechanism of Rat HSC-T6 Cell Apoptosis Induced by FUZHENGHUAYU Tablet

Qi Wang,^{1,2} Hongbo Du,³ Min Li,^{1,2} Yue Li,⁴ Shunai Liu,^{1,2}
Ping Gao,^{1,2} Xiaoli Zhang,⁴ and Jun Cheng^{1,2}

¹ Institute of Infectious Diseases, Beijing Ditan Hospital, Capital Medical University, Beijing 100015, China

² Beijing Key Laboratory of Emerging Infectious Diseases, Beijing 100015, China

³ Department of Traditional Chinese Medicine, Beijing Ditan Hospital, Capital Medical University, Beijing 100015, China

⁴ Beijing Center for Physical and Chemical Analysis, Beijing 100094, China

Correspondence should be addressed to Jun Cheng; jun.cheng.ditan@gmail.com

Received 26 November 2012; Revised 9 April 2013; Accepted 9 April 2013

Academic Editor: Shao Li

Copyright © 2013 Qi Wang et al. This is an open access article distributed under the Creative Commons Attribution License, which permits unrestricted use, distribution, and reproduction in any medium, provided the original work is properly cited.

FUZHENGHUAYU Tablets have been widely used in the treatment of liver fibrosis in China. Here, we investigate the apoptotic effect of FUZHENGHUAYU Tablet in rat liver stellate cell line HSC-T6. HSC-T6 cells were incubated with control serum or drug serum from rats fed with 0.9% NaCl or FUZHENGHUAYU Tablet, respectively. Cells exposed to drug serum showed higher proportions of early and late apoptotic cells than controls. The mRNA levels of collagens I and III, TGF- β 1 and α -SMA were reduced by drug serum compared to control serum. Differentially expressed mRNAs and miRNAs were analyzed by microarray and sequencing, respectively. We identified 334 differentially expressed mRNAs and also 60 GOs and two pathways related to the mRNAs. Seventy-five differentially expressed miRNAs were down-regulated by drug serum and 1963 target genes were predicted. 134 GOs up-regulated in drug serum group were linked to miRNA targets, and drug serum also regulated 43 miRNA signal transduction pathways. Protein levels were evaluated by Western blot. Drug serum down-regulated (phospho-SAPK/JNK)/(SAPK/JNK) and up-regulated phospho-p38/p38 ratios. The study showed that FUZHENGHUAYU Tablet induced apoptosis in rat HSC-T6 cells possibly in part by activating p38 and inhibiting SAPK/JNK.

1. Introduction

Liver fibrosis is a consequence of chronic liver disease characterized by replacement of liver tissue by fibrosis, scar tissue, and regenerative nodules, leading to loss of liver function. The condition is associated with various types of liver injury, including viral hepatitis, alcohol abuse, nonalcoholic steatohepatitis (NASH), autoimmunity, drug intoxication, and primary biliary cirrhosis. While viral hepatitis remains the leading cause of liver transplantation globally, the prevalence of non-alcoholic fatty liver disease (NAFLD) has escalated over the last decade and is increasingly being recognized as a cause of liver cirrhosis and hepatocellular carcinoma (HCC)

[1, 2]. In order to prevent the development of end-stage liver diseases, it is necessary to control or reverse fibrosis. However, there is currently no high-efficient therapy method for this condition.

Liver fibrosis results from chronic damage to the liver in conjunction with the alterations in both the quantity [3] and composition of extracellular matrix (ECM) proteins [4], including collagens (I, III, and IV), fibronectin, undulin, elastin, laminin, hyaluronan, and proteoglycans. Hepatic stellate cells (HSCs) are the main ECM-producing and regulating cells in the injured liver [5]. HSCs reside in the space of Disse (perisinusoidal space) in the normal liver. Following chronic injury, HSCs transdifferentiate into myofibroblast-like cells

and acquire contractile, proinflammatory, and fibrogenic properties [6, 7].

Interactions between different cellular components are thought to be involved in the disease process. A number of abnormal candidate expression genes and miRNAs have been proposed which could affect the progression of hepatic fibrosis [8]. Transforming growth factor-beta 1 (TGF- β 1) from both paracrine and autocrine sources has been shown to be the key mediator of hepatic fibrogenesis [9], and alpha-smooth muscle actin (α -SMA) is an indicator of stellate cell activation [10]. MiR-29b, -199a, -199a*, -200a, and -200b have been reported related to the process of liver fibrosis [11, 12]. It has also been proposed that miRNA changes regulated by negative feedback loops between miRNAs and their downstream genes might play an important role in the steady-state regulation [13]. So, detailed mechanism of liver fibrosis involved in genes and miRNAs still needs to be further clarified. In addition, in mammalian cells, microRNAs (miRNAs) usually bind to complementary sites in the 3' untranslated region (3'-UTR) of specific target genes, resulting in reduced gene translation. Since miRNAs do not generally affect mRNA level, gene expression profiling is not suitable for exploring the target signaling pathways of miRNA. Instead, miRNA-mRNA interaction network analysis is widely used to the medical researches [14]. This is also consistent with the view that the focus of cataloging a "parts list" of genes and proteins should be changed to a strategy of mapping the network of interactions between them [15].

Many kinds of traditional Chinese medicines (TCMs) have been shown to have antifibrotic properties. These include Ganoderma lucidum (Ling Zhi) [16], Sinisan [17] and Shugan-Huayu powder [18]. TCM 319, also known as FUZHENGHUAYU Tablet, is a compound containing six Chinese herbs, including Radix Salviae Miltiorrhizae, Fermentation Mycelium Powder, Semen Persicae, Fructus Schisandrae, Chinensis Pollen pini, and Gynostemma pentaphyllum [19]. Previous studies have shown that FUZHENGHUAYU has antifibrotic effects in rats [19–25]. But there are no reports of the effects of FUZHENGHUAYU on HSC apoptosis, and little is known about the role played by miRNA and mRNA related mechanisms with respect to the effects of FUZHENGHUAYU Tablet. In this study, we used the established methods and other technologies to investigate the molecular mechanisms of FUZHENGHUAYU Tablet in liver fibrosis.

2. Materials and Methods

2.1. Drug Serum and Control Serum Preparation. Twelve male Wistar rats, SPF grade, weighing 300–350 g, were divided equally into control and drug groups. FUZHENGHUAYU Tablet was suspended in distilled water at concentration of 0.04 g/mL. The drug group received FUZHENGHUAYU Tablet dilution at a dose of 2 mL/100 g-wt, twice daily for 3 days. Two hours after the last dose of dilution, serum was collected from the inferior vena cava and inactivated at 56°C for 30 minutes. Serum samples were stored at -70°C

until further processing. The control group rats were treated with 0.9% NaCl and were subjected to the same procedure [22]. This study was performed according to the international, national, and institutional rules considering animal experiments. In present study, drug and control serums were supplied by Dr. Chenghai Liu, Institute of Liver Disease, Shanghai University of Traditional Chinese Medicine, China.

2.2. Cell Culture, Grouping, and Treatment. Rat HSC-T6 cells from our laboratory were cultured in Dulbecco's modified Eagle's medium (DMEM; Gibco) containing 10% fetal bovine serum (FBS; Gibco), 100 U/mL penicillin, and 100 μ g/mL streptomycin (Gibco) in a humidified chamber at 37°C in 5% CO₂. For the control and drug groups, control and drug serums were used instead of FBS, respectively. The cells were cultured for up to 24 h for RNA and protein extraction and for 72 h for apoptosis analysis. Actinomycin D (2 μ L/mL; Sigma) was added into rat HSC-T6 cells exposed to 10% FBS after 12 h as a positive control for the analysis of apoptosis.

2.3. Apoptosis Analysis. Rat HSC-T6 cells treated with drug serum or control serum were washed twice in cold PBS and harvested by exposure to trypsin-EDTA solution. The harvested cells were centrifuged, washed with complete media, and then suspended in Annexin V binding buffer. Apoptosis was assessed using an Annexin V/7-AAD apoptosis kit according to the manufacturer's protocol (Biolegend). Fluorescein isothiocyanate (FITC)-Annexin V, and 7-AAD were added to the cell suspension. The cells were incubated for 30 min at room temperature in the dark and analyzed using a BD FACSCalibur flow cytometer. After fluorescence activated cell sorting (FACS), the percentage of apoptotic cells was assessed using ModFit software.

2.4. Total RNA Extraction. Total RNA was extracted using an EZNA total RNA kit (Omega), according to the manufacturer's instructions. For gene expression microassays and miRNA sequencing, total RNA was extracted using mirVana miRNA isolation kit (Ambion) and checked for RIN number to inspect RNA integrity by an Agilent Bioanalyzer 2100 (Agilent technologies). Only samples with RNA integrity > 7 and with 28S/18S \geq 0.7 were used in the further analysis. RNA samples were stored at -80°C until further processing.

2.5. Real-Time PCR. An SYBR ExScript RT-PCR Kit (TAKARA) and Power SYBR Green PCR Master Mix (ABI) were used for real-time PCR. The primers of rat collagen I, collagen III, TGF- β 1, α -SMA, and β -actin are listed in Table 1 [26]. Beta-actin was used as an endogenous control. Reactions for each sample were performed in triplicate with equal amounts of template cDNA, using the ABI Prism 7500 Sequence Detection System. Real-time PCR conditions were as follows: 95°C for 10 min, followed by 40 cycles at 95°C for 15 s and 60°C for 1 min. Fold induction values were calculated using the 2 ^{$\Delta\Delta$ Ct} method according to the manufacturer's instructions.

TABLE 1: Sequences of primers used for real-time PCR.

Gene	Primer sequence (5'-3')
Collagen I	Sense: TCCTGGCAATCGTGGTTCAA
	Anti-sense: ACCAGCTGGGCCAACATTTTC
Collagen III	Sense: GGTCTCTGCAGGTAACAGTGGTTC
	Anti-sense: TGCTCCAGTTAGCCCTGCAA
TGF- β 1	Sense: TGC GCCTGCAGAGATTCAAG
	Anti-sense: AGGTAACGCCAGGAATTGTTGCTA
α -SMA	Sense: AGCCAGTCGCCATCAGGAAC
	Anti-sense: CCGGAGCCATTGTCACACAC
β -actin	Sense: GGAGATTACTGCCCTGGCTCCTA
	Anti-sense: GACTCATCGTACTCCTGCTTGCTG

2.6. Microarray Hybridization and Data Analysis. Total RNA (100 ng) was amplified, labeled, and purified by using GeneChip 3'IVT Express Kit (Affymetrix) to obtain biotin labeled cRNA. Labeling and hybridization were performed at Shanghai Biochip Company according to the protocols in the Affymetrix Rat 230 2.0 microarray system. Raw data were normalized using the MAS 5.0 algorithm (Gene Spring Software 11.0; Agilent technologies).

After feature extraction (Feature Extraction software), log₂ ratios, representing the ratio of Cy5-processed signal to Cy3-processed signal, were calculated and converted to fold changes. Genes with a log₂ ratio >1 (>2-fold increase) were considered to be upregulated, and those with <-1 (>2-fold decrease) were considered to be downregulated.

2.7. MicroRNA Profile Sequencing and Target Prediction. The small RNA libraries were constructed following the manufacturer's instructions for the Small RNA Sample Prep Kit (Illumina). The small RNAs were ligated with adapters followed by reverse transcription and amplification. The PCR products derived from 22 nt and 30 nt small RNA fragments were purified from 6% Novex TBE PAGE Gel. Purified miRNAs were sequenced on the Illumina Genome Analyzer for 36 cycles. Sequencing was performed at Shanghai Biotechnology Corporation. MiRNAs genes with fold change ≥ 2 or ≤ 0.5 , P value ≤ 0.05 , and FDR ≤ 0.05 were considered to be up-regulated, and miRNAs genes with fold change ≤ 0.5 , P value ≤ 0.05 , and FDR ≤ 0.05 were considered to be down-regulated. Targetscan (<http://www.targetscan.org/>) was used for miRNA target prediction.

2.8. Gene Ontology (GO) Category and Pathway Analysis. DAVID gene database annotation (DAVID Bioinformatics Resources 6.7) was used to interpret the biological effect of mRNAs and target genes of miRNAs. The categorization of the biological process GO of the difference expression genes and target genes was analyzed using the Gene Ontology project (<http://www.geneontology.org/>) which is the key functional classification of the National Center for Biotechnology Information (NCBI). The KEGG genome database was used to identify significant differential genes pathways. In view of the large differences in enrichment numbers, different P -values (≤ 0.05 , ≤ 0.01 , and ≤ 0.001) were used as a threshold

to select significant gene ontology (GO) categories and KEGG pathways, each representing significant differences.

2.9. Western Blot Analysis. Cultured cells were lysed using Proteo JET Mammalian Cell Lysis Reagent (Fermentas) containing a cocktail of proteinase inhibitors (Roche) and phosphatase inhibitor cocktail (Pierce). The debris was discarded and the supernatant containing total proteins was quantified using a BCA kit. The proteins were run on 10% SDS-PAGE and transferred onto PVDF membranes (Millipore, Bedford). After blocking in 5% non-fat milk, the membranes were probed with rabbit monoclonal antibodies against rat p44/42 MAP kinase (137F5) (CST), SAPK/JNK (56G8) (CST), p38 MAP kinase (CST), phospho-p44/42 MAPK (Thr202/Tyr204) (CST), phospho-p38 MAPK (Thr180/Tyr182) (CST), phospho-SAPK/JNK (Thr183/Tyr185) (CST), and mouse monoclonal antibody against rat β -actin (Santa Cruz) as primary antibodies at 1:1000 dilution. Goat anti-rabbit or goat anti-mouse IgG labeled with HRP (1:2000) were used as secondary antibodies. Immunoreactive signals were detected using an Enhanced Chemiluminescence kit (Amersham Pharmacia Biotech) through an ECL system. The results were quantified using the Image J 1.43 software (National Institutes of Health, Bethesda, MD) after densitometric scanning of the films.

2.10. Statistical Analysis. Data were expressed as means \pm SD. Differences between experimental groups were assessed using the two-tailed t -test. Statistical significance was defined as * $P < 0.05$ and ** $P < 0.01$.

3. Results

3.1. FUZHENGHUAYU Tablet Induces Apoptosis in Rat HSC-T6 Cells. In order to analyze whether FUZHENGHUAYU Tablet could induce apoptosis in rat HSC-T6 cells, we treated rat HSC-T6 cells with control or drug serum, respectively. Cells were stained with Annexin V-FITC/7-AAD and gated into lower right (LR) and upper right (UR) quadrants. Cells in LR and UR represented early (Annexin V(+)/7-AAD(-)) and late apoptotic (Annexin V(+)/7-AAD(+)) cells, respectively. Cells in lower left (LL) quadrants were considered to be alive and those in the upper left (UL) quadrants were considered to be necrotic. The extent of apoptosis was expressed as the sum total of the percentages in LR and UR quadrants. The apoptotic rates are showed in Figures 1(a) to 1(f). Cells exposed to drug serum showed more late apoptotic cells (10% \pm 1%) than control serum (5% \pm 1%) ($n = 3$, $P < 0.05$). They also contained a higher proportion of early apoptotic cells (43% \pm 6%) than the controls (26% \pm 4%) ($n = 3$, $P < 0.05$). The total apoptotic cells in the drug group and control group were 53% \pm 6% and 31% \pm 4%, respectively ($n = 3$, $P < 0.01$).

3.2. FUZHENGHUAYU Tablet Decreased mRNA Levels of Collagen I, Collagen III, TGF- β 1, and α -SMA. The levels of collagen I, collagen III, TGF- β 1, and α -SMA were potential markers of the antifibrosis efficacy of FUZHENGHUAYU Tablet. We found that mRNA levels of collagen I, collagen III,

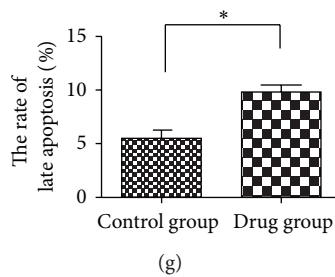
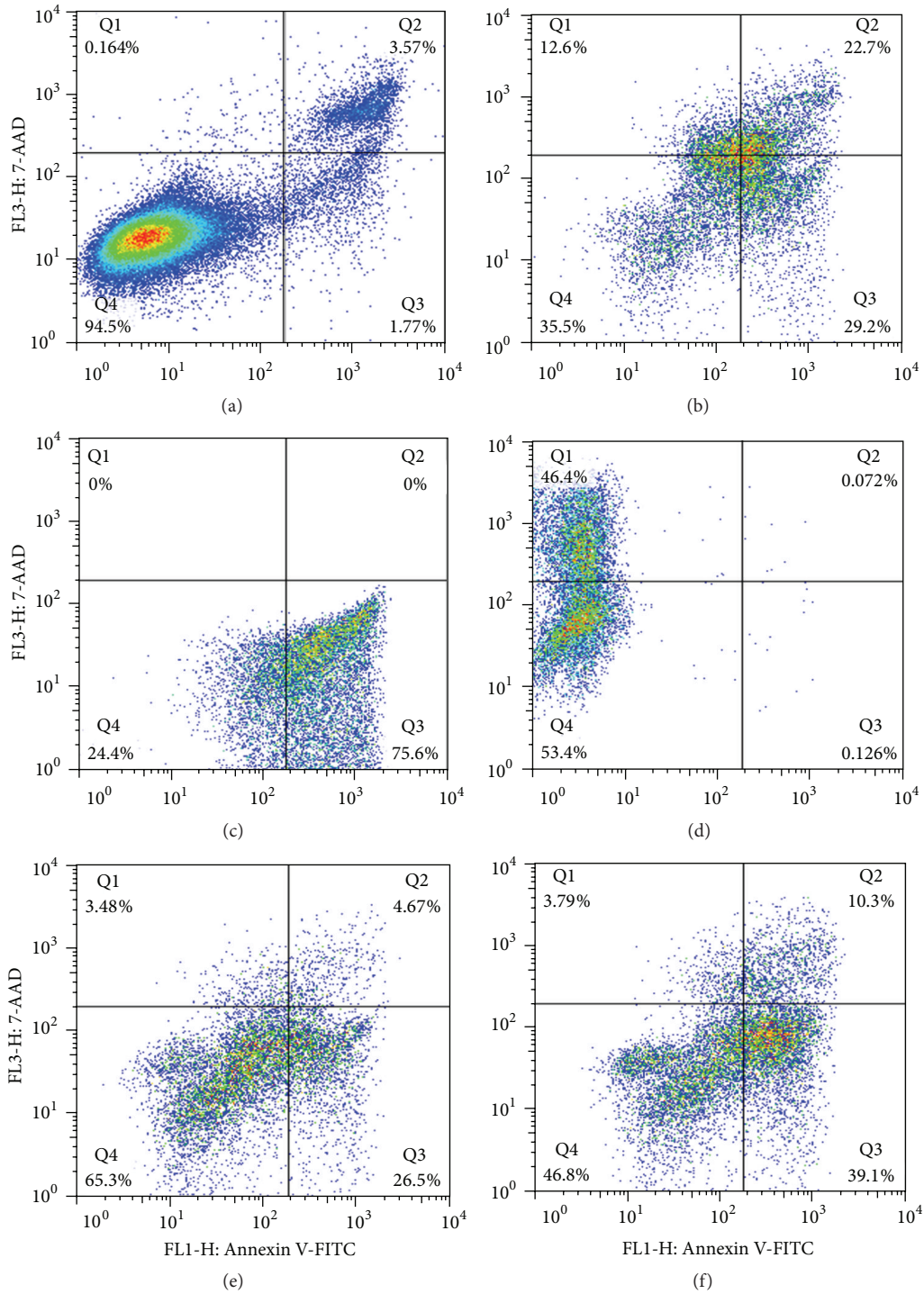


FIGURE 1: Continued.

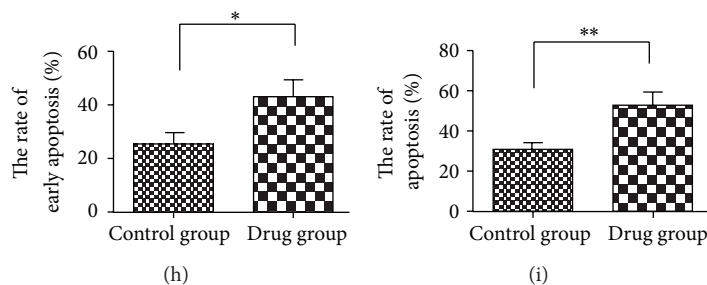


FIGURE 1: FUZHENGHUAYU Tablet induced apoptosis in rat HSC-T6 cells. Cultured rat HSC-T6 cells were divided into control and drug groups. The control group was incubated with DMEM medium containing 10% control serum, and the drug group was cultured with DMEM medium supplemented 10% drug serum for up to 72 h. Apoptosis was assessed using an Annexin V/7-AAD Apoptosis kit and analyzed using a BD FACS Calibur flow cytometer. (a) HSC-T6 cells exposed to 10% FBS and stained with Annexin V(+)/7-AAD(+); (b) HSC-T6 exposed to 10% FBS + 2 μ L/mL actinomycin D and stained with Annexin V(+)/7-AAD(+); (c) HSC-T6 cells exposed to 10% FBS + 2 μ L/mL actinomycin D and stained with Annexin V(+)/7-AAD(-); (d) HSC-T6 cells exposed to 10% FBS + 2 μ L/mL actinomycin D and stained with Annexin V(-)/7-AAD(+); (e) HSC-T6 cells exposed to 10% control serum and stained with Annexin V(+)/7-AAD(+). (f) HSC-T6 cells exposed to with 10% drug serum and stained with Annexin V(+)/7-AAD(+); (g) the late apoptotic cells in the drug (10% \pm 1%) and control groups (5% \pm 1%) ($n = 3$, * $P < 0.05$); (h) the early apoptotic cells in the drug (43% \pm 6%) and control groups (26% \pm 4%) ($n = 3$, * $P < 0.05$); (i) total apoptotic cells in the drug (53% \pm 6%) and control groups (31% \pm 4%) ($n = 3$, ** $P < 0.01$).

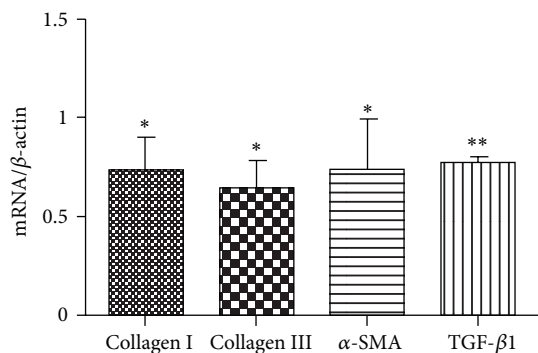


FIGURE 2: FUZHENGHUAYU Tablet serum decreased the mRNA levels of collagen I, collagen III, TGF- β 1, and α -SMA. Data are expressed as mean \pm SD. After incubation with drug serum or control serum for up to 24 h, the mRNA levels of collagen I, collagen III, TGF- β 1, and α -SMA were significantly down-regulated ($n = 3$, * $P < 0.05$, ** $P < 0.01$), being 0.73-, 0.64-, 0.74-, and 0.78-fold lower than the control group, respectively.

TGF- β 1, and α -SMA was significantly down-regulated after exposure of rat HSC-T6 cells to drug serum for up to 24 h. The degree of expression was 0.73-, 0.64-, 0.74-, and 0.78-fold lower than in the control serum group (Figure 2). These findings suggest that apoptosis may be the mechanism of the anti-fibrotic activity of FUZHENGHUAYU Tablet.

3.3. Differentially Expressed mRNA in Control Serum and FUZHENGHUAYU Tablet Serum Groups. Microarray profile analyses of cellular mRNAs in rat HSC-T6 cells identified 334 mRNAs that were differentially expressed between the drug serum group and control serum group; 199 mRNAs were up-regulated and the remainder were down-regulated.

3.4. Differentially Expressed miRNAs in FUZHENGHUAYU Tablet Serum and Control Serum Groups Target Gene Prediction. MicroRNA profile sequencing identified 75 differentially expressed miRNAs, which were down-regulated in drug serum group in comparison with the control serum group. Targetscan (<http://www.targetscan.org/>) prediction of miRNAs identified 1963 potential target genes.

3.5. Bioinformatics Interpretation Revealed the GOs and Signaling Pathways Regulated by Differentially Expressed mRNAs and miRNAs. In order to gain insights into the function of miRNAs and mRNAs, GO term and KEGG pathway annotation were applied.

We have identified 30 up-regulated GOs (Figure 3) and 30 down-regulated GOs (Figure 4) on the differentially expressed mRNAs. These genes were involved in ion transport, necroptosis, cell death, metabolic processes, cell development, differentiation, and adhesion. This form of analysis also identified 134 upregulated GOs by differentially expressed miRNAs target genes (Figure 5), which could be categorized as cell processes, gene expression, cell development, morphogenesis, signaling pathways, cell organization, proliferation, adhesion, and so on. Among all the differentially regulated GOs, those involved in cell development, adhesion, growth, necroptosis, and transport appeared to predominate.

Additional functional analysis of mRNAs using KEGG analysis identified the two signal transduction pathways regulated by drug serum. These were mitogen-activated protein kinases (MAPK) and RIG-I like receptors (Figure 6). In addition, 43 signal transduction miRNA targets were found to be regulated by drug serum. These included MAPK and various cancer signals, as shown in Figure 7.

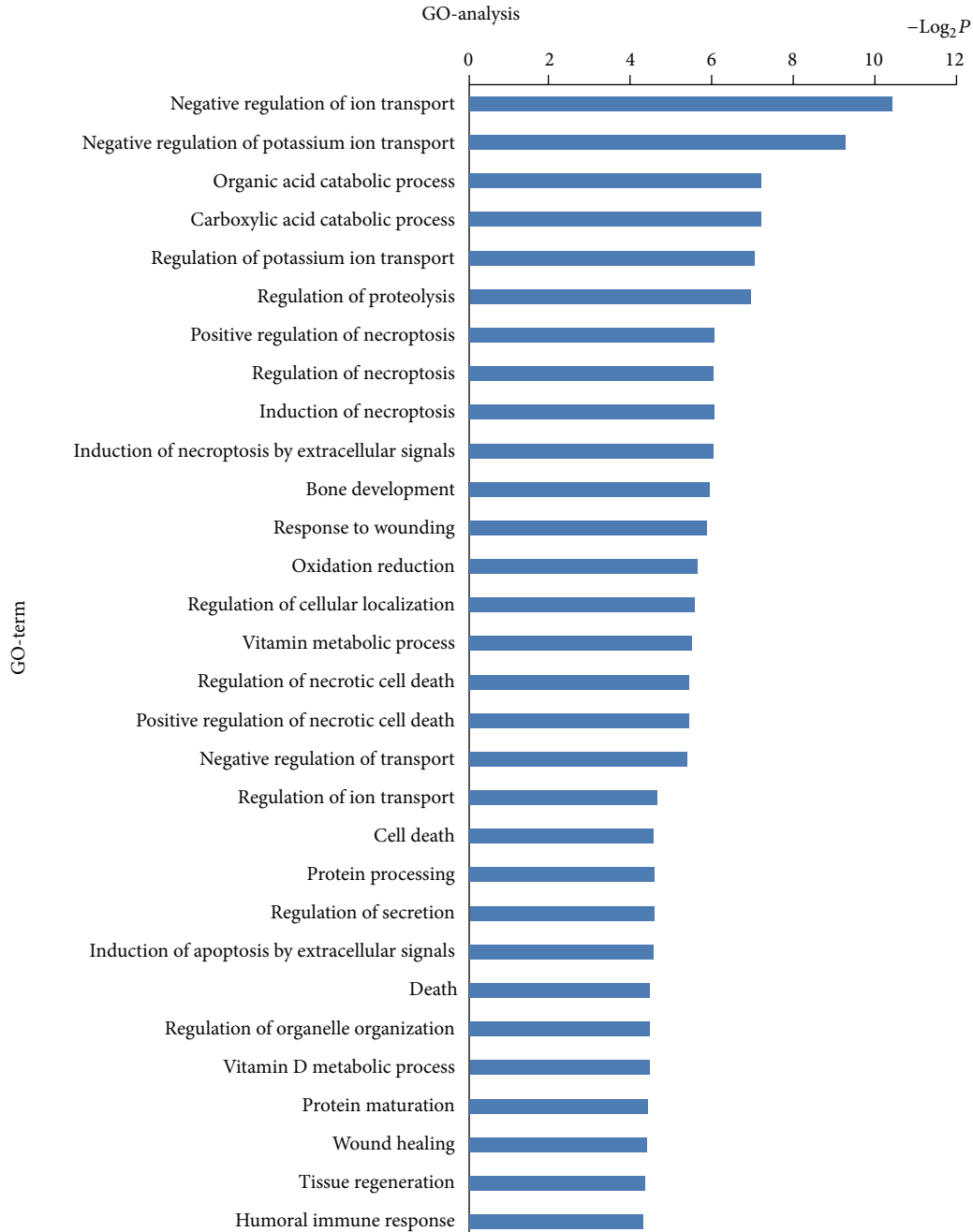


FIGURE 3: Bioinformatics interpretation revealed the GOs regulated by up-regulated expressed mRNAs. Genes with up-regulated expression in the drug and control groups were analyzed by GO. P values ≤ 0.05 were used as a threshold to select significant GO categories.

Enrichment ranking of signaling pathways indicated that MAPK signal transduction pathway was the most prominent. As we know, MAPK signal transduction pathways are involved in a series of important biological effects, such as inflammation, migration, apoptosis, growth, development, and differentiation [27, 28].

The apoptosis results, previous reports, and the results of GO and KEGG analysis all suggested that MAPK signal transduction pathway might be regulated by drug serum, and

this also might be related to the induction of apoptosis in rat HSC-T6 cells.

3.6. MAPK Signal Transduction Pathway Was Regulated by FUZHENGHUAYU Tablet. Mammals express at least four distinctly regulated groups of MAPKs, extracellular signal-related kinases (ERK)-1/2, Jun amino-terminal kinases (JNK1/2/3), p38, and ERK5. MAPKs belong to a large

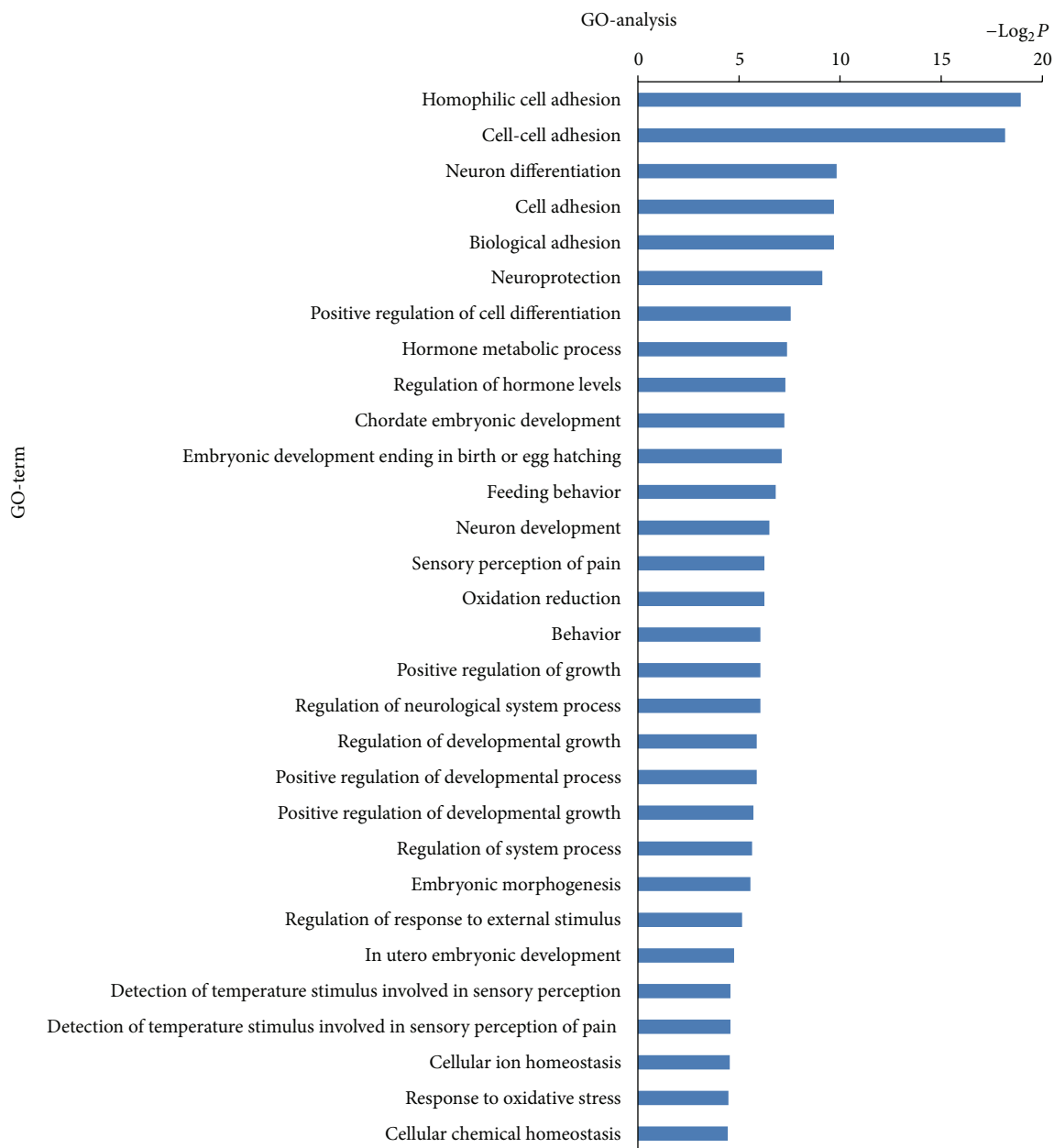


FIGURE 4: Bioinformatics interpretation revealed the GOs regulated by down-regulated expressed mRNAs. Genes with down-regulated expression in the drug and control groups were analyzed by GO. P values ≤ 0.05 were used as a threshold to select significant GO categories.

family of serine/threonine protein kinases. They not only activate/inactivate other proteins but are themselves activated/inactivated by other proteins through phosphorylation/dephosphorylation modification [29].

In order to analyze the hypothesis, the protein levels of rat p44/42, SAPK/JNK, p38, phospho-p44/42, phospho-p38, and phospho-SAPK/JNK were detected by Western blot. The results indicated that the ratio of (phospho-SAPK/JNK)/(SAPK/JNK) was significantly down-regulated and that the ratio of phospho-p38/p38 was significantly up-regulated by drug serum ($n = 3$, $P < 0.05$) (Figure 8). There was no significant change in the (phospho-p44/42)/(p44/42) ratio. These results suggest that changes in SAPK/JNK and

p38 in response to drug serum might be related to its apoptotic effects in rat HSC-T6 cells.

4. Discussion

Traditional Chinese medicine (TCM) uses a holistic approach taking the human body as a self-controlled system network. The goals of biologically based medicine partially overlap the principles of TCM. Bioinformatic and systems biology, therefore, represent an important link between TCM and Western medicine [30]. Bioinformatics and system biology have previously been used to identify disease-related genes or

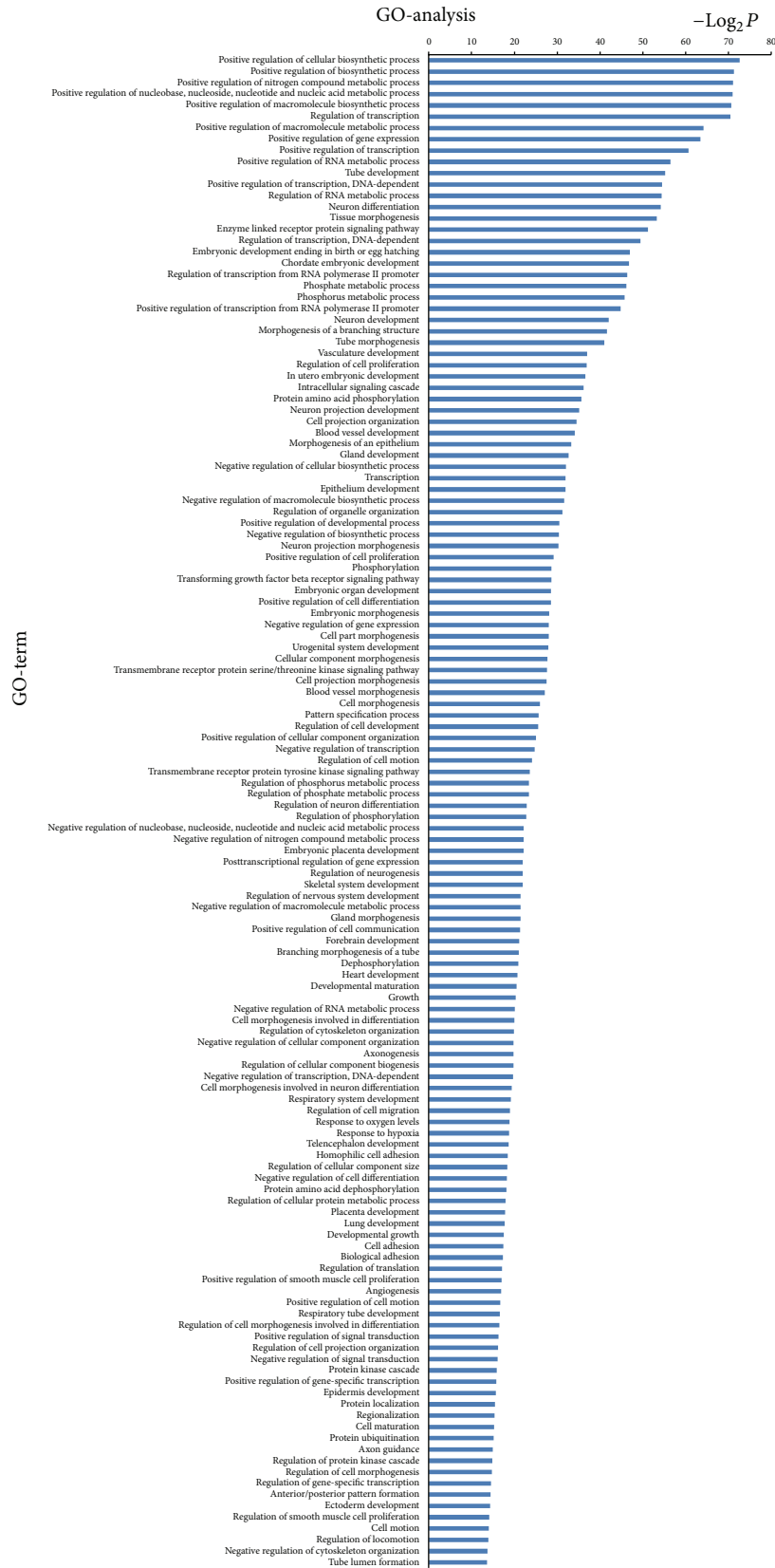


FIGURE 5: Bioinformatics interpretation revealed the GOs regulated by differentially expressed miRNAs target genes. Genes with significant expression difference in the drug and control groups were analyzed by GO. P values ≤ 0.001 and FDR ≤ 0.05 were used as a threshold to select significant GO categories.

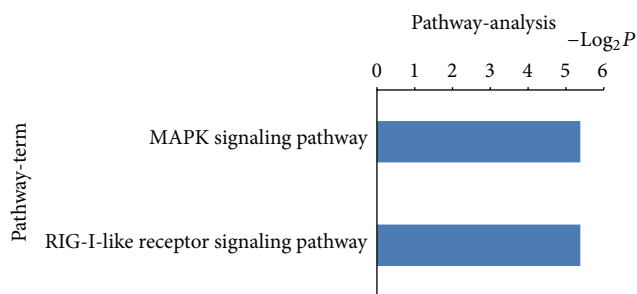


FIGURE 6: Bioinformatics interpretation revealed the KEGG genomes regulated by differentially expressed mRNAs. Genes with significant expression differences in the drug and control groups were analyzed by KEGG. P -values ≤ 0.05 were used as a threshold to select significant KEGG analysis.

functional modules and to recognize redundant, adaptable, and system mechanisms in diseases [31, 32]. The previous reports have supplied us with perfect examples in network pharmacology study.

Liver fibrosis results from the activation of HSCs as part of the wound-healing response to chronic liver injury [33]. It is known that HSCs undergo a transition from a quiescent to an activated phenotype following liver tissue damage [34]. The generation and proliferation of α -SMA positive myofibroblasts from the periportal and perisinusoidal areas also play a central role in the fibrotic process. Previous studies have shown that FUZHENGHUAYU is able to normalize ALT and AST levels in patients with chronic hepatitis B and to some extent reverse the development of liver fibrosis [20, 21]. Another study indicated that FUZHENGHUAYU decoction prevents the autocrine activation of HSCs, possibly by inhibiting secretion of VEGF [22]. A similar study proposed that the anti-fibrotic effects of FUZHENGHUAYU may also be associated with inhibition of liver collagen production. It has also been reported that FUZHENGHUAYU extracts attenuate hepatic fibrosis induced by CCl₄ in rats [19]. The same study showed that the anti-fibrotic effect of FUZHENGHUAYU was associated with down-regulation of mRNA expression of PDGF-B and PDGF-R β and with reduced protein expression of TGF- β 1 [23]. In addition, spontaneous or targeted apoptosis of HSC has been shown to be associated with regression of liver fibrosis in animal models [24, 25].

In the present study we showed for the first time that FUZHENGHUAYU Tablet was able to induce apoptosis in rat HSC-T6 cells. In order to confirm the relationship between the apoptotic and anti-fibrotic effects, we analyzed the mRNA levels of collagen I, collagen III, TGF- β 1, and α -SMA. Our results showed a significant down-regulation in each case.

The miRNAs and their target genes have emerged as key regulators of diverse biological processes, including cancer [35], development [36], cell growth, apoptosis [37], and immune responses [38]. It is known that miRNAs and mRNAs both play essential roles in apoptosis, differentiation, proliferation, and migration in HSCs [8] and also are involved in the process of liver fibrosis [39]. A previous study suggested

that miR-29 regulates liver fibrosis and together with TGF- β and nuclear factor- κ B forms part of a signaling nexus in HSCs [40]. It has also been shown that hepatic levels of miR-29 are significantly increased in mice with CCl₄ induced liver damage and also in the livers of patients with advanced fibrosis. By contrast, miR-29b appears to act as a beneficial factor that protects against liver fibrosis by suppressing the activation of HSCs [11]. It has been suggested that upregulation of miR-199a, -199a*, -200a, and -200b triggers the process of liver fibrosis [12]. Specifically, it has been suggested that miR-16 has the potential to inhibit HSC proliferation and induce apoptosis by inducing Bcl-2 while concurrently reducing cyclin D1 levels [37]. Other evidence suggests that overexpression of miR-181b increases the growth of HSCs by directly targeting p27 [39].

Microarray techniques are increasingly being used as research tools in chemistry and life sciences. The sequencing of the human genome, together with the development of high-throughput technologies, affords a unique opportunity for future research [41]. Microarray and high-throughput sequencing are both based on computational biology and bioinformatics, and both are appropriate for mRNA and miRNA research. In this study, we identified 334 differentially expressed mRNAs. Sequencing identified 75 miRNAs with down-regulated expression in the drug serum group. Online database analysis identified 60 differently regulated GOs from mRNAs and 134 regulated GOs from miRNAs targets that were principally involved in cell development, adhesion, growth, necroptosis, and transport processes. Functional analysis of mRNAs by KEGG revealed that drug serum regulated two signal transduction pathways, involving MAPK and RIG-I like receptors. In addition, drug serum regulated 43 miRNA signal transduction pathways, principally the MAPK pathway and to a lesser extent pathways involved in cancer signals. These findings suggested that drug serum has wide ranging effects on rat HSC-T6 cells, which resulted from differential expression of miRNAs and mRNAs. They also suggested that MAPK signal transduction might be involved in these complex processes. The number of predicted target genes was much higher than the number of differently expressed mRNAs, reflecting differences in the numbers of enriched pathways.

It is possible that liver fibrogenesis is regulated by intracellular signaling pathways, involved in apoptosis, proliferation, migration, or inflammation. Mammals express at least four distinctly regulated groups of MAPKs: ERK-1/2, JNK1/2/3, p38 proteins (p38alpha/beta/gamma/delta), and ERK5. The MAPK cascade is known to be involved in various cellular functions, including cell proliferation, apoptosis, differentiation, and migration. MAPKs have also been shown to modulate major fibrogenic actions of HSCs, but different members of the group have different effects. A previous study showed that ERK stimulation in experimentally induced liver injury mediated the proliferation and migration of HSCs [42]. Other reports have shown that p38-MAPK and caspase-3 both mediate superoxide-induced apoptosis in rat HSCs [43]. Another study showed that TAK1/JNK inhibition decreased HSC proliferation, whereas p38 inhibition increased the rate of HSC proliferation, independently of its activation status

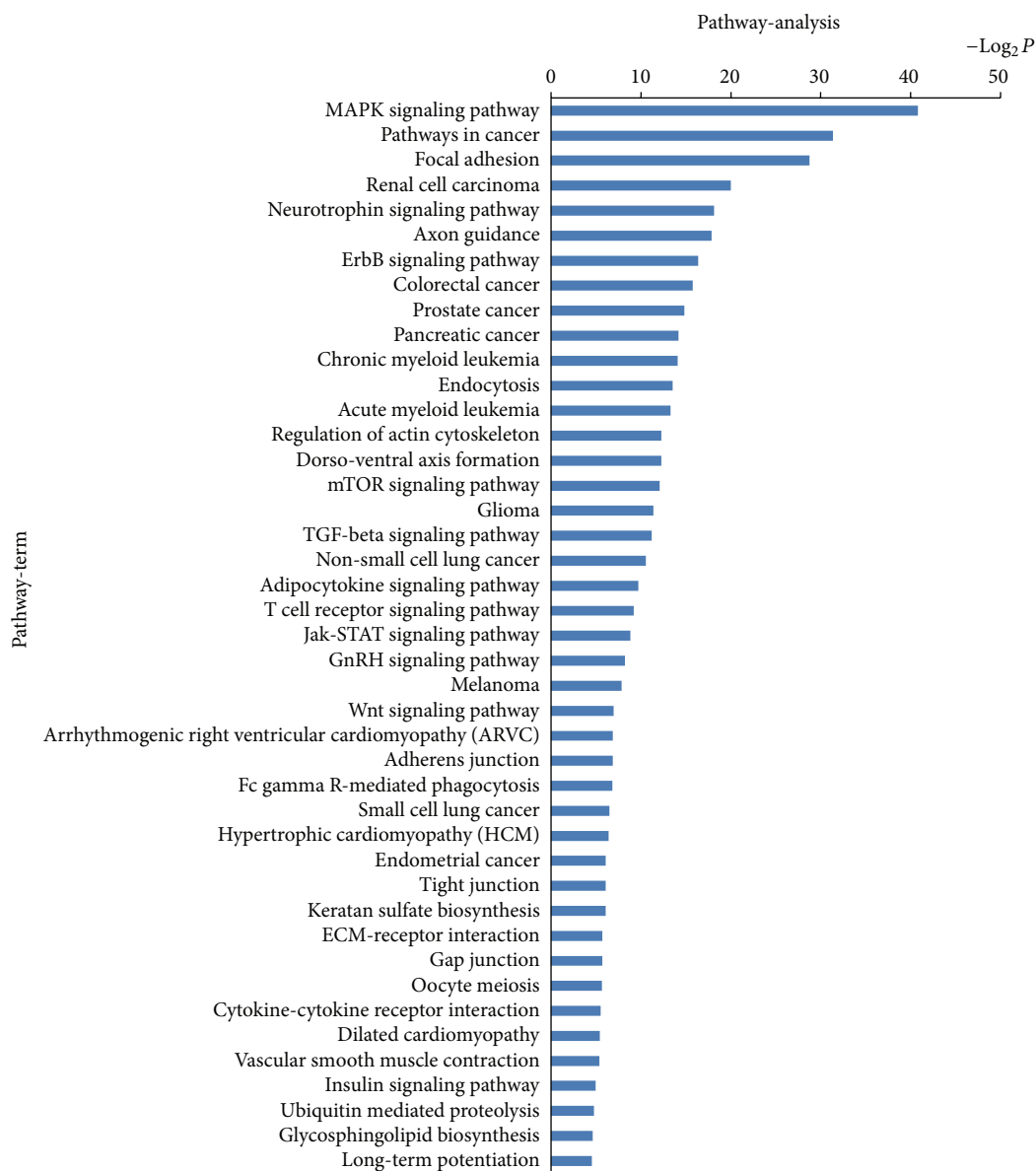


FIGURE 7: Bioinformatics interpretation revealed the KEGG genomes regulated by mRNAs of differentially expressed miRNAs. Genes with significant difference in the drug and control groups were analyzed by KEGG. P -values ≤ 0.01 were used as a threshold to select significant KEGG analysis.

[34]. The same study showed that JNK inhibition increased and p38 inhibition decreased collagen alpha 1 (I) mRNA levels. Additional evidence indicates that c-JNK regulates hepatocyte apoptosis as well as regulating the secretion of inflammatory cytokines by cultured HSCs [44, 45]. Indole-3 carbinol (I3C) is known to inhibit the proliferation of HSC by blocking the NADPH oxidase/reactive oxygen species/p38 MAPK signal pathway [46]. A recent study has shown that p38 may play an important role in the regulation of HSC self-renewal in vitro. Based on this finding, it was suggested that inhibition of p38 activation with a small molecule inhibitor might represent a novel approach to promote ex vivo expansion of HSCs [47]. In our study, drug serum

down-regulated the levels of phospho-SAPK/JNK and up-regulated phospho-p38. There was no change in phospho-p44/42. These results suggest that the changes in phospho-SAPK/JNK and phospho-p38 might in part explain the apoptotic induction effects of TMC 319 in rat HSC-T6 cells.

5. Conclusions

Taken together our results indicate that FUZHENGHUAYU Tablet increases apoptosis of rat HSC-T6 cells by activating p38 and inhibiting SAPK/JNK. These effects may in part

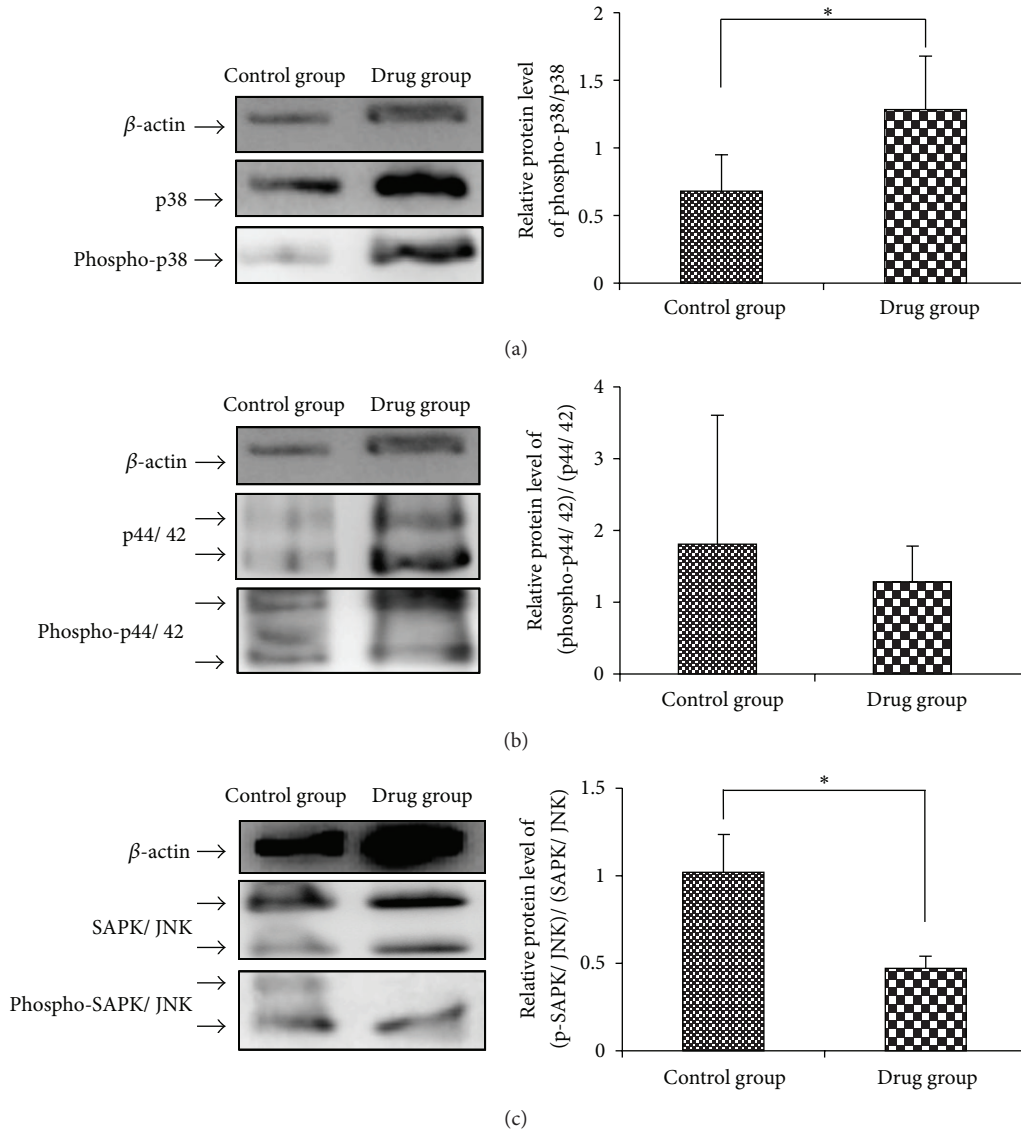


FIGURE 8: The MAPK signal transduction pathway is regulated by FUZHENGHUAYU Tablet. Protein levels of rat p44/42 MAP kinase (137F5), SAPK/JNK (56G8), p38 MAP kinase, phospho-p44/42 MAPK (Thr202/Tyr204), phospho-p38 MAPK (Thr180/Tyr182), and phospho-SAPK/JNK (Thr183/Tyr185) were detected by Western blot.

explain the mechanism by which FUZHENGHUAYU Tablet protects against liver fibrosis.

Abbreviations

TCM: Traditional Chinese Medicine
 HSC: Hepatic stellate cell
 HCC: Hepatocellular carcinoma
 NASH: Non-alcoholic steatohepatitis
 NAFLD: Non-alcoholic fatty liver disease
 ECM: Extracellular matrix
 CCl4: Carbon tetrachloride
 MMP: Matrix metalloproteinase
 TIMP: Tissue inhibitor of metalloproteinase
 ALT: Alanine aminotransferase

AST: Aspartate aminotransferase
 α -SMA: Smooth muscle alpha actin
 β -actin: Beta-actin
 TGF- β : Transforming growth factor-beta
 PDGF: Platelet-derived growth factor
 PDGF-R β : Platelet-derived growth factor receptor beta
 GO: Gene ontology
 miRNA: microRNA
 MAPK: Mitogen-activated protein kinase
 ERK: Extracellular signal regulated kinase
 p38 MAP kinase: p38 mitogen-activated protein kinase
 JNK: Jun N-terminal kinase
 SAPK: Stress-activated protein kinases.

Conflict of Interests

The authors declared that they have no conflict of interests to this work.

Acknowledgments

The authors thank Dr. Chenghai Liu, Institute of Liver Disease, Shanghai University of Traditional Chinese Medicine, China. This work was supported by the Beijing Excellent Talent Program (2011D003034000028), the Research Fund of Capital Medical Top Talent (no. 2009-1-09), and the National Importance Foundation of Infectious Diseases during the Five-Year Plan Period of China (2012ZX10002003 and 2013ZX10002005).

References

- [1] M. Lazo and J. M. Clark, "The epidemiology of nonalcoholic fatty liver disease: a global perspective," *Seminars in Liver Disease*, vol. 28, no. 4, pp. 339–350, 2008.
- [2] C. D. Williams, J. Stengel, M. I. Asike et al., "Prevalence of nonalcoholic fatty liver disease and nonalcoholic steatohepatitis among a largely middle-aged population utilizing ultrasound and liver biopsy: a prospective study," *Gastroenterology*, vol. 140, no. 1, pp. 124–131, 2011.
- [3] S. L. Friedman, "Liver fibrosis: from bench to bedside," *Journal of Hepatology*, vol. 38, supplement 1, pp. S38–S53, 2003.
- [4] R. C. Benyon and J. P. Iredale, "Is liver fibrosis reversible?" *Gut*, vol. 46, no. 4, pp. 443–446, 2000.
- [5] R. Bataller and D. A. Brenner, "Liver fibrosis," *Journal of Clinical Investigation*, vol. 115, no. 2, pp. 209–218, 2005.
- [6] F. Marra, "Hepatic stellate cells and the regulation of liver inflammation," *Journal of Hepatology*, vol. 31, no. 6, pp. 1120–1130, 1999.
- [7] S. Milani, H. Herbst, D. Schuppan, K. Y. Kim, E. O. Riecken, and H. Stein, "Procollagen expression by nonparenchymal rat liver cells in experimental biliary fibrosis," *Gastroenterology*, vol. 98, no. 1, pp. 175–184, 1990.
- [8] Y. He, C. Huang, S. P. Zhang, X. Sun, X. R. Long, and J. Li, "The potential of microRNAs in liver fibrosis," *Cellular Signalling*, vol. 24, no. 12, pp. 2268–2272, 2012.
- [9] Y. Inagaki and I. Okazaki, "Emerging insights into transforming growth factor β Smad signal in hepatic fibrogenesis," *Gut*, vol. 56, no. 2, pp. 284–292, 2007.
- [10] N. Akpolat, S. Yahsi, A. Godekmerdan, M. Yalniz, and K. Demirbag, "The value of α -SMA in the evaluation of hepatic fibrosis severity in hepatitis B infection and cirrhosis development: a histopathological and immunohistochemical study," *Histopathology*, vol. 47, no. 3, pp. 276–280, 2005.
- [11] Y. Sekiya, T. Ogawa, K. Yoshizato, K. Ikeda, and N. Kawada, "Suppression of hepatic stellate cell activation by microRNA-29b," *Biochemical and Biophysical Research Communications*, vol. 412, no. 1, pp. 74–79, 2011.
- [12] Y. Murakami, H. Toyoda, M. Tanaka et al., "The progression of liver fibrosis is related with overexpression of the miR-199 and 200 families," *PLoS ONE*, vol. 6, no. 1, Article ID e16081, 2011.
- [13] J. Shu, B. T. Kren, Z. Xia et al., "Genomewide microRNA down-regulation as a negative feedback mechanism in the early phases of liver regeneration," *Hepatology*, vol. 54, no. 2, pp. 609–619, 2011.
- [14] C. J. Guo, Q. Pan, T. Cheng, B. Jiang, G. Y. Chen, and D. G. Li, "Changes in microRNAs associated with hepatic stellate cell activation status identify signaling pathways," *FEBS Journal*, vol. 276, no. 18, pp. 5163–5176, 2009.
- [15] T. Ideker and R. Sharan, "Protein networks in disease," *Genome Research*, vol. 18, no. 4, pp. 644–652, 2008.
- [16] B. S. Sanodiya, G. S. Thakur, R. K. Baghel, G. B. K. S. Prasad, and P. S. Bisen, "Ganoderma lucidum: a potent pharmacological macrofungus," *Current Pharmaceutical Biotechnology*, vol. 10, no. 8, pp. 717–742, 2009.
- [17] Y. Tang, Y. Liao, N. Kawaguchi-Sakita et al., "Sinisan, a traditional Chinese medicine, attenuates experimental chronic pancreatitis induced by trinitrobenzene sulfonic acid in rats," *Journal of Hepato-Biliary-Pancreatic Sciences*, vol. 18, no. 4, pp. 551–558, 2011.
- [18] C. C. Cheng, N. N. Lin, Y. F. Lee et al., "Effects of Shugan-Huayu powder, a traditional Chinese medicine, on hepatic fibrosis in rat model," *Chinese Journal of Physiology*, vol. 53, no. 4, pp. 223–233, 2010.
- [19] K. F. Cheung, D. W. Ye, Z. F. Yang et al., "Therapeutic efficacy of Traditional Chinese Medicine 319 recipe on hepatic fibrosis induced by carbon tetrachloride in rats," *Journal of Ethnopharmacology*, vol. 124, no. 1, pp. 142–150, 2009.
- [20] P. Liu, Y. Y. Hu, C. Liu et al., "Multicenter clinical study on Fuzhenghuayu capsule against liver fibrosis due to chronic hepatitis B," *World Journal of Gastroenterology*, vol. 11, no. 19, pp. 2892–2899, 2005.
- [21] P. Liu, C. Liu, L. M. Xu et al., "Effects of Fuzheng Huayu 319 recipe on liver fibrosis in chronic hepatitis B," *World Journal of Gastroenterology*, vol. 4, no. 1–6, pp. 348–353, 1998.
- [22] C. Liu, C. M. Jiang, C. H. Liu, P. Liu, and Y. Y. Hu, "Effect for Fuzhenghuayu decoction on vascular endothelial growth factor secretion in hepatic stellate cells," *Hepatobiliary and Pancreatic Diseases International*, vol. 1, no. 2, pp. 207–210, 2002.
- [23] E. Borkham-Kamphorst, J. Herrmann, D. Stoll, J. Treptau, A. M. Gressner, and R. Weiskirchen, "Dominant-negative soluble PDGF- β receptor inhibits hepatic stellate cell activation and attenuates liver fibrosis," *Laboratory Investigation*, vol. 84, no. 6, pp. 766–777, 2004.
- [24] J. B. Chakraborty, F. Oakley, and M. J. Walsh, "Mechanisms and biomarkers of apoptosis in liver disease and fibrosis," *International Journal of Hepatology*, vol. 2012, Article ID 648915, 10 pages, 2012.
- [25] S. L. Friedman, "Evolving challenges in hepatic fibrosis," *Nature Reviews Gastroenterology and Hepatology*, vol. 7, no. 8, pp. 425–436, 2010.
- [26] F. Xiao, K. Yu, F. Dong, Y. Liang, C. Jun, and H. Wei, "The GABAB receptor inhibits activation of hepatic stellate cells," *Digestive Diseases and Sciences*, vol. 55, no. 2, pp. 261–267, 2010.
- [27] L. Min, B. He, and L. Hui, "Mitogen-activated protein kinases in hepatocellular carcinoma development," *Seminars in Cancer Biology*, vol. 21, no. 1, pp. 10–20, 2011.
- [28] L. Santarpia, S. M. Lippman, and A. K. El-Naggar, "Targeting the MAPK-RAS-RAF signaling pathway in cancer therapy," *Expert Opinion on Therapeutic Targets*, vol. 16, no. 1, pp. 103–119, 2012.
- [29] H. J. Schaeffer and M. J. Weber, "Mitogen-activated protein kinases: specific messages from ubiquitous messengers," *Molecular and Cellular Biology*, vol. 19, no. 4, pp. 2435–2444, 1999.
- [30] S. Li, "Network systems underlying traditional Chinese medicine syndrome and herb formula," *Current Bioinformatics*, vol. 4, no. 3, pp. 188–196, 2009.

- [31] X. Wu, R. Jiang, M. Q. Zhang, and S. Li, "Network-based global inference of human disease genes," *Molecular Systems Biology*, vol. 4, article 189, 2008.
- [32] S. Li, L. Wu, and Z. Zhang, "Constructing biological networks through combined literature mining and microarray analysis: a LMMA approach," *Bioinformatics*, vol. 22, no. 17, pp. 2143–2150, 2006.
- [33] E. Albanis and S. L. Friedman, "Hepatic fibrosis: pathogenesis and principles of therapy," *Clinics in Liver Disease*, vol. 5, no. 2, pp. 315–334, 2001.
- [34] B. Schnabl, C. A. Bradham, B. L. Bennett, A. M. Manning, B. Stefanovic, and D. A. Brenner, "TAK1/JNK and p38 have opposite effects on rat hepatic stellate Cells," *Hepatology*, vol. 34, no. 5, pp. 953–963, 2001.
- [35] E. Chan, D. E. Prado, and J. B. Weidhaas, "Cancer microRNAs: from subtype profiling to predictors of response to therapy," *Trends in Molecular Medicine*, vol. 17, no. 5, pp. 235–243, 2011.
- [36] L. A. Goff, S. Boucher, C. L. Ricupero et al., "Differentiating human multipotent mesenchymal stromal cells regulate microRNAs: prediction of microRNA regulation by PDGF during osteogenesis," *Experimental Hematology*, vol. 36, no. 10, pp. 1354–1369, 2008.
- [37] C. J. Guo, Q. Pan, D. G. Li, H. Sun, and B. W. Liu, "miR-15b and miR-16 are implicated in activation of the rat hepatic stellate cell: an essential role for apoptosis," *Journal of Hepatology*, vol. 50, no. 4, pp. 766–778, 2009.
- [38] R. M. O'Connell, D. S. Rao, A. A. Chaudhuri, and D. Baltimore, "Physiological and pathological roles for microRNAs in the immune system," *Nature Reviews Immunology*, vol. 10, no. 2, pp. 111–122, 2010.
- [39] X. W. Wang, N. H. H. Heegaard, and H. Orum, "MicroRNAs in liver disease," *Gastroenterology*, vol. 142, no. 7, pp. 1431–1414, 2012.
- [40] C. Roderburg, G. W. Urban, K. Bettermann et al., "Micro-RNA profiling reveals a role for miR-29 in human and murine liver fibrosis," *Hepatology*, vol. 53, no. 1, pp. 209–218, 2011.
- [41] T. Asselah, I. Bièche, A. Sabbagh et al., "Gene expression and hepatitis C virus infection," *Gut*, vol. 58, no. 6, pp. 846–858, 2009.
- [42] F. Marra, M. C. Arrighi, M. Fazi et al., "Extracellular signal-regulated kinase activation differentially regulates platelet-derived growth factor's actions in hepatic stellate cells, and is induced by in vivo liver injury in the rat," *Hepatology*, vol. 30, no. 4, pp. 951–958, 1999.
- [43] N. M. Jameel, C. Thirunavukkarasu, W. U. Tong, S. C. Watkins, S. L. Friedman, and C. R. Gandhi, "P38-MAPK-and caspase-3-mediated superoxide-induced apoptosis of rat hepatic stellate cells: reversal by retinoic acid," *Journal of Cellular Physiology*, vol. 218, no. 1, pp. 157–166, 2009.
- [44] R. F. Schwabe, B. Schnabl, Y. O. Kweon, and D. A. Brenner, "CD40 activates NF- κ B and c-Jun N-terminal kinase and enhances chemokine secretion on activated human hepatic stellate cells," *Journal of Immunology*, vol. 166, no. 11, pp. 6812–6819, 2001.
- [45] R. F. Schwabe, H. Uchinami, T. Qian, B. L. Bennett, J. J. Lemasters, and D. A. Brenner, "Differential requirement for c-Jun NH2-terminal kinase in TNF α - and Fas-mediated apoptosis in hepatocytes," *The FASEB journal*, vol. 18, no. 6, pp. 720–722, 2004.
- [46] J. Ping, J. T. Li, Z. X. Liao, L. Shang, and H. Wang, "Indole-3-carbinol inhibits hepatic stellate cells proliferation by blocking NADPH oxidase/reactive oxygen species/p38 MAPK pathway," *European Journal of Pharmacology*, vol. 650, no. 2-3, pp. 656–662, 2011.
- [47] Y. Wang, J. Kellner, L. Liu, and D. Zhou, "Inhibition of p38 mitogen-activated protein kinase promotes ex vivo hematopoietic stem cell expansion," *Stem Cells and Development*, vol. 20, no. 7, pp. 1143–1152, 2011.

Research Article

A Computational Drug-Target Network for Yuanhu Zhitong Prescription

Haiyu Xu,¹ Ye Tao,^{1,2} Peng Lu,^{1,3} Peng Wang,² Fangbo Zhang,¹ Yuan Yuan,¹ Songsong Wang,⁴ Xuefeng Xiao,² Hongjun Yang,¹ and Luqi Huang¹

¹ Institute of Chinese Materia Medica, China Academy of Chinese Medical Sciences, No. 16 Nanxiaojie, Dongzhimennei, Beijing 100700, China

² Tianjin University of Traditional Chinese Medicine, Tianjin 300193, China

³ Institute of Automation, Chinese Academy of Sciences, Beijing 100190, China

⁴ Capital Medical University, Beijing 100069, China

Correspondence should be addressed to Hongjun Yang; hongjun0420@vip.sina.com and Luqi Huang; huangluqi@263.net

Received 20 December 2012; Accepted 10 March 2013

Academic Editor: Shao Li

Copyright © 2013 Haiyu Xu et al. This is an open access article distributed under the Creative Commons Attribution License, which permits unrestricted use, distribution, and reproduction in any medium, provided the original work is properly cited.

Yuanhu Zhitong prescription (YZP) is a typical and relatively simple traditional Chinese medicine (TCM), widely used in the clinical treatment of headache, gastralgia, and dysmenorrhea. However, the underlying molecular mechanism of action of YZP is not clear. In this study, based on the previous chemical and metabolite analysis, a complex approach including the prediction of the structure of metabolite, high-throughput *in silico* screening, and network reconstruction and analysis was developed to obtain a computational drug-target network for YZP. This was followed by a functional and pathway analysis by ClueGO to determine some of the pharmacologic activities. Further, two new pharmacologic actions, antidepressant and antianxiety, of YZP were validated by animal experiments using zebrafish and mice models. The forced swimming test and the tail suspension test demonstrated that YZP at the doses of 4 mg/kg and 8 mg/kg had better antidepressive activity when compared with the control group. The anxiolytic activity experiment showed that YZP at the doses of 100 mg/L, 150 mg/L, and 200 mg/L had significant decrease in diving compared to controls. These results not only shed light on the better understanding of the molecular mechanisms of YZP for curing diseases, but also provide some evidence for exploring the classic TCM formulas for new clinical application.

1. Introduction

Traditional Chinese medicine (TCM) is one of the oldest systems of traditional medicines that make use of several herbs to cure a number of ailments for over 2,500 years [1, 2]. Recently, due to its good therapeutic effects and low toxicity, TCM has attracted considerable attention from all over the world [3]. However, the acceptance of TCM is restricted in the Western biomedical practice due to the lack of knowledge of mechanisms of action of the therapeutics as well as the characteristics of the active compounds. In the past, researches worked in the field of TCM had employed phytochemistry which also included separation, structure identification, and pharmacological research. However, those studies ignored the most essential features of multicomponents therapeutics

and in turn the synergistic nature of TCM [4, 5]. The recent studies involving TCM have utilized system biology and network pharmacology to learn the molecular mechanism of TCM, such as TCM syndrome [6, 7], prescription compatibility [8], active substances and their pharmacological actions [9] et al. This approach provided deep understanding of TCM and improved the level of application, as well as promoted the modernization and globalization of TCM [10].

Yuanhu Zhitong prescription (YZP) is a typical and relatively simple TCM formula, consisting of *Radix angelicae dahuricae* and *Rhizoma corydalis* widely used in the clinical treatment of gastralgia, headache, and dysmenorrhea [11]. Alkaloids in *Rhizoma corydalis* and coumarins in *Radix angelicae dahuricae* are the active components in YZP [12, 13]. Recently, we developed a UPLC/Q-TOF-MS method to

construct the chromatographic fingerprint and identify the 21 constituents of YZP [14]; we also developed an RRLC-QQQ technique to detect 17 constituents of YZP tablet [15]. Generally, only the absorbed constituents have more chances to play a role in the therapeutics. Thus, an RRLC-Q-TOF method was developed to identify 15 prototype compounds and some of their metabolites in plasma after oral administration of YZP extracts [16]. Pharmacologically, YZP has a wide variety of actions including antinociceptive [17], anti-inflammatory [18], spasmolysis [19], and vasorelaxation [20]; all of them may be the contributory factor for its therapeutic action. However, the molecular pharmacology of YZP is still unclear. The lack of the compound-target interaction network associated with YZP hindered the knowledge of molecular mechanism of YZP.

In this study, network pharmacology was employed as a tool to understand the active components in YZP and to know how YZP can be better administrated for its optimal therapeutic action. The objective of this study was to better understand the molecular mechanisms of YZP. Based on the known chemical and metabolic knowledge, an integrated model combining the metabolites' structure, virtual screening and validation of compound-target interaction *in silico*, network analysis, construction, and visualization, as well as bioactivity validation, had been performed to shed light on the mystery and effectiveness of YZP.

2. Materials and Methods

The plan of work is depicted in Figure 1.

2.1. Database Construction. The constituents of YZP were derived from our earlier research on the analysis of the prototype constituents and the metabolites of YZP in the plasma [13]. Among them, 7 alkaloids were from *Rhizoma corydalis* and 8 coumarins were from *Radix angelicae dahuricae* (Figure 2). The molecular files of all prototype compounds were downloaded from ChemSpider (<http://www.chemspider.com/>) and saved to a mol format (molecular files). Six metabolites were identified by RRLC-Q-TOF and the Agilent Metabolite ID software (Agilent Technologies, Inc., 2009): 2 from tetrahydroberberine, 2 from tetrahydropalmatine, 1 from protopine, and 1 from oxypeucedanin (Table 1).

2.2. Prediction of Metabolites by Combined Computational Approaches. An ADMET predictor software program (ADMET Predictor, Simulations Plus, Inc., Lancaster, CA, 2012) was employed to predict atomic sites of metabolic reaction for CYP isoforms 1A2, 2C9, 2C19, 2D6, and 3A4. These isoforms account for ~90%–95% of CYP-mediated reactions. The mol files of molecular structure of oxypeucedanin, tetrahydroberberine, protopine, and tetrahydropalmatine were uploaded into the ADMET predictor software. The highest score of the metabolic “soft spot” was selected based on the metabolic type. These molecules were then exported as a mol file.

2.3. Molecular Similarity and Targets Identification. Drug data of 1447 FDA-approved drugs were collected from

DrugBank database (<http://www.drugbank.ca/>, accessed on 2011.10.16). MedChem Studio (MedChem Studio, 3.0; Simulations Plus, Inc., Lancaster, CA, 2012.) could be powerful to quickly identify all molecules that are structurally similar to a reference molecule of interest. We used it to screen similar drugs of YZP by the comparison of 2D structural similarity between the ingredients of YZP (including 15 prototype constituents and 6 metabolites) *in vivo* and drug data. In order to improve the reliability of the results, only high similar drugs were selected according to the similar scores. All therapeutic targets of these similar drugs were also collected as predicted effector molecules of YZP.

2.4. Network Construction and Analysis. The 21 constituents of YZP were classified by 2D chemical structural similarity using MedChem Studio software program. The therapeutic similarity of the target (TST) was established based on an anatomic therapeutic chemical (ATC) classification system corresponding to drug. The potential targets were identified based on the similarity of ATC codes corresponding to the drug by proposing a probabilistic model [21, 22]. The similarity between two ATC codes was derived according to their prior probabilities (frequency) and the probability of their commonality, which was defined as their longest matched prefix:

$$S(\text{atc}_i, \text{atc}_j) = \frac{2 * \log(\text{IC}(\text{prefix}(\text{atc}_i, \text{atc}_j)))}{\log(\text{IC}(\text{atc}_i)) + \log(\text{IC}(\text{atc}_j))}, \quad (1)$$

where prefix (i, j) is the longest matched prefix of ATC code i and j . IC is the information content of ATC code. Note that drugs related to target may have more than one ATC code; we defined the maximum ATC code similarity as TST:

$$\begin{aligned} \text{Target } T_1 &\sim \text{ATC}(T_1) = \{\text{atc}_{11}, \text{atc}_{12}, \dots, \text{atc}_{1m}\}, \\ \text{Target } T_2 &\sim \text{ATC}(T_2) = \{\text{atc}_{21}, \text{atc}_{22}, \dots, \text{atc}_{2n}\}, \end{aligned} \quad (2)$$

$$\text{TST}(T_1, T_2) = \frac{|\text{ATC}(T_1) \cap \text{ATC}(T_2)|}{|\text{ATC}(T_1) \cup \text{ATC}(T_2)|}.$$

ATC (T) represents all the ATC codes belonging to target corresponding to drug.

The potential targets were used to build the compound-target networks (CTN) with the 21 constituents of YZP. CTN was generated by Cytoscape 2.8.1, a standard tool for integrated analysis and visualization of biological networks, which was available for download from <http://cytoscape.org/>. In the graphical network format, nodes represent compounds or targets. Edges encode the compound-target and target-target interactions. From the relationship between chemical structural similarity and the therapeutic similarity, compound combinations and therapeutic targets, the qualitative properties of the networks were analyzed.

2.5. Functional and Pathway Analysis. ClueGO, Cytoscape plug-in, a professional software to facilitate the biological interpretation and to visualize the functionally grouped terms in the form of networks and charts [23], was used to perform

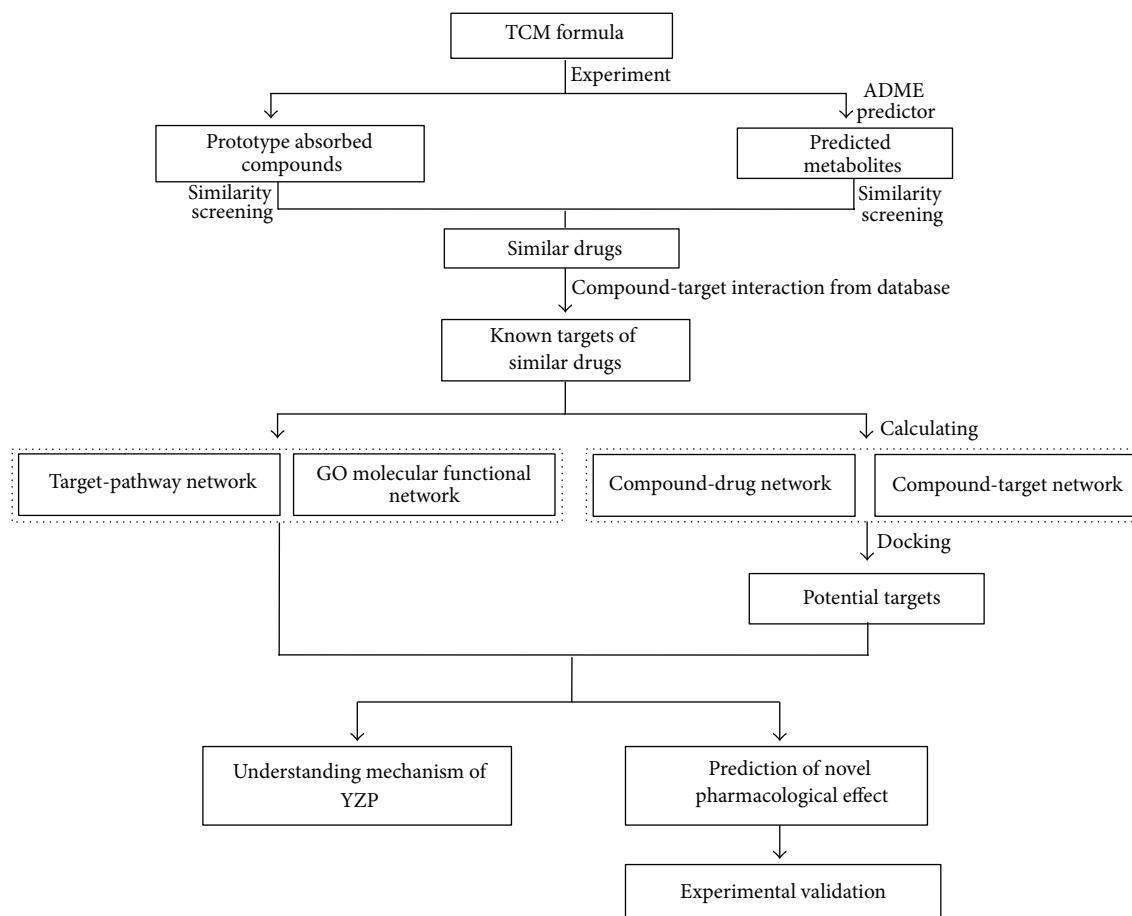


FIGURE 1: Flowchart of the model building.

functional and pathway analysis for the targets related to YZP. Simple text format of the targets in gene identifiers type was directly uploaded into the ClueGO software (Institute for Genomics and Bioinformatics Graz University of Technology, Graz, Austria). Enrichment/depletion tests were conducted for terms and groups as two-sided (enrichment/depletion) tests based on the hypergeometric distribution. The network type was selected as a “Medium” network. To create the annotations network, functional groups were visualized in the network using ClueGO which employed the organic layout algorithm.

3. Target Validation

The molecular docking simulation was further performed to validate the associations of candidate effector molecules with compositive compounds of YZP using eHiTS software program (Version 4.5, SimBioSys Inc., Canada). All the crystal structures of the targets were directly downloaded from RCSB protein data bank (<http://www.pdb.org/>, updated in 2012-6-11) and were carefully checked for their resolutions. The 3D structure of 15 prototype constituents was downloaded from ChemSpider in the mol files. The molecular structure of the metabolites was translated into 3D structure

through CORINA, a fast and powerful 3D structure generator for small and medium sized molecules. A docking score calculated by the customizable scoring function of eHiTS, which combines novel terms (based on local surface point contact evaluation) with traditional empirical and statistical approaches, was used to measure the binding efficiency of each effector molecule to the corresponding compound [24]. While the docking score was lower than -5.0 , these proteins were identified as candidate effector molecules which could bind their corresponding compounds with strong binding efficiency.

4. Bioactivity Validation

4.1. Animals and Housing

4.1.1. Anxiolytic Activity. The anxiolytic activity of YZP was determined by using the AB line zebrafish (*Danio rerio*). Zebrafish were purchased from Harvard Medical School (Boston, MA, USA). The experiments were conducted at Biology Institute of Shandong Academy of Sciences. Zebrafish were kept at approximately 28°C on a 12:12 h light/dark cycle in an automated flow-through continuously filtered water system (Aquatic Habitats, Apopka, FL, USA). During

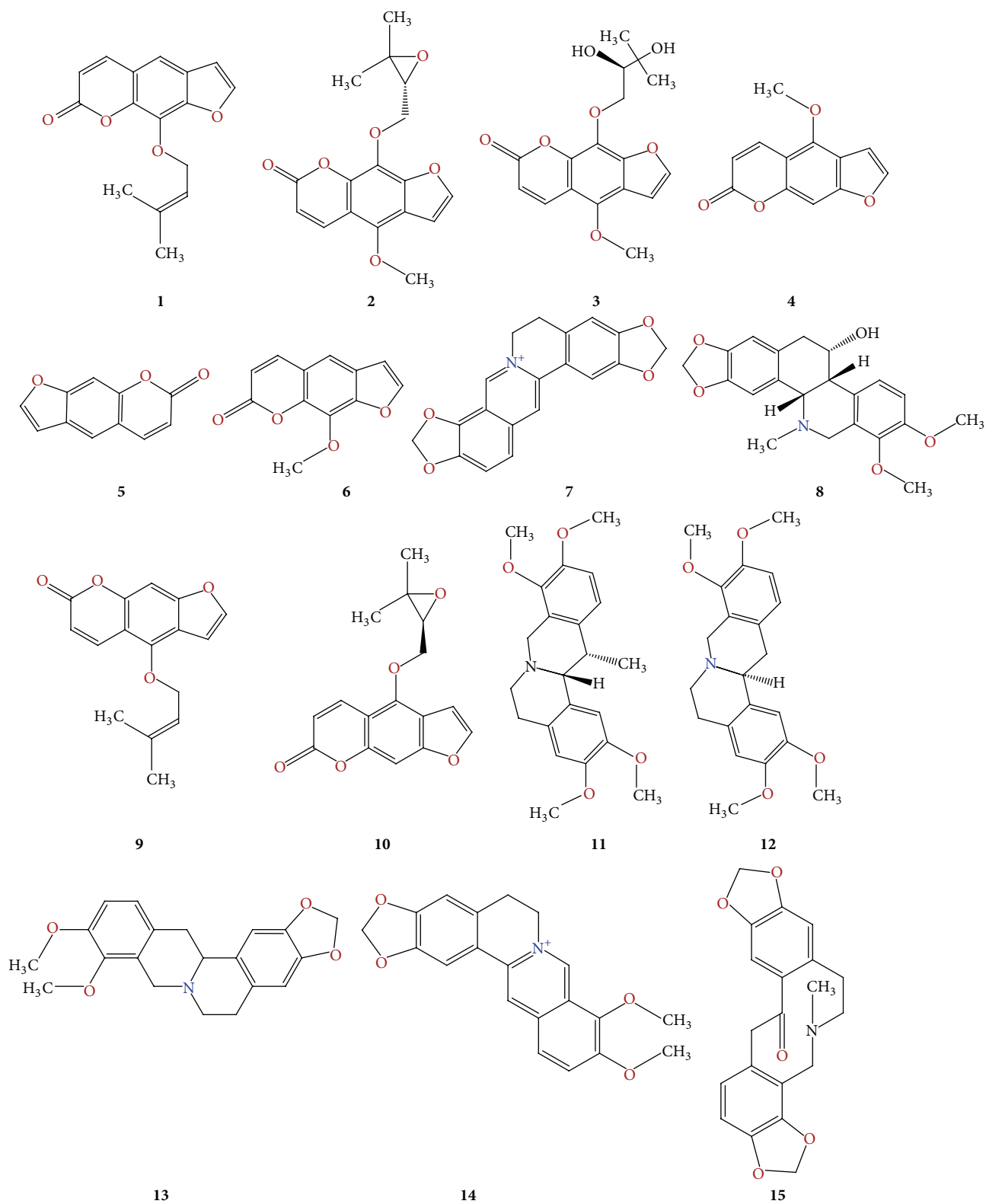


FIGURE 2: The structures of the 15 absorbed compounds and 6 metabolites of YZP: (1) imperatorin; (2) byakangelicol; (3) bykangelicin; (4) bergapten; (5) psoralen; (6) xanthotoxin; (7) coptisine; (8) α -allocryptopine; (9) isoimperatorin; (10) oxypeucedanin; (11) corydaline; (12) tetrahydropalmatine; (13) tetrahydroberberine; (14) berberine; (15) Protopine.

TABLE 1: Six metabolites of YZP detected *in vivo* from the previous experiment.

No.	RT (min)	[M + H] ⁺	Formula	Metabolite name	Formula change	Parent compound	Source
M1	4.1880	342.1333	C ₁₉ H ₁₉ NO ₅	Demethylation, hydrogenation	-CH ₂ +H ₂	Protopine	Plasma
M2	9.08278	342.1691	C ₂₀ H ₂₃ NO ₄	Demethylation	-CH ₂	Tetrahydropalmatine	Plasma
M3	10.6147	342.1695	C ₂₀ H ₂₃ NO ₄	Demethylation	-CH ₂	Tetrahydropalmatine	Plasma, CSF
M4	21.8366	301.0715	C ₁₆ H ₁₂ O ₆	Methylene to ketone	+O-H ₂	Oxypeucedanin	Plasma
M5	5.21887	326.1384	C ₁₉ H ₁₉ NO ₄	Demethylation	-CH ₂	Tetrahydroberberine	Plasma, CSF
M6	8.0093	326.1386	C ₁₉ H ₁₉ NO ₄	Demethylation	-CH ₂	Tetrahydroberberine	Plasma

CSF: cerebrospinal fluid.

the light phase, that is, between 8:00 a.m. and 8:00 p.m., the experiments were carried out to test the drug effect on the behavioral pattern of the Zebrafish. The fish were randomly sorted into treatment groups and vehicle-treated controls for the sake of avoiding any influence of breeding or holding conditions with drug treatment in the study. The tank water was prepared using mixing deionized H₂O and sea salts (Instant Ocean, 1.2 g/20 liters of H₂O). They were housed in 6-liter tanks and fed twice daily with flake fish food. The tanks were maintained under constant filtration and aeration.

4.1.2. Antidepressant Activity. Male C57 black 6 mice were purchased from the Experimental Animal Center of Peking University Health Science Center, Beijing, China. Animals weighing at 18–22 g were housed in a breeding room at temperature of 22 ± 2°C, humidity of 60 ± 5%, and 12/12 h dark-light cycle. In order for the animals to adapt to the laboratory conditions, they were housed under those conditions for three days before starting the experiments. Tap water and food were provided *ad libitum*, but animals were fasted (with free access to water) before the experiments for 12 h. All possible steps were taken to avoid pain and discomfort to animals at every stage of the experiment. The animal experiments complied with the Guide for the Care and Use of Laboratory Animals (National Research Council of the USA, 1996) and related ethical regulations of China Academy of Chinese Medical Sciences.

4.2. Determination of Anxiolytic Activity

4.2.1. Test Apparatus and Procedure [25, 26]. The Zebrafishes were placed in one of two plastic tanks with a capacity of 1.5 liter. The trapezoidal tanks (bottom: 22.9 cm, top: 27.9 cm, height: 15.2 cm, diagonal side: 15.9 cm) were filled with 1,350 mL of home tank water from the fish housing apparatus. It was 6.4 cm wide at the top and tapered to 5.1 cm at the bottom. The tanks were placed in such a way that the diagonal sides were facing each other, with a sheet of white paper blocking the view into the other tank. The tanks were back lit and had a translucent white sheet of plastic as the background so as to improve the performance of the imaging system. EthoVision (Wageningen, The Netherlands), a Samsung 8 mm camcorder, was used to record the image into the Noldus Image Analysis program. The tanks were

positioned 88.5 cm from this camcorder. The Noldus software was applied to assess the swimming behavior (tank location choice). The index of anxiety was evaluated by the choice of position (bottom versus upper levels). Choice of dwelling on the bottom was near a position of safety similar to the position choice of closed versus open arms in the elevated plus maze and positions near the wall (thigmotaxis) versus the center of an open field with rodents. As with the elevated plus maze and open field in rodents there was a separate total activity measure as well.

4.2.2. Drug Administration. In order to administer buspirone HCl (Sigma, St. Louis, MO, USA), Zebrafish were immersed in a beaker containing drug solution (25 mg/L) for 3 min. The extract of YZP was prepared according to the previous study [16] and administered at different concentrations (100, 150, and 200 mg/L) by immersing the Zebrafish for 3 min in a beaker containing YZP. A five-minute pause was obligatory between the end of dosing and the start of the experiment. The fish were exposed to the drug in a separate beaker and then were put into a holding tank without drug during this five-minute interval. For both buspirone and YZP, tank water was used as the vehicle. The control in this study was the exposure to tank water without the drug added. Home tank and the test chamber were completely devoid of any drug exposure. All the fish were drug naïve and each fish was used only once. There were at least 10 fish per condition.

4.3. Determination of Antidepressant Activity. The antidepressant activity was determined by the following behavioral tests: forced swimming test (FST), tail suspension test (TST), and locomotor activity measurement.

4.3.1. Locomotor Activity Measurement. Locomotor activity was measured with locomotor activity system (YLS-1A, Yanyi Science and Technology Co. Ltd., Jinan, China). Animals were placed in the chamber of locomotor activity measurement device to adjust to the environment for 1 minute, followed by recording locomotor counter for 6 min.

4.3.2. FST. The test was performed using the method reported by Porsolt et al. [27]. One hour after the last drug administration, each mouse was placed in an open cylindrical

container (20 cm in height and 12 cm in diameter) filled with 12 cm of water ($22 \pm 1^\circ\text{C}$). A mouse was judged to be immobile when it remained floating in the water, making only the necessary movements to keep its head above water. The animals were constantly observed to ensure no contact between their paws and the base of the cylinder during FST [28].

4.3.3. TST. This test was performed as described previously [29]. Briefly, 1 h after the last drug administration, animals were suspended by the tail from a ledge with adhesive tape (approximately 1 cm from the tip of the tail). The distance between the tip of tail and the floor was approximately 30 cm. Animals were partitioned to avoid interference during the test. Immobility was defined as the absence of movement and was scored over a 6 min trial by an observer blinded to the drug treatment.

4.3.4. Drug Administration. Fluoxetine (30 mg/kg) and YZP at the doses of 4, 8, and 16 g/kg were administered to the mice. Fluoxetine (Fluox) was selected as positive control for depression and saline (0.9% NaCl) as control. Seventy-five mice (five groups of fifteen) were randomized into control and experimental groups. Animals in the control group received normal saline (0.9% NaCl). Animals in the three YZP treatment groups received the YZP at the doses of 4, 8, and 16 g/kg. Animals in the fluoxetine treatment group received fluoxetine at the dose of 30 mg/kg. All drugs and saline were administered i.g. in a volume of 20 mL/kg for seven days before the behavioral tests.

4.3.5. Statistical Analysis. Data were expressed as mean \pm standard error of mean (SEM) and analyzed using SPSS statistical software package. Statistical differences for experiments with more than three groups were determined by analysis of variance (ANOVA). For experiments with two groups, *t*-test was used. Differences were considered significant at *P* value less than 0.05.

5. Results and Discussion

5.1. Identification of Metabolites. Generally, most of TCM herbs are taken orally. It appears that compounds with assumed pharmacological value not only show a good target binding, but also have a chance to reach the target *in vivo*. Thus, detection and identification of the absorbed components and their metabolites are critical steps in the validation of the biological effect and the identification of the mechanism of action of TCM. In most cases, the metabolites play a crucial role in the curative effect. If followed by separation and structure identification, it is an extremely costly and time-consuming process especially for TCM herbs. In recent years, prediction tools based on *in vitro* and *in silico* input parameters have become more popular [30]. ADMET Predictor has emerged as a quick and useful tool to predict metabolic types and sites so as to confer the structure of the metabolites [31]. This comes from Simulations Plus, Inc, a leading provider of simulation and modeling software for pharmaceutical discovery. So far, based on the

available evidence, the results would become more credible if combined with related experimental information [32]. Currently, an RRQC-Q-TOF MS/MS method coupled with Agilent Metabolite ID software was used to rapidly identify these metabolites and accurately speculate the reactive types of metabolism in our previous study. Afterward, ADME/T software has emerged as a quick and useful tool to predict metabolic types and sites so as to confer the structure of the metabolites.

In our previous study [16], 6 metabolites were detected *in vivo* and the types of reactions were concluded by RRQC-Q-TOF and the Agilent Metabolite ID software (Agilent Technologies, Inc., 2009) (Table 1). For example, demethylation reaction of tetrahydroberberine and tetrahydropalmatine happened and two metabolites were identified. Simultaneous demethylation and hydrogenation of protopine occurred and one metabolite was identified. Similarly, methylene to ketone of oxypeucedanin also took place and one metabolite was identified. Metabolic sites of four compounds were inferred by ADME/T software and the higher scores were selected. The structures of six metabolites (compound 16, 17, 18, 19, 20, and 21) were obtained (Figure 3).

5.2. Network Construction and Analysis. With the development of systems biology and the emergence of chemogenomic approaches, high-throughput virtual screening was found to be useful to better understand their possible molecular mechanisms. Recently, a number of computational methods have been developed for drug-target network predictions [33–38]. The similarity principles can be efficient complements for compound-target associations using similarity metrics such as ligand chemical similarity and drug side effects similarity [39]. The DrugBank database is a unique bioinformatics and cheminformatics resource that combines detailed drug data with comprehensive drug target information. Among them, 1447 FDA-approved small molecule drugs are selected and used to calculate the similarities with the constituents of YZP. Similar chemical structures are usually correlated with the therapeutic and pharmacological action [40, 41]. Furthermore, some methods have been developed to build the relationship between chemical structures and the therapeutics using the ATC classification system [42, 43]. In order to further understand the potential relationship between multicomponent and therapeutic effects, a network construction and analysis approach was used to visualize and analyze the interaction data. This approach helped capture the complexity in a simple, compact, and illustrative manner.

The C-T network consisted of 143 nodes and 1049 edges, including 21 candidate compounds (11 from *Rhizoma corydalis* and 10 from *Radix angelicae dahuricae*) and 122 candidate targets. Figure 4 shows a global view of C-T network with color-coded and shape-coded nodes: compounds (green-lozenge) and candidate targets (purple-round). Complex networks are always very huge and have a distributed nature. Clustering is an important data-mining technique used to find data segmentation and pattern identification. Therefore, it is gradually becoming an instant requirement to propose fast network clustering algorithms in the sight

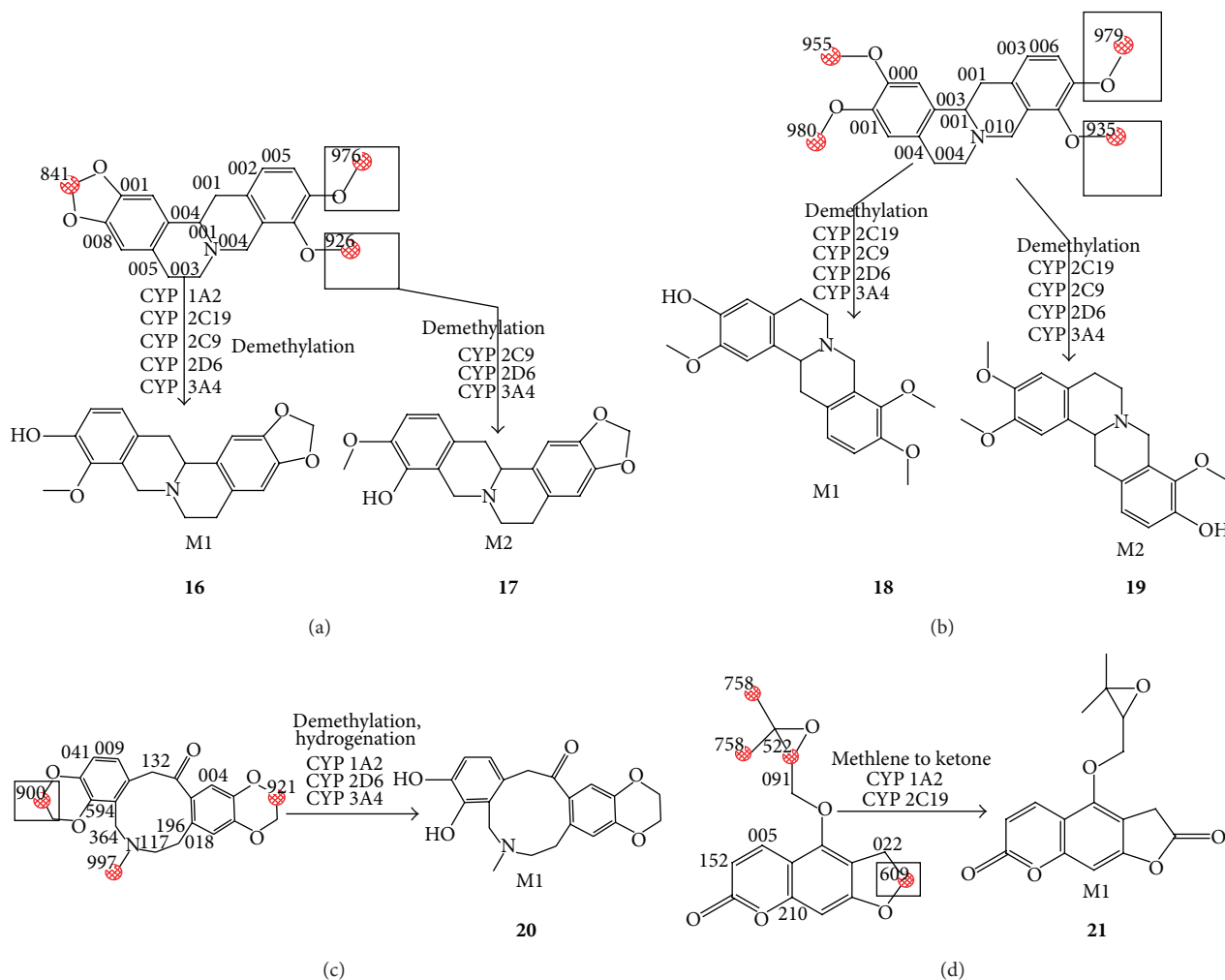


FIGURE 3: The possible metabolic sites and metabolites of six compounds: (16) tetrahydroberberine_M1; (17) tetrahydroberberine_M2; (18) tetrahydropalmatine_M1; (19) tetrahydropalmatine_M2; (20) protopine_M1; (21) oxypeucedanin_M1.

of local view. Data showed that [44–46] similar compounds usually had similar therapeutic and pharmacological action. According to the chemical structure similarity, 21 compounds were classified into three categories: category I included protopine (Compound 15) and its metabolite (Compound 21), category II included the alkaloids (Compounds 7, 8, 11–14, and 17–20) and category III included all coumarins (Compounds 1–6, 9, 10, and 16). Targets were classified as many categories according to ATC classification system and main categories included dopamine receptors (DA) family, 5-hydroxytryptamine receptors (5-HT) family, alpha-adrenergic receptors (AA) family, gamma-aminobutyric acid receptors family, muscarinic acetylcholine receptors (MA) family, phosphodiesterases family, inflammatory activator family for asthma, antibacterial effect family, and antitumor activity family. It was observed that different classes of compounds had some independent targets and the independent therapeutic effect. It was also observed that different classes of compounds had some common targets and therapeutics. But a lot of targets were clustered as a group alone.

Individually, most compounds might possess dozens of potential candidate targets, but a few compounds might have few candidate targets. Compounds 1, 13, 17, and 18 exhibited the highest number of candidate target interactions (73) followed by Compound 12 (with candidate targets of 42). Compound 10 had the least candidate targets (19) but its metabolite (Compound 16) had 34 candidate targets. Compound 7 had no candidate target.

YZP had been clinically used in TCM for the relief of pain, including headache, stomachache, and dysmenorrhea. In this study, C-T network might exhibit the synergy mode of “multicomponents, multitargets” and facilitate the understanding of the possible molecular basis of YZP therapeutic action. In our previous study [12], it was seen that most alkaloids of YZP can enter the brain and can be bound with opioid receptors, DA receptors, 5-HT receptors, GABA receptors, and MA receptors. Tetrahydropalmatine and its metabolites are potential opioid antagonist drugs that had been clinically used for relief of pain [47]. In addition, DA receptors might coordinate motor functions and induce pain inhibition so

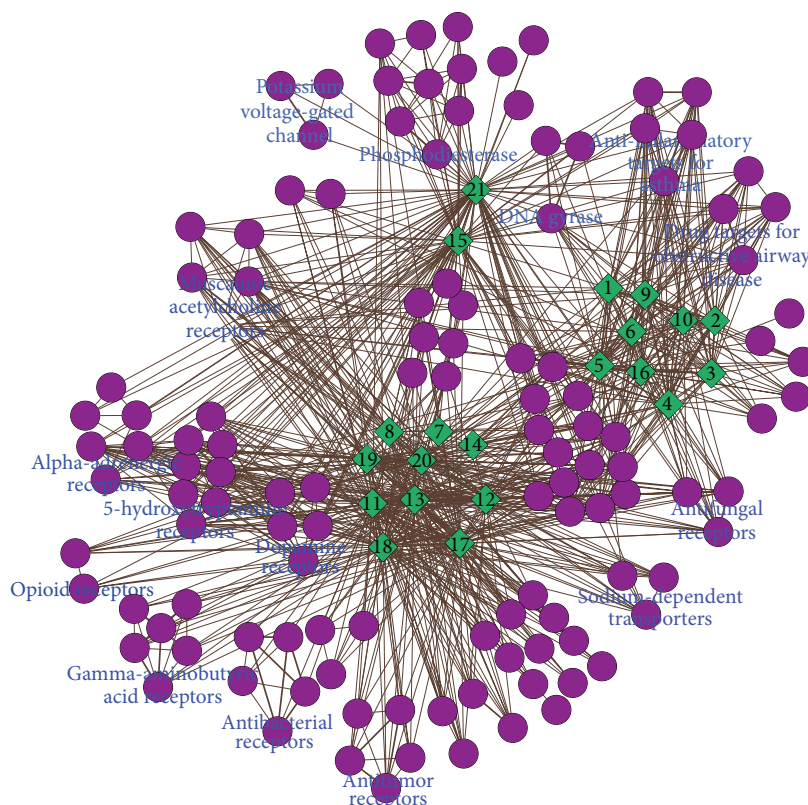


FIGURE 4: Compounds-targets (C-T) network. The C-T network is generated by linking the candidate compounds and all their candidate targets, with color-coded and shape-coded nodes: compounds (green-lozenge), candidate targets (purple-round).

as to relieve pain directly or indirectly [48]. Among AA receptors family, alpha 1 receptors are characteristics of vascular smooth muscle. Alpha 2 receptors are abundant in the brain and are associated with the pain perception [49]. Coumarins of *Rhizoma corydalis* can be primarily connected with the following targets groups: anti-inflammatory targets for asthma, drug targets for obstructive airway disease, antifungal receptors and sodium-dependent transporters, and DNA gyrase. Among them, anti-inflammatory targets for asthma can control chiefly airway responsiveness and reduce airflow resistance and asthma exacerbation [50]. Drug targets can be involved in bronchodilatory and anti-inflammatory effects for obstructive airway disease, which might be possibly related to the TCM theoretics of “regulating Qi.” It is still unclear that how the compound-target interaction of coumarins is responsible for its therapeutic action, which needs further research.

5.3. Molecular Functional and Pathway Analysis. Bioinformatics enrichment tools have played a very important and successful role contributing to the gene functional analysis for TCM biological studies. A number of high-throughput enrichment tools were independently developed as initial studies to address the challenge of functionally analyzing large gene lists [51]. As most of these tools mainly present their results as long lists or complex hierarchical trees, ClueGO, a Cytoscape plug-in, was developed to facilitate

the biological interpretation and to visualize functionally grouped terms in the form of networks and charts [52]. The GO molecular function and Kyoto Encyclopedia of Genes and Genomes (KEGG) analysis for multitargets of YZP are shown in Figure 5(a). The main molecular functions were classified into seven categories: opioid receptor activity, GABA-A receptor activity, benzodiazepine receptor activity, DNA topoisomerase (ATP-hydrolyzing) activity, cholinesterase activity, dopamine receptor activity, and cation channel activity. The main pathways in KEGG were also classified into five categories as follows: linoleic acid metabolism, renin-angiotensin system, gap junction, ligand-receptor interaction, and calcium signaling pathway (Figure 5(b)).

In the practice of TCM, since long time, YZP has been used as an analgesic agent; some animal experiments indicated that YZP possesses the pharmacological action of analgesic [53, 54]. The present study indicated that YZP possesses multipharmacology molecular attributes through different target groups such as opioid receptors, dopamine receptors, and calcium channel. for pain relief. YZP activates opiate receptors to release met-enkephalin which stimulates the pleasure centers for analgesia [55]. Dopamine receptors, which are associated in many neurological processes, including motivation, pleasure, cognition, and memory, are also potential targets of YZP. The main constituents of YZP can pass through the blood brain barrier to exert a pharmacological action [16]. Calcium channel receptors

TABLE 2: The eHiTS scores of potential targets.

NO	Gene name	PDB	Protein name	Compounds	eHiTS score
1	ESR1	1R5K	Estrogen receptor	corydaline	-6.99
2	DRD3	3PBL	D(3) dopamine receptor	corydaline	-6.53
3	CHRM2	3UON	Muscarinic acetylcholine receptor M2	corydaline	-6.33
4	CHRM3	4DAJ	Muscarinic acetylcholine receptor M3	corydaline	-6.28
5	CRYZ	1YB5	Quinone oxidoreductase	oxypeucedanin	-5.59
6	TOP2A	1ZXX	DNA topoisomerase 2-alpha	oxypeucedanin_M1	-5.79
7	VKORC1	3KP9	Vitamin K epoxide reductase complex subunit 1	byakangelicin	-6.04
8	ESR2	1QKM	Estrogen receptor beta	α -Allocryptopine	-6.13
9	ACE	1UZF	Angiotensin-converting enzyme	tetrahydroberberine	-5.69
10	ADRA1A	3SN6	Alpha-1A adrenergic receptor	tetrahydropalmatine	-5.97
11	OPRK1	4DJH	Kappa-type opioid receptor	tetrahydropalmatine	-5.57
12	HRH1	3RZE	Histamine H1 receptor	tetrahydropalmatine	-5.52
13	ADRA2A	3RFM	Alpha-2A adrenergic receptor	Tetrahydropalmatine_M2	-6.90
14	ABCC8	2BBO	ATP-binding cassette transporter subfamily C member 8	protopine_M1	-5.52
15	KCNJ8	3HFC	ATP-sensitive inward rectifier potassium channel 8	protopine_M1	-5.74
16	BCHE	2WIL	Cholinesterase	protopine_M1	-5.42
17	RNASE3	1DYT	Eosinophil cationic protein	protopine_M1	-5.21

and acetylcholine binding can play a crucial role in acute endothelium-dependent vasodilator responses to contract smooth muscle of the blood vessels and change arterial blood flow, which may explain their efficacy in migraine prevention [56].

In addition, a histamine receptor can inhibit gastric acid secretion, promote gastrointestinal motility, and relax gastrointestinal smooth muscle [57]. Cholinesterase receptors can relieve gastrointestinal smooth muscle spasm including the removal of vasospasm and improve microvascular circulation [58]. These could be the potential molecular mechanism by which YZP cures gastralgia.

YZP has the efficacy of “regulating Qi and invigorating blood circulation” in the practice of TCM [11]. In metabolic pathways of KEGG, most targets belonged to two families, linoleic acid metabolism and renin-angiotensin system. Linolenic acid metabolism is a very important metabolic pathway which has many biological effects, including potential immunomodulatory effects. This could change the platelet membrane fluidly, thus changing the number of platelet reactivity and platelet surface receptor stimulation. This in turn effectively prevents the formation of blood clots [59]. Renin-angiotensin system and hormonal regulation system of the human body have vital roles in the regulation of blood pressure, the balance of the electrolyte and fluid, and the development of the cardiovascular system [60].

Further, some new activities were found to be related with YZP, which might provide some evidence for new application of YZP. For example, many alkaloids were connected with GABA receptors group which suggested that YZP might possess anxiolytic action. Among them, dL-tetrahydropalmatine had been reported to have anxiolytic-like action [61]. It was also assumed that YZP might possess antidepressant action because of binding with benzodiazepine receptors in

GO functional analysis (Figure 5(a)). Interestingly, YZP is supposed to have the molecular pharmacology of anticancer action by interaction with DNA topoisomerases which had been reported in the previous studies [62].

5.4. Target Validation. As a complementary medical system to Western medicine, TCM provides a unique theoretical and practical approach to the treatment of diseases over thousands of years. Natural products, containing inherently large-scale structural diversity more than synthetic compounds, have been the major resources of bioactive agents and will continually play as protagonists for discovering new drugs [63]. In order to better understand the profiles of compound-target interaction from the C-T network and provide an efficient approach to drug discovery, molecular docking is an established *in silico* tool used for searching the potentially highly bioactive compounds (Table 2). The results suggested that 17 pairs of compound-target interaction were found and their scores of docking were greater than 5. Similarly, some compounds had several candidate targets. Corydaline could be connected with four targets including CHRM2, CHRM3, ESR1, and DRD3. Protopine_M1 could be connected with 4 targets including ABCC8, BCHE, RNASE3, and KCNJ8. Tetrahydropalmatine could be connected with 3 targets including ADRA1A, OPRK1, and HRH1. But the other constituents had a single target. For example, α -allocryptopine had interacted with ESR2, tetrahydroberberine bound with ACE and oxypeucedanin bound with CRYZ.

5.5. Bioactivity Appraisal. The C-T interaction network and molecular functional analysis suggested that YZP had polypharmacologic actions which were integral to regulate the biological network of disease. Polypharmacologic actions included antinociceptive [17] and vasorelaxation [20]. As per

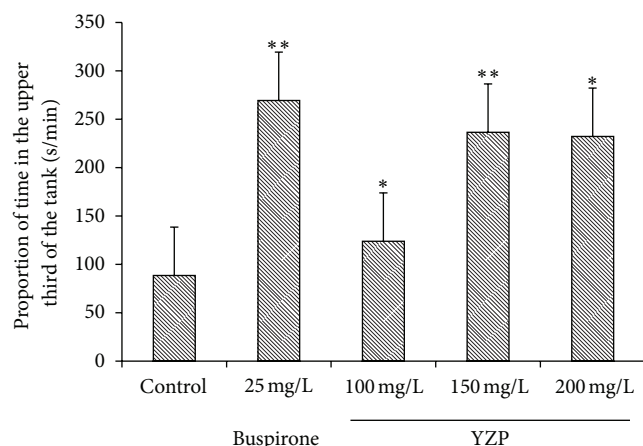


FIGURE 6: Anxiolytic-like effect of YZP. Anxiolytic-like effect of YZP (100 mg/kg, 150 mg/kg, and 200 mg/kg, resp.) on bottom dwelling (sec/min) in zebrafish (mean \pm sem). Significant differences: * $P < 0.05$ and ** $P < 0.01$, compared with the untreated control group.

our understanding, per computational biology, YZP has anxiolytic and antidepressant activity, which could be auxiliary therapy for headache and dysmenorrhea. The computational results indicated that the active constituents were not single but the mixture of multicomponents. Therefore, in the current study, YZP extract was used to validate the anxiolytic and antidepressant activities by animal experiments.

5.6. Assay of Anxiolytic Activity. Zebrafish are widely used in studying the molecular bases of neurobiology with applications in neuropharmacology and neurotoxicology [25, 26]. Bencan et al. [64] had developed a method to assess novel environment diving behavior of Zebrafish as a model of stress response and anxiolytic drug effects. Anxiety-like behavior in Zebrafish has been shown through patterns of swimming along the edge and towards the bottom of novel environments [65, 66]. The present study showed that bupirone at doses of 25 mg/L caused significant ($P < 0.01$) increases in diving compared to controls. Individually compared with control, YZP at doses of 100 mg/L, 150 mg/L, and 200 mg/L caused significant ($P < 0.05$, $P < 0.01$, and $P < 0.01$, resp.) decreases in diving. Even though low dose (100 mg/L) and middle dose (150 mg/L) showed dose-effect relation, there was no significant difference between middle dose and high dose (200 mg/L) (Figure 6). The results suggested that exposure to YZP treatment could reduce anxiety levels in Zebrafish.

5.7. Assay of Antidepressant Activity. Behavioral studies play an important role in the evaluation of antidepressant activity [66]. The FST and the TST are behavioral despair tests, useful for probing the pathological mechanism of depression and for the evaluation of antidepressant drugs [67] and had been widely used as preclinical screening tools for antidepressant drugs [68]. From the FST, it was seen that YZP at doses of 4 g/kg and 8 g/kg exhibited significantly (both $P < 0.01$) shorter duration of immobility and better antidepressive

effect than that of fluoxetine (30 mg/kg) (Figure 7(a)). However, the highest doses (16 g/kg) did not show antidepressant activity. The TST results demonstrated that the immobility time was significantly lower in mice treated with YZP at the doses of 4 and 8 g/kg ($P < 0.05$ and $P < 0.01$, resp.) than mice in control group. However, the highest dose of YZP did not show any such effect (Figure 7(b)). In the FST and TST, false-positive results may exist with certain drugs, in particular psychomotor stimulants, which decrease immobility time by stimulating locomotor activity [69, 70]. Here, the locomotor activity of the mice was measured and the results suggested that YZP at different doses decreased locomotor counters in spontaneous motor activity (Figure 7(c)). These animal studies had revealed the antidepressant effect of YZP. It was also noted that the spontaneous motor activity was inhibited and the highest doses of YZP could not exhibit the antidepressant activity which may be due to the potential sedative activity related to GABA receptors.

6. Conclusions

TCM is regarded as an ancient, vital, and holistic system of health and healing, based on the notion of harmony and balance. Recently, network pharmacology emerged as a powerful tool to uncover molecular mechanisms and connections between the drug constituents and their targeting network. Currently, some researchers obtained the compounds from TCM database but they ignored the contents and pharmacokinetic profiles of the constituents, as well as their metabolites. In this study, 15 prototype constituents existed abundantly in YZP extracts and could be detected in the rat plasma and cerebrospinal fluid. At the same time, 6 metabolites were found *in vivo* and their structures were concluded successfully by high resolution of MS data and ADME/T software. An integrated compound-target interaction network of YZP was reconstructed through similar chemical structure searching based on the prototype compounds and their metabolites *in vivo*. The results of further network analysis based on ATC classification and GO molecular function indicated that similar compounds in YZP possess similar therapeutic action and share the similar pharmacological space. YZP exhibited the synergy mode of “multicomponents, multitargets” in the C-T network and possessed potential multiparmacologic activities. Importantly, many pharmacologic actions could be validated by the data and animal experiments. The findings helped to deeply understand the molecular mechanisms of YZP and also provided some evidence on new potential clinical application. Interestingly, YZP has the anxiolytic and antidepressant activities which would be worth developing and researching.

Conflict of Interests

The authors declare that they have no conflict of interests.

Authors' Contribution

H. Xu, Y. Tao, and P. Lu contributed equally to the work.

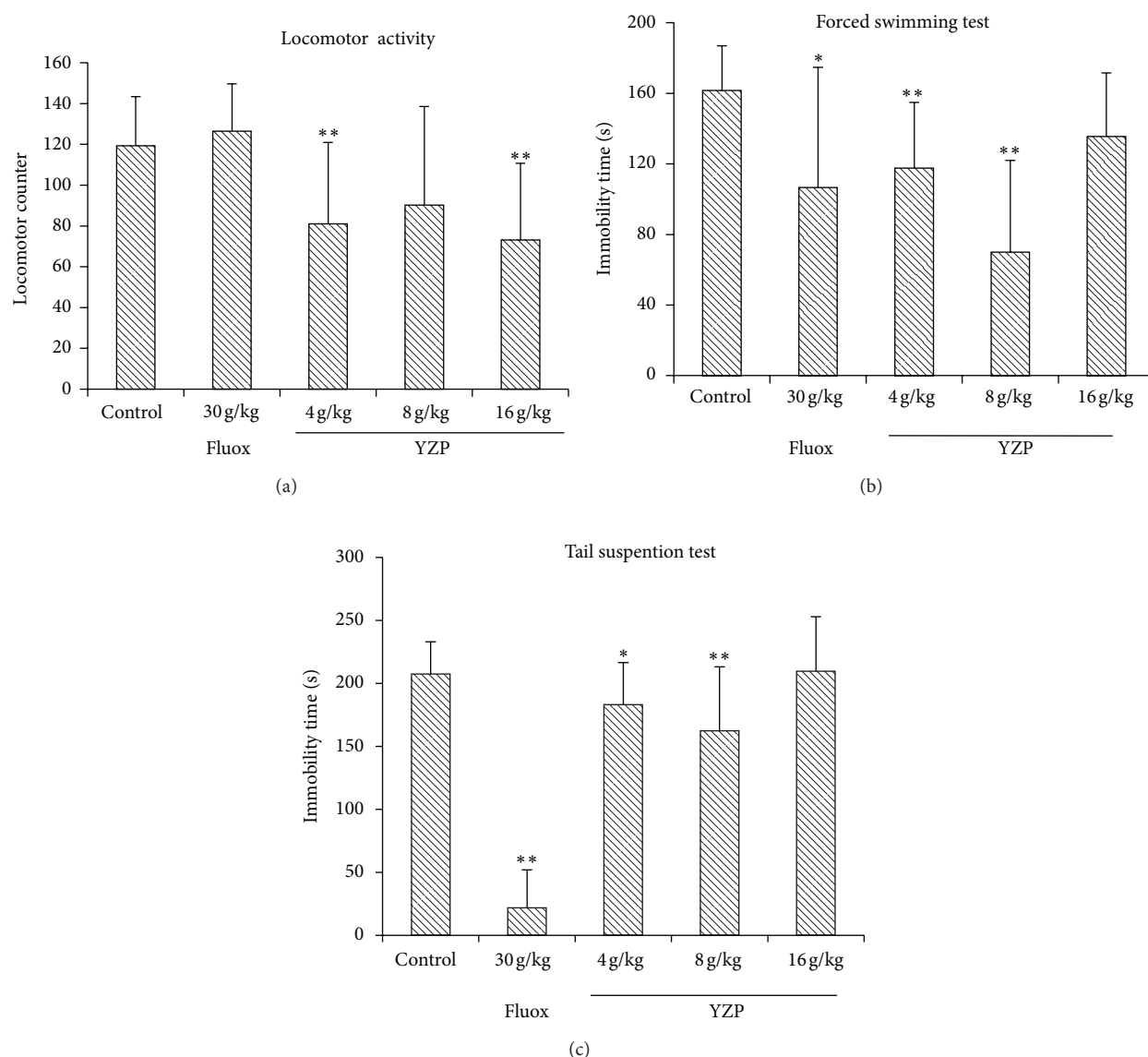


FIGURE 7: Antidepressant-like effect of YZP. (a) Effects of YZP and fluoxetine (Fluox) on locomotor counters in locomotor activity. Significant differences: * $P < 0.05$ and ** $P < 0.01$, compared with the untreated control group. (b) Antidepressant-like effect of YZP (4 g/kg, 8 g/kg and 16 g/kg, resp.) on the FST in mice. Animals were given i.g. YZP or fluoxetine before the tests. The duration of immobility in FST during the last 4 min of the test was recorded. No significant difference was found between Fluoxetine and YZP treated groups. Values were expressed as the mean \pm SEM and analyzed using one-way ANOVA. Significant differences: * $P < 0.05$ and ** $P < 0.01$, compared with the untreated control group. (c) Antidepressant-like effect of YZP (4 g/kg, 8 g/kg, and 16 g/kg, resp.) on the TST in mice. The duration of immobility in TST during the 6 min of the test was recorded. No significant difference was found between Fluoxetine and YZP treated groups. Values were expressed as the mean \pm SEM and analyzed using one-way ANOVA. Significant differences: * $P < 0.05$ and ** $P < 0.01$, compared with the untreated control group.

Acknowledgments

Financial support was provided by Key Projects in the National Science & Technology Pillar Program during the 11th Five-Year Plan Period (no. 2008BAI51B03), the National Natural Science Foundation of China (no. 81202793), and independent topics supported by operational expenses for basic research of China Academy of Chinese Medical Sciences (no. Z02063).

References

- [1] F. Cheung, "TCM: made in China," *Nature*, vol. 480, pp. 82–83, 2011.
- [2] M. Grayson, "Traditional Asian medicine," *Nature*, vol. 480, article 81, 2011.
- [3] S. P. Li, J. Zhao, and B. Yang, "Strategies for quality control of Chinese medicines," *Journal of Pharmaceutical and Biomedical Analysis*, vol. 55, no. 4, pp. 802–809, 2011.

- [4] Y. Tu, "The discovery of artemisinin (QingHaoSu) and gifts from Chinese medicine," *Nature Medicine*, vol. 17, pp. 1217–1220, 2011.
- [5] K. H. Lee, "Research and future trends in the pharmaceutical development of medicinal herbs from Chinese medicine," *Public Health Nutrition*, vol. 3, no. 4, pp. 515–522, 2000.
- [6] S. B. Su, A. P. Lu, S. Li, and W. Jia, "Evidence-based ZHENG: a traditional Chinese medicine syndrome," *Evidence-Based Complementary and Alternative Medicine*, vol. 2012, Article ID 246538, 2 pages, 2012.
- [7] T. Ma, C. Tan, H. Zhang, M. Wang, W. Ding, and S. Li, "Bridging the gap between traditional Chinese medicine and systems biology: the connection of Cold Syndrome and NEI network," *Molecular BioSystems*, vol. 6, no. 4, pp. 613–619, 2010.
- [8] S. Li, B. Zhang, D. Jiang, Y. Wei, and N. Zhang, "Herb network construction and co-module analysis for uncovering the combination rule of traditional Chinese herbal formulae," *BMC Bioinformatics*, vol. 11, supplement 11, article S6, 2010.
- [9] S. Li, B. Zhang, and N. Zhang, "Network target for screening synergistic drug combinations with application to traditional Chinese medicine," *BMC Systems Biology*, vol. 5, no. 1, article S10, 2011.
- [10] X. Li, X. Xu, J. Wang et al., "A system-level investigation into the mechanisms of chinese traditional medicine: compound danshen formula for cardiovascular disease treatment," *PLoS One*, vol. 7, no. 9, pp. 1–16, 2012.
- [11] *Pharmacopoeia Committee of the Ministry of Health of the People's Republic of China, Pharmacopoeia of the People's Republic of China*, vol. 1, Chemical Industry Press, Beijing, China, 2010.
- [12] K. W. Luo, J. G. Sun, J. Y. W. Chan et al., "Anticancer effects of imperatorin isolated from *Angelica dahurica*: induction of apoptosis in HepG2 cells through both death-receptor- and mitochondria-mediated pathways," *Chemotherapy*, vol. 57, pp. 449–459, 2011.
- [13] C. S. Yuan, S. R. Mehendale, C. Z. Wang et al., "Effects of *Corydalis yanhusuo* and *Angelicae dahuricae* on cold pressor-induced pain in humans: a controlled trial," *Journal of Clinical Pharmacology*, vol. 44, no. 11, pp. 1323–1327, 2004.
- [14] Y. C. Zhang, H. Y. Xu, X. M. Chen et al., "Study on the application of intestinal absorption *in vitro* coupled with bioactivity assessment in Yuanhu Zhitong preparation," *Journal of Medicinal Plants Research*, vol. 6, pp. 1941–1947, 2012.
- [15] Y. Zhang, H. Xu, X. Chen et al., "Simultaneous quantification of 17 constituents from Yuanhu Zhitong tablet using rapid resolution liquid chromatography coupled with a triple quadrupole electrospray tandem mass spectrometry," *Journal of Pharmaceutical and Biomedical Analysis*, vol. 56, no. 3, pp. 497–504, 2011.
- [16] Y. Tao, H. Y. Xu, S. S. Wang et al., "Identification of the absorbed constituents after oral administration of Yuanhu Zhitong prescription extract and its pharmacokinetic study by RRLC-QTOF/MS," *Journal of Chromatography, B. Revised*.
- [17] Y. F. Chen, H. Y. Tsai, and T. S. Wu, "Anti-inflammatory and analgesic activities from roots of *Angelica pubescens*," *Planta Medica*, vol. 61, no. 1, pp. 2–8, 1995.
- [18] W. C. Leung, H. Zheng, M. Huen, S. L. Law, and H. Xue, "Anxiolytic-like action of orally administered dl-tetrahydrocannabinol in elevated plus-maze," *Progress in Neuro-Psychopharmacology and Biological Psychiatry*, vol. 27, no. 5, pp. 775–779, 2003.
- [19] K. O. Hiller, M. Ghorbani, and H. Schlicher, "Antispasmodic and relaxant activity of chelidonium, protopine, coptisine, and *Chelidonium majus* extracts on isolated guinea-pig ileum," *Planta Medica*, vol. 64, no. 8, pp. 758–760, 1998.
- [20] H. Nie, L. Z. Meng, J. Y. Zhou, X. F. Fan, Y. Luo, and G. W. Zhang, "Imperatorin is responsible for the vasodilatation activity of *Angelica dahurica* var. *formosana* regulated by nitric oxide in an endothelium-dependent manner," *Chinese Journal of Integrative Medicine*, vol. 15, no. 6, pp. 442–447, 2009.
- [21] D. Lin, "An information-theoretic definition of similarity," in *Proceedings of the 15th International Conference on Machine Learning*, vol. 25, pp. 296–304, Morgan Kaufmann, 1998.
- [22] S. Zhao and S. Li, "Network-based relating pharmacological and genomic spaces for drug target identification," *PLoS ONE*, vol. 5, no. 7, Article ID e11764, 10 pages, 2010.
- [23] G. Bindea, B. Mlecnik, H. Hackl et al., "ClueGO: a cytoscape plug-in to decipher functionally grouped gene ontology and pathway annotation networks," *Bioinformatics*, vol. 25, no. 8, pp. 1091–1093, 2009.
- [24] Z. Zsoldos, D. Reid, A. Simon, S. B. Sadjad, and A. P. Johnson, "eHiTS: a new fast, exhaustive flexible ligand docking system," *Journal of Molecular Graphics and Modelling*, vol. 26, no. 1, pp. 198–212, 2007.
- [25] E. Linney, L. Upchurch, and S. Donerly, "Zebrafish as a neurotoxicological model," *Neurotoxicology and Teratology*, vol. 26, no. 6, pp. 709–718, 2004.
- [26] H. Teraoka, W. Dong, and T. Hiraga, "Zebrafish as a novel experimental model for developmental toxicology," *Congenital anomalies*, vol. 43, no. 2, pp. 123–132, 2003.
- [27] R. D. Porsolt, M. Le Pichon, and M. Jalfre, "Depression: a new animal model sensitive to antidepressant treatments," *Nature*, vol. 266, no. 5604, pp. 730–732, 1977.
- [28] I. Lucki, A. Dalvi, and A. J. Mayorga, "Sensitivity to the effects of pharmacologically selective antidepressants in different strains of mice," *Psychopharmacology*, vol. 155, no. 3, pp. 315–322, 2001.
- [29] L. Steru, R. Chermat, B. Thierry, and P. Simon, "The tail suspension test: a new method for screening antidepressants in mice," *Psychopharmacology*, vol. 85, no. 3, pp. 367–370, 1985.
- [30] S. S. de Buck, V. K. Sinha, L. A. Fenu, R. A. Gilissen, C. E. Mackie, and M. J. Nijsen, "The prediction of drug metabolism, tissue distribution, and bioavailability of 50 structurally diverse compounds in rat using mechanism-based absorption, distribution, and metabolism prediction tools," *Drug Metabolism and Disposition*, vol. 35, no. 4, pp. 649–659, 2007.
- [31] D. D. Stranz, S. Miao, S. Campbell, G. Maydwell, and S. Ekins, "Combined computational metabolite prediction and automated structure-based analysis of mass spectrometric data," *Toxicology Mechanisms and Methods*, vol. 18, no. 2-3, pp. 243–250, 2008.
- [32] H. Han, L. Yang, and Y. Xu, "Identification of metabolites of geniposide in rat urine using ultra-performance liquid chromatography combined with electrospray ionization quadrupole time-of-flight tandem mass spectrometry," *Rapid Communications in Mass Spectrometry*, vol. 25, no. 21, pp. 3339–3350, 2011.
- [33] M. Kuhn, M. Campillos, P. González, L. J. Jensen, and P. Bork, "Large-scale prediction of drug-target relationships," *The FEBS Letters*, vol. 582, no. 8, pp. 1283–1290, 2008.
- [34] M. J. Keiser, V. Setola, J. J. Irwin et al., "Predicting new molecular targets for known drugs," *Nature*, vol. 462, no. 7270, pp. 175–181, 2009.
- [35] Y. C. Wang, Z. X. Yang, Y. Wang, and N. Y. Deng, "Computationally probing drug-protein interactions via support vector machine," *Letters in Drug Design & Discovery*, vol. 7, no. 5, pp. 370–378, 2010.

- [36] Y. C. Wang, C. H. Zhang, N. Y. Deng, and Y. Wang, "Kernel based data fusion improves the drug-protein interaction prediction," *Computational Biology and Chemistry*, vol. 35, no. 6, pp. 353–362, 2011.
- [37] Y. Y. Wang, J. C. Nacher, and X. M. Zhao, "Predicting drug targets based on protein domains," *Molecular BioSystems*, vol. 8, no. 5, pp. 1528–1534, 2012.
- [38] F. X. Cheng, C. Liu, J. Jiang et al., "Prediction of drug-target interactions and drug repositioning via network-based inference," *PLOS Computational Biology*, vol. 8, no. 5, pp. 1–12, 2012.
- [39] T. Cheng, Q. Li, Y. Wang, and S. H. Bryant, "Identifying compound-target associations by combining bioactivity profile similarity search and public databases mining," *Journal of Chemical Information and Modeling*, vol. 51, no. 9, pp. 2440–2448, 2011.
- [40] M. J. Keiser, B. L. Roth, B. N. Armbruster, P. Ernsberger, J. J. Irwin, and B. K. Shoichet, "Relating protein pharmacology by ligand chemistry," *Nature Biotechnology*, vol. 25, no. 2, pp. 197–206, 2007.
- [41] A. Schuffenhauer, P. Floersheim, P. Acklin, and E. Jacoby, "Similarity metrics for ligands reflecting the similarity of the target proteins," *Journal of Chemical Information and Computer Sciences*, vol. 43, no. 2, pp. 391–405, 2003.
- [42] "The Anatomical Therapeutic Chemical (ATC) Classification," <http://www.whocc.no/atcddd/>.
- [43] J. C. Nacher and J. M. Schwartz, "A global view of drug-therapy interactions," *BMC Pharmacology*, vol. 8, article 5, 2008.
- [44] R. J. Gatchel, Y. B. Peng, M. L. Peters, P. N. Fuchs, and D. C. Turk, "The biopsychosocial approach to chronic pain: scientific advances and future directions," *Psychological Bulletin*, vol. 133, no. 4, pp. 581–624, 2007.
- [45] M. D. Sullivan and J. P. Robinson, "Antidepressant and anti-convulsant medication for chronic pain," *Physical Medicine and Rehabilitation Clinics of North America*, vol. 17, no. 2, pp. 381–400, 2006.
- [46] R. Benyamin, A. M. Trescot, S. Datta et al., "Opioid complications and side effects," *Pain Physician*, vol. 11, no. 2, pp. S105–S120, 2008.
- [47] Z. Yang, Y. C. Shao, S. J. Li et al., "Medication of l-tetrahydropalmatine significantly ameliorates opiate craving and increases the abstinence rate in heroin users: a pilot study," *Acta Pharmacologica Sinica*, vol. 29, no. 7, pp. 781–788, 2008.
- [48] M. T. Lin, J. J. Wu, A. Chandra, and B. L. Tsay, "Activation of striatal dopamine receptors induces pain inhibition in rats," *Journal of Neural Transmission*, vol. 51, no. 3–4, pp. 213–222, 1981.
- [49] I. Carroll, S. Mackey, and R. Gaeta, "The role of adrenergic receptors and pain: the good, the bad, and the unknown," *Seminars in Anesthesia, Perioperative Medicine and Pain*, vol. 26, no. 1, pp. 17–21, 2007.
- [50] P. Sharma and A. J. Halayko, "Emerging molecular targets for the treatment of asthma," *Indian Journal of Biochemistry and Biophysics*, vol. 46, no. 6, pp. 447–460, 2009.
- [51] D. W. Huang, B. T. Sherman, and R. A. Lempicki, "Bioinformatics enrichment tools: paths toward the comprehensive functional analysis of large gene lists," *Nucleic Acids Research*, vol. 37, no. 1, pp. 1–13, 2009.
- [52] G. Bindea, B. Mlecnik, H. Hackl et al., "ClueGO: a cytoscape plug-in to decipher functionally grouped gene ontology and pathway annotation networks," *Bioinformatics*, vol. 25, no. 8, pp. 1091–1093, 2009.
- [53] Z. G. Liao, X. L. Liang, J. Y. Zhu et al., "Correlation between synergistic action of Radix Angelica dahurica extracts on analgesic effects of Corydalis alkaloid and plasma concentration of dl-THP," *Journal of Ethnopharmacology*, vol. 129, no. 1, pp. 115–120, 2010.
- [54] Y. Y. Zhu and B. Y. Yu, "Comparative studies on chemistry and pharmacodynamics of the compatibility of Yuanhu Zhitong Prescription," *Journal of China Pharmaceutical University*, vol. 34, no. 5, pp. 461–464, 2003.
- [55] M. Narita and L. F. Tseng, "Evidence for the existence of the β -endorphin-sensitive ' ϵ -opioid receptor' in the brain: the mechanisms of ϵ -mediated antinociception," *Japanese Journal of Pharmacology*, vol. 76, no. 3, pp. 233–253, 1998.
- [56] J. G. R. de Mey, P. M. Schiffers, R. H. P. Hilgers, and M. M. W. Sanders, "Toward functional genomics of flow-induced outward remodeling of resistance arteries," *American Journal of Physiology—Heart and Circulatory Physiology*, vol. 288, no. 3, pp. H1022–H1027, 2005.
- [57] E. Schneider, M. Rolli-Derkinderen, M. Arock, and M. Dy, "Trends in histamine research: new functions during immune responses and hematopoiesis," *Trends in Immunology*, vol. 23, no. 5, pp. 255–263, 2002.
- [58] M. Wienrich, D. Meier, H. A. Ensinger et al., "Pharmacodynamic profile of the M1 agonist talsaclidine in animals and man," *Life Sciences*, vol. 68, no. 22–23, pp. 2593–2600, 2001.
- [59] L. Wan, X. P. Qian, and B. R. Liu, "Progress of research on the chemical constituents and anti-tumor activity of alkaloid fraction of Corydalis," *Modern Oncology*, vol. 20, pp. 1042–1044, 2012.
- [60] W. H. Erik, F. Marc, K. R. Eva et al., "Dietary α -linolenic acid inhibits arterial thrombus formation, tissue factor expression, and platelet activation," *Arteriosclerosis, Thrombosis, and Vascular Biology*, vol. 31, pp. 1772–1780, 2011.
- [61] W. C. Leung, H. Zheng, M. Huen, S. L. Law, and H. Xue, "Anxiolytic-like action of orally administered dl-tetrahydropalmatine in elevated plus-maze," *Progress in Neuro-Psychopharmacology and Biological Psychiatry*, vol. 27, no. 5, pp. 775–779, 2003.
- [62] K. Schmerbach and A. Patzak, "The renin-angiotensin system—a functional jack-of-all-trades," *Acta Physiologica*, vol. 205, no. 4, pp. 453–455, 2012.
- [63] J. Shen, X. Xu, F. Cheng et al., "Virtual screening on natural products for discovering active compounds and target information," *Current Medicinal Chemistry*, vol. 10, no. 21, pp. 2327–2342, 2003.
- [64] Z. Bencan, D. Sledge, and E. D. Levin, "Buspirone, chlor-diazepoxide and diazepam effects in a zebrafish model of anxiety," *Pharmacology Biochemistry and Behavior*, vol. 94, no. 1, pp. 75–80, 2009.
- [65] N. Peitsaro, J. Kaslin, O. V. Anichtchik, and P. Panula, "Modulation of the histaminergic system and behaviour by α -fluoromethylhistidine in zebrafish," *Journal of Neurochemistry*, vol. 86, no. 2, pp. 432–441, 2003.
- [66] E. D. Levin, Z. Bencan, and D. T. Cerutti, "Anxiolytic effects of nicotine in zebrafish," *Physiology and Behavior*, vol. 90, no. 1, pp. 54–58, 2007.
- [67] B. Karolewicz and I. A. Paul, "Group housing of mice increases immobility and antidepressant sensitivity in the forced swim and tail suspension tests," *European Journal of Pharmacology*, vol. 415, no. 2–3, pp. 197–201, 2001.

- [68] P. Willner, "Validity, reliability and utility of the chronic mild stress model of depression: a 10-year review and evaluation," *Psychopharmacology*, vol. 134, no. 4, pp. 319–329, 1997.
- [69] D. Abdulla and K. W. Renton, " β -adrenergic receptor modulation of the LPS-mediated depression in CYP1A activity in astrocytes," *Biochemical Pharmacology*, vol. 69, no. 5, pp. 741–750, 2005.
- [70] R. J. Tynan, S. Naicker, and M. Hinwood, "Chronic stress alters the density and morphology of microglia in a subset of stress-responsive brain regions," *Brain, Behavior, and Immunity*, vol. 24, pp. 1058–1068, 2010.

Research Article

Optimizing Combinations of Flavonoids Deriving from Astragali Radix in Activating the Regulatory Element of Erythropoietin by a Feedback System Control Scheme

Hui Yu,^{1,2} Wendy L. Zhang,³ Xianting Ding,⁴ Ken Y. Z. Zheng,³
Chih-Ming Ho,⁵ Karl W. K. Tsim,³ and Yi-Kuen Lee²

¹ State Key Laboratory of Analytical Chemistry for Life Science, Nanjing University, Nanjing, Jiangsu, China

² Department of Mechanical Engineering, The Hong Kong University of Science and Technology, Clear Water Bay Road, Hong Kong

³ Division of Life Science and Center for Chinese Medicine, The Hong Kong University of Science and Technology, Clear Water Bay Road, Hong Kong

⁴ School of Biomedical Engineering, Med-X Research Institute, Shanghai Jiao Tong University, Shanghai, China

⁵ Center for Cell Control, Mechanical and Aerospace Engineering Department, Biomedical Engineering Department, University of California, Los Angeles, CA 90095-1597, USA

Correspondence should be addressed to Karl W. K. Tsim; botsim@ust.hk and Yi-Kuen Lee; meylee@ust.hk

Received 4 February 2013; Accepted 22 March 2013

Academic Editor: Shao Li

Copyright © 2013 Hui Yu et al. This is an open access article distributed under the Creative Commons Attribution License, which permits unrestricted use, distribution, and reproduction in any medium, provided the original work is properly cited.

Identifying potent drug combination from a herbal mixture is usually quite challenging, due to a large number of possible trials. Using an engineering approach of the feedback system control (FSC) scheme, we identified the potential best combinations of four flavonoids, including formononetin, ononin, calycosin, and calycosin-7-O- β -D-glucoside deriving from Astragali Radix (AR; Huangqi), which provided the best biological action at minimal doses. Out of more than one thousand possible combinations, only tens of trials were required to optimize the flavonoid combinations that stimulated a maximal transcriptional activity of hypoxia response element (HRE), a critical regulator for erythropoietin (EPO) transcription, in cultured human embryonic kidney fibroblast (HEK293T). By using FSC scheme, 90% of the work and time can be saved, and the optimized flavonoid combinations increased the HRE mediated transcriptional activity by ~3-fold as compared with individual flavonoid, while the amount of flavonoids was reduced by ~10-fold. Our study suggests that the optimized combination of flavonoids may have strong effect in activating the regulatory element of erythropoietin at very low dosage, which may be used as new source of natural hematopoietic agent. The present work also indicates that the FSC scheme is able to serve as an efficient and model-free approach to optimize the drug combination of different ingredients within a herbal decoction.

1. Introduction

Traditional Chinese medicine (TCM) has played an important role in primary health care in China of over thousands of years [1]. In contrast to isolated, bioactive, single natural products in Western medicine, TCM uses a mixture of active ingredients; this represents a holistic approach in disease prevention. TCM has attracted a lot of attention for serving as complementary health food supplements with low toxicity and fewer complications [2, 3]. Astragali Radix (AR;

Huangqi), the dried root of *Astragalus membranaceus* (Fisch.) Bunge or *A. membranaceus* (Fisch.) Bunge var. *mongholicus* (Bunge) P. K. Hsiao, is one of the most widely used Chinese herbs as a health food supplement to reinforce “Qi” (vital energy) [4]. Pharmacological study has demonstrated that the water extract of AR possesses many biological functions, including hepatoprotective effects, neuroprotective effects against ischemic brain injury, hematopoietic, antioxidative, antihypertensive, immunological properties, cardiogenic, and antiaging activities [5, 6].

Previous study also showed that the AR extract could improve hematopoietic functions by regulating erythropoietin (EPO) expression. EPO is an erythrocyte-specific hematopoietic growth factor produced by kidney and liver [7]. Failure to increase the amount of circulating EPO under hypoxia stress can lead to anemia [8]. Hypoxia response element (HRE), a critical regulator for EPO transcription, is located on the promoter region of the EPO gene. Under hypoxia condition, the activated hypoxia-induced factor (HIF) binds onto HRE and subsequently initiates EPO gene expression [9]. The AR regulating EPO expression was through an induction of the transcriptional activity of HRE [10]. One of major components in AR was flavonoid, for example, formononetin, ononin, calycosin, and calycosin-7-O- β -D-glucoside. These four flavonoids can induce the expression of EPO [11]; however, the effect of a combination of these flavonoids has not been revealed. Indeed, the combined mixture is mimicking partly the scenario of a herbal mixture.

A major problem in combinatorial therapies lies in the number of possible combinations [12, 13], which becomes more challenging in optimizing Chinese herbal mixtures. Besides, the combined effect of numerous constituents within a herbal composite prescription is hard to validate [14]. Previous study indicated that different experimental methods have been used in discovering combinatorial therapies. Li et al. established an algorithm termed NIMS (Network Target-Based Identification of Multicomponent Synergy) to prioritize synergistic agent combinations in a high throughput way [15]. Both the topology score and agent score were proposed for the evaluation of agent interactions; Yan et al. developed a systematic simplification framework for drug combination design by combining simulation and system reaction network topology analysis [16]. Among different classes of strategy, Wong et al. developed a feedback system control (FSC) scheme to implement an iterative stochastic search [17]. FSC efficiently discovered potent combinations for inhibiting virus infection of fibroblasts, in only tens of iterations out of one hundred thousand possible trials. Recently, Tsutsui et al. further extended the FSC for parallel searching and identified a unique combination of three combined inhibitors that enables the maintenance of human embryonic stem cells [18]. Here, we aimed to optimize a herbal mixture for therapeutic goals by using the FSC scheme, and therefore the optimization of AR-derived flavonoid combinations was evaluated as an initial example. Having the FSC, we were able to quickly pinpoint the optimal flavonoid combinations for maximizing the HRE-mediated transcriptional activity.

2. Materials and Methods

2.1. Plant Materials and Chemicals. Three-year-old AR, the dry roots of *A. membranaceus* var. *mongholicus*, was collected from Shanxi province [4]. The authentication of plant materials was performed morphologically by Dr. Tina Dong of The Hong Kong University of Science and Technology (HKUST) during the field collection. The corresponding voucher no. 02-10-4, as forms of the whole plant were deposited in Center for Chinese Medicine, HKUST. Formononetin, calycosin,

ononin, and calycosin-7-O- β -D-glucoside were purchased from Weikeqi Biotechnology Co. (Sichuan, China). The purities of these marker chemicals, confirmed by high-performance liquid chromatography (HPLC), were higher than 98.0%. Analytical- and HPLC-grade reagents were from Merck (Darmstadt, Germany).

2.2. Preparation of AR Extracts and Chemicals. Dry roots of AR (50 g) were extracted twice with distilled water (400 mL) at 100°C for 2 hours. The extract was centrifuged at 3,000 g for 10 min. The supernatant was freeze-dried (yield = 14.56 g) and kept at -20°C. For standardization of AR extract, an Agilent 1200 series system (Agilent, Waldbronn, Germany), equipped with a degasser, a binary pump, an autosampler, and a thermostated column compartment was used for the analysis. Chromatographic separations were carried out on an Agilent Eclipse XDB-C18 column (4.6 mm \times 250 mm, 5 μ m) with 0.1% formic acid (as Solvent A) and acetonitrile (as Solvent B) at a flow rate of 1.0 mL/min at room temperature. A linear gradient elution was applied from 15%–20% B at 0–10 min, 20% B at 10–20 min, 20%–34% B at 20–45 min, 34%–48% B at 45–55 min, 48%–65% B at 55–70 min, and 65%–80% B at 70–80 min, and the equilibration time of gradient elution was 10 min. Ten μ L of the samples (after filtration with a 0.45 μ m Millipore filter) were injected, and signals were detected at 280 nm with UV detection. A standardized AR extract by calibrating different chemical markers was established. For biological analysis, the dried standardized extract was dissolved in phosphate-buffered saline and filtered through a 0.22 μ m filter before use. The pure flavonoids were dissolved by dimethyl sulfoxide before use.

2.3. DNA Transfection in Culture. Human embryonic kidney (HEK) 293T fibroblast cell is an excellent *in vitro* model in studying the physiological regulation of EPO expression, which is sensitive to hypoxia stress [7]. HEK 293T cell line was obtained from the American Type Culture Collection (ATCC, Manassas, VA) and cultured according to previous reports [11]. The HRE (5'-TCG AGG CCC TAC GTG CTG TCT CAC ACA GCC TGT CTG ACG-3') derived from human EPO gene contains a highly conserved HIF-1 binding site (5'-TAC GTG-3') and other unique cis-acting sequences (5'-CAC AG-3') that are functionally essential for hypoxic induction [11, 19]. Six HREs were synthesized, concatemerized, and then cloned in tandem (head-to-tail orientation) into pBI-GL vectors (BD Biosciences Clontech, San Jose, CA) that had a downstream reporter of firefly luciferase gene [11]. This vector was named as pHRE-Luc [19]. Cultured HEK293T cells were transiently transfected with pHRE-Luc by the calcium phosphate precipitation method [20]. The transfection efficiency was over 80%, as determined by another control plasmid of having a β -galactosidase cDNA, under a cytomegalovirus enhancer promoter. The treatment of flavonoids, or AR extract, was done on transfected HEK293T cells. After 2 days, the cell lysates were collected for luciferase assay. In order to validate the response of the pHRE-Luc in transfected HEK293T cells, the cultures were exposed to hypoxia, serving as a positive control. The authentication of

pHRE-Luc was confirmed by its activation in exposing to mineral oil layering and application of CoCl_2 at 50 mM, and both methods were frequently used to mimic the effect of hypoxia [11].

2.4. Luciferase and Other Assays. The luciferase assay was performed by a commercial kit (Tropix Inc., Bedford, MA). In brief, cultures were lysed by a buffer containing 100 mM potassium phosphate buffer (pH 7.8), 0.2% TritonX-100, and 1 mM dithiothreitol. The cell lysate was centrifuged in 13,200 rpm (16,000 \times g) for 5 min in 4°C, and 50 μ L of the supernatant was transferred to the assay plate and set on the luminance reading machine (FLUOstar OPTIMA, BMG, Germany). The readings of luminance intensity were equalized by the protein concentration of lysates, and the data indicated to the luciferase activities of the samples. Protein concentrations were measured routinely by Bradford's method with a kit from Bio-Rad Laboratories (Hercules, CA).

3. Results

3.1. AR and Flavonoids Induce HRE-Mediated Transcriptional Activity. Calycosin, calycosin-7-O- β -D-glucoside, formononetin, and ononin are the major flavonoids contained within AR water extract (Figure 1(a)), which have inductive effect in EPO expression [10, 11]. HPLC analysis indicated that a standardized AR extract should contain the following marker compounds (μ g/1g; mean \pm SD, $n = 4$) (Figure 1(b)): calycosin (212.69 ± 21.1), calycosin-7-O- β -D-glucoside (238.4 ± 19.5), formononetin (150.12 ± 13.7), and ononin (85.66 ± 8.4). We first examined the abilities of AR extract and the flavonoids in the stimulation of HRE mediated transcriptional activity. The AR extract and four flavonoids, formononetin, ononin, calycosin, and calycosin-7-O- β -D-glucoside, were applied onto pHRE-Luc-transfected fibroblasts for two days. The authentication of pHRE-Luc was confirmed by its activation in exposing to mineral oil layering or CoCl_2 treatment, which was frequently used to mimic the effect of hypoxia [10]. Under the hypoxia by oil layering or CoCl_2 , the expression of pHRE-Luc was robustly induced in a time-dependent manner (Figure 2(a)). The AR extract and flavonoids showed significant induction on the pHRE-Luc activity in a dose-dependent manner (Figures 2(b) and 2(c)). The maximal induction by AR extract was over 70% of increase as compared to the background. Formononetin was the most potent flavonoid in the HRE activation, which induced a maximum over 90% at 1 μ M, and the EC_{50} value was $\sim 0.05 \mu$ M. The EC_{50} of ononin, calycosin, and calycosin-7-O- β -D-glucoside were 0.56, 0.66, and 1.47 μ M, and maximal inductions were 80%, 83%, and 70% of increase, respectively (Figure 2(c)).

3.2. Optimization Strategy with Feedback System Control (FSC) Scheme. The FSC scheme consists of an iterative closed-loop of three operations, including formation of drug combinations, experimental readouts, and search algorithm (Figure 3). As the trials, a group of drug combinations selected from the parametric search space were applied in

cultured cells. Induced cellular activities served as the fitness in drug effect evaluation. Based on the cellular responses, the search algorithm linked the cellular readouts and the drug combinations and therefore generated new combinations for subsequent iteration of experimental tests.

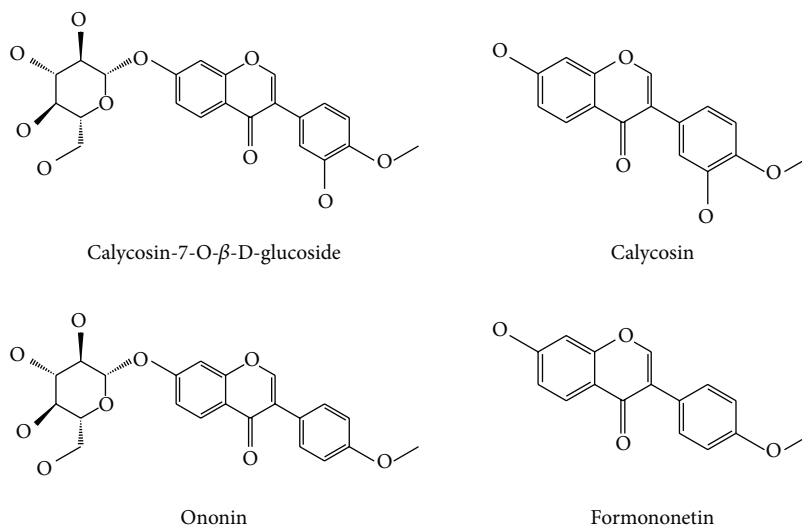
The four flavonoids were mixed and dissolved in dimethyl sulfoxide as the trial combinations. Based on the dose response of individual flavonoids (as from Figure 2(c)), we determined six concentration levels (0, 0.016, 0.08, 0.4, 2, and 10 μ M) of each flavonoid to fully cover the effective range. Flavonoid combinations composed a parametric search space of 1,296 possible trials. The number of possible combinations rapidly increased with the number of flavonoids and concentration levels, as in an exponential form. Six index numbers of 0, 1, 2, 3, 4, 5 were assigned for the concentration levels of 0, 0.016, 0.008, 0.4, 2, 10 μ M, respectively; these index numbers were used later in the differential evolution search algorithm.

The success of FSC scheme heavily relied on the cellular readouts that closely mimicked the desired biological activity and the proper controls to evaluate the effects of the drug combinations. Our goal was to search for potent drug combinations that could stimulate EPO expression, and thus we used the HRE-mediated transcriptional activity as the initial readout. Since HRE is located on the promoter of EPO gene, the induced HRE activity can subsequently trigger the transcription of EPO gene [19].

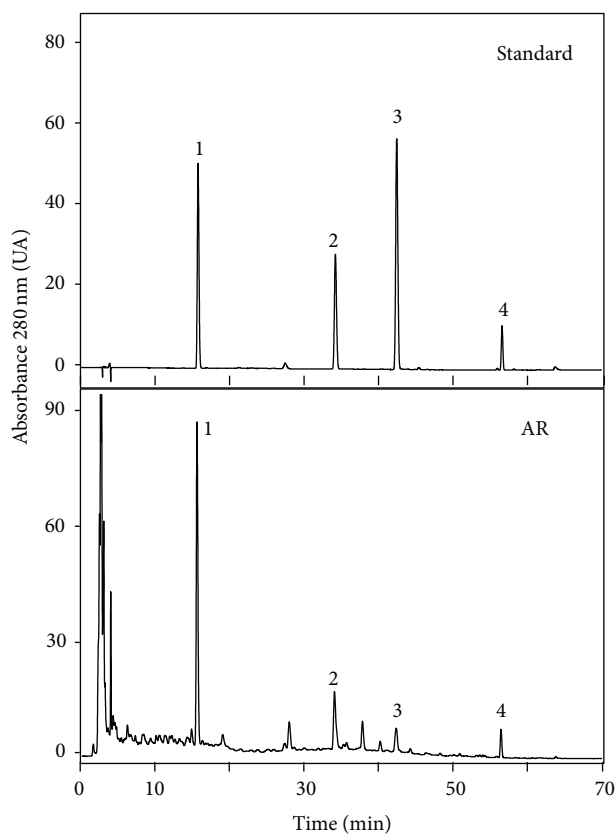
The search algorithm plays an important role in the FSC scheme, which determines the efficiency and accuracy of the exploration. We used the differential evolution algorithm to perform a parallel exploration in the chemical optimization, due to its easy operation and previous successful application [16, 21, 22]. The principle and detailed application of the differential evolution algorithm in our FSC scheme were introduced in the supporting information (Figure 1(S), Supporting information, see supplementary materials available online at <http://dx.doi.org/10.1155/2013/541436>). Parameters, including the number of population (NP) and crossover probability (CR), were modified to better fit our system.

3.3. Optimization of Flavonoid Combination Using FSC. We iteratively evaluated 60 trial combinations in five iterations, each with at least triplicated samples (Figure 4). To determine the collaborative role of four flavonoids on pHRE-Luc-transfected HEK 293T cells, we randomly selected six different combinations of the four flavonoids as trial combinations in the first iteration, using a random number generator in MATLAB (MathWorks). The HRE-mediated transcriptional activities, induced by the combinations, were found to be higher than 130%. The highest response obtained in the first iteration was 232% increase of the control, induced by the 6th combination (0.08, 0.08, 0.4, 10 μ M for formononetin, ononin, calycosin and calycosin-7-O- β -D-glucoside, resp.). Comparing with AR extract and individual flavonoid, higher activities induced by the drug combinations suggested possible collaborative effects among the flavonoids.

In the following iterations, we then attempted to optimize the combinations of the four flavonoids. The trial combinations were generated by the differential evolution (DE)



(a)



(b)

FIGURE 1: Chemical standardization of AR extract by HPLC fingerprint analysis. (a) Calycosin, calycosin-7-O- β -D-glucoside, formononetin, and ononin are the major flavonoids contained within AR water extract. (b) In a HPLC fingerprint at an absorbance of 280 nm, the peaks corresponding to calycosin-7-O- β -D-glucoside (1), ononin (2), calycosin (3), and formononetin (4) were identified as standards (upper panel). The chemical amounts of these four compounds contained within the water extract of AR were calculated according to the HPLC results (lower panel). Representative chromatograms are shown; $n = 3$.

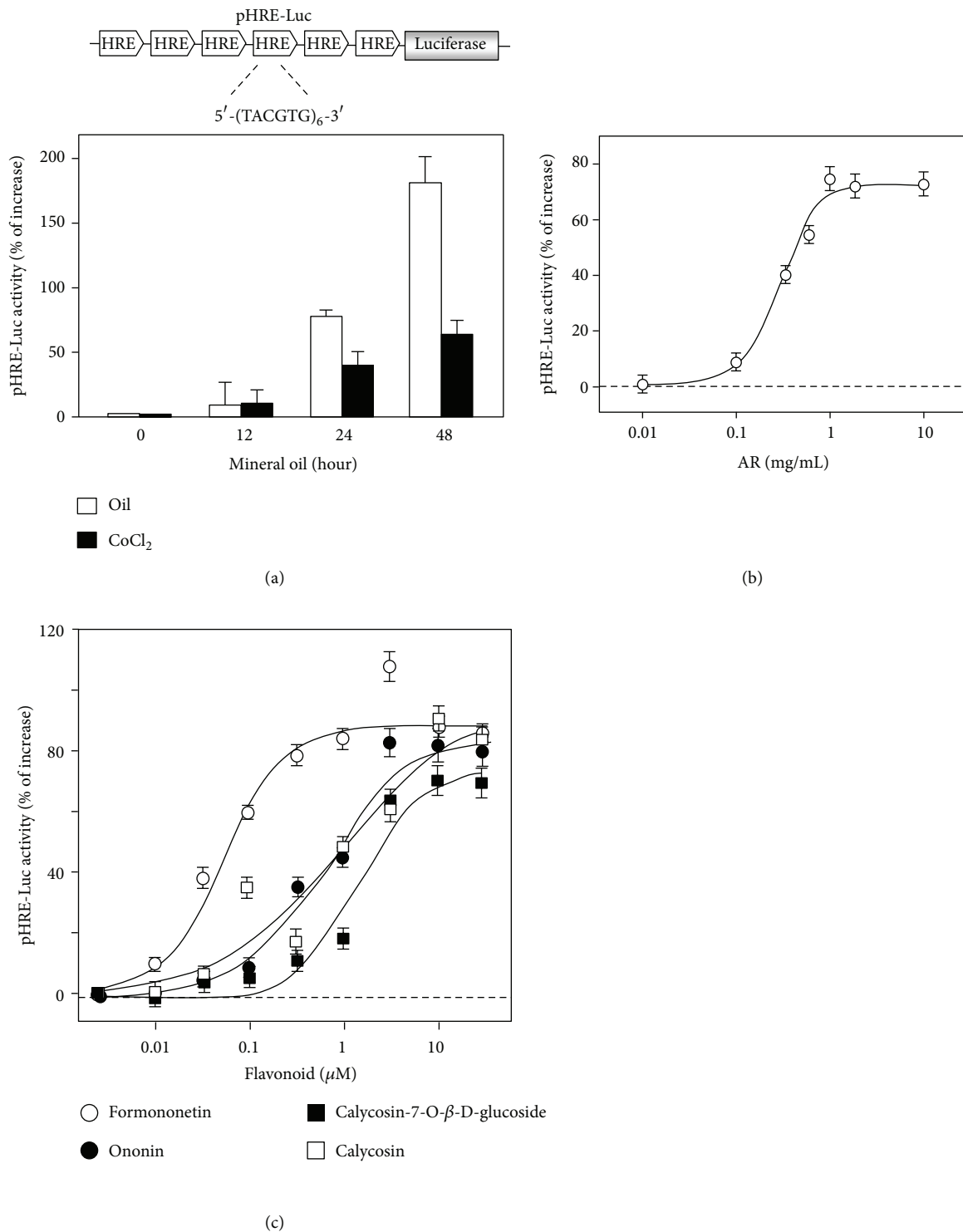


FIGURE 2: The AR extract and flavonoids stimulated the HRE-mediated transcriptional activity in cultured HEK293T cells. (a) Six repeats of hypoxia responsive elements (HRE: 5'-TCG AGG CCC TAC GTG CTG TCT CAC ACA GCC TGT CTG ACG-3') were subcloned in an expression vector of luciferase named as pHRE-Luc (upper panel). Cultured HEK293T cells, transfected with pHRE-Luc, were treated with CoCl₂ (50 mM) or mineral oil layering for 0 to 48 hours. The cell lysates were subjected to luciferase assay to measure the transcriptional activity driven by HRE (lower panel). (b and c) The pHRE-Luc-transfected HEK293T cells were treated with AR extracts (b) and flavonoids (c) for 48 hours to determine the promoter-driven luciferase (pHRE-Luc) activity. Values are expressed as the percentage of increase to basal reading (untreated culture) and in mean ± SD, where *n* = 4, each with triplicate samples.

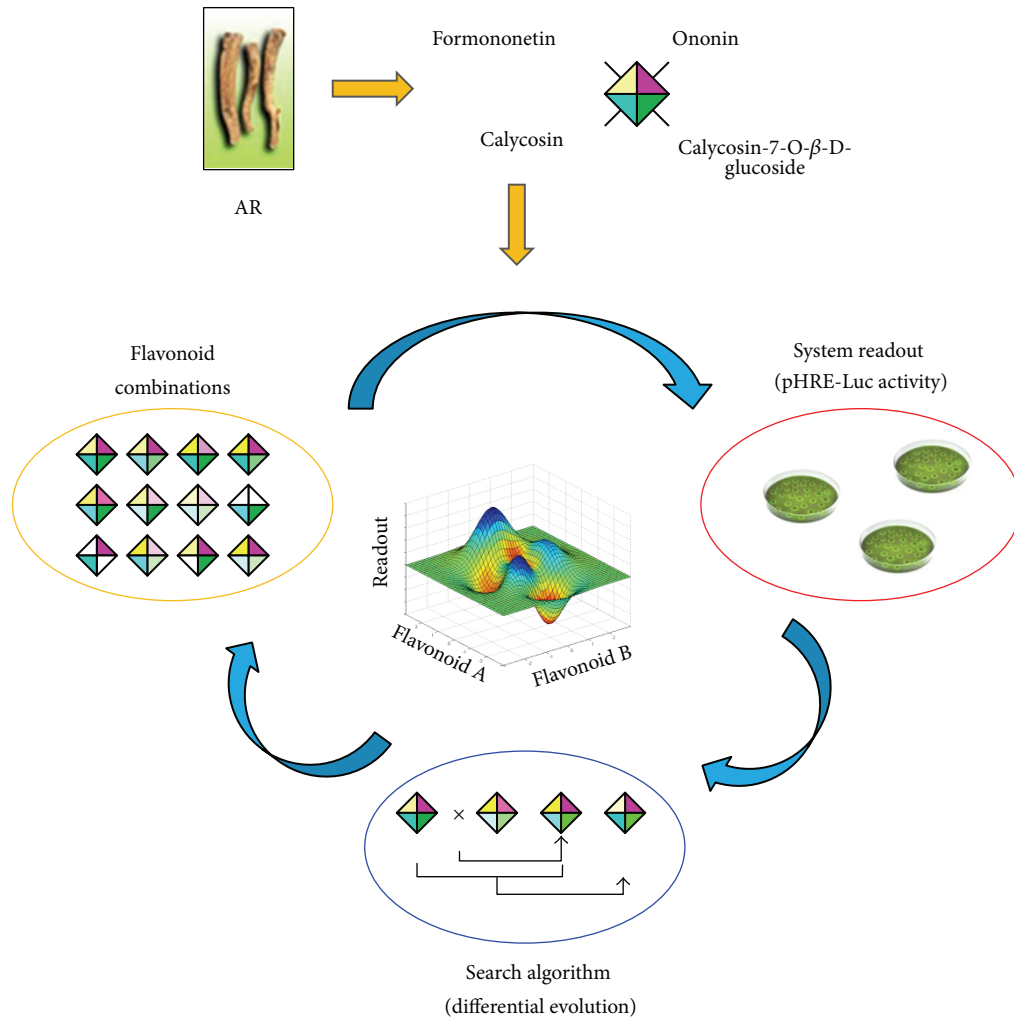


FIGURE 3: Optimization of the flavonoid combination by feedback system control (FSC) scheme. Feedback system control (FSC) scheme was used to optimize the flavonoid combinations. As trial combinations, the drug combinations of four flavonoids were applied onto pHRE-Luc-transfected fibroblasts. The HRE-mediated transcriptional activity was used as the system readout to calculate the fitness of combinations. Differential evolution (DE) algorithm linked the drug combinations and the system readout as to generate new trial combinations in the next iteration.

algorithm, also using the MATLAB. To avoid being trapped in local maximum responses, the number of population was increased from 6 to 12, and finally 18 after iteration 3, and crossover probability was changed from 0.5 to 0.9 after iteration 2. The FSC scheme iteratively updated the potent drug combinations towards better system performance, after the competition between original combinations and trial combinations in each iteration. (Figure 5). After the third iteration, by which we accumulatively tested 24 trials out of 1,296 possible combinations, we identified the 16th combination, that is, 0.08, 0.08, 0.4, 0.08 μM of the four flavonoids. This combination of flavonoids showed a ~3-fold improvement (333%) in stimulating HRE-mediated transcriptional activity compared with individual flavonoids (see Figure 4). This unique combination was carried over through iterations 4 and 5, showing promising drug potency.

Distinct effects of drug combinations in stimulating HRE-mediated transcriptional activity indicated the complicated reciprocity among flavonoids. Out of the 60 trials, we observed that 13 trial combinations induced lower HRE activation than AR and individual flavonoid. The minimum response was observed to be 39% at the 49th combination, that is, 0.016, 2, 0.08, 0.4 μM , which was ~2-fold decrease as compared with individual flavonoid (see Figure 4). Meanwhile, 16 potent combinations induced higher HRE-mediated transcriptional activity than 180% increase of control. Typical dosages of formononetin, ononin, calycosin and calycosin-7-O-β-D-glucoside in 1 mg/mL of AR extract were around 0.56 μM , 0.16 μM , 0.69 μM , and 0.513 μM , respectively [23–25]. Among the 16 potent combinations, the 16th (0.08, 0.08, 0.4, 0.08 μM) and 18th combinations (0.016, 0.4, 0.08, 0 μM) reduced the required dosage by ~10-fold

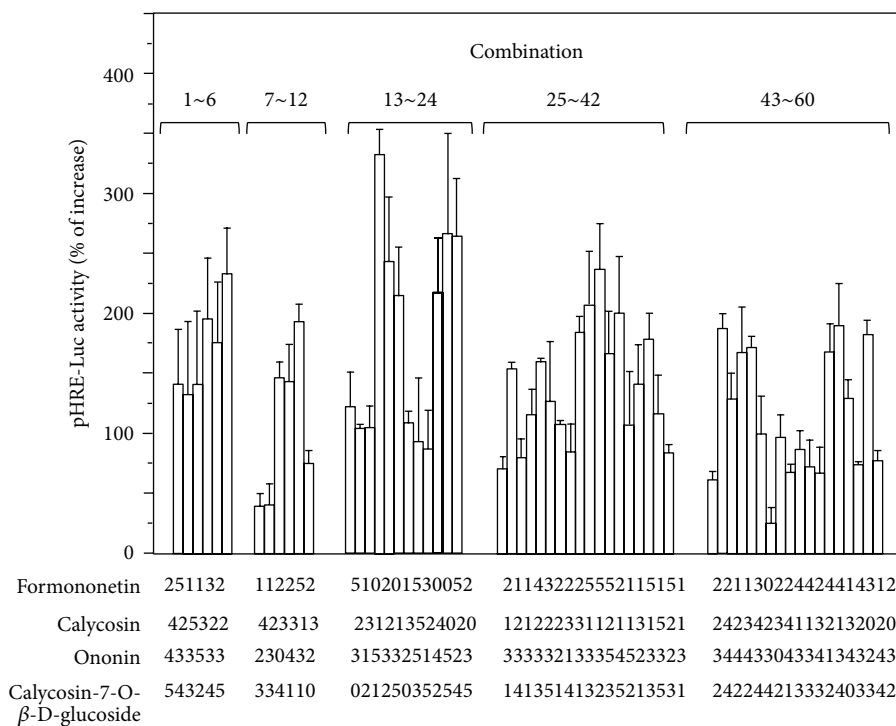


FIGURE 4: The HRE-mediated transcriptional activity induced by the 60 trial combinations in five iterations. The pHRE-Luc-transfected HEK293T cells were treated by the 60 trial combinations in five iterations, that is, 1–6, 7–12, 13–24, 25–42, and 43–60. The integer index of four flavonoids represented the corresponding concentration in each trial shown under each combination, that is, the index numbers of 0, 1, 2, 3, 4, 5 are corresponding to the final concentrations of 0, 0.016, 0.008, 0.4, 2, 10 μ M. After 48 hours, the promoter-driven luciferase (pHRE-Luc) activity was determined. The response to mineral oil layering, a positive control, was as effective as in Figure 2(a). Values are expressed as the percentage of increase to basal reading (untreated culture) and in mean \pm SD, where $n = 4$, each with triplicate samples.

compared with the amounts within AR water extract (see Figure 4).

The AR flavonoids possess a lot of biological functions as described previously [26]; however, the usage of combined flavonoids in a collaborative way is still challenging. To reveal if the flavonoids can work in a synergistic or antagonistic way in activating HRE mediated transcriptional activity, here we used the well-known median-effect equation proposed by Chou [27–30] (Figure 2(S), Supporting information). In Chou's theory, the combination index (CI) was used as the evaluation of synergistic effect. $CI < 1$, $CI = 1$, and $CI > 1$ indicate synergism, additive effect, and antagonism, respectively. The CI values of the 60 trial combinations in our FSC optimization were quite different from each other, ranging from 0.033 to 28.5, showing that the synergistic and antagonistic effects were closely related with the mixing ratio of flavonoids within the drug combinations (Figure 6). Interestingly, the minimum CI values were observed also in the 16th and 18th combinations, to be 0.033 and 0.044, respectively. According to Chou's summary [30], the CI value smaller than 0.1 indicated possible very strong synergism among flavonoids to stimulate the HRE-mediated transcriptional activity, although dose-dependent studies of the combinations were required to obtain further information.

There is no guarantee that the combination we identified would be the best out of the 1,296 possible combinations, until

we have exhaustively tested all the combinations. However, we can testify the effectiveness of this FSC scheme by simulation. Four different benchmark functions were used to mimic the biological system readout. The differential evolution algorithm was implemented exactly the same as used in our flavonoid optimization. Simulation results suggested that the FSC scheme was able to quickly pinpoint the optimal solution (Figure 3(S), Supporting information). Thus, our FSC optimization could be regarded as the stochastic optimal flavonoid combinations of the 1,296 possible combinations.

4. Discussion

The role of flavonoids in regulating the EPO expression has been known [10]. However, the detailed synergistic or antagonistic interaction among flavonoids has not been revealed yet, which therefore stimulates the engineering approach to optimize the flavonoid combinations by FSC scheme. By having FSC approach, we have saved over 90% of the laborious and time-consuming work that is required in exhaustively testing of all possible combinations. Two unique combinations, (0.08, 0.08, 0.4, 0.08) μ M and (0.016, 0.4, 0.08, 0) μ M of formononetin, ononin, calycosin, and calycosin-7-O- β -D-glucoside, were identified to be highly effective in stimulating HRE-mediated transcriptional activity, which

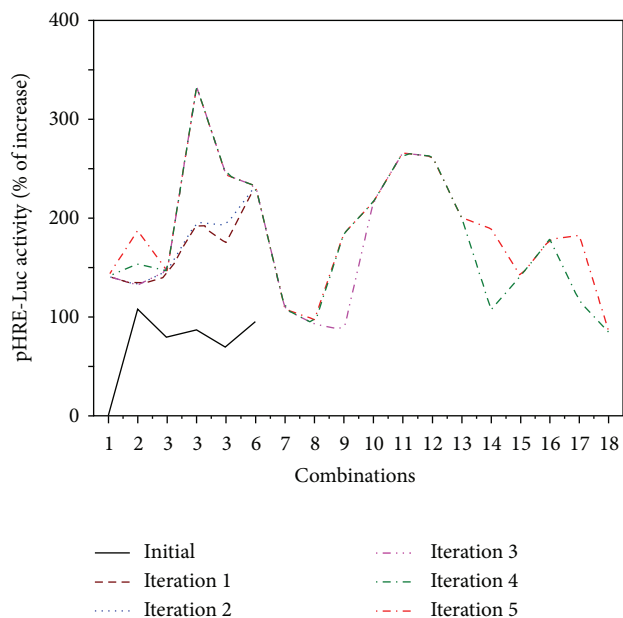


FIGURE 5: The HRE-mediated transcriptional activity induced by the winning population of flavonoid combinations in each iteration. In each iteration, the x -axis represents the i th combination in current winning population. Winning combinations are determined after competition between original combinations and trial combinations, as in Figure 1(S). Values are expressed as the mean value in Figure 4. Initial combinations are comprised of control, AR extract, and individual flavonoid. The FSC scheme iteratively drove combinations in the population towards higher HRE-mediated transcriptional activity; that is, the best response of 3rd combination in the population was found in iteration 3, and carried over through iterations 4 and 5.

was increased ~ 3 -fold by the two optimized combinations, while the AR herbal extract and individual flavonoid can only induce the transcriptional activity by about 80%. The concentration of these four flavonoids that we used here is much lower than that in the herbal extract of AR. Not only in cultured cells, our preliminary results indicated that the application of optimized combination of flavonoids could achieve maximal activation of red blood cell production in animal studies (Zhang et al., unpublished result). By using the FSC scheme as described here, the transcriptional activity of EPO was greatly increased, and the amount of flavonoids used was reduced by ~ 10 -fold.

The successful application of FSC scheme in optimizing the combination of four flavonoids provides hints in study of TCM formulae. According to TCM theory, the herbal formulae should be prepared in a unique methodology having specific combination of different herbs as a formula (named as *Fu Fang*). In general, the combination amongst different herbs within a decoction will directly affect the pharmacological properties of a herbal formula. Indeed, our previous work has supported the usage of the best combination of two herbs in Danggui Buxue Tang, a traditional herbal decoction. Having the best combination of herbs, this herbal decoction possesses enriched chemical and biological properties [23]. However,

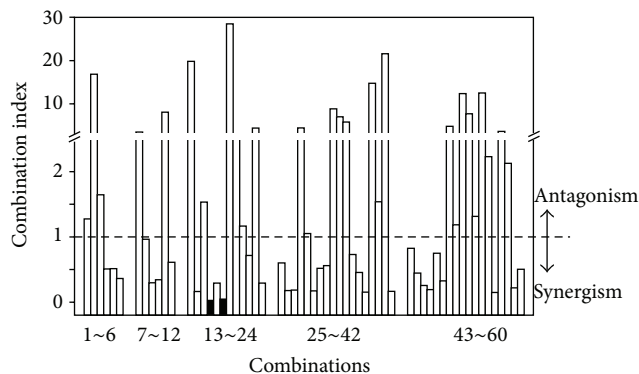


FIGURE 6: Combination index of the 60 trial combinations. The combination indexes (CIs) < 1 , $= 1$, and > 1 indicate synergism, additive effect, and antagonism, respectively. The calculation of CI was accord with the theory of Chou. Sixty combinations out of 5 five iterations are shown here. The 16th and 18th combinations (black bars) showed the strongest synergism, that is, the smallest CI value.

the major problem in the optimization of herbal mixtures is the number of possible combinations. For example, over thousands of possible herb combinations could be found even in a herbal decoction having two herbs. Experimentally, it is impossible to try all these combinations of herbal extracts in optimizing a TCM formula. Having FSC scheme, only about tens of trials are required to optimize the combination, and almost 90% of the work can be trimmed. Thus, the FSC scheme as described here can be used as a new approach to optimize the combination of herbal extracts in TCM formula, which will provide more evidence for the better use of herbal mixture. Moreover, the FSC scheme may be further developed to predict the drug combinations [31].

5. Conclusions

In summary, it can be stated that optimized combinations of flavonoids have a strong HRE-mediated transcriptional activity, which suggests that the optimized flavonoids could have good activity in stimulating the regulatory element of erythropoietin at a very low concentration. The application of FSC scheme could be able to identify potent drug combination of ingredients within herbal medicines, as well as in future its application in finding optimized combination of Chinese herbal mixture.

Authors' Contribution

H. Yu and W. L. Zhang contributed equally to this work.

Conflict of Interest

The authors have no financial or personal relationships with other people or organizations that can inappropriately influence the work presented in the paper.

Acknowledgments

This research was supported by grants from Croucher Foundation (CAS-CF07/08.SC03) to K. W. K. Tsim and a seed grant from HKUST (PROVOST12EG01) to Y. K. Lee.

References

- [1] Y. C. Liu, K. Vian, P. Eckman, T. Y. Fang, and L. D. Chen, *The Essential Book of Traditional Chinese Medicine: Theory, Clinical Practice*, Columbia University Press, New York, NY, USA, 1988.
- [2] T. Xue and R. Roy, "Studying traditional Chinese medicine," *Science*, vol. 300, no. 5620, pp. 740–741, 2003.
- [3] D. Normile, "The new face of traditional Chinese medicine," *Science*, vol. 299, no. 5604, pp. 188–190, 2003.
- [4] X. Q. Ma, Q. Shi, J. A. Duan, T. T. X. Dong, and K. W. K. Tsim, "Chemical analysis of Radix Astragali (Huangqi) in China: a comparison with its adulterants and seasonal variations," *Journal of Agricultural and Food Chemistry*, vol. 50, no. 17, pp. 4861–4866, 2002.
- [5] J. L. Rios and P. G. Waterman, "A review of the pharmacology and toxicology of astragalus," *Phytotherapy Research*, vol. 11, no. 6, pp. 411–418, 1997.
- [6] L. W. Qi, Q. T. Yu, P. Li et al., "Quality evaluation of Radix Astragali through a simultaneous determination of six major active isoflavonoids and four main saponins by high-performance liquid chromatography coupled with diode array and evaporative light scattering detectors," *Journal of Chromatography A*, vol. 1134, no. 1-2, pp. 162–169, 2006.
- [7] C. Dame, K. M. Kirschner, K. V. Bartz, T. Wallach, C. S. Hussels, and H. Scholz, "Wilms tumor suppressor, Wt1, is a transcriptional activator of the erythropoietin gene," *Blood*, vol. 107, no. 11, pp. 4282–4290, 2006.
- [8] W. Jelkmann, "Erythropoietin: structure, control of production, and function," *Physiological Reviews*, vol. 72, no. 2, pp. 449–489, 1992.
- [9] P. Maxwell, "HIF-1: an oxygen response system with special relevance to the kidney," *Journal of the American Society of Nephrology*, vol. 14, no. 11, pp. 2712–2722, 2003.
- [10] K. Y. Z. Zheng, R. C. Y. Choi, A. W. H. Cheung et al., "Flavonoids from radix astragali induce the expression of erythropoietin in cultured cells: a signaling mediated via the accumulation of hypoxia-inducible factor-1 α ," *Journal of Agricultural and Food Chemistry*, vol. 59, no. 5, pp. 1697–1704, 2011.
- [11] K. Y. Z. Zheng, R. C. Y. Choi, H. Q. H. Xie et al., "The expression of erythropoietin triggered by Danggui Buxue Tang, a Chinese herbal decoction prepared from Radix Astragali and Radix Angelicae Sinensis, is mediated by the hypoxia-inducible factor in cultured HEK293T cells," *Journal of Ethnopharmacology*, vol. 132, no. 1, pp. 259–267, 2010.
- [12] J. E. Dancey and H. X. Chen, "Strategies for optimizing combinations of molecularly targeted anticancer agents," *Nature Reviews Drug Discovery*, vol. 5, no. 8, pp. 649–659, 2006.
- [13] J. D. Feala, J. Cortes, P. M. Duxbury, C. Piermarocchi, A. D. McCulloch, and G. Paternostro, "Systems approaches and algorithms for discovery of combinatorial therapies," *Wiley Interdisciplinary Reviews*, vol. 2, no. 2, pp. 181–193, 2010.
- [14] T. Efferth, P. C. H. Li, V. S. B. Konkimalla, and B. Kaina, "From traditional Chinese medicine to rational cancer therapy," *Trends in Molecular Medicine*, vol. 13, no. 8, pp. 353–361, 2007.
- [15] S. Li, B. Zhang, and N. Zhang, "Network target for screening synergistic drug combinations with application to traditional Chinese medicine," *BMC Systems Biology*, vol. 5, supplement 1, p. S10, 2011.
- [16] H. Yan, B. Zhang, S. Li, and Q. Zhao, "A formal model for analyzing drug combination effects and its application in TNF-alpha-induced NFkappaB pathway," *BMC Systems Biology*, vol. 4, article 50, 2010.
- [17] P. K. Wong, F. Yu, A. Shahangian, G. Cheng, R. Sun, and C. M. Ho, "Closed-loop control of cellular functions using combinatory drugs guided by a stochastic search algorithm," *Proceedings of the National Academy of Sciences of the United States of America*, vol. 105, no. 13, pp. 5105–5110, 2008.
- [18] H. Tsutsui, B. Valamehr, A. Hindoyan et al., "An optimized small molecule inhibitor cocktail supports long-term maintenance of human embryonic stem cells," *Nature Communications*, vol. 2, no. 1, article 167, 2011.
- [19] D. E. Post and E. G. Van Meir, "Generation of bidirectional hypoxia/HIF-responsive expression vectors to target gene expression to hypoxic cells," *Gene Therapy*, vol. 8, no. 23, pp. 1801–1807, 2001.
- [20] H. Q. Xie, R. C. Y. Choi, K. W. Leung et al., "Regulation of a transcript encoding the proline-rich membrane anchor of globular muscle acetylcholinesterase: the suppressive roles of myogenesis and innervating nerves," *The Journal of Biological Chemistry*, vol. 282, no. 16, pp. 11765–11775, 2007.
- [21] R. Storn and K. Price, "Differential evolution—a simple and efficient heuristic for global optimization over continuous spaces," *Journal of Global Optimization*, vol. 11, no. 4, pp. 341–359, 1997.
- [22] C. P. Sun, T. Usui, F. Yu et al., "Integrative systems control approach for reactivating Kaposi's sarcoma-associated herpesvirus (KSHV) with combinatory drugs," *Integrative Biology*, vol. 1, no. 1, pp. 123–130, 2009.
- [23] T. T. X. Dong, K. J. Zhao, Q. T. Gao et al., "Chemical and biological assessment of a Chinese herbal decoction containing Radix Astragali and Radix Angelicae Sinensis: determination of drug ratio in having optimized properties," *Journal of Agricultural and Food Chemistry*, vol. 54, no. 7, pp. 2767–2774, 2006.
- [24] Q. Gao, J. Li, J. K. H. Cheung et al., "Verification of the formulation and efficacy of Danggui Buxue Tang (a decoction of Radix Astragali and Radix Angelicae Sinensis): an exemplifying systematic approach to revealing the complexity of Chinese herbal medicine formulae," *Chinese Medicine*, vol. 2, article 12, 2007.
- [25] R. C. Choi, Q. T. Gao, A. W. Cheung et al., "A Chinese herbal decoction, Danggui Buxue Tang, stimulates proliferation, differentiation and gene expression of cultured osteosarcoma cells: genomic approach to reveal specific gene activation," *Evidence-Based Complementary and Alternative Medicine*, vol. 2011, Article ID 307548, 13 pages, 2011.
- [26] H. Wagner, R. Bauer, P. G. Xiao, J. M. Chen, and G. Michler, "Chinese drug monographs and analysis: Radix Astragali (Huangqi)," in *Verlag für Ganzheitliche Medizin Dr. Erich Wühr GmbH*, A. Staudinger, Ed., Kötzing/Bayer, Wald, Germany, 1997.
- [27] T. C. Chou, "The median-effect principle and the combination index for quantitation of synergism and antagonism," in *Synergism and Antagonism in Chemotherapy*, Academic Press, San Diego, Calif, USA, 1991.
- [28] T. C. Chou, "Theoretical basis, experimental design, and computerized simulation of synergism and antagonism in drug

- combination studies," *Pharmacological Reviews*, vol. 58, no. 3, pp. 621–681, 2006.
- [29] T. C. Chou, "The mass-action law based algorithms for quantitative econo-green bio-research," *Integrative Biology*, vol. 3, no. 5, pp. 548–559, 2011.
- [30] T. C. Chou, "The mass-action law based algorithm for cost-effective approach for cancer drug discovery and development," *American Journal of Cancer Research*, vol. 1, no. 7, pp. 925–954, 2011.
- [31] X. M. Zhao, M. Iskar, G. Zeller, M. Kuhn, V. van Noort, and P. Bork, "Prediction of drug combinations by integrating molecular and pharmacological data," *PLoS Computational Biology*, vol. 7, no. 12, Article ID e1002323, 2011.

Research Article

Predicting the Drug Safety for Traditional Chinese Medicine through a Comparative Analysis of Withdrawn Drugs Using Pharmacological Network

Mengzhu Xue,¹ Shoude Zhang,¹ Chaoqian Cai,¹ Xiaojuan Yu,¹ Lei Shan,² Xiaofeng Liu,¹ Weidong Zhang,² and Honglin Li¹

¹ Shanghai Key Laboratory of New Drug Design, State Key Laboratory of Bioreactor Engineering, School of Pharmacy, East China University of Science and Technology, Shanghai 200237, China

² Department of Phytochemistry, School of Pharmacy, Second Military Medical University, Shanghai 200433, China

Correspondence should be addressed to Xiaofeng Liu; xfliu@ecust.edu.cn, Weidong Zhang; wzhangy@hotmail.com and Honglin Li; hlli@ecust.edu.cn

Received 5 March 2013; Accepted 7 April 2013

Academic Editor: Aiping Lu

Copyright © 2013 Mengzhu Xue et al. This is an open access article distributed under the Creative Commons Attribution License, which permits unrestricted use, distribution, and reproduction in any medium, provided the original work is properly cited.

As the major issue to limit the use of drugs, drug safety leads to the attrition or failure in clinical trials of drugs. Therefore, it would be more efficient to minimize therapeutic risks if it could be predicted before large-scale clinical trials. Here, we integrated a network topology analysis with cheminformatics measurements on drug information from the DrugBank database to detect the discrepancies between approved drugs and withdrawn drugs and give drug safety indications. Thus, 47 approved drugs were unfolded with higher similarity measurements to withdrawn ones by the same target and confirmed to be already withdrawn or discontinued in certain countries or regions in subsequent investigations. Accordingly, with the 2D chemical fingerprint similarity calculation as a medium, the method was applied to predict pharmacovigilance for natural products from an in-house traditional Chinese medicine (TCM) database. Among them, Silibinin was highlighted for the high similarity to the withdrawn drug Plicamycin although it was regarded as a promising drug candidate with a lower toxicity in existing reports. In summary, the network approach integrated with cheminformatics could provide drug safety indications effectively, especially for compounds with unknown targets or mechanisms like natural products. It would be helpful for drug safety surveillance in all phases of drug development.

1. Introduction

Drug safety is always a major problem during all the phases of drug development, and its importance has been emphasized in recent years since some approved drugs have to be withdrawn due to severe adverse effects even in the postmarketing phase [1–7]. Although the Food and Drug Administration (FDA) would do drug safety surveillances by report collections on FDA drug safety communications and make consequent decisions on such approved drugs with unexpected safety problems including warnings and withdrawals [8], it should be more efficient for patients and pharmaceutical industry to minimize therapeutic risks if predictive approaches could be used to assess drug safety in the preclinical phase. In fact, there are already some drug

safety predictive approaches developed to this end, which can be roughly divided into quantitative methods and qualitative methods. For the former, toxicologically based QSARs are a typical method to estimate the toxicity of new compounds using the model of a training set of chemicals with known drug-target interactions [9, 10]. Besides, knowledge-based toxicogenomics is also seen as a potent technology, which describes the toxicity of a compound through analyzing responses of the whole genome to the compound at the protein, DNA, or metabolite level and can combine measurements of cheminformatics, bioinformatics, and systems biology [11]. However, there is an obvious limitation to reduce the uses of these methods in *in silico* toxicological predictions; that is, they greatly depend on abundant high-quality experimental data [12]. Thus qualitative methods,

especially network approaches are beginning to thrive in this region [13].

A network is defined as a bipartite graph consisting of nodes to represent molecular objectives and edges to deduce interactions between nodes, which can describe complex interaction events like polypharmacology in a thorough way [14, 15]. Thus, from the network-based viewpoint, toxicity prediction can be described as the identification of novel unexpected drug-target interactions by network topology analysis, machine learning algorithms, cheminformatics, and bioinformatics measurements [16–18]. Till now, there have already been a few methods developed based on network approaches. For example, Campillos et al. constructed a side-effect similarity network to identify common protein targets of unrelated drugs, which is only applicable for marketed drugs with detailed side-effect information [19]. Moreover, Cami et al. developed a predictive pharmacosafety networks (PPNs) which trains a logistic regression model to predict unknown adverse drug events from existing contextual drug safety information [20]. In addition, Yamanishi et al. investigated the relationship between chemical space, pharmacological space, and topology of drug-target interaction networks to develop a new statistical method to predict unknown drug-target interactions, which could be extended to obtain pharmacological information for test datasets with drug candidates based on their chemical structures [21, 22]. Although such existing network approaches are not perfect, it seems quite promising that they are appropriate for drug safety studies and even could be used routinely at all phases of drug discovery. There is hence a great incentive to develop improved network-based methods capable of detecting drug side effects efficiently.

Despite of these predictive methods mentioned above, there have not been special concerns on safety surveillance against medicinal natural products. As we know, traditional Chinese medicine (TCM) has been used in multiple clinical therapies for over 3,000 years, but even till now, there are still sparse research data on effective compositions, biological mechanisms, and adverse drug reactions derived by TCM formulas. Although TCM is regarded as an enormous source for drug discovery which contributes to a lot of anti-inflammatory drugs and anticancer ones, it does not mean that TCM is absolutely safe [23–28]. Presently, therapeutic risks by TCM components have been reviewed owing to the notorious aristolochic acids which were originally used to treat arthritis, rheumatism, hepatitis, and diuresis for a long time but were lately discovered to cause irreversible nephropathy and cancer in humans [29, 30]. Thus it reminds us that the critical problem of pharmacovigilance on active ingredients from TCM formulas should be focused immediately.

To this end, in this study, we firstly constructed a series of networks based on data from the DrugBank database and applied network topology analysis integrated with cheminformatics for drug safety indications [31], including drug-target networks composed by approved drugs with targets and withdrawn drugs with targets, respectively, and a drug-drug network consisting of approved drugs and withdrawn drugs by the same targets. Then 47 approved drugs with

potential therapeutic risks were identified and 34 of them were verified to have already been withdrawn in some countries and regions or in the discontinued phase by reports collection. Ultimately, the approach was applied for an in-home traditional Chinese medicine (TCM) database to indicate pharmacovigilance on natural products extracted from TCM [32]. As a result, 75 natural products with potential risks in therapy were uncovered, especially a drug candidate for hepatitis C virus infection therapy in phase III, Silibinin. Therefore, our method integrating network topology analysis with cheminformatics was proved to be powerful and could provide useful pharmacovigilance indications. Particularly, it is viable to investigate TCM-derived drug safety problem.

2. Materials and Methods

2.1. Datasets. The file for target records, the SDF files of chemical structures annotated with other properties for approved drugs, withdrawn drugs, and small molecular drugs were obtained from the DrugBank database, whereas the structural data for natural products were obtained from the in-home TCM database. Then the small molecular drugs data were used to filter the approved drugs data and the withdrawn drugs data to remove non-small molecular drugs. SMILES and 2D chemical structural fingerprint data for the approved drugs, the withdrawn drugs, and the natural products were prepared by a cheminformatics platform ChemAxon's suite (Academic Version) with default parameters, respectively. Local python scripts were written to format the data files appropriate for network constructions.

2.2. Network Constructions and Network Topology Analysis. drug-target networks consisting of the approved drugs with targets and the withdrawn drugs with targets were constructed with Cytoscape (Version 2.8.2), respectively [33, 34]; then approved drugs and withdrawn drugs by the same targets were identified and integrated into a new network. In particular, for the withdrawn drugs, existing reports were investigated to find out decision factors on drug withdrawals and exhibited by way of a network. Then for the approved drug-target network and the withdrawn-target network, general topology properties were analyzed by Cytoscape, respectively, while CentiBiN (Version 1.4.3) was applied to calculate common vertex centralities for each drug node in the two networks separately [35]. Furthermore, degree distribution profile of drug nodes in each network was analyzed by statistics.

2.3. Cheminformatics Application. In the withdrawn drugs-approved drugs network, such withdrawn drugs that contacted with more than 8 approved drugs were selected for cheminformatics studies, where pairwise fingerprint similarity values would be calculated by Tanimoto coefficient measurements [36, 37]. With the definition by Formula (1), a and b represented occurrences of "1" in binary coded strings i and j , respectively, while c was the occurrence of "1" in the same bit of the two ones. Using 0.7 as the cutoff, the approved drugs greatly similar to certain withdrawn drugs would be

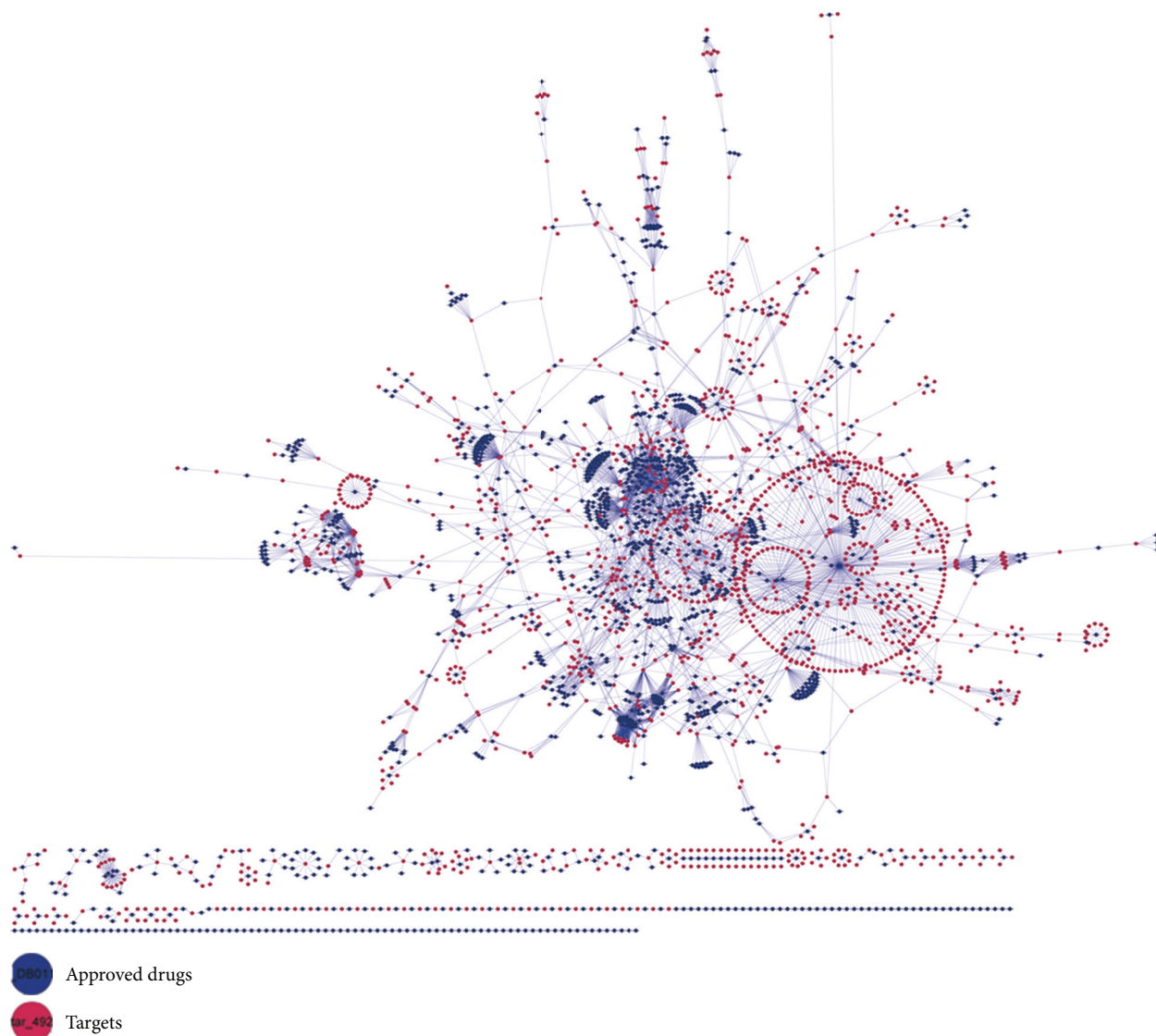


FIGURE 1: The network of approved drugs to targets from DrugBank, in which approved drugs are shown with blue filled spots and targets are exhibited by magenta ones.

picked out for further investigations. Analogously, fingerprint similarity values of natural products from the TCM database against all approved drugs and withdrawn drugs from the DrugBank database were calculated, respectively. For each natural product, hit withdrawn drugs or approved ones would be recorded only when the corresponding Tanimoto coefficients were more than 0.7:

$$\text{Sim}_{\text{Tanimoto}} = \frac{c}{a + b - c}. \quad (1)$$

3. Results

3.1. General Network Topology Analysis on Drug-Target Networks. According to existing information from the DrugBank database, we constructed the approved drug-target network and the withdrawn drug-target network, respectively (Figures 1 and 2). For the former, there are 2889

nodes in total including 1411 drug nodes, whilst there are totally 172 nodes involving 66 drug nodes for the latter. Then general topology properties of the two networks were analyzed for comparisons (Table 1), which adopted multiple characteristics to describe the profile of a network based on graph theory like connectivity, heterogeneity, and centrality [38, 39]. In particular, some topology properties like the shortest paths value obviously depended on the size of each network, so only the ones which are unrelated to sizes or can be regularized by ratios would be discussed below.

In details, isolated nodes in the two networks were noticed first, which made the graphs not connected. Furthermore, it was observed that they were all drug nodes without any associated target nodes. Twenty-three isolated nodes (34.85% of 66 drug nodes) were found in the withdrawn drug-target network, whereas the approved drug-target network possessed a fewer portion of 9.28% (131

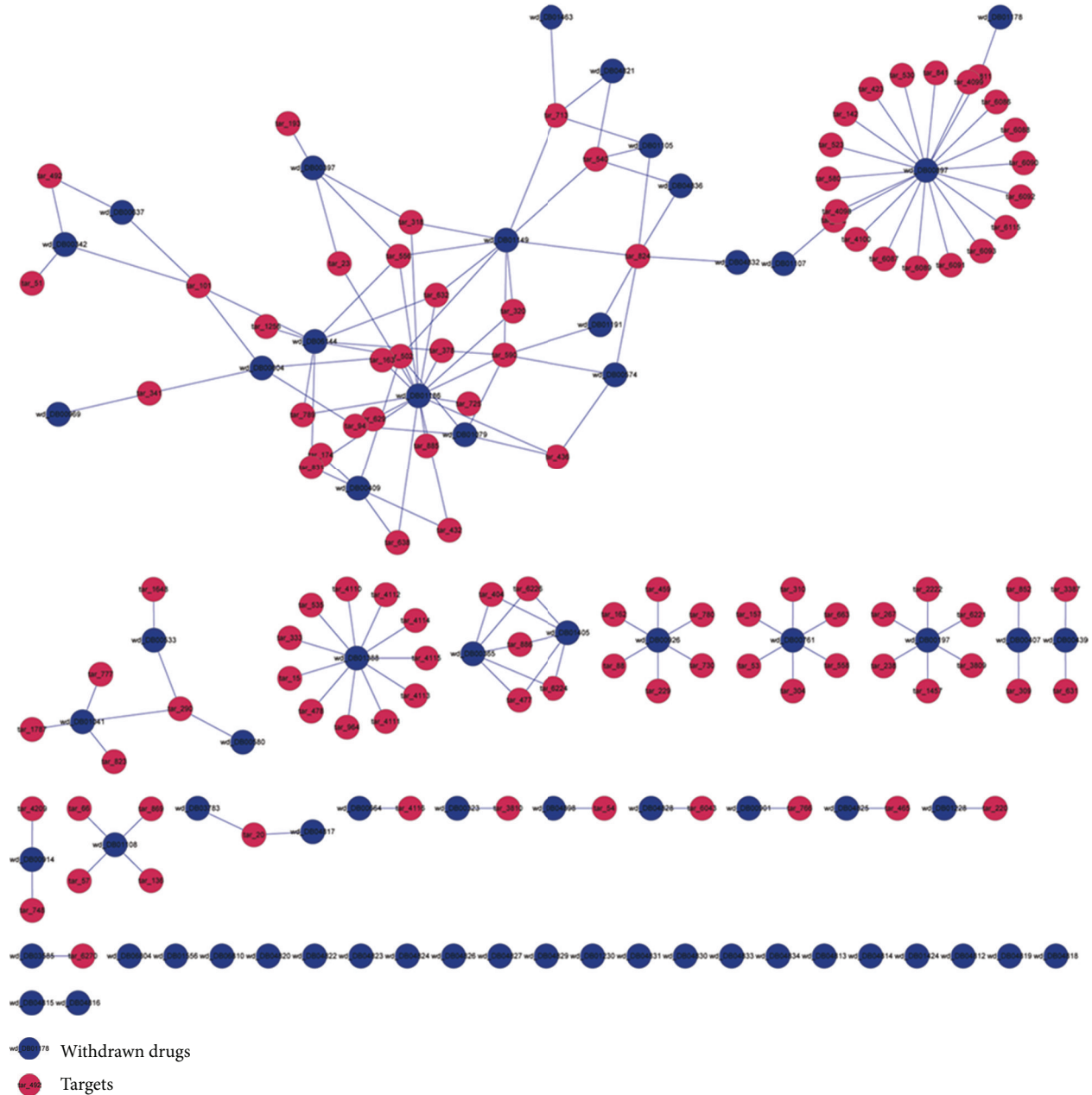


FIGURE 2: The network of withdrawn drugs to targets from DrugBank, where withdrawn drugs are represented by blue filled spots and targets are shown with magenta ones.

ones out of 1411 drug nodes). Besides, all 172 nodes in the withdrawn drug-target network constituted 44 connected components, which on the other hand meant that a connected component had nearly 4 nodes on average, while 2889 ones in the approved drug-target network only made up 217 ones (averagely 13 nodes in a connected component). This observation virtually reflected that nodes in the approved drug-target network were prone to possess more contacts to each other. Moreover, the withdrawn drug-target network had smaller measurements of the characteristic path length (2.914) and the network diameter (7) but a larger network

centralization value (0.107), whilst the ones for the approved drug-target network were 7.510, 23, and 0.054. These results together implicated that the withdrawn drugs were more centralized to fewer targets, even no targets, while approved drugs were more discrete to more targets. Consistent with the surmise above, the higher network density (0.011), the lower network heterogeneity (1.345) and average number of neighbors (1.849) for the withdrawn drug-target network also suggested that nodes in this network are inclined to be crowded in certain regions with fewer interactions to each other and thus exhibited lower irregularity.

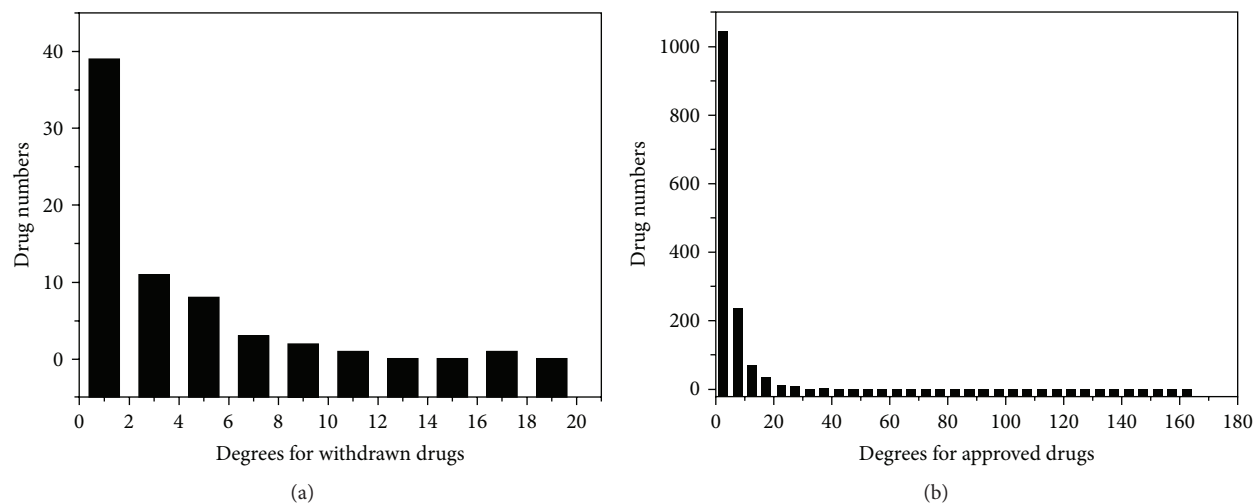


FIGURE 3: Degree distribution statistics for nodes of withdrawn drugs (a) and approved drugs (b) in corresponding drug-target networks, respectively.

TABLE 1: The general network topology analysis on the withdrawn drug-target network and the approved drug-target network by Cytoscape.

Topology properties	Withdrawn drug-target network	Approved drug-target network
Clustering coefficient	0.0	0.0
Connected components	44	217
Network diameter	7	23
Network radius	1	1
Network centralization	0.107	0.054
Shortest paths	2902	5673774
Characteristic path length	2.914	7.510
Avg. number of neighbors	1.849	3.801
Number of nodes	172	2889
Number of drug nodes	66	1411
Network density	0.011	0.001
Network heterogeneity	1.345	1.874
Isolated nodes	23 (34.85%)	131 (9.28%)
Number of self-loops	0	0
Multiedge node pairs	0	0

3.2. Vertex Centralities Studies on Drug-Target Networks.

Furthermore, common vertex centralities for nodes in the two networks were calculated by CentiBin to find more clues [40, 41]. Firstly, degree for each node was measured, and the ones for drug nodes were extracted for degree-distribution investigations in statistics. as illustrated in Table 2 and Figure 3, the withdrawn drug nodes had lower degrees on average and most of them (59.09%) only contacted to 2 target nodes, even less, which validated the lower network heterogeneity and average number of neighbors for the withdrawn drug-target network measured aforementioned

TABLE 2: Degree distribution statistics of drug nodes in the withdrawn drug-target network and the approved drug-target network, respectively.

Degree distribution	Withdrawn drug nodes	Approved drug nodes
Drug nodes in total	66	1411
Average degrees	2.409 ± 3.742	3.891 ± 6.569
Degree ≤ 2	59.09%	37.42%
$2 < \text{degree} \leq 4$	16.67%	30.26%
$4 < \text{degree} \leq 6$	12.12%	11.91%
$6 < \text{degree} \leq 20$	12.12%	18.57%
Degree > 20	0	1.84%

from another point of view. By contrast, approved drug nodes had more interactions with targets, where 63.58% of them contacted to more than 2 targets, especially 1.84% of them could form associations to more than 20 target nodes.

To calculate other vertex centralities planted in the CentiBin, the two networks were formatted into connected graphs according to the indications by CentiBin; thus, isolated nodes and unconnected components were removed and only 45 nodes (17 drug nodes) and 2382 ones (1120 drug nodes) were retained, respectively. Consequently, data from the two networks decreased greatly, especially the one from the withdrawn drug-target network, which was insufficient for further studies but still implied an inferior connectivity of the withdrawn drug-target network. The detailed vertex centralities and network topology properties with corresponding definitions would be listed in Table S1 in the Supplementary Material available online at <http://dx.doi.org/10.1155/2013/256782>.

Moreover, further surveys were taken to detect corresponding diseases and therapeutic intentions derived by certain target nodes in the two connected graphs. Firstly,

28 common ones were extracted, which were almost neurotransmitter receptors or transporters distributing in central and peripheral nervous systems and regulated by agonists or antagonists to treat diseases including depression, Parkinson's syndrome, hypertension, and arrhythmia. Although degrees of these target nodes differed greatly, they acted as "bottlenecks" in the two networks and the connectivity of the graphs would be destroyed if without them. In particular, target nodes with degrees both high in the two networks implied that these targets had attracted plenty of research attentions, but risks of results in failures were high as well, whilst the ones with both lower degrees represented a deficiency of corresponding drugs. Then target nodes which only existed in the connected graph for the approved drug-target network were extracted for similar investigations. Among them, highly connected target nodes ("hubs") represented such therapeutic intentions to develop antibacterial, anti-inflammatory, and antineoplastic agents, which also implied a lower risk of failure for involved drugs.

3.3. 2D Fingerprint Similarity Measurements in the Derived Drug-Drug Network. First of all, decisions on the 66 withdrawn drugs by FDA were collected to find out reasons for withdrawals. Although detailed withdrawal dates for them differed greatly ranging from 1961 to 2010, it was found that all of them were withdrawn due to severe unexpected adverse effects in postmarketing surveillances (Table S2). As a result, the withdrawn drug adverse effect network was built. As illustrated in Figure 4, it was clear that adverse events like hemopathy, cardiovascular toxicity, neurotoxicity, and hepatotoxicity occurred most frequently, whilst each drug mainly induced one adverse event, only two drugs resulted in syndromes of multiple side effects.

To explore potential toxicities derived by approved drugs for pharmacovigilance studies, 2D chemical fingerprint similarity calculations were introduced into the derived network for assistance, which involved withdrawn drugs associated with approved drugs by the same targets. Since the sum of both drugs against the same target somewhat reflected the research interests, withdrawn drugs would be selected for similarity measurements only when they contacted with more than 8 approved drugs. With the Tanimoto coefficient of 0.7 as the cutoff, 47 approved drugs were found greatly similar to withdrawn ones by the same targets in chemical property topologies. Among them, 34 ones (72.3%) have been reported to be in the discontinued phase or even banned in some countries and regions such as Europe, USA, and Canada, while 13 ones (27.7%) are still available in the market but with explicit warnings and strict indications in uses issued by FDA (Figure 5). The detailed remarks on them would be exhibited in Table S3 in the supplementary material.

Besides, side effects occurring frequently for each approved drug of the 47 ones with potential risks were collected from a side effect database SIDER, which contains information on marketed medicines and their recorded adverse drug reactions extracted from dispersed public documents [42]. Consistent to our investigations above, most of the drugs were found to have more than one adverse event records with frequencies in a descending order, especially the

ones which had been discontinued. These results together reaffirmed the severe drug safety problem in the postmarketing phase, and it should be an important subject in the process of drug development. The side-effect collections with highest frequencies for the 47 approved drugs are given in Table S3 in the Supplementary Material as well.

3.4. Drug Safety Indications on Natural Products. The in-house traditional Chinese medicine (TCM) database contains a collection of 2156 natural products isolated from 85 medicinal plants which contributed to several DPP-IV inhibitors by target fishing and RSK2 inhibitors by a virtual screening (unpublished) [32]. Most natural products in the database have physiological activity records but with unknown targets to elucidate mechanisms of action. Thus, we mapped these natural products onto the approved drug-target network and the withdrawn drug-target network by 2D chemical fingerprint similarity calculations to all drugs, respectively. With the same definition and cutoff aforementioned, despite of 988 natural products which did not show high-similarity measurements to approved drugs or to withdrawn drugs, 1092 natural products (50.65%) were found only similar to the approved drugs greatly, which suggested that they might exhibit lower toxicities. Contrarily, 1 natural product was found only alike to the withdrawn drugs. Particularly, 75 ones (3.48%) possessed highly similar features both to the approved drugs and the withdrawn drugs, which highlighted pharmacological activities and potential toxicities simultaneously. Consequently, the 75 natural products were extracted from the database for further investigations, which would be given in Table S4 with records for similar withdrawn drugs in the Supplementary Material.

We searched PubMed and ScienceDirect for published reports about the 75 natural products, but only 25 ones had corresponding literature. Among them, Silibinin which is currently under phase III clinical trials for hepatitis C virus infection therapy had drawn more attentions. In the 2D fingerprint similarity measurements above, Silibinin was found to possess similar chemical features not only to the following approved drugs: Nabilone which is used for control of nausea and vomiting caused by chemotherapeutic agents in the treatment of cancer [43–45], Hesperetin, that is, a cholesterol-lowering flavanoid with antioxidant, anti-inflammatory and anticarcinogenic activities [46–48], and Propafenone which is used in the treatment of atrial and ventricular arrhythmias [49, 50], but also to the withdrawn drug Plicamycin, that is, an antineoplastic antibiotic but has been withdrawn for a dose-related bleeding syndrome [51–53].

In accordance with the similarity calculation results, Silibinin is a flavonolignan extracted from milk thistle seeds, which showed antiviral efficacy, anti-inflammatory activity, anticancer effects, protection against experimental ischemic stroke, and inhibition of A β peptide aggregation with unclear mechanisms [54–60]. Presently, there are no reports on signs of severe toxicity induced by Silibinin, but transient hyperbilirubinemia and mild sensation of heat with infusion were found as the most relevant drug-associated side effects [61, 62]. Combined with our study, although Silibinin was

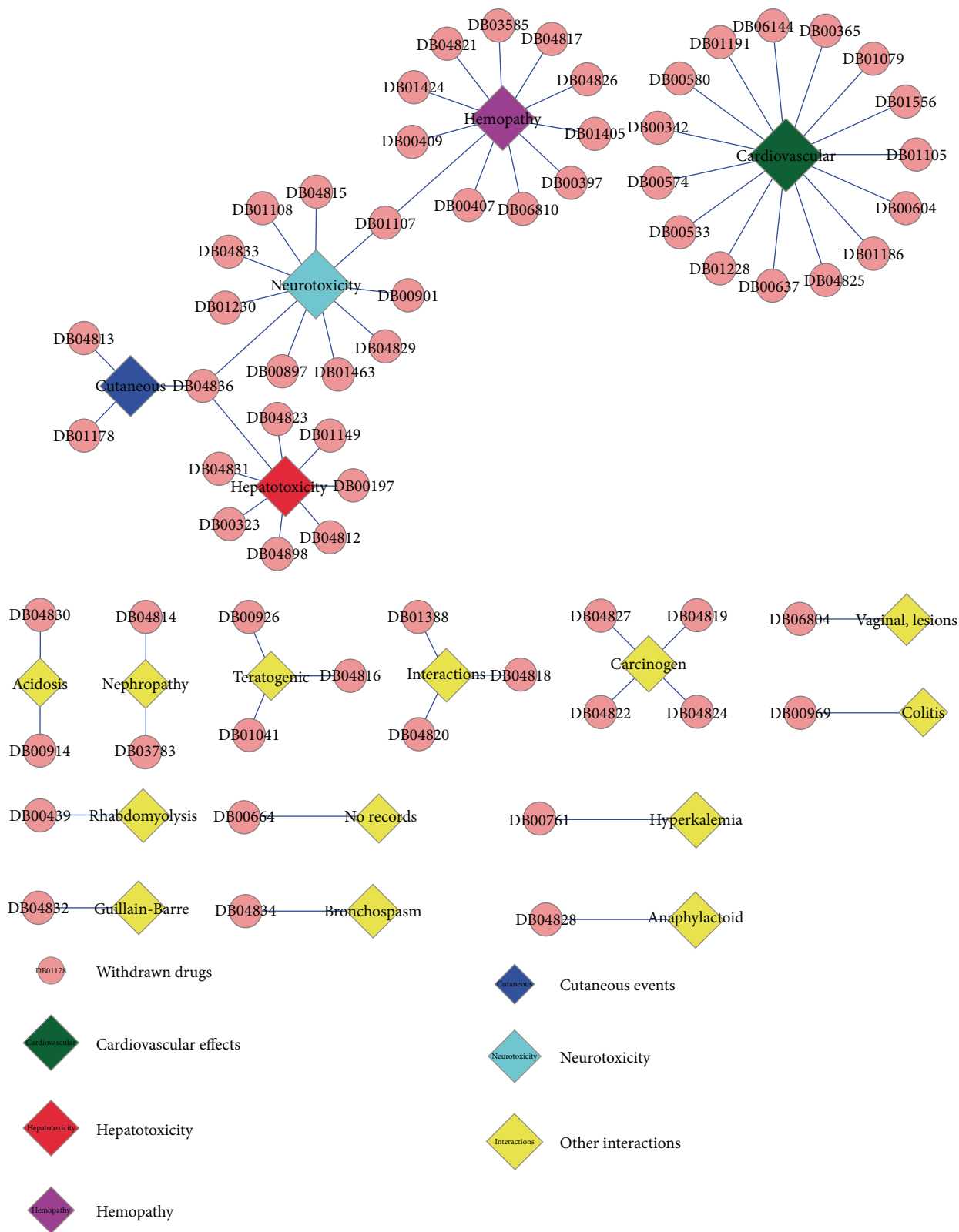


FIGURE 4: The network of critical factors resulting in drug withdrawals to the 66 withdrawn drugs from DrugBank, in which withdrawn drugs are shown with pink filled spots while adverse-effect records for them are exhibited by filled diamonds with different colors.

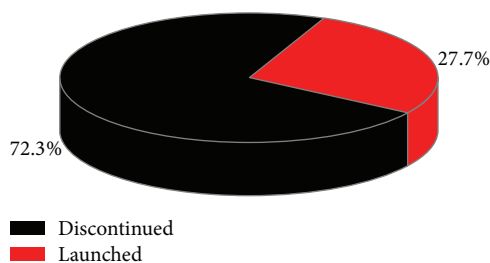


FIGURE 5: Proportion statistics of 47 approved drugs discontinued versus still launched which are greatly similar to withdrawn ones with similarity values more than 0.7, in which discontinued ones are shown in black with launched ones in red.

regarded as a promising drug candidate with a lower toxicity in existing researches, it should be highlighted with the adverse event on hemopathy in progressive clinical surveillances, especially for the old and infants or people with weak metabolism abilities.

4. Discussion

Modern drugs were originally designed for specific targets according to the traditional “one drug, one target, one disease” paradigm. However, drugs may exhibit “off-target” pharmacology, which would result in new therapeutic intentions or unexpected side effects. Thus, network pharmacology model was advocated to elucidate the complexity of biological interaction processes by way of drug-target networks, drug-disease networks, and so on [15]. In this study, based on discrepancies between the approved drug-target network and the withdrawn drug-target network reflected by multiple network topology properties, it is obviously observed that approved drugs tend to contact with more targets, each of which can interact with 3.891 targets on average. In the meantime, “hot” targets only connected by approved drugs mainly distribute in areas of antibacterial, anti-inflammatory, and antineoplastic therapies, while the ones both associated with approved drugs and withdrawn drugs locate in central and peripheral nervous systems for the treatment of diseases such as depression, Parkinson’s syndrome, hypertension, and arrhythmia. This observation would give useful guidance for the research intentions on concrete targets considering risks of failure for involved drugs. Accordingly, combining the results together, it is clear that the network based approach could provide useful information to retain a balance between multiple targeted drug design and adverse side effects, especially in certain therapeutic areas.

Besides, integrated with 2D chemical fingerprint similarity calculations, the two drug-target network models could be used to predict potential targets or pharmacovigilance for marketed drugs or unknown compounds based on their chemical structures. In particular, we investigated drug safety problems induced by natural products extracted from known medicinal plants. As we know, natural products have played a pivotal role in the development of chemotherapies, but for most ones, both bioactive mechanisms and safety boundaries are not known very clearly. Thus with structural

chemical features as mediums, mapping of natural products onto the two drug-target networks would provide more information for elucidations. In cases of natural products from the in-house TCM database, it is observed that they exhibit certain diversity in structures (45.83% of them with Tanimoto coefficient <0.7 against all drugs) which would largely expand the chemical space, whilst 54.17% of them could be selected by chemical similarity measurements for potential pharmacovigilance explorations.

From a technical viewpoint, for the similarity calculation, if 3D geometric shape measurements or other sophisticated functions such as the ones using information mining of medical literature could be considered [63–66], the performance of the method would be better or it would provide all-around information. However, in fact, active conformations of most drugs interacting with targets are not ascertained well. Thus, it could be another major problem to calculate similarity values between conformation sets which would not only exhaust computational sources but also introduce more uncertainties. Moreover, there are few available pharmacology reports on natural products which make it difficult to adopt text mining approaches. Therefore in our studies herein, we tried to simplify these problems and just indicated potential therapeutic risks by drugs qualitatively.

Lastly, compared to adverse drug reaction prediction methods based on sole similarity measurements such as the famous similarity ensemble approach (SEA) [67–71], our methods combined both the advantages of network analysis and cheminformatics, which can not only discover potential side-effect events but also reveal topology properties of targets corresponding to disease modules or pathways. Therefore, it would provide all-around information for drug safety surveillance from the viewpoint of network pharmacology instead of a sole target.

5. Conclusion

To detect the discrepancies between approved drugs and withdrawn drugs, drug-target information from the Drug-Bank database was regularized to construct drug-target networks, and network topology measurements were taken to analyze them. In particular, connectivity-corresponding properties like degrees, connected component numbers, and average neighbor numbers were highlighted because they differentiated each other greatly, which suggested that approved drugs were prone to interact with more targets on average. Then, the withdrawal reasons of these withdrawn drugs were investigated, and it was found that all of them failed due to unexpected adverse effects. Besides, with the chemical structures of withdrawn drugs as probes, 2D fingerprint similarity calculations were adopted for approved drugs and natural products from an in-house TCM database for pharmacovigilance studies, respectively. Consistent with sequent text mining from existing reports, this method was found efficient to provide drug safety indications, especially for compounds with unknown targets or mechanisms like natural products. It is the first time that pharmacovigilance on natural products in large scale is focused and evaluated by network-based approaches. We believe that the network

approach integrated with cheminformatics measurement would be quite useful for drug safety surveillance in all phases of drug development.

Acknowledgments

This work was supported by the National Natural Science Foundation of China (Grants 81230090, 81102375, 21173076, and 81222046), the Twelfth Five-Year National Science & Technology Support Program (Grant 2012BAI29B06), the Shanghai Committee of Science and Technology (Grants 11DZ2260600 and 12401900801), and the 863 Hi-Tech Program of China (Grant 2012AA020308). Honglin Li is also sponsored by Program for New Century Excellent Talents in University (Grant NCET-10-0378).

References

- [1] J. L. Stevens and T. K. Baker, "The future of drug safety testing: expanding the view and narrowing the focus," *Drug Discovery Today*, vol. 14, no. 3-4, pp. 162-167, 2009.
- [2] D. R. Abernethy, J. Woodcock, and L. J. Lesko, "Pharmacological mechanism-based drug safety assessment and prediction," *Clinical Pharmacology and Therapeutics*, vol. 89, no. 6, pp. 793-797, 2011.
- [3] H. Olson, G. Betton, D. Robinson et al., "Concordance of the toxicity of pharmaceuticals in humans and in animals," *Regulatory Toxicology and Pharmacology*, vol. 32, no. 1, pp. 56-67, 2000.
- [4] Z. Lu, "Technical challenges in designing post-marketing eCRFs to address clinical safety and pharmacovigilance needs," *Contemporary Clinical Trials*, vol. 31, no. 1, pp. 108-118, 2010.
- [5] J. Abraham and C. Davis, "A comparative analysis of drug safety withdrawals in the UK and the US (1971-1992): implications for current regulatory thinking and policy," *Social Science and Medicine*, vol. 61, no. 5, pp. 881-892, 2005.
- [6] M. Hauben and A. Bate, "Decision support methods for the detection of adverse events in post-marketing data," *Drug Discovery Today*, vol. 14, no. 7-8, pp. 343-357, 2009.
- [7] J. Moggs, P. Moulin, F. Pognan et al., "Investigative safety science as a competitive advantage for Pharma," *Expert Opinion on Drug Metabolism & Toxicology*, vol. 8, pp. 1071-1082, 2012.
- [8] C. Ishiguro, M. Hall, G. A. Nayarapally et al., "Post-market drug safety evidence sources: an analysis of FDA drug safety communications," *Pharmacoepidemiology and Drug Safety*, vol. 21, pp. 1134-1136, 2012.
- [9] L. G. Valerio Jr., "In silico toxicology for the pharmaceutical sciences," *Toxicology and Applied Pharmacology*, vol. 241, no. 3, pp. 356-370, 2009.
- [10] W. Muster, A. Breidenbach, H. Fischer, S. Kirchner, L. Müller, and A. Pähler, "Computational toxicology in drug development," *Drug Discovery Today*, vol. 13, no. 7-8, pp. 303-310, 2008.
- [11] S. Bureeva and Y. Nikolsky, "Quantitative knowledge-based analysis in compound safety assessment," *Expert Opinion on Drug Metabolism & Toxicology*, vol. 7, no. 3, pp. 287-298, 2011.
- [12] S. Singh and Y. K. Loke, "Drug safety assessment in clinical trials: methodological challenges and opportunities," *Trials*, vol. 13, article 138, 2012.
- [13] N. Chandra and J. Padiadpu, "Network approaches to drug discovery," *Expert Opinion on Drug Metabolism & Toxicology*, vol. 8, pp. 7-20, 2013.
- [14] A. L. Barabási and Z. N. Oltvai, "Network biology: understanding the cell's functional organization," *Nature Reviews Genetics*, vol. 5, no. 2, pp. 101-113, 2004.
- [15] A. L. Hopkins, "Network pharmacology: the next paradigm in drug discovery," *Nature Chemical Biology*, vol. 4, no. 11, pp. 682-690, 2008.
- [16] L. C. Huang, X. Wu, and J. Y. Chen, "Predicting adverse side effects of drugs," *BMC Genomics*, vol. 12, supplement 5, article S11, 2011.
- [17] C. J. Ross, H. Visscher, J. Sistonen et al., "The Canadian Pharmacogenomics Network for Drug Safety: a model for safety pharmacology," *Thyroid*, vol. 20, no. 7, pp. 681-687, 2010.
- [18] J. P. Bai and D. R. Abernethy, "Systems pharmacology to predict drug toxicity: integration across levels of biological organization," *Annual Review of Pharmacology and Toxicology*, vol. 53, pp. 451-473, 2013.
- [19] M. Campillos, M. Kuhn, A. C. Gavin, L. J. Jensen, and P. Bork, "Drug target identification using side-effect similarity," *Science*, vol. 321, no. 5886, pp. 263-266, 2008.
- [20] A. Cami, A. Arnold, S. Manzi et al., "Predicting adverse drug events using pharmacological network models," *Science Translational Medicine*, vol. 3, pp. 114-127, 2011.
- [21] Y. Yamanishi, M. Kotera, M. Kanehisa, and S. Goto, "Drug-target interaction prediction from chemical, genomic and pharmacological data in an integrated framework," *Bioinformatics*, vol. 26, no. 12, pp. i246-i254, 2010.
- [22] Y. Yamanishi, M. Araki, A. Gutteridge, W. Honda, and M. Kanehisa, "Prediction of drug-target interaction networks from the integration of chemical and genomic spaces," *Bioinformatics*, vol. 24, no. 13, pp. i232-i240, 2008.
- [23] H. Itokawa, S. L. Morris-Natschke, T. Akiyama, and K. H. Lee, "Plant-derived natural product research aimed at new drug discovery," *Journal of Natural Medicines*, vol. 62, no. 3, pp. 263-280, 2008.
- [24] M. S. Butler, "The role of natural product chemistry in drug discovery," *Journal of Natural Products*, vol. 67, no. 12, pp. 2141-2153, 2004.
- [25] M. S. Butler, "Natural products to drugs: natural product derived compounds in clinical trials," *Natural Product Reports*, vol. 22, no. 2, pp. 162-195, 2005.
- [26] M. S. Butler, "Natural products to drugs: natural product-derived compounds in clinical trials," *Natural Product Reports*, vol. 25, no. 3, pp. 475-516, 2008.
- [27] H. Lachance, S. Wetzel, K. Kumar et al., "Charting, navigating, and populating natural product chemical space for drug discovery," *Journal of Medicinal Chemistry*, vol. 55, pp. 5989-6001, 2012.
- [28] L. F. Tietze, H. P. Bell, and S. Chandrasekhar, "Natural product hybrids as new leads for drug discovery," *Angewandte Chemie*, vol. 42, no. 34, pp. 3996-4028, 2003.
- [29] F. D. Debelle, J. L. Vanherweghem, and J. L. Nortier, "Aristolochic acid nephropathy: a worldwide problem," *Kidney International*, vol. 74, no. 2, pp. 158-169, 2008.
- [30] Y. H. Hwang, T. Kim, W. K. Cho et al., "In vitro and in vivo genotoxicity assessment of aristolochia manshuriensis kom," *Evidence-Based Complementary and Alternative Medicine*, vol. 2012, Article ID 412736, 9 pages, 2012.
- [31] D. S. Wishart, C. Knox, A. C. Guo et al., "DrugBank: a knowledgebase for drugs, drug actions and drug targets," *Nucleic Acids Research*, vol. 36, no. 1, pp. D901-D906, 2008.

- [32] S. Zhang, W. Lu, X. Liu et al., "Fast and effective identification of the bioactive compounds and their targets from medicinal plants via computational chemical biology approach," *Med-ChemComm*, vol. 2, no. 6, pp. 471–477, 2011.
- [33] M. E. Smoot, K. Ono, J. Ruscchinski, P. L. Wang, and T. Ideker, "Cytoscape 2.8: new features for data integration and network visualization," *Bioinformatics*, vol. 27, no. 3, pp. 431–432, 2011.
- [34] P. Shannon, A. Markiel, O. Ozier et al., "Cytoscape: a software environment for integrated models of biomolecular interaction networks," *Genome Research*, vol. 13, no. 11, pp. 2498–2504, 2003.
- [35] B. H. Junker, D. Koschützki, and F. Schreiber, "Exploration of biological network centralities with CentiBiN," *BMC Bioinformatics*, vol. 7, article 219, 2006.
- [36] C. Ma, L. Wang, and X. Q. Xie, "GPU accelerated chemical similarity calculation for compound library comparison," *Journal of Chemical Information and Modeling*, vol. 51, no. 7, pp. 1521–1527, 2011.
- [37] P. Willett, "Chemical similarity searching," *Journal of Chemical Information and Computer Sciences*, vol. 38, pp. 983–996, 1998.
- [38] T. Aittokallio and B. Schwikowski, "Graph-based methods for analysing networks in cell biology," *Briefings in Bioinformatics*, vol. 7, no. 3, pp. 243–255, 2006.
- [39] E. Estrada, "Quantifying network heterogeneity," *Physical Review E*, vol. 82, Article ID 066102, 2010.
- [40] D. J. Klein, "Centrality measure in graphs," *Journal of Mathematical Chemistry*, vol. 47, no. 4, pp. 1209–1223, 2010.
- [41] P. Hage and F. Harary, "Eccentricity and centrality in networks," *Social Networks*, vol. 17, no. 1, pp. 57–63, 1995.
- [42] M. Kuhn, M. Campillos, I. Letunic, L. J. Jensen, and P. Bork, "A side effect resource to capture phenotypic effects of drugs," *Molecular Systems Biology*, vol. 6, article 343, 2010.
- [43] D. Cunningham, C. J. Bradley, G. J. Forrest et al., "A randomized trial of oral nabilone and prochlorperazine compared to intravenous metoclopramide and dexamethasone in the treatment of nausea and vomiting induced by chemotherapy regimens containing cisplatin or cisplatin analogues," *European Journal of Cancer and Clinical Oncology*, vol. 24, no. 4, pp. 685–689, 1988.
- [44] A. Niiranen and K. Mattson, "Antiemetic efficacy of nabilone and dexamethasone: a randomized study of patients with lung cancer receiving chemotherapy," *American Journal of Clinical Oncology*, vol. 10, no. 4, pp. 325–329, 1987.
- [45] L. H. Einhorn, C. Nagy, B. Furnas, and S. D. Williams, "Nabilone: an effective antiemetic in patients receiving cancer chemotherapy," *Journal of Clinical Pharmacology*, vol. 21, no. 8–9, pp. 64S–69S, 1981.
- [46] Y. Yang, J. Wolfram, H. Shen et al., "Hesperetin: an inhibitor of the transforming growth factor-beta (TGF-beta) signaling pathway," *European Journal of Medicinal Chemistry*, vol. 58, pp. 390–395, 2012.
- [47] B. Zarebczan, S. N. Pinchot, M. Kunnimalaiyaan, and H. Chen, "Hesperetin, a potential therapy for carcinoid cancer," *American Journal of Surgery*, vol. 201, no. 3, pp. 329–333, 2011.
- [48] L. Ye, F. L. Chan, S. Chen et al., "The citrus flavonone hesperetin inhibits growth of aromatase-expressing MCF-7 tumor in ovariectomized athymic mice," *Journal of Nutritional Biochemistry*, vol. 23, pp. 1230–1237, 2012.
- [49] F. Gaita, E. Richiardi, and M. Bocchiardo, "Short- and long-term effects of propafenone in ventricular arrhythmias," *International Journal of Cardiology*, vol. 13, no. 2, pp. 163–170, 1986.
- [50] I. Vassiliadis, P. Papoutsakis, I. Kallikazaros, and C. Stefanadis, "Propafenone in the prevention of non-ventricular arrhythmias associated with the Wolff-Parkinson-White syndrome," *International Journal of Cardiology*, vol. 27, no. 1, pp. 63–70, 1990.
- [51] K. Sampi, M. Hozumi, R. Kumai, Y. Honma, and M. Sakurai, "Differentiation of blasts from patients in myeloid crisis of chronic myelogenous leukemia by in-vivo and in-vitro plicamycin treatment," *Leukemia Research*, vol. 11, no. 12, pp. 1089–1092, 1987.
- [52] J. P. Dutcher, D. Coletti, E. Paietta, and P. H. Wiernik, "A pilot study of alpha-interferon and plicamycin for accelerated phase of chronic myeloid leukemia," *Leukemia Research*, vol. 21, no. 5, pp. 375–380, 1997.
- [53] S. J. Wimalawansa, "Dramatic response to plicamycin in a patient with severe Paget's disease refractory to calcitonin and pamidronate," *Seminars in Arthritis and Rheumatism*, vol. 23, no. 4, 267 pages, 1994.
- [54] R. D. Verschoyle, P. Greaves, K. Patel et al., "Evaluation of the cancer chemopreventive efficacy of silibinin in genetic mouse models of prostate and intestinal carcinogenesis: relationship with silibinin levels," *European Journal of Cancer*, vol. 44, no. 6, pp. 898–906, 2008.
- [55] F. Yin, J. Liu, X. Ji, Y. Wang, J. Zidichouski, and J. Zhang, "Silibinin: a novel inhibitor of A β aggregation," *Neurochemistry International*, vol. 58, no. 3, pp. 399–403, 2011.
- [56] J. Y. Wang, C. C. Chang, C. C. Chiang et al., "Silibinin suppresses the maintenance of colorectal cancer stem-like cells by inhibiting PP2A/AKT/mTOR pathways," *Journal of Cellular Biochemistry*, vol. 113, pp. 1733–1743, 2012.
- [57] M. Dastpeyman, N. Motamed, K. Azadmanesh et al., "Inhibition of silibinin on migration and adhesion capacity of human highly metastatic breast cancer cell line, MDA-MB-231, by evaluation of beta1-integrin and downstream molecules, Cdc42, Raf-1 and D4GDI," *Medical Oncology*, vol. 29, pp. 2512–2518, 2012.
- [58] W. Ai, Y. Zhang, Q. Z. Tang et al., "Silibinin attenuates cardiac hypertrophy and fibrosis through blocking EGFR-dependent signaling," *Journal of Cellular Biochemistry*, vol. 110, no. 5, pp. 1111–1122, 2010.
- [59] A. Tyagi, R. P. Singh, K. Ramasamy et al., "Growth inhibition and regression of lung tumors by silibinin: modulation of angiogenesis by macrophage-associated cytokines and nuclear factor- κ B and signal transducers and activators of transcription 3," *Cancer Prevention Research*, vol. 2, no. 1, pp. 74–83, 2009.
- [60] B. Cheng, H. Gong, X. Li et al., "Silibinin inhibits the toxic aggregation of human islet amyloid polypeptide," *Biochemical and Biophysical Research Communications*, vol. 419, pp. 495–499, 2012.
- [61] R. Barcena, A. Moreno, M. A. Rodriguez-Gandia et al., "Safety and anti-HCV effect of prolonged intravenous silibinin in HCV genotype 1 subjects in the immediate liver transplant period," *Journal of Hepatology*, vol. 58, pp. 421–426, 2013.
- [62] L. Li, J. Zeng, Y. Gao, and D. He, "Targeting silibinin in the antiproliferative pathway," *Expert Opinion on Investigational Drugs*, vol. 19, no. 2, pp. 243–255, 2010.
- [63] X. Liu, H. Jiang, and H. Li, "SHAFTS: a hybrid approach for 3D molecular similarity calculation—1. Method and assessment of virtual screening," *Journal of Chemical Information and Modeling*, vol. 51, pp. 2372–2385, 2011.
- [64] R. A. Copeland, "The dynamics of drug-target interactions: drug-target residence time and its impact on efficacy and safety,"

Expert Opinion on Drug Discovery, vol. 5, no. 4, pp. 305–310, 2010.

- [65] H. Bisgin, Z. Liu, H. Fang et al., “Mining FDA drug labels using an unsupervised learning technique-topic modeling,” *BMC Bioinformatics*, vol. 12, article S11, 2011.
- [66] K. D. Shetty and S. R. Dalal, “Using information mining of the medical literature to improve drug safety,” *Journal of the American Medical Informatics Association*, vol. 18, pp. 668–674, 2011.
- [67] E. Lounkine, M. J. Keiser, S. Whitebread et al., “Large-scale prediction and testing of drug activity on side-effect targets,” *Nature*, vol. 486, pp. 361–367, 2012.
- [68] M. J. Keiser, V. Setola, J. J. Irwin et al., “Predicting new molecular targets for known drugs,” *Nature*, vol. 462, no. 7270, pp. 175–181, 2009.
- [69] M. J. Keiser, B. L. Roth, B. N. Armbruster, P. Ernsberger, J. J. Irwin, and B. K. Shoichet, “Relating protein pharmacology by ligand chemistry,” *Nature Biotechnology*, vol. 25, no. 2, pp. 197–206, 2007.
- [70] J. Hert, M. J. Keiser, J. J. Irwin, T. I. Oprea, and B. K. Shoichet, “Quantifying the relationships among drug classes,” *Journal of Chemical Information and Modeling*, vol. 48, no. 4, pp. 755–765, 2008.
- [71] K. Azzaoui, J. Hamon, B. Faller et al., “Modeling promiscuity based on in vitro safety pharmacology profiling data,” *ChemMedChem*, vol. 2, no. 6, pp. 874–880, 2007.

Research Article

Xiao-Xu-Ming Decoction Protects against Blood-Brain Barrier Disruption and Neurological Injury Induced by Cerebral Ischemia and Reperfusion in Rats

Rui Lan,¹ Jun Xiang,^{1,2} Guo-Hua Wang,¹ Wen-Wei Li,¹ Wen Zhang,¹
Li-Li Xu,¹ and Ding-Fang Cai¹

¹ Department of Integrative Medicine, Zhongshan Hospital, and Laboratory of Neurology, Institute of Integrative Medicine, Fudan University, Shanghai 200032, China

² Longhua Hospital, Shanghai University of Traditional Chinese Medicine, Shanghai 200032, China

Correspondence should be addressed to Ding-Fang Cai; dingfangcai@163.com

Received 10 October 2012; Accepted 22 March 2013

Academic Editor: Aiping Lu

Copyright © 2013 Rui Lan et al. This is an open access article distributed under the Creative Commons Attribution License, which permits unrestricted use, distribution, and reproduction in any medium, provided the original work is properly cited.

Xiao-Xu-Ming decoction (XXMD) is an effective prescription in the treatment of ischemic stroke, but the mechanisms involved are not well known. In the present study, 120 male Sprague-Dawley rats were randomly divided into 5 groups: sham control (sham), ischemia and reperfusion (IR), and IR plus 15, 30, and 60 g/kg/day XXMD. The stroke model was induced by 90 min of middle cerebral artery occlusion followed by reperfusion. The brain lesion areas were evaluated by 2,3,5-triphenyltetrazolium chloride staining, and neurological deficits were observed at different time points after reperfusion. Blood-brain barrier (BBB) disruption was evaluated by assessing brain water content and Evans blue content. Pathological changes in BBB ultrastructure were observed with transmission electron microscopy. MMP-9, -2, and VEGF expression levels were quantitatively determined by western blotting and immunohistochemistry. We found that XXMD (60 g/kg/day) treatment reduced cerebral infarct area, improved behavioral function, and attenuated ultrastructure damage and permeability of BBB following ischemia and reperfusion. Moreover, XXMD downregulated the expression levels of MMP-9, -2, and VEGF. These findings indicate that XXMD alleviates BBB disruption and cerebral ischemic injury, which may be achieved by inhibiting the expression of MMP-9, -2, and VEGF.

1. Introduction

Stroke is a major cause of death and disability worldwide. Numerous researchers have suggested, based on new theories and results, that the stroke therapeutic strategy should shift its focus from neuroprotection of neurons to protection of the neurovascular unit [1–3]. The blood-brain barrier (BBB), a vital element of the neurovascular unit, consists of brain microvessel endothelial cells (BMECs), capillary basement membranes, astrocyte endfeet, endothelial tight junctions, and pericytes [4]. Recent experimental studies indicated that BBB dysfunction was associated with many neurological diseases, such as stroke and Alzheimer's disease [4]. Cerebral ischemia and reperfusion can cause disruption to the BBB [5, 6], with damage to the components of the BBB resulting in an increase in its permeability.

Matrix metalloproteinases (MMPs), a metalloproteinase subfamily, play a crucial role in regulating the activation of growth factors, signaling molecules, and death receptors. They also attack the extracellular matrix, basal lamina, and tight junctions of endothelial cells [7]. Mounting evidence indicates that MMPs, in particular MMP-9 and -2, contribute to BBB disruption and vasogenic edema, hemorrhagic transformation, and cell death induced by cerebral ischemia and reperfusion [7–10].

Vascular endothelial growth factor (VEGF) plays an essential role in angiogenesis. However, VEGF, as a crucial vascular permeability factor, has other effects. For example, VEGF drives BBB disruption and leads to brain edema at the acute phase of stroke [11, 12], and inhibition of endogenous VEGF reduces secondary ischemic brain damage [13–15].

Xiao-Xu-Ming decoction (XXMD) has been widely used in China in the treatment of cerebral diseases for more than 1,000 years. Recently, XXMD has been shown to protect against cerebral ischemic injury and dementia [16–20]. However, the effects of XXMD on BBB disruption are unknown. Thus, in the present study, we sought to investigate the effects of XXMD on cerebral ischemia and reperfusion injury and to determine whether XXMD could attenuate BBB disruption by inhibiting the expression of MMP-9, MMP-2, and VEGF.

2. Materials and Methods

2.1. Preparation of XXMD. The XXMD consists of 12 crude drugs, including *Herba Ephedrae*, *cassia twig*, *Radix Paeoniae Alba*, *Rhizoma Chuanxiong*, *Radix Ginseng*, *Radix Stephaniae Tetrandrae*, *Radix Scutellariae*, *Semen Armeniacae Amarum*, *Radix Aconiti Praeparata*, *Radix Glycyrrhiza*, *Radix Ledebouriellae*, and *fresh Rhizoma Zingiberis Recens* at a ratio of 1:1:1:1:1:1:1:1:1:1:1:1.5:5. The crude drugs were purchased from TCM Pharmacy of Zhongshan Hospital, Fudan University. After the first decoction, conducted for 1 h in a 1:10 (w/v) drug:water ratio, the suspension was gauze filtered. Water was added for the second decoction, which lasted 1 h and which was followed by a third decoction for 1 h. The gruffs were soaked in 75% ethyl alcohol for 24 h, and the liquid was preserved. The filtered and mixed suspension from the three decoctions was collected and centrifuged at 2000 ×g for 20 min to obtain a suspension for the subsequent preparation. Dehydrated alcohol was added slowly with fast agitation until the concentration reached 75% alcohol (v/v). The solution was stirred overnight and the precipitate was discarded. The suspension and the liquid acquired from the gruffs were merged and centrifuged at 2000 ×g for 20 min, then concentrated to a final concentration of 2 g/mL (w/v). The alcohol was recovered simultaneously with a rotary evaporator. Finally, the liquid was autoclaved and stored at –20°C until use.

2.2. Animals. All experiments were performed on adult male Sprague-Dawley rats (Experimental Animal Center, Zhongshan Hospital, Fudan University, China) weighing 230–280 g. One hundred twenty rats were kept in groups of four and maintained on a 12:12 h light:dark cycle at a constant room temperature of 21°C with free access to food and water. The experimental protocols and animal handling procedures were approved by the Animal Care and Use Committee (ACUC) of Fudan University and were consistent with the National Institutes of Health Guide for the Care and Use of Laboratory Animals.

2.3. Drug Administration and Experimental Design. For XXMD treatment, the common human daily dose of XXMD is 165 g/75 kg bodyweight [21]. According to the formula: $d_{\text{rat}} = d_{\text{human}} \times 0.7/0.11$, the common dose of XXMD in rat should be 14.2 g/kg/day. In general, the drug tolerance of a rat is higher than that of human [21], we therefore selected 15, 30, and 60 g/kg/day as the low, medium, and high dosages

in the present study, respectively. Rats were randomly divided into 5 groups: sham control (sham), ischemia and reperfusion (IR), and IR plus XXMD15, XXMD30, and XXMD60. The rats in the XXMD-treated groups were orally administered the corresponding doses of XXMD, and other rats were given the same volume of normal saline. All treatments were performed twice a day at 8:00 and 18:00 for 3 days before the operation and drug administration was continued until animal sacrifice at the conclusion of the experiment. The experimental design of the current study is shown in Figure 1.

2.4. Focal Cerebral Ischemia and Reperfusion. The focal ischemia was induced by left middle cerebral artery occlusion (MCAO) according to previously described methods with minor modifications [22, 23]. The ischemia and reperfusion induction was performed by an operator blind to the animal grouping. Briefly, the rats were anesthetized with 10% chloral hydrate (350 mg/kg, intraperitoneal (i.p.) injection). After the skin incision, the left common carotid artery (CCA) was exposed and carefully separated from nerves and tissue. The external carotid artery (ECA) and internal carotid artery (ICA) were dissected gently. The ECA was clipped, the ECA stump was stretched and aligned with the ICA, and a nylon monofilament was inserted. At this time, the microvascular clip was removed and the thread was advanced until it was about 20 mm from the CCA bifurcation. During the course of the surgery, the rectal temperature, blood gases, and cardiovascular rate of each rat were monitored and maintained. Reperfusion was initiated by withdrawal of the monofilament after 90 min of ischemia. In this study, the rats in the sham group were subjected to the same operation, but the monofilament was not inserted. The other rats in the IR group and the XXMD-treated groups underwent reperfusion following 90 min of cerebral ischemia. During the experiments, 19 rats subjected to focal cerebral ischemia and reperfusion died, and the main causes of death were cerebral infarction with hemorrhage or subarachnoid hemorrhage.

2.5. Quantification of Ischemic Infarct Area and Hemispheric Swelling. Twenty-four hours after reperfusion, the cerebral ischemic infarct areas were evaluated by 2,3,5-triphenyltetrazolium chloride (TTC; Sigma-Aldrich, St. Louis, MO, USA) staining. Briefly, the rats were sacrificed under deeply anesthesia, their brains were quickly removed on ice, and placed at –20°C for 15–20 min. Brains were sectioned into 6 coronal slices of 2 mm thickness and stained with 1% TTC solution in the dark for 20 min at 37°C. Finally, the tissues were fixed in 4% paraformaldehyde (in 0.1 M phosphate buffer, pH 7.4), and the percentage of cerebral infarct area was calculated 24 h later with microscope image analysis software (Image-Pro Plus, USA) according to the formula: $[\text{contralateral hemisphere area} - (\text{ipsilateral hemisphere area} - \text{infarct area})] / \text{contralateral hemisphere area} \times 100\%$. Hemispheric swelling was assessed in slices stained by TTC according to the formula: $100\% \times (\text{ipsilateral volume} - \text{contralateral volume}) / \text{contralateral volume}$ [24, 25].

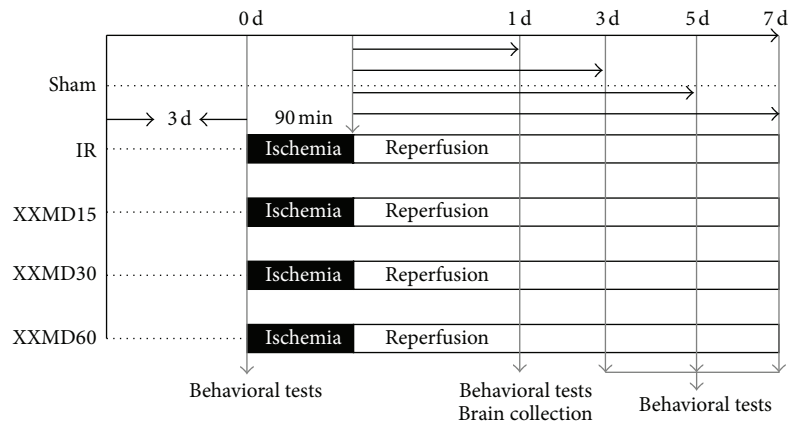


FIGURE 1: Diagram showing the experimental design of the present study. The rats ($n = 120$) were randomly divided into 5 groups. Different doses of XXMD were orally administered to rats in the XXMD-treated groups for 3 days prior to the operation until the end of the experiments. And the others were given the distilled water. The rats in the IR and XXMD-treated groups were subjected to reperfusion following 90 min of middle cerebral artery occlusion, while the rats in the sham group underwent the same surgical procedure without monofilament occlusion. Brain tissues were collected for subsequent investigations, such as TTC staining, evaluation of brain water content, BBB leakage and BBB ultrastructure changes, western blot analysis, and immunohistochemistry. In addition, behavioral tests were performed at the indicated time points.

2.6. Behavioral Observations. Cerebral ischemia and reperfusion can cause motor asymmetry. In the present study, behavioral observations involving three tests were performed by two investigators who were unaware of the animal grouping at different time points after reperfusion. Rats were gently handled and trained daily for 3 days before the operation to accustom the animals to being handled.

2.6.1. Neurological Deficit Scores. Neurological examinations were performed at 0, 1, 3, 5, and 7 days after reperfusion. The neurological deficits were assessed on a 5-point scale described by Longa et al. [22] as follows: 0 = no deficit; 1 = failure to extend left forepaw; 2 = circling to the left; 3 = falling to the left; 4 = no spontaneous walking with a depressed level of consciousness. In the study, 5 rats that underwent MCAO without any detectable neurological deficits were excluded from the following investigations and analysis to exclude operative failures.

2.6.2. Vibrissae-Elicited Forelimb Placing Test. This test was performed as previously described with slight modifications [26–28]. Briefly, when the vibrissae on each side of each rat were gently brushed against the edge of a table, they reflexively placed their forelimbs on that side onto the countertop. However, the reflex could not be induced contralateral to the ischemic injury. The reflex was tested 20 times on each side per trial, and two trials were performed per test session. If muscle tension or struggling occurred, the rats were held and stroked until they relaxed and the trial was resumed. The number of vibrissae stimulations in which a paw placement occurred was counted, and the percentage was calculated.

2.6.3. Tail Hang Test. Tail hang tests were assessed at different time points according to the method described by Zhao et al. and Borlongan et al. [27, 29] with minor modifications. Each

rat was lifted 5–10 cm above the table. An ischemia-damaged rat will immediately turn to the right side. The large right turn is accompanied by a twisting of the body and a raise of the head toward the holding hand. “Turns” were counted when the angle reached 90° or more. Smaller turns were not counted. The rat was lifted no more than 5 s on each trial and was released for a few seconds before the next trial. The test was repeated 20 times per testing day. The percentage of trials during which a right turn occurred was calculated.

2.7. Brain Water Content Measurement. Brain water content was measured with the dry-wet weight method 24 h after reperfusion. After being anesthetized, the animals were sacrificed, and the brain tissues were removed and separated into ischemic and nonischemic hemispheres, which were immediately weighed to obtain the wet weight (WW). Then the tissues were placed in an oven at 100°C for 24 h and reweighed to obtain the dry weight (DW). The brain water content was assessed with the following formula: $100\% \times (\text{WW} - \text{DW}) / \text{WW}$.

2.8. BBB Integrity. To measure BBB permeability, the Evans blue content was assessed. Briefly, 2% Evans blue solution (4 mL/kg), dissolved in normal saline, was administered intravenously at 23 h after reperfusion. The rats were deeply anesthetized 1 h later and transcardially perfused with normal saline to wash away the remaining dye in the blood vessels. Ischemic and nonischemic hemispheres were dissected and weighed. The ischemic brain tissues were placed in formamide (1 mL/100 mg) at 55°C for 24 h. Finally, the absorption of the tissue was calculated at the 620 nm wavelength with a luminescence spectrometer (Flex Station 3, Molecular Devices, Sunnyvale, CA, USA) according to the standard curve of Evans blue content, with formamide as negative control.

2.9. Ultrastructural Alterations of BBB. Transmission electron microscopy was used to determine BBB ultrastructural alterations. Rats were deeply anesthetized and transcardially perfused by normal saline followed by cold 1% glutaraldehyde/3% paraformaldehyde solution 24 h after reperfusion. The brain tissues were removed and postfixed in the above solution. Coronal sections of 1.0 m³ in volume and located 1.2 mm to 0.2 mm rostral to bregma were prepared to obtain the peri-infarct tissue of the ipsilateral cortex. The tissue was postfixed in 2% osmium for 1.5 h, dehydrated, and embedded in Epon 812 Resin (TAAB, Berks, UK). Ultrathin (0.06 μm) sections were cut with a diamond knife, stained with uranyl acetate and lead citrate, and observed with an electron microscope (H-7100S; Hitachi, Tokyo, Japan).

2.10. Western Blotting Analysis. Western blotting was used to assess the expression levels of MMP-9, MMP-2, and VEGF 24 h after cerebral ischemia and reperfusion. The ischemic hemisphere tissues were prepared in lysis buffer with protease inhibitors (Beyotime, Haimen, Jiangsu, China) and centrifuged at 13,000 ×g for 5 min. The supernatant was collected. Protein concentrations were determined with a BCA kit (Beyotime). Fifty micrograms of protein solution were separated by electrophoresis in different concentrations of polyacrylamide gel and transferred to polyvinylidene fluoride membranes (Millipore, Bedford, MA, USA). After blocking for 2 h with a 5% solution of skim milk, prepared with Tris-buffered saline with 0.1% Tween-20 (TBST), the primary antibodies polyclonal rabbit anti-MMP-9, -MMP-2, and -VEGF (all diluted 1:1000; Abcam, HK, China) were incubated with the membranes at 4°C overnight. The membranes were incubated with the secondary antibody conjugated with horseradish-peroxidase (Beyotime) after washing with TBST three times for 10 min each. The targeted antigens were detected by standard chemical luminescence methods (Beyotime) with Fluor Chem FC2 gel imaging system (Alpha Innotech, Santa Clara, CA, USA). The expression of the targeted proteins was determined by using the GAPDH protein as a loading control. Western blots were duplicated with three independent sets. Band intensities were measured with Quantity One software (Bio-Rad Laboratories, Hercules, CA, USA).

2.11. Immunohistochemistry. Immunohistochemical staining was used to evaluate whether treatment with XXMD changes the expression of MMP-9, MMP-2, and VEGF after cerebral ischemia and reperfusion. Rat brain tissues were postfixed in 4% paraformaldehyde for 24 h and then immersed in 30% sucrose solution with phosphate buffer saline (PBS, pH 7.4) for 24 h. Coronal sections (10 μm thick) at the level of the anterior commissure in the infarct region were obtained. For immunohistochemistry, sections were deparaffinized and incubated with 0.3% H₂O₂ in PBS. After blocking with 5% normal goat serum, the sections were incubated with rabbit polyclonal anti-MMP-9 antibody (diluted 1:100; Abcam), anti-MMP-2 antibody (diluted 1:300; Abcam), or anti-VEGF antibody (diluted 1:100; Abcam) at 4°C overnight. After washing in PBS, the sections were incubated with the

secondary antibody conjugated with horseradish-peroxidase (Beyotime) for 1 h at 37°C, and then visualized using 3,3'-diaminobenzidine tetrahydrochloride (DAB kit; Beyotime). The sections were photographed and observed with a light microscope (Olympus/BX51, Tokyo, Japan).

2.12. Statistical Analysis. Values are shown as the means ± standard error of the mean (SEM). Differences in quantitative data obtained from cerebral infarct area, hemispheric swelling, behavioral tests, brain water content, BBB integrity, and integrated densities of protein bands from western blots were evaluated by one-way analysis of variance (ANOVA) followed by Student's *t*-test and post hoc Fisher's tests. *P* < 0.05 was considered statistically significant. Statistical analysis was performed with SPSS version 11.5 for Windows (SPSS, Chicago, IL, USA).

3. Results

3.1. XXMD Reduced Cerebral Infarct Area and Hemispheric Swelling. Cerebral infarct area and hemispheric swelling, induced by MCAO, were evaluated through the use of TTC staining. XXMD (30 g/kg/day and 60 g/kg/day) significantly reduced both the infarct area in the territory of the middle cerebral artery and hemispheric swelling compared to the IR group (Figure 2).

3.2. XXMD Improved Neurological Function. The effects of XXMD on behavioral tests after reperfusion were studied. Compared to the IR group, the XXMD30 and XXMD60 treatment had significantly reduced neurological deficit scores at 0, 1, 3, 5, and 7 days after reperfusion (Figure 3(a)). The forelimb placing of the nonischemic hemisphere induced by vibrissae brushing was disrupted and gradually improved from 3 days to 7 days after stroke induction. However, XXMD30 and XXMD60 treatment notably decreased the number of contralateral forelimb placements from 1 to 7 days after reperfusion (Figure 3(b)). In the tail test, the percentage of large right turns was significantly attenuated in the XXMD30 and XXMD60 groups compared to the IR group (Figure 3(c)). Thus, these results indicated that XXMD improved neurological function and motor asymmetry induced by ischemia and reperfusion.

3.3. XXMD Reduced Brain Water Content and BBB Disruption. Brain water content and Evans blue content were evaluated 24 h after reperfusion. The brains of rats administered XXMD (60 g/kg/day) had a lower water content than those of the IR group. The nonischemic hemispheres were not significantly different between groups. The Evans blue content results were similar to those of the brain water content. BBB disruption occurred and was remarkably increased 24 h after reperfusion. XXMD treatment (60 g/kg/day) significantly decreased Evans blue content compared with the IR group (3.99 ± 0.67 μg/g tissue versus 7.89 ± 0.68 μg/g tissue) in the ischemic hemisphere. However, there were no significant differences between the nonischemic hemispheres of different groups (Figure 4).

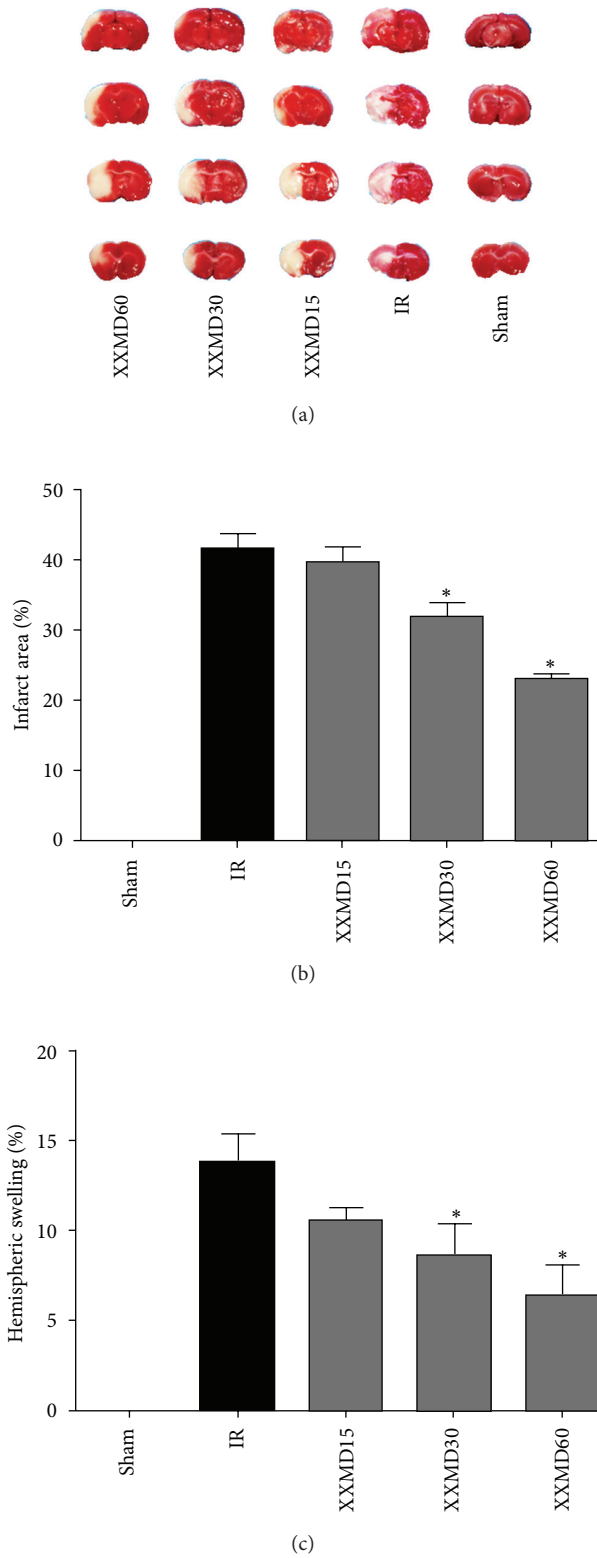


FIGURE 2: Effects of XXMD on cerebral infarct area and hemispheric swelling 24 h after reperfusion. (a) Representative images of TTC-stained brain slices. (b) The quantitative analysis of cerebral infarct area. (c) The quantitative analysis of hemispheric swelling. The images indicated that XXMD remarkably reduced cerebral infarct area and hemispheric swelling. Data are reported as the mean \pm SEM, $n = 4$ for each group. * $P < 0.05$ versus the IR group.

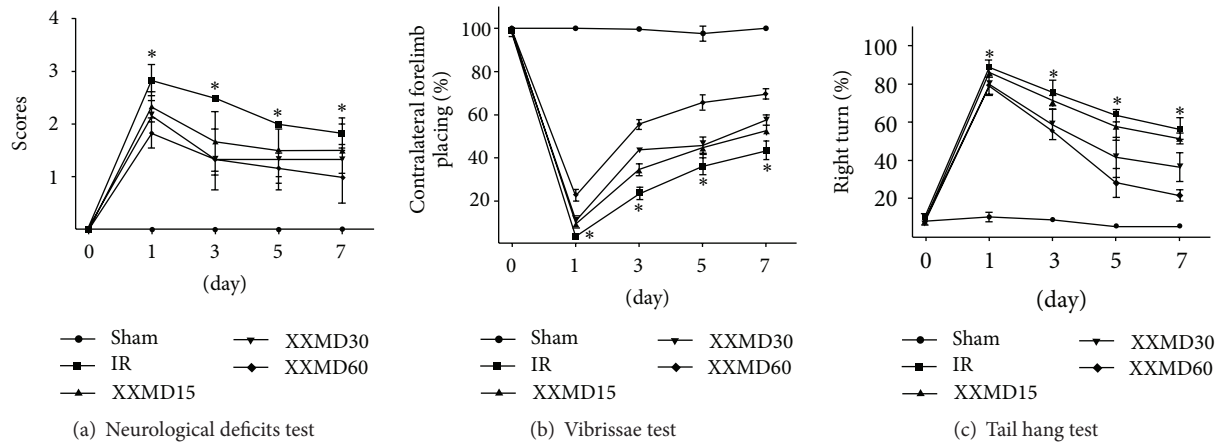


FIGURE 3: The behavioral tests of the 5 groups at different time points. (a) The neurological deficits test. (b) The vibrissae test. (c) The tail hang test. The results indicated that XXMD significantly improved neurological function in injured rats. Data represent the mean \pm SEM, $n = 4-5$ for each group. * $P < 0.05$ versus the XXMD30 and XXMD60 groups.

3.4. XXMD Attenuated the Changes in the BBB Ultrastructure. Transmission electron microscopy was used to detect BBB ultrastructural alterations. The cortical microvessels in the sham group were normal, with a continuous basal lamina, regular endothelial cells, and astrocyte endfeet. However, a series of changes indicative of BBB disruption were observed in the IR group. For example, the capillary lumen was deflated and edema was easily detected around the capillary. In addition, astrocyte endfeet surrounding the capillaries appeared markedly swollen, and some showed vacuolar changes. The tight junctions between endothelial cells were unclear, and swollen Golgi complexes were observed. These damages were alleviated in the XXMD60 group; the integrity of the capillary endothelium was almost normal with a regular capillary lumen and continuous base membrane. Furthermore, the edema around the capillary and the swelling of astrocyte foot processes were decreased (Figure 5).

3.5. XXMD Downregulated the Expression of MMP-9, MMP-2, and VEGF. Western blotting was used to investigate the expression levels of MMP-9, MMP-2, and VEGF 24 h after reperfusion. The results and subsequent analysis of the western blots showed that MMP-9, MMP-2, and VEGF were increased after ischemia and reperfusion. However, XXMD treatment (30 and 60 g/kg/day) blocked the increases in MMP-9, MMP-2, and VEGF expressions (Figure 6), suggesting that reducing the increased levels of these proteins may be one of the mechanisms underlying the neuroprotection of XXMD against BBB disruption and ischemic injury.

3.6. XXMD Reduced the Distribution of MMP-9, MMP-2, and VEGF. The next experiments were used to study the distribution of MMP-9, MMP-2, and VEGF in the ischemic cortex by immunohistochemistry. Extensive ischemic damage was evident in these regions. In the sham group, there was almost no MMP-9 immunostaining in the cortex. However, in the IR group, it was intense and mainly localized to the cytoplasm of neurons and glial cells, though cerebral

vessels were also notably stained. Most cells showed ischemic changes. However, MMP-9 staining was less intense in the XXMD60 group compared with the IR group (Figure 7(a)).

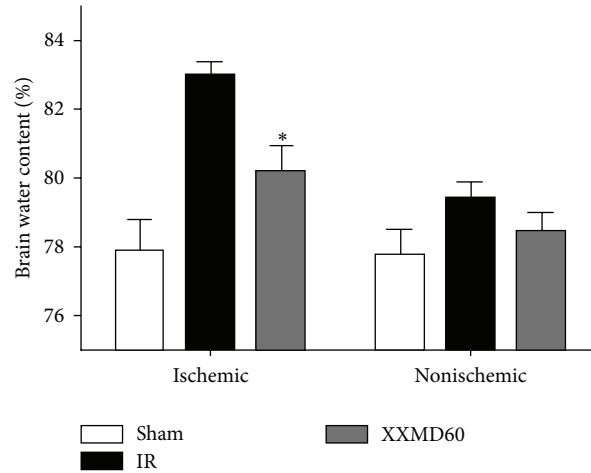
The MMP-2 immunostaining results were similar to those of MMP-9. In the sham groups, MMP-2 immunostaining was mainly localized to the cytoplasm of a few glial cells and to neurons with normal morphological appearance. Twenty-four hours after reperfusion, MMP-2 immunostaining was increased and many neurons in the ischemic cortex showed ischemic changes, such as shrinkage of the nucleus and cytoplasm, in an area in which many ischemic neurons, glial cells, and cerebral vessels were clearly stained. Although MMP-2 staining was intense in the XXMD60 group, the extent was reduced compared to that of the IR group, and the majority of positive cells were glial cells and neurons, the number of which was less than the IR group (Figure 7(b)).

VEGF immunostaining was absent in the sham rat cortex. However, in the IR group, VEGF immunostaining was increased and intensely located in ischemic cerebral vessels, neurons, and reactive astrocytes. VEGF immunostaining was weaker in the XXMD60 group than in the IR group (Figure 7(c)).

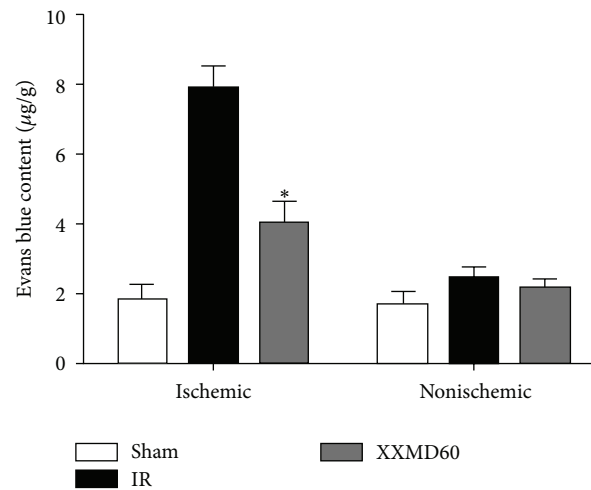
4. Discussion

In the present study, we demonstrated that XXMD treatment significantly attenuated neurological injury induced by cerebral ischemia and reperfusion. XXMD reduced the cerebral infarct area and hemispheric swelling and improved behavioral function. Furthermore, the data showed that XXMD treatment attenuated BBB disruption, which may be associated with the downregulation of the expression of MMP-9, MMP-2, and VEGF. XXMD may protect against cerebral ischemia and reperfusion injury by reducing the levels of these proteins.

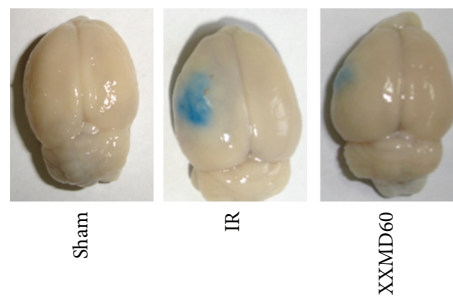
BBB, which is essential for the function of the central nervous system, plays an important role in the maintenance of homeostasis [30]. BBB disruption is induced at the onset



(a)



(b)



(c)

FIGURE 4: Brain water content and Evans blue content 24 h after reperfusion. (a) The quantitative analysis of brain water content. (b) The quantitative analysis of Evans blue content. (c) Representative images of Evans blue extravasation. The results indicated that XXMD (60 g/kg/day) treatment attenuated the increase in brain water content and Evans blue content induced by cerebral ischemia and reperfusion. Data are reported as the mean \pm SEM, $n = 4$ for each group. * $P < 0.05$ versus the IR group.

of cerebral ischemia and reperfusion. When BBB breakdown occurs, many serum proteins that are detrimental to neurons pass through the barrier, further worsening brain injury. The data of the present study consistently indicated that Evans blue content, as an indicator of BBB permeability,

distinctly increased and that brain edema rapidly formed at the early stage of ischemia and reperfusion injury. These events were significantly blocked by XXMD treatment. The crucial components of the BBB, such as astrocytes and basement membranes, and the primary barrier, which is

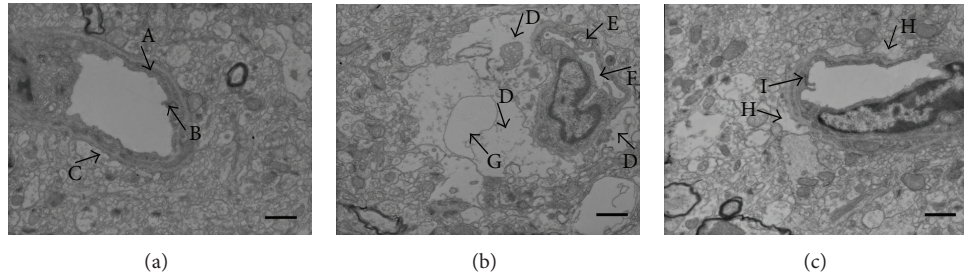


FIGURE 5: The ultrastructural variations of the BBB 24 h after reperfusion. (a) The ultrastructure of the BBB in the sham group. Strong integrity of the basement membrane (A), a clear tight junction (B), and normal astrocyte endfeet (C) were observed. (b) The ultrastructure of the BBB in the IR group. The edema around the capillary was marked in the IR group, the astrocyte endfeet surrounding the capillaries were swollen (D), and some endfeet showed vacuolar changes. Moreover, the Golgi complex was swollen (E), the capillary lumen was shrunk (F), and the tight junction could not be observed in the images. (c) The ultrastructure of the BBB in the XXMD60 group. The edema was mitigated (H) and a regular capillary lumen, continuous base membrane, and clear tight junction (I) could be found. $n = 4$ for each group. Scale bar = $1 \mu\text{m}$.

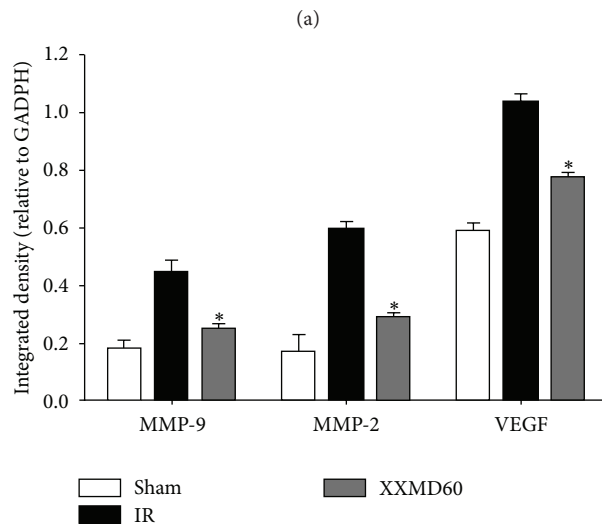
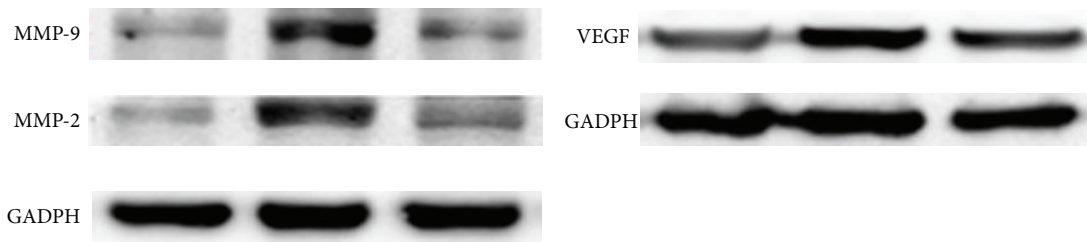


FIGURE 6: Effects of XXMD on MMP-9, MMP-2, and VEGF expressions 24 h after reperfusion. (a) Representative protein bands from western blotting for MMP-9, -2, and VEGF in the penumbra of the ischemic cortex. (b) Integrated density for MMP-9,-2, and VEGF. The expression levels of MMP-9, MMP-2, and VEGF under XXMD treatment were significantly reduced compared to the IR group. Data are reported as the mean \pm SEM, $n = 3$ for each group. * $P < 0.05$ versus the IR group.

formed by endothelia cells in capillaries, contribute to the integrity and physical function of the BBB [31]. However, a series of changes rapidly occur after reperfusion. The transmission electron microscope images showed marked edema of astrocyte endfeet and crushed microvessels, changes that

eventually lead to microcirculation dysfunction. XXMD treatment substantially alleviated the morphological changes and blocked the decrease in brain blood flow. Therefore, we conclude that XXMD protected against disruption to both the structure and function of the BBB.

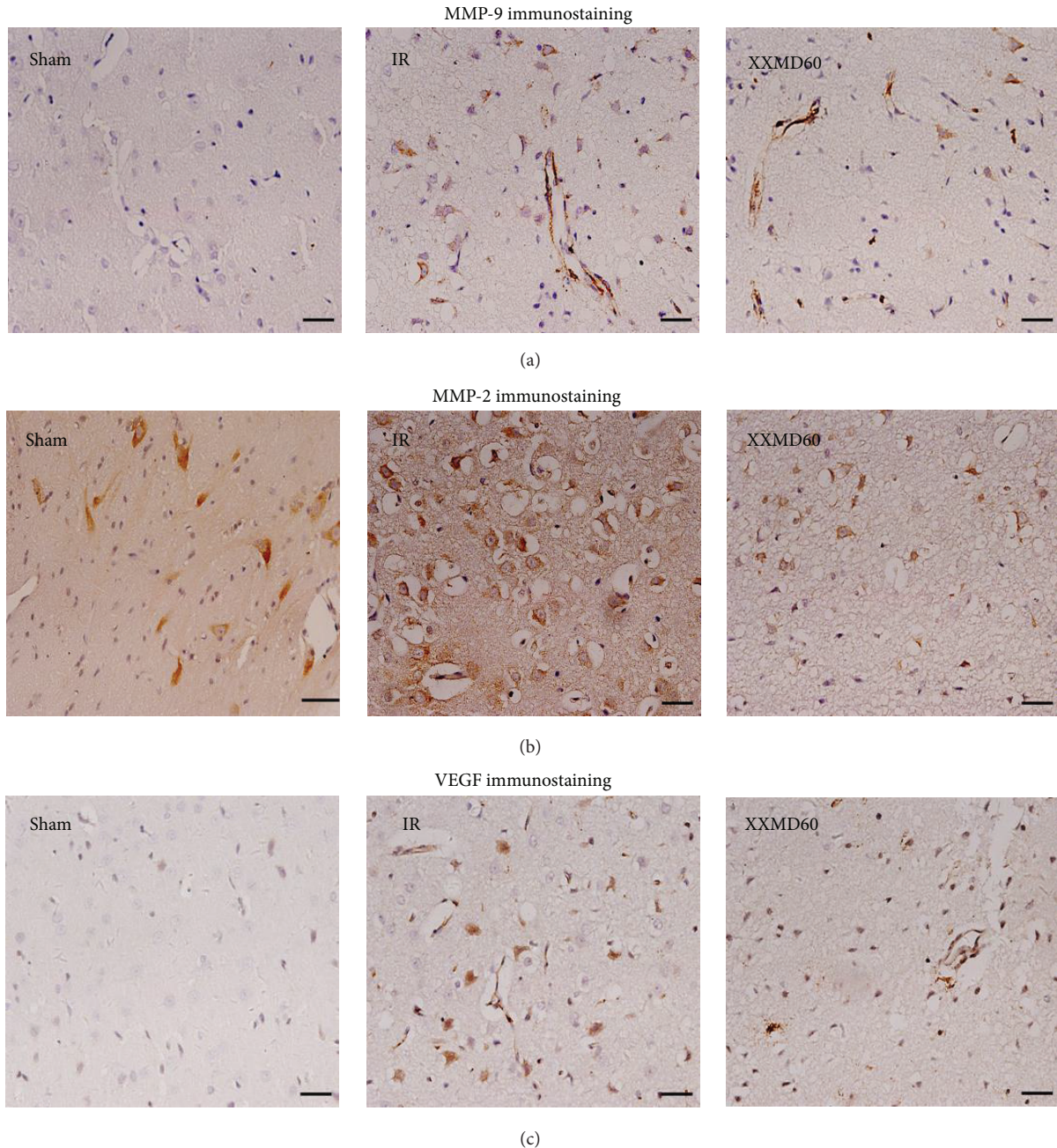


FIGURE 7: MMP-9, MMP-2, and VEGF immunohistochemistry in the ischemic cortex 24 h after reperfusion. (a) Representative images of MMP-9 immunohistochemistry in different groups. The images showed intense staining of neurons, glial cells, and cerebral vessels after ischemia and reperfusion. However, there were fewer stained neurons and glial cells in the XXMD60 group than in the IR group. (b) Representative images of MMP-2 immunohistochemistry. In the sham group, there was less staining in the cortex. MMP-2 immunostaining was enhanced 24 h after reperfusion in the IR group. The intensity of the MMP-2 staining was reduced in the XXMD60 group, with only a small number of strongly stained neurons and astrocytes. (c) Representative images of VEGF immunohistochemistry. There was almost no staining in the cortex in the sham group. VEGF immunostaining was intensely increased in ischemic cerebral vessels, neurons and reactive astrocytes in the IR group. In the XXMD treatment groups, VEGF immunostaining was reduced in intensity with a similar pattern for cell bodies and processes as in the IR group. $n = 6$, scale bar = $20 \mu\text{m}$.

Following reperfusion, MMPs and free radicals that may mediate the attack on the capillaries are released [10, 31]. The increase in MMP-9 and -2 degrades tight junction proteins that strengthen the endothelial cell wall and form the endothelial barrier. Degradation of these proteins results

in BBB disruption, further vasogenic edema formation, and neuronal damage in stroke with reperfusion [10, 32, 33].

Angiogenesis is a potent process in stroke. VEGF, a substantial mediator of angiogenesis, plays bidirectional roles in different stages of cerebral ischemia and reperfusion.

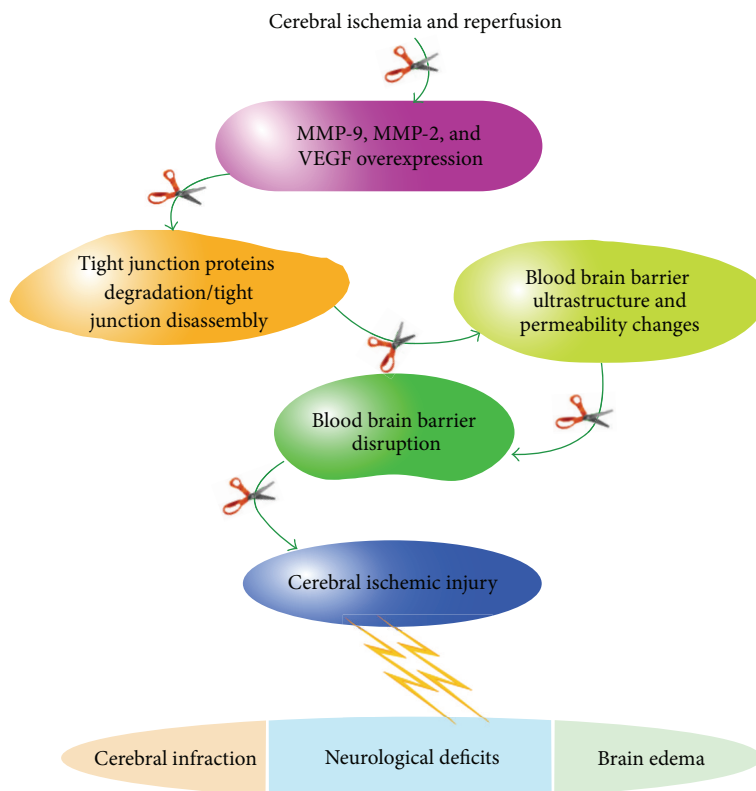


FIGURE 8: The mechanisms underlying the neuroprotection of XXMD against BBB disruption and ischemic injury induced by focal cerebral ischemia and reperfusion. Briefly, focal cerebral ischemia and reperfusion resulted in increase in MMP-9, MMP-2, and VEGF at the early stage of cerebral ischemia and reperfusion, which degraded the tight junction proteins or led to tight junction disassembly, further caused changes to the BBB ultrastructure and increased BBB permeability. Eventually, these alterations led to BBB disruption and ischemic injury, which includes cerebral infarction, neurological deficits, and brain edema. Interestingly, XXMD administration notably downregulated the expression levels of MMP-9, -2, and VEGF, further enhanced the tight junction and minimized BBB ultrastructure and permeability changes. As a result, XXMD administration inhibited BBB disruption and alleviated ischemic injury. The open scissors indicate the effects of XXMD treatment on cerebral injury following stroke and reperfusion.

It markedly enhances angiogenesis and reduces neurological deficits during the recovery stage [34, 35]. However, it not only increases BBB permeability and the incidence of hemorrhagic transformation but also aggravates secondary ischemic insults at the acute stage of stroke [36, 37]. Like MMP-9 and -2, VEGF increases the permeability of the BBB due to tight junction disassembly [38].

Mounting evidence indicates that VEGF upregulates the releases and expressions of MMP-9 and -2 [39–42]. In the current study, we studied the expression levels and distribution of MMP-9, MMP-2, and VEGF at the same time point as for Evans blue leakage. The data showed that MMP-9, MMP-2, and VEGF proteins were upregulated and markedly expressed by neurons, astrocytes, and cerebral vessels 24 h after reperfusion. XXMD treatment significantly inhibited the expressions of MMP-9, MMP-2, and VEGF. These results support the view that MMP-9, MMP-2, and VEGF are involved in the BBB breakdown after cerebral ischemia and reperfusion. Thus, the data further suggested that XXMD preserved BBB integrity after reperfusion which may be partly through blocking MMP-9, MMP-2 and VEGF expressions (Figure 8).

In conclusion, the current study demonstrated that XXMD, as a drug of multiple targets, improved neurological function and exerted a protective effect on the BBB by downregulation of MMP-9, -2, and VEGF after cerebral ischemia and reperfusion injury.

Acknowledgment

This work was supported by the National Natural Science Foundation of China (Grants no. 81173389 and no. 81202813).

References

- [1] G. Z. Del, "Stroke and neurovascular protection," *The New England Journal of Medicine*, vol. 354, no. 6, pp. 553–555, 2006.
- [2] E. H. Lo, T. Dalkara, and M. A. Moskowitz, "Mechanisms, challenges and opportunities in stroke," *Nature Reviews Neuroscience*, vol. 4, no. 5, pp. 399–415, 2003.
- [3] J. Lok, P. Gupta, S. Guo et al., "Cell-cell signaling in the neurovascular unit," *Neurochemical Research*, vol. 32, no. 12, pp. 2032–2045, 2007.

- [4] P. Ballabh, A. Braun, and M. Nedergaard, "The blood-brain barrier: an overview: structure, regulation, and clinical implications," *Neurobiology of Disease*, vol. 16, no. 1, pp. 1–13, 2004.
- [5] T. Kuroiwa, P. Ting, H. Martinez, and I. Klatzo, "The biphasic opening of the blood-brain barrier to proteins following temporary middle cerebral artery occlusion," *Acta Neuropathologica*, vol. 68, no. 2, pp. 122–129, 1985.
- [6] L. Belayev, R. Busto, W. Zhao, and M. D. Ginsberg, "Quantitative evaluation of blood-brain barrier permeability following middle cerebral artery occlusion in rats," *Brain Research*, vol. 739, no. 1-2, pp. 88–96, 1996.
- [7] G. A. Rosenberg, "Matrix metalloproteinases and their multiple roles in neurodegenerative diseases," *The Lancet Neurology*, vol. 8, no. 2, pp. 205–216, 2009.
- [8] V. Lucivero, M. Prontera, D. M. Mezzapesa et al., "Different roles of matrix metalloproteinases-2 and -9 after human ischaemic stroke," *Neurological Sciences*, vol. 28, no. 4, pp. 165–170, 2007.
- [9] J. Montaner, J. Alvarez-Sabín, C. A. Molina et al., "Matrix metalloproteinase expression is related to hemorrhagic transformation after cardioembolic stroke," *Stroke*, vol. 32, no. 12, pp. 2762–2767, 2001.
- [10] G. A. Rosenberg, E. Y. Estrada, and J. E. Dencoff, "Matrix metalloproteinases and TIMPs are associated with blood-brain barrier opening after reperfusion in rat brain," *Stroke*, vol. 29, no. 10, pp. 2189–2195, 1998.
- [11] A. T. Argaw, L. Asp, J. Zhang et al., "Astrocyte-derived VEGF-A drives blood-brain barrier disruption in CNS inflammatory disease," *Journal of Clinical Investigation*, vol. 122, no. 7, pp. 2454–2468, 2012.
- [12] Z. G. Zhang, L. Zhang, Q. Jiang et al., "VEGF enhances angiogenesis and promotes blood-brain barrier leakage in the ischemic brain," *Journal of Clinical Investigation*, vol. 106, no. 7, pp. 829–838, 2000.
- [13] Y. Chiba, T. S. S. Miyake, J. Koyama, T. Kondoh, K. Hosoda, and E. Kohmura, "Anti-VEGF receptor antagonist (VGA1155) reduces infarction in rat permanent focal brain ischemia," *Kobe Journal of Medical Sciences*, vol. 54, no. 2, pp. E136–E146, 2008.
- [14] O. Z. Chi, C. Hunter, X. Liu, and H. R. Weiss, "Effects of anti-VEGF antibody on blood-brain barrier disruption in focal cerebral ischemia," *Experimental Neurology*, vol. 204, no. 1, pp. 283–287, 2007.
- [15] J. Koyama, S. Miyake, T. Sasayama, Y. Chiba, T. Kondoh, and E. Kohmura, "The novel VEGF receptor antagonist, VGA1155, reduces edema, decreases infarct and improves neurological function after stroke in rats," *Kobe Journal of Medical Sciences*, vol. 56, no. 1, pp. 1–11, 2010.
- [16] K. Du, C. Wu, C. Ding, S. Zhao, H. Qin, and J. Zhang, "Simultaneous LC-MS analysis and of wogonin and oroxylin a in rat plasma, and pharmacokinetic studies after administration of the active fraction from *Xiao-Xu-Ming* decoction," *Chromatographia*, vol. 69, no. 11-12, pp. 1259–1266, 2009.
- [17] Y. Wang, C. Ding, K. Du et al., "Identification of active compounds and their metabolites by high-performance liquid chromatography/electrospray ionization Fourier transform ion cyclotron resonance mass spectrometry from *Xiao-Xu-Ming* decoction (XXMD)," *Rapid Communications in Mass Spectrometry*, vol. 23, no. 17, pp. 2724–2732, 2009.
- [18] Z. Li, K. Ni, and G. Du, "Simultaneous analysis of six effective components in the anti-Alzheimer's disease effective component group of *Xiao-Xu-Ming* decoction," *Chinese Journal of Chromatography*, vol. 25, no. 1, pp. 80–83, 2007 (Chinese).
- [19] D. F. Cai, Y. K. Yang, and X. X. Gu, "Clinical trial on treatment of acute cerebral infarction with TCM treatment according to syndrome differentiation combining Western medicine by staging," *Chinese Journal of Integrated Traditional and Western Medicine*, vol. 27, no. 9, pp. 789–792, 2007.
- [20] X. M. Shi, D. F. Cai, W. Dai et al., "Effect of QFTL TCP on endothelin and gene expression in acute cerebral ischemia," *China Journal of Modern Medicine*, vol. 13, no. 5, pp. 6–9, 2003.
- [21] X. H. Zhu, S. J. Li, H. H. Hu, L. R. Sun, M. Das, and T. M. Gao, "Neuroprotective effects of *Xiao-Xu-Ming* decoction against ischemic neuronal injury in vivo and in vitro," *Journal of Ethnopharmacology*, vol. 127, no. 1, pp. 38–46, 2010.
- [22] E. Z. Longa, P. R. Weinstein, S. Carlson, and R. Cummins, "Reversible middle cerebral artery occlusion without craniectomy in rats," *Stroke*, vol. 20, no. 1, pp. 84–91, 1989.
- [23] M. R. Bigdeli, S. Hajizadeh, M. Froozandeh, B. Rasulian, A. Heidarianpour, and A. Khoshbaten, "Prolonged and intermittent normobaric hyperoxia induce different degrees of ischemic tolerance in rat brain tissue," *Brain Research*, vol. 1152, no. 1, pp. 228–233, 2007.
- [24] Z. Huang, P. L. Huang, N. Panahian, T. Dalkara, M. C. Fishman, and M. A. Moskowitz, "Effects of cerebral ischemia in mice deficient in neuronal nitric oxide synthase," *Science*, vol. 265, no. 5180, pp. 1883–1885, 1994.
- [25] S.-Y. Li, D. Yang, Z. J. Fu, T. Woo, D. Wong, and A. C. Y. Lo, "Lutein enhances survival and reduces neuronal damage in a mouse model of ischemic stroke," *Neurobiology of Disease*, vol. 45, no. 1, pp. 624–632, 2012.
- [26] T. Schallert, S. M. Fleming, J. L. Leasure, J. L. Tillerson, and S. T. Bland, "CNS plasticity and assessment of forelimb sensorimotor outcome in unilateral rat models of stroke, cortical ablation, parkinsonism and spinal cord injury," *Neuropharmacology*, vol. 39, no. 5, pp. 777–787, 2000.
- [27] H. Zhao, T. Shimohata, J. Q. Wang et al., "Akt contributes to neuroprotection by hypothermia against cerebral ischemia in rats," *Journal of Neuroscience*, vol. 25, no. 42, pp. 9794–9806, 2005.
- [28] X. Gao, H. Zhang, T. Takahashi et al., "The Akt signaling pathway contributes to postconditioning's protection against stroke; the protection is associated with the MAPK and PKC pathways," *Journal of Neurochemistry*, vol. 105, no. 3, pp. 943–955, 2008.
- [29] C. V. Borlongan, Y. Tajima, J. Q. Trojanowski, V. M. Y. Lee, and P. R. Sanberg, "Transplantation of cryopreserved human embryonal carcinoma-derived neurons (NT2N cells) promotes functional recovery in ischemic rats," *Experimental Neurology*, vol. 149, no. 2, pp. 310–321, 1998.
- [30] B. T. Hawkins and T. P. Davis, "The blood-brain barrier/neurovascular unit in health and disease," *Pharmacological Reviews*, vol. 57, no. 2, pp. 173–185, 2005.
- [31] H. H. Ji, W. H. Sang, and S. K. Lee, "Free radicals as triggers of brain edema formation after stroke," *Free Radical Biology and Medicine*, vol. 39, no. 1, pp. 51–70, 2005.
- [32] J. Liu, X. Jin, K. J. Liu, and W. Liu, "Matrix metalloproteinase-2-mediated occludin degradation and caveolin-1-mediated claudin-5 redistribution contribute to blood-brain barrier damage in early ischemic stroke stage," *Journal of Neuroscience*, vol. 32, no. 9, pp. 3044–3057, 2012.
- [33] Y. Yang and G. A. Rosenberg, "MMP-mediated disruption of claudin-5 in the blood-brain barrier of rat brain after cerebral ischemia," *Methods in Molecular Biology*, vol. 762, pp. 333–345, 2011.

- [34] J. P. Yang, H. J. Liu, and X. F. Liu, "VEGF promotes angiogenesis and functional recovery in stroke rats," *Journal of Investigative Surgery*, vol. 23, no. 3, pp. 149–155, 2010.
- [35] Y. Q. Wang, H. R. Cui, S. Z. Yang et al., "VEGF enhance cortical newborn neurons and their neurite development in adult rat brain after cerebral ischemia," *Neurochemistry International*, vol. 55, no. 7, pp. 629–636, 2009.
- [36] Z. Li, R. Wang, S. Li et al., "Intraventricular pre-treatment with rAAV-VEGF induces intracranial hypertension and aggravates ischemic injury at the early stage of transient focal cerebral ischemia in rats," *Neurological Research*, vol. 30, no. 8, pp. 868–875, 2008.
- [37] O. Z. Chi, C. Hunter, X. Liu, and H. R. Weiss, "Effects of deferoxamine on blood-brain barrier disruption and VEGF in focal cerebral ischemia," *Neurological Research*, vol. 30, no. 3, pp. 288–293, 2008.
- [38] W. Wang, W. L. Dentler, and R. T. Borchardt, "VEGF increases BMEC monolayer permeability by affecting occludin expression and tight junction assembly," *The American Journal of Physiology*, vol. 280, no. 1, pp. H434–H440, 2001.
- [39] H. Wang and J. A. Keiser, "Vascular endothelial growth factor upregulates the expression of matrix metalloproteinases in vascular smooth muscle cells: role of flt-1," *Circulation Research*, vol. 83, no. 8, pp. 832–840, 1998.
- [40] W. J. Lamoreaux, M. E. C. Fitzgerald, A. Reiner, K. A. Hasty, and S. T. Charles, "Vascular endothelial growth factor increases release of gelatinase A and decreases release of tissue inhibitor of metalloproteinases by microvascular endothelial cells in vitro," *Microvascular Research*, vol. 55, no. 1, pp. 29–42, 1998.
- [41] H. K. Rooprai, G. J. Rucklidge, C. Panou, and G. J. Pilkington, "The effects of exogenous growth factors on matrix metalloproteinase secretion by human brain tumour cells," *British Journal of Cancer*, vol. 82, no. 1, pp. 52–55, 2000.
- [42] S. Valable, J. Montaner, A. Bellail et al., "VEGF-induced BBB permeability is associated with an MMP-9 activity increase in cerebral ischemia: both effects decreased by Ang-1," *Journal of Cerebral Blood Flow and Metabolism*, vol. 25, no. 11, pp. 1491–1504, 2005.

Research Article

A Systematic, Integrated Study on the Neuroprotective Effects of Hydroxysafflor Yellow A Revealed by ^1H NMR-Based Metabonomics and the NF- κB Pathway

Yuanyan Liu,^{1,2} Zeqin Lian,¹ Haibo Zhu,¹ Yinghong Wang,¹ Shishan Yu,¹ Tingting Chen,¹ Jing Qu,¹ Jianbei Li,¹ Shuanggang Ma,¹ and Xianhong Chen¹

¹ State Key Laboratory of Bioactive Substance and Function of Natural Medicines, Institute of Materia Medica, Chinese Academy of Medical Sciences and Peking Union Medical College, Beijing 100050, China

² School of Chinese Materia Medica, Beijing University of Chinese Medicine, Beijing 100102, China

Correspondence should be addressed to Yinghong Wang; wyh@imm.ac.cn and Shishan Yu; yushishan@imm.ac.cn

Received 5 February 2013; Accepted 2 March 2013

Academic Editor: Aiping Lu

Copyright © 2013 Yuanyan Liu et al. This is an open access article distributed under the Creative Commons Attribution License, which permits unrestricted use, distribution, and reproduction in any medium, provided the original work is properly cited.

Hydroxysafflor yellow A (HSYA) is the main active component of the Chinese herb *Carthamus tinctorius* L.. Purified HSYA is used as a neuroprotective agent to prevent cerebral ischemia. Injectable safflor yellow (50 mg, containing 35 mg HSYA) is widely used to treat patients with ischemic cardiocerebrovascular disease. However, it is unknown how HSYA exerts a protective effect on cerebral ischemia at the molecular level. A systematical integrated study, including histopathological examination, neurological evaluation, blood-brain barrier (BBB), metabonomics, and the nuclear factor- κB (NF- κB) pathway, was applied to elucidate the pathophysiological mechanisms of HSYA neuroprotection at the molecular level. HSYA could travel across the BBB, significantly reducing the infarct volume and improving the neurological functions of rats with ischemia. Treatment with HSYA could lead to relative corrections of the impaired metabolic pathways through energy metabolism disruption, excitatory amino acid toxicity, oxidative stress, and membrane disruption revealed by ^1H NMR-based metabonomics. Meanwhile, HSYA treatment inhibits the NF- κB pathway via suppressing proinflammatory cytokine expression and p65 translocation and binding activity while upregulating an anti-inflammatory cytokine.

1. Introduction

Stroke is one of the leading causes of adult disability and death in developing countries. Vascular cognitive impairment is recognized as a widespread and preventable syndrome [1]. With the increasingly rapid aging process, cerebrovascular disease, such as stroke, is a very important public health and societal problem. The flower of the safflower plant, *Carthamus tinctorius* L., and its extracts have been extensively used in traditional Chinese medicine for the treatment of cerebrovascular and cardiovascular diseases [2]. Previous work has indicated that HSYA, the main chemical component of the safflower yellow pigment, can antagonize binding of the platelet activating factor to its receptor [3], produce antihypotensive and antithrombotic effects, inhibit platelet aggregation [4], and exhibit neuroprotective effects after

permanent middle cerebral artery occlusion (pMCAO) in rats [5, 6]. Injectable safflor yellow (50 mg, containing 35 mg HSYA) has been widely used in Chinese medicine, and it was approved as a new drug by the State Food and Drug Administration (SFDA) for treating patients with ischemic cardiocerebrovascular disease in 2005. Moreover, a second clinical study of HSYA has been approved by the China SFDA for the treatment of diseases of blood vessels in the brain. The subchronic toxicity study of HSYA indicated that it is generally well tolerated [7].

In cerebral ischemia, there is ample evidence for the activation of the NF- κB [8, 9]. NF- κB induces the expression of both proinflammatory genes and genes related to apoptosis [10]. In peripheral cells, NF- κB is crucial for inflammation reactions [11] but increases excitotoxic damage in the hippocampus [12]. Although it has been established that

inflammation contributes to cerebral ischemic injury and that HSYA is an effective neuroprotectant, it is not known how HSYA exerts a protective effect at the molecular level and if it can travel across the BBB. It is also not known if NF- κ B is altered or if the inflammatory factors are affected in order to achieve neuroprotection.

Metabonomics is a well-established field in systems biology [13] and has been applied to observe meaningful and relevant biochemical changes due to disease, toxicity, nutrition, and other variables [14]. It is an important methodology for measuring the relative concentrations of endogenous small molecules in biofluids and characterizing changes in the metabolites in organisms [15]. Nuclear magnetic resonance spectroscopy (NMR) and high-performance liquid chromatography coupled with multistage tandem mass spectrometry (HPLC-MSⁿ) have been used to study such changes, allowing for metabolite screening to be performed over a wide range of concentration [9, 13]. Metabonomics studies can provide invaluable information towards understanding molecular mechanisms and novel insights into the status of dysfunction in biological systems.

In this study, the effect of HSYA on the infarct volume and neurological score of rats with focal cerebral ischemic injury was investigated. Specifically, an HPLC-MSⁿ method was developed for detecting HSYA transport across the BBB in different rat brain tissues after intravenous injection. Furthermore, a metabonomics method was employed to characterize the metabolic profile associated with MCAO-induced cerebral ischemia and observe the protective effects of HSYA in brain tissue. The metabolic disturbance was studied using high-resolution magic-angle spinning (HR MAS) NMR spectroscopy combined with pattern recognition methods. Based on the previous studies, the role of HSYA in the NF- κ B pathway after pMCAO was investigated.

2. Materials and Methods

2.1. Animals. Male Sprague-Dawley (SD) rats, 12 weeks old, weighing 280–290 g were housed in an environmentally controlled room and food and water ad libitum. The rats underwent permanent MCAO as described in Supplementary Materials (MCAO model construction) available online at <http://dx.doi.org/10.1155/2013/147362> [16]. All protocols in this study were approved by the Medical Ethic Committee of Peking Union Medical College and were in accordance with National Institutes of Health regulations for the care and use of animals in research.

2.2. Drug Administration. The *Carthamus tinctorius* samples were purchased from the Beijing Tongrentang Medicine Corporation Ltd. (Beijing, China). HSYA was isolated and purified in our laboratory and confirmed by HRMSⁿ and ¹H, ¹³C NMR (purity > 98%, HPLC). HSYA was dissolved in normal saline and administered intravenously (i.v.) at doses of 10 mg/kg (pretreated), 10 mg/kg (posttreated), 50 mg/kg (posttreated), and 10 mg/kg (5 times posttreated). Pyrrolidine dithiocarbamate ammonium salt (PDTC, Sigma), a potent

NF- κ B suppressor [17], followed the same dosage regimen as HSYA to be compared to each other at equal pace. Normal control and the sham-operation animals received vehicle in the same manner as the drug-treated group.

2.3. Samples. After animal sacrificed, brains were rapidly removed and immersed in chilled artificial cerebrospinal fluid (118 mM NaCl, 4.8 mM KCl, 2.0 mM CaCl₂, 1.2 mM MgSO₄, 25.0 mM NaHCO₃, and 12.0 mM KH₂PO₄). The brain was sectioned into 3 mm coronal slices and targeted brain regions were dissected. All samples were snap-frozen in liquid nitrogen and stored at –80°C. The remaining tissues from the coronal slices were stored in formalin solution (0.026 mM NaH₂PO₄, 0.042 mM Na₂HPO₄, 1.322 mM NaCl, and 9% formaldehyde) for histologic stained.

20–50 mg frozen tissue samples was homogenized at 1000 rpm in 6 min in mixed solvent (CH₃CN : H₂O = 1 : 1). The supernatants were removed and dried under a stream of nitrogen before lyophilizing.

2.4. HPLC-MSⁿ Analyses. An Agilent 1100 Series liquid chromatography system was utilized. HPLC separation was carried on an Agilent Zorbax SB-C₁₈ column (2.1 × 150 mm, 5 μm) with a Phenomenex C₁₈ guard column (4 × 20 mm, 5 μm); the column was set at 35°C. The mobile phase was acetonitrile, 0.1% formic acid water (8 : 92, v/v). The flow rate was 0.4 mL/min, and the effluent was monitored at 275, 320, and 400 nm.

The ESI-MSⁿ experiment was performed on an Agilent 1100 Series LC/MSD Trap mass spectrometer (Santa Clara, CA, USA). The ESI conditions were as follows: HV capillary voltage 3.5 kV, drying temperature 350°C, drying gas (N₂) 9.0 L/min, nebulizer gas (N₂) 50 psi, and capillary exit voltage –124.8 V (negative). The function of smart fragmentation was set on (Smart Frag Ampl was 30%–200%).

2.5. ¹H NMR Spectroscopy. Lyophilized brain tissue extracts weighing 40–80 μg were reconstituted in 50 μL of D₂O containing 0.1% sodium 3-trimethylsilyl-2,2,3,3-d₄-propionate (TSP, an internal standard, δ 0.0 ppm), and 40 μL of each supernatant was transferred to narrow-mouth 4 mm rotors (Varian Inc., America). ¹H-NMR spectra of liver tissues were recorded using the Carr-Purcell-Meiboom-Gill (CPMG) pulse sequence, with 256 transients, a spin-echo delay (τ) of 400 μs, and a total spin-spin relaxation delay (2nτ) of 100 ms. The data were acquired with 128 scans and a spectral width of 8000 Hz and digitized into 64 K data points by a nano probe on a Varian INOVA-500 spectrometer (Varian Inc., America) operating at a proton frequency of 500.13 MHz. The samples were spun at 2–3 KHz and maintained at 300 K throughout the experiment. The FIDs were weighted by an exponential function with a 0.3 Hz line-broadening factor prior to Fourier transformation. Spectra were manually rephased, and the baseline was corrected before reducing the data.

The biochemical data were expressed as the mean ± SD of five rats per group. Statistical analysis was performed using a one-way ANOVA. A calculated *P* value of less than 0.05 was considered statistically significant.

2.6. Data Analysis. The acquired NMR spectra were referenced to the chemical shift of TSP. Following phase and baseline correction, the $^1\text{H-NMR}$ spectra were automatically reduced to ASCII files using VNMR software (Varian, Inc.). The spectra were divided into 800 segments, each of 0.005 ppm wide, over a spectral window ranging from 0.5 to 4.5 ppm. The generated ASCII files were imported into Microsoft EXCEL for the addition of labels and then imported into SIMCA-P12.0 (Umetrics, Umeå, Sweden) for the pattern recognition analysis. Prior to the analysis, the values of all variables were centered and scaled.

Partial least square discriminant analysis (PLS-DA) was used to find differential metabolites between groups. PLS-DA is a frequently used PLS-based classification method where the response variable is a categorical one (dummy variables describing the categories) expressing the class membership of the statistical units. PLS-DA aims to find the best possible discriminant function (model) that separates classes of observations based on their X variables. When group separation was not satisfied based on PLS-DA, the data were further preprocessed using orthogonal partial least-squares discriminant analysis (OPLS-DA) to remove linear combinations of variables X that were orthogonal to the Y vector of the dependent variables, to eliminate the intersubject variability and describe maximum separation based on class [18]. Two-dimensional score plots are proved to be an efficient means of visualizing classification of the samples and investigating regions of the spectra that were altered as a result of compound dosing. The corresponding loading plots were used to identify which spectral variables contribute to the positioning of samples on the score plot and hence the variables that influence any observed separation in the data set.

2.7. Measurement of Infarct Size and Neurological Function.

After 24 h of pMCAO, the neurological deficit score of each rat was obtained according to Longa's et al. method [16]. The neurologic findings were scored on a five-point scale: a score of 0 indicated no neurologic deficit, a score of 1 (failure to extend left forepaw fully) a mild focal neurologic deficit, a score of 2 (circling to the left) a moderate focal neurologic deficit, and a score of 3 (falling to the left) a severe focal deficit; rats with a score of 4 did not walk spontaneously and had a depressed level of consciousness. The brain slices were stained with a 2% solution of 2,3,5-triphenyl tetrazolium chloride (TTC) (Sigma) in saline at 37°C for 30 min and photographed. The volume of infarction was calculated according to the following formula $V = \sum_{i=1}^{n-1} ((A_i + A_{i+1})/2h)$, where V is the volume of fraction; A_i is the infarct area of each slice; and h is slice thickness.

2.8. Western Blot Analysis. Tissues were prepared as described in a previous report [19]. The blocked membranes were incubated overnight at 4°C with primary antibodies (1:400 dilution) against NF- κB p65 or phospho-I κB - α (Santa). Following 1 h secondary antibody (1:5000 dilution) incubation, the immunodetection was carried out by using

enhanced chemiluminescence detection reagents. β -action was used as a loading control.

2.9. RNA Isolation and Semiquantitative NF- κB p65, IL-1 β , and IL-10 RT-PCR. Cerebral cortex RNA extraction was prepared by using Trizol reagent (Invitrogen). Equal aliquots of the cDNA were amplified by PCR using specific primers (provided in supplemental Table 1S) at different cycles (30 cycles for p65, 35 cycles for IL-1 β and IL-10, and 23 cycles for glyceraldehyde-3-phosphate dehydrogenase (GAPDH)). PCR products were then separated using a 1.5% agarose gel by gel electrophoresis, and band intensity was semiquantified by densitometry using GeneTools (Syngene) gel analysis software which was normalized by using GAPDH as an endogenous reference.

2.10. Nuclear Factor Binding Assay. NF- κB DNA binding activity was assessed using Trans-AM transcription factor assay kits (Active Motif) according to the manufacturer's instructions. Five or ten micrograms of brain tissue nuclear extracts were added to 96-well plates. Antibody binding was measured using a luminometer. The specificity of nuclear factors activation was determined by competition experiments using wild-type and mutant consensus oligonucleotides provided with the kit.

2.11. Statistical Analysis. All the results were obtained by a single experimenter, who was blinded to the experimental treatment groups and indicated at least three independent experiments expressing as mean \pm SD. The unpaired t -test was performed to evaluate statistically significant differences; statistical significance was set at $P < 0.05$.

3. Results and Discussion

3.1. Effect of HSYA on the Infarct Volume and Neurological Score. TTC staining was used to evaluate the volume of infarction to compare the effect of different administrations of HSYA on pMCAO. As shown in Figures 1(a) and 1(b), the normal and sham-operated rats did not show any lesions in either hemisphere. However, 24 h after pMCAO, there was significant infarction ($230 \pm 20 \text{ mm}^3$), as shown in the TTC-stained coronal brain section. Different treatments of HSYA, 10 mg/kg (pretreated), 10 mg/kg (posttreated), 50 mg/kg (posttreated), and 10 mg/kg (5 times posttreated), decreased the infarct volume by 21.3% ($P < 0.05$), 20.4% ($P < 0.05$), 21.5% ($P < 0.05$), and 30.9% ($P < 0.01$), respectively, compared to vehicle-treated MCAO rats. Successive administration of HSYA decreased the infarct volume more significantly than a single injection. Therefore, primarily successive administration of HSYA was used in subsequent experiments.

Meanwhile, the time point (24 h) and dosage regimen (i.v. successive administration, 10 mg/kg/30 min, 5 times) were determined; the effect of HSYA and PDTC on the infarct volume and neurological score after pMCAO was observed. As shown in Figures 1(c) and 1(d), normal and sham-operated rats did not show any lesions in either hemisphere, while 24 h after pMCAO, there was significant infarction

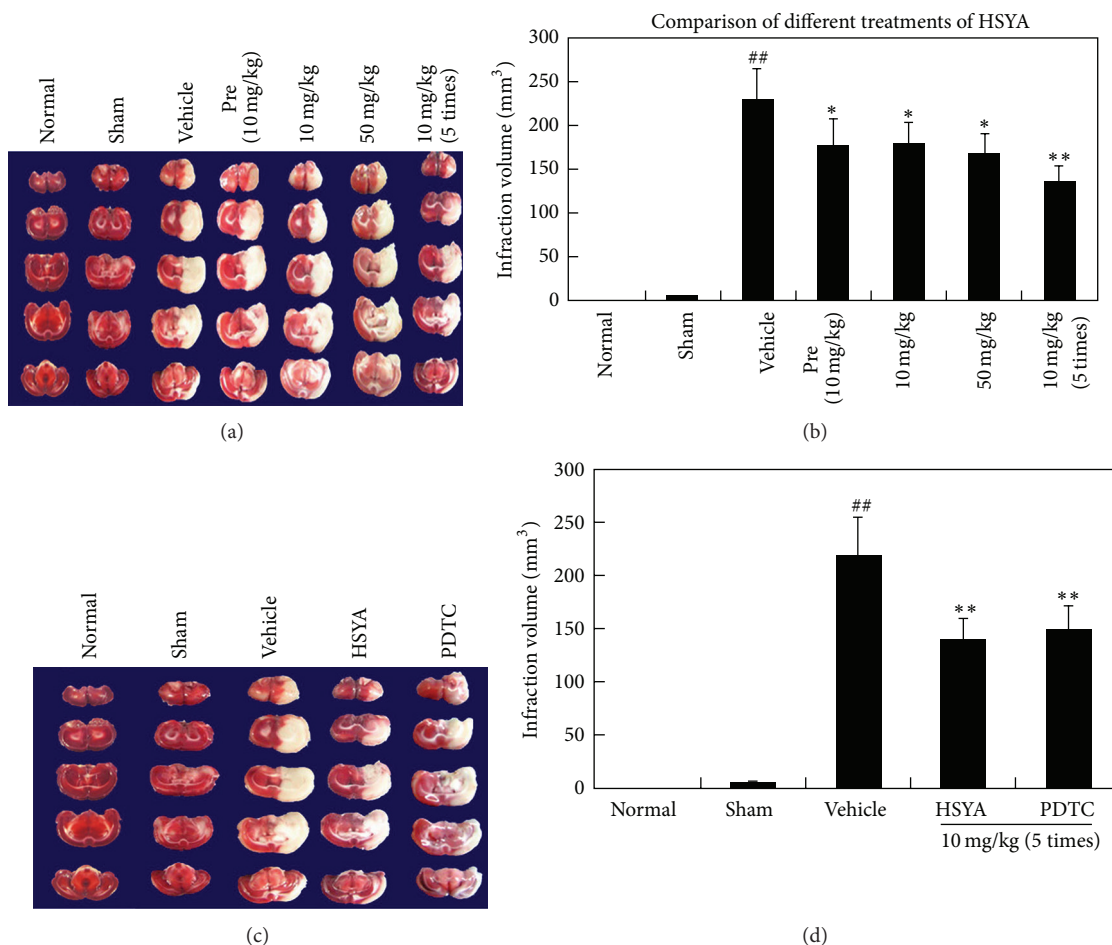


FIGURE 1: Effect of different administrations of HSYA and PDTC on infarct volume. (a, b) different administrations of HSYA; (c, d) HSYA and PDTC. A well-defined pale area was considered to be the infarct in the right hemisphere representative of TTC-stained sections after 24 h of pMCAO. ^{##} $P < 0.01$ compared with sham group; ^{*} $P < 0.05$, ^{**} $P < 0.01$ compared with vehicle-treated pMCAO group.

($230 \pm 20 \text{ mm}^3$) in TTC-stained coronal brain sections. A neurological deficit score of 8.16 ± 0.75 was observed in vehicle-treated MCAO rats (provided in supplemental Table 2S). Clearly, HSYA and PDTC treatment decreased the infarct volume by 30.9% and 28.4%, respectively, and produced significant improvements in neurological functions ($P < 0.01$) compared to vehicle-treated MCAO rats. The effect of HSYA and PDTC on the infarct volume and neurological score did not show a significant difference when compared to each other.

3.2. Detection of HSYA in Different Rat Brain Tissues. HSYA was detected in different rat brain tissues using HPLC/ESI-MSⁿ and HPLC/HRMSⁿ methods. The relationship between the structural characteristics and fragmentation behavior was investigated for HSYA. The HPLC/ESI-MSⁿ method is a reliable means of characterizing HSYA even in minute quantities. In addition, HPLC/HRMSⁿ was applied to verify the proposed fragmentation pathways. As shown in Figures 2(a)–2(c), HSYA with a retention time of 7.2 min was

detected at m/z 611 $[M-H]^-$ in HPLC/(-)ESI-MSⁿ and m/z 611.1593 in HPLC/HRMSⁿ, suggesting a molecular weight of 612 Da and a molecular formula of $C_{27}H_{31}O_{16}$. In the product ion mass spectra of $[M-H]^-$, a prominent ion at m/z 491 (i.e., 611–120) was observed in the MS² spectrum. Furthermore, a peak at m/z 491.1182 in HPLC/HRMS² suggested a molecular formula of $C_{23}H_{23}O_{12}$ and indicated that this was a diagnostic ion of HSYA. Accordingly, the proposed fragmentation pathways of HSYA are shown in Figure 2(d). HSYA was able to be unambiguously identified in extracts or biopsies based on its retention time, characteristic $[M-H]^-$ ion at m/z 611, fragment ion at m/z 491, and the constant neutral loss of 120 Da. The limit of detection was 0.87 ng (signal/noise = 3.6). This validated method was applied to detect HSYA in different brain tissues (brain stem, cortex, hippocampus, and cerebellum) after i.v. administration of HSYA to vehicle-treated MCAO rats and normal rats. It was found that HSYA could be detected in each of the four brain tissues both for ischemic and normal groups.

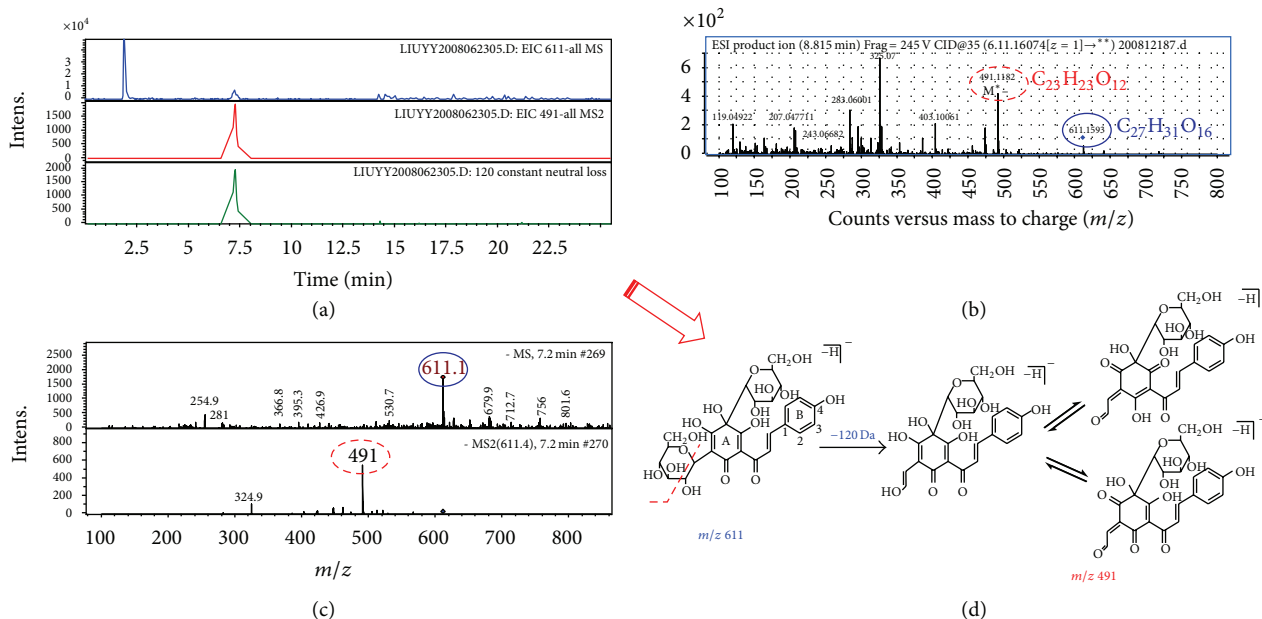


FIGURE 2: (a) HPLC/DAD/ESI-MSⁿ analyses of sample solution; (b) HPLC/ESI-MSⁿ spectra of [M-H]⁻ (m/z 611) ion in negative ion mode; (c) HPLC/HRMS data of [M-H]⁻ ion and its product ions for HSYA; (d) proposed fragmentation pathways for HSYA based on HPLC/HRMS data (m/z 611 \rightarrow 491).

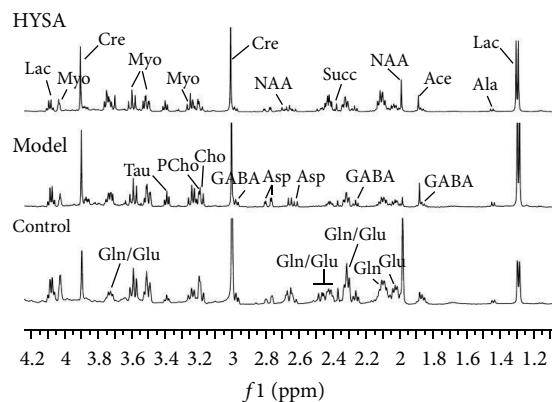


FIGURE 3: Typical 500 MHz ¹H NMR CPMG spectra of brain tissue samples.

3.3. ¹H MAS NMR Metabonomics and Multivariate Statistical Analysis. In the previous studies, HSYA was verified to travel across the BBB and exhibit a protective effect on cerebral ischemia according to histopathological examination and neurological evaluation. Next, we examined the influence of HSYA on the endogenous small molecules in brain tissue. Here, we evaluated the beneficial effects of HSYA using ¹H NMR-based metabonomics at a molecular level in brain samples.

Figure 3 shows low-frequency regions of typical CPMG spectra of the polar metabolites extracted from rat brain tissues of control, ischemia and HSYA-treated rats. Based on literature reports [20, 21] and using the Chenomx NMR Suite software (Chenomx, Calgary, Canada), the major metabolites

in brain tissues were identified, as shown in Figure 3 and Table 3S. Furthermore, a multivariate statistical method was applied to analyze the spectra more comprehensively and to identify metabolite signals that could efficiently differentiate between the treatment groups.

We analyzed the metabolic variations in extracts of different brain tissues, including the cerebellum, cortex, hippocampus, and stem, after permanent focal cerebral ischemia using ¹H-NMR spectroscopy and a multivariate statistical analysis. The OPLS-DA statistical analysis demonstrated that there were significant differences between the metabolic profiles of ischemia and control rats in the cerebellum, cortex, and hippocampus samples (Figures 4(a), 4(d), and 4(g)). The group that was administered HSYA deviated from the model group (Figures 4(b), 4(e), and 4(h)) and approached the control group, showing a trend of metabolic recovery (Figures 4(c), 4(f), and 4(i)). The metabolic profiles of the stem samples of ischemic and control animals were mostly the same, as the stem is a region of the brain that is resistant to hypoxia/ischemia [22]. Multivariate statistical algorithms were used to classify ¹H NMR spectra of the brain cerebellum, cortex, and hippocampus in rats and identify distinct metabolic profiles for the three different regions. Loading plots from the OPLS-DA of the NMR spectra are provided in the supplementary materials Figure 1S.

The OPLS-DA scores and loading plot of the ¹H-NMR data of cerebellum samples of ischemic rats showed an apparent higher level of lactate (Lac), alanine (Ala), choline (Cho), and phosphocholine (Pcho) along with a lower level of *N*-acetyl aspartate (NAA), Myo-inositol (Myo), creatine (Cre), and taurine (Tau) than in control rats. The model had an overall goodness of fit, R^2Y , of 89% and an overall

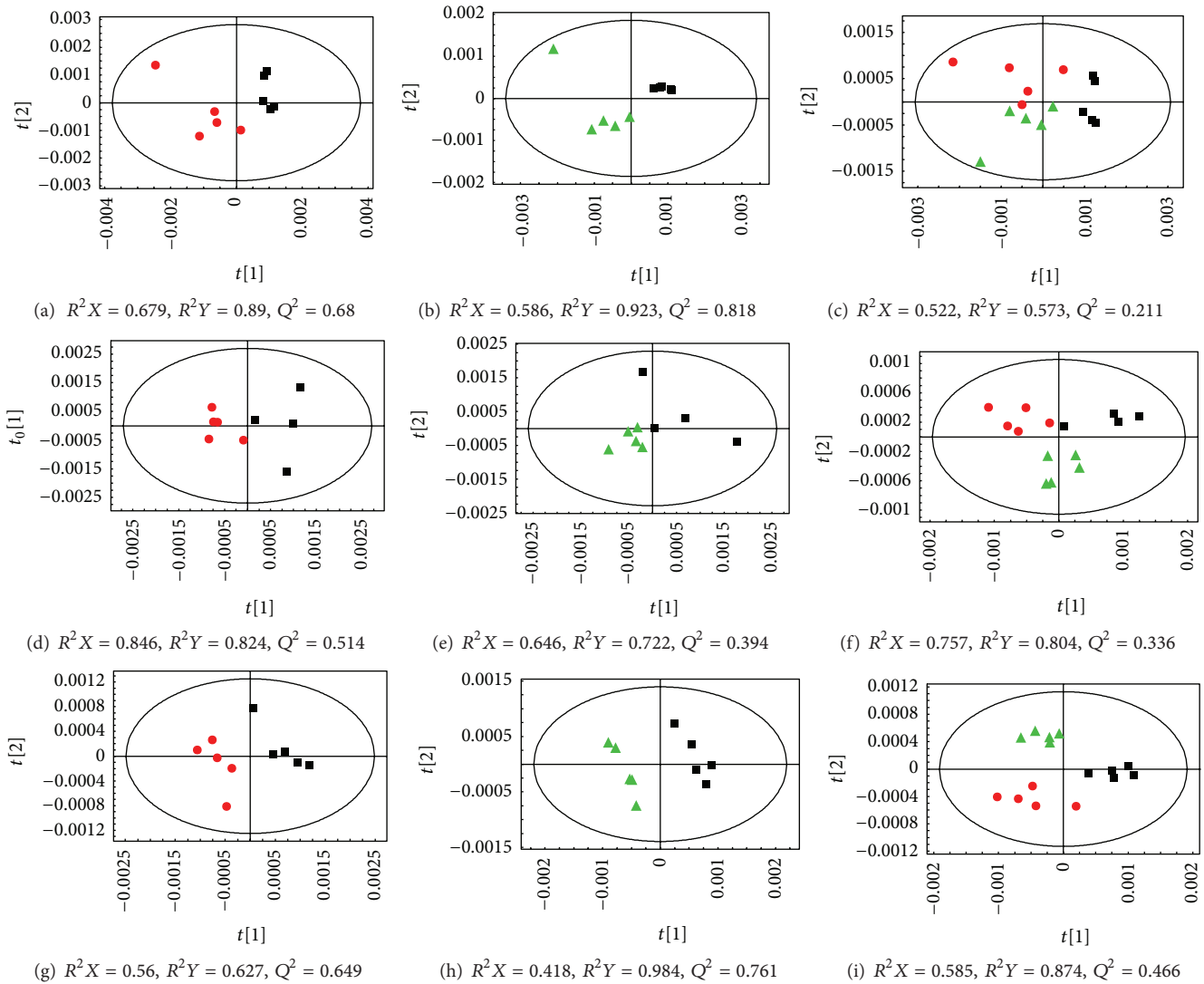


FIGURE 4: OPLS-DA scores plots from the analyses of the processed NMR spectra. (a–c) cerebellum, (d–f) cortex, and (g–i) hippocampus tissue extracts derived from three groups of rats: red circle, control; black square, ischemia; green triangle, HSYA.

cross-validation coefficient, Q^2 , of 68%. Treating ischemic animals with HSYA reverted some of the ischemic effects on the metabolite concentrations in the OPLS-DA loading plot. Compared with the ischemia group, the levels of Lac, Ala, Cho, and Pcho in the treatment group were significantly reduced and the levels of NAA, Cre, Myo, and Tau remarkably increased.

The predominant changes identified in the OPLS-DA analysis of cortex samples from ischemic rats included an increase in the signal intensities of Lac, acetate (Ace), Ala, glutamate (Glu), and aspartate (Asp), accompanied by a reduction in the intensities of NAA, Myo, Cre, Tau, and Gamma-aminobutyric acid (GABA). A general comparison between HSYA-treated and ischemic rats using an OPLS-DA model resulted in a clear differentiation between the two groups. The loading plot showed a decrease in Lac, Ace, Glu, and Asp and an increase in NAA, Cre, Myo, Tau, and GABA with treatment.

The metabolic changes in the hippocampus included a significant increase in the signal intensities of Lac, Ace, Cre, Glu, Glu/Gln, and Ala, accompanied by signal reductions of NAA, Tau, and GABA in ischemic animals. Moreover, significant differences were observed with HSYA treatment. Compared to ischemic rats without HSYA treatment, Lac, Ace, Glu, and Ala were remarkably reduced and NAA, Tau, and GABA were significantly increased in the treatment group as seen in the OPLS-DA loading plot.

Ischemic stroke causes a significant amount of cell damage resulting from an insufficient supply of glucose and oxygen to central nervous system (CNS) tissue. Lac is often used as an indicator of cerebral anoxia or hypoxia [23]. Overflow metabolism results in an incomplete oxidation of glucose, leading to the accumulation of Lac, Ace, Ala, and Glu and other incompletely oxidized metabolites associated with the glycolytic pathway [24]. They are the products of glycolysis and increase rapidly during hypoxia and ischemia

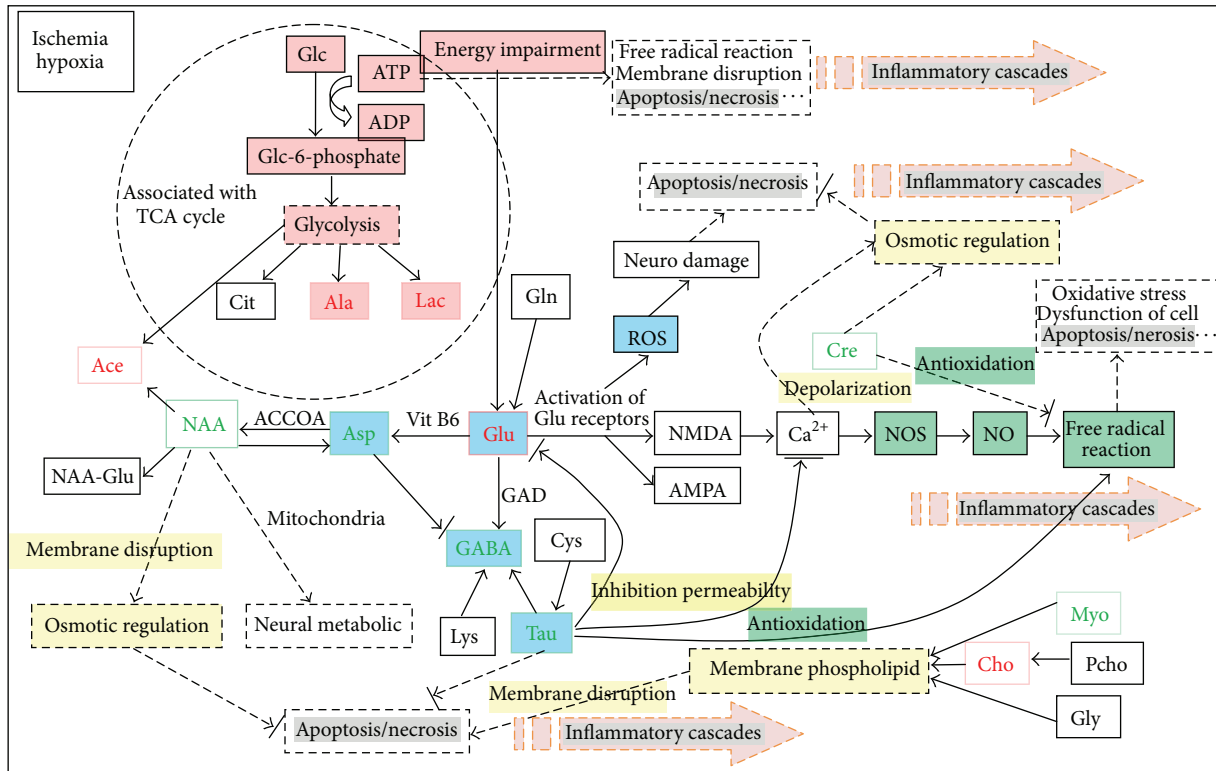


FIGURE 5: Summary of the metabolic pathways in which the metabolites described in this paper are involved. Red indicates metabolites with increased levels due to cerebral ischemia. Black indicates metabolites not found or not identified. Green indicates lowered metabolites due to cerebral ischemia. The pathways associated with energy metabolism, excitotoxicity, oxidative stress, and membrane disruption are labeled in red, blue, green, and yellow background, respectively.

to accommodate the extra energy demand required during ischemia [25]. The cells of the ischemic core undergo anoxic depolarization and are destined to die due to lack of energy [26]. As the number of depolarization increases, the infarcts grow larger [27]. As shown in Figure 5, a network map identified the tricarboxylic acid (TCA) cycle as playing a central role in the proposed signaling pathway that also interacts with numerous other pathways. Interestingly, the level of Lac in ischemic rats after treatment with HSYA significantly decreased, returning toward the normal level. This indicates that HSYA can modulate the changes in energy metabolism induced by ischemia and even reduce the infarct volume.

Following cerebral ischemia, there is an excessive release of Glu [28] and breakdown of astrocytic functions [29] that results in impaired Glu uptake by astrocytes [30]. Glu uptake reduces the glucose supply and exacerbates the energy impairment but can also lead to excitotoxicity [31]. Glu excitotoxicity is a significant determinant of ischemia pathophysiology. The increased levels of extracellular Glu most likely contribute directly to cell damage by calcium overload through excessive NMDA receptor activation or indirectly through initiating cascades such as free radical formation (Figure 5) [32]. An increase in the amount of oxygen free radicals leads to prompt dysfunction of the cellular membrane, resulting in necrosis [33]. Many studies

have showed that the decreased Glu release might contribute to the neuroprotective effect of HSYA [34]. Spontaneous Glu release during ischemia could lead to excitotoxicity and perturbation of neural network functions [35].

On the contrary, Tau has been suggested to be a neuroprotective chemical [36], and its effects include calcium modulation, apoptosis inhibition, and protection against oxidative stress via its antioxidant properties [37]. Tau has also been implicated in the mechanism of cell shrinkage during apoptosis in several cell types, including cerebellar granule neurons [38]. Cell shrinkage is a distinctive characteristic of apoptotic cells. It is thought that changes in ion channel fluxes play a major role in this shrinkage [39]. Therefore, decreased Tau in the cerebellum and cortex of ischemic rats may not only indicate some deleterious information but also reflect part of the adaptive measures taken by the CNS.

GABA, a key mediator of inhibitory neurotransmission in the mammalian central nervous system, is generated from Glu in GABAergic neurons by glutamic acid decarboxylase [40]. It is worth noting that this involves converting the principal excitatory neurotransmitter (Glu) into the principal inhibitory neurotransmitter (GABA). GABAergic agents protect against the delayed death of the CA1 hippocampal neurons elicited by ischemia. The changes in GABA during and after ischemia are sufficient to cause CNS depression or excitation [41]. In addition, Tau and lysine can increase both

GABA synthesis and effects, while Asp and Glu most likely inhibit GABA effects [42]. In the present study, increased inhibitory neurotransmitter levels such as GABA and Tau accompanied with decreased excitatory neurotransmitter levels of Glu and Asp are associated with a better outcome of stroke when treated with HSYA.

Cerebral ischemia in particular is responsible for oxidative stress due to the generation of free radicals [43], which result in deleterious effects during pathogenesis [44]. Cre and Tau possess antioxidant properties in the brain [45]. Cre is thought to have a multifaceted role in the brain. Apart from being involved in brain osmoregulation, it has recently been implicated in energy homeostasis and protection from oxidative stress through acting directly as an antioxidant [46]. In the present study, Cre increased markedly in the hippocampus but decreased in the cerebellum and cortex of ischemic rats. An increase in Cre may reflect a protective mechanism against the enhanced oxidation, whereas a decline may indicate the exhaustion of Cre and lack of antioxidation in certain brain regions of ischemic rats. HSYA intervention could relatively elevate the levels of these two antioxidative markers.

NAA, a metabolite synthesized in the mitochondria, is commonly used as a marker of neuronal viability [47]. Extracellular NAA is transported into astrocytes [48] where it is rapidly hydrolyzed into Ace and Asp [49]. Considerable evidence shows that NAA has multiple roles in neurons, including neural metabolic function in mitochondria, osmoregulation, and axon-glia signaling [50, 51]. The reduction in NAA in a visible infarct was related to the reduction in blood flow to the infarct, which in turn was related to the infarct extent and clinical outcome [52]. Notably, NAA levels have clearly recovered after HSYA treatment, indicating that the disturbance of neuronal activity can be modified by HSYA.

Myo is a significant intracellular osmolyte, whose change may indicate fluctuations in tissue osmolarity [47]. It has been reported that Pcho, Myo, and glycerol are precursors used for the synthesis of membrane phospholipids in the cell and their levels play a role in lipid metabolism [47, 53]. For example, Pcho contributes to the Cho resonance, which may act as a biomarker for membrane phospholipid metabolism [54]. Therefore, changes in Pcho, Cho, and Myo in this study may arise from the cell membrane disruption caused by ischemia. Moreover, the disruption of the membrane would subsequently cause cellular contents to leak into the surrounding tissue resulting in an inflammatory response.

Collectively, the progression of ischemic injury has been thought to involve many molecular pathways that play roles in the death of neurons [55]. As shown in Figure 5 cerebral ischemia triggers a complex series of biochemical and molecular disorders that impairs the neurological functions through a breakdown of cellular integrity mediated by energy metabolism, excitotoxic glutamatergic signalling, ionic imbalance, oxidative stress, membrane disruption, osmotic regulation, and so forth [33]. Treatment with HSYA could lead to relative corrections to the changes in these metabolic pathways induced by ischemia. Reversals of metabolic disturbances in the brain after therapy may provide new insights into therapeutic targets for ischemia.

3.4. Inhibition of HSYA on the NF- κ B Pathway. NF- κ B activation requires nuclear translocation of the p65 subunit. In this study, the translocation ability of NF- κ B p65 subunit from the cytoplasm to the nucleus was investigated by western blotting at different times after pMCAO. As shown in Figure 6(a), expression of the p65 subunit in the cerebral cortex of the ischemic side exhibited an increasing trend in the nucleus. NF- κ B was activated as early as 3 h, reached its peak point at 24 h after pMCAO, and then declined. In contrast, p65 expression in the cytoplasm showed the opposite trend; expression reached its lowest point at 24 h. Both in the nucleus and the cytoplasm, NF- κ B remained activated at 48 h. These results indicated that NF- κ B was activated and translocated from the cytoplasm to the nucleus. Consistent with the infarct volume, the 24 h time point was the most significant ($P < 0.01$) compared to the others ($P < 0.05$). Therefore, the effect of HSYA was evaluated at 24 h after cerebral occlusion in the following experiments.

To determine whether HSYA treatment can interfere with the ischemia-induced activation of the NF- κ B p65 subunit, the effect of HSYA on the cytosolic and nuclear pools of p65 protein was evaluated by western blot analysis in the injured ipsilateral cerebral cortex of animals 24 h after artery occlusion. As shown in Figure 6(b), pMCAO considerably increased the nuclear and decreased the cytosolic p65 protein levels. Treatment with HSYA (10 mg/kg/30 min, 5 times) inhibited the increase and decrease of the nuclear and cytosolic p65 levels 24 h after MCAO, respectively. These results suggested that HSYA blocked the nuclear translocation of the p65 from cytoplasm.

Subsequently, we assessed the effect of HSYA on the total p65 mRNA and protein expression by RT-PCR and western blot analysis, respectively. The total p65 mRNA and protein expression levels were increased (Figures 6(c) and 6(d)) during cerebral ischemia, indicating that, 24 h after pMCAO, p65 transcriptional and protein synthesis was induced. However, no effect of HSYA on total p65 mRNA and protein expression was observed. The effect of HSYA on cytokine mRNA expression is displayed in Figure 7.

Activation of NF- κ B is due to increased DNA binding of NF- κ B after its release from I κ B. Because the p65 subunit, which has potent transcriptional activation domains, is known to be important in ischemia [56, 57], we used a p65-specific antibody to assess DNA binding in a microwell colorimetric assay. The NF- κ B wild-type and mutated consensus oligonucleotides were used to monitor the specificity of the assay. Wild-type oligonucleotide competed for NF- κ B binding to the probe immobilized on the plate, but the mutated consensus oligonucleotide had no effect on NF- κ B binding. After 24 h of MCAO, specific NF- κ B binding activity was increased in ischemic brains (Figure 2S). When HSYA was continuously administered after ischemia, p65 binding activity decreased by 33.5% ($P < 0.05$). PDTC, the potent NF- κ B suppressor was used as a positive control and showed a more significant inhibition of 50.4% ($P < 0.01$).

NF- κ B/Rel proteins are transcription factors involved in the activation of an exceptionally large number of genes in response to inflammation, viral and bacterial infections, and other stressful situations requiring rapid reprogramming

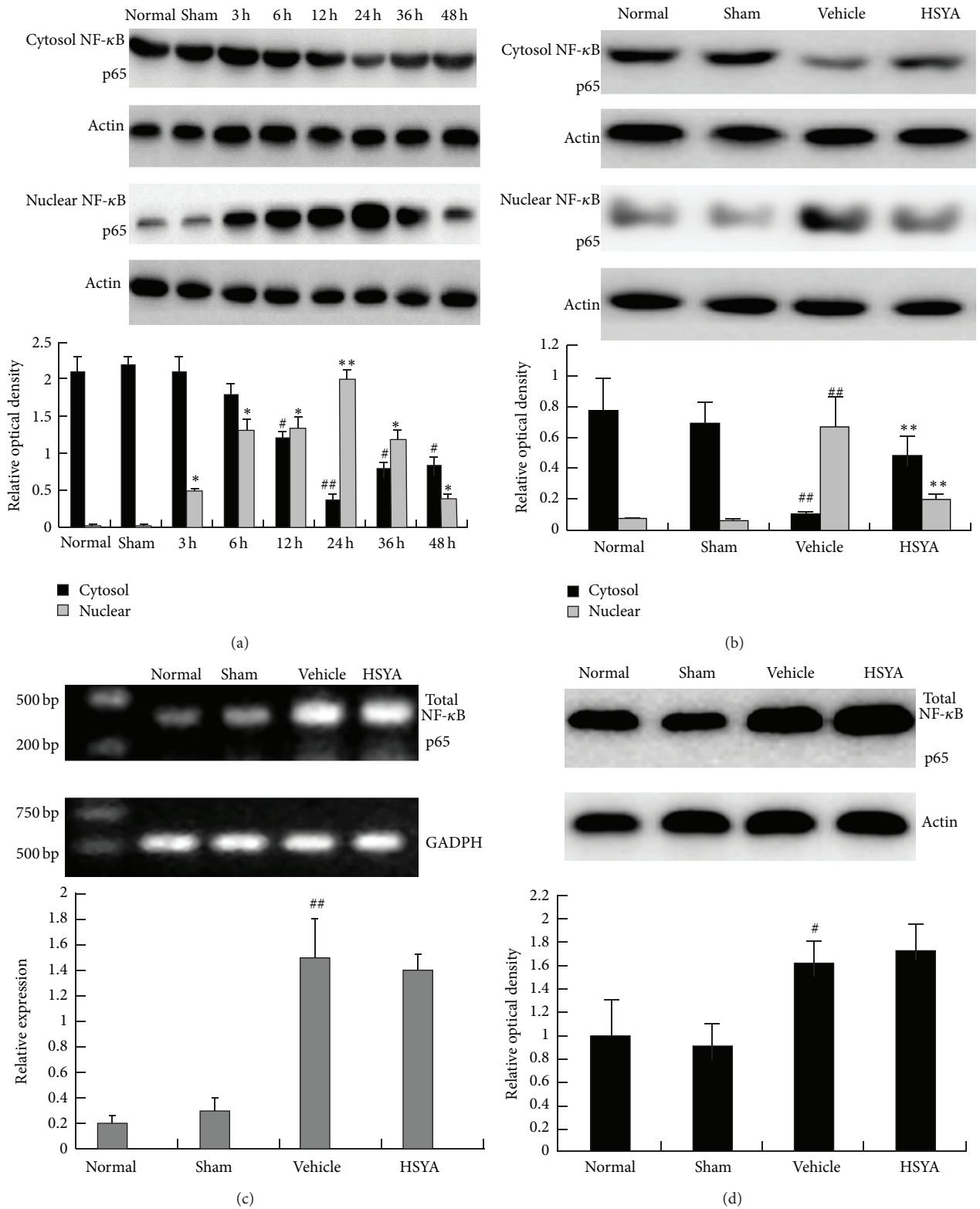


FIGURE 6: (a) Time course of NF-κB activation, (b) NF-κB p65 activation, (c) total NF-κB p65 mRNA, and (d) protein expression. Data represent $\bar{x} \pm s.n = 6$ each group; results represent at least three independent experiments. ## $P < 0.01$ compared with sham group in the cytoplasm or in the nucleus. * $P < 0.05$, ** $P < 0.01$ compared with model group in the cytoplasm or in the nucleus.

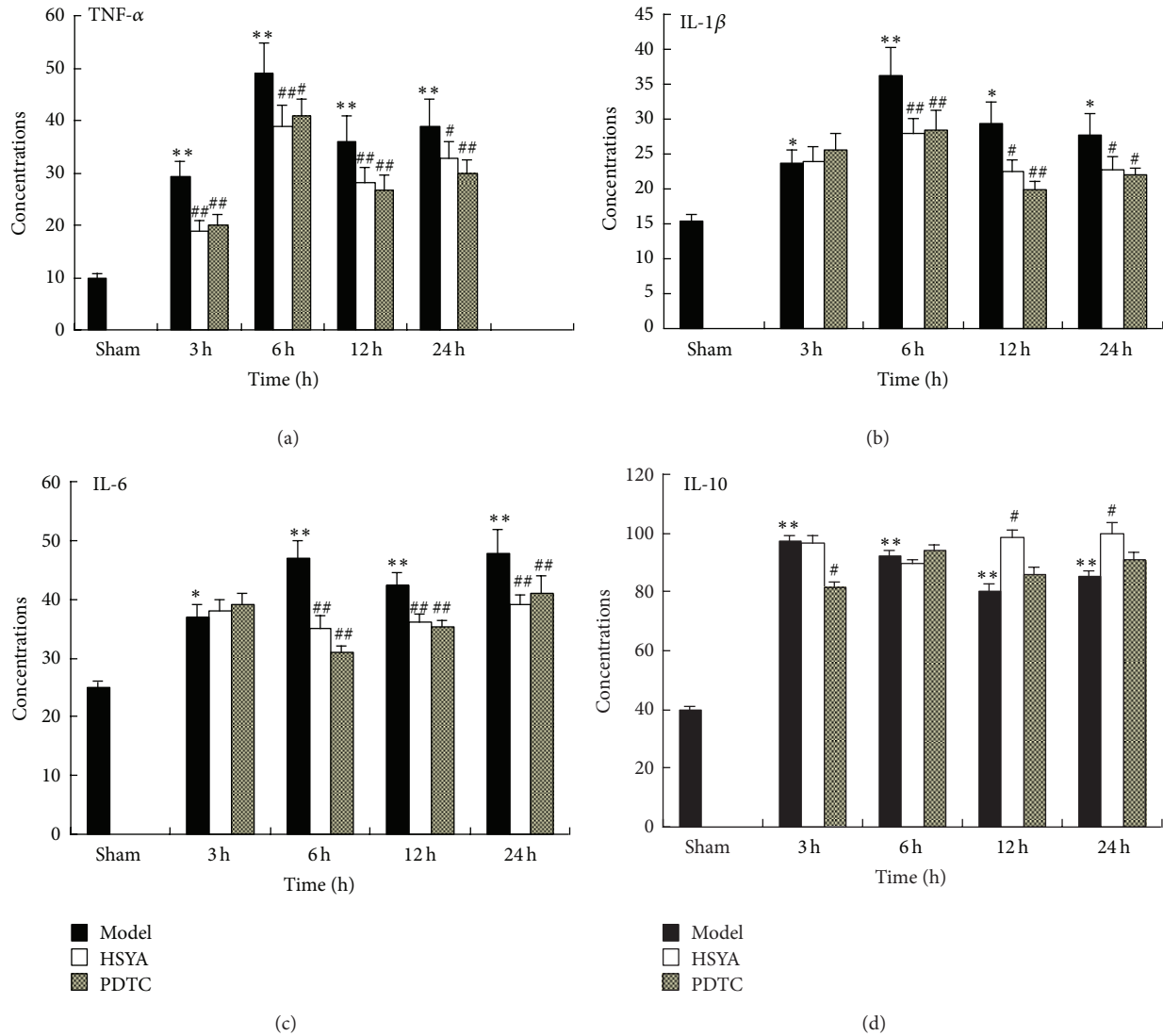


FIGURE 7: Effect of HSYA on cytokine mRNA expression at 3 h, 6 h, 12 h, and 24 h. (a) TNF- α mRNA expression, (b) IL-1 β mRNA expression, (c) IL-6 mRNA expression, and (d) IL-10 mRNA expression. Data represent $\bar{x} \pm s$, $n = 6$ each group; results represent at least three independent experiments. ## $P < 0.01$ compared with sham group. * $P < 0.05$, ** $P < 0.01$ compared with model group.

of gene expression. Stimulation leads to the rapid phosphorylation and, ultimately, proteolytic degradation of I κ B, which frees NF- κ B to translocate to the nucleus and activate the transcription of its target genes. In the brain, NF- κ B regulates the expression of antiapoptotic, proapoptotic, and proinflammatory genes, thereby playing a dual role in neuronal survival [10, 58].

In a few hours after the onset of cerebral ischemia, a multifaceted inflammatory reaction emerges. The transcription of numerous inflammatory mediators is induced [59]. The inflammation contributes to the breakdown of the BBB in cerebral ischemia [60] and is closely interrelated with neuronal cell death, thereby promoting a neurological deficit. The transcription factor NF- κ B, as a key regulator of hundreds of genes involved in inflammation, is activated in the hippocampal CA1 neurons after cerebral ischemia [59, 61].

Studies have demonstrated that IL-1 β and IL-6 genes expressions were induced early following MCAO [62]. TNF- α is a deleterious cytokine in stroke [63]. It might activate a cytokine network in the postischemic brain and contribute to an increased sensitivity to and risk of ischemic brain injury [64]. Inhibition of TNF- α may represent a novel pharmacological strategy to treat ischemic stroke [65]. Moreover, it is well accepted that IL-10, an anti-inflammatory cytokine, can attenuate brain infarction [66] and provide neuroprotection in ischemic stroke [67]. It is commonly accepted that inhibition of NF- κ B will prevent proinflammatory cytokine production, thereby contributing to neuroprotection [68].

In the present study, we noted that HSYA suppressed the translocation of the NF- κ B p65 protein from the cytoplasm to the nucleus by western blotting. Additionally, HSYA suppressed p65 DNA-binding activity and the transcription

and protein levels of the proinflammatory cytokines TNF- α , IL-1 β , and IL-6. HSYA also promoted both the transcription and protein expression of the anti-inflammatory cytokine IL-10. In the brain, activated NF- κ B acted on genes encoding cytokines, cyclooxygenase-2, nitric oxide synthase, and apoptotic proteins [10, 69]. Cerebrovascular inflammation plays a central role in the pathogenesis of cerebral ischemia [70]. Our results suggest that HSYA is also neuroprotective through suppression of the inflammatory NF- κ B signaling pathway. This might be one of the mechanisms for the inhibition of apoptosis and protection of cells from ischemic damage.

Here, we propose neuroprotective mechanisms of HSYA through metabolomics studies combined with an examination of its anti-inflammatory effect through the inhibition of the NF- κ B pathway. First, the energy failure or drastic decrease in cellular ATP and glucose levels due to a rapid decrease in glucose uptake following ischemia is responsible for the underlying mechanism of necrosis in the core region [71]. Second, Glu-mediated excitotoxicity could force the effected cell to self-destruct and lead to neuronal damage and eventual cell death. Third, oxidative stress has been shown to activate several intracellular signaling cascades that may have deleterious effects on the cellular homeostasis. One such event leads to activation of MAPKs [71], which are responsible for transmitting extracellular signals into the nucleus. Finally, the changes in the metabolites associated with membrane disruption may cause leakage of cellular contents into the surrounding tissue and invariably a consequent inflammatory response.

4. Conclusion

Collectively, cerebral ischemia triggers a complex series of biochemical and molecular mechanism that impairs the neurological functions through breakdown of cellular integrity mediated by energy metabolism, excitotoxic glutamatergic signalling, free-radical reactions, and so forth and then might initiate a series of inflammatory cascades associated with apoptosis or necrosis (Figure 5). On the other hand, NF- κ B is a ubiquitously expressed transcription factor that regulates expression of genes involved in inflammation, cell survival, and apoptosis [72, 73]. Our data suggest that HSYA treatment inhibits the NF- κ B pathway via suppressing proinflammatory cytokine expression and p65 translocation and binding activity while upregulating an anti-inflammatory cytokine, thereby exhibiting an anti-inflammatory effect, ultimately leading to reduced apoptosis-like cell death. The previous complementary studies suggest that the neuroprotective effect of HSYA is related to the inhibition of neuronal apoptosis or necrosis by modulating inflammatory cascades.

The progression of ischemic injury has been proven to involve many molecular pathways that play roles in the death of neurons. We present new insights into the pathophysiological mechanisms through a systematic integration of histopathological examination, neurological evaluation, BBB permeability studies, metabolomics, and studies of the NF- κ B pathway involved in the neuroprotective effect of HSYA after ischemia. The therapeutic effect of HSYA is not

a series of independent and isolated metabolic pathways but instead is a complex interconnected network. However, certain limitations exist in the present studies. How does HSYA travel across the BBB? We have detailed an effective method for detecting HSYA in brain samples and verified that HSYA could cross the BBB of ischemic and normal rats. As such, the mechanism of how HSYA, a small, water-soluble compound, can cross the BBB and whether its neuroprotective effect can be enhanced by an improvement in BBB permeability and integrity still needs to be investigated in future. The duration of ischemia is an important prognosis determinant. Reperfusion also plays a prominent role in damage distribution and is responsible for oxidative stress due to the generation of free radicals [57]. The reperfusion-induced inflammatory infarction is much more harmful and complicated than ischemia. In the present study, a series of metabolic pathways associated with inflammation were found during brain ischemia. In the future, changes in the stage of reperfusion and the precise mechanisms of how HSYA protects against focal cerebral ischemia need to be further investigated.

Abbreviations

HSYA:	Hydroxysafflor yellow A
BBB:	Blood-brain barrier
NF- κ B:	Nuclear factor- κ B
pMCAO:	Permanent middle cerebral artery occlusion
SFDA:	State Food and Drug Administration
NMR:	Nuclear magnetic resonance spectroscopy
HPLC-MS ⁿ :	High-performance liquid chromatography coupled with multistage tandem mass spectrometry
HR MAS:	High-resolution magic-angle spinning
PDTC:	Pyrrrolidine dithiocarbamate ammonium salt
TSP:	3-trimethylsilyl-2,2,3,3-d ₄ -propionate
CPMG:	Carr-Purcell-Meiboom-Gill
OPLS-DA:	Orthogonal partial least-squares discriminant analysis
TTC:	2,3,5-triphenyl tetrazolium chloride
GAPDH:	Glyceraldehyde-3-phosphate dehydrogenase
CNS:	Central nervous system
Lac:	Lactate
Ala:	Alanine
GABA:	Gamma-aminobutyric acid
Ace:	Acetate
NAA:	<i>N</i> -acetyl aspartate
Glu:	Glutamate
Gln:	Glutamine
Asp:	Aspartate
Cre:	Creatine
Cho:	Choline
Pcho:	Phosphocholine
Tau:	Taurine
Myo:	Myo-inositol.

Conflict of Interests

All authors declare that they have no Conflict of interests.

Author's Contribution

Yuanyan Liu, Zeqin Lian, and Haibo Zhu contributed equally to this work.

Acknowledgments

The work was supported by Grants from the National Science and Technology Project of China (nos. 2012ZX09301002-002 and 2012ZX09301002-003) and Natural Sciences Foundation of Beijing, China (Grant Number: 7122114).

References

- [1] V. Hachinski, C. Iadecola, R. C. Petersen et al., "National institute of neurological disorders and stroke-Canadian stroke network vascular cognitive impairment harmonization standards," *Stroke*, vol. 37, no. 9, pp. 2220–2241, 2007.
- [2] K. Kazuma, T. Takahashi, K. Sato, H. Takeuchi, T. Matsumoto, and T. Okuno, "Quinochalcones and flavonoids from fresh florets in different cultivars of *Carthamus tinctorius* L.," *Bioscience, Biotechnology and Biochemistry*, vol. 64, no. 8, pp. 1588–1599, 2000.
- [3] B. X. Zang, M. Jin, N. Si, Y. Zhang, W. Wu, and Y. Z. Piao, "Antagonistic effect of hydroxysafflor yellow a on the platelet activating factor receptor," *Yao Xue Xue Bao*, vol. 37, no. 9, pp. 696–699, 2002.
- [4] J. Tian, W. Jang, Z. Wang, C. Wang, and F. Fu, "Effects of safflower flavone on local cerebral ischemia and thrombosis formation in rats," *Chinese Traditional and Herbal Drugs*, vol. 34, pp. 741–743, 2003.
- [5] H. Zhu, Z. Wang, C. Ma et al., "Neuroprotective effects of hydroxysafflor yellow a: *in vivo* and *in vitro* studies," *Planta Medica*, vol. 69, no. 5, pp. 429–433, 2003.
- [6] X. Wei, H. Liu, X. Sun et al., "Hydroxysafflor yellow A protects rat brains against ischemia-reperfusion injury by antioxidant action," *Neuroscience Letters*, vol. 386, no. 1, pp. 58–62, 2005.
- [7] Z. Liu, C. Li, M. Li, D. Li, and K. Liu, "The subchronic toxicity of hydroxysafflor yellow A of 90 days repeatedly intraperitoneal injections in rats," *Toxicology*, vol. 203, no. 1–3, pp. 139–143, 2004.
- [8] A. Nurmi, P. J. Lindsberg, M. Koistinaho et al., "Nuclear factor- κ B contributes to infarction after permanent focal ischemia," *Stroke*, vol. 35, no. 4, pp. 987–991, 2004.
- [9] J. C. Lindon, E. Holmes, and J. K. Nicholson, "Metabonomics techniques and applications to pharmaceutical research & development," *Pharmaceutical Research*, vol. 23, no. 6, pp. 1075–1088, 2006.
- [10] M. P. Mattson, "NF- κ B in the survival and plasticity of neurons," *Neurochemical Research*, vol. 30, no. 6–7, pp. 883–893, 2005.
- [11] M. A. Collart, P. Baeuerle, and P. Vassalli, "Regulation of tumor necrosis factor alpha transcription in macrophages: involvement of four κ B-like motifs and of constitutive and inducible forms of NF- κ B," *Molecular and Cellular Biology*, vol. 10, no. 4, pp. 1498–1506, 1990.
- [12] Z. Yu, D. Zhou, A. J. Bruce-Keller, M. S. Kindy, and M. P. Mattson, "Lack of the p50 subunit of nuclear factor- κ B increases the vulnerability of hippocampal neurons to excitotoxic injury," *Journal of Neuroscience*, vol. 19, no. 20, pp. 8856–8865, 1999.
- [13] J. C. Lindon and J. K. Nicholson, "Analytical technologies for metabonomics and metabolomics, and multi-omic information recovery," *TrAC—Trends in Analytical Chemistry*, vol. 27, no. 3, pp. 194–204, 2008.
- [14] E. Holmes, R. L. Loo, J. Stamler et al., "Human metabolic phenotype diversity and its association with diet and blood pressure," *Nature*, vol. 453, no. 7193, pp. 396–400, 2008.
- [15] J. K. Nicholson, J. C. Lindon, and E. Holmes, "Metabonomics: understanding the metabolic responses of living systems to pathophysiological stimuli via multivariate statistical analysis of biological NMR spectroscopic data," *Xenobiotica*, vol. 29, no. 11, pp. 1181–1189, 1999.
- [16] E. Z. Longa, P. R. Weinstein, S. Carlson, and R. Cummins, "Reversible middle cerebral artery occlusion without craniectomy in rats," *Stroke*, vol. 20, no. 1, pp. 84–91, 1989.
- [17] H. W. L. Ziegler-Heitbrock, T. Sternsdorf, J. Liese et al., "Pyrrolidine dithiocarbamate inhibits NF- κ B mobilization and TNF production in human monocytes," *Journal of Immunology*, vol. 151, no. 12, pp. 6986–6993, 1993.
- [18] C. L. Gavaghan, I. D. Wilson, and J. K. Nicholson, "Physiological variation in metabolic phenotyping and functional genomic studies: use of orthogonal signal correction and PLS-DA," *FEBS Letters*, vol. 530, no. 1–3, pp. 191–196, 2002.
- [19] S. Z. Kong, Y. F. Xian, S. P. Ip et al., "Protective effects of hydroxysafflor yellow A on β -amyloid-induced neurotoxicity in PC12 cells," *Neurochemical Research*, 2013.
- [20] H. Seegers, E. Grillon, Y. Trioullier, A. Vãth, J. M. Verna, and D. Blum, "Nuclear factor- κ B activation in permanent intraluminal focal cerebral ischemia in the rat," *Neuroscience Letters*, vol. 288, no. 3, pp. 241–245, 2000.
- [21] Y. Li, Z. Y. Zhang, and J. I. Zhang, "Determination of hydroxysafflor yellow A in rat plasma and tissues by high-performance liquid chromatography after oral administration of safflower extract or safflor yellow," *Biomedical Chromatography*, vol. 21, no. 3, pp. 326–334, 2007.
- [22] Z. Yu, X. Gao, Y. Zhao, and K. Bi, "HPLC determination of safflor yellow A and three active isoflavones from TCM Naodesheng in rat plasma and tissues and its application to pharmacokinetic studies," *Biomedical Chromatography*, vol. 21, no. 6, pp. 577–584, 2007.
- [23] B. R. S. Broughton, D. C. Reutens, and C. G. Sobey, "Apoptotic mechanisms after cerebral ischemia," *Stroke*, vol. 40, no. 5, pp. e331–e339, 2009.
- [24] L. B. Gladden, "Lactate metabolism: a new paradigm for the third millennium," *The Journal of Physiology*, vol. 558, no. 1, pp. 5–30, 2004.
- [25] B. Zhang, S. Halouska, C. E. Schiaffo, M. R. Sadykov, G. A. Somerville, and R. Powers, "NMR analysis of a stress response metabolic signaling network," *Journal of Proteome Research*, vol. 10, no. 8, pp. 3743–3754, 2011.
- [26] J. L. Griffin and R. A. Kauppinen, "A metabolomics perspective of human brain tumours," *FEBS Journal*, vol. 274, no. 5, pp. 1132–1139, 2007.
- [27] K. Ohta, R. Graf, G. Rosner, and W. D. Heiss, "Calcium ion transients in peri-infarct depolarizations may deteriorate ion homeostasis and expand infarction in focal cerebral ischemia in cats," *Stroke*, vol. 32, no. 2, pp. 535–543, 2001.
- [28] G. Mies, T. Iijima, and K. A. Hossmann, "Correlation between peri-infarct DC shifts and ischaemic neuronal damage in rat," *NeuroReport*, vol. 4, no. 6, pp. 709–711, 1993.
- [29] S. L. Budd, "Mechanisms of neuronal damage in brain hypoxia/ischemia: focus on the role of mitochondrial calcium accumulation," *Pharmacology and Therapeutics*, vol. 80, no. 2, pp. 203–229, 1998.

- [30] R. G. Giffard and R. A. Swanson, "Ischemia-induced programmed cell death in astrocytes," *Glia*, vol. 50, no. 4, pp. 299–306, 2005.
- [31] T. Mori, N. Tateishi, Y. Kagamiishi et al., "Attenuation of a delayed increase in the extracellular glutamate level in the peri-infarct area following focal cerebral ischemia by a novel agent ONO-2506," *Neurochemistry International*, vol. 45, no. 2-3, pp. 381–387, 2004.
- [32] T. M. Bliss, M. Ip, E. Cheng et al., "Dual-gene, dual-cell type therapy against an excitotoxic insult by bolstering neuroenergetics," *Journal of Neuroscience*, vol. 24, no. 27, pp. 6202–6208, 2004.
- [33] T. K. McIntosh, M. Juhler, and T. Wieloch, "Novel pharmacologic strategies in the treatment of experimental traumatic brain injury: 1998," *Journal of Neurotrauma*, vol. 15, no. 10, pp. 731–769, 1998.
- [34] S. L. Mehta, N. Manhas, and R. Raghurir, "Molecular targets in cerebral ischemia for developing novel therapeutics," *Brain Research Reviews*, vol. 54, no. 1, pp. 34–66, 2007.
- [35] Z. J. Yang, Y. Xie, G. M. Bosco, C. Chen, and E. M. Camporesi, "Hyperbaric oxygenation alleviates MCAO-induced brain injury and reduces hydroxyl radical formation and glutamate release," *European Journal of Applied Physiology*, vol. 108, no. 3, pp. 513–522, 2010.
- [36] H. Ye, S. Jalini, L. Zhang, M. Charlton, and P. L. Carlen, "Early ischemia enhances action potential-dependent, spontaneous glutamatergic responses in CA1 neurons," *Journal of Cerebral Blood Flow and Metabolism*, vol. 30, no. 3, pp. 555–565, 2010.
- [37] J. Zhou, Y. Li, G. Yan et al., "Protective role of taurine against morphine-induced neurotoxicity in C6 cells via inhibition of oxidative stress," *Neurotoxicity Research*, vol. 20, no. 4, pp. 334–342, 2011.
- [38] F. Lang, J. Madlung, D. Siemen, C. Ellory, A. Lepple-Wienhues, and E. Gulbins, "The involvement of caspases in the CD95(Fas/Apo-1)-but not swelling-induced cellular taurine release from Jurkat T-lymphocytes," *Pflugers Archiv European The Journal of Physiology*, vol. 440, no. 1, pp. 93–99, 2000.
- [39] M. B. Friis, C. R. Friborg, L. Schneider et al., "Cell shrinkage as a signal to apoptosis in NIH 3T3 fibroblasts," *The Journal of Physiology*, vol. 567, no. 2, pp. 427–443, 2005.
- [40] M. Gómez-Angelats and J. A. Cidlowski, "Invited review: cell volume control and signal transduction in apoptosis," *Toxicologic Pathology*, vol. 30, no. 5, pp. 541–551, 2002.
- [41] S. Sá Santos, U. Sonnewald, M. J. T. Carrondo, and P. M. Alves, "The role of glia in neuronal recovery following anoxia: *in vitro* evidence of neuronal adaptation," *Neurochemistry International*, vol. 58, no. 6, pp. 665–675, 2011.
- [42] L. L. Sternau, W. D. Lust, A. J. Ricci, and R. Ratcheson, "Role for γ -aminobutyric acid in selective vulnerability in gerbils," *Stroke*, vol. 20, no. 2, pp. 281–287, 1989.
- [43] A. Pitkanen, P. J. Riekkinen, T. Halonen, A. Ylinen, T. Ruutinen, and M. Lehtinen, "Amino acid levels in human CSF after generalized seizure," *Journal of Neural Transmission*, vol. 70, no. 3-4, pp. 313–319, 1987.
- [44] D. A. I. Nita, V. Nita, S. Spulber et al., "Oxidative damage following cerebral ischemia depends on reperfusion—a biochemical study in rat," *Journal of Cellular and Molecular Medicine*, vol. 5, no. 2, pp. 163–170, 2001.
- [45] P. H. Chan, "Reactive oxygen radicals in signaling and damage in the ischemic brain," *Journal of Cerebral Blood Flow and Metabolism*, vol. 21, no. 1, pp. 2–14, 2001.
- [46] C. Guidi, L. Potenza, P. Sestili et al., "Differential effect of creatine on oxidatively-injured mitochondrial and nuclear DNA," *Biochimica et Biophysica Acta*, vol. 1780, no. 1, pp. 16–26, 2008.
- [47] X. Zhang, H. Liu, J. Wu, X. Zhang, M. Liu, and Y. Wang, "Metabonomic alterations in hippocampus, temporal and prefrontal cortex with age in rats," *Neurochemistry International*, vol. 54, no. 8, pp. 481–487, 2009.
- [48] M. J. Lan, G. A. McLoughlin, J. L. Griffin et al., "Metabonomic analysis identifies molecular changes associated with the pathophysiology and drug treatment of bipolar disorder," *Molecular Psychiatry*, vol. 14, no. 3, pp. 269–279, 2009.
- [49] W. Huang, H. Wang, R. Kekuda et al., "Transport of N-acetylaspartate by the Na^+ -dependent high-affinity dicarboxylate transporter NaDC3 and its relevance to the expression of the transporter in the brain," *Journal of Pharmacology and Experimental Therapeutics*, vol. 295, no. 1, pp. 392–403, 2000.
- [50] M. A. Jalil, L. Begumi, L. Contreras et al., "Reduced N-acetylaspartate levels in mice lacking aralar, a brain- and muscle-type mitochondrial aspartate-glutamate carrier," *The Journal of Biological Chemistry*, vol. 280, no. 35, pp. 31333–31339, 2005.
- [51] C. Demougeot, C. Marie, M. Giroud, and A. Beley, "N-acetylaspartate: a literature review of animal research on brain ischaemia," *Journal of Neurochemistry*, vol. 90, no. 4, pp. 776–783, 2004.
- [52] J. R. Moffett, B. Ross, P. Arun, C. N. Madhavarao, and A. M. A. Namboodiri, "N-Acetylaspartate in the CNS: from neurodiagnostics to neurobiology," *Progress in Neurobiology*, vol. 81, no. 2, pp. 89–131, 2007.
- [53] M. R. Pears, J. D. Cooper, H. M. Mitchison, R. J. Mortishire-Smith, D. A. Pearce, and J. L. Griffin, "High resolution ^1H NMR-based metabolomics indicates a neurotransmitter cycling deficit in cerebral tissue from a mouse model of batten disease," *The Journal of Biological Chemistry*, vol. 280, no. 52, pp. 42508–42514, 2005.
- [54] J. M. Wardlaw, I. Marshall, J. Wild, M. S. Dennis, J. Cannon, and S. C. Lewis, "Studies of acute ischemic stroke with proton magnetic resonance spectroscopy: relation between time from onset, neurological deficit, metabolite abnormalities in the infarct, blood flow, and clinical outcome," *Stroke*, vol. 29, no. 8, pp. 1618–1624, 1998.
- [55] R. Senaratne, A. M. Milne, G. M. MacQueen, and G. B. C. Hall, "Increased choline-containing compounds in the orbitofrontal cortex and hippocampus in euthymic patients with bipolar disorder: a proton magnetic resonance spectroscopy study," *Psychiatry Research—Neuroimaging*, vol. 172, no. 3, pp. 205–209, 2009.
- [56] A. Schneider, A. Martin-Villalba, F. Weih, J. Vogel, T. Wirth, and M. Schwaninger, "NF- κ B is activated and promotes cell death in focal, cerebral ischemia," *Nature Medicine*, vol. 5, no. 5, pp. 554–559, 1999.
- [57] N. J. Mulcahy, J. Ross, N. J. Rothwell, and S. A. Loddick, "Delayed administration of interleukin-1 receptor antagonist protects against transient cerebral ischaemia in the rat," *The British Journal of Pharmacology*, vol. 140, no. 3, pp. 471–476, 2003.
- [58] J. M. Lee, M. C. Grabb, G. J. Zipfel, and D. W. Choi, "Brain tissue responses to ischemia," *Journal of Clinical Investigation*, vol. 106, no. 6, pp. 723–731, 2000.
- [59] U. Dirnagl, C. Iadecola, and M. A. Moskowitz, "Pathobiology of ischaemic stroke: an integrated view," *Trends in Neurosciences*, vol. 22, no. 9, pp. 391–397, 1999.

- [60] D. A. Ridder and M. Schwaninger, "NF- κ B signaling in cerebral ischemia," *Neuroscience*, vol. 158, no. 3, pp. 995–1006, 2009.
- [61] E. Candelario-Jalil, Y. Yang, and G. A. Rosenberg, "Diverse roles of matrix metalloproteinases and tissue inhibitors of metalloproteinases in neuroinflammation and cerebral ischemia," *Neuroscience*, vol. 158, no. 3, pp. 983–994, 2009.
- [62] T. Ueno, Y. Sawa, S. Kitagawa-Sakakida et al., "Nuclear factor- κ B decoy attenuates neuronal damage after global brain ischemia: a future strategy for brain protection during circulatory arrest," *Journal of Thoracic and Cardiovascular Surgery*, vol. 122, no. 4, pp. 720–727, 2001.
- [63] Q. H. Zhai, N. Futrell, and F. J. Chen, "Gene expression of IL-10 in relationship to TNF- α , IL-1 β and IL-2 in the rat brain following middle cerebral artery occlusion," *Journal of the Neurological Sciences*, vol. 152, no. 2, pp. 119–124, 1997.
- [64] H. Uno, T. Matsuyama, H. Akita, H. Nishimura, and M. Sugita, "Induction of tumor necrosis factor- α in the mouse hippocampus following transient forebrain ischemia," *Journal of Cerebral Blood Flow and Metabolism*, vol. 17, no. 5, pp. 491–499, 1997.
- [65] S. D. Lavine, F. M. Hofman, and B. V. Zlokovic, "Circulating antibody against tumor necrosis factor- α protects rat brain from reperfusion injury," *Journal of Cerebral Blood Flow and Metabolism*, vol. 18, no. 1, pp. 52–58, 1998.
- [66] F. C. Barone, B. Arvin, R. F. White et al., "Tumor necrosis factor- α : a mediator of focal ischemic brain injury," *Stroke*, vol. 28, no. 6, pp. 1233–1244, 1997.
- [67] H. Ooboshi, S. Ibayashi, T. Shichita et al., "Postischemic gene transfer of interleukin-10 protects against both focal and global brain ischemia," *Circulation*, vol. 111, no. 7, pp. 913–919, 2005.
- [68] Y. C. Chang and C. C. Huang, "Perinatal brain injury and regulation of transcription," *Current Opinion in Neurology*, vol. 19, no. 2, pp. 141–147, 2006.
- [69] J. E. Carroll, D. C. Hess, E. F. Howard, and W. D. Hill, "Is nuclear factor- κ B a good treatment target in brain ischemia/reperfusion injury?" *NeuroReport*, vol. 11, no. 9, pp. R1–R4, 2000.
- [70] H. E. de Vries, J. Kuiper, A. G. de Boer, T. J. C. van Berkel, and D. D. Breimer, "The blood-brain barrier in neuroinflammatory diseases," *Pharmacological Reviews*, vol. 49, no. 2, pp. 143–156, 1997.
- [71] J. Cao, J. I. Viholainen, C. Dart, H. K. Warwick, M. L. Leyland, and M. J. Courtney, "The PSD95-nNOS interface: a target for inhibition of excitotoxic p38 stress-activated protein kinase activation and cell death," *Journal of Cell Biology*, vol. 168, no. 1, pp. 117–126, 2005.
- [72] T. C. Nichols, "NF- κ B and reperfusion injury," *Drug News and Perspectives*, vol. 17, no. 2, pp. 99–104, 2004.
- [73] M. S. Hayden and S. Ghosh, "Signaling to NF- κ B," *Genes and Development*, vol. 18, no. 18, pp. 2195–2224, 2004.

Research Article

An Integrative Platform of TCM Network Pharmacology and Its Application on a Herbal Formula, *Qing-Luo-Yin*

Bo Zhang,^{1,2} Xu Wang,¹ and Shao Li¹

¹ Bioinformatics Division and Center for Synthetic and Systems Biology, TNLIST/Department of Automation, Tsinghua University, Room 1-107, FIT Building, Beijing 100084, China

² Joint Computational Center of Drug Discovery, Tianjin International Joint Academy of Biotechnology & Medicine, Tianjin 300457, China

Correspondence should be addressed to Shao Li; shaoli@mail.tsinghua.edu.cn

Received 6 January 2013; Accepted 4 February 2013

Academic Editor: Aiping Lu

Copyright © 2013 Bo Zhang et al. This is an open access article distributed under the Creative Commons Attribution License, which permits unrestricted use, distribution, and reproduction in any medium, provided the original work is properly cited.

The scientific understanding of traditional Chinese medicine (TCM) has been hindered by the lack of methods that can explore the complex nature and combinatorial rules of herbal formulae. On the assumption that herbal ingredients mainly target a molecular network to adjust the imbalance of human body, here we present a self-developed TCM network pharmacology platform for discovering herbal formulae in a systematic manner. This platform integrates a set of network-based methods that we established previously to catch the network regulation mechanism and to identify active ingredients as well as synergistic combinations for a given herbal formula. We then provided a case study on an antirheumatoid arthritis (RA) formula, *Qing-Luo-Yin* (QLY), to demonstrate the usability of the platform. We revealed the target network of QLY against RA-related key processes including angiogenesis, inflammatory response, and immune response, based on which we not only predicted active and synergistic ingredients from QLY but also interpreted the combinatorial rule of this formula. These findings are either verified by the literature evidence or have the potential to guide further experiments. Therefore, such a network pharmacology strategy and platform is expected to make the systematical study of herbal formulae achievable and to make the TCM drug discovery predictable.

1. Introduction

Traditional Chinese medicine (TCM) is a whole medical system deriving from thousands of years of clinical application that has evolved independently from or parallel to allopathic conventional medicine and has been considered as one of the main items of the complementary or alternative medical system [1, 2]. The treatments of TCM formulate the therapeutic use of herbs using the combinatorial principle of Sovereign-Minister-Assistant-Envoy (*Jun-Chen-Zuo-Shi* in Chinese) on the basis of a patient's syndrome (*ZHENG* in Chinese) and attempt to regain the balance state of life and body functions [3]. However, unlike modern drugs developed by targeting a specific protein, understandings of the molecular basis of traditional herbal formulae are still very limited, posing a serious challenge for the modernization of TCM [4]. With the

recent advent of high-throughput technologies, experimental analyses of the active ingredients screening and the mechanisms of action of herbal formulae have become increasingly various. Investigators often examine a herbal formula from different facets by combining chemical or metabolic fingerprint [5, 6], pharmacodynamic and pharmacokinetic technology [7, 8], and genomic, proteomic or metabolomics analyses [9–11]. However, herbal formulae with numerous chemical compounds are too complex to be examined solely by conventional experimental approaches. Moreover, a herbal formula contains hundreds of chemical compounds and its therapeutic effects are mainly produced by complex interactions among ingredients [12]. Current experimental methods are restricted to tap into the deeper well and comprehensively elucidate the molecular mechanisms of TCM. The dearth of modern methods in TCM study and deconvolution of

complexity of TCM urgently requires new strategies and appropriate approaches.

As the beginning of TCM network pharmacology, we proposed the possible relationship between TCM and molecular networks in 1999 [13] and established a network-based herbal formulae research framework illustrated by a network-based case study on Cold/Hot herbal formulae and Hot/Cold syndromes in 2007 [14, 15]. Shortly after, the age of “network pharmacology” has clearly begun [16, 17], we believe network pharmacology approaches, focused on examining the network connectivity and dynamics as components of drug targets and designing the optimal therapeutic strategies, can reveal the underlying complex relationships between a herbal formula and the whole body. Thus, we further explored the new subject of TCM network pharmacology by updating the research paradigm from current “one target, one drug” to “network target, multicomponent therapeutics,” which refers to the comprehensive analysis for therapeutic effects of herbal formulae on the basis of the identification of the network target underlying a given disease or TCM syndrome as well as the target network of a given herbal formula [15, 18–20]. To date, accumulating evidence suggests that the network pharmacology analysis is a powerful way to study the molecular mechanisms that are responsible for combinational effects of herbal formula [18, 20–25]. For example, Sun et al. presented a network analysis to explore the mechanism of anti-Alzheimer herbal ingredients by evaluating the distance between the herbal targets and “Alzheimer-related proteins” in the protein interaction network [21]. Wang et al. used a systems biology model integrating oral bioavailability and drug-likeness screening, target identification, and network methods to analyze the synergistic mechanism of four herbs in combined treatment of cardiovascular disease [22].

In this work, to better recognize the active ingredients in herbal formula and uncover the combinational rules of ingredients, we integrate our previous methods into a TCM network pharmacology platform to illustrate network connections between multiple targets of ingredients in herbal formula and multiple genes of a specific disease. The methods we created for TCM network pharmacology in the past years include network-based disease gene prediction, drug target prediction, drug-gene-disease comodule association, herb network analysis, and synergistic drug combination screening [20, 25–31]. The good performance of these methods had been demonstrated in discovery of bioactive compounds and elucidation of action mechanism for herbal formulae [23, 32].

We further apply this integrative platform to unveil the molecular mechanisms of antirheumatoid arthritis (RA) formula named *Qing-Luo-Yin* (Q-L-Y), including four herbs: Ku-Shen (*Sophora flavescens*), Qing-Feng-Teng (*Sinomenium acutum*), Huang-Bai (*Phellodendron chinensis*) and Bi-Xie (*Dioscorea collettii*) [33]. Here, we revealed the target network of QLY against RA-related key processes including angiogenesis, inflammatory response, and immune response and report that the four herbs may produce interactions for enhancing efficiency and reducing toxicity through acting in concert on the target network closely associated with RA. The *Jun* herb, Ku-Shen, treats the main causes of RA, for example,

inflammatory response, immune response, and angiogenesis. The *Chen* herb, Qing-Feng-Teng, serves to augment the anti-inflammatory and antiangiogenesis effects of *Jun*. The *Zuo-Shi* herbs, Huang-Bai and Bi-Xie, are used to modulate the therapeutic effects of *Jun-Chen* herbs and to counteract the side effects of Ku-Shen possibly by targeting some off-target genes (i.e., PTGS1). Moreover, we found that the synergism among major ingredients from Ku-Shen and Qing-Feng-Teng may derive from the feedback loop and compensatory mechanisms (i.e., TNF-, IL1B-, and VEGFA induced NF- κ B pathways). We also identified several ingredient groups such as Saponins and Alkaloids that act as active components in QLY using the cluster analysis of their target profiles. The above findings are either verified by the literature evidence or have the potential to guide further experiments. Hopefully, our platform is eventually extensible to other herbal formulae, which provides a reliable and practical strategy to identify active herbal ingredients and potential synergistic pairs, to reveal the mechanisms of herbal formulae and to facilitate TCM drug discovery and modernization as well.

2. Materials and Methods

2.1. Inputs of the Integrative Platform of TCM Network Pharmacology. To address the challenges in the study of the molecular basis and combinatorial principle of herbal formulae, we developed a network-based integrative strategy to provide a unified framework as a platform for TCM network pharmacology (Figure 1). This platform contains two different types of entities as inputs: herbal ingredients with known chemical structure, disease-specific genes, and targets of drug treating this disease. Previously, we built a HerbBioMap database to collect the chemical ingredients in 621 herbs [34]. For QLY, we select all available ingredients for each of four herbs in this formula from HerbBioMap and the available literature on the four herbs [34–37]. We also conducted chemical analysis to identify and determine the major ingredients in QLY, for example, Matrine, Kurarinone, Sinomenine, Berberine, and Diosgenin [38, 39]. Finally, after excluding the repeated ingredients, a total of 235 ingredients with 112 in Ku-Shen, 49 in Qing-Feng-Teng, 54 in Huang-Bai, and 20 in Bi-Xie were collected in this study. The structure, canonical name, and CID number of these ingredients were obtained from PubChem [40]. For RA, known RA-related genes were retrieved from the OMIM Morbid Map [41]. Putative RA genes were predicted by our CIPHER method [27]. The known targets of RA drugs were obtained from DrugBank database [42]. For RA disease network construction, these genes and gene products are treated as seeds to obtain their partner genes in the context of the human protein-protein interaction network (HPRD, Release 7) [43].

2.2. Predicting Target Profiles for Each Ingredients in QLY. Comprehensively determining compound-target interaction profiles and mapping these on signaling and metabolic pathways will become increasingly necessary for elucidating the mechanisms of action of drugs [44]. *In silico* prediction

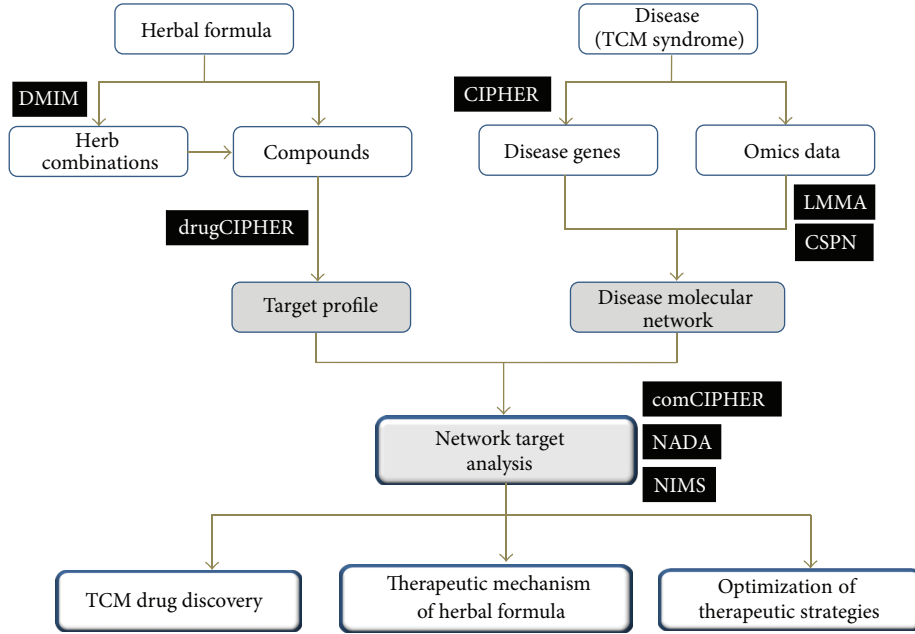


FIGURE 1: A schematic map of the integrative TCM network pharmacology platform that is based on our network target theory and combined some of our self-developed methods including CIPHER, drugCIPHER, comCIPHER, DMIM, NIMS, NADA, LMMA, and CSPN.

of target profiles of small molecular compounds especially is a critical step for the study of TCM network pharmacology. Recently, we developed a regression model called drugCIPHER that can predict the links between drugs and target proteins by combining the drug chemical similarity and protein-protein interaction information in a heterogeneous network that correlates chemical, pharmacological, and genomic spaces [26]. In accordance with the rationale of “like attracts like,” this method is based on the hypothesis that drugs with similar chemical structures or therapeutic effects tend to bind to functionally related or modularized target proteins in the molecular network. Thus, drugCIPHER can infer the target profile for a given herbal ingredient with known structure by integrating and making full use of all available FDA-approved drug structures, drug-target interactions, and human protein-protein interactions. The prediction principle of drugCIPHER is also featured in the TCM holism thinking.

In this study, we used the drugCIPHER-CS step in our drugCIPHER method to predict the target profile for each herbal ingredient from QLY. The drugCIPHER-CS score refers to the likelihood of ingredient-target interaction calculated from the correlation between the query ingredient’s structure similarity vector in the drug space and the target-related gene’s closeness vector in the target space. The resulting proteins with high likelihoods are considered as potential targets of the herbal ingredient. We selected the top 100 proteins with high precision rate as a target profile for each ingredient [26]. We then assembled the target profiles of all available ingredients in every of four herbs and resulted in an integrative target profiles of QLY.

2.3. Principal Component Analysis (PCA). To classify the herbal ingredients from QLY using the predicted target

profiles, PCA was performed to reduce the dimensionality of multivariate data into a multidimensional space, allowing for clear visualization of the variation between different herbal ingredients. In this step, we use PCA to reduce the dimension of the target profile of each ingredient in QLY while most of the variance is preserved by linearly transforming the variables into a smaller number, say n , of variables that we denote by z_1, \dots, z_n :

$$z_i = \sum_{j=1}^m \omega_{ij} x_j, \quad \forall i = 1, \dots, n, \quad (1)$$

where $x = [x(1), \dots, x(m)]^T$ denotes the target profile of each ingredient in QLY and ω_{ij} is transforming weights with the property of the orthogonality and unit norm:

$$\begin{aligned} \sum_j \omega_{ij}^2 &= 1, \quad \forall i, \\ \sum_j \omega_{ij} \omega_{kj} &= 0, \quad \forall i \neq k. \end{aligned} \quad (2)$$

2.4. Network Target Analysis. To better elucidate the holistic therapeutic effects of QLY, we attempted to figure out the target network and mechanism of action of QLY by our platform. First, genes or proteins involved in RA were compiled by combining RA-causing genes from OMIM and CIPHER prediction [27, 41] and the target proteins of anti-RA drugs from DrugBank [42]. Second, RA-related genes or proteins were used as seeds to fish their partner interacting proteins in the HPRD [43]. The searching of such partner proteins resulted in an expanded network as the RA-specific network. Third, the candidate targets of chemical compounds in each herb predicted by drugCIPHER were mapped into

the RA-specific network and were used as a new query to identify the target network of each herb, respectively. Fourth, in order to understand the possible biological functions of each herb, the functional distribution of these target networks was further examined. Finally, the combinational rationale of QLY was interpreted according to the detailed analysis of comodule associations and enriched biological functions.

2.5. Biological Function Enrichment Analysis. For biological functional analysis of QLY, we use the functional enrichment tool of the DAVID database to analyze the enriched GO (Gene Ontology) terms for the assembled target-related proteins of QLY with a false discovery rate less than 0.05 by the Fisher exact test [45, 46]. We only selected the GO functional terms with P value less than 0.05 after Benjamini's correction.

3. Results

3.1. A Self-Developed Platform of TCM Network Pharmacology. The concept of "network target" that we proposed [15, 18–20] is the core of the integrative platform of TCM network pharmacology, by which we hypothesize that the relationship between a herbal formula and a disease or TCM syndrome can be transferred into a network context. The key modules in a disease-specific molecular network are considered as the therapeutic target of a given herbal formula. Thus, we can disclose the action mechanisms and the active ingredients as well as their combinations in a herbal formula from the network target viewpoint. This platform fully integrates our developed methods, in which the good performance has been validated, respectively [25–32], for understanding the therapeutic mechanism of herbal formula from the following three aspects (Figure 1).

- (1) Network target construction: the construction of a disease-specific network as the therapeutic target, such as the prioritization of candidate genes for a given disease (CIPHER) [27], and construction of disease-specific networks in the molecular level (LMMA) [28] or in the pathway-pathway interaction level (CSPN) [29] by combined knowledge and high-throughput omics data.
- (2) Target prediction and herbal pair extraction: the prediction of target profiles of herbal ingredients (drugCIPHER) [26, 47] as well as the extraction of common herbal pairs from herbal formulae treating specific diseases (DMIM) [25].
- (3) Comodule analysis based on the network target: such as drug-gene-disease comodule analysis between drug (ingredient) targets from herbal formula and disease-specific network target (comCIPHER) [31] and network target-based computational screening of active ingredients (NADA) [30] and synergistic therapeutic combinations (NIMS) [20, 48].

Different from conventional herbal formulae research strategies that find active ingredients based on a certain disease, our network target strategy [25–32] can lead to more

discoveries of active ingredients against various diseases in a network level by capturing each ingredient's target profile in a genome-wide scale. Thus, our platform has two significant characteristics: discovery-oriented and generally applicable, especially in predicting active ingredients, synergistic ingredient combinations as well as active ingredient groups from a given formula, and providing the comprehensive molecular mechanisms of the formula. Here, we examine the *Qing-Luo-Yin* as a case study in the following sections.

3.2. Clustering Active Ingredients in QLY Based on the Target Profiles. QLY, which derives from a Xin'an medical family [49], is an effective formula in the treatment of arthritis and a typical antiangiogenic herbal formula in TCM [50]. This formula is composed of Ku-Shen (*Sophora flavescens*), Qing-Feng-Teng (*Sinomenium acutum*), Huang-Bai (*Cortex Phellodendri Chinensis*), and Bi-Xie (*Dioscorea tokoro Makino*) (Figure 2(a)) [51]. Our previous studies have revealed the antiangiogenic and anti-inflammatory effects [33] and the network regulation actions of QLY [14].

To further understand the molecular details about how QLY can be administrated on RA, we used our platform to predict the target profiles of each ingredient in QLY and utilized PCA to visually assess the distinction of target profiles of each herb and determine whether herbal ingredients can be grouped. The analysis of dimensionality of all target profiles showed that two first components could account for >60% of the variance present in all targets contained within the target profiles. To see whether the variation retained in the two components contains relevant information about the mechanism of QLY, each ingredient is projected onto the two components as illustrated in Figure 2(b). The PCA analysis showed that four herbs cannot be separated into four independent clusters only according to the target profiles (Figure 2(b)), suggesting that the features of target profiles of the ingredients from different herbs are overlapped. Further, to determine whether the herbal ingredients with the similar chemical properties can be clustered together, the results showed that most herbal ingredients in QLY can be roughly divided into three groups, which exactly were mapped to three types of chemical components, namely, saponins, glycosides, and alkaloids (Figure 2(c)). Figure 2(c) showed that the herbal ingredients in each well-separated cluster may have similar mechanisms of action and can affect different stages or pathological processes of RA in the form of active ingredient groups. Together, these findings indicate that predicted target profiles can be used to identify active ingredient groups leading to similar effects in a herbal formula.

3.3. Predicting Active and Synergistic Ingredients from QLY. To examine what ingredients can produce synergistic effects on key pathological processes involving RA, angiogenesis, inflammatory, and immune response and what are the synergistic mechanisms among them, we took advantage of the previous conclusion that synergism may arise from modulations of compensatory actions or feedback loops in the network [20, 52] to estimate the interaction between

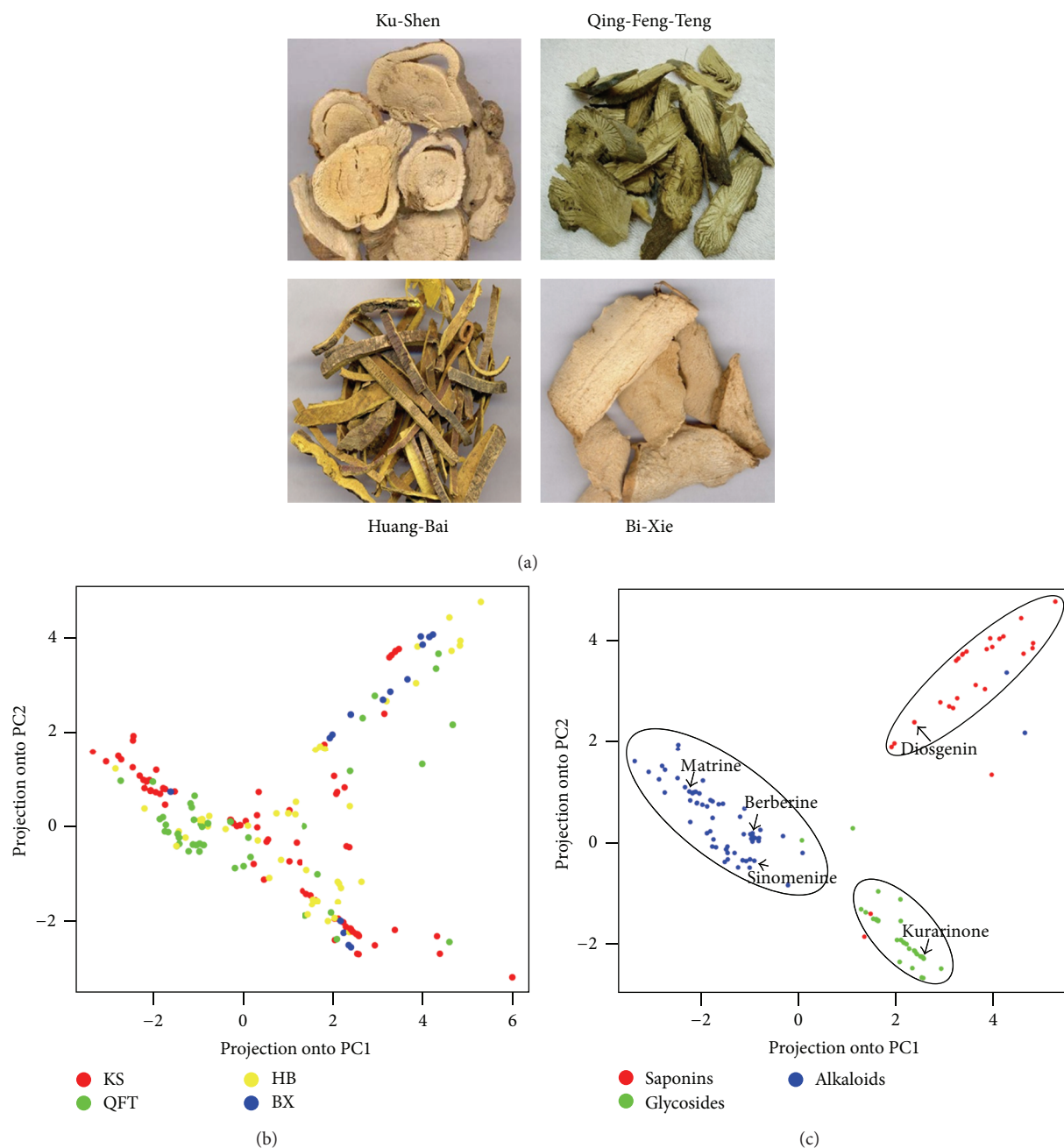


FIGURE 2: (a) Four herbs Ku-Shen (*Sophora flavescens*), Qing-Feng-Teng (*Sinomenium acutum*), Huang-Bai (*Cortex Phellodendri Chinensis*), and Bi-Xie (*Dioscorea tokoro Makino*) in QLY. (b) and (c) Principal component analysis of the target profiles for each herbal ingredient in QLY. Each dot represents one herbal ingredient plotted against its target profile. Ingredients are color coded according to the four herbs (b) and the three types of the chemicals (c) in QLY. Samples were distributed by their similarity in target profiles using dimensionality reduction. The different chemical types cluster in terms of target profiles can be separated from each other. The four herb clusters in terms of target profiles are partially intermix with each other.

ingredients. Adapting such criteria, we derived an ingredient-ingredient interaction network in terms of target proteins of each ingredient (Figure 3). We identified six potentially synergistic pairs between main ingredients from Ku-Shen and other herbs, including Matrine and Sinomenine, Matrine and Kurarinone, Matrine and Berberine, Kurarinone and Sinomenine, Kurarinone and Berberine, and Kurarinone and

Diosgenin. These prediction results can be supported by the literature evidence. For example, Matrine and Sinomenine were evaluated as a synergistic combination by endothelial cell proliferation assay in previous studies [20] and were confirmed from the mechanism here. As shown in Figure 3, the prediction showed that Matrine can bind to the IL1R1, which suppresses inflammatory and immune response by

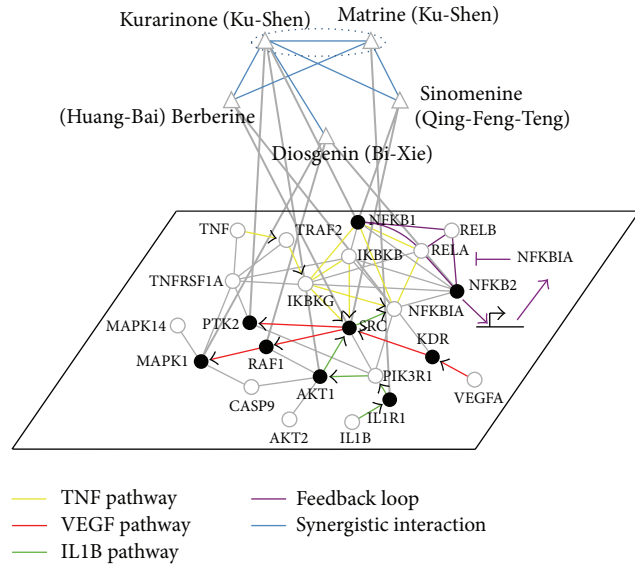


FIGURE 3: Putative therapeutic mechanism for selected major active ingredients in QLY and potential synergistic pairs. The upper network is the ingredient synergy network (including Kurarinone and Matrine in Ku-Shen, Sinomenine in Qing-Feng-Teng, Berberine in Huang-Bai, and Diosgenin in Bi-Xie), and the lower network is RA-specific molecular network which was constructed manually based on the RA-related pathways and the potential targets of the major ingredients. Herbal ingredients and RA-related genes were represented as triangle and circle, respectively. TNF-, IL1B-, and VEGF-induced pathways were highlighted in color line as indicated. NFKB1, NFKB2, RELA, and RELB can form heterogeneous complex as an important transcription factor in the development of RA. The blue line linking two ingredients indicated synergy with the width of the line correlating with the number of synergistic mechanisms: the wider line represented feedback and compensatory mechanisms and the narrow line represented feedback or compensation.

blocking the NF- κ B pathway activated by IL1B. Sinomenine can suppress angiogenesis and inflammation by inhibiting NFKB1 and SRC. Sinomenine may complement Matrine-induced inactivation of NF- κ B to reduce its induction of angiogenesis, inflammation, and immune response. In particular, two ingredients from Ku-Shen, Kurarinone and Matrine, may lead to potent synergistic interaction with each other, thus reflecting interactions from different ingredients in the same herb. Because some studies indicated the relationship between NF- κ B and oxidative stress in rheumatoid arthritis [53], we inferred that Kurarinone as an antioxidant [54] is likely to inhibit NF- κ B activation in terms of predicted target profiles. Kurarinone can inhibit AKT1 and PTK2, which is downstream of IL1B. This may sensitize the effect of Matrine via modulation of NF- κ B and AKT1. In addition, four other synergistic pairs were also identified by network-based synergism hypothesis. For example, Matrine and Berberine act on different targets (IL1R1 and KDR) of two cross-talk pathways (IL1B and VEGFA pathway) that regulate the SRC activity. Kurarinone and Sinomenine act on different targets (AKT1 and SRC) of the same pathway (AKT1-SRC-PTK2 pathway) that regulates the NFKB1. Kurarinone and Berberine act on different targets (NFKB1 and KDR) of two related pathways

(VEGF and NF- κ B pathway) that regulate different targets (SRC and NFKB1). Kurarinone and Diosgenin act on the same type of target (NFKB1 and NFKB2) in the feedback loop (NFKB1-NFKB2-RELA-RELB complex) and different targets (PTK2 and RAF1) of two related pathways.

3.4. Target Networks and Combinatorial Rules of QLY. Different from the conventional trial-and-error drug studies, our network-based strategy tries to make the TCM drug discovery predictable and to make the systematical study of combinatorial rules in herbal formulae achievable. As shown in Figure 4, the network target analysis of 235 ingredients in QLY herbs indicated the detailed mechanisms of herb combinations with increased efficacy and decreased toxicity in RA therapy. Ku-Shen, as *Jun* herbs in QLY, acts on the principle RA pathological processes, such as inflammation, immune response, and angiogenesis. Qing-Feng-Teng as a *Chen* herb and Huang-Bai and Bi-Xie as *Zuo-Shi* herbs seem to augment or modulate the therapeutic effects of *Jun* herb through targeting RA-related genes including NFKB1, HTR3A, CASP1, and PPARG. Interestingly, these results of network target analysis demonstrate an unexpected mechanism of QLY for RA therapies, in which Aryl hydrocarbon receptor (AHR) contributing to the pathogenesis of RA [55] is regulated by multiple ingredients in QLY (e.g., Kuraridin, Sophoraflavanone and Xanthohumol in Ku-Shen, Salicylaldehyde and Allantoin in Qing-Feng-Teng, β -Elemene in Huang-Bai, and Piperitol in Bi-Xie). Besides, the pharmacological activities of Ku-Shen, Qing-Feng-Teng, and Bi-Xie are associated with targeting the NF- κ B pathway. These results demonstrated the synergistic effects among the four herbs of QLY. Our predictions also include the mechanisms of decreased toxicity of *Zuo* and *Shi* herb in QLY. For instance, Xanthohumol in *Jun* herb may cause adverse drug reactions through affecting off-target genes such as PTGS1, resulting in gastrointestinal haemorrhage, haematuria, and abdominal pain [56]. In the target network, we found that cis-limonene oxide phellochinin A and ferulic acid in Huang-Bai may neutralize the adverse effects of Ku-Shen through modulating PTGS1.

In addition, by examining the functional distribution of the potential targets of QLY, we found that the significantly enriched GO terms QLY acted include the key processes in the development of RA, such as inflammatory response, regulation of cytokine production, regulation of angiogenesis, and leukocyte activation (Table 1). Therefore, by modulating these pathological processes, QLY may promote the recovery of network balance from a disease state to a normal state. Together, these results reveal not only the target network of QLY against RA-related angiogenesis, inflammatory response, immune response, and NF- κ B activity but also the “*Jun-Chen-Zuo-Shi*” principle of QLY from the connections of functional modules in the network target.

4. Discussion

Many common diseases such as cancer and rheumatoid arthritis as well as cardiovascular diseases are complex biological systems caused by multiple molecular abnormalities

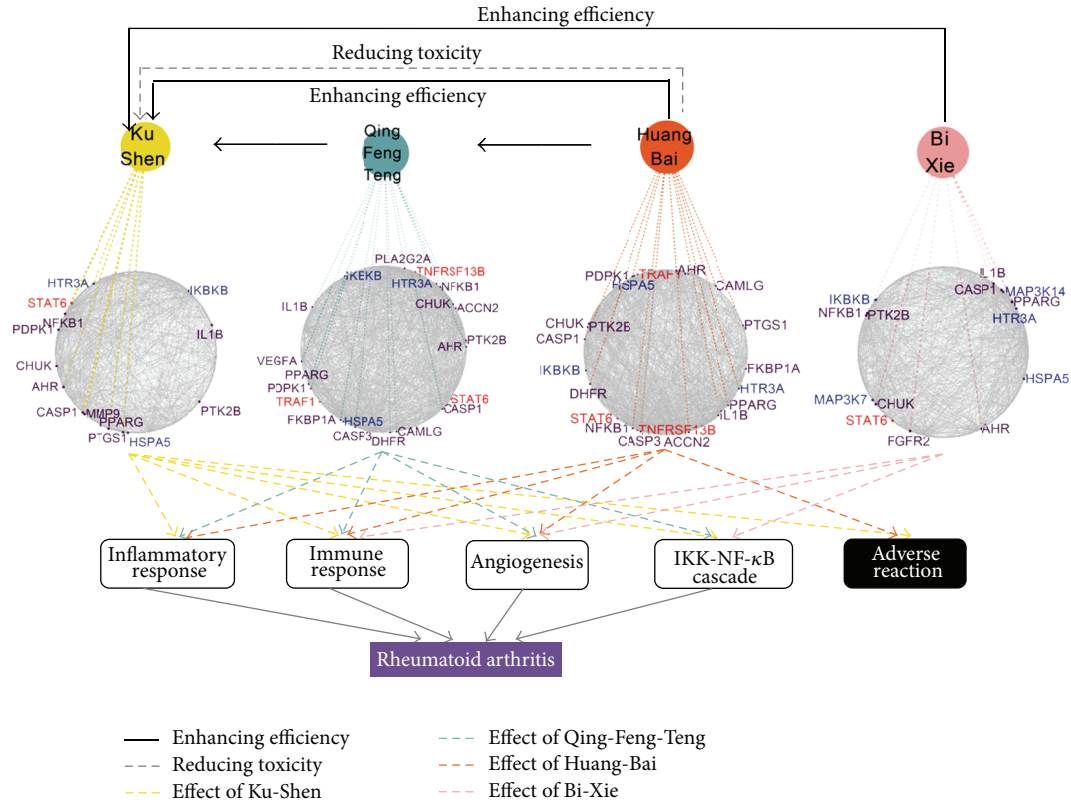


FIGURE 4: Target network and functional enrichment of the four herbs from QLY. A target network of each herb was uniquely identified by mapping the possible targets of each herb into RA-specific molecular network. The functions for the target networks were obtained by the functional enrichment tool (DAVID). These enriched biological functions are associated with RA. Targeting PTGS1 may lead to some adverse effects. Genes labeled in red color denote RA genes collected from OMIM, genes labeled in purple color denote the targets of the FDA-approved drugs for treating RA, and genes labeled in blue color represent RA genes predicted by CIPHER.

TABLE 1: Enriched RA-related GO terms in the *Qing-Luo-Ying* target network.

Function category	GO term ID	GO terms	P value (Benjamini's correction)
Angiogenesis	GO:0009611	Response to wounding	1.30E - 29
	GO:0045765	Regulation of angiogenesis	1.62E - 04
	GO:0010594	Regulation of endothelial cell migration	0.002
Inflammatory response	GO:0006954	Inflammatory response	1.23E - 13
	GO:0001817	Regulation of cytokine production	1.42E - 04
	GO:0006955	Immune response	0.002
	GO:0045321	Leukocyte activation	1.17E - 05
	GO:0001816	Cytokine production	0.004
	GO:0051249	Regulation of lymphocyte activation	0.001
	GO:0006952	Defense response	2.88E - 12
	GO:0042981	Regulation of apoptosis	2.32E - 17
NF-κB activity	GO:0051092	Positive regulation of NF-κB transcription factor activity	0.037

[57, 58]. During the therapy, many drugs that modulate a single target might not always yield the desirable outcome even if they completely interdict the functions of their direct targets [59, 60]. From a network perspective, the entity that needs to be targeted and modulated must shift from single proteins to entire disease molecular networks [61,

62]. The efficacy of such therapies can be explained by the fact that drugs targeting different proteins in the disease network or pathway could trigger a synergistic response, and their combinations can eliminate compensatory reactions and feedback controls, thereby overcoming the robustness of diseases [63, 64]. These perspectives illuminate that the level

of complexity of the proposed therapies should be increased. Interestingly, the properties of TCM herbal formula are consistent with the coming network-based therapeutic strategies. However, currently it is hard to unveil the complex systems embedded in the TCM repertoire, especially the interactions between the complex biological systems of human body and the complex chemical systems of herbal formulae.

To provide a novel route for the systematic studies of herbal formulae, here we report a self-developed integrative platform of TCM network pharmacology (Figure 1) to acquire a better understanding of the underlying mechanisms and combinatorial rules of herbal formula. To the best of our knowledge, this is the first self-developed TCM network pharmacology platform for studying herbal formulae [47, 48, 65]. Indeed, the performance of all methods in the platform have been properly tested, respectively [25–32], and some key methods have been recognized as one of the leading approaches in network biology and network pharmacology [66, 67]. For instance, CIPHER achieves a high-precision accuracy in disease gene prediction that outperforms the state-of-art methods [27], drugCIPHER takes the lead in the genome-wide drug target prediction [26], and NIMS is regarded as a novel method in network pharmacology [67]. These methods can help solve challenging problems in studying chemical and biological basis of herbal formula. For example, drugCIPHER provides a new way to identify target profiles of most ingredients in herbal formulae [26, 47].

In this work, by QLY as a case study, we demonstrate that this platform is effective on identifying bioactive ingredients, synergistic ingredient pairs, and ingredient groups (Figures 2 and 3) and elaborating the combinatorial rules of QLY (Figure 4), which tentatively validated by statistical approaches as well as literature. For example, the previous experimental studies have shown the anti-inflammatory actions of Matrine, the antiangiogenic effect and anti-IL1B expression of Sinomenine, the immune-regulatory effect of Berberine [68–71], and synergistic effects between Matrine and Sinomenine [20], which proved the outputs of our platform. Although the target networks of QLY need to be further experimentally determined, this platform is useful for uncovering the systematic-level mechanisms that are not easily detectable in experimental studies. For instance, our analysis revealed that not only Ku-Shen and three other herbs may synergize by targeting different biological processes (e.g., angiogenesis, inflammatory, and immune response), but also Huang-Bai may antagonize the adverse reaction of Ku-Shen through some off-target genes (e.g., PTGS1) that deserve further experimental testing.

The aim of herbal formulae treatment is to adjust an imbalance state of disease-specific network, which refers to the network interaction and node activity or expression in a given disease context deviating from health status (Figure 5). Recent studies of cancer therapy have shown that disease-specific networks are dynamic and can change with time and space in order to adapt to different interventions, resulting in compensatory effects and drug resistance [72, 73]. For a given disease-specific molecular network, the combination of interventions can best restore the disease network to a desired normal state. Thus, our platform can be used to reveal the

behavior of network balance regulation featured by herbal formulae. Our results suggest that various ingredients in QLY may weakly target different proteins within the RA molecular network, shut down the whole pathological process by network interaction or biochemical synergism, then maintain a delicate balance of the human body, and finally activate its own capability of disease resistance. In this study, we clarified that the synergistic effects among six main ingredients in QLY are caused by acting on the compensatory pathway and feedback loop in the TNF/IL1B/VEGF-induced NF- κ B pathways involved in RA and the synergistic mechanism of QLY is partially associated with the modulation of NF- κ B imbalanced network (Figures 3 and 4). Recently, the combination intervention of NF- κ B system has provided the evidence for the efficiency of network balance regulation in cancer therapy. For instance, NF- κ B-blocking therapies against tumors with constitutive or chemotherapy-induced NF- κ B activation represent one of the few examples where inhibition of NF- κ B network serves as a homeostatic switch for enhancing genotoxic damage but promotes the secretion of protumorigenic factor, IL-1 β [74, 75]. In this case, NF- κ B inhibition combined with anti-IL-1 therapy will rebalance the adverse effects of perturbed NF- κ B network [76]. Indeed, the adjustment of dysregulated NF- κ B network implicated in other diseases can help to understand the effects of QLY on RA. QLY is most likely to modulate angiogenesis within inflammation or tumor environment owing to its modulation of the NF- κ B network. It is noted that the *Jun-Chen* herb (Ku-Shen and Qing-Feng-Teng) in QLY has shown the therapeutic benefits on tumor development [70, 77]. Recently we also identified and experimentally verified a novel angiogenesis inhibitor, vitexicarpin, from a herb paired with Huang-Bai in QLY [32]. We believe that integrative adjustment of the imbalanced network is expected to be one of the trends of future drug discovery, especially discovery of combinatory drugs from herbal formulae.

In addition, we can also capture the formula-syndrome relationship from a network target viewpoint. The treatment strategy of herbal formula is characterized by guiding the combination of herbs in the light of the imbalance state of the human body, such as TCM Cold and Hot syndromes. We investigated the imbalanced molecular network associated with Cold syndrome and Hot syndrome in the context of the neuroendocrine-immune system and identified several key Hot syndrome-related molecules, such as IL1B, TNF, and VEGF [14]. Our previous results demonstrated that QLY can suppress angiogenesis and inflammation in collagen induced arthritis rats [33]. The present work also demonstrates at the molecular level that QLY as a Cold-natured formula is likely to modulate these network hub molecules of Hot syndrome (IL1B, TNF, and VEGF), aiming to expel the “pathogenetic hot” for curing Hot syndrome-related RA and exert the antiangiogenesis, anti-inflammation, and immune-regulatory actions (Figure 4 and Table 1). All together, these findings evidenced that the mechanism of QLY can be interpreted by its actions on a therapeutic network and its adjustment of the network imbalance state.

As illustrated by *Qing-Luo-Yin*, we demonstrate that the implementation of our TCM network pharmacology

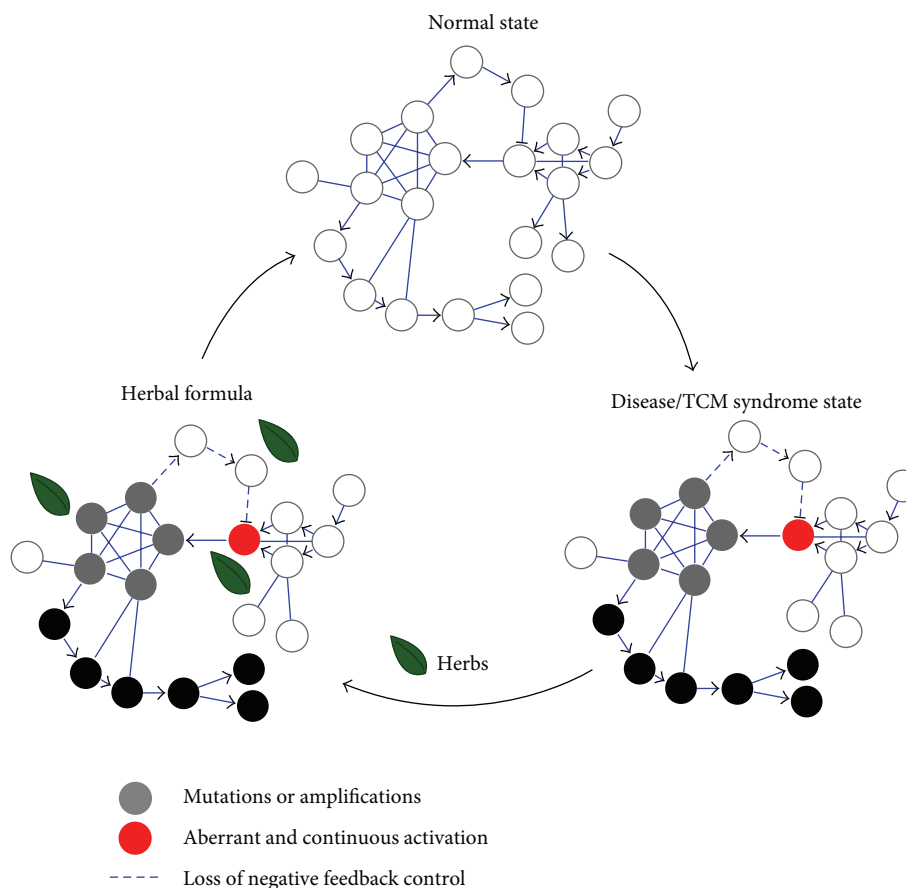


FIGURE 5: Regulation of network imbalance as an important therapeutic principle of herbal formula. Mutation/amplification and aberrant signal transduction cause the multiple changes of the normal network structure, leading to the imbalance of health state. Combinations of herbs used in herbal formula (substantially certain chemical compounds) can weakly target different proteins within the disease-specific network so as to restore the imbalanced disease state.

platform can not only recover the known knowledge but also provide new findings that deserve further experimental validations for discovering the active ingredients and therapeutic mechanism of herbal formulae. Therefore, this sustainable development platform coupling with the rich experience of TCM is hopeful of shifting the paradigm for conquering complex diseases from the conventional “one target, one drug” to the “network target, multicomponent therapeutics,” offering bright prospects and solid supports for translating TCM from experience-based to evidence-based medicine and accelerating TCM drug discovery as well.

Conflict of Interests

The authors declare that they have no conflict of interests.

Acknowledgments

This work is supported by the National Natural Science Foundation of China (nos. 81225025, 60934004, and 91229201), the CATCM project, and the SATCM key discipline of “TCM Bi-Bing” in Yijishan Hospital of Wannan Medical College.

References

- [1] P. M. Barnes, E. Powell-Griner, K. McFann, and R. L. Nahin, “Complementary and alternative medicine use among adults: United States, 2002,” *Advance Data*, no. 343, pp. 1–19, 2004.
- [2] US Food and Drug Administration, Guidance for industry on complementary and alternative medicine products and their regulation by the Food and Drug Administration, 2006.
- [3] J. Qiu, “Traditional medicine: a culture in the balance,” *Nature*, vol. 448, no. 7150, pp. 126–128, 2007.
- [4] T. W. Corson and C. M. Crews, “Molecular understanding and modern application of traditional medicines: triumphs and trials,” *Cell*, vol. 130, no. 5, pp. 769–774, 2007.
- [5] D. K. W. Mok and F. T. Chau, “Chemical information of Chinese medicines: a challenge to chemist,” *Chemometrics and Intelligent Laboratory Systems*, vol. 82, no. 1–2, pp. 210–217, 2006.
- [6] J. L. Zhang, M. Cui, Y. He, H. L. Yu, and D. A. Guo, “Chemical fingerprint and metabolic fingerprint analysis of Danshen injection by HPLC-UV and HPLC-MS methods,” *Journal of Pharmaceutical and Biomedical Analysis*, vol. 36, no. 5, pp. 1029–1035, 2005.
- [7] L. Zhou, Z. Zuo, and M. S. S. Chow, “Danshen: an overview of its chemistry, pharmacology, pharmacokinetics, and clinical use,”

- Journal of Clinical Pharmacology*, vol. 45, no. 12, pp. 1345–1359, 2005.
- [8] J. Kamei, A. Saitoh, T. Asano et al., “Pharmacokinetic and pharmacodynamic profiles of the antitussive principles of *Glycyrrhizae radix* (licorice), a main component of the Kampo preparation Bakumondo-to (Mai-men-dong-tang),” *European Journal of Pharmacology*, vol. 507, no. 1–3, pp. 163–168, 2005.
- [9] T. Efferth, Y. J. Fu, Y. G. Zu, G. Schwarz, V. S. B. Konkimalla, and M. Wink, “Molecular target-guided tumour therapy with natural products derived from traditional Chinese medicine,” *Current Medicinal Chemistry*, vol. 14, no. 19, pp. 2024–2032, 2007.
- [10] W. C. S. Cho, “Application of proteomics in Chinese medicine research,” *The American Journal of Chinese Medicine*, vol. 35, no. 6, pp. 911–922, 2007.
- [11] M. Wang, R. J. A. N. Lamers, H. A. A. J. Korthout et al., “Metabolomics in the context of systems biology: bridging traditional Chinese medicine and molecular pharmacology,” *Phytotherapy Research*, vol. 19, no. 3, pp. 173–182, 2005.
- [12] Z. Xu, “Modernization: one step at a time,” *Nature*, vol. 480, no. 7378, pp. S90–S92, 2011.
- [13] S. Li, “Possible relationship between traditional Chinese medicine ZHENG and molecular networks,” in *Proceedings of the 1st Academic Annual Meeting of the China Association for Science and Technology*, 1999.
- [14] S. Li, Z. Q. Zhang, L. J. Wu, X. G. Zhang, Y. D. Li, and Y. Y. Wang, “Understanding ZHENG in traditional Chinese medicine in the context of neuro-endocrine-immune network,” *IET Systems Biology*, vol. 1, no. 1, pp. 51–60, 2007.
- [15] S. Li, “Framework and practice of network-based studies for Chinese herbal formula,” *Journal of Chinese Integrative Medicine*, vol. 5, no. 5, pp. 489–493, 2007.
- [16] A. L. Hopkins, “Network pharmacology: the next paradigm in drug discovery,” *Nature Chemical Biology*, vol. 4, no. 11, pp. 682–690, 2008.
- [17] A. L. Hopkins, “Network pharmacology,” *Nature Biotechnology*, vol. 25, no. 10, pp. 1110–1111, 2007.
- [18] S. Li, “Network systems underlying traditional Chinese medicine syndrome and herb formula,” *Current Bioinformatics*, vol. 4, no. 3, pp. 188–196, 2009.
- [19] S. Li, “Network target: a starting point for traditional Chinese medicine network pharmacology,” *Zhongguo Zhong Yao Za Zhi*, vol. 36, pp. 2017–2020, 2011.
- [20] S. Li, B. Zhang, and N. B. Zhang, “Network target for screening synergistic drug combinations with application to traditional Chinese medicine,” *BMC Systems Biology*, vol. 5, supplement 1, article S10, 2011.
- [21] Y. Sun, R. Zhu, H. Ye et al., “Towards a bioinformatics analysis of anti-Alzheimer’s herbal medicines from a target network perspective,” *Briefings in Bioinformatics*, vol. 8, pp. 1–17, 2012.
- [22] X. Wang, X. Xu, W. Y. Tao, Y. Li, Y. H. Wang, and L. Yang, “A systems biology approach to uncovering pharmacological synergy in herbal medicines with applications to cardiovascular disease,” *Evidence-Based Complementary and Alternative Medicine*, vol. 2012, Article ID 519031, 15 pages, 2012.
- [23] Y. Wang, Z. Liu, C. Li et al., “Drug target prediction based on the herbs components: the study on the multitargets pharmacological mechanism of qishenkeli acting on the coronary heart disease,” *Evidence-Based Complementary and Alternative Medicine*, vol. 2012, Article ID 698531, 10 pages, 2012.
- [24] J. Zhao, P. Jiang, and W. Zhang, “Molecular networks for the study of TCM pharmacology,” *Briefings in Bioinformatics*, vol. 11, no. 4, Article ID bbb063, pp. 417–430, 2009.
- [25] S. Li, B. Zhang, D. Jiang, Y. Wei, and N. Zhang, “Herb network construction and co-module analysis for uncovering the combination rule of traditional Chinese herbal formulae,” *BMC Bioinformatics*, vol. 11, supplement 11, article S6, 2010.
- [26] S. Zhao and S. Li, “Network-based relating pharmacological and genomic spaces for drug target identification,” *PLoS ONE*, vol. 5, no. 7, Article ID e11764, 2010.
- [27] X. Wu, R. Jiang, M. Zhang, and S. Li, “Network-based global inference of human disease genes,” *Molecular Systems Biology*, vol. 4, article 189, 2008.
- [28] S. Li, L. Wu, and Z. Zhang, “Constructing biological networks through combined literature mining and microarray analysis: a LMMA approach,” *Bioinformatics*, vol. 22, no. 17, pp. 2143–2150, 2006.
- [29] Y. Huang and S. Li, “Detection of characteristic sub pathway network for angiogenesis based on the comprehensive pathway network,” *BMC Bioinformatics*, vol. 11, supplement 1, article S32, 2010.
- [30] L. S. Li, N. B. Zhang, and S. Li, “Ranking effects of candidate drugs on biological process by integrating network analysis and gene ontology,” *Chinese Science Bulletin*, vol. 55, no. 26, pp. 2974–2980, 2010.
- [31] S. Zhao and S. Li, “A co-module approach for elucidating drug-disease associations and revealing their molecular basis,” *Bioinformatics*, vol. 28, no. 7, pp. 955–961, 2012.
- [32] B. Zhang, L. Liu, S. Zhao, X. Wang, L. Liu, and S. Li, “Vitexicarpin acts as a novel angiogenesis inhibitor and its target network,” *Evidence-Based Complementary and Alternative Medicine*, vol. 2012, Article ID 278405, 13 pages, 2012.
- [33] S. Li, A. P. Lu, Y. Y. Wang, and Y. D. Li, “Suppressive effects of a Chinese herbal medicine Qing-Luo-Yin extract on the angiogenesis of collagen-induced arthritis in rats,” *The American Journal of Chinese Medicine*, vol. 31, no. 5, pp. 713–720, 2003.
- [34] S. Li, B. Zhang, and J. Yuan, “HerbBioMap database,” China Copyright of Computer Software, 2011SR076502.
- [35] X. Chen, C. Yi, X. Yang, and X. Wang, “Liquid chromatography of active principles in *Sophora flavescens* root,” *Journal of Chromatography B*, vol. 812, no. 1–2, pp. 149–163, 2004.
- [36] X. X. Zhao, C. Peng, H. Zhang, and L. P. Qin, “Sinomenium acutum: a review of chemistry, pharmacology, pharmacokinetics, and clinical use,” *Pharmaceutical Biology*, vol. 50, no. 8, pp. 1053–1061, 2012.
- [37] J. Zhao, Q. C. Pang, J. Ma, X. W. Zheng, Q. X. Meng, and C. M. Liu, “Main active constituent detection of cortex phellodendri chinensis by spectral imaging technology,” *Acta Optica Sinica*, vol. 28, no. 12, pp. 2288–2291, 2008.
- [38] M. Wu, C. Ma, Y. Wu, and S. Li, “Simultaneous LC analysis of five bioactive alkaloids in an anti-angiogenesis herbal formula, Qing-Luo-Yin,” *Chromatographia*, vol. 68, no. 7–8, pp. 579–585, 2008.
- [39] S. Yang, K. Li, Y. Zhang, S. Li, and Y. Shi, “Identification and determination of the major constituents in an antiangiogenesis herbal formula, Qing-Luo-Fang, by HPLC-DAD-ESI/MS,” *Journal of Liquid Chromatography and Related Technologies*, vol. 33, no. 20, pp. 1842–1853, 2010.
- [40] Y. Wang, J. Xiao, T. O. Suzek, J. Zhang, J. Wang, and S. H. Bryant, “PubChem: a public information system for analyzing bioactivities of small molecules,” *Nucleic Acids Research*, vol. 37, supplement 2, pp. W623–W633, 2009.

- [41] A. Hamosh, A. F. Scott, J. S. Amberger, C. A. Bocchini, and V. A. McKusick, "Online Mendelian Inheritance in Man (OMIM), a knowledgebase of human genes and genetic disorders," *Nucleic Acids Research*, vol. 33, supplement 1, pp. D514–D517, 2005.
- [42] D. S. Wishart, C. Knox, A. C. Guo et al., "DrugBank: a knowledgebase for drugs, drug actions and drug targets," *Nucleic Acids Research*, vol. 36, supplement 1, pp. D901–D906, 2008.
- [43] T. S. K. Prasad, R. Goel, K. Kandasamy et al., "Human protein reference database—2009 update," *Nucleic Acids Research*, vol. 37, supplement 1, pp. D767–D772, 2009.
- [44] U. Rix and G. Superti-Furga, "Target profiling of small molecules by chemical proteomics," *Nature Chemical Biology*, vol. 5, no. 9, pp. 616–624, 2009.
- [45] D. W. Huang, B. T. Sherman, and R. A. Lempicki, "Systematic and integrative analysis of large gene lists using DAVID bioinformatics resources," *Nature Protocols*, vol. 4, no. 1, pp. 44–57, 2009.
- [46] M. Ashburner, C. A. Ball, J. A. Blake et al., "Gene ontology: tool for the unification of biology," *Nature Genetics*, vol. 25, no. 1, pp. 25–29, 2000.
- [47] S. Li and S. Zhao, "Network-based identification of drug target and drug action," Invention Patent: 201010218468.X.
- [48] S. Li, N. Zhang, and B. Zhang, "Network-based identification of synergistic drug combination," Invention Patent: ZL200810239284. 4.
- [49] Y. Li and Y. Liu, "Experience of Professor Li Ji-Ren in the treatment of Bi-ZHENG," *Journal of Beijing University of Traditional Chinese Medicine (Clinical Medicine)*, vol. 14, no. 5, pp. 21–23, 2007.
- [50] T. P. Fan, J. C. Yeh, K. W. Leung, P. Y. K. Yue, and R. N. S. Wong, "Angiogenesis: from plants to blood vessels," *Trends in Pharmacological Sciences*, vol. 27, no. 6, pp. 297–309, 2006.
- [51] S. Li, A. Lu, and H. Jia, "Therapeutic actions of the Chinese herbal formulae with cold and heat properties and their effects on ultrastructures of synoviocytes in rats of the collagen-induced arthritis," *Journal of Traditional Chinese Medicine*, vol. 22, no. 4, pp. 296–302, 2002.
- [52] H. Yan, B. Zhang, S. Li, and Q. Zhao, "A formal model for analyzing drug combination effects and its application in TNF- α -induced NF κ B pathway," *BMC Systems Biology*, vol. 4, article 50, 2010.
- [53] L. G. Darlington and T. W. Stone, "Antioxidants and fatty acids in the amelioration of rheumatoid arthritis and related disorders," *The British Journal of Nutrition*, vol. 85, no. 3, pp. 251–269, 2001.
- [54] X. L. Piao, X. S. Piao, S. W. Kim, J. H. Park, H. Y. Kim, and S. Q. Cai, "Identification and characterization of antioxidants from *Sophora flavescens*," *Biological and Pharmaceutical Bulletin*, vol. 29, no. 9, pp. 1911–1915, 2006.
- [55] T. Nakahama, A. Kimura, N. T. Nguyen et al., "Aryl hydrocarbon receptor deficiency in T cells suppresses the development of collagen-induced arthritis," *Proceedings of the National Academy of Sciences of the United States of America*, vol. 108, no. 34, pp. 14222–14227, 2011.
- [56] E. Lounkine, M. J. Keiser, S. Whitebread et al., "Large-scale prediction and testing of drug activity on side-effect targets," *Nature*, vol. 486, no. 7403, pp. 361–367, 2012.
- [57] H. Kitano, "Biological robustness," *Nature Reviews Genetics*, vol. 5, no. 11, pp. 826–837, 2004.
- [58] H. Kitano, "Cancer as a robust system: implications for anti-cancer therapy," *Nature Reviews Cancer*, vol. 4, no. 3, pp. 227–235, 2004.
- [59] J. Lehár, A. Krueger, G. Zimmermann, and A. Borisy, "High-order combination effects and biological robustness," *Molecular Systems Biology*, vol. 4, article 215, 2008.
- [60] P. Csermely, V. Ágoston, and S. Pongor, "The efficiency of multi-target drugs: the network approach might help drug design," *Trends in Pharmacological Sciences*, vol. 26, no. 4, pp. 178–182, 2005.
- [61] A. del Sol, R. Balling, L. Hood, and D. Galas, "Diseases as network perturbations," *Current Opinion in Biotechnology*, vol. 21, no. 4, pp. 566–571, 2010.
- [62] R. B. Russell and P. Aloy, "Targeting and tinkering with interaction networks," *Nature Chemical Biology*, vol. 4, no. 11, pp. 666–673, 2008.
- [63] A. F. Fliri, W. T. Loging, and R. A. Volkman, "Cause-effect relationships in medicine: a protein network perspective," *Trends in Pharmacological Sciences*, vol. 31, no. 11, pp. 547–555, 2010.
- [64] R. P. Araujo, C. Doran, L. A. Liotta, and E. F. Petricoin, "Network-targeted combination therapy: a new concept in cancer treatment," *Drug Discovery Today: Therapeutic Strategies*, vol. 1, no. 4, pp. 425–433, 2004.
- [65] S. Li, N. Zhang, and B. Zhang, "Method of network-based identification of multicomponent synergy and compositions for use as effective component of anti-angiogenesis medicines," Invention Patent: US, 8112230 B2, 2009.
- [66] A. L. Barabási, N. Gulbahce, and J. Loscalzo, "Network medicine: a network-based approach to human disease," *Nature Reviews Genetics*, vol. 12, no. 1, pp. 56–68, 2011.
- [67] C. Morel, F1000.com/12166956, 2011.
- [68] C. Y. Chuang, J. G. Xiao, and G. C. Y. Chiou, "Ocular anti-inflammatory actions of matrine," *Journal of Ocular Pharmacology*, vol. 3, no. 2, pp. 129–134, 1987.
- [69] T. W. Kok, P. Y. K. Yue, N. K. Mak, T. P. D. Fan, L. Liu, and R. N. S. Wong, "The anti-angiogenic effect of sinomenine," *Angiogenesis*, vol. 8, no. 1, pp. 3–12, 2005.
- [70] X. J. Li, P. Y. K. Yue, W. Y. Ha et al., "Effect of sinomenine on gene expression of the IL-1 β -activated human synovial sarcoma," *Life Sciences*, vol. 79, no. 7, pp. 665–673, 2006.
- [71] Z. Hu, Q. Jiao, J. Ding et al., "Berberine induces dendritic cell apoptosis and has therapeutic potential for rheumatoid arthritis," *Arthritis and Rheumatism*, vol. 63, no. 4, pp. 949–959, 2011.
- [72] P. Lito, C. A. Pratilas, E. W. Joseph et al., "Relief of profound feedback inhibition of mitogenic signaling by RAF inhibitors attenuates their activity in BRAFV600E melanomas," *Cancer Cell*, vol. 22, no. 5, pp. 668–682, 2012.
- [73] A. Britschgi, R. Andraos, H. Brinkhaus et al., "JAK2/STAT5 inhibition circumvents resistance to PI3K/mTOR blockade: a rationale for cotargeting these pathways in metastatic breast cancer," *Cancer Cell*, vol. 22, no. 6, pp. 796–811, 2012.
- [74] F. R. Greten, M. C. Arkan, J. Bollrath et al., "NF- κ B is a negative regulator of IL-1 β secretion as revealed by genetic and pharmacological inhibition of IKK β ," *Cell*, vol. 130, no. 5, pp. 918–931, 2007.
- [75] L. C. Hsu, T. Enzler, J. Seita et al., "IL-1 β -driven neutrophilia preserves antibacterial defense in the absence of the kinase IKK β ," *Nature Immunology*, vol. 12, no. 2, pp. 144–150, 2011.
- [76] Y. Ben-Neriah and M. Karin, "Inflammation meets cancer, with NF- κ B as the matchmaker," *Nature Immunology*, vol. 12, no. 8, pp. 715–723, 2011.

- [77] L. P. Zhang, J. K. Jiang, J. W. O. Tam et al., "Effects of matrine on proliferation and differentiation in K-562 cells," *Leukemia Research*, vol. 25, no. 9, pp. 793–800, 2001.

Research Article

A Systems Biology-Based Investigation into the Pharmacological Mechanisms of Wu Tou Tang Acting on Rheumatoid Arthritis by Integrating Network Analysis

Yanqiong Zhang, Danhua Wang, Shufang Tan, Haiyu Xu, Chunfang Liu, and Na Lin

Institute of Chinese Materia Medica, China Academy of Chinese Medical Sciences, No. 16, Nanxiaojie, Dongzhimennei, Beijing 100700, China

Correspondence should be addressed to Na Lin; linna888@163.com

Received 11 January 2013; Accepted 20 February 2013

Academic Editor: Aiping Lu

Copyright © 2013 Yanqiong Zhang et al. This is an open access article distributed under the Creative Commons Attribution License, which permits unrestricted use, distribution, and reproduction in any medium, provided the original work is properly cited.

Aim. To investigate pharmacological mechanisms of Wu Tou Tang acting on rheumatoid arthritis (RA) by integrating network analysis at a system level. **Methods and Results.** Drug similarity search tool in Therapeutic Targets Database was used to screen 153 drugs with similar structures to compositive compounds of each ingredient in Wu Tou Tang and to identify 56 known targets of these similar drugs as predicted molecules which Wu Tou Tang affects. The recall, precision, accuracy, and F1-score, which were calculated to evaluate the performance of this method, were, respectively, 0.98, 0.61, 59.67%, and 0.76. Then, the predicted effector molecules of Wu Tou Tang were significantly enriched in neuroactive ligand-receptor interaction and calcium signaling pathway. Next, the importance of these predicted effector molecules was evaluated by analyzing their network topological features, such as degree, betweenness, and k -coreness. We further elucidated the biological significance of nine major candidate effector molecules of Wu Tou Tang for RA therapy and validated their associations with compositive compounds in Wu Tou Tang by the molecular docking simulation. **Conclusion.** Our data suggest the potential pharmacological mechanisms of Wu Tou Tang acting on RA by combining the strategies of systems biology and network pharmacology.

1. Introduction

Rheumatoid arthritis (RA) is a systemic autoimmune disease characterized by the presence of inflammatory synovitis, the predominance of proerosive mediators, and the progressive destruction of cartilage and bone [1]. Traditional Chinese Medicine (TCM) has been extensively used for centuries in the treatment of arthritic diseases. On the concept of TCM, RA is categorized as “arthromyodynia” (Bi Zheng, Bi syndrome, or blockage syndrome) [2]. Various TCM-based herbal formulas and the extracts or the ingredients of herbs, such as Wu Tou Tang, Guizhi Shaoyao Zhi Mu Tang, Du Huo Ji Sheng Tang, Fangji Huangqi Tang, and extracts of the herb *Tripterygium Wilfordii* Hook f. (TWHF) have been demonstrated to be effective for relieving the severity of RA [3–5]. The use of a combination of multiple herbs in TCM formulas is designed to exploit the additive or synergistic activities of individual herbs, as well as to balance

or neutralize the toxic effects of certain herbal components by others in the mixture [6]. It is of great significance to screen effective ingredients from natural herbs and investigate their therapeutic mechanisms.

Wu Tou Tang as a classic TCM formula from Chinese medical sage Zhang Zhongjing is prepared from a basic formula of five Chinese herbs, including Radix Aconiti (Wu Tou), Herba Ephedrae (Ma Huang), Radix Astragali (Huang Qi), Radix Paeoniae Alba (Bai Shao), and Radix Glycythizae (Gan Cao). It is widely produced in China in accordance with the China Pharmacopoeia standard of quality control and is extensively used for the treatment of RA, hemicranias, and constitutional hypotension [7]. In TCM theory, multiple agents contained in one formula must work synergistically. With regard to Wu Tou Tang, Radix Aconiti is the primary component and is believed to be effective in treating rheumatic arthritis and RA; Herba Ephedrae serves as the ministerial component to intensify the analgesic function

of Radix Aconiti; Radix Astragali acts as the adjunctive component to invigorate qi (vital energy), strengthen the body, and reinforce the effect of Radix Aconiti and Herba Ephedrae; Radix Paeoniae Alba and Radix Glycythizae are both messenger drugs which can either focus the actions of the formula on a certain area of the body or harmonize and integrate the actions of the other ingredients of the formula [8, 9]. There have been a large number of studies which were carried out to investigate in active monomers among ingredients of Wu Tou Tang and made great progresses. For example, Aconitine (monomer of Radix Aconiti) is found to greatly lighten the hyperalgesia of the rat adjuvant arthritis [10]; Ephedrine (monomer of Herba Ephedrae) is an alkaloid that functions as a decongestant, an antitussive, a central nervous system (CNS) stimulant, and an appetite suppressant [11]. However, monomer pharmacological effects cannot present overall efficacy of the whole formula. There is an urgent need for investigations involving all the compounds of Wu Tou Tang.

TCM, characterized by the use of herbal formula (Fu-Fang), is multicomponent and multitarget agents, essentially achieving the therapeutic effectiveness through collectively modulating the molecular network of the body system using its active ingredients. Which the development in high-throughput detection methods, many researchers have investigated the multitarget and synergetic actions of multicomponent in TCM formula at a molecular level. However, these studies have confronted several great challenges as following. First, it is very labor-intensive, time-consuming and costly to isolate and identify chemical constituents with desirable pharmacological effects, because most medicinal herbs may contain tens of thousands of constituents; then, it is very difficult to investigate its pharmacological and toxicological effects, because a certain component in TCM formula may act on multiple biological targets; finally, there may be a complex and highly dynamic ingredient-ingredient interaction network underlying the overall clinical effects because TCM formulas are administrated as an integrated prescription for treating diseases traditionally. In this context, it is necessary to develop a novel method which can understand the biological processes of the interactions among genes, proteins, and environmental factors at a system level in order to discover the molecular mechanisms related to the therapeutic efficacy of TCM. Network pharmacology, a novel research field which elucidates the underlying mechanisms of biological systems by analyzing various biological networks such as ingredient-ingredient, ingredient-target, target-target interaction networks, may have the potentials to address the relationship between multicomponents and drug synergistic effects [12, 13]. There are two kinds of approaches in network pharmacology. (1) Bottom-up: addition of well-known molecular drugs and observation of synergistic effects; (2) top-down: reduction of more general formula to its minimal elements that keep its beneficial properties [14, 15]. As TCM formula is considered to be an empirical system of multicomponent therapeutics which potentially meets the demands of treating a number of complex diseases in an integrated manner, the methodologies of network pharmacology are suitable for pursuing a priori knowledge about the

combination rules embedded in TCM [16]. Therefore, we here intend to investigate the pharmacological mechanisms of Wu Tou Tang acting on RA by integrating network analysis.

2. Materials and Methods

The technical strategy of this study was shown in Figure 1.

2.1. Data Preparation

2.1.1. Structural Information of the Compositive Compounds of Each Ingredient in Wu Tou Tang. Structural information (*.mol or *.sdf files) of the compositive compounds of each ingredient in Wu Tou Tang was obtained from TCM Database@Taiwan [17] (<http://tcm.cmu.edu.tw/>, Updated in 2012-06-28), which is currently the largest noncommercial TCM database worldwide. TCM Database@Taiwan is based on information collected from Chinese medical texts and scientific publications and contains more than 20,000 pure compounds isolated from 453 TCM ingredients. In total, we collected the structural information of 17 compounds for Radix Aconiti, 29 compounds for Herba Ephedrae, 22 compounds for Radix Astragali, 15 compounds for Radix Paeoniae Alba and 82 compounds for Radix Glycythizae.

2.1.2. Known Therapeutic Targets Approved by FDA for the Treatment of RA. Known therapeutic targets were obtained from DrugBank database [18] (<http://www.drugbank.ca/>, version: 3.0). We only used those drug-target interactions whose drugs are FDA approved for the treatment of RA and whose targets are human genes/proteins. In total, we obtained 58 known therapeutic targets. The detailed information on these known therapeutic targets is described in Supplementary Table S1 in Supplementary Material available online at <http://dx.doi.org/10.1155/2013/548498>.

2.1.3. Protein-Protein Interaction (PPI) Data. PPI data were imported from eight existing PPI databases including Human Annotated and Predicted Protein Interaction Database (HAPPI) [19], Reactome [20], Online Predicted Human Interaction Database (OPHID) [21], IntAct [22], Human Protein Reference Database (HPRD) [23], Molecular Interaction Database (MINT) [24], Database of Interacting Proteins (DIP) [25], and PDZBase [26]. The detailed information on these PPI databases is described in Supplementary Table S2. In total, we obtained 6713 interactions between 3231 proteins.

2.2. Pharmacological Mechanism Analysis

2.2.1. Screening of Similar Drugs and Prediction of Effector Molecules for Wu Tou Tang. We used drug similarity search tool in Therapeutic Targets Database [27] (TTD, <http://xin.cz3.nus.edu.sg/group/cjttd/ttd.asp>, Version 4.3.02 release on Aug 25th 2011) to screen similar drugs of Wu Tou Tang through the structural similarity comparison. TTD provides comprehensive information about efficient targets and the corresponding approved, clinical trial, and investigative drugs. All information provided in TTD is fully

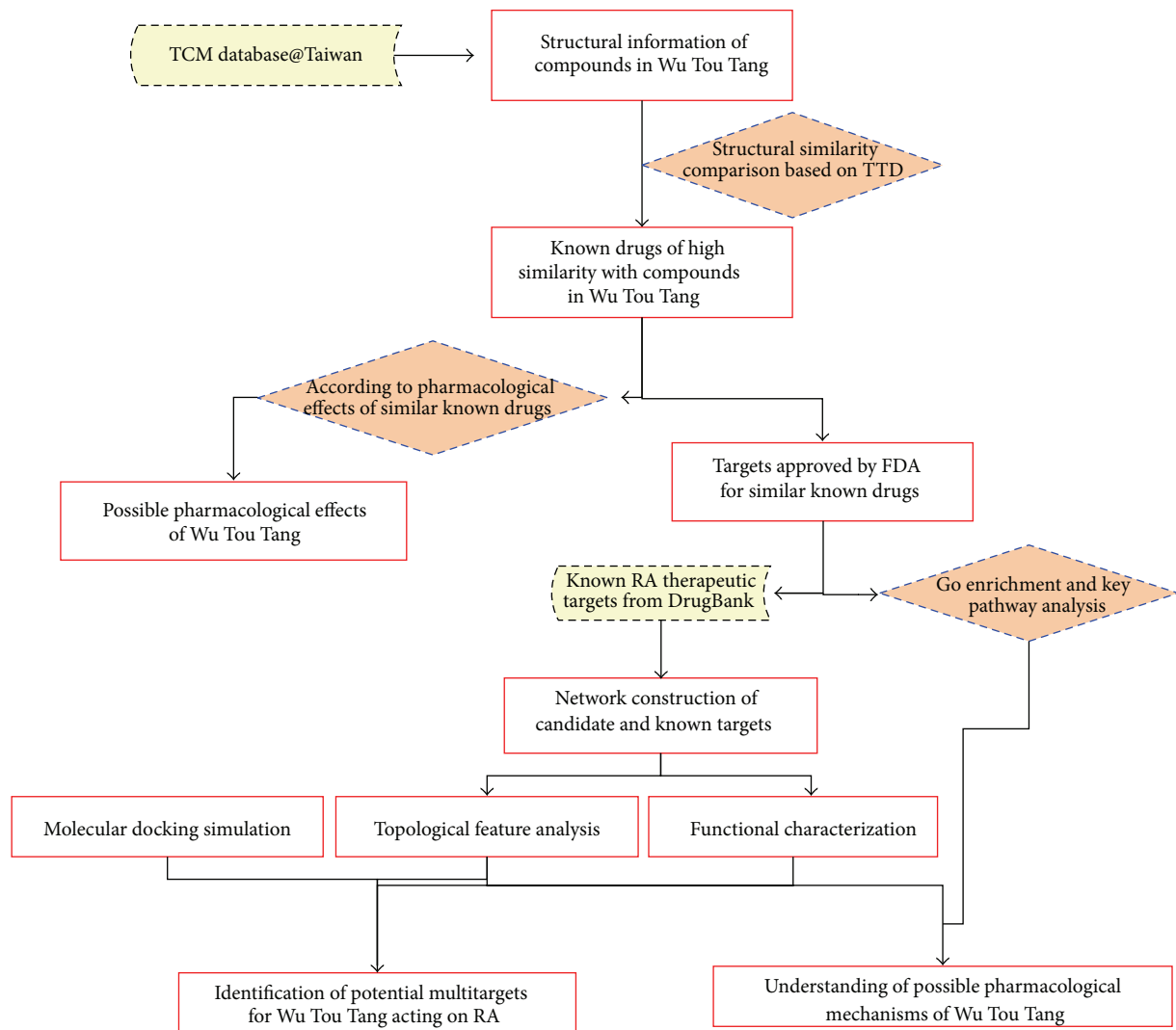


FIGURE 1: A schematic diagram of this systems biology-based investigation into the pharmacological mechanisms of Wu Tou Tang acting on rheumatoid arthritis by integrating multitarget identification and network analysis.

referenced. We only selected the drugs with high similar score (>0.85 , similar ~ very similar) in the comparison with the structures of composite compounds of each ingredient in Wu Tou Tang. The therapeutic targets of these similar drugs were also collected as predicted effector molecules of Wu Tou Tang. In total, we obtained 153 similar drugs and 56 predicted effector molecules of Wu Tou Tang. The detailed information on these similar drugs and predicted effector molecules is described in Supplementary Table S3.

In order to evaluate the performance of this prediction method, 59 FDA-approved drugs and their known targets were randomly collected from TTD (http://bidd.nus.edu.sg/group/cjttd/TTD_Download.asp). The detailed information on these FDA-approved drugs and their known targets is described in Supplementary Table S4). As a certain drug may have or be predicted to have multiple targets, we used a multilabel evaluation measure which can rate predictions as “half-right” when only a portion of the correct

labels were recovered or more labels than the correct ones were predicted. The overall accuracy (ACC) which is the percentage of correctly predicted instances, the recall (REC), the precision (PRE), and the average $F1$ -score ($F1$) which is the harmonic mean of REC and PRE were calculated according to the previous study [28]. Let D denote a dataset with n instances. In addition, let Y_i and Z_i be the set of correct labels and the set of predicted labels of instance $i \in D$, respectively. Consequently, we can define the ACC, REC, PRE, and $F1$ for label k as follows:

$$ACC = \sum_{(i/i \in D)} \frac{|Y_i \cap Z_i|}{|Y_i \cup Z_i|}, \quad (f1)$$

$$REC_k = \sum_{(i/i \in D \& k \in Y_i)} \frac{|Y_i \cap Z_i|}{|Z_i|}, \quad (f2)$$

$$\text{PRE}_k = \sum_{(i|i \in D \& k \in Z_i)} \frac{|Y_i \cap Z_i|}{|Z_i|}, \quad (f3)$$

$$F1 = \frac{2(\text{REC})(\text{PRE})}{\text{REC} + \text{PRE}}. \quad (f4)$$

2.2.2. Gene Ontology (GO) and Pathway Enrichment Analysis for Candidate Effector Molecules of Wu Tou Tang. We used Database for Annotation, Visualization, and Integrated Discovery [29] (DAVID, <http://david.abcc.ncifcrf.gov/home.jsp>, version 6.7) for GO enrichment analysis. DAVID now provides a comprehensive set of functional annotation tools for investigators to understand biological meaning behind a large list of genes. We also performed pathway enrichment analysis using pathway data obtained from the FTP service of KEGG [30] (Kyoto Encyclopedia of Genes and Genomes, <http://www.genome.jp/kegg/>, last updated: October 16, 2012). The KEGG pathway section is a collection of manually constructed pathway maps representing information on molecular interaction and reaction networks.

2.3. Network Construction. We first constructed a PPI network for known targets of RA and candidate effector molecules of Wu Tou Tang based on their PPI data obtained from eight existing PPI databases as mentioned above. Then, we applied Navigator software (Version 2.2.1) to visualize the PPI network.

2.4. Defining Features Set. For each node i in the above PPI network, we defined three measures for assessing its topological property. (1) "Degree" is defined as the number of links to node i ; (2) "betweenness" is defined as the number of edges running through node i . Both degree and betweenness centrality can measure a protein's topological importance in the network. The larger a protein's degree/betweenness centrality is, the more important the protein is in the PPI network [31]. (3) K -core analysis is an iterative process in which the nodes are removed from the networks in order of least connected [32]. The core of maximum order is defined as the main core or the highest k -core of the network. A k -core subnetwork of the original network can be generated by recursively deleting vertices from the network whose degree is less than k . This results in a series of subnetworks that gradually reveal the globally central region of the original network. On this basis, " K value" is used to measure the centrality of node i .

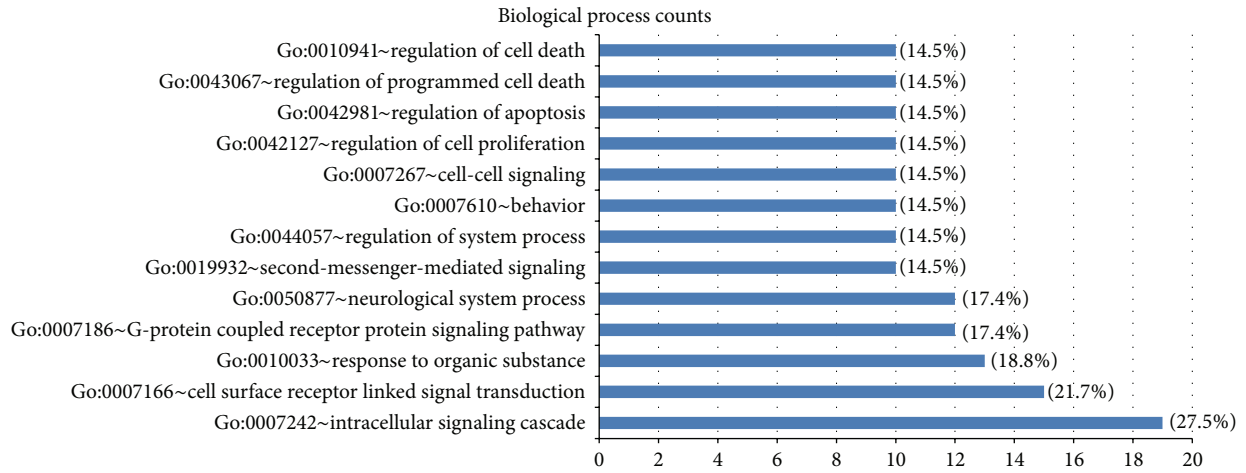
2.5. Molecular Docking Simulation. eHiTS software [33] (Version 4.5, SimBioSys Inc. Canada) was used to validate the associations of candidate effector molecules with compositive compounds in Wu Tou Tang. All the protein structures were obtained from RCSB protein data bank [34] (<http://www.pdb.org/>, been updated in 2012-11-06) and have carefully checked for their resolutions. The 3D structures (*.mol files) of the compositive compounds of each ingredient in Wu Tou Tang were obtained from TCM Database@Taiwan [17] (<http://tcm.cmu.edu.tw/>, Updated in 2012-06-28). A docking score calculated by the customizable

scoring function of eHiTS, which combines novel terms (based on local surface point contact evaluation) with traditional empirical and statistical approaches [33], was used to measure the binding efficiency of each effector molecule to the corresponding compound. For candidate effector molecules, when the docking score was higher than the median value, these proteins were identified be able to bind their corresponding compounds with strong binding efficiency.

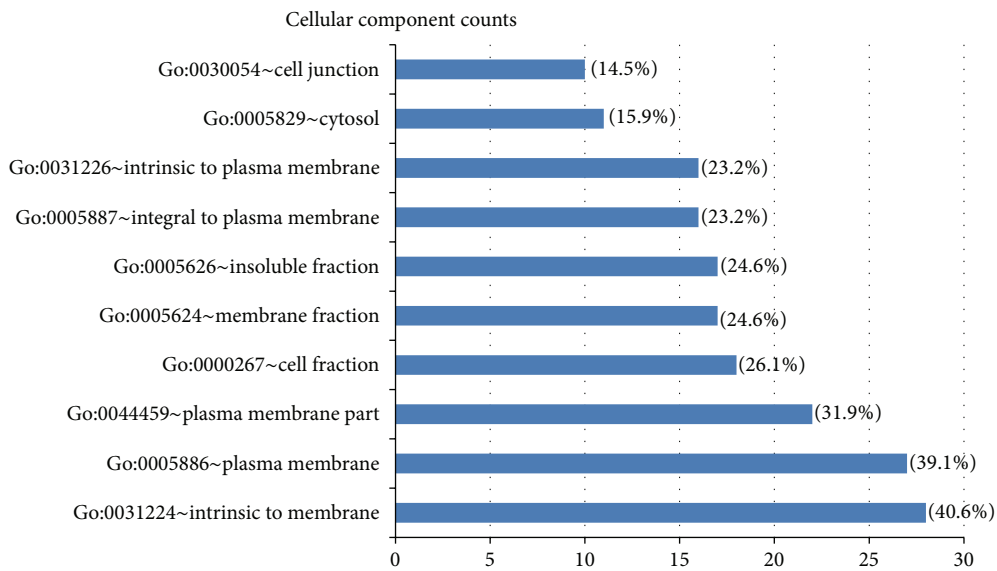
3. Results and Discussion

3.1. Identification of the Underlying Pharmacological Mechanisms of Wu Tou Tang. In order to demonstrate the reliability of our prediction system, we firstly evaluated its performance by the multilabel measure. As the result of the independent set test, the recall value of our prediction system was 0.98, indicating that it could screen the effector molecules of drugs correctly; however, its precision (0.61) and overall accuracy (59.67%) were slightly low because of several false positive prediction results. The $F1$ score is a measure of a test's accuracy. It considers both the precision and the recall of the test to compute the score. The $F1$ score can be interpreted as a weighted average of the precision and recall, where an $F1$ score reaches its best value at 1 and worst score at 0. It is better suited than the overall accuracy, especially for unbalanced datasets, because the overall accuracy often biases towards an overrepresented class [28]. Our data have shown that the $F1$ score of our prediction system was 0.76.

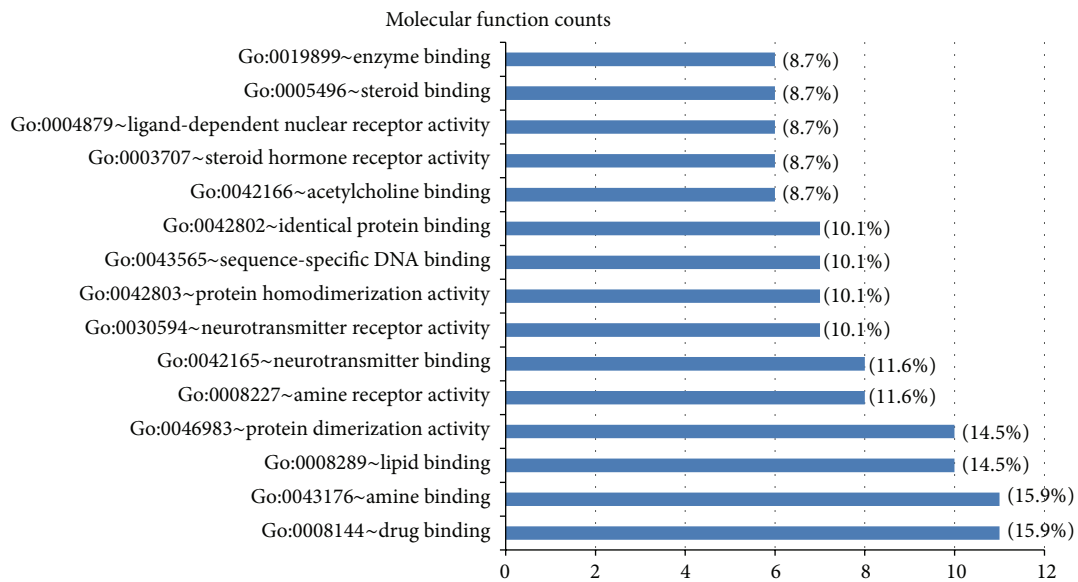
Using this prediction system, 153 similar drugs of compositive compounds (data shown in Supplementary Table S3) and 56 candidate effector molecules (data shown in Supplementary Table S3) for Wu Tou Tang were screened to reveal their underlying molecular mechanisms. According to the therapeutic effects of these similar drugs, we found that all five ingredients in Wu Tou Tang could act as anti-inflammatory, antibacterial, and hypoglycemic agents. Especially, both Radix Aconiti and Herba Ephedrae could be used as analgesics and corticosteroids; Radix Astragali had deintoxication; both Radix Paeoniae Alba and Radix Glycythizae could function as analgesics, immune regulator, and dietary supplement. In addition, we researched the functional distribution of candidate effector molecules of Wu Tou Tang by GO enrichment analysis. The GO annotation system uses a controlled and hierarchical vocabulary to assign function to genes or gene products in any organism. It contains three independent categories: biological processes, molecular function, and cellular components. Figure 2 shows enriched GO terms of predicted effector molecules of Wu Tou Tang. The top three significantly enriched GO biological processes of them include intracellular signaling cascade, cell surface receptor linked signal transduction, and response to organic substance (Figure 2(a)); most of these predicted effector molecules are localized on the cellular membrane (Figure 2(b)) and function as binding components (Figure 2(c)). These annotations are all related with the processes of different molecular signal transmissions, indicating that Wu Tou Tang may intervene in these pathological progresses.



(a)



(b)



(c)

FIGURE 2: Continued.

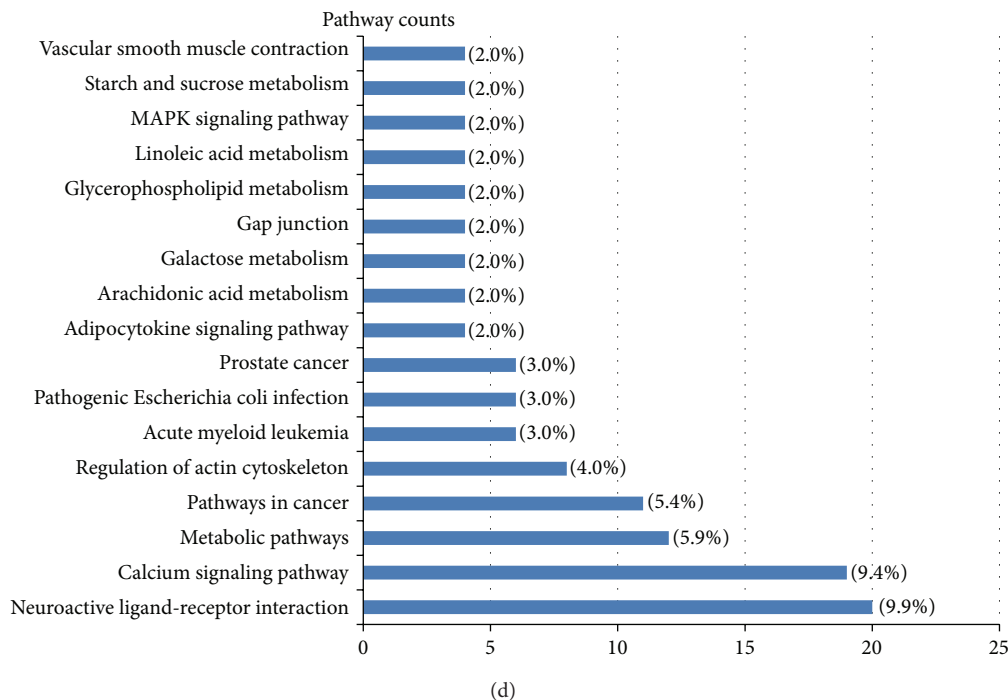


FIGURE 2: Enriched Gene Ontology terms for biological processes (a), for cellular components (b), and for molecular functions (c) and KEGG pathways (d) on the candidate effector molecules of Wu Tou Tang.

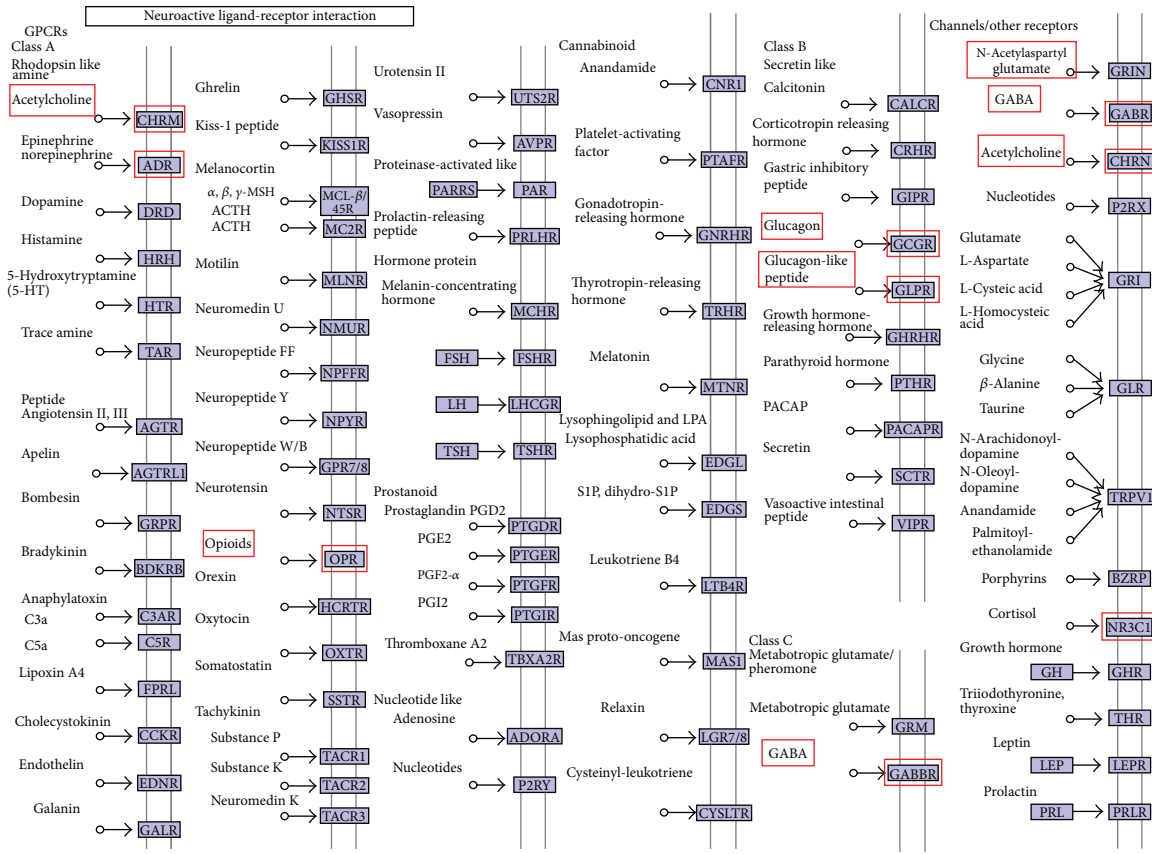
Pathway information is important for understanding gene and protein function. Therefore, we analyzed the enriched KEGG biological pathways among these predicted effector molecules of Wu Tou Tang. As shown in Figure 2(d), the most associated pathway was neuroactive ligand-receptor interaction, which had 20 (20/56, 35.71%) predicted effector molecules associated with it. The second-most frequent associations were calcium signaling pathway, followed by metabolic pathways, pathways in cancer, regulation of actin cytoskeleton, pathogenic *Escherichia coli* infection, and so on.

Among these pathways, the importance of neuroactive ligand-receptor interaction in the development and progress of RA has been reported. In TCM theory, patients suffering from RA can be categorized into Cold-ZHENG-related RA who are treated by the cold-warming herbal formulas and Hot-ZHENG-related RA who are treated by the hot-cooling herbal formulas [35]. Li et al. [36] found that genes shared by both Cold-ZHENG and Hot-ZHENG are significantly enriched in the pathway of neuroactive ligand-receptor interaction. In the present study, we mapped the predicted effector molecules of Wu Tou Tang onto KEGG pathways. Figure 3(a) shows the effects of the active compounds in Wu Tou Tang on the system of neuroactive ligand-receptor interaction. These active compounds act on different receptors so as to regulate the uptake and transport systems of neurotransmitters such as acetylcholine, norepinephrine and opioid, suggesting that Wu Tou Tang may block the reuptake of multiple neurotransmitters and stimulate the release of these neurotransmitters in a multitarget pattern. In addition, it has been demonstrated

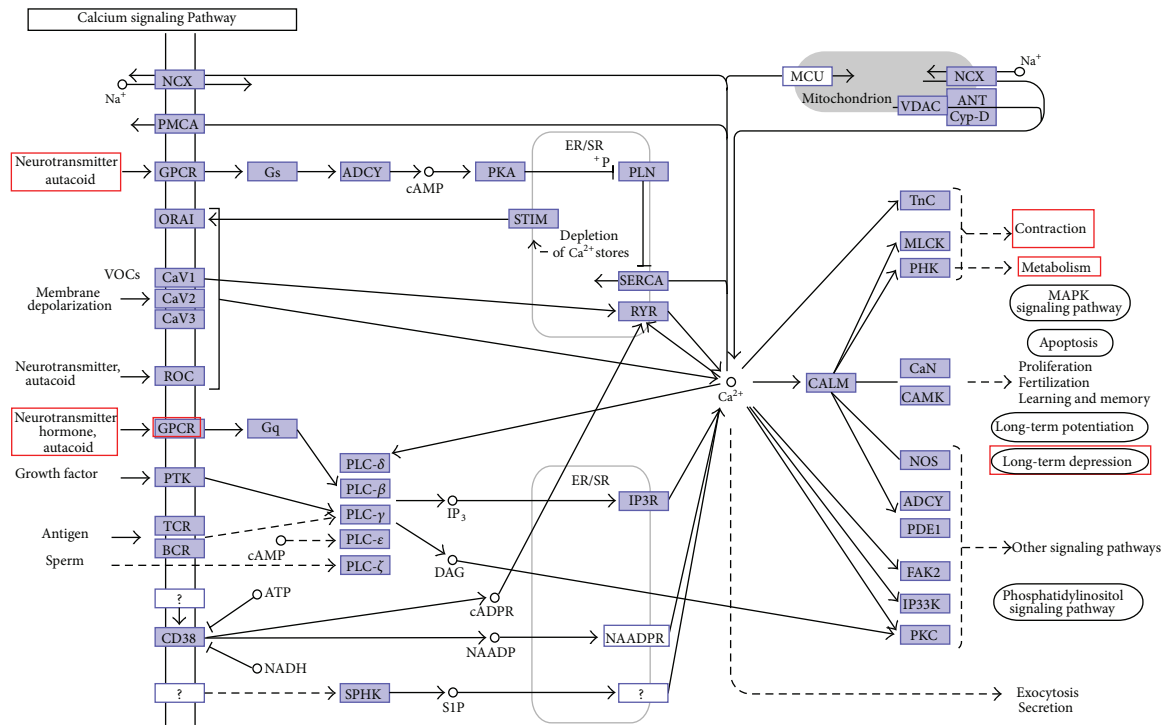
that calcium signaling pathway plays an important role in RA progression. Ca^{2+} signals are essential for diverse cellular functions including differentiation, effector function, and gene transcription in the immune system. Davies and Hallett [37] found that cytosolic Ca^{2+} signaling could trigger neutrophil responses in RA. Lu et al. [38] also indicated that calcium signaling pathway may be related with heat pattern of RA. As shown in Figure 3(b), the predicted effector molecules of Wu Tou Tang mapped in this pathway such as adrenergic receptor and opioid receptor are closely related to the progression of RA.

3.2. Importance of the Candidate Effector Molecules for Wu Tou Tang Acting on RA Therapy. We constructed a PPI network for known targets of RA and candidate effector molecules of Wu Tou Tang based on their PPI data. In total, there are 6713 interactions between 3231 proteins (Figure 4(a)). According to the previous study of Li et al. [36], we identified a node as a hub protein if its degree is more than 2-fold of the median degree of all nodes in a network. As the results, there are 129 hub proteins, the interactions among which are shown in Figure 4(b).

Analysis on topological features may improve the identification of essential proteins in PPI networks. Based on the characteristic of biological network, nodes with higher degree and K -coreness are the center of network and their removal may disrupt a number of essential pathways to break network [32, 39]. In addition, some global topological features such as closeness/betweenness centrality have been



(a)



(b)

FIGURE 3: Effects of active compounds in Wu Tou Tang on neuroactive ligand-receptor interaction (a) and calcium signaling pathway (b) by their candidate effector molecules marked with red panes. This plot is modified from KEGG pathway map.

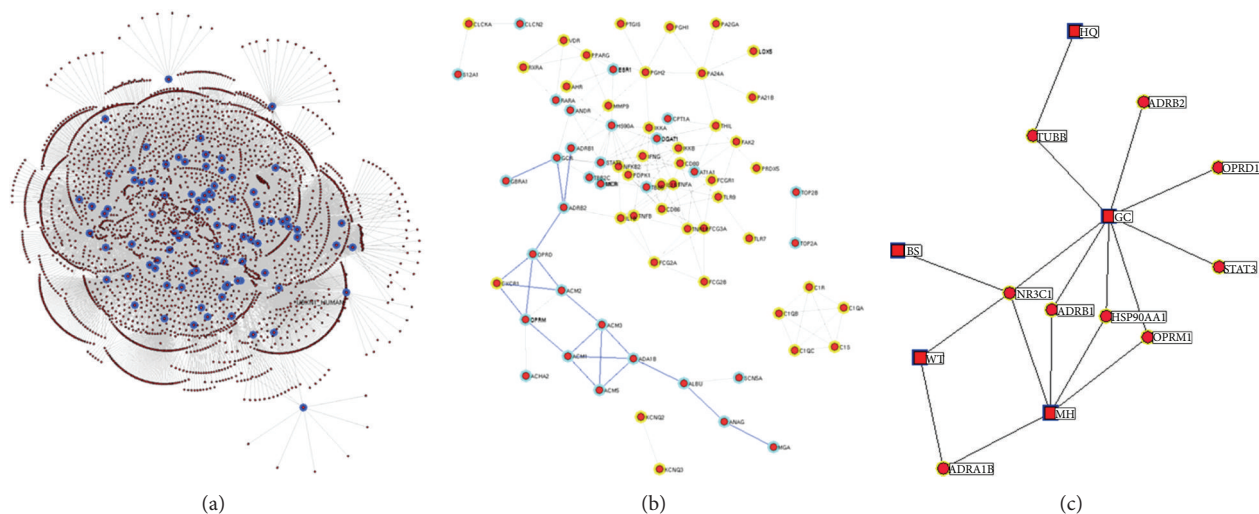


FIGURE 4: (a) The protein-protein interaction (PPI) network of known targets of rheumatoid arthritis (RA) and candidate effector molecules of Wu Tou Tang based on their PPI data. In total, there are 6713 interactions between 3231 proteins in the PPI network. (b) The PPI network of 129 hub proteins obtained from (a). Yellow nodes refer to known targets of RA, and green nodes refer to candidate effector molecules of Wu Tou Tang. Pathway with blue edges refer to neuroactive ligand-receptor interaction, which is the most associated pathway of candidate effector molecules of Wu Tou Tang according to the pathway enrichment analysis. (c) The interaction network of five ingredients in Wu Tou Tang and nine major candidate effector molecules of Wu Tou Tang on RA therapy. Square nodes refer to ingredients in Wu Tou Tang, and circular nodes refer to major candidate effector molecules of Wu Tou Tang on RA therapy.

put forward. Closeness/betweenness centrality correlates more closely with essentiality than degree, exposing critical nodes that usually belong to the group of scaffold proteins or proteins involved in crosstalk between signaling pathways [31]. Nodes with higher value of closeness/betweenness centrality can be identified as initial candidates for drug targets [40]. Thus, we calculated the degree, the betweenness, and the K -coreness of candidate effector molecules in order to demonstrate their importance in PPI network. The nodes with all the three feature values (“Degree”, “Betweenness” and “ K value”) higher than their corresponding medians were identified as major candidate effector molecules of Wu Tou Tang acting on RA. As the result, nine proteins, ADRB1_HUMAN (official gene symbol, OGC: ADRB1), ADRB2_HUMAN (OGC: ADRB2), OPRM1_HUMAN (OGC: OPRM1), OPRD1_HUMAN (OGC: OPRD1), ADRA1B_HUMAN (OGC: ADRA1B), HSP90AA1_HUMAN (OGC: HSP90AA1), STAT3_HUMAN (OGC: STAT3), NR3C1_HUMAN (OGC: NR3C1), and TUBB5_HUMAN (OGC: TUBB), were identified as major candidate effector molecules of Wu Tou Tang on RA therapy. The detailed information on these proteins and their corresponding compounds in Wu Tou Tang is described in Supplementary Table S5. As shown in Figure 4(c), NR3C1 was the common effector molecules of four ingredients in Wu Tou Tang, including Radix Aconiti, Herba Ephedrae, Radix Paeoniae Alba, and Radix Glycythizae; ADRA1B was the common effector molecules of Radix Aconiti and Herba Ephedrae; ADRB1, HSP90AA1, and OPRM1 were all the common effector molecules of Herba Ephedrae and Radix Glycythizae; TUBB was the common effector molecules of Radix Glycythizae and Radix Astragali. All these data indicate that the therapeutic effects

of Wu Tou Tang on RA may be based on the synergistic interactions of different ingredients.

3.2.1. Biological Interpretations of Major Candidate Effector Molecules. Among nine major candidate effector molecules of Wu Tou Tang on RA therapy, ADRB2, ADRA1B, HSP90AA1, STAT3, NR3C1, and TUBB have been demonstrated to be associated with RA progression. We would like to illustrate their biological significance in RA.

ADRB2, named as beta-2 adrenergic receptor, is a member of the group of G-protein-coupled receptors [41]. It is present on skeletal and cardiac muscle cells and on peripheral blood lymphocytes. ADRB2 may represent a link between the sympathetic nervous system and the immune system [42]. In RA patients, Baerwald et al. [43] detected the reduced number of ADRB2 on peripheral blood mononuclear cells, which may be associated with disease activity and defective suppressor cell functions. Pont-Kingdon et al. [44] also indicated that ADRB2 might be a factor affecting RA by impairing the control of the immune response. These involvements of ADRB2 in RA imply a potential importance of its genetic variation in this disease. Xu et al. [45] showed an association of ADRB2 SNPs with RA in a population from the northern part of Sweden. Malysheva et al. [46] further demonstrated a correlation between ADRB2 polymorphisms and RA in conjunction with human leukocyte antigen-DRB1 shared epitope. These findings suggest the associations between RA and variants in the gene encoding ADRB2.

ADRA1B, named as alpha-1B adrenergic receptor, mediates its action by association with G proteins that activate a phosphatidylinositol-calcium second messenger system [47].

Its effect is mediated by G(q) and G(11) proteins. Nuclear ADRA1A-ADRA1B hetero-oligomers regulate phenylephrine (PE)-stimulated ERK signaling in cardiac myocytes. Previous studies demonstrated that the expression of ADRA1B mRNA in PBMC during chronic inflammation in juvenile rheumatoid arthritis (JRA) may be associated with altered responses of the immune system to stress [48].

HSP90AA1, named as heat shock protein HSP 90-alpha (Hsp90 α), belongs to the heat shock protein 90 family [49]. It is a highly conserved and abundant protein, constituting approximately 1% of the total intracellular protein. This protein is localized in cytoplasm and melanosome of human cells. In the cytoplasm, Hsp90 α has more than 200 interacting proteins, and it commonly functions in concert with various cochaperones including Hsp70, Hsp40, Hop, Hip, and p23, which can form a complex and subsequently bind to the interacting proteins and assist in their folding or activation [50]. Functionally, Hsp90 α promotes the maturation, structural maintenance, and proper regulation of specific target proteins involved for instance in cell cycle control and signal transduction. Accumulating studies have indicated the intracellular role of Hsp90 α in tumorigenesis. In 2011, Sedlackova et al. [51] detected the HSP expression profile by real-time quantitative reverse transcription polymerase chain reaction in RA, osteoarthritis, and healthy controls. Their data showed the significantly increased Hsp90 α mRNA level in RA synovial tissues. This upregulation together with the downregulation of Hsp70 and the elevated HspBP1/Hsp70 mRNA ratios can be used to differentiate between RA patients and healthy individuals through analysis of peripheral blood samples, suggesting that the differential expression of Hsp90 α may be a promising diagnostic marker for RA patients.

STAT3, named as signal transducer and activator of transcription 3, belongs to the transcription factor STAT family and contains one SH2 domain [52]. Among seven known STAT proteins, STAT3 has been demonstrated to be active in synovial lining cells in adjuvant arthritis and RA and in freshly isolated RA SFs [53]. It is activated by a number of cytokines and growth factors expressed in RA synovitis, including IL-6, oncostatin M, EGF, and PDGF [54]. STAT3 is one of components in the Janus kinase (JAK)-STAT signal transduction pathway, which functionally regulates gene expression and various cellular processes, including cell activation, proliferation, and differentiation. In RA, this pathway plays a critical role in synovial membrane proliferation. Emerging experimental results demonstrate that JAK-STAT inhibitors may exhibit dramatic effects on RA in clinical trials [55].

NR3C1, named as glucocorticoid receptor, has a dual mode of action, as a transcription factor that binds to glucocorticoid response elements and as a modulator of other transcription factors [56]. It affects inflammatory responses, cellular proliferation, and differentiation in target tissues. Glucocorticoids are extensively used in the treatment of inflammatory bone diseases, such as RA. Rauch et al. [57] indicated that the anti-inflammatory selective glucocorticoid receptor modulator may preserve osteoblast differentiation.

TUBB, named as tubulin beta chain, belongs to the tubulin family. Tubulin is the major constituent of microtubules

[58]. It binds two moles of GTP, one at an exchangeable site on the beta chain and one at a nonexchangeable site on the alpha chain. In 1992, Ramos-Ruiz et al. [59] found the decreased tubulin synthesis in synoviocytes from adjuvant-induced arthritic rats. By proteomic analysis, Kamada et al. [60] further found that the expression levels of tubulin protein in bone marrow-adherent cells were increased in osteoarthritis compared to RA.

3.2.2. Validation by Molecular Docking Simulation. Molecular docking simulation, as one of structure-based methods, is an invaluable tool in drug discovery and design. Computational docking technique is flexible ligand docking, where the candidate ligands are fitted to the 3D structure of the target receptor with allowance for the conformational flexibility of the ligands [61]. Thus, it is of great importance to investigate ligand-protein interactions and elucidate binding mechanisms. eHiTS, one of the molecular docking softwares, systematically covers the part of the conformational and positional search space that avoids severe steric clashes, producing highly accurate docking poses at a speed practical for virtual high-throughput screening [33]. For these reasons, the molecular docking simulation was performed in this study to validate the associations of major candidate effector molecules with compositive compounds of Wu Tou Tang on RA therapy using eHiTS software. As a result, 26 pairs of compound-candidate effector molecules interactions were deleted either because their structural information was unavailable or because negative results were output from eHiTS. The positive docking results for other interactions were summarized in Supplementary Table S6. The median value of all docking scores was -4.41 kcal/mol, and there were 13 pairs of compound-candidate effector molecules interactions with strong binding free energy. Among these, GCR_HUMAN could effectively bind with five "candidate compounds" (Aconitine from Radix Aconiti, Methyl-7-epiganoderate from Herba Ephedrae, Paeoniflorin from Radix Paeoniae Alba, Isoramanone from Radix Glycythizae, and Aldohypaconitine from Radix Aconiti); ADRB1_HUMAN could also efficiently bind with five "candidate compounds" (Isogosferol from Radix Glycythizae, Neohancoside A from Radix Glycythizae, delta-Terpineol from Herba Ephedrae, Neoisopulegol from Radix Glycythizae, and trans-beta-Terpineol from Herba Ephedrae); STAT3_HUMAN could effectively bind with two compounds in Radix Glycythizae (Methyl glycyrrhetate and Glycyrrhetol); ADRB2_HUMAN could efficiently bind with one compound in Radix Glycythizae (2-Methyl-1,3,6-tri). Especially, the binding free energy of the Aconitine-GCR_HUMAN (-8.81 kcal/mol), Methyl-7-epiganoderate-GCR_HUMAN (-8.27 kcal/mol), and Paeoniflorin-GCR_HUMAN interactions (-6.75 kcal/mol) were all higher than 1.5-fold of the median value of docking scores.

4. Conclusion

Different from western medicine, TCM is an independent system of theory, which treats the function and dysfunction

of living organisms in a more holistic way. It is very difficult to understand the therapeutic mechanisms of TCM because of the complexity of the chemical components and their actions *in vivo*. Many studies have applied monomer in herbs to elucidate the pharmacological efficacy of the whole TCM formula. However, this method ignored the multitarget characteristic of the multicomponent TCM formula. At present, to develop an effective method for understanding the TCM system as a whole is still the “bottleneck” of modern TCM study. Currently, we combined the strategies of systems biology and network pharmacology to investigate the complicated multitarget mechanisms of Wu Tou Tang. Our main findings are (1) to develop a novel strategy which is used to investigate into the therapeutic mechanisms of Wu Tou Tang from chemical structures, genomic, proteomic, and pharmacological data in an integrated framework. (2) This strategy can pinpoint out the underlying pharmacological effects of the ingredients in Wu Tou Tang based on the synergistic interactions of the ingredients, targets, and pathways. The results indicate that Radix Aconiti shares the most common effector molecules with Herba Ephedrae, while less common effector molecules with Radix Glycythizae and Radix Paeoniae Alba. Moreover, it is important to note that there may be the most common effector molecules between Radix Glycythizae and Herba Ephedrae. These findings suggest that five Chinese herbs in Wu Tou Tang together probably display synergistic actions and our network-based approach may facilitate to generate hypothesis to optimize and reformulate the herbal formula by elucidating the compatible mechanism of the complex prescription. (3) We also provide a list of candidate effector molecules for Wu Tou Tang; some of them backed experimental evidence reported in the literature and were validated by the molecular docking simulation. Although there are potentially interesting associations between these effector molecules and RA, cautious interpretation should be performed as our strategy is based on statistical analysis. Therefore, further experimental studies are required to test these hypotheses. Taken together, this study may support further assessments of clinical application of Wu Tou Tang, and enable further research on TCM formulas in a more timely and cost-effective manner.

Conflict of Interests

The authors do not have any conflict of interests with the content of the paper.

Acknowledgments

This study was supported by the National Natural Science Foundation of China (no. 81173628), the National Basic Research Program of China (973 Program) (2011CB505300 and 2011CB505305), and the Joint Innovation Project of Visiting Professor in China Academy of Chinese Medical Sciences.

References

- [1] C. Böhler, H. Radner, M. Ernst et al., “Rheumatoid arthritis and falls: the influence of disease activity,” *Rheumatology*, vol. 51, no. 11, pp. 2051–2057, 2012.
- [2] J. Liu and R. L. Liu, “The potential role of Chinese medicine in ameliorating extra-articular manifestations of rheumatoid arthritis,” *Chinese Journal of Integrative Medicine*, vol. 17, no. 10, pp. 735–737, 2011.
- [3] S. Y. Zhang and J. Liu, “Clinical observation of modified Wu Tou Tang in the treatment of active rheumatoid arthritis,” *Chinese Journal of Traditional Medical Science and Technology*, vol. 17, pp. 326–327, 2010.
- [4] W. D. Hu, C. S. Lin, D. Q. Kong et al., “Clinical observation of modified Guizhishao yao zhi decoction in the treatment of active rheumatoid arthritis,” *Chinese Journal of Primary Medicine and Pharmacy*, vol. 12, pp. 1699–1700, 2005.
- [5] N. Lin, C. Liu, C. Xiao et al., “Triptolide, a diterpenoid triepoxide, suppresses inflammation and cartilage destruction in collagen-induced arthritis mice,” *Biochemical Pharmacology*, vol. 73, no. 1, pp. 136–146, 2007.
- [6] Y. P. Zhu and H. J. Woerdenbag, “Traditional Chinese herbal medicine,” *Pharmacy World and Science*, vol. 17, no. 4, pp. 103–112, 1995.
- [7] Z. Zheng, T. Yan, W. Chen, L. Ye, L. Tang, and Z. Liu, “Pharmacokinetic determination of ephedrine in Herba Ephedrae and Wu Tou Tang decoctions in rats using ultra performance liquid chromatography tandem mass spectrometry,” *Xenobiotica*, vol. 42, no. 8, pp. 775–783, 2012.
- [8] C. Elder, C. Ritenbaugh, M. Aickin et al., “Reductions in pain medication use associated with traditional chinese medicine for chronic pain,” *The Permanente Journal*, vol. 16, no. 3, pp. 18–23, 2012.
- [9] H. J. Wang and B. H. Chiang, “Anti-diabetic effect of a traditional Chinese medicine formula,” *Food & Function*, vol. 3, no. 11, pp. 1161–1169, 2012.
- [10] H. Shi, C. Zhou, Y. Li, G. Wang, and Y. Sun, “Anti-inflammatory effect of aconitines,” *Zhongguo Zhong Yao Za Zhi*, vol. 15, no. 3, pp. 174–192, 1990.
- [11] J. Hallas, L. Bjerrum, H. Støvring, and M. Andersen, “Use of a prescribed ephedrine/caffeine combination and the risk of serious cardiovascular events: a registry-based case-crossover study,” *American Journal of Epidemiology*, vol. 168, no. 8, pp. 966–973, 2008.
- [12] W. Tao, X. Xu, X. Wang et al., “Network pharmacology-based prediction of the active ingredients and potential targets of Chinese herbal Radix Curcumae formula for application to cardiovascular disease,” *Journal of Ethnopharmacology*, vol. 145, no. 1, pp. 1–10, 2013.
- [13] Z. H. Liu and X. B. Sun, “Network pharmacology: new opportunity for the modernization of traditional Chinese medicine,” *Yao Xue Xue Bao*, vol. 47, pp. 696–703, 2012.
- [14] S. Zhao and S. Li, “Network-based relating pharmacological and genomic spaces for drug target identification,” *PLoS ONE*, vol. 5, no. 7, Article ID e11764, 2010.
- [15] S. Li, B. Zhang, and N. Zhang, “Network target for screening synergistic drug combinations with application to traditional Chinese medicine,” *BMC Systems Biology*, vol. 5, supplement 1, p. S10, 2011.
- [16] S. Li, B. Zhang, D. Jiang, Y. Wei, and N. Zhang, “Herb network construction and co-module analysis for uncovering

- the combination rule of traditional Chinese herbal formulae," *BMC Bioinformatics*, vol. 11, supplement 11, p. S6, 2010.
- [17] C. Y.-C. Chen, "TCM database Taiwan: the world's largest traditional Chinese medicine database for drug screening In Silico," *PLoS ONE*, vol. 6, no. 1, Article ID e15939, 2011.
- [18] D. S. Wishart, C. Knox, A. C. Guo et al., "DrugBank: a knowledgebase for drugs, drug actions and drug targets," *Nucleic Acids Research*, vol. 36, no. 1, pp. D901–D906, 2008.
- [19] J. Y. Chen, S. R. Mamidipalli, and T. Huan, "HAPPI: an online database of comprehensive human annotated and predicted protein interactions," *BMC Genomics*, vol. 10, supplement 1, p. S16, 2009.
- [20] L. Matthews, G. Gopinath, M. Gillespie et al., "Reactome knowledgebase of human biological pathways and processes," *Nucleic Acids Research*, vol. 37, no. 1, pp. D619–D622, 2009.
- [21] K. R. Brown and I. Jurisica, "Online predicted human interaction database," *Bioinformatics*, vol. 21, no. 9, pp. 2076–2082, 2005.
- [22] B. Aranda, P. Achuthan, Y. Alam-Faruque et al., "The IntAct molecular interaction database in 2010," *Nucleic Acids Research*, vol. 38, no. 1, Article ID gkp878, pp. D525–D531, 2009.
- [23] T. S. Keshava Prasad, R. Goel, K. Kandasamy et al., "Human protein reference database-2009 update," *Nucleic Acids Research*, vol. 37, no. 1, pp. D767–D772, 2009.
- [24] A. Ceol, A. Chatr Aryamontri, L. Licata et al., "MINT, the molecular interaction database: 2009 update," *Nucleic Acids Research*, vol. 38, no. 1, Article ID gkp983, pp. D532–D539, 2009.
- [25] B. Lehne and T. Schlitt, "Protein-protein interaction databases: keeping up with growing interactomes," *Human Genomics*, vol. 3, no. 3, pp. 291–297, 2009.
- [26] T. Beuming, L. Skrabanek, M. Y. Niv, P. Mukherjee, and H. Weinstein, "PDZBase: a protein-protein interaction database for PDZ-domains," *Bioinformatics*, vol. 21, no. 6, pp. 827–828, 2005.
- [27] F. Zhu, Z. Shi, C. Qin et al., "Therapeutic target database update 2012: a resource for facilitating target-oriented drug discovery," *Nucleic Acids Research*, vol. 40, no. 1, pp. D1128–D1136, 2012.
- [28] S. Briesemeister, J. Rahnenführer, and O. Kohlbacher, "Going from where to why—interpretable prediction of protein subcellular localization," *Bioinformatics*, vol. 26, no. 9, Article ID btq115, pp. 1232–1238, 2010.
- [29] G. Dennis Jr., B. T. Sherman, D. A. Hosack et al., "DAVID: database for annotation, visualization, and integrated discovery," *Genome Biology*, vol. 4, no. 5, p. P3, 2003.
- [30] J. Wixon and D. Kell, "The Kyoto encyclopedia of genes and genomes—KEGG," *Yeast*, vol. 17, no. 1, pp. 48–55, 2000.
- [31] Y. Wang, Z. Liu, C. Li et al., "Drug target prediction based on the herbs components: the study on the multitargets pharmacological mechanism of qishenkeli acting on the coronary heart disease," *Evidence-Based Complementary and Alternative Medicine*, vol. 2012, Article ID 698531, 10 pages, 2012.
- [32] S. Wuchty and E. Almaas, "Evolutionary cores of domain co-occurrence networks," *BMC Evolutionary Biology*, vol. 5, p. 24, 2005.
- [33] Z. Zsoldos, D. Reid, A. Simon, B. S. Sadjad, and A. P. Johnson, "eHiTS: an innovative approach to the docking and scoring function problems," *Current Protein and Peptide Science*, vol. 7, no. 5, pp. 421–435, 2006.
- [34] P. W. Rose, B. Beran, C. Bi et al., "The RCSB protein data bank: redesigned web site and web services," *Nucleic Acids Research*, vol. 39, no. 1, pp. D392–D401, 2011.
- [35] S. B. Su, A. Lu, S. Li, and W. Jia, "Evidence-based ZHENG: a traditional Chinese medicine syndrome," *Evidence-Based Complementary and Alternative Medicine*, vol. 2012, Article ID 246538, 2 pages, 2012.
- [36] S. Li, Z. Q. Zhang, L. J. Wu, X. G. Zhang, Y. D. Li, and Y. Y. Wang, "Understanding ZHENG in traditional Chinese medicine in the context of neuro-endocrine-immune network," *IET Systems Biology*, vol. 1, no. 1, pp. 51–60, 2007.
- [37] E. V. Davies and M. B. Hallett, "Cytosolic Ca²⁺ signalling in inflammatory neutrophils: implications for rheumatoid arthritis (Review)," *International Journal of Molecular Medicine*, vol. 1, no. 2, pp. 485–490, 1998.
- [38] C. Lu, C. Xiao, G. Chen et al., "Cold and heat pattern of rheumatoid arthritis in traditional Chinese medicine: distinct molecular signatures identified by microarray expression profiles in CD4-positive T cell," *Rheumatology International*, pp. 1–8, 2010.
- [39] S. H. Yeh, H. Y. Yeh, and V. W. Soo, "A network flow approach to predict drug targets from microarray data, disease genes and interactome network-case study on prostate cancer," *Journal of Clinical Bioinformatics*, vol. 2, no. 1, p. 1, 2012.
- [40] P. Holme, B. J. Kim, C. N. Yoon, and S. K. Han, "Attack vulnerability of complex networks," *Physical Review E*, vol. 65, no. 5, Article ID 056109, pp. 056109/1–056109/14, 2002.
- [41] A. M. Malfait, A. S. Malik, L. Marinova-Mutafchieva, D. M. Butler, R. N. Maini, and M. Feldmann, "The β_2 -adrenergic agonist salbutamol is a potent suppressor of established collagen-induced arthritis: mechanisms of action," *Journal of Immunology*, vol. 162, no. 10, pp. 6278–6283, 1999.
- [42] M. Wahle, G. Hanefeld, S. Brunn et al., "Failure of catecholamines to shift T-cell cytokine responses toward a Th2 profile in patients with rheumatoid arthritis," *Arthritis Research and Therapy*, vol. 8, no. 5, p. R138, 2006.
- [43] C. G. O. Baerwald, M. Wahle, T. Ulrichs et al., "Reduced catecholamine response of lymphocytes from patients with rheumatoid arthritis," *Immunobiology*, vol. 200, no. 1, pp. 77–91, 1999.
- [44] G. Pont-Kingdon, J. Bohnsack, K. Sumner et al., "Lack of association between beta 2-adrenergic receptor polymorphisms and juvenile idiopathic arthritis," *Scandinavian Journal of Rheumatology*, vol. 38, no. 2, pp. 91–95, 2009.
- [45] B. Xu, L. Ärleth, S. B. Rantapää-Dahlquist, and A. K. Lefvert, " β_2 -adrenergic receptor gene single-nucleotide polymorphisms are associated with rheumatoid arthritis in northern Sweden," *Scandinavian Journal of Rheumatology*, vol. 33, no. 6, pp. 395–398, 2004.
- [46] O. Malysheva, M. Pierer, U. Wagner, M. Wahle, U. Wagner, and C. G. Baerwald, "Association between β_2 adrenergic receptor polymorphisms and rheumatoid arthritis in conjunction with human leukocyte antigen (HLA)-DRB1 shared epitope," *Annals of the Rheumatic Diseases*, vol. 67, no. 12, pp. 1759–1764, 2008.
- [47] D. Lorton, C. Lubahn, and D. L. Bellinger, "Potential use of drugs that target neural-immune pathways in the treatment of rheumatoid arthritis and other autoimmune diseases," *Current Drug Targets-Inflammation & Allergy*, vol. 2, no. 1, pp. 1–30, 2003.
- [48] C. Roupe Van Der Voort, C. J. Heijnen, N. Wulffraat, W. Kuis, and A. Kavelaars, "Stress induces increases in IL-6 production by leukocytes of patients with the chronic inflammatory disease juvenile rheumatoid arthritis: a putative role for α_1 -adrenergic receptors," *Journal of Neuroimmunology*, vol. 110, no. 1-2, pp. 223–229, 2000.

- [49] R. Beck, N. Dejeans, C. Glorieux et al., "Hsp90 is cleaved by reactive oxygen species at a highly conserved N-terminal amino acid motif," *PLoS One*, vol. 7, no. 7, Article ID e40795, p. 1, 2012.
- [50] S. Solier, K. W. Kohn, B. Scroggins et al., "Heat shock protein 90 α (HSP90 α), a substrate and chaperone of DNA-PK necessary for the apoptotic response," *Proceedings of the National Academy of Sciences of the United States of America*, vol. 109, no. 32, pp. 12866–12872, 2012.
- [51] L. Sedlackova, A. Sosna, P. Vavrincova et al., "Heat shock protein gene expression profile may differentiate between rheumatoid arthritis, osteoarthritis, and healthy controls," *Scandinavian Journal of Rheumatology*, vol. 40, no. 5, pp. 354–357, 2011.
- [52] V. Nicolaidou, M. M. Wong, A. N. Redpath et al., "Monocytes induce STAT3 activation in human mesenchymal stem cells to promote osteoblast formation," *PLoS One*, vol. 7, no. 7, Article ID e39871, 2012.
- [53] M. Seddighzadeh, A. Gonzalez, B. Ding et al., "Variants within STAT genes reveal association with anticitrullinated protein antibody-negative rheumatoid arthritis in 2 European populations," *Journal of Rheumatology*, vol. 39, no. 8, pp. 1509–1516, 2012.
- [54] H. Wang, Y. Fang, Y. Wang et al., "Inhibitory effect of curcumol on Jak2-STAT signal pathway molecules of fibroblast-like synoviocytes in patients with rheumatoid arthritis," *Evidence-Based Complementary and Alternative Medicine*, vol. 2012, Article ID 746426, 8 pages, 2012.
- [55] H. Yoshida, A. Kimura, T. Fukaya et al., "Low dose CP-690, 550 (tofacitinib), a pan-JAK inhibitor, accelerates the onset of experimental autoimmune encephalomyelitis by potentiating Th17 differentiation," *Biochemical and Biophysical Research Communications*, vol. 418, no. 2, pp. 234–240, 2012.
- [56] S. R. Witzmann, J. D. Turner, S. B. Mériaux, O. C. Meijer, and C. P. Muller, "Epigenetic regulation of the glucocorticoid receptor promoter 17 in adult rats," *Epigenetics*, vol. 7, no. 11, pp. 1290–1301, 2012.
- [57] A. Rauch, V. Gossye, D. Bracke et al., "An anti-inflammatory selective glucocorticoid receptor modulator preserves osteoblast differentiation," *FASEB Journal*, vol. 25, no. 4, pp. 1323–1332, 2011.
- [58] E. Oda, Y. Nakamura, M. Yamamoto, and M. Kojiro, "Immunohistochemical distribution of tubulin beta II in human normal and neoplastic tissues," *Kurume Medical Journal*, vol. 52, no. 4, pp. 117–125, 2005.
- [59] R. Ramos-Ruiz, J. Avila, J. P. Lopez-Bote, C. Bernabeu, and V. Larraga, "Decreased tubulin synthesis in synoviocytes from adjuvant-induced arthritic rats," *Biochimica et Biophysica Acta*, vol. 1138, no. 3, pp. 184–190, 1992.
- [60] T. Kamada, M. S. Kurokawa, T. Kato et al., "Proteomic analysis of bone marrow-adherent cells in rheumatoid arthritis and osteoarthritis," *International Journal of Rheumatic Diseases*, vol. 15, no. 2, pp. 169–178, 2012.
- [61] R. J. Bienstock, "Computational drug design targeting protein-protein interactions," *Current Pharmaceutical Design*, vol. 18, no. 9, pp. 1240–1254, 2012.

Research Article

Metabolism of Genipin in Rat and Identification of Metabolites by Using Ultraperformance Liquid Chromatography/Quadrupole Time-of-Flight Tandem Mass Spectrometry

Yue Ding,^{1,2} Jian-Wei Hou,¹ Yong Zhang,¹ Li-Ying Zhang,² Tong Zhang,¹ Yi Chen,² Zhen-Zhen Cai,¹ and Li Yang³

¹ Experiment Center for Teaching and Learning, Shanghai University of Traditional Chinese Medicine, Shanghai 201203, China

² School of Pharmacy, Shanghai University of Traditional Chinese Medicine, Shanghai 201203, China

³ Institute of Chinese Materia Medica, Shanghai University of Traditional Chinese Medicine, Shanghai 201203, China

Correspondence should be addressed to Tong Zhang; zhangtdmj@hotmail.com and Yi Chen; liver1220@hotmail.com

Received 17 October 2012; Accepted 10 February 2013

Academic Editor: Wei Jia

Copyright © 2013 Yue Ding et al. This is an open access article distributed under the Creative Commons Attribution License, which permits unrestricted use, distribution, and reproduction in any medium, provided the original work is properly cited.

The *in vivo* and *in vitro* metabolism of genipin was systematically investigated in the present study. Urine, plasma, feces, and bile were collected from rats after oral administration of genipin at a dose of 50 mg/kg body weight. A rapid and sensitive method using ultraperformance liquid chromatography coupled with electrospray ionization quadrupole time-of-flight tandem mass spectrometry (UPLC-Q/TOF MS) was developed for analysis of metabolic profile of genipin in rat biological samples (urine, plasma, feces, and bile). A total of ten metabolites were detected and identified by comparing their fragmentation patterns with that of genipin using MetaboLynx software tools. On the basis of the chromatographic peak area, the sulfated and glucuronidated conjugates of genipin were identified as major metabolites. And the existence of major metabolites G1 and G2 was confirmed by the *in vitro* enzymatic study further. Then, metabolite G1 was isolated from rat bile by semipreparative HPLC. Its structure was unambiguously identified as genipin-1-o-glucuronic acid by comparison of its UV, IR, ESI-MS, ¹H-NMR, and ¹³C-NMR spectra with conference. In general, genipin was a very active compound that would transform immediately, and the parent form of genipin could not be observed in rats biological samples. The biotransformation pathways of genipin involved demethylated, ring-opened, cysteine-conjugated, hydroformylated, glucuronidated, and sulfated transformations.

1. Introduction

Genipin is an aglycone derived from an iridoid glycoside called geniposide, which is present in the fruit of *Gardenia jasminoides* Ellis. Intestinal bacteria in animals can transform geniposide to its aglycone genipin [1]. In our laboratory, geniposide could be transformed into genipin by immobilized β -Glucosidase in a two-phase aqueous-organic system [2]. Genipin has been proven to possess multiple bioactivities including antitumor [3, 4], neuroprotective [5], choleric [6], and anti-inflammatory effects [7–9]. It is also an excellent natural cross-linker for proteins, collagen, gelatin, and chitosan cross-linking. It is much less toxic than glutaraldehyde and many other commonly used synthetic cross-linking reagents [10]. Genipin-chitosan delivery systems are useful to control the release of such different drugs as clarithromycin, tramadol

hydrochloride, and low-molecular-weight heparin loaded in spray-dried microspheres [11].

In our previous studies, the parent form of genipin could not be detected directly in all plasma specimens of rats as it had been transformed to other forms such as conjugated genipin. The conjugated genipin could be hydrolyzed with sulfatase to genipin [12]. So, it can be assumed that some metabolites could exert stronger bioactivities. Therefore, investigation of the metabolites of genipin is of great significance in elucidation of its pharmacological mechanisms and discovering novel drugs from the metabolites. However, the metabolism of genipin has not been fully investigated as no report has been seen in the literature that comprehensively and comparatively investigated the *in vivo* and *in vitro* metabolic profile of this compound.

In the present study, metabolism of genipin was investigated systematically by using ultraperformance liquid chromatography coupled with electrospray ionization quadrupole time-of-flight tandem mass spectrometry (UPLC-Q/TOF MS). The *in vivo* metabolites were detected in plasma, bile, urine, and feces. One phase I metabolite and nine phase II metabolites were detected totally and their structures were identified. The *in vitro* incubation and enzymatic hydrolysis analysis also confirmed the existence of two phase II metabolites. And one major phase II metabolite (genipin-1- α -glucuronic acid) had been prepared by preparative chromatography technology, and its structure was unambiguously identified by comparison of its UV, IR, ESI-MS, $^1\text{H-NMR}$, and $^{13}\text{C-NMR}$ spectra with conference [13]. The biotransformation pathways of genipin involved demethylated, ring-opened, cysteine-conjugated, hydroformylated, glucuronidated, and sulfated transformations.

2. Experimental

2.1. Chemicals and Reagents. Genipin with a purity of 98.0% by HPLC was supplied by Wako Pure Chemical Industries Ltd (Japan). Sulfatase (type H-1 from *Helix pomatia*, containing 26.290 units/g) and β -glucuronidase (type B-1, from bovine liver, containing 1.240.000 units/g), UDPGA (Uridine 5'-diphosphoglucuronic acid trisodium salt), alamethicin (from *Trichoderma viride*), and saccharolactone were purchased from Sigma Chemical Co. Ltd (St Louis, MO, USA). HPLC-grade methanol and acetonitrile were purchased from Merck (Darmstadt, Germany). Ultrapure water was prepared with Milli-Q Ultrapure water purification system (Millipore, Bedford, MA, USA) and used for all analyses. Pooled human liver microsomes (HLM) protein (10 mg/mL) was supplied by the Research Institute for Liver diseases (Shanghai, CA). Potassium phosphate and MgCl_2 (magnesium chloride) were supplied by Sinopharm Chemical Reagents Co. Ltd.

2.2. In Vivo Experiment

2.2.1. Animals. Twenty-four male Sprague-Dawley rats weighing 180–220 g were obtained from the Laboratory Animal Center of the Shanghai University of Traditional Chinese Medicine (TCM). These rats were kept in an air-conditioned animal quarter at a temperature of 22–24°C and a relative humidity of $50 \pm 10\%$ and had access to the standard laboratory food and water. The rats were divided into four groups at random. Rats in the first group ($n = 6$) were kept in metabolic cages. Before the experiment, the blank urine and feces samples from each rat were collected for 12 h using a metabolic cage, and 300 μL blood samples were collected from the suborbital veniplex in heparinized tubes. Then, rats were given a single dose of genipin solution at 50 mg/kg of body weight by gavage into the stomach. After administration, food and water were provided freely, and the drug-containing urine and feces samples were collected during the time of 0–24 h. The drug-containing blood samples were collected at 10, 60, 240, and 720 min after administration. Rats in the second group ($n = 6$) were orally administered distilled water at 2 mL/100 g. The blank

bile samples were collected by bile duct cannulation surgery. Rats in the third group ($n = 6$) were orally administered genipin solution at 50 mg/kg of body weight, and the drug-containing bile samples were collected. Rats in the fourth group ($n = 6$) were given a single dose of genipin solution at 10 mg/kg by intravenous administration, and the blank blood samples were collected before administration, while the drug-containing blood samples were collected at 10, 60, 240, and 720 min after administration of genipin. Animal experiments were carried out in accordance with the local institutional guidelines for animal care of Shanghai University of Traditional Chinese Medicine. Plasma was separated from blood placed in heparinized Eppendorf tubes after centrifuging at 4000 $\times g$ for 10 min. All samples were kept at -80°C .

2.2.2. Sample Preparation. Plasma, urine, and bile 400 μL samples were precipitated with 3 volumes of methanol. The supernatant was separated after vortex-mixed and centrifuging. Feces 500 mg 0–48 h sample was grounded and extracted by ultrasonication with 1 mL water for 30 min each time, and the extracted solution was precipitated with 3 volumes of methanol. The supernatant was separated after vortex-mixed and centrifuging. Extracting solutions with different pretreatment methods described the earlier were all dried under nitrogen gas over a water bath of 37°C. The residues were reconstituted in 100 μL solution consisted of acetonitrile and water (15:85) and centrifuged at 10000 $\times g$ for 10 min prior to analysis.

2.3. In Vitro Incubation Experiment. Glucuronidation catalyzed by the UDP-glucuronosyltransferases (UGTs) was a major pathway for drug metabolism and elimination in humans. We added 100 μL of genipin (2.25 $\mu\text{g}/\text{mL}$) dissolved in methanol to empty incubation tubes (1.5 mL polypropylene microcentrifuge tube) and dried it under nitrogen gas over a water bath of 37°C. We placed the incubation tubes on ice and added 50 μg of pooled human liver microsomes (HLM) protein, 2.5 μg alamethicin (2.5 $\mu\text{g}/\mu\text{L}$ methanol; 50 μg alamethicin/mg microsomes protein), and balanced to a volume of 50 μL with 50 mM potassium phosphate buffer (pH 7.5, which included protein at final concentration of 0.5 mg/mL). We preincubated the tubes at 37°C for 5 min. We started reaction by adding 50 μL of UDPGA cofactor solution (including 0.645 mg UDPGA, 10 μL 50 mM magnesium chloride solution, 10 μL 50 mM saccharolactone, 25 μL 100 mM potassium phosphate buffer, pH 7.5., and 5 μL water), mixed the tube by gentle flicking, capped tube, and incubated it for up to 6 h. The incubated solution was immediately treated with stop solution (ice-cold acetonitrile) after vortex and centrifuged at 14000 $\times g$ for 10 min. We transferred 200 μL supernatant to tubes, dried it under nitrogen gas over a water bath of 37°C, then reconstituted it with 100 μL solution consisted of acetonitrile: water (15:85), centrifuged at 10000 $\times g$ for 10 min prior to analysis. To better identify the glucuronide metabolite peak, there were also three negative controls that (1) contained no UDPGA, (2) contained no substrate, and (3) were not incubated. The samples were analyzed by using UPLC-Q/TOF MS.

2.4. Enzymatic Hydrolysis Analysis. Enzymatic hydrolysis analysis was performed when searching and confirming the presence of phase II metabolites. The experiment initiated with collecting the drug-containing bile samples of rats in the third group. A 400 μL bile sample was mixed with 50 μL of β -glucuronidase or sulfatase (1000 units/mL in pH 5.0 acetate buffer) and incubated at 37°C for 30 min. After incubation, protein precipitation and redissolution procedures were identical to those described in the part of Section 2.2.2. Another 400 μL of the same bile sample was processed with the same procedures only except without adding β -glucuronidase or sulfatase for incubation. 5 μL of posttreated sample was injected in UPLC-Q/TOF MS for analysis. The effect of the glucuronidase or sulfatase was studied by comparing the UPLC-Q/TOF MS peak intensities for compounds of interests before and after the enzymatic incubation. The compounds of interest included glucuronidated conjugates or sulfated conjugates and their nonconjugated forms (hydrolyzed forms).

2.5. Chromatographic and Mass Spectrometry Conditions. The chromatographic system used was Waters Acquity UPLC (Waters, Milford, MA, USA) equipped with binary solvent manager, sample manager, column manager, and PDA detector, which was also coupled with a Q/TOF mass spectrometer. For the separation of metabolites in biological samples, chromatographic analysis was performed with an acquity UPLC HSS C18 column (100 mm \times 2.1 mm i.d., 1.8 μm particle size, Waters Corporation, Milford, MA, USA). The column was eluted with gradient conditions: 0–10 min, linear from 98% to 92% A; 10–17 min, linear from 92% to 88% A; 17–22 min, linear from 88% to 5% A; 22–25 min, held at 5% A for 3 min; 25–26 min, linear from 5% to 98% A; 26–35 min, held at 98% A for 9 min to prepare equilibration of the column for next analysis, where mobile phase A consisted of 0.005% formic acid in de-ionized water and mobile phase B consisted of acetonitrile. The flow rate was 500 $\mu\text{L}/\text{min}$ and the column temperature was maintained at 40°C, while the sample-tray temperature was kept at 4°C.

A Waters acquity Synapt G2 quadrupole time-of-flight (Q/TOF) tandem mass spectrometry (Waters Corp., Manchester, UK) was connected to the UPLC system via an electrospray ionization (ESI) interface and controlled by MassLynx software (Version 4.1). The ESI source was operated in the negative ionization mode, and optimized conditions for maximum detection of metabolites were as follows: capillary voltage, 3.0 kV; sample cone, 25 V; extraction cone, 4 V; source temperature, 150°C; desolvation temperature, 450°C. The cone and desolvation gas (N_2) flows were set at 50 and 850 (L/H). Leucine-enkephalin was used as the lock mass generating a reference ion in positive mode at m/z 556.2771 and introduced by a lockspray at 5 $\mu\text{L}/\text{min}$ for accurate mass acquisition.

The mass spectrometer and UPLC system were controlled by MassLynx 4.1 software. Data were collected in centroid mode, and the MS^E approach using dynamic ramp of collision energy was carried out in two scan functions—Function 1 (low energy): mass-scan range: 100–1000; scan time: 0.2 s;

inter-scan delay: 0.05 s; collision energy: 4 V; Function 2 (high energy): mass-scan range: 100–1000; scan time: 0.2 s; inter-scan delay: 0.05 s; collision energy ramp of 15–30 V. MS/MS experiments were operated for major metabolites to obtain additional information from product ions. Comparison of fragment ion spectra between genipin and metabolites further aided in the identification of metabolite structures and site (s) of modifications in the parent molecule.

2.6. Isolation of the Major Metabolite from Rat Bile. Twenty male Sprague-Dawley rats weighing 180–220 g were given a single dose of genipin solution at 50 mg/kg of body weight by gavage into the stomach. After administration, the bile samples were collected by bile duct cannulation surgery. semipreparative HPLC (high performance liquid chromatography) was performed on an Agilent 1100 system consisting of a G1379A degasser, a G1311A quaternary pump, a 7725i manual sampler, and a G1316A thermostated column compartment with a G1315D DAD (Diode Array Detector) detector. Rat bile samples (100 mL) were first extracted three times by ethyl acetate and butyl alcohol. The ethyl acetate and butyl alcohol solution were removed later. The water soluble fraction was subjected to a macroporous absorption resin chromatography in an elution liquid (Ethanol/Water, 10/90 v/v). Metabolite G1 in elution was purified by semipreparative HPLC using an Agilent Eclipse XDB-C18 ODS column (250 mm \times 9.4 mm, 5 μm) and gradient conditions consisting of (A) acetonitrile and (B) water: 0–15 min, linear from 4% to 60% A at a flow rate of 3 mL/min to isolate the major metabolite in rat bile. Its purity would be determined by the high performance liquid chromatography-variable wavelength detector (HPLC-VWD) analysis. Its chemical structure was identified by comparison of their UV, IR, ESI-MS, $^1\text{H-NMR}$, and $^{13}\text{C-NMR}$ spectra with the conference [13].

3. Results and Discussion

3.1. UPLC-Q/TOF MS Analysis of Genipin. To identify the metabolites of genipin, the chromatographic and MS fragmentation behaviors of the parent compound genipin were first investigated. The retention time of genipin was 13.37 min under the chromatographic conditions employed. In the MS^2 fragmentation mode, genipin formed a pseudomolecule weight of $[\text{M-H}]^-$ at m/z 225.0774. The elemental compositions, double bond equivalents (DBEs), the experimental masses and calculated masses, and the mass errors of the pseudomolecular ion and its fragment ions were displayed in Table 1. The maximum of mass errors between measured and calculated values was less than 15 ppm (≤ 2.0 mDa), which signified high resolution and good accuracy. Figure 1(a) showed the product ion spectrum of genipin under the high collision energy scan. On the basis of the high resolution mass spectral information, a tentative pathway for the formation of the most informative fragment ions of genipin is proposed in Figure 1(b). The product ion at m/z 207.0674 was generated by the loss of an OH radical (C-1) from the pseudomolecular ion at m/z 225.0774. The presence of a product ion at m/z 175.0414

TABLE 1: The predicted elemental compositions, measured masses and calculated masses, double-bond equivalents (DBEs), and mass errors of pseudo molecule of genipin and its fragment ions.

Elemental composition	Measured mass (Da)	Calculated mass (Da)	DBE	Error (mDa)	Error (ppm)
C ₁₁ H ₁₃ O ₅ ⁻	225.0774	225.0763	4.5	1.1	4.9
C ₁₁ H ₁₁ O ₄ ⁻	207.0674	207.0657	6.5	1.7	8.2
C ₁₀ H ₁₁ O ₄ ⁻	195.0673	195.0657	5.5	1.6	8.2
C ₁₀ H ₇ O ₃ ⁻	175.0414	175.0395	7.5	1.9	10.9
C ₉ H ₇ O ₂ ⁻	147.0456	147.0446	6.5	1.0	6.8
C ₇ H ₇ O ₂ ⁻	123.0456	123.0446	4.5	1.0	8.1
C ₄ H ₅ O ₃ ⁻	101.0248	101.0239	2.5	0.9	8.9

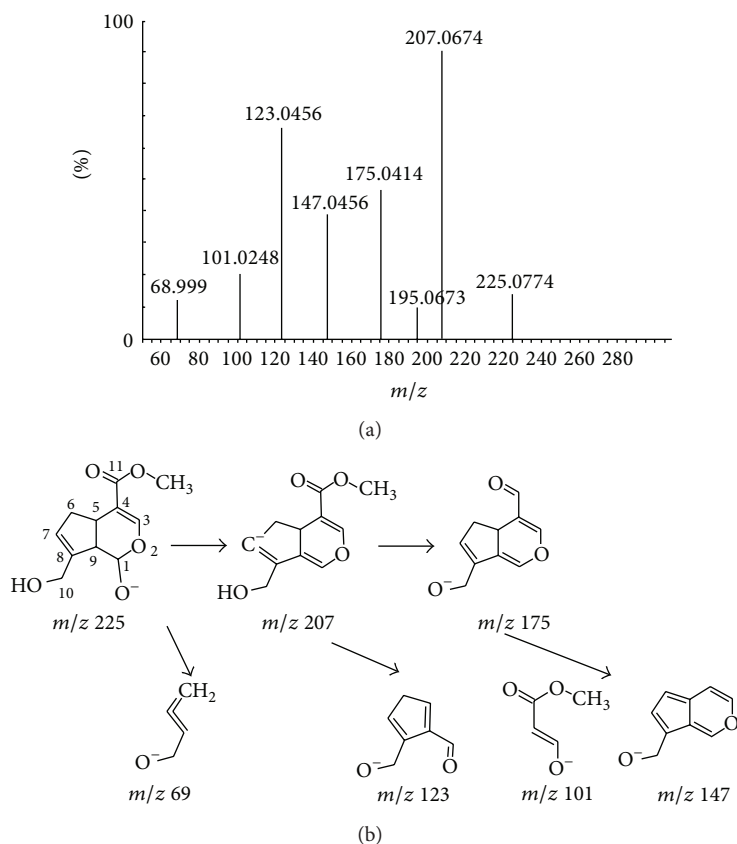


FIGURE 1: (a) Mass spectrum of genipin obtained on Q-TOF mass spectrometry at high collision energy. (b) Proposed fragmentation pathways of genipin.

was probably resulted from a cleavage of methylol group on C-11 from the ion at m/z 207.0674. And the major moiety ion at m/z 225.0774 may have undergone a successive loss of an OH radical on C-1 and a methyl ester on C-4 to produce the ion exhibiting m/z 147.0456. In addition, two other fragment ions gave m/z 123.0456 and m/z 101.0248 (Table 1), which could serve as characteristic ions for screening and identifying metabolites with similar skeletons.

3.2. Identification of Metabolites in Rat Bile, Blood, Feces, and Urine. The UPLC and MS conditions were optimized to obtain a full overview of metabolites by comparing the drug-containing biological samples with blank biological samples.

As shown in Figure 2, ten metabolites of genipin were detected in rat bile samples. Extracted ion chromatogram of genipin and its metabolites are presented in Figure 3. Table 2 lists the detailed information of these metabolites, including the retention times, proposed elemental compositions, and the characteristic fragment ions.

Metabolite G1. G1 was the most abundant metabolite in rat's bile on the basis of the chromatographic peak area. It was eluted at 10.95 min with a molecular weight $[H-1]^-$ of 401.1102 and a derived formula of C₁₇H₂₁O₁₁. High collision energy analysis revealed a characteristic product ion at 225.0765 with neural loss of a glucuronide unit with 176 Da in the MS/MS

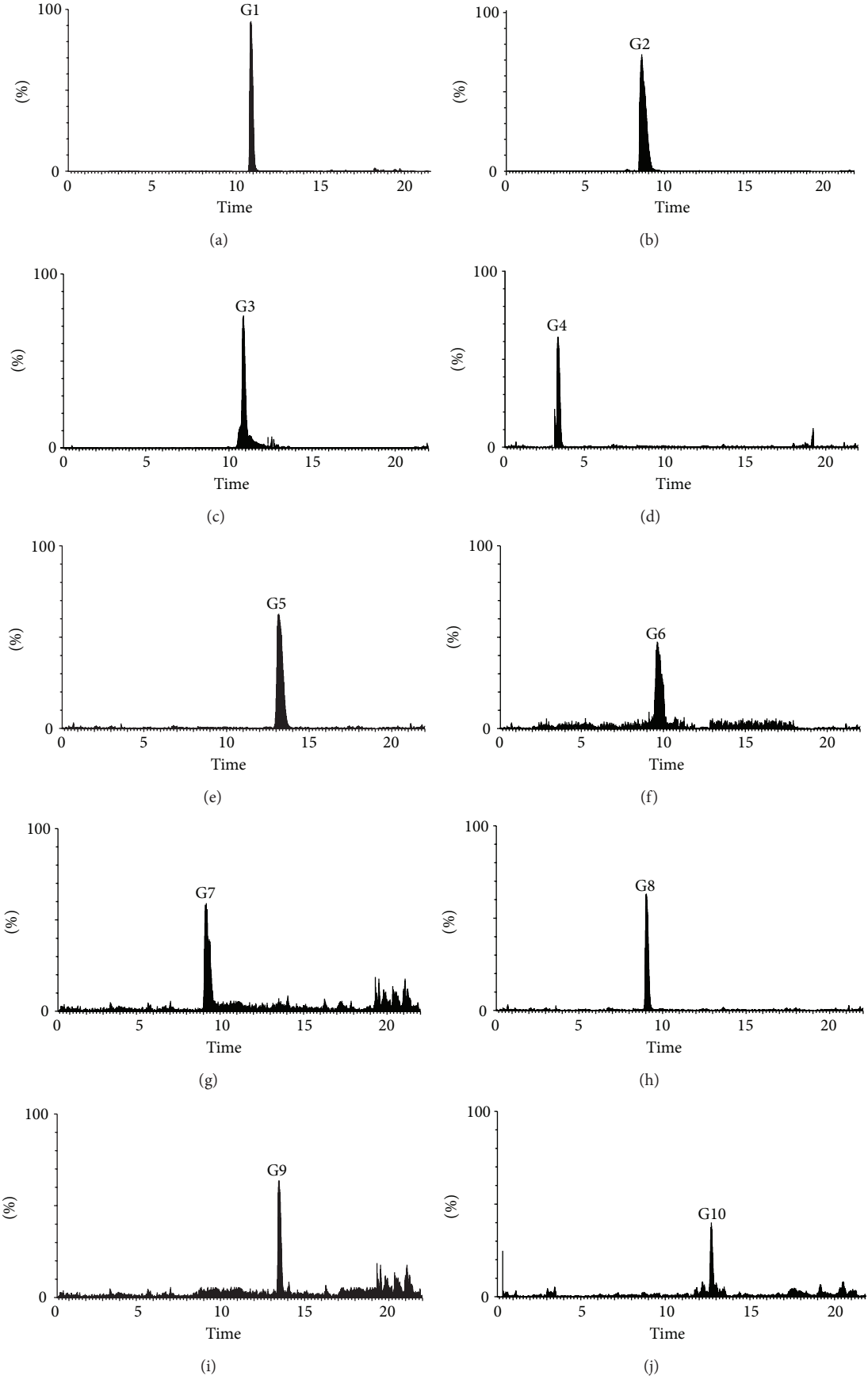


FIGURE 2: Extracted ion chromatograms of ten metabolites of genipin.

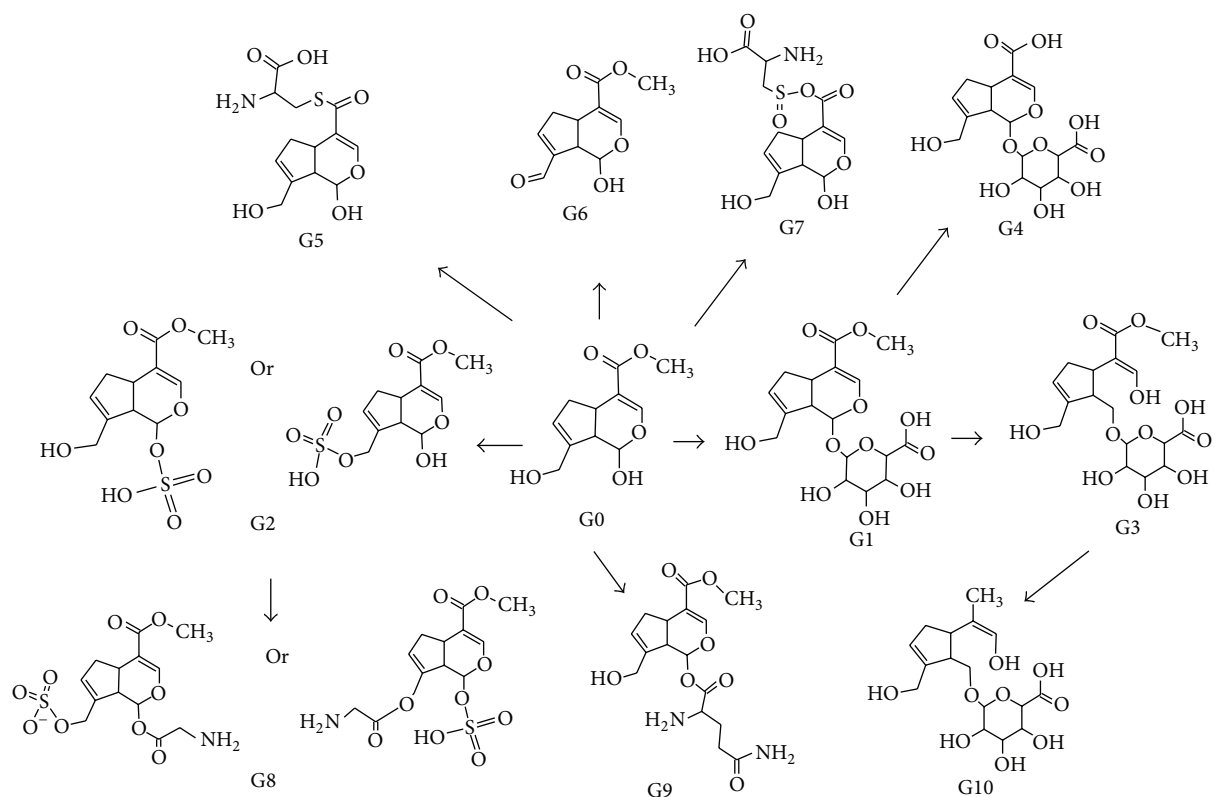


FIGURE 3: The possible metabolic pathways of genipin in rat bile.

spectra. Fragment ions at m/z 207.0673, 147.0450, 123.0450, and 101.0247 were the same as those of genipin. Therefore, G1 was identified as monoglucuronidated conjugate of genipin. But the accurate site of glucuronated action could not be confirmed because it could be occurred on the hydroxyl groups of both C-1 and C-10 positions.

Metabolite G2. G2 had a retention time of 8.76 min and showed an $[M-H]^-$ ion at m/z 305.0348, corresponding to the elemental composition of $C_{11}H_{13}SO_8$. In the MS/MS spectra of G2, the fragment ion at m/z 225.0767 was generated from the $[M-H]^-$ ion by the loss of a sulfate unit with 80 Da from metabolite G2. And high collision energy analysis revealed product ions at 207.0668, 147.0445, 123.0461, and 101.0254 that were the same as those of genipin. Metabolite G2 was tentatively identified as monosulfated conjugate of genipin.

Metabolite G3. G3 was eluted at 9.74 min and displayed a molecular ion at m/z 403.1197. Accurate mass measurement showed that the chemical formula was $C_{17}H_{23}O_{11}$, suggesting the addition of two hydrogen atoms on metabolite G1. The product ion at m/z 227.0595 was the base peak in the MS/MS spectrum, with a loss of 176 Da, indicating that a glucuronic acid was attached to the aglycone moiety. The product ions of G3 at m/z 227.0595, 209.0769, and 149.0576 were all 2 Da greater compared with product ions m/z 225.0767, 207.0668, and 147.0445 from genipin. Hence, it could be inferred that metabolite G3 was ring-opened derivative of G1. The

glucuronated action can be occurred on the hydroxyl groups of both C-1 and C-10 positions. However, the site of the glucuronated action could not be characterized from the MS/MS spectra.

Metabolite G4. G4 was eluted at 3.55 min and displayed a molecular ion at m/z 387.0903. Accurate mass measurement showed that the chemical formula was $C_{16}H_{19}O_{11}$, suggesting the loss of CH_2 from metabolite G1. The product ions of G4 at m/z 211.0586 and 193.0312 were all 14 Da lower compared with product ions of genipin at m/z 225.0767 and 207.0668. Moreover, the character product ion of genipin at m/z 147.0461 was also observed in the MS/MS spectrum of metabolite G4. Hence, it could be inferred that metabolite G4 was demethylation derivative of metabolite G1.

Metabolite G5. G5 with a retention time at 13.01 min had a molecular ion ($[M-H]^-$) at m/z 314.0723. Accurate mass measurement showed that the chemical formula of G5 was $C_{13}H_{16}NO_6S$. The molecular ion at m/z 314.0723 could have lost an H_2O molecule to generate a product ion at m/z 296.0621. It was notable that $[M-H]^-$ ion of G5 could generate a product ion at m/z 195.0672 by losing a $C_3H_5NO_2S$ unit. It indicated that there was a cysteine group in G5. High collision energy analysis revealed product ions at 227.0374, 209.0254, 195.0672, and 177.0523 with the proposed fragmentation pathways of G5 was shown in Figure 4(a). Hence, G5 was identified as cysteine conjugate of demethylol-genipin.

TABLE 2: The retention times, accurate measurements, and elemental formula of protonated molecules and product ions by Q-TOF MS/MS analysis of metabolites.

Compound no.	t_R (min)	Molecular ions m/z (Da)	Fragment ions m/z (Da)	Formula	Error (mDa)	Error (ppm)
G0 (genipin)	13.37	225.0774		$C_{11}H_{13}O_5$	1.1 mDa	4.9 ppm
			207.0674	$C_{11}H_{11}O_4$	1.7 mDa	8.2 ppm
			195.0673	$C_{10}H_{11}O_4$	1.6 mDa	8.2 ppm
			175.0414	$C_{10}H_7O_3$	-1.5 mDa	-8.6 ppm
			147.0456	$C_9H_7O_2$	1.0 mDa	6.8 ppm
			123.0456	$C_7H_7O_2$	1.3 mDa	10.6 ppm
			101.0248	$C_4H_5O_3$	0.9 mDa	8.9 ppm
G1	10.95	401.1102		$C_{17}H_{21}O_{11}$	1.8 mDa	4.5 ppm
			383.1001	$C_{17}H_{19}O_{10}$	2.3 mDa	6.0 ppm
			369.0831	$C_{16}H_{17}O_{10}$	0.9 mDa	2.4 ppm
			225.0765	$C_{11}H_{13}O_5$	0.2 mDa	0.9 ppm
			207.0673	$C_{11}H_{11}O_4$	1.6 mDa	7.7 ppm
			147.0450	$C_9H_7O_2$	0.4 mDa	2.7 ppm
			123.0450	$C_7H_7O_2$	0.3 mDa	3.3 ppm
101.0247	$C_4H_5O_3$	0.8 mDa	7.9 ppm			
G2	8.76	305.0348		$C_{11}H_{13}SO_8$	1.7 mDa	5.6 ppm
			287.0241	$C_{11}H_{11}SO_7$	1.6 mDa	5.6 ppm
			273.0085	$C_{10}H_9SO_7$	1.6 mDa	5.9 ppm
			225.0767	$C_{11}H_{13}O_5$	0.4 mDa	1.8 ppm
			207.0668	$C_{11}H_{11}O_4$	1.1 mDa	5.3 ppm
			147.0445	$C_9H_7O_2$	-0.1 mDa	-0.7 ppm
			123.0461	$C_7H_7O_2$	1.0 mDa	8.1 ppm
101.0254	$C_4H_5O_3$	0.5 mDa	4.9 ppm			
G3	9.74	403.1197		$C_{17}H_{23}O_{11}$	4.3 mDa	-10.7 ppm
			227.0595	$C_{11}H_{15}O_5$	-3.1 mDa	13.7 ppm
			209.0769	$C_{11}H_{13}O_4$	-4.5 mDa	9.1 ppm
			197.0808	$C_{10}H_{13}O_4$	-0.6 mDa	-3.0 ppm
			177.0552	$C_{10}H_9O_3$	0.1 mDa	0.6 ppm
149.0576	$C_9H_9O_2$	-2.7 mDa	-18.1 ppm			
G4	3.55	387.0903		$C_{16}H_{19}O_{11}$	-2.4 mDa	-6.2 ppm
			343.1046	$C_{15}H_{19}O_9$	1.7 mDa	5.0 ppm
			325.0938	$C_{15}H_{17}O_8$	1.5 mDa	4.6 ppm
			211.0586	$C_{10}H_{11}O_5$	-2.0 mDa	-9.5 ppm
			193.0312	$C_{10}H_9O_4$	-1.1 mDa	-5.7 ppm
175.0404	$C_{10}H_7O_3$	-0.9 mDa	-5.1 ppm			
147.0461	$C_9H_7O_2$	1.5 mDa	10.2 ppm			
G5	13.01	314.0723		$C_{13}H_{16}NO_6S$	2.5 mDa	8.0 ppm
			296.0621	$C_{13}H_{14}NO_5S$	2.8 mDa	9.5 ppm
			282.0397	$C_{12}H_{12}NO_5S$	-3.9 mDa	-13.8 ppm
			264.0335	$C_{12}H_{10}NO_4S$	0.4 mDa	1.5 ppm
			252.0331	$C_{11}H_{10}NO_4S$	2.0 mDa	7.9 ppm
			227.0374	$C_{10}H_{11}O_4S$	-0.4 mDa	-1.8 ppm
			209.0254	$C_{10}H_9O_3S$	-1.8 mDa	-8.6 ppm
195.0672	$C_{10}H_{11}O_4$	1.5 mDa	7.7 ppm			
177.0523	$C_{10}H_9O_3$	-0.9 mDa	-5.1 ppm			

TABLE 2: Continued.

Compound no.	t_R (min)	Molecular ions m/z (Da)	Fragment ions m/z (Da)	Formula	Error (mDa)	Error (ppm)
G6	9.60	223.0611		$C_{11}H_{11}O_5$	0.5 mDa	2.2 ppm
			205.0509	$C_{11}H_9O_4$	0.8 mDa	3.9 ppm
			193.0531	$C_{10}H_9O_4$	0.8 mDa	3.9 ppm
			175.0388	$C_{10}H_5O_3$	-0.7 mDa	-4.0 ppm
			147.0437	$C_9H_7O_2$	-0.9 mDa	-6.1 ppm
			121.0299	$C_7H_5O_2$	0.9 mDa	7.4 ppm
			101.0237	$C_4H_5O_3$	-0.2 mDa	-2.0 ppm
G7	9.26	346.0406		$C_{13}H_{16}NO_8S$	-0.1 mDa	-0.3 ppm
			328.0516	$C_{13}H_{14}NO_7S$	2.5 mDa	7.6 ppm
			284.0632	$C_{12}H_{14}NO_5S$	2.5 mDa	7.6 ppm
			252.0351	$C_{11}H_{10}NO_4S$	2.0 mDa	7.9 ppm
			211.0614	$C_{10}H_{11}O_5$	0.8 mDa	3.8 ppm
			193.0504	$C_{10}H_9O_4$	0.3 mDa	1.6 ppm
			175.0411	$C_{10}H_7O_3$	1.6 mDa	9.1 ppm
G8	9.21	362.0593		$C_7H_7O_2$	-0.2 mDa	-1.6 ppm
				$C_{13}H_{16}NO_9S$	4.3 mDa	13.0 ppm
			305.0350	$C_{11}H_{13}SO_8$	1.9 mDa	6.2 ppm
			287.0219	$C_{11}H_{11}SO_7$	-0.6 mDa	-2.1 ppm
			207.0655	$C_{11}H_{11}O_4$	-0.2 mDa	-1.0 ppm
G9	13.59	353.1381		$C_7H_7O_2$	0.1 mDa	0.8 ppm
			123.0447	$C_4H_5O_3$	0.2 mDa	2.0 ppm
				$C_{16}H_{21}N_2O_7$	3.2 mDa	9.1 ppm
			335.1288	$C_{16}H_{19}N_2O_6$	4.5 mDa	13.4 ppm
			207.0674	$C_{11}H_{11}O_4$	1.7 mDa	8.2 ppm
G10	12.7	359.1354	195.0673	$C_{10}H_{11}O_4$	1.6 mDa	8.2 ppm
			175.0414	$C_{10}H_7O_3$	-1.5 mDa	-8.6 ppm
			147.0456	$C_9H_7O_2$	1.0 mDa	6.8 ppm
				$C_{16}H_{23}O_9$	1.2 mDa	3.3 ppm
			183.1024	$C_{10}H_{15}O_3$	0.3 mDa	1.6 ppm
	$C_{10}H_{13}O_2$	1.0 mDa	6.1 ppm			
	$C_9H_{11}O$	0.9 mDa	6.7 ppm			

Metabolite G6. G6 had a retention time of 9.60 min and showed an $[M-H]^-$ ion at m/z 223.0611, corresponding to the elemental composition of $C_{11}H_{11}O_5$. As shown in Table 3, the molecular ion of G6 lost H_2O , a molecule of methoxy, and aldehyde to form product ions at m/z 205.0509, m/z 193.0531, and 147.0437. The proposed fragmentation pathways of G6 were shown in Figure 4(b). Hence, G6 was identified as 10-aldehyde-genipin.

Metabolite G7. G7 had a retention time of 9.26 min and showed an $[M-H]^-$ ion at m/z 346.0406, corresponding to the elemental composition of $C_{13}H_{16}NO_8S$. The $[M-H]^-$ ion of G7 could lose H_2O to generate the fragment ion at m/z 328.0516 and a molecule of $HCOOH$ subsequently to generate the fragment ions at m/z 284.0632. And another product ion at m/z 211.0614 was generated by losing $C_3H_5NO_3S$ from the precursor ion at m/z 346.0406. Fragment ions at m/z

175.0411 and 123.0444 were the same to those from genipin. Hence, G7 was identified as cysteinesulfinic acid conjugate of demethylol-genipin.

Metabolite G8. G8 had a retention time of 9.21 min and showed an $[M-H]^-$ ion at m/z 362.0593, corresponding to the elemental composition of $C_{13}H_{16}NO_9S$. In the MS/MS spectra of G8, the fragment ion at m/z 305.0350 was generated from the $[M-H]^-$ ion by the loss of C_2H_3NO unit from Metabolites G8. The major fragment ion at m/z 305.0350 was the same as that of G2. Moreover, fragment ions at m/z 207.0655, 123.0447, and 101.0241 were same to those from G2. Therefore, G8 was identified as glycine conjugate of G2.

Metabolite G9. G9 had a retention time of 13.59 min and showed an $[M-H]^-$ ion at m/z 353.1381, corresponding to the elemental composition of $C_{16}H_{21}N_2O_7$. The $[M-H]^-$ ion

TABLE 3: The metabolites in different biological samples of rats.

	Formula	Bile	Urine	Plasma*	Feces	Plasma**
G0	C ₁₁ H ₁₄ O ₅ (genipin)	–	–	–	–	–
G1	C ₁₇ H ₂₂ O ₁₁	+	+	+	–	+
G2	C ₁₁ H ₁₄ SO ₈	+	+	+	+	–
G3	C ₁₇ H ₂₄ O ₁₁	+	+	–	–	–
G4	C ₁₆ H ₂₀ O ₁₁	+	–	–	–	–
G5	C ₁₃ H ₁₇ NO ₆ S	+	+	–	–	–
G6	C ₁₁ H ₁₂ O ₅	+	–	–	–	–
G7	C ₁₃ H ₁₇ NO ₈ S	+	+	–	–	–
G8	C ₁₃ H ₁₇ NO ₉ S	+	–	–	–	–
G9	C ₁₆ H ₂₂ N ₂ O ₇	+	+	–	–	–
G10	C ₁₆ H ₂₄ O ₉	+	–	–	–	–

+: found; –: not found.

Plasma* were from rats given single dose of genipin solution at 50 mg/kg of body weight by gavage into the stomach.

Plasma** were from rats given single dose of genipin solution at 10 mg/kg of body weight by intravenous administration.

of G9 could lose H₂O to generate the fragment ion at m/z 335.1288. Moreover, the character product ions of genipin at m/z 207.0674, 175.0414, and 147.0456 were also observed in the MS/MS spectrum of metabolite G9. Hence, it could be inferred that metabolite G9 was glutamine conjugate of genipin.

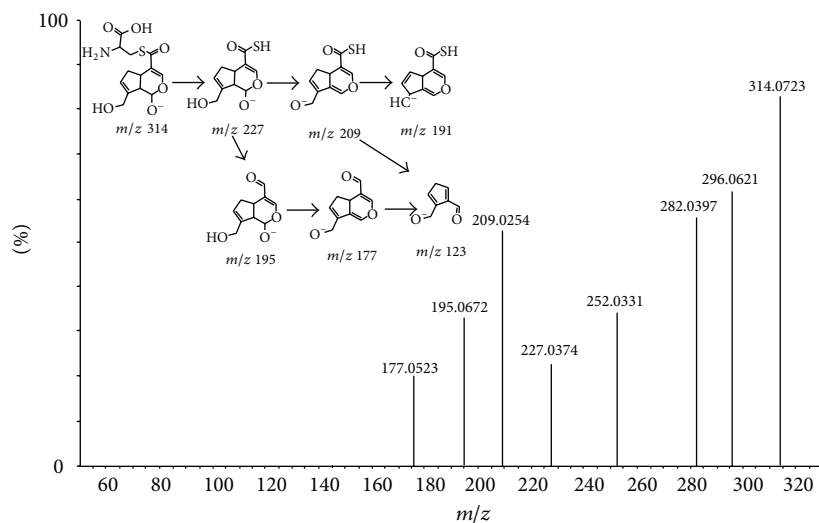
Metabolite G10. A minor compound with the retention time of 12.7 min in the chromatogram was observed as metabolite G10 with a molecule ion at m/z 359.1354, corresponding to the elemental composition of C₁₆H₂₃O₉. The product ion at m/z 183.1024 was also observed in the MS/MS spectrum, with a loss of 176 Da, indicating that a glucuronic acid was attached to the aglycone moiety. The product ion at m/z 165.0926 of G10 was formed by the loss of an H₂O unit from the product ion m/z 183.1024, followed by the loss of one CH₂O unit to form m/z 135.0810. The proposed fragmentation pathways of G10 were shown in Figure 4(c).

After analysis of the metabolites of genipin in rats urine, feces, and plasma samples, the result showed that all metabolites excluding G1 to G10 appeared in other samples could be detected in bile. The result was shown in Table 3. There were six metabolites (G1, G2, G3, G5, G7, and G9) in urine, two metabolites (G1 and G2) in plasma, and one metabolite (G1) in feces. And the plasma samples from rats which were administrated genipin by intravenous administration in the fourth group were also analyzed. Only one metabolite (G1) was identified whereas the parent form of genipin was absent.

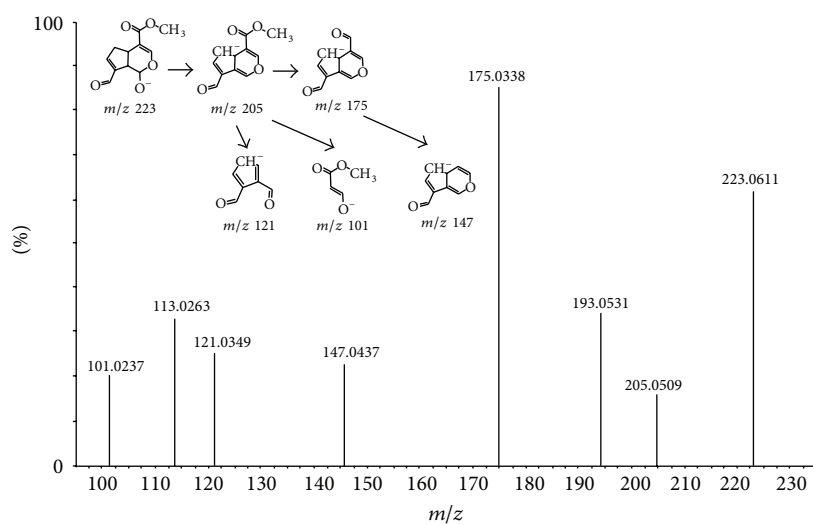
In this metabolism study of genipin, it could conclude that genipin was an active compound that could be metabolized to other forms wholly and immediately. On the basis of the chromatographic peak area, the sulfated and glucuronidated conjugates of genipin were major metabolites and there were other 8 metabolites. According to the result, demethylated, ring-opened, cysteine-conjugated, hydroformylated, glucuronidated, and sulfated transformations were proposed to be the possible metabolic pathways of genipin in rat, which would improve our knowledge about the *in vivo* metabolism of genipin.

3.3. Metabolism of Genipin In Vitro in Human Liver Microsomes. Incubations of genipin in human liver microsomes (HLM) protein were performed to determine the hepatic contribution to the overall disposition of this drug. Comparing with the three negative control samples, metabolite G1 was detected in HLM incubations with the amount of genipin decreasing. Using the UPLC-QTOF/MS, metabolite G1 had a retention time of 10.95 min and showed an [M-H][–] ion at m/z 401.1102 with fragment ions at m/z 207.0673, 147.0450, 123.0450, and 101.0247. Glucuronidation represents one of the major pathways for drug metabolism in humans and other mammalian species. Here, we found that genipin was metabolized in human liver microsomes immediately as the metabolite G1 that could be detected after 1 h incubation. And amount of metabolite G1 could not increase indicated that incubations of genipin in human liver microsomes (HLM) protein had been finished in 6 h. The result also confirmed that glucuronidated transformations were proposed to be the possible major metabolic pathways of genipin in rats.

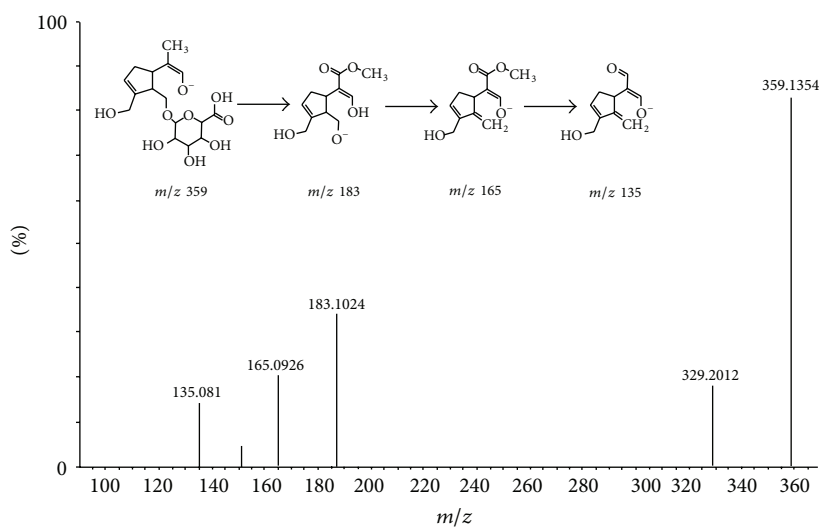
3.4. Enzymatic Hydrolysis Analysis. The metabolism study of genipin showed that the parent form of genipin could not be detected in biological samples (bile, urine, plasma, and feces). In order to confirm the existence of major metabolite G1 and G2, the drug-containing urine samples were hydrolyzed with β -glucuronidase or sulfatase. After UPLC-QTOF/MS analysis, the appearance of genipin (m/z 225.0774) with the retention time at 13.25 min (Figure 5) was all detected in the drug-containing urine samples after β -glucuronidase or sulfatase hydrolysis. When β -glucuronidase was added to urine samples with the same processing, metabolite G1 was hydrolyzed to genipin as metabolite G2 could not be hydrolyzed by β -glucuronidase (Figure 6). On the contrary, when sulfatase was added to urine samples with the same processing, some amount of metabolite G2 could be hydrolyzed to genipin which was showed with the decrease of the peak area of metabolite G2 (Figure 7).



(a)



(b)



(c)

FIGURE 4: Representative MS/MS spectrum of $[M-H]^-$ ion at m/z 314.0723 for metabolite G5 (a); MS/MS spectrum of $[M-H]^-$ ion at m/z 223.0611 for metabolite G6 (b); MS/MS spectrum of $[M-H]^-$ ion at m/z 359.1354 for metabolite G10 (c).

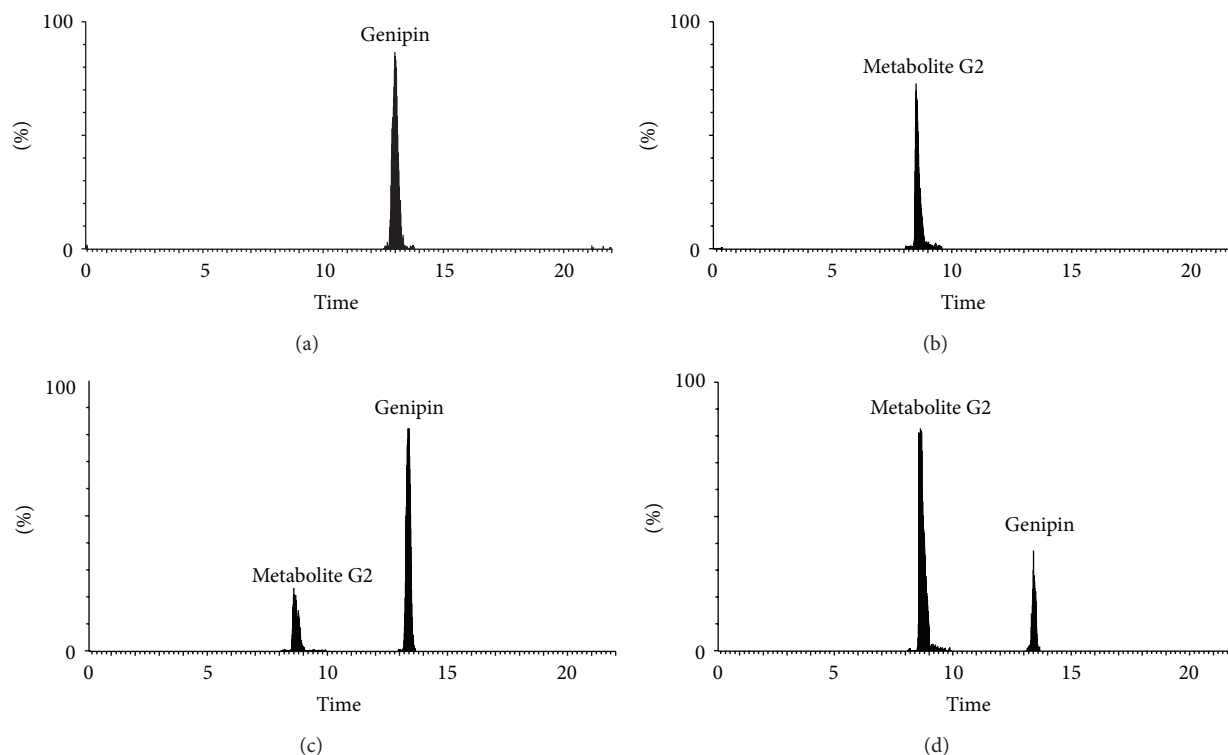


FIGURE 5: The extracted ion chromatogram of m/z 225 of bile treated accordingly to experimental schemes. (a) the standard solution with genipin at concentration of 50 ng/mL; (b) the drug-containing bile; (c) the drug-containing urine hydrolyzed by sulfatase; (d) the drug-containing urine hydrolyzed with β -glucuronidase.

3.5. Identification of the Structure of Metabolite G1. Metabolite G1 was the most abundant metabolite in rat bile on the basis of the chromatographic peak area, and it was isolated from rats bile as described in Section 2.6. From the following experimental data, it was confirmed that metabolite G1 was genipin-1-*o*-glucuronic acid. Its structure was shown in Figure 8. IR ν_{\max}^{KBr} cm^{-1} : 3400, 1710, 1630. UV $\lambda_{\max}^{\text{MeOH}}$ (log ϵ): 240 nm (4.96). ^1H NMR (400 MHz, CD_3OD): δ 7.49 (s, 1H, 3-H), 5.78 (s, 1H, 7-H), 5.28 (d, $J = 7.2$ Hz, 1H, 1-H), 4.70 (d, $J = 7.9$, 1H, 1'-H), 4.32 (d, $J = 14.4$ Hz, 1H, 10-Ha), 4.15 (d, $J = 14.8$ Hz, 1H, 10-Hb), 3.70 (s, 3H, $-\text{OCH}_3$), 3.58 (d, $J = 9.2$ Hz, 1H, 5'-H), 3.48–3.39 (m, 2H, 3'-H, 4'-H), 3.27–3.14 (m, 2H, 2'-H, 5-H), 2.82–2.72 (m, 2H, 6-Ha, 9-H), 2.14–2.08 (m, 1H, 6-Hb); ^{13}C NMR (100 MHz, CD_3OD): δ 36.35 (5-C), 39.64 (6-C), 47.06 (9-C), 51.68 (OCH_3), 61.32 (10-C), 73.56, 74.71, 76.26, 77.62 ($2' \sim 5'$ -C), 98.07 (1-C), 100.32 (1'-C), 112.65 (4-C), 128.23 (7-C), 144.86 (8-C), 153.36 (3-C), 169.59 (11-C), 176.5 ($6'$ -C). The HMBC correlation of genipin-1-*o*-glucuronic acid was shown in Figure 9.

4. Conclusions

In the present study, metabolism of genipin in the rat was extensively studied by using UPLC-QTOF/MS. Accurate masses along with mass fragmentation were applied to elucidate the structures of metabolites with the aid of MetaboLynx software tools. Ten metabolites (G1–G10) were found in rat

bile, and their structures were elucidated based on the retention times on the UPLC system, the accurate molecular mass, and characteristic fragment ions. And six metabolites (G1, G2, G3, G5, G7, and G9) in urine, two metabolites (G1 and G2) in plasma, and one metabolite (G1) in feces were detected. Among the ten metabolites, the sulfated and glucuronidated conjugates of genipin were major metabolites on the basis of the chromatographic peak area. Demethylated, ring-opened, cysteine-conjugated, hydroformylated, glucuronidated, and sulfated transformations were proposed to be the possible metabolic pathways of genipin in rat.

In the *in vitro* experiment, genipin can be transformed to metabolite G1 after incubation in human liver microsomes with UDP-glucuronosyltransferases. In the drug-containing bile samples, metabolite G1 could be hydrolyzed to genipin by β -glucuronidase, and metabolite G2 could be hydrolyzed to genipin by sulfatase. It confirmed the existence of major metabolite G1 and G2 in the drug-containing bile samples.

At last, the major metabolite G1 was isolated by a semipreparative HPLC using an Agilent Eclipse XDB-C18 ODS column. Its purity was up to 98% which was determined by the high performance liquid chromatography-variable wavelength detector (HPLC-VWD) analysis. And its chemical structure was identified by comparison of their UV, IR, ESI-MS, ^1H -NMR, and ^{13}C -NMR spectra with the conference. Metabolite G1 was confirmed as genipin-1-*o*-glucuronic acid.

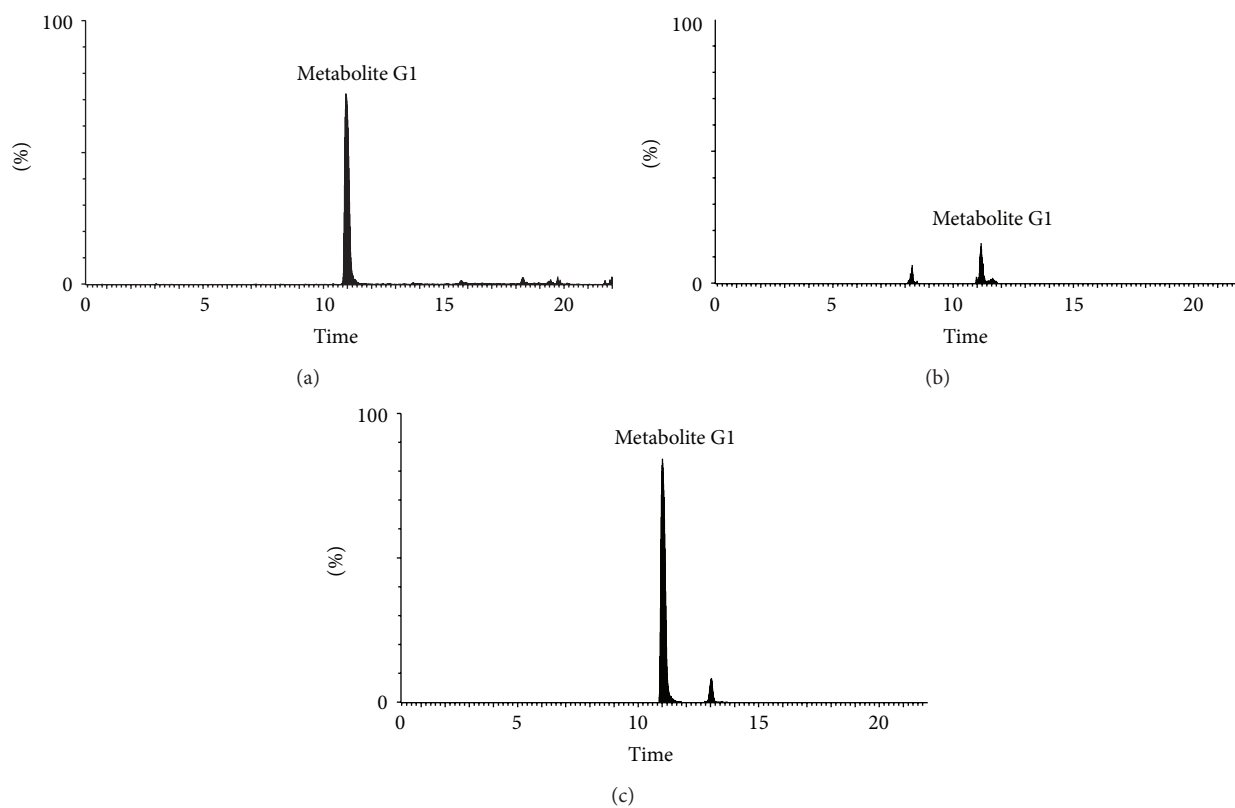


FIGURE 6: The extracted ion chromatogram of m/z 401 of bile treated accordingly to experimental schemes. (a) the drug-containing bile; (b) The drug-containing urine hydrolyzed by β -glucuronidase; (c) the drug-containing urine hydrolyzed with sulfatase.

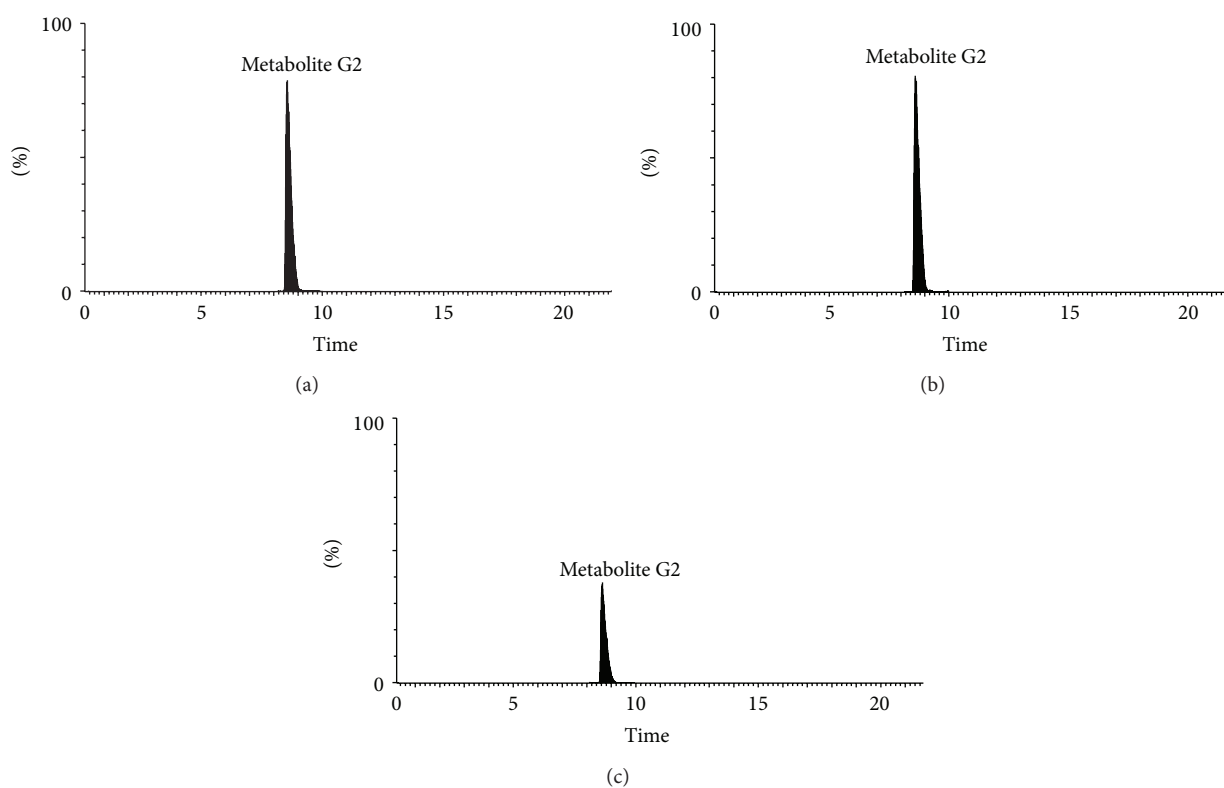


FIGURE 7: The extracted ion chromatogram of m/z 305 of bile treated accordingly to experimental schemes. (a) the drug-containing bile; (b) The drug-containing urine hydrolyzed by β -glucuronidase; (c) the drug-containing urine hydrolyzed with sulfatase.

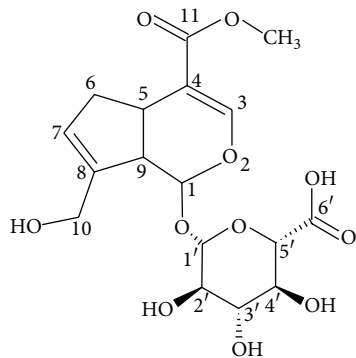


FIGURE 8: Chemical structure of genipin-1-o-glucuronic acid.

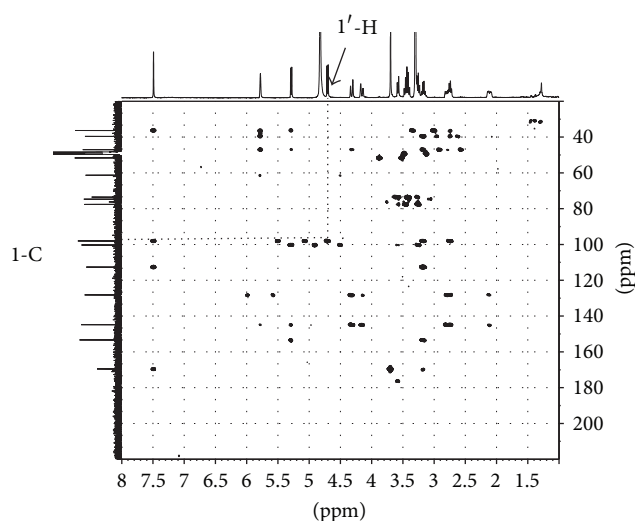


FIGURE 9: Key HMBC correlations of genipin-1-o-glucuronic acid. The coupling from 1'-H to 1-C was observed, which confirms the attachment of a glucuronic acid group to 1-C.

Conflict of Interests

No potential conflict of interests was disclosed.

Acknowledgments

This work was financially supported by the programs of National Natural Science Foundation of China (Project nos. 81173561 and 81274200), Foundation of the Ministry of Education of China (NCET-10-0944), and the Shanghai Municipal Education Commission (Project nos. 2010JW21 and 10SG40).

References

[1] T. Akao, K. Kobashi, and M. Aburada, "Enzymic studies on the animal and intestinal bacterial metabolism of geniposide," *Biological and Pharmaceutical Bulletin*, vol. 17, no. 12, pp. 1573–1576, 1994.

[2] Y. S. Yang, T. Zhang, S. C. Yu et al., "Transformation of geniposide into genipin by immobilized β -glucosidase in a two-phase aqueous-organic system," *Molecules*, vol. 16, no. 5, pp. 4295–4304, 2011.

[3] R. J. Mailloux, C. N. K. Adjeitey, and M. E. Harper, "Genipin-induced inhibition of uncoupling protein-2 sensitizes drug-resistant cancer cells to cytotoxic agents," *PLoS ONE*, vol. 5, no. 10, Article ID e13289, 2010.

[4] H. Cao, Q. Feng, W. Xu et al., "Genipin induced apoptosis associated with activation of the c-Jun NH2-terminal kinase and p53 protein in HeLa cells," *Biological and Pharmaceutical Bulletin*, vol. 33, no. 8, pp. 1343–1348, 2010.

[5] M. Tanaka, M. Yamazaki, and K. Chiba, "Neuroprotective action of genipin on tunicamycin-induced cytotoxicity in neuro2a cells," *Biological and Pharmaceutical Bulletin*, vol. 32, no. 7, pp. 1220–1223, 2009.

[6] H. Goto and H. Takikawa, "Effect of genipin on cholestasis induced by estradiol-17 β -glucuronide and lithocholate-3-O-glucuronide in rats," *Hepatology Research*, vol. 40, no. 5, pp. 524–529, 2010.

[7] H. J. Koo, Y. S. Song, H. J. Kim et al., "Antiinflammatory effects of genipin, an active principle of gardenia," *European Journal of Pharmacology*, vol. 495, no. 2-3, pp. 201–208, 2004.

[8] H. J. Koo, K. H. Lim, H. J. Jung, and E. H. Park, "Anti-inflammatory evaluation of gardenia extract, geniposide and genipin," *Journal of Ethnopharmacology*, vol. 103, no. 3, pp. 496–500, 2006.

[9] K. N. Nam, Y. S. Choi, H. J. Jung et al., "Genipin inhibits the inflammatory response of rat brain microglial cells," *International Immunopharmacology*, vol. 10, no. 4, pp. 493–499, 2010.

[10] F. Mwale, M. Iordanova, C. N. Demers, T. Steffen, P. Roughley, and J. Antoniou, "Biological evaluation of chitosan salts cross-linked to genipin as a cell scaffold for disk tissue engineering," *Tissue Engineering*, vol. 11, no. 1-2, pp. 130–140, 2005.

[11] R. Harris, E. Lecumberri, and A. Heras, "Chitosan-genipin microspheres for the controlled release of drugs: clarithromycin, tramadol and heparin," *Marine Drugs*, vol. 8, no. 6, pp. 1750–1762, 2010.

[12] Y. Ding, T. Zhang, J. S. Tao, B. Tan, C. R. Guo, and L. Yang, "HPLC-MS/MS method to determine genipin in rat plasma after hydrolysis with sulfatase and its application to a pharmacokinetic study," *Biomedical Chromatography*, vol. 26, no. 7, pp. 816–825, 2012.

[13] S. Takeda, T. Endo, and M. Aburada, "Pharmacological studies on iridoid compounds. III. The choleric mechanism of iridoid compounds," *Journal of Pharmacobio-Dynamics*, vol. 4, no. 8, pp. 612–623, 1981.

Research Article

Metabolomic Study of Collagen-Induced Arthritis in Rats and the Interventional Effects of Huang-Lian-Jie-Du-Tang, a Traditional Chinese Medicine

Rongcai Yue,¹ Ling Zhao,^{1,2} Yaohua Hu,¹ Peng Jiang,¹ Shuping Wang,¹ Li Xiang,¹ Wencong Liu,² Lei Shan,¹ Weidong Zhang,^{1,3} and Runhui Liu¹

¹ School of Pharmacy, Second Military Medical University, 325 Guo-He Road, Shanghai 200433, China

² College of Traditional Chinese Medicine, Jilin Agricultural University, Changchun 130118, China

³ School of Pharmacy, Shanghai Jiao Tong University, Shanghai 200030, China

Correspondence should be addressed to Weidong Zhang; wdzhangy@hotmail.com and Runhui Liu; lyliurh@126.com

Received 18 September 2012; Revised 28 January 2013; Accepted 28 January 2013

Academic Editor: Wei Jia

Copyright © 2013 Rongcai Yue et al. This is an open access article distributed under the Creative Commons Attribution License, which permits unrestricted use, distribution, and reproduction in any medium, provided the original work is properly cited.

Huang-Lian-Jie-Du-Tang (HLJDT) is a traditional Chinese medicine (TCM) with anti-inflammatory activity. The present study used a metabolomic approach based on LC-Q-TOF-MS to profile rheumatoid-arthritis- (RA-) related metabolic changes and to investigate the interventional mechanisms of HLJDT in collagen-induced arthritis rats. Forty male Wistar rats were randomly divided into five groups: (1) a model group, (2) a normal control group, (3) a dexamethasone group, (4) a HLJDT group, and (5) a group that received 13 components of HLJDT. Plasma samples were collected 8, 15, and 22 days after the rats were injected with bovine type II collagen. By combining variable importance in the projection values with partial least squares discriminant analysis, 18 potential biomarkers were identified in the plasma samples. The biomarkers were primarily involved in glycerophospholipid metabolism, fatty acid metabolism, tryptophan metabolism, linoleic acid metabolism, phenylalanine metabolism, purine metabolism, arachidonic acid metabolism, and bile acid biosynthesis. Using the potential biomarkers as a screening index, the results suggest that HLJDT can potentially reverse the process of RA by partially regulating fatty acid oxidation and arachidonic acid metabolism. This study demonstrates that a metabolomic strategy is useful for identifying potential RA biomarkers and investigating the underlying mechanisms of a TCM in RA treatment.

1. Introduction

Rheumatoid arthritis (RA) is an autoimmune disease characterized by persistent synovitis, systemic inflammation, and autoantibodies [1, 2]. RA primarily affects the small diarthrodial joints of the hands and feet, causing swelling and pain. If left untreated, RA may result in deformity. Several studies have investigated the pathogenetic mechanisms of RA, particularly collagen-induced arthritis (CIA) in humans and in animal models [3–5]. Although some important biomarkers and novel therapeutic methods have been identified and developed for RA diagnosis and treatment [6–8], the occurrence of RA-induced deformity remains high. Moreover, current RA treatment medications are limited by

several well-characterized clinical side effects, such as hepatotoxicity [9, 10], gastrointestinal effects [11], and cardiotoxic effects [12]. Therefore, further investigation of the biological processes related to RA, as well as its clinical diagnosis and treatment, is needed to understand its disease mechanism, identify new biomarkers, and explore new anti-RA drugs.

Metabolomics focuses on the comprehensive measurement of all small molecular weight compounds, including endogenous and exogenous species, which are present in a biological system. Furthermore, it provides a functional readout of abnormal, disease-related physiological states in the human body and may provide new insights into the global effects of disease related to metabolic pathways [13]. In recent years, metabolomics has been used to identify disease-related

biomarkers and shows significant potential for the early diagnosis, therapeutic monitoring and pathogenic understanding of many diseases, including RA [14–16]. Among the analytical techniques used in metabolomic research, LC-MS is recognized as one of the most selective, sensitive, and reproducible methods [17] due to its enhanced reproducibility of retention times [18]. This reproducibility is especially important for large-scale, untargeted metabolic profiling.

Huang-Lian-Jie-Du-Tang is an aqueous extract that consists of four herbal materials: *Rhizoma Coptidis*, *Radix Scutellariae*, *Cortex Phellodendri*, and *Fructus Gardeniae*. In our previous study, LC-DAD and LC-ESI-MS methods were developed and validated for the chromatographic fingerprinting and quantitative analysis of HLJDT [19]. Furthermore, HLJDT's potentially active components were identified in a plasma-based pharmacochemical study [20]. In addition, the anti-inflammatory activities, component herbs and active components of HLJDT were also investigated [21, 22]. However, a proper approach for evaluating the holistic efficacy of such a multicomponent medicine is urgently needed. In the present study, we used a metabolomic approach to investigate the biochemical abnormalities associated with RA and to assess the therapeutic effects of HLJDT and its components in CIA rats.

2. Experimental Methods

2.1. Reagents and Materials. HPLC-grade methanol and acetonitrile were purchased from J.T. Baker (NJ, USA). Ultrapure water (18.2 M Ω) was prepared with a Milli-Q water purification system (Millipore, MA, USA). The following HLJDT components were purchased from the National Institute for the Control of Pharmaceutical and Biological Products (Beijing, China): geniposide, coptisine, phellodendrine, jatrorrhizine, magnoflorine, palmatine, berberine, baicalin, chlorogenic acid, crocin, wogonoside, baicalein, and wogonin. The following standard metabolites were obtained from Sigma-Aldrich (St. Louis, MO, USA): choline, carnitine, L-phenylalanine, arachidonic acid, hippuric acid, uric acid, allantoin, 5-hydroxy tryptophan, and L-tryptophan.

Rhizoma Coptidis (*Rhizoma* of *Coptis chinensis* Franch.), *Radix Scutellariae* (*Radix* of *Scutellaria baicalensis* Georgi.), *Cortex Phellodendri* (*Cortex* of *Phellodendron chinense* Schneid.), and *Fructus Gardeniae* (*Fructus* of *Gardenia jasminoides* Ellis.) were purchased from Bozhou (Anhui province, China) and were authenticated by Professor HanMing Zhang (Second Military Medical University, Shanghai, China). Voucher specimens of *Rhizoma coptidis*, *Radix scutellariae*, *Cortex phellodendri*, and *Fructus gardeniae* were stored at the Second Military Medical University, Shanghai, China (no. HL20070523, HQ20070523, HB20070523, and ZZ20070523, resp.). HLJDT extract was prepared from the four medicinal herbs (*Rhizoma Coptidis*, *Radix Scutellariae*, *Cortex Phellodendri*, and *Fructus Gardeniae* in a 3:2:2:3 ratio) as previously described in [19, 20]. All TCM mixtures were maintained under careful quality control to ensure their identification throughout the experiments.

2.2. Animals. Adult male Wistar rats (140–160 g) were purchased from the SLAC Laboratory Animal Co. (Shanghai, China). Rats were kept in SPF-grade Experimental Animal Houses (the Second Military Medical University, Shanghai) with free access to food and water under standard temperature conditions (22°C) and a 12 h light/dark cycle. The animal experiments were conducted in strict accordance to the National Institutes of Health's Guide to the Care and Use of Laboratory Animals. The animal experiments were approved by the local institutional review board at the authors' affiliated institutions.

2.3. CIA Model and Drug Administration. Type II collagen (Chondrex, Redmond, WA, USA) was emulsified with incomplete Freund's adjuvant at a 1:1 ratio. Rats were intradermally injected with 2 mg/kg of collagen-IFA suspension at the base of the tail (day 0). A boost injection with 1 mg/kg of the collagen-IFA suspension was given on day 7 in the same manner.

Forty rats were randomly divided into 5 groups of 8 rats each: (1) rats without CIA immunization (normal control group, NG), (2) rats with CIA immunization (CIA model group, MG), (3) CIA rats treated with 270 mg/kg of HLJDT (HLJDT group, HG), (4) CIA rats treated with the 13 main components of HLJDT (components group, CG), and (5) rats treated with 0.05 mg/kg of dexamethasone (Sine Phama Lab Co., Ltd., Shanghai, China) (positive control group, DG). A dry powder of HLJDT was dissolved in 0.5% carboxymethyl cellulose sodium (CMC-Na), stirred at 37°C for 1 h and administered orally to the CIA rats. This 270 mg/kg dose was explored in the animal experiment and is considered within the MTD (2 g/kg) for oral administration. Based on the quantitative analysis of HLJDT [19] and a dosage of 270 mg/kg of HLJDT, 13 main components were identified: 5.67 mg/kg of geniposide, 0.24 mg/kg of coptisine, 0.35 mg/kg of phellodendrine, 1.2 mg/kg of jatrorrhizine, 1.31 mg/kg of magnoflorine, 2.07 mg/kg of palmatine, 12.97 mg/kg of berberine, 10.55 mg/kg of baicalin, 1.05 mg/kg of chlorogenic acid, 0.39 mg/kg of crocin, 2.39 mg/kg of wogonoside, 1.45 mg/kg of baicalein, and 0.88 mg/kg of wogonin. The components were mixed, dissolved in 0.5% CMC-Na solution, and administered intragastrically to the CIA rats. The NG and MG rats received oral administrations of an equal volume of 0.5% CMC-Na aqueous solution. All of the drug treatments were administered daily from day 0 to 28.

2.4. Assessment of Arthritis in Rats. After the second immunization, the rats were checked for the development of arthritis based on the extent of edema and/or erythema in their paws. The incidence and severity of arthritis were evaluated by observing changes in their arthritis scores every 2 days, measuring hind paw volumes every 4 days and measuring body weight every 3 days (only when arthritic signs were present). The observed severity of the arthritis was assessed by a semiquantitative score as follows: 0, normal, with no macroscopic signs of arthritis or swelling; 1, mild but distinct redness and swelling of the ankle or apparent redness and swelling of the individual digits, regardless of the number

of affected digits; 2, moderate redness and swelling of the ankle; 3, redness and swelling of the entire paw, including the digits; and 4, maximally inflamed limb with the involvement of multiple joints. In these studies, the maximum score was 8, which represents the sum of the scores of both hind paws in each animal. The hind paw volumes were measured with a plethysmometer (7140UGO, Basile, Comerio, Italy) and were recorded as the mean volume displacement of both hind paws in each rat. A precision balance (Sartorius AG, Goettingen, Germany) was used to monitor changes in body weight.

2.5. Lipid Peroxide Assay and Antioxidant Enzyme Activity Assays. The plasma samples were obtained by centrifuging blood samples for 10 min at 3500 rpm and 4°C. The supernatant was used in the subsequent bioassays. Malondialdehyde (MDA), superoxide dismutase (SOD), and glutathione peroxidase (GSH-Px) assays were performed using commercially available kits according to their manufacturer's instructions (Jiancheng Bioengineering Institute, Nanjing, China). Briefly, the lipid peroxide content was determined by measuring the concentration of thiobarbituric-acid- (TBA-) reactive substances. The TBA-reactive content was expressed in terms of MDA content using 1,1,3,3-tetraethoxypropane as a standard. The absorbance was measured at 532 nm and the values were expressed as nmol of MDA per mg of protein. The SOD assay was based on SOD's inhibitory effects on the spontaneous autoxidation of 6-hydroxydopamine. One IU of SOD is required to inhibit the initial rate of 6-hydroxydopamine autoxidation by 50%. The GSH-Px activity assay is based on measurements of decreasing absorbance at 340 nm due to the consumption of NADPH.

2.6. Sample Preparation. The plasma samples were collected from the NG, MG, DG, HG, and CG on days 8, 15, and 22. The samples were stored at -80°C prior to analysis. One-hundred-microliter aliquots of plasma were diluted with 300 µL of methanol. After vortex-mixing the solution for 1 min and centrifuging it at 12000 rpm for 10 min, the supernatant was transferred to autosampler vials. A quality control (QC) sample was prepared by mixing 20 µL aliquots from each group with plasma and handled in the same manner described above. The QC sample was used for monitoring the stability of sequence analysis and was continuously analyzed 6 times to validate the repeatability of the equipment.

2.7. LC-Q-TOF-MS Conditions. LC-Q-TOF-MS analysis was performed on an Agilent-1290 LC system (Agilent Technologies, Palo Alto, CA, USA) coupled with an electrospray ionization (ESI) source and an Agilent-6530 Q-TOF mass spectrometer. Chromatographic separation was performed on a Zorbax SB-C18 column (1.8 µm, 2.1 mm × 150 mm, Agilent) with the column temperature set at 40°C. Ultrapure water with 0.1% formic acid (A) and acetonitrile (B) was used in the mobile phase according to the following gradient program: 0–2 min, 5% B; and 2–5 min, 5–50% B; and 5–6 min, 50% B; 6–17 min, 50–95% B; followed by a 5-min reequilibration step. The mobile phase flow rate was 0.3 mL/min, and the sample injection volume was 4 µL.

Positive and negative ion modes were used in mass detection. The source parameters were set as follows: drying gas flow rate, 11 L/min; gas temperature, 350°C; pressure of nebulizer gas, 45 psig; Vcap, 4000 V in positive mode and 3000 V in negative mode; fragmentor, 120 V; skimmer, 45 V; and scan range, m/z 50–1000. The MS/MS analysis was acquired in targeted MS/MS mode with the collision energy ranging from 10 V to 40 V.

2.8. Data Processing, Multivariate Data Analysis and Biomarker Identification. The MS spectra were processed using Agilent's Mass Hunter Qualitative Analysis Software (Version B.03.01, Agilent Technologies, USA) for peak detection. A list of detected peak intensities was generated using the retention time m/z data pairs as identifiers. The resultant normalized peak intensities formed a single matrix with retention time m/z pairs for each file in the data set. All of the processed data were normalized and scaled for each chromatogram prior to multivariate statistical analysis. Integrated raw mass spectrometric data were processed using Agilent's Mass Profiler Software (Version B.02.00, Agilent Technologies, USA). The intensity of each ion was normalized with respect to the total ion count to generate a data matrix consisting of the retention time, the m/z value, and the normalized peak area. The ion intensity of each peak was normalized to 10,000 and to the sum of its peak intensities within the sample. The processed data were exported and further processed by PCA and PLS-DA using the SIMCA-P software package (Version 11, Umetrics AB, Umeå, Sweden). The data were processed by unit variance scaling and were mean-centered using the SIMCA-P software. Model quality was evaluated based on the relevant values of R^2 and Q^2 . Potential markers of interest were extracted from the values of variable importance in the projections (VIP > 1), which were constructed from PLS-DA analysis. P values were obtained from Student's t -test ($P < 0.05$). The exact molecular mass data from redundant m/z peaks, which correspond to the formation of different parent and product ions, were used to confirm the molecular mass of the metabolites. MS/MS data analysis highlighted neutral losses or product ions, which are characteristic of metabolite groups and can be used to discriminate between database hits. The identities of specific metabolites were confirmed by comparing their mass spectra and chromatographic retention times to commercially available reference standards. The metabolites were also identified at the Scripps Center for Metabolomics and Mass Spectrometry (METLIN). The biochemical reactions associated with these metabolites were obtained from the Kyoto Encyclopedia of Genes and Genomes (KEGG) and the Human Metabolome Database (HMDB). The fold changes were calculated as $\text{Fold} = \log_2$ (average peak intensity of group A/average peak intensity of group B).

2.9. Statistical Analysis. All quantitative data were expressed as the mean ± SD as indicated. The comparisons between the two groups were analyzed by an unpaired Student t -test and multiple comparisons were analyzed by one-way analysis of

TABLE 1: Effects of HLJDT and its components on MDA levels and antioxidant enzymes' activities on day 22.

Groups	MDA (nmol/mL)	SOD (U/mL) ^a	GSH-Px (U/mL) ^b
Normal control	2.71 ± 0.34	4.56 ± 0.24	7.72 ± 0.71
Model control	4.98 ± 0.53 ^{##}	2.95 ± 0.22 ^{##}	4.97 ± 1.56 [#]
Dexamethasone	2.62 ± 0.28 ^{**}	4.23 ± 0.33 ^{**}	7.69 ± 1.38 [*]
HLJDT	2.99 ± 0.38 ^{**}	4.74 ± 0.29 ^{**}	7.30 ± 1.13 [*]
Components of HLJDT	2.91 ± 0.42 ^{**}	5.27 ± 0.22 ^{**}	6.82 ± 0.91 [*]

SOD: superoxide dismutase; GSH-Px: glutathione peroxidase. * $P < 0.05$, ** $P < 0.01$, [#] $P < 0.05$, and ^{##} $P < 0.01$ ([#]: compared with normal control group; *): compared with model control group).

^aOne unit of SOD activity is defined as amount of SOD when SOD inhibition ratio reaches 50% in 1 mL reaction solution.

^bOne unit of GSH-Px activity is defined as amount of enzyme required to degrade 1 $\mu\text{mol/L}$ of GSH per min subtracting nonenzymatic reaction at 37°C.

variance (ANOVA) followed by Tukey's HSD post hoc test. Statistical significance was established as $P < 0.05$.

3. Results and Discussion

3.1. Assessment of the CIA Model. Immunization with bovine type II collagen (coadministered with incomplete Freund's adjuvant) started producing severe arthritis 10 days after primary immunization and reached a peak on day 22 in the model group (Figure 1(a)). The decrease of arthritis in CIA rats that were treated with HLJDT and its components was further examined. Compared to the model group, swollen paws were significantly reduced in the dexamethasone, HLJDT, and component groups: ($P < 0.05$) (Figure 1(b)). Furthermore, after type II collagen immunization, the arthritis scores of CIA rats in the dexamethasone, HLJDT and components groups were significantly lower than those in the model group on days 16–22 ($P < 0.01$, $P < 0.05$, and $P < 0.05$ versus model group, resp.) (Figure 1(c)).

3.2. Effects of HLJDT and Its Components on Lipid Peroxide and Antioxidant Enzyme Activities. Immunization with bovine type II collagen caused a significant decrease in the activities of SOD (2.95 ± 0.22 versus 4.56 ± 0.24 , $P < 0.01$) and GSH-Px (4.97 ± 1.26 versus 7.72 ± 0.71 , $P < 0.05$) and a significant increase in MDA levels (4.98 ± 0.53 versus 2.71 ± 0.34 , $P < 0.01$) in comparison to the normal group on day 22 (Table 1). Compared to the test groups, the administration of HLJDT and its components caused an increase in SOD and GSH-Px activity and a decrease in MDA levels in the model control group. These findings indicate that HLJDT and its components possess potent antioxidant activities in CIA rats.

3.3. Assessment of the Repeatability and Stability of the LC-Q-TOF-MS Method. The repeatability and stability of the LC-Q-TOF-MS method were validated by analyzing 6 injections of identical QC samples that were prepared according to the same protocol. The relative standard deviations of the peak retention times and areas were less than 1.0% and 5.0%, respectively. Thus, the precision and repeatability of the proposed method were satisfactory for metabolomic analysis.

Fingerprints of the plasma samples were acquired in positive and negative modes. After comparing our results between both nodes, we observed higher noise, fewer peaks,

and a matrix effect in the negative mode, whereas the total ionic chromatogram (TIC) of the positive mode was more suitable for analysis (Figure 2). Moreover, most of the metabolites that were detected in the plasma samples were less polar than those observed in the urine samples described in our previous study [23].

3.4. Multivariate Statistical Analysis and Potential Biomarker Identification. Ions were generated in the LC-Q-TOF-MS analysis. PLS-DA, a supervised method, is frequently used to classify groups that show metabolic differences and to extract potential biomarkers. After PLS-DA processing, the CIA model group was clearly separated from the normal control group on day 22 (Figure 3). Variables were also generated based on the values of variable importance in the projection (VIP > 1). Then, by combining Student's t -test with the selected variables, distinct metabolites were identified ($P < 0.05$) and selected for further study.

The three steps to identify these biomarkers were as follows. First, the MS² spectrum of significantly different metabolic ions was obtained using a targeted MS/MS mode. Next, several online databases, such as METLIN (<http://metlin.scripps.edu/>), HMDB (<http://www.hmdb.ca/>), and KEGG (<http://www.kegg.jp/>), were used for initial determination of the markers. Finally, the metabolites were compared to the standard MS² spectrum (see Figure 4 for an example using carnitine at m/z 162 to illustrate the identification process).

Following the identification process, 18 unique metabolites were identified (Table 2), including 11 identified in the positive mode and 7 identified in the negative mode. Three of the metabolites (L-phenylalanine, allantoin, and indoxyl sulfate) were repeatedly detected in the urine samples described in our previous study. Furthermore, 13 metabolites were upregulated, and 5 metabolites were downregulated in the model group compared to the normal control group (Figure 5). These metabolites were mainly associated with glycerophospholipid metabolism, fatty acid metabolism, tryptophan metabolism, linoleic acid metabolism, phenylalanine metabolism, purine metabolism, arachidonic acid metabolism, and bile acid biosynthesis pathways and may indicate the potential efficacy of the medication in RA.

Overproduction of oxidants leads to oxidative tissue damage at the molecular level. A growing number of reports

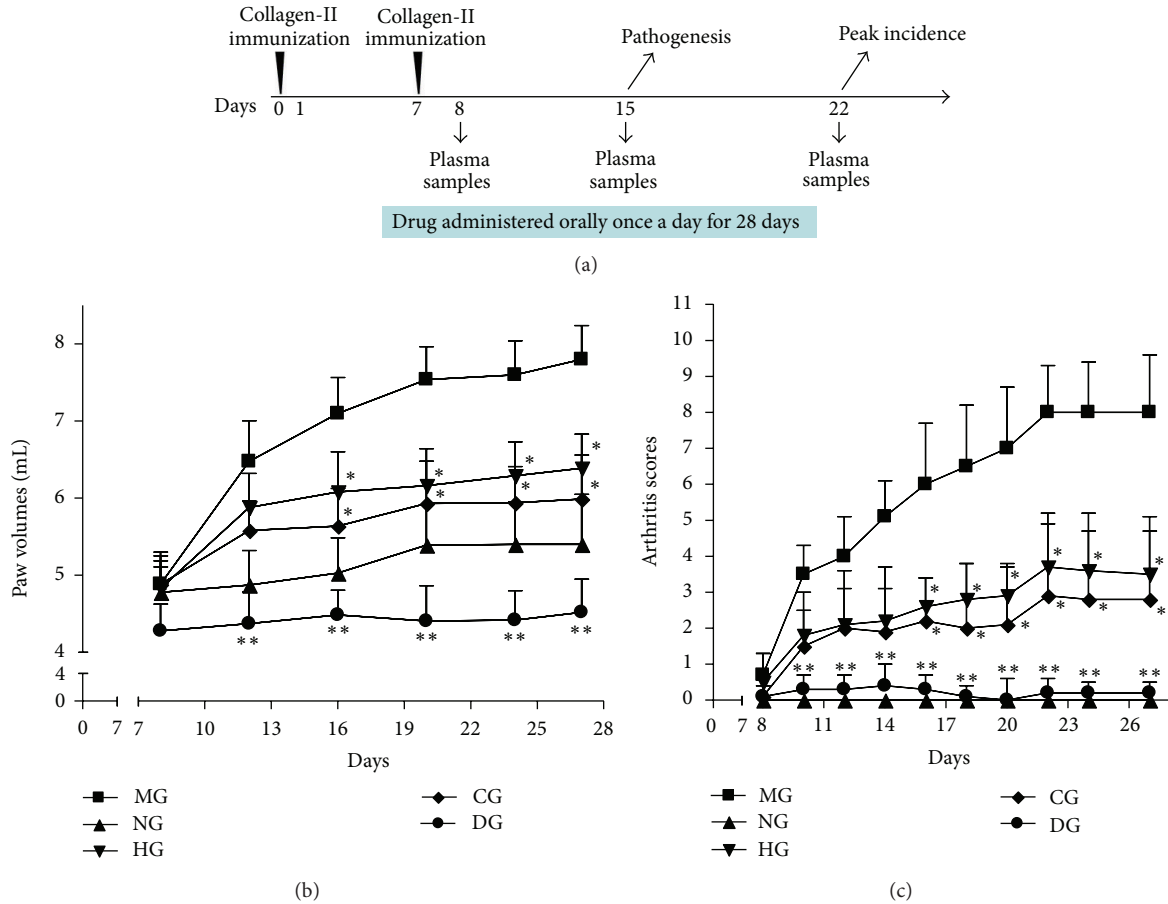


FIGURE 1: (a) Time schedule for CIA immunization, pathogenesis, peak incidence, drug administration, and sample collection for examinations. Wistar rats were immunized with bovine type II collagen with incomplete Freund's adjuvant and randomly divided into normal control, model, dexamethasone (0.05 mg/kg), HLJDT (270 mg/kg), and its 13-component groups on the day of arthritis onset (day 0, $n = 8$). (b) Hind paw volumes of each rat were evaluated every 4 days. Oral treatment of CIA rats with dexamethasone (0.05 mg/kg), HLJDT (270 mg/kg), and its components daily significantly ameliorated the severity and development of arthritis from day 16 ($P < 0.05$ versus model control). (c) Arthritis was scored every 2 days. Oral treatment of CIA rats with dexamethasone (0.05 mg/kg), HLJDT (270 mg/kg), and its components daily significantly reduced arthritis from day 16 ($P < 0.01$, $P < 0.05$, and $P < 0.05$ versus model group, resp.). NG, normal control group; MG, model group; DG, dexamethasone group; HG, HLJDT group; CG, components group.

have provided evidence that implicates oxidative injury as a major pathogenic mechanism in RA [24–27]. Therefore, protecting joints from oxidative injury may provide a useful therapeutic potential for RA prevention and treatment [28, 29]. Biomarkers related to glycerophospholipid metabolism (e.g., choline and glycerophosphocholine) and fatty acid metabolism (e.g., carnitine, acetylcarnitine, palmitoyl-L-carnitine and palmitic acid methyl ester) were all upregulated in CIA rats (except for carnitine), indicating that RA caused increased lipid catabolism. Uric acid and allantoin also contributed to oxidative injury *in vivo* [30–32]. Uric acid protected the DNA against free-radical damage [33, 34], while allantoin, which was detected and measured in biological fluids and tissues, was produced after uric acid oxidation. Therefore, the downregulation of uric acid and the upregulation of allantoin observed in the model group indicate that oxidative reactions led to serious damage in CIA rats. This observation also demonstrates that urate plays the

role of a natural antioxidant related to purine metabolism *in vivo*. Carnitine is required for the transport of long chain fatty acids and acyl coenzyme A derivatives across the inner mitochondrial membrane. Several reports have shown that carnitine has protective effects against oxidative damage [35]. Carnitine not only participates in the metabolism of reactive oxygen species [14] but also plays a role in fatty acid energy metabolism [36, 37]. Other studies have shown that plasma carnitine levels were significantly lower in RA patients than in a control group [38], whereas long chain acylcarnitine levels were higher in RA patients [39]. These results are consistent with the ionic response trends that were observed in the present study. Notably, bile acid promotes the digestion and absorption of fatty acids and has an ameliorating effect on RA [40]. Bile acid biosynthesis (e.g., glycocholic acid and deoxycholic acid) was downregulated in CIA rats, indicating a disruption in fatty acid metabolism. Phenylalanine and tryptophan metabolism was discussed in our previous study

TABLE 2: Potential biomarkers in response to RA and their metabolic pathways.

Mode	Number	t_R /min	m/z	Formula	Identification	Fold ^a	P value ^a	Related pathway
ESI(+)	1	1.16	104.1076	C ₅ H ₁₄ NO	Choline ^b	26.11	0.000	Glycerophospholipid metabolism
	2	1.19	162.1129	C ₇ H ₁₅ NO ₃	Carnitine ^b	-0.84	0.000	Fatty acid metabolism, oxidative injury
	3	1.20	258.1108	C ₈ H ₂₁ NO ₆ P	Glycerophosphocholine ^c	25.39	0.000	Glycerophospholipid metabolism
	4	1.73	204.1235	C ₉ H ₁₇ NO ₄	Acetylcarnitine ^c	0.819	0.006	Fatty acid metabolism, oxidative injury
	5	3.06	166.0869	C ₉ H ₁₁ NO ₂	L-Phenylalanine ^b	0.81	0.005	Phenylalanine metabolism
	6	5.07	180.0661	C ₉ H ₉ NO ₃	Hippuric acid ^b	25.27	0.007	Phenylalanine metabolism
	7	5.30	194.0820	C ₁₀ H ₁₁ NO ₃	Phenylacetyl glycine ^c	-0.93	0.004	Phenylalanine metabolism
	8	10.13	357.2796	C ₂₄ H ₃₆ O ₂	DHA ethyl ester ^c	3.19	0.002	Alpha linolenic acid and linoleic acid metabolism
	9	14.89	400.3427	C ₂₃ H ₄₅ NO ₄	Palmitoyl-L-carnitine ^c	0.57	0.003	Fatty acid metabolism
	10	16.58	305.2481	C ₂₀ H ₃₂ O ₂	Arachidonic acid ^b	0.94	0.002	Arachidonic acid metabolism
	11	16.79	271.2637	C ₁₇ H ₃₄ O ₂	Palmitic acid methyl ester ^c	4.09	0.000	Fatty acid metabolism
ESI(-)	12	1.24	157.0361	C ₄ H ₆ N ₄ O ₃	Allantoin ^b	2.13	0.000	Purine metabolism, oxidative injury
	13	1.74	167.0207	C ₅ H ₄ N ₄ O ₃	Uric acid ^b	-1.16	0.004	Purine metabolism, oxidative injury
	14	2.19	219.0775	C ₁₁ H ₁₂ N ₂ O ₃	5-Hydroxy tryptophan ^b	0.99	0.008	Tryptophan metabolism
	15	4.51	203.0831	C ₁₁ H ₁₂ N ₂ O ₂	L-Tryptophan ^b	1.61	0.003	Tryptophan metabolism
	16	8.34	212.0025	C ₈ H ₇ NO ₄ S	Indoxyl sulfate ^c	1.27	0.003	Tryptophan metabolism
	17	6.21	464.3024	C ₂₆ H ₄₃ NO ₆	Glycocholic acid ^c	-0.38	0.022	Bile acid biosynthesis
	18	10.14	391.2855	C ₂₄ H ₄₀ O ₄	Deoxycholic acid ^c	-0.44	0.046	Bile acid biosynthesis

^a Fold changes (calculated as \log_2 (average peak intensity of model group/average peak intensity of normal control group)) and P value compared with normal control group on day 22.

^b Metabolites validated with standards.

^c Metabolites putatively annotated.

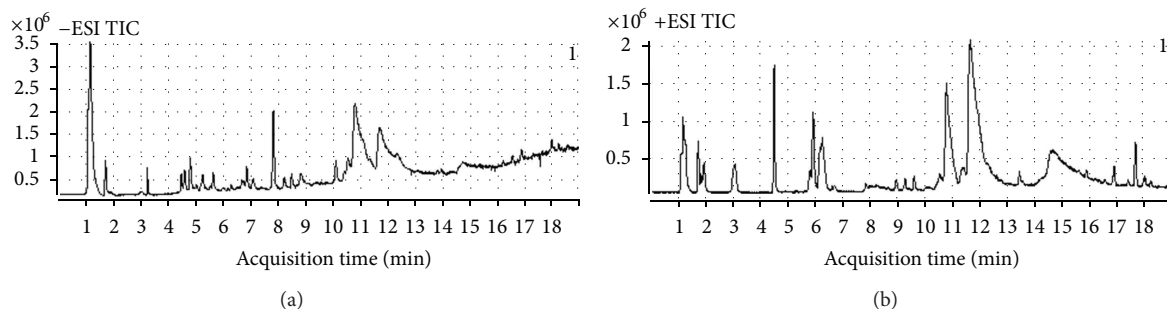


FIGURE 2: Representative base peak intensity chromatogram of the rat plasma obtained in ESI negative mode (a) and ESI positive mode (b) based on LC-Q-TOF-MS.

of urine metabolomics; the results obtained here were complementary to our earlier study [23].

In summary, 18 potential biomarkers were identified. These markers are mainly associated with glycerophospholipid metabolism, fatty acid metabolism, tryptophan metabolism, linoleic acid metabolism, phenylalanine metabolism, purine metabolism, arachidonic acid metabolism, and bile acid biosynthesis and reveal RA regulating network *in vivo*.

3.5. Metabolomic Analysis of HLJDT and Its Treatment Components. PCA, an unsupervised pattern recognition method, was used to observe trends in mean metabolite pattern changes across various time points (Figure 6). PLS-DA, a supervised pattern recognition method, was used to display

the metabolic state of CIA rats on days 8, 15, and 22 (Figure 7). The location marked with an arrow in Figure 6 indicates the trend in mean metabolite pattern changes. On day 8, each group's metabolic state had changed from its initial position (day 0). This change indicates that RA had disrupted endogenous substance metabolism and had significantly altered the metabolic fingerprints of the plasma compared to its normal state. From day 8 to day 22, the direction of the trajectory gradually moved towards the initial space. The trajectory then returned to the initial space, indicating a recovery from the disrupted metabolic state. Compared to the model control group, the three drug treatment groups showed better recovery performance from the CIA-induced metabolic state. This result can be observed by comparing the dynamic

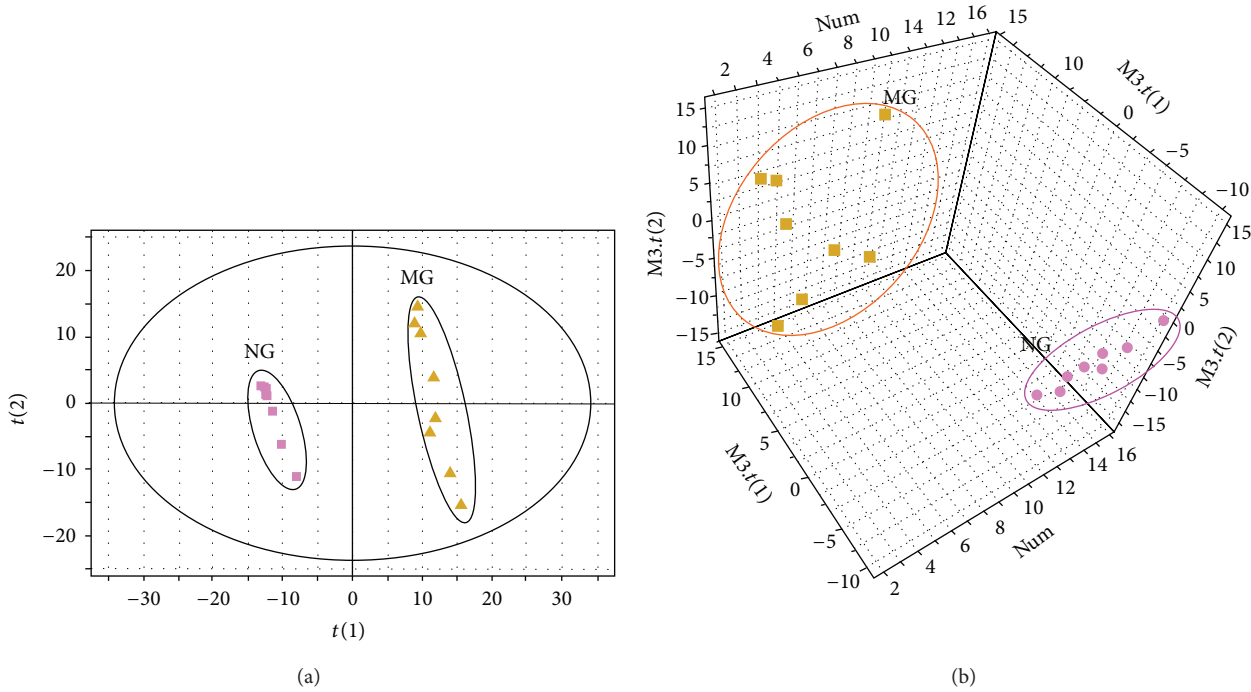


FIGURE 3: Results of multiple pattern recognition of plasma biomarkers between normal control group and model group on day 22. PLS-DA score plot ($R^2X = 0.253$, $R^2Y = 0.997$, $Q_2 = 0.875$, $n = 8$) of NG and MG. NG, normal control group; MG, model group.

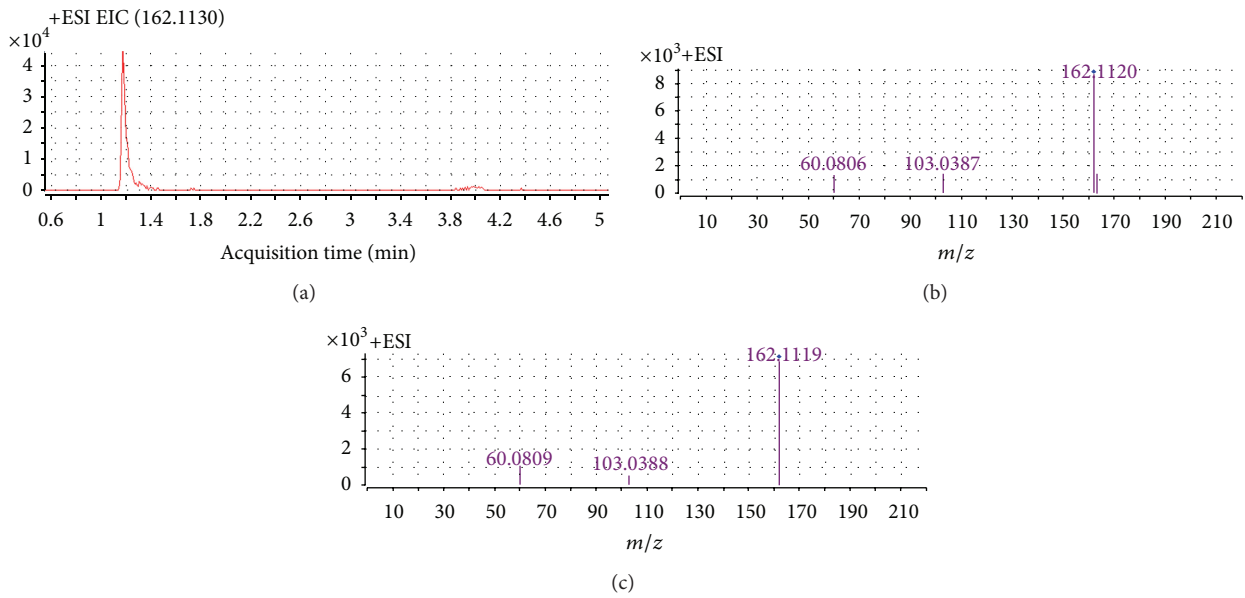


FIGURE 4: Identification of a selected biomarker (m/z 162.1129). (a) Extracted ion chromatogram (EIC) of m/z 162.113 ($t_R = 1.19$ min); (b) MS/MS spectrum of the ion; (c) MS/MS spectrum of a commercial standard carnitine. The collision energy was 10 V.

trajectories in Figures 6 and 7(c). While the dexamethasone group had the advantage of rapid treatment, the toxic side effects of long-term dexamethasone administration led to a metabolic state that deviated from normal rats on day 22. Furthermore, HLJDT and its components resulted in better recovery performance from the CIA-induced metabolic state than dexamethasone on day 22 (Figure 7(c)).

Nine metabolites were reversed by HLJDT, and 7 were reversed by its components (Table 3). This result indicates that the component group could largely replace the effects of the complete formula. The metabolites that were reversed are primarily involved in phenylalanine metabolism, glycerophospholipid metabolism, fatty acid metabolism, and arachidonic acid metabolism, which indicate that the

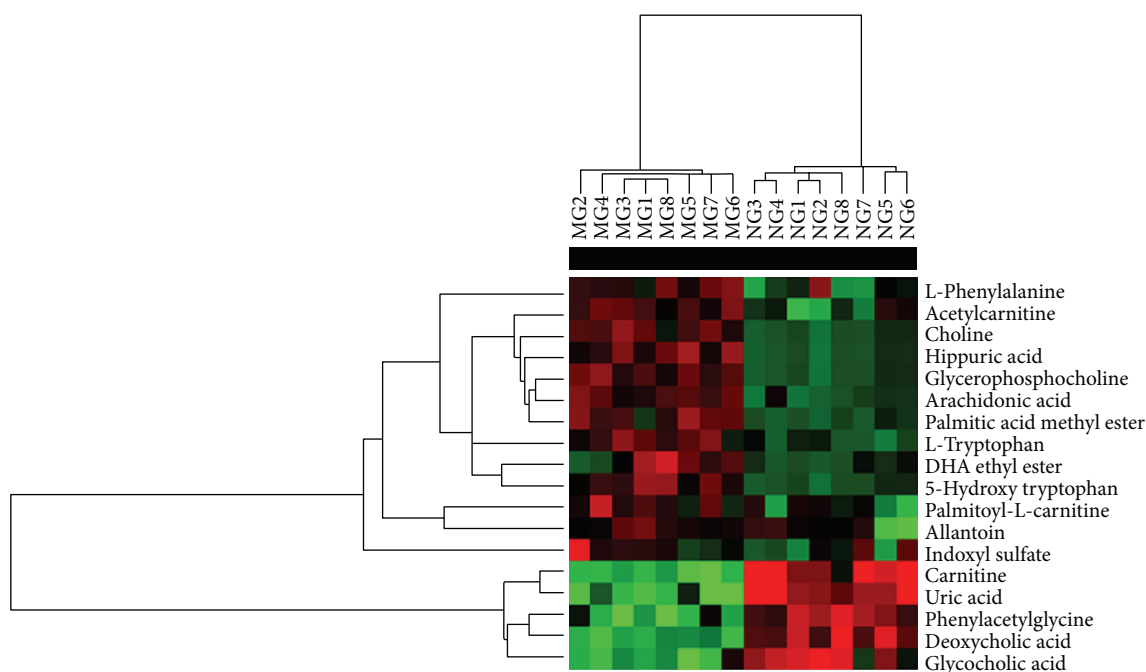


FIGURE 5: All the potential biomarkers in response to RA detected by cluster analysis. The columns show the expression levels and each row represents a biomarker. The red color indicates upregulated biomarkers compared with normal control group, while the green color represents downregulated biomarkers compared with normal control group. NG, normal control group; MG, model group; $n = 8$.

TABLE 3: Summary of potential biomarkers in HLJDT and its components' groups on day 22.

Biomarkers	HLJDT		Components of HLJDT	
	Fold ^a	<i>P</i> value ^a	Fold ^b	<i>P</i> value ^b
Choline	-20.24	0.041	—	—
Carnitine	0.40	0.000	0.18	0.003
Glycerophosphocholine	-19.87	0.001	-16.79	0.009
Acetylcarnitine	-0.76	0.003	-0.15	0.002
L-Phenylalanine	-0.28	0.012	-0.19	0.043
Hippuric acid	-20.17	0.004	-18.87	0.006
Palmitoyl-L-carnitine	-0.56	0.002	-0.01	0.022
Allantoin	-0.12	0.018	—	—
Arachidonic acid	-0.24	0.002	-0.14	0.003

^a Fold changes calculated as \log_2 (average peak intensity of HLJDT group/average peak intensity of model group) and *P* value compared with model group on day 22.

^b Fold changes calculated as \log_2 (average peak intensity of components of HLJDT group/average peak intensity of model group) and *P* value compared with model group on day 22.

effectiveness of HLJDT and its components as an RA treatment partially depends on restoring imbalances related to oxidative injury and the arachidonic acid pathway. HLJDT was reported to have protective and therapeutic effects on peripheral inflammation and hepatotoxin-induced liver injuries [41, 42]. *Rhizoma coptidis* and *Radix scutellariae* were responsible for the suppressive effect of HLJDT on eicosanoid generation. Some of their pure components,

including baicalein, baicalin, wogonoside, wogonin, coptisine, and magnoflorine, were also shown to inhibit eicosanoid generation in rat macrophages via the arachidonic acid cascade [21].

The results from a lipid peroxide assay, antioxidant enzyme activity assays, and metabolomic analysis demonstrate that HLJDT and its components have extensive effects in RA treatment by regulating the pathway disruptions associated with oxidative injury and arachidonic acid metabolism.

4. Conclusions

In this study, metabolomic analysis with LC-Q-TOF-MS was used to profile RA-related metabolic changes in the plasma and to investigate the interventional mechanisms of HLJDT and its components. After multiple levels of statistical analysis, 18 significant biomarkers (11 metabolites detected in the positive mode and 7 metabolites detected in the negative mode) were identified. These biomarkers are primarily involved in glycerophospholipid metabolism, fatty acid metabolism, tryptophan metabolism, linoleic acid metabolism, phenylalanine metabolism, purine metabolism, arachidonic acid metabolism, and bile acid biosynthesis. Potential biomarkers-related glycerophospholipid metabolism and fatty acid metabolism, namely, carnitine, acetylcarnitine, allantoin, uric acid, choline, and glycerophosphocholine, appear to have diagnostic and/or prognostic values for RA and require further investigation in clinical studies. Using the potential biomarkers identified in this study as a screening index, we hypothesize that HLJDT

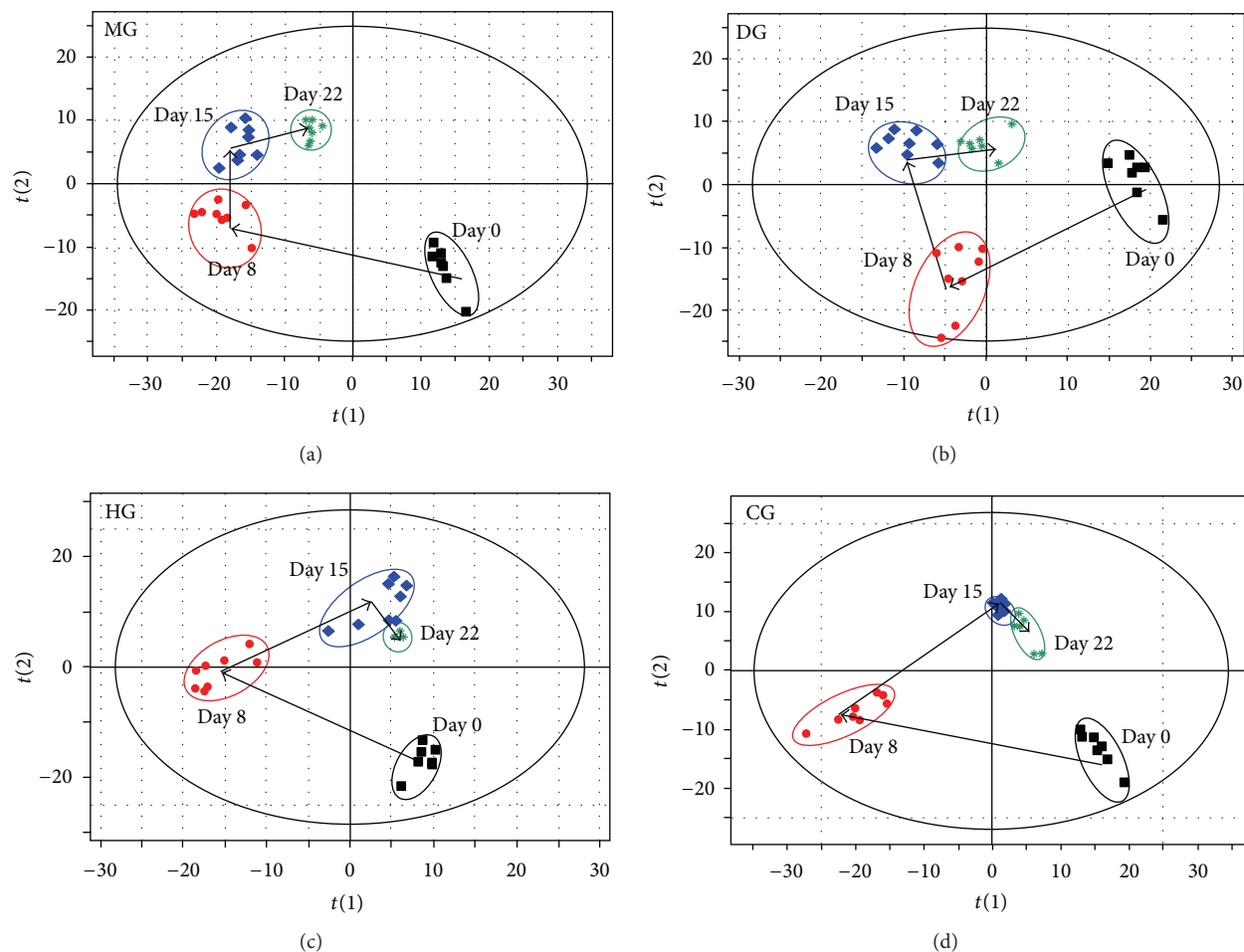


FIGURE 6: Dynamic PCA scores' plots of plasma metabolites impacted by different groups from day 0 to 22. (a) HLJDT group, (b) dexamethasone group, (c) components group, and (d) model group. HG, HLJDT group; DG, dexamethasone group; CG, components group; MG, model group.

and its components can limit the pathological process of RA by partially reversing metabolite levels and regulating pathway disruptions. The metabolomic results presented here provide a systemic view of the development and progression of RA as well as a theoretical basis for the prevention or treatment of RA.

Abbreviations

RA:	Rheumatoid arthritis
CIA:	Collagen-induced arthritis
LC-Q-TOF-MS:	Liquid chromatography quadrupole time-of-flight mass spectrometry
HLJDT:	Huang-Lian-Jie-Du-Tang formula
NG:	Normal group
MG:	Model group
DG:	Dexamethasone group
HG:	HLJDT group
CG:	Components group
TCM:	Traditional Chinese medicine
PCA:	Principal component analysis

PLS-DA: Partial least squares discriminant analysis

GSH-Px: Glutathione peroxidase

SOD: Superoxide dismutase

MDA: Malondialdehyde

TBA: Thiobarbituric acid.

Conflict of Interest

The authors declare that they have no conflict of interests.

Authors' Contribution

R. Yue and L. Zhao contributed equally to this paper.

Acknowledgments

This work was supported by NSFC (81102865, 81230090, and 30725045), partially supported by Global Research Network for Medicinal Plants (GRNMP), Shanghai Leading Academic Discipline Project (B906), FP7-PEOPLE-IRSES-2008

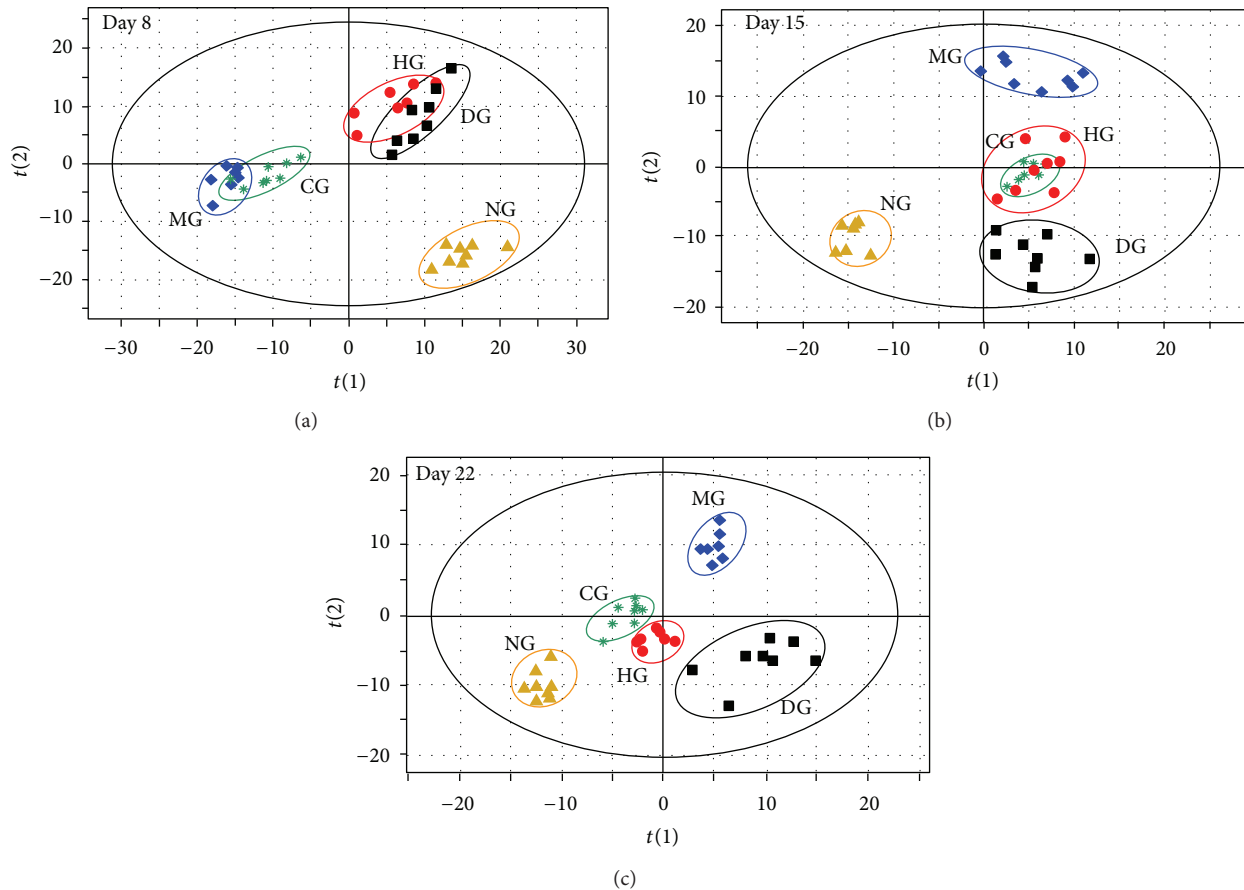


FIGURE 7: Comparison of PLS-DA scores plots of rat plasma data of different groups on days 8, 15, and 22. (a) Day 8 ($Q^2Y_{(cum)} = 0.777$, $R^2X_{(cum)} = 0.428$, $R^2Y_{(cum)} = 0.98$). (b) Day 15 ($Q^2Y_{(cum)} = 0.796$, $R^2X_{(cum)} = 0.41$, $R^2Y_{(cum)} = 0.985$). (c) Day 22 ($Q^2Y_{(cum)} = 0.804$, $R^2X_{(cum)} = 0.439$, $R^2Y_{(cum)} = 0.993$). NG, normal control group; MG, model group; DG, dexamethasone group; HG, HLJDT group; CG, components group.

(TCMCANCER Project 230232), Key Laboratory of Drug Research for Special Environments, PLA, Shanghai Engineering Research Center for the Preparation of Bioactive Natural Products (10DZ2251300), the Scientific Foundation of Shanghai China (09DZ1975700, 09DZ1971500, and 10DZ1971700), National Major Project of China (2011ZX09307-002-03), and the Twelfth Five-Year National Science and Technology Support Program (2012BAI29B06).

References

- [1] F. C. Arnett, S. M. Edworthy, D. A. Bloch et al., "The American Rheumatism Association 1987 revised criteria for the classification of rheumatoid arthritis," *Arthritis and Rheumatism*, vol. 31, no. 3, pp. 315–324, 1988.
- [2] D. L. Scott, F. Wolfe, and T. W. J. Huizinga, "Rheumatoid arthritis," *The Lancet*, vol. 376, no. 9746, pp. 1094–1108, 2010.
- [3] M. A. van Maanen, M. C. Lebre, T. van der Poll et al., "Stimulation of nicotinic acetylcholine receptors attenuates collagen-induced arthritis in mice," *Arthritis and Rheumatism*, vol. 60, no. 1, pp. 114–122, 2009.
- [4] W. Q. Lai, A. W. Irwan, H. H. Goh, A. J. Melendez, I. B. McInnes, and B. P. Leung, "Distinct roles of sphingosine kinase 1 and 2 in murine collagen-induced arthritis," *Journal of Immunology*, vol. 183, no. 3, pp. 2097–2103, 2009.
- [5] H. Kelchtermans, L. Geboes, T. Mitera, D. Huskens, G. Leclercq, and P. Matthys, "Activated CD4+CD25+ regulatory T cells inhibit osteoclastogenesis and collagen-induced arthritis," *Annals of the Rheumatic Diseases*, vol. 68, no. 5, pp. 744–750, 2009.
- [6] L. G. M. van Baarsen, C. A. Wijbrandts, T. C. G. Timmer, T. C. T. M. van der Pouw Kraan, P. P. Tak, and C. L. Verweij, "Synovial tissue heterogeneity in rheumatoid arthritis in relation to disease activity and biomarkers in peripheral blood," *Arthritis and Rheumatism*, vol. 62, no. 6, pp. 1602–1607, 2010.
- [7] V. C. Willis, A. M. Gizinski, N. K. Banda et al., "N- α -benzoyl-N5-(2-chloro-1-iminoethyl)-L-ornithine amide, a protein arginine deiminase inhibitor, reduces the severity of murine collagen-induced arthritis," *Journal of Immunology*, vol. 186, no. 7, pp. 4396–4404, 2011.
- [8] A. Augello, R. Tasso, S. M. Negrini, R. Cancedda, and G. Pennesi, "Cell therapy using allogeneic bone marrow mesenchymal

- stem cells prevents tissue damage in collagen-induced arthritis," *Arthritis and Rheumatism*, vol. 56, no. 4, pp. 1175–1186, 2007.
- [9] C. Salliot and D. van der Heijde, "Long-term safety of methotrexate monotherapy in patients with rheumatoid arthritis: a systematic literature research," *Annals of the Rheumatic Diseases*, vol. 68, no. 7, pp. 1100–1104, 2009.
- [10] N. Alcorn, S. Saunders, and R. Madhok, "Benefit-risk assessment of leflunomide: an appraisal of leflunomide in rheumatoid arthritis 10 years after licensing," *Drug Safety*, vol. 32, no. 12, pp. 1123–1134, 2009.
- [11] D. Schaffer, T. Florin, C. Eagle et al., "Risk of serious NSAID-related gastrointestinal events during long-term exposure: a systematic review," *Medical Journal of Australia*, vol. 185, no. 9, pp. 501–506, 2006.
- [12] P. A. Scott, G. H. Kingsley, C. M. Smith, E. H. Choy, and D. L. Scott, "Non-steroidal anti-inflammatory drugs and myocardial infarctions: comparative systematic review of evidence from observational studies and randomised controlled trials," *Annals of the Rheumatic Diseases*, vol. 66, no. 10, pp. 1296–1304, 2007.
- [13] C. Gieger, L. Geistlinger, E. Altmaier et al., "Genetics meets metabolomics: a genome-wide association study of metabolite profiles in human serum," *PLoS Genetics*, vol. 4, no. 11, Article ID e1000282, 2008.
- [14] A. M. Weljie, R. Dowlatbadi, B. J. Miller, H. J. Vogel, and F. R. Jirik, "An inflammatory arthritis-associated metabolite biomarker pattern revealed by 1H NMR spectroscopy," *Journal of Proteome Research*, vol. 6, no. 9, pp. 3456–3464, 2007.
- [15] M. B. Lauridsen, H. Bliddal, R. Christensen et al., "1H NMR spectroscopy-based interventional metabolic phenotyping: a cohort study of rheumatoid arthritis patients," *Journal of Proteome Research*, vol. 9, no. 9, pp. 4545–4553, 2010.
- [16] X. Li, S. Yang, Y. Qiu et al., "Urinary metabolomics as a potentially novel diagnostic and stratification tool for knee osteoarthritis," *Metabolomics*, vol. 6, no. 1, pp. 109–118, 2010.
- [17] G. Theodoridis, H. G. Gika, and I. D. Wilson, "LC-MS-based methodology for global metabolite profiling in metabolomics/metabolomics," *Trends in Analytical Chemistry*, vol. 27, no. 3, pp. 251–260, 2008.
- [18] A. Nordström, G. O'Maille, C. Qin, and G. Siuzdak, "Non-linear data alignment for UPLC-MS and HPLC-MS based metabolomics: quantitative analysis of endogenous and exogenous metabolites in human serum," *Analytical Chemistry*, vol. 78, no. 10, pp. 3289–3295, 2006.
- [19] S. Dou, L. Liu, P. Jiang, W. Zhang, and R. Liu, "LC-DAD and LC-ESI-MS chromatographic fingerprinting and quantitative analysis for evaluation of the quality of Huang-Lian-Jie-Du-Tang," *Chromatographia*, vol. 69, no. 7-8, pp. 659–664, 2009.
- [20] Y. Hu, P. Jiang, S. Wang et al., "Plasma pharmacochrometry based approach to screening potential bioactive components in Huang-Lian-Jie-Du-Tang using high performance liquid chromatography coupled with mass spectrometric detection," *Journal of Ethnopharmacology*, vol. 141, no. 2, pp. 728–735, 2012.
- [21] H. Zeng, S. Dou, J. Zhao et al., "The inhibitory activities of the components of Huang-Lian-Jie-Du-Tang (HLJDT) on eicosanoid generation via lipoxygenase pathway," *Journal of Ethnopharmacology*, vol. 135, no. 2, pp. 561–568, 2011.
- [22] H. Zeng, X. Liu, S. Dou et al., "Huang-Lian-Jie-Du-Tang exerts anti-inflammatory effects in rats through inhibition of nitric oxide production and eicosanoid biosynthesis via the lipoxygenase pathway," *Journal of Pharmacy and Pharmacology*, vol. 61, no. 12, pp. 1699–1707, 2009.
- [23] R. Yue, L. Zhao, Y. Hu et al., "Rapid-resolution liquid chromatography TOF-MS for urine metabolomic analysis of collagen-induced arthritis in rats and its applications," *Journal of Ethnopharmacology*, vol. 145, no. 2, pp. 465–475, 2013.
- [24] C. A. Hitchon and H. S. El-Gabalawy, "Oxidation in rheumatoid arthritis," *Arthritis Research and Therapy*, vol. 6, no. 6, pp. 265–278, 2004.
- [25] G. Baskol, H. Demir, M. Baskol et al., "Investigation of protein oxidation and lipid peroxidation in patients with rheumatoid arthritis," *Cell Biochemistry and Function*, vol. 24, no. 4, pp. 307–311, 2006.
- [26] H. R. Griffiths, "Is the generation of neo-antigenic determinants by free radicals central to the development of autoimmune rheumatoid disease?" *Autoimmunity Reviews*, vol. 7, no. 7, pp. 544–549, 2008.
- [27] K. Hadjigogos, "The role of free radicals in the pathogenesis of rheumatoid arthritis," *Panminerva Medica*, vol. 45, no. 1, pp. 7–13, 2003.
- [28] L. Gail Darlington and T. W. Stone, "Antioxidants and fatty acids in the amelioration of rheumatoid arthritis and related disorders," *British Journal of Nutrition*, vol. 85, no. 3, pp. 251–269, 2001.
- [29] E. A. Ostrakhovitch and I. B. Afanasev, "Oxidative stress in rheumatoid arthritis leukocytes: suppression by rutin and other antioxidants and chelators," *Biochemical Pharmacology*, vol. 62, no. 6, pp. 743–746, 2001.
- [30] B. N. Ames, R. Cathcart, E. Schwiers, and P. Hochstein, "Uric acid provides an antioxidant defense in humans against oxidant- and radical-caused aging and cancer: a hypothesis," *Proceedings of the National Academy of Sciences of the United States of America*, vol. 78, no. 11, pp. 6858–6862, 1981.
- [31] M. Grootveld and B. Halliwell, "Measurement of allantoin and uric acid in human body fluids. A potential index of free-radical reactions in vivo?" *Biochemical Journal*, vol. 243, no. 3, pp. 803–808, 1987.
- [32] G. K. Glantzounis, E. C. Tsimoyiannis, A. M. Kappas, and D. A. Galaris, "Uric acid and oxidative stress," *Current Pharmaceutical Design*, vol. 11, no. 32, pp. 4145–4151, 2005.
- [33] A. M. Cohen, R. E. Aberdroth, and P. Hochstein, "Inhibition of free radical-induced DNA damage by uric acid," *FEBS Letters*, vol. 174, no. 1, pp. 147–150, 1984.
- [34] K. J. A. Davies, A. Sevanian, S. F. Muakkassah-Kelly, and P. Hochstein, "Uric acid-iron ion complexes. A new aspect of the antioxidant functions of uric acid," *Biochemical Journal*, vol. 235, no. 3, pp. 747–754, 1986.
- [35] N. Tastekin, N. Aydogdu, D. Dokmeci et al., "Protective effects of l-carnitine and alpha-lipoic acid in rats with adjuvant arthritis," *Pharmacological Research*, vol. 56, no. 4, pp. 303–310, 2007.
- [36] C. R. Bruce, A. J. Hoy, N. Turner et al., "Overexpression of carnitine palmitoyltransferase-1 in skeletal muscle is sufficient to enhance fatty acid oxidation and improve high-fat diet-induced insulin resistance," *Diabetes*, vol. 58, no. 3, pp. 550–558, 2009.
- [37] F. Le Borgne, A. Ben Mohamed, M. Logerot, E. Garnier, and J. Demarquoy, "Changes in carnitine octanoyltransferase activity induce alteration in fatty acid metabolism," *Biochemical and Biophysical Research Communications*, vol. 409, no. 4, pp. 699–704, 2011.

- [38] A. Klzllltunc, S. Cogalgil, and L. Cerrahoglu, "Carnitine and antioxidants levels in patients with rheumatoid arthritis," *Scandinavian Journal of Rheumatology*, vol. 27, no. 6, pp. 441–445, 1998.
- [39] S. Krähenbühl, B. Willer, P. Brühlmann, H. Hoppeler, and G. Stucki, "Carnitine homeostasis in patients with rheumatoid arthritis," *Clinica Chimica Acta*, vol. 279, no. 1-2, pp. 35–45, 1999.
- [40] A. Bruusgaard and R. B. Andersen, "Effect of an intravenously administered bile acid (chenodeoxycholic acid) on rheumatoid arthritis," *Scandinavian Journal of Rheumatology*, vol. 4, no. 3, pp. 169–173, 1975.
- [41] Y. Dai, K. Miki, T. Fukuoka et al., "Suppression of neuropeptides' mRNA expression by herbal medicines in a rat model of peripheral inflammation," *Life Sciences*, vol. 66, no. 1, pp. 19–29, 1999.
- [42] S. C. Lin, C. C. Lin, F. J. Lu, Y. H. Lin, and C. H. Chen, "Protective and therapeutic effects of huanglian-jie-du-tang on hepatotoxin-induced liver injuries," *American Journal of Chinese Medicine*, vol. 24, no. 3-4, pp. 219–229, 1996.

Research Article

Metabolomic Strategy for Studying the Intervention and the Synergistic Effects of the Shexiang Baoxin Pill for Treating Myocardial Infarction in Rats

Li Xiang,¹ Peng Jiang,¹ Shuping Wang,¹ Yaohua Hu,¹ Xiaojun Liu,¹ Rongcai Yue,¹ Weidong Zhang,^{1,2,3} and Runhui Liu¹

¹ School of Pharmacy, Second Military Medical University, No. 325 Guohe Road, Shanghai 200433, China

² School of Pharmacy, Shanghai Jiao Tong University, Shanghai 200030, China

³ Department of Pharmacognosy, King Saud University, Riyadh 11451, Saudi Arabia

Correspondence should be addressed to Weidong Zhang; wdzhangy@hotmail.com and Runhui Liu; lyliurh@126.com

Received 7 October 2012; Revised 3 January 2013; Accepted 17 January 2013

Academic Editor: Wei Jia

Copyright © 2013 Li Xiang et al. This is an open access article distributed under the Creative Commons Attribution License, which permits unrestricted use, distribution, and reproduction in any medium, provided the original work is properly cited.

A metabolomic approach has been developed for evaluating the therapeutic effects of the bioactive components and the synergistic efficacy of the Shexiang Baoxin Pill (SBP) on myocardial infarction (MI) in rats. The MI rats were administered the SBP, muscone, cinnamic acid, bufalin, ginsenoside Re, ginsenoside Rb1, cholic acid, borneol, and a combined version of these bioactive components (SFSBP). Liquid chromatography/quadrupole time-of-flight mass spectrometry (LC-Q-TOF/MS) was used to obtain the mass data from the rats' serum. The number of biomarkers that were reversed by SFSBP was greater than any of the monotherapy groups. The PLS-DA score plots demonstrated that the SFSBP group results were located closer to the sham group than any of the monotherapy groups and that the SBP group was located closer to the sham group than the SFSBP treatment group. The reversing results observed with SFSBP showed synergistic effects when compared with those of the individual bioactive components that were used as monotherapy. Meanwhile, the SBP displayed superior regulation efficacy to SFSBP in MI rats, indicating that there must be other active components in the SBP that were responsible for the treatment of MI that were not included in the SFSBP treatment.

1. Introduction

Traditional Chinese Medicines (TCMs) have a long-standing use in clinical practice, and their effectiveness has also been confirmed [1–5]. TCMs hold an important position in the health care tradition of many countries, particularly in Asia [6]. As each TCM employs a large number of chemical compounds and as these components are its pharmacodynamic material basis, TCM itself is definitely a multi-component agent. Characteristically, TCMs focus on body's response to pathogenic factors more than on the pathological mechanisms, and TCM regulates them in a more holistic way with minimal side effects [7]. Although the therapeutic effectiveness of TCM has been recognized significantly for thousands of years, its synergistic effects have not been sufficiently clarified.

The Shexiang Baoxin Pill (SBP), which consists of seven herbal medicines, including *Moschus*, *Radix Ginseng*, *Calculus Bovis*, *Styrax*, *Cortex Cinnamomi*, *Venenum Bufonis*, and *Borneolum Syntheticum*, has been widely used for treating coronary heart disease (CHD) in China for many years [8–12]. The therapeutic mechanisms of the SBP have been studied in our lab for approximately ten years. Although Peng Jiang et al. [13] and Li Xiang et al. [14] have demonstrated that the therapeutic mechanisms of the SBP were involved mainly in inhibiting dysfunctions in energy metabolism, oxidative injury, and inflammation in the development of myocardial infarction (MI), the advantages of the synergistic efficacy of the SBP had not been investigated. There are hundreds of compounds in the SBP, but most of them are nonbioactive ingredients. In other words, they are not useful therapeutically. Therefore, we hope to rebuild a simplified

formula of an SBP (SFSBP) using the bioactive ingredients to attempt to clarify the advantages of the synergistic efficacy of the SBP.

It has been reported that there are hundreds of compounds in the SBP [15, 16]. Compounds such as muscone, cinnamic acid, bufalin, ginsenoside Re, ginsenoside Rb1, cholic acid, and borneol are the principal active components in the ingredients (*Moschus*, *Cortex Cinnamomi*, *Styrax*, *Venenum Bufonis*, *Radix Ginseng*, *Calculus Bovis*, and *Borneolum Syntheticum*), and they are also responsible for the therapeutic effectiveness of the SBP [17]. In this study, these 7 bioactive compounds were combined into a simplified formula of the Shexiang Baoxin Pill (SFSBP) according to their proportions in the SBP [15, 16].

Metabolomics is a systematic approach that can be used for understanding processes ranging from the analysis of metabolic profiles *in vivo* to the dynamic responses to pathophysiological stimuli or drug interventions [18]. It provides insights into the global metabolic condition of the entire organisms, which is reasonably coincident with the systemic and integrative nature of TCM [19]. Metabolomics has been applied to the study of the potential mechanisms of many TCMs, such as the Shuanglong formula [20], the Sini Decoction [21], and the Compound Danshen Tablets [22, 23].

As part of an ongoing study, a metabolomic methodology has been employed to investigate the synergistic efficacy of the multiple components of SBP in MI rats. Through a comparative study of the holistic intervention effects of the SBP, the SFSBP, and the 7 single bioactive compounds on MI rats, the synergistic efficacy of the multicomponent properties of the SBP has been clarified preliminarily.

2. Experiment

2.1. Materials and Reagents. HPLC grade methanol and acetonitrile were purchased from Honeywell (NJ, USA). Spectroscopic grade formic acid and leucine enkephalin were purchased from Sigma-Aldrich (St. Louis, MO, USA). Ultrapure water was prepared with a Milli-Q water purification system (MA, USA). The assay kits used for creatine kinases (CK) and lactate dehydrogenase (LDH) were purchased from Nanjing Jiancheng Bioengineering Institute (Nanjing, China). The Shexiang Baoxin Pill (SBP) was kindly donated by Shanghai Hutchison Pharmaceuticals (Shanghai, China). Muscone, cinnamic acid, bufalin, ginsenoside Re, ginsenoside Rb1, cholic acid, and borneol (purity > 98%) were purchased from Shanghai Ronghe Biopharmaceutical Co., LTD (Shanghai, China).

2.2. Animals. Eighty male Sprague-Dawley rats (200 ± 20 g) were purchased from SLAC Laboratory Animal Co., Ltd (Shanghai, China). All of the animals were kept in an animal room with a constant temperature of $23 \pm 2^\circ\text{C}$ and a 12 h dark-light cycle with free access to food and water. The animal facilities and protocols were used with the permission of the Institutional Animal Care and Use Committee of the Second Military Medical University. All of the animals were treated with humane care throughout the experiment under the previous conditions for a 2-week acclimation period.

2.3. MI Model and Drug Administration. An MI model was induced by the left anterior descending coronary artery (LADCA) ligation [24, 25]. First, animals were anesthetized with ether, immobilized on a pad and positioned on their backs. Then, the heart was exteriorized immediately after thoracotomy in the fourth left intercostal space. After the heart was returned to its normal position, a 4–0 black silk ligature was securely ligated in the MI group rats. To ascertain that the MI model had been successful, electrocardiograms (ECGs) were recorded using a MPA 2000 biosignal analysis system (Alcott Biotech Co. Ltd., Shanghai, China) to obtain an abnormal Q wave (less than 0.3 mV). The sham group was operated upon using the same process as previously mentioned, except for the ligation step. In total, 64 MI rats and 8 sham rats survived.

Fifty-six MI rats were randomly grouped and treated with 9 types of medicines: SBP (28 mg/kg/day, $n = 7$), SFSBP (40 mg/kg/day, $n = 7$, composed of muscone (2.28 mg), cinnamic acid (2.57 mg), bufalin (1.16 mg), ginsenoside Re (7.87 mg), ginsenoside Rb1 (3.20 mg), cholic acid (10.20 mg), and borneol (12.72 mg)), muscone (150 mg/kg/day, $n = 6$), cinnamic acid (50 mg/kg/day, $n = 6$), bufalin (10 mg/kg/day, $n = 6$), ginsenoside Re (20 mg/kg/day, $n = 6$), ginsenoside Rb1 (40 mg/kg/day, $n = 6$), cholic acid (80 mg/kg/day, $n = 6$), or borneol (100 mg/kg/day, $n = 6$). The nine types of medicines were ground into fine powders and dissolved in a 0.5% carboxymethyl cellulose sodium salt (CMC-Na) aqueous solution. The remaining 8 MI rats were treated as an MI model group, and 0.5% CMC-Na was orally administered, as was performed for the 8 sham rats. All of the rats were orally gavaged for 15 consecutive days.

2.4. Sample Collection. Blood was collected from the ophthalmic venous plexus after all the rats were anaesthetized with ether on the 15th day. The blood was then centrifuged at 3,500 rpm for 10 min at 4°C , 1 h after the blood collection. Then, 200 μL of the supernatant serum obtained was collected and stored at -20°C for analysis of CK and LDH. The remaining serum (>200 μL) was stored in a -80°C refrigerator for LC-Q-TOF/MS analysis. The hearts of 72 rats were excised and immediately fixed in 10% formalin for the analysis of the histopathology.

2.5. Preparation of Metabolomic Samples. The serum samples were thawed before analysis. Each 100 μL of serum aliquot was added to 1000 μL of methanol. The mixture was vortexed for 2 min and centrifuged at 12,000 rpm for 10 min at 4°C . The supernatant was stored at -80°C for at least 24 hours before analysis.

The blank sample was acetonitrile, and it was run after every two serum sample injections to minimize carryover. Equal volumes of methanol and ultrapure water were mixed as a needle cleaning phase and were washed for 1 min during every injection.

A volume of 10 μL was pooled as a quality control (QC) sample from each serum sample. The preparation process for the QC samples was the same as for the analysis samples. The QC samples were injected randomly during the analysis sequence to ensure the stability of the instrument that was

used to evaluate the mass, the retention time, and the ionic intensity.

2.6. LC-Q-TOF/MS Analysis. Metabolomic analysis was performed on an Agilent-1200 LC system coupled to an Agilent-6520 Q-TOF mass spectrometer (Agilent Technologies, Palo Alto, CA, USA) and equipped with an electrospray ionization source. Separation of all of the serum samples was performed on an Eclipse plus C₁₈ column (1.8 μm, 2.1 mm × 100 mm, Agilent). The column temperature was maintained at 45°C. Ultrapure water (a) with 0.1% formic acid and acetonitrile (b) with 0.1% formic acid were used as the mobile phase, and the flow rate was set at 0.25 mL/min. The gradient program was as follows: 0–1.5 min, 2% B; 1.5–9 min, 100% B; 9–11 min, 85% B; 11–13 min, 80% B; 13–18 min, 2% B; 18–22 min, 2% B in positive mode and 0–1.5 min, 2% B; 1.5–9 min, 85% B; 9–12 min, 100% B; 12–15 min, 100% B; 15–19 min, 2% B; 19–23 min, 2% B in negative mode. The sample injection volume was 1 μL.

The parameters for mass detection were set as follows: the gas temperature was 330°C; the drying gas (N₂) flow rate was 8 L min⁻¹; the nebulizer gas pressure was 35 psig, the Vcap was 3,700 V in the negative mode and 3,900 V in the positive mode; the skimmer was 65 V; the fragmentor was 160 V; and the mass scan range was *m/z* 50–1000. Leucine enkephalin was used as the lock mass (*m/z* 554.2615 in the negative mode and 556.2771 in the positive mode). The MS/MS analysis was acquired in the targeted MS/MS mode with three collision energies: 10 ev, 20 ev and 40 ev.

2.7. Method Validation. Validation of the method was carried out to confirm the suitability of long batch analysis. In this study, six extracted ions, including *m/z* 269.05 (homocysteine, positive mode), *m/z* 118.07 (L-valine, positive mode), *m/z* 282.27 (oleamide, positive mode), *m/z* 608.3631 (PGPC, negative mode), *m/z* 188.0768 (3-indolepropionic acid, negative mode), and *m/z* 165.046 (3-methylxanthine, negative mode), were chosen to assess the repeatability and stability of the established method by assessing the variations in peak areas and retention times.

Six parallel samples that were obtained from the same sample were prepared using the same extraction method and were injected continuously for the assessment of the repeatability. QC samples were injected after every 6 serum sample injections to evaluate the stability of the sequence analysis.

2.8. Data Processing. The LC-Q-TOF/MS data were analyzed by Agilent Mass Hunter Qualitative Analysis Software (Agilent Technologies, Palo Alto, CA, USA). The parameters for the data collection were set as follows: mass ranging from 50 to 1000 amu and retention time ranging from 0 to 12 min, and mass tolerance was 0.05 Da, retention time tolerance was 0.1 min, and peak relative height was ≥1.5%. Mass data (*m/z*) and retention time (*t_R*) were listed as the identifiers for each peak. Before the multivariate analysis, the ion intensities for each peak were normalized to the total area to correct for the MS response shift through sequence

analysis due to the long duration of this metabolomic study. Partial least squares discriminant analysis (PLS-DA) was performed through SIMCA-P (version 11.0, Umetrics, Umea, Sweden) for multivariate analysis. One-way analyses of variance (ANOVAs) were performed using a Bonferroni correction of the SPSS 13.0 package for Windows (SPSS Inc., Chicago, IL, USA) for the analysis of significance. Differences were considered significant at values of *P* < 0.05.

3. Results and Discussion

3.1. Pharmacology Study

3.1.1. Serum Enzyme Measurements. The activities of the serum enzymes CK and LDH are considered to be important parameters in the assessment of myocardial injury [26, 27]. In the present study, the serum concentrations of CK and LDH were measured to evaluate both the validity of the MI model and the therapeutic effectiveness of different treatments. As shown in Figure 1, the concentrations of CK and LDH were significantly increased (*P* < 0.01, compared with the sham group) in the MI group (B), which indicated that the MI model had been successfully induced. The cinnamic acid (H) group only acquired a significant restoration effect on LDH when compared with the MI group (*P* < 0.01). The cholic acid (K) group not only showed a significant difference from the MI group but also showed a significant difference when compared with the sham group (*P* < 0.01), suggesting that cholic acid had over-regulated the disturbed balance of LDH and CK *in vivo* that was induced by the MI and that there might be side effects during regulation. However, the reducing effects of the SBP (C), the SFSBP (D), and the ginsenoside Re (E) groups seemed more robust than did the remaining groups (*P* < 0.01, compared with the sham group).

3.1.2. Effects of MI on Myocardial Tissue. As shown in Figure 2, histological sections of myocardial tissue from the MI group can be differentiated clearly from those of the sham group. There was serious swelling of the fibroblasts and the fibroblastic hyperplasia in the MI group, while subendocardial necrosis, infiltrated leukocytes, chronic inflammatory cells, edema, and vacuoles could be clearly observed. However, these symptoms, induced by myocardial injury, were almost completely lacking in the sham group. Histopathological examination of the SBP and SFSBP groups was very similar to that of the sham group; slight subendocardial damage was observed, and a reduction of inflammatory cells was observed, which indicated that the SBP and SFSBP groups had experienced decreased myocardial damage. The fibrotic and necrotic effects were slightly reversed in the ginsenoside Rb1, ginsenoside Re, and cinnamic acid groups, which demonstrated that these 3 drugs showed therapeutic effects on MI, but they were not as effective as were the SBP and the SFSBP. Meanwhile, fibrotic and necrotic tissues were clearly observed in the borneol, bufalin, and muscone groups. All of the results demonstrated that the therapeutic performance was much lower in regulating myocardial damage when using the single components individually.

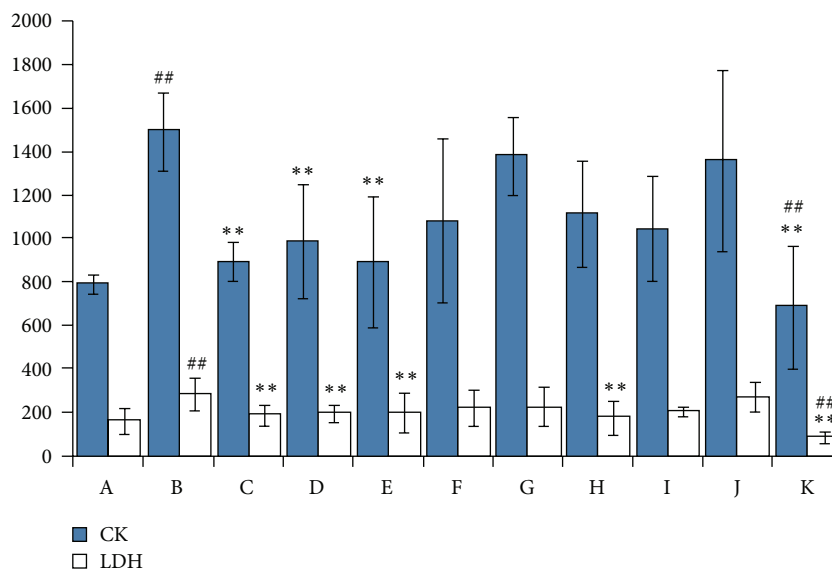


FIGURE 1: CK and LDH results in rat serum from MI group. LDH: lactate dehydrogenase and CK: and creatine kinases. (A) sham group, (B) MI group, (C) SBP group, (D) SFSBP group, (E) ginsenoside Re, (F) ginsenoside Rb1, (G) bufalin group, (H) cinnamic acid group, (I) muscone group, (J) borneol group, and (K) cholic acid group. ** $P < 0.01$ versus MI group and ## $P < 0.01$ versus sham group.

3.2. Method Validation for Stability and Repeatability of Sequence Analysis Using LC-Q-TOF/MS. The stability of sequence analysis using the LC-Q-TOF/MS system was validated by the variations in peak area and retention time of six extracted ions (m/z 269.05 (homocysteine, positive mode), m/z 118.07 (L-valine, positive mode), m/z 282.27 (oleamide, positive mode), m/z 608.3631 (PGPC, negative mode), m/z 188.0768 (3-indolepropionic acid, negative mode), and m/z 165.046 (3-methylxanthine, negative mode)). The relative standard deviations (RSDs) of the peak areas of the six extracted ions were all less than 13% in both the negative and the positive modes, while the relative standard deviations (RSDs) of the retention times of the six extracted ions were all less than 2% [14].

The repeatability of the LC-Q-TOF/MS system was validated by a reduplicated analysis of six parallel samples. The relative standard deviations (RSDs) of the peak areas of the six extracted ions were less than 15% in both the positive and the negative modes, while the relative standard deviations (RSDs) of the retention times of the six extracted ions were all less than 1% [14].

All of the results demonstrated that the stability and the repeatability of the proposed method were satisfactory for the metabolomic study.

3.3. Metabolomics Study

3.3.1. Biomarkers Contributed by MI. In our previous study, 8,302 ion signals in the positive mode and 7,289 ion signals in the negative mode were detected in both the MI model and the sham groups. Multivariate statistical analyses of a partial least squares discriminate analysis (PLS-DA) were performed by SIMCA-P software. Variable biomarkers were selected between the MI and the sham groups based on their variable importance in the projection threshold (VIP > 1).

Eventually, 27 biomarkers (see Supplementary Table 1 available online at <http://dx.doi.org/10.1155/2013/823121>) were identified (14 in the positive and 13 in the negative) by searching through the Biofluid Metabolites Database (<http://metlin.scripps.edu/>) and the Human Metabolome Database (<http://www.hmdb.ca/>) for information on the MS and the MS/MS results in our previous study [14]. These biomarkers primarily involved 4 pathological pathways. Five biomarkers, including homocysteine [28–31], PGPC [32–34], 5-methylcytosine [35], hippuric acid [36], and allantoin [37], were related to oxidative injury from myocardial dysfunction. Five biomarkers, including AIR, hypoxanthine [38, 39], allantoin, lactic acid [40–42], and 3-methylxanthine, participated in energy metabolism dysfunctions induced by MI. Three biomarkers, including PGE2, leukotriene A4 methyl ester, and 12(S)-HETE, which are found in arachidonic acid metabolism, were involved in the inflammation that relates to MI. Five biomarkers, including L-proline, L-isoleucine, homocysteine, pyroglutamic acid, and L-valine, are amino acids which indicate that the formation of a MI has broken the balance of the amino acid metabolism.

In this study, the different therapeutic effects of the 9 treatment groups have been evaluated through monitoring the changes in the 27 identified biomarkers.

3.3.2. Different Therapeutic Effects of SFSBP and Its 7 Constituent Groups on MI. The PLS-DA score plots (Figure 3) that were built to holistically evaluate the regulatory effects of SFSBP and its constituent treatment groups on MI in both positive and negative modes showed clear results. Although some of the monotherapy groups (ginsenoside Rb1, ginsenoside Re, bufalin, cinnamic acid, muscone, borneol and cholic acid treated groups) overlapped slightly with the SFSBP-group, none of the monotherapy groups were located

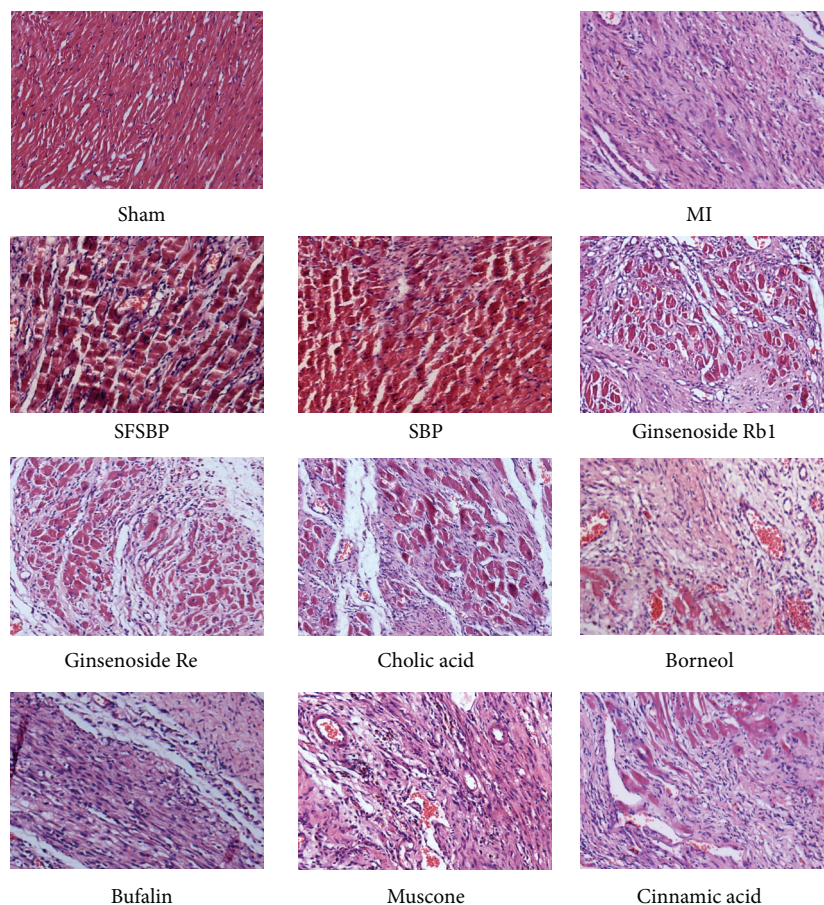


FIGURE 2: Myocardial tissues of 11 groups under light microscopy.

closer to the sham group than the SFSBP-treated group was in either mode.

The mean levels of the 27 identified biomarkers were also analyzed to evaluate the therapeutic effects of SFSBP and its 7 monocomponents. Nineteen of the biomarkers were significantly reduced to the level of the sham group by SFSBP, while the number of biomarkers reduced by ginsenoside Rb1, ginsenoside Re, bufalin, cinnamic acid, muscone, borneol, and cholic acid was 8, 6, 6, 8, 11, 5, and 6, respectively. As shown in Figure 5, the therapeutic effects of ginsenoside Rb1, ginsenoside Re, and cholic acid were primarily focused on regulating the biomarkers that relate to the oxidative injury (hippuric acid, homocysteine, and 5-methylcytosine) from MI, while bufalin and cinnamic acid were primarily focused on inhibiting the dysfunctions in energy metabolism (lactic acid) that are induced by MI. Furthermore, muscone achieved a significant therapeutic effect on the regulation of the oxidative injury (hippuric acid and 5-methylcytosine) and the dysfunctions in energy metabolism (lactic acid) related to MI, while borneol achieved scarcely any therapeutic effects on MI. Additionally, as shown in Figure 4, the mean levels of 2 biomarkers (pyroglutamic acid and 3-indolepropionic acid) in the SFSBP-treated group were reduced closer to the level of the sham group than they were in the monotherapy groups. Meanwhile, 4 biomarkers, including PGPC, PGE2,

L-isoleucine, and L-proline were only significantly reduced to the level of the sham group by SFSBP. PGPC and PGE2 were involved in the oxidative injury and the inflammation from MI, respectively, indicating that the therapeutic effects of SFSBP came primarily from regulating the oxidative injury and the inflammation induced by MI.

All of the results indicated that SFSBP showed a stronger and more stable therapeutic effect for treating myocardial injury than did the monotherapies. Although each single therapy treated group was dosed at a higher dose concentration than was the SFSBP group, the SFSBP group showed the highest degree of recovery among the 8 treated groups. These results were consistent with pharmacology results that suggested that SFSBP could amplify the therapeutic effects of each of its constituents and exert synergistic therapeutic efficacies.

3.3.3. Evaluation of Therapeutic Effectiveness of SFSBP on MI by Comparison with the SBP. Another PLS-DA model was built to evaluate the therapeutic effectiveness of the SFSBP and the SBP on MI. As shown in Figure 6, the SBP and the SFSBP groups were far from the MI group on the PLS-DA score plots. The SBP-treated group was closer to the sham group than it was to the SFSBP-treated group. Overlap between the two groups was also observed, revealing that the

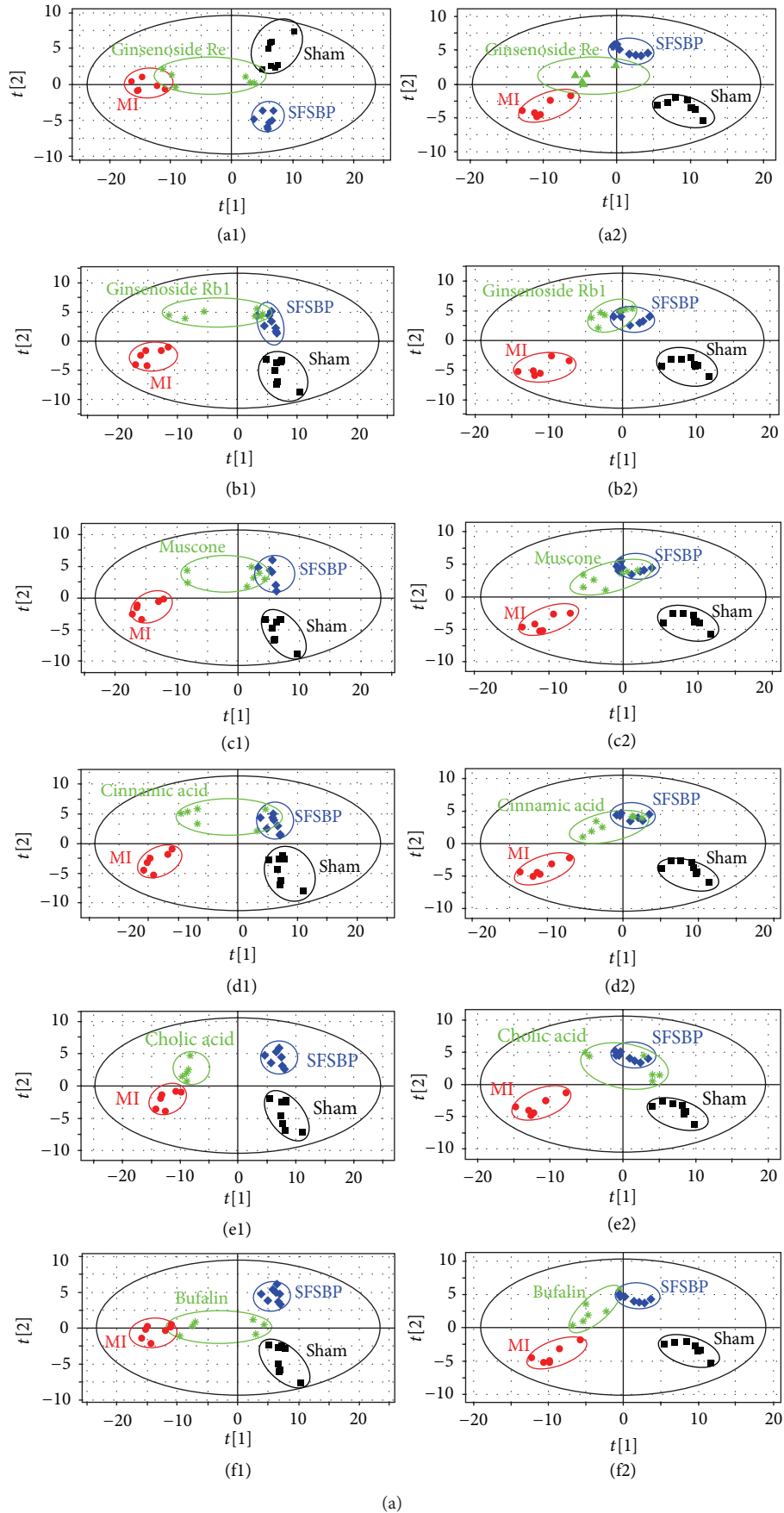


FIGURE 3: Continued.

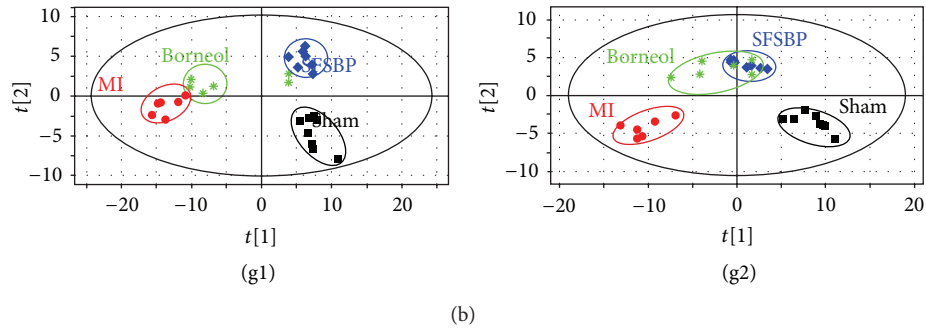


FIGURE 3: PLS-DA score plots of rat serum on day 15 in both positive and negative modes. (Parameters of each score plot were shown in Supplementary Material.)

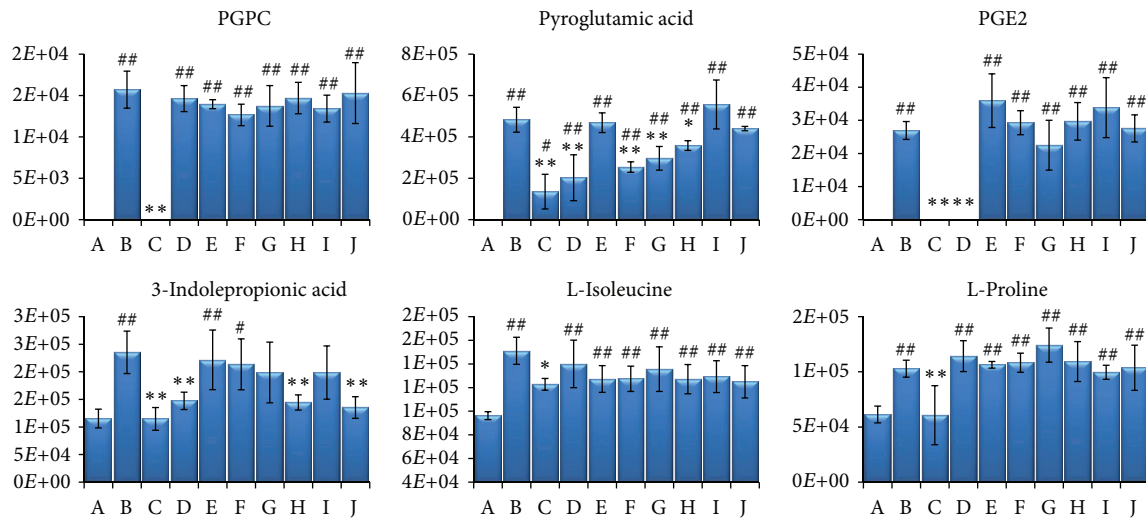


FIGURE 4: The six biomarkers that were regulated differently in SFSBP and its constituent groups. (A) sham group, (B) MI group, (C) SFSBP group, (D) ginsenoside Rb1, (E) ginsenoside Re, (F) bufalin, (G) cinnamic acid, (H) muscone, (I) borneol, and (J) cholic acid. * $P < 0.05$ and ** $P < 0.01$ when compared with MI group; # $P < 0.05$, ## $P < 0.01$ when compared with sham group. The number on the y -axis represents the peak areas of these biomarkers.

SBP achieved more effective therapeutic performance during the recovery from the MI surgery than did the SFSBP.

The mean levels of the 27 identified biomarkers were also examined to evaluate the therapeutic effectiveness of the SFSBP and the SBP on MI. Nineteen biomarkers were significantly ($P > 0.05$, compared to sham group) reduced to the level of the sham group by either the SBP or the SFSBP. Among these biomarkers, 16 biomarkers (Figure 7) were reduced to the level of the sham group in both groups. Leukotriene A4 methyl ester, oleamide, and 3-methylxanthine (Figure 8) were reduced to the level of the sham group by the SBP ($P > 0.05$, SBP-treated group versus sham group), while L-proline, 5-aminoimidazole ribonucleotide, and taurocholic acid (Figure 8) were regulated to the level of the sham group in the SFSBP-treated group ($P > 0.05$, SFSBP-treated group versus sham group), and the remaining five biomarkers, hypoxanthine, niacinamide, 12(S)-HETE, 2-furoic acid, and allantoin, were not able to be restored by either the SBP or the SFSBP treatments.

Among those biomarkers that were significantly reduced by the SBP and the SFSBP, lactic acid is involved in energy metabolism, hippuric acid, homocysteine, 5-methylcytosine, and PGPC are involved in oxidative injury, and PGE2 is involved in inflammation, which indicates that the SBP and the SFSBP might offer therapeutic effects on the dysfunctions in energy metabolism, oxidative injury, and inflammation induced by MI. Additionally, leukotriene A4 methyl ester (involved in inflammation) and 3-methylxanthine (involved in energy metabolism) can be reduced to the level of the sham group by the SBP but not by the SFSBP (Figure 8), indicating that the therapeutic effectiveness of the SBP may be superior to that of the SFSBP in inhibiting the inflammation and the dysfunctions in energy metabolism.

The results demonstrated that the SBP and the SFSBP did have significant therapeutic efficacy in the MI rats and that their therapeutic mechanism was focused on inhibiting the dysfunctions in energy metabolism, oxidative injury, and inflammation from MI. Considering the fact that the

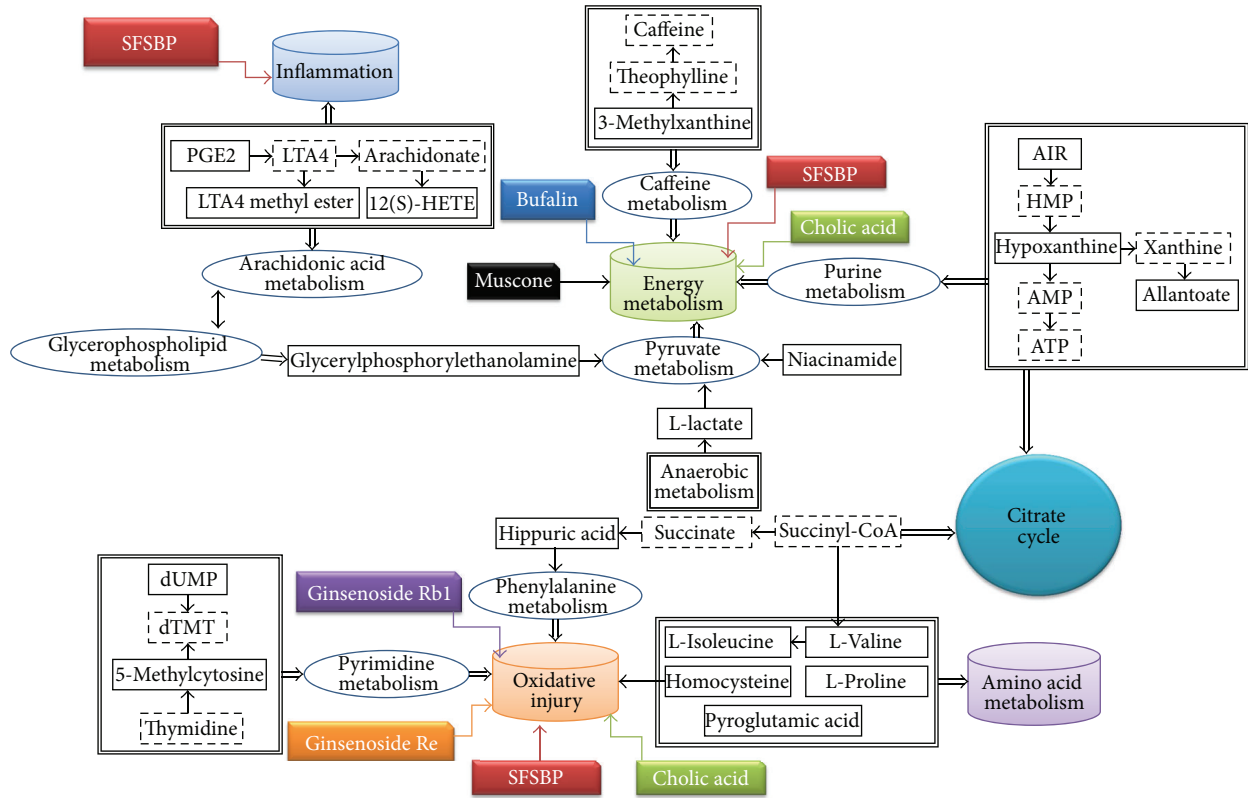


FIGURE 5: The distribution of regulation effects using different treatments. The solid-line squares represent the identified biomarkers; the cylinders represent pathogenesis induced by MI; the dashed squares represent different treatments.

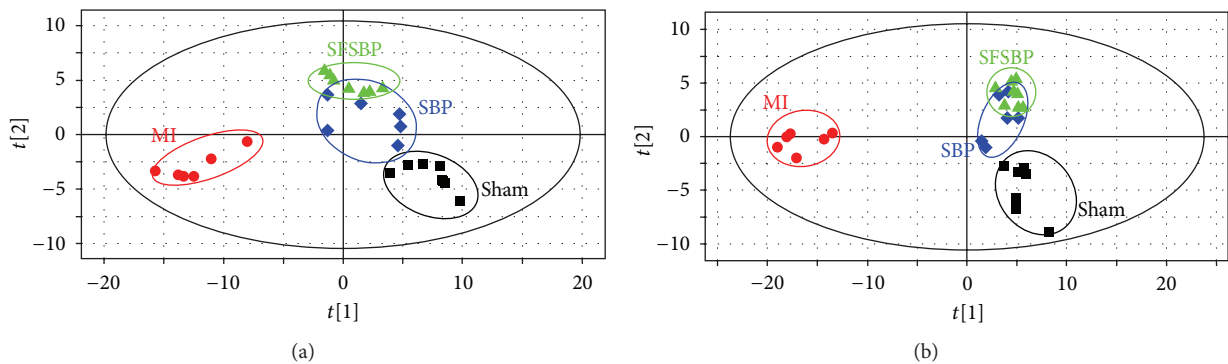


FIGURE 6: PLS-DA score plots of rat serum on day 15 in positive and negative modes. (a) PLS-DA score plot of rat serum of the SFSBP group in positive mode ($R^2 X_{(cum)} = 0.596, R^2 Y_{(cum)} = 0.977, Q^2 Y_{(cum)} = 0.573$); (b) PLS-DA score plot of rat serum of the SFSBP group in negative mode ($R^2 X_{(cum)} = 0.516, R^2 Y_{(cum)} = 0.975, Q^2 Y_{(cum)} = 0.583$).

SFSBP has the composition of the SBP, we can conclude that the SBP might also have synergistic effects in MI rats. However, the regulatory efficacy of the SBP on MI rats was superior to that of the SFSBP, according to the PLS-DA score plots. One of the reasons for this might be that there are other bioactive compounds in the SBP exerting therapeutic effects on MI, so that the composition of SFSBP needs to be further optimized. In consideration of the fact that the concentrations of 7 bioactive compounds in the SFSBP were much higher than those in the SBP, the therapeutic efficacy

of the SFSBP was not as strong as that of the SBP, indicating the rationality of the TCM formula and the likelihood that it cannot simply be substituted with a combination of several bioactive compounds from its formula.

4. Conclusions

In this study, a metabolomic strategy has been performed to investigate the therapeutic and the synergistic effects of a TCM formula. This study revealed that the therapeutic effects

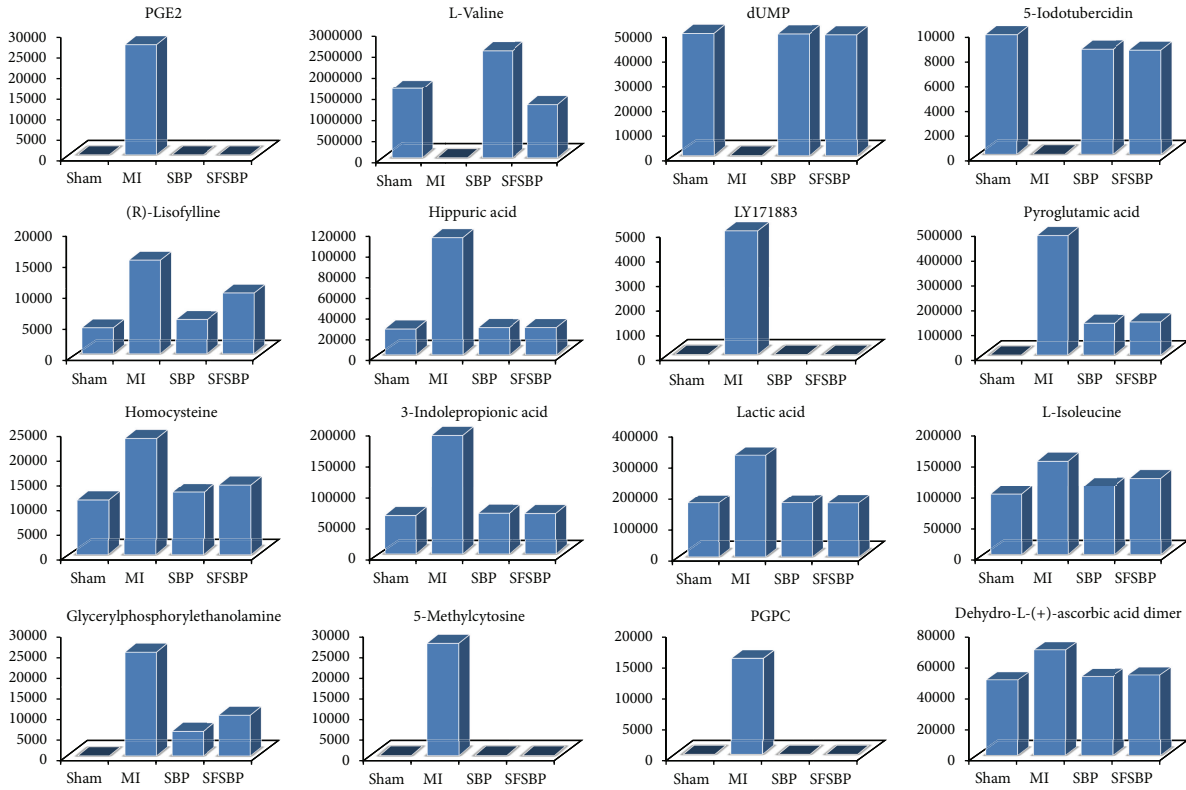


FIGURE 7: The sixteen biomarkers that were significantly reduced by both SBP and SFSBP. The number on the *y-axis* represents the peak areas of these biomarkers.

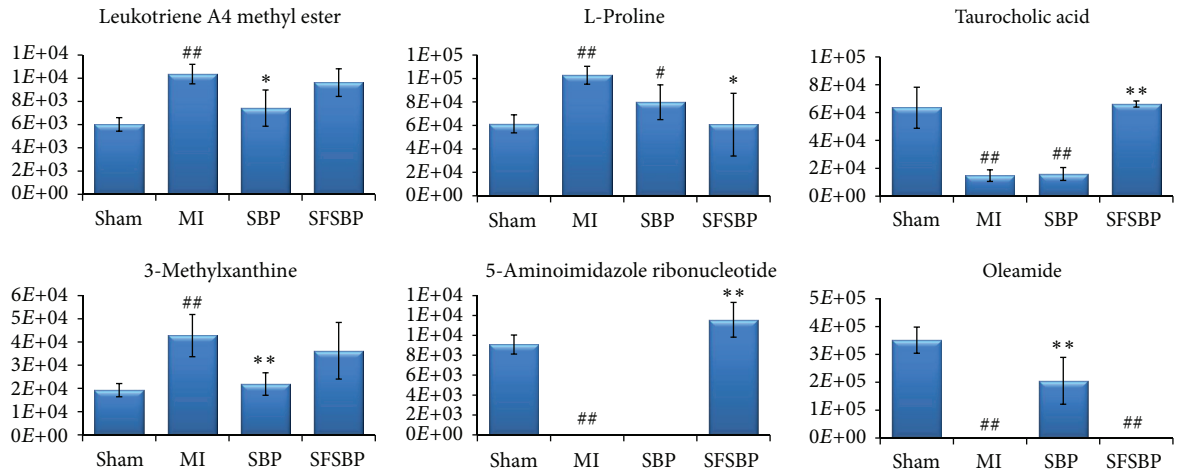


FIGURE 8: The six biomarkers that were differently regulated between the SBP- and SFSBP-treated groups. **P* < 0.05 and ***P* < 0.01 when compared with the MI group; #*P* < 0.05 and ##*P* < 0.01 when compared with the sham group. The number on the *y-axis* represents the peak areas of these biomarkers.

of multicomponent medicines were greater than the effects of single components and that they exert a synergistic effect, in accordance with our previous study [14], which also indicated that TCM did have advantages in regulating the dysfunctions induced by complicated diseases. Finally, we believe that such a metabolomic-based approach is an efficacious strategy for the study of TCM.

Acknowledgments

This work was supported by the NSFC (81102865), NSFC (81230090), partially supported by the Global Research Network for Medicinal Plants (GRNMP) and by King Saud University, the Shanghai Leading Academic Discipline Project (B906), FP7-PEOPLEIRSES-2008 (TCMCANCER Project

230232), the Key laboratory of drug research for special environments, PLA, the Shanghai Engineering Research Center for the Preparation of Bioactive Natural Products (10DZ2251300), and the Scientific Foundation of Shanghai China (09DZ1975700, 09DZ1971500, and 10DZ1971700).

References

- [1] F. Salameh, D. Perla, M. Solomon et al., "The effectiveness of combined Chinese herbal medicine and acupuncture in the treatment of atopic dermatitis," *The Journal of Alternative and Complementary Medicine*, vol. 14, no. 8, pp. 1043–1048, 2008.
- [2] I. Cohen, M. Tagliaferri, and D. Tripathy, "Traditional Chinese medicine in the treatment of breast cancer," *Seminars in Oncology*, vol. 29, no. 6, pp. 563–574, 2002.
- [3] X. M. Li and L. Brown, "Efficacy and mechanisms of action of traditional Chinese medicines for treating asthma and allergy," *Journal of Allergy and Clinical Immunology*, vol. 123, no. 2, pp. 297–306, 2009.
- [4] Y. J. Kang, "Herbogenomics: from traditional Chinese medicine to novel therapeutics," *Experimental Biology and Medicine*, vol. 233, no. 9, pp. 1059–1065, 2008.
- [5] M. P. Sheehan, M. H. A. Rustin, D. J. Atherton et al., "Efficacy of traditional Chinese herbal therapy in adult atopic dermatitis," *The Lancet*, vol. 340, no. 8810, pp. 13–17, 1992.
- [6] V. E. Tyler, "Herbal medicine: from the past to the future," *Public Health Nutrition*, vol. 3, no. 4A, pp. 447–452, 2000.
- [7] K.-H. Lee, "Research and future trends in the pharmaceutical development of medicinal herbs from Chinese medicine," *Public Health Nutrition*, vol. 3, pp. 515–522, 2000.
- [8] *Editorial Committee of Pharmacopoeia of Ministry of Health P. R. China*, Part 1, China Chemical Industry Press, Beijing, China, 2010.
- [9] D. J. Wu, H. S. Hong, and Q. Jiang, "Effect of shexiang baoxin pill in alleviating myocardial fibrosis in spontaneous hypertensive rats," *Chinese Journal of Integrated Traditional and Western Medicine*, vol. 25, no. 4, pp. 350–353, 2005.
- [10] H. T. Song, T. Guo, and H. M. Zhao, "Pharmacodynamic studies on Heart-protecting Musk Pills with myocardial blood flow perfusion in rats," *Pharmaceutical Journal of Chinese People's Liberation Army*, vol. 18, pp. 137–139, 2002.
- [11] Y. Yang, Y. D. Ye, and L. M. Mao, "Shexiangbaoxinwan to AMI thrombolysis future ventricle configuration and function influence," *Chinese Journal of the Practical Chinese with Modern Medicine*, vol. 18, p. 1583, 2005.
- [12] R. Y. Ye, "Effect of heart-protecting Musk Pill on cardiac function of ischemic heart disease," *Zhejiang Journal of Integrated Traditional Chinese and Western Medicine*, vol. 16, pp. 734–735, 2006.
- [13] P. Jiang, W. Dai, S. Yan et al., "Potential biomarkers in the urine of myocardial infarction rats: a metabolomic method and its application," *Molecular BioSystems*, vol. 7, no. 3, pp. 824–831, 2011.
- [14] L. Xiang, P. Jiang, C. Zhan et al., "The serum metabolomic study of intervention effects of the traditional Chinese medicine Shexiang Baoxin Pill and a multi-component medicine poly pill in the treatment of myocardial infarction in rats," *Molecular BioSystems*, vol. 8, pp. 2434–2442, 2012.
- [15] S. K. Yan, W. D. Zhang, R. H. Liu, and Y. C. Zhan, "Chemical fingerprinting of Shexiang Baoxin Pill and simultaneous determination of its major constituents by HPLC with evaporative light scattering detection and electrospray mass spectrometric detection," *Chemical and Pharmaceutical Bulletin*, vol. 54, no. 7, pp. 1058–1062, 2006.
- [16] S. Yan, Y. Yang, Y. Wu, R. Liu, and W. Zhang, "Chemical fingerprinting and quantitative analysis of volatiles in Shexiang Baoxin Pill by gas chromatography with flame ionization and mass spectrometric detection," *Journal of Analytical Chemistry*, vol. 64, no. 2, pp. 149–155, 2009.
- [17] P. Jiang, R. Liu, S. Dou et al., "Analysis of the constituents in rat plasma after oral administration of Shexiang Baoxin pill by HPLC-ESI-MS/MS," *Biomedical Chromatography*, vol. 23, no. 12, pp. 1333–1343, 2009.
- [18] J. K. Nicholson and J. C. Lindon, "Systems biology: metabolomics," *Nature*, vol. 455, no. 7216, pp. 1054–1056, 2008.
- [19] R. Verpoorte, Y. H. Choi, and H. K. Kim, "Ethnopharmacology and systems biology: a perfect holistic match," *Journal of Ethnopharmacology*, vol. 100, no. 1–2, pp. 53–56, 2005.
- [20] X. Liang, X. Chen, Q. Liang et al., "Metabonomic study of Chinese Medicine Shuanglong Formula as an effective treatment for myocardial infarction in rats," *Journal of Proteome Research*, vol. 10, no. 2, pp. 790–799, 2011.
- [21] G. Tan, Z. Lou, W. Liao et al., "Hydrophilic interaction and reversed-phased ultraperformance liquid chromatography TOF-MS for serum metabolomic analysis of myocardial infarction in rats and its application," *Molecular BioSystems*, vol. 8, pp. 548–556, 2012.
- [22] Y. Lu, X. Liu, X. Liang, L. Xiang, and W. Zhang, "Metabolomic strategy to study therapeutic and synergistic effects of tanshinone IIA, salvianolic acid B and ginsenoside Rb1 in myocardial ischemia rats," *Journal of Ethnopharmacology*, vol. 134, no. 1, pp. 45–49, 2011.
- [23] Y. Lv, X. Liu, S. Yan et al., "Metabolomic study of myocardial ischemia and intervention effects of Compound Danshen Tablets in rats using ultra-performance liquid chromatography/quadrupole time-of-flight mass spectrometry," *Journal of Pharmaceutical and Biomedical Analysis*, vol. 52, no. 1, pp. 129–135, 2010.
- [24] J. Wang, X. Liu, B. Ren, H. Rupp, N. Takeda, and N. S. Dhalla, "Modification of myosin gene expression by imidapril in failing heart due to myocardial infarction," *Journal of Molecular and Cellular Cardiology*, vol. 34, no. 7, pp. 847–857, 2002.
- [25] K. Ytrehus, "Models of myocardial ischemia," *Drug Discovery Today: Disease Models*, vol. 3, no. 3, pp. 263–271, 2006.
- [26] H. Y. Zhang, X. Chen, P. Hu et al., "Metabolomic profiling of rat serum associated with isoproterenol-induced myocardial infarction using ultra-performance liquid chromatography/time-of-flight mass spectrometry and multivariate analysis," *Talanta*, vol. 79, no. 2, pp. 254–259, 2009.
- [27] B. C. Wexler, J. T. Judd, and G. W. Kittinger, "Myocardial necrosis induced by isoproterenol in rats," *Angiology*, vol. 19, no. 12, pp. 665–682, 1968.
- [28] C. J. Boushey, S. A. A. Beresford, G. S. Omenn, and A. G. Motulsky, "A quantitative assessment of plasma homocysteine as a risk factor for vascular disease: probable benefits of increasing folic acid intakes," *Journal of the American Medical Association*, vol. 274, no. 13, pp. 1049–1057, 1995.
- [29] W. Eqrton, J. Silberberg, R. Cheryl Ray et al., "Serial measures of plasma homocyst(e)ine after acute myocardial infarction," *American Journal of Cardiology*, vol. 77, pp. 759–761, 1996.
- [30] A. Lindgren, L. Brattström, B. Norrving et al., "Plasma homocysteine in the acute and convalescent phases after stroke," *Stroke*, vol. 26, pp. 795–800, 1995.

- [31] J. E. Graeber, J. H. Slott, and R. E. Ulane, "Effect of homocysteine and homocystine on platelet and vascular arachidonic acid metabolism," *Pediatric Research*, vol. 16, no. 6, pp. 490–493, 1982.
- [32] V. N. Bochkov, A. Kadl, J. Huber, F. Gruber, B. R. Binder, and N. Leitinger, "Protective role of phospholipid oxidation products in endotoxin-induced tissue damage," *Nature*, vol. 419, no. 6902, pp. 77–81, 2002.
- [33] G. O. Fruhwirth, A. Moutzi, A. Loidl, E. Ingolic, and A. Hermetter, "The oxidized phospholipids POVPC and PGPC inhibit growth and induce apoptosis in vascular smooth muscle cells," *Biochimica et Biophysica Acta—Molecular and Cell Biology of Lipids*, vol. 1761, no. 9, pp. 1060–1069, 2006.
- [34] J. Hartwich, A. Dembinska-Kiec, A. Gruca et al., "Regulation of platelet adhesion by oxidized lipoproteins and oxidized phospholipids," *Platelets*, vol. 13, no. 3, pp. 141–151, 2002.
- [35] A. P. Sampson, "Leukotrienes in cardiovascular disease," *Clinical and Experimental Allergy Reviews*, vol. 1, no. 2, pp. 170–174, 2001.
- [36] M. P. Gonthier, V. Cheynier, J. L. Donovan et al., "Microbial aromatic acid metabolites formed in the gut account for a major fraction of the polyphenols excreted in urine of rats fed red wine polyphenols," *Journal of Nutrition*, vol. 133, no. 2, pp. 461–467, 2003.
- [37] R. J. Johnson, D. H. Kang, D. Feig et al., "Is there a pathogenetic role for uric acid in hypertension and cardiovascular and renal disease?" *Hypertension*, vol. 41, no. 6, pp. 1183–1190, 2003.
- [38] O. D. Saugstad, "Hypoxanthine as a measurement of hypoxia," *Pediatric Research*, vol. 9, no. 4, pp. 158–161, 1975.
- [39] O. D. Saugstad, "Hypoxanthine in umbilical cord plasma as a measurement of intrauterine hypoxia," *Acta Obstetrica et Gynecologica Scandinavica*, vol. 54, p. 26, 1975.
- [40] B. D. Guth, J. A. Wisneski, R. A. Neese et al., "Myocardial lactate release during ischemia in swine. Relation to regional blood flow," *Circulation*, vol. 81, no. 6, pp. 1948–1958, 1990.
- [41] I. M. Cheifetz, F. H. Kern, S. R. Schulman, W. J. Greeley, R. M. Ungerleider, and J. N. Meliones, "Serum lactates correlate with mortality after operations for complex congenital heart disease," *Annals of Thoracic Surgery*, vol. 64, no. 3, pp. 735–738, 1997.
- [42] R. A. Kreisberg, "Lactate homeostasis and lactic acidosis," *Annals of Internal Medicine*, vol. 92, no. 2, pp. 227–237, 1980.

Research Article

Vitexicarpin Acts as a Novel Angiogenesis Inhibitor and Its Target Network

Bo Zhang,^{1,2} Lu Liu,¹ Shiwen Zhao,¹ Xu Wang,¹ Liyang Liu,¹ and Shao Li¹

¹ MOE Key Laboratory of Bioinformatics and Bioinformatics Division, TNLIST, Department of Automation, Tsinghua University, Beijing 100084, China

² Joint Computational Center of Drug Discovery, Tianjin International Joint Academy of Biotechnology & Medicine, Tianjin 300457, China

Correspondence should be addressed to Shao Li; shaoli@mail.tsinghua.edu.cn

Received 22 October 2012; Accepted 20 November 2012

Academic Editor: Weidong Zhang

Copyright © 2013 Bo Zhang et al. This is an open access article distributed under the Creative Commons Attribution License, which permits unrestricted use, distribution, and reproduction in any medium, provided the original work is properly cited.

Vitexicarpin (VIT) isolated from the fruits of *Vitex rotundifolia* has shown antitumor, anti-inflammatory, and immunoregulatory properties. This work is designed to evaluate the antiangiogenic effects of VIT and address the underlying action mechanism of VIT by a network pharmacology approach. The results validated that VIT can act as a novel angiogenesis inhibitor. Firstly, VIT can exert good antiangiogenic effects by inhibiting vascular-endothelial-growth-factor- (VEGF-) induced endothelial cell proliferation, migration, and capillary-like tube formation on matrigel in a dose-dependent manner. Secondly, VIT was also shown to have an antiangiogenic mechanism through inhibition of cell cycle progression and induction of apoptosis. Thirdly, VIT inhibited chorioallantoic membrane angiogenesis as well as tumor angiogenesis in an allograft mouse tumor model. We further addressed VIT's molecular mechanism of antiangiogenic actions using one of our network pharmacology methods named drugCIPHER. Then, we tested some key molecules in the VEGF pathway targeted by VIT and verified the inhibition effects of VIT on AKT and SRC phosphorylation. Taken together, this work not only identifies VIT as a novel potent angiogenesis inhibitor, but also demonstrates that network pharmacology methods can be an effective and promising approach to make discovery and understand the action mechanism of herbal ingredients.

1. Introduction

Antiangiogenic therapeutics proposed in 1971 has been widely used for the treatment of excessively angiogenic diseases such as cancer, psoriasis, and rheumatoid arthritis [1, 2]. In recent years, bioactive compounds of traditional Chinese medicine (TCM) herbs as a source of Antiangiogenic agents have played an important role in the discovery and development of anti-cancer drugs [3, 4]. For example, ginsenosides Rb1, Rb2, and Rg3 from *Panax ginseng* can inhibit tumor angiogenesis and metastasis by inhibiting the release of VEGF from tumour cells [5, 6]. Triptolide purified from *Tripterygium wilfordii* Hook F inhibits VEGF expression and secretion from endothelial cells (ECs) and decreases the expression of COX-1, COX-2, and 5-lipoxygenase [7, 8]. More recently, we and others found that sinomenine from *Sinomenium acutum* is a potent angiogenesis inhibitor and exerts synergistic

inhibitory effects on ECs proliferation when combined with matrine from *Sophora flavescens* [9–11]. Thus, bioactive phytochemicals can serve as valuable lead compounds for developing derivatives, constituting a major source for discovering, and developing new antiangiogenic and anticancer drugs. Elucidation of the mechanisms of action of bioactive phytochemicals derived from TCM not only offers new insights into the action mechanism of herbs but also facilitates the ensuing use of bioactive phytochemicals as leads in drug development.

A variety of flavonoid substances, particularly those present in Chinese medicinal herbs, are hypothesized to be the potent kinase inhibitors and show a preventive effect on cancer [12]. Vitexicarpin is a flavonoid from the fruits of *Vitex rotundifolia* (Man Jing Zi), which is structurally typical flavones backbone (Figure 1). It has been documented that vitexicarpin exhibits broad cytotoxicity against human cancer

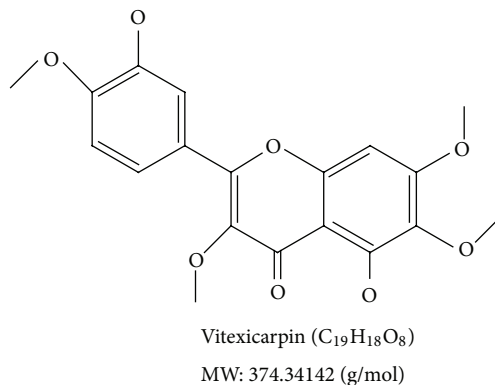


FIGURE 1: The chemical structure of vitexicarpin, a compound from *Vitex rotundifolia* (Man Jing Zi).

cell lines [13, 14], exerts an inhibitory effect on T-lymphocyte proliferation [15], and prevents the TNF- α -induced vascular inflammation [16]. In addition to these activities, we firstly discovered that vitexicarpin inhibits the VEGF-induced ECs proliferation at a half-maximal inhibitory concentration (IC₅₀) of 3.4 μ M [17]. It is speculated that vitexicarpin could inhibit tumor growth and inflammation responses by negatively regulating angiogenesis. However, the antiangiogenic mechanism of vitexicarpin remains elusive, and how to determine the promiscuous target-related proteins of vitexicarpin is also a challenge due to the less specific and low binding properties of small molecular compounds [18].

With the rapid development of network pharmacology [19] and systems pharmacology [20], recent works have demonstrated the value in using network approaches to provide a systematic insight into the molecular mechanisms of complex diseases (e.g., arrhythmias) [21], as well as therapeutic drugs (e.g., bafetinib) [22]. The information retrieved from biological network has been proven important for understanding the links between complex diseases and therapeutic drugs in a relatively unbiased and systematic manner [23, 24]. Therefore, network approaches leave room for *in silico* elucidation of drug action mechanisms, offering a new opportunity for drug discovery and development, especially for natural products and traditional Chinese medicine researches [25–28]. In our previous works, we proposed a novel theory of “Network Target” to analyze the mechanisms of action of herbal formula and its ingredients, and subsequently established a series of network-based methods as a starting point for TCM network pharmacology [11, 17, 23, 25, 26, 28, 29]. For example, we recently established a drugCIPHER method that can effectively predict target profiles for a drug or herbal compound [29]. The rationale of drugCIPHER is given a protein, if most of its neighbor proteins in the protein-protein interaction network are actually the known targets of FDA-approved drugs with similar chemical structures or therapeutic effects to a given compound, then this protein is most likely to be the target of this compound [29]. Thus, given a query drug or herbal compound, drugCIPHER can assign a score to each protein in the interaction network and describe the importance of the protein to the mechanism of actions of this drug or herbal compound.

Here, we tried to give an example of the application of TCM network pharmacology on the research of herbal compounds and took a “top-down” approach to identify the Anti-angiogenic target network of vitexicarpin. Taking advantage of the *in vitro* and *in vivo* models of angiogenesis, we systematically examined the effects of vitexicarpin on different steps and players involved in angiogenesis. We then used drugCIPHER to predict the target profiles of vitexicarpin and found that pathways enriched in target profiles can explain the therapeutic activities of vitexicarpin. We also addressed the molecular mechanisms underlying vitexicarpin’s Anti-angiogenic effect by identifying the possible target network involved in VEGF pathway. Eventually, experimental validation of the target network revealed that reduced phosphorylation states of SRC and AKT are in response to the anti-angiogenesis actions of vitexicarpin.

2. Materials and Methods

2.1. Cell Lines, Cell Culture, and Reagents. Primary human umbilical vascular endothelial cells (HUVECs) were purchased from ScienCell Research Laboratories. HUVECs were grown onto gelatin-coated 10 cm² culture dishes in a standard endothelial cell medium (ECM) supplemented with 5% fetal bovine serum (FBS; Hyclone Laboratories), 50 μ g/mL endothelial cell growth supplement (ECGS; Sigma), 50 IU/L penicillin, and 50 mg/L streptomycin at 37°C in a humidified 5% CO₂/95% air incubator. Vitexicarpin was purchased from National Institute for the Control of Pharmaceutical and Biological Products, Beijing, China. A 50 mM solution of vitexicarpin was prepared in DMSO, stored at –20°C and protected from light, and then diluted as needed concentrations in culture medium.

2.2. In Vitro Angiogenesis Assay

2.2.1. Migration Analysis by Wound Healing and Transwell Assay. HUVECs migration was evaluated by both the CytoSelect 24-well Wound Healing Assay and Transwell Migration Assay. A CytoSelect Wound Healing Assay kit (CBA-120-5) purchased from Cell Biolabs (San Diego) was used for this assay. HUVECs suspended in culture medium containing 5%

FBS were seeded at 10,000 cells per well on 24-well culture dishes precoated with 0.1% gelatin (Sigma), and then put the CytoSelect™ Wound Healing Insert into the plate wells. After overnight incubation, the inserts were removed from the well to generate a 0.9 mm “Wound field.” The cells were incubated with 20 µg/mL mitomycin C for 1 h to deactivate HUVEC proliferation. After that, the cells were washed with PBS to remove debris and incubated with or without VEGF and different concentrations of vitexicarpin. After 12 h of incubation, images were taken by a phase contrast microscope (Olympus) and the wound size was determined [30].

The chemotactic motility of HUVECs was assayed using Transwell chamber with 6.5 mm diameter noncoated filter membrane (pore size, 8 µm; Corning, Inc.). Endothelial cell medium with 0.1% FBS supplemented with 10 ng/mL VEGF was used as chemoattractant in the bottom chamber, and 5×10^4 HUVECs pretreated with mitomycin C in 200 µL ECM (0.1% FBS) with different concentrations of vitexicarpin were seeded in the top chamber. The cells were migrated for 4 h and the nonmigrated cells on the top surface of the membrane were removed by wiping with a cotton swab. The migrated cells on the lower side of the membrane were fixed with cold 4% paraformaldehyde for 1 h and then stained with hematoxylin and eosin (H&E). Chemotaxis was quantified by manually counting the migrated cells with inverted microscope at $\times 200$ magnification. Four independent areas were counted for each assay.

2.2.2. Apoptosis Analysis by Annexin V/Propidium Iodide (PI), Hoechst 33342, and DNA Ladder. Vitexicarpin-induced apoptotic death of HUVECs was detected by Annexin V and PI staining and flow cytometry. After vitexicarpin treatment, floating and adherent cells were collected and washed with PBS twice, and stained by using Vybrant Apoptosis Assay Kit (Invitrogen) following the standard protocol provided by the manufacturer. After staining, apoptotic cells were quantified by flow cytometry and examined using Olympus fluorescence microscope. The rates of early-stage apoptosis cells were demonstrated to be Annexin V positive and PI negative. Vitexicarpin-induced DNA condensation of apoptotic cells was assessed by Hoechst 33342 staining. HUVECs were starved with 0.1% FBS culture medium and then treated with or without VEGF (10 ng/mL) and different concentrations of vitexicarpin. After incubation for another 12 h, both floating and adherent cells were pooled and stained with Hoechst 33342 (Molecular Probes, Eugene, OR). The nuclei of apoptotic cells with characteristic nuclear fragmentation were counted in randomly chosen fields using an Olympus fluorescence microscope and expressed as a percentage of the total cell number. For assays of DNA ladder, cells were collected and lysed. RNase was added to the lysate and incubated for 30 minutes at 37°C. Proteinase K and SDS were added, followed by incubation at 50°C for 16 hours. DNA was extracted, precipitated, and electrophoresed. The stained gel was visualized by ultraviolet (UV) light and photographed.

2.3. Ex and In Vivo Angiogenesis Assay

2.3.1. Tube Formation Assay. A matrigel tube formation assay was performed to assess *ex vivo* angiogenesis. Growth

factor-reduced Matrigel was thawed at 4°C and placed in prechilled 24-well culture plates (200 µL/well) and set at 37°C for 30 min. The tube formation assay was performed employing HUVECs within six passages. A suspension of 5×10^4 HUVECs in 500 µL ECM (supplemented with 0.1% FBS and 10 ng/mL or 50 ng/mL VEGF) were seeded in duplicate into Matrigel-precoated 24-well plates in the presence of different concentrations of vitexicarpin. After 16 h of interventions, the cultures were photographed using $\times 40$ Olympus inverted microscope. The length of the tube was calculated by importing digital images into NIH ImageJ. Inhibition percentage was expressed using solvent control as 100%.

2.3.2. CAM Assay. As described by Richardson and Singh [31], fertilized White Leghorn chicken eggs (8 per group) were incubated at 37°C at constant humidity. On day 3, a square window was opened in the shell after removal of 2–3 mL of albumen in order to detach the developing CAM from the shell. The window was sealed with a glass, and the eggs were returned to the incubator. On day 8, growing CAMs were treated as follows: 1 mm³ sterilized gelatin sponges were implanted on top of the growing CAMs and adsorbed with 2 µL PBS with 0.1% DMSO as vehicle control, 2 µL PBS containing 50 ng VEGF as angiogenic model control, 2 µL PBS admixed to VEGF and VIT at 0.1 µM to 5 µM. At day 12, CAMs fixed with Bouin’s fluid were photographed with a stereomicroscope equipped with a CCD camera and image analyser system (Olympus). The angiogenic response was assessed as the number of vessels converging toward the sponges.

2.3.3. Allograft Model. Murine sarcoma S180 cells (1×10^7 cells/body) were suspended in a mixture of DPBS and Matrigel (BD BioSciences, San Jose, CA, USA) and subcutaneously implanted into the axilla of female Kunming mice (3-month old, 15–25 g) from Experimental Animal Center of the Academy of Military Medical Sciences (Beijing, China) on day 0. Tumor-bearing animals were randomized into vehicle or vitexicarpin treatment groups (10 mice per group) on day 1. Mice were injected intraperitoneally with vehicle (Normal saline, NS) or dilutions of vitexicarpin (100, 150 mg/kg body weight, dissolved 70% DMSO and 30% NS) on every other day for 2 weeks. Mice were monitored daily and tumor volumes were measured twice weekly. Tumors were harvested after two weeks and either formalin-fixed and paraffin-embedded and snap-frozen for H&E staining and immunohistochemical analysis.

2.4. Western Blot and Gelatin Zymography. Cell lysates were prepared in 100 µL of denaturing lysis buffer (2% SDS, 50 mM Tris, 2 mM EDTA). The protein extracts were subjected to SDS-PAGE and transferred to a nitrocellulose membrane (Pall Corp.). After the transfer, the membranes were incubated with blocking solution and probed with various antibodies followed by washing. Protein levels were assessed by immunoblotting with the specific antibodies and detected by the chemiluminescence detection system. Anti-AKT1, anti-phospho-AKT1, anti-SRC, anti-phospho-SRC,

anti-procaspase3, anti-procaspase7, anti-PARP, anti-cleaved-PARP, and anti- β -actin antibodies were purchased from Cell Signaling Technology.

Gelatin zymography was used to examine the activity of MMP2. All media were collected and subjected to SDS-PAGE using 0.01% w/v gelatin containing 10% polyacrylamide gel. After electrophoresis, the gels were equilibrated in 50 mM Tris-HCl (pH 7.5) with 2.5% Triton X-100 for 30 min at room temperature. Gels were then incubated at 37°C for 20 h in an incubation buffer [50 mM Tris-HCl (pH 7.5), 150 mM NaCl, and 10 mM CaCl₂, 1 mM ZnCl₂ and 0.02% NaN₃], and then stained with 0.25% Coomassie Blue R250.

2.5. The Target Network of Vitexicarpin and Functional Analysis. The target-related proteins of vitexicarpin were predicted using the drugCIPHER-CS step in our drugCIPHER method, whose good performance on target prediction was demonstrated in our previous work [29]. Briefly, based on the “Like attracts like” rationale, the drugCIPHER method predicts the target profile for a given compound mainly by correlating the drug similarity network around this compound and genome-wide proteins in the protein-protein interaction network. The drugCIPHER score refers to the likelihood of compound-target interaction calculated from the correlation between the query compound’s structure similarity vector in the drug space and the target-related gene’s functional similarity vector in the target space. The resulting target proteins with high likelihoods are considered as the potential drug targets. In this study, we obtain the known drug-target interactions from DrugBank (version: January, 2012) [32]. The chemical structure relation is calculated based on Tanimoto coefficient [33]. The human protein interaction network is constructed from HPRD [34], BIND [35], IntAct [36], MINT [37], and OPHID [38]. The assumption is that drugs with similar target profiles predicted by drugCIPHER may target a common network. In order to construct the target network of VIT when inhibiting VEGF-induced angiogenesis, we selected FDA-approved drugs whose target proteins can fall into the VEGF pathway defined by KEGG. Then, we used the Pearson’s linear correlation coefficient between the predicted target profiles of each selected drug and vitexicarpin as a measure of drugCIPHER-based compound-drug similarity. It is calculated by the following equations

$$r = \frac{N(\sum XY) - (\sum X)(\sum Y)}{\sqrt{[N\sum X^2 - (\sum X)^2][N\sum Y^2 - (\sum Y)^2]}} \quad (1)$$

where X , Y denote the drugCIPHER-CS score of vitexicarpin and FDA-approved drugs, respectively, and N is the total number of proteins in the target profiles.

For functional analysis, we use DAVID web server to analyze the enriched KEGG pathways for the top 10% target-related proteins of vitexicarpin with a false discovery rate less than 0.05 by the Fisher Exact test [39]. We only selected the KEGG pathways with P value less than 0.05 after Bonferroni’s correction.

2.6. Docking Analysis. The high-resolution protein structures of SRC and AKT1 were obtained from the refined X-ray

crystal structure of 2H8H.pdb and 3MVH.pdb, which is available from the Protein Data Bank. The Autodock 4.0 suite of programs uses an automated docking approach that allows ligand flexibility as described to a full extent elsewhere [40]. Default parameters were used as described in the AutoDock manual. The protein structure was prepared using the PyMol and AutoDockTools and used for flexible docking studies with AutoDock 4.0 after extraction of the crystal ligand.

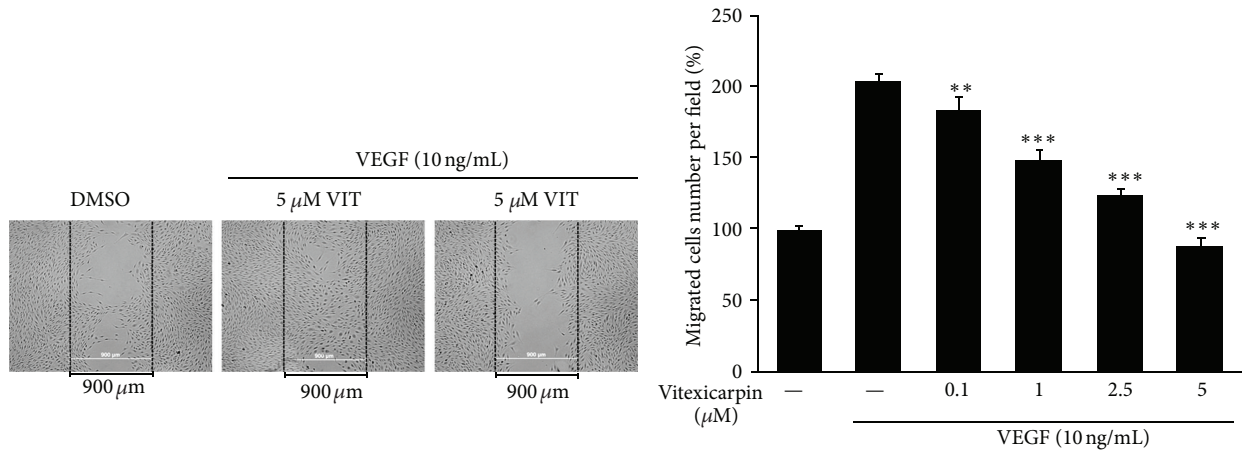
2.7. Statistical Analysis. The data are presented as mean \pm SD, and statistical comparisons between groups were performed using Student’s t -test. $P < 0.05$ was considered statistically significant.

3. Results

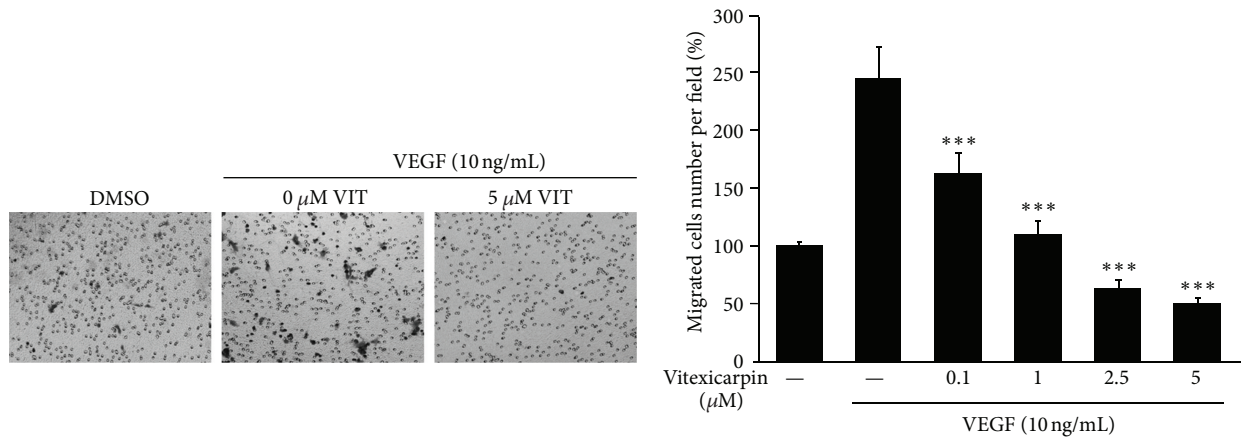
3.1. Vitexicarpin Inhibits VEGF-Induced Lateral, Longitudinal Migration and Tube Formation of Endothelial Cells. To evaluate the effect of vitexicarpin on VEGF-stimulated endothelial cell migration, wound healing and transwell cell migration assays were performed to explore whether vitexicarpin could inhibit the VEGF-induced motility of HUVECs. As shown in Figure 2(a), vitexicarpin inhibits VEGF-induced HUVECs migration in a concentration-dependent manner, with half-maximal inhibition at $\sim 2.5 \mu\text{M}$. Vitexicarpin significantly inhibited VEGF-induced lateral migration and decreased wound healing potential at $5 \mu\text{M}$ (Figure 2(a)). Next, the effects of vitexicarpin on the longitudinal migration of endothelial cells were investigated using transwell assays. The number of HUVECs that migrated in the Transwell assay was higher in the presence of VEGF than in the control. At $0.1 \mu\text{M}$, vitexicarpin reduced the longitudinal EC migration induced by VEGF (Figure 2(b)). These results suggested that vitexicarpin inhibited cell migration by inhibiting the SRC pathway downstream protein kinase activities.

To examine the potential effects of vitexicarpin on the capillary structure formation of endothelial cells, we investigated how vitexicarpin affects VEGF-induced tube formation using a Matrigel assay. When HUVECs are seeded on Matrigel, they should form elongated and robust capillary-like structures. This phenomenon can be facilitated by the proangiogenic factor VEGF, whereas vitexicarpin effectively blocked the VEGF-induced tube formation after 16 h of incubation (Figure 2(c)). $0.1 \mu\text{M}$ vitexicarpin partly inhibited endothelial tube formation on Matrigel and $1 \mu\text{M}$ vitexicarpin completely blocked the formation of the tubular structures. To further understand the inhibitory effects of vitexicarpin on tube formation, we also examined the effect of vitexicarpin on the activity of MMP2 which results in the extracellular matrix degradation and enhances tube formation. As shown in Figure 2(d), we found that vitexicarpin inhibited the activity of MMP2 and thus caused an inhibitory action of tube formation. These results demonstrated that vitexicarpin can block VEGF-induced *in vitro* and *ex vivo* angiogenesis by inhibiting lateral, longitudinal migration and tube formation of endothelial cells.

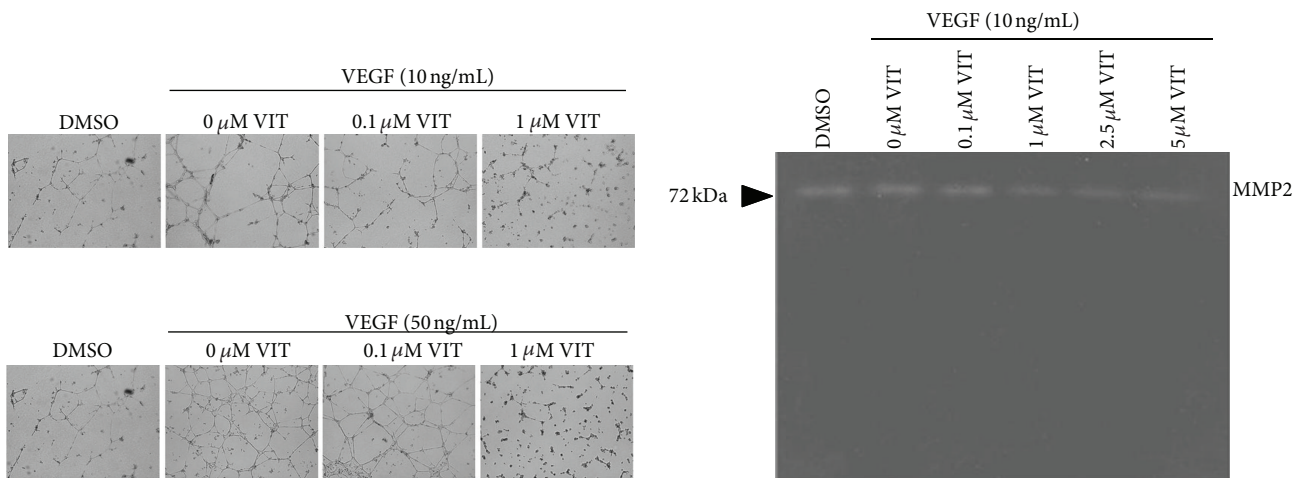
3.2. Vitexicarpin Inhibits VEGF-Induced HUVECs Proliferation and Induces Cell Cycle Arrest. To evaluate the antiproliferative effect of vitexicarpin on VEGF-stimulated endothelial



(a)



(b)



(c)

(d)

FIGURE 2: Vitexicarpin inhibits VEGF-induced migration and tube formation. Vitexicarpin at a range of concentrations (0.1 μM –5 μM) concentration dependently inhibits HUVEC migration caused by wound healing (a) and HUVEC invasion using transwell chamber chemotaxis assay (b). (c) Vitexicarpin inhibits VEGF-induced tube formation of HUVECs. Representative results of HUVECs on Matrigel in the absence or presence of 10 ng/mL or 50 ng/mL VEGF plus different concentrations of vitexicarpin. (d) Vitexicarpin inhibits the enzyme activity of MMP2. Gel Zymography analysis of the effect of vitexicarpin on MMP2 activity. ** $P < 0.01$; *** $P < 0.001$ compared with VEGF group. Error bars represent \pm SD of experiments.

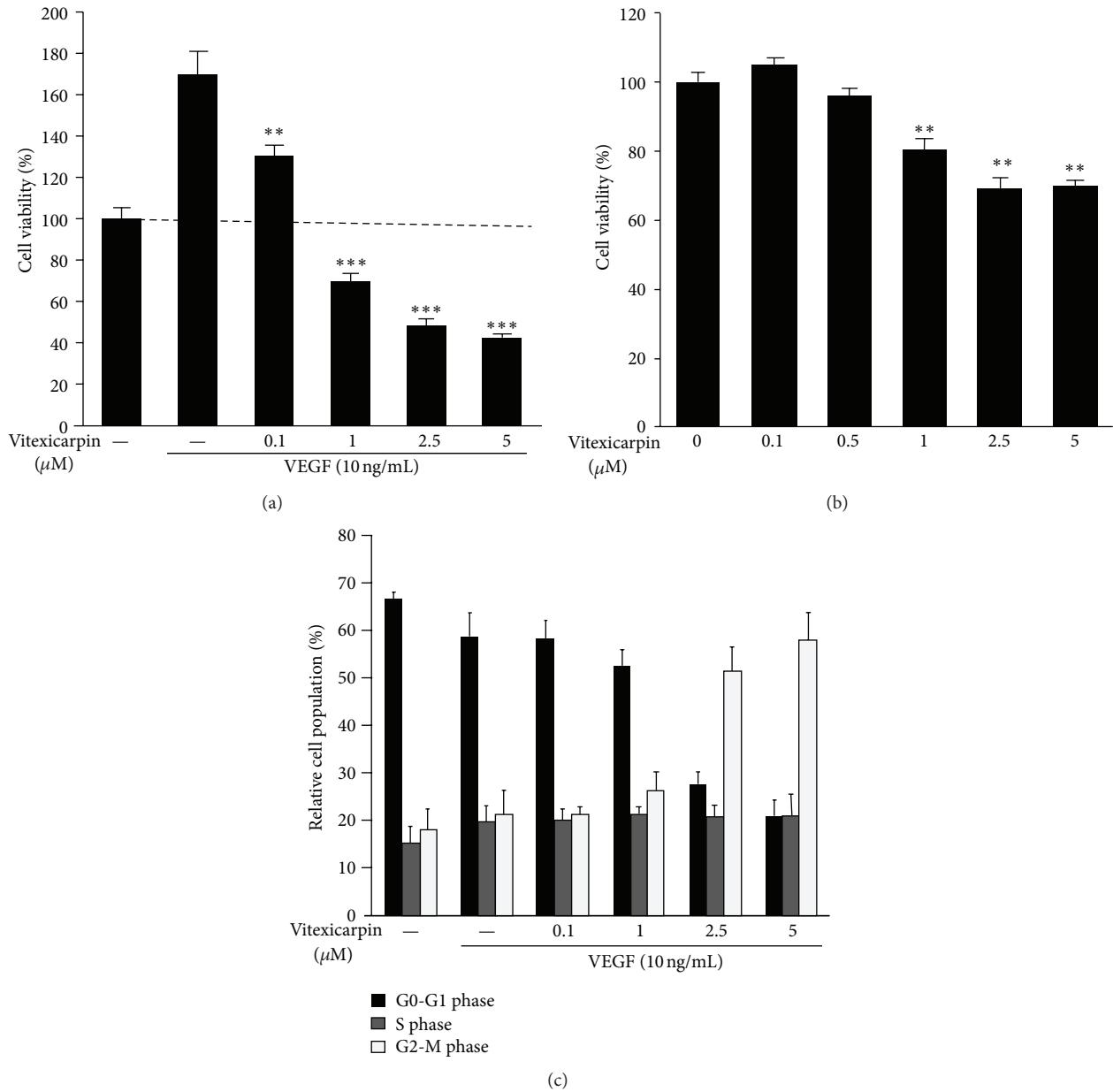


FIGURE 3: Vitexicarpin inhibits VEGF-induced proliferation of endothelial cells. (a) Vitexicarpin inhibits VEGF-induced endothelial cells viability in a dose-dependent manner. Cell viability was quantified by CCK-8 assay. (b) Effects of vitexicarpin at indicated concentrations on endothelial cells viability under normal culture conditions. (c) Cell cycle analysis showing G2/M arrest in cells treated with vitexicarpin at indicated concentrations. ** $P < 0.01$; *** $P < 0.001$ compared with VEGF control.

cells, we examined the inhibitory effects of vitexicarpin on the viability of HUVECs stimulated with VEGF165 by using CCK-8. HUVECs (2×10^4 cells/well) were incubated for 24 h in 96-well microplates with various final concentrations of vitexicarpin (0, 0.1, 1, 2.5, and 5 μM). As shown in Figure 3(a), vitexicarpin can significantly inhibit VEGF-mediated HUVECs viability at concentrations as low as 1 μM , with an IC_{50} of approximately 2.5 μM . As a solvent control, we also examined the effect of 0.1% DMSO on cell viability. Upon supplementation of the culture medium with 0.1% DMSO, our data indicated that 0.1% DMSO has no effects on HUVEC proliferation and viability. The

cytotoxic activity of vitexicarpin against HUVECs was assessed without the supplementation of proangiogenic factors in 5% FBS-containing endothelial cell medium (condition did not support proliferation). Vitexicarpin treatment at 5 μM for 24 h only decreased the percentage of metabolically viable HUVECs by approximately 25% (Figure 3(b)). To assess whether vitexicarpin regulated cell cycle progression, we additionally performed PI analysis by FACS. After HUVECs were treated with 10 ng/mL VEGF in the presence or absence of various concentrations of vitexicarpin for 24 h, the percentage of cells in G0/G1, S, and G2-M phases was monitored. Vitexicarpin reduced the percentage

of G0–G1 phase cell from 59.24 to 19.81%, and a concomitant accumulation of cells in G2-M phase from 20.98 to 59.55% was observed. VEGF induced HUVECs to enter S phase, whereas the addition of vitexicarpin did not reduce S phase entry (Figure 3(c)). These results suggest that vitexicarpin could arrest the cell cycle progression.

3.3. Vitexicarpin Induced the Apoptotic Death of HUVECs.

To verify the proapoptotic effects of vitexicarpin on VEGF-stimulated HUVECs, we evaluated the apoptotic cell death effect of vitexicarpin by annexin V-PI staining and flow cytometry, in which only annexin V-stained cells were considered as early apoptotic cells (Figure 4(a)). We also visualized the apoptotic effects of vitexicarpin by using Hoechst 33342 staining. HUVECs were treated with a range of concentrations of the vitexicarpin for 24 h. Examination of the HUVECs upon vitexicarpin treatment revealed that the appearance of morphologic characteristics of apoptosis, such as plasma membrane disintegration, chromatin condensation, and nuclear fragmentation, was significantly induced by 1 μ M vitexicarpin, as indicated in Figure 4(b). These results suggest that vitexicarpin induces early-stage apoptosis in HUVECs in the presence of VEGF. DNA electrophoresis using samples isolated from vitexicarpin (5 μ M)-treated HUVECs confirmed DNA fragmentation (Figure 4(c)). To gain more insight into how vitexicarpin induces apoptosis in endothelial cells, we pretreated cells with the pan-caspase inhibitor Z-VAD-fmk. This inhibitor reduced the percentage of annexin V-positive cells among vitexicarpin-induced apoptotic HUVECs, indicating that the classical caspase pathway was required for the apoptosis induced by vitexicarpin (Figure 4(a)). The potential mechanisms of vitexicarpin-mediated apoptosis were explored by Western blot analysis of some of the proteins involved in the apoptotic process (Figure 4(d)). A clear decrease in pro-caspase-3 and pro-caspase-7 expression was observed using 2.5 μ M and 5 μ M vitexicarpin, respectively. We also observed a concentration-dependent increase in the expression of the cleaved-poly (ADP-ribose) polymerase (PARP). These results demonstrated that vitexicarpin inhibited proliferation and induced early and late apoptosis in VEGF-induced HUVECs.

3.4. Vitexicarpin Inhibits VEGF-Induced Angiogenesis Ex and In Vivo .

To assess the effect of vitexicarpin on angiogenesis *in vivo*, blood vessel growth was stimulated on the chorioallantoic membranes (CAMs) with VEGF in the presence or absence of different concentrations of vitexicarpin (0.1–5 μ M). This assay measures developmental angiogenesis, and it is routinely used to obtain the first indication of angiogenic activity *in vivo*. VEGF induced a robust angiogenic response, whereas vitexicarpin disrupted VEGF-mediated angiogenesis (Figure 5(a), right panel). Quantitative analysis revealed that VEGF caused a 3.2-fold increase in the number of newly formed blood vessels compared with that of medium alone (Figure 5(a), left panel; $P < 0.001$). The development of vasculature at day 10 treated with 0.1 μ M, 1 μ M, 2.5 μ M, and 5 μ M vitexicarpin caused a 24, 36, 45, and 84% reduction in the infiltration of blood vessels, respectively. These

results suggested that vitexicarpin is a potent antiangiogenic molecule *ex vivo*.

To examine the inhibitory effect of vitexicarpin on tumor angiogenesis and growth, we used an allograft mouse tumor model. The primary tumors (after 14 days) were dissected, fixed, and imbedded. Tumors from the mice with vitexicarpin treatment were smaller than that from NS group, suggesting that vitexicarpin inhibits tumor growth *in vivo*. H&E staining showed that treatment of tumors with vitexicarpin appeared to increase the extent of necrosis within tumor (Figure 5(b)). Furthermore, there were profound differences in the number of blood vessels in the tumor tissue from NS and vitexicarpin group (Figure 5(b)). Based on anti-CD31 staining, microvessel density (MVD) in tumor tissue from NS group was 34.4 ± 4.4 mm²/field, whereas that in vitexicarpin-treated group was 10 ± 2.7 mm²/field (P value = $6.14E - 06$; Figure 5(b)), indicating that vitexicarpin significantly inhibited tumor angiogenesis.

3.5. Predicted Target Profiles Reveal the Antitumor and Antiangiogenic Activities of Vitexicarpin.

To identify the target-related proteins of vitexicarpin, we used drugCIPHER-CS [29] to calculate its likelihood to bind to all the 13,388 proteins in the interaction network. Here we only assembled and ranked the 2,039 druggable proteins which are often known targets in the DrugBank. 204 target proteins (top 10%) represented the potential targets of vitexicarpin.

Enrichment analysis helps to better understand the biological functions of target proteins and pathways involved in the activities of vitexicarpin. By establishing a set of the known angiogenesis-related drug targets (i.e., the known targets of angiogenic drugs in DrugBank), we found that top 10% target proteins are significantly enriched in the set of known angiogenesis-related drug targets ($P = 3.63E - 05$). By using top 10% targets of vitexicarpin, we also found significantly enriched KEGG pathways vitexicarpin may affect cancer-related pathways (e.g., Non-small cell lung cancer, Prostate cancer, Glioma, Pathways in cancer, etc.), T cell receptor signaling pathway, and VEGF signaling pathway. Interestingly, it has been previously reported that vitexicarpin exhibits broad cytotoxicity against human cancer cell lines and exerts an inhibitory effect on T-lymphocyte proliferation. The comparison results with literature suggest that target profiles predicted by drugCIPHER can reveal the polypharmacological activities of vitexicarpin.

3.6. Target Network Prediction and Validation of Vitexicarpin When Inhibiting Angiogenesis.

Having shown that the target profiles predicted by drugCIPHER can help improve the capacity to comprehensively understand the mechanisms of herbal compounds, we further set out to elucidate the Antiangiogenic mechanisms of vitexicarpin by network pharmacology approach. According to the principle of drugCIPHER, we identified the possible target network by which vitexicarpin can exert inhibition effects on VEGF-induced angiogenesis. First, we collected 58 FDA-approved drugs directly targeting 18 proteins which can fall into the VEGF pathway. Among the 18 proteins, 11 of them can link together into one network

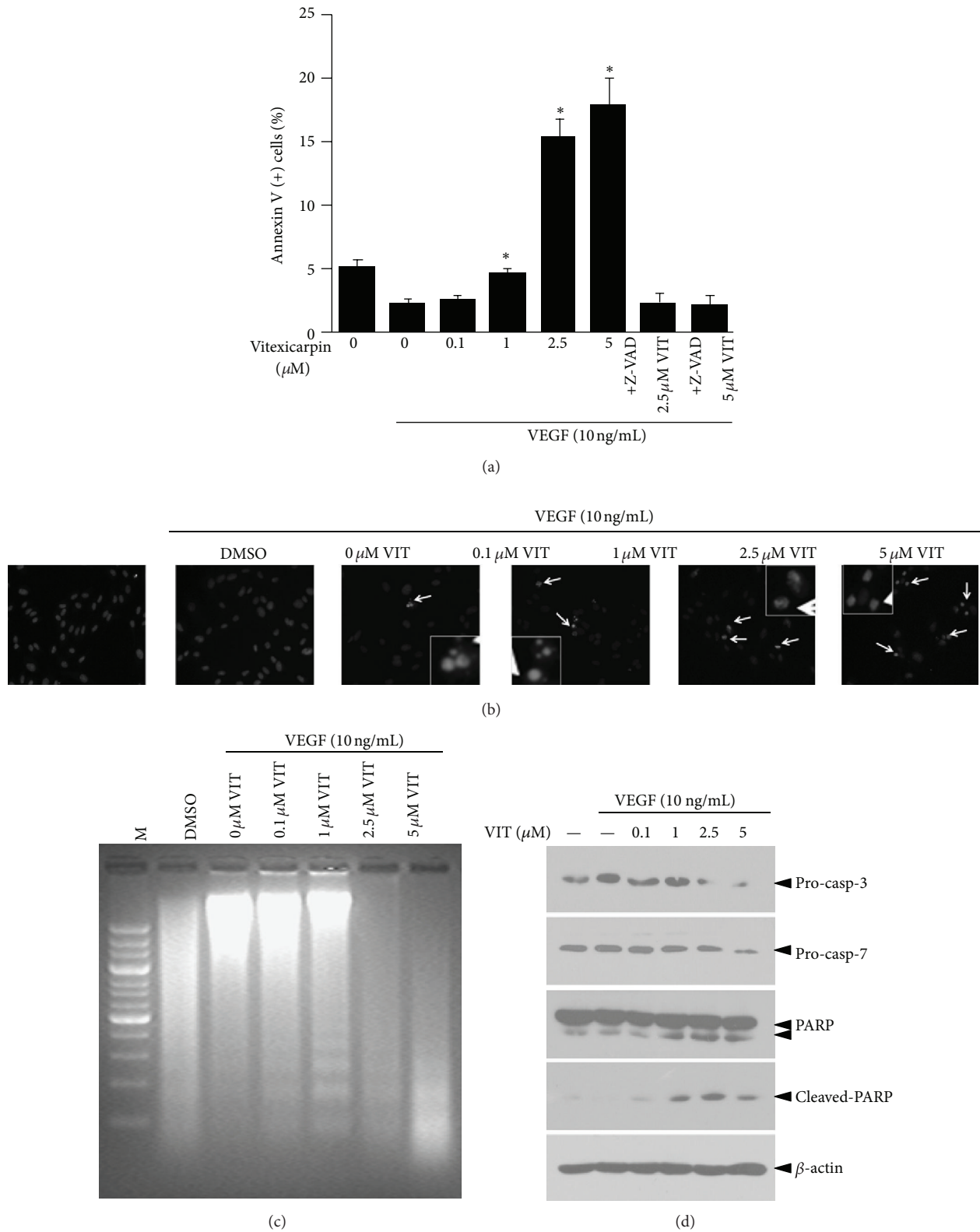
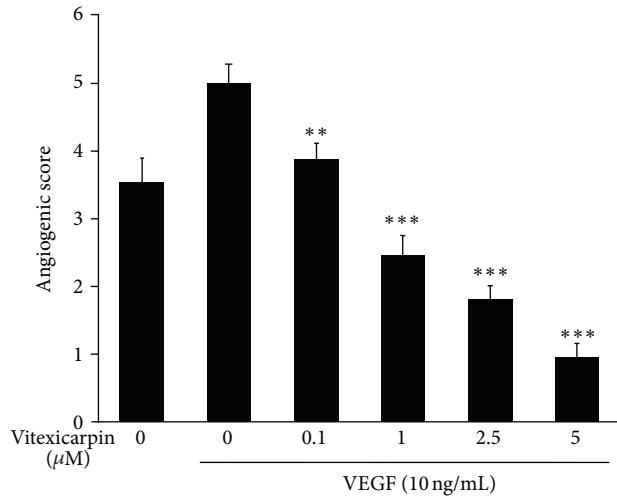
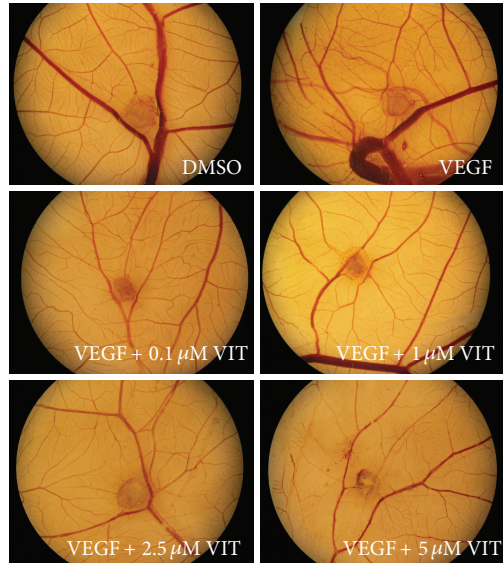
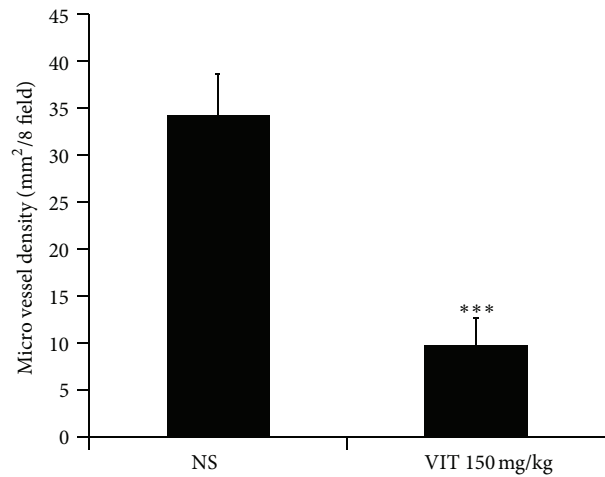
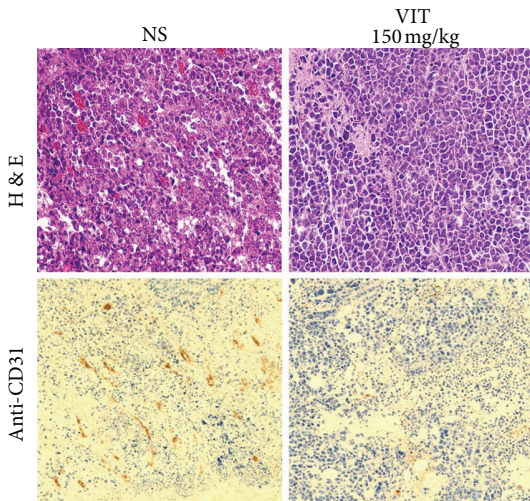


FIGURE 4: Vitexicarpin induces apoptosis of VEGF-stimulated endothelial cells. (a) Vitexicarpin increases annexin V (+) cells at indicated concentrations. (b) Hoechst 33342 staining of apoptotic endothelial cells. Cells are magnified in inset figure. (c) DNA fragment in endothelial cells treated with vitexicarpin at indicated concentrations for 12 h. (d) Effects of vitexicarpin on pro-casp-3, pro-casp-7, PARP, and cleaved-PARP. β -actin is used as a loading control. ** $P < 0.01$; *** $P < 0.001$ compared with VEGF group.



(a)



(b)

FIGURE 5: Vitexicarpin inhibits VEGF-induced angiogenesis *ex vivo* and *in vivo*. (a) Vitexicarpin inhibits VEGF-induced angiogenesis in the CAM assay *in vivo*. In comparison to DMSO group, the application of VEGF (10 ng/mL) induced a strong vascularization. In contrast, the simultaneous application of VEGF and vitexicarpin blocked VEGF-induced angiogenesis. ** $P < 0.01$; *** $P < 0.001$ compared with VEGF group; bars, \pm SD. (b) H&E staining (upper panels) and anti-CD31 stained blood vessels (lower panels) of tumor sections from NS and vitexicarpin (150 mg/kg). Vitexicarpin inhibits tumor angiogenesis in allograft mouse tumor model. All images, $\times 200$ magnification. *** $P < 0.001$ compared with NS group; Error bars, \pm SD.

through direct protein physical interaction at the protein interaction level (Figure 6(a)). Then, we calculated the correlations between 58 FDA-approved drugs' and vitexicarpin's profiles. Direct target proteins of FDA-approved drugs that tend to be more similar to vitexicarpin in profile clustering are the potential targets of vitexicarpin. We therefore reasoned that a specific network that can connect all the direct target proteins of drugs with profiles highly similar to vitexicarpin could be used to estimate its possible targeting functional

network, for example, VEGF pathway. Using this principle, we identified the target network composed of 11 proteins, suggesting that vitexicarpin can achieve the Antiangiogenic effects through targeting key molecules in this network target embedded in the VEGF pathway (Figure 6(a)).

To preliminarily assess the predicted targets of vitexicarpin, we selected two key kinase molecules in VEGF-induced ECs migration and proliferation pathways, SRC and AKT, whose drugCIPHER scores are ranked top 2 in this

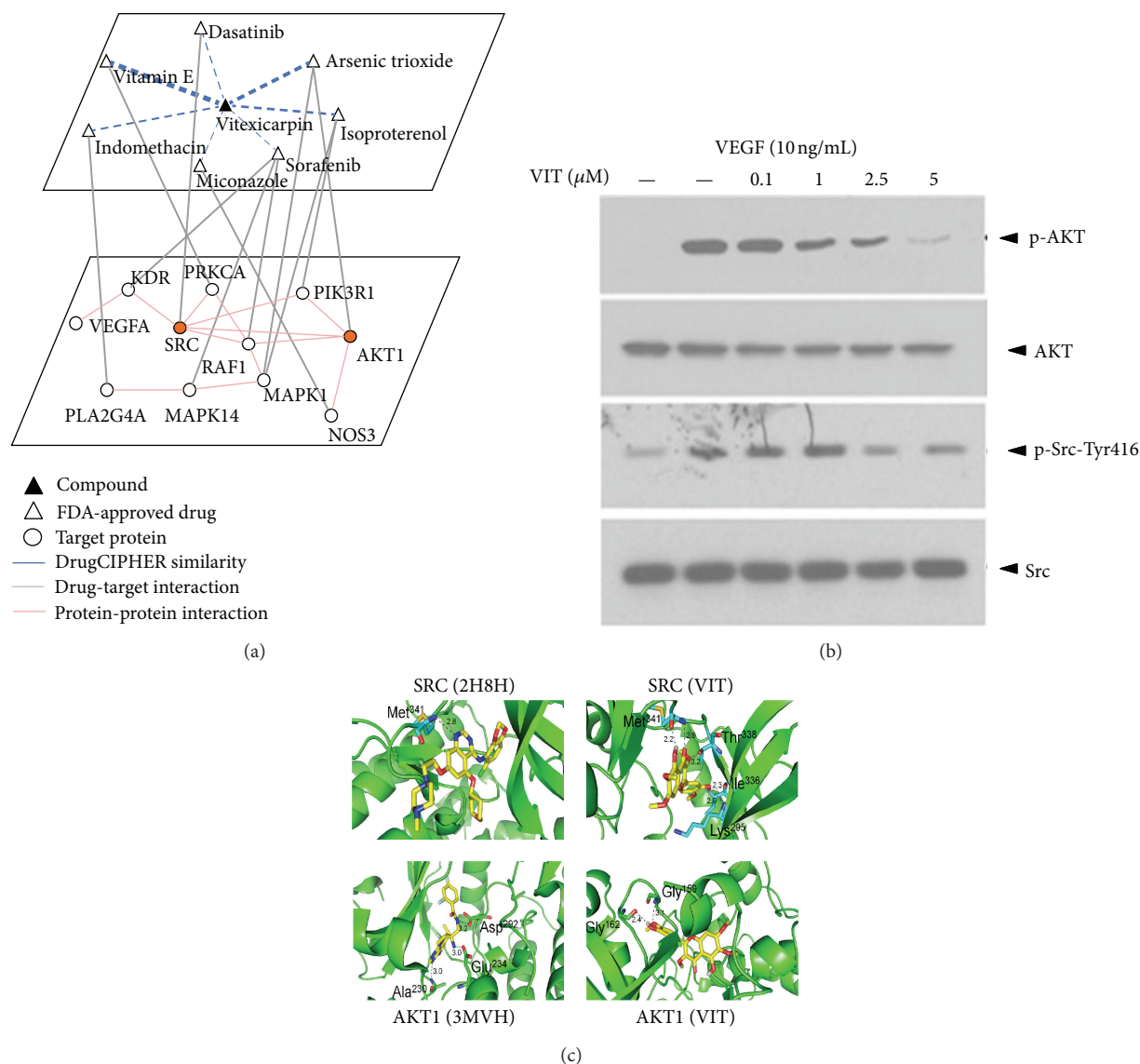


FIGURE 6: The constructed target angiogenesis-related network of vitexicarpin and experimental validation of two key molecules. (a) Network diagram showing vitexicarpin targeting network when inhibiting angiogenesis. The dot line thickness denoted by drugCIPHER similarities is the drugCIPHER scores' correlation coefficients between drugs and vitexicarpin. (b) Western blot analysis was performed to examine the changes of phosphoprotein levels of p-SRC and p-AKT in the vitexicarpin-treated HUVECs. Proteins were extracted from the cultured HUVEC at 30 min after vitexicarpin treatment and probed with proper dilutions of specific antibodies. Vitexicarpin inhibits VEGF-induced p-SRC and p-AKT phosphorylation in a dose-dependent manner. (c) Comparison of binding interactions of quinazoline inhibitor (PDB 2H8H) and vitexicarpin with SRC kinase (upper panel) and comparison of binding interactions of WFE (PDB 3MVH) and vitexicarpin with AKT1 (lower panel). Vitexicarpin is in stick. Carbon atom for vitexicarpin (yellow). Hydrogen bonds are displayed (dark dashed lines). The value on the dashed lines denotes the distance (Å) of H-bonds.

network target. The experimental results demonstrated that VEGF significantly increased SRC kinase phosphorylation at Tyr416, but this increase was blocked by vitexicarpin in a concentration-dependent manner (Figure 6(b)). Half-maximal effects were obtained at a concentration of $\sim 2.5 \mu\text{M}$. Consistently, AKT1, which is a key signal mediator in VEGF-stimulated HUVECs, was phosphorylated by VEGF, and AKT1 activation was suppressed by vitexicarpin in a concentration-dependent manner (Figure 6(b)). The result showed that vitexicarpin significantly inhibited VEGF-induced cell

migration and proliferation and induced apoptosis through inhibition of the SRC and AKT pathway downstream molecules.

To evaluate the possibility of SRC and AKT1 as the direct targets of vitexicarpin, we performed docking analysis to examine the mode of vitexicarpin-binding SRC and AKT1. The available X-ray crystal structures of kinases from the PDB database were used for validation of target prediction results. We found that the binding energy of vitexicarpin with SRC and AKT1 is -9.23 kcal/mol and -9.21 kcal/mol ,

respectively. Vitexicarpin was docked into the ligand-binding sites and occupied the hydrophobic pocket of SRC and AKT1 (Figure 6(c)). Compared to published complex of SRC (2H8H), vitexicarpin was able to maintain five hydrogen bonds with Met³⁴¹, Lys²⁹⁵, Ile³³⁶, and Thr³³⁸ at the active site of SRC. In addition, the vitexicarpin/AKT1 model generated two hydrogen bonds with Gly¹⁵⁹ and Gly¹⁶² and two π - π interactions compared with AKT1 complex (3MVH). These results indicate the potential of SRC and AKT1 as direct targets of vitexicarpin, which deserve further experimental verifications.

4. Discussion

In recent years, substantial effort has been dedicated to identifying Antiangiogenic agents from TCM herbs [4, 41]. Vitexicarpin is a bioactive flavonoid from *V. rotundifolia*, which can inhibit tumor growth and inflammation. However, little information is known about its functions in angiogenesis. In this study, we demonstrate that vitexicarpin (0.1–5 μ M) exhibited Antiangiogenic activities *in vitro*, as shown in the results of endothelial cells migration, proliferation, and Matrigel tube formation assays (Figures 2 and 3). Further studies using flow cytometric analysis, DNA fragment, and caspase-3 blotting indicated that vitexicarpin (0.1–5 μ M) inhibited ECs proliferation via cell cycle arrest and induction of apoptosis (Figure 4). Consistent with our *in vitro* results, 5 μ M vitexicarpin inhibited the angiogenesis sprouting from CAM (Figure 5(a)). In addition, vitexicarpin impaired vascularization in allograft mouse tumor model (Figure 5(b)). It should be noted that therapeutic effects of Man Jing Zi as an antiarthritis herb, described in Ri-Hua-Zi-Ben-Cao, are deciphered by the Antiangiogenic activity of vitexicarpin.

At present, one of the major challenges in the use of herbal compounds in drug discovery is the unexpected interactions with on-target and off-target proteins due to the less specific binding characteristics of small molecules [18, 42]. In addition, herbal compounds have more complex stereochemical and physicochemical properties compared to synthetic small molecules [18, 43]. Thus, exploiting the promiscuous targets of herbal compounds enables a deeper understanding of the global perturbation of these compounds induced at the molecular level [44, 45]. Now, an important task is to elucidate how these herbal compounds perturb these pathways by computationally modeling their interactions with their target proteins [46]. Here, we show that unbiased target profiles can be systematically predicted through integrating chemical similarity information and the relatedness of drug targets in the protein-protein interaction network. The target profiles identified by drugCIPHER [29] can provide a comprehensive understanding of the pharmacology effects and side effects or toxicities for a given herbal compound with rigid chemical structure. Computational scoring of target proteins using our approach led to the identification of vitexicarpin-interacting proteins at a genome-wide level. The method is cost effective, highly flexible, and applicable to all kinds of herbal compounds with known chemical structure, and it can be used with mechanisms analysis of any herbal compounds or TCM formulae of interest.

The top 10% target-related proteins of vitexicarpin are significantly enriched in the 38 KEGG pathways. 14 cancer-related pathways and T cell receptor signaling pathway exactly account for the known biological functions of vitexicarpin. Interestingly, VEGF signaling pathway can partly elaborate the Antiangiogenic mechanisms of vitexicarpin, consistent with our experimental results. Of the remaining pathways, Neurotrophin signaling pathway, Insulin signaling pathway, and Type II diabetes mellitus are enriched by target-related proteins of vitexicarpin, suggesting that it may be potentially used for the diabetes therapy. Thus, vitexicarpin's result provides an example of how "target profiles" predicted by drugCIPHER can comprehensively shed light on the mechanisms of action of herbal compounds.

The available target profile makes it possible to infer the mechanism of a herbal compound of interest by comparing profiles with existing FDA-approved drugs. As shown in Figure 6(a), drugs such as vitamin E, dasatinib, arsenic trioxide, isoproterenol, sorafenib, and indomethacin have similar target profiles with vitexicarpin and these drugs also show certain Antiangiogenic activities [47–52]. The drugCIPHER method can give the measurement of compound-protein associations, including information on direct protein physical interactions and functional interactions. Recent work has shown that drug's effects can pass either within a protein or across several proteins, to achieve specific interactions (enhance or inhibit) along a network [53]. Therefore, functionally interacting proteins with the compounds may be close to directly interacting proteins in the network. In this study, we show that vitexicarpin can inhibit the phosphorylation of SRC and AKT, which partly elucidate the Antiangiogenic action of vitexicarpin, although the direct targets of vitexicarpin are still uncertain and need further investigation.

In summary, this work suggests that vitexicarpin is an angiogenesis inhibitor *in vitro* and *in vivo*. We successfully applied drugCIPHER to predict and experimentally validate key proteins SRC and AKT in the target network of vitexicarpin, revealing a previously unreported anti-angiogenesis molecular basis of vitexicarpin on vascular endothelial cell migration, apoptosis, and proliferation. This work also highlights the considerable potential for future herb medicine researches in terms of TCM network pharmacology.

Conflict of Interests

The authors declare that they have no conflict of interests.

Acknowledgments

This work is supported by the National Natural Science Foundation of China (nos. 81225025, 60934004, and 61021063) and CATCM project.

References

- [1] R. K. Jain, "Normalizing tumor vasculature with anti-angiogenic therapy: a new paradigm for combination therapy," *Nature Medicine*, vol. 7, no. 9, pp. 987–989, 2001.

- [2] P. Carmeliet, "Angiogenesis in life, disease and medicine," *Nature*, vol. 438, no. 7070, pp. 932–936, 2005.
- [3] S. Wang, Z. Zheng, Y. Weng et al., "Angiogenesis and anti-angiogenesis activity of Chinese medicinal herbal extracts," *Life Sciences*, vol. 74, no. 20, pp. 2467–2478, 2004.
- [4] T. P. Fan, J. C. Yeh, K. W. Leung, P. Y. K. Yue, and R. N. S. Wong, "Angiogenesis: from plants to blood vessels," *Trends in Pharmacological Sciences*, vol. 27, no. 6, pp. 297–309, 2006.
- [5] M. Mochizuki, Yung Choon Yoo, K. Matsuzawa et al., "Inhibitory effect of tumor metastasis in mice by saponins, ginsenoside-Rb2, 20(R)- and 20(S)-ginsenoside-Rg3, of Red ginseng," *Biological and Pharmaceutical Bulletin*, vol. 18, no. 9, pp. 1197–1202, 1995.
- [6] M. W. Chen, L. Yang, L. Ni, and C. Huang, "The effects of 20(R)-Rg3 on lung carcinoma A549 cell line and endogenous VEGF secreted by tumor cells," *Journal of Sichuan University*, vol. 37, no. 1, pp. 60–62, 2006.
- [7] K. B. Hu, Z. H. Liu, D. Liu, and L. S. Li, "Inhibition of vascular endothelial growth factor expression and production by triptolide," *Planta Medica*, vol. 68, no. 4, pp. 368–369, 2002.
- [8] B. Wang, L. Ma, X. Tao, and P. E. Lipsky, "Triptolide, an active component of the Chinese herbal remedy Tripterygium wilfordii Hook F, inhibits production of nitric oxide by decreasing inducible nitric oxide synthase gene transcription," *Arthritis and Rheumatism*, vol. 50, no. 9, pp. 2995–3003, 2004.
- [9] S. Li, A. P. Lu, Y. Y. Wang, and Y. D. Li, "Suppressive effects of a Chinese herbal medicine Qing-Luo-Yin extract on the angiogenesis of collagen-induced arthritis in rats," *American Journal of Chinese Medicine*, vol. 31, no. 5, pp. 713–720, 2003.
- [10] T. W. Kok, P. Y. K. Yue, N. K. Mak, T. P. D. Fan, L. Liu, and R. N. S. Wong, "The anti-angiogenic effect of sinomenine," *Angiogenesis*, vol. 8, no. 1, pp. 3–12, 2005.
- [11] S. Li, B. Zhang, and N. Zhang, "Network target for screening synergistic drug combinations with application to traditional Chinese medicine," *BMC Systems Biology*, vol. 5, supplement 1, article S10, 2011.
- [12] D. X. Hou and T. Kumamoto, "Flavonoids as protein kinase inhibitors for cancer chemoprevention: direct binding and molecular modeling," *Antioxidants and Redox Signaling*, vol. 13, no. 5, pp. 691–719, 2010.
- [13] F. Díaz, D. Chávez, D. Lee et al., "Cytotoxic flavone analogues of vitexicarpin, a constituent of the leaves of *Vitex negundo*," *Journal of Natural Products*, vol. 66, no. 6, pp. 865–867, 2003.
- [14] J. Kobayakawa, F. Sato-Nishimori, M. Moriyasu, and Y. Matsukawa, "G2-M arrest and antimetabolic activity mediated by casticin, a flavonoid isolated from *Vitex rotundifolia* (Linne fil.)," *Cancer Letters*, vol. 208, no. 1, pp. 59–64, 2004.
- [15] K. M. You, K. H. Son, H. W. Chang, S. S. Kang, and H. P. Kim, "Vitexicarpin, a flavonoid from the fruits of *Vitex rotundifolia*, inhibits mouse lymphocyte proliferation and growth of cell lines *in vitro*," *Planta Medica*, vol. 64, no. 6, pp. 546–550, 1998.
- [16] S. M. Lee, Y. J. Lee, Y. C. Kim, J. S. Kim, D. G. Kang, and H. S. Lee, "Vascular Protective Role of Vitexicarpin Isolated from *Vitex rotundifolia* in Human Umbilical Vein Endothelial Cells," *Inflammation*, vol. 35, pp. 584–593, 2011.
- [17] S. Li, B. Zhang, D. Jiang, Y. Wei, and N. Zhang, "Herb network construction and co-module analysis for uncovering the combination rule of traditional Chinese herbal formulae," *BMC Bioinformatics*, vol. 11, supplement 11, article S6, 2010.
- [18] I. Paterson and E. A. Anderson, "The renaissance of natural products as drug candidates," *Science*, vol. 310, no. 5747, pp. 451–453, 2005.
- [19] A. L. Hopkins, "Network pharmacology: the next paradigm in drug discovery," *Nature Chemical Biology*, vol. 4, no. 11, pp. 682–690, 2008.
- [20] J. van der Greef and R. N. McBurney, "Rescuing drug discovery: *in vivo* systems pathology and systems pharmacology," *Nature Reviews Drug Discovery*, vol. 4, no. 12, pp. 961–967, 2005.
- [21] S. I. Berger, A. Ma'ayan, and R. Iyengar, "Systems pharmacology of arrhythmias," *Science Signaling*, vol. 3, no. 118, p. ra30, 2010.
- [22] T. R. Burkard, U. Rix, F. P. Breitwieser, G. Superti-Furga, and J. Colinge, "A computational approach to analyze the mechanism of action of the kinase inhibitor bafetinib," *PLoS Computational Biology*, vol. 6, no. 11, Article ID e1001001, 2010.
- [23] X. Wu, R. Jiang, M. Q. Zhang, and S. Li, "Network-based global inference of human disease genes," *Molecular Systems Biology*, vol. 4, pp. 189–199, 2008.
- [24] A. L. Barabási, N. Gulbahce, and J. Loscalzo, "Network medicine: a network-based approach to human disease," *Nature Reviews Genetics*, vol. 12, no. 1, pp. 56–68, 2011.
- [25] S. Li, "Framework and practice of network-based studies for Chinese herbal formula," *Journal of Chinese Integrative Medicine*, vol. 5, no. 5, pp. 489–493, 2007.
- [26] S. Li, "Network systems underlying traditional Chinese medicine syndrome and herb formula," *Current Bioinformatics*, vol. 4, no. 3, pp. 188–196, 2009.
- [27] J. Zhao, P. Jiang, and W. Zhang, "Molecular networks for the study of TCM pharmacology," *Briefings in Bioinformatics*, vol. 11, no. 4, Article ID bbp063, pp. 417–430, 2009.
- [28] S. Li, "Network target: a starting point for traditional Chinese medicine network pharmacology," *Zhongguo Zhong Yao Za Zhi*, vol. 36, pp. 2017–2020, 2011.
- [29] S. Zhao and S. Li, "Network-based relating pharmacological and genomic spaces for drug target identification," *PLoS ONE*, vol. 5, no. 7, Article ID e11764, 2010.
- [30] F. A. Fierro, S. Kalomoiris, C. S. Sondergaard, and J. A. Nolte, "Effects on proliferation and differentiation of multipotent bone marrow stromal cells engineered to express growth factors for combined cell and gene therapy," *Stem Cells*, vol. 29, no. 11, pp. 1727–1737, 2011.
- [31] M. Richardson and G. Singh, "Observations on the use of the avian choriallantoic membrane (CAM) model in investigations into angiogenesis," *Current Drug Targets—Cardiovascular and Haematological Disorders*, vol. 3, no. 2, pp. 155–185, 2003.
- [32] D. S. Wishart, C. Knox, A. C. Guo et al., "DrugBank: a knowledgebase for drugs, drug actions and drug targets," *Nucleic Acids Research*, vol. 36, no. 1, pp. D901–D906, 2008.
- [33] X. Q. Xie and J. Z. Chen, "Data mining a small molecule drug screening representative subset from NIH PubChem," *Journal of Chemical Information and Modeling*, vol. 48, no. 3, pp. 465–475, 2008.
- [34] T. S. Keshava Prasad, R. Goel, K. Kandasamy et al., "Human protein reference database—2009 update," *Nucleic Acids Research*, vol. 37, no. 1, pp. D767–D772, 2009.
- [35] G. D. Bader, D. Betel, and C. W. V. Hogue, "BIND: the biomolecular interaction network database," *Nucleic Acids Research*, vol. 31, no. 1, pp. 248–250, 2003.
- [36] S. Kerrien, B. Aranda, L. Breuza et al., "The IntAct molecular interaction database in 2012," *Nucleic Acids Research*, vol. 40, no. D1, pp. D841–D846, 2012.

- [37] A. Ceol, A. Chatr Aryamontri, L. Licata et al., "MINT, the molecular interaction database: 2009 update," *Nucleic Acids Research*, vol. 38, no. 1, Article ID gkp983, pp. D532–D539, 2009.
- [38] K. R. Brown and I. Jurisica, "Online predicted human interaction database," *Bioinformatics*, vol. 21, no. 9, pp. 2076–2082, 2005.
- [39] D. W. Huang, B. T. Sherman, and R. A. Lempicki, "Systematic and integrative analysis of large gene lists using DAVID bioinformatics resources," *Nature Protocols*, vol. 4, no. 1, pp. 44–57, 2009.
- [40] G. M. Morris, D. S. Goodsell, R. S. Halliday et al., "Automated docking using a Lamarckian genetic algorithm and an empirical binding free energy function," *Journal of Computational Chemistry*, vol. 19, no. 14, pp. 1639–1662, 1998.
- [41] J. C. Yeh, T. Cindrova-Davies, M. Belleri et al., "The natural compound n-butylidenephthalide derived from the volatile oil of *Radix Angelica sinensis* inhibits angiogenesis *in vitro* and *in vivo*," *Angiogenesis*, vol. 14, no. 2, pp. 187–197, 2011.
- [42] E. Zamir and P. I. H. Bastiaens, "Reverse engineering intracellular biochemical networks," *Nature Chemical Biology*, vol. 4, no. 11, pp. 643–647, 2008.
- [43] T. W. Corson and C. M. Crews, "Molecular understanding and modern application of traditional medicines: triumphs and trials," *Cell*, vol. 130, no. 5, pp. 769–774, 2007.
- [44] U. Rix and G. Superti-Furga, "Target profiling of small molecules by chemical proteomics," *Nature Chemical Biology*, vol. 5, no. 9, pp. 616–624, 2009.
- [45] S. A. Canny, Y. Cruz, M. R. Southern, and P. R. Griffin, "PubChem promiscuity: a web resource for gathering compound promiscuity data from PubChem," *Bioinformatics*, vol. 28, no. 1, Article ID Article numberbtr622, pp. 140–141, 2012.
- [46] K. W. Lee, A. M. Bode, and Z. Dong, "Molecular targets of phytochemicals for cancer prevention," *Nature Reviews Cancer*, vol. 11, no. 3, pp. 211–218, 2011.
- [47] F. Y. Tang and M. Meydani, "Green tea catechins and vitamin E inhibit angiogenesis of human microvascular endothelial cells through suppression of IL-8 production," *Nutrition and Cancer*, vol. 41, no. 1-2, pp. 119–125, 2001.
- [48] A. S. Chung and N. Ferrara, "Targeting the tumor microenvironment with Src kinase inhibition," *Clinical Cancer Research*, vol. 16, no. 3, pp. 775–777, 2010.
- [49] G. J. Roboz, S. Dias, G. Lam et al., "Arsenic trioxide induces dose- and time-dependent apoptosis of endothelium and may exert an antileukemic effect via inhibition of angiogenesis," *Blood*, vol. 96, no. 4, pp. 1525–1530, 2000.
- [50] F. L. Minnear, M. A. A. DeMichele, D. G. Moon, C. L. Rieder, and J. W. Fenton, "Isoproterenol reduces thrombin-induced pulmonary endothelial permeability *in vitro*," *American Journal of Physiology*, vol. 257, no. 5, part 2, pp. H1613–H1623, 1989.
- [51] D. L. Ou, Y. C. Shen, J. D. Liang et al., "Induction of Bim expression contributes to the antitumor synergy between sorafenib and mitogen-activated protein kinase/extracellular signal-regulated kinase kinase inhibitor CI-1040 in hepatocellular carcinoma," *Clinical Cancer Research*, vol. 15, no. 18, pp. 5820–5828, 2009.
- [52] H. R. Pearce, N. Kalia, K. D. Bardhan, and N. J. Brown, "Effects of aspirin and indomethacin on endothelial cell proliferation *in vitro*," *Journal of Gastroenterology and Hepatology*, vol. 18, no. 10, pp. 1180–1187, 2003.
- [53] R. Nussinov, C. J. Tsai, and P. Csermely, "Allo-network drugs: harnessing allostery in cellular networks," *Trends in Pharmacological Sciences*, vol. 32, pp. 686–693, 2011.

Review Article

Traditional Chinese Medicine-Based Network Pharmacology Could Lead to New Multicomponent Drug Discovery

Jian Li,¹ Cheng Lu,² Miao Jiang,² Xuyan Niu,² Hongtao Guo,² Li Li,² Zhaoxiang Bian,³ Na Lin,⁴ and Aiping Lu^{2,3}

¹ School of Basic Medical Sciences, Beijing University of Chinese Medicine, Beijing 100029, China

² Institute of Basic Research of Clinical Medicine, China Academy of Chinese Medical Sciences, Beijing 100700, China

³ School of Chinese Medicine, Hong Kong Baptist University, Kowloon, Hong Kong

⁴ Institute of Materia Medica, China Academy of Chinese Medical Sciences, Beijing 100700, China

Correspondence should be addressed to Aiping Lu, lap64067611@126.com

Received 24 September 2012; Accepted 18 October 2012

Academic Editor: Shao Li

Copyright © 2012 Jian Li et al. This is an open access article distributed under the Creative Commons Attribution License, which permits unrestricted use, distribution, and reproduction in any medium, provided the original work is properly cited.

Current strategies for drug discovery have reached a bottleneck where the paradigm is generally “one gene, one drug, one disease.” However, using holistic and systemic views, network pharmacology may be the next paradigm in drug discovery. Based on network pharmacology, a combinational drug with two or more compounds could offer beneficial synergistic effects for complex diseases. Interestingly, traditional Chinese medicine (TCM) has been practicing holistic views for over 3,000 years, and its distinguished feature is using herbal formulas to treat diseases based on the unique pattern classification. Though TCM herbal formulas are acknowledged as a great source for drug discovery, no drug discovery strategies compatible with the multidimensional complexities of TCM herbal formulas have been developed. In this paper, we highlighted some novel paradigms in TCM-based network pharmacology and new drug discovery. A multiple component drug can be discovered by merging herbal formula-based pharmacological networks with TCM pattern-based disease molecular networks. Herbal formulas would be a source for multiple component drug candidates, and the TCM pattern in the disease would be an indication for a new drug.

1. Introduction

Completed in 2003, the human genome project plunged the world into the postgenomic era aimed at understanding the global function of the genome through systems biology, mathematics, and computational techniques [1]. The large-scale generation and integration of genomic, proteomic, signaling, and metabolomic data suggest that most diseases are much more complex than initially anticipated and that most disease genes vary in their expression patterns [2]. Besides, organic life is a nonlinear system involving all kinds of interactions between networks of biomacromolecules, cells, drugs, and each other [3], and the “one drug for one gene for one disease” model failed to work because one drug often has many targets, and many protein targets are targeted by more than one drug [4, 5]. These insights triggered a major change in the strategies adopted in the new drug discovery: the shift from single compound drugs to multiple compound drugs.

Based on these concerns, network pharmacology emerged as the next paradigm in new drug discovery with its elucidation capacity in the complexity of biological process [6]. Network pharmacology, a system biology-based methodology, is a new approach to drug design that encompasses the construction of disease networks, drug-target networks, and drug-disease networks. In the network pharmacology-based new drug discovery, a biological network of a disease and a pharmacological network of the candidate are crucial since the candidate showing the well-matched its pharmacological network with some certain disease biological network, would be developed into a new drug [7, 8].

Multiple component drugs, considered as a future direction for new drug discovery, have received widely spread reported [9–11]. Polypill was reported to be an alternative for real therapeutics [12, 13]. Traditional Chinese medicine (TCM), with its unique theory and long history, identifies the patients with Bian Zheng (also called pattern or syndrome

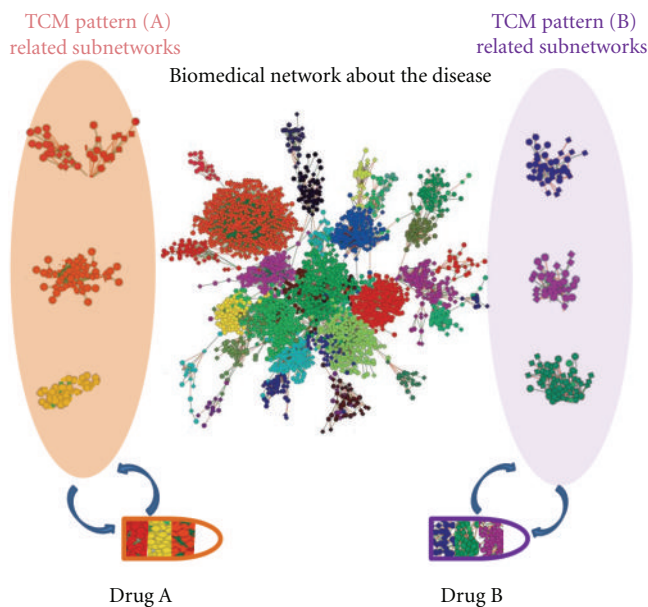


FIGURE 1: A diagram of drug discovery based on TCM-based network pharmacology. Each circle or diamond represents one gene or protein. Functionally interconnected genes or proteins are grouped by bioinformatics and shown in different colors. The biological networks in a disease include the general biological network of the disease (middle part) and TCM pattern network of the disease (Pattern (A) and (B) as an example). The shared disease biological networks and TCM pattern networks are shown in different colors. Drug A and drug B (in lower part) is targeting to the general biological network of the disease and molecular network of TCM pattern (A) and (B) in the disease respectively, and thus the drug A could be good for the disease with TCM pattern (A) and drug B could be good for the disease with pattern (B).

differentiation) which diagnoses the patients based on TCM information, such as symptoms, tongue appearances, and pulse feelings, and TCM treats the patients accordingly with herbal formulas (which contains multiple components) targeting to the TCM pattern [14]. In another word, TCM uses multiple compound herbal products to treat the pattern in the disease. Thus it is reasonable to suggest finding new multiple compound drugs from herbal formulas for treating a subgroup (TCM pattern) of the patients in a certain of disease.

The major hurdles in the multiple compound new drug discoveries are how to identify the TCM pattern in a disease and build up the pharmacological network of herbal formula. TCM pattern in a disease can be identified with biological network biomarkers, and the pharmacological network of herbal formula can be built up with newly network pharmacological approaches. Thus, by integrating the TCM pattern molecular network and the pharmacological network of herbal formulas, which we would like to call as TCM-based network pharmacology, could be a novel way to lead to multiple compound drug discoveries.

2. TCM Pattern-Based Disease Molecular Networks

Currently, the integration of TCM pattern classifications and biomedical diagnoses is becoming a common clinical diagnostic model in China and has produced better clinical outcomes [15]. As a case, clinical research on rheumatoid

arthritis (RA) suggests that RA patients should be treated by different therapies based on their TCM patterns [16]. Thus, TCM pattern classification in a disease could be a more precise indication when designing and evaluating a drug candidate. As a diagnostic result in TCM pattern classification, TCM patterns could link up the corresponding subnetworks of a specific disease in the context of molecular medicine. The present information about a disease could be collected to establish molecular networks underlying the disease. For example, the molecular network of RA has been established [17, 18]. The network of a disease could help identify the corresponding pharmacological network for therapeutic intervention, by merging the disease molecular network and the intervention pharmacological networks. In recent years, many researchers have paid more attention to the molecular networks built on the TCM pattern in some diseases [19]. A wide variety of TCM pattern-based disease molecular network applications have already been reported and bridged the gap between TCM patterns of Chinese medicine and diagnostic parameters of western medicine for example, we and others have surveyed plentiful typical cold and hot TCM pattern patients and examined *omics* information, such as genomics [20–23] or metabolomics [24, 25]. According to the cold and hot patterns-based bionetwork we could not only open out the mechanism of TCM pattern, but also understand the complexity of life processes [26, 27]. Furthermore, at another example, the biochemical changes are identified in kidney deficiency syndromes animal model through chemometric analysis [28]. In such a case, the integration of next generation *omics* technique will yield

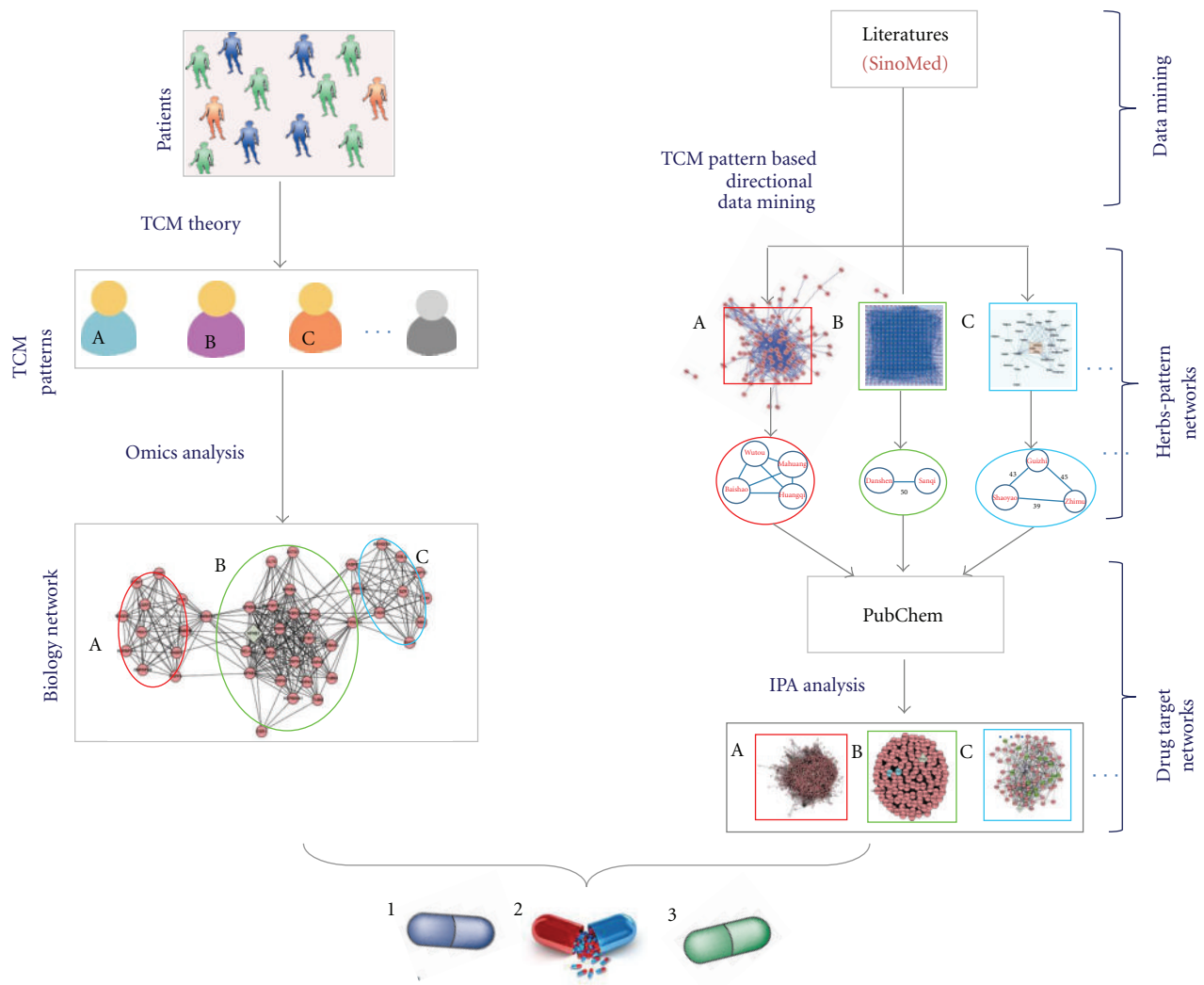


FIGURE 2: A conceptual model for multiple compound drug discovery using TCM-based network pharmacology. In the left of the paradigm, the molecular network of the disease-TCM pattern (lower left) can be constructed by analyzing the omics data from patients classified with the TCM pattern or related information from public databases. The typical and major TCM patterns (indicated as A, B, and C in the middle left) can be determined based on an expert consensus or literature analysis. In the right of the diagram, the most commonly used TCM herbal combinations for the treatment of a disease with specific TCM patterns can be found using text mining based on publications from SinoMed database (indicated as A, B, and C, middle right). All of the targeted proteins for the active compounds in the TCM herbal formula can be obtained in PubChem, and these targeted proteins can be used to build up the pharmacological networks for potential multiple-compound drug candidates from the herbal formulas (lower right). By matching the pharmacological networks of herbal compound combinations from the herbal formula with the disease-pattern molecular network, those well-matched compound combinations might be found for new drug candidates (capsule 1, 2, and 3 in lower part).

fundamental insights into the TCM pattern-based disease molecular networks. Then, with the help of TCM pattern-based networks in a disease, it seems to not only translate between different diagnostic readouts in TCM and western medicine, but also discover potential drug candidates.

3. Herbal Formula-Based Pharmacological Networks

More studies have shown that herbal formulas are effective in treating some diseases. As the cases, Lam et al. reported that

a four-herb Chinese medicine PHY906 could reduce gastrointestinal toxicity induced by chemotherapy drug CPT-11 through multiple mechanisms including inhibiting CPT-11-triggered inflammation, promoting intestinal recovery, and intestinal progenitor cell repopulation [29]; Wang et al. explored the molecular mechanism and synergistic effects of each ingredient in Realgar-Indigo naturalis formula (RIF), a well-known and clinically proven TCM formulae for leukaemia therapy, and found that arsenic in Realgar directly attacked the receptor on coprotein in leukaemia cells, Indirubin in Indigo antagonized the toxicity of arsenic and slowed leukaemia cell growth and Tanshinone

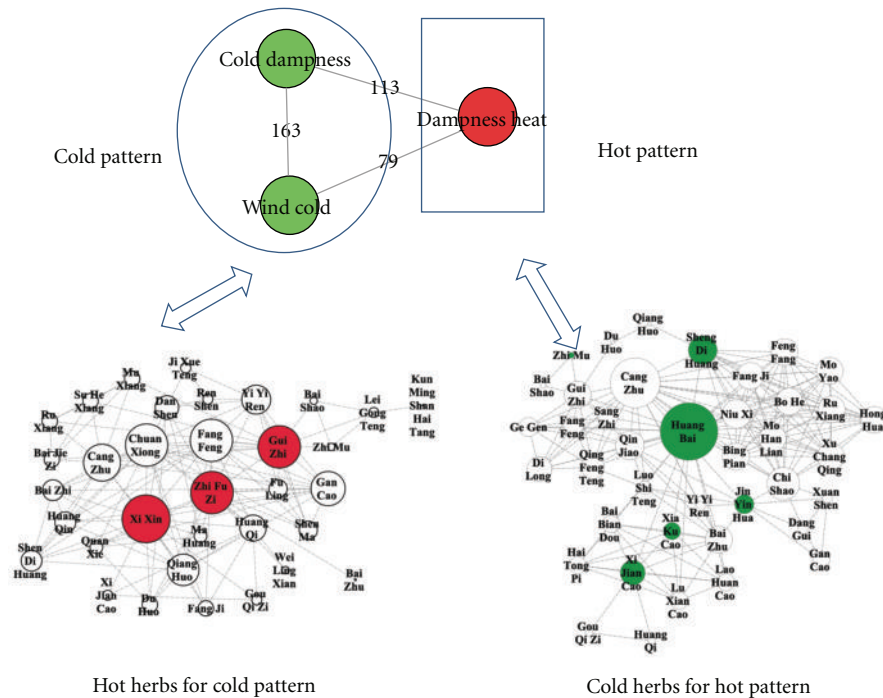


FIGURE 3: The common herbal formula for the treatment of RA with TCM cold and heat pattern obtained by text mining. All publications about clinical trials in SinoMed were collected, and common combinations of herbs (herbal formula) for the treatment of RA with TCM cold and heat pattern were found.

in red sage root restored pathways that stop leukaemia from spreading [30]. However, the conventional methods are hard to elucidate the pharmacological mechanism for multiple compound containing herbal formulas, and it has been believed that systems biology could be helpful in pharmacological study. Using a metabolomic method of reversed-phase liquid chromatography/quadrupole time-of-flight mass spectrometry (LC-Q-TOF-MS), Jiang et al. reported that Shexiangbaoxin Pill (SBP) could be used to treat myocardial infarction (MI) through regulating the perturbed pathway of energy metabolism, and five biomarkers, including creatine, uridine, glutamate, oxalosuccinic acid and nicotinamide mononucleotide, were completely reversed to normal levels in MI rats administrated with SBP for 15 days [31]. Li et al. established a method called distance-based mutual information model (DMIM), and through which they demonstrated that six herbs in Liu-wei-di-huang (LWDH) formula connected closely with common responsive genes enriched in cancer pathways and neuroendocrine-immune pathways, and also LWDH formula-treated diseases shared an overlapped molecular basis associated with the angiogenic processes as well as the imbalance of the human body [32]. In this respect, systems biology could be helpful in not only pharmacological mechanism study, but also new drug discovery.

Though still fairly new, researchers have been trying to explore some new paradigm in drug discovery with the aid of pharmacology biology, a part of systems biology, in

which comparative reverse systems pharmacology and drug-combination studies, guided by system response profiles (SRPs), might be the two effective ways [33]. Another strategy, targeting at the human genome-microbiome axis, might also become a novel ways to discover new drugs from traditional chinese medicine (TCM) using systems biology [34]. These newly developed pharmacological networks are not only used to explore the pharmacological activity of a single compound drug, but they can also be used to examine combination therapy (drug combinations) [35, 36]. TCM herbal formulas with multiple compounds are pharmacologically targeting biological networks, instead of single target. Aided by information from genomics, proteomics, and metabolomics, researchers are seeking a methodology to build molecular pharmacological networks for herbal formulas or combination therapy [37]. For example, *Salvia miltiorrhiza* (SM) and *Panax notoginseng* (PN) in combination (SMPN) have been widely used (primarily in TCM) for the treatment of coronary heart disease, and we combined text mining with bioinformatics to build functional networks for SMPN [38]. These results suggest that the pharmacological activity of SMPN is the outcome of the interactions between SM and PN in the multiple pathways and biological processes during the treatment of coronary heart disease. With the help of pharmacological networks, we would know more about the pharmacological activities of the multiple compound drug candidates from herbal formulas.

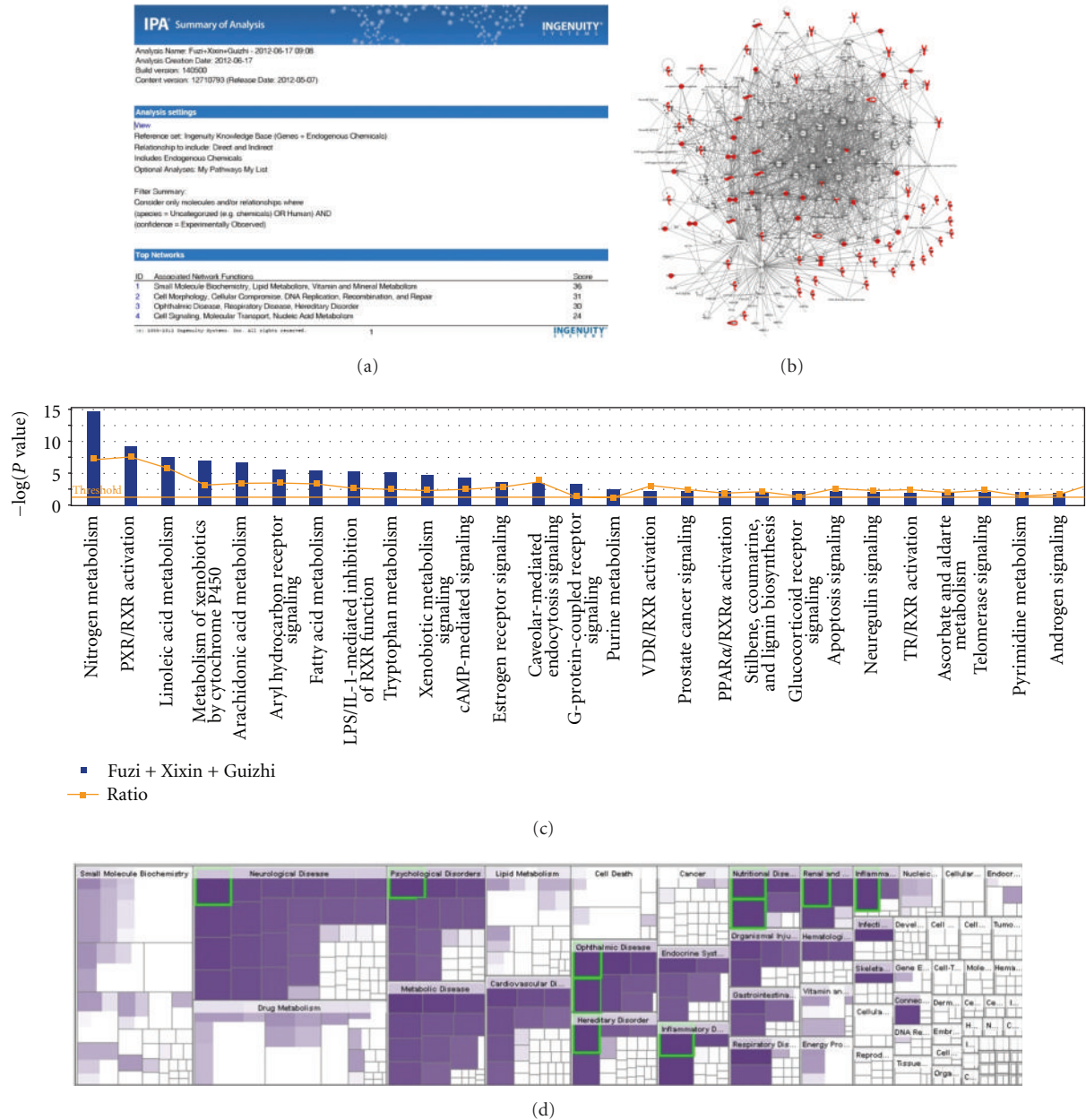


FIGURE 4: The summary on the network based on the protein targets of Fuzi, Xixin, and Guizhi built up with IPA software. (a) The summary of network analysis results; (b) the merged networks of the protein targets; (c) the canonical pathways related with the protein targets; (d) the hot map of biofunctions related with the protein targets.

4. TCM-Based Network Pharmacology in Multiple Compound New Drug Discovery

Based on the integration of the biological network of a disease with specific TCM patterns and the pharmacological network of TCM herbal formulas, TCM-based pharmacology network could lead to a new approach for the multiple compound new drug discoveries. Figure 1 shows a diagram illustrating the role of the combination of TCM pattern networks in a disease and TCM herbal formula networks in the new drug discovery. The biological network in a disease

can be divided into two parts: the biological network of the disease shared by all TCM patterns in the disease, and the TCM pattern network of the disease. The common shared disease biological network can also be divided into subnetworks, and the biological network of the TCM pattern can be also divided into different subnetworks. We can then determine the pharmacological networks of multiple-compound drug candidates (such as candidate drug A and B in the lower part of Figure 1). Drug A, with its pharmacological networks, can regulate a part of the shared disease networks and all three of the TCM pattern (A)

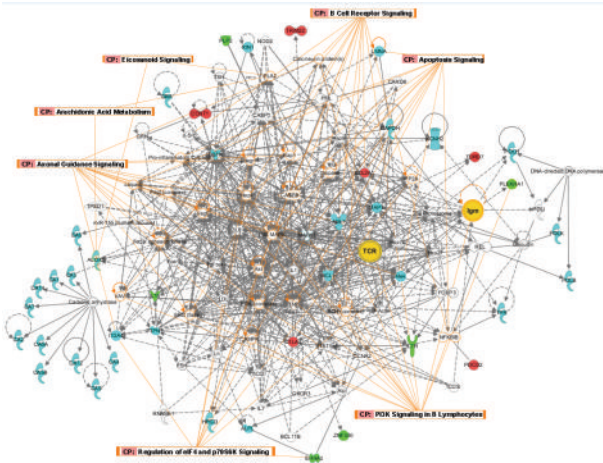


FIGURE 5: The merged networks of identified differentially expressed genes in RA-cold pattern and protein targets of Fuzi, Xixin, and Guizhi. Red color shows the upregulated genes in RA-cold pattern compared with health; green: the downregulated genes in RA-cold pattern compared with health; Blue color shows the protein targets of Fuzi, Xixin, and Guizhi; yellow color shows the common molecular both in networks of RA-cold pattern and networks of protein targets of Fuzi, Xixin, and Guizhi. (CP: the common canonical pathways related with differentially expressed genes in RA-cold pattern and protein targets of Fuzi, Xixin, and Guizhi both; orange lines: the molecular involved in the common canonical pathways.)

networks. Thus, drug A could be developed as an effective treatment for the disease categorized in TCM pattern (A). Similarly, drug B could be developed as an effective treatment for the disease categorized in TCM pattern (B). Therefore, building up the molecular networks of TCM patterns in a specific disease and herbal formula-based pharmacological network could lead to a new strategy of multiple compound drug discoveries. Furthermore, TCM pattern classification could specify the therapeutic scope of a drug candidate. TCM herbal formulas, with multiple compounds and clinically proven effectiveness when used in treating the corresponding TCM pattern in a disease, could be an important source for the new drug discovery. The basic process of TCM network pharmacology-based multiple-component drug discovery includes several steps (Figure 2), mainly the build-up of the disease-TCM pattern molecular networks and the pharmacological networks of the multiple-compound drug candidates from the TCM herbal formulas, and then merging of the multiple-compound drug candidate pharmacological networks with disease-TCM pattern molecular networks. If the pharmacological networks of multiple-compound drug candidates from the TCM formula (indicated as A, B, and C in the right of Figure 2) can be matched to the disease-TCM pattern networks (indicated as A, B, and C in the left of Figure 2), then new drugs (indicated as 1, 2, and 3 with capsules in the bottom of Figure 2) might be discovered.

To give an example of this, take RA for instance. Following the TCM clinical practice, the RA patients can be classified into two main patterns: the cold and hot patterns.

The gene expression profiles of blood cell from typical cold and hot pattern RA patients were performed to obtain a systematic view of the molecular signatures separately. The differentially expressed candidate genes from microarray chips were explored using DAVID, GeneSpring, and ingenuity pathway analysis (IPA) software, to analyze the protein-protein interactions (PPI)-related network. Thus, the molecular network of the RA-cold and -hot pattern based on genomics data could be identified. In addition, many public databases are available for disease-related network analysis. In particular, the PubMed, a free service, provides an access to the medline database of citations, abstracts, and some full-text articles on life sciences and biomedical topics. Take all these into consideration, a relatively complete molecular network of the RA-cold and -hot pattern could be achieved.

For new drug discovery, the major cold or hot patterns in RA are used to build up the molecular networks for merging with the herbal formula pharmacological network. The following questions are that how to find out best potential herbal formula candidates. Figure 3 showed the potential herbal formula used for cold pattern treatment of RA, and the potential herbal formula used for heat pattern of RA in TCM by text mining. With the support from PubChem bioassay [39], we can study polypharmacological behavior in the PubChem collection via cross-assay analysis [40–42], which can be an important source of drug discovery. Based on PubChem bioassay, researchers can develop a network representation of the assay collection and then apply a bipartite mapping between this network and various biological networks as well as artificial networks (i.e., drug-target network). Mapping to a drug-target network allowed researchers to prioritize new selective compounds, while mapping to other biological networks enabled them to observe interesting target pairs and their associated compounds in the context of biological systems [40]. This approach could be a useful way to build up and investigate the pharmacological network for the multiple compound new drug candidates. As a case, we have chosen protein targets of the compounds in the herbal formula consisting of *Radix Aconiti Praeparata* (Fuzi), *Herba Asari* (Xixin), and *Ramulus Cinnamomi* (Guizhi) which were found good for the treatment of RA with cold pattern by text mining, then pharmacological networks for the multiple compound new drug candidates were built up by IPA (ingenuity pathway analysis software) and protein-protein interaction analysis after collecting their target proteins from PubChem. Furthermore, the functions of the networks and the relationships between the herbal formula networks and disease-pattern networks were analyzed to find new drug candidates for the cold pattern of RA in TCM. As shown in the result of text mining, there were 78 target proteins in the herbal formula (the detail information of every target protein was shown in Table 1). We uploaded the total 78 target proteins to the IPA software online and built up the molecular networks of those target proteins. The analysis results of IPA of the target proteins of the herbal formula (including Fuzi, Xixin, and Guizhi) were shown in Figure 4, in which there were shown the summary of analysis results (Figure 4(a)), the merged

TABLE 1: Target proteins of Fu Zi, Xi Xin, and Gui Zhi searched in PubChem.

Active compounds	Homosapiens proteins name	GI number
Higenamine	D(2) dopamine receptor	118206
Fuziline	Orexin receptor type 1	222080095
Safrole	Caspase 8	2493531
	Vitamin D3 receptor isoform VDRA	63054845
	Microtubule-associated protein tau	92096784
	Corticotropin-releasing hormone receptor 2	38349113
	Aldehyde dehydrogenase 1 family, member A1	30582681
	Euchromatic histone-lysine N-methyltransferase 2	168985070
	Corticotropin releasing factor-binding protein	30219
Methyleugenol	Farnesoid X nuclear receptor	325495553
	Sentrin-specific protease 8	262118306
	AR protein	124375976
Asaricin	Cytochrome P450 3A4 isoform 1	13435386
Asarinin	Sentrin-specific protease 8	262118306
	Cytochrome P450 1A2	73915100
	Cytochrome P450 2D6 isoform 1	40805836
	Cytochrome P450 2C9 precursor	13699818
	Cytochrome P450 2C19 precursor	4503219
Cinnamaldehyde	Transient receptor potential cation channel subfamily A member 1	313104269
	cGMP-specific 3',5'-cyclic phosphodiesterase	317373261
	Lamin isoform A delta 10	27436948
	Prothrombin	339641
	Glucocorticoid receptor	311348376
	Aldehyde dehydrogenase 1 family, member A1	30582681
	Chain A, crystal structure of the human 2-oxoglutarate oxygenase Loc390245	221046486
	Glucocerebrosidase	496369
Cinnamic acid	Thromboxane-A synthase	254763392
	Heat shock protein HSP 90-alpha isoform 2	154146191
	Melanocortin receptor 4	119508433
	Lysosomal alpha-glucosidase preproprotein	119393891
	Alkaline phosphatase, tissue-nonspecific isozyme isoform 1 precursor	116734717
	Tyrosine-protein kinase ABL1 isoform a	62362414
	Nuclear receptor coactivator 3 isoform a	32307126
	Nuclear receptor coactivator 1 isoform 1	22538455
	MPI protein	16878311
	Glyceraldehyde-3-phosphate dehydrogenase isoform 1	7669492
	Glutathione S-transferase omega-1 isoform 1	4758484
	Tyrosinase	401235
	Arachidonate 5-lipoxygenase	126407
	Carbonic anhydrase 2	115456
	Cytochrome P450 2A6	308153612
	Carbonic anhydrase 3	134047703
	Carbonic anhydrase 6	116241278
	Carbonic anhydrase 9	83300925
	Hydroxycarboxylic acid receptor 2	74762622
	Carbonic anhydrase 5B, mitochondrial	8928041
	Carbonic anhydrase 14	8928036
	5-hydroxytryptamine receptor 7	8488960
	Epidermal growth factor receptor	2811086
Carbonic anhydrase 7	1168744	
Carbonic anhydrase 5A, mitochondrial	461680	
Tyrosine-protein phosphatase non-receptor type 1	131467	

TABLE 1: Continued.

Active compounds	Homosapiens proteins name	GI number
	Carbonic anhydrase 4	115465
	Carbonic anhydrase 1	115449
	Adenosine receptor A2b	112938
	Lethal(3)malignant brain tumor-like protein 1 isoform I	117938328
	5-hydroxytryptamine receptor 5A	13236497
	potassium voltage-gated channel subfamily H member 2 isoform d	325651834
	DNA polymerase iota	154350220
	DNA polymerase kappa	7705344
	DNA polymerase eta	5729982
	DNA polymerase beta	4505931
	Estrogen receptor beta isoform 1	10835013
	Nuclear receptor subfamily 0 group B member 1	5016090
	Thyroid hormone receptor beta	189491771
	15-hydroxyprostaglandin dehydrogenase [NAD+] isoform 1	31542939
	FAD-linked sulphhydryl oxidase ALR	54112432
	Ras and Rab interactor 1	68989256
	Integrin alpha-4 precursor	67191027
	Chain A, human Ape1 endonuclease with bound abasic DNA And Mn2+ Ion	6980812
	Mcl-1	7582271
	Chain A, structure of human Recq-like helicase in complex with a DNA Substrate	282403581
	Chain A, Jmjd2a tandem tTudor domains in complex with a trimethylated histone H4-K20 peptide	162330054
	Euchromatic histone-lysine N-methyltransferase 2	168985070
	Chain B, the structure of wild-type human Hadh2 bound to Nad+ At 1.2 A	122921311
	Chain A, the structure of wild-type human Hadh2 bound to Nad+ At 1.2 A	122921310
	Bromodomain adjacent to zinc finger domain 2B	6683500
	Carbonic anhydrase 12	5915866

network (Figure 4(b)), the canonical pathways (Figure 4(c)), and the hot map of biofunctions related with protein targets of the herbal formula by IPA platform (Figure 4(d)).

Actually, it is obvious that the literature-derived network is relatively crude and redundant for the main reason of the quality control in the text/data mining approaches. Regarding this, it is important to define criteria of literature included and excluded. On the other hand, it is helpful to combine literature mining and *omics* analysis, such as literature mining combined microarray analysis system (LMMA system) [43]. In further, integrating both the experimental data and the literature knowledge seems to be an effective way to reduce noises of data in biological network modeling [44].

5. Merging the Molecular Disease Network with the Pharmacological Network of the Candidate Drugs

Recently, the essence of life had increasingly been studied from a systems perspective across different scientific disciplines [45]. Plenty of work had been done to provide the practical frameworks for applying “systems thinking” to human diseases and drug discovery [45–47]. The published report showed the relationships between drug targets and

disease-gene products, which measured the shortest distance between both sets of proteins in current models of the human protein-protein interaction (PPI) network [4]. Significant differences in distance were found between etiological and palliative drugs, and recent trend toward more rational drug design was observed in the research. Indeed, the method of using the concepts of network biology to integrate data of drug targets and disease-related genes or proteins had been an important way for no matter the discovery of new drug, or repurposing of old drugs. For example, we merged the networks of protein targets of Fuzi, Xixin, and Guizhi and the network of identified differentially expressed genes in RA with TCM cold pattern versus health. As shown in Figure 5, two common molecular (TCR and IgM) and seven common canonical pathways were all found related with the two networks. We considered that the common molecular and canonical pathways might be the potential therapeutic targets of Fuzi, Xixin, and Guizhi to treat RA with cold pattern.

On the other hand, drug repurposing, which is the use of established drugs for new indications, would be realized with network pharmacology approaches. Development of a new pharmaceutical product requires at least from 10 to 15 years and costs from \$500 million to \$2 billion [48–50], yet the number of new drugs approved by the FDA has been declining year by year [51]. Existing drugs already

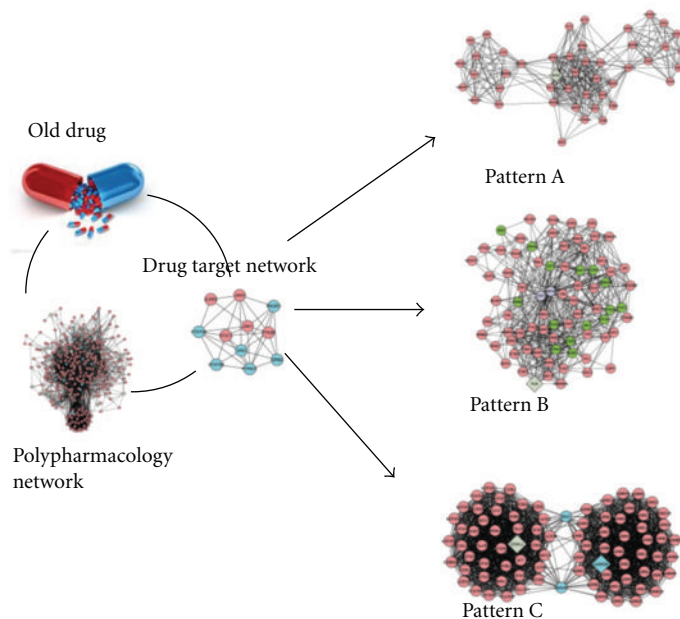


FIGURE 6: A conceptual paradigm for the repurposing of old drugs based on TCM network pharmacology. The pharmacological networks of an old drug can be built up with bioinformatics approaches (left). By merging the pharmacological networks of the old drug with the disease-TCM pattern molecular network (indicated with (A), (B), and (C) in the right), a better indication based on TCM pattern classification might be found.

have clinical data and therefore require much less time and money to be approved for a new indication [52]. Researchers have proposed inverse docking models as a novel method to evaluate previously approved drugs for new therapeutic indications [53–55]. Methotrexate (MTX) and sulfasalazine (SSZ) combination therapy is a common treatment for RA, and we found that this combination was more effective for treating RA patients with the TCM cold pattern [56, 57]. In order to find the biological mechanism with network pharmacology, the pharmacological networks of MTX and SSZ were matched with the molecular network of RA with TCM cold pattern, and the network-based pharmacological mechanism result supports the clinical finding [58]. Similarly we can apply the model to screen other existed drug and see which TCM pattern or indication would be better for the drug. Thus we propose a strategy that uses TCM-based network pharmacology for repurposing a marketed “old” drug (Figure 6). Briefly, the pharmacological networks of the marketed drugs can be built based on the information about the pharmacological activity of these drugs from established databases. By matching the pharmacological network of the old drugs and the TCM pattern molecular networks in the disease, we can determine which subgroup of patients would be better candidates for the drugs. In the right of Figure 6, TCM pattern (A), (B), and (C) indicate the molecular networks for the disease with TCM pattern (A), (B), and (C), respectively. If the pharmacological network of the marketed drug can be matched with pattern (A), then the marketed drug could be further investigated clinically for the treatment of the disease with TCM pattern (A). Similarly, we can find new indications for other marketed drugs. Thus,

the marketed “old” drug can be regarded as a new drug because it can be used with a new specified indication.

6. Perspectives and Conclusions

TCM pattern classification, as a diagnostic approach, could be used to classify patients based on their disease diagnosis in biomedicine. As a result, the TCM pattern could be a potential drug therapeutic target. Additionally, TCM herbal formulas are a vast, promising, and natural resource for drug discovery. More importantly, with their clinically approved effectiveness and safety, they are containing multiple compounds and would be the multiple compound drug candidates. Thus, new drug discovery should put a greater emphasis on TCM pattern classification in certain disease and multiple-compound drug candidates from TCM herbal formulas. We expect that, along the advancement of TCM based network pharmacology, a novel multiple compound drugs would be discovered in the near future.

Authors’ Contribution

J. Li and C. Lu contributed equally to this work.

Acknowledgments

This work was partially supported by the National Science Foundation of China (nos. 30825047 and 90709007), and National Key Project for New Drug Development of The Ministry of Science and Technology (2009zx09502-019).

References

- [1] L. Hood, J. R. Heath, M. E. Phelps, and B. Lin, "Systems biology and new technologies enable predictive and preventative medicine," *Science*, vol. 306, pp. 640–643, 2004.
- [2] K. I. Goh, M. E. Cusick, D. Valle, B. Childs, M. Vidal, and A. L. Barabasi, "The human disease network," *Proceedings of the National Academy of Sciences of the United States of America*, vol. 104, pp. 8685–8690, 2007.
- [3] T. Pawson and R. Linding, "Network medicine," *FEBS Letters*, vol. 582, pp. 1266–1270, 2008.
- [4] M. A. Yildirim, K. I. Goh, M. E. Cusick, A. L. Barabasi, and M. Vidal, "Drug-target network," *Nature Biotechnology*, vol. 25, pp. 1119–1126, 2007.
- [5] C. G. Wermuth, "Multitargeted drugs: the end of the "one-target-one-disease" philosophy?" *Drug Discovery Today*, vol. 9, no. 19, pp. 826–827, 2004.
- [6] A. L. Hopkins, "Network pharmacology," *Nature Biotechnology*, vol. 25, pp. 1110–1111, 2007.
- [7] A. L. Hopkins, "Network pharmacology: the next paradigm in drug discovery," *Nature Chemical Biology*, vol. 4, pp. 682–690, 2008.
- [8] F. Sams-Dodd, "Target-based drug discovery: is something wrong?" *Drug Discovery Today*, vol. 10, no. 2, pp. 139–147, 2005.
- [9] Y. Wang, X. Fan, H. Qu, X. Gao, and Y. Cheng, "Strategies and techniques for multi-component drug design from medicinal herbs and traditional Chinese medicine," *Current Topics in Medicinal Chemistry*, vol. 12, no. 12, pp. 1356–1362, 2012.
- [10] K. Lan and W. Jia, "An integrated metabolomics and pharmacokinetics strategy for multi-component drugs evaluation," *Current Drug Metabolism*, vol. 11, pp. 105–114, 2010.
- [11] X. Y. Tian and L. Liu, "Drug discovery enters a new era with multi-target intervention strategy," *Chinese Journal of Integrative Medicine*. In press.
- [12] H. Jaques, "The polypill concept: the future," *European Heart Journal*, vol. 32, pp. 2732–2733, 2011.
- [13] K. M. Carey, M. R. Comee, J. L. Donovan, and A. Kanaan, "A polypill for all? Critical review of the polypill literature for primary prevention of cardiovascular disease and stroke," *The Annals of Pharmacotherapy*, vol. 46, pp. 688–695, 2012.
- [14] A. Lu, M. Jiang, C. Zhang, and K. Chan, "An integrative approach of linking traditional Chinese medicine pattern classification and biomedicine diagnosis," *Journal of Ethnopharmacology*, vol. 141, no. 2, pp. 549–556, 2011.
- [15] A. P. Lu and K. J. Chen, "Integrative medicine in clinical practice: from pattern differentiation in traditional Chinese medicine to disease treatment," *Chinese Journal of Integrative Medicine*, vol. 15, no. 2, article 152, 2009.
- [16] Y. T. He, Q. L. Zha, J. P. Yu, Y. Tan, C. Lu, and A. P. Lu, "Principal factor analysis of symptoms of rheumatoid arthritis and their correlations with efficacy of traditional Chinese medicine and Western medicine," *Journal of Chinese Integrative Medicine*, vol. 6, pp. 32–36, 2008.
- [17] C. H. Huang, L. Cong, J. Xie, B. Qiao, S. H. Lo, and T. Zheng, "Rheumatoid arthritis-associated gene-gene interaction network for rheumatoid arthritis candidate genes," *BMC Proceedings*, vol. 3, supplement 7, p. S75, 2009.
- [18] G. Wu, L. Zhu, J. E. Dent, and C. Nardini, "A comprehensive molecular interaction map for rheumatoid arthritis," *PLoS ONE*, vol. 5, Article ID e10137, 2010.
- [19] J. Zhao, P. Jiang, and W. Zhang, "Molecular networks for the study of TCM pharmacology," *Briefings in Bioinformatics*, vol. 11, pp. 417–430, 2010.
- [20] C. Lu, X. Niu, C. Xiao et al., "Network-based gene expression biomarkers for cold and heat patterns of rheumatoid arthritis in traditional Chinese medicine," *Evidence-Based Complementary and Alternative Medicine*, vol. 2012, Article ID 203043, 17 pages, 2012.
- [21] G. Chen, C. Lu, Q. Zha et al., "A network-based analysis of traditional Chinese medicine cold and hot patterns in rheumatoid arthritis," *Complementary Therapies in Medicine*, vol. 20, pp. 23–30, 2012.
- [22] M. Jiang, C. Xiao, G. Chen et al., "Correlation between cold and hot pattern in traditional Chinese medicine and gene expression profiles in rheumatoid arthritis," *Frontiers of Medicine*, vol. 5, pp. 219–228, 2011.
- [23] C. Lu, C. Xiao, G. Chen et al., "Cold and heat pattern of rheumatoid arthritis in traditional Chinese medicine: distinct molecular signatures indentified by microarray expression profiles in CD4-positive T cell," *Rheumatology International*, vol. 32, no. 1, pp. 61–68, 2012.
- [24] Y. Gu, C. Lu, Q. Zha et al., "Plasma metabolomics study of rheumatoid arthritis and its Chinese medicine subtypes by using liquid chromatography and gas chromatography coupled with mass spectrometry," *Molecular BioSystems*, vol. 8, pp. 1535–1543, 2012.
- [25] H. van Wietmarschen, K. Yuan, C. Lu et al., "Systems biology guided by Chinese medicine reveals new markers for subtyping rheumatoid arthritis patients," *Journal of Clinical Rheumatology*, vol. 15, no. 7, pp. 330–337, 2009.
- [26] T. Ma, C. Tan, H. Zhang, M. Wang, W. Ding, and S. Li, "Bridging the gap between traditional Chinese medicine and systems biology: the connection of Cold Syndrome and NEI network," *Molecular BioSystems*, vol. 6, pp. 613–619, 2010.
- [27] S. Li, Z. Q. Zhang, L. J. Wu, X. G. Zhang, Y. D. Li, and Y. Y. Wang, "Understanding ZHENG in traditional Chinese medicine in the context of neuro-endocrine-immune network," *IET Systems Biology*, vol. 1, pp. 51–60, 2007.
- [28] M. Chen, L. Zhao, and W. Jia, "Metabonomic study on the biochemical profiles of a hydrocortisone-induced animal model," *Journal of Proteome Research*, vol. 4, pp. 2391–2396, 2005.
- [29] W. Lam, S. Bussom, F. Guan et al., "Chemotherapy: the four-herb Chinese medicine PHY906 reduces chemotherapy-induced gastrointestinal toxicity," *Science Translational Medicine*, vol. 2, no. 45, Article ID 45ra59, 2010.
- [30] L. Wang, G. B. Zhou, P. Liu et al., "Dissection of mechanisms of Chinese medicinal formula Realgar-Indigo naturalis as an effective treatment for promyelocytic leukemia," *Proceedings of the National Academy of Sciences of the United States of America*, vol. 105, no. 12, pp. 4826–4831, 2008.
- [31] P. Jiang, W. Dai, S. Yan et al., "Potential biomarkers in the urine of myocardial infarction rats: a metabolomic method and its application," *Molecular BioSystems*, vol. 7, no. 3, pp. 824–831, 2011.
- [32] S. Li, B. Zhang, D. Jiang, Y. Wei, and N. Zhang, "Herb network construction and co-module analysis for uncovering the combination rule of traditional Chinese herbal formulae," *BMC Bioinformatics*, vol. 11, no. 11, article S6, 2010.
- [33] J. van der Greef and R. N. McBurney, "Rescuing drug discovery: in vivo systems pathology and systems pharmacology," *Nature Reviews Drug Discovery*, vol. 4, no. 12, pp. 961–967, 2005.
- [34] L. Zhao, J. K. Nicholson, A. Lu et al., "Targeting the human genome-microbiome axis for drug discovery: inspirations from global systems biology and traditional Chinese medicine," *Journal of proteome research*, vol. 11, no. 7, pp. 3509–3519, 2012.

- [35] S. Zhao and R. Iyengar, "Systems pharmacology: network analysis to identify multiscale mechanisms of drug action," *Annual Review of Pharmacology and Toxicology*, vol. 52, pp. 505–521, 2012.
- [36] H. Z. Ye, C. S. Zheng, X. J. Xu, M. X. Wu, and X. X. Liu, "Potential synergistic and multitarget effect of herbal pair Chuanxiong Rhizome-Paeonia Albiflora Pall on osteoarthritis disease: a computational pharmacology approach," *Chinese Journal of Integrative Medicine*, vol. 17, pp. 698–703, 2011.
- [37] L. B. C. Gao, J. Miao, T. Yong, and L. Aiping, "Functional networks for *Salvia miltiorrhiza* and *Panax notoginseng* in combination explored with text mining and bioinformatical approach," *Journal of Medicinal Plants Research*, vol. 5, article 10, 2011.
- [38] G. Chen and A. P. Lu, "Prediction of the mechanisms of *salvia miltiorrhiza* against atherosclerosis using text mining and network-based analysis," *Journal of Algorithms and Computational Technology*, vol. 5, no. 1, pp. 139–144, 2011.
- [39] <http://www.ncbi.nlm.nih.gov/pubchem>.
- [40] B. Chen, D. Wild, and R. Guha, "PubChem as a source of polypharmacology," *Journal of Chemical Information and Modeling*, vol. 49, no. 9, pp. 2044–2055, 2009.
- [41] Q. Li, T. Cheng, Y. Wang, and S. H. Bryant, "PubChem as a public resource for drug discovery," *Drug Discovery Today*, vol. 15, no. 23–24, pp. 1052–1057, 2010.
- [42] Y. Pouliot, A. P. Chiang, and A. J. Butte, "Predicting adverse drug reactions using publicly available PubChem bioassay data," *Clinical Pharmacology and Therapeutics*, vol. 90, no. 1, pp. 90–99, 2011.
- [43] S. Li, L. Wu, and Z. Zhang, "Constructing biological networks through combined literature mining and microarray analysis: a LMMA approach," *Bioinformatics*, vol. 22, no. 17, pp. 2143–2150, 2006.
- [44] P. Le Phillip, A. Bahl, and L. H. Ungar, "Using prior knowledge to improve genetic network reconstruction from microarray data," *In Silico Biology*, vol. 4, no. 3, pp. 335–353, 2004.
- [45] J. van der Greef and R. N. McBurney, "Rescuing drug discovery: in vivo systems pathology and systems pharmacology," *Nature Reviews Drug Discovery*, vol. 4, no. 12, pp. 961–967, 2005.
- [46] T. Ideker, T. Galitski, and L. Hood, "A new approach to decoding life: systems biology," *Annual Review of Genomics and Human Genetics*, vol. 2, pp. 343–372, 2001.
- [47] H. Kitano, "Computational systems biology," *Nature*, vol. 420, pp. 206–210, 2002.
- [48] C. P. Adams and V. V. Brantner, "Estimating the cost of new drug development: is it really 802 million dollars?" *Health Affairs*, vol. 25, pp. 420–428, 2006.
- [49] M. Dickson and J. P. Gagnon, "The cost of new drug discovery and development," *Discovery Medicine*, vol. 4, pp. 172–179, 2004.
- [50] I. Kola and J. Landis, "Can the pharmaceutical industry reduce attrition rates?" *Nature Reviews Drug Discovery*, vol. 3, no. 8, pp. 711–715, 2004.
- [51] K. I. Kaitin, "Obstacles and opportunities in new drug development," *Clinical Pharmacology and Therapeutics*, vol. 83, pp. 210–212, 2008.
- [52] T. T. Ashburn and K. B. Thor, "Drug repositioning: identifying and developing new uses for existing drugs," *Nature Reviews Drug Discovery*, vol. 3, no. 8, pp. 673–683, 2004.
- [53] Y. Z. Chen and D. G. Zhi, "Ligand-protein inverse docking and its potential use in the computer search of protein targets of a small molecule," *Proteins*, vol. 43, pp. 217–226, 2001.
- [54] Y. Y. Li, J. An, and S. J. Jones, "A large-scale computational approach to drug repositioning," *Genome Informatics*, vol. 17, no. 2, pp. 239–247, 2006.
- [55] E. Dubus, I. Ijjaali, O. Barberan, and F. Petitet, "Drug repositioning using in silico compound profiling," *Future Medicinal Chemistry*, vol. 1, no. 9, pp. 1723–1736, 2009.
- [56] C. Lu, Q. Zha, A. Chang, Y. He, and A. Lu, "Pattern differentiation in Traditional Chinese Medicine can help define specific indications for biomedical therapy in the treatment of rheumatoid arthritis," *Journal of Alternative and Complementary Medicine*, vol. 15, pp. 1021–1025, 2009.
- [57] C. Lu, C. Xiao, G. Chen et al., "Cold and heat pattern of rheumatoid arthritis in traditional Chinese medicine: distinct molecular signatures indentified by microarray expression profiles in CD4-positive T cell," *Rheumatology International*, pp. 1–8, 2010.
- [58] C. L. Miao Jiang, G. Chen, C. Xiao et al., "Understanding the molecular mechanism of interventions in treating rheumatoid arthritis patients with corresponding traditional Chinese medicine patterns based on bioinformatics approach," *Evidence-Based Complementary and Alternative Medicine*, vol. 2012, Article ID 129452, 11 pages, 2012.